

Scientific Editors/ Éditeurs Scientifiques

Ingmar GRENTHE

Ignasi PUIGDOMENECH

Royal Institute of Technology, Stockholm (Sweden)

Contributors/Collaborateurs

Bert ALLARD

Linköping University, Linköping (Sweden)

Steven A. BANWART

University of Bradford, Bradford (United Kingdom)

Jordi BRUNO

QuantiSci SL, Cerdanyola (Spain)

James H. EPHRAIM

Linköping University, Linköping (Sweden)

Rolf GRAUER [†]

Paul Scherrer Institut, Villigen (Switzerland)

Ingmar GRENTHE

Royal Institute of Technology, Stockholm (Sweden)

Jörg HADERMANN

Paul Scherrer Institut, Villigen (Switzerland)

Wolfgang HUMMEL
Paul Scherrer Institut, Villigen (Switzerland)

Andreas JAKOB
Paul Scherrer Institut, Villigen (Switzerland)

Theo KARAPIPERIS
Paul Scherrer Institut, Villigen (Switzerland)

Andrey V. PLYASUNOV
Royal Institute of Technology, Stockholm (Sweden)

Ignasi PUIGDOMENECH
Royal Institute of Technology, Stockholm (Sweden)

Joseph A. RARD
Lawrence Livermore National Laboratory, Livermore, California (USA)

Surendra SAXENA
University of Uppsala, Uppsala (Sweden)

Kastriot SPAHIU
Swedish Nuclear Fuel & Waste Management Co. (SKB), Stockholm (Sweden)

Secretariat/Secrétariat

M. C. Amaia SANDINO
Ignasi PUIGDOMENECH
OECD/NEA Data Bank (France)

Text processing and layout Traitement de texte et mise en pages

Cécile LOTTEAU
OECD/NEA Data Bank (France)

Preface

In 1992 the OECD Nuclear Energy Agency published the first volume (*Chemical Thermodynamics of Uranium* [92GRE/FUG]) in a series of critical reviews of thermodynamic data of elements of particular importance for the safety assessment of nuclear waste disposal systems. Another volume appeared in 1995 (*Chemical Thermodynamics of Americium* [95SIL/BID]) and two more volumes are expected in the near future (*Chemical Thermodynamics of Technetium* and *Chemical Thermodynamics of Neptunium and Plutonium*). These compilations are known as the NEA Thermochemical Data Base (TDB) project [90WAN]. Thermodynamic data are important for the modelling of the chemical processes in the engineered part of nuclear waste repository systems (the “near-field” region), and also to describe the effect of the “far-field”, *i.e.* how the chemical change in ground and surface water systems may affect the transport of toxic elements from the repository to the biosphere. Hence, the TDB project has been sponsored by the Radioactive Waste Management Committee (RWMC) of the NEA, and its Performance Assessment Advisory Group (PAAG), and the reviews are being coordinated by the NEA Data Bank.

The thermodynamic database of the NEA, like most databases of its kind, includes only data where precise, quantitative experimental information is available. Experimentalists have seldom used the same conditions when studying a given chemical system, and the numerical data in general cannot be directly compared to one another. It is necessary to establish methods that allow a recalculation of such data to a common standard state. These methods should also be used when selected thermodynamic data are extrapolated to the “working” conditions in specific systems.

In order to build a reliable chemical model of a system it is necessary to include all relevant processes. In practice this requires the use, not only of quality-assessed numerical data, but also of established scientific theories to estimate quantities for which precise experimental information is not available.

With these facts in mind one of us (I.G.) suggested that the NEA compilations of chemical thermodynamic data should be supplemented by a text describing both how data estimates can be made, and how extrapolation methods can be used to recalculate thermodynamic data to the specific conditions used in a model. The scientific basis and the accuracy of such estimation and extrapolation methods and their limitations should be outlined.

The description/modelling of interactions between metal ions and “small” ligands is reasonably straightforward; this is not the case for humic/fulvic acids. There are a large

number of different models used to transform experimental data into “equilibrium” or “binding” constants. These are described and compared with one another in Chapters V and VI.

We hope that the present volume may be used as a “compendium” of estimation and extrapolation procedures. The comparisons between different techniques might also be useful for those who are not experts in the various disciplines covered. All authors have been encouraged to include examples in their texts, which may serve as tutorials for the readers.

Most of the authors have participated in multidisciplinary research work involving environmental issues, particularly related to nuclear waste repository systems. All of us are, or have been, “laboratory” chemists/physicists. In discussions with colleagues we have often noticed that the concept “model” and the requirements of the scientific enquiry are described in somewhat different terms in “pure” and “applied” science. We therefore thought it worthwhile to include some more general chapters on the principles governing function and performance assessment, modelling strategies, and the results of the modelling of some complex systems.

Transport of chemical substances from a repository to the biosphere is the key element in safety and performance assessment. We have therefore included two chapters on such processes. One is more “traditional”, based on continuum mechanics (Chapter XII), while the other is based on a microscopic modelling (Chapter XI).

For use in waste management it is necessary to use procedures that are quality assessed. This has normally been achieved through some scientific review process before the methods have been published in the scientific literature. In keeping with the previous volumes, we have also asked outside reviewers to comment on the various chapters. Their suggestions and the action taken by the authors in response to them have been compiled at the NEA. The editors, the authors, and the NEA appreciate the helpful criticism of the review team, which is listed on pages ix-x.

Stockholm, April 1997

The Scientific Editors

Préface

En 1992, l'Agence de l'OCDE pour l'énergie nucléaire a publié le premier volume (*Chemical Thermodynamics of Uranium* [92GRE/FUG]) d'une série d'études critiques sur des données thermodynamiques d'éléments particulièrement importants pour l'évaluation de sûreté dans le traitement des déchets nucléaires. Un autre volume a été publié en 1995 (*Chemical Thermodynamics of Americium* [95SIL/BID]) et deux autres volumes sont attendus bientôt (*Chemical Thermodynamics of Technetium* et *Chemical Thermodynamics of Neptunium and Plutonium*). Ces compilations sont connues sous le nom de projet de Banque de données thermodynamique de l'AEN (TDB) [90WAN]. Les données thermodynamiques sont importantes pour la modélisation des processus chimiques dans la partie conception des systèmes de stockage des déchets radioactifs (la région du "champ proche"), et aussi pour décrire les effets dans le "champ lointain", c'est-à-dire, comment une modification chimique dans les systèmes des eaux souterraines et de surface pourrait affecter le transport d'éléments toxiques du dépôt vers la biosphère. C'est pourquoi le projet TDB est subventionné par le Comité de la gestion des déchets radioactifs de l'AEN (RWMC), et son Groupe consultatif sur l'évaluation des performances des systèmes d'évacuation des déchets radioactifs (PAAG), et la réalisation des études est coordonnée par la Banque de données de l'AEN.

La base de données thermodynamique de l'AEN, comme la plupart des bases de données de ce type, ne comprend que les données pour lesquelles des informations expérimentales quantitatives et précises sont disponibles. Les expérimentateurs n'ont utilisé que rarement les mêmes conditions pour étudier un système chimique donné, et, en général, les valeurs numériques ne peuvent pas être comparées directement entre elles. Il faut établir des méthodes qui permettent un nouveau calcul de ces données dans un état standard commun. Ces méthodes peuvent aussi être utilisées quand les données thermodynamiques choisies sont extrapolées aux conditions "de travail" dans des systèmes spécifiques.

De manière à construire un modèle chimique fiable d'un système, il faut inclure tous les processus utiles. En pratique, ceci demande non seulement l'utilisation de valeurs numériques de qualité contrôlée, mais aussi l'utilisation de théories scientifiques établies afin d'estimer les quantités pour lesquelles on n'a pas de valeur expérimentale précise.

Une fois ceci précisé, l'un de nous (I.G.) a suggéré que les compilations de l'AEN de données thermodynamiques soient complétées par un texte décrivant, à la fois, comment des estimations de données peuvent être réalisées et comment des méthodes d'extrapolation peuvent être utilisées pour recalculer des données thermodynamiques dans

les conditions spécifiques utilisées dans un modèle. Le cadre scientifique ainsi que la précision de telles méthodes d'estimation et d'extrapolation et de leurs limitations pourraient être présentés brièvement.

La description/modélisation des interactions entre les ions métalliques et les “petits” ligands est relativement simple ; ce n'est pas le cas pour les acides humiques/fulviques. Il existe un grand nombre de modèles différents utilisés pour transformer des données expérimentales en constantes “d'équilibre” ou “de complexation”. Celles-ci sont décrites et comparées entre elles dans les Chapitres V et VI.

Nous espérons que ce livre puisse être utilisé comme un “mode d'emploi” des procédures d'estimation et d'extrapolation. Les comparaisons entre différentes techniques peuvent aussi être utiles à ceux qui ne sont pas experts dans toutes les disciplines employées. Tous les auteurs ont été encouragés à utiliser, dans leurs textes, des exemples qui peuvent servir de travaux dirigés pour le lecteur.

La plupart des auteurs ont participé à des travaux de recherches multidisciplinaires sur des problèmes d'environnement, particulièrement liés aux systèmes de dépôt des déchets nucléaires. Chacun de nous est, ou a été, chimiste ou physicien “en laboratoire”. En discutant avec des collègues, nous avons souvent remarqué que l'on parle du concept “modèle” et des besoins de la recherche scientifique avec des termes quelque peu différents en science “fondamentale” ou “appliquée”. Par conséquent, nous avons pensé qu'il était intéressant d'écrire quelques chapitres généraux supplémentaires sur les principes régissant l'évaluation du fonctionnement et de la performance, les stratégies de modélisation, et les résultats de la modélisation de quelques systèmes complexes.

Le transport de substances chimiques d'un dépôt vers la biosphère est l'élément clé dans l'évaluation de la sûreté et de la performance. Nous avons donc ajouté deux chapitres sur de tels processus. L'un, basé sur la mécanique des milieux continus, est plus “traditionnel” (Chapitre XII), alors que l'autre est basé sur une modélisation microscopique (Chapitre XI).

Pour être utilisées en gestion des déchets, il faut des procédures de qualité contrôlée. Normalement, ceci a été fait par un examen scientifique avant que ces méthodes ne soient publiées dans la littérature scientifique. Comme dans les volumes précédents, nous avons aussi demandé à des experts extérieurs leurs avis sur les différents chapitres. Leurs suggestions et les modifications des auteurs, en réaction à celles-ci, ont été réunies à l'AEN. Les éditeurs, les auteurs et l'AEN ont apprécié la critique constructive de l'équipe d'experts dont la liste se trouve en pages xi-xii.

Avril 1997, Stockholm

Les Éditeurs Scientifiques

Acknowledgements

We are grateful to the members of both the NEA Radioactive Waste Management Committee and its Performance Assessment Advisory Group for their suggestions and assistance in seeking financial support for this book. We thank the following persons within the NEA for their support and encouragement: Dr. Kunihiro Uematsu, Director General; Dr. Philippe Savelli, Deputy Director, Science, Computing and Development; Mr. Jean-Pierre Olivier, Head of the Division for Radiation Protection and Radioactive Waste Management; Mr. Claes Nordborg of the Nuclear Science Division and Dr. Nigel Tubbs of the Data Bank.

The editors would especially like to thank Dr. M.C. Amaia Sandino and Cécile Lotteau at the NEA Data Bank for their patience when the authors did not follow the agreed time schedule, and when they suggested extensive revisions of their texts. Without their assistance the book would not have appeared in print.

Each of the chapters in this book (excluding Chapter IV) has been reviewed by one or more of the following experts:

Prof. M. T. Beck	Kossuth Lajos University, Debrecen, Hungary
Prof. L. Ciavatta	Universita di Napoli, Napoli, Italia
Dr. E. Curti	Paul Scherrer Institut, Villigen, Switzerland
Prof. V. Cvetkovic	Royal Institute of Technology, Stockholm, Sweden
Dr. M. Filella	Université de Genève, Switzerland
Dr. J. Hadermann	Paul Scherrer Institut, Villigen, Switzerland
Dr. W. Heer	Paul Scherrer Institut, Villigen, Switzerland
Dr. W. Hummel	Paul Scherrer Institut, Villigen, Switzerland
Prof. G. de Marsily	Université Pierre et Marie Curie, Paris, France
Dr. F. Karlsson	Swedish Nuclear Fuel & Waste Management Co., Stockholm, Sweden
Dr. F. J. Pearson, Jr.	Paul Scherrer Institut, Villigen, Switzerland
Dr. J. A. Rard	Lawrence Livermore National Laboratory, California, USA
Prof. W. Stumm	EAWAG, Duebendorf, Switzerland
Dr. B. Sundman	Royal Institute of Technology, Stockholm, Sweden

Dr. P. Tremaine	Memorial University of Newfoundland, St. John's, Newfoundland, Canada
Dr. O. Wahlberg	Royal Institute of Technology, Stockholm, Sweden
Dr. H. Wanner	Swiss Federal Nuclear Safety Inspectorate, Villigen, Switzerland

The NEA, the editors and the authors thank the reviewers for their helpful criticism.

Thanks are expressed to the Swedish Nuclear Fuel and Waste Management Co. for its financial support of editing efforts during the later stages of this project.

This book has been prepared with \LaTeX computer typesetting software [94LAM]. Some of the graphs were produced with the GNUPLOT plotting program, originally written by T. Williams and C. Kelly (\LaTeX output option written by D. Kotz and R. Lang). During the development process of the book, the following public domain software has also been used: GsView by R. Lang; Ghostscript by L.P. Deutsch of Aladdin Enterprises; DviWin by H. Sendoukas; DviPS by T. Rokicki; MicroEmacs by D.M. Lawrence; TeXCAD by G. Horn and J. Winkelmann; and gTeX by Y.U. Ryu.

We would also like to thank the following parties for granting permission to reproduce copyright material:

- American Geophysical Union, Washington, DC, USA, for their permission to reprint Figure XII.3.
- Elsevier Science-NL, Sara Burgerhartstraat 25, 1055 KV Amsterdam, The Netherlands, for their permission to reprint Figures VII.2, VII.3, VII.4, XI.2, and XI.8.
- Kluwer Academic Publishers, Dordrecht, The Netherlands, for their permission to reprint Figures VII.1, VII.9, VII.10, and VII.11.
- Marcel Dekker, Inc., New York, U.S.A., for their permission to reprint Figure VI.1.
- The National Cooperative for the Disposal of Radioactive Waste (Nagra), Hardstrasse 73, CH-5430 Wettingen, Switzerland, for their permission to reprint Figure XII.1

Stockholm, April 1997

The Scientific Editors

Remerciements

Nous sommes reconnaissants aux membres du Comité de la gestion des déchets radioactifs de l'AEN et de son Groupe consultatif sur l'évaluation de la performance des systèmes d'évacuation des déchets radioactifs pour leurs suggestions et l'aide qu'ils nous ont apportées dans la recherche d'un financement pour ce livre. Nous voulons remercier les personnes de l'AEN suivantes pour leur soutien et leurs encouragements : Dr. Kunihiro Uematsu, Directeur général ; Dr. Philippe Savelli, Directeur adjoint, Sciences, informatique et développement ; M. Jean-Pierre Olivier, Chef de la Division de la protection radiologique et de la gestion des déchets radioactifs ; M. Claes Nordborg de la Division des sciences nucléaires et Dr. Nigel Tubbs de la Banque de données.

Les éditeurs voudraient remercier tout particulièrement Dr. M.C. Amaia Sandino et Cécile Lotteau de la Banque de données de l'AEN pour leur patience quand les auteurs n'ont pas respecté le planning prévu, et quand ils ont suggéré de considérables modifications de leurs textes. Sans leur aide, ce livre n'aurait jamais été publié.

Tous les chapitres de ce livre (sauf le Chapitre IV) ont été revus par au moins l'un des experts suivants:

Prof. M. T. Beck	Kossuth Lajos University, Debrecen, Hongrie
Prof. L. Ciavatta	Universita di Napoli, Napoli, Italie
Dr. E. Curti	Paul Scherrer Institut, Villigen, Suisse
Prof. V. Cvetkovic	Royal Institute of Technology, Stockholm, Suède
Dr. M. Filella	Université de Genève, Suisse
Dr. J. Hjadermann	Paul Scherrer Institut, Villigen, Suisse
Dr. W. Heer	Paul Scherrer Institut, Villigen, Suisse
Dr. W. Hummel	Paul Scherrer Institut, Villigen, Suisse
Prof. G. de Marsily	Université Pierre et Marie Curie, Paris, France
Dr. F. Karlsson	Swedish Nuclear Fuel & Waste Management Co., Stockholm, Suède
Dr. F. J. Pearson, Jr.	Paul Scherrer Institut, Villigen, Suisse
Dr. J. A. Rard	Lawrence Livermore National Laboratory, California, USA
Prof. W. Stumm	EAWAG, Duebendorf, Suisse
Dr. B. Sundman	Royal Institute of Technology, Stockholm, Suède

Dr. P. Tremaine	Memorial University of Newfoundland, St John's, Newfoundland, Canada
Dr. O. Wahlberg	Royal Institute of Technology, Stockholm, Suède
Dr. H. Wanner	Swiss Federal Nuclear Safety Inspectorate, Villigen, Suisse

L'AEN, les éditeurs et les auteurs remercient les experts pour leurs critiques constructives.

Nous voudrions aussi remercier la compagnie Swedish Nuclear Fuel & Waste Management Co. pour son soutien financier aux efforts d'édition pendant les dernières étapes de ce projet.

Ce livre a été réalisé avec le logiciel de mise en pages \LaTeX [94LAM]. Certains graphiques ont été réalisés avec le logiciel de dessin GNUPLOT, écrit, à l'origine, par T. Williams and C. Kelly (l'option de sortie compatible avec \LaTeX a été écrite par D. Kotz et R. Lang). Pendant la conception de ce livre, les logiciels du domaine public suivants ont aussi été utilisés : GsView par R. Lang ; Ghostscript par L.P. Deutsch d'Aladdin Enterprises ; DviWin par H. Sendoukas ; DviPS par T. Rokicki ; MicroEmacs par D.M. Lawrence ; TeXCAD par G. Horn et J. Winkelmann ; et gTeX par Y.U. Ryu.

Nous tenons aussi à remercier les organismes suivants pour avoir permis la reproduction de graphiques protégés par copyright :

- American Geophysical Union, Washington, DC, USA, pour leur autorisation de reproduire la Figure XII.3.
- Elsevier Science-NL, Burgerharstraat 25, 1055 KV Amsterdam, Pays-Bas, pour leur autorisation de reproduire les Figures VII.2, VII.3, VII.4, XI.2 et XI.8.
- Kluwer Academic Publishers, Dordrecht, Pays-Bas, pour leur autorisation de reproduire les Figures VII.1, VII.9, VII.10 et VII.11.
- Marcel Dekker, Inc., New York, USA, pour leur autorisation de reproduire la Figure VI.1.
- The National Cooperative for the Disposal of Radioactive Waste (Nagra), Hardstrasse 73, CH-5430 Wettingen, Suisse, pour leur autorisation de reproduire la Figure XII.1.

Avril 1997, Stockholm

Les Éditeurs Scientifiques

Foreword

The NEA Data Bank provides a number of services that may be useful to the reader of this book: among others, a library of computer programs in various areas. This includes geochemical codes such as PHREEQE, EQ3/6, MINEQL, MINTEQ, PHRQPITZ, *etc.* These computer codes can be obtained on request from the NEA Data Bank.

The TDB Data Base is now accessible on-line through Internet at <http://www.nea.fr/html/dbtdb>.

For requests of data, computer programs, on-line access or further information, please write to:

OECD Nuclear Energy Agency, Data Bank
Le Seine-St. Germain
12, boulevard des Îles
F-92130 Issy-les-Moulineaux, France

or by electronic mail to: **tdb@nea.fr**

More information about the NEA is available at <http://www.nea.fr>.

The opinions and conclusions expressed are those of the authors only, and do not necessarily reflect the views of any Member country or international organisation. This volume is published on the responsibility of the Secretary-General of the OECD.

Paris, April 1997

The NEA Secretariat

Avant-propos

La Banque de données de l'AEN offre nombre de services qui peuvent être utiles au lecteur de ce livre : parmi d'autres, une bibliothèque de logiciels dans plusieurs domaines. Cela comprend des codes géochimiques tels que PHREEQE, EQ3/6, MINEQL, MINTEQ, PHRQPITZ, *etc.* Ces codes de calculs peuvent être obtenus sur demande à la Banque de données de l'AEN.

La Banque de données TDB est maintenant accessible en ligne sur Internet à l'adresse: <http://www.nea.fr/html/dbtdb>.

Pour tout renseignement sur des données, logiciels, possibilités de connexion ainsi que toute information complémentaire vous pouvez écrire à :

Agence de l'OCDE pour l'énergie nucléaire
Banque de données
Le Seine-St. Germain
12, boulevard des Îles
F-92130 Issy-les-Moulineaux, France

ou par courrier électronique à : tdb@nea.fr

Des informations sur l'AEN sont disponibles à <http://www.nea.fr>.

Les opinions et conclusions exprimées dans ce rapport n'engagent que les auteurs, et ne représentent pas nécessairement celles d'un pays Membre ou d'une organisation internationale. Ce rapport est publié sous la responsabilité du Secrétaire général de l'OCDE.

Avril 1997, Paris

Le Secrétariat de l'AEN

Contents

I Introduction

<i>by: Ingmar GRENTHE and Ignasi PUIGDOMENECH</i>	1
I.1 Models and modelling	1
I.1.1 The need for models	3
I.1.2 Verification and validation of models	3
I.1.3 Modelling stages for complex systems	4
I.2 Laboratory systems <i>vs.</i> complex systems encountered in nature and in science/technology	5
I.3 Modelling methodologies for complex systems	8
I.4 Some simple physical and chemical models	12
I.5 Under what circumstances can we make predictions of the time evolution of chemical systems?	13
I.6 Some additional considerations on chemical modelling	18
I.6.1 Sources of thermodynamic data	19
I.6.2 Using tabulated thermodynamic data	21
I.7 Chapitre I : Introduction (French translation of Chapter I)	22

II Symbols, Standards, and Conventions

<i>by: Ingmar GRENTHE and Ignasi PUIGDOMENECH</i>	35
II.1 Symbols, terminology and nomenclature	35
II.1.1 Symbols and terminology	35
II.1.2 Reference codes	35
II.1.3 Chemical formulae and nomenclature	38
II.1.4 Phase designators	38
II.1.5 Systems and their components	40
II.1.5.1 Components in redox reactions	41
II.1.6 Processes	41
II.1.7 Thermodynamic data	41
II.1.8 Equilibrium constants	43
II.1.8.1 Protonation of a ligand	44
II.1.8.2 Formation of metal ion complexes	44
II.1.8.3 Solubility constants	46
II.1.8.4 Equilibria involving the addition of a gaseous ligand	46
II.1.8.5 Surface coordination reactions	47
II.1.8.6 Redox equilibria	48
II.1.9 pH	53
II.2 Units and conversion factors	54
II.3 Standard and reference conditions	56
II.3.1 Standard state	56
II.3.2 Standard state pressure	58

II.3.3	Reference temperature	58
II.4	Fundamental physical constants	58
II.5	Graphical representations of equilibrium systems	58
III Chemical Background for the Modelling of Reactions in Aqueous Systems		
	<i>by: Ingmar GRENTHE, Wolfgang HUMMEL and Ignasi PUIGDOMENECH</i>	69
III.1	Introduction	69
III.2	Factors that influence the equilibrium properties of chemical reactions in aqueous systems	72
III.2.1	Chemical characteristics of metal ions	72
III.2.2	Water as a solvent	75
III.2.2.1	Solvation and complex formation, ion-ion and ion-dipole interactions	75
III.2.2.2	Ion-ion and ion-dipole interactions	77
III.2.2.3	Ligands and their chemical characteristics	79
III.2.2.4	Qualitative features of complex formation reactions	82
III.3	Classification of metal complexes	85
III.4	The thermodynamics of complex formation reactions	88
III.5	Complex formation, a competitive process	89
III.5.1	The pH dependence of complex formation reactions	91
III.5.2	Polynuclear complex formation	91
III.5.3	The stoichiometry of hydroxide complexes	91
III.5.4	Competition between different metal ions for the same ligand	94
III.6	Theoretical framework for the estimation of equilibrium constants	96
III.6.1	On the magnitude of equilibrium constants and the ratios between equilibrium constants for successive complex formation reactions	96
III.6.2	Estimation of equilibrium constants for ternary complexes	98
III.6.3	On the use of correlations for the prediction of equilibrium constants	103
III.6.3.1	Correlations based on the size and charge of the metal ion	104
III.6.3.2	Ligand field theory and Irving and Williams series	107
III.6.4	Correlations based on properties of the ligand	108
III.6.5	Correlations between equilibrium constants, $\log_{10} K$, of different metal ions	109
III.6.6	Correlations between successive equilibrium constants	113
III.6.7	An example of the use of estimation methods for the modelling of a complex aquatic system, the influence of oxalate on U(VI) speciation	114
III.7	Some aspects of chemical kinetics	124
III.7.1	Reactions in homogeneous aqueous systems	125
III.7.2	The temperature dependence of rate constants	126
III.7.2.1	Dynamics of acid/base and complex formation reactions	126
III.7.2.2	Dynamics of electron transfer reactions	127
III.7.2.3	Catalysis and biologically mediated reactions	128
III.7.2.4	Photochemical reactions	128
III.7.3	The steady-state concept for flow systems	128
III.7.4	Rates and mechanisms of heterogeneous equilibria	129
IV Solubility Limitations: An “Old Timer’s” View		
	<i>by: Rolf GRAUER</i>	131
IV.1	Einleitung	131
IV.2	Über Inhalt und Qualität von geochemischen Datenbasen	133
IV.2.1	“The Law of Mythical Numbers”	133
IV.2.2	... and “The Handbook of Unstable, Exotic and Nonexistent Compounds”	135
IV.2.3	Der Vergleich von Datenbasen: Ein Weg zu besseren Werten ?	135

IV.3	Löslichkeitslimiten im Nahfeld: Das Beispiel Americium	136
IV.3.1	Löslichkeitsbestimmende Phasen	136
IV.3.2	Die Rolle der Lanthaniden	137
IV.3.3	Verglaste Abfälle	138
IV.3.4	Löslichkeitslimiten im Nahfeld: welche Festphasen ?	138
IV.4	Löslichkeitslimiten im Fernfeld: Das Beispiel Nickel	138
IV.4.1	Die Modellierung der Nickel-Löslichkeit	139
IV.4.2	Zur Geochemie des Nickels	140
IV.4.3	Löslichkeitslimiten im Fernfeld ?	141
IV.5	Schlussbemerkungen	141
IV.6	Solubility limitations: An “old timer’s” view (English translation of Chapter IV)	144
V	Binding Models for Humic Substances	
	<i>by: Wolfgang HUMMEL</i>	153
V.1	Introduction	153
V.2	What are humic substances ?	154
V.3	Metal ion binding of humic substances	155
V.3.1	The experimental data	155
V.3.2	Variations in component concentration	157
V.3.2.1	The simplest model	157
V.3.2.2	Mixed-ligand models	161
V.3.2.3	Variable stoichiometry models	163
V.3.2.4	The multi-site models	166
V.3.2.5	The continuous distribution models	169
V.3.3	Variations in pH	174
V.3.3.1	Empirical functions	174
V.3.3.2	Proton exchange reactions	175
V.3.3.3	Electrostatic effects	179
V.3.4	Variations in ionic strength	185
V.3.4.1	Empirical functions	186
V.3.4.2	Electrostatic effects	186
V.3.5	What is the best humic binding model?	188
V.4	Problem solving strategies	190
V.4.1	Models used as research tools	190
V.4.2	Models used as assessment tools	191
V.4.2.1	The “conservative roof” approach for performance assessment	191
V.4.2.2	Competition of other complexes	195
V.4.2.3	Application of laboratory data in performance assessment	201
VI	Metal Ion Binding by Humic Substances	
	<i>by: James H. EPHRAIM and Bert ALLARD</i>	207
VI.1	Introduction	207
VI.2	General overview	208
VI.2.1	Isolation and extraction of humic substances	209
VI.2.2	Characterisation methods	209
VI.2.3	Redox properties of humic substances	212
VI.3	Solution chemistry of humic substances	213
VI.3.1	Proton interactions with humic substances	213
VI.3.1.1	Discrete ligand models	213
VI.3.1.2	Continuous distribution models	221
VI.3.1.3	Discrete models versus continuous distribution models	222
VI.3.2	Models for the interaction of metals with humic/fulvic acids	223

VI.3.2.1	Discrete ligand models	225
VI.3.2.2	Continuous distribution models	226
VI.3.2.3	Factors affecting the overall complex formation function	226
VI.3.2.4	Competitive binding of various metal ions to humic substances	227
VI.3.3	Data needs for modelling the role of humic substances	228
VI.3.3.1	Review of studies on interactions between humic substances and metal ions	231
VI.4	Modelling example: speciation of Eu^{3+} in the environment in presence of humic substances and Ca^{2+}	232
VI.4.1	Relevance of the exercise	241
VI.5	Summary	241
VII	Aqueous Speciation at the Interface Between Geological Solids and Groundwater	
	<i>by: Steven A. BANWART</i>	245
VII.1	Introduction	245
VII.2	Theoretical background	246
VII.2.1	Intermolecular forces at the solid-solution interface	246
VII.2.2	Mass balances for adsorbing substances: The concept of surface excess	246
VII.2.3	Stoichiometric adsorption reactions and the thermodynamic law of mass action	249
VII.2.4	Combining mass balances and thermodynamic mass laws: The adsorption isotherm	252
VII.2.4.1	The Langmuir adsorption isotherm	252
VII.2.4.2	A linear adsorption isotherm: The distribution coefficient	253
VII.2.5	The influence of solution speciation on adsorption	253
VII.3	Surface complexation	254
VII.3.1	Chemisorption of water: Formation of variable charged surfaces	254
VII.3.2	Adsorption of ligands and metals at the hydrated surface	254
VII.3.3	The pH dependence of adsorption	258
VII.3.4	Competitive adsorption	264
VII.3.5	Non-ideal behaviour: Activity corrections for surface coverage	267
VII.3.6	Charged surfaces and ion exchange	272
VII.3.6.1	Origins of surface charge	272
VII.3.6.2	The electrical double layer	275
VII.3.6.3	Ion exchange reactions	275
VII.3.7	Thermodynamic descriptions of complex adsorption systems	280
VII.4	Surface precipitation	281
VII.4.1	The transition from adsorption to surface precipitation	281
VII.4.2	The conditional solubility constant for surface precipitation/co-precipitation	282
VII.5	Implications for contaminant hydrogeology	283
VII.5.1	Reversible partitioning of contaminants	283
VII.5.2	Irreversible adsorption	286
VII.5.3	Coupling geochemistry and hydrogeology	287
VIII	Systematization and Estimation of Thermochemical Data on Silicates	
	<i>by: Surendra K. SAXENA</i>	289
VIII.1	Introduction	289
VIII.2	A systematized data base	291
VIII.2.1	Thermodynamics	292
VIII.2.1.1	Temperature dependence of the Gibbs free energy	292
VIII.2.1.2	Heat capacity at high temperature	292

VIII.2.2	The regression technique	295
VIII.2.3	The optimization technique	296
VIII.2.4	Data base	300
VIII.3	Estimation of enthalpy of silicates	300
VIII.3.1	Principles underlying empirical correlation	300
VIII.3.2	Tardy's method	300
VIII.3.3	The polyhedral approach	314
VIII.3.3.1	Chermak-Rimstidt method	314
VIII.3.3.2	A new polyhedral method	316
VIII.4	Estimation of entropy	320
VIII.4.1	Example of a calculation	321
VIII.5	Estimation of heat capacities of solids	322
VIII.6	Conclusions	322
IX Estimations of Medium Effects on Thermodynamic Data		
	<i>by: Ingmar GRENTHE, Andrey V. PLYASUNOV and Kastriot SPAHIU</i>	325
IX.1	Introduction	325
IX.2	On the estimation of activity coefficients in electrolyte systems	327
IX.3	The Brønsted-Guggenheim-Scatchard model (SIT)	331
IX.3.1	Determination of ion interaction coefficients	341
IX.4	Other equations, approximately equivalent with the SIT model	345
IX.5	On the magnitude of the specific ion interaction coefficients	347
IX.5.1	Correlations among specific ion interaction parameters for cations	347
IX.5.2	Correlations among specific ion interaction parameters for complexes	350
IX.5.3	Correlations between $\Delta\varepsilon$ -values for chemical reactions	352
IX.6	The Pitzer equations	352
IX.7	Comparison of the SIT and the Pitzer models for the description of concentration-dependence of equilibrium constants of complex formation reactions in ionic media	355
IX.7.1	The determination of the Pitzer and the SIT parameters from the $\log_{10} K$ data	366
IX.8	The relationship between the SIT $\varepsilon(i, j)$ and the Pitzer $\beta_{ij}^{(0)}$ and $\beta_{ij}^{(1)}$ parameters for mean-activity coefficients	378
IX.8.1	The relationship between the $\Delta\varepsilon$ values in the SIT model and the $\Delta\beta^{(0)}$ and $\Delta\beta^{(1)}$ values in the Pitzer models for complex formation reactions at "trace" concentrations of reactants/products	383
IX.9	The use of the SIT at elevated temperatures	397
IX.9.1	Osmotic coefficient	397
IX.9.2	The analytical statements for partial and apparent molar properties of single electrolytes on the basis of the SIT model	398
IX.9.3	The Debye-Hückel limiting law slopes	400
IX.10	The concentration dependence of heats of reactions	406
IX.10.1	The calculation of the standard enthalpy of reaction from experimental $\Delta_r H_m$ data using the Pitzer equation	410
IX.10.2	The calculation of the standard enthalpy of a reaction from experimental $\Delta_r H_m$ data using the SIT model	412
IX.10.3	The extrapolation equations for the determination of the standard enthalpy of reaction from the experimental $\Delta_r H_m$ data based on the Pitzer and the SIT models	417
IX.11	Conclusions	424

X	Temperature Corrections to Thermodynamic Data and Enthalpy Calculations	427
	<i>by: Ignasi PUIGDOMENECH, Joseph A. RARD, Andrey V. PLYASUNOV and Ingmar GRENTHE</i>	
X.1	Introduction	427
X.2	Second-law extrapolations	429
X.2.1	The hydrogen ion convention	432
X.2.2	Approximations	434
X.2.2.1	Constant enthalpy of reaction	434
X.2.2.2	Constant heat capacity of reaction	434
X.2.2.3	Isoelectric and isocoulombic reactions	437
X.2.3	Calculation of $\Delta_{\text{sol}}H_{\text{m}}$ from temperature dependence of solubility	444
X.2.4	Alternative heat capacity expressions for aqueous species	447
X.2.4.1	DQUANT Equation	447
X.2.4.2	The revised Helgeson–Kirkham–Flowers model	448
X.2.4.3	The Ryzhenko–Bryzgalin model	455
X.2.4.4	The density or “complete equilibrium constant” model	465
X.3	Third-law method	469
X.3.1	Evaluation from high and low-temperature calorimetric data	470
X.3.2	Evaluation from high-temperature data	473
X.3.3	A brief comparison of enthalpies derived from the second and third-law methods	475
X.4	Estimation methods	476
X.4.1	Estimation methods for heat capacities	476
X.4.1.1	Heat capacity estimations for solid phases	476
X.4.1.2	Heat capacity estimations for aqueous species	477
X.4.1.3	Heat capacity estimation methods for reactions in aqueous solutions	482
X.4.2	Entropy estimation methods	483
X.4.2.1	Entropy estimation methods for solid phases	483
X.4.2.2	Entropy estimation methods for aqueous species	485
X.4.3	Examples	490
X.5	Concluding remarks	492
X.6	Acknowledgements	493
XI	Cellular Automaton Models of Reaction-Transport Processes	495
	<i>by: Theo KARAPIPERIS</i>	
XI.1	Introduction	495
XI.2	Cellular automata	498
XI.2.1	Historical development	498
XI.2.2	Elementary examples	499
XI.3	Cellular automata for transport with chemical reactions	503
XI.3.1	Models	503
XI.3.1.1	Transport	503
XI.3.1.2	Chemical reactions	507
XI.3.2	Applications	510
XI.3.2.1	$a + b \rightarrow c$	510
XI.3.2.2	Autocatalytic reactions	511
XI.3.2.3	Reactions with mineral surfaces	514
XI.4	Conclusion	522
XI.5	Acknowledgements	524

XII	Modelling Solute Transport Using the Double Porous Medium Approach	525
	<i>by: Andreas JAKOB</i>	
XII.1	Introduction	525
XII.2	Classification of transport phenomena	527
XII.3	Mass transport due to a concentration gradient	529
XII.3.1	Fickian dispersion	529
XII.3.2	Scale dependent dispersivity	537
XII.3.3	The problem of local averaging	538
XII.3.4	Sorption equations used in transport modelling	539
XII.3.5	The double porosity medium concept	545
XII.3.6	Effects of matrix diffusion and the effective surface sorption approximation	554
XII.3.7	Modelling methodology and further examples	564
XII.4	Acknowledgments	574
XII.5	Glossary	574
XIII	The Pillars of Safety	577
	<i>by: Jörg HADERMANN</i>	
XIII.1	Introduction	577
XIII.2	Reduction of release rate at the source	584
XIII.3	Retardation during transport	585
XIII.4	Dilution	588
XIV	Trace Element Modelling	593
	<i>by: Jordi BRUNO</i>	
XIV.1	Why are we concerned about trace metals ?	593
XIV.2	Some general aspects of (geo)chemical modelling	594
XIV.2.1	How did all this start ?	594
XIV.3	The methodology of geochemical modelling	596
XIV.3.1	The building blocks	596
XIV.3.2	The system data	596
XIV.3.3	The chemical and physical variability of subsurface environments	597
XIV.3.3.1	Physical conditions	597
XIV.3.3.2	Biological conditions	597
XIV.3.3.3	Variability of chemical conditions	597
XIV.3.4	Getting a feeling for the system. The conceptual model	599
XIV.3.4.1	The geological setting	600
XIV.3.4.2	The hydrogeological condition	603
XIV.3.4.3	A quantitative description of local disequilibrium. The Peclet, Damkohler and Lichtner parameters	605
XIV.3.4.4	The interaction of trace metals with major component solid phases	607
XIV.4	The objective of geochemical modelling efforts. Interpretation <i>vs.</i> prediction	612
XIV.4.1	An example of assessing the potential impact of an anthropogenic disturbance on a high-level nuclear waste repository. The effects of acid rain in the granitic geosphere	612
XIV.4.2	An example of calculating the maximum release concentrations of critical radionuclides from spent fuel disposal. How information from natural system studies can be used to narrow down unrealistic predictions.	615
XIV.5	Acknowledgments	621
XV	Authors List	623
XVI	Reference List	655

Table des matières

I Introduction

<i>par : Ingmar GRENTHE et Ignasi PUIGDOMENECH</i>	1
I.1 Modèles et modélisation	1
I.1.1 Le besoin des modèles	3
I.1.2 Vérification et validation des modèles	3
I.1.3 Étapes de la modélisation de systèmes complexes	4
I.2 Systèmes de laboratoire <i>vs.</i> systèmes complexes rencontrés dans la nature et en science/technologie	5
I.3 Méthodologies de modélisation pour systèmes complexes	8
I.4 Quelques modèles physiques et chimiques simples	12
I.5 Sous quelles conditions pouvons-nous faire des prévisions sur l'évolution des systèmes chimiques au cours du temps ?	13
I.6 Considérations supplémentaires sur la modélisation	18
I.6.1 Sources de données thermodynamiques	19
I.6.2 Utilisation de données thermodynamiques présentées en tableaux	21
I.7 Chapitre I : Introduction (version française)	22

II Symboles, normes et conventions

<i>par : Ingmar GRENTHE et Ignasi PUIGDOMENECH</i>	35
II.1 Symboles, terminologie et nomenclature	35
II.1.1 Symboles et terminologie	35
II.1.2 Codes des références	35
II.1.3 Formules chimiques et nomenclature	38
II.1.4 Désignation des phases	38
II.1.5 Les systèmes et leurs constituants	40
II.1.5.1 Les constituants dans les réactions d'oxydoréduction	41
II.1.6 Processus	41
II.1.7 Données thermodynamiques	41
II.1.8 Constantes d'équilibre	43
II.1.8.1 Capture d'un proton par un ligand	44
II.1.8.2 Formation de complexes d'ions métalliques	44
II.1.8.3 Constantes de solubilité	46
II.1.8.4 Équilibre faisant intervenir l'addition d'un ligand gazeux	46
II.1.8.5 Réactions de coordination en surface	47
II.1.8.6 Équilibres redox	48
II.1.9 pH	53
II.2 Unités et facteurs de conversion	54
II.3 Conditions standards et de référence	56
II.3.1 État standard	56
II.3.2 Pression de l'état standard	58
II.3.3 Température de référence	58
II.4 Constantes physiques fondamentales	58

II.5	Représentations graphiques de systèmes d'équilibre	58
III	Notions chimiques pour la modélisation de réactions dans des systèmes aqueux <i>par : Ingmar GRENTHE, Wolfgang HUMMEL et Ignasi PUIGDOMENECH</i>	69
III.1	Introduction	69
III.2	Facteurs affectant les propriétés d'équilibre des réactions chimiques dans les systèmes aqueux	72
III.2.1	Caractéristiques chimiques des ions métalliques	72
III.2.2	L'eau en tant que solvant	75
III.2.2.1	Solvatation et formation de complexes, interactions ion-ion et dipôle-ion	75
III.2.2.2	Interactions ion-ion et dipôle-ion	77
III.2.2.3	Les ligands et leurs caractéristiques	79
III.2.2.4	Caractéristiques qualitatives des réactions de complexation ..	82
III.3	Classification des complexes métalliques	85
III.4	Thermodynamique des réactions de complexation	88
III.5	La complexation, un processus de compétitions	89
III.5.1	Dépendance en fonction du pH des réactions de complexation	91
III.5.2	Formations de complexes polynucléaires	91
III.5.3	Stoichiométrie des complexes hydroxydes	91
III.5.4	Compétition entre différents ions métalliques pour le même ligand	94
III.6	Cadre théorique pour l'estimation des constantes d'équilibre	96
III.6.1	À propos des valeurs des constantes d'équilibre et de leurs rapports pour des réactions de complexation successives	96
III.6.2	Estimation de constantes d'équilibre pour des complexes ternaires	98
III.6.3	À propos de l'utilisation de corrélations pour la prévision de constantes d'équilibre	103
III.6.3.1	Corrélations basées sur la taille et la charge de l'ion métallique	104
III.6.3.2	Théorie du champ de ligands et séries d'Irving et de Williams	107
III.6.4	Corrélations basées sur les propriétés des ligands	108
III.6.5	Corrélations entre constantes d'équilibre, $\log_{10} K$, de différents ions métalliques	109
III.6.6	Corrélations entre constantes d'équilibre successives	113
III.6.7	Exemple d'utilisation de méthode d'estimation pour la modélisation d'un système aquatique complexe, influence de l'ion oxalate sur les formes chimiques de l'U(VI)	114
III.7	Quelques aspects de la cinétique chimique	124
III.7.1	Réactions en systèmes aqueux homogènes	125
III.7.2	Dépendance des constantes de vitesse en fonction de la température ..	126
III.7.2.1	Dynamique des réactions acido/basique et de complexation	126
III.7.2.2	Dynamique des réactions de transfert d'électrons	127
III.7.2.3	Réactions par voies catalytiques et biochimiques	128
III.7.2.4	Réactions photochimiques	128
III.7.3	Le concept du régime permanent pour les systèmes d'écoulements	128
III.7.4	Vitesses et mécanismes d'équilibres hétérogènes	129
IV	Les limitations de la solubilité : l'opinion d'un "vieux briscard"	
	<i>par : Rolf GRAUER</i>	131
IV.1	Einleitung	131

IV.2	Über Inhalt und Qualität von geochemischen Datenbasen	133
IV.2.1	“The Law of Mythical Numbers”	133
IV.2.2	... and “The Handbook of Unstable, Exotic and Nonexistent Compounds”	135
IV.2.3	Der Vergleich von Datenbasen : Ein Weg zu besseren Werten ?	135
IV.3	Löslichkeitslimiten im Nahfeld : Das Beispiel Americium	136
IV.3.1	Löslichkeitsbestimmende Phasen	136
IV.3.2	Die Rolle der Lanthaniden	137
IV.3.3	Verglaste Abfälle	138
IV.3.4	Löslichkeitslimiten im Nahfeld : welche Festphasen ?	138
IV.4	Löslichkeitslimiten im Fernfeld : Das Beispiel Nickel	138
IV.4.1	Die Modellierung der Nickel-Löslichkeit	139
IV.4.2	Zur Geochemie des Nickels	140
IV.4.3	Löslichkeitslimiten im Fernfeld	141
IV.5	Schlussbemerkungen	141
IV.6	Les limitations de la solubilité : l’opinion d’un “vieux briscard” (version anglaise)	144
V	Modèles pour liaisons avec des substances humiques	
	<i>par : Wolfgang HUMMEL</i>	153
V.1	Introduction	153
V.2	Que sont les substances humiques	154
V.3	Liaisons d’un ion métallique avec des substances humiques	155
V.3.1	Les données expérimentales	155
V.3.2	Variations des concentrations des constituants	157
	V.3.2.1 Le modèle le plus simple	157
	V.3.2.2 Modèles à mélange de ligands	161
	V.3.2.3 Modèles à stoechiométrie variable	163
	V.3.2.4 Modèles multi-sites	166
	V.3.2.5 Modèles à distribution continue	169
V.3.3	Variations de pH	174
	V.3.3.1 Fonctions empiriques	174
	V.3.3.2 Réactions d’échanges de protons	175
	V.3.3.3 Effets électrostatiques	179
V.3.4	Variations de force ionique	185
	V.3.4.1 Fonctions empiriques	186
	V.3.4.2 Effets électrostatiques	186
V.3.5	Quel est le meilleur modèle pour les liaisons humiques ?	188
V.4	Stratégies de résolutions de problèmes	190
V.4.1	Modèles en tant qu’outils de recherche	190
V.4.2	Modèles en tant qu’outils d’évaluation	191
	V.4.2.1 L’approche conservative dans l’évaluation de la performance ..	191
	V.4.2.2 Compétition d’autres complexes	195
	V.4.2.3 Application des données de laboratoire dans l’évaluation de la performance	201
VI	Liaisons d’un ion métallique avec des substances humiques	
	<i>par : James H. EPHRAIM et Bert ALLARD</i>	207
VI.1	Introduction	207
VI.2	Vue d’ensemble générale	208
	VI.2.1 Isolation et extraction des substances humiques	209

VI.2.2	Méthodes de caractérisation	209
VI.2.3	Propriétés d'oxydoréduction des substances humiques	212
VI.3	Chimie des solutions des substances humiques	213
VI.3.1	Interactions des protons avec les substances humiques	213
VI.3.1.1	Modèles à ligands discrétisés	213
VI.3.1.2	Modèles à distribution continue	221
VI.3.1.3	Modèles discrétisés contre modèles à distribution continue ..	222
VI.3.2	Modèles pour l'interaction des métaux avec les acides humiques/ fulviques	223
VI.3.2.1	Modèles à ligands discrétisés	225
VI.3.2.2	Modèles à distribution continue	226
VI.3.2.3	Facteurs affectant le mécanisme général de complexation ..	226
VI.3.2.4	Compétition entre différents ions métalliques pour la formation de liaisons avec les substances humiques	227
VI.3.3	Les besoins en données pour modéliser le rôle des composés humiques	228
VI.3.3.1	Examen critique d'études sur les interactions entre substances humiques et ions métalliques	231
VI.4	Exemple de modélisation : détermination des formes chimiques de l'Eu ³⁺ présentes dans un milieu contenant des substances humiques et Ca ²⁺	232
VI.4.1	Intérêt de l'exercice	241
VI.5	Résumé	241
VII	Espèces chimiques en solution à l'interface entre solides géologiques et eaux souterraines par : Steven A. BANWART	245
VII.1	Introduction	245
VII.2	Contexte théorique	246
VII.2.1	Forces intermoléculaires à l'interface solide-solution	246
VII.2.2	Bilans massiques des composés adsorbés : Le concept d'excès de surface	246
VII.2.3	Réactions d'adsorption stochiométrique et la loi thermodynamique d'action de masse	249
VII.2.4	Combinaisons des bilans massiques et des lois d'actions de masse : L'isotherme d'adsorption	252
VII.2.4.1	L'isotherme d'adsorption de Langmuir	252
VII.2.4.2	Une isotherme d'adsorption linéaire : Le coefficient de distribution	253
VII.2.5	Influence des espèces chimiques en solution sur l'adsorption	253
VII.3	Complexation en surface	254
VII.3.1	Chimisorption de l'eau : Formation de surfaces chargées de façon variable	254
VII.3.2	Adsorption de ligands et de métaux à la surface hydratée	254
VII.3.3	Dépendance de l'adsorption en fonction du pH	258
VII.3.4	Adsorption compétitive	264
VII.3.5	Comportement non-idéal : Corrections d'activité dues au recouvrement de la surface	267
VII.3.6	Surfaces chargées et échange ionique	272
VII.3.6.1	Origines de la charge de la surface	272
VII.3.6.2	La double couche électrique	275
VII.3.6.3	Réactions d'échange ionique	275

VII.3.7	Descriptions thermodynamiques des systèmes d'adsorption complexes	280
VII.4	Précipitation en surface	281
VII.4.1	La transition de l'adsorption à la précipitation en surface	281
VII.4.2	La constante conditionnelle de solubilité pour la précipitation/ coprécipitation en surface	282
VII.5	Implications pour l'hydrogéologie des polluants	283
VII.5.1	Partage réversible des polluants	283
VII.5.2	Adsorption irréversible	286
VII.5.3	Combinaison de la géochimie et de l'hydrogéologie	287
VIII	Systématisation et estimation de données thermochimiques de silicates	
	<i>par : Surendra K. SAXENA</i>	289
VIII.1	Introduction	289
VIII.2	Une banque de données systématisée	291
VIII.2.1	Thermodynamique	292
VIII.2.1.1	Dépendance en fonction de la température de l'énergie libre de Gibbs	292
VIII.2.1.2	Capacité calorifique à hautes températures	292
VIII.2.2	La technique de régression	295
VIII.2.3	La technique d'optimisation	296
VIII.2.4	Banque de données	300
VIII.3	Estimation d'enthalpie de silicates	300
VIII.3.1	Principes sous-jacents de la corrélation empirique	300
VIII.3.2	Méthode de Tardy	300
VIII.3.3	L'approche polyédrique	314
VIII.3.3.1	Méthode de Chermak-Rimstidt	314
VIII.3.3.2	Nouvelle méthode polyédrique	316
VIII.4	Estimation d'entropie	320
VIII.4.1	Exemple de calcul	321
VIII.5	Estimation de capacités calorifiques de solides	322
VIII.6	Conclusions	322
IX	Estimation de l'influence du milieu sur les données thermodynamiques	
	<i>par : Ingmar GRENTHE, Andrey V. PLYASUNOV et Kastriot SPAHIU</i>	325
IX.1	Introduction	325
IX.2	À propos de l'estimation des coefficients d'activité dans les systèmes	327
IX.3	Le modèle de Brønsted-Guggenheim-Scatchard (SIT)	331
IX.3.1	Détermination des coefficients d'interaction ionique	341
IX.4	Autres équations, à peu près équivalentes au modèle SIT	345
IX.5	À propos de l'ordre de grandeur des coefficients spécifiques d'interaction ionique	347
IX.5.1	Corrélations entre paramètres spécifiques d'interaction ionique pour cations	347
IX.5.2	Corrélations entre paramètres spécifiques d'interaction ionique pour complexes	350
IX.5.3	Corrélations entre valeurs de $\Delta\epsilon$ pour réactions chimiques	352
IX.6	Les équations de Pitzer	352
IX.7	Comparaison entre les modèles de Pitzer et SIT pour la description de la dépendance en fonction de la concentration des constantes d'équilibre des réactions de complexation en milieu ionique	355

IX.7.1	Détermination des paramètres de Pitzer et SIT à partir des valeurs des $\log_{10} K$	366
IX.8	Relations entre les paramètres $\varepsilon_{(i,j)}$ du SIT et $\beta_{ij}^{(0)}$ $\beta_{ij}^{(1)}$ pour des coefficients d'activité moyenne	378
IX.8.1	Relations entre les valeurs de $\Delta\varepsilon$ du modèle SIT et celles de $\Delta\beta^{(0)}$ et $\Delta\beta^{(1)}$ du modèle de Pitzer pour les réactions de complexation avec des "traces" de réactifs/produits	383
IX.9	Utilisation du SIT à températures élevées	397
IX.9.1	Coefficient osmotique	397
IX.9.2	Expressions analytiques pour les propriétés molaires apparentes et partielles d'électrolytes seuls basés sur le modèle SIT	398
IX.9.3	Pentes des lois-limite de Debye-Hückel	400
IX.10	Dépendance en fonction de la concentration des chaleurs de réaction	406
IX.10.1	Calcul de l'enthalpie standard de réaction à partir des données expérimentales de $\Delta_r H_m$ en utilisant l'équation de Pitzer	410
IX.10.2	Calcul de l'enthalpie standard de réaction à partir des données expérimentales de $\Delta_r H_m$ en utilisant le modèle SIT	412
IX.10.3	Equations d'extrapolation pour la détermination de l'enthalpie standard de réaction à partir des données expérimentales de $\Delta_r H_m$ basées sur les modèles de Pitzer et SIT	417
IX.11	Conclusions	424
X	Corrections de température sur les données thermodynamiques et les calculs d'enthalpies par : Ignasi PUIGDOMENECH, Joseph A. RARD, Andrey V. PLYASUNOV et Ingmar GRENTHE	427
X.1	Introduction	427
X.2	Extrapolations de la deuxième loi de la thermodynamique.....	429
X.2.1	La convention de l'ion hydrogène	432
X.2.2	Approximations	434
X.2.2.1	Enthalpie constante de réaction	434
X.2.2.2	Capacité calorifique constante de réaction	434
X.2.2.3	Réactions isoélectrique et isocoulombique	437
X.2.3	Calcul de $\Delta_{sol} H_m$ à partir de la dépendance de la solubilité en fonction de la température	444
X.2.4	Autres possibilités d'expression de la capacité calorifique pour composés aqueux	447
X.2.4.1	Équation de DQUANT.....	447
X.2.4.2	Le modèle de Helgeson-Kirkham-Flowers révisé	448
X.2.4.3	Le modèle de Ryzhenko-Bryzgalin	455
X.2.4.4	Le modèle de densité ou de "constante d'équilibre atteint" ..	465
X.3	La méthode de la troisième loi de la thermodynamique	469
X.3.1	Évaluation à partir de données calorimétriques hautes et basses températures	470
X.3.2	Évaluation à partir de données hautes températures	473
X.3.3	Brève comparaison entre enthalpies tirées des méthodes des deuxième et troisième lois de la thermodynamique	475
X.4	Méthodes d'estimation	476
X.4.1	Méthodes d'estimation pour capacités calorifiques	476
X.4.1.1	Estimations de capacités calorifiques de phases solides	476
X.4.1.2	Estimations de capacités calorifiques de composés aqueux ..	477

	X.4.1.3	Méthodes d'estimations de capacités calorifiques pour réactions en solution aqueuse	482
	X.4.2	Méthodes d'estimation d'entropies	483
	X.4.2.1	Méthodes d'estimation d'entropies de phases solides ...	483
	X.4.2.2	Méthodes d'estimation d'entropies de composés aqueux	485
	X.4.3	Exemples	490
X.5		Conclusions	492
X.6		Remerciements	493
XI		Modèles d'automates cellulaires pour les processus de réaction-transport	
		<i>par : Theo KARAPIPERIS</i>	495
XI.1		Introduction	495
XI.2		Les automates cellulaires	498
	XI.2.1	Développement historique	498
	XI.2.2	Exemples élémentaires	499
XI.3		Automates cellulaires pour le transport avec réactions chimiques	503
	XI.3.1	Modèles	503
	XI.3.1.1	Transport	503
	XI.3.1.2	Réactions chimiques	507
	XI.3.2	Applications	510
	XI.3.2.1	$a + b \rightarrow c$	510
	XI.3.2.2	Réactions autocatalytiques	511
	XI.3.2.3	Réactions avec les surfaces minérales	514
XI.4		Conclusions	522
XI.5		Remerciements	524
XII		Modélisation du transport de solutés avec l'approche du milieu	
		doublement poreux <i>par : Andreas JAKOB</i>	525
XII.1		Introduction	525
XII.2		Classification des phénomènes de transport	527
XII.3		Transport de matière causé par un gradient de concentration	529
	XII.3.1	Dispersion de Fickian	529
	XII.3.2	Dispersivité en fonction des échelles	537
	XII.3.3	Le problème des moyennes locales	538
	XII.3.4	Équations de sorption utilisées dans la modélisation du transport	539
	XII.3.5	Le concept du milieu à double porosité	545
	XII.3.6	Effets de la diffusion dans la matrice et l'approximation de la surface effective de sorption	554
	XII.3.7	Méthodologie de la modélisation et exemples supplémentaires	564
XII.4		Remerciements	574
XII.5		Glossaire	574
XIII		Les piliers de la sûreté	
		<i>par : Jörg HADERMANN</i>	577
XIII.1		Introduction	577
XIII.2		Réduction des vitesses de rejets à la source	584
XIII.3		Retard pendant le transport	585
XIII.4		Dilution	588

XIV	Modélisation des éléments présents sous forme de traces	593
	<i>par : Jordi BRUNO</i>	
XIV.1	En quoi les métaux présents sous forme de traces nous concernent-ils ? ...	593
XIV.2	Quelques aspects généraux de la modélisation (géo)chimique	594
XIV.2.1	Comment tout cela a-t-il commencé ?	594
XIV.3	Méthodologie de la modélisation géochimique	596
XIV.3.1	Les pierres de l'édifice	596
XIV.3.2	Les données du système	596
XIV.3.3	Variabilité chimique et physique des environnements souterrains	597
XIV.3.3.1	Conditions physiques	597
XIV.3.3.2	Conditions biologiques	597
XIV.3.3.3	Variabilité des conditions chimiques	597
XIV.3.4	Ressentir le système. Le modèle conceptuel	599
XIV.3.4.1	Le cadre géologique	600
XIV.3.4.2	La condition hydrogéologique	603
XIV.3.4.3	Description quantitative du déséquilibre local. Les paramètres de Peclet, Damkohler et Lichtner	605
XIV.3.4.4	Interaction des métaux présents sous forme de traces avec les constituants majeurs des phases solides	607
XIV.4	L'objectif des efforts de modélisation géochimique. Interprétations <i>vs.</i> prévisions	612
XIV.4.1	Exemple de l'évaluation de l'impact potentiel d'une perturbation anthropogénique sur un dépôt de déchets hautement radioactifs. Effets des pluies acides sur la géosphère granitique	612
XIV.4.2	Exemple de calcul des concentrations maximales de rejet de radioéléments critiques provenant d'un dépôt de combustible usagé. Comment utiliser des informations tirées d'études sur des systèmes naturels pour limiter les prévisions irréalistes	615
XIV.5	Remerciements	621
XV	Liste des auteurs	623
XVI	Listes des références	655

List of Tables

I.1	Processes affecting the stability of metal containers	17
II.1	Symbols and terminology	36
II.2	Abbreviations for chemical processes	42
II.3	Unit conversion factors	54
II.4	Conversion factors of molarity to molality	55
II.5	Reference states for the elements	57
II.6	Fundamental physical constants	59
III.1	Coordination numbers and geometry for some metal ions and their complexes	74
III.2	Thermodynamic data for complex formation reactions	90
V.1	List of model assumptions	158
VI.1	Comparison of experimentally based overall degree of dissociation of Laurentide fulvic acid with the summation of computed contributions of five different acid sites to overall degree of dissociation	224
VI.2	Concentrations and equilibrium constants used in the calculation of the speciation of Eu(III) in ground and surface waters	235
VI.3	Parameters used in describing/modelling metal ion binding by humic substances	243
VII.1	Functional groups at the solid-water interface	256
VII.2	Stoichiometry, thermodynamic laws of mass action and capacity factors for solution and surface coordination reactions	259
VII.3	Cr ³⁺ and CrO ₄ ²⁻ adsorption on iron hydroxide	261
VII.4	Adsorption competition between sulfate and carbonate ions	265
VII.5	Non-ideal behaviour for sulphate adsorption on soil	270
VII.6	The relationship between surface charge and electrical double-layer potential	276
VII.7	Ion-exchange equilibria during dilution of saline groundwaters	279
VII.8	Comparison of reversible and irreversible adsorption effects on contaminant retardation	285
VIII.1	A thermochemical data base on silicates standard state enthalpy of formation from elements and molar entropy at 298.15 K	301
VIII.2	Results of regressed data on lattice energy and fictive polyhedral parameters	310
VIII.3	Regressed lattice enthalpy of the polyhedral units	319
VIII.4	Some estimated results	320
VIII.5	Data for use with Holland's entropy model	321
VIII.6	Coefficients for calculating the heat capacity of a solid	323
IX.1	Ion interaction coefficients, ε , for cations	335

IX.2	Ion interaction coefficients, ε , for anions	339
IX.3	Equilibrium constants for $\text{UO}_2^{2+} + \text{Cl}^- \rightleftharpoons \text{UO}_2\text{Cl}^+$	342
IX.4	Equilibrium constants for the dissociation of water in KCl solutions	369
IX.5	Regression results of data in Table IX.4	371
IX.6	Equilibrium constants for $\text{H}^+ + \text{SO}_4^{2-} \rightleftharpoons \text{HSO}_4^-$ in NaClO_4 solutions	373
IX.7	Regression results for data in Table IX.6	374
IX.8	Quantitative relationship between the Pitzer parameters $\beta^{(0)}$ and $\beta^{(1)}$ and the SIT ε_γ parameters for different ion combinations	379
IX.9	Relation between the Pitzer and the SIT parameters for the complex formation reaction studied in different 1-1 supporting electrolytes	384
IX.10	Equilibrium constants for reaction $\text{Cd}^{2+} + \text{NO}_2^- \rightleftharpoons \text{CdNO}_2^+$ in NaClO_4 solutions	387
IX.11	Equilibrium constants for reaction $\text{Fe}^{3+} + \text{Cl}^- \rightleftharpoons \text{FeCl}^{2+}$ in HClO_4 solutions	389
IX.12	Equilibrium constants for reaction $\text{Cd}^{2+} + \text{Cl}^- \rightleftharpoons \text{CdCl}^+$ in NaClO_4 , LiClO_4 and $\text{Mg}(\text{ClO}_4)_2$ media	393
IX.13	Test of the SIT approach for some reactions at elevated temperatures in NaCl media	405
IX.14	Values of L_1 for some common electrolytes	409
IX.15	Results of the calculation of the $\Delta_r H_m^\circ$ value for $\text{H}_2\text{O}(\text{l}) \rightleftharpoons \text{H}^+ + \text{OH}^-$ in NaCl medium	418
IX.16	Results of the experimental determinations of the $\Delta_r H_m$ for $\text{H}_2\text{O}(\text{l}) \rightleftharpoons \text{H}^+ + \text{OH}^-$ in NaClO_4 medium	420
IX.17	Results of the least square determination of unknowns in fitting equations	421
IX.18	Experimental values of the enthalpy change for $\text{Hg}^{2+} + \text{Cl}^- \rightleftharpoons \text{HgCl}^+$ in NaClO_4 ionic medium	423
X.1	Temperature contributions in Eq. (X.20)	437
X.2	Equilibrium constants for the ionisation of carbonic acid	444
X.3	Ionic polarisabilities	456
X.4	T and p variation of the density and dielectric constant of liquid water	460
X.5	The calculated and experimental values of $\Delta_r S_m^\circ$, $\Delta_r C_{p,m}^\circ$ and $\Delta_r V_m^\circ$ for reaction $\text{Al}^{3+} + 4\text{OH}^- \rightleftharpoons \text{Al}(\text{OH})_4^-$ at 298.15 K and 1 bar	463
X.6	Sublimation data of ruthenium	472
X.7	Third-law extrapolation of ruthenium data	472
X.8	Thermodynamic values for the reanalysis of sublimation data for ruthenium	474
X.9	Third-law extrapolation of ruthenium data without fixing entropies	474
X.10	Heat capacity parameters	479
X.11	Parameters for Khodakovskiy's equations	482
X.12	Contributions to entropies of solids	484
X.13	Magnetic (electronic) contributions to entropies at 298.15 K	486
XII.1	Table of coupled processes	528
XII.2	Values for some transport parameters used in the double porosity medium approximation (see text)	563
XII.3	Comparison of the volume-based sorption equilibrium distribution coefficient, K_d , for strontium from different laboratory experiments and from the Grimsel migration experiment	569
XII.4	Values of the best-fitting parameters and the minimum value for the χ^2 -merit function for two alternative calculations for iodide breakthrough in the Finnsjön migration experiment assuming either one or two preferential flow path(s)	574

XIII.1	Example compilation of features, events and processes for a deep geological repository	579
XIII.2	Maximum release rates from the near-field for some isotopes	585
XIII.3	Comparison of different sorption distribution constants as measured in the field and in the laboratory	589
XIII.4	Dose conversion factors for a hypothetical release	590
XIV.1	Ranges of physical, biological and chemical variables in subsurface environments	598
XIV.2	Characteristic reaction times for geochemical processes derived from primary data . . .	604
XIV.3	Average residence times of water in main reservoirs	605
XIV.4	Characteristic reaction times for the processes describing the interaction of trace metals with major component solid phases	608
XIV.5	Comparison of the surface complexation model by [90DZO/MOR] and the conditional solubility constant approach	610
XIV.6	Modelling the effect of soil acidification on the stability of a granitic nuclear waste repository	614

Liste des tableaux

I.1	Processus affectant la stabilité des conteneurs métalliques	17
II.1	Symboles et terminologie	36
II.2	Abréviations pour les processus chimiques	42
II.3	Facteurs de conversions d'unités	54
II.4	Facteurs de conversion de molarité en molalité	55
II.5	États de références pour les éléments	57
II.6	Constantes physiques fondamentales	59
III.1	Nombres de coordination et géométrie de quelques ions métalliques et de leurs complexes	74
III.2	Données thermodynamiques pour des réactions de complexation	90
V.1	Liste des hypothèses des modèles	158
VI.1	Comparaison du degré global de dissociation de l'acide fulvique Laurentide obtenu expérimentalement, avec la somme des contributions calculées par ordinateur de cinq sites acides différents à leurs degrés globaux de dissociation	224
VI.2	Concentrations et constantes d'équilibre utilisées dans la détermination des espèces chimiques de l'Eu(III) dans les eaux souterraines et de surface	235
VI.3	Paramètres utilisés dans la description/modélisation de la liaison entre ions métalliques et substances humiques	243
VII.1	Groupes fonctionnels à l'interface eau-solide	256
VII.2	Stoichiométrie, lois thermodynamiques d'action de masse et facteurs de capacité pour les réactions de coordination en solution et en surface	259
VII.3	Adsorption de Cr^{3+} et CrO_4^{2-} sur l'hydroxyde de fer	261
VII.4	Compétition entre l'adsorption des ions sulfate et carbonate	265
VII.5	Comportement non idéal de l'adsorption de sulphates sur la terre	270
VII.6	Relations entre la charge de surface et le potentiel électrique de double couche	276
VII.7	Échange ionique pendant la dilution des eaux souterraines salines	279
VII.8	Comparaison des effets d'adsorption réversibles et irréversibles sur le retard à la contamination	285
VIII.1	Une banque de données d'enthalpies standards de formation de silicates à partir des éléments et d'entropies molaires à 298.15 K	301
VIII.2	Résultats d'une régression sur des données d'énergies de maille et des paramètres des polyèdres fictifs	310
VIII.3	Enthalpies de maille des unités polyédriques obtenues par régression	319
VIII.4	Quelques résultats d'estimations	320
VIII.5	Données pour l'utilisation du modèle de l'entropie de Holland	321

VIII.6	Coefficients pour calculer la capacité calorifique d'un solide	323
IX.1	Coefficients d'interaction ionique, ε , pour cations	335
IX.2	Coefficients d'interaction ionique, ε , pour anions	339
IX.3	Constantes d'équilibre de $\text{UO}_2^{2+} + \text{Cl}^- \rightleftharpoons \text{UO}_2\text{Cl}^+$	342
IX.4	Constantes d'équilibre de la dissociation de l'eau dans des solutions de KCl	369
IX.5	Résultats d'une régression sur des données du Tableau IX.4	371
IX.6	Constantes d'équilibre de $\text{H}^+ + \text{SO}_4^{2-} \rightleftharpoons \text{HSO}_4^-$ dans des solutions de NaClO_4	373
IX.7	Résultats d'une régression sur des données du Tableau IX.6	374
IX.8	Relation quantitative entre les paramètres de Pitzer, $\beta^{(0)}$ et $\beta^{(1)}$, et ceux du SIT, ε_γ , pour différentes combinaisons d'ions	379
IX.9	Relation entre les paramètres de Pitzer et du SIT de la réaction de complexation étudiée dans différents électrolytes-support 1-1	384
IX.10	Constantes d'équilibre de la réaction $\text{Cd}^{2+} + \text{NO}_2^- \rightleftharpoons \text{CdNO}_2^+$ dans des solutions de NaClO_4	387
IX.11	Constantes d'équilibre de la réaction $\text{Fe}^{3+} + \text{Cl}^- \rightleftharpoons \text{FeCl}^{2+}$ dans des solutions de HClO_4	389
IX.12	Constantes d'équilibre de la réaction $\text{Cd}^{2+} + \text{Cl}^- \rightleftharpoons \text{CdCl}^+$ en milieux NaClO_4 , LiClO_4 et $\text{Mg}(\text{ClO}_4)_2$	393
IX.13	Test de l'approche SIT pour quelques réactions à températures élevées en milieux NaCl	405
IX.14	Valeurs de L_1 pour quelques électrolytes courants	409
IX.15	Résultats des calculs des valeurs de $\Delta_r H_m^\circ$ de $\text{H}_2\text{O}(\text{l}) \rightleftharpoons \text{H}^+ + \text{OH}^-$ en milieux NaCl	418
IX.16	Résultats des déterminations expérimentales des $\Delta_r H_m$ de $\text{H}_2\text{O}(\text{l}) \rightleftharpoons \text{H}^+ + \text{OH}^-$ en milieu NaCl	420
IX.17	Résultats obtenus par la méthode des moindres carrés sur les inconnues dans les équations paramétrées	421
IX.18	Valeurs expérimentales de la variation d'enthalpie au cours de $\text{Hg}^{2+} + \text{Cl}^- \rightleftharpoons \text{HgCl}^+$ en milieu NaClO_4 ionique	423
X.1	Contributions de la température dans l'Eq. (X.20)	437
X.2	Constantes d'équilibre pour l'ionisation de l'acide carbonique	444
X.3	Polarisabilités ioniques	456
X.4	Variation en fonction de T et p de la densité et de la constante diélectrique de l'eau liquide	460
X.5	Valeurs expérimentales et calculées de $\Delta_r S_m^\circ$, $\Delta_r C_{p,m}^\circ$, et $\Delta_r V_m^\circ$ pour la réaction $\text{Al}^{3+} + 4\text{OH}^- \rightleftharpoons \text{Al}(\text{OH})_4^-$ à 298.15 K et 1 bar	463
X.6	Données sur la sublimation du ruthénium	472
X.7	Extrapolation de la troisième loi de la thermodynamique pour des données sur le ruthénium	472
X.8	Valeurs thermodynamiques pour une nouvelle analyse des données sur la sublimation du ruthénium	474
X.9	Extrapolation de la troisième loi de la thermodynamique pour des données sur le ruthénium sans fixer les entropies	474
X.10	Paramètres pour les capacités calorifiques	479
X.11	Paramètres pour les équations de Khodakovskiy	482
X.12	Contributions aux entropies de solides	484
X.13	Contributions magnétiques (électroniques) aux entropies à 298.15 K	486
XII.1	Tableau des processus couplés	528

XII.2	Valeurs de quelques paramètres de transport utilisés dans l'approximation du milieu doublement poreux (voir texte)	563
XII.3	Comparaison des coefficients de distribution des équilibres de sorption basés sur le volume, K_d , pour le strontium dans différentes expériences de laboratoire et dans l'expérience de migration de Grimsel	569
XII.4	Valeurs des paramètres optimisés et valeur minimum de la fonction χ^2 -merit pour deux calculs possibles du passage des iodures dans l'expérience de migration de Finnsjön en considérant un ou deux chemin(s) préférentiel(s)	574
XIII.1	Compilation d'exemple de caractéristiques, d'événements et de processus pour un dépôt géologique profond	579
XIII.2	Vitesses maximales de rejets provenant du champ proche pour quelques isotopes ...	585
XIII.3	Comparaison de différentes constantes de distribution de sorption mesurées sur le terrain et en laboratoire	589
XIII.4	Facteurs de conversion de doses pour une hypothétique émission	590
XIV.1	Ordres de grandeur de variables physiques, biologiques et chimiques dans un environnement souterrain	598
XIV.2	Temps de réaction caractéristiques pour processus géologiques tirés de données primaires	604
XIV.3	Temps de séjour moyen de l'eau dans les principaux réservoirs	605
XIV.4	Temps de réaction caractéristiques pour les processus décrivant les interactions des traces de métaux avec les composants principaux des phases solides	608
XIV.5	Comparaison du modèle de complexation en surface de [90DZO/MOR] et de l'approche de la constante de solubilité conditionnelle	610
XIV.6	Modélisation de l'effet de l'acidification de la terre sur la stabilité d'un dépôt de déchets nucléaires granitique	614

List of Figures

I.1	Schematic features of the modelling and validation of a simple (laboratory) system . . .	2
I.2	Outline of the procedures used for describing properties/functioning of complex systems	4
I.3	The characteristic features of laboratory systems and more complex systems encountered in nature and in the scientific/technological world	6
I.4	Standard fault tree	9
I.5	Simplified process influence diagram	10
I.6	Construction of interaction diagrams of the “RES”-type	11
I.7	Example of a phase diagram	14
I.8	Schematic outline of an underground waste repository	15
I.9	Pourbaix diagrams for iron and copper	16
II.1	Distribution functions	60
II.2	Ligand average curve	61
II.3	Logarithmic diagram for copper(II)	62
II.4	Pourbaix diagram for iron	63
II.5	Predominance diagram	67
III.1	Solvation of cations in (a) protic, and (b) polar aprotic solvents	76
III.2	Distribution diagram of the various species formed in the Co(II)-edta ⁴⁻ system	80
III.3	Some less common coordination geometries for UO ₂ ²⁺	82
III.4	Some less common coordination geometries: Fe(III)-edta	83
III.5	Some less common coordination geometries: Ho(SO ₄) ₂ (H ₂ O) ₄ ⁻	84
III.6	Common bonding geometries for the carbonate ion	85
III.7	The distribution of acceptor ions in the periodic table	86
III.8	Relative stability of chloride and fluoride complexes for hard and soft acceptors	87
III.9	Distribution diagram for Hg(II) <i>versus</i> total chloride concentration	88
III.10	Uranium(VI) phosphate complexes	92
III.11	Isomorphic substitution in (UO ₂) ₃ (CO ₃) ₆ ⁶⁻	93
III.12	The structures of (UO ₂) ₃ (O)(OH) ₃ ⁺ and (UO ₂) ₂ (OH) ₂ ²⁺ in the solid state	94
III.13	Distribution diagrams for lead(II) hydrolysis	95
III.14	The stability of the carbonate complexes of calcium(II) and cerium(III)	97
III.15	Statistically expected equilibrium constant K_{stat} for $\text{MA}_2 + \text{MB}_2 \rightleftharpoons 2\text{MAB}$	100
III.16	Compositions of complexes formed in the Al ³⁺ -Cl ⁻ -dimethylformamide system	102
III.17	The coordination geometry of uranyl oxalate complexes. I. UO ₂ (oxalate)F ₃ ³⁻	103
III.18	The coordination geometry of uranyl oxalate complexes. II. UO ₂ (oxalate) ₂ H ₂ O ²⁻	104
III.19	The coordination geometry of uranyl oxalate complexes. III. UO ₂ (oxalate) ₃ ⁴⁻	105
III.20	Dependence of log ₁₀ K_1 for the formation of hydroxide complexes on $z_i/d_{\text{M-O}}$	106
III.21	Dependence of log ₁₀ K_1 for fluoride complexation on $z_i/d_{\text{M-F}}$	107
III.22	The constancy of the equilibrium constant for Reaction (III.4)	108

III.23	$\log_{10} K_1$ of some glycine complexes <i>versus</i> the ionisation potential of the metal	109
III.24	$\log_{10} K_1$ of some glycine complexes <i>versus</i> electronegativities of metal cations	110
III.25	$\log_{10} \beta_2$ for complexes of bivalent transition metal cations with several ligands	110
III.26	Correlation plot of Fe(III)-phenolate and -salicylate complexes	111
III.27	$\log_{10} K_{\text{CuL}}$ <i>versus</i> $\log_{10} K_{\text{NiL}}$	112
III.28	Correlation of $\log_{10} K$ for organic complexes of Ca and Sr	113
III.29	Correlation between $\log_{10} K$ for edta and dcta	114
III.30	Correlation of stability constants for nta- and edta-complexes	115
III.31	Coordination geometry of $\text{Ni}(\text{nta})_2^{4-}$	116
III.32	Coordination geometry of $\text{Fe}(\text{nta})_2^{3-}$	116
III.33	Coordination geometry of $\text{Zr}(\text{nta})_2^{2-}$	117
III.34	Coordination geometry of $\text{Nd}(\text{nta})_2\text{H}_2\text{O}^{3-}$	117
III.35	Coordination geometry of $\text{VO}_2\text{edta}^{3-}$	118
III.36	The structure of the dinuclear complex $(\text{UO}_2)_2\text{edtaF}_4^{4-}$	119
III.37	Correlations between $\log_{10} K_n$ and $\log_{10} K_{(n-1)}$ for oxalate, citrate and nta complexes	120
III.38	3D-plot of the oxalate concentration necessary to bind 50% of $[\text{U(VI)}]_{\text{total}}$ as oxalate complexes (including estimated ternary complexes)	121
III.39	Contour plot of the oxalate concentration necessary to bind 50% of $[\text{U(VI)}]_{\text{total}}$ as oxalate complexes (including estimated ternary complexes)	122
III.40	3D-plot of the oxalate concentration necessary to bind 50% of $[\text{U(VI)}]_{\text{total}}$ as oxalate complexes (excluding ternary complexes)	123
III.41	Effect of excluding ternary $\text{UO}_2\text{-OH-oxalate}$ complexes on the contour plot of the oxalate concentration necessary to bind 50% of $[\text{U(VI)}]_{\text{total}}$ as oxalate complexes	124
V.1	Metal concentration dependence of humic complexation. Eu, Am and Cm complexation with humic and fulvic acids (single and two site models)	167
V.2	Metal concentration dependence of humic complexation. Eu, Am and Cm complexation with humic and fulvic acids (continuous distribution model)	172
V.3	The pH dependence of humic complexation. Eu, Am and Cm complexation with humic and fulvic acids	177
V.4	A synopsis of experimental data of Eu, Am and Cm complexation with humic and fulvic acids at ionic strength 0.1 M	193
V.5	The “conservative roof” approach for performance assessment	194
V.6	Schematic representation of competitive effects in metal-humic binding models: cation and anion competition	198
V.7	Schematic representation of competitive effects in metal-humic binding models: ternary complexes	199
V.8	Schematic representation of competitive effects in metal-humic binding models: competition of mineral surface sites	200
V.9	Complete sketch of mutual interactions of toxic metals, humic substances, other cations and anions, and mineral surface sites	201
V.10	Scoping calculations of humic complexation with Eu at trace concentration level	204
V.11	Contour plot of the concentration of humic substance (\log_{10} g/l) necessary to bind 90% of the total dissolved Eu	206
VI.1	Structure of fulvic acid as proposed by Schnitzer and Kahn	210
VI.2	Structure of Bersbo fulvic acid	211
VI.3	One-electron step reactions	212
VI.4	Stages of the program	218
VI.5	Examples of site heterogeneity assignments to a number of fulvic acid samples	220
VI.6	$\text{p}K_a^{\text{app}}$ <i>vs.</i> α for Laurentide fulvic acid	222

VI.7	δpK vs. α for Laurentite fulvic acid	223
VI.8	Effect of ionic strength on metal-humate interaction	228
VI.9	pK_a^{app} vs. α for 12 fulvic acids	230
VI.10	Speciation of Eu(III) in surface water	236
VI.11	Speciation of Eu(III) in surface water	236
VI.12	Speciation of Eu(III) in surface water	237
VI.13	Speciation of Eu(III) in groundwater	238
VI.14	Speciation of Eu(III) in groundwater	239
VI.15	Speciation of Eu(III) in groundwater	239
VI.16	Speciation of Eu(III) with low concentration of humics	240
VI.17	Speciation of Eu(III) with low concentration of humics	240
VI.18	Speciation of Eu(III) with low concentration of humics	241
VII.1	Adsorption reactions depend on the chemical nature of the adsorbing solute (adsorbate) and of the solid surface (adsorbent)	247
VII.2	Schematic diagram of a flow-through reactor system used to study adsorption on mineral surfaces	249
VII.3	Breakthrough of total dissolved Cr with time for Cr(VI) adsorption on iron oxide	250
VII.4	Surface excess of Cr on colloidal goethite	251
VII.5	Hydroxide ions chemically bound to terminal Fe(III) sites on the surface of iron oxide	255
VII.6	The pH dependence of Cr^{3+} and CrO_4^{2-} adsorption on iron oxide	263
VII.7	The dependence of surface carbonate and sulphate species on $p\text{CO}_2$	267
VII.8	Non-ideal behaviour for sulphate adsorption on soil	271
VII.9	The origins of surface charge	273
VII.10	Qualitative diagrams for titration of hydroxyl groups at mineral surfaces	274
VII.11	The relation between interfacial charge and potential distribution through the electrical double-layer	277
VII.12	The ratio of sodium and calcium activity in solution, plotted according to the thermodynamic mass law given in Table VII.7	278
VII.13	Thermodynamic modelling of the sodium and calcium ion-exchange reaction during groundwater dilution at the Äspö Hard Rock Laboratory	280
VII.14	A conceptual isotherm describing the transition between adsorption equilibrium and surface-precipitation equilibrium at the mineral-water interface	282
VIII.1	The experimental data and extrapolations on C_p and C_V of corundum	294
VIII.2	Comparison of phase equilibrium computations with experimental data for $\text{Br} \rightleftharpoons \text{Per} + \text{H}_2\text{O}(\text{l})$	296
VIII.3	Comparison of phase equilibrium computations with experimental data for $\text{Ms} \rightleftharpoons \text{Cor} + \text{San} + \text{H}_2\text{O}(\text{f})$	298
VIII.4	Comparison of phase equilibrium computations with experimental data for $\text{Ms} + \text{Q} \rightleftharpoons \text{San} + \text{Sill} + \text{H}_2\text{O}(\text{f})$	299
VIII.5	Comparison of phase equilibrium computations with experimental data for $\text{Ms} + \text{Q} \rightleftharpoons \text{San} + \text{And} + \text{H}_2\text{O}(\text{f})$	299
VIII.6	The pyroxene structure showing the silicon tetrahedral chain and the M1 and M2 octahedra	317
IX.1	Variation of $\log_{10} \gamma_{\pm}$ for some 1:1 electrolytes	328
IX.2	Plot of $(\log_{10} \gamma_{\pm} - Z_M Z_X D)$ vs. I_m	329
IX.3	Concentration dependence of the SIT coefficient for a number of electrolytes	333
IX.4	Determination of the SIT coefficient from the mean activity coefficients for HCl	341
IX.5	Extrapolation to $I = 0$: An example	343

IX.6	Correlations between interaction coefficients for monovalent cations	348
IX.7	Correlations between interaction coefficients for monovalent cations	348
IX.8	Correlations between interaction coefficients for divalent cations	349
IX.9	Correlations between interaction coefficients for trivalent cations	349
IX.10	Correlations between interaction coefficients and the ion potential Z/r	350
IX.11	Correlations between interaction coefficients and the ion potential Z/r	351
IX.12	Correlations between interaction coefficients and the ion potential Z/r	351
IX.13	Concentration dependence of $\log_{10} \gamma$ of $\text{CO}_2(\text{aq})$ in NaCl solutions	359
IX.14	Comparison of the experimental and calculated values of $\log_{10} K$ using the Pitzer approach and the SIT model for $\text{H}_2\text{O}(\text{l}) + \text{CO}_2(\text{aq}) \rightleftharpoons \text{H}^+ + \text{HCO}_3^-$	360
IX.15	Comparison of the experimental and calculated values of $\log_{10} K$ using the Pitzer approach and the SIT model for $\text{HCO}_3^- \rightleftharpoons \text{H}^+ + \text{CO}_3^{2-}$	362
IX.16	Comparison of the experimental and predicted values of $\log_{10} K$ using the Pitzer approach with the available from the literature values of the mixing terms and the SIT model for $\text{H}_2\text{O}(\text{l}) + \text{CO}_2(\text{aq}) \rightleftharpoons \text{H}^+ + \text{HCO}_3^-$	364
IX.17	Comparison of the experimental and predicted values of $\log_{10} K$ using the Pitzer approach with the available data from the literature values of the mixing terms and the SIT model for $\text{HCO}_3^- \rightleftharpoons \text{H}^+ + \text{CO}_3^{2-}$	365
IX.18	Parametrization of the SIT and different variants of the Pitzer models for $\text{H}_2\text{O}(\text{l}) \rightleftharpoons \text{H}^+ + \text{OH}^-$	370
IX.19	Parametrization of the SIT and different variants of the Pitzer models for $\text{H}^+ + \text{SO}_4^{2-} \rightleftharpoons \text{HSO}_4^-$	373
IX.20	Relative contributions of the Debye-Hückel term to $\ln \gamma_{\pm}$ for the SIT and the Pitzer models	376
IX.21	Concentration dependence of function Y for the typical 1-1 and 2-1 electrolytes	376
IX.22	The comparison of the quality of the reproduction of experimental data of mean activity coefficients for different electrolytes	377
IX.23	Relationship between parameters for the Pitzer and SIT models for 1-1 electrolytes	380
IX.24	Relationship between parameters for the Pitzer and SIT models for 2-1 and 1-2 electrolytes	380
IX.25	Relationship between parameters for the Pitzer and SIT models for 3-1 and 1-3 electrolytes	381
IX.26	The comparison of “predicted” and “experimental” values of the $\beta^{(1)}$ parameter as a function of temperature	382
IX.27	Relationship between parameters for the Pitzer and SIT models from $\log_{10} K$ in 1-1 background electrolytes	384
IX.28	Comparison of experimental and calculated values of the $\log_{10} K$ obtained using the SIT and the simplified Pitzer models for $\text{Cd}^{2+} + \text{NO}_2^- \rightleftharpoons \text{CdNO}_2^+$ in NaClO_4 solutions	388
IX.29	Comparison of experimental and calculated values of $\log_{10} K$ for $\text{Fe}^{3+} + \text{Cl}^- \rightleftharpoons \text{FeCl}^{2+}$ in HClO_4 solutions	390
IX.30	Comparison of experimental and predicted values of the difference in $\log_{10} K$ values for $\text{Fe}^{3+} + \text{Cl}^- \rightleftharpoons \text{FeCl}^{2+}$ in pure HClO_4 and mixed HClO_4 - NaClO_4 media	391
IX.31	The values of function Y calculated from the $\log_{10} K$ data for $\text{Cd}^{2+} + \text{Cl}^- \rightleftharpoons \text{CdCl}^+$ in NaClO_4 , LiClO_4 and $\text{Mg}(\text{ClO}_4)_2$ media based on the SIT model	394
IX.32	The values of function Y calculated from the $\log_{10} K$ data for $\text{Cd}^{2+} + \text{Cl}^- \rightleftharpoons \text{CdCl}^+$ in NaClO_4 , LiClO_4 and $\text{Mg}(\text{ClO}_4)_2$ media based on the Pitzer model	395
IX.33	Comparison of experimental and smoothed values of activity coefficients for NaCl solutions on the basis of the SIT model	402

IX.34	Comparison of experimental and smoothed values of relative apparent molar enthalpies for NaCl solutions on the basis of the SIT model	403
IX.35	Comparison of experimental and smoothed values of apparent molar volumes for NaCl solutions on the basis of the SIT model	403
IX.36	Comparison of experimental and smoothed values of the apparent molar heat capacities for NaCl solutions on the basis of the SIT model	404
IX.37	Differences between experimental and smoothed using the SIT values of $\log_{10} K$ for $\text{CO}_2 + \text{H}_2\text{O}(\text{l}) \rightleftharpoons \text{H}^+ + \text{HCO}_3^-$	406
IX.38	Differences between experimental and smoothed using the SIT values of $\log_{10} K$ for $\text{HCO}_3^- \rightleftharpoons \text{H}^+ + \text{CO}_3^{2-}$	407
IX.39	Differences between experimental and smoothed using the SIT values of $\log_{10} K$ for $\text{HSO}_4^- \rightleftharpoons \text{H}^+ + \text{SO}_4^{2-}$	407
IX.40	Parametrization of the SIT and different variants of the Pitzer models from the experimental values of $\Delta_r H_m$ for $\text{H}_2\text{O}(\text{l}) \rightleftharpoons \text{H}^+ + \text{OH}^-$ in NaClO_4 medium	422
IX.41	Concentration dependence of the fitting function Y for $\text{Hg}^{2+} + \text{Cl}^- \rightleftharpoons \text{HgCl}^+$ in NaClO_4 solutions based on the Pitzer model	424
IX.42	Concentration dependence of the fitting function Y for $\text{Hg}^{2+} + \text{Cl}^- \rightleftharpoons \text{HgCl}^+$ in NaClO_4 solutions based on the SIT model	425
X.1	Equilibrium constants for $\text{CO}_3^{2-} + \text{UO}_2^{2+} \rightleftharpoons \text{UO}_2\text{CO}_3(\text{aq})$	436
X.2	Temperature dependence for the dielectric constant of water	438
X.3	Equilibrium constants for reaction $\text{H}_2\text{O}(\text{l}) + \text{UO}_2^{2+} \rightleftharpoons \text{H}^+ + \text{UO}_2\text{OH}^+$	441
X.4	Equilibrium constants for reaction $\text{CO}_3^{2-} + \text{UO}_2^{2+} \rightleftharpoons \text{UO}_2\text{CO}_3(\text{aq})$	441
X.5	Equilibrium constants for $\text{UO}_2^{2+} + \text{CO}_2(\text{aq}) \rightleftharpoons \text{UO}_2\text{CO}_3(\text{aq}) + 2\text{H}^+$	443
X.6	Equilibrium constants for $\text{CO}_3^{2-} + \text{UO}_2^{2+} \rightleftharpoons \text{UO}_2\text{CO}_3(\text{aq})$	443
X.7	Equilibrium constants for $\text{CO}_3^{2-} + \text{UO}_2^{2+} \rightleftharpoons \text{UO}_2\text{CO}_3(\text{aq})$	449
X.8	Comparison of experimental equilibrium constants for calcite dissolution	453
X.9	Equilibrium constants for $\text{ZnO}(\text{cr}) + \text{H}^+ \rightleftharpoons \text{ZnOH}^+$	454
X.10	Equilibrium constants for the hydrolysis of $\text{CO}_2(\text{aq})$	455
X.11	Comparison of experimental formation constants of AlOH^{2+} with the the Ryzhenko-Bryzgalin model	461
X.12	Comparison of experimental formation constants of $\text{Al}(\text{OH})_4^-$ with the Ryzhenko-Bryzgalin model	462
X.13	Comparison of experimental equilibrium constants for $\text{Al}(\text{OH})_4^- \rightleftharpoons \text{AlOH}^{2+} + 3\text{OH}^-$ with the Ryzhenko-Bryzgalin model	462
X.14	Comparison of experimental equilibrium constants for $\text{Fe}^{2+} + \text{CH}_3\text{COO}^- \rightleftharpoons \text{FeCH}_3\text{COO}^+$ with the Ryzhenko-Bryzgalin model	464
X.15	Comparison of experimental equilibrium constants for $\text{Fe}^{2+} + 2\text{CH}_3\text{COO}^- \rightleftharpoons \text{Fe}(\text{CH}_3\text{COO})_2(\text{aq})$ with the Ryzhenko-Bryzgalin model	465
X.16	The temperature dependence of parameter $k(T)$ of Eq. (X.52) for $\text{H}_2\text{O}(\text{l})$ and $\text{NH}_4\text{OH}(\text{aq})$	467
X.17	Equilibrium constants for $\text{CO}_2(\text{aq}) + \text{H}_2\text{O}(\text{l}) \rightleftharpoons \text{HCO}_3^- + \text{H}^+$	468
X.18	Experimental equilibrium constants for reaction $\text{U}^{4+} + \text{H}_2\text{O}(\text{l}) \rightleftharpoons \text{UOH}^{3+} + \text{H}^+$	492
XI.1	Initial random distribution of 50% live cells and distribution after 10, 100 and 1000 iterations of “Life”	501
XI.2	(a) Updating rule for CA implementation of “billiard-ball” model of computation; (b) Propagation and collision of particles according to this rule	502
XI.3	One- and two-armed spirals evolving out of isolated lines of activated cells (white) buffered by lines of quiescent cells (grey)	503
XI.4	a -density for a one-dimensional, homogeneous system reacting via $a + b \rightarrow c$, as a function of time	512

XI.5	Spatial concentration pattern obtained from two-dimensional simulation of the Schnackenberg model	514
XI.6	Turing pattern reorganisation (from four to three stripes) caused by density fluctuations	515
XI.7	Profile of solute concentration and the “concentration” of solid per m^3 of rock	518
XI.8	Oscillations in CO surface density obtained from two-dimensional simulation of CO catalytic oxidation on the Pt(100) plane	521
XII.1	Sections through a drillcore of granite from the Grimsel underground laboratory (Switzerland)	530
XII.2	Spreading and shape of the peak due to mechanical dispersion for a short tracer pulse with initial release time T	534
XII.3	Longitudinal dispersivity <i>vs.</i> scale with data classified by reliability	537
XII.4	Schematic $S(C)$ <i>vs.</i> C diagrams for the linear, Freundlich and (one site) Langmuir isotherm	542
XII.5	Sketch of the influence of a possible fracture infill in the water-conducting zone to matrix diffusion	548
XII.6	The (x,z) -geometry for transport in a fractured rock	549
XII.7	The qualitative behaviour of the retardation functions $R(C)$ for three often used isotherms as depicted in the diagrams	552
XII.8	Effects of matrix diffusion in a 1D-advection model and neglecting (longitudinal) dispersion for a non-decaying solute migrating in a semi-infinite medium	558
XII.9	The influence of (limited) matrix diffusion for a migrating stable solute taking into account only 1D-advection, 1D-matrix diffusion, neglecting dispersion, and including sorption onto fracture surfaces and onto inner surfaces of the porous rock matrix	559
XII.10	The effect of limited matrix diffusion on ^{237}Np breakthrough	562
XII.11	Comparison of the effective surface sorption approximation essa with calculations assuming matrix diffusion for various penetration depths d	565
XII.12	Schematic overview of the Grimsel migration experiment showing the laboratory drift, some of the boreholes drilled for the hydrogeological characterisation and the tracer experiments	566
XII.13	Effect of matrix diffusion on tracer breakthrough for a conservative (uranine) and for a weakly sorbing tracer (strontium)	567
XII.14	Prediction of uranine and cesium breakthrough in the Grimsel migration experiment using the double-porosity medium concept for a smaller and faster dipole flow field	570
XII.15	Plot of a best-fit curve for iodide breakthrough in a Finnsjön migration experiment in the frame of a single-porosity medium approximation	572
XII.16	A calculation using the same experimental data as in Figure XII.15 but including a second preferential flow path	573
XIII.1	Typical model chain for the groundwater scenario	582
XIII.2	Radiotoxicity index (RTI) for vitrified high-level wastes	583
XIII.3	Typical effect of physical retardation by matrix diffusion	586
XIV.1	Periodic table of trace elements considered to be biologically interesting elements	594
XIV.2	Concentration of dissolved solids as a function of mean annual runoff for different rock types	601
XIV.3	A Piper plot of European bottled waters and their relationship to the parent rock type	602
XIV.4	Plot of $\log_{10} K_{\text{int}}$ for the surface complexation reactions of trace elements with various solid surfaces	609

XIV.5	Measured <i>vs.</i> calculated U concentrations from a 3% in mole U(VI)-Fe(III) oxyhydroxide coprecipitate, comparison between surface complexation and conditional solubility constant approach from [95BRU/PAB]	611
XIV.6	Idealised view of the time dependence of the formation of solid phases under granitic groundwater conditions	616
XIV.7	Calculated U concentrations by assuming equilibrium with U_3O_8 <i>versus</i> measured U content in the selected groundwaters at Poços de Caldas [91BRU/CRO]	619
XIV.8	Calculated U concentrations by assuming U(VI)/Fe(OH) ₃ coprecipitation of <i>versus</i> measured U content in the selected groundwaters at Poços de Caldas	620
XIV.9	El Berrocal. Calculated solubilities by using individual (schoepite/autunite) solid phases and by assuming U(VI)/Fe(OH) ₃ coprecipitation compared with the measured U concentrations	620

Liste des figures

I.1	Caractéristiques schématiques de la modélisation et de la validation d'un système simple (de laboratoire)	2
I.2	Schéma des procédures utilisées pour la description des propriétés/fonctionnements de systèmes complexes	4
I.3	Les caractéristiques de systèmes de laboratoire et d'autres, plus complexes, rencontrés dans la nature et dans le monde scientifique/technologique	6
I.4	Arbre des erreurs type	9
I.5	Diagramme simplifié d'influence de processus	10
I.6	Construction des diagrammes d'interactions du type "RES"	11
I.7	Exemple d'un diagramme de phases	14
I.8	Croquis schématique d'un dépôt de déchets souterrain	15
I.9	Diagrammes de Pourbaix du cuivre et du fer	16
II.1	Fonctions de distribution	60
II.2	Courbe des ligands moyens	61
II.3	Diagramme logarithmique pour le cuivre(II)	62
II.4	Diagramme de Pourbaix du fer	63
II.5	Diagramme de prédominance	67
III.1	Solvatation de cations par des solvants (a) protiques (b) polaires aprotiques	76
III.2	Diagramme de distribution des différentes espèces formées dans le système Co(II)-edta ⁴⁻	80
III.3	Quelques géométries de coordinations peu courantes de UO ₂ ²⁺	82
III.4	Quelques géométries de coordinations peu courantes : Fe(III)-edta	83
III.5	Quelques géométries de coordinations peu courantes : Ho(SO ₄) ₂ (H ₂ O) ₄ ⁻	84
III.6	Géométries courantes de liaison de l'ion carbonate	85
III.7	La répartition des ions accepteurs dans le tableau périodique	86
III.8	Stabilité relative des complexes chlorés et fluorés pour des accepteurs durs et mous ..	87
III.9	Diagramme de distribution de Hg(II) vs. la concentration totale en chlore	88
III.10	Complexes phosphatés d'uranium(VI)	92
III.11	Substitution isomorphique dans (UO ₂) ₃ (CO ₃) ₆ ⁶⁻	93
III.12	Les structures à l'état solide de (UO ₂) ₃ (O)(OH) ₃ ⁺ et (UO ₂) ₂ (OH) ₂ ²⁺	94
III.13	Diagrammes de distribution de l'hydrolyse du plomb(II)	95
III.14	Stabilité des complexes carbonatés du calcium(II) et du cerium(III)	97
III.15	Constante d'équilibre statistiquement prévue K_{stat} pour $\text{MA}_2 + \text{MB}_2 \rightleftharpoons 2\text{MAB}$	100

III.16	Compositions des complexes formés dans le système $\text{Al}^{3+}\text{-Cl}^{-}\text{-diméthylformamide}$.	102
III.17	Géométrie de coordination des complexes oxalates d'uranyle. I. $\text{UO}_2(\text{oxalate})\text{F}_3^{3-}$.	103
III.18	Géométrie de coordination des complexes oxalates d'uranyle. II. $\text{UO}_2(\text{oxalate})_2\text{H}_2\text{O}^{2-}$.	104
III.19	Géométrie de coordination des complexes oxalates d'uranyle. III. $\text{UO}_2(\text{oxalate})_3^{4-}$.	105
III.20	Dépendance de $\log_{10} K_1$ pour la formation de complexes hydroxydes en fonction de $z_i/d_{\text{M-O}}$.	106
III.21	Dépendance de $\log_{10} K_1$ pour la complexation par fluorures en fonction de $z_i/d_{\text{M-F}}$	107
III.22	L'invariabilité de la constante d'équilibre de la réaction (III.4) .	108
III.23	$\log_{10} K_1$ de quelques complexes de glycine <i>vs.</i> potentiel d'ionisation du métal .	109
III.24	$\log_{10} K_1$ de quelques complexes de glycine <i>vs.</i> électronégativité des cations métalliques .	110
III.25	$\log_{10} \beta_2$ de complexes de cations métalliques de transition bivalents avec plusieurs ligands .	110
III.26	Courbe de corrélation des complexes Fe(III)-phénolate et -salicylate .	111
III.27	$\log_{10} K_{\text{CuL}}$ <i>vs.</i> $\log_{10} K_{\text{NiL}}$.	112
III.28	Corrélation de $\log_{10} K$ pour des complexes organiques de Ca et de Sr .	113
III.29	Corrélation entre $\log_{10} K$ pour l'edta et la dcta .	114
III.30	Corrélation de constantes de stabilité pour des complexes de nta et d'edta .	115
III.31	Géométrie de coordination de $\text{Ni}(\text{nta})_2^{4-}$.	116
III.32	Géométrie de coordination de $\text{Fe}(\text{nta})_2^{3-}$.	116
III.33	Géométrie de coordination de $\text{Zr}(\text{nta})_2^{2-}$.	117
III.34	Géométrie de coordination de $\text{Nd}(\text{nta})_2\text{H}_2\text{O}^{3-}$.	117
III.35	Géométrie de coordination de $\text{VO}_2\text{edta}^{3-}$.	118
III.36	Structure du complexe dinucléaire $(\text{UO}_2)_2\text{eddt}\text{F}_4^{4-}$.	119
III.37	Corrélations entre $\log_{10} K_n$ et $\log_{10} K_{(n-1)}$ pour des complexes avec des ligands oxalate, citrate et nta .	120
III.38	Courbe 3-D de la concentration en ion oxalate nécessaire pour complexer 50% de [U(VI)] _{totale} (en tenant compte des complexes ternaires estimés) en complexes de ligands oxalate .	121
III.39	Courbe de niveau de la concentration en ion oxalate nécessaire pour complexer 50% de [U(VI)] _{totale} (en tenant compte des complexes ternaires estimés) en complexes de ligands oxalate .	122
III.40	Courbe 3-D de la concentration en ion oxalate nécessaire pour complexer 50% de [U(VI)] _{totale} (sans tenir compte des complexes ternaires) en complexes de ligands oxalate .	123
III.41	Effet de la non prise en compte des complexes ternaires $\text{UO}_2\text{-OH-oxalate}$ sur la courbe de niveau de la concentration nécessaire à la complexation de 50% de [U(VI)] _{totale} en complexes de ligands oxalate .	124
V.1	Dépendance de la complexation humique en fonction de la concentration du métal. Complexation de Eu, Am et Cm avec des acides fulviques et humiques (modèles à un et deux sites) .	167
V.2	Dépendance de la complexation humique en fonction de la concentration du métal. Complexation de Eu, Am et Cm avec des acides fulviques et humiques (modèles à distribution continue) .	172
V.3	Dépendance de la complexation humique en fonction du pH. Complexation de Eu, Am et Cm avec des acides fulviques et humiques .	177
V.4	Résumé des données expérimentales sur la complexation de l'Eu, l'Am et du Cm avec des acides humiques et fulviques à une force ionique de 0.1 M .	193

V.5	L'approche conservative pour l'évaluation de la performance	194
V.6	Représentation schématique d'effets compétitifs sur les modèles de liaison métallique-humique : compétition entre cations et anions	198
V.7	Représentation schématique d'effets compétitifs sur les modèles de liaison métallique-humique : complexes ternaires	199
V.8	Représentation schématique d'effets compétitifs sur les modèles de liaison métallique-humique : compétition entre sites de surface minérale	200
V.9	Croquis complet des interactions mutuelles entre métaux toxiques, substances humiques, autres cations et anions, et sites de surface minérale	201
V.10	Diagrammes 3-D de la complexation humique de traces d'Eu	204
V.11	Courbe de niveau de la concentration en substances humiques (\log_{10} g/l) nécessaire à la complexation de 90% de la totalité de l'Eu dissous	206
VI.1	Structure d'acide fulvique proposée par Schnitzer et Kahn	210
VI.2	Structure de l'acide fulvique de Berbsø	211
VI.3	Réactions d'échange mono-électronique	212
VI.4	Étapes du programme	218
VI.5	Exemples d'affectations d'hétérogénéité dans les sites à quelques échantillons d'acides fulviques	220
VI.6	pK_a^{app} vs. α pour l'acide fulvique Laurentide	222
VI.7	δpK vs. α pour l'acide fulvique Laurentide	223
VI.8	Effet de la force ionique sur l'interaction métallique-humique	228
VI.9	pK_a^{app} vs. α pour 12 acides fulviques	230
VI.10	Espèces chimiques de l'Eu(III) dans les eaux de surface	236
VI.11	Espèces chimiques de l'Eu(III) dans les eaux de surface	236
VI.12	Espèces chimiques de l'Eu(III) dans les eaux de surface	237
VI.13	Espèces chimiques de l'Eu(III) dans les eaux souterraines	238
VI.14	Espèces chimiques de l'Eu(III) dans les eaux souterraines	239
VI.15	Espèces chimiques de l'Eu(III) dans les eaux souterraines	239
VI.16	Espèces chimiques de l'Eu(III) avec une faible concentration en produits humiques ..	240
VI.17	Espèces chimiques de l'Eu(III) avec une faible concentration en produits humiques ..	240
VI.18	Espèces chimiques de l'Eu(III) avec une faible concentration en produits humiques ..	241
VII.1	Les réactions d'adsorption dépendent de la nature chimique du soluté (adsorbé) et de la surface solide (adsorbant)	247
VII.2	Diagramme schématique d'un système de réacteur à flux continu utilisé pour étudier l'adsorption sur surfaces minérales	249
VII.3	Passage de la totalité du Cr dissous au cours du temps pour l'adsorption du Cr(VI) sur de l'oxyde de fer	250
VII.4	Excès de surface de Cr sur de la goethite colloïdale	251
VII.5	Ions hydroxydes chimiquement liés à des sites terminaux de Fe(III) à la surface d'oxyde de fer	255
VII.6	Dépendance de l'adsorption de Cr^{3+} et de CrO_4^{2-} sur oxyde de fer en fonction du pH	263
VII.7	Dépendance des espèces carbonatés et sulfatés en surface en fonction de p_{CO_2}	267
VII.8	Comportement non-ideal de l'adsorption de sulfates sur la terre	271
VII.9	Origines de la charge de surface	273
VII.10	Diagrammes qualitatifs pour le titrage des groupes hydroxyles sur les surfaces minérales	274
VII.11	Relation entre la charge interfaciale et la distribution de potentiel au travers de la double couche électrique	277

VII.12	Rapport des activités du sodium et du calcium en solution, tracé selon la loi thermodynamique d'action de masse donnée dans le Tableau VII.7	278
VII.13	Modélisation thermodynamique de la réaction d'échange ionique entre le sodium et le calcium pendant la dilution des eaux souterraines au laboratoire d'Äspö Hard Rock	280
VII.14	Isotherme conceptuelle décrivant la transition entre les équilibres d'adsorption et de précipitation en surface à l'interface eau-minéral	282
VIII.1	Données expérimentales et extrapolations sur le C_p et le C_V du corindon	294
VIII.2	Comparaison entre données expérimentales et calculées par ordinateur pour $\text{Br} \rightleftharpoons \text{Per} + \text{H}_2\text{O}(\text{l})$	296
VIII.3	Comparaison entre données expérimentales et calculées par ordinateur pour $\text{Ms} \rightleftharpoons \text{Cor} + \text{San} + \text{H}_2\text{O}(\text{f})$	298
VIII.4	Comparaison entre données expérimentales et calculées par ordinateur pour $\text{Ms} + \text{Q} \rightleftharpoons \text{San} + \text{Sill} + \text{H}_2\text{O}(\text{f})$	299
VIII.5	Comparaison entre données expérimentales et calculées par ordinateur pour $\text{Ms} + \text{Q} \rightleftharpoons \text{San} + \text{And} + \text{H}_2\text{O}(\text{f})$	299
VIII.6	Structure du pyroxène montrant la chaîne de silicium tétraédrique et les octaèdres M1 et M2	317
IX.1	Variation de $\log_{10} \gamma_{\pm}$ pour quelques électrolytes 1:1	328
IX.2	Représentation graphique de $(\log_{10} \gamma_{\pm} - Z_M Z_X D)$ vs. I_m	329
IX.3	Dépendance du coefficient de SIT en fonction des concentrations pour quelques électrolytes	333
IX.4	Détermination du coefficient de SIT à partir des coefficients moyens d'activité pour HCl	341
IX.5	Extrapolation à $I = 0$: un exemple	343
IX.6	Corrélations entre coefficients d'interaction pour cations monovalents	348
IX.7	Corrélations entre coefficients d'interaction pour cations monovalents	348
IX.8	Corrélations entre coefficients d'interaction pour cations divalents	349
IX.9	Corrélations entre coefficients d'interaction pour cations trivalents	349
IX.10	Corrélations entre coefficients d'interaction et le potentiel ionique Z/r	350
IX.11	Corrélations entre coefficients d'interaction et le potentiel ionique Z/r	351
IX.12	Corrélations entre coefficients d'interaction et le potentiel ionique Z/r	351
IX.13	Dépendance en fonction de la concentration de $\log_{10} \gamma$ de $\text{CO}_2(\text{aq})$ dans des solutions de NaCl	359
IX.14	Comparaison des valeurs expérimentales et calculées de $\log_{10} K$ utilisant l'approche de Pitzer et le modèle SIT pour $\text{H}_2\text{O}(\text{l}) + \text{CO}_2(\text{aq}) \rightleftharpoons \text{H}^+ + \text{HCO}_3^-$	360
IX.15	Comparaison des valeurs expérimentales et calculées de $\log_{10} K$ utilisant l'approche de Pitzer et le modèle SIT pour $\text{HCO}_3^- \rightleftharpoons \text{H}^+ + \text{CO}_3^{2-}$	362
IX.16	Comparaison des valeurs expérimentales et prévues de $\log_{10} K$ utilisant l'approche de Pitzer avec les valeurs disponibles dans la littérature sur les termes de mélanges et le modèle SIT pour $\text{H}_2\text{O}(\text{l}) + \text{CO}_2(\text{aq}) \rightleftharpoons \text{H}^+ + \text{HCO}_3^-$	364
IX.17	Comparaison des valeurs expérimentales et prévues de $\log_{10} K$ utilisant l'approche de Pitzer avec les valeurs disponibles dans la littérature sur les termes de mélanges et le modèle SIT pour $\text{HCO}_3^- \rightleftharpoons \text{H}^+ + \text{CO}_3^{2-}$	365
IX.18	Paramétrisation du modèle SIT et de différentes variantes du modèle de Pitzer pour $\text{H}_2\text{O}(\text{l}) \rightleftharpoons \text{H}^+ + \text{OH}^-$	370
IX.19	Paramétrisation du modèle SIT et de différentes variantes du modèle de Pitzer pour $\text{H}^+ + \text{SO}_4^{2-} \rightleftharpoons \text{HSO}_4^-$	373

IX.20	Contributions relatives du terme de Debye-Hückel à $\ln \gamma_{\pm}$ pour les modèles SIT et de Pitzer	376
IX.21	Dépendance en fonction des concentrations de la fonction Y pour les électrolytes-types 1-1 et 1-2	376
IX.22	Comparaison de la qualité de la reproduction de données expérimentales des coefficients moyens d'activité pour différents électrolytes	377
IX.23	Relations entre les paramètres des modèles de Pitzer et SIT pour des électrolytes 1-1 ..	380
IX.24	Relations entre les paramètres des modèles de Pitzer et SIT pour des électrolytes 2-1 et 1-2	380
IX.25	Relations entre les paramètres des modèles de Pitzer et SIT pour des électrolytes 3-1 et 1-3	381
IX.26	Comparaison de valeurs "prévues" et "expérimentales" du paramètre $\beta^{(1)}$ en fonction de la température	382
IX.27	Relations entre paramètres des modèles de Pitzer et SIT d'après $\log_{10} K$ dans des électrolytes de type 1-1	384
IX.28	Comparaisons des valeurs expérimentales et calculées de $\log_{10} K$ obtenues en utilisant les modèles SIT et de Pitzer simplifié pour $\text{Cd}^{2+} + \text{NO}_2^- \rightleftharpoons \text{CdNO}_2^+$ dans des solutions de NaClO_4	388
IX.29	Comparaisons des valeurs expérimentales et calculées de $\log_{10} K$ pour $\text{Fe}^{3+} + \text{Cl}^- \rightleftharpoons \text{FeCl}^{2+}$ dans des solutions de HClO_4	390
IX.30	Comparaisons des valeurs expérimentales et prévues de la différence en valeur de $\log_{10} K$ pour $\text{Fe}^{3+} + \text{Cl}^- \rightleftharpoons \text{FeCl}^{2+}$ en milieux HClO_4 pur et $\text{HClO}_4\text{-NaClO}_4$	391
IX.31	Valeurs de la fonction Y calculées à partir des données de $\log_{10} K$ en milieux NaClO_4 , LiClO_4 et $\text{Mg}(\text{ClO}_4)_2$ en utilisant le modèle SIT pour $\text{Cd}^{2+} + \text{Cl}^- \rightleftharpoons \text{CdCl}^+$	394
IX.32	Valeurs de la fonction Y calculées à partir des données de $\log_{10} K$ en milieux NaClO_4 , LiClO_4 et $\text{Mg}(\text{ClO}_4)_2$ en utilisant le modèle de Pitzer pour $\text{Cd}^{2+} + \text{Cl}^- \rightleftharpoons \text{CdCl}^+$	395
IX.33	Comparaison entre valeurs expérimentales et lissées des coefficients d'activité dans des solutions de NaCl d'après le modèle SIT	402
IX.34	Comparaison entre valeurs expérimentales et lissées d'enthalpies molaires apparentes relatives dans des solutions de NaCl d'après le modèle SIT	403
IX.35	Comparaison entre valeurs expérimentales et lissées de volumes molaires apparents dans des solutions de NaCl d'après le modèle SIT	403
IX.36	Comparaison entre valeurs expérimentales et lissées de capacités calorifiques apparentes dans des solutions de NaCl d'après le modèle SIT	404
IX.37	Différences entre les valeurs expérimentales et lissées en utilisant SIT de $\log_{10} K$ pour $\text{CO}_2 + \text{H}_2\text{O}(\text{l}) \rightleftharpoons \text{H}^+ + \text{HCO}_3^-$	406
IX.38	Différences entre les valeurs expérimentales et lissées en utilisant SIT de $\log_{10} K$ pour $\text{HCO}_3^- \rightleftharpoons \text{H}^+ + \text{CO}_3^{2-}$	407
IX.39	Différences entre les valeurs expérimentales et lissées en utilisant SIT de $\log_{10} K$ pour $\text{HSO}_4^- \rightleftharpoons \text{H}^+ + \text{SO}_4^{2-}$	407
IX.40	Paramétrisation du modèle SIT et de différentes variantes de celui de Pitzer à partir des valeurs expérimentales de $\Delta_r H_m$ pour $\text{H}_2\text{O}(\text{l}) \rightleftharpoons \text{H}^+ + \text{OH}^-$ en milieu NaClO_4 ...	422
IX.41	Dépendance de la fonction d'ajustement Y en fonction des concentrations pour $\text{Hg}^{2+} + \text{Cl}^- \rightleftharpoons \text{HgCl}^+$ dans des solutions de NaClO_4 basée sur le modèle de Pitzer	424
IX.42	Dépendance de la fonction d'ajustement Y en fonction des concentrations pour $\text{Hg}^{2+} + \text{Cl}^- \rightleftharpoons \text{HgCl}^+$ dans des solutions de NaClO_4 basée sur le modèle SIT	425
X.1	Constantes d'équilibre pour $\text{CO}_3^{2-} + \text{UO}_2^{2+} \rightleftharpoons \text{UO}_2\text{CO}_3(\text{aq})$	436
X.2	Dépendance de la constante diélectrique de l'eau en fonction de la température	438
X.3	Constantes d'équilibre pour la réaction $\text{H}_2\text{O}(\text{l}) + \text{UO}_2^{2+} \rightleftharpoons \text{H}^+ + \text{UO}_2\text{OH}^+$	441

X.4	Constantes d'équilibre pour la réaction $\text{CO}_3^{2-} + \text{UO}_2^{2+} \rightleftharpoons \text{UO}_2\text{CO}_3(\text{aq})$	441
X.5	Constantes d'équilibre pour $\text{UO}_2^{2+} + \text{CO}_2(\text{aq}) \rightleftharpoons \text{UO}_2\text{CO}_3(\text{aq}) + 2\text{H}^+$	443
X.6	Constantes d'équilibre pour $\text{CO}_3^{2-} + \text{UO}_2^{2+} \rightleftharpoons \text{UO}_2\text{CO}_3(\text{aq})$	443
X.7	Constantes d'équilibre pour $\text{CO}_3^{2-} + \text{UO}_2^{2+} \rightleftharpoons \text{UO}_2\text{CO}_3(\text{aq})$	449
X.8	Comparaison de constantes d'équilibre expérimentales pour la dissolution de la calcite	453
X.9	Constantes d'équilibre pour $\text{ZnO}(\text{cr}) + \text{H}^+ \rightleftharpoons \text{ZnOH}^+$	454
X.10	Constantes d'équilibre pour l'hydrolyse de $\text{CO}_2(\text{aq})$	455
X.11	Comparaison de constantes de formation expérimentales d' AlOH^{2+} avec le modèle de Ryzhenko-Bryzgalin	461
X.12	Comparaison de constantes de formation expérimentales d' $\text{Al}(\text{OH})_4^-$ avec le modèle de Ryzhenko-Bryzgalin	462
X.13	Comparaison de constantes d'équilibre expérimentales avec le modèle de Ryzhenko-Bryzgalin pour $\text{AlOH}_4^- \rightleftharpoons \text{AlOH}^{2+} + 3\text{OH}^-$	462
X.14	Comparaison de constantes d'équilibre expérimentales avec le modèle de Ryzhenko-Bryzgalin pour $\text{Fe}^{2+} + \text{CH}_3\text{COO}^- \rightleftharpoons \text{FeCH}_3\text{COO}^+$	464
X.15	Comparaison de constantes d'équilibre expérimentales avec le modèle de Ryzhenko-Bryzgalin pour $\text{Fe}^{2+} + 2\text{CH}_3\text{COO}^- \rightleftharpoons \text{Fe}(\text{CH}_3\text{COO})_2$	465
X.16	Dépendance du paramètre $k(T)$ de l'Eq. (X.52) pour $\text{H}_2\text{O}(\text{l})$ et $\text{NH}_4\text{OH}(\text{aq})$ en fonction de la température	467
X.17	Constantes d'équilibre pour $\text{CO}_2(\text{aq}) + \text{H}_2\text{O}(\text{l}) \rightleftharpoons \text{HCO}_3^- + \text{H}^+$	468
X.18	Constantes d'équilibre expérimentales pour la réaction $\text{U}^{4+} + \text{H}_2\text{O}(\text{l}) \rightleftharpoons \text{UOH}^{3+} + \text{H}^+$	492
XI.1	Distribution initiale aléatoire de 50% des cellules vivantes et distribution après 10, 100 et 1000 itérations de "Life"	501
XI.2	(a) Dernière règle pour la mise en œuvre des CA du modèle de calcul de la "boule de billiard" ; (b) Propagation et collision de particules selon cette règle	502
XI.3	Spirales à un et deux bras évoluant en dehors des lignes isolées des cellules activées (blanches) tamponnées par des lignes de cellules au repos	503
XI.4	Densité- a pour un système homogène à une dimension réagissant selon $a + b \rightarrow c$, en fonction du temps	512
XI.5	Figure spatiale des concentrations obtenues par une simulation à deux dimensions du modèle de Schnackenberg	514
XI.6	Réorganisation des figures de Turing (de quatre à trois rayures) causée par des fluctuations de densité	515
XI.7	Profil de la concentration de soluté et la "concentration" de solide par m^3 de roche ..	518
XI.8	Oscillations de la densité superficielle de CO obtenues par simulation à deux dimensions de l'oxydation catalytique de CO sur le plan Pt(100)	521
XII.1	Sections d'une carotte de granite provenant du laboratoire souterrain de Grimsel (Suisse)	530
XII.2	Propagation et forme du pic dues à la dispersion mécanique pour une brève injection de traceur avec l'instant de début de rejet T	534
XII.3	Dispersivité longitudinale <i>vs.</i> la distance avec classification des données selon leur fiabilité	537
XII.4	Diagrammes schématiques de $S(C)$ <i>vs.</i> C pour l'isotherme linéaire de Freundlich et de Langmuir (à un site)	542
XII.5	Croquis de l'influence d'un possible remplissage de faille dans la zone qui amène l'eau à la matrice de diffusion	548
XII.6	Géométrie selon x et z pour le transport dans une roche fracturée	549
XII.7	Comportement qualitatif des fonctions de retard $R(C)$ pour trois isothermes souvent utilisées comme le représentent les diagrammes	552

XII.8	Effets de la diffusion dans la matrice dans un modèle à advection 1-D et en négligeant la dispersion (longitudinale) pour un soluté qui ne se désintègre pas migrant dans un milieu semi-infini	558
XII.9	Influence d'une diffusion (limitée) dans la matrice pour un soluté stable en migration en ne considérant que l'advection 1-D, la diffusion 1-D dans la matrice, en négligeant la dispersion, et en incluant la sorption sur les surfaces de fracture et sur les surfaces internes de la matrice de la roche poreuse	559
XII.10	Effet de la diffusion limitée dans la matrice sur le passage du ^{237}Np	562
XII.11	Comparaison de l'approximation de la surface effective de sorption (ases) avec des calculs en admettant la diffusion dans la matrice pour plusieurs profondeurs de pénétration d	565
XII.12	Vue d'ensemble schématique de l'expérience de migration de Grimsel montrant la galerie du laboratoire, quelques trous de forages creusés pour la caractérisation hydrogéologique et les expériences avec traceurs	566
XII.13	Effet de la matrice de diffusion sur le passage d'un traceur pour un traceur pénalisant (uranine) et un qui n'est que légèrement absorbé (strontium)	567
XII.14	Prévision du passage de l'uranine et du césium dans l'expérience de migration de Grimsel en utilisant le concept du milieu doublement poreux pour un champ de débits de dipôles plus petit et plus rapide	570
XII.15	Représentation de la courbe la mieux ajustée pour le passage des iodures dans une expérience de migration de Finnsjön dans le cadre de l'approximation du milieu simplement poreux	572
XII.16	Calcul utilisant les mêmes données expérimentales que dans la Figure XII.15 mais qui comprend un second chemin préférentiel de circulation de fluide	573
XIII.1	Chaîne de modèles typiques pour les scénarios des eaux souterraines	582
XIII.2	Index de radiotoxicité (IRT) pour les déchets vitrifiés hautement radioactifs	583
XIII.3	Effet typique du retard physique par la diffusion dans la matrice	586
XIV.1	Tableau périodique des éléments traceurs considérés comme étant biologiquement intéressants	594
XIV.2	Concentration des solides dissous en fonction de la moyenne annuelle du ruissellement pour différents types de roche	601
XIV.3	Représentation graphique de Piper des eaux européennes mises en bouteilles et de leurs relations avec le type de roche d'où elles proviennent	602
XIV.4	Représentation graphique de $\log_{10} K_{\text{int}}$ pour les réactions de complexation en surface d'éléments traceurs avec plusieurs surfaces solides	609
XIV.5	Concentrations en U mesurées <i>vs.</i> des concentrations en U calculées d'un coprécipité oxyhydroxide U(VI)-Fe(III) à 3% en mole, comparaison entre la surface de complexation et l'approche de la constante conditionnelle de solubilité de [95BRU/PAB]	611
XIV.6	Vue idéalisée de la dépendance en fonction du temps de la formation de phases solides dans les conditions des eaux souterraines granitiques	616
XIV.7	Concentrations en U calculées en admettant l'équilibre avec U_3O_8 <i>vs.</i> teneur en U mesurée dans les eaux souterraines sélectionnées de Poços de Caldas [91BRU/CRO] ..	619
XIV.8	Concentrations en U calculées en admettant la coprécipitation U(VI)/Fe(OH)_3 <i>vs.</i> teneur en U mesurée dans les eaux souterraines sélectionnées de Poços de Caldas	620
XIV.9	El Berrocal. Solubilités calculées en utilisant des phases solides particulières (schoepite /autunite) et en supposant la coprécipitation U(VI)/Fe(OH)_3 comparées avec les concentrations en U mesurées	620

Chapter I

Introduction

Ingmar GRENTHE
Department of Inorganic Chemistry
Royal Institute of Technology
S-100 44 Stockholm (Sweden)

Ignasi PUIGDOMENECH ¹
OECD Nuclear Energy Agency
Le Seine – Saint Germain
12, boulevard des Iles
F-92130 Issy-les-Moulineaux (France)

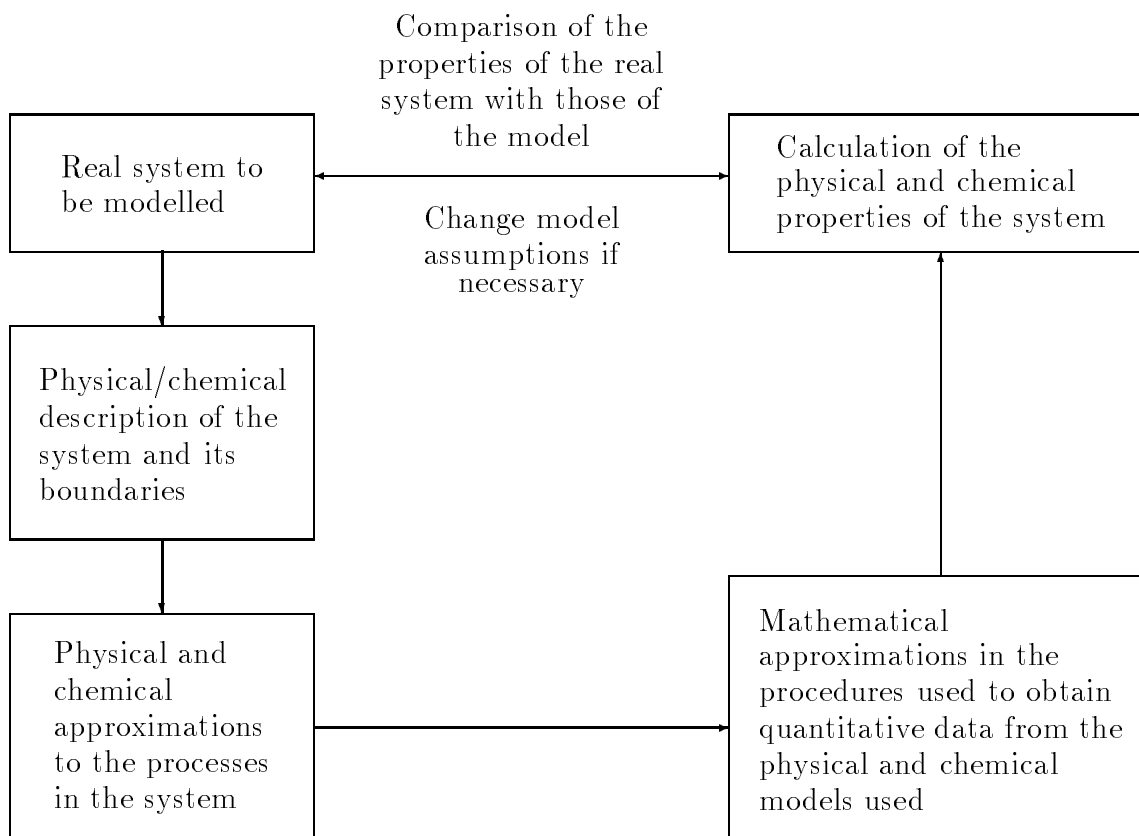
I.1. Models and modelling

Modelling is essential when trying to understand complex systems and phenomena and in order to take action on the information obtained. Human activity, to a large part driven by technology and population growth, influences our surroundings both on local and global scales. In order to describe, model, understand and change these processes it is necessary to combine many different scientific disciplines, *e.g.* by forming multidisciplinary teams which must be able to engage the various stake-holders in the understanding/decision-making process. This is a difficult and complex task where modelling is a key element in establishing a common “language” among those involved.

This book deals with the modelling of aqueous chemical systems in nature and elsewhere. Their degree of complexity may vary considerably from simple laboratory systems, *via* technical systems (*e.g.*, hydrometallurgical systems, energy systems of various kinds, and waste systems) to large scale systems in nature (*e.g.*, global geochemical cycles, and the transport of metal containing species and other chemicals in ground and surface water systems). The emphasis is on modelling of *chemical* reactions and equilibria and the main part of the text will therefore be devoted to chemical issues. However, *physical* processes such as mass transport (diffusion, advection and dispersion) are important for the chemical evolution of ground and surface waters, and will therefore also be discussed. Before

¹ Permanent address: Department of Inorganic Chemistry, Royal Institute of Technology, S-100 44 Stockholm, Sweden.

Figure I.1: Schematic features of the modelling and validation of a simple (laboratory) system.



entering into the details of chemical modelling we will describe some of the terminology and modelling strategies used.

A *system* is that part of the physical world that the modeller wants to describe, and where all the relevant processes in the model are assumed to take place. *Boundary conditions* are the quantitative data about the initial state and about the physical boundaries of the system. Boundary conditions are necessary to make statements about the behaviour of the model (and in an incomplete way also about the physical world).

There are formalised procedures that may be used in the analysis and description of complex systems – there is even a scientific discipline, *system or operation analysis* that is devoted to issues of this type. An analysis of a system in principle follows the scheme given in Figures I.1 and I.2. In this chapter we will present a first discussion of various types of models and how, and in what contexts, they are used.

Models are used in science and technology as tools; they are by choice and necessity incomplete and describe only those aspects of “reality” which the modeller finds to be relevant for the understanding and description of the “real” system. From this follows that

modelling may be performed on different levels of sophistication, and necessary elements are the approximations of various kinds, based on the conceptions of the problem at hand.

1.1.1. The need for models

Why then do we use models? Oreskes, Shrader-Frechette and Belitz [94ORE/SHR] state that “Models can corroborate a hypothesis by offering evidence to strengthen what may be already partly established through other means. Models can elucidate discrepancies in other models. Models can also be used for sensitivity analysis – for exploring ‘what if questions’ – thereby illuminating which aspects of the system are most in need of further study, and where more data are most needed. Thus, the primary goal of models is heuristic: models are representations, useful for guiding further study but not susceptible to proof.” This is a reasonable statement from the natural science point of view. However, models are not only used to guide further studies, but also to evaluate the performance of systems as a function of time, to investigate compliance with *performance criteria* and to help in *decision-making*, as indicated in Figure I.2.

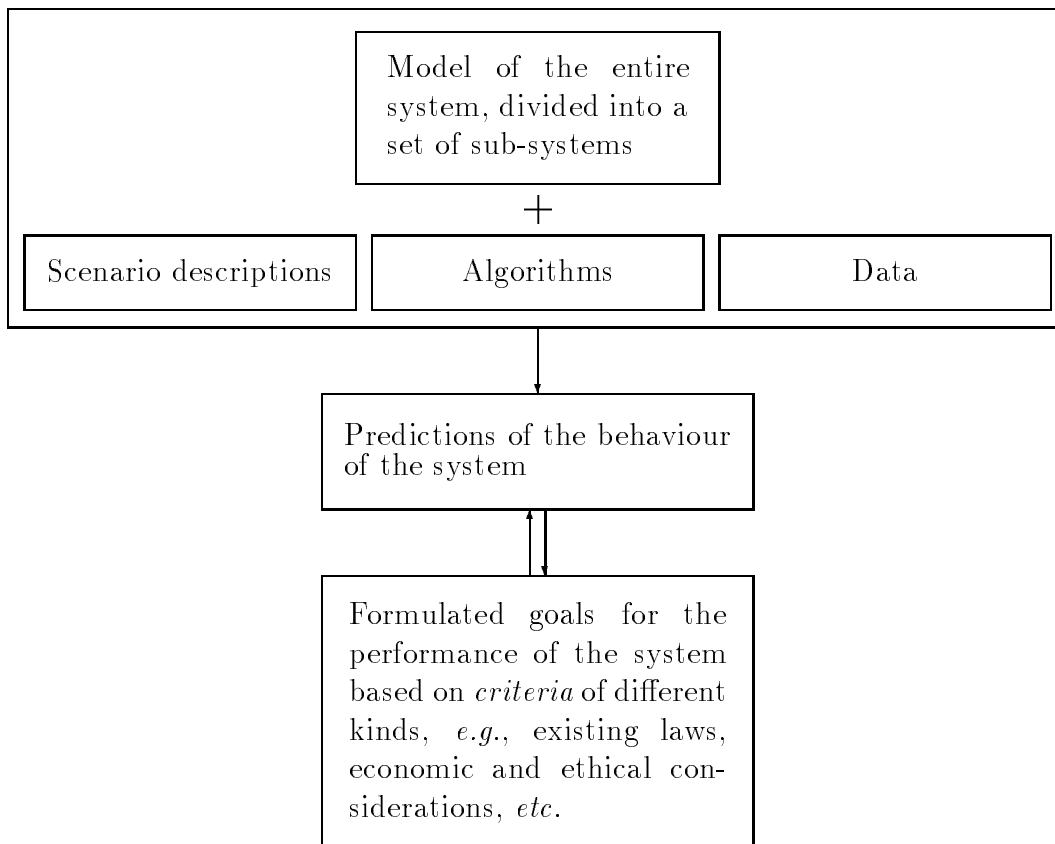
Decision-making is often regarded as a rational choice between known alternatives. This is a very simplistic view, many decisions have to be taken (not to take the decision is also a decision!) against a background of genuine uncertainty in the data and models. One remedy is the use of “conservative” assumptions. Examples are found in the management of toxic, including radioactive, wastes where the models often may be “unrealistic” in some details, but this is accepted provided that the models err on the conservative side (*i.e.*, they overestimate the negative effect of a decision).

1.1.2. Verification and validation of models

Verification and validation are important issues when discussing and using models. One difficulty is that the terms have different connotations to different individuals. *Verify* according to most dictionaries means an assertion or establishment of truth. To say that a model is verified implies that its truth has been established, and that it can be used as a basis for decision-making, or as a component in other models. Verification is also used to denote the ability of a certain computer code to solve correctly the governing equations. This is made by comparing numerical solutions within benchmark studies or with analytical solutions, and demonstrating that they are equivalent under the conditions where the model is used.

Validation does not necessarily denote the establishment of truth, but implies that the model does not contain detectable flaws and errors of logic. In nuclear waste management the term is used in a different way. The US Nuclear Regulatory Commission defines it as the process of obtaining “assurance that a model, as embodied in a computer code, is a correct representation of the process or system for which it is intended”, while the US Department of Energy defines validation as “a process whose objective is to ascertain that the code or model indeed reflects the behaviour of the real world”. The International Atomic Energy Agency states that models are validated when it is confirmed that they

Figure I.2: Outline of the procedures used for describing properties/functioning of complex systems.



“provide a good representation of the actual processes occurring in the real system”. The terminology used within the nuclear waste community is unfortunate because it tends to be misleading to scientists and laymen outside the area. There are interesting discussions of these issues by Konikow and Bredehoft [92KON/BRE], de Marsily, Combes and Goblet [92MAR/COM], and by Oreskes, Shrader-Frechette and Belitz [94ORE/SHR]. Let us make a quote from the last of these references: “no general empirical proposition about the natural world can ever be certain. No matter how much data we have, there will always be the possibility that more than one theory can explain the available observations.”

I.1.3. Modelling stages for complex systems

Figure I.1 describes reasonably well the modelling situations encountered when trying to describe fairly simple systems such as those encountered in *laboratory* investigations. Most systems encountered in nature have a much higher degree of complexity, and the modelling approach must be modified/elaborated accordingly. Figure I.2 gives a better, albeit schematic, description of the procedure.

The essential part of this process is a *formulation of objectives* for the model, the *documentation* of the scientific basis for the analysis, and the *expert judgements* made. These form the rationale behind the model, which must be transparent to all users.

The analysis can be made using the following set of “procedures”:

- Choice of *scenarios*. This is a description in word of the system and the FEPs (**F**eatures, **E**vents and **P**rocesses) taking place in it. The “main” FEPs are defined (or assumed) by the modeller, based on the current general level of description/understanding of the system, but also on performance criteria. See for example Table XIII.1 on p. 579.

The FEPs can vary widely, from those that may be formulated in scientific/technical terms, to others that deal with, *e.g.*, social and behavioural issues. We will only discuss the first types. However, the latter may often be more important for both the performance of the system, and for the ultimate decision of implementing a certain technical system, or not.

- Choice of *conceptual models*. This is the process where the modeller selects the appropriate scientific theories, models and data that will be used to describe the processes defined in the various scenario descriptions. This process in general also involves various physical and chemical approximations. The data are in many cases model-dependent and it is not always possible to use data from experiments evaluated with one model, in a different one.
- Transfer to mathematical models. The process where the modeller transfers the conceptual models into a suitable form for calculating relevant system properties under the given assumptions. This nearly always requires mathematical approximations of various kinds.
- Calculations. This is seemingly the most straightforward part of the exercise. However, it is essential to use computer codes that are well tested and do not suffer from problems of numerical instability [92KON/BRE]. A particular difficult problem is the coupling of different processes, *e.g.*, chemical reactions and mass-transport processes such as diffusion and advection. This problem will be discussed in Chapter XII.

The design of models should be dictated by the questions the model is supposed to answer, a key task is to separate the significant features from the less important.

I.2. Laboratory systems *vs.* complex systems encountered in nature and in science/technology

It is necessary to be aware of the very large differences between laboratory systems, and other much more complex systems such as those encountered in nature or in science/technology. This section is only intended to give the reader an idea of the nature of these differences, and how they affect modelling strategies.

Figure I.3: The characteristic features of laboratory systems and more complex systems encountered in nature and in the scientific/technological world.

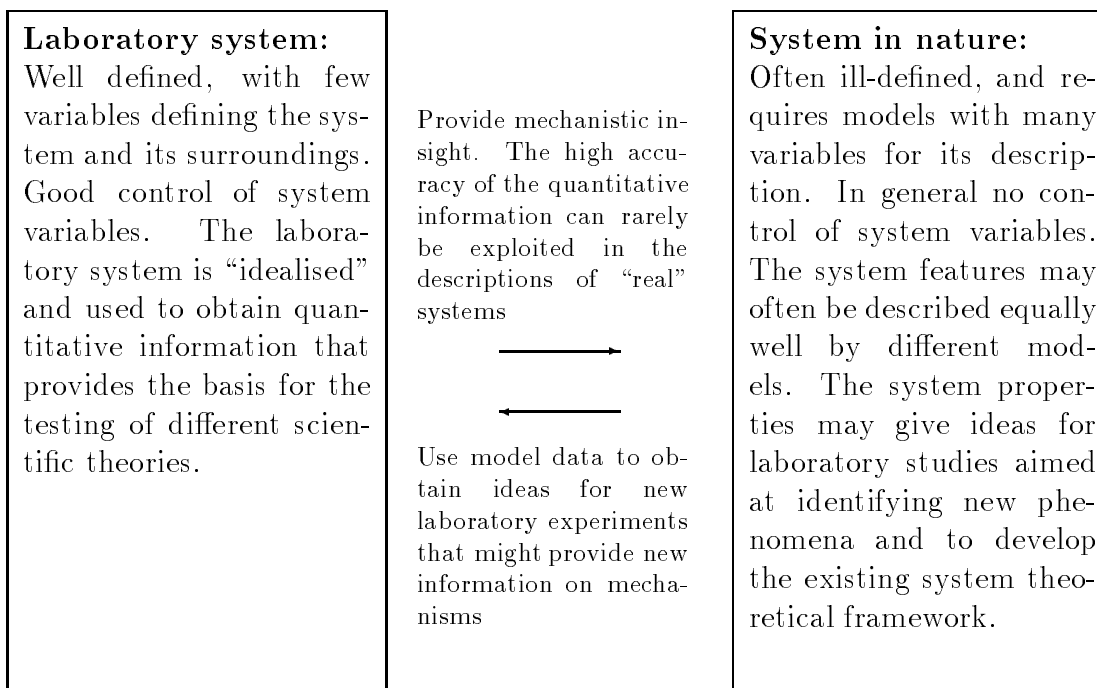


Figure I.3 demonstrates the characteristics of laboratory systems and of systems in nature.

“Laboratory” systems are used for developing new scientific theories, or to extend or further develop already existing ones. This is done by simplifying and controlling the system as far as possible within the scope of the problem. A characteristic feature is that detailed experimental observations are used to make a synthesis in the form of a new, or extended theory, *i.e.*, laboratory data allow the extension of models to describe more complex systems by a “bottom-up” approach.

Example 1:

Equilibrium analysis [61ROS/ROS, 71SIL, 71ROS/ROS, 80HAR/BUR], *i.e.*, the interpretation of solution chemical data in terms of a solution chemical model, is a typical example of a laboratory model. The solution chemical data might be for example spectrophotometric or electromotive force (emf) data, like pH measurements. The data are interpreted in terms of equilibrium reactions (acid-base, complex formation, solubility, *etc.*) to obtain values of equilibrium constants. See also Section II.1.8.

Another example is the determination of the *speciation*, *i.e.*, the chemical form of the various components in a system *at equilibrium*, by the use of already existing solution chemical data (equilibrium constants). See for example Figure II.3 on p.62. In systems with many components this requires the use of a suitable computer code, but it also requires models for the recalculation of the available equilibrium

constants so they are valid at the ionic strength/ionic medium composition and the temperature in the system. It may be also necessary to *estimate* the composition and thermodynamic data for species that are chemically reasonable, but for which no quantitative data are available.

Models of this type are often submodels in the more complex models. The scientific information and understanding on which these models are based are usually fairly good, and an important part of this book is devoted to the description of the characteristic features of models of this type.

Typical computer codes for this type of model (calculation of chemical speciation at equilibrium) are HALTAFALL, developed by Sillén *et al.* [67ING/KAK, 70EKE/SIL, 71WAR/ING], SOLGAS and SOLGASWATER, by Eriksson [75ERI, 79ERI], EQ3/6 by Wollery [83WOL, 86WOL, 90WOL/JAC], PHREEQE by Plummer *et al.* [80PAR/THO, 83FLE/PLU, 88PLU/PAR, 90PLU/PAR], *etc.* The codes MINEQL by Westall *et al.* [76WES/ZAC, 79WES, 84SCH, 86WES] (*cf.* <http://www.agate.net/~ersoftwr/homepage.html>), HYDRAQL by Leckie and co-workers [88PAP/HAY], and MINTEQ [87PET/HOS] are also of this type, but they also include the possibility to model *surface speciation*, *cf.* Chapter VII. Nordstrom *et al.* have discussed and compared codes of this type [79NOR/PLU, 84NOR/BAL].

Example 2:

Hydrological models describe *dynamic* events, *i.e.*, the movement of water in media of different types. They may also be classified as “simple” models in the sense that they depict only one particular process in a system. This does not imply that the physical or mathematical approximations required to describe the system and to calculate the model properties are simple, *cf.* [92KON/BRE] and [92MAR/COM]. A summary of the characteristic features of this type of models is given in Chapters XI and XII.

Systems that require coupling between mass transport and chemical reactions fall in another category than those mentioned in Examples 1 and 2. The computational problems that arise when calculating the system properties are now severe and require a careful consideration of the time-scale of the chemical events as compared to the transport, and also of the dimensionality of the problem, *i.e.*, if a particular problem requires a three-dimensional model, or if a two-, or one-dimensional model will be sufficient. The difference in numerical stability and requirement of computer time will be very different for these three cases. This area is outside the main scope of this book, and the readers are referred to the bibliography in Chapters XI and XII for more details. “Simple” problems of this type are well-known in chemical engineering for the description of column operations of various kinds, such as ion-exchange and liquid-liquid extraction. The problems are simple in the sense that the physical and chemical processes in the system are well known and understood.

“Complex” systems represent something very different, and cannot be tackled with the “bottom-up” method. There are several reasons for this:

- The high degree of complexity may result in unknown interactions between the components and the processes. The higher the degree of complexity the more such unknown interactions may be of importance.
- The high complexity makes it impossible to use models that rely on detailed mechanistic description of the chemical and physical processes in the system, because the collection of the necessary information might change the properties of the system. In order to obtain detailed information of an underground waste repository it would be necessary to make extensive use of drilling operations, or excavations, which would change the properties of the site. An additional problem is that the expenditures for computer time increases rapidly with increasing complexity.
- The observed macroscopic properties of the system may be compatible with different models, *i.e.*, there is a problem with the uniqueness of the models.

In these cases, the description/modelling of the complex system must start from its macroscopic behaviour/function, and the key issue is really to break-down the system into smaller parts (sub-systems), in such a way that all relevant factors that might influence their behaviour are taken into account. This is a “top-down”, or objective-based, approach. The description/modelling must be *open* in the sense that there is a continuous reevaluation of the approach used as new information becomes available: hypothesis testing and synthesis form a closed loop.

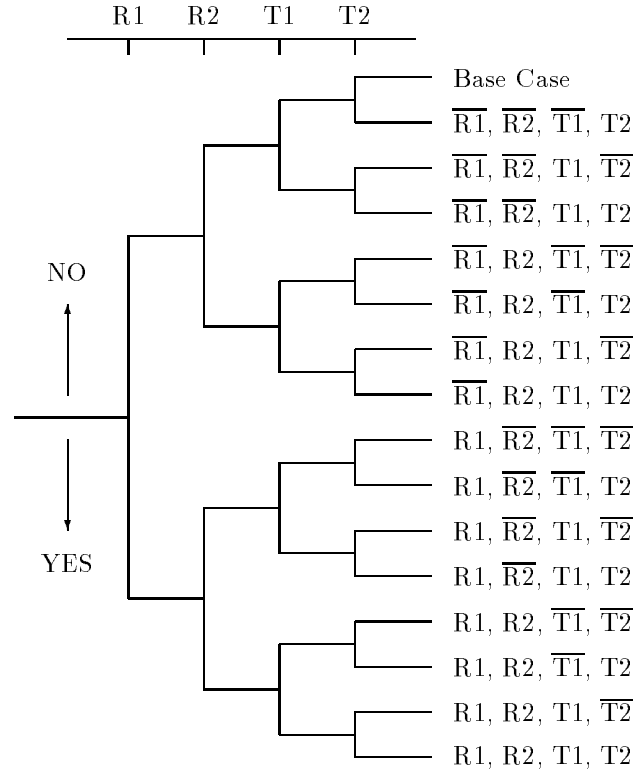
I.3. Modelling methodologies for complex systems

Special methodologies have been developed to keep track of the different events and parameters that might influence the function of complex systems, and to identify the most important of these. It is essential to undertake this process in such a way that all steps taken, and the rationale behind all decisions are well documented. This leads to a *chain* of (sub)models. The degree of detail must be consistent within the model chain and tailored to the problem at hand. The process must be “transparent” so that it can be back-tracked if necessary.

This type of “cause - effect” analysis is very helpful for the examination of complex problems. The relative importance of the various interactions can also be assessed qualitatively, or quantitatively. This is a necessary step in order to simplify the system before beginning the systematic calculations. The following methods are widely used to build models for complex systems:

- *Event or fault tree analysis.* This methodology is used to describe the system behaviour in terms of FEPs which are well-known, or can be estimated with a high degree of certainty. Fault-tree analysis has been developed for risk analysis and safety assessment of large scale industrial structures such as chemical plants (*e.g.*, for the production of explosives

Figure I.4: A standard fault tree showing all possible combinations of four FEPs: two release processes (R1 and R2) and two mass-transport phenomena (T1 and T2). From [80CRA/GUZ].



and petrochemical products) and nuclear power installations. Figure I.4 shows a standard fault tree analysis for scenario descriptions of a system with four FEPs, and it illustrates how chains of events might take place. Note the “binary” structure, events either do take place with a certain probability, or they do not take place. It is notoriously difficult to assign probabilities to geological, or human related FEPs.

- *Process influence diagrams with linked documentation.* Another way to describe a system and its function is to construct PIDs (**P**rocess **I**nfluence **D**iagrams), where the FEPs are represented by boxes, and interactions by lines between the boxes [95CHA/AND]. A highly simplified PID is illustrated in Figure I.5, and another example is given in Chapter XIII. The following procedure is used:

- a systematic review and documentation of FEPs and of the interactions that can influence the performance of the system;
- documentation of decisions made in the development of scenarios in order to ensure traceability of the process;
- construction of a basic influence diagram, and from this, scenario influence diagrams;

Figure I.5: Simplified process influence diagram (PID) giving a schematic description of a system. The boxes contain documentation on the various FEPs, and the lines represents interactions between them. The system boundary is defined by some measurable properties; within the system there is a significant change of properties as compared to the undisturbed situation. In a repository for radioactive waste, external FEPs may be the change in hydraulic conductivity in the geological medium as a result of seismic events, or the change in the composition and amount of infiltrating surface water from changes in the atmospheric conditions. An internal FEPs may be the corrosion of waste canisters resulting from chemical gradients within the repository, caused for instance by radiolysis. From Eng *et al.* [94ENG/HUD].

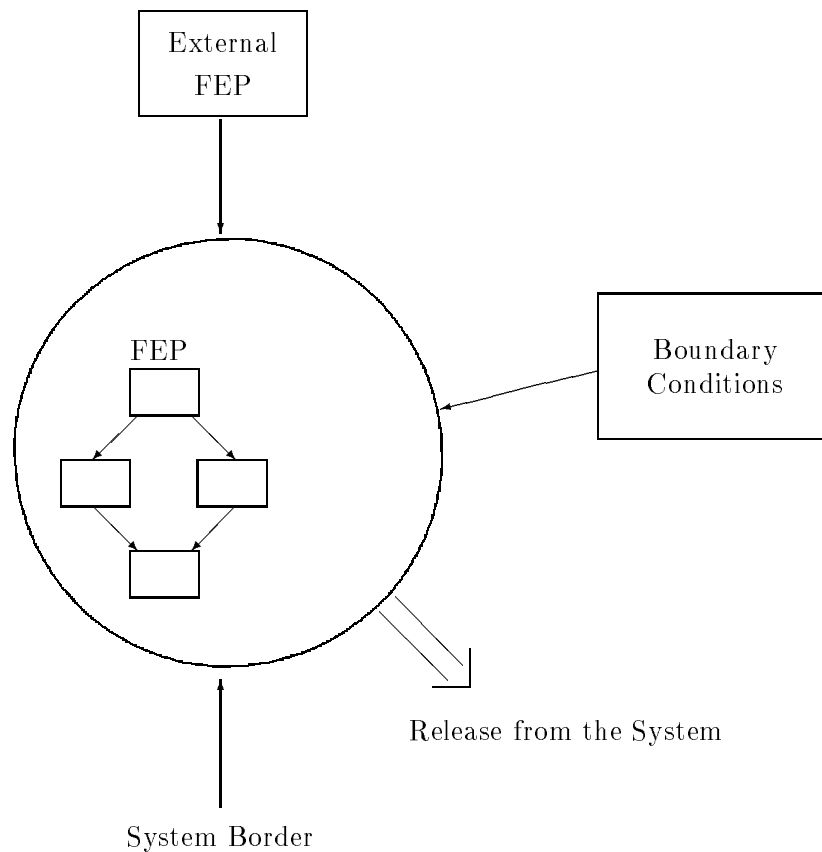
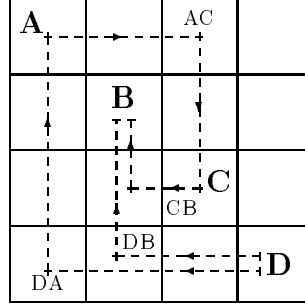


Figure I.6: Construction of interaction diagrams of the “RES”-type. The main components (FEPs) of the system are listed along the diagonal, and interactions among them are shown in the off-diagonal elements (AC is the interaction of **A** on **C**, and CA is the effect of **C** on **A**, which in general are not equivalent). The figure shows two possible effects of component **D** on **B**. The diagonal elements for a high-level radioactive waste repository might for example be: the UO₂-matrix (**A**); the canister materials (**B**); water (**C**); and radiation (**D**). In this case, DA and DB would correspond to different types of radiation damage, AC would be the reducing power of the spent fuel (sink of aqueous oxidants), and CB the corrosion of the canister. From [94ENG/HUD].



– formulation of scenarios and calculation cases.

- *The interaction diagram or “Rock Engineering Systems” (RES) approach.* This is another type of interaction diagrams, where a square matrix is used to describe the FEPs and their interactions. A complete description of these diagrams is given in [92HUD]. The FEPs are located on the diagonal of a square matrix and the interactions are represented by the off-diagonal terms. Figure I.6 represents a system with four FEPs and twelve (16 - 4) off-diagonal terms. See [94ENG/HUD]. Assume that we are interested in how variable **D** affects variable **B**. This will occur in two ways, by the direct off-diagonal interaction **DB**, or indirectly through the other FEPs in the system. One such influence pathway (**D-A-C-B**) is indicated in the Figure. Variable **D** affects variable **B** through three interactions **DA**, **AC** and **CB**. The way in which a particular variable affects all the others is described by the interactions along the matrix row through the variable. The way in which a particular variable is affected by all other variables is given by the interactions in the column through that variable.

In addition to modelling methodologies there are also uncertainties to be taken into account:

- Uncertainty in the scenarios used. This in turn will influence the other types of uncertainty.
- Uncertainty in the definition of the system. This is the key uncertainty when trying to describe systems in nature. It is related to the heterogeneity of the system and

the lack of proper information on all its parts. The same fundamental types of uncertainty are also present in the system boundaries.

- Uncertainty in the data, *e.g.*, in equilibrium constants, flow porosity, *etc.* Part of this book will be devoted to discussions of the uncertainty in chemical data.
- Uncertainty in the understanding of the mechanisms of the processes taking place in the system. This may be a problem already in the laboratory systems; however, fundamental scientific inquiries are made in order to resolve issues of this type. It is not simple to obtain a detailed mechanistic insight in many systems encountered in nature. This problem is aggravated when descriptions extending over long periods of time are required. This is the case *e.g.*, when modelling the impact of technological systems on the environment. The mechanistic understanding also constitutes an important part of the chemistry sections in this book.

The modeller must be able to cope with uncertainties and also with the simplifications required to make a scientific interpretation of complex systems possible. The following Chapters of this book will mainly be concerned with the scientific basis for relatively simple models. However, these are often sub-models in more complex model structures, even if they do not enter directly into them. In the next section we will give some additional examples that might be helpful to the reader.

I.4. Some simple physical and chemical models

There is an important difference between models that are used for *interpolations* within a specific system, and those used for making *extrapolations* or *predictions* of the system behaviour under conditions outside those studied. The first type of model does not necessarily require detailed knowledge of what goes on inside a system, and the values of the system properties at any point within the system are deduced from the experimental data using some empirical function.

The connotations of extrapolation and prediction are somewhat different, the first implying a process based on a solid scientific basis, the latter indicating something more vague. However, the two terms are often used as synonymous of one another.

When discussing extrapolation and prediction in the context of this book, we are assuming that the systems are reasonably “well-behaved”, *i.e.*, that the driving forces acting on, or within the system, are so small that it does not behave in a chaotic fashion.

Let us study a simple example to illustrate the points mentioned above.

Example 3: Radioactive decay

Through experimental observations we know that certain elements are not stable, and that they are transformed by processes in their nuclei into new elements, which in turn also may be instable. The chain of instable nuclides finally end up in a stable element. The theory describing radioactive decay gives the following rate of decay of a parent nucleus to its daughter element

$$\frac{dN}{dt} = -\lambda N \quad (\text{I.1})$$

where λ is a constant and N the number of parent nuclei at time t . Let us now assume that we have an isolated system of a certain radioactive element. For given boundary conditions (known values of λ and of N_0 , *i.e.*, N at $t = 0$) we can integrate the previous equation, and calculate the number of atoms in our system at any given point in the future. The precision of our prediction depends on how well we know the quantities λ and N_0 . This is a simple system, and the scientific community would certainly agree that it is possible to make very precise predictions of its future behaviour, even over extremely long periods of time. This is not uninteresting. We do know how the radioactivity of the elements in future repositories for nuclear material will behave over time.

Scientists have used the same physical theory to date geological and other systems. The ^{238}U and ^{232}Th decay series have been used for dating purposes. In an undisturbed geological system which is sufficiently old the activity of a parent nuclide is the same as that of all its daughter nuclides (secular equilibrium). However, in an open system, the different chemistry of parent and daughter elements may result in preferential losses of some nuclides, and the activity ratio is no longer equal to unity [92OSM/IVA], and we need additional information on its chemistry, geology and hydrology in order to date the system. These data are much more uncertain than the theory of radioactive decay. Hence, the age determinations are rather uncertain, even though the theory behind Eq. (I.1) is very well established.

I.5. Under what circumstances can we make predictions of the time evolution of chemical systems?

The time evolution of chemical systems depends on the possibility of chemical reactions. When discussing reactions, chemists often distinguish between two limiting situations, whether they are under *thermodynamic*, or *kinetic* control.

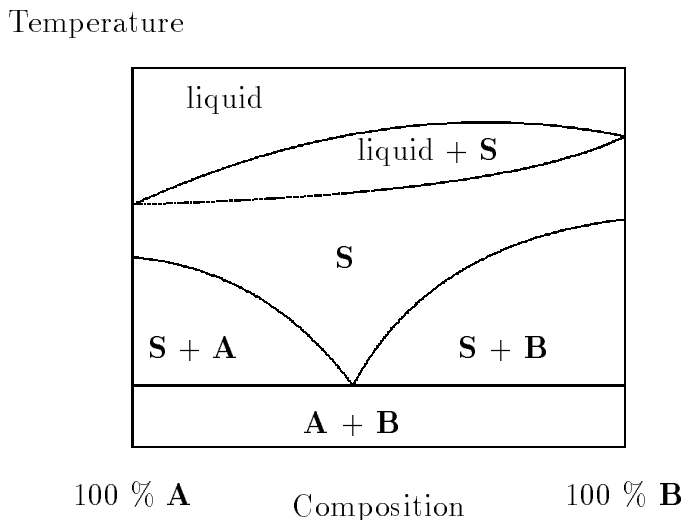
Example 4:

As an example of a system under thermodynamic control, we can select a phase diagram for a binary system of two pure solids **A** and **B**, and a solid solution, **S**, as shown in Figure I.7. The system is at constant pressure and there is no exchange of matter with the surroundings. We can always predict the behaviour of this system over time. Within the phase boundaries nothing will happen when we change the system variables. When a phase boundary is crossed the system will change as indicated in the diagram. However, the diagram does not tell us how fast this process is. The example may seem trivial, but it has technical implications.

The technical life time of materials is often controlled by the rate of corrosion and it is important to be able to estimate this in order to select the proper material for different types of installations. To evaluate the long-time durability of materials one often uses *accelerated testing*. This is based on the simple principle that the rates of chemical reactions increase with increasing temperature. In this way one can “compress” the time-scale for the testing. This is an excellent method, provided that the mechanism of corrosion is the same in the investigated temperature range. However, if there is a phase change when the temperature is increased, there is no reason to believe that the corrosion mechanism remains unchanged.

Corrosion processes are in general controlled by kinetic factors, and in order to describe them one must have a detailed knowledge of the chemical events at the atomic/molecular level. Knowledge of this type is nearly always restricted to very simple systems, and predictions of the time behaviour of more complicated systems is therefore both difficult

Figure I.7: Example of a phase diagram for a system with two components **A** and **B** (pure solid phases), where **S** represents a solid solution.



and uncertain.

Example 5: Estimation of the corrosion of metallic materials over long periods of time

The problem concerns the prediction of the long time durability of metal containers for toxic wastes. The containers may be deposited either on the bottom of the oceans, or in a rock repository for nuclear waste in some geological medium. Figure I.8 shows schematically the outline of an underground repository.

In order to assess the chemical conditions and reactions of importance for the long-time safety of the repository:

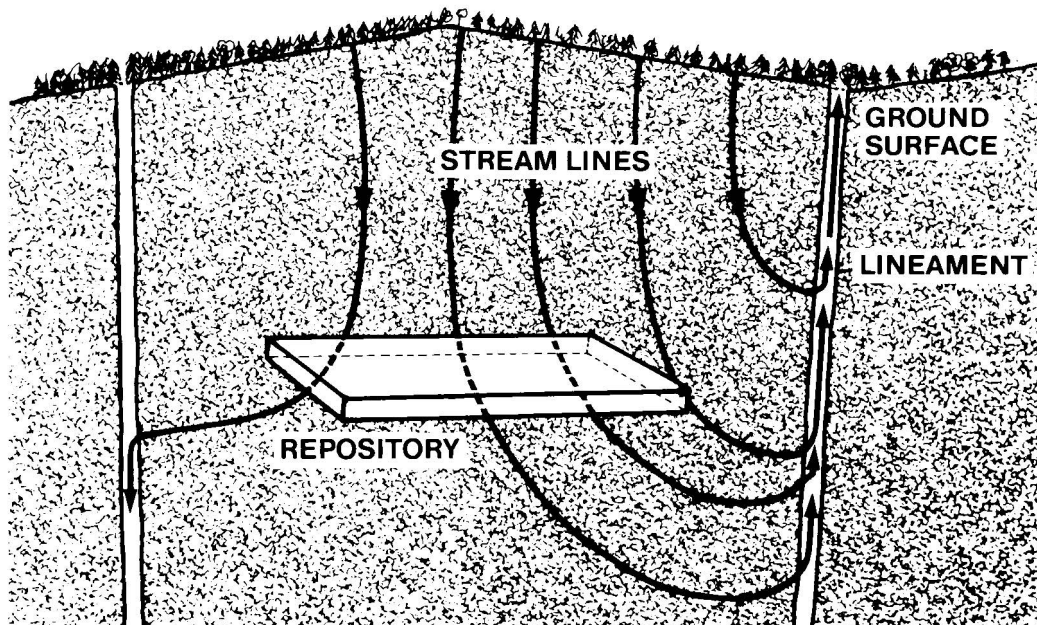
- The system and its surroundings must be described, including a decision on the system boundary.
- The key chemical parameters in the system must be identified.
- It must be decided if the corrosion is governed by thermodynamics or kinetics.

Corrosion is a chemical process which depends on the choice of canister material and on the physical and chemical properties of the surroundings. The latter are determined by the location of the repository. This will also determine the hydraulic gradients in the repository, *i.e.*, the driving force for groundwater flow and therefore, the transport of potential corroding chemical agents to the canister, and once its walls have been penetrated, of toxic material from the canister (both as particles and in dissolved form).

A chemist will quickly be able to identify important chemical parameters in systems of this type, *e.g.*, pH, the redox potential of the system and the presence of specific substances that might cause strong corrosion.

Figure I.9 contains simplified Pourbaix-diagrams, (*cf.* Chapter II, *p.*62), which show the corrosion properties of iron and copper in pure water. Diagrams for other metals can be found in Pourbaix's "Atlas" [74POU]. This Figure indicates areas where corrosion is thermodynamically impossible (*immunity*), areas where corrosion leads to the formation of a layer of corrosion products that may inhibit further corrosion (the technical term is *passivation*), and finally, the area where there is *active corrosion*. When a metal is passivated the corrosion is always kinetically controlled. In the region where a material is

Figure I.8: Schematic outline of an underground repository [83KBS]. The stream lines for groundwater flow through the system are outlined. The rate of flow depends on hydraulic gradients, the presence of water carrying fractures (“lineaments”) and the amount of surface water infiltration.

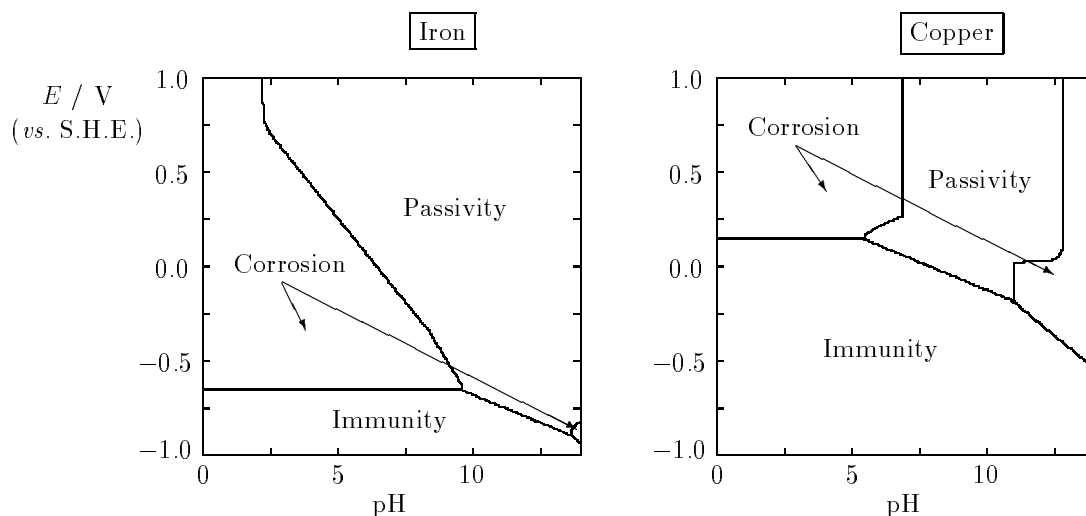


thermodynamically stable it is straightforward to predict the long-time behaviour: no changes will occur as long as the external conditions remain the same. Through diagrams of this type, we can also identify the conditions where corrosion occurs. For the case of copper, both oxygen and sulphide may give rise to corrosion. However, the diagram does not provide information on the rate of this process.

In the system we are discussing, there are two types of kinetic processes. One is determined by the rate of chemical reactions at the interface between the canister and the water, and the other by the rate of transport of corrosive substances in the water to the surface of the canister.

The system is more complicated than most laboratory systems, especially if we consider processes that take place over long periods of time. Long, in this context is anything beyond 100 years. We may ask how to judge if the predictions are reasonable, or not. Table I.1 gives some guidance on judgements of this type, the estimated “accuracy” is only based on estimates by the authors. A more detailed discussion of copper corrosion in underground systems is given in [94WER/SPA], by using a model where both chemical processes and transport are taken into account.

Figure I.9: Pourbaix diagrams for iron and copper at 25°C.



Let us now make a summary:

- Extrapolations over long time periods must use models based on theory.
- The more complicated the system, the more difficult it is to make accurate predictions.
- The uncertainty in the prediction depends on the uncertainty in theories, models and boundary conditions.

Figure I.1 indicates how “validation” is made in simple systems. In complicated systems, this procedure cannot be used. It is not possible to test the model predictions of the system development when changes take place in the surroundings, or its behaviour, over very long periods of time. We have to rely on other methods, most of which are based on the assumption that if we can describe the present state of the system, then the same models may be used to predict its behaviour when the system variables are changed. Extrapolations of the behaviour of systems over long periods of time are often made by using artifacts and *natural analogues*. The question is then whether we can use information from *postdictions* (“history matching”) in one system to make assessments of the accuracy of *predictions* in the same, or similar, systems.

The long-time corrosion of copper may be evaluated from archaeological artifacts, provided there is information on the chemical surroundings over the period of interest. Such information is available, *e.g.*, for artifacts found in marine surroundings (in bottom sediments, or in the water) [88HAL/OES]. By studying the extent of corrosion of these artifacts one obtains information both of the extent of corrosion and its distribution over the surface of the material (“pitting”).

Table I.1: Processes affecting the stability of metal containers for toxic wastes.

Process	Time scale	“Control method”	Accuracy
Corrosion	0 - 100(?) years	Material testing	Often high, but material dependent
	up till 3000(?) years	Archaeological artifacts	Strongly dependent on “boundary conditions”
	geological time frame	Natural analogues (“float copper”, the Oklo-reactor sites)	Strongly dependent on “boundary conditions”
Chemical composition of the atmosphere and surface water	0 - 100 years	Extrapolations of technology and population development	Good for most components
Climate changes over long time periods		Theory based	Poor, judging from geological data on drill cores from the Greenland ice

From the previous, it is obvious that we can never verify the predicted behaviour of complicated systems over long periods of time. Nevertheless, it may be necessary to make predictions of this type. Extrapolations of the behaviour of active technical systems do not seem necessary over time periods longer than 10 (for the technology components in systems) to 100 (*e.g.*, dam systems) years. Systems which have to be evaluated over longer periods, in general have important non-technological components, *e.g.*, the effects of loss of biological diversity, socio-economical effects of the large societal systems for transport, energy production, agriculture *etc.* The main issues in systems of this type are political, not scientific.

We are convinced that for decisions on systems of this type it does not make sense to discuss the accuracy of the predictive models in absolute terms. Such models can only be used to compare the consequences of the different options available when a decision has to be taken.

I.6. Some additional considerations on chemical modelling

Chemical modelling can be made on different levels of detail. It may involve a description of a *dynamic* situation, where the chemical system is in continuous evolution, *e.g.*, as a result of ongoing chemical reactions and/or the transport of chemical constituents into or out of the system.

It can also be an essentially *static* description, a snap-shot of an actual situation in a system where some variables, *e.g.*, the total concentration of the chemical components are assumed to be constant.

These descriptions (or models) have their counterparts among chemical theories — in order to make quantitative statements about chemical changes the chemists are using two fundamental disciplines: *chemical thermodynamics* and *chemical kinetics*. The first describes the conditions under which chemical reactions are possible and the extent of the reactions when *equilibrium* is attained. Hence, thermodynamics provides a measure of the maximum chemical change that takes place in the system under specified external conditions. As a byproduct one obtains information on the concentrations of all chemical species under the given conditions.

The rates of chemical reactions may vary over a very wide range (with characteristic time constants from $\sim 10^{-9}$ to $\sim 10^9$ sec), and some reactions take place very slowly even on a geological time scale. In order to model the time evolution of a chemical system we must know all the factors that influence the various rates of reaction and also the rate constants for the reactions. Information of this type is seldom available for complex systems. If this is a problem, or not, depends on the time-scale of the model – in many systems the rate of processes are not dominated by chemical reactions but by the rate of mixing (*e.g.*, the chemical change in a lake caused by the mixing of an inflow with a different composition than the bulk). The time constants for many chemical reactions in homogeneous solution are less than minutes/a few hours, a time scale that is very short in comparison with the rates of mixing in most systems in nature. From a modelling point of view we may then regard these chemical reactions as instantaneous. This is important from a modelling point of view because it allows the modeller to regard the chemical reactions and the rate of mixing as uncoupled processes. If we want to model the chemical evolution in the system caused by mixing, we must of course know the rate of the physical mixing process.

There are also a number of chemical reactions that in the absence of catalysts occur so slowly that there is no observable reaction in the time scale of the model. In this situation the modeller does not have to take the chemical reaction into account in the model – we have a state of *metastable equilibrium*.

Reactions in heterogeneous systems (some solubility/precipitation reactions, weathering reactions, and gas/liquid equilibria) often have much slower rates of reaction than those in homogeneous solution and the modelling of such a system may then be much more complicated. These issues will be discussed further in Chapter III.

All attempts to model a complex system should begin with a thermodynamic model because this provides a first idea of the chemical reactions that are most important for the

system, and those that can safely be disregarded. Thermodynamic modelling is in many respects a straightforward procedure: there are a large number of well tested computer codes that may be used to handle even very complicated equilibrium systems. Hence, the success, or failure, of the modelling depends on the quality of the thermodynamic database used. The database must be complete in the sense that information on all relevant chemical reactions must be known. The quantitative thermodynamic information must also have a satisfactory accuracy. We will discuss this point shortly.

Other input data for chemical modelling is information on the total concentrations of the various components in a system. For the conditions prevalent to-day, this is essentially a problem of analytical chemistry. However, when describing the time evolution of a system it is necessary to understand if and how the total concentrations may change as a result of anthropogenic input, or by other events.

1.6.1. Sources of thermodynamic data

Chemical thermodynamics is a well established scientific discipline and quantitative data have appeared in the chemical literature for more than a century. Thermodynamic data on various compounds and chemical reactions are found in various data compilations.

Stability Constants [64SIL/MAR, 71SIL/MAR, 79PER3, 82HOG] provide information about equilibrium constants of various types. These compilations contain information on essentially all published data for a given system, and the authors have not made any attempts of critical evaluation of the quality of the data (except for an occasional question mark). The experimental information on ionic medium and temperature are reported along with the experimental method used. Nearly all the reported equilibrium constants are expressed in concentration units (*cf.* Chapter II) and the numerical values are therefore only valid when used in the same conditions as when they were determined. A computer-held version of the *Stability Constants* is maintained by the IUPAC Commission on Equilibrium Data. This electronic database is available through Academic Software, Sourby Old Farm, Timble, Otley, Yorkshire LS21 2PW, United Kingdom (<http://www.cityscape.co.uk/users/gr71>).

Critical Stability Constants [74MAR/SMI, 75MAR/SMI, 76SMI/MAR, 77MAR/SMI, 82MAR/SMI, 89SMI/MAR] is another compilation of equilibrium constants taken from *Stability Constants* but where the authors have made a selection of the “best” values at certain specified ionic strengths. Unfortunately there is no information on the rationale used in the selection of the data. A computer-held version of the *Critical Stability Constants* is maintained by the National Institute of Standards and Technology. This electronic database is available through Standard Reference Data Program, NIST, Gaithersburg, MD 20899-0001, USA (<http://www.nist.gov/srd>)

The *IUPAC Commission on Equilibrium Data* have published a set of critical evaluations of equilibrium constants for a few selected metal – ligand systems (fluoride [80BON/HEF], edta [77AND], *etc.*). In the same series, Perrin [82PER] has made a compilation of equilibrium dissociation constants for inorganic acids and bases which contain similar information as *Stability Constants*. These compilations give a good discussion of

the various experimental studies, but make no attempt to reduce the data to a common reference state.

The following compilations contain thermodynamic information in the form of Gibbs energies of formation, enthalpies of formation, entropies, heat capacities, *etc.*: U. S. Bureau of Standards [82WAG/EVA], JANAF [85CHA/DAV], CODATA [89COX/WAG], and the books by Knacke *et al.* [91KNA/KUB], Barin [93BAR], and Kubaschewski *et al.* [93KUB/ALC]. CODATA's "key-values" [89COX/WAG] have been selected after a very thorough evaluation of the existing thermodynamic data for each compound. Another important source is *Termicheskie konstanty veshchestv* (*Thermal constants of substances*), in 10 volumes, Academy of Sciences, Moscow, 1965 to 1981, edited by V. P. Glushko. This is an extensive compilation of thermodynamic data for solid phases, aqueous solutions and gases, comprising twenty books of tables and references. The same editor started in 1981 the series *Termodinamicheskie svoistva individualnykh veshchestv* (*Thermodynamic properties of individual substances*), now consisting of eight books containing tables of data and a discussion of the selection of the most reliable values and their uncertainties. An updated and revised version of this work has been published in English [93GUR/VEY].

Thermodynamic properties of minerals and aqueous reactions of interest for geochemist may be found in [68ROB/WAL, 78HEL/DEL, 78ROB/HEM, 82HEL, 82HEM/HAA, 90HOL/POW, 90NOR/PLU, 92JOH/OEL, 94NOR/MUN, 95ROB/HEM].

The last two paragraphs give references which contain thermodynamic data at standard state conditions, and at a temperature of 298.15 K and a pressure of 0.10000 MPa. Data for aqueous species are referred to the infinite dilution standard state. Details about definitions of various types of equilibrium constants and a discussion of standard state conditions are given in Chapter II.

Information on thermodynamic data for actinides, both for the elements and for their compounds and aqueous species (including inorganic complexes) has been compiled by the International Atomic Energy Agency (IAEA) in Vienna [66RAN, 68LAV/GER, 72GER/LAV, 73SPE, 75RAN, 76ALC/JAC, 76FUG/OET, 76OET/RAN, 78COR/OHA, 80BRE/LAM2, 81CHI/AKH, 81SPE, 83FUG/PAR, 83KUB, 84FLO/HAS, 84GRO/DRO, 84HOL/RAN, 85HIL/GUR, 92FUG/KHO].

Thermodynamic data for the actinides uranium, neptunium, plutonium and americium, as well as technetium are being reviewed by the Nuclear Energy Agency (NEA) of the Organisation for Economic Co-operation and Development (OECD) in Paris. The reviews include both the elements and their compounds and aqueous species (including inorganic complexes). Withing this project [88WAN] both thermodynamic data and their uncertainties are being selected in consistency with the CODATA values mentioned above. So far reviews for uranium and americium have been published, [92GRE/FUG, 95SIL/BID].

I.6.2. Using tabulated thermodynamic data

An important problem that the chemical modeller has to deal with is the consistency of thermodynamic data: erroneous results may be obtained when using values from several different sources and combining them in a model. This is discussed by Grauer, in Chapter IV.

Despite the large amount of information available the modeller might find that important information is missing. This lack of information may be of two different kinds:

- Methods might be available to recalculate thermodynamic data from the values given under *standard state conditions* and at a reference temperature. These are the values usually found in thermodynamic compilations. Such recalculations are necessary because the systems to be modelled are rarely at standard state conditions or at the reference temperature. This means that the existing thermodynamic information must be corrected so that it is valid at the temperature, pressure and ionic strength of the actual system. Methods to perform these corrections are described in Chapters IX and X.
- Information on the stoichiometric composition and on the equilibrium constants involving species that the modeller has good chemical reasons to believe might be formed in the system, but for which no quantitative data are available.

What to do when important information is missing? The poorest solution is to include only information that is available in the databases – a much better solution is to use chemical theories to predict reasonable estimates of the quantities needed, and then to find out how sensitive the model result (*e.g.* a mineral solubility, or a total element concentration) is to variations in the unknown model parameters. If these parameters turn out to be important for the modelling it may be necessary to determine them experimentally. The examples in Chapters III and X demonstrate that also estimations of thermodynamic quantities may give valuable insight into the chemical behaviour of a complex system.

Expressed in another way: in thermodynamic modelling it is important to use not only the quantitative data available in databases, but also the qualitative or semi-quantitative information that can be extracted from the established chemical theories. The use of extrapolation methods for thermodynamic data is important and we have therefore described the methods for estimating activity factors and for making estimates of the temperature dependence of thermodynamic quantities in Chapters IX and X, respectively. Estimates of the chemical composition of dissolved species require a short background on some general chemical principles. These are described in Chapter III, where references to monographs/text-books which provide more detailed information are also given.

I.7. Chapitre I : Introduction

I.1 Modèles et modélisation

La modélisation est essentielle lorsqu'on essaye de comprendre des systèmes et des phénomènes complexes et afin de traiter les informations obtenues. L'activité humaine, principalement commandée par la technologie et la croissance démographique, influence notre environnement à la fois à l'échelle locale et globale. Pour décrire, modéliser, comprendre et modifier ces processus, il faut combiner beaucoup de disciplines scientifiques différentes, par exemple, en créant des équipes multidisciplinaires qui doivent être capables de faire le lien entre les différentes pièces dans le processus de compréhension/prise de décision. C'est une tâche complexe et difficile où la modélisation joue un rôle essentiel dans l'établissement d'un "langage" commun parmi tous les autres utilisés.

Ce livre parle de la modélisation des systèmes chimiques aqueux dans la nature et ailleurs. Leur degré de complexité peut varier considérablement de simples systèmes de laboratoire, *via* les systèmes techniques (par exemple, les systèmes hydrométallurgiques, différents types de systèmes énergétiques et les systèmes de déchets), à des systèmes plus vastes dans la nature (par exemple, les cycles géochimiques globaux, et le transport de composés contenant des métaux et d'autres produits chimiques dans les systèmes des eaux de surface et souterraines). L'accent est mis sur la modélisation des réactions *chimiques* et des équilibres, et la majeure partie de ce livre traitera donc des problèmes chimiques. Cependant, les processus *physiques* tels que le transport de matière (diffusion, convection et dispersion) sont importants dans l'évolution chimique des eaux souterraines et de surface, et ils seront donc aussi traités. Avant d'entrer dans les détails de la modélisation chimique, nous détaillerons une partie de la terminologie employée et certaines stratégies de modélisation employées.

Un *système* est la partie du monde physique que le modélisateur veut décrire et où tous les processus importants du modèle sont supposés avoir lieu. Les *conditions aux limites* sont les données quantitatives de l'état initial et des limites physiques du système. Les conditions aux limites sont nécessaires pour exposer le fonctionnement du modèle (et, de façon incomplète, celui du monde physique).

Il existe des procédures officielles qui peuvent être utilisées dans l'analyse et la description de systèmes complexes – il existe même une discipline scientifique, *analyse de systèmes ou d'opérations*, qui traite des problèmes de ce type. En principe, l'analyse d'un système suit le schéma donné dans les Figures I.1 et I.2 (pages 2 et 4). Dans ce chapitre, nous présenterons une première argumentation sur plusieurs types de modèles et comment, et dans quels contextes, ils sont utilisés.

Les modèles sont utilisés en science et en technologie comme des outils ; par choix et par nécessité, ils sont incomplets et décrivent seulement les aspects de la "réalité" que le modélisateur considère utiles à la compréhension et à la description du système "réel". Il en découle que la modélisation peut être effectuée à différents niveaux de sophistication, et que les éléments nécessaires sont des approximations de plusieurs sortes, basées sur les conceptions du problème considéré.

I.1.1 Le besoin des modèles

Pourquoi donc utilisons-nous des modèles ? Oreskes, Shrader-Frechette et Belitz [94ORE/SHR] exposent que "Les modèles peuvent corroborer une hypothèse en apportant des preuves pour renforcer ce qui peut déjà être établi par d'autres moyens. Les modèles peuvent aussi expliquer les divergences d'autres modèles. Les modèles peuvent aussi être utilisés pour des études de sensibilité – pour répondre aux questions "qu'est-ce qui se passerait si...?" – mettant ainsi en évidence les points du système qui ont besoin d'être étudiés et où l'on a besoin de plus de données. Ainsi, le premier but des modèles est heuristique : les modèles sont des représentations utiles pour diriger des recherches plus approfondies, mais pas susceptibles d'apporter des preuves". C'est un exposé raisonnable du point de vue des sciences naturelles. Cependant les modèles ne sont pas seulement utilisés pour conduire des études plus approfondies, mais aussi pour évaluer les performances d'un système dans le temps, pour vérifier sa conformité avec les *critères de performance* et d'aider à la *prise de décisions*, comme le montre la Figure I.2 (p.4).

La prise de décisions est souvent vue comme un choix rationnel entre plusieurs possibilités connues. C'est une vision très simpliste, beaucoup de décisions doivent être prises (ne pas prendre de décision en est une !) dans un contexte de véritable incertitude sur les données et les modèles. Un remède est l'utilisation d'hypothèses "conservatives". On peut trouver des exemples dans la gestion des déchets toxiques, comprenant les déchets nucléaires, où les modèles sont souvent "irréalistes" sur certains détails, mais ceci est toléré à condition que les modèles fassent des erreurs du côté conservatif (c'est-à-dire, ils surestiment les effets négatifs d'une décision).

1.1.2 Vérification et validation des modèles

La vérification et la validation sont des problèmes importants lorsque l'on examine et que l'on utilise des modèles. Une difficulté est que les termes ont différentes connotations pour différentes personnes. *Vérifier*, selon la plupart des dictionnaires, signifie affirmer ou établir la vérité. Dire qu'un modèle est vérifié implique que son exactitude a été établie et qu'il peut être utilisé comme base pour la prise de décisions, ou comme composant dans d'autres modèles. La vérification est aussi utilisée pour montrer la capacité d'un certain code de calculs à résoudre correctement les équations régissant. Pour cela, on compare les solutions numériques avec celles d'études de références ou avec des solutions analytiques, et on montre qu'elles sont équivalentes sous les conditions dans lesquelles le modèle est utilisé.

Par *validation*, on n'entend pas forcément établissement de l'exactitude, mais montrer que le modèle n'a pas de défaut détectable ou d'erreur de logique. En gestion des déchets nucléaires, ce terme est employé dans un autre sens. La Commission de la réglementation nucléaire des États-Unis (US Nuclear Regulatory Commission) la définit comme le processus pour obtenir "l'assurance qu'un modèle, utilisé dans un code de calcul, est une représentation correcte du processus ou du système pour lequel il est destiné", alors que le Ministère de l'énergie des États-Unis (US Department of Energy) définit la validation comme "un processus dont l'objectif est d'établir que le code ou le modèle reflète effectivement le fonctionnement du monde réel". L'Agence internationale de l'énergie atomique considère que des modèles sont validés quand on est sûr qu'ils "donnent une bonne représentation des véritables processus qui se produisent dans le système réel". La terminologie employée par les professionnels des déchets nucléaires est maladroite car elle a tendance à induire en erreur les scientifiques et les personnes qui n'ont pas de connaissance dans ce domaine. Il existe des argumentations intéressantes sur ces problèmes par Konikow et Bredehoft [92KON/BRE], de Marsily, Combes et Goblet [92MAR/COM], et par Oreskes, Shrader-Frechette et Belitz [94ORE/SHR]. Voici une citation tirée de la dernière de ces références : "aucune proposition générale empirique sur le monde naturel ne peut être certaine. Cela ne dépend pas du nombre d'informations que l'on a, il y aura toujours la possibilité que plus d'une théorie puisse expliquer les observations effectuées".

1.1.3 Les phases de la modélisation pour des systèmes complexes

La Figure I.1, p.2, décrit raisonnablement bien les situations rencontrées en modélisation lorsqu'on essaye de décrire des systèmes relativement simples tels que ceux que l'on trouve dans les recherches *en laboratoire*. La plupart des systèmes rencontrés dans la nature ont des degrés de complexité bien plus importants et l'approche de la modélisation doit être modifiée/élaborée de façon adaptée. La Figure I.2, p.4, donne une meilleure, bien que schématique, description de la procédure.

La partie essentielle de ce processus est la *formulation des objectifs* pour le modèle, la *documentation* sur le cadre scientifique pour l'analyse, et les jugements d'experts effectués. C'est la logique du modèle, elle doit être transparente pour tous les utilisateurs.

L'analyse peut être faite en utilisant l'ensemble des "procédures" suivantes :

- Choix des *scénarios*. C'est une description avec des mots du système et des FEPs (Features, Events and Processes) qui ont lieu dans celui-ci. Les "principaux" FEPs sont définis (ou posés comme hypothèses) par le modélisateur qui se base sur le niveau actuel de description/compréhension du système, mais aussi sur des critères de performance (voir Tableau XIII.1 p. 579, par exemple).

Introduction

Les FEPs peuvent varier largement de ceux qui peuvent être formulés en termes scientifiques/techniques à ceux qui traitent des problèmes sociaux et de comportement. Nous ne traiterons que des premiers. Cependant, les derniers sont peut-être souvent plus importants pour la réalisation d'un système et pour la décision finale d'implanter ou non un certain système technique.

- Choix des modèles *conceptuels*. C'est le processus par lequel le modélisateur choisit les théories scientifiques appropriées, les modèles et les données qui seront utilisés pour décrire les processus définis dans les divers scénarios de description. En général, celui-ci nécessite aussi diverses approximations physiques et chimiques. Dans beaucoup de cas, les données sont dépendantes du modèle, et il n'est pas toujours possible d'utiliser des données expérimentales évaluées par un modèle dans un autre.
- Transcription en modèles mathématiques. C'est le processus par lequel le modélisateur transcrit les modèles conceptuels dans une forme appropriée pour calculer les propriétés utiles d'un système avec des hypothèses données. Ceci requiert à peu près toujours des approximations mathématiques de toutes sortes.
- Calculs. C'est apparemment la partie la plus simple de cet exercice. Cependant il faut utiliser des codes de calculs qui sont bien testés et qui n'ont pas de problèmes d'instabilités numériques [92KON/BRE]. Un problème particulier et difficile est le couplage de différents processus, par exemple, les processus réactionnels chimiques et ceux de transfert de matière tels que la diffusion et la convection. Ce problème sera traité dans le Chapitre XII.

La conception des modèles devrait être dictée par les questions auxquelles le modèle est supposé répondre, une tâche clé est de séparer les caractéristiques significatives des moins importantes.

I.2 Systèmes de laboratoire *vs.* systèmes complexes rencontrés dans la nature et en science/technologie

Il faut être conscient des très grandes différences entre les systèmes de laboratoire et d'autres bien plus compliqués tels que ceux rencontrés dans la nature ou en science/technologie. Cette partie a seulement pour but de donner au lecteur une idée de la nature de ces différences et de comment elles agissent sur les stratégies de modélisation.

La Figure I.3, *p.* 6, montre les caractéristiques des systèmes de laboratoire et de ceux de la nature.

Les systèmes "de laboratoire" sont utilisés pour développer de nouvelles théories scientifiques ou pour étendre ou approfondir celles qui existent déjà. Pour cela, on simplifie et on contrôle le système autant que possible à l'intérieur du champ d'application du problème. Une caractéristique est que les observations expérimentales détaillées sont utilisées pour faire sous la forme d'une nouvelle ou d'une amélioration d'une théorie, c'est-à-dire, les données de laboratoire permettent le développement des modèles pour décrire des systèmes plus complexes par une approche "ascendante".

Exemple 1 :

Étude d'un équilibre [61ROS/ROS, 71SIL, 71ROS/ROS, 80HAR/BUR], c'est-à-dire, l'interprétation de données chimiques sur une solution en termes modèle chimique de solution, est un exemple typique de modèle de laboratoire. Les données sur la solution chimique pourraient être, par exemple, des données spectrophotométriques ou de forces électromotrices (fém) comme des mesures de pH. Elles sont interprétées en termes de réactions équilibrées (acides/bases, complexation, solubilité, *etc.*) pour obtenir des valeurs de constantes d'équilibre (voir aussi la partie II.1.8).

Un autre exemple est la détermination des *espèces* chimiques, c'est-à-dire, la forme chimique des différents constituants d'un système à l'équilibre, en utilisant des données, déjà existantes, sur des solutions chimiques (des constantes d'équilibre). Voir la Figure II.3, *p.* 62, par exemple. Dans des systèmes qui ont beaucoup de constituants, il faut utiliser un code de calcul adapté, mais il faut aussi des modèles

pour recalculer les constantes d'équilibre disponibles pour qu'elles soient correctes dans le milieu ionique/à la force ionique et à la température du système. Il peut aussi être nécessaire *d'estimer* la composition et les données thermodynamiques des espèces chimiquement raisonnables, mais, pour lesquelles, aucune donnée quantitative n'est disponible.

Les modèles de ce type sont souvent des sous-modèles dans les modèles plus complexes. L'information et la compréhension scientifiques, sur lesquels ces modèles sont basés, sont souvent assez bonnes, et une importante partie de livre traite de la description des caractéristiques des modèles de ce type.

Les codes de calculs typiques pour ce type de modèle (détermination des espèces chimiques présentes à l'équilibre) sont HALTAFALL, développés par Sillén *et al.* [67ING/KAK, 70EKE/SIL, 71WAR/ING], SOLGAS et SOLGASWATER, par Eriksson [75ERI, 79ERI], EQ3/6 par Wollery [83WOL, 86WOL, 90WOL/JAC], PHREEQE, par Plummer *et al.* [80PAR/THO, 83FLE/PLU, 88PLU/PAR, PLU/PAR], *etc.* Les codes MINEQL de Westall *et al.* [76WES/ZAC, 79WES, 84SCH, 86WES] (voir <http://www.agate.net/~ersoftwr/homepage.html>), HYDRAQL de Lecckie et son équipe [88PAP/HAY], et MINTEQ [87PET/HOS] sont aussi de ce type, mais ils comprennent aussi la possibilité de modéliser les *espèces chimiques présentes sur une surface* (voir Chapitre VII). Nordstrom *et al.* ont aussi examiné et comparé des codes de ce type [79NOR/PLU, 84NOR/BAL].

Exemple 2 :

Les modèles hydrologiques décrivent des événements *dynamiques*, c'est-à-dire, le mouvement de l'eau dans des milieux de différents types. Ils peuvent aussi être classés dans la catégorie des modèles "simples", c'est-à-dire qu'ils décrivent seulement un processus particulier dans un système. Ceci ne veut pas dire que les approximations physiques et mathématiques nécessaires pour décrire le système et pour calculer les propriétés du modèle sont simples, voir [92KON/BRE] et [92MAR/COM]. Un résumé des caractéristiques de ce type de modèles est donné dans les Chapitres XI et XII.

Les systèmes où l'on doit coupler les transferts de matière et les réactions chimiques ne tombent pas dans la même catégorie que ceux des Exemples 1 et 2. Les problèmes informatiques qui surviennent quand on calcule les propriétés du système sont maintenant sérieux et requièrent une prise en compte précautionneuse de l'échelle de temps des réactions chimiques comparée à celle du transport et aussi des dimensions du problème, c'est-à-dire, si un problème particulier nécessite un modèle tri-dimensionnel, ou si un bi- ou un mono- ne suffit pas. La différence en stabilité numérique et en temps de calcul sera très importante entre ces trois cas. Ce domaine est, ici, hors sujet et les lecteurs peuvent consulter la bibliographie des Chapitres XI et XII pour plus de détails. Des problèmes "simples" de ce type sont bien connus en génie chimique pour la description d'opérations en colonne de plusieurs sortes telles que l'échange ionique et l'extraction liquide-liquide. Les problèmes sont simples, c'est-à-dire que les processus chimiques et physiques du système sont bien connus et compris.

Les systèmes "complexes" représentent quelque chose de très différent et ne peuvent pas être attaqués avec la méthode "ascendante", et, ceci pour plusieurs raisons :

- Le haut degré de complexité peut conduire à des interactions inconnues entre les processus et les constituants. Plus le degré de complexité est grand, plus ces interactions inconnues peuvent être d'importance.
- La grande complexité rend l'utilisation de modèles, qui dépendent de la description mécanistique détaillée des processus chimiques et physiques du système, impossible, car le rassemblement des informations nécessaires peut changer les propriétés du système. Pour obtenir des informations sur un dépôt de déchets souterrain, il faudrait faire d'importants forages ou excavations qui changeraient les propriétés du site. Un problème supplémentaire est que le coût en temps d'utilisation d'ordinateurs augmente rapidement avec la complexité.
- Les propriétés macroscopiques observées du système peuvent être compatibles avec différents modèles, c'est-à-dire, il y a un problème avec l'unicité des modèles.

Dans ces cas, la description/modélisation d'un système complexe doit commencer avec son comportement/son fonctionnement macroscopique, et le problème clé est réellement de morceler le système (en sous-systèmes), de telle façon que tous les facteurs utiles qui peuvent influencer leur fonctionnement soient pris en compte. C'est une approche "descendante" ou basée sur les objectifs. La description/modélisation doit être *ouverte*, en ce sens qu'il y a une réévaluation continue de l'approche utilisée au fur et à mesure que de nouvelles informations deviennent disponibles : tester les hypothèses et les synthèses forment une boucle sans fin.

I.3 Méthodologie pour la modélisation de systèmes complexes

Des méthodologies spéciales ont été développées pour se tenir au courant des différents événements et paramètres qui pourraient affecter la fonction des systèmes complexes, et pour identifier les plus importants d'entre-eux. Il faut entreprendre ce processus de manière à ce que toutes les mesures prises et la logique de toute décision soient bien décrites. Ceci conduit à une *chaîne* de (sous)modèles. Le degré de détail doit être cohérent à l'intérieur de la chaîne de modèles et adapté au problème considéré. Le processus doit être "transparent" pour être repris si nécessaire.

Cette analyse de "cause à effet" est très utile pour l'examen des problèmes complexes. L'importance relative des différentes interactions peut aussi être évaluée qualitativement ou quantitativement. C'est une étape nécessaire pour simplifier le système avant de commencer les calculs systématiques. Les méthodes suivantes sont largement utilisées pour construire des modèles pour des systèmes complexes :

- *Analyse par événements ou par arbre des erreurs.* Cette méthodologie est utilisée pour décrire le comportement d'un système en termes de FEPs qui sont bien connus ou qui peuvent être estimés avec un haut degré de certitude. L'analyse par arbre des erreurs a été développée pour l'analyse de risques et l'évaluation de sûreté de structures industrielles à grande échelle telles que les usines chimiques (par exemple, pour la production d'explosifs et de produits pétrochimiques) et les centrales nucléaires. La Figure I.4, p.9, montre une analyse standard, par arbre des erreurs, pour les descriptions de scénarios d'un système à quatre FEPs, et illustre comment la chaîne des événements peut avoir lieu. Remarquez la structure "binaire", soit les événements ont lieu avec une certaine probabilité, soit ils n'ont pas lieu. Il est bien connu qu'il est difficile de donner des probabilités à des FEPs en rapport avec la géologie ou avec l'homme.
- *Diagrammes d'influence des processus avec la documentation qui s'y rapporte.* Un autre moyen pour décrire un système et sa fonction est de construire des PIDs (**P**rocess **I**nfluence **D**iagrams), où les FEPs sont représentés par des boîtes et les interactions par des flèches entre les boîtes [95CHA/AND]. Un PID très simplifié est présenté par la Figure I.5, p.10, et un autre exemple est donné au Chapitre XIII. On utilise la procédure suivante :
 - un examen et une documentation systématiques sur les FEPs et sur les interactions qui peuvent affecter la performance du système ;
 - documentation sur les décisions prises au cours du développement des scénarios pour s'assurer la possibilité de revenir sur le processus ;
 - construction d'un diagramme des influences fondamentales, et à partir de là, les diagrammes d'influence sur les scénarios ;
 - formulation des scénarios et les cas de calculs.
- *Le diagramme d'interactions ou l'approche des "Rock Engineering Systems" (RES).* C'est un autre type de diagrammes d'interactions où l'on utilise une matrice carrée pour décrire les FEPs et leurs interactions. Une description complète de ces diagrammes est donnée dans [92HUD]. Les FEPs sont placés sur la diagonale de la matrice carrée et les interactions sont représentées par les termes non diagonaux. La Figure I.6, p.11, représente un système à quatre FEPs et douze (16 - 4) termes

Quelques modèles physiques et chimiques simples

non-diagonaux. Voir [94ENG/HUD]. Supposons que nous voulions savoir comment une variable D agit sur B. Cela peut se produire par une interaction directe non-diagonale DB ou, indirectement, au travers d'autres FEPs du système. Un chaîne d'influence de ce type (D-A-C-B) est indiquée sur la Figure. La variable D affecte la variable B par l'intermédiaire de trois interactions DA, AC et CB. Les façons dont une certaine variable influence les autres sont décrites par les interactions situées dans la ligne de cette variable. Les façons dont une certaine variable est influencée par les autres sont décrites par les interactions situées dans la colonne de cette variable.

En plus de ces méthodologies de modélisation, il faut aussi tenir compte d'incertitudes :

- L'incertitude sur les scénarios utilisés. Celle-ci influencera, tour à tour, les autres types d'incertitudes.
- L'incertitude sur la définition du système. C'est la principale incertitude lorsque l'on veut décrire des systèmes de la nature. Elle est liée à l'hétérogénéité du système et au manque d'information propre sur toutes ces parties. On trouve les mêmes types fondamentaux d'incertitudes dans les limites du système.
- L'incertitude sur les données, par exemple, les constantes d'équilibre, la porosité eu égard à l'écoulement, *etc.* Une partie de ce livre traitera des incertitudes sur les données chimiques.
- L'incertitude sur la compréhension des mécanismes des processus qui ont lieu dans le système. Cela peut déjà être un problème dans les systèmes de laboratoire ; cependant, des recherches scientifiques fondamentales sont entreprises pour résoudre les problèmes de ce type. Il n'est pas simple d'obtenir un aperçu mécanistique détaillé de nombreux systèmes rencontrés dans la nature. Ce problème est encore plus grave lorsque des descriptions sur une longue période sont nécessaires. C'est le cas, par exemple, lorsque l'on veut modéliser l'impact des systèmes technologiques sur l'environnement. La compréhension des mécanismes constitue aussi une part importante des parties qui traitent de chimie dans ce livre.

Le modélisateur doit être capable de se débrouiller avec les incertitudes et aussi avec les simplifications nécessaires pour rendre possible une interprétation scientifique des systèmes complexes. Les Chapitres suivants de ce livre traiteront principalement de la base scientifique pour les modèles relativement simples. Cependant, ces derniers sont souvent des sous-modèles dans des structures de modèles plus compliquées, même s'ils n'en font pas directement partie. Dans la partie suivante, nous donnerons quelques exemples supplémentaires qui pourront être utiles au lecteur.

I.4 Quelques modèles physiques et chimiques simples

Il y a une importante différence entre les modèles qui sont utilisés pour des *interpolations* dans un système spécifique et ceux utilisés pour faire des *extrapolations* ou des *prévisions* sur le comportement du système en dehors des conditions qui ont été étudiées. Les premiers ne requièrent pas nécessairement de connaissance détaillée de ce qui se passe dans le système, et les valeurs des propriétés n'importe où dans le système sont déduites des valeurs expérimentales en utilisant une fonction empirique quelconque.

Les connotations d'extrapolation et de prévision sont quelque peu différentes, la première s'applique à un processus fondé sur une solide base scientifique, la dernière indique quelque chose de plus vague. Cependant, ces deux termes sont souvent utilisés comme synonymes.

Quand nous traitons d'extrapolation et de prévision dans le contexte de ce livre, nous supposons que les systèmes "se comportent raisonnablement bien", c'est-à-dire, les forces agissant sur, ou à l'intérieur du système sont si faibles que le système ne se comportera pas de façon chaotique.

Etudions un exemple simple pour illustrer les points mentionnés ci-dessus.

Introduction

Exemple 3 : Décroissance radioactive

Grâce à certaines observations expérimentales, nous savons que certains éléments ne sont pas stables et qu'ils sont transformés par des processus intranucléaires en nouveaux éléments qui, à leur tour, peuvent aussi être instables. La chaîne des éléments instables se termine finalement par un élément stable. La théorie qui décrit la décroissance radioactive donne la vitesse de décroissance suivante du noyau père à l'élément fils :

$$\frac{dN}{dt} = -\lambda N \quad (\text{I.1})$$

où λ est une constante et N le nombre de noyaux pères au temps t . Supposons maintenant que nous ayons un système isolé, composé d'un certain élément radioactif. Pour des conditions aux limites données (valeurs connues de λ et de N_0 , c'est-à-dire, N à $t = 0$) nous pouvons intégrer l'équation précédente et calculer le nombre d'atomes de notre système à n'importe quel instant dans le futur. La précision de nos prévisions dépend de celle avec laquelle nous connaissons λ et de N_0 . C'est un système simple, et la communauté scientifique serait certainement d'accord pour dire qu'il est possible de faire des prévisions très précises sur son comportement futur, même sur des périodes extrêmement longues. Ce n'est pas inintéressant. Nous savons ce que deviendra la radioactivité au cours du temps dans les futurs dépôts pour déchets nucléaires.

Les scientifiques ont utilisé la même théorie scientifique pour dater des systèmes géologiques et d'autres encore. Les séries de décroissance radioactive de l' ^{238}U et du ^{232}Th ont été utilisées en datation. Dans un système géologique non modifié, suffisamment vieux, l'activité du nucléide père est la même que celle de chacun de ses nucléides descendants (équilibre séculaire). Cependant, dans un système ouvert, les différences chimiques entre le nucléide père et ses nucléides descendants peuvent conduire à des pertes préférentielles en certains éléments, et les rapports d'activités ne valent plus un [92OSM/IVA], et nous devons en savoir plus sur la chimie, la géologie et l'hydrologie du système pour le dater. Ces données sont bien plus incertaines que la théorie de la décroissance radioactive. C'est pourquoi, les datations sont plutôt incertaines, même si la théorie derrière l'Eq. I.1 est très bien établie.

I.5 Dans quelles circonstances pouvons nous faire des prévisions sur l'évolution des systèmes chimiques au cours du temps ?

L'évolution des systèmes chimiques dans le temps dépend de la possibilité des réactions chimiques. Quand ils parlent de réactions, les chimistes distinguent deux situations limites, les réactions sous contrôle *thermodynamique* et celles sous contrôle *cinétique*.

Exemple 4 :

Comme exemple de système sous contrôle thermodynamique, nous pouvons prendre un diagramme de phase pour un système binaire de deux solides purs **A** et **B**, et une solution solide **S**, comme le montre la Figure I.7, p.14. Le système est à pression constante et il n'y a pas d'échange de matière avec l'extérieur. Nous pouvons toujours prédire l'évolution de ce système au cours du temps. Dans les limites d'une phase, rien n'arrivera si nous changeons les variables du système. Quand une frontière de phase est franchie, le système changera comme c'est indiqué sur le diagramme. Cependant, ce diagramme ne nous dit rien sur la vitesse de ce processus. Cet exemple peut sembler trivial, mais il a des applications techniques.

La durée de vie technique des matériaux est souvent contrôlée par la vitesse de corrosion et il est important d'être capable de l'estimer pour choisir le bon matériau pour différents types d'installations. Pour évaluer la longévité des matériaux, on utilise des *tests accélérés*. Ils sont basés sur le simple principe que les vitesses des réactions chimiques augmentent avec la température. De cette façon, on

peut “comprimer” l'échelle de temps pour faire les tests. C'est une excellente méthode, à condition que le mécanisme de corrosion soit le même dans le domaine de température utilisée. Cependant, s'il y a un changement de phase quand la température augmente, il n'y a aucune raison de croire que le mécanisme de corrosion reste inchangé.

En général, les processus de corrosion sont contrôlés par des facteurs cinétiques et, pour les décrire, on a besoin de connaissances détaillées de ce qui se passe au niveau atomique/moléculaire. La plupart du temps, on ne peut accéder à de telles connaissances que pour des systèmes très simples, et les prévisions concernant le comportement au cours du temps de systèmes plus compliqués est donc à la fois difficile et incertain.

Exemple 5 : Estimation de la corrosion de matériaux métalliques sur de longues périodes de temps

Le problème concerne la prévision de la durabilité des conteneurs en métal pour déchets toxiques. Les conteneurs peuvent être soit déposés au fond des océans soit dans un dépôt pour déchets nucléaires, creusé dans la roche, dans un milieu géologique quelconque. La Figure I.8, p.15, montre schématiquement le croquis d'un dépôt souterrain.

De façon à évaluer les conditions chimiques et les réactions importantes pour la sûreté du dépôt sur de longues périodes de temps :

- Le système et ses environs doivent être décrits, ce qui comprend une décision sur les limites du système.
- Les paramètres chimiques clés du système doivent être identifiés.
- Il faut décider si la corrosion est sous contrôle thermodynamique ou cinétique.

La corrosion est un processus chimique qui dépend du matériau du conteneur métallique et des propriétés physiques et chimiques de son environnement. Ces dernières sont déterminées par la localisation du dépôt. Ceci déterminera aussi les gradients hydrauliques dans le dépôt, c'est-à-dire, les forces agissant sur le flux des eaux souterraines et, donc, le transport d'éventuels produits chimiques corrosifs vers le conteneur et, une fois ses parois franchies, de produits toxiques du conteneur (aussi bien sous forme de particules que dissoute).

Un chimiste serait rapidement capable d'identifier les paramètres chimiques importants dans des systèmes de ce type, par exemple, pH, le potentiel d'oxydoréduction du système et la présence de produits spécifiques qui peuvent causer une corrosion importante.

La Figure I.9, p.16, présente des diagrammes de Pourbaix simplifiés, (voir Chapitre II, p. 62), qui montrent les propriétés de la corrosion du fer et du cuivre dans l'eau pure. Des diagrammes pour d'autres métaux se trouvent dans “L'Atlas” de Pourbaix [74POU]. Cette Figure indique les domaines où la corrosion est thermodynamiquement impossible (*immunité*), ceux où la corrosion forme une couche protectrice qui arrête sa propagation (le terme technique est *passivation*), et, finalement, ceux où il y a de la *corrosion active*. Quand un métal est passivé, la corrosion est toujours sous contrôle cinétique. Dans la région où un matériau est thermodynamiquement stable, il est facile de prédire son comportement sur de longues périodes de temps : rien ne changera tant que les conditions extérieures resteront inchangées. Avec des diagrammes de ce type, nous pouvons aussi distinguer les conditions dans lesquelles la corrosion se produit. Pour le cas du cuivre, l'oxygène et le soufre peuvent accroître la corrosion. Cependant, le diagramme ne donne pas d'informations sur la vitesse de ce processus.

Dans le système que nous examinons, il y a deux types de processus cinétiques. L'un est déterminé par la vitesse des réactions chimiques à l'interface entre le conteneur et l'eau, l'autre par la vitesse de transport de substances corrosives dans l'eau jusqu'à la surface du conteneur.

Le système est plus compliqué que la plupart des systèmes de laboratoire, en particulier si nous considérons que le processus durera longtemps. Dans ce contexte, longtemps signifie plus de 100 ans. Nous pouvons nous demander comment juger si les prévisions sont raisonnables ou non. Le Tableau I.1 donne des conseils sur ces jugements, la “précision” estimée est seulement basée sur des estimations réalisées

par les auteurs. Un examen plus détaillé sur la corrosion du cuivre dans les systèmes souterrains est donné dans [94WER/SPA], en utilisant un modèle où les processus, à la fois, chimiques et de transport sont pris en compte.

Faisons, maintenant, un résumé :

- Les extrapolations sur une longue période de temps doivent utiliser des modèles basés sur une théorie.
- Plus le système est compliqué, plus il est difficile de faire des prévisions précises.
- L'incertitude sur une prévision dépend des incertitudes sur les théories, les modèles et les conditions aux limites.

La Figure I.1, p.2, indique comment on procède pour “valider” un système simple. Dans les systèmes compliqués, on ne peut pas utiliser cette procédure. Il n'est pas possible de tester les prévisions du développement du système, réalisées avec un modèle, alors que des modifications ont lieu dans son environnement, ou dans son comportement, sur de très longues périodes de temps. Nous devons nous appuyer sur d'autres méthodes dont la plupart sont basées sur l'hypothèse que si nous pouvons décrire l'état actuel du système, alors les mêmes modèles pourront être utilisés pour prévoir son comportement quand les variables du système seront changées. Les extrapolations sur de longues périodes de temps sur le comportement des systèmes sont souvent réalisées en utilisant des artéfacts et des *analogues naturels*. La question est alors de savoir si on peut utiliser les informations collectées par *postdictions* (“déductions du passé”) sur un système pour évaluer la précision des *prévisions* sur le même ou sur des systèmes similaires.

La corrosion du cuivre sur de longues périodes de temps peut être évaluée d'après des artéfacts archéologiques, à condition qu'il y ait des informations sur la chimie de son environnement sur la période considérée. De telles informations sont disponibles, par exemple, pour les objets trouvés dans les milieux marins (dans l'eau ou dans les sédiments déposés) [88HAL/OES]. En étudiant l'étendue de la corrosion de ces objets, on obtient des informations à la fois sur l'ampleur de la corrosion et sur sa distribution sur la surface du matériau (“piqûres”).

D'après ce que nous avons vu, il est évident que l'on ne peut jamais vérifier, sur de longues périodes de temps, le comportement prévu de systèmes compliqués. Malgré tout, il peut être nécessaire de faire des prévisions de ce type. Les extrapolations du comportement de systèmes techniques en service ne semblent pas nécessaires sur plus de 10 (pour les composants technologiques d'un système) à 100 ans (par exemple, les systèmes de barrages). Les systèmes qui doivent être évalués sur de longues périodes ont, en général, d'importants composants non technologiques, par exemple, les effets de la perte de diversité biologique, les effets socio-économiques de grands systèmes sociétaux pour les transports, la production d'énergie, l'agriculture, *etc.* Les principaux problèmes des systèmes de ce type sont politiques, non scientifiques.

Nous sommes convaincus que pour prendre des décisions à propos de ces systèmes, il est inutile de discuter la précision des modèles de prévisions en termes absolus. De tels modèles peuvent aussi être utilisés pour comparer les conséquences des différentes options possibles quand une décision doit être prise.

I.6 Considérations supplémentaires sur la modélisation chimique

La modélisation chimique peut être utilisée à des niveaux plus ou moins détaillés. Cela peut impliquer la description d'une situation *dynamique* où le système chimique est en évolution continue, par exemple, causé par des réactions chimiques en cours et/ou le transport de produits chimiques vers ou hors du système.

Il peut aussi s'agir d'une description essentiellement *statique*, une photographie instantanée d'une situation réelle d'un système où quelques variables, par exemple, les concentrations totales en constituants chimiques, sont supposées rester constantes.

Ces descriptions (ou modèles) ont leur équivalent parmi les théories chimiques — afin de faire des exposés quantitatifs sur les modifications chimiques, les chimistes utilisent deux disciplines fondamentales la *thermodynamique chimique* et la *cinétique chimique*. La première décrit les conditions sous lesquelles les réactions chimiques sont possibles et le taux de transformation des réactions quand l'*équilibre* est atteint. Ainsi, la thermodynamique donne une mesure de la modification chimique maximum qui peut avoir lieu dans un système sous des conditions extérieures spécifiées. On obtient comme sous-produits des informations sur les concentrations de toutes les espèces chimiques sous les conditions données.

Les vitesses des réactions chimiques peuvent varier énormément (avec des constantes de vitesses caractéristiques de $\sim 10^{-9}$ à $\sim 10^9$ s), et quelques réactions peuvent avoir lieu très lentement même à l'échelle de temps géologique. Pour modéliser l'évolution dans le temps d'un système chimique, nous devons connaître tous les facteurs, qui affectent les différentes vitesses de réactions ainsi que leur constante de vitesse. On ne possède que rarement des informations de ce type pour des systèmes complexes. Que ce soit un problème ou non dépend de l'échelle de temps du modèle. Dans beaucoup de systèmes, les vitesses des processus ne sont pas régies par les réactions chimiques mais par la vitesse de mélange (par exemple, les modifications chimiques d'un lac causées par l'arrivée d'un fluide de composition différente de celle du lac). Les constantes de vitesses de beaucoup de réactions en solution homogène sont inférieures à quelques minutes/heures, une échelle de temps qui est très courte en comparaison des vitesses de mélanges dans la plupart des systèmes de la nature. D'un point de vue modélisation, nous pouvons alors considérer ces réactions chimiques comme instantanées. Pour la modélisation, ceci est très important, car le modélisateur peut découpler les réactions chimiques et les processus de mélange. Si nous voulons modéliser l'évolution chimique d'un système causée par un mélange, nous devons, bien sûr, connaître la vitesse du processus physique de mélange.

Il y a aussi un certain nombre de réactions chimiques qui, en l'absence de catalyseurs, ont lieu si lentement qu'elles ne sont pas observées à l'échelle de temps du modèle. Dans ce cas, le modélisateur n'a pas à prendre en compte la réaction chimique dans son modèle ; on parle alors d'état d'*équilibre métastable*.

Les réactions dans des systèmes hétérogènes (quelques réactions de solubilité/précipitation, réactions causées par des processus d'altération météorique, et des équilibres liquide/gaz) ont souvent des vitesses de réactions bien plus courtes que celles qui se produisent en solution homogène et la modélisation de tels systèmes pourra alors être bien plus compliquée. Ces problèmes seront traités plus loin dans le Chapitre III.

Toute tentative de modélisation d'un système complexe devrait commencer avec un modèle thermodynamique car cela donne une idée des réactions chimiques les plus importantes pour le système et de celles que l'on peut négliger sans problème. La modélisation thermodynamique est, à beaucoup d'égard, une procédure simple : il existe un grand nombre de codes de calculs validés qui peuvent être utilisés pour traiter des systèmes d'équilibres même très compliqués. Ainsi, la réussite ou l'échec de la modélisation dépend de la qualité de la banque de données thermodynamiques utilisée. La banque de donnée doit être complète, c'est-à-dire que toute réaction chimique importante doit être connue. Les données thermodynamiques quantitatives doivent aussi avoir une précision satisfaisante. Nous examinerons ce point rapidement.

D'autres informations à fournir pour la modélisation chimique sont des données sur les concentrations totales des divers constituants du système. On considère, aujourd'hui que c'est essentiellement un problème de chimie analytique. Cependant, quand on décrit l'évolution dans le temps d'un système, il faut comprendre si et comment les concentrations totales peuvent changer à cause d'une action anthropogénique ou d'autres événements.

1.6.1 Sources de données thermodynamiques

La thermodynamique chimique est une discipline scientifique très bien établie et des données quantitatives sont apparues dans la littérature chimique depuis plus d'un siècle. Des données thermodynamiques sur divers composés et réactions chimiques se trouvent dans de nombreuses compilations de données.

Introduction

Stability Constants [64SIL/MAR, 71SIL/MAR, 79PER3, 82HOG] donne des informations sur des constantes d'équilibre de plusieurs types. Ces compilations contiennent des informations sur à peu près toutes les données publiées pour un système donné, et les auteurs n'ont fait aucune tentative d'évaluation critique de la qualité de ces données (sauf avec d'occasionnels points d'interrogation). Les informations expérimentales sur le milieu ionique et la température ont été reportées partout avec la méthode expérimentale utilisée. À peu près toutes les constantes d'équilibre reportées sont exprimées en unités de concentrations (voir Chapitre II) et les valeurs numériques ne sont donc valables que dans les conditions dans lesquelles elles ont été déterminées. Une version des *Stability Constants* est disponible sur ordinateur et mise à jour par *IUPAC Commission on Equilibrium Data*. Cette banque de données informatisée est disponible chez : Academic Software, Sourby Old Farm, Timble, Otley, Yorkshire LS21 2PW, United Kingdom (<http://www.cityscape.co.uk/users/gr71>).

Critical Stability Constants [74MAR/SMI, 75MAR/SMI, 76SMI/MAR, 77MAR/SMI, 82MAR/SMI, 89SMI/MAR] est une autre compilation de constantes d'équilibre tirées de *Stability Constants*, mais les auteurs ont fait une sélection des “meilleures” valeurs à certaines forces ioniques spécifiées. Malheureusement, on ne sait rien sur la logique utilisée pour faire cette sélection de données. Une version de *Critical Stability Constants* est disponible sur ordinateur et mise à jour par le *National Institute of Standards and Technology*. Cette banque de données informatisées est disponible à : Standard Reference Data Program, NIST, Gaithersburg, MD 20899-0001, USA (<http://www.nist.gov/srd>).

IUPAC Commission on Equilibrium Data, a publié un jeu d'évaluations critiquées de constantes d'équilibre pour quelques systèmes métal - ligand choisis (fluorure [80BON/HEF], edta [77AND], etc.). Dans la même série, Perrin [82PER] a fait une compilation des constantes d'équilibre de dissociation d'acides et bases inorganiques qui contient des informations du type de celles rencontrées dans *Stability Constants*. Ces compilations donnent une bonne analyse des diverses études expérimentales, mais n'essayent pas de mettre ces données dans un état de référence commun.

Les compilations suivantes contiennent des informations thermodynamiques sous la forme d'énergies de Gibbs de formation, enthalpies de formation, entropies, capacités calorifiques, etc. : US Bureau of Standards [82WAG/EVA], JANAF [85CHA/DAV], CODATA [89COX/WAG], et les livres écrits par Knacke *et al.* [91KNA/KUB], Barin [93BAR], et Kubaschewski *et al.* [93KUB/ALC]. Les “valeurs clés” de CODATA [89COX/WAG] ont été choisies après une évaluation très minutieuse des données thermodynamiques existantes pour chaque composé. Une autre source importante est *Termicheskie konstanty veshesty* (*Thermal Constants of Substances*), en 10 volumes, Academy of Sciences, Moscow, de 1965 à 1981, édité par V. P. Glushko. C'est une grande compilation de données thermodynamiques pour des phases solides, des solutions aqueuses et gazeuses, comprenant vingt livres de tableaux et de références. Le même éditeur a commencé en 1981 la série des *Termodinamicheskie svoistva individualnykh veshestv* (*Thermodynamic properties of individual substances*), qui est, maintenant, composée de huit livres contenant des tableaux de données ainsi qu'une analyse des choix des meilleures valeurs et de leur incertitudes. Une version révisée et mise à jour de ce travail a été publiée en anglais [93GUR/VEY].

Les propriétés thermodynamiques des minéraux et des réactions aqueuses intéressantes pour un géochimiste peuvent être trouvées dans [68ROB/WAL, 78HEL/DEL, 78ROB/HEM, 82HEL, 82HEM/HAA, 90HOL/POW, 90NOR/PLU, 92JOH/OEL, 94NOR/MUN, 95ROB/HEM].

Les deux derniers paragraphes donnent des références qui contiennent des données thermodynamiques dans les conditions de l'état standard, et à une température de 298.15 K et une pression de 0.10000 MPa. Les données pour des espèces aqueuses se réfèrent à l'état standard de dilution infinie. Des détails sur les définitions de différents types de constantes d'équilibre et une analyse des conditions de l'état standard sont données au Chapitre II.

Des informations sur les données thermodynamiques pour des actinides, à la fois pour les éléments, leurs composés et leurs espèces aqueuses (dont les complexes inorganiques) ont été compilées par l'Agence internationale de l'énergie atomique (IAEA) à Vienne [66RAN, 68LAV/GER, 72GER/LAV, 73SPE, 75RAN, 76ALC/JAC, 76FUG/OET, 76OET/RAN, 78COR/OHA, 80BRE/LAM2, 81CHI/AKH, 81SPE, 83FUG/PAR, 83KUB, 84FLO/HAS, 84GRO/DRO, 84HOL/RAN, 85 HIL/GUR, 92FUG/KHO].

Des données thermodynamiques sur les actinides uranium, neptunium, plutonium et américium, ainsi

que celles du technétium sont collectées dans une série d'études critiques par l'Agence pour l'énergie nucléaire (AEN) de l'Organisation pour la coopération et le développement économiques (OCDE) à Paris. Les études critiques traitent à la fois des éléments, de leurs composés et de leurs espèces aqueuses (dont les complexes inorganiques). Dans ce projet [88WAN] les données thermodynamiques et leurs incertitudes sont choisies en cohérence avec les valeurs de CODATA mentionnées ci-dessus. Pour l'instant, seuls les tomes de l'uranium et du technétium ont été publiés [92GRE/FUG, 95SIL/BID].

1.6.2 Utilisation des données thermodynamiques disponibles

Le chimiste modélisateur fait face à un problème important qui est la cohérence des données thermodynamiques : on peut obtenir des résultats erronés quand on utilise des valeurs de sources différentes en les associant dans un modèle. Grauer traite de ce sujet dans le Chapitre IV.

Malgré la grande quantité d'informations disponibles, le modélisateur peut trouver qu'il lui manque des informations importantes. Ce manque d'informations peut être de deux sortes :

- On doit avoir des méthodes pour recalculer les données thermodynamiques données dans les conditions de l'état standard et à la température de référence. Ce sont ces valeurs que l'on trouve souvent dans les compilations de données thermodynamiques. De tels nouveaux calculs sont nécessaires car les systèmes à modéliser sont rarement dans les conditions de l'état standard ou à la température de référence. Cela veut dire que les données thermodynamiques existantes doivent être corrigées pour être valides à la température, à la pression et à la force ionique du système réel. Des méthodes pour réaliser ces corrections sont décrites dans les Chapitres IX et X.
- Des informations sur la composition stoechiométrique et sur les constantes d'équilibres faisant intervenir des espèces pour lesquelles le modélisateur a de bonnes raisons chimiques de croire qu'elles peuvent se former dans le système, mais pour lesquelles il ne possède aucune données quantitatives.

Que faire quand des informations importantes manquent ? La plus mauvaise solution consiste à n'utiliser que les informations que l'on a trouvées dans les banques de données. Une bien meilleure solution est d'utiliser des théories chimiques pour prévoir des estimations raisonnables des données dont on a besoin et, ensuite, de voir combien le modèle est sensible (par exemple la solubilité d'un minéral, ou la concentration totale en un élément) aux variations des paramètres inconnus du modèle. Si ces paramètres s'avèrent trop importants pour la modélisation, il peut être nécessaire de les déterminer expérimentalement. Les exemples des Chapitres III et X démontrent qu'en plus, les estimations de données thermodynamiques peuvent donner une bonne idée du fonctionnement chimique d'un système.

En d'autres termes, en modélisation thermodynamique il est important de ne pas utiliser seulement les données quantitatives disponibles dans les banques de données, mais aussi les informations qualitatives ou semi-quantitatives qui peuvent être tirées des théories chimiques établies. L'utilisation de méthodes d'extrapolation pour les données thermodynamiques est importante et nous avons, par conséquent, décrit les méthodes pour estimer des coefficients d'activité et pour faire des estimations sur la dépendance en fonction de la température des données thermodynamiques, dans les Chapitres IX et X respectivement. Des estimations de la composition chimique d'espèces dissoutes requiert une petite connaissance des principes généraux de la chimie. Ils sont décrits au Chapitre III où l'on donne aussi des références de monographies/manuels qui les expliquent plus en détails.

Chapter II

Symbols, Standards, and Conventions [†]

Ingmar GRENTHE
Department of Inorganic Chemistry
Royal Institute of Technology
S-100 44 Stockholm (Sweden)

Ignasi PUIGDOMENECH *
OECD Nuclear Energy Agency
Le Seine – Saint Germain
12, boulevard des Iles
F-92130 Issy-les-Moulineaux (France)

This chapter specifies and lists the symbols, terminology and nomenclature, the units and conversion factors, the standard conditions and the reference temperature, and the fundamental physical constants used in this book.

II.1. Symbols, terminology and nomenclature

II.1.1. *Symbols and terminology*

The symbols for physical and chemical quantities used in this book follow the recommendations of the International Union of Pure and Applied Chemistry, IUPAC [79WHI2, 88MIL/CVI]. They are summarised in Table II.1.

II.1.2. *Reference codes*

The reference list in this book has been automatically created by a computer program that scans the reference codes cited in the text and retrieves the corresponding citations from a data base at the NEA. This procedure is necessary to ensure compatibility of

[†] A substantial portion of this Chapter originates from an NEA report (TDB-5) and from the published NEA reviews on the thermochemistry of uranium and americium [92GRE/FUG, 95SIL/BID].

* Permanent address: Department of Inorganic Chemistry, Royal Institute of Technology, S-100 44 Stockholm, Sweden.

Table II.1: Symbols and terminology.

thermodynamic temperature, absolute temperature	T
Celsius temperature	t
Avogadro constant	N_A
(molar) gas constant	R
Boltzmann constant	k
Faraday constant	F
chemical potential of substance B	μ_B
(molar) Gibbs energy	G_m
(molar) entropy	S_m
(molar) enthalpy	H_m
(molar) heat capacity at constant pressure	$C_{p,m}$
(molar) volume	V_m
density (mass divided by volume)	ρ
amount of substance B ^(a)	n_B
mole fraction of substance B: $n_B/\sum_i n_i$	x_B
pressure	p
partial pressure of substance B: $x_B p$	p_B
fugacity of substance B	f_B
fugacity coefficient: f_B/p_B	$\gamma_{f,B}$
molarity or concentration of a solute substance B (amount of B divided by the volume of the solution) ^(b)	$c_B, [B]$
molality of a solute substance B (amount of B divided by the mass of the solvent) ^(c)	m_B
mean ionic molality ^(d) , $m_{\pm}^{(\nu_+ + \nu_-)} = m_+^{\nu_+} m_-^{\nu_-}$	m_{\pm}
activity of substance B	$a_B, \{B\}$
activity coefficient, molality basis: a_B/m_B	γ_B
activity coefficient, concentration basis: a_B/c_B	y_B
mean ionic activity ^(d) , $a_{\pm}^{(\nu_+ + \nu_-)} = a_+^{\nu_+} a_-^{\nu_-}$	a_{\pm}
mean ionic activity coefficient ^(d) , $\gamma_{\pm}^{(\nu_+ + \nu_-)} = \gamma_+^{\nu_+} \gamma_-^{\nu_-}$	γ_{\pm}
osmotic coefficient, molality basis	ϕ
stoichiometric coefficient of substance B (negative for reactants, positive for products)	ν_B
general equation for a chemical reaction	$0 = \sum_B \nu_B B$
equilibrium constant ^(e)	K
electromotive force	E
rate constant	k

Table II.1 (continued)

charge number of an ion B (positive for cations, negative for anions)	Z_B
ionic strength: $I_m = \frac{1}{2} \sum_i m_i Z_i^2$ or $I_c = \frac{1}{2} \sum_i c_i Z_i^2$	I
pH = $-\log_{10}[a_{H^+}/(\text{mol} \cdot \text{kg}^{-1})]$, <i>cf.</i> Section II.1.9	pH
superscript for standard state ^(f)	°

(a)	<i>cf.</i> Sections 1.2 and 3.6 of the IUPAC manual [79WHI2].
(b)	This quantity is called “amount-of-substance concentration” in the IUPAC manual [79WHI2]. A solution with a concentration equal to $0.1 \text{ mol} \cdot \text{dm}^{-3}$ is called a 0.1 molar solution or a 0.1 M solution.
(c)	A solution having a molality equal to $0.1 \text{ mol} \cdot \text{kg}^{-1}$ is called a 0.1 molal solution or a 0.1 m solution.
(d)	For an electrolyte $N_{\nu_+} X_{\nu_-}$ which dissociates into $\nu_{\pm} (= \nu_+ + \nu_-)$ ions, in an aqueous solution with concentration m , the individual cationic molality and activity coefficient are $m_+ (= \nu_+ m)$ and $\gamma_+ (= a_+/m_+)$. A similar definition is used for the anionic symbols. Electrical neutrality requires that $\nu_+ Z_+ = \nu_- Z_-$.
(e)	Special notations for equilibrium constants are outlined in Section II.1.8. In some cases, K_c is used to indicate a concentration constant in molar units, and K_m a constant in molal units.
(f)	See Section II.3.1 “Standard state”.

references among all NEA TDB reviews, it avoids the duplication of any given reference in several chapters, and it facilitates the production of the book.

The reference codes cited are ordered chronologically and alphabetically by the first two authors within each year, as described by CODATA [87GAR/PAR]. A reference code is made up of the final two digits of the year of appearance (if the publication is not from the 20th century, the year will be put in full). The year is followed by the first three letters of the first two authors, separated by a slash. If there are multiple reference codes, a “2” will be added to the second one, a “3” to the third one, and so forth. Reference codes are always enclosed in square brackets.

The assignment of the reference codes is done automatically by the NEA updating computer programs for the TDB data base. It is therefore possible that multiple reference codes in the TDB data base do not occur in multiple form in the present book. The designators “2”, “3”, *etc.*, are nevertheless retained for reasons of compatibility with the TDB data base.

II.1.3. Chemical formulae and nomenclature

The recommendations made by IUPAC [71JEN, 77FER, 90LEI] on the nomenclature of inorganic compounds and complexes are followed in this book, except for the following items:

- i) The formulae of coordination compounds and complexes are not enclosed in square brackets [71JEN, Rule 7.21].
- ii) The prefixes “oxy-” and “hydroxy-” are retained if used in a general way, *e.g.*, “gaseous oxyfluorides”. For specific formula names, however, the IUPAC recommended name [71JEN, Rule 6.42] is used, *e.g.*, “uranium(IV) difluoride oxide” for $\text{UF}_2\text{O}(\text{cr})$.

An IUPAC rule that is often not followed [71JEN, Rules 2.163 and 7.21] is recalled here: the order of arranging ligands in coordination compounds and complexes is the following: central atom first, followed by ionic ligands and then by the neutral ligands. If there are more than one ionic or neutral ligand, the alphabetical order of the symbols of the ligating atoms determines the sequence of the ligands. For example, $(\text{UO}_2)_2\text{CO}_3(\text{OH})_3^-$ is standard, while $(\text{UO}_2)_2(\text{OH})_3\text{CO}_3^-$ is non-standard.

Abbreviations of names for organic ligands appear sometimes in formulae. Following the recommendations by IUPAC, lower case letters are used and, if necessary, the ligand abbreviation is enclosed within parentheses. Hydrogen atoms that can be replaced by the metal atom are shown in the abbreviation with an upper case “H”, for example: H_3edta^- , $\text{Am}(\text{Hedta})(\text{s})$ (where edta stands for ethylenediaminetetraacetate).

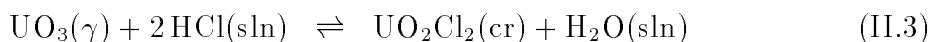
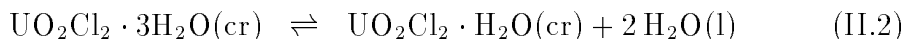
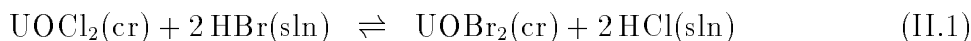
II.1.4. Phase designators

Chemical formulae may refer to different chemical species and are often required to be specified more clearly in order to avoid ambiguities. For example, UF_4 occurs as a gas, a solid, and an aqueous complex. The distinction between the different phases is made by phase designators that immediately follow the chemical formula and appear in parentheses. The only formulae that are not provided with a phase designator are aqueous ions, since they are the only charged species in this book. The use of the phase designators is described below.

- The designator (l) is used for pure liquid substances, *e.g.*, $\text{H}_2\text{O}(\text{l})$.
- The designator (aq) is used for undissociated, uncharged aqueous species, *e.g.*, $\text{U}(\text{OH})_4(\text{aq})$, $\text{CO}_2(\text{aq})$. Since ionic gases are not discussed in this book, all ions may be assumed to be aqueous and are not designed with (aq). If a chemical reaction refers to a medium other than H_2O (*e.g.*, D_2O , 90% ethanol/10% H_2O), then (aq) is replaced by a more explicit designator, *e.g.*, “(in D_2O)” or “(sln)”. In the case of (sln), the composition of the solution is described in the text.

- The designator (sln) is used for substances without specifying the actual equilibrium composition of the substance in the solution. Note the difference in the designation of H₂O in Eqs. (II.2) and (II.3). H₂O(l) in Reaction (II.2) indicates that H₂O is present as a pure liquid, *i.e.*, no solutes are present, whereas Reaction (II.3) involves a HCl solution, in which the thermodynamic properties of H₂O(sln) may not be the same as those of the pure liquid H₂O(l). In dilute solutions, however, this difference in the thermodynamic properties of H₂O can be neglected, and H₂O(sln) may be approximated as pure H₂O(l).

Examples:



- The designators (cr), (am), (vit), and (s) are used for solid substances. (cr) is used for crystalline, (am) for amorphous, and (vit) for glassy substances. Otherwise, the general designator (s) is used.
- In some cases, more than one crystalline form of the same chemical composition may exist. In such a case, the different polymorphs are distinguished by separate designators to identify them. If the crystal has a mineral name, the designator (cr) is replaced by the first four characters of the mineral name in parentheses, *e.g.*, SiO₂(quar) for quartz and SiO₂(chal) for chalcedony. If there is no mineral name, the designator (cr) is replaced by a Greek letter preceding the formula and indicating the structural phase, *e.g.*, α -UF₅, β -UF₅.

Phase designators are also used in conjunction with thermodynamic symbols to define the state of aggregation of a compound to which a thermodynamic quantity refers. The notation is in this case the same as outlined above. In an extended notation (*cf.* [82LAF]) the reference temperature is usually given in addition to the state of aggregation of the composition of a mixture.

Examples:

$\Delta_f G_m^\circ(\text{Na}^+, \text{aq}, 298.15 \text{ K})$	standard molar Gibbs energy of formation of aqueous Na ⁺ at 298.15 K
$S_m^\circ(\text{UO}_2\text{SO}_4 \cdot 2.5\text{H}_2\text{O}, \text{cr}, 298.15 \text{ K})$	standard molar entropy of UO ₂ SO ₄ · 2.5H ₂ O(cr) at 298.15 K
$C_{p,m}^\circ(\text{UO}_3, \alpha, 298.15 \text{ K})$	standard molar heat capacity of α -UO ₃ at 298.15 K
$\Delta_f H_m(\text{HF}, \text{sln}, \text{HF} \cdot 7.8\text{H}_2\text{O})$	enthalpy of formation of HF diluted 1:7.8 with water

II.1.5. Systems and their components

As mentioned in Chapter I, a *system* is that part of the physical world that the scientist wants to describe. The quantitative definition of a system requires not only the chemical composition of the substances in it but also the amount of each of the phases (minerals, fluids, *etc.*). A system is *isolated* if neither energy nor matter is exchanged with its surroundings. A *closed* system has constant mass and bulk composition, while energy may be exchanged with its surroundings. In *open* systems both matter and energy may be exchanged through their boundaries.

The number of components in a thermodynamic system is the minimum number of constituents required to describe its composition. Hence,

each species in the system should have a unique formula with respect to the components chosen, or equivalently, none of the chosen components should be expressible as a combination of the others.

For a system containing N_{spe} species with N_{react} *independent* reactions between the species, the number of components is $N_{\text{comp}} = N_{\text{spe}} - N_{\text{react}}$. The mathematical criterion of linear independence of the components is that the determinant of the composition matrix of the species related to the chosen components should not be zero.

The solvent is usually present in a very large excess. As the concentration of water in a dilute solution is approximately 55 M, it is not practical to use water as a species when describing the composition of aquatic systems. Water should therefore **always** be chosen as a component. In general, any species with fixed activity should be chosen as a component: pure phases (solids present in large excess), a solvent (like water which has $a_{\text{H}_2\text{O}} \approx 1$), a gas at constant fugacity (like atmospheric CO_2), *etc.* It is also practical to choose H^+ as a component because its activity is often used as a master variable when modelling aqueous systems. In the same way it is **practical** (but not necessary) to select the components of the system as species not capable of further dissociation (like PO_4^{3-} , Ca^{2+} , *etc.*).

Example: HCO_3^- and CO_3^{2-} could both be selected as components, but it would be quite impractical to use, say, C^{4+} and O^{2-} as components, because the stoichiometric definition of species then becomes cumbersome.

The maximum number of phases in thermodynamic systems at equilibrium is given by the Gibbs phase rule, which states that the number of independent properties that can be varied in a system (the number of *degrees of freedom*, N_f) is given by

$$N_f = 2 + N_{\text{comp}} - N_{\text{phases}}$$

where N_{comp} is the number of components, and N_{phases} the number of phases present in the system. The degrees of freedom are two intensive properties (like T and p , or T and ρ) and the chemical potential of each component. A result of the Gibbs phase rule, of

interest in modelling equilibrium systems at fixed T and p , is that the number of species with fixed activities must be smaller than the number of components.

The choice of components is reflected in the notation used for the equilibrium constants, *cf.* Section II.1.8. The subscripts (in $\beta_{q,m}$ for example) denote the stoichiometric coefficients for the components.

It is essential that the numerical values of all equilibrium constants used in a model are based on the same components, if not, they have to be recalculated to a common set of components before meaningful chemical equilibrium calculations can be performed.

II.1.5.1. Components in redox reactions

Many chemical elements occur in different oxidation states and it is therefore practical to use the electron as a component (even though it does not occur in free form in chemical systems). This can be illustrated by the following two choices of components, used to describe the species UO_2^{2+} in a system:

UO_2^{2+} is equal to $(\text{UO}_3)_1(\text{H}^+)_2(\text{H}_2\text{O})_{-1}$, (in a system with $\text{UO}_3(\text{cr})$, $\text{H}_2\text{O}(\text{l})$ and H^+ as components, related by the reaction: $\text{UO}_3(\text{cr}) + 2\text{H}^+ - \text{H}_2\text{O}(\text{l}) \rightleftharpoons \text{UO}_2^{2+}$).

UO_2^{2+} is equal to $(\text{U}^{4+})_1(\text{e}^-)_{-2}(\text{H}^+)_{-4}(\text{H}_2\text{O})_2$ (in a system, with $\text{H}_2\text{O}(\text{l})$, H^+ , e^- and U^{4+} as components, related by the reaction: $\text{U}^{4+} - 2\text{e}^- - 4\text{H}^+ + 2\text{H}_2\text{O}(\text{l}) \rightleftharpoons \text{UO}_2^{2+}$).

The terminology used for equilibrium constants and reduction potentials for redox reactions is described in Section II.1.8.6.

II.1.6. Processes

Chemical processes are denoted by the operator Δ , written before the symbol for a property, as recommended by IUPAC [82LAF]. An exception to this rule is the equilibrium constant, *cf.* Section II.1.8. The nature of the process is denoted by annotation of the Δ , *e.g.*, the Gibbs energy of formation, $\Delta_{\text{f}}G_{\text{m}}$, the enthalpy of sublimation, $\Delta_{\text{sub}}H_{\text{m}}$, *etc.* The abbreviations of chemical processes are summarised in Table II.2.

The most frequently used symbols for processes are $\Delta_{\text{f}}G$ and $\Delta_{\text{f}}H$, the Gibbs energy and the enthalpy of formation of a compound or complex from the elements in their reference states (*cf.* Table II.5).

II.1.7. Thermodynamic data

The following parameters, valid at the reference temperature of 298.15 K and at the standard pressure of 1 bar, are usually considered:

Table II.2: Abbreviations used as subscripts of Δ to denote the type of chemical processes.

Subscript of Δ	Chemical process
at	separation of a substance into its constituent gaseous atoms (atomisation)
dehyd	elimination of water of hydration (dehydration)
dil	dilution of a solution
f	formation of a compound from its constituent elements
fus	melting (fusion) of a solid
hyd	addition of water of hydration to an unhydrated compound
mix	mixing of fluids
r	chemical reaction (general)
sol	process of dissolution
sub	sublimation (evaporation) of a solid
tr	transfer from one solution or liquid phase to another
trs	transition of one solid phase to another
vap	vaporisation (evaporation) of a liquid

$\Delta_f G_m^\circ$	the standard molar Gibbs energy of formation from the elements in their reference state	(kJ · mol ⁻¹)
$\Delta_f H_m^\circ$	the standard molar enthalpy of formation from the elements in their reference state	(kJ · mol ⁻¹)
S_m°	the standard molar entropy	(J · K ⁻¹ · mol ⁻¹)
$C_{p,m}^\circ$	the standard molar heat capacity at constant pressure	(J · K ⁻¹ · mol ⁻¹)

For aqueous neutral species and ions, the values of $\Delta_f G_m^\circ$, $\Delta_f H_m^\circ$, S_m° and $C_{p,m}^\circ$ correspond to the standard partial molar quantities, and for individual aqueous ions they are relative quantities, defined with respect to the aqueous hydrogen ion, according to the convention [89COX/WAG] that $\Delta_f H_m^\circ(\text{H}^+, \text{aq}, T) = 0$, and that $S_m^\circ(\text{H}^+, \text{aq}, T) = 0$. Furthermore, for an *ionized solute* B containing any number of different cations and anions:

$$\begin{aligned}\Delta_f H_m^\circ(\text{B}_\pm, \text{aq}) &= \sum_+ \nu_+ \Delta_f H_m^\circ(\text{cation}, \text{aq}) + \sum_- \nu_- \Delta_f H_m^\circ(\text{anion}, \text{aq}) \\ S_m^\circ(\text{B}_\pm, \text{aq}) &= \sum_+ \nu_+ S_m^\circ(\text{cation}, \text{aq}) + \sum_- \nu_- S_m^\circ(\text{anion}, \text{aq}).\end{aligned}$$

A chemical reaction “ r ”, involving reactants and products “ B ”, can be abbreviated as

$$0 = \sum_B \nu_{r,B} B \quad (\text{II.4})$$

where the stoichiometric coefficients $\nu_{r,B}$ are positive for products, and negative for reactants. The reaction parameters considered include:

$\log_{10} K_r^\circ$	the equilibrium constant of the reaction, logarithmic
$\Delta_r G_m^\circ$	the molar Gibbs energy of reaction (kJ · mol ⁻¹)
$\Delta_r H_m^\circ$	the molar enthalpy of reaction (kJ · mol ⁻¹)
$\Delta_r S_m^\circ$	the molar entropy of reaction (J · K ⁻¹ · mol ⁻¹)
$\Delta_r C_{p,m}^\circ$	the molar heat capacity of reaction (J · K ⁻¹ · mol ⁻¹)

The equilibrium constant, K_r° , is related to $\Delta_r G_m^\circ$ according to the following relation,

$$\log_{10} K_r^\circ = -\frac{\Delta_r G_m^\circ}{RT \ln(10)}$$

and can be calculated from the individual values of $\Delta_f G_m^\circ(B)$ according to,

$$\log_{10} K_r^\circ = -\frac{1}{RT \ln(10)} \sum_B \nu_{r,B} \Delta_f G_m^\circ(B).$$

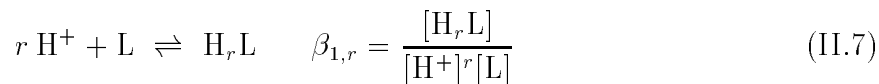
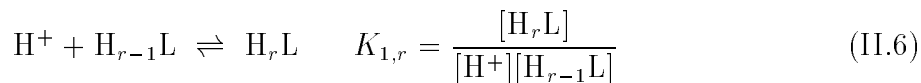
II.1.8. Equilibrium constants

The IUPAC has not explicitly defined the symbols and terminology for equilibrium constants of reactions in aqueous solution. The NEA has therefore adopted the conventions that have been used in *Stability constants of metal ion complexes* by Sillén and Martell [64SIL/MAR, 71SIL/MAR]. An outline is given in the paragraphs below. Note that, for some simple reactions, there may be different correct ways to index an equilibrium constant. It may sometimes be preferable to indicate the number of the reaction the data refer to, especially in cases where several ligands participate in the reaction. For example, for the equilibrium



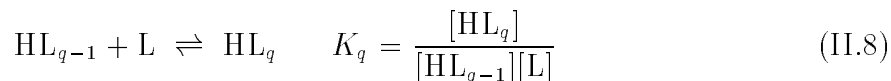
both $\beta_{q,m}$ and $\beta(\text{II.5})$ would be appropriate, and $\beta_{q,m}(\text{II.5})$ is accepted, too. Note that, in general, K is used for the consecutive or stepwise formation constant, and β is used for the cumulative or overall formation constant. In the following outline, charges are only given for actual chemical species, but are omitted for species containing general symbols (M, L).

II.1.8.1. Protonation of a ligand

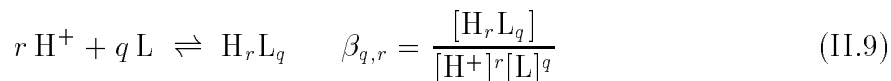


This notation has been proposed and used by Sillén and Martell [64SIL/MAR], but it has been simplified later by the same authors [71SIL/MAR] from $K_{1,r}$ to K_r . This book retains, for the sake of consistency, *cf.* Eqs. (II.8) and (II.9), the older formulation of $K_{1,r}$.

For the addition of a ligand, the notation shown in Eq.(II.8) is used.

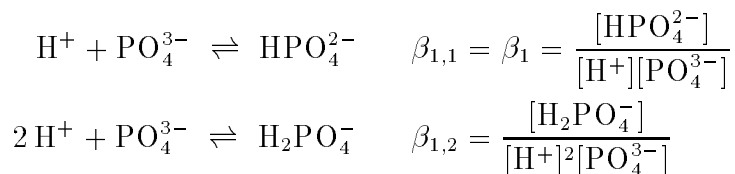


Eq. (II.9) refers to the overall formation constant of the species H_rL_q .

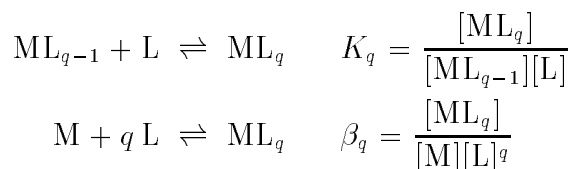


In Eqs. (II.6), (II.7) and (II.9), the second subscript r can be omitted if $r = 1$, as shown in Eq. (II.8).

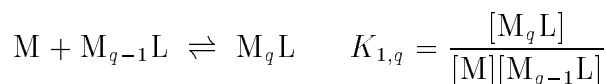
Examples:



II.1.8.2. Formation of metal ion complexes



For the addition of a metal ion, *i.e.*, the formation of polynuclear complexes, the following notation is used, analogous to Eq.(II.6):



Eq. (II.10) refers to the overall formation constant of a complex M_mL_q .

$$m M + q L \rightleftharpoons M_mL_q \quad \beta_{q,m} = \frac{[M_mL_q]}{[M]^m[L]^q} \quad (\text{II.10})$$

The second index can be omitted if it is equal to 1, *i.e.*, $\beta_{q,m}$ becomes β_q if $m = 1$.

The formation constants of mixed ligand complexes are not indexed. In this case, it is necessary to list the chemical reactions considered and to refer the constants to the corresponding reaction numbers.

It has been customary to use negative values for the indices of the protons to indicate complexation with hydroxide ions, OH^- . However, if OH^- occurs as a reactant, the notation becomes clearer if OH^- is treated like a normal ligand L:

$$m M + n OH^- \rightleftharpoons M_m(OH)_n \quad \beta_{n,m} = \frac{[M_m(OH)_n]}{[M]^m[OH^-]^n}$$

If H_2O occurs as a reactant to form hydroxide complexes, H_2O is considered as a protonated ligand, HL, so that the reaction is treated as described below in Eqs. (II.11) to (II.13).

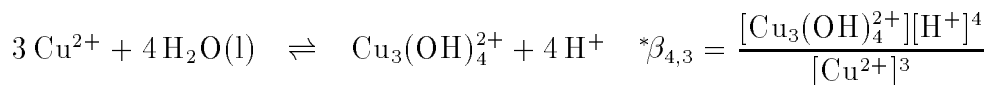
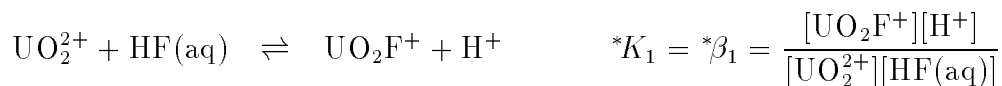
In many experiments, the formation constants of metal ion complexes are determined by adding a ligand in its protonated form to a metal ion solution. The complex formation reactions thus involve a deprotonation reaction of the ligand. In this case, the equilibrium constant is supplied with an asterisk, as shown in Eqs. (II.11) and (II.12) for mononuclear and in Eq. (II.13) for polynuclear complexes.

$$ML_{q-1} + HL \rightleftharpoons ML_q + H^+ \quad {}^*K_q = \frac{[ML_q][H^+]}{[ML_{q-1}][HL]} \quad (\text{II.11})$$

$$M + q HL \rightleftharpoons ML_q + q H^+ \quad {}^*\beta_q = \frac{[ML_q][H^+]^q}{[M][HL]^q} \quad (\text{II.12})$$

$$m M + q HL \rightleftharpoons M_mL_q + q H^+ \quad {}^*\beta_{q,m} = \frac{[M_mL_q][H^+]^q}{[M]^m[HL]^q} \quad (\text{II.13})$$

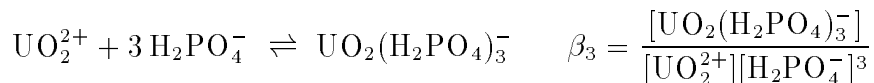
Examples:



Note that an asterisk is only assigned to the formation constant if the protonated ligand is deprotonated during the reaction. If a protonated ligand is added and coordinated as such to the metal ion, the asterisk has to be omitted, as shown in Eq. (II.14).

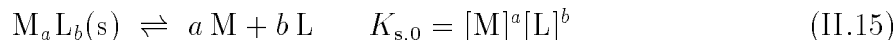
$$M + q H_rL \rightleftharpoons M(H_rL)_q \quad \beta_q = \frac{[M(H_rL)_q]}{[M][H_rL]^q} \quad (\text{II.14})$$

Example:

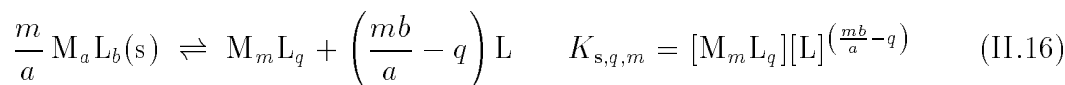


II.1.8.3. Solubility constants

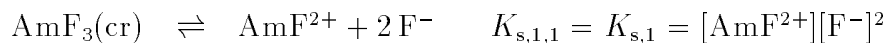
Conventionally, equilibrium constants involving a solid compound are denoted as “solubility constants” rather than as formation constants of the solid. An index “s” to the equilibrium constant indicates that the constant refers to a dissolution process, as shown in Eqs. (II.15) to (II.17).



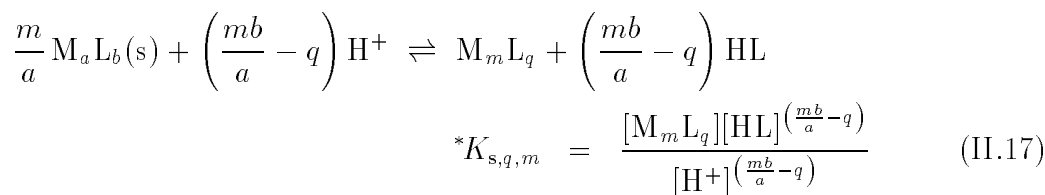
$K_{\text{s},0}$ is the conventional solubility product, and the subscript “0” indicates that the equilibrium reaction involves only uncomplexed aqueous species. If the solubility constant includes the formation of aqueous complexes, a notation analogous to that of Eq. (II.10) is used:



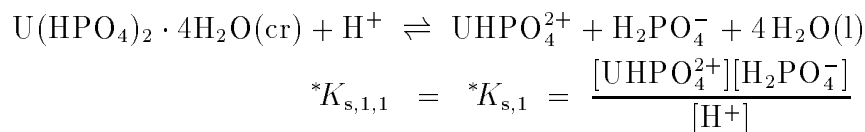
Example:



Similarly, an asterisk is added to the solubility constant if it simultaneously involves a protonation equilibrium:

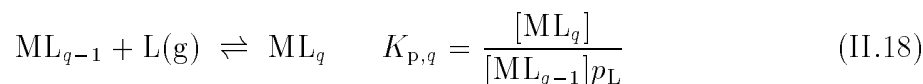


Example:



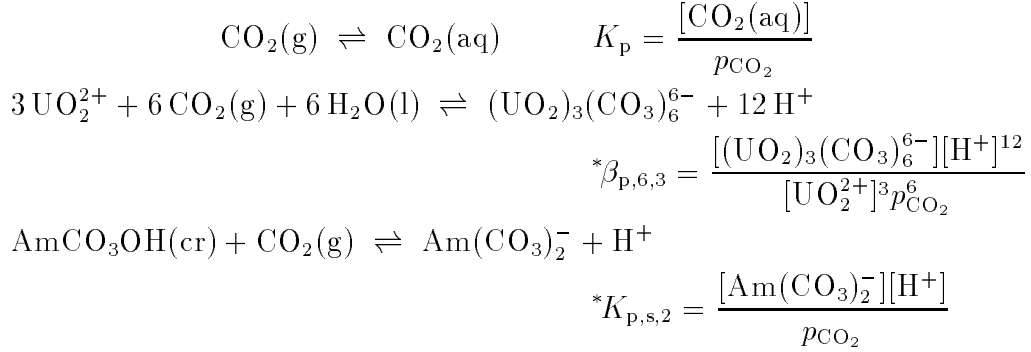
II.1.8.4. Equilibria involving the addition of a gaseous ligand

A special notation is used for constants describing equilibria that involve the addition of a gaseous ligand, as outlined in Eq. (II.18).



where p_L is the partial pressure of the gaseous species L. The subscript “p” can be combined with any other notations given above.

Examples:



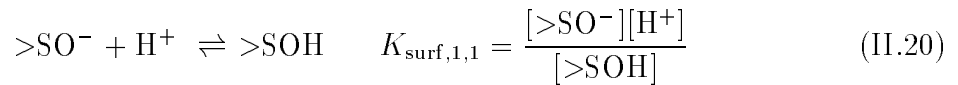
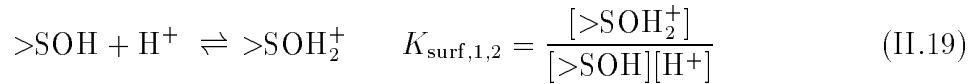
In cases where the subscripts become complicated, it is recommended that K or β be used with or without subscripts, but always followed by the equation number of the equilibrium to which it refers.

II.1.8.5. Surface coordination reactions

Equilibrium constants for reactions involving a solid surface are denoted as “surface coordination constants”. An index “surf” to the equilibrium constant indicates that the constant refers to a surface coordination/dissociation process.

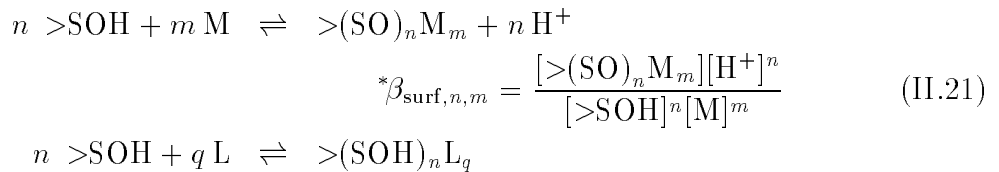
The surface site is represented here as “>SOH”, and it is treated like any other ligand. In general all concentration terms appearing in equilibrium constants for surface reactions (Eqs. (II.19) to (II.23)) are expressed in $\text{mol} \cdot \text{l}^{-1}$.

The proton coordination/dissociation reactions are:



These equations are equivalent to Eq. (II.6), with $L \equiv >\text{SO}^-$.

Due to the nature of the surface sites, most surface coordination reactions involve simultaneous deprotonation, and similarly to other reactions, an asterisk is added to the notation of the equilibrium constant. Metal, anion, and metal complex coordination are expressed as:

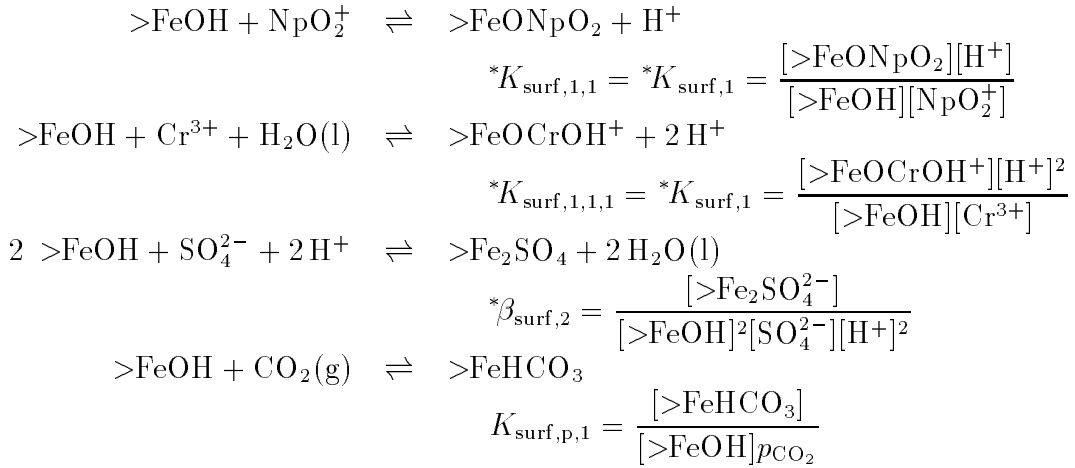


$$\beta_{\text{surf},n,q} = \frac{[>(\text{SOH})_n\text{L}_q]}{[>\text{SOH}]^n[\text{L}]^q} \quad (\text{II.22})$$

$$n >\text{SOH} + m \text{M} + q \text{L} \rightleftharpoons >(\text{SO})_n\text{M}_m\text{L}_q + n \text{H}^+ \\ {}^*\beta_{\text{surf},q,m,n} = \frac{[>(\text{SO})_n\text{M}_m\text{L}_q][\text{H}^+]^n}{[>\text{SOH}]^n[\text{M}]^m[\text{L}]^q} \quad (\text{II.23})$$

As usual, the last index in the equilibrium constant may be omitted if it is equal to one. In cases where the subscripts become complicated, it is recommended that K or β be used with or without subscripts, but always followed by the equation number of the equilibrium to which it refers.

Examples:



where p_{CO_2} is the partial pressure of carbon dioxide.

II.1.8.6. Redox equilibria

Thermodynamic data for redox reactions are presented in different ways:

- as *normal*, or *standard* potentials
- as standard Gibbs energies of reaction, $\Delta_r G_m^\circ$
- as equilibrium constants
- as pe° values

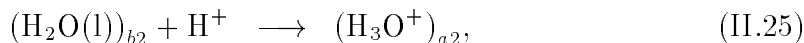
In the following section we will make a brief review of these concepts.

It is not possible to determine **absolute** values for the Gibbs energy of chemical species, we can only determine **changes**, *e.g.*, as a result of chemical reactions in a system. If we want to express the redox properties of a system we must therefore introduce an arbitrary zero point. The procedure is analogous to those used when:

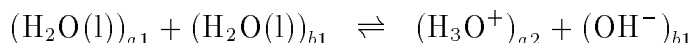
- tabulating standard Gibbs energies of formation of chemical compounds ($\Delta_f G_m^\circ$), where we define the zero point by assigning the value zero to the standard free energy of formation of all elements in their stable form at the temperature 298.15 K and the pressure 1 bar.
- assigning a zero-point for acid/base reactions in aqueous solutions. In this case we relate the strength of an acid and a base to its ability to release, respectively take up, *protons*. For the case of water we have:



and

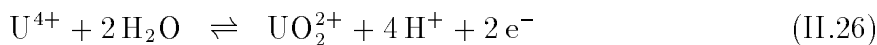


where $a1/b1$ and $a2/b2$ denote corresponding acid–base pairs. By combining the two equations we eliminate the free proton[†], which like the free electron does not exist in the kind of chemistry we are interested in. We have:



The equilibrium constant for this equation is measurable and is known as the *ionic product of water*, denoted K_w . If the equilibrium constants for the proton release and proton uptake are denoted $K(\text{II.24})$ and $K(\text{II.25})$, we have: $K_w = K(\text{II.24}) \times K(\text{II.25})$. We can define $K(\text{II.25}) = 1$, and will in this way use water as the reference base through which we compare the strength of all acids in *water*. We can also use water as a reference acid, through which we can compare the strengths of different bases in water.

It is not possible to study the formation of free electrons, *e.g.*, in reactions such as:



because they cannot occur in ordinary aqueous chemical systems. This is in complete analogy with the previous example on acid/base equilibria where H^+ is a fictive species. However, the reaction may take place as a *half-cell reaction* in an electrochemical cell. The electrons released in one half-cell are taken up by the reactant(s) in a second half-cell. The zero point is defined by the choice of the second half-cell. By international definition the half-cell reaction between the aqueous hydrogen ion and hydrogen gas is used as a reference:



[†] Note that in most reactions H^+ denotes the *hydrated* proton, which is a real species, *c.f.* p.52, while in Eqs. (II.24) and (II.25) H^+ denotes the *free* proton.

The equilibrium constant for this half-cell reaction is defined as unity:

$$K^\circ(\text{II.27}) = \frac{a_{\text{H}^+} a_{\text{e}^-}}{\sqrt{p_{\text{H}_2}}} = 1 \quad (\text{by definition}) \quad (\text{II.28})$$

In addition, $\Delta_r G_m^\circ(\text{II.27}) = E^\circ(\text{II.27}) = \Delta_r H_m^\circ(\text{II.27}) = \Delta_r S_m^\circ(\text{II.27}) = 0$ by definition, at all temperatures.

By combining Reactions (II.26) and (II.27) we obtain:

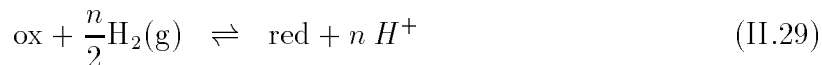


In contrast to Reaction (II.26), the equilibrium constant of the last equation can be measured. In the same way as for acid–base reactions it can be considered as the product of two equilibrium reactions but in this case involving free electrons rather than free protons.

Redox reactions like (II.26) are usually quantified in terms of their standard electrode (half-cell) potential, E° , which is identical to the electromotive force (emf) of a standard galvanic cell in which the reference electrode is the standard hydrogen electrode, SHE[†], in accordance with the “1953 Stockholm Convention” [88MIL/CVI]. This means that electrode potentials are given as *reduction potentials* relative to the standard hydrogen electrode, which acts as an electron donor (Reaction (II.27)). The sign of the standard electrode potential, E° , is that of the observed sign of its polarity when coupled with the standard hydrogen electrode. Several compilations of E° values may be found in the literature [71CHA/COL, 85BAR/PAR, 89BRA, *etc.*]. It must be noted that some older compilations of redox data report *oxidation* potentials instead (notably that of Latimer: *Oxidation Potentials of the Elements* [52LAT]).

In the standard hydrogen electrode (Reaction (II.27)), $\text{H}_2(\text{g})$ is at unit fugacity (an ideal gas at unit pressure, 1 bar); H^+ is at unit activity (*cf.* Section II.3.1); and the galvanic cell where the SHE is used has a negligible liquid junction potential. In general one does not use the standard hydrogen electrode in experimental studies, but secondary standards (*e.g.*, the Ag/AgCl electrode, or the calomel electrode) which are easy to work with, and whose electrode potentials are accurately known on the standard hydrogen electrode scale.

A general redox reaction between an oxidant “ox” and a reductant “red” may be written as:



The change in the Gibbs energy for this reaction is:

$$\Delta_r G_m(\text{II.29}) = \Delta_r G_m^\circ(\text{II.29}) + RT \ln \left(\frac{a_{\text{red}} a_{\text{H}^+}^n}{a_{\text{ox}} p_{\text{H}_2}^{n/2}} \right)$$

[†] The SHE stands for the standard hydrogen electrode, and SCE for the saturated calomel electrode. The abbreviation NHE has been widely used for the “normal hydrogen electrode”, which is by definition identical to the SHE. It should nevertheless be noted that NHE customarily refers to a standard state pressure of 1 atm, whereas SHE always refers to a standard state pressure of 1 bar (0.1 MPa).

The electrode potential is related to the Gibbs energy change, $\Delta_r G_m$, and to the equilibrium constant, K , as outlined in Eq. (II.30).

$$E(\text{II.29}) = -\frac{1}{nF} \Delta_r G_m(\text{II.29}) = \frac{RT \ln(10)}{nF} \log_{10} K(\text{II.29}) \quad (\text{II.30})$$

Setting p_{H_2} and a_{H^+} equal to unity:

$$\begin{aligned} \Delta_r G_m(\text{II.29}) &= \Delta_r G_m^\circ(\text{II.29}) - RT \ln \left(\frac{a_{\text{ox}}}{a_{\text{red}}} \right) \\ E(\text{II.29}) &= E^\circ(\text{II.29}) + \frac{RT}{nF} \ln \left(\frac{a_{\text{ox}}}{a_{\text{red}}} \right) \end{aligned} \quad (\text{II.31})$$

where the last equation is the familiar Nernst equation.

As described above, Reaction (II.29) may formally be written as two half-cell reactions:



The equilibrium constants for these reactions are denoted $K^\circ(\text{II.32})$ and $K^\circ(\text{II.27})$, respectively. They cannot be measured experimentally because we cannot measure the concentration/activity of free electrons in ordinary chemical systems.

The equilibrium constant for Eq. (II.29) is on the other hand a measureable quantity, and it is related to the equilibrium constants for the two half-cell reactions:

$$K^\circ(\text{II.29}) = (K^\circ(\text{II.27}))^n \times K^\circ(\text{II.32})$$

Introducing Eq. (II.28):

$$K^\circ(\text{II.29}) = K^\circ(\text{II.32}) = \frac{a_{\text{red}}}{a_{\text{ox}} a_{e^-}^n} \quad (\text{II.33})$$

In the literature on geochemical modelling of natural waters, it is customary to represent the “electron activity” of an aqueous solution with the symbol “pe” or “p ε ” (*defined* as: $\text{pe} = -\log_{10} a_{e^-}$) by analogy with pH ($= -\log_{10} a_{\text{H}^+}$), while the redox potential of an aqueous solution relative to the standard hydrogen electrode is usually denoted by either “Eh” or “ E_{H} ” (see for example [81STU/MOR, 82DRE, 84HOS, 94NOR/MUN]). The variable “pe” may be introduced in Eq. (II.33):

$$-\log_{10} a_{e^-} = \text{pe} = \frac{1}{n} \left(\log_{10} K^\circ + \log_{10} \frac{a_{\text{ox}}}{a_{\text{red}}} \right) \quad (\text{II.34})$$

At standard conditions the activities of reactants and products are unity ($a_{\text{red}} = a_{\text{ox}} = 1$), and the relation between pe° and E° is obtained:

$$\text{pe}^\circ = \frac{1}{n} \log_{10} K^\circ = \frac{FE^\circ}{RT \ln(10)} \quad (\text{II.35})$$

pe° may be introduced into Eq. (II.34):

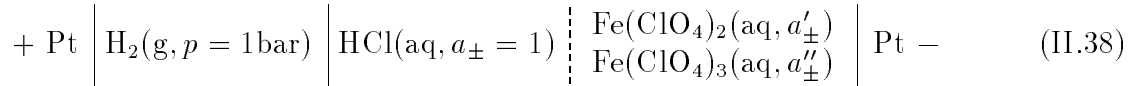
$$\text{pe} = \text{pe}^\circ + \frac{1}{n} \log_{10} \frac{a_{\text{ox}}}{a_{\text{red}}} \quad (\text{II.36})$$

Finally, the relation between a_{e^-} and the redox potential against the standard hydrogen electrode, E , may be obtained from Eqs. (II.31), (II.34), and (II.35):

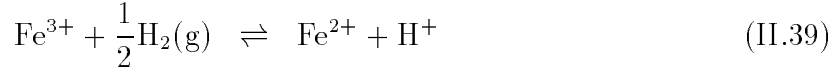
$$-\log_{10} a_{\text{e}^-} = \frac{F E}{RT \ln(10)} \quad (\text{II.37})$$

In chemical equilibrium modelling, both “ e^- ” and “ H^+ ” can be chosen as components and they can be treated numerically in a similar way: equilibrium constants, mass balance, *etc.* may be defined for both. However, while “ H^+ ” represents the hydrated proton in aqueous solution, “ e^- ” is not an aqueous species, and it is necessary to set its concentration to *zero* during the calculations (arbitrary values, however, may be assigned to a_{e^-} which are then related to E by Eq. (II.37)).

Example: For the hypothetical galvanic cell



(where “ $\left| \right|$ ” denotes a liquid junction; “ $\left| \right|$ ” a phase boundary; and a_{\pm} , a'_{\pm} , and a''_{\pm} are the mean ionic activities of HCl and of the ferrous and ferric perchlorates respectively), the cell reaction is:



For convenience Reaction (II.39) can be represented by half-cell reactions, each involving an equal number of “electrons”, as shown in the following equations



Equilibrium constants may be written for these half-cell reactions in the following way:

$$K^\circ(\text{II.40}) = \frac{a_{\text{Fe}^{2+}}}{a_{\text{Fe}^{3+}} a_{\text{e}^-}} \quad (\text{II.41})$$

$$K^\circ(\text{II.27}) = \frac{a_{\text{H}^+} a_{\text{e}^-}}{\sqrt{p_{\text{H}_2}}} = 1 \quad (\text{by definition}) \quad (\text{II.28})$$

and it follows that $K^\circ(\text{II.40}) = K^\circ(\text{II.39})$.

The following equation describes the redox potential of Reaction (II.39), if p_{H_2} and a_{H^+} are equal to unity (*cf.* Eq. (II.31)):

$$E(\text{II.39}) = E^\circ(\text{II.39}) + \frac{RT}{F} \ln \left(\frac{a_{\text{Fe}^{3+}}}{a_{\text{Fe}^{2+}}} \right)$$

The “activity of electrons” in Eqs. (II.28), (II.33), (II.34), and (II.41) may be interpreted to represent the relative tendency for a dissolved oxidant to accept electrons, or for electrons to “leave” the half-cell electrode. Alternatively, the symbol “ a_{e^-} ” might just be considered to be a mathematical representation of the function “ $\sqrt{p_{H_2}}/a_{H^+}$ ” (*cf.* Eq. (II.28)), and may therefore also be seen as equivalent to the standard electrode potential of the half-cell (*cf.* Eq. (II.37)).

II.1.9. pH

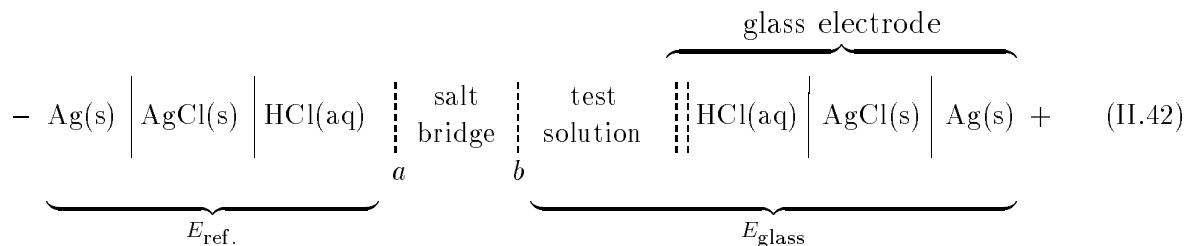
Because of the importance of potentiometric methods in the determination of the acidity of aqueous solutions, a short discussion on the definition of “pH” and a simplified description of the experimental techniques used to measure pH will be given here.

The acidity of aqueous solutions is often expressed in a logarithmic scale of the hydrogen ion activity. The definition of pH is

$$\text{pH} = -\log_{10} a_{H^+} = -\log_{10}(m_{H^+} \gamma_{H^+})$$

The activity can only be estimated from the known concentration of H^+ in the limited range of the Debye-Hückel equation (that is, in extremely diluted solutions). In practice the use of pH values requires extra assumptions on the values for single ion activities.

The determination of pH is often performed by emf measurements of galvanic cells involving liquid junctions [69ROS, 73BAT]. A common setup is a cell made up of a reference half-cell (*e.g.*, $\text{Ag(s)}/\text{AgCl(s)}$ in a solution of constant chloride concentration), a salt bridge, the test solution, and a glass electrode (which encloses a solution of constant acidity and an internal reference half-cell) corresponding to the following galvanic cell:



where “ \mid ” denotes a liquid junction, and “ \vdots ” stands for a glass membrane (permeable to hydrogen ions). The emf of such a cell is given by

$$E(II.42) = E_{\text{glass}} - E_{\text{ref.}} + E_j = E^{\circ'} + \frac{RT}{nF} \ln a_{H^+} + E_j$$

where $E_{\text{ref.}}$ and E_{glass} are the half cell potentials of the reference cell and the test solution half-cell, respectively, $E^{\circ'}$ is a constant, and E_j is the junction potential. The purpose of the salt bridge is to minimise the junction potentials in junctions “ a ” and “ b ” when the concentration in the test solution is varied. The method often used to reduce and control the value of E_j consists of using a saturated (or nearly saturated) solution of potassium chloride as salt bridge.

Because of the problems in eliminating the liquid junction potentials and in defining individual ionic activity coefficients, an “operational” definition of pH is given by IUPAC [88MIL/CVI]. This definition involves the measurement of pH differences between the test solution and standard solutions of known pH and similar ionic strength (in this way similar values of γ_{H^+} and E_j cancel each other when emf values are subtracted).

II.2. Units and conversion factors

Thermodynamic data are given according to the *Système International d’Unités* (SI units). The unit of energy is the joule. Some basic conversion factors, also for non-thermodynamic units, are given in Table II.3.

Table II.3: Unit conversion factors.

To convert from (non-SI unit symbol)	to (SI unit symbol)	multiply by
ångström (Å)	metre (m)	1×10^{-10} (exactly)
standard atmosphere (atm)	pascal (Pa)	1.01325×10^5 (exactly)
bar (bar)	pascal (Pa)	1×10^5 (exactly)
thermochemical calorie (cal)	joule (J)	4.184 (exactly)
entropy unit (e.u. $\equiv \text{cal} \cdot \text{K}^{-1} \cdot \text{mol}^{-1}$)	$\text{J} \cdot \text{K}^{-1} \cdot \text{mol}^{-1}$	4.184 (exactly)

Since a large part of the NEA-TDB project deals with the thermodynamics of aqueous solutions, the units describing the amount of dissolved substance are used very frequently. For convenience, this book uses “M” as an abbreviation of “ $\text{mol} \cdot \text{dm}^{-3}$ ” for molarity, c , and “m” as an abbreviation of “ $\text{mol} \cdot \text{kg}^{-1}$ ” for molality, m . It is often necessary to convert concentration data from molarity to molality and vice versa. This conversion is used for the ionic strength extrapolation of equilibrium constants by the specific ion interaction model which assumes molality units (*cf.* Chapter IX) and is made in the following way. Molality of a solute B, m_B , is defined as m_B moles of substance B dissolved in 1000 grams of pure water. Molarity, c_B , is defined as n_B moles of substance B dissolved in $(1000\rho - n_B M)$ grams of pure water, where ρ is the density of the solution and M the molar weight of the solute. From this it follows that

$$m_B = \frac{1000c_B}{1000\rho - c_B M}$$

Baes and Mesmer [76BAE/MES, p.439] give a table with conversion factors (from molarity to molality) for nine electrolytes and various ionic strengths. Conversion factors at 298.15 K for twenty one electrolytes, calculated using the density equations reported by Söhnel and Novotný [85SOH/NOV], are reported in Table II.4.

Table II.4: Factors ϱ for the conversion of molarity, c_B , to molality, m_B , of a substance B, in various media (calculated from densities in [85SOH/NOV]).

$c \text{ (M)}$	$\varrho = m_B/c_B \text{ (dm}^3 \text{ of solution per kg of H}_2\text{O)}$						
	HClO ₄	NaClO ₄	LiClO ₄	NH ₄ ClO ₄	Ba(ClO ₄) ₂	HCl	NaCl
0.10	1.00766	1.00753	1.00737	1.00912	1.01076	1.00478	1.00462
0.25	1.01472	1.01451	1.01409	1.01862	1.02307	1.00756	1.00722
0.50	1.02657	1.02646	1.02559	1.03508	1.04496	1.01231	1.01177
0.75	1.03860	1.03878	1.03743	1.05230	1.06846	1.01718	1.01654
1.00	1.05081	1.05148	1.04961	1.07028	1.09360	1.02215	1.02149
1.50	1.07588	1.07802	1.07504	1.10863	1.14911	1.03239	1.03189
2.00	1.10189	1.10617	1.10193		1.21248	1.04301	1.04292
3.00	1.15706	1.16776	1.16053		1.36888	1.06538	1.06677
4.00	1.21705	1.23743	1.22645			1.08925	1.09303
5.00	1.28264	1.31674				1.11471	1.12177
6.00	1.35474	1.40774				1.14184	
$c \text{ (M)}$	LiCl	KCl	NH ₄ Cl	MgCl ₂	CaCl ₂	HNO ₃	NaNO ₃
0.10	1.00488	1.00569	1.00663	1.00488	1.00435	1.00562	1.00578
0.25	1.00779	1.00991	1.01225	1.00798	1.00689	1.00974	1.01016
0.50	1.01272	1.01720	1.02187	1.01354	1.01187	1.01686	1.01775
0.75	1.01774	1.02477	1.03177	1.01949	1.01757	1.02425	1.02565
1.00	1.02285	1.03258	1.04196	1.02578	1.02390	1.03188	1.03383
1.50	1.03331	1.04894	1.06317	1.03929	1.03821	1.04784	1.05101
2.00	1.04408	1.06624	1.08552	1.05396	1.05459	1.06471	1.06925
3.00	1.06659	1.10372	1.13389	1.08670	1.09339	1.10123	1.10899
4.00	1.09041	1.14528	1.18768	1.12412	1.14065	1.14168	1.15340
5.00	1.11561		1.24767		1.19738	1.18646	1.20300
6.00	1.14226					1.23611	1.25852
$c \text{ (M)}$	LiNO ₃	NH ₄ NO ₃	H ₂ SO ₄	Na ₂ SO ₄	(NH ₄) ₂ SO ₄	H ₃ PO ₄	Na ₂ CO ₃
0.10	1.00587	1.00775	1.00635	1.00438	1.00816	1.00743	1.00273
0.25	1.01030	1.01506	1.01164	1.00713	1.01660	1.01428	1.00295
0.50	1.01784	1.02760	1.02087	1.01275	1.03191	1.02606	1.00427
0.75	1.02556	1.04054	1.03054	1.01936	1.04856	1.03825	1.00645
1.00	1.03345	1.05389	1.04061	1.02682	1.06648	1.05086	1.00935
1.50	1.04975	1.08184	1.06193	1.04406	1.10620	1.07731	1.01698
2.00	1.06673	1.11157	1.08482		1.15138	1.10550	1.02680
3.00	1.10285	1.17689	1.13553		1.26099	1.16755	
4.00	1.14202	1.25124	1.19353		1.40372	1.23827	
5.00	1.18458	1.33648	1.26000			1.31937	
6.00	1.23091	1.43508	1.33654			1.41313	

Examples:

$$\begin{aligned} 1.00 \text{ M NaClO}_4 &\equiv 1.05 \text{ m NaClO}_4 \\ 1.00 \text{ M NaCl} &\equiv 1.02 \text{ m NaCl} \\ 4.00 \text{ M NaClO}_4 &\equiv 4.95 \text{ m NaClO}_4 \\ 6.00 \text{ M NaNO}_3 &\equiv 7.55 \text{ m NaNO}_3 \end{aligned}$$

Equilibrium constants, unless they are dimensionless, need also to be converted if the concentration scale is changed from molarity to molality or vice versa. For a general equilibrium reaction, $0 = \sum_{\text{B}} \nu_{\text{B}} \text{B}$, the equilibrium constants can be expressed either in molarity or molality units, K_c or K_m , respectively:

$$\begin{aligned} \log_{10} K_c &= \sum_{\text{B}} \nu_{\text{B}} \log_{10} c_{\text{B}} \\ \log_{10} K_m &= \sum_{\text{B}} \nu_{\text{B}} \log_{10} m_{\text{B}} \end{aligned}$$

With $(m_{\text{B}}/c_{\text{B}}) = \varrho$, or $(\log_{10} m_{\text{B}} - \log_{10} c_{\text{B}}) = \log_{10} \varrho$, the relationship between K_c and K_m becomes very simple, as shown in Eq. (II.43).

$$\log_{10} K_m = \log_{10} K_c + \sum_{\text{B}} \nu_{\text{B}} \log_{10} \varrho \quad (\text{II.43})$$

$\sum_{\text{B}} \nu_{\text{B}}$ is the sum of the stoichiometric coefficients of the reaction, *cf.* Eq. (II.4), and the values of ϱ are the factors for the conversion of molarity to molality as tabulated in Table II.4 for several electrolyte media at 298.15 K. The uncertainty introduced by the use of Eq. (II.43) in the values of $\log_{10} K_m$ is probably $\leq \pm 0.001 \sum_{\text{B}} \nu_{\text{B}}$.

From the values in Table II.4 it can be seen that when dealing with very dilute solutions, molarity and molality may be used interchangeably, and $K_m \approx K_c$.

II.3. Standard and reference conditions

II.3.1. Standard state

A precise definition of the term “standard state” has been given by IUPAC [82LAF]. The fact that only changes in thermodynamic parameters, but not their absolute values, can be determined experimentally, makes it important to have a well-defined standard state, a “base line” to which the variations can be referred. The IUPAC [82LAF] definition of the standard state has been adopted in this book. The standard state pressure, $p^\circ = 0.1 \text{ MPa}$ (1 bar), has therefore also been adopted, *cf.* Section II.3.2. The application of the standard state principle to pure substances and mixtures is summarised below. It should be noted that the standard state is always linked to a reference temperature, *cf.* Section II.3.3.

- The standard state for a gaseous substance, whether pure or in a gaseous mixture, is the pure substance at the standard state pressure and in a (hypothetical) state in which it exhibits ideal gas behaviour.

Table II.5: Reference states for the elements at the reference temperature of 298.15 K [82WAG/EVA, 89COX/WAG].

O ₂	gaseous	Pb	crystalline, cubic
H ₂	gaseous	B	β , crystalline, rhombohedral
He	gaseous	Al	crystalline, cubic
Ne	gaseous	Zn	crystalline, hexagonal
Ar	gaseous	Cd	crystalline, hexagonal
Kr	gaseous	Hg	liquid
Xe	gaseous	Cu	crystalline, cubic
F ₂	gaseous	Ag	crystalline, cubic
Cl ₂	gaseous	Fe	crystalline, cubic
Br ₂	liquid	V	crystalline, cubic
I ₂	crystalline, orthorhombic	Ti	crystalline, hexagonal
S	crystalline, orthorhombic	U	crystalline, orthorhombic
Se	crystalline, hexagonal (“black”)	Th	crystalline, cubic
Te	crystalline, hexagonal	Be	crystalline, hexagonal
N ₂	gaseous	Mg	crystalline, hexagonal
P	crystalline, cubic (“white”)	Ca	crystalline, cubic
As	crystalline, rhombohedral (“grey”)	Sr	crystalline, cubic
Sb	crystalline, rhombohedral	Ba	crystalline, cubic
Bi	crystalline, rhombohedral	Li	crystalline, cubic
C	crystalline, hexagonal (graphite)	Na	crystalline, cubic
Si	crystalline, cubic	K	crystalline, cubic
Ge	crystalline, cubic	Rb	crystalline, cubic
Sn	crystalline, tetragonal (“white”)	Cs	crystalline, cubic

- The standard state for a pure liquid substance is (ordinarily) the pure liquid at the standard state pressure.
- The standard state for a pure solid substance is (ordinarily) the pure solid at the standard state pressure.
- The standard state for a solute B in a solution is defined as a hypothetical solution, at the standard state pressure, in which $m_B = m^\circ = 1 \text{ mol} \cdot \text{kg}^{-1}$, and in which the activity coefficient γ_B is unity. In order to compare thermodynamic data for a solute B in different aqueous ionic media it is necessary to use a common standard state, often that with pure water as the solvent.

It should be emphasised that the use of “ $^\circ$ ”, *e.g.*, in $\Delta_f H_m^\circ$, implies that the compound in question is in the standard state and that the elements are in their reference states. The reference states of the elements at the reference temperature (*cf.* Section II.3.3) are listed in Table II.5.

II.3.2. Standard state pressure

The standard state pressure recommended by the International Union of Pure and Applied Chemistry IUPAC [82LAF] is 0.1 MPa (1 bar). However, the majority of the thermodynamic data published in the scientific literature refer to the old standard state pressure of 1 “standard atmosphere” (= 0.101325 MPa). The difference between the thermodynamic data for the two standard state pressures is not large and lies in most cases within the experimental uncertainty limits. In practice the parameters affected by the change between these two standard state pressures are the Gibbs energy and entropy changes of all processes that involve gaseous species. Consequently, changes occur also in the Gibbs energies of formation of species that consist of elements whose reference state is gaseous (H, O, F, Cl, N, and the noble gases). No other parameters are affected significantly. A discussion on the procedure to convert thermodynamic data for the small pressure change from 1 atm to 1 bar (0.1 MPa) is given in [82WAG/EVA], see also Freeman [84FRE] and the NEA reviews on the thermochemistry of uranium and americium [92GRE/FUG, 95SIL/BID].

II.3.3. Reference temperature

The definitions of standard states given in Section II.3 make no reference to fixed temperature. Hence, it is theoretically possible to have an infinite number of standard states of a substance as the temperature varies. It is, however, convenient to complete the definition of the standard state in a particular context by choosing a reference temperature. As recommended by IUPAC [82LAF], the reference temperature chosen in this book is $T = 298.15$ K or $t = 25^\circ\text{C}$. Where necessary for the discussion, values of experimentally measured temperatures are reported after conversion to the IPTS-68 [69COM]. The relation between the absolute temperature T (K, kelvin) and the Celsius temperature t ($^\circ\text{C}$) is defined by $t = (T - T_0)$ where $T_0 = 273.15$ K.

II.4. Fundamental physical constants

The fundamental physical constants are taken from a recent publication by CODATA [86COD]. Those relevant to this book are listed in Table II.6.

II.5. Graphical representations of equilibrium systems

It is practical to use graphical displays of various types to obtain an overview of the chemistry of equilibrium systems. There is an abundance of computer programs that allow the user to make virtually any type of display with any chosen set of variables. We will only give a few examples here. The reader will find many more equilibrium diagrams in the following Chapters.

In this context *master variables* is an important concept [52SIL, 59SIL]. These are usually the activities of components and they determine the ratios of the various species

Table II.6: Values for some fundamental physical constants. These values have been taken from CODATA [86COD]. The digits in parentheses are the one-standard-deviation uncertainty in the last digits of the given value.

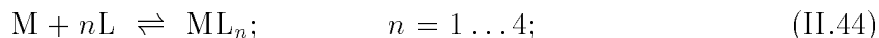
Quantity	Symbol	Value	Units
speed of light in vacuum	c	299 792 458	$\text{m} \cdot \text{s}^{-1}$
permeability of vacuum	μ_0	$4\pi \times 10^{-7}$ $= 12.566\,370\,614 \dots$	$10^{-7} \text{ N} \cdot \text{A}^{-2}$
permittivity of vacuum	ϵ_0	$1/\mu_0 c^2$ $= 8.854\,187\,817 \dots$	$10^{-12} \text{ C}^2 \cdot \text{J}^{-1} \cdot \text{m}^{-1}$
Planck constant	h	6.626 0755(40)	$10^{-34} \text{ J} \cdot \text{s}$
elementary charge	e	1.602 177 33(49)	10^{-19} C
Avogadro constant	N_A	6.022 1367(36)	10^{23} mol^{-1}
Faraday constant, $N_A \times e$	F	96 485.309(29)	$\text{C} \cdot \text{mol}^{-1}$
molar gas constant	R	8.314 510(70)	$\text{J} \cdot \text{K}^{-1} \cdot \text{mol}^{-1}$
Boltzmann constant, R/N_A	k	1.380 658(12)	$10^{-23} \text{ J} \cdot \text{K}^{-1}$
Non-SI units used with SI:			
electron volt, $(e/C) \text{ J}$	eV	1.602 177 33(49)	10^{-19} J
atomic mass unit, $1\text{u} = m_{\text{u}} = \frac{1}{12} m(^{12}\text{C})$	u	1.660 5402(10)	10^{-27} kg

in a chemical equilibrium system. For example, in acid-base equilibria pH is a master variable, and for metal complex formation the activity of the free ligand is another master variable.

A common simplification when constructing equilibrium diagrams is to use standard conditions (for aqueous solutions this implies that activity coefficients are assumed constant and ≈ 1). This assumption seldom affects the usefulness of the chemical information displayed in the diagram.

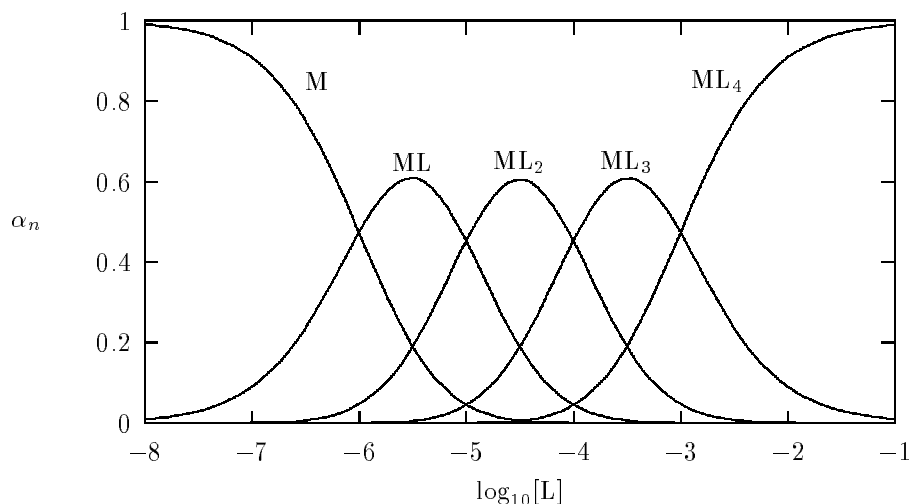
Species distribution diagrams and plots of the *average number of ligands* bonded to a metal ion are often useful, both when evaluating published information and for describing chemical aspects of more complex systems.

Example: We will illustrate the principle by constructing such diagrams for a binary, mononuclear system where the following reactions occur:



and where the overall equilibrium constants for these reactions are: $\log_{10} \beta_n = 6, 11, 15$, and 18 (for $n = 1 \dots 4$).

Figure II.1: Distribution functions for metal complexes



The most useful master variable in this system is the *free ligand concentration* $[L]$. The species distribution curves may be expressed as:

$$\alpha_n = \frac{[ML_n]}{[M] + \sum [ML_n]} = \frac{[ML_n]}{[M]_{\text{total}}} \quad (\text{II.45})$$

where α_n is the fraction of the total metal in the complexed form “ ML_n ”. The *average ligand number*, \bar{n} , is defined as follows:

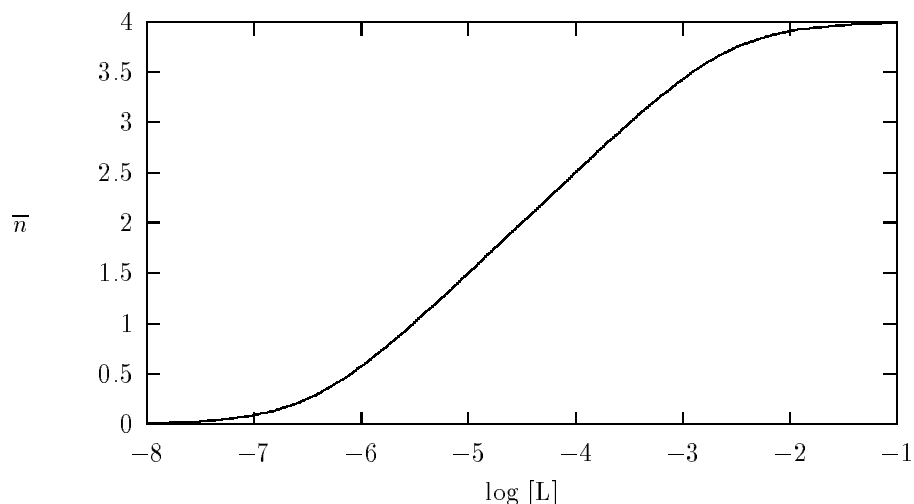
$$\bar{n} = \frac{\sum n[ML_n]}{[M] + \sum [ML_n]} = \frac{[L]_{\text{total as complex}}}{[M]_{\text{total}}} \quad (\text{II.46})$$

where \bar{n} is the ratio of non-free ligand (*i.e.*, ligand in complexes) to the total metal concentration.

Figures II.1 and II.2 illustrate how complexes are formed and transformed when the ligand concentration changes. The $\bar{n}([L])$ function demonstrates both the maximum number of ligands that can be coordinated, and the “rest-bonding” capacity of the metal ion. The function can also be used to get a quick estimate of the predominating complexes in a given system. If $\bar{n} = 1.5$ in a mononuclear system, the predominating complexes are in general ML and ML_2 .

The distribution curves show how the concentration of the various species change with varying free ligand concentration. This information is important when assessing the quality of experimental equilibrium data used to obtain equilibrium constants. In order to determine an equilibrium constant for a certain complex accurately, it is necessary that the complex is present in measurable amounts in the test solutions. This can always be

Figure II.2: Ligand average curve for the same metal complexation system displayed in Figure II.1



ascertained by calculating the distribution functions for the conditions used in the experiments. If an equilibrium constant has been reported from data where the complex is present in very low concentration, it should be looked upon with caution.

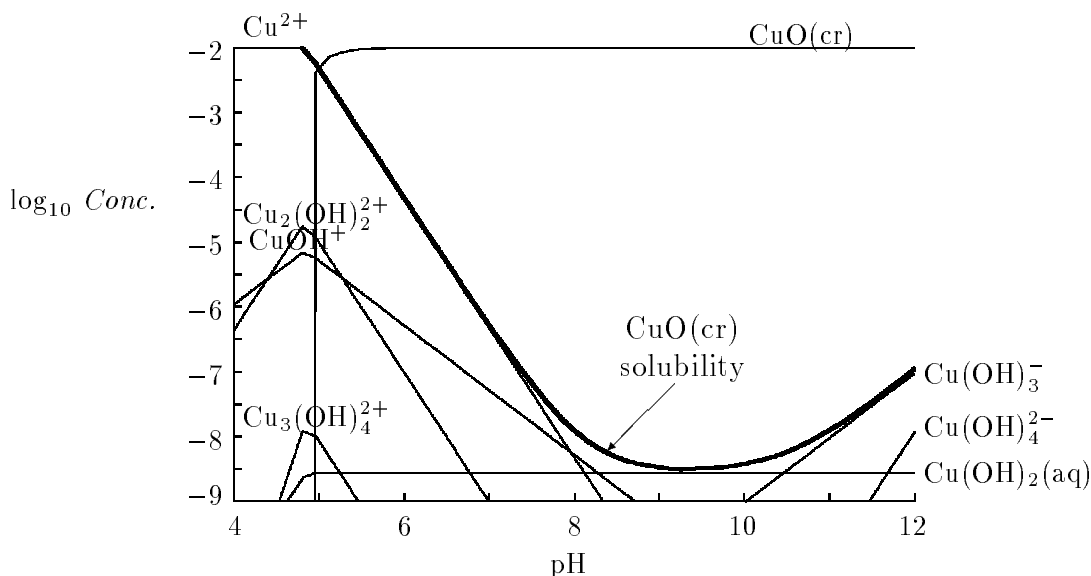
Distribution curves in systems where polynuclear complexes are formed may be calculated according to:

$$\alpha_{n,m} = \frac{m [M_m L_n]}{[M] + \sum m [M_m L_n]} = \frac{m [M_m L_n]}{[M]_{\text{total}}} \quad (\text{II.47})$$

and $\alpha_{n,m}$ depends both on the free ligand concentration **and** the total concentration of metal ion, and therefore, distribution curves in polynuclear systems require a three-dimensional representation. A practical way to achieve this is to calculate a set of distribution curves where one variable is kept constant, *e.g.*, $\alpha_{n,m} = f([L]_M)$, where the subscript “M” denotes that the distribution diagram has been calculated at a specific, constant value of the total concentration of M.

Logarithmic diagrams are perhaps easier to construct manually because they consist mostly of straight lines. In these diagrams, the logarithm of the concentration of aqueous species is plotted against the logarithm of the concentration of an appropriate master variable. A logarithmic diagram that illustrates the hydrolysis of Cu(II) is shown in Figure II.3. Similar diagrams for most metal cations are found in the review of metal hydrolysis by Baes and Mesmer [76BAE/MES]. To illustrate how logarithmic diagrams may be constructed, the curve corresponding to CuOH^+ in Figure II.3 will be used as an example. This curve can be divided into two pH ranges:

Figure II.3: Logarithmic diagram for copper(II) at $[\text{Cu}^{2+}]_{TOT} = 0.01 \text{ M}$ and at 25°C (neglecting activity coefficients). The diagram shows both the logarithm of the concentrations of copper(II) species and the solubility of $\text{CuO}(\text{cr})$ as a function of pH.



- at $\text{pH} < 5$ the reaction to be considered is: $\text{Cu}^{2+} + \text{H}_2\text{O}(\text{l}) \rightleftharpoons \text{CuOH}^+ + \text{H}^+$, with $\log_{10} {}^*K_1 = -7.96$, and

$$\log_{10}[\text{CuOH}^+] = 7.96 + \text{pH} + \log_{10}[\text{Cu}^{2+}]$$

As it can be assumed that $[\text{CuOH}^+] \ll [\text{Cu}^{2+}]$, that is, $[\text{Cu}^{2+}] \approx [\text{Cu}^{2+}]_{TOT}$, it follows that $\log_{10}[\text{CuOH}^+]$ can be represented as a line of slope +1 against pH.

- at $\text{pH} > 5$ and at $[\text{Cu}^{2+}]_{TOT} = 0.01 \text{ M}$, the oxide of copper(II), $\text{CuO}(\text{cr})$, precipitates and the following reaction must be considered: $\text{CuO}(\text{cr}) + \text{H}^+ \rightleftharpoons \text{CuOH}^+$, with $\log_{10} {}^*K_{s,1} = -0.29$, and

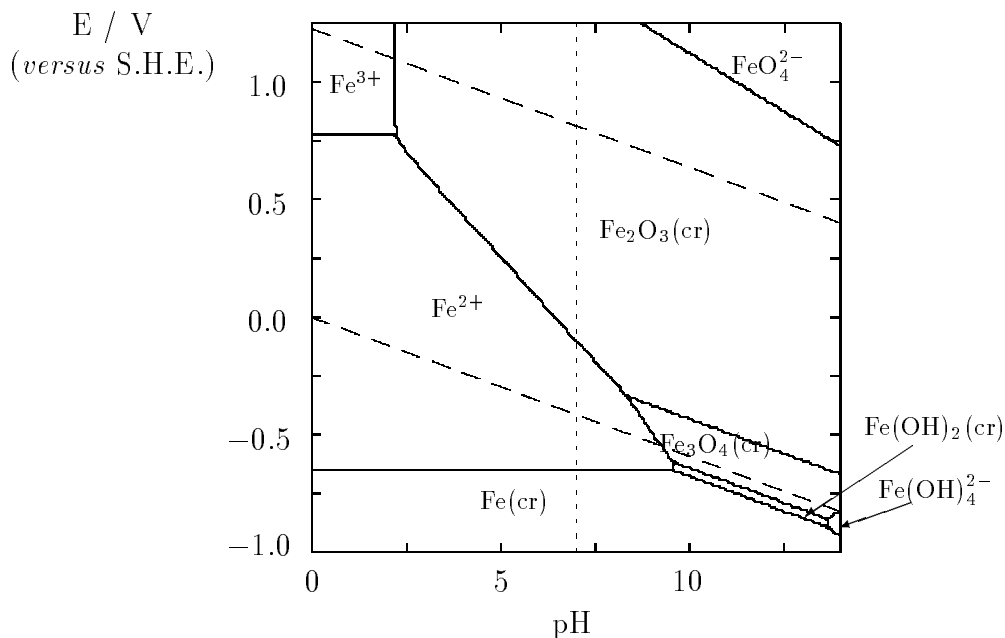
$$\log_{10}[\text{CuOH}^+] = -0.29 - \text{pH}.$$

Therefore $\log_{10}[\text{CuOH}^+]$ in this pH range can be represented by a line of slope -1 in Figure II.3.

Predominance area diagrams are used to display the chemical characteristics of systems that require at least two independent variables for their description, one for each axis.

The stability areas of solid phases can be given in a predominance area diagram as contour lines for specific total concentrations, in a way analogous to that used to describe the elevation on a topographic map. This procedure is used *e.g.*, to construct Pourbaix diagrams, usually by setting $[\text{M}]_{TOT} = 10^{-6} \text{ M}$. Pourbaix diagrams are also called potential/pH diagrams because of the choice of variables on the axes of the diagrams, and

Figure II.4: Pourbaix diagram (potential/pH predominance diagram) for iron at $[\text{Fe}]_{TOT} = 10^{-6}$ M and at 25°C (assuming unity for all activity coefficients). The vertical dotted line shows the neutral pH, that is, the value at which $a_{\text{H}^+} = a_{\text{OH}^-}$. The sloping dashed lines show the stability area of water. Adapted from [96BEV/PUI].



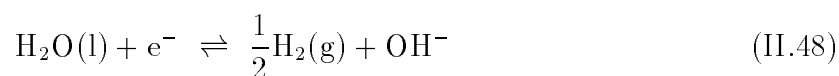
they are extensively used in corrosion science. Diagrams for most metallic elements can be found in Pourbaix's "Atlas" [74POU], as well as in refs. [65GAR/CHR, 83CHE/ARA, 88BRO, 92SAT, *etc.*].

Figure II.4 shows an example of a Pourbaix diagram.

These diagrams indicate areas where corrosion is thermodynamically impossible (the area where $\text{Fe}(\text{cr})$ is stable in Figure II.4; this has very little practical importance in the iron system since it is outside the stability range of water), areas where the reaction product is a solid phase that may inhibit the corrosion (passivation by the formation of a solid diffusion barrier, *e.g.*, in the case of iron: magnetite, $\text{Fe}_3\text{O}_4(\text{cr})$, and hematite, $\text{Fe}_2\text{O}_3(\text{cr})$), and finally areas where there is active corrosion (*i.e.*, where a dissolved species is the stable product). The reader should compare the iron diagrams in Figures I.9 and II.4.

The technique used to draw Pourbaix diagrams has been described in the literature [50DEL/POU, 65GAR/CHR, 74VAL, 81STU/MOR, *etc.*]. The method will be outlined here.

The stability field of water will be used first as an example. Water can be reduced according to:



Alternatively, and adding the ionic product of water ($\text{H}_2\text{O(l)} \rightleftharpoons \text{H}^+ + \text{OH}^-$):

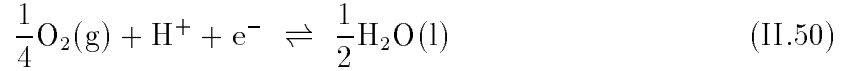


From Eq. (II.31), and taking into account that the equilibrium constant for the last reaction is equal to one by definition (*cf.* Eq. (II.28)) and that its redox potential against the standard hydrogen electrode is $E^\circ(\text{II.27}) = 0$:

$$E(\text{II.27}) = -\frac{RT \ln(10)}{F} (0.5 \log_{10} p_{\text{H}_2} + \text{pH}) \quad (\text{II.49})$$

By setting the partial pressure of hydrogen gas constant and equal to 1 bar, this equation represents a line with a slope [†] of -0.06 V/pH in the potential/pH diagram, represented by the lower dashed sloping line in Pourbaix diagrams, *cf.* Figure II.4. At potentials below this line $\text{H}_2(\text{g})$ evolution is possible ($p_{\text{H}_2} > 1 \text{ bar}$).

The upper sloping dashed line in Pourbaix diagrams is that corresponding to water oxidation

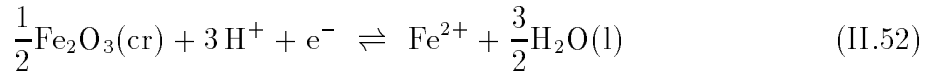


and from Eq. (II.31):

$$E(\text{II.50}) = E^\circ(\text{II.50}) - \frac{RT \ln(10)}{F} (\text{pH} - 0.25 \log_{10} p_{\text{O}_2}) \quad (\text{II.51})$$

Again, by setting the partial pressure of oxygen gas constant and equal to 1 bar, this equation represents a line with slope -0.06 in the potential/pH diagram. At potentials above this line $\text{O}_2(\text{g})$ evolution is possible ($p_{\text{O}_2} > 1 \text{ bar}$).

The following reaction shows an example involving an aqueous species and a solid phase:



Again, Eq. (II.31) is used:

$$E(\text{II.52}) = E^\circ(\text{II.52}) - \frac{RT \ln(10)}{F} (3 \text{pH} + \log_{10} a_{\text{Fe}^{2+}}) \quad (\text{II.53})$$

This equation constitutes a line of slope -0.18 V/pH in the Pourbaix diagrams (Figure II.4) for any given value of the activity of Fe^{2+} . Usually the activity of Fe^{2+} is set equal to 10^{-6} M , the limit at which corrosion is considered to be noticeable.

The line represented by Eq. (II.50) will appear in the Pourbaix diagram under the following conditions:

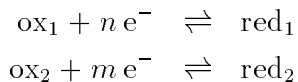
- $a_{\text{Fe}^{2+}} = [\text{Fe}]_{\text{TOT}} = 10^{-6} \text{ M}$, which is appropriate only at potentials where Fe^{2+} predominates over Fe^{3+} .

[†] $RT \ln(10)/F = 0.05916 \text{ V} \approx 0.06 \text{ V}$ at $T = 298.15 \text{ K}$ (25.00°C).

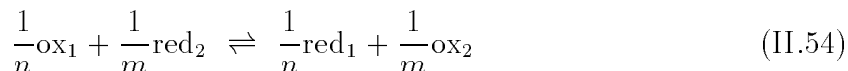
- At acidities where no Fe(II) hydrolysis occurs (ferrous iron starts to hydrolyze at $\text{pH} \geq 8$ [76BAE/MES]).

It may be seen in Figure II.4 that these two conditions are fulfilled between $\text{pH} \approx 2$ and 8, where the line between Fe^{2+} and $\text{Fe}_2\text{O}_3(\text{cr})$ has been drawn.

An interesting property of potential/pH diagrams is that they show which oxidations are thermodynamically possible, for example by superposing diagrams for two elements. This may be seen by considering two redox reactions:



with standard redox potentials E_1° and E_2° . These two equilibria may be combined into a single reaction:

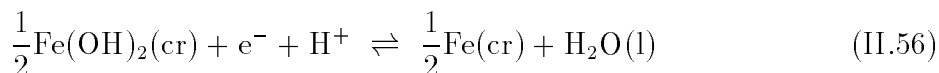


with the following equilibrium constant:

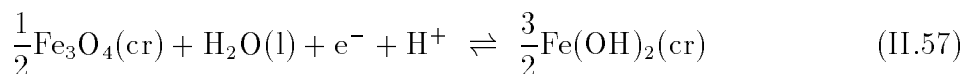
$$\log_{10} K^\circ(\text{II.54}) = (E_1^\circ - E_2^\circ) \frac{F}{RT \ln(10)} \quad (\text{II.55})$$

It follows that if $E_1^\circ > E_2^\circ$, then Reaction (II.54) will proceed to the right, and the oxidant “ox₁” will react with “red₂”. For example, a comparison of the $\text{Fe}^{3+}/\text{Fe}^{2+}$ line with the lower sloping dotted line in Figure II.4 shows that acidic Fe(III) aqueous solutions will react with $\text{H}_2(\text{g})$ to produce Fe^{2+} and H^+ .

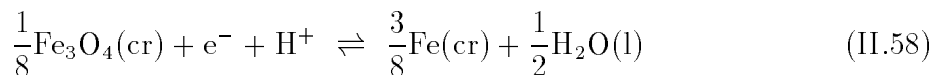
Finally, the stability area of $\text{Fe}(\text{OH})_2(\text{cr})$ will be discussed. When studying the corrosion properties of iron at near neutral pH, it is of interest to find out if the oxidation of iron can proceed through the formation of iron(II) hydroxide:



followed eventually by further oxidation to magnetite,



perhaps continued by oxidation into hematite, *etc.*, or if thermodynamic considerations indicate that iron metal oxidation might result in the direct formation of magnetite:



Reactions (II.56) to (II.57) have all been written as one electron reductions, because then:

$$E = E^\circ - \frac{RT \ln(10)}{F} \text{pH}$$

for all three reactions, each with a different value of E° . All three reactions may then be represented by parallel lines of slope -0.06 V/pH in the Pourbaix diagram of iron. For any given pH-value, Eq. (II.31) (the Nernst equation) indicates that:

- At $E > E^\circ(\text{II.56})$ iron metal will be oxidized to $\text{Fe}(\text{OH})_2(\text{cr})$.
- At $E > E^\circ(\text{II.57})$ ferrous hydroxide will be oxidized to magnetite.
- At potentials above $E^\circ(\text{II.58})$ the oxidant (magnetite, $\text{Fe}_3\text{O}_4(\text{cr})$) predominates over the reductant (iron metal).

To find out the thermodynamic ranking of the oxidation products of $\text{Fe}(\text{cr})$ we may use the rule expressed by Eq. (II.55). In the example, where the pH dependence is the same in all three reactions, we find that if $E^\circ(\text{II.56}) < E^\circ(\text{II.57})$ then $\text{Fe}(\text{OH})_2(\text{cr})$ will be formed. Note that thermodynamic data from different compilations may be contradictory. For example,

- From the data listed in the NBS tables [82WAG/EVA]: $E^\circ(\text{II.56}) = -0.06 \text{ V}$, and $E^\circ(\text{II.57}) = -0.16 \text{ V}$, indicating that $\text{Fe}(\text{OH})_2(\text{cr})$ is not stable and it should decompose into magnetite and iron metal.
- From the JANAF tables [85CHA/DAV]: $E^\circ(\text{II.56}) = -0.09 \text{ V}$, and $E^\circ(\text{II.57}) = -0.08 \text{ V}$, indicating a narrow range of existence for $\text{Fe}(\text{OH})_2(\text{cr})$.

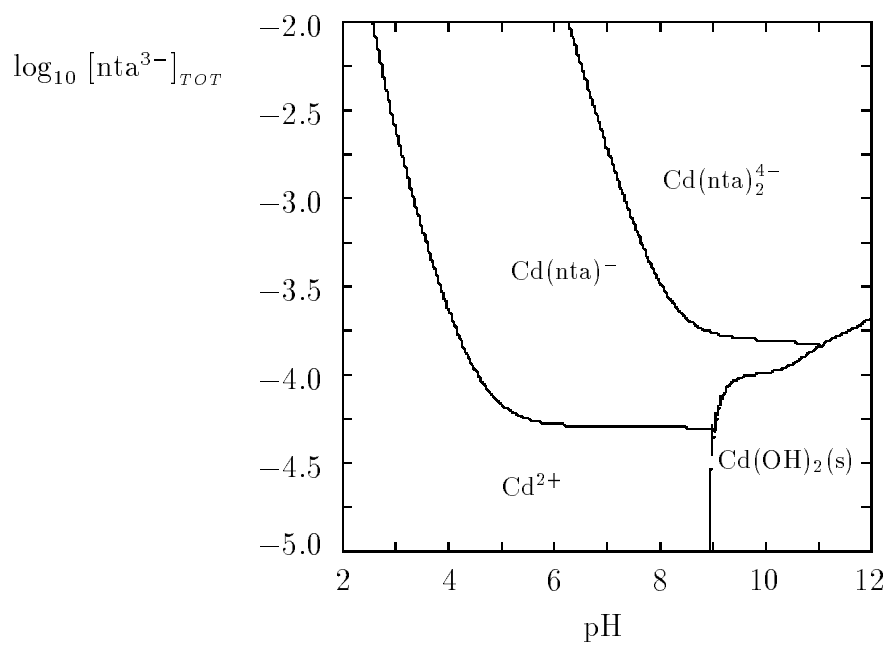
The stability area for iron(II) hydroxide, shown in Figure II.4), is therefore in agreement with the data in the JANAF tables, but not with those in the NBS tables.

Predominance area diagrams can be drawn using any type of variables on the axes. One example is shown in Figure II.5, which depicts the regions of predominance for cadmium complexes as the total ligand/metal concentration ratio is increased.

In Figures II.4 and II.5 the lines between two aqueous species represent equilibria between the species on both sides, *along* the line their concentrations are equal. Within the areas, one or the other aqueous species is present at a larger concentration. As mentioned earlier, lines separating a solid and an aqueous species are contour lines showing the coordinates at which the solid reaches saturation. Lines between two solids show their respective limits of stability.

Chemical equilibrium diagrams (Figures II.3 to II.5) have been drawn here with computer software [83PU1] using the chemical compositions calculated with the SOLGASWATER algorithm [79ERI]. This technique differs slightly from the procedures described above because the computer programs must be able to deal with a wide range of chemical possibilities. Nevertheless, the basic principles behind the programs are those given above.

Figure II.5: Predominance diagram for the system Cd^{2+} - OH^- - nta^{3-} for $[\text{Cd}^{2+}]_{TOT} = 10^{-4} \text{ M}$, at standard conditions and at 25°C (nta^{3-} stands for the nitrilotriacetate anion)



Chapter III

Chemical Background for the Modelling of Reactions in Aqueous Systems

Ingmar GRENTHE
Department of Inorganic Chemistry
Royal Institute of Technology
S-100 44 Stockholm (Sweden)

Ignasi PUIGDOMENECH
Department of Inorganic Chemistry
Royal Institute of Technology
S-100 44 Stockholm (Sweden)

Wolfgang HUMMEL
Waste Management Laboratory
Paul Scherrer Institut
CH-5232 Villigen PSI (Switzerland)

III.1. Introduction

Chemistry, like all sciences, has its particular set of theories, procedures and experimental methods which form the “language” used to communicate chemical information and ideas. It is necessary to be familiar both with the “grammar” and the “vocabulary” of this language in order to use and develop chemical information. For this reason we have included a chapter dealing with fundamental chemical concepts, some of which may already be known to the reader. These will be used to provide a framework useful for a discussion of the chemistry of aqueous solutions and the modelling of aquatic systems. The discussion will be short, but the reader should be able to obtain a more comprehensive picture by using the references.

Most chemical information has been obtained in laboratory systems under well defined conditions, where one in general has tried to reduce the number of variables as much as possible in order to reduce the complexity of the system and to focus on the *particular* aspects of interest in the study. This may result in a bias of the available experimental

information; as an example there is an abundance of thermodynamic data for complex formation reactions in binary systems, but comparatively few for ternary and higher systems. This imbalance does *not* reflect the relative importance of the two groups, but rather the interests of the experimentalists.

Chemists have developed precise *analytical tools* for the determination of the total concentrations of various components, and also in very complicated systems such as the ones encountered in nature. This information is *one* essential component for the understanding and description of the chemical processes taking place there. But more is required. It is necessary to describe the *chemical interactions* between the components, a task that requires both an understanding of *why* and *how* chemical reactions occur. This is a formidable task which cannot be solved by “brute force”, *i.e.*, investigations in the laboratory of all possible chemical events that may take place. It is often necessary to simplify the description of the system by identifying the most important processes. Laboratory data, but also chemical theories, play an important role in this step. The properties of such a *model* of the real system, *cf.* Chapter I, can then be compared with those of the real system, *e.g.*, by confirmatory experiments.

This exercise requires the use of various types of heuristic chemical models, as described in this chapter. Note that a model is a device used to describe some particular aspects of a complex issue; a model is based on certain assumptions; these have to be specified and checked for relevance; each model has its own range of applications. There is nothing contradictory in the use of different models to describe a certain system, because they emphasise different aspects of its properties. The only requirement on the model is that it should be self-consistent and produce useful results, such as describing a given set of experimental observations and being able to predict the outcome of new ones.

Chemistry deals with the properties of chemical elements and their compounds. A key point in *any* chemical discussion is the understanding of chemical reactivity, *i.e.*, how chemical elements react to form chemical compounds, and how these compounds may be transformed into new ones. Chemical reactivity is obviously important also for the understanding of aquatic systems because these obtain many of their properties as a result of chemical transformations.

The phenomenological description of chemical systems relies on the two scientific disciplines, *chemical thermodynamics* (which “explains” why chemical reactions occur) and *chemical kinetics* (which explains how they occur). Classical chemical thermodynamics (as used in this book) deals only with *two* states of the chemical system, the *initial* and the *final* state. The initial state represents the condition where all reactants are present, but where *no* reaction has yet occurred. In the same way the final state represents the system when the possible chemical reactions have occurred (within the time-frame of interest, *cf.* the concept *pseudo-equilibrium* on p.127) and no further changes takes place (equilibrium systems). Thermodynamics provides information about the *possible* changes in the system, expressed in terms of changes in the thermodynamic properties used to describe it.

It is common knowledge that chemical reactions which have a net thermodynamic driving force do not always occur with measurable rates. One example is a mixture of

hydrogen and oxygen, where no reaction takes place unless the reaction is *initiated* by a spark, or the introduction of a catalyst, such as a speck of platinum. Another is an aqueous system containing sulfate and hydrogen sulfide, where it is impossible to attain redox equilibrium, unless the temperature is well above 200°C, *cf.* p.127.

The corollary to these observations is that chemical reactions may be controlled both by thermodynamics and kinetics. We will come back to this issue in Section III.7.

By using tabulated thermodynamic data it is possible to decide *if* a particular reaction may occur, or not, and also the extent of that reaction. Thermodynamic data are tabulated for specific *standard conditions* which often differ from those in the system studied. Thermodynamics, in combination with physico-chemical theories such as the Debye-Hückel model, also provides the framework for recalculation of standard state data to any desired condition as described in Chapters IX and X.

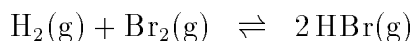
Chemical thermodynamics is a well established discipline both experimentally and theoretically. The extensive information included in thermodynamic databases and compilations of equilibrium constants for chemical reactions (*cf.* Section I.6.1) are impressive examples of its experimental success.

Chemists and physicists have always been interested to link thermodynamics to information on the atomic/molecular level, and in a following section we will outline how such connections may be established for solution chemical data. The importance of the procedures described there is that they provide a framework for *estimating* data where no experimental information is available.

The first step in any description of a complex chemical system is usually based on a thermodynamic model. There are several reasons for this:

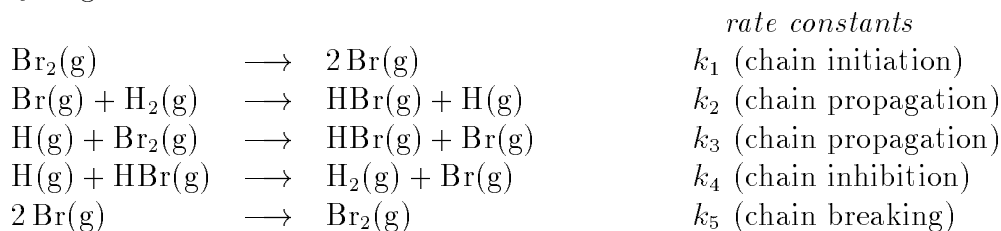
- The thermodynamic model provides information on the possible reactions that may take place in the system, and their relative importance, provided that the equilibrium assumption is valid. Hence, it is often possible to *reduce* the complexity of the system by neglecting interactions between some of the components.
- There may be no information on rates and mechanisms of the reactions taking place in the system and the modeller is therefore *forced* to use a simpler approach, such as that provided by thermodynamics.

All chemical reactions involve the breaking and creation of chemical bonds – the reaction between hydrogen and bromine can be described on two levels of sophistication, the first indicates only the *reactants* and the *products*, and their mass balance, *i.e.*,:



Stoichiometric equations of this type are sufficient for the thermodynamic characterisation of the reaction. They indicate the obvious that chemical bonds are both broken and formed in the reaction, but they do not tell us *how these events take place*. Such information may be deduced from experiments where the rate of reaction is studied as a function of the concentrations of the species present in the system, and the temperature. This is the area of chemical kinetics.

The set of *elementary reactions* describing the transformation of hydrogen and bromine to hydrogen bromide are:



This sequence of elementary reactions is compatible with the experimental *rate law*

$$\begin{aligned}\frac{d[\text{HBr}]}{dt} &= \frac{k_a[\text{H}_2][\text{Br}_2]^{1/2}}{k_b + [\text{HBr}][\text{Br}_2]^{-1}} \\ &= 2 \frac{k_2 k_3 k_4^{-1} k_1^{1/2} k_5^{-1/2} [\text{H}_2][\text{Br}_2]^{1/2}}{k_3 k_4^{-1} + [\text{HBr}][\text{Br}_2]^{-1}}\end{aligned}$$

which describes how the rate of reaction is influenced by the various rate constants k_i , and the concentrations of the components. This example illustrates the important difference in complexity between thermodynamics and kinetics. In Section III.7 we will make some general comments on the importance of chemical kinetics for the description of processes in aquatic systems.

In chemistry we are interested to relate the chemical processes to the properties of the particular reactants (and products), or sometimes to a particular reaction center in a complex molecule or ion. The “translation” of macroscopic information from thermodynamics to “molecular” theories is not straightforward (the reverse process is dealt with in statistical thermodynamics). The following sections will illustrate the reasoning, but also point out some inherent weaknesses in these procedures.

III.2. Factors that influence the equilibrium properties of chemical reactions in aqueous systems

The following discussion deals with equilibrium reactions involving acid/base, complex formation, and redox processes in both homogeneous and heterogeneous systems. The reactants are in general *metal ions* and *ligands* of various types. We will mainly be concerned with phenomena that are common for a large group of these reactions. Chemical reactions depend on the chemical characteristics of *both* metal ions and ligands, but also on the special properties of the solvent, as indicated in the following.

III.2.1. Chemical characteristics of metal ions

In this section we will discuss the *charge*, *size*, *coordination number*, *acceptor properties* and *hydration* characteristics of metal ions.

Chemists use two “limiting” models to describe chemical bonding. One extreme is the *ionic model*, where classical electrostatics is used to describe ion-ion and ion-dipole interactions [65PHI/WIL, 87COT/WIL]; the other extreme is the *covalent model*, where chemical bonding is described as a result of the “sharing” of electrons between the atoms forming the bond. Neither of these models is the “right” one – they describe different aspects of the chemical bond.

The charge of a metal ion is determined by, but not always equal to, its oxidation state.

Example 1:

The alkali metals occur in aqueous solution as single charged ions M^+ , *i.e.* the oxidation state +1. The chemistry of zirconium and hafnium is dominated by the oxidation state +4, and they occur in strongly acid aqueous solution as aquo ions M^{4+} (the reason for the statement about the acidity is explained on p.78). Uranium may occur in four different oxidation states +3, +4, +5, and +6. The corresponding aquo ions are U^{3+} , U^{4+} , UO_2^+ and UO_2^{2+} . The actual oxidation state of a given element, and the occurrence of elements with different oxidation states is determined by the electron configuration of the element. Textbooks on general chemistry provide more details (*e.g.*, [84GRE/EAR, 88COT/WIL]). It should also be pointed out that some of the oxidation states may not be stable in aqueous solutions because of redox reactions with the solvent, *e.g.*, aqueous U^{3+} reduces water rapidly, with the formation of hydrogen and U^{4+} aquo ions.

A metal ion is also characterised by its size. The *ionic radius* is deduced from experimental determinations of bond distances in different compounds. It is not a true constant, but varies with the coordination number (this variation is known and tabulations of ionic radii always refer to a specific coordination number). There is also a slight variation, often less than a few percent, between different chemical compounds. A list of ionic radii for the elements is provided by Prewitt and Shannon [69SHA/PRE, 76SHA].

The ionic radius is important for a discussion of the *coordination number* of metal ions. This is defined as the number of atoms that are bonded to the metal ion in a given compound. Small coordination numbers are in general found for ions of small radii (often in combination with large donor atoms), while large coordination numbers are encountered for the larger ions. Lanthanide and actinide elements in oxidation states +3 and +4 have large radii for their high charge and their coordination numbers are therefore high – eight and nine are common, and even twelve coordination may occur for certain ligands, *e.g.*, nitrate. The coordination number is often a constant for a given metal ion, but exceptions do occur, some examples of the characteristic coordination numbers for different metal ions are given in Table III.1.

The coordination number depends not only on the characteristics of the metal ion, but also on the properties of the ligand, *e.g.*, the cadmium(II) aquo ion, $Cd(H_2O)_6^{2+}$, is octahedral while the highest iodide complex, CdI_4^{2-} , is tetrahedral. Hg(II) is another example where the coordination geometry ranges from octahedral in $Hg(H_2O)_6^{2+}$, via a trigonal bipyramid geometry in $HgI_2(aq)$ and HgI_3^- to tetrahedral in HgI_4^{2-} . It is necessary to be

Table III.1: Coordination numbers and geometry for some metal ions and their complexes. The less common coordination numbers are given within parenthesis.

Metal ion	Coordination number	Coordination geometry	Examples
Li^+	4	tetrahedral	$\text{Li}(\text{H}_2\text{O})_4^+$
Ca^{2+}	6 to 8	distorted from octahedral to square antiprism	
Cr^{2+}	6	octahedral	$\text{Cr}(\text{H}_2\text{O})_6^{2+}$
Cr^{3+}	6	octahedral	$\text{Cr}(\text{H}_2\text{O})_6^{3+}$
Cr(VI)	4	tetrahedral	CrO_4^{2-} , $\text{Cr}_2\text{O}_7^{2-}$
Mn^{2+}	6	octahedral	$\text{Mn}(\text{H}_2\text{O})_6^{2+}$
Fe^{2+}	6	octahedral	$\text{Fe}(\text{H}_2\text{O})_6^{2+}$
Fe^{3+}	(4), 6, (7)	tetrahedral octahedral, distorted	FeCl_4^- $\text{Fe}(\text{H}_2\text{O})_6^{3+}$, $\text{Fe}(\text{edta})\text{OH}^{2-}$
Co^{2+}	(4), 6	tetrahedral octahedral	CoCl_4^{2-} $\text{Co}(\text{H}_2\text{O})_6^{2+}$
Co^{3+}	6	octahedral	$\text{Co}(\text{H}_2\text{O})_6^{3+}$
Ni^{2+}	4, 6	(tetrahedral) square planar octahedral	NiCl_4^{2-} $\text{Ni}(\text{CN})_4^{2-}$ $\text{Ni}(\text{NH}_3)_6^{2+}$
Cd^{2+}	4, 6	tetrahedral octahedral	CdI_4^{2-} $\text{Cd}(\text{H}_2\text{O})_6^{2+}$

aware of the possibility of changes in coordination geometry because this will influence both the possible stoichiometry of complexes and the thermodynamics for their formation.

The acceptor properties of the various metal ions are discussed in Section III.2.2.4.

III.2.2. Water as a solvent

Water is an excellent solvent for many ionic and polar compounds. This is due both to its high dielectric permittivity and its donor properties (ability to act as a ligand, *cf.* Section III.2.2.4).

Water is a *structured* medium through the formation of an extensive network of hydrogen bonds. This network may be changed or disrupted either by solutes, or by changing the temperature.

Solvent-solute interactions in aqueous systems can be described surprisingly well by electrostatic models. Positive ions are surrounded by a primary layer of water molecules with the negative end of the dipole, the oxygen atom, pointing towards the cation. This water is in general considered to be chemically bonded to the cation, and the first solvation layer is therefore often called the inner coordination sphere, and is characterised by its coordination geometry.

The water in the first solvation shell is hydrogen bonded to external water molecules. However, the solvated ions do not “fit” into the hydrogen-bond network of pure liquid water. Hence, there is a layer of more or less “disrupted” water between the primary solvation layer and the “bulk” solvent. This region is characterised by a gradual change in structure, as indicated by Figure III.1.a. For metal ions that bind water molecules strongly it is often possible to identify a second hydration layer outside the first. The structure around the dissolved metal ions is very different in polar, aprotic solvents. These form strong bonds with metal ions, but do not have the protons required to form hydrogen bonds, *cf.* Figure III.1.b, and therefore no second solvation sphere can be formed. Examples of such solvents are dimethylsulfoxide, (DMSO), $(\text{CH}_3)_2\text{SO}$ and acetonitrile CH_3CN [78AHR].

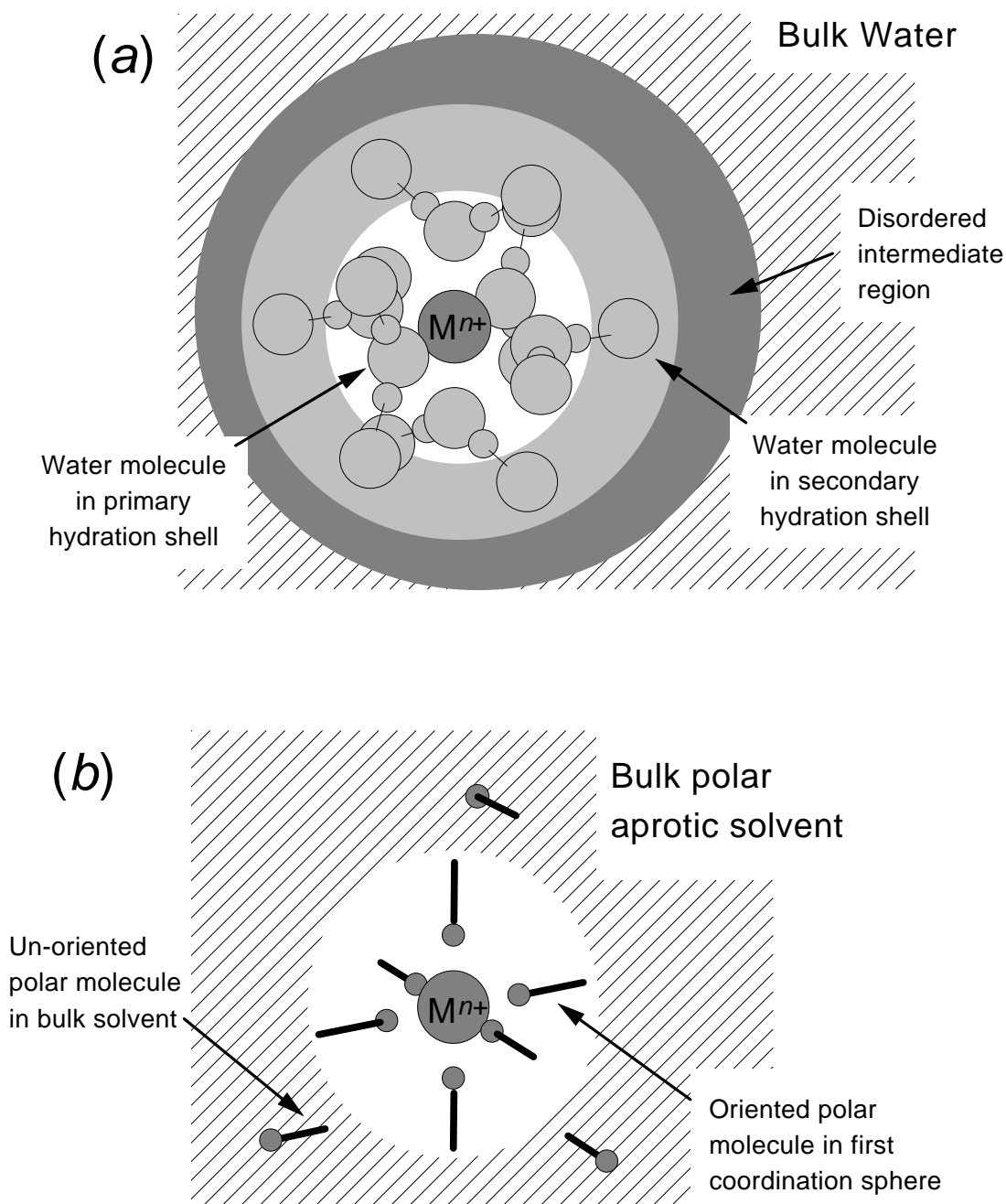
Despite its structural features, water is often modelled as a *structureless dielectricum*, because this is often found to be a very efficient model when describing the thermodynamics of reactions in water.

III.2.2.1. Solvation and complex formation, ion-ion and ion-dipole interactions

In the simplest electrostatic models the ion-ion and ion-dipole interactions are governed by electrostatics where the water is considered as a dielectric continuum with a macroscopic dielectric constant. The attractive force between ions of charges Z_+ and Z_- is given by the Coulomb law:

$$F = -\frac{1}{4\pi\epsilon\epsilon_0} \frac{Z_+Z_-}{r_{\text{A-B}}^2}$$

Figure III.1: Drawings illustrating the solvation of cations in (a) protic, and (b) polar aprotic solvents. Adapted from [74COX/HED, 77BOC/RED, 90BEC/NAG, 93MOR/HER]. The central ion is shown octahedrally coordinated by six solvent molecules. Diagram (a) displays a second hydration shell coordinated to the first one by hydrogen bonds (represented by thin lines).



The total energy consist of two main contributions, an attractive Coulomb energy and a repulsion energy term. E_{tot} is equal to

$$E_{\text{tot}} \approx \frac{1}{4\pi\epsilon\epsilon_0} \frac{Z_+Z_-}{r_{\text{A-B}}} - \frac{B_{\text{A-B}}}{r_{\text{A-B}}^n}$$

where $r_{\text{A-B}}$ is the distance between the two ions A and B, ϵ and ϵ_0 are the relative dielectric permittivity (the dielectric constant) in the solvent and the permittivity in vacuum, respectively. $B_{\text{A-B}}$ and n are constants, where the latter may be estimated theoretically [65PHI/WIL, p.148].

III.2.2.2. Ion-ion and ion-dipole interactions

Electrostatic models are used in both qualitative and quantitative ways. We have just described some of the quantitative features. For additional information, the reader is referred to [65PHI/WIL, 87COT/WIL]. Ion-ion and ion-dipole interactions are used when discussing chemical bonding in terms of “ionicity” *versus* “covalency”, and when making correlations of various types between chemical and physical quantities, *cf.* Section III.6.7.

Quantitative electrostatic models are also used when describing the thermodynamic properties of electrolyte solutions. The Debye-Hückel model and the various variations of this are the best known examples of this category, *cf.* Chapter IX.

In the simple Debye-Hückel theory, water is also considered to be a structureless dielectricum and no account is taken of solvation. In the more elaborate models, *e.g.*, the Helgeson-Kirkham-Flowers model [81HEL/KIR] the following features are included:

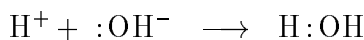
- the intrinsic properties of the electrolyte, which are independent of the solvent;
- cavity formation, electrostriction collapse, and local disruption of the solvent structure by the solute;
- orientation of disordered H₂O dipoles to form hydration shells around the dissolved ions;
- long- and short-range interactions of the solvated ions with one another;
- ion association (complex formation).

The reader is referred to [81HEL/KIR] and Chapters IX and X for additional information.

Not only ionic species but also most uncharged molecules are *solvated* (in aqueous solution *hydrated*) in solution. Solvation is introduced indirectly also in the continuum models by taking *dielectric saturation* close to the ions into account. Solvation and complex formation involve the same kind of chemical interactions at the microscopic level. The chemical interactions between metal ions and water may be described in different ways, ranging from purely electrostatic ion-dipolar interactions to a well defined chemical bond involving electron delocalisation from the lone-pairs on the water molecule to the metal ion. In the following we will use the latter model, where bonding between metal

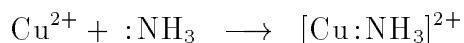
ion and ligand is a result of a donation of an electron pair from a *Lewis base* (the ligand) to a *Lewis acid* (the metal ion). The following example illustrates the origin of the terminology.

- We may write the reaction between an acid and a base in the following way



where the two dots denote an electron pair on the base. An acid base reaction may then be described in two ways, either as a reaction involving a proton transfer (the Brønsted-Lowry concept), or as a reaction involving the donation of an electron pair from a donor (the base) to an acceptor, the (Lewis) acid.

Complex formation reactions between a metal ion and a ligand also involve a donation of an electron pair from a donor (the ligand) to an acceptor (the metal ion), *e.g.*:



If we look on the chemical processes at the “electron pair level” we see that both acid/base reactions and complex formation reactions can be described in the same way. The Lewis acid/base concept is more general than the Brønsted-Lowry concept.

Complex formation reactions involve the *replacement* of a coordinated water molecule by another ligand. The only exceptions are metal-ion hydrolysis, and some reactions involving deprotonation of a ligand already bonded to a metal ion, as described below. The properties of the solvent are thus essential for the understanding of complex formation reactions.

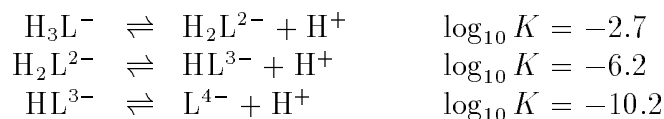
Hydrated metal ions are *acids* – a simple chemical explanation is that a water molecule bonded to a positively charged metal ion increases its acidity due to an increased electrostatic repulsion between the metal center and the hydrogen atoms (or as a result of redistribution of electrons from the region between oxygen and hydrogen in the water molecule to the region close to the metal ion).

The acidity of the coordinated water, *i.e.*, the hydrolysis of the metal ions increases with increasing charge and decreasing ionic radius of the metal ion. This is in qualitative agreement with the expectations from an electrostatic point of view. The same electrostatic “explanation” may be used to describe the fact that ligands containing hydrogen atoms that can participate in protolytic reactions *always* show an increase in acidity when coordinated to metal ions.

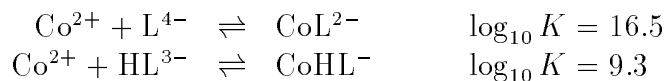
These general statements are useful because they allow us to make chemical predictions.

Example 2:

The ligand edta^{4-} , ethylenediamine tetraacetate, contains four carboxylate groups and two nitrogen donors. In the pH region $3 \leq \text{pH} \leq 11$ the relevant acid dissociation constants are:



In the same pH region cobalt(II) forms the following complexes with edta:



All equilibrium constants in this example have been obtained from [77AND] for $I = 0.1$ M and 20°C . From the last three equilibrium constants we obtain for the reaction:



i.e., the proton dissociation constant of HL^{3-} increases by 7.2 logarithmic units on coordination to Co(II). The acid/base properties of coordinated ligands are important when discussing the possible stoichiometry and bonding of ligands containing more than one protolytic functional group. The distribution diagram in Figure III.2 shows that CoL^{2-} is the predominant complex in solutions where the predominant forms of the free ligand are L^{4-} , HL^{3-} and H_2L^{2-} .

In most environmental system one encounters organic ligands that contain protolytic groups. It is then essential to keep the possibility of protolytic reactions in mind. An example of the modelling of such a system is given in Section III.6.7.

Remark:

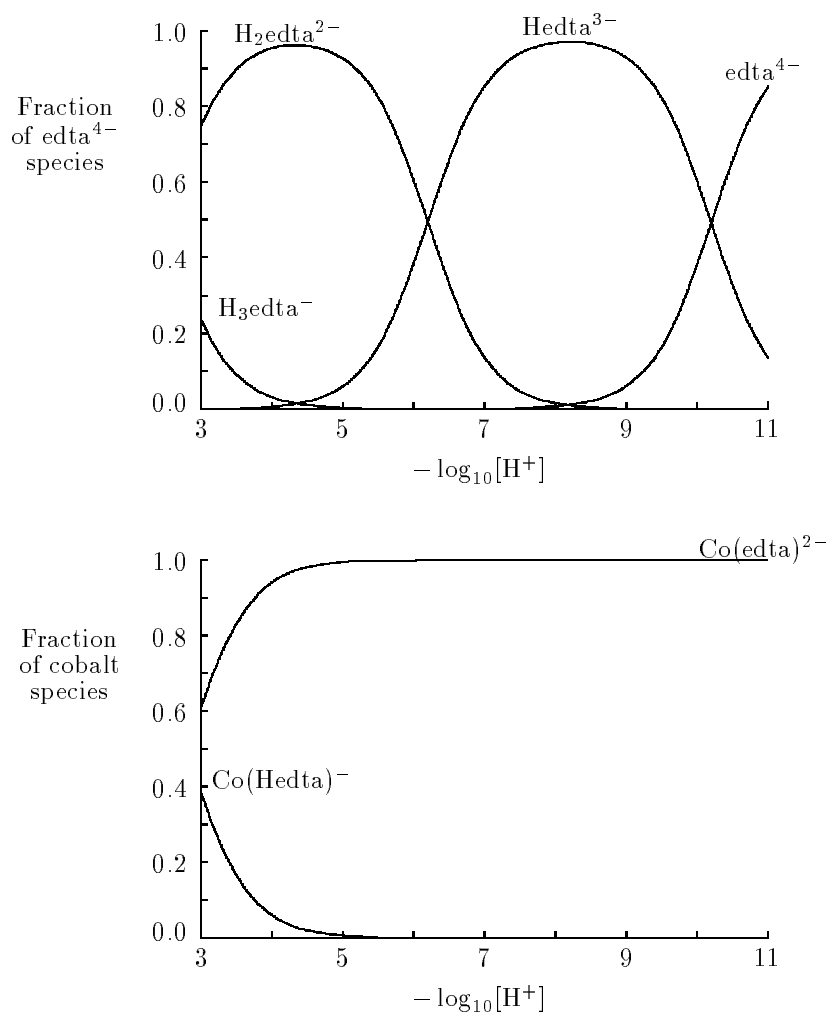
The strength of acids is known to increase strongly with increasing temperature and this is also true for hydrolysis reactions. This point is discussed in Chapter X.

III.2.2.3. Ligands and their chemical characteristics ¹

Reactants bonded to a particular metal-ion reaction center are called *ligands*. They may be either a single atom ion like F^- , or multi-atom ions or molecules. In the latter case one always can identify a smaller number of atoms that are bonded to the metal-ion center. These atoms are called *donor atoms*, and always contain electron pairs, *i.e.*, they are Lewis bases. The ordinary electron-pair bond is usually a single-bond (called a sigma-bond), but some ligands may also form multiple bonds (π -bonds) resulting in a larger electron redistribution in the coordinative bond.

¹ The examples of coordination geometries shown here of metal complexes with organic and inorganic molecules (Figures III.3 to III.5, III.17 to III.19, and III.31 to III.36) are taken from crystal structure data. Sources of such data are CSD, the Cambridge Structural Database [79ALL/BEL], and ISCD, the Inorganic Crystal Structure Database [83BER/SIE].

Figure III.2: Distribution diagrams of the various species formed in the Co(II)-edta⁴⁻ system. The diagrams refer to calculations where the total concentrations of metal ion and ligand are 10⁻⁵ M and 10⁻³ M, respectively.



Example 3:

The ligand F^- , contains only one atom, which obviously is the one involved in reactions where fluoride complexes are formed. The sulfate ion, SO_4^{2-} , contains five atoms, a central sulfur atom surrounded by four oxygen atoms forming a regular tetrahedron – only the oxygen atoms can bind to metal ions. The thiocyanate ion, SCN^- , contains two different donor atoms, sulfur and nitrogen, linked by carbon (which cannot bind to metal ions in this case), the actual mode of bonding is determined by the chemical characteristics of the metal ion, *vide infra* (Section III.2.2.4). The ligand cannot bind with both S and N to the same metal ion because of steric restrictions. However, the ligand may act as a *bridge* between two metal ions. The anion edta^{4-} contains eight oxygen donors from the four carboxylate groups, and two nitrogen donors. A maximum of *four* oxygen and *two* nitrogen donors may be bonded simultaneously to a given metal ion. The actual number is determined by the size and coordination geometry of the metal ion, *cf.* Figures III.4, III.35 and III.36.

A ligand is *unidentate* if only one of its donor atom is bonded to a metal ion. The ligand forms a *chelate* if more than one donor atom is bonded to the same metal ion. Chelate formation may result in the formation of very stable complexes. However, this requires that the ligand geometry and the coordination geometry of the metal ion match one another. The reason for this has been discussed by Schwarzenbach [52SCH], and Adamson [54ADA].

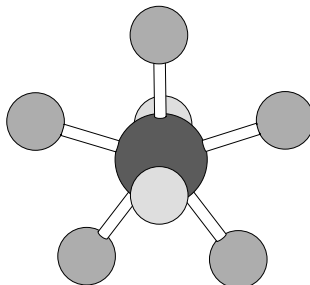
There are only few inorganic ligands that may form chelates, in general only the oxo-anions like sulfate, sulfite, selenate, selenite, phosphate, carbonate, *etc.*

There is an abundance of organic ligands that may form chelates. Many of these are especially designed to bind selectively to particular metal ions, depending on their preferred choice of donor atoms and coordination geometry. Most organic ligands have a considerable freedom to adapt their conformation to the desired coordination geometry. However, the more donor atoms they contain, the more difficult it is to exploit all of them in bonding. A rule of thumb is that the strongest complexes are formed when the donor atoms are not separated by more than two other atoms (usually carbon atoms), forming a five-membered chelate ring together with the metal ion. Figures III.3, III.4 and III.5 illustrate the coordination geometry and ligand bonding for some simple inorganic ligands and for some organic ligands containing from one to six donor atoms.

Some ligands may act as *bridges* between different metal atoms and lead to the formation of *polynuclear* complexes. Hydroxide/oxide and oxo-anions are all good bridging ligands. Fluoride is an excellent bridging ligand in the solid state but not in complexes in solution. Bridging with organic ligands in general occurs in polydentate ligands where all functional groups cannot bind to the same metal ion for steric reasons. Figures III.6 and III.36 demonstrate different bridging situations.

It is obvious that both the location of the donor atoms in the ligand, and the coordination characteristics of the metal ion, will determine which donor atoms are actually

Figure III.3: Example of some less common coordination geometries: Coordination around the linear UO_2^{2+} ion. The picture shows the complex $\text{UO}_2\text{F}_5^{3-}$ where all ligands are placed in a plane perpendicular to the linear O-U-O axis. This pentagonal bipyramid geometry is common for compounds of the linear dioxoactinoid (V) and (VI) ions.

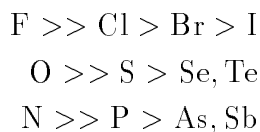


bonded. The chemical composition of ligands may vary considerably from the very simple like fluoride, to the structurally very complicated like peptides or humic/fulvic acids, the later are discussed in Chapters V and VI.

III.2.2.4. Qualitative features of complex formation reactions

There exists a set of *empirical* rules that give a *qualitative* description of the chemical interactions between metal ions and various donor atoms. Donor atoms may be arranged in two ways, depending on the relative strength of their bonding to metal ions, in the same way metal ions may be ordered in two groups depending on their ability to bind the various donor atoms.

One group of metal ions (class (a), or *hard acceptors* [87COT/WIL, p.216–217], or Lewis acids) forms complexes which decrease in stability depending on the donor atom as follows



F, O and N are *hard donors*, with small polarisability values and a general tendency for “ionic” interactions, while I, S, P, *etc.* are soft donors, with high polarisabilities and a tendency to form “covalent” bonds.

The other group of metal ions (class (b), or *soft acceptors*, or Lewis acids) have the reverse order of stability, *i.e.*,

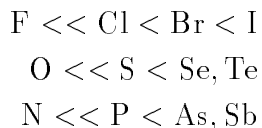
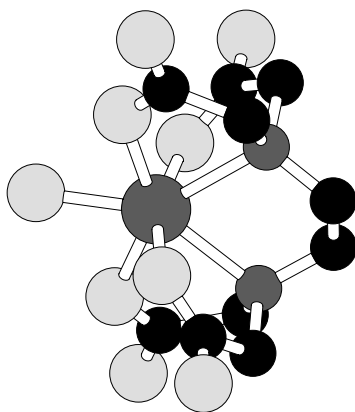


Figure III.4: Example of some less common coordination geometries: Coordination geometry of the Fe(III) edta complex (edta = ethylenediaminetetraacetate) $\text{Fe}(\text{edta})(\text{H}_2\text{O})^-$. Fe(III) is *seven* coordinate (the most common coordination geometry is octahedral). The reason for the increased coordination number is probably that the Fe(III) ion does not fit into the “basket” formed by the two nitrogen and four oxygen donors from the ligand. The ligand is located asymmetrically on one side of the Fe(III) and there is room for an additional water on the other side. This type of coordination is very common in edta complexes, for which non-octahedral geometries are the rule, rather than the exception. The black circles in the edta-ligand denote carbon atoms, the light grey oxygen atoms and the remaining two, nitrogen atoms. The single atom bonded to Fe(III) is a water oxygen.



The donor atoms in periods three and higher in the periodic table, have a much larger polarisability than those in period two, *i.e.*, they are “softer” and tend to form covalent bonds.

The positions of hard and soft Lewis acids in the periodic table are shown in Figure III.7.

General rule:

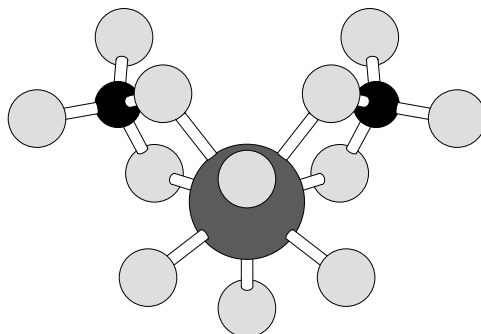
The strongest complexes are formed between donors and acceptors that belong to the same group. We can understand this in terms of the two models of chemical bonding, where hard – hard interactions are mainly “electrostatic” and soft – soft interactions mainly “covalent”. This general rule is very useful, when discussing the possible interactions between ligands and metal ions in complex chemical systems.

Example 4:

Soft metal ions such as Pt and Hg, and the “border region” elements Cd, Pb and Bi (Figure III.7), are highly toxic, presumably because they can bind strongly to peptides/proteins, some of which contain sulfur.

The *actinide* elements, and many of the elements formed in nuclear fission are examples

Figure III.5: Example of some less common coordination geometries: Geometry of $\text{Ho}(\text{SO}_4)_2(\text{H}_2\text{O})_4^-$ with eight donor atoms around Ho(III). High coordination numbers are common for the lanthanides and the actinides. Each sulfate ligand is coordinated through two of its oxygen donors and thus forms a chelate. The black circles denote sulfur atoms. The four light grey circles bonded only to the dark grey Ho(III) denote oxygen atoms in coordinated water molecules.



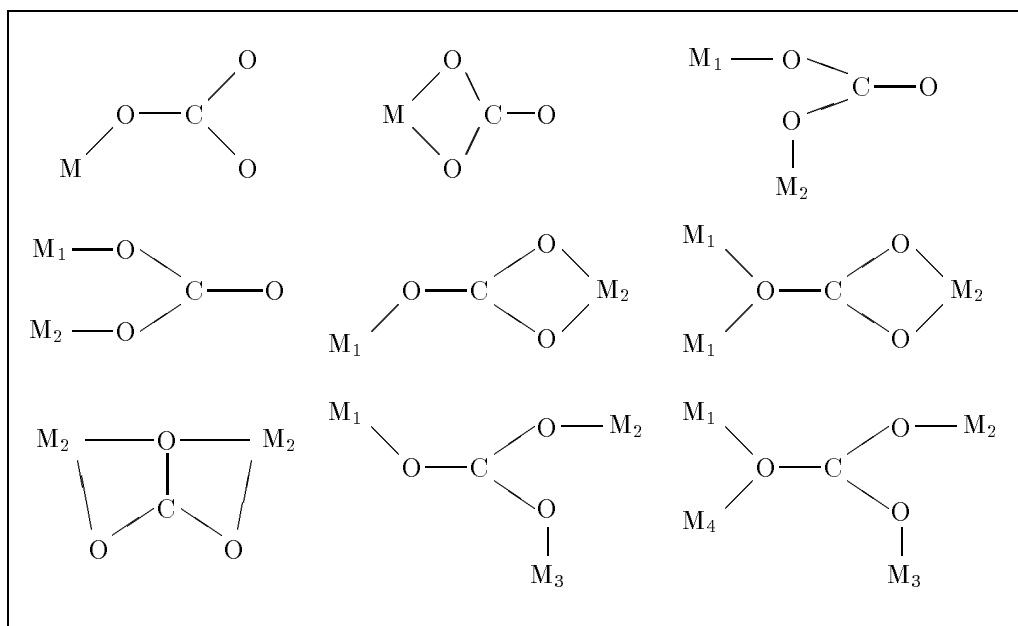
of hazardous elements which belong to the group of hard Lewis acids. From the general chemical systematics outlined above, we can conclude that the actinide elements will form strong complexes only with ligands containing “hard” donor atoms. Of the *inorganic* ligands occurring in nature we then only have to consider the fluoride ion and those containing oxygen (hydroxide, sulfate, nitrate/nitrite, phosphate, carbonate and silicate). Inorganic ligands containing nitrogen donors are rare (ammonia, and nitrite) and nearly always present in very low concentrations in natural water systems.

Organic ligands of various types are present in ground and surface water systems. Some of them are there as a result of human and industrial activities (detergents, industrial chemicals, *etc.*); others are produced in the biosphere by microbiological and other processes. The ligands have a range of molecular weights, varying from low-molecular compounds to polymers. They contain essentially three different types of donor atoms O, S and N, where the first is predominant.

Humic/fulvic acids are high-molecular organic ligands known to be good complexing agents for most metal ions, *cf.* Chapters VI and V. They contain a number of strong metal binding *functional groups* (phenol-, carboxylate-, aldehyde-, keto-, amino-, *etc.*) which also can participate in protolytic equilibria. The high molecular weight and the large number of functional groups give them *polyelectrolyte* properties, which must be taken into account when modelling the metal – humate/fulvate interactions, *cf.* Chapters VI and V. There is an extensive literature that will be discussed in these two Chapters. A recent book by Buffle “Complexation reactions in aquatic systems: An analytical approach” [88BUF], and the proceedings from the OECD-NEA workshop “Binding models concerning natural organic substances in performance assessment” [95NEA] give a review of the area.

Hard Lewis acids such as the actinides are preferentially bonded to oxygen and nitrogen

Figure III.6: Common bonding geometries for the carbonate ion [83PAL/ELD].



donors in these ligands.

The stability of metal complexes also depends on the charges of metal ion and ligand. In general the stability increases with increasing charge as expected from electrostatic considerations, hence nitrate/nitrite complexes are much weaker than sulfate complexes, and the former may be neglected when modelling, *e.g.*, the species distribution of actinides in a ground water system.

However, one must be careful when using electrostatic considerations – because the hardness/softness characteristics are a property of the oxidation state of the donors and acceptors (*i.e.*, their charge). For example, copper(I) is a softer Lewis acid than copper(II) and therefore forms *stronger* chloride complexes than Cu(II).

Figure III.8 illustrates that for UO_2^{2+} the formation of chloride complexes in most environments is negligible in comparison with the formation of fluoride complexes (and this holds for other hard acceptors), while the chloride complexes are totally predominant for Hg(II) (and other soft acceptors).

III.3. Classification of metal complexes

Complex formation in aqueous solution takes place according to the following general (stoichiometric) scheme. For simplicity, we have considered a two-component system where only mononuclear complexes are formed (charges have been omitted for brevity):

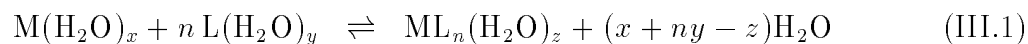
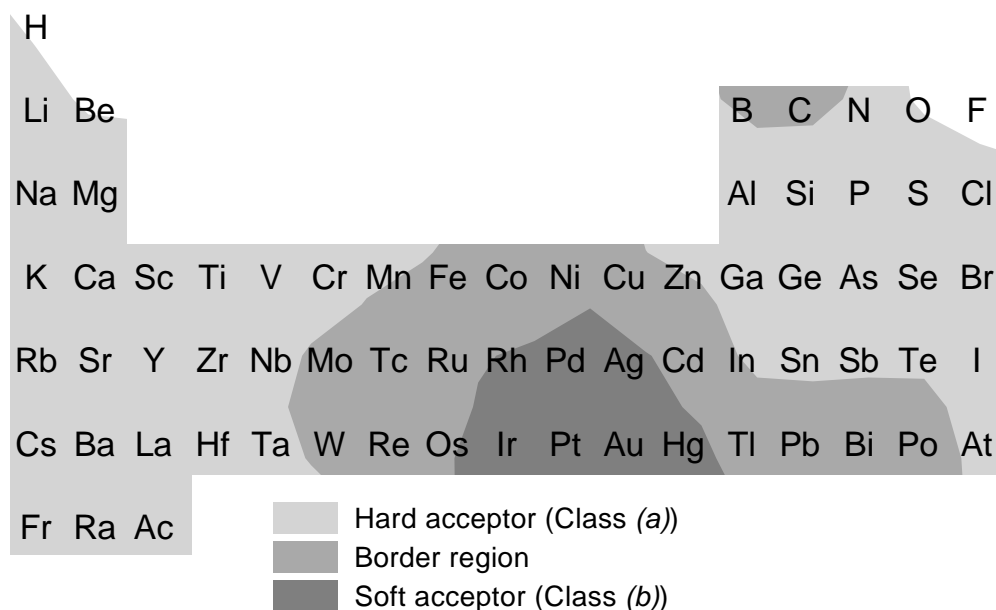


Figure III.7: The distribution of acceptor atoms in the periodic table. Adapted from [58AHR/CHA]. The lanthanides and actinides, which are not shown in this figure, belong to class (a), *i.e.* they are hard acceptors.



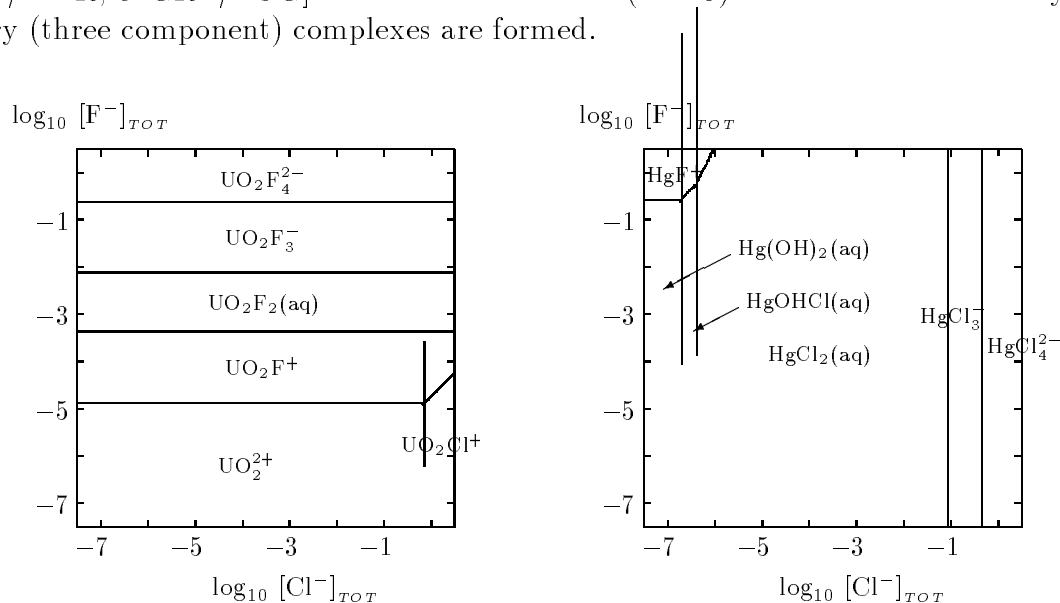
This equation emphasises that ions in solution are hydrated, a fact influencing the thermodynamics of Eq. (III.1) to a large extent [73AHR]. Eq. (III.1) may be interpreted as describing a “release” of water molecules from the hydration spheres of cations and anions to the “bulk” solvent. The term “release” is used to describe the fact that the water in the solvation spheres has a different freedom of translation movement as compared to the bulk water. A similar difference is found between ice and liquid water. The melting of ice results in a large increase in entropy. Similarly, the “release” of water molecules in complex formation reactions is often accompanied by a large and positive entropy change, which increases with the number of water molecules released.

Metal complexes containing different metal ions, different ligands and with a variety of stoichiometric compositions have been studied by chemists during more than one hundred years. In order to use this enormous amount of information it is practical to make a classification of metal complexes based on their composition/bonding characteristics. We will use the following indicators:

- the number of components;
- the bonding of the ligand, monodentate, chelating, or bridging;
- the number of metal ions in the complex, *i.e.*, mononuclear *vs.* polynuclear.

Eq. (III.1) indicates that more than one ligand can bind to the central ion M. Complex

Figure III.8: Relative stability of chloride and fluoride complexes for hard and soft acceptors. The figure shows predominance area diagrams for UO_2^{2+} and Hg^{2+} (which are examples of hard and soft metal ions respectively). The diagrams have been calculated at $\text{pH} = 3.5$ (to avoid the formation of strong hydroxide complexes) and at a total metal concentration of 10^{-8} M. Values for the equilibrium constants are from [76BAE/MES, 76SMI/MAR, 92GRE/FUG] in the standard state ($I = 0$). Note that both binary and ternary (three component) complexes are formed.



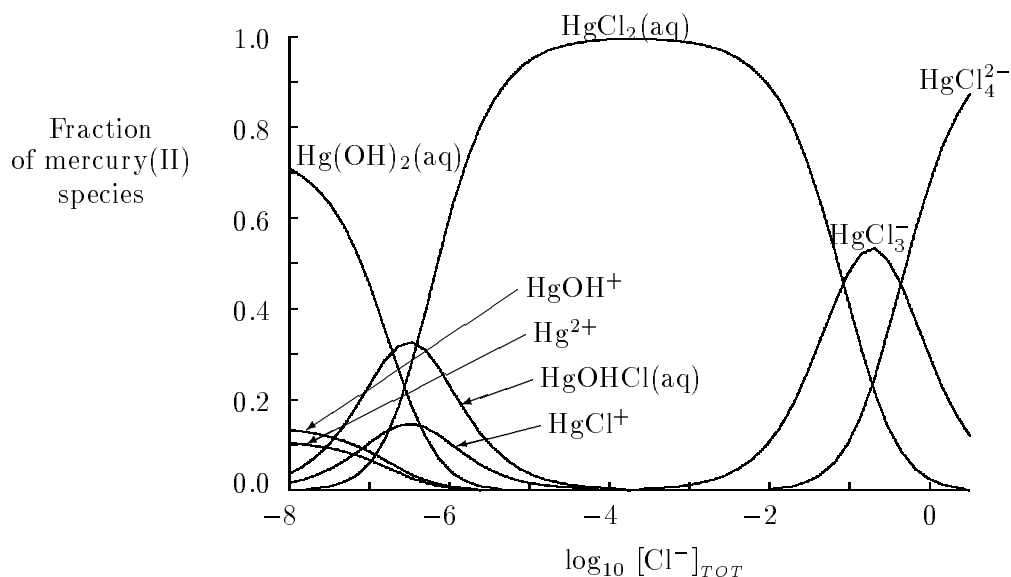
formation reactions take place in a *stepwise* fashion, where one ligand is added at a time, until the *maximum number* is reached. This number is related to the coordination number of the metal ion. In octahedral geometry at most six mono-dentate, three bidentate and two three-dentate ligands may bind to the central metal ion.

The stepwise formation of complexes can be represented graphically in a *distribution diagram*, using the free ligand concentration as a “master variable”, as described in Section II.5 (p.59). An example of such diagrams is given in Figure III.9.

The number of ligands that can be bonded to a metal ion depends both on the electron structure of the metal ion, the relative sizes of central ion and ligand, and the geometry of the ligand, when it contains more than one donor atom. Most metal ions have one (or two) characteristic coordination numbers, each with a special coordination geometry as indicated in Table III.1.

Classical solution chemical studies only give information about the *constitution* of the complexes formed. Information about the detailed bonding of the ligand and the geometry of the complexes formed require additional experimental information, *e.g.*, provided by spectroscopic (IR, Raman, multi-nuclear NMR, spectroscopic information on d-d spectra, *etc.*) and diffraction techniques (X-ray and neutron diffraction, EXAFS, large angle X-ray scattering of solutions, *etc.*). Much experimental information on the structure of complexes has been obtained from X-ray diffraction studies of solid compounds. There

Figure III.9: The distribution of mercury(II) species in aqueous solutions as a function of the total chloride concentration. Diagram calculated at the same conditions as the predominance diagram for Hg(II) in Figure III.8, but in the absence of fluoride ions.



are important differences in the intermolecular forces in the solid state and in solution which might result in structural differences. However, in situations where a complex of a given stoichiometry occurs both in the solid state (as “isolated” units that interact rather weakly with surrounding ions/molecules) and in solution, there is usually a good agreement between their structures.

III.4. The thermodynamics of complex formation reactions

The standard free energy of reaction is equal to

$$\Delta_r G_m^\circ = \Delta_r H_m^\circ - T \Delta_r S_m^\circ$$

where $\Delta_r H_m^\circ$ and $\Delta_r S_m^\circ$ are the standard enthalpies and entropies of reaction, respectively. It is practical to have some method to estimate these quantities if experimental data are not available. Qualitative estimates of the entropy changes for complex formation reactions may be obtained as indicated below.

Reaction (III.1) illustrates that complex formation reactions result in changes in the solvation of both reactants and products.

In Sections III.2.2.1 and III.2.2.2 we discussed a simple electrostatic model of ion solvation. The strength of bonding of the water in the first coordination sphere should increase with increasing ionic charge and decreasing ionic radius. The “ordering” effect

of the electrostatic field should extend also outside the first sphere. The qualitative conclusion from this model is that in a reaction, the differences in the properties between the bulk water and the water in the first and second solvation spheres will be larger the larger the differences in electrostatic potential between reactants and products.

From a microscopic point of view we can describe Reaction (III.1) as a reaction where “ordered” water in the first and second coordination spheres is transferred to the less “ordered” state in the bulk solvent. This process results in an increase in entropy for the system, in the same way as when a gas is expanded from a small volume to a larger one, or when solid ice is transformed to liquid water.

We would then expect the values of $\Delta_r S_m^\circ$ between a set of different metal ions with a given ligand to increase with increasing charge and decreasing ionic radius of the central ion. The entropy changes should also decrease between consecutive complex formation reactions, because of the decrease in charge and solvation and the increase in size, when more ligands are added to the central ion.

For ligands that contain different number of donor atoms we expect the entropy change to increase with the number of coordinated donor atoms. The data in Table III.2 indicates that the experimental findings confirm these expectations.

The data in the table indicates that complexes between hard donors and hard acceptors have large positive entropy contributions, while the enthalpy term usually is fairly small. On the other hand, in complexes formed between soft donors and soft acceptors the enthalpy term gives a major contribution to the stability of the complexes, while the entropy contribution is smaller. Enthalpies of reaction involving the proton, e.g. protonation of bases are usually fairly large but always less than the enthalpy of protonation of hydroxide.

Information of the type discussed above is useful to estimate the temperature dependence of a reaction when no experimental enthalpy of reaction is known. More detailed discussion of the thermodynamics of complex formation reactions is given by Åhrland [67AHR, 68AHR]. The conclusions drawn above relate to aqueous solutions; non-aqueous systems behave in a different way, as discussed also by Åhrland [79AHR, 82AHR].

III.5. Complex formation, a competitive process

Most experimental investigations of complex formation reactions have been made on binary systems, and information on ternary and higher systems is scarce. The one exception is for ligands which are polyprotic acids, H_nL , either organic or inorganic. For these ligands, all the different species L^{n-} , $HL^{(n-1)-}$, $H_2L^{(n-2)-}$, ... are potential ligands, and in any careful experimental study the investigators have to decide if complexes of the type MH_pL_q are formed, or not. One also has to ascertain if a coordinated water molecule can be deprotonated with the formation of ternary hydroxide complexes, $M(OH)_pL_q$, as shown in Figures III.8 and III.9. The occurrence of ternary complexes in nature is probably more common than indicated by published equilibrium data. Experimentalists often try to avoid them by selecting the experimental conditions in such a way that their formation is minimised. For the user of equilibrium data it is essential to keep this in mind,

Table III.2: Thermodynamic data for complex formation reactions. The first group of data illustrates how the thermodynamic quantities depend on the charge of the positive ion. The second and third groups show how the thermodynamic quantities vary for the stepwise reactions, and for ligands containing a different number of donor atoms, respectively. The fourth group demonstrates how the thermodynamic quantities vary with the hardness of the ligand for a typical soft acceptor.

Reaction	$\Delta_r G_m^\circ$ kJ · mol ⁻¹	$\Delta_r H_m^\circ$ kJ · mol ⁻¹	$T \Delta_r S_m^\circ$ kJ · mol ⁻¹
Charge dependence:			
$H^+ + F^- \rightleftharpoons HF(aq)$	-16.57	12.26	28.8
$Be^{2+} + F^- \rightleftharpoons BeF^+$	-28.79	-1.7	27.1
$Al^{3+} + F^- \rightleftharpoons AlF^{2+}$	-35.02	4.60	39.6
Stepwise reactions:			
$Tl^{3+} + Cl^- \rightleftharpoons TlCl^{2+}$	-42.76	-25.27	17.5
$TlCl^{2+} + Cl^- \rightleftharpoons TlCl_2^+$	-32.97	-16.95	16.0
$TlCl_2^+ + Cl^- \rightleftharpoons TlCl_3(aq)$	-19.37	-4.52	14.9
$TlCl_3(aq) + Cl^- \rightleftharpoons TlCl_4^-$	-15.86	-0.71	15.2
Chelate formation:			
$Cu^{2+} + ac^- \rightleftharpoons Cu ac^+$	-10.71	4.35	15.1
$Cu^{2+} + mal^{2-} \rightleftharpoons Cu mal(aq)$	-32.17	11.92	44.1
$Cu^{2+} + edta^{4-} \rightleftharpoons Cu edta^{2-}$	-105.5	-34.10	71.4
Hardness/softness:			
$Hg^{2+} + F^- \rightleftharpoons HgF^+$	-5.82	3.8	9.6
$Hg^{2+} + Cl^- \rightleftharpoons HgCl^+$	-38.49	-23.0	15.5
$Hg^{2+} + Br^- \rightleftharpoons HgBr^+$	-51.46	-42.68	8.8
$Hg^{2+} + I^- \rightleftharpoons HgI^+$	-73.22	-75.31	-2.1

because outside the concentration ranges used in the laboratory studies, different species may form. If quantitative data on them are not given in the literature it is necessary to *estimate* both possible stoichiometries, and the magnitude of the equilibrium constants. This procedure is facilitated when one of the components is present in large excess over the others, a situation typical for the modelling of the speciation of *trace metals* in aquatic systems.

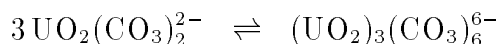
III.5.1. The pH dependence of complex formation reactions

For ligands that are anions of weak acids (hydroxide, fluoride, carbonate, phosphate, silicate, and the anions of most organic acids), there is always a competition between metal ions and hydrogen ions for the given ligand, and the complex formation reactions will be strongly pH dependent. This is one of the reasons why pH is an important “master variable” for the description of equilibria in aqueous solution. Phosphate is the most important of the inorganic ligands in this group; complexes containing H_2PO_4^- , HPO_4^{2-} and PO_4^{3-} are known. The ligands with the largest negative charge always form the most stable complexes. On the other hand these are also the strongest bases, with the strongest competition from H^+ . For this reason, H_2PO_4^- and HPO_4^{2-} are important ligands in most aquatic systems. Figure III.10 shows the distribution of dioxouranium(VI) phosphate complexes as a function of pH at a total concentration of phosphate of $5 \cdot 10^{-6}$ M (0.5 ppm).

III.5.2. Polynuclear complex formation

The metal ions in polynuclear complexes may be of the same type, or different. However, few complexes containing different metal ions are known, one example [86GRE/RIG] is the formation of $(\text{UO}_2)_2(\text{MO}_2)(\text{CO}_3)_6^{6-}$, where M is Np or Pu. In this case we can describe the complexes as formed by an isomorphic substitution of UO_2^{2+} in $(\text{UO}_2)_3(\text{CO}_3)_6^{6-}$, with NpO_2^{2+} or PuO_2^{2+} , *cf.* Figure III.11. This is a process analogous to isomorphic substitutions in the solid state.

The relative importance of polynuclear, as compared to mononuclear complexes increases with increasing total concentration of metal ions. For example, the equilibrium



is shifted towards the right with increasing total concentration of uranium.

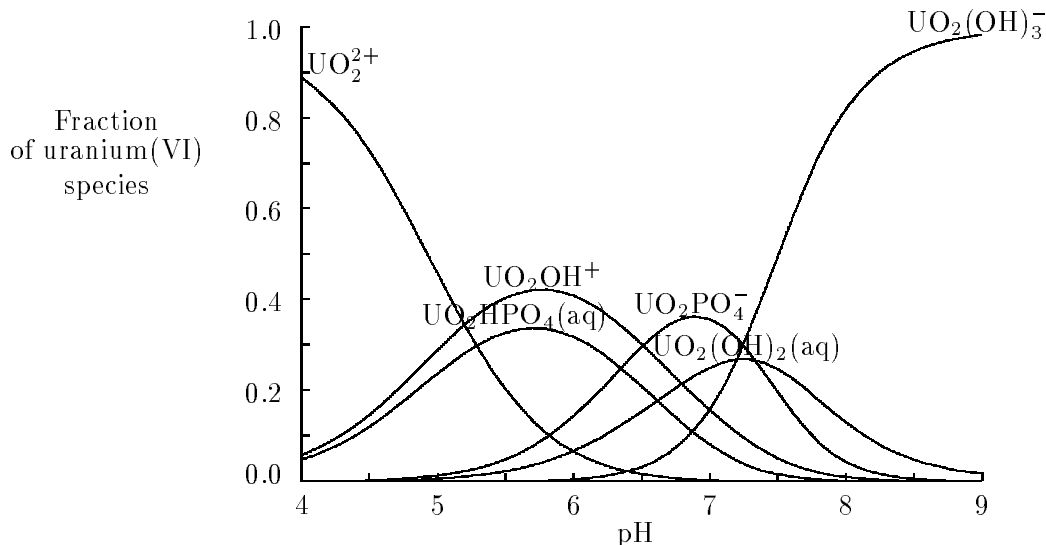
At trace concentration levels most complexes are mononuclear.

The chemistry of the metal hydroxides is dominated by polynuclear complexes. An excellent review of the field has been given by Baes and Mesmer [76BAE/MES].

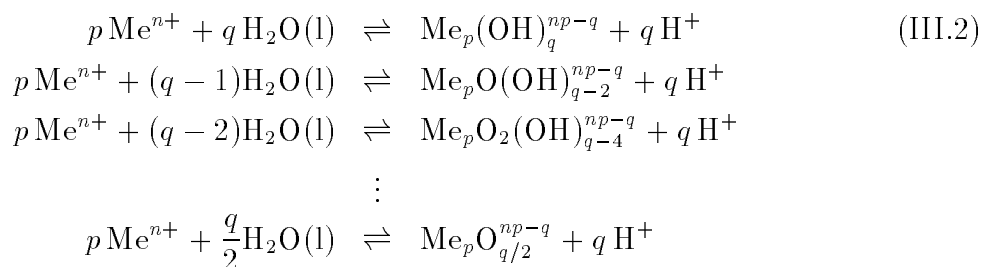
III.5.3. The stoichiometry of hydroxide complexes

Most hydrolysis equilibria are studied experimentally by measuring the hydrogen ion concentration, *cf.* Eq. (III.2). In this type of experiment one measures the concentration of

Figure III.10: The stabilities of the phosphate complexes of dioxouranium(VI). The diagram has been calculated at $[\text{PO}_4^{3-}]_{\text{total}} = 5 \cdot 10^{-6} \text{ M}$, and at $[\text{UO}_2^{2+}]_{\text{total}} = 10^{-8} \text{ M}$. Values for the equilibrium constants are those given in [92GRE/FUG] in the standard state ($I = 0$).



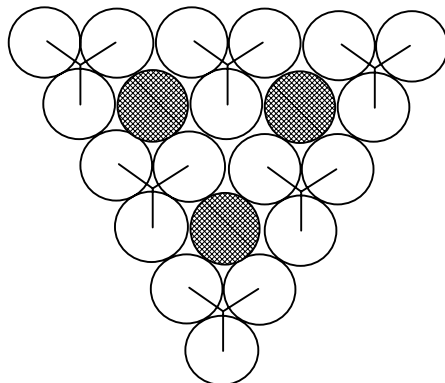
hydrogen ions released during the hydrolysis reaction. This quantity gives no information as to whether the released protons come from coordinated water or hydroxide. In this particular type of experiment the following equations are therefore *equivalent* from a *thermodynamic* and modelling point of view. However, the constitution of the complexes and their chemical properties will be very different:



It is important to realise that the stoichiometric formulas above are equivalent in order to avoid the same complex being included more than once in the mass balance equations used in speciation codes.

In some cases there are additional data that can be used to deduce the chemically correct stoichiometry. This is of great importance for *chemical* discussions of structure and bonding. One example is offered by $(\text{UO}_2)_3(\text{OH})_5^+$, which is a predominant hydrolysis complex in the pH range 4-7. This complex has been studied by X-ray scat-

Figure III.11: Isomorphous substitution of UO_2^{2+} with NpO_2^{2+} or PuO_2^{2+} in $(\text{UO}_2)_3(\text{CO}_3)_6^{6-}$. One or possibly two uranyl ions may be replaced by another actinide(VI)yl-ion with the overall geometry retained [83ABE/FER]. The filled circles denote MO_2^{2+} ions and the open circles the carbonate oxygen atoms.



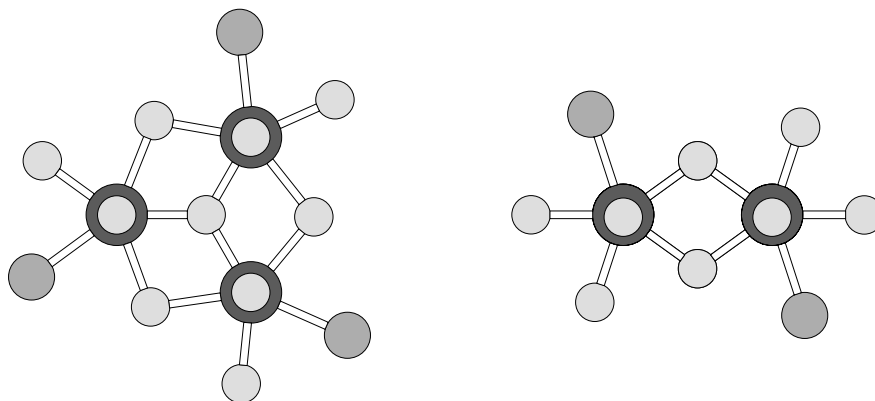
tering in solution [70ABE] and found to have a planar geometry and the stoichiometry $(\text{UO}_2)_3(\text{O})(\text{OH})_3^+$, *cf.* Figure III.12.

General information on the coordination may sometimes be used to ascertain whether a proposed stoichiometry is chemically reasonable or not. An example from Grenthe and Lagerman [91GRE/LAG] is given in *Chemical Thermodynamics of Uranium* [92GRE/FUG], where the chemical composition of the ternary complex $(\text{UO}_2)_{11}(\text{CO}_3)_6(\text{OH})_{12}^{2-}$ proposed in a aqueous-solution study was justified through a chemical-structure reasoning.

The composition of the complexes formed in polynuclear metal hydroxide systems depends on the pH and the total concentration of the metal ion. This is shown in the distribution diagrams (Figure III.13) for the hydrolysis of lead(II) at two different total concentrations, 0.10 M and 1×10^{-5} M, respectively.

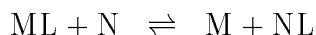
In many modelling situations it is interesting to describe the behaviour of an element present in trace concentrations. Under these circumstances we expect hydroxide complexes to occur mainly in mononuclear form. However, when studying hydrolysis in the laboratory it is often an experimental necessity to use much higher concentrations, where the hydrolysis is dominated by the formation of polynuclear species, *cf.* Figure III.13. The experimental determination of equilibrium constants for mononuclear species may then be impossible, or accompanied by large uncertainties. As a result the database for mononuclear hydroxide complexes is often rather poor, and it may be necessary to estimate the constants, we will come back to this in Section III.6.3.

Figure III.12: The structures of $(\text{UO}_2)_3(\text{O})(\text{OH})_3^+$ and $(\text{UO}_2)_2(\text{OH})_2^{2+}$ in the solid state (Uranium atoms are represented by the darker and larger spheres, Oxygen atoms by the small light-gray spheres, and Chlorine atoms are shown by the spheres of intermediate shade and size). In the left figure, the central oxygen atom represents an oxide ion and the bridging oxygen atoms are hydroxide groups. The remaining coordination positions are occupied by water oxygens and chloride ions. The bridging oxygen atoms in the figure to the right belong to hydroxide ions. The X-ray technique used does not allow the determination of hydrogen atom positions [70ABE].



III.5.4. Competition between different metal ions for the same ligand

We can illustrate this process by the following simple exchange reaction between two metal ions M and N and a ligand L:

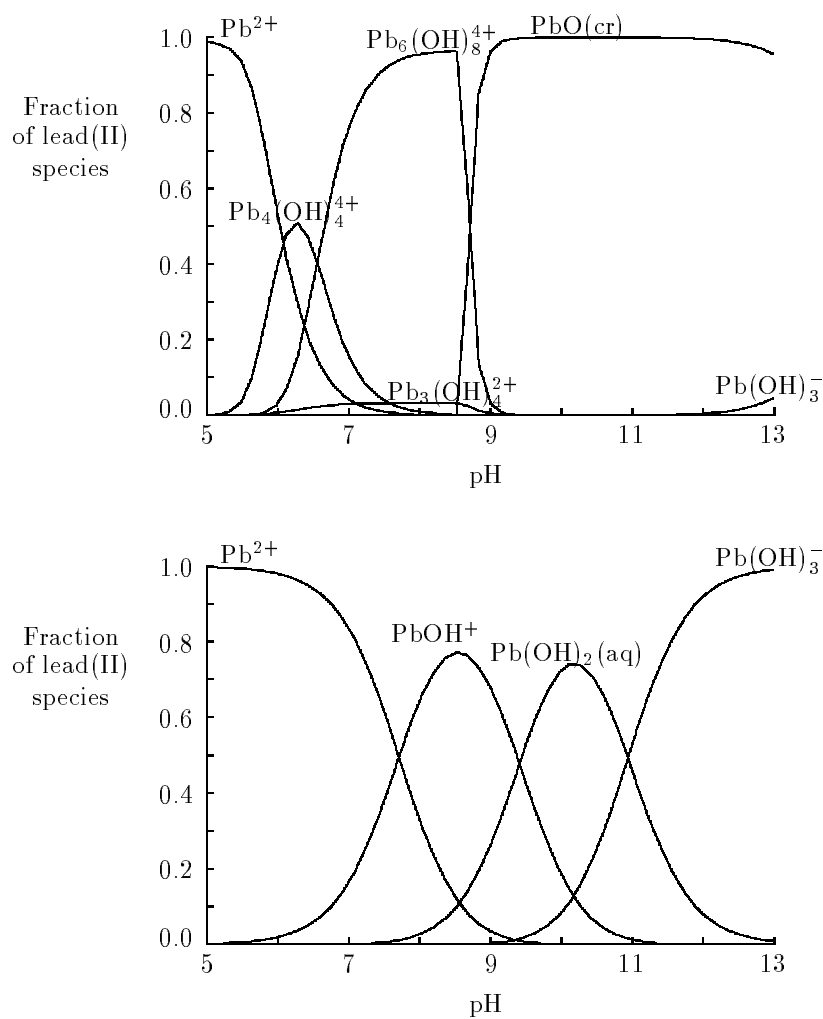


with the equilibrium constant

$$K = \beta_{\text{N}}/\beta_{\text{M}} = \frac{[\text{NL}][\text{M}]}{[\text{ML}][\text{N}]}$$

The relative amounts of the species ML and NL depend *both* on the equilibrium constants, *and* the total concentrations of M and N. As a result a metal ion like Ca^{2+} that is present in fairly large amounts in many ground and surface water systems may have an important influence on the speciation of a trace element, even if the complex formation constants of this are much larger than for Ca^{2+} .

Figure III.13: Distribution diagrams for lead(II) hydrolysis at two total metal concentrations: 0.10 M (upper diagram) and 1×10^{-5} M (lower diagram). The source for the hydrolysis equilibrium constants is Ref. [76BAE/MES].



Example 5:

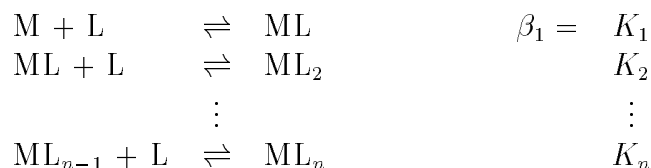
Calcium(II) and Cerium(III) are both present in ground and surface water systems. Both elements form complexes with carbonate (a component in these systems), but of very different strength: $\log_{10} \beta_1(\text{Ca}^{2+}) \approx 3.2$, and $\log_{10} \beta_1(\text{Ce}^{3+}) \approx 7.6$, $\log_{10} \beta_2(\text{Ce}^{3+}) \approx 12.2$, for the formation of $\text{CaCO}_3(\text{aq})$, CeCO_3^+ and $\text{Ce}(\text{CO}_3)_2^-$, respectively. Figure III.14 shows the relative amounts of $\text{CaCO}_3(\text{aq})$ and CeCO_3^+ as a function of $\log_{10}[\text{CO}_3^{2-}]$ when the total concentrations of Ca(II) and Ce(III) are $1 \times 10^{-5} \text{ M}$ and $1 \times 10^{-8} \text{ M}$ respectively.

III.6. Theoretical framework for the estimation of equilibrium constants

The varying chemical conditions in nature may result in the formation of totally new species for which no laboratory data are available. When modelling chemical processes it is essential to keep this possibility in mind. Thermodynamic databases may thus be *incomplete* and it is necessary for the modeller to be able to judge *if* and *where* such lack of data may occur. This requires knowledge both of the general chemical principles, which often are qualitative, and methods to *estimate* the stoichiometry of complexes and their corresponding thermodynamic data.

III.6.1. On the magnitude of equilibrium constants and the ratios between equilibrium constants for successive complex formation reactions

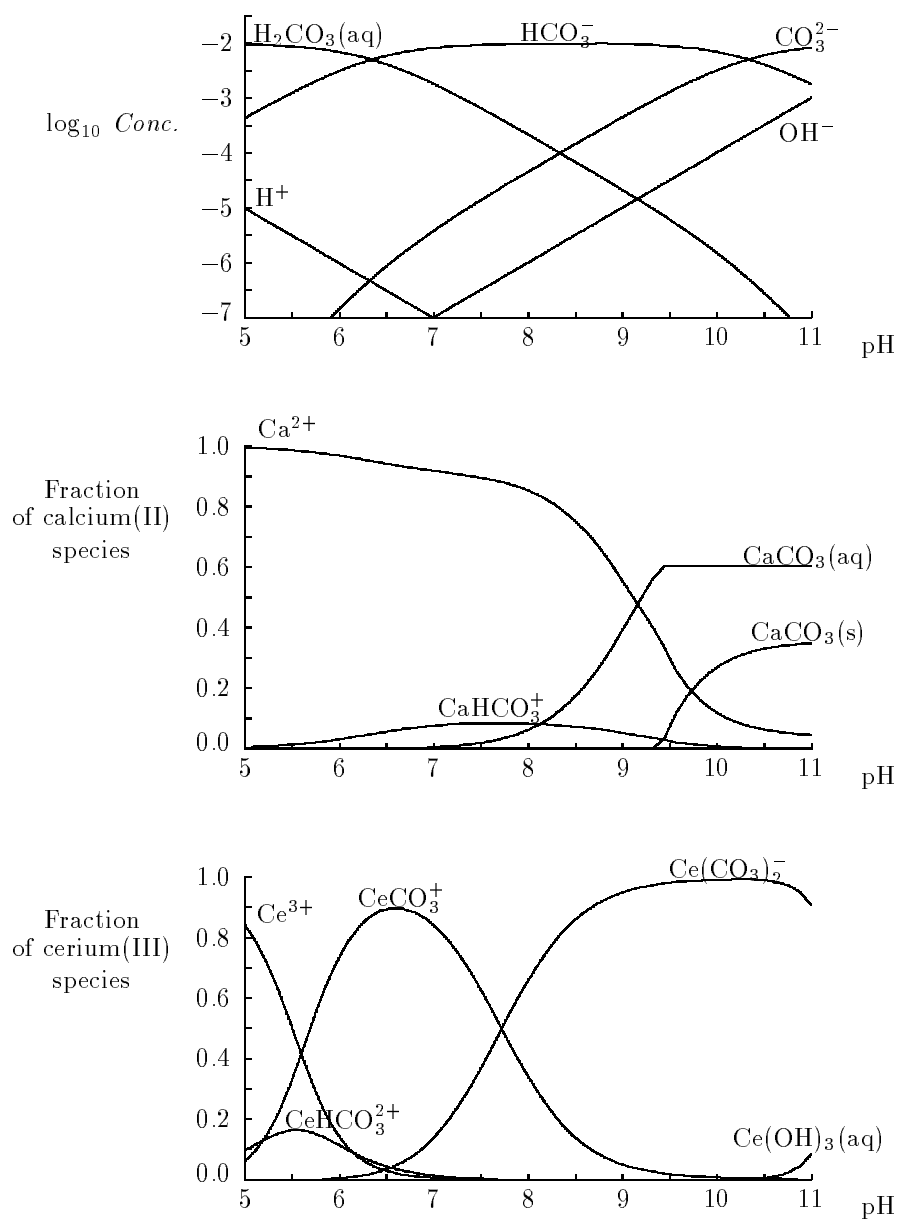
In systems where more than one ligand is bonded to the metal ion we can define equilibrium constants for the consecutive reactions, which are of the type:



And we have $\beta_n = K_1 K_2 \dots K_n$.

With few exceptions these equilibrium constants decrease in the order $K_1 > K_2 > \dots > K_n$. The exceptions are found mainly among the mononuclear hydrolysis reactions (where the quality of the data are not always as good as would be desired), for systems containing π -bonding ligands such as cyanide, and for some reactions involving Hg(II) and Tl(III). This empirical finding is useful when estimating equilibrium constants for higher complexes in situations where there is only experimental information for the formation of the first complex. We can go a step further and explore the expected ratios between equilibrium constants for consecutive complex formation reactions in chemical systems where we have a well defined coordination geometry, assuming that these are based on statistical considerations alone.

Figure III.14: Carbonate complexes of calcium(II) and cerium(III). The pH-dependence of the free carbonate concentration is shown in the upper plot under the same conditions as the lower graphs (note that $[\text{CO}_3^{2-}]$ changes by a factor $> 10^6$ in this pH-range). All three diagrams have been calculated at $[\text{CO}_3^{2-}]_{\text{total}} = 0.01 \text{ M}$, and the two lower diagrams with $[\text{Ca(II)}]_{\text{total}} = 10^{-5} \text{ M}$, and $[\text{Ce(III)}]_{\text{total}} = 10^{-8} \text{ M}$ for both. Note that calcite (CaCO_3) precipitates at $\text{pH} > 9.2$ under these conditions. Setting $[\text{Ca(II)}]_{\text{total}} = 0$ does not affect the lower diagram because the carbonate/Ca(II) ratio is large. Equilibrium constants (at $I = 0$ and 25°C) are from [78KRA/DEC, 90WOO, 93MOR/HER].



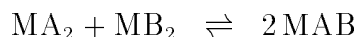
Example 6:

Let us consider the case discussed by Beck and Nagypál [90BEC/NAG]: the coordination of a bidentate ligand to a metal ion with octahedral coordination geometry (an octahedron has six corners and twelve edges). The first ligand molecule can bind along any of the edges, and it can dissociate in only one way. The second ligand molecule can then bind along any of the five remaining edges, where no corner is occupied by the first ligand, and the dissociation can occur in two different ways. If the complex formation is determined by statistical factors alone we expect the ratio between the first two constants to be: $K_1/K_2 = \frac{12}{1} \times \frac{2}{5} = 4.8$.

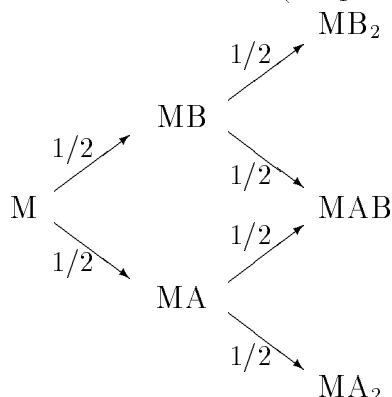
The third ligand can only be bonded in one way, but dissociate in three. This statement must be modified for the case where the two ligands are bonded in trans-position to one another. The two free positions in the coordination polyhedron are then opposite one another and not along a common edge. This distance is so large that the ligand cannot span it. One out of the five possibilities of binding the second ligand gives rise to this trans-bonding. Hence, the expected ratio between K_2 and K_3 based on statistical considerations is: $K_2/K_3 = \frac{5}{2} \times \frac{3}{1} \times \frac{5}{4} = 9.375$.

III.6.2. Estimation of equilibrium constants for ternary complexes

It is also possible to calculate the *statistical* value of the equilibrium constant for a mixed complex from the equilibrium constants of the corresponding binary complexes, *e.g.*,



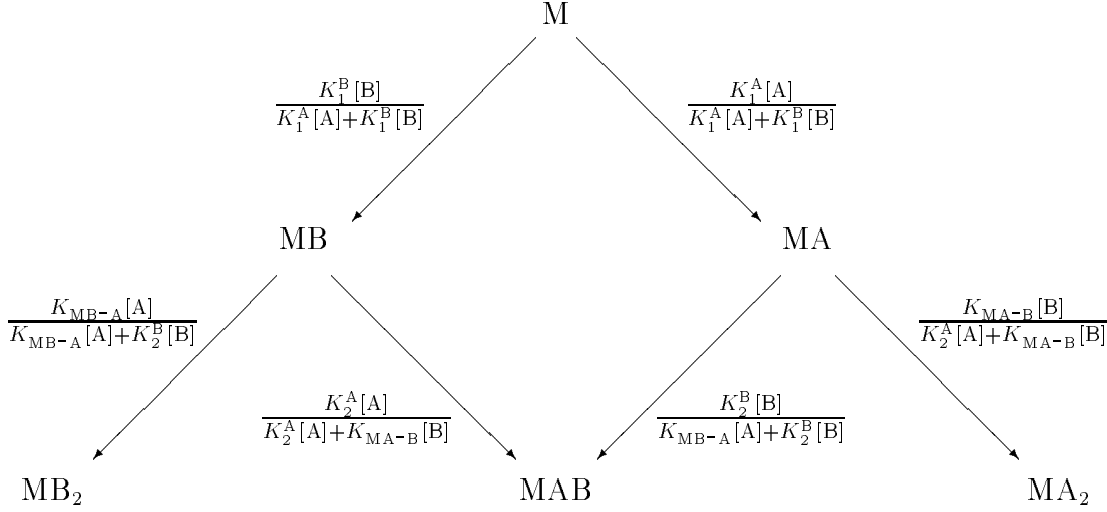
If we select ligands that give complexes with the same number of donor atoms we have the following probabilities for the various reactions (adapted from [90BEC/NAG]):



i.e., the probabilities of formation of MA_2 and MB_2 are both proportional to $\frac{1}{2} \times \frac{1}{2} = \frac{1}{4}$, while the probability of formation of MAB is proportional to $2 \times \frac{1}{4} = \frac{1}{2}$. The statistical value for the equilibrium constant is then $(\frac{1}{2})^2 / (\frac{1}{4})^2 = 4$, or $\beta_{\text{MAB}}^2 = 4 \times \beta_{\text{MA}_2} \times \beta_{\text{MB}_2}$.

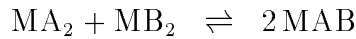
Experimental observations indicate that the ratio between successive equilibrium constants often deviates significantly from the statistical value – the reason is that the chemical interactions in general are *specific*.

In most cases the behaviour of the binary systems are experimentally known. In this situation one can modify the statistical procedure for estimating the equilibrium constant of the mixed complexes. The procedure for a three component system is outlined in the following scheme (adapted from [90BEC/NAG]):



where the quantities K_{MA-B} and K_{MB-A} are equilibrium constants which describe the affinities of MA for B and MB for A, respectively. If MA and MB bind A and B equally we have $K_{MA-B} = K_2^A$ and $K_{MB-A} = K_2^B$. If B binds with the same strength to MA and MB we have $K_{MA-B} = K_2^B$ and for A $K_{MB-A} = K_2^A$. If we do not know the real bond strength we can use $K_{MA-B} = K_{MB-A} = \sqrt{K_2^A \cdot K_2^B}$ as a reasonable estimate. K_1 and K_2 are the stepwise equilibrium constants in the binary systems.

Beck and Nagypál [90BEC/NAG] give an extensive discussion, and we will just present their results for reactions of the type depicted in the previous scheme. The statistical value for the equilibrium constant for the reaction



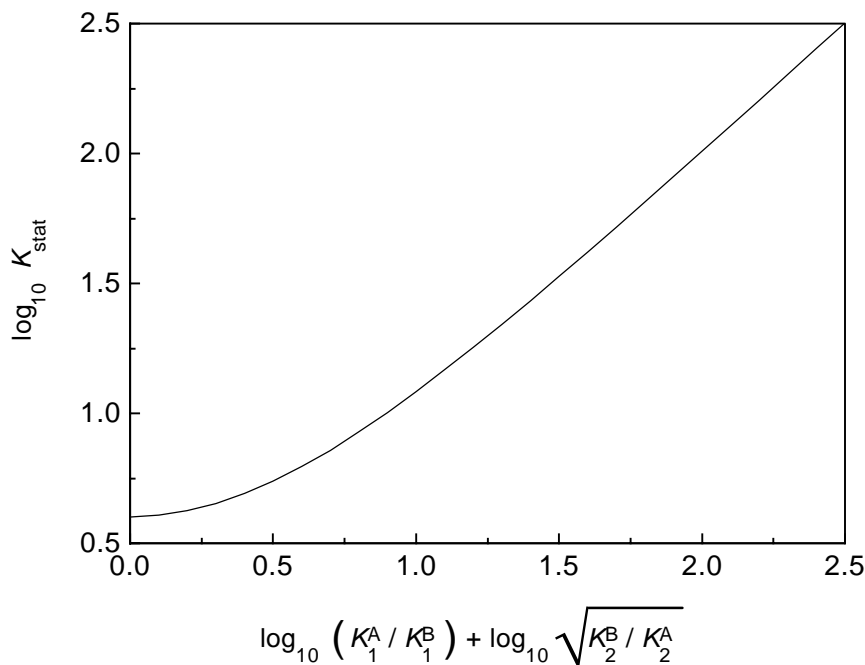
is equal to

$$K_{\text{stat}} = 2 + \frac{K_1^A}{K_1^B} \cdot \sqrt{\frac{K_2^B}{K_2^A}} + \frac{K_1^B}{K_1^A} \cdot \sqrt{\frac{K_2^A}{K_2^B}} \quad (\text{III.3})$$

From this expression we find that $K_{\text{stat}} = 4$ only holds if $K_1^A/\sqrt{K_2^A} = K_1^B/\sqrt{K_2^B}$. In all other cases the value of K_{stat} is larger.

Figure III.15 shows the value of $\log_{10} K_{\text{stat}}$ if the formation of the ternary complexes is governed by statistical factors only and $K_{MA-B} = K_{MB-A} = \sqrt{K_2^A \cdot K_2^B}$. This curve could be used as a guideline for estimating such equilibrium constants, when the behaviour of the binary systems are known. The ternary system $\text{Hg(II)}\text{-Cl}^-\text{-OH}^-$, cf. Figure III.9, is

Figure III.15: The statistically expected equilibrium constant K_{stat} for $\text{MA}_2 + \text{MB}_2 \rightleftharpoons 2\text{MAB}$ as a function of $\log_{10}((K_1^A/K_1^B) \cdot \sqrt{K_2^B/K_2^A})$. Adapted from [90BEC/NAG].



an example where the magnitude of the equilibrium constant for the ternary complex $\text{HgOHCl}(\text{aq})$ deviates strongly from the statistical value.

We can use data for the U(VI)-oxalate and carbonate systems to estimate the equilibrium constant for the formation of the complex $[\text{UO}_2(\text{ox})\text{CO}_3]^{2-}$.

Example 7:

Estimate the equilibrium constants for the formation of $\text{UO}_2(\text{oxalate})(\text{CO}_3)^{2-}$ from the following equilibrium constants for the binary systems (data at $I = 0$, carbonate and oxalate constants are taken from [92GRE/FUG] and [69HAV], respectively):

$$\begin{aligned} \log_{10} \beta_1(\text{UO}_2\text{CO}_3) &= 9.7 ; & \log_{10} \beta_2(\text{UO}_2(\text{CO}_3)_2^{2-}) &= 16.9 ; \\ \log_{10} K_2(\text{UO}_2(\text{CO}_3)_2^{2-}) &= 7.2 \\ \log_{10} \beta_1(\text{UO}_2(\text{oxalate})) &= 7.2 ; & \log_{10} \beta_2(\text{UO}_2(\text{oxalate})_2^{2-}) &= 11.9 ; \\ \log_{10} K_2(\text{UO}_2(\text{oxalate})_2^{2-}) &= 4.7. \end{aligned}$$

- If we assume that the stepwise complexes in *both* the binary systems and in the ternary complex are formed statistically we have

$$\begin{aligned}\beta^{\text{stat}}(\text{UO}_2(\text{oxalate})\text{CO}_3^{2-}) &= 2\sqrt{\beta_2(\text{UO}_2(\text{oxalate})_2^{2-})\beta_2(\text{UO}_2(\text{CO}_3)_2^{2-})} \\ \log_{10} \beta(\text{UO}_2(\text{oxalate})\text{CO}_3^{2-}) &= 14.7\end{aligned}$$

- If we use the experimental ratios of the stepwise constants we will have a different result because these are quite different in the two systems. For the carbonate system we have

$$\log_{10} \beta_1(\text{UO}_2\text{CO}_3) - \frac{1}{2} \log_{10} K_2(\text{UO}_2(\text{CO}_3)_2^{2-}) = 6.1$$

and in the oxalate system

$$\log_{10} \beta_1(\text{UO}_2(\text{oxalate})) - \frac{1}{2} \log_{10} K_2(\text{UO}_2(\text{oxalate})_2^{2-}) = 4.9$$

By using the curve in Figure III.15 and the experimental quantity

$$\log_{10} \frac{\beta_1(\text{UO}_2\text{CO}_3)}{\beta_1(\text{UO}_2(\text{oxalate}))} \sqrt{\frac{K_2(\text{UO}_2(\text{oxalate})_2^{2-})}{K_2(\text{UO}_2(\text{CO}_3)_2^{2-})}}$$

we obtain $\log_{10} K^{\text{stat}} = 1.25$ and $\log_{10} \beta(\text{UO}_2(\text{oxalate})\text{CO}_3^{2-}) = 15.0$.

This example may give an idea of the uncertainty in this type of estimations !

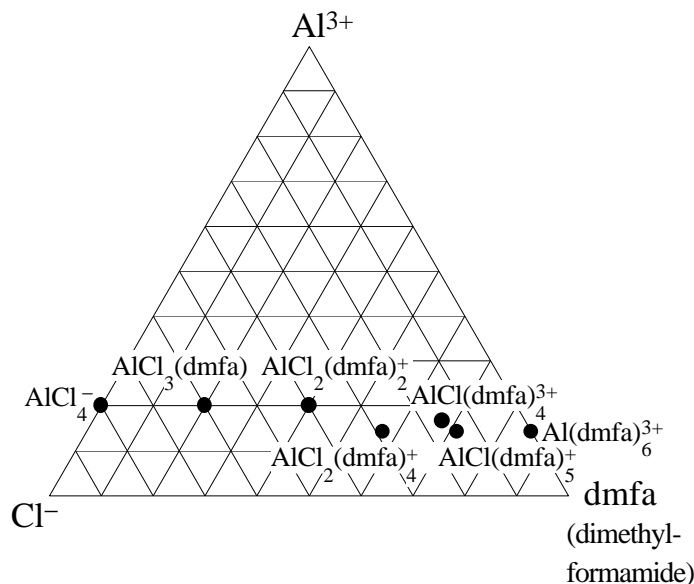
A “phase diagram”, *cf.* Figure III.16, where the components, a metal ion and two ligands are placed in the corners of an equilateral triangle, may be used to describe different ternary systems:

- if only binary interactions occur in the system, all compositions fall along two of the sides of the triangle. The properties of the three-component system are then the sum of those of the constituent binary systems.
- if the metal cation, Me, forms ternary complexes with the two ligands, X and Y, there will be composition points inside the ternary diagram, and the system is not additive. In the absence of experimental information, it is necessary to use the general theories from coordination chemistry to estimate the stoichiometry and equilibrium constants of the possible complexes that may form in these systems.

In systems where ternary complexes are formed, the properties of the ternary system will be equal to the sum of the Me–X and Me–Y systems only when the concentration of the ternary species is negligible in comparison with the binary complexes.

In general one finds that the system is additive when the bonding strength between the metal cation and the two ligands differs considerably. The formation of predominating amounts of ternary complexes (with the exception of H^+ and OH^- containing species)

Figure III.16: Compositions of complexes formed in the Al^{3+} - Cl^- -dimethylformamide system. Adapted from [90BEC/NAG].

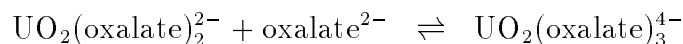


requires a close balance between ligand geometry, bonding strength and concentrations, and this situation is likely to be rare.

In many modelling situations one has a rather large number of components, and there is in general no information on the possible ternary, or higher interactions among all these components. The discussion above indicates that to describe ternary interactions, only a small number of the components need to be taken into account – the *choice* of these components must be based on general chemical knowledge.

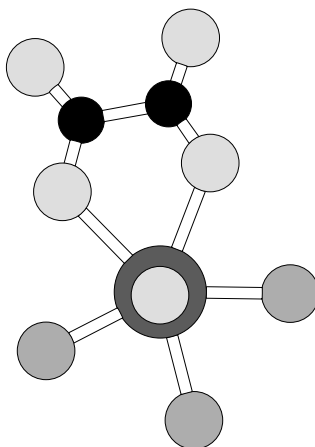
Example 8:

Estimate the possible stoichiometric compositions for a ternary system containing UO_2^{2+} , a bidentate ligand (oxalate, carbonate), and a strong binding monodentate ligand like fluoride or hydroxide. The coordination geometry around U(VI) is a pentagonal, or hexagonal bipyramid. Figures III.17, III.18 and III.19 illustrate the geometry of some binary and ternary complexes studied in the solid state. The uranium(VI) oxalate system has been studied in solution by Havel [69HAV] who found that the equilibrium constant for the reaction



was only $\log_{10} K_3 = 0.4$, *i.e.*, much smaller than those for the formation of the first two oxalate complexes (which are $\log_{10} K_1 = 6.0$ and $\log_{10} K_2 = 4.7$, all data at $I = 1 \text{ M}$). This finding fits nicely with the structural information (Figures III.17 to III.19) which indicates that the third ligand can only use one of its carboxylate groups in bonding, with

Figure III.17: The coordination geometry of uranyl oxalate complexes. I. $\text{UO}_2(\text{oxalate})\text{F}_3^{3-}$. All ligands are located in a plane perpendicular to the linear O-U-O axis, forming a pentagonal bipyramid.



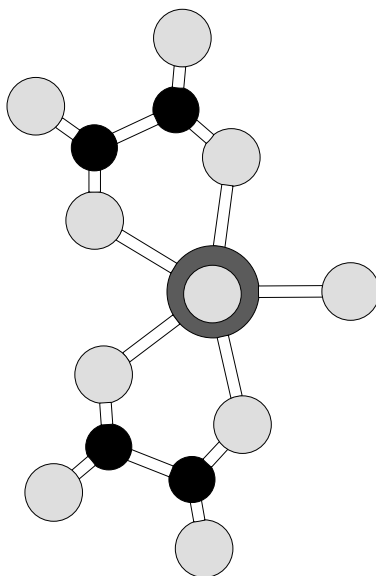
a much lower equilibrium constant as a result. This is an example of steric interference. There is not room for three oxalate groups bonded by both their carboxylate groups. The ligand bite is at least 0.2 \AA smaller when the oxalate uses a carboxylate group that is bonded “end-on” and this makes it possible to bind the third ligand.

Based on structural information alone, one might therefore expect the following ternary complexes to be formed: $\text{UO}_2(\text{oxalate})\text{F}^-$, $\text{UO}_2(\text{oxalate})\text{F}_2^{2-}$, $\text{UO}_2(\text{oxalate})\text{F}_3^{3-}$, $\text{UO}_2(\text{oxalate})_2\text{F}^{3-}$. F^- can be replaced by hydroxide. For carbonate, the same stoichiometries are possible. In the four component system U(VI)-carbonate-oxalate-fluoride, the ternary complex $\text{UO}_2(\text{oxalate})\text{CO}_3^{2-}$ might also be formed.

III.6.3. On the use of correlations for the prediction of equilibrium constants

The equilibrium constant is a characteristic of a *reaction*, nevertheless it is often possible to correlate the values of $\log_{10} K$ for a series of reactions with some property(ies) of the metal ion or the ligand. Correlations of this type are always based on a chemical model/theory, and they are useful because they summarise the properties of a large group of data in a concise way, at the same time as they provide a rationale for *predicting* the values of equilibrium constants for which no experimental data are available. It must be emphasised that the *efficient* use of correlations *requires* chemical information about coordination geometry, donor-acceptor characteristics, information of the structure and conformation freedom of the ligand, *etc.* It is within classes of reactions that share some common characteristics that correlations are most precise. In the following section we will give examples of some of the correlations used by coordination chemists.

Figure III.18: The coordination geometry of uranyl oxalate complexes. II. $\text{UO}_2(\text{oxalate})_2\text{H}_2\text{O}^{2-}$. All ligands are located in a plane perpendicular to the O-U-O axis, forming a pentagonal bipyramid.



III.6.3.1. Correlations based on the size and charge of the metal ion

The theoretical idea behind these type of correlations is the *ionic model* of chemical bonding, *i.e.*, a model where the chemical forces between atoms are largely of electrostatic type. We then expect that the bond energy, E , between a certain ligand and a series of different metal ions will be governed by the size and charge of the reactants as follows:

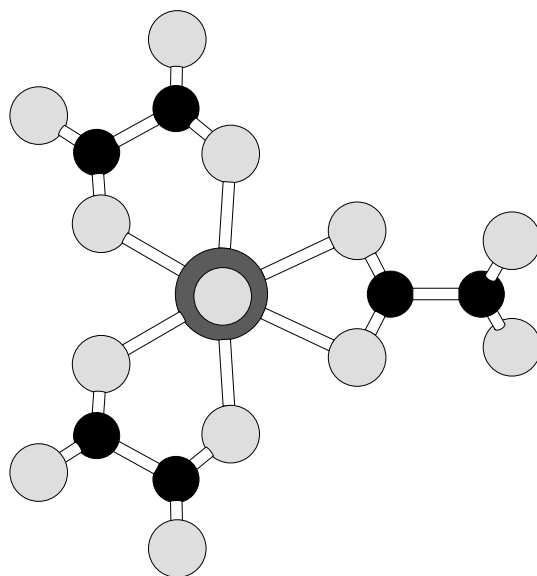
$$E \propto Z_{\text{M}}Z_{\text{L}}/d_{\text{M-L}}$$

where Z_{M} and Z_{L} are the charges of metal ion and ligand, respectively, and $d_{\text{M-L}}$ is the bond distance between them, *cf.* p.75. When comparing complexes between different metal ions and the same ligand we expect that: $E \propto Z_{\text{M}}/d_{\text{M-L}}$.

Correlations of this type should work best for chemical systems where the general chemical behaviour indicates a significant electrostatic component in the chemical bonding, *e.g.*, the bonding between hard acceptors and hard donors.

A theory based on this concept was developed by Kossiakoff and Harker [38KOS/HAR] to describe the protolytic behaviour of inorganic acids of the type $\text{MO}_p(\text{OH})_q^{(2p+q-z)-}$. This theory was used and extended by Baes and Mesmer to describe the variations of the first hydrolysis constants of metal-hydroxide complexes with the “ion-potential”, $z/d_{\text{M-O}}$ of the metal ion. Figure III.20 illustrates the results of this type of correlations. It should be pointed out that the uncertainty in the experimental

Figure III.19: The coordination geometry of uranyl oxalate complexes. III. $\text{UO}_2(\text{oxalate})_3^{4-}$. The three oxalate ligands are placed in a plane approximately perpendicular to the O-U-O axis, forming a hexagonal bipyramid. The third ligand can only use one of its carboxylate groups in bonding. This ligand is no longer planar as the other two.

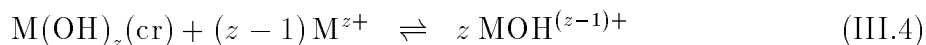


equilibrium constants may be large, because the predominant reactions in these systems involve polynuclear species.

Fluoride complexes are also expected to show a similar behaviour and Figure III.21 shows the dependence of the equilibrium constant for the formation of MF^{n+} complexes for several metal cations with $z/d_{\text{M-F}}$.

Baes and Mesmer have made extensive use of “electrostatic” type of correlations in their discussions of the chemistry of metal-ion hydrolysis and the solubility of hydrous metal oxides.

For the reaction:



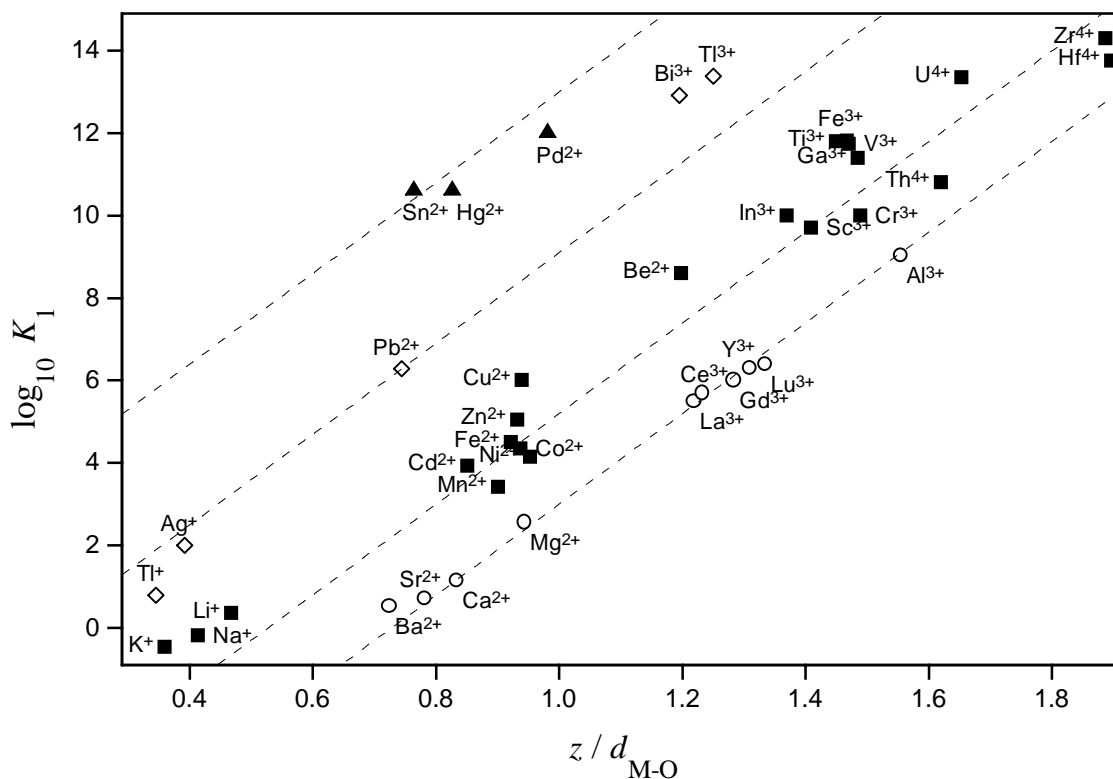
we have

$$K(\text{III.4}) = \frac{[\text{MOH}^{(z-1)+}]^z}{[\text{M}^{z+}]^{z-1}} = K_1^z K_{s,0}$$

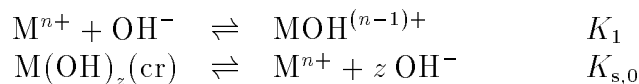
and

$$\log_{10} K(\text{III.4}) = z \log_{10} K_1 + \log_{10} K_{s,0} \quad (\text{III.5})$$

Figure III.20: The linear dependence of $\log_{10} K_1$ for reaction: $M^{n+} + OH^- \rightleftharpoons MOH^{(n-1)+}$, on the ratio of the charge to the M-O distance for four groups of cations. The dashed lines show the correlations given by Baes and Mesmer [76BAE/MES], *cf.* their Figure 18.4.



where K_1 and $K_{s,0}$ correspond to the following two equilibria respectively:



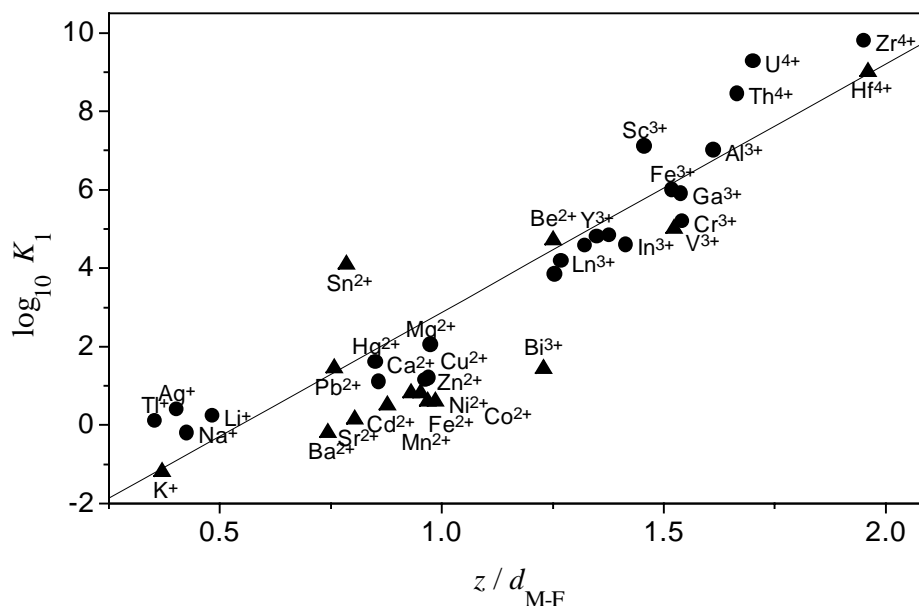
The value of $\log_{10}(K_1^z K_{s,0})$ is -5.6 for most metal cations, as indicated by the plot of $\frac{1}{z}(\log_{10} K_{s,0} + 5.6)$ *vs.* $\log_{10} K_1$ shown in Figure III.22.

Correlations of this type are very useful to predict $\log_{10} K_1$ (which often are difficult to measure experimentally) from $\log_{10} K_{s,0}$ (which often can be determined experimentally with high precision).

For further details about these and other correlations for this important group of complexes, the reader is referred to Chapter 18 in the classic book by Baes and Mesmer: “The Hydrolysis of Cations” [76BAE/MES].

There are other correlations between the ionic properties of metal cations, *e.g.*, between the ionic radius and the electronic configuration, the charge, the electronegativity, and the ionisation potential. Hence, one also expects correlations between equilibrium constants and these quantities, an example is the following correlation (van Panthaleon

Figure III.21: The dependence of $\log_{10} K_1$ for the formation of metal fluoride complexes, MF^{n+} , with the ratio of the charge to the M-F distance. Ionic radii are from [69SHA/PRE], and stability constants are from [76SMI/MAR, 82MAR/SMI, 89SMI/MAR] (circles: data at $I = 0$, triangles: data at $I > 0$).



van Eck [53PAN]):

$$\log_{10} K_1 = p(I_n - q)$$

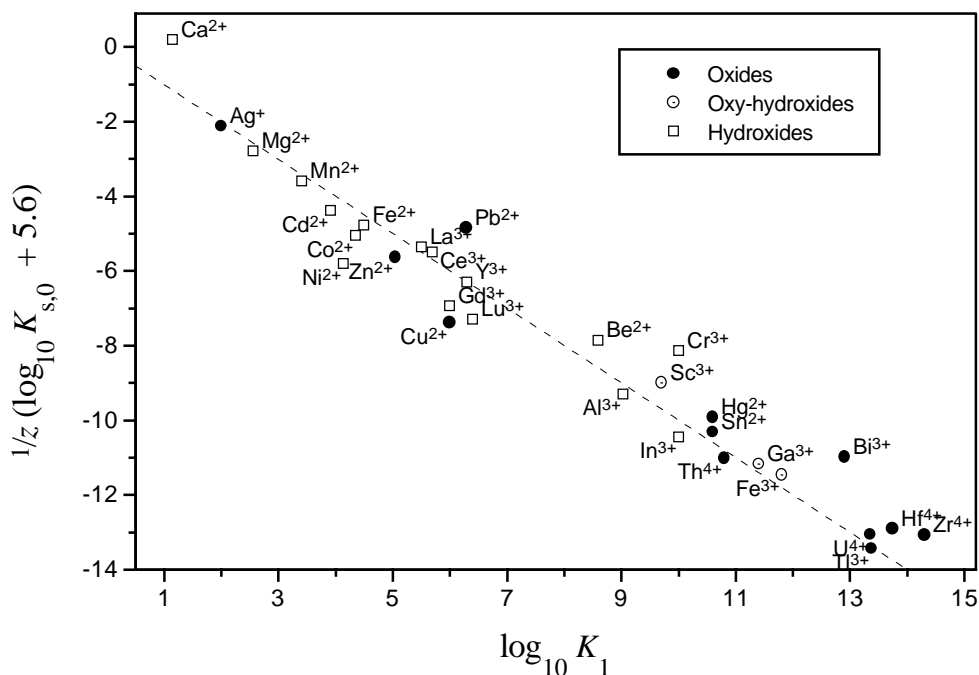
where K_1 is the equilibrium constant for the formation of the complex ML , I_n is the n :th ionisation potential of the cation M^{n+} , and p and q are constants which depend on the ligand and the experimental conditions. An example of this kind of correlation is given in Figure III.23 for some complexes of glycine. The same equilibrium constants are plotted as a function of the electronegativity of the metal cation in Figure III.24 as an example of another type of correlation between equilibrium constants and ionic properties.

III.6.3.2. Ligand field theory and Irving and Williams series

The equilibrium constants for the 3-d transition elements from Mn(II) to Zn(II) vary in a regular way as indicated in Figure III.25.

The observed variations can qualitatively be explained by using the ligand-field theory. According to this the observed variations are a result of the different d -electron configurations of the central ion. This theory is useful for describing the variation of thermodynamic quantities for transition elements with partially filled d -orbitals. More details may be found in standard textbooks [84GRE/EAR, *p.*1096; 86COT/WIL, *p.*467]. The general increase in stability from Mn(II) to Zn(II) may be looked upon as a result

Figure III.22: The constancy of the equilibrium constant for Reaction (III.4): $M(OH)_z(cr) + (z-1)M^{z+} \rightleftharpoons zMOH^{(z-1)+}$. The line corresponds to $K(III.4) = K_1^z K_{s,0} = 10^{-5.6}$, cf. Eq. (III.5). Data from [76BAE/MES] at $I = 0$ and $25^\circ C$.

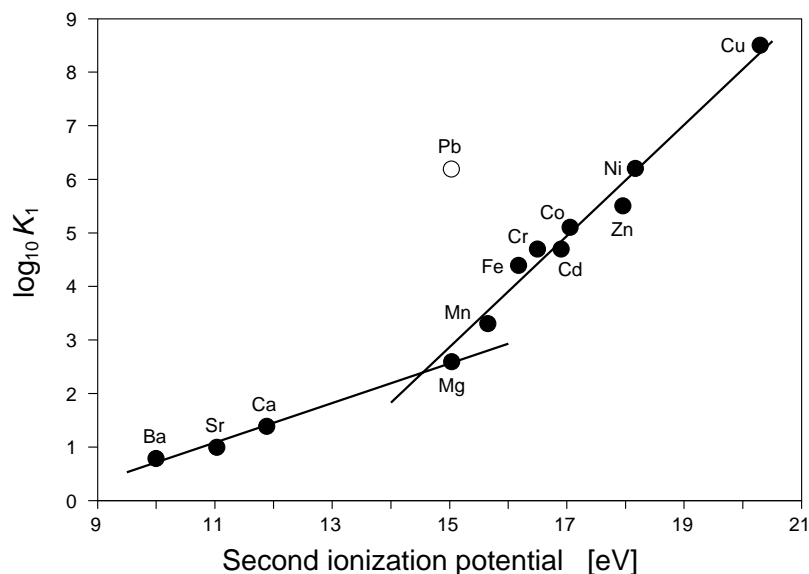


of the decreasing ionic radius from Mn^{2+} to Zn^{2+} , while the other variations are a result of differences in the d -electron configurations among the metal ions. The variations observed depend on the donor atoms in the ligands and the coordination geometry. Hence interpolations may only be made for a series of complexes of the same stoichiometry and coordination geometry. Correlations may be made not only for stability constants, but also for other thermodynamic quantities [53IRV/WIL, 95JOH/NEL].

III.6.4. Correlations based on properties of the ligand

The most important of these correlations is between the $\log_{10} K$ values for the formation of metal complexes between the same metal and different ligands and the $\log_{10} K$ for the protonation of the same ligands. The theoretical concept behind this is that both the binding of a proton and a metal ion to the ligand are chemically similar processes, a Lewis acid/base reaction involving the donation of an electron pair from a donor (the ligand) to an acceptor (the proton, or a metal ion). This and other correlations assume that *one* characteristic property is responsible for the variation of the $\log_{10} K$ -values. This is seldom the case. However, the correlations are most likely to work for complexes containing only few ligands that do not contain too many donor atoms, so that steric interference is less important. We will now give examples of correlations of this type and

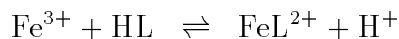
Figure III.23: The dependence of the stability constants, $\log_{10} K_1$, of some M(II)-glycine complexes as a function of the second ionisation potential of the central metal ion. The stability constants are taken from [91KIS/SOV]. Distinct correlations are found for alkaline earth metals and transition metals of oxidation state +2. Pb(II) does not fit in either correlation.



also discuss the observed deviations.

Figure III.26 shows correlations between the equilibrium constants for the formation of Fe(III) complexes with substituted phenols and salicylic acids. The donor atoms and the coordination geometry are the same for each ligand, but the protonation constants and the metal complexation varies by changing substituents in the non-bonding part of the ligands.

The two lines shown in Figure III.26 have a slope of one, *i.e.*, the equilibrium constants are strictly proportional to the protonation constants of the ligand. Hence, the equilibrium constant for the reactions



has the same value for all substituted salicylates. It is not uncommon to find slopes which differ from unity.

III.6.5. Correlations between equilibrium constants, $\log_{10} K$, of different metal ions

There are two types of correlations, the first between two metal ions of similar chemical characteristics (hardness/softness, charge and coordination geometry) and different ligands (Figures III.27 and III.28), and the second between ligands of similar chemical

Figure III.24: The dependence of the stability constants, $\log_{10} K_1$, of some M(II)-glycine complexes as a function of the electronegativities of the central metal ion. The stability constants are taken from [91KIS/SOV]. The electronegativities stem from [60PAU] (for Cu(II)) and [61ALL] (all other metal cations).

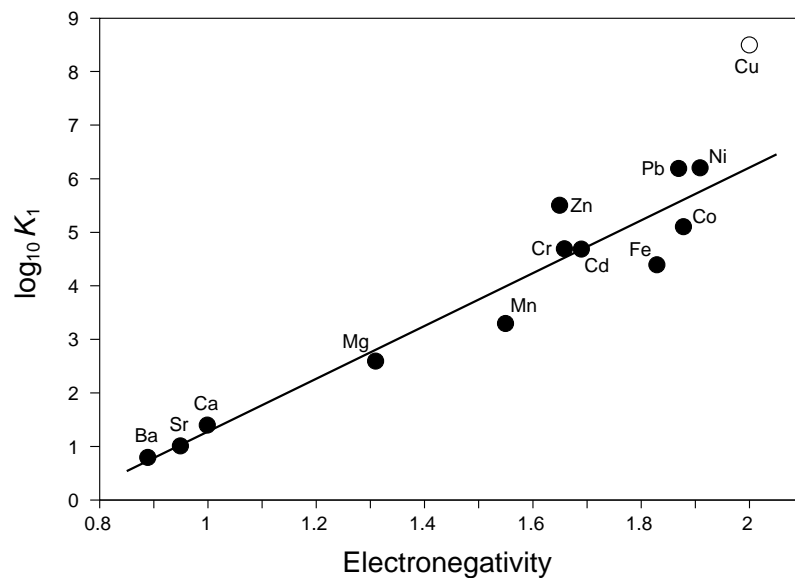


Figure III.25: The dependence of $\log_{10} \beta_2$ for complexes of bivalent transition metal cations with a few ligands. Values of $\log_{10} \beta_2$ originate from [89SMI/MAR]. Figure adapted from [81STU/MOR, 90BEC/NAG].

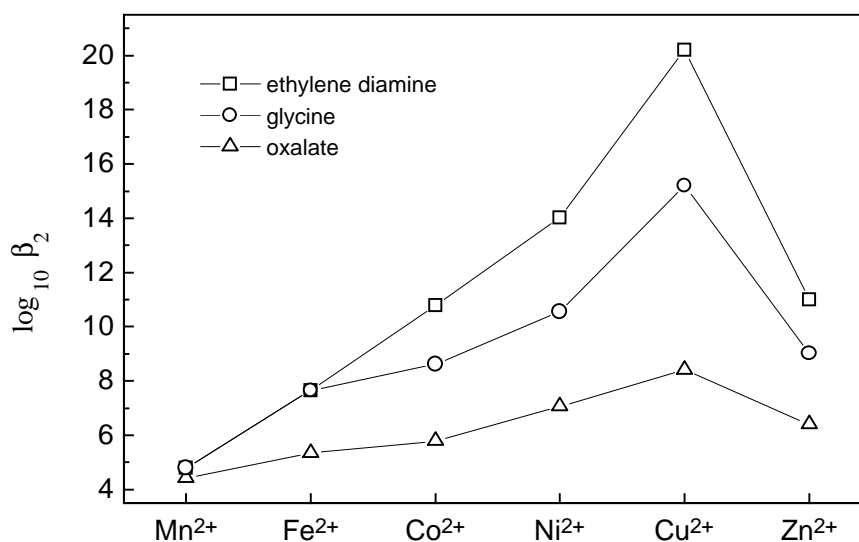
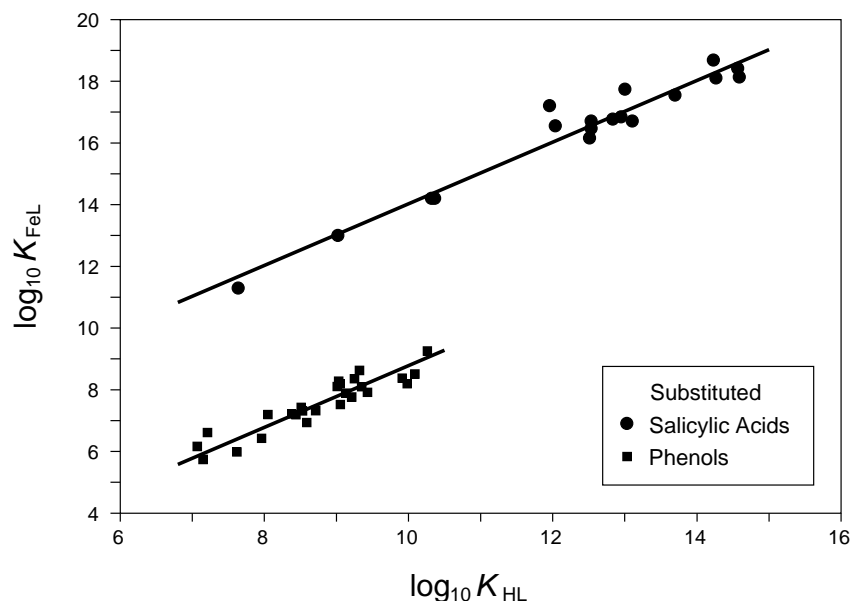


Figure III.26: Correlations between equilibrium constants for the formation of Fe(III) complexes with substituted phenols and salicylic acids and the first protonation constant of these acids. The data refer to zero ionic strength, and are from [77MAR/SMI, 82MAR/SMI, 89SMI/MAR]. Lines of unity slope are added for illustrative purposes.

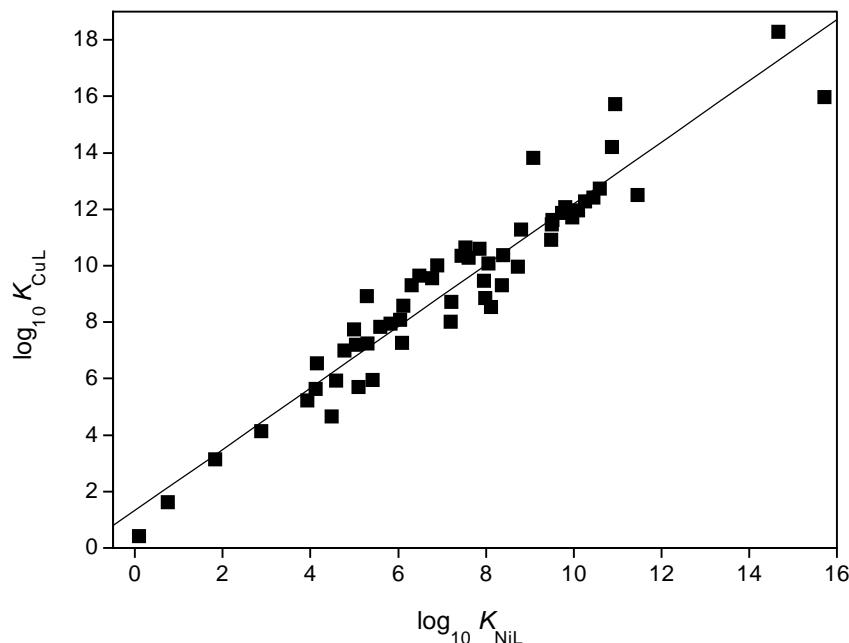


characteristics (hardness/softness, chelate rings and coordination geometry) and different metal ions (Figures III.29 and III.30).

The first diagram contains information about a large number of complexes of Cu(II) and Ni(II) with ligands containing different numbers and types of donor atoms (Figure III.27), the second diagram is a correlation between Sr^{2+} and Ca^{2+} complexes of different ligands (Figure III.28). The good correlation between the two metal ions indicate that the variation in chemical properties are rather similar (a fact known also from other chemical observations). This type of diagram is useful for the prediction of unknown stability constants for one metal, from known data for the other.

Other types of correlations are shown in Figures III.29 and III.30. The first shows the correlations between equilibrium constants for the ligands edta and dcta (1,2-diaminocyclohexane-N,N,N',N'-tetraacetate) for different metal ions. The two ligands contain the same number and type of donor atoms (two nitrogen atoms from the amino groups and four oxygens, one from each acetate group). The similarity in the ligand characteristics results in similar variations among the stability constants for a large group of different metal ions. There seems to be a systematic difference in stability of about 1.1 logarithmic units in favour of dcta. The metal ions given in the diagram are able to use all the available donor atoms. This is not the case for all metal ions, as illustrated by the following correlation diagram between edta and nta (nitrilo-triacetate) complexes.

Figure III.27: The relationship between equilibrium constants for copper and nickel complexes of several organic ligands. Adapted from [56IRV/ROS].

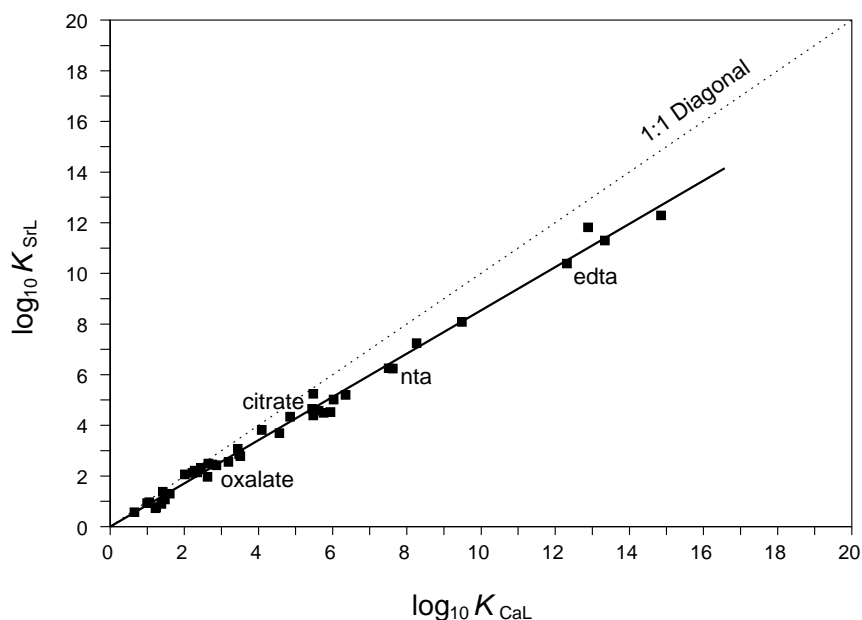


Both these ligands contain the same type of donor atoms, but their number and geometrical location are quite different: $(-\text{OCOCH}_2)_2\text{NCH}_2\text{CH}_2\text{N}(\text{CH}_2\text{COO}^-)_2$ for edta *versus*. $\text{N}(\text{CH}_2\text{COO}^-)_3$ for nta.

Figures III.31 to III.34 show the structures of some nta complexes. The nta/edta correlation line in Figure III.30 with a slope of 0.6 shows that the nta complexes are less stable than the corresponding edta complexes – this is no doubt due to the coordination of the six donor atoms in edta *versus* at most four in nta. However, the “-yl” complexes (NpO_2^+ , UO_2^{2+} and VO_2^+) of edta and nta are close to the 1:1 diagonal, indicating a similar coordination of the ligands. Figures III.35 and III.36 show that there is a mismatch between the coordination geometry of edta and the “yl”-cations. In the U(VI)-complex only one $\text{N}(\text{CH}_2\text{COO})_2$ group of the edta molecule can bind for sterical reasons. In the corresponding nta-complexes one presumably has the same type of coordination.

A comparison of the structure of $\text{VO}_2\text{edta}^{3-}$ (Figure III.35) with the coordination geometry of nta indicates that both ligands may bind with a similar geometry – Four bonded donor groups in both edta and nta should result in equilibrium constants of similar magnitude, which is confirmed by the experimental data.

Figure III.28: Correlation of stability constants for complexes of calcium and strontium with several organic ligands. The data refer to zero ionic strength, and are from [74MAR/SMI, 75SMI/MAR, 77MAR/SMI, 82MAR/SMI, 89SMI/MAR].

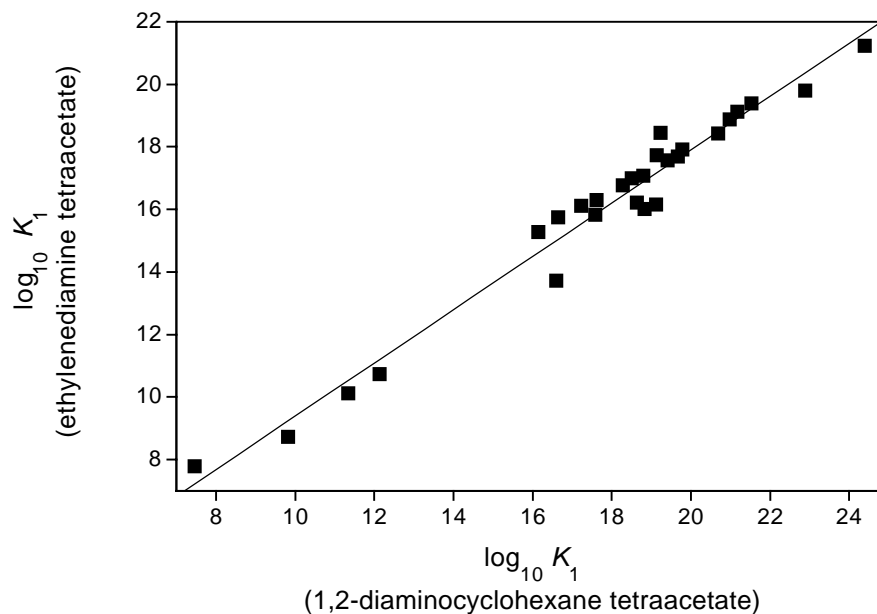


III.6.6. Correlations between successive equilibrium constants

In systems where mononuclear constants of the type ML_n are formed one often finds regularities between the successive equilibrium constants provided that there are no major changes in coordination geometry due to steric interference between the metal ions and the ligands, *cf.* Section III.6.1 on *p.*96. Figure III.37 illustrates this for $\log_{10} K_1$, and $\log_{10} K_2$ for oxalate, citrate and nta complexes for a set of different metal ions. The regression lines between the two sets of $\log_{10} K$ have a slope close to unity, and an intercept indicating that the difference between the two sets is nearly constant (however, the value differs to some extent from the one expected from statistical considerations alone). It is interesting to observe that the largest deviations from the correlations are found for the tetra-dentate nta ligand which has a structure that does not permit the coordination of all donor atoms in complexes of octahedral (Fe^{3+}) or square planar geometry (Pd(II)). The lack of correlation between $\log_{10} K_3$ and $\log_{10} K_2$ for the “yl”-ions is certainly related to their coordination geometry as illustrated in Figs. III.18 and III.19.

The observation of large variations in stability of nta complexes also correlates nicely with the molecular structures of such complexes (Figures III.31 to III.34). Cations with large ionic radii like the lanthanides, Zr(IV), ter- and tetravalent actinides, have coordination numbers of eight and higher and also large values of $\log_{10} K_2$. These complexes seem to follow a similar linear relation as found, *e.g.*, for citrates. All cations with maximum

Figure III.29: Correlation between $\log_{10} K$ for ethylenediaminetetraacetate (edta) and 1,2-diaminocyclohexane-N,N,N',N'-tetraacetate (dcta) complexes. The line has a unit slope. The data refer to 20°C and at $I = 0.1$ M. Adapted from [56IRV/ROS].

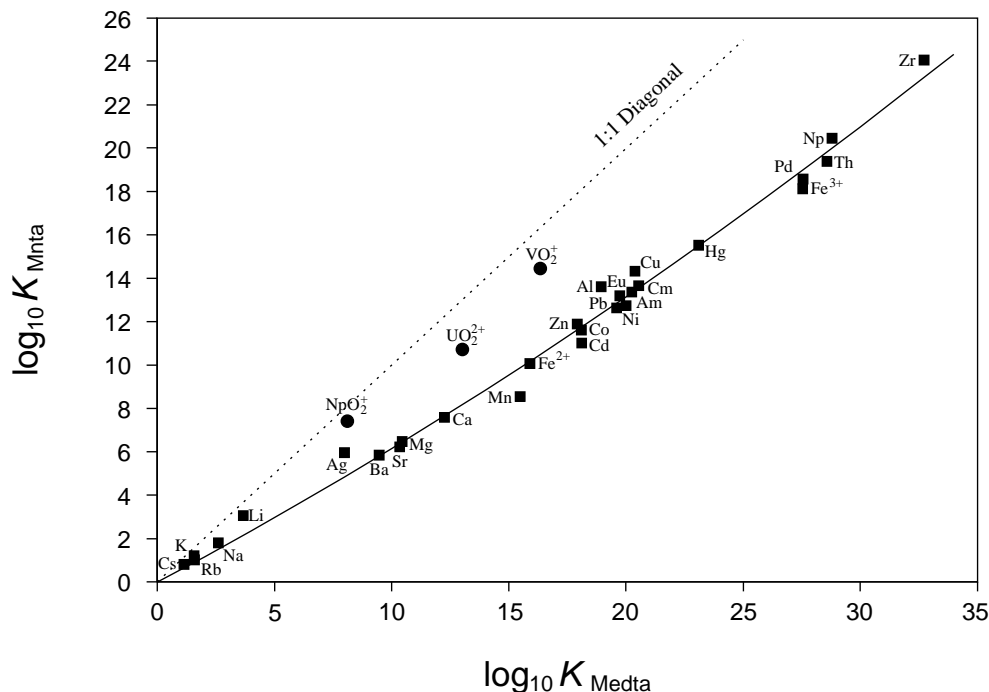


coordination numbers smaller than eight have low $\log_{10} K_2$ values.

III.6.7. An example of the use of estimation methods for the modelling of a complex aquatic system, the influence of oxalate on U(VI) speciation

We want to estimate the influence of oxalate on aqueous U(VI) speciation for a range of typical groundwaters. U(VI) is taken as an example of actinides; its inorganic complexation behaviour is discussed in Grenthe *et al.* [92GRE/FUG]. Oxalate belongs to the class of simple carboxylic acids. It occurs naturally in plants but was also found to be the most important product of radiolytic degradation of bitumen [91LOO/KOP]. The main geochemical parameters of groundwaters included in this example are pH, p_{CO_2} and the concentration of alkaline earth metals. Uranium is thought to be present in low concentration (10^{-6} M). Thus, we have to consider U(VI)-hydroxide, -carbonate and -oxalate complexes, including the possible formation of mixed ligand (ternary) complexes. In order to keep the example simple, the influence of fluoride, phosphate or sulfate complexes is neglected here. We want to estimate the minimum concentration of oxalate in groundwaters necessary to cause a significant influence on the speciation of U(VI). The level of significance is somewhat arbitrarily chosen as 50% U(VI)-oxalate complexation. If we know the minimum oxalate concentrations as a function of the main geochemical parameters of groundwaters, we are able to decide under which conditions, if at all, oxalate will influence U(VI) speciation.

Figure III.30: Correlation of stability constants for complexes of nta and edta. Complexes of “-yl” cations are shown as circles, all other complexes shown as squares. The data refer to $I = 0$ and are taken from [74MAR/SMI, 82MAR/SMI, 89SMI/MAR].



In a first step we have to consider all possible complexes in the chemical system.

U(VI) is known to form hydroxide complexes $\text{UO}_2(\text{OH})_n^{2-n}$ up to $n = 4$. There are also a series of polynuclear hydroxo complexes, but for total U(VI) concentrations less than 10^{-5} M they are minor species contributing less than 10% to the total speciation. Carbonate complexes $\text{UO}_2(\text{CO}_3)_m^{2-2m}$ are formed up to $m = 3$. A well established trinuclear carbonate species is negligible at low U(VI) concentrations. All data are taken from Grenthe *et al.* [92GRE/FUG], except the value for $\text{UO}_2(\text{OH})_2(\text{aq})$, where a better estimate is taken from [95PAS/KIM].

Oxalate complexes $\text{UO}_2(\text{ox})_p^{2-2p}$ are also formed up to $p = 3$, but in contrast to carbonate the tri-oxalate complex is very weak due to stereochemical reasons, *cf.* Figure III.37. The equilibrium constants for the U(VI)-oxalate system were taken from Havel [69HAV]. Note that this spectrophotometric study was performed at low pH (less than 5) and atmospheric CO_2 partial pressure in order to avoid complications due to U(VI) hydrolysis and carbonate complexation. Hence, these experimental data give no information whether ternary complexes involving hydroxide or carbonate play a role in systems of higher pH and p_{CO_2} , or not.

Ca and Mg also form oxalate complexes. As can be seen in Figure III.37 (K_1 - K_2 correlations, Section III.6.6), the stability constants of Ca, Mg and Sr oxalate complexes are rather similar, but the Sr constant is somewhat lower, according to the overall Ca-Sr

Figure III.31: Coordination geometry of $\text{Ni}(\text{nta})_2^{4-}$. Ni(II) has a coordination number of six, forming an almost perfect octahedral coordination with the two nta ligands. Each nta molecule therefore is coordinated with only one $\text{N}(\text{CH}_2\text{COO})_2$ group, the third carboxylate group is not bound in this complex.

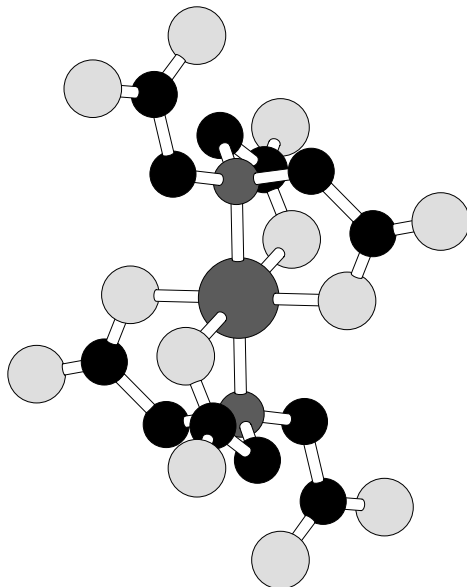


Figure III.32: Coordination geometry of $\text{Fe}(\text{nta})_2^{3-}$. Fe(III) is seven coordinate with two nta ligands. Note, that the same coordination number is also found for edta (Figure III.4). One nta ligand is bonded with four donor groups, the second one with only three donor groups, *i.e.*, one carboxylate group of this second ligand is not coordinated in this complex.

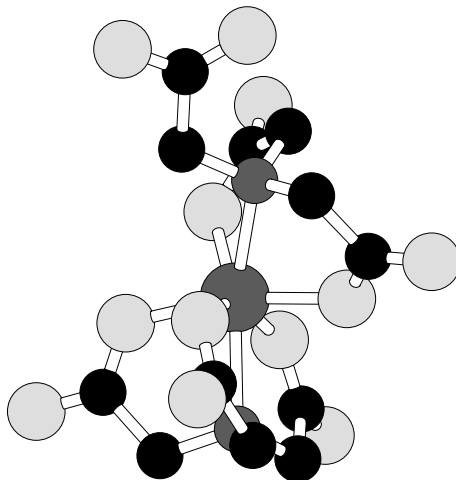


Figure III.33: Coordination geometry of $\text{Zr}(\text{nta})_2^{2-}$. Zr(IV) shows a coordination number of eight. All four donor groups of both nta ligands are bonded to the metal cation. The increase in coordination number from Fe(III) (Figure III.32) to Zr(IV) is correlated with an increasing ionic radius.

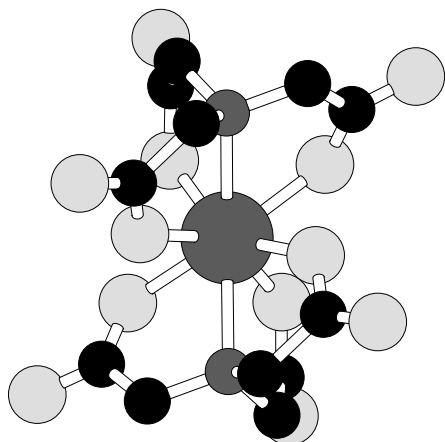


Figure III.34: Coordination geometry of $\text{Nd}(\text{nta})_2\text{H}_2\text{O}^{3-}$. The further increase in the ionic radius compared to Fe(III) and Zr(IV) results in a coordination number of nine. All four donor groups of both nta ligands are bonded to the metal cation and in addition a water molecule is coordinated.

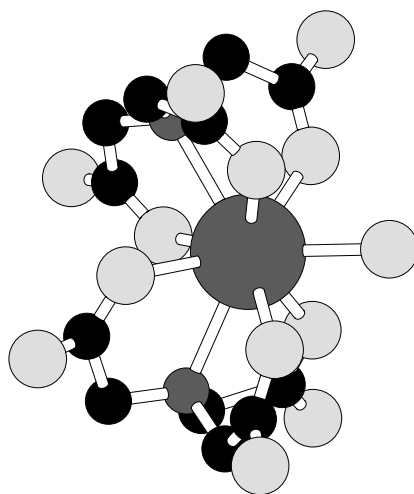
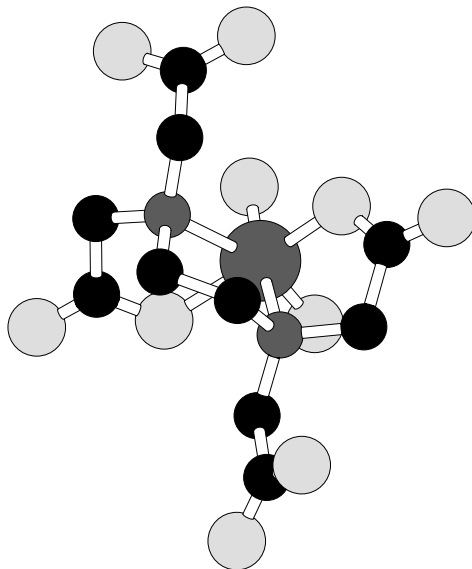
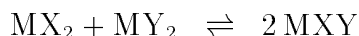


Figure III.35: Coordination geometry of $\text{VO}_2\text{edta}^{3-}$. Only four donor groups (two carboxylate oxygens and two nitrogen atoms) in edta are coordinated to the VO_2^+ ion. The two other carboxylate groups of edta are not bound in this complex. Note that in contrast to the linear UO_2^{2+} ion, the VO_2^+ ion is bent with an O-V-O angle of about 107° [71SCH/COU].



relation observed for a large range of ligands (Figure III.28, Ca-Sr relation, Section III.6.5). Therefore, the competition of Ca, Mg and Sr can be summarised by two “alkaline earth constants” (1:1 and 1:2 complexes) in the model.

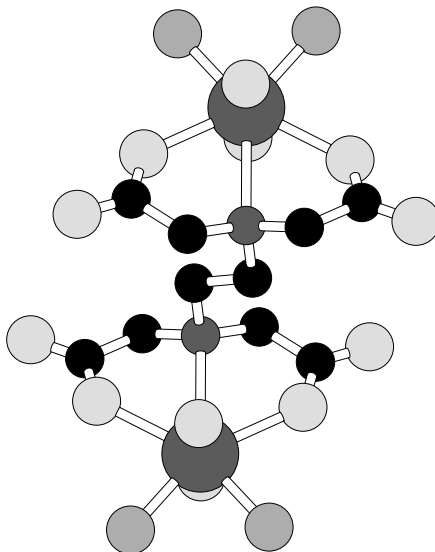
There are many precise investigations reported in the literature on the binary systems U(VI)-carbonate and U(VI)-oxalate, but there are no data available concerning the ternary U(VI)-carbonate-oxalate system. Based on the similarity of the two ligands the formation of ternary complexes has to be considered (*cf.* Example 7 in *p.*100). As discussed in Section III.6.1, the formation of 1:1:2 and 1:2:1 complexes is unlikely due to sterical reasons. The formation of 1:1:1 complexes, however, may significantly influence the speciation of U(VI). The equilibrium constant for the reaction



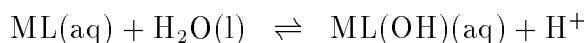
was estimated in two different ways in Example 7, *p.*100, resulting in $\log_{10} K_{1,1,1} = 14.7$ and $\log_{10} K_{1,1,1} = 15.0$, respectively.

We have also to consider the possible formation of ternary complexes involving hydroxide, in addition to oxalate or carbonate. In the uranium(VI) system we have information, or estimates, of the equilibrium constants for the formation of UO_2OH^+ , $\text{UO}_2(\text{OH})_2(\text{aq})$, $\text{UO}_2(\text{OH})_3^-$ and $\text{UO}_2(\text{OH})_4^{2-}$. It seems reasonable to assume that the acidity of, *e.g.*, $\text{UO}_2\text{L}(\text{H}_2\text{O})_3$, is not larger than that of $\text{UO}_2(\text{H}_2\text{O})_5^{2+}$. As a matter of fact, the experimen-

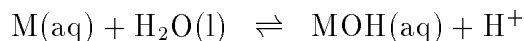
Figure III.36: The structure of the dinuclear complex $(\text{UO}_2)_2\text{edtaF}_4^{4-}$. The coordination geometry of the UO_2^{2+} ion only allows the bonding of “half” of the ligand, the $-\text{N}(\text{CH}_2\text{COO}^-)_2$ group to each metal ion. The remaining two coordination sites are occupied by two fluoride ions. Note the pentagonal bipyramid geometry of both UO_2^{2+} ions.



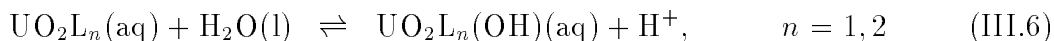
tal information [64RAJ/MAR, 70FRA/LOU] indicates that the equilibrium constant for a reaction of the type



is at least a factor of ten smaller than for the reaction



An estimate of the equilibrium constants for the reactions



is then obtained from the corresponding hydrolysis reaction of UO_2^{2+}



For all Reactions (III.6) we have assumed $\log_{10} K \approx -6$. This assumption is probably quite adequate for a neutral ligand, L. If the ligand is charged, however, this assumption will represent the maximum effect of the mixed ligand complexation.

There is no experimental information allowing an estimate of the equilibrium constants for reactions of the type

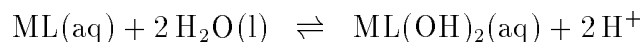


Figure III.37: Correlations between $\log_{10} K_n$ and $\log_{10} K_{(n-1)}$ for oxalate, citrate and nta complexes. The data refer to $I = 0$, and are taken from [74MAR/SMI, 77MAR/SMI, 82MAR/SMI, 89SMI/MAR], except oxalate data for Ca, Co, Ni, Eu, and U(VI) which are the result of re-evaluations of the original literature.

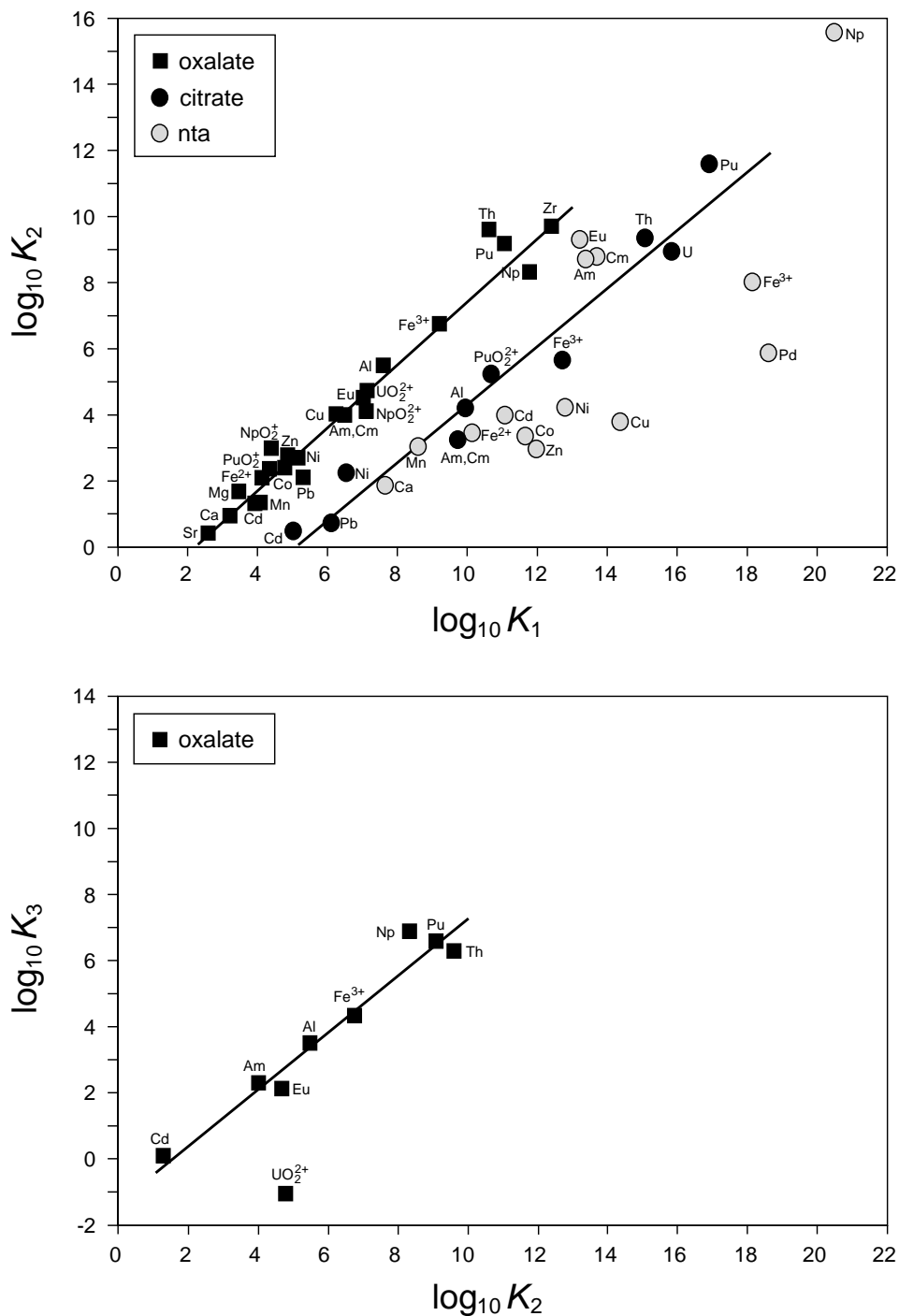
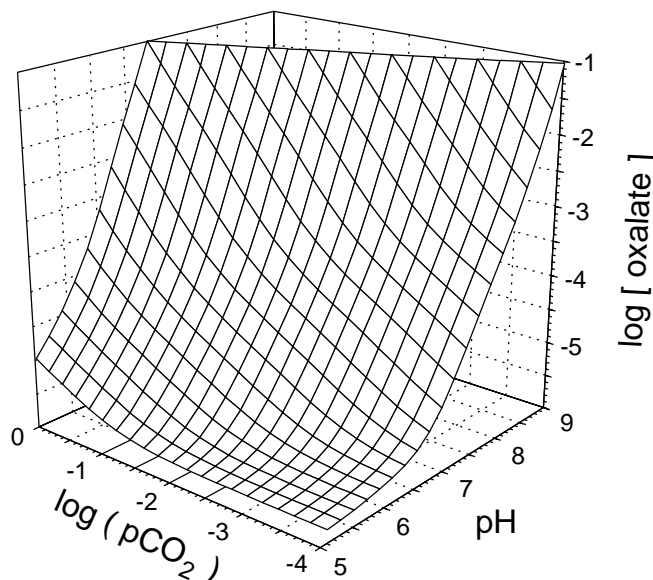
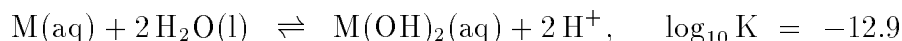


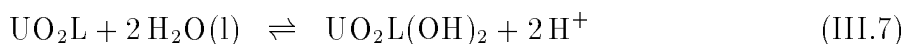
Figure III.38: Concentration of oxalate necessary to bind 50% of $[U(VI)]_{\text{total}}$ as oxalate complexes (including estimated ternary complexes). The diagram illustrates the pH and p_{CO_2} values where this takes place.



Also for these reactions it seems probable that the equilibrium constants are orders of magnitude smaller than for the reactions



This would, for the present case, indicate that the equilibrium constants for the reactions

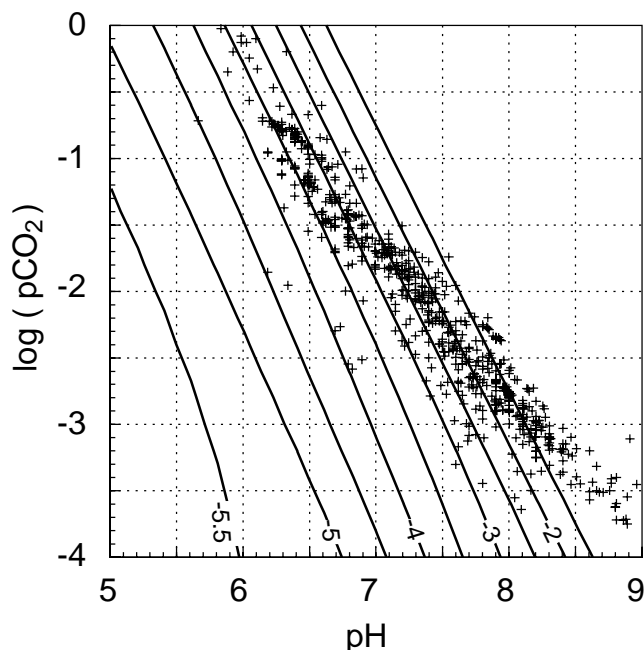


are $\log_{10} K(III.7) < -16$. hence, these species are not important in ground water systems.

Ternary complexes $UO_2L(OH)_3$ are geometrically possible, using the previous line of argument they are not likely to be present in appreciable amounts at the pH values encountered in natural water systems.

The concentration of oxalate necessary to complex 50% of the total concentration of U(VI) is shown in Figure III.38 as a function of pH and p_{CO_2} at $I = 0.1$ M. At pH=5 and $p_{CO_2} = 10^{-4}$ bar, there is no competition of U(VI)-hydroxide and -carbonate complexes, and thus very low oxalate concentrations are sufficient to complex 50% of U(VI), mainly as UO_2ox (where “ox” stands for the oxalate anion). With increasing pH at low p_{CO_2} , U(VI) hydroxo complexes act as competitors to U(VI)-oxalate and $UO_2-(OH)$ -ox complexes. In the region where both pH and $\log_{10} p_{CO_2}$ increase, the carbonate complexes dominate and U(VI) hydroxo complexes become minor species. In this range a dramatic increase in oxalate concentration is required to obtain 50% oxalate containing U(VI) species. This is

Figure III.39: Contour plot of the concentration of oxalate necessary to bind 50% of $[\text{U(VI)}]_{\text{total}}$ as complexes containing oxalate, including estimated ternary complexes (the lines show projections of the $\log_{10}[\text{oxalate}]$ levels in Fig. III.38). Crosses correspond to analyses for more than 700 Swiss groundwater samples.



due to the fact that $\text{UO}_2(\text{ox})_2^{2-}$ and the very weak $\text{UO}_2(\text{ox})_3^{4-}$ complex cannot compete with the very stable $\text{UO}_2(\text{CO}_3)_3^{4-}$.

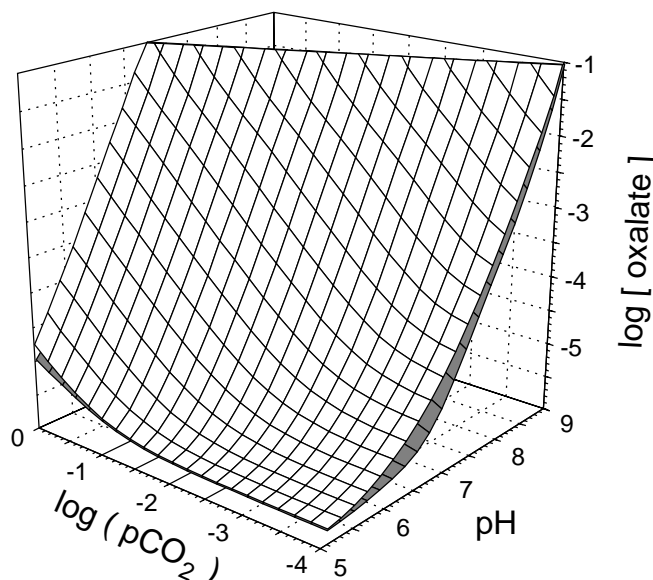
Model calculations made by varying the concentration of Ca using the common “alkaline earth constants” mentioned previously showed that the competition of alkaline earth metals remains negligible as long as $[\text{Ca}] + [\text{Mg}] + [\text{Sr}] \leq 10^{-2}$ M. Natural groundwaters seldom exceed this value. Figures III.38 to III.41 have therefore been calculated with $[\text{Ca}] + [\text{Mg}] + [\text{Sr}] = 10^{-2}$ M.

If the three-dimensional surface in Figure III.38 is projected onto the pH- p_{CO_2} plane, contour plots can be drawn, as is shown in Figure III.39. In addition, data derived from more than 700 Swiss groundwater analyses are added. As can be seen in the contour plot, more than 10^{-4} M oxalate is needed for almost all groundwaters in order to complex 50% of U(VI). Such high oxalate concentrations are never encountered under natural conditions.

The groundwater data show a strong correlation of p_{CO_2} with pH. It may be shown that these values can approximately be described as a closed system in equilibrium with calcite, and it follows that these systems are *not* in equilibrium with air, where $p_{\text{CO}_2} = 10^{-3.5}$ bar.

The influence of the ternary complexes, whose stability constants are only estimated, is shown in Figures III.40 and III.41. The 3-D surfaces in Figure III.40 show the results of model calculations without ternary complexes (white surface) on the background of

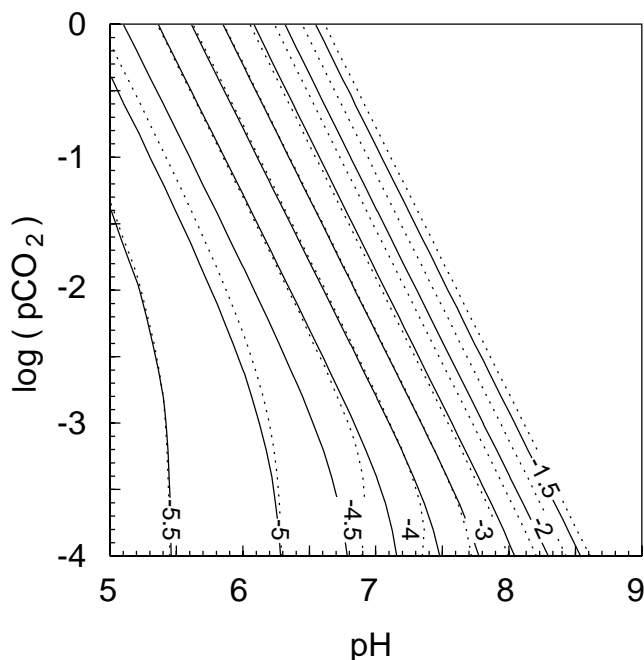
Figure III.40: Concentration of oxalate necessary to bind 50% of $[U(VI)]_{\text{total}}$ in oxalate containing species (excluding ternary complexes). The diagram illustrates the pH and p_{CO_2} values where this takes place. The darker surface in the background is that shown in Fig. III.38, where ternary complexes (of estimated stability) are included.



the previous results (ternary complexes included, dark surface taken from Figure III.38). When the ternary complexes are not included there is an increase in the concentration of oxalate needed in order to complex 50% of U(VI). The magnitude of this difference varies, although in general it is rather small: it becomes more than a factor of two at low p_{CO_2} and in the pH range of 6 to 8. In this parameter range the complex $\text{UO}_2(\text{OH})(\text{ox})^-$ predominates. In order to examine the effect of $\text{UO}_2(\text{CO}_3)\text{ox}^{2-}$ alone, contour lines for two different model calculations are shown in Figure III.41. The solid lines are contours of the white surface in Figure III.40, where calculations without any ternary complexes have been made. The dotted lines show results of calculations with $\text{UO}_2(\text{CO}_3)\text{ox}^{2-}$ added to the model. The influence is rather small; its maximum of half a log-unit, is seen between pH 6.8 and 8.4 when $10^{-4.5}$ to $10^{-2.5}$ M oxalate is needed for 50% U(VI) complexation. The model calculations indicate clearly that only two ternary complexes UO_2^{2+} -oxalate- OH^- and UO_2^{2+} -oxalate-carbonate affect the modelling, but that their influence is fairly small.

One may ask if it is necessary to improve the modelling by additional laboratory experiments of the ternary systems. It depends – as long as there is no indication that the ternary complexes are much stronger than estimated here, and as long as common groundwaters are discussed, there is no need for such studies. In the worst case (Figure III.39) more than 10^{-4} M oxalate is needed in order to see any significant influence of oxalate on the U(VI) speciation. In groundwaters containing at least 10^{-4} M Ca, calcium oxalate

Figure III.41: Contour plot of the concentration of oxalate necessary to bind 50% of $[\text{U(VI)}]_{\text{total}}$ as complexes containing oxalate. The continuous lines, drawn without any ternary complexes, show projections of the $\log_{10}[\text{oxalate}]$ levels in the upper surface of Fig. III.40, the dotted lines have been obtained including $\text{UO}_2\text{CO}_3\text{ox}^{2-}$ as the only ternary complex.



minerals (Whewellite $\text{Ca}(\text{ox}) \cdot \text{H}_2\text{O}$ or Weddellite $\text{Ca}(\text{ox}) \cdot 2\text{H}_2\text{O}$, both having solubility constants $\log_{10} K_{s,0} < -8$) will precipitate, limiting the concentration of the oxalate to values below 10^{-3} M in any case.

These conclusions cannot be generalised with respect to other cation-ligand systems. However, the importance of different species may be checked by the procedures and model calculations outlined above. This type of modelling should be made before undertaking time-consuming and costly laboratory experiments.

III.7. Some aspects of chemical kinetics

Aquatic systems in nature are rarely static. Water moves in the geological media as a result of differences in hydraulic gradients. Water from different sources are mixed, and these physical processes results in very complex dynamic systems, *cf.* Chapters XI and XII. The description and modelling of these systems is facilitated if the chemical reactions taking place there are much slower, or much faster than those characterising the physical processes, *i.e.*, they are for all purposes independent from one another: they are *uncoupled*. A first stage in any attempt to model aquatic processes in nature is to decide the extent of coupling between physical and chemical processes. This requires

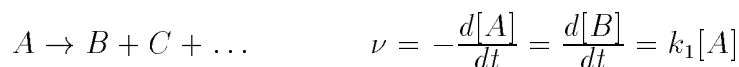
knowledge of the dynamics of the physical transport processes (Chapters XI and XII) and the chemical reactions.

The previous sections in this chapter have mainly dealt with chemical issues of importance for the description of chemical equilibrium systems. These provide “boundary” conditions for a discussion/description of rate processes in such systems. This section will deal with the rate of reactions between dissolved species in solution and a brief introduction to chemical reaction mechanisms.

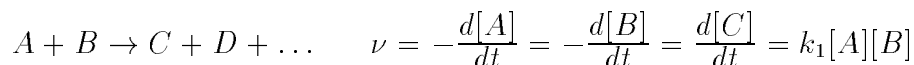
III.7.1. Reactions in homogeneous aqueous systems

In the introduction we indicated that stoichiometric equations do not give information on how the transformation from reactants to products takes place at the molecular level. Such information may be obtained from chemical kinetics. This is an important field in chemistry and the reader must consult specialised texts in order to obtain more information than this short introduction can provide. General introductions are given in standard textbooks such as [88COT/WIL, 89ATK] and in more specialised texts such as [72TOB, 74WIL, 87KAT/GOR]. In general the *mechanism* of reaction consists of a sequence of reactions (often called *elementary reactions*, each one with its particular *rate-constant*) that add up to the given stoichiometry. The elementary reaction with the smallest rate of reaction will determine the overall rate of the reaction and is called the *rate-determining step* in the mechanism. Two types of elementary reactions are of particular interest, *mono-molecular* and *bi-molecular* reactions, exemplified by:

mono-molecular reaction:



bi-molecular reaction:



The transformation of reactants to products may occur as a sequence of consecutive elementary reactions, but also along two or more parallel pathways. In the latter case each pathway has its own rate determining step with its own characteristic transition state.

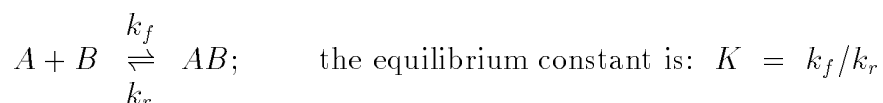
The rate of reaction, ν , is dependent on the concentration of the reactant(s) and the magnitude of the temperature-dependent rate constants k_1 and k_2 . The upper limit for the rate of reaction is determined by the maximum rate of *encounters* between the reactants. In aqueous solution this is determined by their rates of diffusion; such reactions are therefore called *diffusion controlled*. At room temperature the corresponding bimolecular rate constant is $\approx 10^{10} \text{ M}^{-1}\text{s}^{-1}$. From this value we can estimate the maximum rate of reaction between two reactants at given concentrations and temperature.

Example 9:

Estimate the maximum rate for a bimolecular reaction between two components A and B present at an initial concentration of 10^{-7} M.

We have: $\nu_{t=0} = 10^{10} \times 10^{-7} \times 10^{-7} = 10^{-4} \text{ M} \cdot \text{s}^{-1}$, which is a very high rate of reaction, even at trace concentrations of the reactants.

The equilibrium constant for a given chemical reaction provides a relationship between the rate constants for the reaction. This is illustrated by the following simple example, where the mechanism consists of only two elementary reactions (with rate constants k_f and k_r), where one is the reverse of the other:



For mechanisms containing many elementary reactions, the corresponding relationship between the rate constants and the equilibrium constant for the overall reaction may be more complicated and specialised textbooks should be consulted for more details. The gas-phase reaction between hydrogen and bromine discussed on page 71 is an example of such a reaction.

III.7.2. The temperature dependence of rate constants

The rate constant is strongly dependent on the temperature and often follows the Arrhenius equation

$$k_i = B_i e^{-E_a/RT}$$

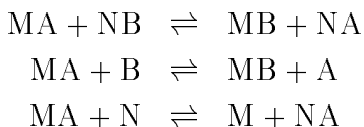
where k_i is the rate constant, B_i the *pre-exponential* factor, and E_a the *activation energy*. The deduction of the reaction mechanism and its temperature is a major experimental undertaking even in superficially “simple” reactions, *cf. p. 71*. It does not seem feasible to obtain the mechanistic details of all the reactions that might take place in a complicated multi-component system like those encountered in most ground and surface water systems. Fortunately, this is rarely necessary when describing the speciation and transport characteristics of solutes in these systems.

III.7.2.1. Dynamics of acid/base and complex formation reactions

Chemical reactions involving acid/base equilibria are, in general, diffusion controlled, and thus very fast even at trace concentrations of the reactants. Their characteristic time constants are often shorter than 10^{-6} sec. Complex formation reactions are also in general very fast, but slower than the diffusion controlled limit. Their rates vary with

the ligand. The bonding of a monodentate ligand is always much faster than that of a multidentate one. One may imagine that the “wrapping” of the multidentate ligand around the metal ion requires many steps, some of which may be slow. The rate of reaction is also metal-ion dependent, and decreases in general with increasing charge and decreasing ionic radius of the metal ion. Certain metal ions are characterised by very slow reactions (Cr(III), Co(III), and their homologues; Pd(II) and Pt(II), and Au(I) and Au(III)), with characteristic time scales of hours, or days for 50% completion of the reactions. For more details the reader should consult [72TOB, 87KAT/GOR].

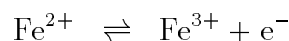
Most metal ions in ground and surface water systems are present as complexes and not as aqua ions. Hence it is necessary to consider also exchange reactions of the type



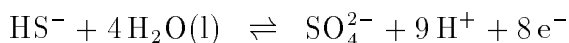
where M and N are two different metal ions and A and B two different (multi-dentate) ligands. Exchange reactions of this type are often slow, especially at trace concentration levels of the reactants. This is due both to the concentration of the reactants but also to the fact that the ligands have to be “wrapped”/“unwrapped” for the exchange to take place [93MOR/HER, p.395–405].

III.7.2.2. Dynamics of electron transfer reactions

Redox processes are another important group of reactions, where those involving the transfer of *one* electron in general are very fast, *e.g.*,



while those involving the transfer of more electrons and major chemical rearrangement between the reduced and oxidised state *always* are slow. This is because multi-electron transfer only occurs one electron at the time, and therefore take place in several steps which requires many successive encounters between electron donor and electron acceptor, resulting in a slow overall reaction. An example of a reaction of this type is



This is so slow that equilibrium between hydrogen sulfide and sulfate has never been observed in any system below 200°C.

In order to facilitate the description/modelling of a system, it is practical to identify the chemical reactions which are so slow that they cannot attain equilibrium within the time scale of the model, and exclude them before making an equilibrium model. Such systems are said to be in *pseudo-equilibrium*.

The reader must be aware that *many redox reactions in nature are kinetically controlled and cannot be described by equilibrium models*. An important exception is redox equilibria involving Fe(II) and Fe(III). It should be pointed out that many of these electron transfer reactions are heterogeneous reactions taking place at the interface between the solution and Fe(II) / Fe(III) containing minerals, *cf.* Hering and Stumm [90HER/STU], White [90WHI], Bancroft and Hyland [90BAN/HYL], and Waite [90WAI].

III.7.2.3. Catalysis and biologically mediated reactions

Catalysis is as important in ground and surface waters, as in other chemical systems. A special type of “catalysis” is offered by chemical transformations mediated by the microbiological systems in soil and water. Microorganisms can increase the rate of reactions which proceed “downhill” from a thermodynamic point of view, *i.e.*, with a decrease in Gibbs free energy. However, they can also mediate reactions that involve an *increase* in Gibbs energy by coupling this reaction to other reactions in such a way that the *combined* reaction has a negative free energy change. For example, sulfate reducing bacteria can couple the free energy released in metabolising organic material in the water to reduce sulfate to sulfide under ambient conditions where inorganic sulfate reduction is not thermodynamically possible. In the same way, organic ligands in ground and surface water systems can be formed and transformed through the mediation of microbiological processes. These cannot be described with equilibrium models and the characteristic time scale of these processes must be ascertained from case to case.

A discussion of the importance of microbiological processes in the aquatic sulfate – sulfide system is given by Pedersen [95PED/KAR].

III.7.2.4. Photochemical reactions

Photochemical reactions may be very important in surface water systems, particularly for reactions in the manganese and iron cycles. For more details the readers are referred to the recent edition of *Aquatic Chemistry* by Stumm and Morgan [96STU/MOR, p.726] and White [90WHI].

III.7.3. The steady-state concept for flow systems

It is important to distinguish between the steady-state approximation used in chemical kinetics and the steady-state concept used in open systems. In the steady-state approximation, the time derivatives are assumed to be zero for the reactive intermediates in the reaction mechanism. For example, $d[\text{H}]/dt = 0$ and $d[\text{Br}]/dt = 0$ for the reaction mechanism of the gas-phase reaction between hydrogen and bromine discussed on page 71.

The steady-state model in open systems, such as surface water systems, is based on the experimental observations that the concentrations of many components are constant over long periods of time. These systems are not equilibrium systems – there is a balance between the rates of addition to, and removal from the system of the various components. Examples of such systems are discussed in Stumm and Morgan [96STU/MOR].

III.7.4. Rates and mechanisms of heterogeneous equilibria

This is an important field for the understanding of chemical processes in aquatic systems in nature and in many engineering applications. *Corrosion* of materials is one example, *dissolution*, *precipitation* and *sorption*, *mineral weathering* and *diagenesis* are others. Solubility and sorption are discussed in the Chapters by Grauer (Chapter IV) and Banwart (Chapter VII).

A characteristic feature of many reactions in heterogeneous systems is that the rate of reaction is proportional to the surface area in contact with the aqueous phase. This is easy to understand, because the reactions take place at the interface between the solid and the solution, and the number of encounters leading to reaction is then proportional to the exposed surface and the concentration of the reactants in solution. All parts of the exposed surface do not have the same reactivity even if the solid is a single well-defined phase. Each part of the surface can be characterised by its particular density of atoms and structure and has therefore its own reactivity. The geometrical surface can be determined experimentally in a laboratory system, and possibly also in sediments and other porous media. It is *not possible* to determine the exposed area in fractured media, like bedrock aquifers. The “wetted” surface, and hence the “surface area” is a model parameter, which cannot be determined *a priori*.

Kinetic models for the weathering of minerals have been developed by Helgeson *et al.* [79HEL], and excellent introductions to the field are given in *Kinetics of Geochemical Processes*, edited by Lasaga and Kirkpatrick [81LAS/KIR] and in *Aqueous Surface Chemistry* edited by Stumm [87STU, pp.197–312].

There is a considerable scattering among thermodynamic data for the solubility of hydrous oxides of various types. This is partly due to variations in particle size [67SCH, 71LAN/WHI], but also to slow re-crystallisation processes where the freshly precipitated hydrous oxide “ages” with time, which results in a decrease of its solubility. The “aging” process often involves a decrease in water content of the solid phase. This process is faster at elevated temperatures, *e.g.*, in hydrothermal systems, but very little quantitative information is available about the rates of transformation at lower temperatures. The effect of solid-phase aging on its solubility may be very large, and results in changes of the solubility over several orders of magnitude with changing crystallinity. A corollary is that hydrous oxides precipitate at much higher pH than expected from the solubility product measured for a well crystalline solid phase. When modelling aquatic systems it is therefore imperative to decide on the state of the solubility limiting solid phases. These are rarely the high-temperature phases used in most laboratory investigations.

Chapter IV

Solubility Limitations: An “Old Timer’s” View

Rolf GRAUER[†]
Paul Scherrer Institut
CH-5232 Villigen PSI (Switzerland)

IV.1. Einleitung

Ein wesentlicher Aspekt der Sicherheitsanalyse von Endlagern ist die Prognose maximal möglicher Nuklidkonzentrationen im Nah- und Fernfeld. Besonderes Gewicht wird dabei auf die Löslichkeitslimiten der einzelnen Elemente gelegt (Kapitel XIV, Hadermann), die mit Hilfe eines thermodynamischen Modells vorausgesagt werden.

An der theoretischen Grundlage solcher Modelle ist nicht zu zweifeln. Das Fundament der Gleichgewichtsthermodynamik ist fest gefügt. Lewis und Randall [61LEW/RAN] geben deshalb in ihrem klassischen Lehrbuch den Ratschlag “... to reach this frontier (of a growing science) one must pass over well-traveled roads; of these one of the safest is the broad highway of thermodynamics”.

Dennoch sind Löslichkeitsberechnungen häufig falsch, und die Versuche zur Modellvalidierung führen an natürlichen Analogenen, oder auch schon an einfachen Becherglassituationen, zu fragwürdigen oder gar unbrauchbaren Ergebnissen. Die Gründe dafür liegen auf verschiedenen Ebenen; sie sollen hier aufgezeigt und an ausgewählten Beispielen diskutiert werden.

Die Problemstellung erscheint trivial. Zur Berechnung einer Löslichkeit benötigt man die folgenden Kenntnisse:

- die Zusammensetzung der löslichkeitsbestimmenden Festphase und ihr Löslichkeitsprodukt
- alle in dem System möglichen Komplexe des interessierenden Kations sowie seiner Konkurrenten und ihre Stabilitätskonstanten

- die Konzentrationen der einzelnen Liganden und der konkurrierenden Kationen. Dies ist im wesentlichen ein analytisches Problem und wird hier nicht diskutiert.

In der Praxis treten überall Probleme auf: Bezüglich der löslichkeitslimitierenden Festphase bestehen grosse Unsicherheiten bis hin zur Unkenntnis. Die Frage nach der stabilen Phase kann meist nur für einfache Becherglassituationen beantwortet werden.

In komplexen Systemen werden sich im allgemeinen Mischphasen bilden, die Spurenbestandteile mit aufnehmen. *z.B.* sind Hydroxidfällungen aus Lösungen mit mehreren Kationen keine reinen Verbindungen. So enthalten natürliche feindisperse Goethite und Hämatite neben Aluminium auch die zweiwertigen Übergangsmetalle von Mangan bis Zink [88COR].

Es zeigt sich, dass es wegen der Bildung (metastabiler) Mischphasen kaum möglich ist, die Zusammensetzung der Lösung und des Bodenkörpers für ein Fällungsexperiment mit n Kationen und m Liganden in stark unterschiedlichen Ausgangskonzentrationen vorauszusagen. Es wird vielleicht gelingen, das Verhalten der Hauptbestandteile mit einiger Genauigkeit oder wenigstens grössenordnungsmässig zu prognostizieren. Das Verhalten der Spurenelemente kann aber bestenfalls abgeschätzt oder auch nur vermutet werden.

Grosse Unsicherheiten bestehen auch hinsichtlich der Stöchiometrie und der Stabilität der Komplexe von wichtigen Kationen. So wird beispielsweise diskutiert, ob gemischte Hydroxo-Carbonato-Komplexe von Uran(VI) reell sind, oder ob sie lediglich “error absorbers” für die Modellierung von Becherglasexperimenten darstellen [92KRA/BIS]. Der Komplex $\text{U}(\text{OH})_5^-$, früher bei hohen pH-Werten als wichtig erachtet, hat an Bedeutung verloren [87BRU/CAS], weil seine Stabilität offensichtlich überschätzt wurde. Auch der Katalog der Phosphato-Komplexe von Uran(VI) musste kürzlich grundlegend revidiert werden [92SAN/BRU]. (“Metal speciation is the analytical chemist’s answer for eternal employment” [90BRO/GUC]).

Ein Kernproblem liegt ferner im Inhalt und in der Qualität der zur Modellierung verwendeten Datenbasen. Mit diesem Thema befasst sich der nächste Abschnitt.

Als letzter Punkt sei schliesslich festgehalten, dass vielen Anwendern und Compilern thermodynamischer Datenbasen ein breites und solides Wissen in allgemeiner anorganischer Chemie fehlt. Die führt zu zahlreichen, zwar mathematisch genauen, aber chemisch unsinnigen Prognosen.

Nach dieser Aufzählung mag es beinahe aussichtslos erscheinen, gesicherte Angaben über Löslichkeitslimiten zu geben (mehr dazu in den Abschnitten IV.3 und IV.4). Es kann auch nicht das Ziel eines kurzen Aufsatzes sein, auf einen Schlag alle Probleme zu lösen. Ich möchte im folgenden nur zeigen, wie sich wenigstens die grössten Fehler in diesem Business vermeiden lassen. Der Schlüssel dazu sind breite Kenntnisse in Stoffchemie, die früheren Chemikergenerationen im Rahmen der analytischen Grundausbildung vermittelt worden sind. Vieles davon findet sich in vergriffenen Lehrbüchern der qualitativen Analyse [14TRE, 47TRE, 57CHA], im altbewährten Lehrbuch von Remy [50REM], oder im neueren Werk von Greenwood und Earnshaw [84GRE/EAR]. Allein mit diesen persönlichen Werkzeugen liessen sich am Schreibtisch viele Fragen lösen und viele Fehler vermeiden. Kommt man auch damit nicht weiter, so ist ein Gang zur Biblio-

thek zu empfehlen, um die Informationen in Gmelins Handbuch der anorganischen Chemie anzuzapfen.

Ich plädiere für eine bessere chemische Allgemeinbildung, für den intensiven Gebrauch der chemischen Vernunft und für die Prioritäten der chemischen Evidenz vor Gleichgewichtskonstanten dubioser Herkunft. Was im einzelnen damit gemeint ist, wird in den nächsten Abschnitten gezeigt.

IV.2. Über Inhalt und Qualität von geochemischen Datenbasen

Eine geochemische Datenbasis enthält quantitative Informationen über die chemischen Eigenschaften von Elementen und Verbindungen. Sie sollte in sich konsistent, d.h. widerspruchsfrei und auch möglichst vollständig sein. Von dieser Idealvorstellung sind wir weit entfernt. Die Aufgabe, aus verstreuten, lückenhaften Informationen von teilweise schlechter Qualität konsistente Daten zusammenzustellen ist alles andere als trivial. Die Forderung nach Vollständigkeit bedeutet, das alle geochemisch relevanten Verbindungen erfasst sein sollten. Auch dies ist eine Sisypheus-Arbeit. Dagegen erscheint es recht einfach, geochemisch irrelevante Verbindungen aus solchen Datenbasen zu verbannen. Leider wird das nicht gemacht, und deshalb enthalten Datenbasen neben vielen falschen Zahlen auch viel unnötigen Ballast.

Eine Menge solcher Fehler liesse sich vermeiden. Dies soll an einigen Beispielen gezeigt werden. Die ausgewählten Fälle sind exemplarisch. Keine Datenbasis ist frei von solchen Beispielen, und man könnte aus dem vollen schöpfen. Es wäre somit unfair, wenige ausgewählte Autoren hier an den Pranger zu stellen. Entgegen der üblichen Gepflogenheit wird deshalb nicht jede Aussage belegt.

IV.2.1. “The Law of Mythical Numbers” ...

Thermodynamische Datenbasen basieren in der Regel nicht auf Originalarbeiten, sondern auf älteren Datensammlungen, die aus früheren Kompilationen zusammengestellt worden sind, die wiederum ... Dazu ein Beispiel:

“**CARBONATES:** The NEA compilation lists 4 values for nickel carbonate in a rather broad range (from -603.0 to -637.6 $\text{kJ} \cdot \text{mol}^{-1}$). The data from Wagman *et al.* [82WAG/EVA] and from Naumov *et al.* [71NAU/RYZ] are the same and are in very good agreement with the solubility product given by Smith and Martell [76SMI/MAR]. As Naumov *et al.* [71NAU/RYZ] also report standard heat of formation and entropy values his data has been selected here”.

Wahrhaftig eine überzeugende Argumentation ! Der ausgewählte Wert ist grob falsch (s. Abschnitt IV.4.1), und weil dieses Vorgehen bei der Auswahl die Regel ist, sind falsche Werte keine Ausnahme. So enthält beispielsweise die Sammlung von Kotrlý und Šucha [85KOT/SUC], die ihrerseits wieder auf den “Critical Stability Constants” [74MAR/SMI, 75SMI/MAR, 76SMI/MAR, 77MAR/SMI, 82MAR/SMI, 89SMI/MAR] beruht, Löslichkeitskonstanten für die Carbonate der Übergangsmetalle von Mangan

bis Zink, die bis auf einen einzigen Wert falsch sind [94GRA]. Falsch ist auch der Wert für Cadmiumcarbonat ($\log_{10} K_{s,0} = -13.74$), der sich seit 1935 hartnäckig fortgepflanzt hat. Andere Tabellen (z.B. [82WAG/EVA]) geben dafür einen ebenfalls falschen Wert von $\log_{10} K_{s,0} = -11.20$. Kürzlich haben Stipp *et al.* [93STI/PAR] den Stammbaum der Löslichkeits- “Konstanten” von Cadmiumcarbonat sorgfältig rekonstruiert und gezeigt, dass die heute gängigen Tabellenwerte im wesentlichen auf einer Bestimmung der Lösungswärme im Jahre 1883 beruhen. Unterschiede in der Beurteilung dieser einen Arbeit und die Verwendung unterschiedlicher Zahlen für die Hilfsgrößen im Laufe der Zeit führen zu der angegebenen Variationsbreite von $\log_{10} K_{s,0}$. Die Löslichkeit von Cadmiumcarbonat ist erstmals 1965 experimentell bestimmt worden [65GAM/STU]. Danach ist $\log_{10} K_{s,0} = 12.00 \pm 0.15$, ein Wert, der erst 1991 und 1993 bestätigt wurde (s. [93STI/PAR]). Diese Fallstudie erhärtet das Gesetz der Mythischen Zahlen [82SIN] (“An expert opinion, once referenced, becomes fact despite evidence to the contrary”) und sie erschüttert das Vertrauen in “kritische” Datensammlungen.

Vielleicht lassen sich mythische Zahlen in Datenbasen nie ganz vermeiden. Zu ihrer Verminderung gibt es aber ein sehr einfaches Rezept: Es sind die Originalarbeiten zu sichten und mit chemischem Sachverstand zu beurteilen. Dabei ist es stets hilfreich, sich nicht nur auf eine Verbindung zu konzentrieren, die gerade interessant erscheint, sondern Vergleiche mit ähnlichen Substanzen anzustellen. Mit diesem Vorgehen liessen sich die oben erwähnten Fehler in [85KOT/SUC] nicht nur erkennen, sondern auch beseitigen [94GRA].

Neben mythischen Zahlen, die “nur” um einige Größenordnungen falsch sind, schleichen sich in Datenbasen auch absurde Zahlen ein. Dazu zwei Beispiele.

In einer Datenbank findet man die Freie Bildungsenthalpie von Palladium(II)-chlorid ($\Delta G^\circ = -126.4 \text{ kJ} \cdot \text{mol}^{-1}$). Daraus ergibt sich für das Löslichkeitsprodukt $\log_{10} K_{s,0} = -7.09$. Die Verbindung ist aber offensichtlich leicht löslich. Im Lehrbuch von Remy [50REM2] ist nachzulesen, dass nicht nur das Dihydrat, sondern auch das wasserfreie, bei Rotglut aus den Elementen synthetisierte Palladiumchlorid “in Wasser leicht löslich und zerfliesslich” ist.

Mindestens zwei Datenbasen geben für Zinn(II)-sulfat eine Freie Bildungsenthalpie von -908.19 kJ/mol an. Daraus ergibt sich $\log_{10} K_{s,0} = -23.93$. Man wundert sich, dass in der klassischen Analytik diese ausserordentliche Schwerlöslichkeit nicht ausgenutzt wird, und dass keine Zinnsulfat-Lagerstätten bekannt sind. Der “old timer” weiss aus seinem Anfängerpraktikum, dass Zinn(II)-sulfat an feuchter Luft zerfliesst. Das “greenhorn” könnte sich anhand der Trivalliteratur [50REM3, 87WEA] über die hohe Löslichkeit dieser Verbindung orientieren. Im Chemie Lexikon [92ROM] findet er auch den Hinweis, dass die Verbindung u.a. zur galvanischen Verzinnung und zur elektrolytischen Einfärbung von anodisiertem Aluminium verwendet wird. Diese Prozesse setzen wohl eine gute Löslichkeit voraus.

Der Wert $\Delta G^\circ = -908.16 \text{ kJ} \cdot \text{mol}^{-1}$ beruht vermutlich auf einem Druckfehler. Man findet in der Literatur $\Delta G^\circ = -193.4 \text{ kcal} \cdot \text{mol}^{-1}$ [75GME]. Mit übertriebener Zahlenschärfe umgerechnet erhält man exakt $\Delta G^\circ = -809.16 \text{ kJ} \cdot \text{mol}^{-1}$! Auch mit diesem Wert wird allerdings die Verbindung noch nicht leichtlöslich ($\log_{10} K_{s,0} = -6.6$).

IV.2.2. ... and “The Handbook of Unstable, Exotic and Nonexistent Compounds”

Neben mythischen Zahlen für bekannte Verbindungen enthalten Datensammlungen auch nichtexistierende Verbindungen mit den zugehörigen thermodynamischen Daten. Ein klassisches Beispiel ist das Kupfer(II)-carbonat, dessen Löslichkeit seit mindestens 1935 mit $\log_{10} K_{s,0} \approx -9.6$ (mit kleineren Variationen) angegeben wird. Es ist nicht klar, auf welchen Feststoff sich diese Zahl bezieht. Erst 1973 ist die Hydrothermalsynthese von Kupfercarbonat gelungen [73EHR/JOH], und 1980 wurde seine Löslichkeit bestimmt: $\log_{10} K_{s,0} = -11.45$ [81REI/JOH]. Die mythische Zahl für die imaginäre Verbindung erscheint aber 1985 wieder in einer Tabelle [85KOT/SUC], und wird 1990 in einer Monographie zitiert [90MOR/MAC].

Zu den nichtexistierenden Verbindungen gehört beispielweise das Nickelsilicat NiSiO_3 . Es ist ein hypothetisches Endglied der Pyroxen-Reihe, und seine thermodynamischen Daten sind Schätzwerte [77TAR/GAR]. In einer geochemischen Datenbasis sind sie ohne jeden Nutzen. Von geringem Nutzen sind auch Hochtemperatur-Phasen wie Spinelle oder das Nickel-orthosilicat Ni_2SiO_4 . Für diese Verbindung werden gar die Daten von zwei polymorphen Formen angegeben (Olivin- und Spinellstruktur). Die Spinellstruktur erhält man nur bei hohen Drücken: bei 650°C beispielsweise bei 18 kbar [66GME, p.937]. Ein Löslichkeitsgleichgewicht bei Umgebungsbedingungen ist illusorisch.

Viele geochemische Datenbasen enthalten unnötigen Ballast in Form von leichtlöslichen Salzen oder instabilen, hydrolysierbaren Verbindungen. Beispiele sind Nickelchlorid und -sulfat sowie deren Hydrate, Selen(IV)-oxid und -chlorid oder Diphosphate. Das fleissige Sammeln von Bildungsenthalpien anstelle von Löslichkeitskonstanten verbaut die Einsicht in das Verhalten dieser Stoffe.

Zum Ballast gehören auch Verbindungen, die sich aus den Elementen, nicht aber aus wässriger Lösung herstellen lassen. Das Selen(IV)-chlorid wurde eben erwähnt. Der Katalog ähnlicher Beispiele ist lang; als besondere Rosine in diesem Kuchen ist das Siliciumselenid, SiSe_2 , zu erwähnen. Sammlerfleiss, ungetrübt von chemischem Sachverstand, führt zu derartigen Auswüchsen.

IV.2.3. Der Vergleich von Datenbasen: Ein Weg zu besseren Werten ?

In den heutigen geochemischen Datenbasen steckt ein immenser Arbeitsaufwand, der von ungezählten Personen im Laufe vieler Jahre erbracht worden ist. Es ist deprimierend, dass die Ergebnisse nicht besser ausgefallen sind.

Es muss nun nochmals ein grosser Aufwand getrieben werden, um die Datenbasen von ihren Fehlern und von ihrem Ballast zu befreien. Einfache Regeln für ein erfolgreiches Vorgehen lassen sich nicht aufstellen; es soll hier aber festgehalten werden, was *nicht* zum Ziel führt, obschon die Methode zu den “well-traveled roads” gehört und offenbar von vielen als “one of the safest broad highways” gehalten wird (s. Abschnitt IV.1).

Aus den Ausführungen über die Genese von Datenbasen und über das Gesetz der Mythischen Zahlen folgt zwingend, dass ein blosser Vergleich verschiedener Datenbasen die Situation nicht verbessert. Dennoch wird viel Zeit in solche Übungen investiert

[92PEA/BER]. Der Befund “ $\Delta \log_{10} K = 0$ ” ist kein Qualitätskriterium. Er besagt nur, dass die verglichenen Basen die gleichen Zahlen enthalten, die aber beliebig falsch, oder - wie im Beispiel von Zinnsulfat - gar unsinnig sein können.

Eine zum öffentlich ausgetragenen Gesellschaftsspiel entartete Variante des Datenbasen-Vergleichs ist das “Blind Modelling”. Die Spielregeln sind einfach: An alle Teilnehmer wird eine Wasseranalyse verteilt, und sie erhalten den Auftrag, diesem Wasser je 1 μg /Liter von verschiedenen Elementen (z.B. Selen, Zinn, Uran) zuzusetzen. Jeder Mitspieler berechnet dann mit seiner Datenbasis die Speziation, er identifiziert die löslichkeitslimitierende Festphase und gibt als Endergebnis den Sättigungsindex SI an ($\text{SI} = \log_{10}(Q/K)$. Q : aktuelles Ionenprodukt; K : Löslichkeitskonstante). In diesem Spiel gibt es keine Sieger. Auch hier bürgen übereinstimmende Ergebnisse nicht für die Qualität der Daten. Häufig variieren aber die Sättigungsindices in weiten Grenzen [92ALE/DAY], z.B. von -7.6 bis $+163.7$ (!) für Selen, -3.3 bis $+34.7$ für Zinn und -33.7 bis $+10.3$ für Uran. Solche Diskrepanzen sind peinlich; sie sollten nicht in einer geochemischen Zeitschrift einer breiten Öffentlichkeit bekanntgemacht, sondern in einer verschwiegenen Klausur bereinigt werden. Neben Modellierern sollten auch kompetente Chemiker daran teilnehmen.

IV.3. Löslichkeitslimiten im Nahfeld: Das Beispiel Americium

Das Americium ist mit seinen Isotopen 241 ($t_{1/2} = 433$ a) und 243 ($t_{1/2} = 7370$ a) für die Sicherheitsanalyse eines Endlagers nicht besonders wichtig. Es wurde hier vor allem wegen seiner übersichtlichen Chemie aus didaktischen Gründen als Beispiel ausgewählt.

IV.3.1. Löslichkeitsbestimmende Phasen ¹

In natürlichen Wässern ist je nach dem Kohlendioxid-Partialdruck das Carbonat oder das Hydroxidcarbonat des Americiums stabil. Der Grenzwert steht noch nicht eindeutig fest. Unsicherheiten bestehen auch über die Stabilität der gemischten Hydroxo-Carbonato-Komplexe [90FEL/RAI]. Die berechneten Americium-Löslichkeiten im Nahfeld [95BER, 92BRU/SEL] sind deshalb nicht als definitiv zu betrachten.

Neben der Forderung nach verlässlichen Löslichkeitsdaten stellt sich hier die generelle Frage, wie sich das Löslichkeitsverhalten eines Feststoffs ändert, wenn seine Kationen zerfallen. Die Tochterkerne unterscheiden sich chemisch von der Mutter, so dass Stöchiometrie und Struktur der Ausgangssubstanz nicht erhalten bleiben. (Übung: Berechne die Löslichkeit von $^{241}\text{Am}(\text{OH})\text{CO}_3$ in einem gegebenen Wasser nach 400 und 800 Jahren).

Der α -Zerfall wirkt sich besonders gravierend auf die Feststoffeigenschaften aus. Die α -Teilchen verlieren ihre Energie vorwiegend durch Ionisationsprozesse in einem Bereich bis etwa 20 μm ; sie können deshalb aus einer mikrokristallinen Substanz austreten, ohne grossen Schaden anzurichten. Dagegen wird die Energie der Rückstosskerne (≈ 0.1 MeV)

¹ Die Herausgeber möchten darauf hinweisen, daß der hier vorliegende Text vor der Veröffentlichung der kritischen Übersicht der NEA über die Thermodynamik des Americium [95SIL/BID] verfaßt wurde.

im Nahbereich (10 nm) durch Stossprozesse abgegeben. Dabei ereignen sich etwa 2000 Atomverschiebungen pro Zerfall, die in kristallinen Stoffen Gitterschäden verursachen [82ROY]. Für eine Reihe von Verbindungen ist gezeigt worden, dass sie nach einer α -Dosis von etwa 10^{19} Zerfällen pro cm^3 amorph werden. Die amorphe Phase hat eine höhere Löslichkeit als das kristalline Ausgangsprodukt.

Elektronenmikroskopische Untersuchungen an $^{241}\text{Am}(\text{OH})_3$ haben gezeigt, dass die Kristalle beim Aufbewahren in Lösung nach sechs Monaten vollständig fragmentiert waren [77HAI/LLO]. In dieser Zeit sind weniger als 0.1% des Americiums zerfallen! Strukturschäden durch den α -Zerfall wirken sich also viel früher aus als die Transmutation.

IV.3.2. Die Rolle der Lanthaniden

In den Abfalloxiden der aufgearbeiteten Brennelemente liegt der Massenanteil von Americiumoxid in der Grössenordnung von 1%. Daneben sind aber bedeutend grössere Mengen von Lanthanid-Oxiden vorhanden, die zum grössten Teil inaktiv sind [82ROY, 83HER]. Das Stoffmengenverhältnis Ln/Am beträgt etwa 50.

Es gehört zum etablierten Lehrbuchwissen, dass sich das Americium chemisch, aufgrund der Ionenradienverhältnisse vor allem auch kristallchemisch, sehr ähnlich verhält wie die dreiwertigen Lanthaniden. Wenn sich in einem Endlager geordnete Verbindungen bilden können, so werden dies (Ln, Am)-Mischphasen sein. Dieser Aspekt bleibt bei Löslichkeitsberechnungen häufig unberücksichtigt, was mitunter zu erstaunlichen Ergebnissen führt: Für ein bestimmtes Modellwasser wurde für Samarium eine Löslichkeit von 2×10^{-4} M berechnet, und als limitierende Phase wird $\text{Sm}_2(\text{CO}_3)_3$ angegeben [92BRU/SEL]. Die für das gleiche Wasser berechnete Americium-Löslichkeit beträgt 2×10^{-8} M mit AmCO_3OH als stabiler Festphase. Der Widerspruch zwischen diesen beiden Angaben ist offensichtlich; er hätte bei einer Qualitätskontrolle erkannt werden müssen.²

Berücksichtigt man das hohe Ln/Am-Verhältnis im Abfall, so erscheint es naheliegend, sich in erster Linie um die Stabilität der Festphasen im System Ln(III)- H_2O - CO_2 zu kümmern. Es ist unsinnig, sich allein auf Samarium zu konzentrieren, weil es zufällig ein radioaktives Isotop enthält, und daneben die hohen Anteile an inaktivem Cer, Praseodym und Neodym zu übersehen. Solange für diese Elemente keine zuverlässigen und kohärenten Löslichkeitsdaten vorliegen, kann auch kein verlässlicher Wert für die Löslichkeit von Americium angegeben werden. Neuere Arbeiten über die Löslichkeit von Neodym in Hydrogencarbonatlösungen [93CAR, 93MEI/TAK] stimmen zuversichtlich.

² Anmerkung der Herausgeber: Aufgrund der tragischen Umstände war es nicht möglich, den Autor zu ersuchen, diese harte Aussage nochmals zu überdenken. Bruno und Sellin [92BRU/SEL] haben die Analogie zwischen Am und Sm sowie auch die Diskrepanz zwischen den beiden errechneten Löslichkeiten diskutiert. Das leichter lösliche, aber gut bekannte, $\text{Sm}_2(\text{CO}_3)_3$ wurde von Bruno und Sellin anstelle von SmCO_3OH gewählt. Für letzteres waren die Zahlenwerte zur damaligen Zeit nicht erhältlich. Die höhere Löslichkeit des Sm war eher das Ergebnis einer absichtlichen "konservativen" Entscheidung, als das einer fehlenden Qualitätskontrolle. Der an dieser Thematik interessierte Leser sei auch auf die Referenz [96MER/FUG] hingewiesen.

IV.3.3. Verglaste Abfälle

Es ist fraglich, ob sich in einem Endlager mit verglastem Abfall definierte (Ln, Am)-Phasen bilden. Die Borosilicatgläser enthalten etwa 12% Abfall-Calcinat, und als Hauptbestandteile rund 50% SiO_2 und 15% B_2O_3 . Bei der Hydrolyse solcher Gläser entstehen silicatreiche, amorphe Umwandlungsprodukte. Zwar bestehen keine Zweifel, dass die Löslichkeit von Schwermetallen des Abfalls durch die Einlagerung in Sekundärphasen begrenzt wird. Dies ist insbesondere auch für Lanthan gezeigt worden [82SAV/ROB, 89PET/DRA, 91DAU/CRO].

Löslichkeitsberechnungen sind aber nicht möglich. Die Hoffnung, es würden sich im Laufe der Zeit definierte kristalline Phasen bilden, ist der Strohalm, an dem sich die Modellierer festhalten. In der Natur finden sich aber genügend Beispiele dafür, dass metastabile Phasen geologische Zeiträume überdauern.

IV.3.4. Löslichkeitslimiten im Nahfeld: welche Festphasen ?

Beim verglasten Abfall werden die Actiniden und Spaltprodukte durch die Glaskorrosionsprodukte stark verdünnt. Die Berechnung von Löslichkeiten mit einfachen Verbindungen ist für diese Situation somit unrealistisch.

In einem Endlager für abgebrannten Brennstoff sind Spaltprodukte und Transurane durch das Uran noch stärker verdünnt als im Glas, und die Bildung eigenständiger Gleichgewichtsphasen ist ebenfalls unwahrscheinlich. Dieser Schluss ist nicht neu. Grenthe [91GRE] schreibt dazu: “It is not likely that actinides (with the exception of U) and fission products will form separate mineral phases, they will rather be incorporated into minerals formed as a result of chemical interactions along the flow-path of the groundwater. The information on these phases is scarce or non-existing, on the other hand the formation of these secondary minerals from the ions transported from the repository is most probably controlled by *kinetic* factors”. Und an anderer Stelle [92GRE/FUG]: “The thermodynamic data of pure uranium minerals may be of limited value for geochemical modelling, because most of these are unlikely to form from the uranium released from nuclear waste repositories. Leached uranium is more likely to be found in association with iron(III)-oxide hydrates, a common secondary phase in water carrying fractures”.

IV.4. Löslichkeitslimiten im Fernfeld: Das Beispiel Nickel

Im Fernfeld liegen die Radionuklide aus dem Endlager in hoher Verdünnung vor. Sie werden auf ihrem Weg an Mineraloberflächen adsorbiert und möglicherweise auch in die Wirtsphase eingebaut. Sie begegnen einer grossen Anzahl natürlicher Spurenelemente mit z.T. ähnlichem chemischem Verhalten, und es ist deshalb unwahrscheinlich, dass Elemente aus dem Abfall im Fernfeld eigenständige definierte Festphasen bilden. Dazu müssten kritische Keimbildungskonzentrationen überschritten werden, und das anschliessende Kristallwachstum müsste ohne Interferenz durch die zahlreichen Lösungsgenossen erfolgen. Dennoch wird immer wieder versucht, die Löslichkeit kritischer Nuklide in einer solchen komplexen

Umgebung mit einem sehr einfachen Modell zu berechnen.

Das Nickel ist hier als Beispiel gewählt worden, weil einerseits das Nuklid ^{59}Ni mit einer Halbwertszeit von 7.5×10^4 Jahren von Interesse ist. Es gelangt als Aktivierungsprodukt von ^{58}Ni aus Strukturkomponenten in den Abfall. Andererseits ist das Nickel kein exotisches Element: Es kommt in Spurenkonzentration überall vor, und seine Geochemie ist eingehend untersucht worden [67GME, 78WED].

IV.4.1. Die Modellierung der Nickel-Löslichkeit

Im Rahmen der umfangreichen Poços-de-Caldas-Analogstudie [91CHA/MCK] wurden für verschiedene Wässer die Löslichkeiten von neun Spurenelementen berechnet und mit den Analysenwerten verglichen [91BRU/CRO]. In einem bestimmten Wasser wurde eine Nickelkonzentration von 5×10^{-9} M ermittelt. Dieser Wert liegt im Bereich der typischen Konzentrationen in natürlichen Wässern ($\approx 10^{-8}$ M [78WED]).

Die Löslichkeitsberechnung durch vier Arbeitsgruppen ergab die folgenden Resultate [91BRU/CRO]:

Gruppe	[Ni(II)]	Festphase
A	3.0×10^{-14}	NiFe_2O_4
B	5.1×10^{-2}	$\text{Ni}(\text{OH})_2$
C	3.6×10^{-4}	NiO
D	2.7×10^{-2}	$\text{Ni}(\text{OH})_2$

Die Ergebnisse der Modellrechnungen überstreichen zwölf Größenordnungen und weichen drastisch von der Realität ab. Der Grund liegt in der Auswahl von unrealistischen löslichkeitslimitierenden Festphasen.

Der Trevorit NiFe_2O_4 gehört zu den Spinellen. Er ist eine typische Hochtemperaturphase und kein Verwitterungsprodukt. Es ist deshalb ein vermeidbarer Kunstfehler, den Nickelgehalt eines Grundwasser mit dieser Festphase zu modellieren.

Das Nickeloxid kommt als seltenes Mineral in der Natur vor (Bunsenit). Er lässt sich aber unter Umgebungsbedingungen nicht aus wässriger Lösung fällen. In Hydrothermalexperimenten geht das Hydroxid erst bei 285°C in das Oxid über, und Nickeloxid, das sich als Korrosionsprodukt in NaOH-Schmelzen gebildet hat, hydrolysiert mit Wasser zum Hydroxid [77OSW/ASP]. NiO gehört deshalb zu den unrealistischen Verbindungen.

Nickelhydroxid scheint in der Natur nicht vorzukommen. Es entsteht bei der Hydroxidfällung in Form sehr dünner, kleiner Plättchen mit einem Durchmesser von etwa 100 nm. Gut kristalline Produkte entstehen erst unter hydrothermalen Bedingungen. Dementsprechend schwanken die Löslichkeitsangaben von $\log_{10} K_{s,0} = -14.7$ für frische Fällungen bis $\log K_{s,0} = -17.2$ für gealterte Produkte.

Das Nickelhydroxid ist in hydrogencarbonathaltigen Wässern instabil. Es reagiert bereits an der Luft ($\log_{10} p\text{CO}_2 = -3.5$) zu einem nicht näher charakterisierten Hydroxidcarbonat [77OSW/ASP], und bei Nickelfällungen mit Hydrogencarbonat entstehen Hydroxidcarbonate [66GME, p.844]. Diese Substanzklasse ist variantenreich, und Löslichkeitsdaten scheinen nicht vorzuliegen. Einige Vertreter kommen in der Natur vor, so der Nullaganit ($\text{Ni}_2(\text{OH})_2\text{CO}_3$) und der Zaritit ($\text{Ni}_3(\text{OH})_4\text{CO}_3 \cdot 4\text{H}_2\text{O}$). Der Otwayit ist ein gemischtes (Ni, Mg)-Hydroxidcarbonat.

Das wasserfreie Nickelcarbonat findet sich in der Natur in einer verunreinigten Variante (Gaspeit: $(\text{Ni}, \text{Mg}, \text{Fe})\text{CO}_3$ [91STR/ZIM]). In reiner Form lässt es sich nur hydrothermal herstellen [66GME, p.844, 80REI]; es ist deshalb geochemisch irrelevant, und es stört nicht, dass die gängigen Löslichkeitsprodukte ($\log_{10} K_{s,0} = -6.87$ [85KOT/SUC]) grob falsch sind: Sie beziehen sich auf das Hexahydrat, und nicht auf die wasserfreie Verbindung. (Ein realistischer Schätzwert für NiCO_3 ist $\log_{10} K_{s,0} = -11.2 \pm 0.3$; er ist konsistent mit den Löslichkeiten in der Reihe MnCO_3 - ZnCO_3 [94GRA, 80REI]).

Die Modellierung der Nickellöslichkeit ist also, wie sich mit wenig Aufwand zeigen liess, mit unrealistischen Festphasen durchgeführt worden. Die viel zu hohen Konzentrationen der Modellrechnung mit NiO und $\text{Ni}(\text{OH})_2$ dürfen nicht dahingehend interpretiert werden, dass das Modell zu “konservativen” Aussagen führt: Das Modell hat versagt ! Die Frage ist jetzt nur, ob man es besser machen kann.

IV.4.2. Zur Geochemie des Nickels

Der mittlere Nickelgehalt der Erdkruste beträgt etwa 100 ppm. In den Primärmineralien findet man es als Sulfideinschlüsse in Silicaten, oder anstelle von Eisen(II), bzw. Magnesium in Silicatstrukturen [89SPO]. Bei der Verwitterung wird es in Hydroxiden und Oxiden mitgefällt [78WED]; in Form von nickelhaltigem Limonit, $(\text{Fe}, \text{Ni})\text{O}(\text{OH}) \cdot n\text{H}_2\text{O}$, kommt es als abbauwürdiges Erz vor [84GRE/EAR]. Wegen der Ähnlichkeit der Ionenradien wird Nickel auch in sekundären Dreischichtsilicaten anstelle von Magnesium eingebaut (Ionenradien: Ni^{2+} : 80 pm, Mg^{2+} : 77 pm). In Ausnahmefällen können in Smectiten bis zu 50% der Oktaederplätze durch Nickel belegt sein [87DEC/COL]. Das Silicaterz Garnierit, $(\text{Ni}, \text{Mg})_6\text{Si}_4\text{O}_{10}(\text{OH})_8$, ist ebenfalls ein Verwitterungsprodukt.

Diese Verhältnisse zeigen, dass die Berechnung der Nickel-Löslichkeit in einem oxischen System wenig aussichtsreich ist. Natürliche Hämatite und Goethite enthalten ja nicht nur Nickel, sondern auch weitere Uebergangselemente [88COR], und die Berechnung der Löslichkeit von Smectiten ist ein aussichtsloses Unterfangen [88GRA].

Unter reduzierenden Bedingungen bildet Nickel wegen seines B-Charakters schwerlösliche Sulfide, die aber bei kleinen Konzentrationen nicht in reiner Form anfallen werden. Die kritische Durchsicht der Sulfidlöslichkeiten wäre vermutlich eine dankbare Aufgabe.

IV.4.3. Löslichkeitslimiten im Fernfeld ?

Was hier am Beispiel des Nickels gezeigt worden ist, lässt sich sinngemäss auch auf andere Spurenelemente in der Geosphäre übertragen.

Die Bemühungen, die Konzentration von Spurenelementen in natürlichen Wässern mit Hilfe von Löslichkeitsgleichgewichten reiner, individueller Festphasen zu erklären sind als gescheitert zu betrachten. Darüber dürfen auch gelegentliche Uebereinstimmungen zwischen Modell und Realität nicht hinwegtäuschen.

Von einem tauglichen Modell wäre zu erwarten, dass es die Konzentrationen einer ganzen Reihe von Spurenelementen in einer Vielzahl von Wässern mindestens auf die Grössenordnung richtig voraussagt. Das ist offensichtlich nicht der Fall.

Der Hauptgrund für das Versagen der Löslichkeitsmodelle dürfte in der Annahme liegen, dass die Konzentration von Spurenelementen durch individuelle Festphasen festgelegt wird. Die Auswahl solcher Phasen durch die Modellierer ist zudem meist willkürlich, und im Laufe einer Modellvalidierung, die diesen Namen verdient, wäre der löslichkeitsbestimmende Feststoff zu identifizieren und sauber nachzuweisen.

In natürlichen Systemen werden Spurenelemente nur in Ausnahmefällen eigenständige Phasen bilden. Sie sind entweder in Wirtsphasen in hoher Verdünnung eingebaut, oder an der Oberfläche von anderen Feststoffen adsorbiert. In der Praxis dürfte die Unterscheidung dieser beiden Fälle nicht immer einfach sein. Zu den Ausnahmen gehört möglicherweise das Thorium, sofern es als Oxid vorliegt. Es ist auch vermutet worden, dass die Lanthaniden im Meerwasser als Phosphate gefällt werden [93BYR/KIM]. Die vorgebrachten Argumente stützen diese Hypothese. Der Beweis für ihre Richtigkeit wäre aber erst erbracht, wenn die postulierte Festphase nachgewiesen würde. Die Ansicht, dass die Konzentration der Lanthaniden im Meerwasser, wie diejenige anderer Spurenelemente, durch Adsorptionsprozesse reguliert wird [91LI], ist deshalb nicht widerlegt.

IV.5. Schlussbemerkungen

Die Bilanz aus den Kapiteln IV.2 bis IV.4 ist unerfreulich ! Es hat sich gezeigt, dass Löslichkeitslimiten mit naiven chemischen Konzepten und mit schlechten Daten berechnet werden. Ein Modell sollte helfen, bestimmte Phänomene besser zu verstehen; hier aber bricht zwischen Berechnen und Begreifen eine tiefe Kluft auf. Mangelnde chemische Kenntnisse der Akteure und mangelnde Selbstkritik sind die Gründe dafür.

Der Schaden, der dadurch entsteht, kann gross werden. Schliesslich steht die Glaubwürdigkeit der ganzen Sicherheitsanalyse auf dem Spiel, wenn Kritiker vom fahrlässigen Umgang mit Löslichkeitslimiten auf die Qualität des Ganzen schliessen. Wir brauchen also ein glaubhaftes Modellkonzept, und wir brauchen glaubhafte Daten.

Es muss sich die Einsicht durchsetzen, dass das Konzept der Löslichkeitslimiten mit einfachen Feststoffen eine grobe Annäherung an die Realität ist. Ebenso muss sich die Einsicht durchsetzen, dass sich die Welt wegen der "intellektuellen Unschärferelation" [79SIT] nicht zugleich genau und verstehbar beschreiben lässt. Eine Modellrechnung wird keine Aussage darüber machen, "wie es ist" oder "wie es sein wird", sondern nur darüber,

“wie es unter den getroffenen vereinfachenden Annahmen sein *könnte*”.

Bekanntlich lassen sich Theorien und auch Modelle nicht im strengen Sinne validieren, sondern nur widerlegen [59POP, 94ORE/SHR]. Es ist deshalb eine Minimalanforderung, dass ein Modell nicht im Widerspruch steht zu evidenten Befunden. Mindestens darauf hin wären Modellrechnungen zu überprüfen. Dazu bieten sich in erster Linie übersichtliche Becherglassituationen an. Zeigen sich hier schon krasse Widersprüche, so ist das Modell eben falsch !

Der erste Schritt auf dem Weg zu glaubwürdigen Daten ist das Ausmisten der Datenbasen³. Es herrscht offensichtlich die Meinung, dass eine gute Datenbasis möglichst umfangreich ist. Ein Umdenken ist unumgänglich. Qualität steht vor Quantität, und das Motto heisst: “*Pauca, sed matura*”⁴.

Zu einer Feststoff-Datenbasis gehört eine ausführliche Dokumentation. Dort ist zu begründen, weshalb eine bestimmte Verbindung aufgenommen worden ist. Ihre geochemische Relevanz, bzw. ihre Bedeutung für das Endlager ist zu beurteilen, und wünschenswert wären Angaben über ihre Bildungsbedingungen. Aus dieser Dokumentation sollte die Herkunft der Daten klar hervorgehen, und es muss ersichtlich sein, mit welchen Methoden die Daten ermittelt wurden. Ein Hinweis wie *z.B.* “Wagman *et al.* 1982” [82WAG/EVA] genügt nicht, denn er ist kein Gütesiegel. Schliesslich wäre auch zu begründen, weshalb eine bestimmte Arbeit gegenüber anderen bevorzugt worden ist. - Zu all dem sind fundierte chemische und geochemische Kenntnisse unerlässlich. Kein “broad highway” führt daran vorbei, und auch die “well-traveled roads” des naiven Datenbasen-Vergleichs führen nicht zum Ziel.

Die Löslichkeitslimiten werden zu den “Pillars of Safety” eines Endlagers gezählt. Es zeigt sich aber, dass diese Säule nicht besonders tragfähig ist. Vermutlich wird sich nur für wenige Nuklide und nur für das Nahfeld überzeugend nachweisen lassen, dass die Löslichkeitsbegrenzung für die Nuklidfreisetzung wirksam wird. Wirksam ist aber, auch im Fernfeld bei hohen Verdünnungen, die Sorption am Verfüllmaterial und am Gestein. Obschon auch hier offene Fragen und Unsicherheiten bestehen, fallen grundsätzliche Schwierigkeiten weg, die bei Löslichkeitsabschätzungen kaum quantifizierbar sind: man braucht sich keine Gedanken zu machen über kritische Keimbildungs-Konzentrationen, über den kristallisationshemmenden Einfluss der Kieselsäure, über komplex aufgebaute, nichtideale Mischphasen und über die Änderung des Löslichkeitsverhaltens der Festphasen als Folge des radioaktiven Zerfalls.

³ Ein Hinweis auf die griechische Mythologie drängt sich auf: während dreissig Jahren hatte sich der Mist von dreitausend Rindern in den Ställen des Augias angehäuft. Herakles hat den ganzen Dreck an einem einzigen Tag ausgeräumt. Wohl nur dank seinen verwandtschaftlichen Beziehungen zum Olymp konnte er diese Aufgabe so speditiv und effizient erledigen. Wir, weder Götter noch Heroen, werden uns mit den Datenbasen länger beschäftigen müssen. Ob dabei ein Lorbeerkrantz zu gewinnen ist ? Lang ist die Liste der Ruhmestaten des Herakles, und sein Name hat deshalb die Jahrtausende überdauert. Ueberdauert hat aber auch der Name des Augias: nur, weil er einen Augias-Stall hatte !

⁴ Motto auf dem Siegel von C.F. Gauss (“Wenig, das aber ausgereift”).

Schlussbemerkungen

Es wäre deshalb sinnvoller, mehr Zeit und Arbeit in die Adsorption zu investieren als in sophistische und unsichere Löslichkeitsmodelle. Doch wie steht es mit der Qualität von Sorptionsdaten ? Das Spiel wiederholt sich, und Herakles ist auf's neue gefordert !

Editors comments:

Two weeks after finishing this chapter, Rolf Grauer died of a heart attack while mountaineering in Berner Oberland. He intended to have his text translated into English, but the editors decided to leave it as received. By presenting it “frisch vom Fass” we hope that the readers will catch not only Rolf’s profound scientific insights, but also his spirituality. In the next section, the English translation is also included.

IV.6. Solubility limitations: an “old timer’s” view

IV.1 Introduction

Predicting the maximum possible nuclide concentrations in the near and far fields is an important aspect in the safety assessment of final repositories. Particular emphasis is placed on the various elements’ solubility limits (Chapter XIV, Hadermann) which are predicted by means of thermodynamic model.

The theoretical basis for such models is not in doubt. The foundations of equilibrium thermodynamics are firmly established. Lewis and Randall [61LEW/RAN] therefore give the following piece of advice in their standard textbook: “...to reach this frontier (of a growing science), one must pass over well-travelled roads; of these, one of the safest is the broad highway of thermodynamics”.

Yet solubility calculations are frequently wrong, and attempts to validate models by means of natural analogues or even simple laboratory experiments lead to questionable or even unusable results. There are a number of different reasons why this is so; they will be pointed out and discussed by means of selected examples in this paper.

The problem seems to be quite straightforward. The following information is required for a solubility calculation:

- the composition of the solid phase determining solubility and its solubility product,
- all the possible complexes of the cation concerned as well as of competing cations and their stability constants,
- the concentrations of the various ligands and competing cations; this is basically an analytical problem and is not discussed here.

In practice, problems arise all along the line: there are considerable uncertainties or even a complete lack of knowledge with regard to the solid phase which determines solubility. Answers concerning the stable phase can usually be given only for simple laboratory experiments.

Mixed phases that take up trace elements will usually be formed in complex systems. For example, hydroxides precipitated from solutions with several cations are not pure compounds. Natural, finely dispersed goethite and hematite contain not only aluminium but also the bivalent transition elements ranging from manganese to zinc [88COR].

Owing to the formation (of metastable) mixed phases, it is scarcely possible to predict the composition of the solution and the remaining solid in a precipitation experiment with n cations and m ligands in quite different initial concentrations. It will perhaps be possible to predict the behaviour of the main constituents with some accuracy or at least as an order of magnitude. But the behaviour of the trace elements can at best be estimated or even only guessed.

Considerable uncertainties also exist with regard to the stoichiometry and stability of the complexes of important cations. For instance, it is not certain whether mixed uranium (VI) hydroxide-carbonate complexes are real, or whether they are only “error absorbers” for the modelling of simple laboratory experiments [92KRA/BIS]. The significance of the complex $\text{U}(\text{OH})_5^-$ which was previously considered important at high pH values has declined [87BRU/CAS] as its stability was obviously overestimated. Recently the catalogue of uranium(VI) phosphate complexes also had to be thoroughly revised [92SAN/BRU]. (“Metal speciation is the analytical chemist’s answer for eternal employment” [90BRO/GUC]).

Another basic problem concerns the content and quality of the databases used for modelling, a topic which is discussed in the next section.

The last point which should be remembered is that many users and compilers of thermodynamic databases do not have a sound general knowledge of inorganic chemistry. This leads to very many predictions which are mathematically accurate but absurd in terms of chemistry.

After these comments, it may seem virtually impossible to give reliable data on solubility limits (see Sections IV.3 and IV.4 for more details on this subject). Neither can a short article be expected to solve every problem in one go. In this paper, I should simply like to show how at least the worst mistakes in this field can be avoided. The answer is to have the extensive knowledge of analytical chemistry which was

passed on to earlier generations of chemists in the course of their basic training. Much of this knowledge is to be found in qualitative analysis textbooks that are out of print [14TRE, 47TRE, 57CHA], in Remy's standard textbook [50REM], or in more recent work by Greenwood and Earnshaw [84GRE/EAR]. Many questions could be answered and many mistakes avoided simply by consulting one's own copies of these works. If these are to no avail, it is advisable to visit a library and assimilate the information in Gmelin's textbook on inorganic chemistry.

Here I am pleading for better basic training and the intensive use of reason in chemistry, and for the priority of chemical evidence over equilibrium constants of doubtful origin. What is exactly meant by this statement is discussed below.

IV.2 Content and quality of geochemical databases

A geochemical database contains quantitative information on the chemical characteristics of elements and compounds. The data should be consistent, *i.e.*, non-conflicting, and also as complete as possible. We still have a very long way to go before achieving this ideal. Compiling consistent data from dispersed, patchy information which is sometimes of poor quality is not an easy task. The completeness requirement means that all geochemically relevant compounds should be included. This is also a monumental operation. On the other hand, it does seem quite easy to exclude geochemically irrelevant compounds from such databases. Unfortunately, this is not done, so that databases contain much unnecessary ballast in addition to many wrong figures.

A great many such mistakes could be avoided, as will be shown by a few examples. The selected cases are typical, and examples of the same kind could be found in every database. It would be unfair to pillory a few selected authors. Contrary to the usual practice, we shall therefore not give the source for each statement.

IV.2.1 "The law of mythical numbers" ...

Thermodynamic databases are usually not based on original work but on older data collections which have been collated from earlier compilations, which in their turn have been reproduced... Following is an example:

"CARBONATES: The NEA compilation lists 4 values for nickel carbonate in a rather broad range (from -603.0 to -637.6 $\text{kJ} \cdot \text{mol}^{-1}$). The data from Wagman *et al.* [82WAG/EVA] and from Naumov *et al.* [71NAU/RYZ] are the same and are in very good agreement with the solubility product given by Smith and Martell [76SMI/MAR]. As Naumov *et al.* [71NAU/RYZ] also report standard heat of formation and entropy values his data has been selected here".

What a convincing argument ! The selected value is quite wrong (*cf.* Section IV.4.1), and since this is the usual data selection procedure, wrong values are no exception. For example, the compilation by Kotly and Sucha [85KOT/SUC], which is itself based on "Critical Stability Constants" [74MAR/SMI, 75SMI/MAR, 76SMI/MAR, 77MAR/SMI, 82MAR/SMI, 89SMI/MAR], contains solubility constants for the carbonates of the transition metals ranging from manganese to zinc that are all wrong with one exception [94GRA]. The value for cadmium carbonate ($\log_{10} K_{s,0} = -13.74$), which has stubbornly persisted since 1935, is also wrong, as is the other value of $\log_{10} K_{s,0} = -11.20$ given in other tables (*e.g.* [82WAG/EVA]). Stipp *et al.* [93STI/PAR] recently carefully reconstructed the diagram for the solubility constants of cadmium carbonate and showed that today's current table values are mostly based on a heat of solution determined in the year 1883. Differences in the assessment of this single work and the use of different numbers for the auxiliary constants over the years result in the spread of values given for $\log_{10} K_{s,0}$. The solubility of cadmium carbonate was determined experimentally for the first time in 1965 [65GAM/STU]. The result was $\log_{10} K_{s,0} = 12.00 \pm 0.15$, a value which was not confirmed until 1991 and 1993 (*cf.* [93STI/PAR]). This case study confirms the law of mythical numbers [82SIN] ("an expert

opinion, once referenced, becomes fact despite evidence to the contrary”) and undermines confidence in “critical” sets of data.

Perhaps mythical numbers can never be completely avoided in databases. But there is a very simple way of reducing their frequency, which is to examine the original work and assess it as a scientist. In doing so, it is always advantageous not to focus on a single compound just because it appears to be interesting, but to make comparisons with similar substances. If this procedure was used, the mistakes referred to above [85KOT/SUC] would not only be spotted but eliminated [94GRA].

In addition to mythical numbers, which are “only” slightly wrong, databases are also infiltrated by absurd numbers. Two examples can be given.

One database gives the free energy of formation for palladium(II) chloride ($\Delta G^\circ = -126.4 \text{ kJ} \cdot \text{mol}^{-1}$). This gives a solubility product of $\log_{10} K_{s,0} = -7.09$. But the compound is obviously easily soluble. According to Remy [50REM2], not only the dihydrate but also the anhydrous palladium chloride synthesised by red heat from the elements “are easily dissolved in water”.

At least two databases give a free energy of formation of $-908.19 \text{ kJ} \cdot \text{mol}^{-1}$ for tin(II) sulfate. Therefore $\log_{10} K_{s,0} = -23.93$. It is surprising that this extraordinary low solubility is not exploited in conventional analytical technique and that there are no known tin sulfate ore deposits. The “old timer” knows from his beginning studies that tin(II) sulfate dissolves in damp air. The “greenhorn” could obtain information on the high solubility of this compound from standard literature [50REM3, 87WEA]. The “Chemie Lexikon” [92ROM], will also tell him that the compound is used, among other things, for electroplating and electrolytic tinting of anodised aluminium. These processes obviously require good solubility.

The value $\Delta G^\circ = -908.16 \text{ kJ} \cdot \text{mol}^{-1}$ is presumably due to a printing mistake. The value $\Delta G^\circ = -193.4 \text{ kcal} \cdot \text{mol}^{-1}$ is found in literature. With too many significant digits, the conversion gives exactly $\Delta G^\circ = -809.16 \text{ kJ} \cdot \text{mol}^{-1}$! However, the compound is not easily soluble either with this value ($\log_{10} K_{s,0} = -6.6$).

IV.2.2 ... and “The Handbook of Unstable, Exotic and Nonexistent Compounds”

In addition to mythical numbers for known compounds, databases also contain non-existent compounds with the associated thermodynamic data. A classic example is copper(II) carbonate, whose solubility has been given at least since 1935 as $\log_{10} K_{s,0} \approx -9.6$ (with small variations). It is not clear to which solid this number refers. The hydrothermal synthesis of copper carbonate was not achieved until 1973 [73EHR/JOH], and its solubility was determined in 1980: $\log_{10} K_{s,0} = -11.45$ [81REI/JOH]. But the mythical number for the imaginary compound again appeared in a table in 1985 [85KOT/SUC], and was cited in a monograph in 1990 [90MOR/MAC].

The non-existent compounds include, for example, nickel silicate NiSiO_3 which is a hypothetical end member of the pyroxene group. Its thermodynamic data are estimated values [77TAR/GAR] and are of no use whatsoever in a geochemical database. Neither are high-temperature phases such as spinel and nickel orthosilicate Ni_2SiO_4 of very much use. The data for two polymorphic forms are even given for this compound (olivine and spinel structure). The spinel structure is obtained only at high pressures: for example at 18 kbar at 650°C [66GME, p.937]. A solubility equilibrium in ambient conditions is illusory.

Many geochemical databases contain unnecessary ballast in the form of easily soluble salts or unstable hydrolyzable compounds, such as nickel chloride and sulfate as well as their hydrates, selenium(IV) oxide and chloride or diphosphate. The laborious compilation of free energies of formation instead of solubility constants obstructs the view of how these substances behave.

The ballast also includes compounds which are produced from the elements but not from an aqueous solution. Selenium(IV) chloride has just been mentioned. There are many similar examples; silicon selenide SiSe_2 should be mentioned as a special currant in this cake. Laborious compilation, untouched by chemical expertise, leads to such excesses.

IV.2.3 Database comparisons: a way to better values?

Today's geochemical databases are the outcome of a tremendous effort made by great numbers of people over the years. It is depressing to see that the results of this effort are so unsatisfactory.

A further great effort must now be made to rid the databases of their mistakes and ballast. It is not possible to define simple rules to ensure that the operation will be a success; but what should be borne in mind is what does *not* lead to the goal, although the method belongs to "the well-travelled roads" and is obviously seen by many as "one of the safest broad highways" (*cf.* Section IV.1).

It necessarily follows from the comments on the genesis of databases and the law of mythical numbers that the situation cannot be improved simply by comparing different databases. Yet much time is spent on such exercises [92PEA/BER]. The finding " $\Delta \log_{10} K = 0$ " is no quality criterion. It simply says that the bases compared contain the same figures which may be completely wrong or - as in the example of tin sulfate - quite absurd.

One variant of the database comparison which has degenerated into a public parlour game is "blind modelling". The rules of the game are simple. A water analysis is distributed to every player and they are instructed to add 1 $\mu\text{g/liter}$ of various elements (*e.g.*, selenium, tin, uranium) to this water. Each player then calculates the speciation with his database, identifies the solid phase which limits solubility and gives as the final result the saturation index SI ($\text{SI} = \log_{10}(Q/K)$ where Q is the ion activity product and K the solubility constant). There is no winner in this game. And neither do identical results guarantee the quality of data. But saturation indices often vary considerably [92ALE/DAY], *e.g.*, from -7.6 to $+163.7$ (!) for selenium, from -3.3 to $+34.7$ for tin, and from -33.7 to $+10.3$ for uranium. Such discrepancies are embarrassing; they should not be broadcast to a wide public by a geochemical journal but be discreetly ironed out. In addition to modellers, qualified chemists should also take part in such an exercise.

IV.3 Solubility limits in the near field: the example of americium

With its isotopes ^{241}Am ($t_{1/2} = 433$ yr) and ^{243}Am ($t_{1/2} = 7370$ yr), americium is not particularly important for the safety assessment of a final storage facility. It has been chosen here as an instructive example mainly because of its clear chemical behaviour.

IV.3.1 Phases determining solubility⁵

The carbonate or the hydroxy-carbonate of americium are the stable solid phases in natural waters depending on the partial pressure of carbon dioxide. The limit value has not yet been clearly fixed. There are also uncertainties about the stability of mixed hydroxide-carbonate complexes [90FEL/RAI]. The solubilities in the near field calculated for americium [92BRU/SEL, 95BER] are therefore not to be seen as definitive values.

In addition to the requirement for reliable solubility data, there is the general problem of how the solubility behaviour of a solid changes when its cations decay. The daughter nuclei differ chemically from the mother so that the stoichiometry and the structure of the initial substance are not maintained. (Exercise: calculate the solubility of $^{241}\text{Am}(\text{OH})\text{CO}_3$ in a given type of water after 400 and 800 years).

The α -decay has a particularly serious effect on the characteristics of the solid. The α -particles lose their energy, mainly as a result of ionisation, within a range of up to roughly 20 μm ; they can therefore be released from a microcrystalline substance without causing any great damage. However, the energy from the recoil nuclei (≈ 0.1 MeV) is given off in the immediate vicinity (10 nm) due to collision processes. The resulting 2000 atomic displacements per decay cause lattice damage in crystalline substances [82ROY].

⁵ The Editors want to point out that this text was written before the NEA's critical review on americium thermodynamics [95SIL/BID] had been published.

Solubility Limitations: An “Old Timer’s” View

It has been shown that a series of compounds become amorphous after a dose of some 10^{19} decays per cm^3 . The amorphous phase has a higher solubility than the initial crystalline product.

Electron microscope studies on $^{241}\text{Am}(\text{OH})_3$ have shown that the crystals were completely fragmented after six months in a solution [77HAI/LLO]. Within this period less than 0.1 per cent of the americium had decayed ! Structural damage caused by α -decay therefore occurs much earlier than transmutation.

IV.3.2 The role of lanthanides

The mass fraction of americium oxide in the residual oxides of processed fuel elements is about 1 per cent. But significantly greater quantities of lanthanide oxides, which are mostly inactive, are also present [82ROY, 83HER]. The proportion of Ln to Am is about 50:1.

It is an established fact that the chemical behaviour of americium is very similar to that of trivalent lanthanides, especially its crystal chemical behaviour owing to the similarities of ionic radii. If ordered compounds are formed in a final storage facility, they will be (Ln, Am) mixed phases. This factor is frequently disregarded in solubility calculations, which leads to surprising results: in one particular model a solubility of 2×10^{-4} M was calculated for samarium in water, and $\text{Sm}_2(\text{CO}_3)_3$ was given as the limiting phase [92BRU/SEL]. The americium solubility calculated for the same water amounts to 2×10^{-8} M with AmCO_3OH as a stable solid phase. The contradiction between these two results is obvious and should have been spotted in the course of a quality check.⁶

If the high Ln/Am ratio in the waste is taken into account, it seems obvious that the first step should be to examine the stability of the solid phases in the system $\text{Ln(III)}-\text{H}_2\text{O}-\text{CO}_2$. It is absurd to focus entirely on the samarium because it happens to contain a radioactive isotope, and at the same time to overlook the high proportions of inactive cerium, praseodymium and neodymium. As long as there are no reliable and coherent solubility data for these elements, no reliable value can be given either for the solubility of americium. More recent work on the solubility of neodymium in bicarbonate solutions [93CAR, 93MEI/TAK] strikes a confident note.

IV.3.3 Vitrified waste

It is questionable whether defined (Ln, Am) phases are formed from vitrified waste. Borosilicate glass contains about 12 per cent residual calcinate and approximately 50 per cent SiO_2 and 15 per cent B_2O_3 as its main constituents. The hydrolysis of such glass results in the formation of amorphous alteration products with a high silicate content. There is no doubt that the solubility of heavy metals in the waste is limited by the formation of secondary phases. This has also been demonstrated particularly in the case of lanthanum [82SAV/ROB, 89PET/DRA, 91DAU/CRO]. But it is not possible to calculate solubilities. The hope that defined crystalline phases will be formed in the course of time is the straw at which modellers clutch. But nature provides sufficient examples to show that metastable phases outlive geological eras.

IV.3.4 Solubility limits in the near field: which solid phases?

The concentration of actinides and fission products in vitrified waste is greatly reduced by the presence of glass corrosion products. Solubility calculations with simple compounds are therefore unrealistic in

⁶ Note by the Editors: due to the tragic circumstances it is not possible to ask the author to reconsider this harsh sentence. Bruno and Sellin [92BRU/SEL] discussed the analogy between Am and Sm, as well as the discrepancy between the two calculated solubilities. The more soluble, but well known, $\text{Sm}_2(\text{CO}_3)_3$ was selected by Bruno and Sellin instead of SmCO_3OH , for which quantitative information was not available at that time. The higher Sm-solubility was the result of a deliberate “conservative” decision, rather than a lacking “quality check”. The reader interested in this subject should also be aware of Ref. [96MER/FUG].

such a case.

In a final repository for spent fuel, fission and transuranium products are diluted even more by the presence of uranium than in the glass form, and the formation of independent equilibrium phases is also improbable. This conclusion is not a new finding. As Grenthe says [91GRE]: “It is not likely that actinides (with the exception of U) and fission products will form separate mineral phases, they will rather be incorporated into minerals formed as a result of chemical interactions along the flowpath of the groundwater. The information on these phases is scarce or non-existing, on the other hand the formation of these secondary minerals from the ions transported from the repository is most probably controlled by *kinetic* factors”. According to another source [92GRE/FUG], “The thermodynamic data of pure uranium minerals may be of limited value for geochemical modelling, because most of these are unlikely to form from the uranium released from nuclear waste repositories. Leached uranium is more likely to be found in association with iron(III)-oxide hydrates, a common secondary phase in water-carrying fractures”.

IV.4 Solubility limits in the far field: the example of nickel

In the far field, the radionuclides released from the repository will be present in low concentrations. In the course of their migration, they will be adsorbed on to mineral surfaces and also possibly incorporated into host phases. They encounter a large number of natural trace elements which to some extent behave chemically in a similar way, and it is therefore unlikely that in the far field, elements from the waste will form pure defined solid phases. For this to happen, critical nucleation concentrations would have to be exceeded, and the ensuing crystal growth would have to take place without interference from the numerous solution associates. Nevertheless, attempts are made time after time to calculate the solubility of critical nuclides in such a complex environment using a very simple model.

Nickel has been selected as an example here firstly because the nuclide ^{59}Ni with a half-life of 7.5×10^4 years is of interest. It enters the waste as an activation product of ^{58}Ni from the structural components. Secondly, nickel is not an exotic element as it is found everywhere in trace concentrations and its geochemistry has been thoroughly studied [67GME, 78WED].

IV.4.1 Modelling of nickel solubility

In the comprehensive Poços de Caldas analogue study [91CHA/MCK], the solubilities of nine trace elements were calculated for various types of water and compared with the analytical values [91BRU/CRO]. A nickel concentration of 5×10^{-9} M was obtained in one particular type of water. This value lies within the range of typical concentrations in natural waters ($\approx 10^{-8}$ M [78WED]).

The solubilities calculated by four working groups were as follows [91BRU/CRO]:

Group	[Ni(II)]	Solid phase
A	3.0×10^{-14}	NiFe_2O_4
B	5.1×10^{-2}	$\text{Ni}(\text{OH})_2$
C	3.6×10^{-4}	NiO
D	2.7×10^{-2}	$\text{Ni}(\text{OH})_2$

The model computation results cover 12 orders of magnitude and deviate extremely from reality. The explanation for this is the choice of unrealistic solubility-limiting solid phases.

Trevorite, NiFe_2O_4 , belongs to the spinel family. It forms under high temperature conditions and it is not a weathering product. Therefore, it is avoidable malpractice to model the nickel content of groundwater with this solid phase.

Solubility Limitations: An “Old Timer’s” View

Nickel oxide occurs naturally as a rare mineral (bunsenite). But it cannot be precipitated under ambient conditions from an aqueous solution. In hydrothermal experiments, nickel hydroxide is transformed into oxide only at 285°C, and nickel oxide, which forms as a corrosion product in NaOH solutions, hydrolyzes with water into hydroxide [77OSW/ASP]. NiO therefore forms part of the unrealistic compounds.

Nickel hydroxide does not seem to occur naturally. By hydroxide precipitation, it takes the form of very thin, small platelets with dimensions of about 100 nm. Good crystalline products develop only under hydrothermal conditions. Accordingly, the solubility data range from $\log_{10} K_{s,0} = -14.7$ for fresh precipitations to $\log_{10} K_{s,0} = -17.2$ for products that have aged.

Nickel hydroxide is unstable in waters containing bicarbonate. It already reacts in air ($\log_{10} p\text{CO}_2 = -3.5$) to form a non-specified hydroxy-carbonate [77OSW/ASP]. Also hydroxy-carbonates are formed when nickel is precipitated with bicarbonate [66GME, p.844]. This class of substance has a great many variants, and solubility data do not appear to be available. A few specimens occur naturally, such as nullaganite ($\text{Ni}_2(\text{OH})_2\text{CO}_3$) and zaritite ($\text{Ni}_3(\text{OH})_4\text{CO}_3 \cdot 4\text{H}_2\text{O}$). Otwayite is a mixed (Ni, Mg)-hydroxy-carbonate.

Anhydrous nickel carbonate occurs naturally in an impure form (gaspeite: $(\text{Ni}, \text{Mg}, \text{Fe})\text{CO}_3$ [91STR/ZIM]). Its pure form can be produced only hydrothermally [66GME, p.844, 80REI]. It is therefore geochemically irrelevant and it does not matter if the current solubility products ($\log_{10} K_{s,0} = -6.87$ [85KOT/SUC]) are completely wrong: they refer to the hexahydrate and not to the anhydrous compound. (A realistic estimated value for NiCO_3 is $\log_{10} K_{s,0} = -11.2 \pm 0.3$; it is consistent with solubilities in the series $\text{MnCO}_3 - \text{ZnCO}_3$ [80REI, 94GRA]).

As has been shown at little cost, nickel solubility has therefore been modelled with unrealistic solid phases. The excessively high concentrations obtained by the model computation with NiO and $\text{Ni}(\text{OH})_2$ must not be taken to mean that the model leads to “conservative” data: the model has gone wrong. Now the only question is whether it can be improved.

IV.4.2 The geochemistry of nickel

The average nickel content of the earth’s crust is about 100 ppm. In primary minerals it is found as sulfide inclusions in silicates, or it replaces iron(II) or magnesium in silicate structures [89SPO]. As weathering occurs, it is precipitated in hydroxides and oxides [78WED]; in the form of nickel-bearing limonite ($\text{Fe}, \text{Ni})\text{O}(\text{OH}) \cdot n\text{H}_2\text{O}$), it occurs as an economically valuable ore [84GRE/EAR]. Owing to the similarity of the ionic radii, nickel is also incorporated instead of magnesium in secondary three-layer silicates (ionic radii: Ni^{2+} : 80 pm, Mg^{2+} : 77 pm). In exceptional cases, smectites may have occupied with nickel up to 50 per cent of the octahedron sites [87DEC/COL]. The silicate ore garnierite, $(\text{Ni}, \text{Mg})_6\text{Si}_4\text{O}_{10}(\text{OH})_8$, is also a weathering product.

These conditions show that there is little hope of calculating nickel solubility in an oxide system. Natural hematite and goethite also contain other transition metals [88COR] as well as nickel, and calculating the solubility of smectites is a hopeless task [88GRA].

Under reducing conditions, the *b* character of nickel results in the formation of low-solubility sulfides. Due to the low nickel concentration, these solids will not be obtained in a pure form. A critical examination of sulfide solubilities would probably be a worthwhile exercise.

IV.4.3 Solubility limits in the far field?

What has been demonstrated with the example of nickel can also be logically transposed to other trace elements in the geosphere.

The efforts to explain the concentration of trace elements in natural waters by means of the solubility equilibria of pure, individual solid phases must be seen as a failure. Occasional agreements between models and reality should not obscure the fact.

A useful model would be expected to predict correctly at least an order of magnitude for the concentrations of a whole series of trace elements in many kinds of water. This is obviously not the case.

Concluding remarks

Probably the main reason for the failure of solubility models is the assumption that trace element concentrations are determined by pure individual solid phases. In addition, the choice of such phases by the modeller is mostly arbitrary, and in the course of any model validation worthy of the name, the solid which determines solubility would have to be properly identified and properly checked out.

In natural systems trace elements will form pure single phases only in exceptional cases. They are either incorporated in a highly diluted form in host phases or adsorbed on the surfaces of other solids. In practice, it will probably not always be easy to differentiate between these two cases. The exceptions possibly include thorium, as long as it is present as oxide. It is also supposed that lanthanides are precipitated in seawater as phosphates [93BYR/KIM]. The arguments presented support this hypothesis. However, this cannot be proved correct until the presence of the hypothetical solid phase is demonstrated. The view that the concentration of lanthanides in seawater is regulated by adsorption processes as in the case of other trace elements [91LI] is therefore not disproved.

IV.5 Concluding remarks

The findings in Sections IV.2 to IV.4 are disappointing. It has transpired that naive scientific approaches and poor data are used to calculate solubility limits. A model should make it easier to understand certain phenomena; but here the gap between calculation and understanding is wide. The reasons for this are that modellers do not know enough about chemistry and are not self-critical enough.

The resulting damage may be serious. Finally, the credibility of the safety assessment as a whole is at stake when critics of the negligent treatment of solubility limits draw conclusions about the quality of the entire system. We therefore need a credible modelling scheme and we need credible data.

It must be realised that the use of solubility limits based on pure solid phases is a rough approximation to reality. It must also be realised that, because of the “intellectual uncertainty principle” [79SIT], the world cannot be described in both exact and understandable terms. A model computation cannot say “how things are” or “how things will be”, but only “how things *could* be subject to given simplifying assumptions.”

As everybody knows, theories and models cannot be validated in the strict sense but only refuted [59POP, 94ORE/SHR]. It is therefore a minimum requirement that a model should not conflict with facts that are obvious. Accordingly, the least that can be done is to check out model calculations, firstly by means of simple laboratory experiments. If they already reveal serious conflicts, the model is just wrong !

The first step towards credible data is to clear out the databases⁷. Apparently the prevailing opinion is that to be good, a database should be all-embracing. A change in thinking is imperative. Quality should come before quantity, and the motto should be: “*Pauca, sed matura*”⁸.

A database of solids requires detailed documentation stating the grounds for including any particular compound. The geochemical relevance of this information and its significance for the final repository must be judged, and details on its formation should be provided. The data source and the methods used to determine the data should be clearly stated in the documentation. A reference such as, for example, “Wagman et al. 1982” [82WAG/EVA] is not sufficient, for it is no quality guarantee. Finally, the reasons for preferring one particular work to another should also be stated. Sound knowledge of chemistry and geochemistry is essential for all this. No “broad highway” shows the way ahead, and the “well-travelled roads” of simple database comparisons are not the answer either.

⁷ A reference to Greek mythology is called for: for 30 years the dung from 3000 cattle had piled up in the Augean stables. Hercules cleared it all out in a single day. It was only because of his family ties with Olympus that he was able to perform this task so quickly and efficiently. We who are neither gods nor heroes will have to busy ourselves for a much longer time with databases. Will there be a laurel wreath at the end of our labours ? The list of Hercules’ glorious deeds is long, and his name has therefore been remembered for thousands of years. The name of Augeas has also survived, but only because of his stables !

⁸ Motto on the seal of C.F. Gauss (“Few in number but sound”).

Solubility Limitations: An “Old Timer’s” View

Solubility limits are one of the “pillars of safety” in a final repository. But it transpires that this pillar is not particularly stable. It is probably only in the case of a few radionuclides and in the near field, that we can convincingly demonstrate the effectiveness of defining solubilities for radionuclide release. However, the sorption on backfill and on rock is also a relevant process in the far field where concentrations of radionuclides will be very low. Although there are still uncertainties in this area, basic difficulties that are hardly quantifiable in solubility estimates are cleared up: there is no need to worry about critical nucleation concentrations, the crystallisation-inhibiting influence of silicic acid, complex, non-ideal mixed phases, and the change in the solubility behaviour of solid phases as a result of radioactive decay.

It would therefore make more sense to devote more time and effort to adsorption than to sophisticated and unreliable solubility models. But what is the position with regard to sorption data ? So here we go again, and Hercules is faced with a new challenge !

Chapter V

Binding Models for Humic Substances

Wolfgang HUMMEL
Waste Management Laboratory
Paul Scherrer Institut
CH-5232 Villigen PSI (Switzerland)

V.1. Introduction

Humic substances are the largest fraction of natural organic matter in water. They are important for water quality, for chemical weathering in natural environments, and as complexing agents for trace metals. The latter property requires that humic substances are included in thermodynamic modelling of aqueous systems. However, in general thermodynamic databases, do not contain equilibrium constants for complexation of metal ions with humic substances. Any attempt to remedy this omission inevitably pulls the modeller into a veritable jungle of humic binding models, published in a plethora of journal articles. Obviously there must be some differences between metal ion binding by “ordinary” or “simple” ligands like carbonate or acetate, which is described in terms of “classical” equilibrium thermodynamics, and binding of metal ions by humic substances.

This chapter is intended to guide the modeller through the multitude of humic binding models by emphasising the differences between complexation models of simple organic ligands and binding models of humic substances. The modeller should understand (1) why, from a thermodynamic point of view, humic substances cannot be treated the same way as simple organic or inorganic complex forming ligands; (2) why and for what purpose the various binding models were developed; and (3) what problem solving strategy could be followed in a particular modelling problem. As all current humic binding models are just fitting models, consistent treatment of experimental data is emphasised as a prerequisite to deriving a reliable set of model parameters tailored to the problem at

hand.

The general discussion of humic binding models will be useful in modelling metal-humic interactions in any aquatic system. The example discussed in detail throughout this chapter is taken from ongoing work in the assessment of radionuclide behaviour in the environment. Likewise, the problem solving strategy proposed in the last part of this chapter focuses on this topic, although it is not at all limited to radioactive waste problems.

V.2. What are humic substances ?

Humic substances occur in rotting vegetable matter and can be detected in the black slime of an ordinary compost pit in a home garden. They are found in the brown organic matter of a variety of soils, as well as in peat, lignite and brown coals. The concentration of humic substances in natural waters varies over three orders of magnitude [85THU]: Ground waters and marine waters are lowest in concentration with 0.03 to 0.6 mg/l of humic substances expressed as dissolved organic carbon (DOC). Streams, rivers, and lakes vary from 0.5 to 4.0 mg/l. Tea-colored waters, such as marshes, bogs, and swamps vary from 10 to 30 mg/l DOC as humic substances. As a group humic substances account for approximately 30 to 50 percent of the DOC of most natural waters, except in colored waters, where they contribute 50 to 90 percent of the DOC.

What is the chemical composition of these “humic substances”? This is a difficult question. Humic substances are the product of decomposition chemistry, not the ordered chemistry of biological products. Thus, no chemical labeled “humic substances” exists, and there are no simple methods of analysis for humic substances. The first problem is to define, in some limited yet useful way, what humic substances are. Humic substances may be defined operationally [85THU]: They are colored, polyelectrolytic, organic acids isolated from water on XAD resins¹, weak-base ion-exchange resins, or a comparable procedure. Alternatively, they are extracted from soil by sodium hydroxide (typically 0.1 M). In both cases a further fractionation divides humic substances into two classes, which are humic and fulvic acid. Humic acid is the fraction that precipitates at pH 2.0 or less, the fraction remaining in solution is fulvic acid. Other classification schemes emphasise the origin of humic substances (soil, aquatic, sediment, *etc.*) rather than pure operational classifications. For an in-depth discussion of this topic see [88BUF].

The knowledge concerning the structure of humic substances may be summarised according to Thurman [85THU] as follows. Fulvic acids have a range of molecular weight from 500 to 2000 g/mol, whereas humic acids are larger and often colloidal, with molecular weight from 2000 to 5000 g/mol, and sometimes much larger, up to 100,000. The major

¹ XAD resins are nonionic methacrylate polymers that adsorb organic matter from water by hydrophobic bonding. The pH of the water is lowered to 2.0, and the humic substances adsorb onto the XAD resin. Then, the humic substances are desorbed quantitatively with base and studied by various techniques. Because approximately 30% of the dissolved organic carbon of a natural water are organic acids that are not retained by XAD resins at pH 2.0, they have been called the “hydrophilic acids”. Little is known about the nature of these hydrophilic acids and their study has only begun.

functional groups include: carboxylic acids, phenolic hydroxyl, carbonyl, and aliphatic hydroxyl groups. On the average, fulvic acid contains 5.5 mM of carboxyl groups per gram. This corresponds to one carboxylic acid group per 6 carbon atoms, or one group per aromatic ring, if distributed evenly. If not, there may be as many as two or three carboxylic-acid groups on some aromatic rings, and none on others. The ^{13}C -NMR spectra indicate that the aromatic to aliphatic ratio is 1:2. Hence, approximately 65 percent of the carbon is aliphatic, and many of the carboxyl and hydroxyl groups are on aliphatic carbons. The average phenolic content in fulvic acids is 1.2 mM/g based on NMR and titration data, this is 1 phenolic functional group for every 30 carbon atoms, or only two phenolic groups per fulvic acid molecule, as the molecular size of less than 2000 suggests that up to 60 carbon atoms are involved in the structure with probably 3 to 4 aromatic rings. This is not a large molecule, rather, it is a medium-sized, water-soluble acid. Hydroxyl and carbonyl groups, summed together, are as abundant in fulvic acid as carboxyl groups. This information is based on ^{13}C -NMR spectra of several samples. The amount corresponds to 5 to 7 mM/g. This suggests that the fulvic acid mixture contains molecules with either carboxyl, carbonyl, and hydroxy groups for every 3 carbon atoms. Fulvic acid from water is probably a mixture of many different molecules, with the average characteristics listed above. The number of compounds that constitute the fulvic acid fraction may be 10, 100, 1000 or more compounds, and the structure of fulvic acid remains an interesting unresolved question. Humic acid is less soluble than fulvic acid. On the average, it contains fewer carboxyl groups than fulvic acid, but a somewhat larger phenolic content. Degradation experiments do not show radically different products for humic and fulvic acid, suggesting that the cores of both humic and fulvic acid are similar. Therefore, in the following discussion of binding models the term “humic substances” comprises both, humic and fulvic acid.

This short summary of knowledge about the nature of humic substances foreshadows the difficulties encountered when their binding properties with metal ions are studied experimentally, and when the experimental results are subsequently modelled by means of thermodynamic approaches [88BUF].

V.3. Metal ion binding of humic substances

V.3.1. The experimental data

The minimal set of experimental data needed to describe the interaction of a metal ion, M , with a humic substance, HS , comprises $[\text{MHS}]$, the concentration of metal bound to a certain humic substance, $[\text{M}]$, the concentration of free metal in the aqueous phase, and $(\text{HS})_{\text{total}}$, the total concentration of humic substance. $[\text{MHS}]$ and $[\text{M}]$ can be quantified on the molar scale [mol/l], but $(\text{HS})_{\text{total}}$ is known only as mass per unit volume (g/l). Note, that [] is used in the following for molarity units and () for mass per unit volume. One of the two molar concentrations, $[\text{MHS}]$ or $[\text{M}]$, is usually derived directly from measured quantities, whereas the other is calculated from mass balance equations involving the total concentration of metal in the system, $[\text{M}]_{\text{total}}$, and the concentration of aqueous metal

complexes formed. The experimental procedures to measure these quantities and the subsequent mass balance calculations also contain some model assumptions; but these, like the complexation behaviour of the metal ion with ligands other than HS, can be checked independently of the humic binding model which is used to interpret the experimental data.

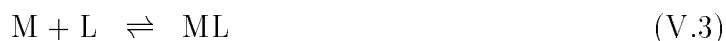
This minimal set of experimental information can be described by a constant cK , defined as the number of moles of metal bound per gram of humic substance divided by the concentration of free metal in solution:

$${}^cK = \frac{[\text{MHS}]}{[\text{M}] \cdot (\text{HS})_{\text{total}}} \quad (\text{V.1})$$

The unit of cK therefore is volume per mass, usually given as l/g. The coefficient cK closely resembles the well known stability constant

$$K = \frac{[\text{ML}]}{[\text{M}] \cdot [\text{L}]} \quad (\text{V.2})$$

of a metal-ligand complex formation for the reaction



However, there are two fundamental differences between the formally similar Eqs. (V.1) and (V.2).

First, in the case of simple organic ligands, like acetate, oxalate or edta, the molecular structure of the ligand L and thus, the nature and number of functional groups S is well known. The stereochemistry of the possible metal - ligand complexes can be deduced from this molecular structure information. The complexes predominating within a certain experimentally investigated region of chemical parameter space (component concentrations, pH, ionic strength, *etc.*) are usually determined by data fitting procedures using a number of alternative complexation models characterised by different sets of possible complexes. In cases where there are only small differences between the best fits of these alternative complexation models, additional evidence for verification of the existence of certain species like ML, ML₂, MHL, M(OH)L, *etc.*, may be obtained from spectroscopic studies and crystal structure determinations of the metal-organic compounds. In contrast to these well-defined ligands, “humic substances” serves just as a label for an operationally defined class of a naturally occurring mixture of large size molecules. The molecular structure models proposed so far for humic substances are rather dissimilar and indicate the lack of knowledge and the complexity of the subject (see, for example, “Kleinhempel’s model” [70KLE], also in [88BUF] *p.*175, a “random molecular model” [83MUR/LIN], a “pseudomicellar structure model” [94ENG/WAN], or a “flexible carbon network structure” [94SCH]). The nature and number of functional groups S involved in metal binding by humic substances are, at best, uncertain. That is, the stereochemistry of M - HS complexes is largely unknown. By analogy to small molecules, the functional groups involved in binding a metal ion may be called a “ligand”. A 1:1 complex in the case of humic

substances is defined as a metal ion bound to a certain (unknown) number of functional groups within the same humic molecule.

The second difference between Eqs. (V.1) and (V.2), is closely related to the first one, and concerns the concentration of free ligand, $[L]$, and the total concentration of humic substance $(HS)_{\text{total}}$. The latter provides information about experimental conditions; the mass of humic substance added per unit volume of solution. In order to convert this mass number into the total molar concentration of “ligands” or binding sites available for complexation with the metal ion, $[L]_{\text{total}}$, we need to know the number of complexing sites per unit mass of the humic substance. Analytical methods like pH - titration, elemental analysis or radioactive labeling, measure, or at least allow an estimate, of the total concentrations of different kinds of functional groups. These total concentrations, however, only give upper limits for the concentrations of the binding sites $[L]_{\text{total}}$. The only method to directly measure these quantities would involve the metal ion under study as a probe: Suppose we know the stereochemistry of the MHS complex formed and its equilibrium constant, the molar concentration of binding sites could then easily be derived from the measurements. But the stereochemistry, *i.e.* the nature and number of functional groups involved in metal binding, and their associated complexation strength are the unknowns in this game. The total molar concentration of binding sites, $[L]_{\text{total}}$, cannot be measured independently of the model assumptions. Hence, the concentration of free binding sites $[L]$ is a model dependent parameter.

Summarising laboratory experiments on selected humic substances, the coefficient ‘ K ’ is found to vary with changes in component concentrations, pH, and ionic strength. These changes are described in the various binding models of humic substances. The different *concepts* to describe these changes are presented in the following sections in a systematic manner. We begin with variations in component concentrations, *i.e.* the concentrations of metal ions and humic substances, at constant pH and ionic strength. Then we proceed to pH variations and finally we discuss the treatment of ionic strength effects. Humic binding models may comprise any combination of these concepts. If we attempted to discuss published *binding models* in a systematic manner, we would end up with a classification scheme consisting of such complicated classes as “discrete heterogeneous non-electrostatic models”, for example. The intent is not to give a detailed review of all humic binding models developed so far but merely to discuss some important aspects of published models, in the hope of providing the reader with a pathway through the multitude of humic binding models.

V.3.2. Variations in component concentration

V.3.2.1. The simplest model

Any useful binding model for humic substances contains a number of assumptions, but relies ultimately on experimental data. This seems to be a rather trivial statement, but while struggling along with the different humic binding models, the reader of the literature in the field may get the impression that a clear-cut distinction between measured data

and more or less plausible model assumptions is all but impossible. In some cases model assumptions intermingle with experimental results; in most cases at least some of the basic assumptions are never explicitly stated. In the hope of clearing this thicket, an effort is made here to clearly state the assumptions and to discuss their plausibility and consequences.

Table V.1: List of model assumptions.

Assumption	Description of assumption
{A1}	The metal ion M forms only 1:1 complexes with ligand sites L of the humic molecule. The humic molecule consists of a number of functional groups S . This number is not specified in the model, but is assumed to be fixed within the pH and metal concentration range where the model is applied.
{A2}	For each metal ion M under study, only one kind of ligand site L predominates within the parameter range where the model is used.
{A3}	The complexing strength of the ligand sites L is constant, and does not vary with the location within the humic molecule, <i>i.e.</i> the influence of different substituents and varying stereochemistry on L is ignored.
{A4}	Chemical changes of the humic molecules have no influence on the number of active ligand sites available for metal complexation.
{A5}	The functional groups S involved in metal binding do not undergo any proton exchange reactions in the pH range of interest.
{A6}	There are no interactions between functional groups S of the humic molecule, <i>i.e.</i> electrostatic effects that change the binding characteristics of S are ignored.

The simplest version of a humic binding model, based on assumptions {A1} to {A6} (Table V.1), considers metal-humic interactions as a reaction between a metal ion and a unique ligand site L to form a 1:1 complex, as described by Eqs. (V.2) and (V.3). In other words, the simplest humic binding model, sometimes called a “single site model”,

treats humic substance like a simple organic ligand with unknown molecular weight.

The amount of metal bound to the humic substance is then given by

$$[\text{MHS}] = [\text{ML}] \quad (\text{V.4})$$

and the total concentration of ligand sites is simply the sum of free ligand sites and metal bound to humic substance

$$[\text{L}]_{\text{total}} = [\text{L}] + [\text{ML}] \quad (\text{V.5})$$

The total concentration of humic substance, $(\text{HS})_{\text{total}}$, is related to the total concentration of ligand sites $[\text{L}]_{\text{total}}$ by

$$(\text{HS})_{\text{total}} \cdot \text{SCC} = [\text{L}]_{\text{total}} \quad (\text{V.6})$$

where the Site Complexation Capacity SCC is the amount of active binding sites per unit mass of humic substance (mol/g). As discussed in Section V.3.1, $[\text{L}]_{\text{total}}$ and thus SCC is a model dependent adjustable parameter. According to assumption {A4}, the simplest model described here, treats SCC as a constant, independent of the concentrations of metal and humic substance. Combining Eqs. (V.2), (V.5) and (V.6) gives

$$(\text{HS})_{\text{total}} \cdot \text{SCC} = [\text{L}] (1 + K \cdot [\text{M}]) \quad (\text{V.7})$$

Finally, combining Eqs. (V.1), (V.2), (V.4) and (V.7) and rearranging shows the relation between the measured data ${}^{\circ}K$ and $[\text{M}]$ and the adjustable model parameters K and SCC:

$${}^{\circ}K = \frac{K}{1 + K \cdot [\text{M}]} \cdot \text{SCC} \quad (\text{V.8})$$

Experimental data plotted in a $\log_{10} {}^{\circ}K$ - $\log_{10}[\text{M}]$ diagram, which extends over a sufficiently large range of free metal concentration, will give various information: In the region of very low metal loading the free ligand sites predominate, $[\text{L}] > [\text{ML}]$ or $K \cdot [\text{M}] < 1$, and Eq. (V.8) reduces to

$${}^{\circ}K = K \cdot \text{SCC} \quad (\text{V.9})$$

The model predicts that ${}^{\circ}K$ is constant in the range of trace metal concentrations. In the region of high metal loading close to metal saturation, the ligand sites are to a large extent bonded to metal ions, *i.e.* $[\text{ML}] > [\text{L}]$ or $K \cdot [\text{M}] > 1$, and Eq. (V.8) reduces to

$${}^{\circ}K = \frac{1}{[\text{M}]} \cdot \text{SCC} \quad (\text{V.10})$$

Thus, in the region of high metal loading, $\log_{10} {}^{\circ}K$ decreases with increasing $\log_{10}[\text{M}]$ by slope -1 . As can be seen from Eq. (V.10), in the region of metal saturation ${}^{\circ}K$ no longer depends on the parameter K but is determined by SCC, the site complexation capacity,

alone. As a consequence of the model assumptions, the site complexation capacity is defined as the maximum number of moles of metal ions bound per unit mass of humic substance

$$\text{SCC} = [\text{MHS}]_{\text{max}}/(\text{HS})_{\text{total}} \quad (\text{V.11})$$

at metal saturation $[\text{L}]_{\text{total}} \approx [\text{ML}] = [\text{MHS}]_{\text{max}}$. The parameter SCC, in this model, is therefore usually associated with terms like “total metal-binding capacity” [91BID/GRE], “complexing capacity” [95MOU/MOU], or “loading capacity” [96KIM/CZE].

In theory, the parameter SCC can be adjusted in the region of metal saturation (Eq. (V.11)), whereas the parameter K may be derived from data in the range of trace metal concentrations (Eq. (V.9)). In practice, however, the analytical window of a given experimental technique used to study metal-humic interactions usually does not permit measurements over many orders of magnitude in component concentration. In the region of high metal loading especially, metal saturation can only approximately be achieved, due to coagulation and precipitation of humic substances and Eq. (V.11) cannot be applied directly. Most studies published so far present data measured over two to three orders of magnitude in component concentration, and the model parameters K and SCC are obtained by fitting these data for given pH and ionic strength values.

For example, Bidoglio *et al.* [91BID/GRE] interpret their equilibrium titration curves of the lanthanides Eu(III) and Tb(III) with fulvic acids in terms of this simple model. They denote the site complexation capacity SCC as c , the total metal-binding capacity of fulvic acid, and their conditional constant K' is identical with our parameter K . The same type of model is used by Moulin and Moulin [95MOU/MOU] to interpret data of Am(III), Cm(III), Dy(III), Np(V) and U(VI) complexation with humic substances. The site complexation capacity SCC is named W , the complexing capacity, and the conditional interaction constant β is identical with our parameter K . The approach used by Kim and coworkers [96CZE/KIM, 96KIM/CZE] to model data of Am(III), Cm(III), Np(V) and U(VI) complexation with humic acid looks somewhat different at a first glance. A loading capacity LC is defined as a dimensionless number, the maximum number of moles of metal ions bound per moles of humic substance

$$\text{LC} = [\text{MHS}]_{\text{max}}/[\text{HS}]_{\text{total}} \quad (\text{V.12})$$

where $[\text{HS}]_{\text{total}}$ is the total concentration of humic substance in mol/l. The conversion from the analytical concentration of humic substance in g/l, $(\text{HS})_{\text{total}}$, to the molar concentration, $[\text{HS}]_{\text{total}}$, is operationally defined as

$$[\text{HS}]_{\text{total}} = (\text{HS})_{\text{total}} \cdot \text{PEC}/z \quad (\text{V.13})$$

PEC is the proton exchange capacity in mol/g at pH 7, derived from pH titration of the humic substance. The parameter z is thought to be the number of functional groups (with charge minus one) coordinating to a metal ion. Local charge neutralisation is assumed in the model, *i.e.* $z = 3$ for trivalent ions like Am^{3+} , $z = 2$ for divalent ions like UO_2^{2+} , and

$z = 1$ for monovalent ions like NpO_2^+ . The total concentration of ligand sites $[\text{L}]_{\text{total}}$ is defined in terms of the loading capacity

$$[\text{L}]_{\text{total}} = [\text{HS}]_{\text{total}} \cdot \text{LC} \quad (\text{V.14})$$

Combining Eqs. (V.12) and (V.14), reveals that the total concentration of ligand sites is defined as the maximum concentration of metal ions bound to humic substance, $[\text{L}]_{\text{total}} = [\text{MHS}]_{\text{max}}$, in accordance with our model. Thus, the conceptual models used in [91BID/GRE, 95MOU/MOU, 96KIM/CZE] are the same despite some differing definitions of conversion relations and adjustable parameters. The conditional interaction constants K' or β in all these models are numerically identical if fitted to the same data sets. Note, that β values derived by Kim and Czerwinski [96KIM/CZE] are independent of the actual value of PEC and the number chosen for z . The assumption of local charge neutralisation cannot be verified or falsified by experimental data. The fit of any experimental data set results in the same values of β irrespective of the value chosen for z .

The fitting parameter K should turn out to be constant over large component concentration ranges if the assumptions of our model are valid. Experimental investigations at relatively high metal loading by Bidoglio *et al.* [91BID/GRE] and Kim and coworkers [96CZE/KIM, 96KIM/CZE] indeed result in constant parameters K over the entire range of metal concentration. However, in the range of low metal loading, Moulin and Moulin [95MOU/MOU] report an increase in the fitted K values with decreasing metal concentration! Contrary to the claim in [96CZE/KIM] this change in K cannot be ascribed to different definitions of the humic substance concentration, because these differences have no influence on the fitted K values. Our simple model therefore seems not to be an adequate description of metal-humic complexation behaviour from metal saturation down to very low metal loading. This is not surprising, we cannot expect that humic substances behave just as a simple monofunctional organic ligand.

V.3.2.2. Mixed-ligand models

In the simplest model of metal-humic binding, {A1}, we assumed that the metal ion M only forms 1:1 complexes with ligand sites L of the humic molecule. However, it is possible that a metal ion bound to a ligand site L exchanges coordinated water molecules for low molecular weight ligands X, thereby forming mixed-ligand L-M-X complexes. If we skip assumption {A1}, such complexes may be described by the equilibrium



where X is an anion like CO_3^{2-} , oxalate, *etc.* The conditional stability constant of this mixed-ligand equilibrium is

$$K_{\text{mix}} = \frac{[\text{MLX}]}{[\text{ML}] \cdot [\text{X}]} \quad (\text{V.16})$$

The concentration of metal bound to the humic substance thus is now given by

$$[\text{MHS}] = [\text{ML}] + [\text{MLX}] \quad (\text{V.17})$$

and the total concentration of ligand sites is simply the sum of free ligand sites and metal bound to the humic substance

$$[\text{L}]_{\text{total}} = [\text{L}] + [\text{ML}] + [\text{MLX}] \quad (\text{V.18})$$

The relation between the measured data cK and $[\text{M}]$ and the three adjustable model parameters K , K_{mix} and SCC is now:

$${}^cK = \frac{K(1 + K_{\text{mix}} \cdot [\text{X}])}{1 + K(1 + K_{\text{mix}} \cdot [\text{X}]) \cdot [\text{M}]} \cdot \text{SCC} \quad (\text{V.19})$$

In the region of high metal loading where the ligand sites are predominantly occupied by metal ions, we have $[\text{ML}] + [\text{MLX}] > [\text{L}]$ or $K(1 + K_{\text{mix}} \cdot [\text{X}]) \cdot [\text{M}] > 1$, and Eq. (V.19) reduces to Eq. (V.10) in the previous model. In this parameter range, no influence of the additional ligand X on the experimental cK values is expected. In other words, in the region of high metal loading experimental data do not allow us to distinguish between metal ions bound via 1:1 complexes only, or mixed-ligand complexes. However, in the region of very low metal loading, the free ligand sites predominate, $[\text{L}] > [\text{ML}] + [\text{MLX}]$ or $K(1 + K_{\text{mix}} \cdot [\text{X}]) \cdot [\text{M}] < 1$, and Eq. (V.19) reduces to

$${}^cK = K(1 + K_{\text{mix}} \cdot [\text{X}]) \cdot \text{SCC} \quad (\text{V.20})$$

Here, we expect an increase of cK when the concentration of the additional ligand X is increased above a certain threshold, which is given by $[\text{MLX}] > [\text{ML}]$ or $K_{\text{mix}} \cdot [\text{X}] > 1$. Therefore, only experimental data at low metal loading are appropriate to decide whether mixed-ligand complexes are formed, or not, within a certain range of X concentrations.

Information about the formation of MLX complexes in the literature is scarce. Experimental evidence for the existence of such complexes was first provided by acid-base titrations combined with ion-selective measurement of Cu^{2+} concentration [73MAN/RAM]. Powell and Town [91POW/TOW] postulated from data obtained by spectroscopic and voltammetric techniques that MLX complexes were formed in significant amounts. However, no attempt was made by the authors to derive stability constants from their data, [91POW/TOW]. Buffle [80BUF] corrected literature data for the complexation of $\text{Cu}(\text{II})$ by humic substance in the presence of X by introducing mixed-ligand complexes. He tentatively assumed that the stability constant for the reaction between ML and X is the same as for the addition of X to the metal aqua ion. As a result, the corrected data fit better to the binding models used in that study. Recently, Glaus, Hummel and Van Loon [95GLA/HUM] showed in an experimental study of the complexation of humic substances with $\text{Co}(\text{II})$, $\text{Eu}(\text{III})$ and $\text{U}(\text{VI})$, and carbonate, oxalate, nta and edta as anion X, that MLX complexes are rather weak compared with complexes formed by the low molecular

weight ligands X alone. In all cases studied so far, $K_{\text{mix}} < K_2$, where K_2 is the stepwise stability constant for the equilibrium between MX and MX_2 , *i.e.*

$$K_2 = \frac{[\text{MX}_2]}{[\text{MX}] \cdot [\text{X}]} \quad (\text{V.21})$$

If the relation $K_{\text{mix}} < K_2$ is valid in general for any metal/ligand combination, it will be possible to estimate the threshold concentration of X, above which mixed ligand complexes become important in metal-humic systems, even for cases where K_{mix} is not known.

V.3.2.3. Variable stoichiometry models

If we assume that X is not a low molecular weight ligand, but a second ligand site L of the humic substance that coordinates to the metal ion M, we postulate the formation of classical 1:2 complexes according to:



The conditional stability constant of equilibrium (V.22) is

$$\beta_2 = \frac{[\text{ML}_2]}{[\text{M}] \cdot [\text{L}]^2} \quad (\text{V.23})$$

The concentration of metal bound to the humic substance thus is now given by

$$[\text{MHS}] = [\text{ML}] + [\text{ML}_2] \quad (\text{V.24})$$

and the total concentration of ligand sites is the sum of free ligand sites and metal bound to the humic substance

$$[\text{L}]_{\text{total}} = [\text{L}] + [\text{ML}] + 2[\text{ML}_2] \quad (\text{V.25})$$

The relation between the measured data cK and $[\text{M}]$ and the three adjustable model parameters K , β_2 and SCC is:

$${}^cK = \frac{K + \beta_2 \cdot [\text{L}]}{1 + (K + \beta_2 \cdot 2[\text{L}]) \cdot [\text{M}]} \cdot \text{SCC} \quad (\text{V.26})$$

This type of model is sometimes called a “multidentate model” [86TUR/VAR]. The term is misleading since we do not know *a priori* how many functional groups S constitute a ligand site L of a humic substance. If more than one functional group S is coordinating, even a simple 1:1 complex ML is a multidentate complex. We therefore recommend using the term “variable stoichiometry models” for models comprising other than simple 1:1 complexes.

In the region of high metal loading close to metal saturation, the ligand sites are predominantly occupied by metal ions, *i.e.* $[\text{ML}] + 2[\text{ML}_2] > [\text{L}]$ or $(K + \beta_2 \cdot 2[\text{L}]) \cdot [\text{M}] > 1$,

but Eq. (V.26) does not simply reduce to Eq. (V.10), as in the cases discussed so far. We have to distinguish two cases. If the 1:1 complex predominates, *i.e.* if $[ML] > 2 \cdot [ML_2]$ or $K > \beta_2 \cdot 2[L]$, Eq. (V.26) reduces to Eq. (V.10):

$${}^cK = \frac{1}{[M]} \cdot SCC$$

If the 1:2 complex predominates, *i.e.* if $[ML] < 2 \cdot [ML_2]$ or $K < \beta_2 \cdot 2[L]$, Eq. (V.26) reduces to

$${}^cK = \frac{1}{[M]} \cdot \frac{SCC}{2} \quad (V.27)$$

Hence, the site complexation capacity is divided by a factor of two as compared to Eq. (V.10), because two complexing sites are involved in the formation of 1:2 complexes. A factor of two in experimental cK values will in general be within the scatter in the experimental data. Thus, the existence of 1:2 complexes is very difficult to prove unambiguously.

In the region of very low metal loading, the free ligand sites predominate, and $[L] > [ML] + 2[ML_2]$ or $(K + \beta_2 \cdot 2[L]) \cdot [M] < 1$, Eq. (V.26) reduces to

$${}^cK = (K + \beta_2 \cdot [L]) \cdot SCC \quad (V.28)$$

In this range the concentration of free binding sites is close to the total concentration of binding sites, $[L] \approx [L]_{\text{total}} = (HS)_{\text{total}} \cdot SCC$, and Eq. (V.28) can be written as

$${}^cK = (K + \beta_2 \cdot (HS)_{\text{total}} \cdot SCC) \cdot SCC \quad (V.29)$$

A linear increase with slope one of the experimental cK values with increasing total concentration of humic substance is predicted in this concentration range if 1:2 complexes predominate. This behaviour differs from that in the simple model discussed above, Eq. (V.9), where experimental cK values are predicted to be independent of the total concentration of humic substance $(HS)_{\text{total}}$. An increase of experimental cK values with increasing total concentration of humic substance, can also be interpreted in terms of multiple sites. In this conceptual model, as discussed in detail in the next section, increasing concentration of humic substance at constant total metal concentration results in a decrease in the overall metal loading of the humic substance. As a consequence, the ratio strong/weak complexing sites is shifted towards the (few) strong sites and the overall effect is an increase of experimental cK values.

In summary, discrimination between models including complexes with variable stoichiometry, and models including (multiple) 1:1 complexes only, can only be achieved by varying *both*, the total concentration of humic substance *and* the total concentration of metal, at low metal loading, over several orders of magnitude. Unfortunately, all attempts published so far to model data with 1:2 complexes were made with data sets consisting of either variable metal concentrations but constant humic substance concentration alone,

or vice versa. No unique model can be obtained from these data sets. The existence and potential importance of 1:2 metal-humic complexes has not yet been shown from experimental data. In addition, the concepts of 1:2 complexes presented by different authors are rather inconsistent. A few representative examples illustrating this unfortunate situation follow.

We begin with an example representing the clearest discussion of variable stoichiometry models found in the literature. Buffle, Greter and Haerdi [77BUF/GRE] measured the complexation properties of fulvic acids with lead and copper ion-selective electrodes. The experimental data consist of metal and pH titrations at constant humic substance concentration (and constant ionic strength). They were interpreted in terms of 1:1 and 1:2 complexes, including proton exchange equilibria (see Section V.3.3.2). The authors [77BUF/GRE] assumed that the fulvic acid molecules contain only one coordinating site, and thus the site complexation capacity parameter, SCC, is inversely proportional to the mean molecular weight, M_w , of the fulvic acid: $SCC = 1/M_w$. As a consequence, the 1:2 complexes are thought to involve two molecules of fulvic acid which “is physically possible since the molecular weight of the complexing molecules of fulvic acid is always low (generally less than 1000 g/mol)”. Three parameters were fitted to the metal titration data, the two stability constants for 1:1 and 1:2 complexes and M_w . However, the authors were aware of the fact that metal titration data alone cannot prove or disprove the existence of 1:2 complexes. After deriving Eq. (V.29), Buffle, Greter and Haerdi [77BUF/GRE] stated that this equation was checked by plotting “ K / SCC versus $(HS)_{total} \cdot SCC$ for various water samples. “Good straight lines were obtained”, but no data or plots of this kind are shown in the paper.

Stevenson [76STE] reports potentiometric titration data for complexes between Cu, Pb and Cd and three humic acids at various ionic strengths but constant humic acid concentrations. The results were interpreted in terms of 1:1 and 1:2 complexes according to Eq. (V.26), including proton exchange equilibria (see Section V.3.3.2). [76STE] states “it should be noted that, in coordination chemistry, 1:1 and 1:2 complex refer to the number of molecules necessary to satisfy the coordination number of the metal ion. As used herein, the relationship denotes the number of *ligand* sites per metal ion”. Although not stated clearly in the paper, further discussions in [76STE] indicate that the author thinks his postulated 1:2 complex consists of two adjacent acidic groups, most probably of the structure type of phthalic or salicylic acid, which is the definition of a two-dentate 1:1 complex. In essence, a conceptual two site model, as discussed in the next section, is formally treated in terms of a variable stoichiometry model. The same misleading terminology, mixing up the concept of variable stoichiometry and multiple sites, is used by Yoon *et al.* [94YOO/MOO]. They interpret spectroscopic data of Eu(III) - fulvic acid complexation in terms of “two types of carboxylate moieties for the binding of metal ions on fulvic acid which formed 1:1 (EuL^{2+} ; L = carboxylate) and 1:2 (EuL_2^+)”. Misleading terminology adds further to the already rather complicated topic and should be avoided.

The interaction of humic and fulvic acids with Eu(III) and Am(III) at trace metal concentration was measured by Bertha and Choppin, [78BER/CHO], using Schubert’s method. The total metal concentration was held approximately constant while the con-

centration of humic substance was varied over about one order of magnitude. The experimental data were interpreted as a 1:m complex, with m between 1.4 and 1.8. Bertha and Choppin [78BER/CHO] therefore assumed that the complex species are ML and ML₂. In addition, they state “since we cannot *a priori* choose whether these two types of sites are identical or not, we designate the 1:1 sites as X and the 1:2 sites as Y”. In fact, this represents a combination of a variable stoichiometry model with a multiple site model. This model was abandoned in later publications of the same group in favor of a formal variable stoichiometry model. For example, Torres and Choppin [84TOR/CHO], measuring Eu(III) and Am(III) humate complexation by a liquid/liquid distribution method at approximately constant trace metal concentrations but varying pH, state “the experimental data was fitted satisfactorily by a second order analysis leading to values of β_1 and β_2 but did not require any further parameter, *e.g.* β_3 ”. This misleading formal treatment of experimental data is still presented in recent publications. For example, Tao, Du and Li [96TAO/DU] report 1:1 and 1:2 stability constants for uranyl-fulvic acid complexation, formally derived from data obtained by an ion exchange method. These models add very little to our understanding of metal-humic interactions.

V.3.2.4. The multi-site models

The conceptual models discussed so far treat humic substances as a simple organic ligand with an unknown molecular weight, which forms primarily 1:1 complexes with metal ions. Variations in experimental cK values at low metal loading lead either to variable fitting parameters K in the simplest model, Eq. (V.8), or are treated by formally introducing 1:2 complexes as in Eq. (V.26). The following is an alternative to variable “constants” K or the controversial concept of variable stoichiometry, *e.g.* 1:2 complexes.

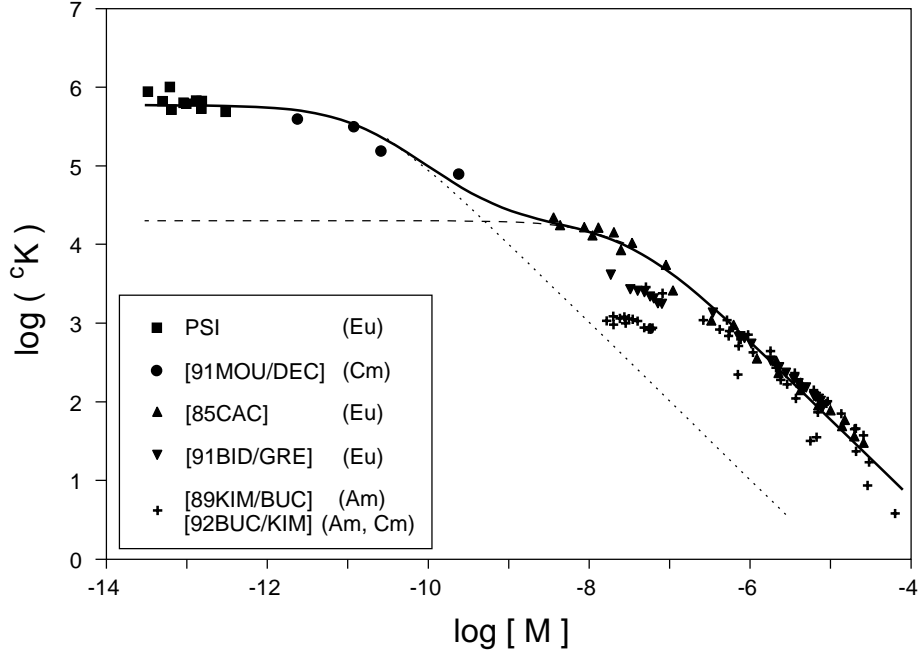
For illustration, Eu, Am and Cm data in the pH range 5 - 5.5 and at ionic strength 0.1 M were collected from several publications. These data have been obtained using different experimental methods. All experimental data are expressed in terms of cK and $[M]$ as a common basis. As can be seen in Figure V.1, the experimental data show a consistent pattern. However, it is not possible to model the entire range of data by the simple single site approach (Eq. (V.8)). If we split the data set into the concentration ranges $[M] > 10^{-9}$ M and $[M] < 10^{-9}$ M, the single site model nicely fits both data sets separately but with two rather different sets of parameters in Eq. (V.8), namely $\log_{10} K = 7.5$, $\log_{10} SCC = -3.2$ (dashed line in Figure V.1) and $\log_{10} K = 10.8$, $\log_{10} SCC = -5.0$ (dotted line in Figure V.1).

If we want to describe the entire range of experimental data we have to drop the assumption {A2}, and consider more than one kind of ligand site. The total amount of metal bound to the humic substance is given by the sum of metal bound to different ligand sites i

$$[MHS] = \sum_i [ML_i] \quad (V.30)$$

As before, the total concentration of a given ligand site i is the sum of the concentration

Figure V.1: Metal concentration dependence of humic complexation. Eu, Am and Cm complexation with humic and fulvic acids. Symbols: Experimental data in the pH range 5.0 - 5.5 and at ionic strength 0.1 M from several publications. PSI: M.A. Glaus, W. Hummel and L.R. Van Loon, Paul Scherrer Institute (1996) unpublished data. Lines: Model calculations using Eq. (V.8), single site model, with $\log_{10} K = 7.5$ and $\log_{10} SCC = -3.2$ (dashed line) and $\log_{10} K = 10.8$ and $\log_{10} SCC = -5.0$ (dotted line), or using Eq. (V.33), two site model, with the same parameters (solid line).



of the free ligand site i and of the metal bound to humic substance at site i

$$[L]_{\text{total},i} = [L_i] + [ML_i] \quad (\text{V.31})$$

The total concentration of humic substance, $(\text{HS})_{\text{total}}$, is related to the total concentration of ligand site $[L]_{\text{total},i}$ by

$$(\text{HS})_{\text{total}} \cdot \text{SCC}_i = [L]_{\text{total},i} \quad (\text{V.32})$$

where SCC_i is the site complexation capacity of binding site i in mol/g. The single site model (Eq. (V.8)) is then extended to a multi-site model:

$$^{\circ}K = \sum_i \frac{K_i}{1 + K_i \cdot [M]} \cdot \text{SCC}_i \quad (\text{V.33})$$

In essence, the multi-site model, Eq. (V.33), considers humic substance as a mixture of simple organic ligands with unknown molecular weights, where each component of the mixture is characterised by two fitting parameters, K_i and SCC_i .

The simplest version of Eq. (V.33), a two site model ($i = 2$) contains the two parameter sets derived above (solid line in Figure V.1). The main feature of this model is that it interprets the experimental data by assuming a high concentration of weak sites and a low concentration of strong sites. The weak sites determine the behaviour of humic complexation at high metal loading, whereas the strong sites, even though their concentration is only in the range of a few percent of the weak sites, determine the complexation strength of humic substances at low metal loading, *i.e.* at trace metal concentrations.

This type of model is very often used in the literature. For example, Li, Victor and Chakrabarti [80LI/VIC] interpret their data on U(IV) and U(VI) complexation with humic, fulvic and tannic acids by graphical analysis (Scatchard plots) in terms of a 2-site model according to Eq. (V.33). Using the same type of graphical analysis, Mantoura and Riley [75MAN/RIL] interpret their data on complexation of Co, Ni and Zn with humic acids of different origins in terms of a 2-site model. Note that their parameter n_i is the number of metal binding sites per molecule of humic acid. Although not clearly stated in their paper, they must have used an average molecular weight of 5000 g/mol to convert $(\text{HS})_{\text{total}}$ (g/l) into M_{HA} , the molar concentration of humic acid. The stability constants derived by Mantoura and Riley [75MAN/RIL] are identical with the K_i in Eq. (V.33), however, their n_i has to be multiplied by 0.0002 to be compatible with the definition of SCC_i used here. The complexation behaviour of humic acid towards Eu^{3+} is described by Caceci [85CAC] in terms of a 2-site model. The data were fitted numerically to Eq. (V.33). In addition, experimental $^{\circ}K$ data are published, which are called K^* by Caceci [85CAC]. McKnight *et al.* [83MCK/FED] investigated the copper-complexing properties of aquatic humic substances isolated from eighteen different environments. They did numerical fits using a model containing two types of Cu(II)-binding sites and found that all data sets could be described by one set of constants according to Eq. (V.33). Note that the site complexation capacity SCC_i is given as L_i , moles of Cu(II) binding sites per milligram carbon of aquatic fulvic acid. The complexation of copper(II) with dissolved organic ligands in seawater is interpreted by Van den Berg [84BER4] in terms of two complexing ligands. He did not determine the mass of the dissolved organic ligands, but rather the concentration of Cu(II) bound to organic ligands and the concentration of free copper. Thus, instead of fitting data to Eq. (V.33), Van den Berg [84BER4] used Eq. (V.34), derived by multiplying Eq. (V.33) by $(\text{HS})_{\text{total}}$. Note, that Van den Berg [84BER4] uses the term ‘complexing capacity’, CL_x , for the total concentration of ligand sites, $[\text{L}]_{\text{total},i}$.

$$\frac{[\text{MHS}]}{[\text{M}]} = {}^{\circ}K \cdot (\text{HS})_{\text{total}} = \sum_i \frac{K_i}{1 + K_i \cdot [\text{M}]} \cdot [\text{L}]_{\text{total},i} \quad (\text{V.34})$$

These examples show, that even though the same conceptual model is used, great care has to be taken when comparing results. Different terms and definitions are used by different authors, and sometimes the total concentration of humic substance is converted into molar units by more or less plausible model assumptions. All these items have to be ‘translated’ to a common basis before any comparisons of data and models can be made.

The good agreement between the solid line for the two-site model in Figure V.1 and the experimental data may be an artifact. There is no obvious reason why binding of metal

ions by humic substances should be dominated by just *two* different types of sites. A numerically more accurate fit would probably be based on a multi-site model containing more than two sites. For example, Cabaniss and Shuman [88CAB/SHU] quantitatively model copper binding by Suwannee River fulvic acids using a 5-site model according to Eq. (V.33) with ten adjustable parameters. This model fits the data used to calibrate it, quantitatively describes results from other experiments, and can be used to describe data which cover three orders of magnitude of copper concentration and one order of magnitude of DOC. Cabaniss and Shuman [88CAB/SHU] note that a good fit does not imply that the “sites” determined correspond to chemical reality; the parameters may be useful for equilibrium modelling, but should not be used to make inferences about molecular structure.

A disadvantage of multi-site models is the two added adjustable parameters for each additional site. An approach to reduce the number of adjustable parameters is proposed by Mattigod and Sposito [79MAT/SPO]. They select a number of simple organic ligands which are thought to represent the major types of binding sites of humic substances. Specifically, they used nine organic acids as a model for sludge-derived fulvic acid [79MAT/SPO]. This represents a 9-site model according to Eq. (V.33) where all the K_i values are fixed by the selection of a set of aromatic, aliphatic, and amino acids whose functional groups are expected to simulate closely the metal-complexing groups in the fulvic acid fraction of a sewage sludge. Nine adjustable SCC_i parameters remain. These were fitted to a “reference fulvic acid” and the concentration of each model acid is given in terms of the total concentration of ligand sites, $[L]_{total,i}$. The actual $[L]_{total,i}$ or SCC_i parameters have to be calculated from the reference $[L]_{total,i}$ and reference $(HS)_{total}$, and the actually measured $(HS)_{total}$.

At a first glance, a huge difference seems to exist between a 9-site model according to Eq. (V.33) with 18(!) adjustable parameters and the mixture model of Mattigod and Sposito [79MAT/SPO] where all parameters are fixed. However, this difference is only apparent. Choosing the reference ligands out of a large set of simple organic acids only replaces the numerical fit of K_i values with a “fit-by-selection” procedure. And fitting the concentrations of these selected simple organic acids to a reference humic substance is equivalent to a fit of SCC_i parameters to a reference humic substance. The degree of freedom is the same in both approaches, only the technique of parameter fitting is different.

V.3.2.5. The continuous distribution models

The heterogeneous mixture labeled “humic substance” may comprise 10, 100, 1000 or more compounds, all with slightly different molecular structure and stereochemistry of their binding sites. There is no theoretical limit of the number of different ligand sites used to represent the metal binding properties of humic substances. In fact, a very large number of different ligand sites characterised by varying parameters K_i may be envisioned in humic binding models. The discrete distribution of sites in the multi-site model discussed above, characterised by site complexation capacities SCC_i , may then be

replaced by a continuous distribution of ligand sites, characterised by a differential site complexation capacity $\text{SCC}(K)$, defined as

$$\text{SCC}_i = \text{SCC}(K) dK \quad (\text{V.35})$$

In the mathematical description of the binding model, the sum of Eq. (V.33) therefore is replaced by an integral

$$^cK = \int_0^\infty \frac{K}{1 + K \cdot [\text{M}]} \cdot \text{SCC}(K) dK \quad (\text{V.36})$$

The actual evaluation of the differential site complexation capacity $\text{SCC}(K)$ depends on the model assumptions. To begin with, one may assume that one kind of binding site predominates the interactions of a metal ion with humic substances. In contrast to our simplest binding model discussed in Section V.3.2.1, we assume that the complexing strength of the ligand site is not a fixed number, but varies around a mean value due to the influence of different substituents and varying stereochemistry in the large number of different molecules comprising “humic substance”. If we therefore drop assumption {A3} (Table V.1), we expect some sort of single-mode distribution of $\text{SCC}(K)$ as function of K . Any analytical form of the distribution can be assumed. Following Perdue and coworkers [83PER/LYT2, 84PER/REU] a normal distribution is described by

$$\text{SCC}(\log_{10} K) = \frac{\text{SCC}_0}{\sigma_{\log_{10} K} \sqrt{2\pi}} \cdot \exp \left[-\frac{1}{2} \left(\frac{\log_{10} K - \log_{10} K_0}{\sigma_{\log_{10} K}} \right)^2 \right] \quad (\text{V.37})$$

where $\log_{10} K_0$ is the mean $\log_{10} K$ value, $\sigma_{\log_{10} K}$ is the standard deviation for the distribution of $\log_{10} K$ values about the mean value, and SCC_0 is a proportionality factor for the site complexation capacities in g/mol. Note, that the distribution is defined in logarithmic units of K . Thus, when Eq. (V.37) is substituted in Eq. (V.36), the integration variable has to be changed to $\log_{10} K$ and the integral evaluated from minus to plus infinity:

$$\begin{aligned} ^cK = & \frac{\text{SCC}_0}{\sigma_{\log_{10} K} \sqrt{2\pi}} \int_{-\infty}^{+\infty} \frac{10^{\log_{10} K}}{1 + 10^{\log_{10} K} [\text{M}]} \times \\ & \exp \left[-\frac{1}{2} \left(\frac{\log_{10} K - \log_{10} K_0}{\sigma_{\log_{10} K}} \right)^2 \right] d \log_{10} K \end{aligned} \quad (\text{V.38})$$

No analytical solution for Eq. (V.38) is known, and a numerical solution has to be found for any given value of $[\text{M}]$, and given values for the three adjustable parameters $\log_{10} K_0$, $\sigma_{\log_{10} K}$ and SCC_0 .

A modified version of the normal distribution model is available which remedies this problem. A distribution function was proposed by Sips [48SIP] which closely resembles

a normal distribution but has the advantage that it can be integrated analytically. The Sips distribution is given by

$$\text{SCC}(K) = \frac{\text{SCC}_s}{\pi} \frac{\sin(\pi\alpha)}{K^\alpha/K_s + 2\cos(\pi\alpha) + K_s/K^\alpha} \quad (\text{V.39})$$

where K_s , α and SCC_s are constants. The distribution represented by Eq. (V.39) has a quasi-Gaussian shape with an apex at $K_s^{1/\alpha}$. $K_s^{1/\alpha}$ is thus analogous to the mean K_0 of the normal distribution Eq. (V.37), and the index of heterogeneity, α ($0 \leq \alpha \leq 1$), is analogous to the standard deviation $\sigma_{\log_{10} K}$. If this form of $\text{SCC}(K)$ is substituted into Eq. (V.36), a modified Freundlich binding expression is obtained² upon (non-trivial !) integration [48SIP]:

$${}^cK = \frac{K_s \cdot [\text{M}]^{\alpha-1}}{1 + K_s \cdot [\text{M}]^\alpha} \cdot \text{SCC}_s \quad (\text{V.40})$$

When $\alpha = 1$, corresponding to identical sites which may be mathematically represented by a Dirac delta function distribution of $\text{SCC}(K)$, Eq. (V.40) reduces to the Eq. (V.8) of the simplest model.

In the region of high metal loading close to metal saturation, the ligand sites are predominantly occupied by metal ions, *i.e.* $K_s \cdot [\text{M}]^\alpha > 1$, and Eq. (V.40) reduces to Eq. (V.10) for all α values. In other words, at high metal loading no difference between a simple single-site model and a continuous distribution model is expected. In the region of very low metal loading the free ligand sites predominate, *i.e.* $K_s \cdot [\text{M}]^\alpha < 1$, and Eq. (V.40) reduces to

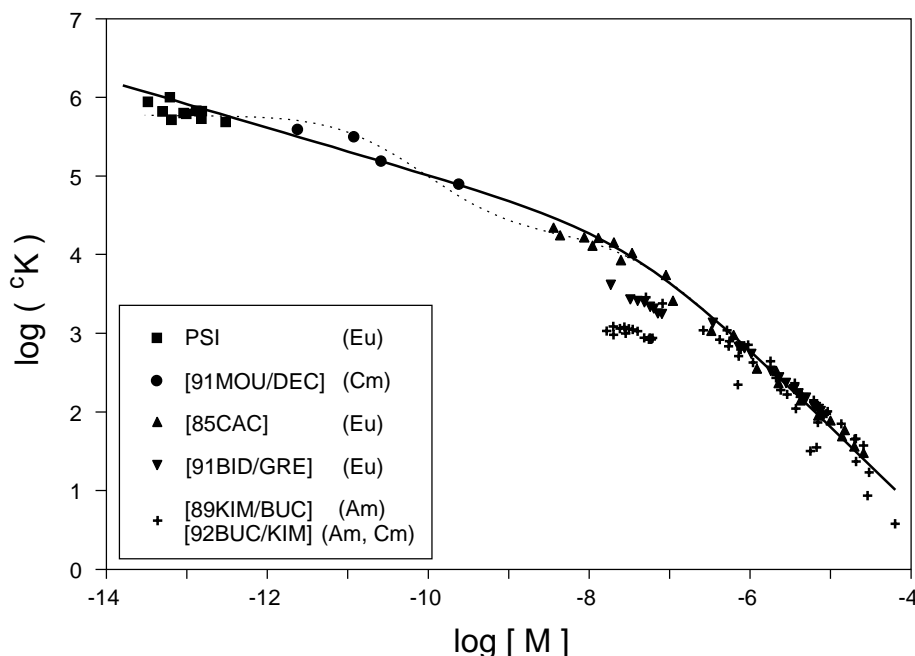
$${}^cK = K_s \cdot \text{SCC}_s \cdot [\text{M}]^{\alpha-1} \quad (\text{V.41})$$

At low metal loading cK reaches a constant value only if $\alpha = 1$. In all other cases, $\log_{10} {}^cK$ varies linearly with varying $\log_{10} [\text{M}]$ with slope $\alpha - 1$. This increase in $\log_{10} {}^cK$ with decreasing $\log_{10} [\text{M}]$ is steeper the smaller the parameter α is, *i.e.* the broader the distribution of $\text{SCC}(K)$ as function of K .

For illustration, the data of Figure V.1 are presented in Figure V.2 together with a fitted curve based on Eq. (V.40), the Freundlich type binding expression (solid line in Figure V.2 with $\log_{10} K_s = 5.2$, $\log_{10} \text{SCC}_s = -3.2$, $\alpha = 0.7$). For comparison, the result of the two-site model of Figure V.1 is added (dotted line). As can be seen, the two-step appearance is gone and a smooth dependence of cK on free metal concentration is obtained. An infinitely increasing cK coefficient with decreasing metal loading is predicted by this model. This is clearly in contradiction with chemical reality, as there are no infinitely strong binding

² Actually, the derivation of the Sips distribution went the other way round. Sips started from the observation that adsorption of gas molecules on catalyst surfaces can be described by (purely empirical) Freundlich isotherms. By applying an inverse Stieltjes-Laplace transform to the mathematical expression known as Freundlich isotherm, Sips obtained a distribution function which is now known as Sips distribution and which happened to be very similar to the Gaussian normal distribution function [48SIP].

Figure V.2: Metal concentration dependence of humic complexation. Eu, Am and Cm complexation with humic and fulvic acids. Symbols: Experimental data in the pH range 5.0 - 5.5 and at ionic strength 0.1 M from several publications. PSI: M.A. Glaus, W. Hummel and L.R. Van Loon, Paul Scherrer Institute (1996) unpublished data. Lines: Model calculations using Eq. (V.33), two site model, with parameters given in Figure V.1 (dotted line), or using Eq. (V.40), a continuous distribution model, with $\log_{10} K_s = 5.2$, $\log_{10} SCC_s = -3.2$ and $\alpha = 0.7$ (solid line).



sites. An upper limit of binding strength will be reached at some low metal loading, and beyond this limit $^{\circ}K$ is expected to remain constant. Thus, we have remedied the chemically unrealistic two-site model by creating a chemically unrealistic infinite increase of the $^{\circ}K$ coefficient. If we want to solve this new problem, we have to replace the infinite upper boundary in Eqs. (V.36) or (V.38) by a finite boundary. This adds another adjustable parameter to our model, effectively modifying it to a “truncated” continuous distribution model. But we not only increase the number of adjustable parameters, we also lose the advantage of the analytical expression, Eq. (V.40), as no analytical solutions of truncated $SCC(K)$ distributions are known.

Until now we have assumed that only one class of binding site predominates, according to assumption {A2} (Table V.1). If we drop this assumption by postulating the existence of more than one class of ligands, we arrive at multiple site continuous distribution models. For the simplest case, a two site model, we expect bimodal distributions of $SCC(K)$ as function of K . A pronounced bimodal distribution is actually reported by Perdue,

Reuter and Parrishi [84PER/REU] as the final result of their statistical model of proton binding by humic substances. They found two maxima of $\text{SCC}(K)$ around $\log_{10} K_0 = 4$ and $\log_{10} K_0 = 12$ by extending Eq. (V.38) to a two-site Gaussian distribution model. This result can be interpreted as representing proton binding by carboxylic and phenolic binding sites. Similar results are reported by Nederlof *et al.* [93NED/WIT] using a double Freundlich binding expression based on Eq. (V.40). They found two maxima of $\text{SCC}(K)$ around $\log_{10} K_0 = 3$ and $\log_{10} K_0 = 10$, both maxima appearing at the edges of their experimental window. Results for metal binding of humic substances are less clear-cut than proton binding. Perdue and Lytle [83PER/LYT2] report results for copper binding by humic substances and state that the “data sets were fit reasonably well by a single-mode Gaussian distribution model (one class of ligands), although minor improvement in the degree of fit was obtained with the bimodal distribution model”. The free copper concentrations in their measurements range between 10^{-2} M and 10^{-6} M. In a recent study, Benedetti *et al.* [95BEN/MIL] extended the free copper concentration down to 10^{-14} M and found a pronounced bimodal distribution using a Freundlich type binding expression according to Eq. (V.40). Similar results are obtained for Cd, whereas Ca binding can be described by a monomodal Sips distribution [95BEN/MIL].

All these results depend on *a priori* assumptions about the distribution function $\text{SCC}(K)$. If no assumptions are made beforehand about the type of distribution, the function $\text{SCC}(K)$ has to be derived from experimental data. Mathematically, finding $\text{SCC}(K)$ implies the inversion of Eq. (V.36), which cannot be achieved analytically. Good results are obtained with numerical methods only for very accurate data that cover the whole range of concentrations of interest. By making some approximations it is also possible to solve Eq. (V.36) analytically for $\text{SCC}(K)$. Numerous methods have been proposed and applied to experimental data, such as the affinity spectrum method [83SHU/COL, 86DZO/FIS, 86FIS/DZO], the differential equilibrium function [70GAM, 88ALT/BUF], the logarithmic symmetrical approximation [90NED/RIE], and the site occupation distribution function [90BUF/ALT]. These and some other “semianalytical” methods are compared and discussed in some detail in [86DZO/FIS, 86FIS/DZO, 90BUF/ALT, 92NED/RIE]. In an ideal world of accurate data and infinitely wide analytical windows, these methods would allow the derivation of chemically meaningful $\text{SCC}(K)$ distributions, which in turn would provide valuable information for the development or selection of an appropriate humic binding model. In reality, however, all these methods suffer severely from artifacts due to narrow analytical windows and spurious peaks in the distribution function generated by experimental errors. The problem of truncated and error prone data sets was a topic of discussion during the last ten years, as documented in [86FIS/DZO, 86TUR/VAR, 90BUF/ALT, 94NED/RIE]. Despite all efforts made to eliminate these problems by using spline functions to smooth the experimental data [86FIS/DZO, 94NED/RIE], or by introducing new methods [90BUF/ALT], it still remains to be seen if these approaches contribute to our understanding of metal-humic binding and promote the development of chemically more realistic and more accurate binding models.

V.3.3. Variations in pH

A general observation made in investigations of metal-humic complexation is that the experimental K values vary with pH. Different concepts were developed to describe, to explain, and to model this observed pH dependence of K values. The ideas can roughly be divided into concepts assuming variable pH dependent concentration of complexing sites and concepts ascribing the behaviour of K values to variable pH dependent conditional stability constants. This pH dependence of conditional stability constants is modelled by empirical functions, by assuming proton exchange reactions or by introducing electrostatic effects.

V.3.3.1. Empirical functions

In some models the concentration of complexing sites is identified with the maximum concentration of metal ions bound to humic substances. It is observed that the latter quantity, which is proportional to quantities like “complexing capacity” or “loading capacity”, changes with pH. Consequently, the complexing capacity W [95MOU/MOU] or the loading capacity LC [96CZE/KIM] is evaluated experimentally and used to define the amount of humic substance available for complexation under a given set of experimental conditions. The resulting empirical functions of pH, *i.e.* $W = f(\text{pH})$ and $LC = f(\text{pH})$, are found to be highly non-linear.

A similar approach is chosen by Choppin and coworkers [84TOR/CHO, 95RAO/CHO] who assume that the site complexation capacity, SCC, of a humic substance is proportional to the degree of ionisation, α , of the humic substance at a particular pH, *i.e.* $\text{SCC} = f(\alpha)$, or more precisely $\text{SCC} = \text{PEC} \cdot \alpha$, where PEC is the proton exchange capacity or the “total carboxylate capacity” [84TOR/CHO]. Both α and PEC, are evaluated experimentally by pH titration. α is also an empirical function of pH which is highly non-linear [84TOR/CHO].

These concepts implicitly drop assumption {A4}, that the number of active binding sites is constant under varying chemical conditions. Although not always clearly stated (with the commendable exception of [96CZE/KIM]), the common assumption underlying these concepts, is that metal ions may interact only with deprotonated, or dissociated, functional groups of the humic substance. At a given pH, where the potential ligand sites are only partially dissociated, all proton exchange sites, PEC, are not fully available for metal complexation, and thus the experimental K values vary with pH. Metal-proton exchange reactions of the type $\text{M} + \text{HL} \rightleftharpoons \text{ML} + \text{H}$, with strongly complexing functional groups like phenolic or alcoholic OH groups, are not considered in this concept. This means that assumption {A5}, no proton exchange reactions, is valid even at increasing pH.

This model seems to work fairly well at high metal loading close to metal saturation. In this parameter range, where the metal-humic interactions most probably are dominated by weak complexes with carboxylic acid groups, a “stability constant” independent of pH is found when the concentration of complexing sites is defined by the empirical loading

capacity [89KIM/BUC, 96KIM/CZE] or the degree of ionisation [95RAO/CHO]. At trace metal concentrations, *i.e.* very low metal loading, however, the “stability constants” are found to change drastically with pH even if the concentration of binding sites is defined by the degree of ionisation [84TOR/CHO]. This is strong evidence that metal-proton exchange reactions play some role in this pH/concentration range.

Nevertheless, the pH dependence of conditional stability constants is sometimes described by empirical functions. For example, Torres and Choppin [84TOR/CHO] found that the pH variation of the conditional stability constants $\log_{10} \beta$ for uranyl-humate complexation, corrected for the degree of ionisation, α , is a linear function of this parameter α , *i.e.* $\log_{10} \beta = \text{intercept} + \text{slope} \cdot \alpha$. This model just serves as a simple description of experimental data and no explanation of the empirical linear function in chemical terms was attempted by Torres and Choppin [84TOR/CHO].

V.3.3.2. Proton exchange reactions

All concepts discussed so far assume, {A5}, that metal-proton exchange reactions do not influence the metal complexation behaviour of humic substances. On the other hand, it is well known that the formation of strong metal complexes with small organic ligands like salicylic acid or edta involves proton exchange reactions of the type



with an equilibrium constant

$$K_{\text{exch}} = \frac{[\text{ML}] \cdot [\text{H}]}{[\text{M}] \cdot [\text{HL}]} \quad (\text{V.43})$$

We drop the assumption {A5} and postulate that proton exchange reactions, *e.g.* with phenolic OH groups, dominate metal complexation with humic substance within a certain pH range. Within this pH range, all free ligand sites of the humic substance are protonated, *i.e.* $[\text{L}]_{\text{total}} = [\text{HL}] + [\text{ML}]$, and thus the model described by, Eq. (V.8), is modified to

$${}^{\circ}K = \frac{K_{\text{exch}} \cdot [\text{H}]^{-1}}{1 + K_{\text{exch}} \cdot [\text{M}]/[\text{H}]} \cdot \text{SCC} \quad (\text{V.44})$$

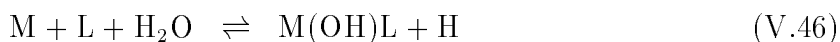
In the region of high metal loading, the same behaviour of ${}^{\circ}K$ as in the case of the model described by Eq. (V.10) is expected. In the region of low metal loading the protonated ligand sites predominate, *i.e.* $[\text{HL}] > [\text{ML}]$ and we expect an increase of $\log_{10} {}^{\circ}K$ with increasing pH with a slope of one:

$$\log_{10} {}^{\circ}K = \log_{10} K_{\text{exch}} + \log_{10} \text{SCC} + \text{p}[\text{H}] \quad (\text{V.45})$$

Metal-proton exchange reactions are often assumed to be the predominant equilibria in the more complex humic binding models. For example, Stevenson [76STE] includes proton

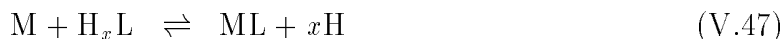
exchange in his variable stoichiometry model, which is already discussed in Section V.3.2.3. Chemical equilibria in Tipping's Model V [92TIP/HUR] are also expressed in terms of metal-proton exchanges. In this model, two classes of binding sites are assumed, single proton-dissociating A sites (monodentate) according to Eq. (V.42), and, when the single groups are sufficiently close, bidentate B sites which are assumed to release two protons when complexing a metal ion. Two separate exchange constants for type A and type B sites, K_{MHA} and K_{MHB} respectively, are included in Model V as adjustable parameters.

Experimental results for the complexation of humic substance with Eu, Am and Cm at trace metal concentrations may serve as an illustration of the pH dependence of ${}^{\circ}K$. Data measured by different authors on humic and fulvic acids from various sources within the pH range 3.8 to 7 at an ionic strength 0.1 M exhibit a very strong pH dependence, even in the acidic pH range (Figure V.3). In Figure V.3, $\log_{10} {}^{\circ}K$ increases with pH with a slope of one, which corroborates the assumption of predominating metal-proton exchange reactions according to equilibrium (V.42). However, the interpretation is not unambiguous. Bulk thermodynamic data alone cannot discriminate between a model describing the observed variability of ${}^{\circ}K$ by assuming a proton exchange reaction according to equilibrium (V.42) and a model assuming the formation of ternary complexes with OH^- according to equilibrium (V.46):



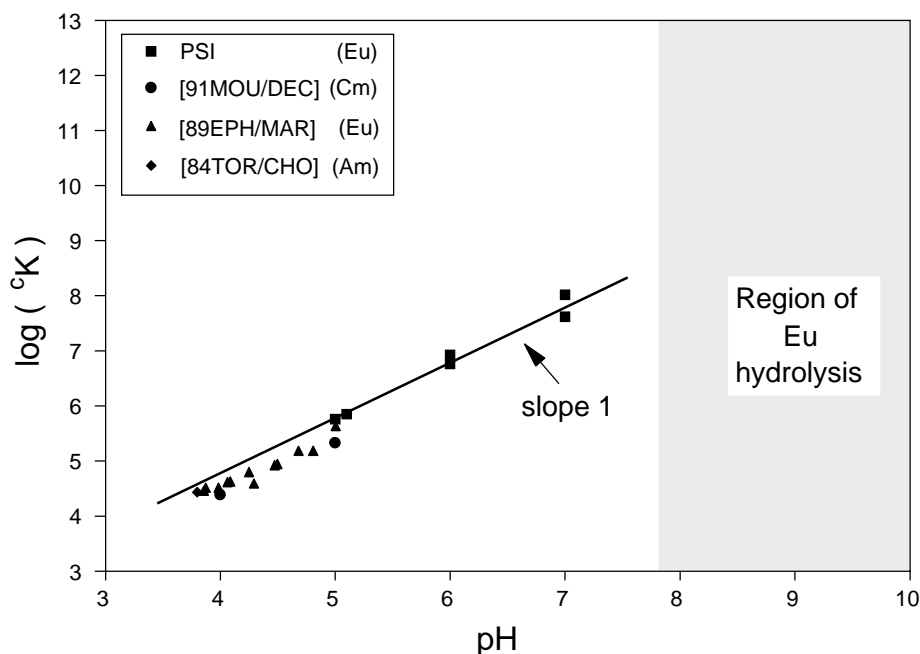
There are additional chemical arguments which allow a choice between the two models. These go as follows: In the case of U(VI) one observes an increase of $\log_{10} {}^{\circ}K$ with pH with a slope of one below pH 5.5 at trace metal concentration [93HIG/KIN]. According to our own experimental results, the increase of $\log_{10} {}^{\circ}K$ by slope 1 extends up to pH 10 for both U(VI) and Eu. The hydrolysis of Eu^{3+} and UO_2^{2+} aquo ions commences at completely different pH values, *i.e.* above pH 4 for UO_2^{2+} and beyond pH 7 for Eu^{3+} . If the formation of ternary hydroxo complexes predominated in the pH range investigated here, one would expect that different hydrolysis behaviour would somehow be reflected in the variation of $\log_{10} {}^{\circ}K$ with pH. Since this was not observed, we assume proton exchange reactions according to Eq. (V.42) in both cases over the whole pH range investigated.

This simple model fails if it is applied to other metal ions like Ca or Pb, or transition metals like Ni, Co, and Cu. Experimental results of humic complexation with these metals *consistently* show a pH dependency of $\log_{10} {}^{\circ}K$, but with a slope significantly less than one (see for example [77BUF/GRE] or [93HIG/KIN]). One may argue that the measured bulk properties do not reflect a single metal-proton exchange reaction, but a mixture of many slightly different reactions which may or may not release protons while binding a metal ion. The observed net result is an average number, x , of protons released during metal binding



where x may be a non-integer number. This model contains, besides K_{exch} and SCC, a

Figure V.3: The pH dependence of humic complexation. Eu, Am and Cm complexation with humic and fulvic acids. Symbols: Experimental data in the range of trace metal concentration and at ionic strength 0.1 M from several publications. PSI: M.A. Glaus, W. Hummel and L.R. Van Loon, Paul Scherrer Institute (1996) unpublished data. The solid line with slope one corroborates the assumption of metal-proton exchange reactions as the dominating complexation process.



third adjustable parameter x :

$$^{\circ}K = \frac{K_{\text{exch}} \cdot [\text{H}]^{-x}}{1 + K_{\text{exch}} \cdot [\text{M}]/[\text{H}]^x} \cdot \text{SCC} \quad (\text{V.48})$$

which at low metal loading can be adjusted in such a way that the observed pH dependence is described by the model:

$$\log_{10} ^{\circ}K = \log_{10} K_{\text{exch}} + \log_{10} \text{SCC} + x \cdot \text{p}[\text{H}] \quad (\text{V.49})$$

Buffle, Greter and Haerdi [77BUF/GRE] included x in a variable stoichiometry model (see Section V.3.2.3) and determined its value from the titration of samples at constant concentration of the metal ion. They report values of x between 0.6 and 0.8 for Cu and Pb.

In the foregoing discussion we dropped assumption {A2} by introducing a non-integer stoichiometry coefficient x for proton release. Alternatively, we may drop assumption {A3}, and assume that K_{exch} has a continuous distribution of values due to the influence of different substituents and varying stereochemistry. If we further assume a Sips

distribution, Eq. (V.39), then our original continuous distribution model without proton exchange reactions, Eq. (V.40), is equal to

$${}^cK = \frac{K_{s,\text{exch}} \cdot [M]^{\alpha-1} [H]^{-\alpha}}{1 + K_{s,\text{exch}} \cdot ([M]/[H])^{\alpha}} \cdot \text{SCC}_s \quad (\text{V.50})$$

At low metal loading, Eq. (V.50) reduces to

$$\log_{10} {}^cK = \log_{10} K_{s,\text{exch}} + \log_{10} \text{SCC}_s + (\alpha - 1) \cdot \log_{10} [M] + \alpha \cdot \text{p}[H] \quad (\text{V.51})$$

In contrast to the concepts discussed so far, in which cK is independent of the metal concentration at low metal loading, we now have a coupled dependency of cK on pH and the metal concentration. If $\log_{10} {}^cK$ increases with pH by slope α , a variation with $\log_{10} [M]$ of slope $\alpha - 1$ is expected. In other words, the “flatter” the pH dependency becomes, the steeper $\log_{10} [M]$ dependency would be expected.

So far we assumed that metal-proton exchange reactions predominate over the entire parameter range of interest, resulting in a linear pH dependence of $\log_{10} {}^cK$ to very high pH values. From a chemical point of view this is a rather unrealistic assumption, because beyond some pH range the predominating functional groups may be deprotonated and metal complexation may take place at free ligand sites. This effect may be accounted for in humic binding models as follows: The equilibrium described by Eq. (V.42) can be interpreted as a competition between a simple metal-ligand formation, Eq. (V.3), and a protonation reaction according to



with a protonation constant

$$K^{\text{H}} = \frac{[\text{HL}]}{[\text{H}] \cdot [\text{L}]} \quad (\text{V.53})$$

The total concentration of ligand sites is now the sum of free and protonated ligand sites and metal bound to the humic substance

$$[\text{L}]_{\text{total}} = [\text{L}] + [\text{HL}] + [\text{ML}] \quad (\text{V.54})$$

and the model, Eq. (V.8), extends to

$${}^cK = \frac{K}{1 + K^{\text{H}} \cdot [\text{H}] + K \cdot [\text{M}]} \cdot \text{SCC} \quad (\text{V.55})$$

At low metal loading, $\log_{10} {}^cK$ as a function of pH now varies between slope one, if all free ligand sites are protonated, and slope zero, if all free ligand sites are deprotonated. The transition between these two regions is determined by the value of the protonation constant K^{H} .

Any shape of the $\log_{10} {}^cK$ - pH curves can be obtained if we assume multiple sites and extend our single site model, Eq. (V.55), to a multiple site model

$${}^cK = \sum_i \frac{K_i}{1 + K_i^H \cdot [H^+] + K_i \cdot [M]} \cdot SCC_i \quad (V.56)$$

However, increasing the number of sites increases the number of adjustable parameters by three for each site.

In order to circumvent this parameter increase, one may try to combine the concept of individual protonation constants, Eq. (V.53), with the concept of continuous distributions of stability constants. In general, the resulting two-dimensional distribution functions of K and K^H cannot be solved analytically. The numerical evaluation of these expressions is not an insurmountable technical problem, but puts serious obstacles in the way of evaluating conceptual models in terms of chemical plausibility. Only if we assume that both, K and K^H , have identical distribution functions, thus reducing the two-dimensional case to a one-dimensional one, and assume a Sips distribution, Eq. (V.39), can we obtain an analytical solution. The derivation of this “multicomponent equation” is discussed in detail by van Riemsdijk *et al.* [86RIE/BOL].

None of the more complicated approaches to model the pH dependence of cK , as described by Eqs. (V.50), (V.55), (V.56) or multicomponent equations [86RIE/BOL], has been thoroughly evaluated in the literature. If these approaches are used at all, they are incorporated into even more complex models, *e.g.* [95BEN/MIL], and the reasons for the usual resulting “good fit of experimental data” is not analysed in terms of individual contributions of conceptual “compartments” of the composite model. Whether the general trend of pH and metal concentration effects, found experimentally for a large set of metal ions over a wide range of pH, can be described *consistently* by any one of the models discussed above or any plausible combination of them, is still an open question.

V.3.3.3. Electrostatic effects

A completely different concept to explain the observed pH (and ionic strength) dependence of experimental cK values emerges if the overall charge of a humic macromolecule is considered. The following reasoning was originally developed for sorption of metal ions on solid surfaces, *e.g.* [90DZO/MOR], but may be also applied with some small modifications to the complexation of metal ions to humic substances.

The basic idea is that the concentrations of protons and free metal ions in the vicinity of humic binding sites are different from the proton and free metal concentrations of the bulk solution. Energy is required to move ions through potential gradients near charged regions of macromolecules, so the overall charge of humic substance affects the tendency of binding sites to coordinate or dissociate protons and metal ions. With increasing negative charge of the humic molecule, caused by progressive dissociation of protonated functional groups with increasing pH, it becomes more difficult to dissociate protons and metal ions. Although it is impossible to separate the chemical and electrostatic contributions to the total binding energy experimentally, it is useful to separate them theoretically in order to

obtain a specific (*i.e.*, chemical) interaction term that does not vary with overall charge, and a variable electrostatic interaction term [90DZO/MOR].

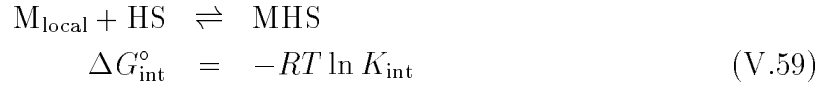
The total free energy of complexation, $\Delta G_{\text{total}}^\circ$, is separated into its component parts

$$\Delta G_{\text{total}}^\circ = \Delta G_{\text{int}}^\circ + \Delta G_{\text{coul}}^\circ \quad (\text{V.57})$$

where $\Delta G_{\text{int}}^\circ$ is the chemical or “intrinsic” free-energy term and $\Delta G_{\text{coul}}^\circ$ is the variable electrostatic or “coulombic” term. In other words, the overall complex formation equilibrium



is separated into an equilibrium with “local” concentration of metal ions, $[\text{M}]_{\text{local}}$, either at the surface of an impenetrable region, or within a penetrable phase,



and an equilibrium between this “local” concentration and the bulk concentration of ions

$$\begin{aligned} \text{M} &\rightleftharpoons \text{M}_{\text{local}} \\ \Delta G_{\text{coul}}^\circ &= Z \cdot F \cdot \psi \end{aligned} \quad (\text{V.60})$$

The theoretical expression for the coulombic term, Eq. (V.60), is derived from the electrostatic work in transporting ions through the interfacial potential gradient. Combining Eqs. (V.57) to (V.60) we get

$$K = K_{\text{int}} \cdot \exp(-\Delta Z F \psi / RT) \quad (\text{V.61})$$

where R is the gas constant, T the absolute temperature, F the Faraday constant, ψ the electrostatic potential, K_{int} an intrinsic (adjustable) equilibrium constant which is assumed not to depend on the overall charge of the humic molecule, and ΔZ the change in the charge of the binding site due to the complexation reaction. In the case of simple metal ion coordination, Eq. (V.58), ΔZ is simply the charge Z of the free metal ion. In the case of metal-proton exchange reactions, ΔZ is the difference between the charge of the metal ion and the number of protons released.

Eq. (V.61) is the basic expression in all electrostatic models, and all further problems are related to the question of how to evaluate the electrostatic potential ψ . This question is discussed in detail by Bartschat, Cabaniss and Morel [92BAR/CAB] and the following short summary follows their reasoning. The key variable for calculating the coulombic effect on the free energy of a reaction, the electrostatic potential ψ , is usually obtained as the solution of a Poisson-Boltzmann equation.

When the potential ψ is small, so that $\exp(F\psi/RT) \approx 1 + F\psi/RT$, the Poisson-Boltzmann equation can be linearised to an equation with analytical solutions for planar,

cylindrical, and spherical geometries. The impenetrable sphere concept was first used by Debye and Hückel to derive their well-known limiting laws for the activity coefficients of strong ions in solution. More recently, the Debye-Hückel equation³ was applied to humic substances by Tipping, Reddy and Hurley [90TIP/RED] and Falck [91FAL]. This Debye-Hückel equation contains three adjustable parameters, the radius of the humic molecule, the distance of closest approach of a small ion to the humic molecule, and the charge in mol/g of the humic molecule. The latter parameter may be estimated from the total charge of the humic substance, measured by pH titration, and the average molecular weight of the humic substance. Whereas the distance of closest approach of small ions is expected to vary little from ion to ion, the radius and molecular weight of a humic molecule are essentially two fitting parameters in the Debye-Hückel equation. The effects of varying these parameters when fitting proton dissociation data of humic substances is discussed in some detail by Tipping, Reddy and Hurley [90TIP/RED].

However, when ψ is large, as may be the case when considering humic molecules with many deprotonated functional groups at high pH, the linear approximation might be inappropriate.

Unfortunately, the only nonlinear Poisson-Boltzmann equation for which an analytical solution has been found is for an infinite plane with equally distributed charges. This solution was used by Gouy and Chapman in their original theory, which is the basis of surface complexation models describing sorption of ions on mineral surfaces [90DZO/MOR]. The charge on a surface is determined by proton transfer reactions and by surface coordination reactions with other cations and anions. If a diffuse layer of counterion charges is assumed to be located on the solution side of the interface, the relationship between surface charge and potential is fixed by the electrical double-layer theory. According to the Gouy-Chapman theory (for a symmetrical electrolyte with valence z), the surface charge density (σ , in C/m²) is related to the potential at the surface (ψ , in volts) at 25°C by

$$\sigma = 0.1174 \cdot \sqrt{c} \cdot \sinh(z \cdot \psi \cdot 19.46) \quad (\text{V.62})$$

where c is the molar electrolyte concentration [90DZO/MOR]. A more general discussion of charge density expressions including asymmetrical electrolytes is given by de Levie

³ Note some potential pitfalls when dealing with equations referring to electrostatic effects. In the older literature, *e.g.* in Tanford's comprehensive textbook [61TAN], the Debye-Hückel equations and variants thereof are derived in CGS electrostatic units (esu). This not only involves a factor of 4π in the equations, but also the fundamental physical constants like ϵ_0 , e , and k have different units and different numerical values than in the SI system (see Table II.6). Tipping, Reddy and Hurley [90TIP/RED] and Falck [91FAL], however, just take equations from [61TAN] without stating this fact. In addition, in both publications the formula for the Debye parameter κ is wrongly copied from [61TAN]. Tipping, Reddy and Hurley [90TIP/RED] present an equation (2) for κ which does not refer to the ionic strength I , but to N ions per cubic centimeter (Eq. 26-16 in [61TAN]). Falck [91FAL] presents an equation (6) for κ where a scaling factor of $\sqrt{1000}$ is dropped (Eq. 26-32 in [61TAN]) and thus I is implicitly defined in mol per cubic centimeter. In addition, the numerical value of the Debye parameter at 25°C (in SI units !) is wrong in [91FAL], probably by a factor of $\sqrt{10}$. In summary, great care has to be taken when considering electrostatic theory from the older literature, otherwise one may easily introduce numerical errors of many orders of magnitude in binding models.

[90LEV]. The surface charge density σ cannot be measured directly, but is an adjustable parameter in binding models that include the Gouy-Chapman electrostatic term. In principle, σ can be evaluated by two methods. The first, more empirical one, considers the total charge of the humic substance, measured as a function of pH by titration. The second method, employed in surface complexation models, calculates the net charge on the surface by mass balance equations of (postulated) surface complexation equilibria [90DZO/MOR]. Both methods need the specific surface area A (m^2/g) to convert the total charge of the surface into the surface charge density σ . In the case of sorption of ions on mineral surfaces some methods are proposed which allow an estimate of the specific surface area within one order of magnitude, at least for pure metal oxides [90DZO/MOR]. The specific surface area A of humic substances has to be treated as an empirical fitting parameter. Due to conformational changes of humic molecules with varying chemical conditions, A is probably not a constant, even for a specific sample, but may vary with pH and the ionic strength.

Modeling humic substances as infinite planes seems to be justified for large humic acid molecules, but is a poor approximation for the smaller size fraction of fulvic acids.

A completely different concept for electrostatic interactions is promoted by Marinsky and coworkers [86EPH/ALE, 86EPH/MAR, 86MAR/EPH, 89CAB/MOR]. Humic substances are treated as a microphase gel [84MAR/RED2] based on a macroscopic two-phase gel model originally developed for the physicochemical description of synthetic cross-linked polyelectrolytes like ion exchange resins [84MAR/RED]. It is assumed that enough counterions accumulate in the charged gel phase to neutralise it, and based on this electroneutrality assumption, the distribution of protons and metal ions between the gel phase and the bulk solution can be described by Donnan potentials. The Donnan potential term, the ratio of the metal ion activities in the two phases, *i.e.* $\{M\}_{\text{gel}}/\{M\}_{\text{solution}}$, is used to evaluate the exponential term in Eq. (V.61). For low ionic strength the concentration of counterions in the gel phase is approximately equal to the concentration of charge of the humic substance, and ψ is related to ρ_0 , the volume charge density of the gel, by Bartschat, Cabaniss and Morel [92BAR/CAB]:

$$-\rho_0/I = \exp(-F\psi/RT) \quad (\text{V.63})$$

The concentration of counterions in the gel phase, which, by the electroneutrality assumption, is equal to the volume charge density of the gel, cannot be measured. To calculate this quantity, the total charge of the humic substance, measured by pH titration in mol/g, and the specific volume, V_{gel} , of the gel phase in l/g are needed. In the case of macroscopic two-phase gels, the density of the gel can be measured in a pycnometer [84MER/MAR], or the volume of the remaining solution can be measured with a spectrophotometer after adding a macromolecular dye which cannot diffuse into the gel phase [84ALE/ESC]. Both methods lead to an independent determination of V_{gel} . In the case of a peat, the volume of the gel phase could only be estimated by assuming that it corresponds to the quantity of water contained by the fully hydrated sample (“wet peat”) [80MAR/WOL]. In contrast to ion exchange resins and similar cross-linked synthetic polymers, simple linear

polymers and humic substances are one-phase solutions, and do not exhibit a macroscopic gel phase. However, one may envision the large molecules of linear polymers and humic substances as microphase gels. The phase boundary of these microphase gels must be defined arbitrarily [80SLO/MAR]. In other words, the specific volume of a humic substance, V_{gel} , is a model dependent adjustable parameter, like the specific surface area, A , in the Gouy-Chapman theory discussed above. Within the scope of Marinsky's gel model for humic substances, the exponential term in Eq. (V.63), named the "electrostatic deviation term (ΔpK)" [86EPH/ALE, 89EPH/BOR]

$$\Delta\text{pK} = -F\psi/RT \quad (\text{V.64})$$

is derived from experimental data in the following manner: At high ionic strengths (1 M and higher), experimental titration data are found to be insensitive to ionic strength. It is assumed that in this region the electrolyte concentration in the bulk solution and in the gel phase are the same, *i.e.* the Donnan potential vanishes and thus ΔpK is zero. Therefore, the experimental data at high ionic strength are taken as a "reference line" and all deviations of experimental data at lower ionic strength are interpreted as due to the electrostatic deviation term ΔpK (see Figure 24 in [86EPH/ALE] or Figure 4 in [89EPH/BOR]). In other words, although it is never clearly stated in the publications of Marinsky and coworkers, the specific volume, V_{gel} , of a humic substance "gel" is considered to be an empirical function of pH and ionic strength and is used to express the deviation between the experimental data at lower ionic strength from the "reference line" at high ionic strength.

All treatments of electrostatic effects discussed so far can be considered as limiting cases, or special solutions of the Poisson-Boltzmann equation, limited to small potentials as in the Debye-Hückel theory, or to infinite flat interfaces as in the Gouy-Chapman flat plate model or Marinsky's gel model. Unfortunately, all more general cases of the Poisson-Boltzmann equation do not have analytical solutions and we must resort to numerical methods for their solution. The case of rigid impenetrable spheres of arbitrary electrostatic potential is described by de Wit *et al.* [90WIT/RIE], and both penetrable and impenetrable spheres and their limiting cases are discussed in detail by Bartschat, Cabaniss and Morel [92BAR/CAB]. In the case of an impenetrable sphere, the relevant charge parameter is σ , the surface charge density on the sphere, which is assumed to be uniform. In the case of a penetrable sphere, the relevant charge parameter is ρ_0 , the density of the charge contained in the volume of the sphere in the absence of counterions. In both cases the charge parameters can be evaluated from experimental titration data by assuming an average radius and an average molecular weight of the humic substance. If size distributions are to be considered, a third model dependent parameter enters the game, to describe the relationship between the size of the humic molecule and the charge parameter, σ or ρ_0 . If it is assumed that the number of charged sites is proportional to the molecular weight and that the molecular weight of the molecule is proportional to its volume, the volume charge density ρ_0 of the penetrable sphere will not vary with size. In the case of the impenetrable sphere, the surface charge density σ will increase in direct proportion to the radius of the humic molecule. However, additional assumptions are

hidden here not stated by Bartschat, Cabaniss and Morel [92BAR/CAB], namely that proportionality between the number of charged sites and the volume holds also for an *impenetrable* sphere and that *all* these charged sites contribute to the surface charge. By contrast, if we assume that the number of charged sites is proportional to the surface area of the humic molecule, the surface charge density σ will not vary with size. As is shown by Bartschat, Cabaniss and Morel [92BAR/CAB], both the penetrable and impenetrable sphere models can elegantly describe the effect of size distributions and provide an intermediate solution for medium sized molecules not described well by either Debye-Hückel or polyelectrolyte models. The behaviour of such molecules is of the Debye-Hückel type for small-sized molecules, and is described as either the Donnan model (penetrable spheres) or the Gouy-Chapman model (impenetrable spheres) when their radius becomes very large. As in all other approaches towards more “realistic” humic binding models discussed in the preceding sections, the advantage of considering size distributions of humic molecules is offset by the increase of the number of empirical fitting parameters in the model.

A more general problem inherent in all the electrostatic concepts is the question, “What is the ‘surface’ or the ‘volume’ of a humic molecule?”. From the viewpoint of macroscopic properties, *e.g.* the filtration behaviour of humic colloids, envisioning humic substance as composed of spherical particles is perfectly valid. On the microscopic level, metal-humic bonding is described using functional groups, or “local” molecular properties. Electrostatic effects on macromolecules are described on a scale between these two extremes. The geometrical distribution of charges in the near and intermediate neighborhood of a chosen local reference point influences the binding properties of this functional group. As the molecular structure of humic substance is not known, we cannot infer the geometrical distribution of charges in the intermediate neighborhood from local functional groups. What may appear to be spheres from a distance will blur when we “approach” our objects of research, and finally might look more like cotton wad than like billiard-balls. In fact, humic substances may be described in terms of fractal geometry over about two orders of magnitude in size [93RIC/LIN, 94OST/MOR]. Fractals are geometric representations of strongly disordered systems with structures that can be described by non-integral dimensions [94SEN]. A fundamental tenet of fractal geometry is that disorder exists at any characterisation scale used to examine the substance. Regardless of the “magnification” used, the disorder of a fractal object cannot be resolved. From this perspective, disorder is seen as an inherent characteristic of a fractal material rather than as a perturbation phenomenon forced upon it. Experimental results show [93RIC/LIN, 94OST/MOR] that humic substances can be described as fractal materials exactly in the size range that causes electrostatic effects on metal-humic binding. Thus, the mental construct of humic molecules as simple geometrical objects having well-defined “surfaces” and “volumes” may be quite inappropriate. But no attempt has yet been made to model electrostatic effects in terms of fractal geometry.

To circumvent the geometrical problems, one may resort to a purely empirical treatment of electrostatic effects. In an early approach of this type Wilson and Kinney [77WIL/KIN]

used the empirical relation

$$2\omega Z = F\psi/RT \quad (\text{V.65})$$

where ω is the electrostatic interaction factor and Z is the average charge on a humic molecule at a given pH. The average charge Z cannot be evaluated without knowledge of the average molecular weight of the humic molecules. If one assumes that protons are the only cationic species in solution and that only one type of carboxylic acid groups is present, the molecular charge at a given pH can be represented as

$$Z = -\alpha \cdot n_{\text{COOH}} \quad (\text{V.66})$$

where n_{COOH} is the (not measurable) total number of carboxylic acid groups per molecule, and α is the (measurable) fraction of species dissociated. As a consequence, the product $\omega \cdot n_{\text{COOH}}$ can be derived as an empirical fitting parameter from titration curves [77WIL/KIN]. However, the product cannot be resolved further without additional model assumptions, *e.g.* of the average molecular weight.

More recently, Tipping used the empirical relation, Eq. (V.65), in his Model V [92TIP/HUR], and defined the electrostatic interaction factor ω as

$$\omega = P \cdot \log_{10} I \quad (\text{V.67})$$

where I is the ionic strength and P is an adjustable parameter for optimisation. In contrast to the product, $\omega \cdot n_{\text{COOH}}$, in [77WIL/KIN], we have now two independent fitting parameters in Model V [92TIP/HUR], the average molecular weight of the humic molecule and the purely empirical parameter P .

A final remark on electrostatic effects: Pure polyelectrolyte models assume a single repeated functional group, *i.e.* assumptions {A1} to {A5} are valid, and all measured pH variations of K are thought to be due to electrostatic interactions. This is a valid description of synthetic polyelectrolytes, but humic substances are more complex. Therefore, humic binding models usually combine electrostatic effects with functional group heterogeneity in one way or another. A few examples may illustrate this point. In Morel's "oligoelectrolyte model" [92BAR/CAB] electrostatic terms are combined with a multiple site model. Tipping's "Model V" [92TIP/HUR] contains electrostatic terms and discrete distributions of two classes of metal-proton exchange sites. Van Riemsdijk and coworkers [90WIT/RIE] propose a humic binding model which comprises electrostatic interactions and continuous (Sips) distributions of binding sites.

V.3.4. Variations in ionic strength

The variation of experimental K values with ionic strength is a general observation made in investigations of metal-humic complexation. The ideas developed to model the measured ionic strength effects can be divided into concepts assuming that the concentration of complexing sites is dependent on ionic strength and concepts ascribing the behaviour of

$^{\circ}K$ values to conditional stability constants that depend on ionic strength due to electrostatic effects. All models that account for both pH and ionic strength effects have already been discussed in the preceding section. Here we focus solely on the special ionic strength aspects of these models.

V.3.4.1. Empirical functions

In some of the models the concentration of complexing sites is identified with the maximum concentration of metal ions bound to humic substance. It is observed that this is proportional to quantities like “complexing capacity” or “loading capacity”, and changes with varying pH and ionic strength. Consequently, the complexing capacity W [95MOU/MOU] or the loading capacity LC [96CZE/KIM] is evaluated experimentally and used to define the amount of humic substance available for complexation under a given set of experimental conditions. The resulting empirical functions of pH and ionic strength, *i.e.* $W = f(\text{pH}, I)$ and $LC = f(\text{pH}, I)$, are found to be non-linear in pH, but little was known about their ionic strength dependence until recently.

Measurements are reported for the complexation of Cm(III) with humic acid in 0.1 M and 0.001 M NaClO₄ at pH 5. W values of 1.2 and 1.6 meq/g, and $\log_{10} \beta$ values of 8.5 and 8.0 l/eq, respectively, were found by Moulin *et al.* [91MOU/DEC]. All other measurements of Moulin and coworkers were carried out in 0.1 M electrolyte medium [95MOU/MOU]. Additional data have been reported for the complexation of Am(III) with humic acid in 0.1 M and 1.0 M NaClO₄ at pH 6 [89KIM/BUC]. Two almost identical complexation constants were derived from these two data sets. Almost all later investigations of Kim and coworkers were made only in 0.1 M NaClO₄, but the claim of the complexation constants “being independent of ionic strength” is repeated also for other metal ions like neptunyl and uranyl without experimental verification [91KIM/SEK, 92BUC/KIM, 94CZE/BUC]. Recently, the effect of ionic strength on the complexation of Am(III) and Cm(III) by humic acid was investigated at pH 6 [96CZE/KIM]. The ionic strength I was varied from 0.001 M to 5.0 M NaClO₄ and the loading capacity LC was found to change with I according to $LC = \text{intercept} + \text{slope} \cdot \sqrt{I}$. In contrast to earlier claims, an ionic strength dependence of the complexation constants was observed which is larger than the scatter of the experimental data.

V.3.4.2. Electrostatic effects

All electrostatic model concepts discussed in Section V.3.3.3 were developed mainly to “correct” measured data for ionic strength effects. Authors of the different electrostatic models regard concomitant pH effects as less important. The reason for this emphasis on ionic strength effects is the hope, that the “intrinsic” stability constants, K_{int} , of Eq. (V.61) will turn out to be independent of ionic strength (and pH) at the end of successful modelling, so that they can be treated in the same way as the thermodynamic stability constants, K° , of simple metal-ligand equilibria. This hope has failed so far for two reasons.

First, at constant pH the Gouy-Chapman flat plate model and the Donnan gel model predict that the apparent stability constant $\log_{10} K$, Eq. (V.61), is proportional to $\log_{10} I$

$$\log_{10} K = \text{const} - \Delta Z \cdot \log_{10} I \quad (\text{V.68})$$

provided that the geometric parameters of these models do not vary greatly with ionic strength. The same relation holds for spherical models as long as the spheres have a sufficiently large radius. The model approaches Debye-Hückel behaviour only for small spheres, and, under those conditions, the variation of $\log_{10} K$ with $\log_{10} I$ becomes less pronounced [92BAR/CAB]. In general, experimental data do not behave according to this model prediction. For example, Ephraim *et al.* [86EPH/ALE] modified their Donnan gel model by introducing a purely empirical “fractional contribution of end and charged surface effects in the molecule” in order to explain, why they found a much smaller variation of $\log_{10} K$ with $\log_{10} I$ for protonation equilibria of fulvic acid than predicted by the model. The same problem in copper binding data, but combined with large ionic strength variations, was described by Bartschat, Cabaniss and Morel [92BAR/CAB] assuming that the protons bind to small molecules, and copper ions bind to large molecules of the same fulvic acid sample. Their conclusion from this modelling exercise is that “if proton and metal binding are dominated by different size fractions (and this seems to be the only way to explain the data sets), it is futile to try to apply electrostatic information extracted from a pH titration (such as conclusions about size and charge of molecules) to a metal titration”. This is in marked contrast to Tipping’s Model V [92TIP/HUR], where pH titration data are used to “calibrate” the model. When modelling metal complexation data, these parameters remain fixed and only two intrinsic stability constants per metal ion are fitted. In summary, according to [92BAR/CAB] and [92TIP/HUR] there are insufficient data available to properly evaluate ionic strength effects and to resolve the above mentioned contradictions. The “intrinsic stability constants” reported by various authors still have to be regarded as model dependent adjustable parameters rather than “true” thermodynamic constants.

Even if this problem could be resolved, a second obstacle prevents a direct comparison of “intrinsic” stability constants, K_{int} , with thermodynamic stability constants, K° , of simple metal-ligand equilibria. As discussed by Bartschat, Cabaniss and Morel [92BAR/CAB] the remaining important difference is the reference state for the binding constants. In the Debye-Hückel theory the electrostatic potential ψ has a finite value at zero ionic strength, and this value is included in the “intrinsic” binding constant, K° , by defining activity coefficients of exactly 1 at ionic strength zero. In the case of the impenetrable sphere model [92BAR/CAB], one also could define constants that use zero ionic strength as a reference state. However, this is impossible for other geometries, infinite planes and cylinders, for which the surface potential approaches infinity as the ionic strength approaches zero. Therefore, electrostatic models for macromolecules do not “subtract out” the contribution at zero ionic strength. Hence, the reference state for the macromolecule is the condition where ψ is actually zero. Then, and only then the apparent binding constant K of Eq. (V.61) equals the intrinsic binding constant K_{int} . In order to be able to compare K_{int} values with stability constants of simple ligands, the latter have to be transformed

to a reference state of zero potential. From a mathematical point of view, the reference state of zero potential is reached as the ionic strength approaches infinity. Consequently, Bartschat, Cabaniss and Morel [92BAR/CAB] propose to “correct” thermodynamic constants, K° , with activity coefficients calculated by the Debye-Hückel equation at infinite ionic strength. Although mathematically correct, this procedure ignores the fact that the electrostatic theory fails at high ionic strength due to the increasing importance of non-coulombic interactions. The difficult problems of ionic strength corrections beyond the “Debye-Hückel concentration range” are discussed in detail in Chapter IX. From a practical point of view, the apparent binding constant cannot be distinguished from the intrinsic binding constant, K_{int} , at sufficiently high ionic strength. What is “sufficiently high”? In the scope of Marinsky’s gel model, an ionic strength of 1 M is used implicitly as reference state [86EPH/ALE, 89EPH/BOR], but the topic is not discussed any further. In summary, the problem of reference states seems to be largely ignored. Apart from the above mentioned proposals no discussion of this topic has been found in the literature concerning humic binding models.

V.3.5. What is the best humic binding model?

At the end of this survey of concepts and approaches to the binding of metal ions with humic substances, the reader might like some recommendations concerning the “best” humic binding model. Papers presenting reviews and extensive numerical testing of different models usually conclude that the problem of metal-humic complexation is not yet solved in a satisfactory manner, and that a better humic binding model still waits to be developed. This ideal model should be chemically correct, numerically accurate and simple to use in predictive modelling. Is there any hope that we may see this ultimate humic binding model? The answer is simply no! This unconditional no is based on the idea that there exists a kind of “uncertainty principle” for humic binding models which may be stated as follows:

It is not possible to achieve an accurate *and* simple description of metal-humic binding.

Accurate in this context does not only mean the numerical accuracy of fitted and predicted results, but also the chemical correctness of the conceptual model. The term “simple” means simplicity when using the model for solving “real world” problems. This has two aspects: the amount of experimental data needed to calibrate a model with respect to the special problem under study, and the mathematical simplicity of the model. The often debated issue of mathematical simplicity of a model is judged to be a problem of decreasing importance in the age of powerful personal computers. Even the most complicated mathematical model needs to be integrated into user-friendly software just once. Then the user is not forced to bother with computational details anymore. On the other hand, if a model requires many site-specific data that requires an elaborate time and money-consuming effort to collect, the model cannot be termed “simple” regardless of its degree of mathematical simplicity.

The ultimate microscopic chemical model of humic bonding requires a detailed description of the molecular structures of site-specific mixtures of large but varying numbers of natural organic compounds. To attain this level of knowledge is hardly feasible, even in a very ambitious research program. Ignoring reality for a moment, we may dream of reaching this utopian goal by some not yet developed experimental techniques. Then we would end up with the most complicated humic binding models, because we would have to redo the entire sequence of site-specific molecular structure determinations for each and every case under study in order to apply this “detailed molecular binding model” in its full beauty and accuracy. Any attempt to decrease the load of experimental work needed to calibrate this model would lead to an “averaged molecular binding model” in which the individual molecular features are replaced by averages within certain parameter ranges. The prize for this decrease in experimental cost, which is a gain in terms of simplicity, is a concomitant loss in chemical and numerical accuracy of the model.

If this (hypothetical) process of averaging of molecular properties is driven far enough, we finally reach the realm of the humic binding models in use today. The common feature of these models is that they describe the heterogeneity of humic substances by empirical distributions of molecular properties. The distributions are considered in terms of distributions of equilibrium constants leading to “affinity spectra” or “differential equilibrium functions”, or in terms of molecular size distributions influencing “electrostatic terms” *etc.*, as already discussed in the preceding sections. Compared to our hypothetical “detailed molecular binding model” these models are already far from chemical and numerical accuracy but the experimental effort needed to calibrate them is on the verge of current technology. Thus, leaving utopia and coming back to reality, these “site specific distribution models” are at present those of highest accuracy and “best value for invested research money”.

If we are heading towards simpler models, the process of averaging must go on. This can be done in different ways. The continuous distributions may be replaced by discrete values. Alternatively, some sort of “averaged distribution functions” may be used, which to a certain degree level out the heterogeneity of samples of different origin. Of course, any combination of discrete values and continuous distribution functions may be used as well. In any case, the simplicity of the model is increased at the expense of accuracy. Reaching the extreme case of averaging, all adjustable parameters of the humic binding model are fixed, and we describe some sort of “global average humic substance”. Now the simplicity is at its maximum, but the chemical and the numerical accuracy are both very low.

In summary, there is no such thing as the “best humic binding model”. We always struggle with the tradeoff between accuracy and simplicity. The choice of the “best model” depends on the intention of the modeller, and the purpose of the model. In the following, problem solving strategies are outlined for two cases: models used as research tools, and models used as tools to assess behaviour in nature.

V.4. Problem solving strategies

V.4.1. Models used as research tools

Scientific research projects on humic substances usually aim at increasing our understanding of chemical features and processes governing metal-humic interactions. Within such projects binding models are important research tools. In an ideal case, several different models may be analysed theoretically and tested by comparison with measurable quantities. Hence, experimental data may validate or refute the various model assumptions. In an iterative process, model assumptions and experimental procedures are refined until a satisfactory description of metal-humic interactions is reached. In the real world of limited funding, however, this iterative process is usually stopped by practical constraints. In addition to economic limitations there are two other potential obstacles to progress. First, many scientists adopt a favorite idea at some stage of their work and dwell upon this idea in their further research. Different “schools” develop this way. If these schools tend to ignore each other instead of engaging in open scientific dispute, there is a real danger that progress will be limited. Second, the result may be ambiguous if too small a data set is used to test the various models. A typical example is found in [84CAB/SHU], where eight different models were used to analyse the experimental results of a copper-into-ligand titration of estuarine dissolved organic matter. The metal titration was carried out at a single fixed pH and ionic strength. As it is shown by Cabaniss, Shuman and Collins [84CAB/SHU], the eight models all fit this small data set well, in spite of their being based on contradictory assumptions.

In summary, in order to achieve a deeper understanding of metal-humic binding, a thorough analysis of contradictory conceptual models is needed based on large experimental data sets, comprising different metal ions with sufficient variation in key parameters like metal concentration, pH and ionic strength. Using humic binding models as research tools in this way leads to chemically and numerically more accurate descriptions of metal-humic binding at the expense of simplicity. Examples of this type of research tools are the “differential equilibrium function” approach of Buffle [88ALT/BUF] designed to explore the distribution of binding sites, Marinsky’s “unified physicochemical description of complexation equilibria of natural organic acids” [86EPH/ALE, 86EPH/MAR, 86MAR/EPH] aiming at a consistent description of binding site heterogeneity and electrostatic effects, the “oligoelectrolyte model” of Morel [92BAR/CAB] emphasising the molecular size heterogeneity of humic substances, or models such as the recently published Non-Ideal Competitive Adsorption (NICA) model [95BEN/MIL] developed by van Riemsdijk’s group to explore the chemical heterogeneity of humic substances with respect to competitive binding processes.

Tipping’s Model V, “a unifying model of cation binding by humic substances” [92TIP/HUR, 94TIP] is a research tool on the verge of being an assessment tool. The model includes something of each of the concepts discussed in Section V.3: binding site heterogeneity, metal-proton exchange equilibria, electrostatic terms accounting for charge, and ionic strength effects and counterion accumulation. In addition, metal ion competi-

tion effects can be explored with this model [93TIP]. As a research tool, Model V contains a large number of adjustable parameters. However, in order to cope with the limited experimental data available, most of these parameters are fixed at “reasonable” values. The remaining parameters are adjusted by analysing large numbers of experimental data sets [92TIP/HUR, 93HIG/KIN, 93TIP2] with the hope of extracting from them a data base of “best values” defining a sort of “global average humic substance”. Whether this approach will finally result in a valuable assessment tool or not, remains to be seen.

V.4.2. Models used as assessment tools

Assessment of metal behaviour in the environment is a task rather different from basic research. Here, the metal-humic interaction is just one feature out of many others to be considered in assessing the behaviour of environmental systems. For example, to develop concepts for the remediation of metal-polluted areas or to assess the performance of future waste repositories, models which predict orders of magnitude are generally sufficient. Of course, models predicting metal-humic interactions with higher accuracy might be welcome, but if the amount of site-specific data needed to calibrate these models exceeds a certain limit they cannot be used in assessments of environmental system behaviour. In the case of large metal-polluted areas important geochemical parameters, like pH, DOC and metal concentrations, may show considerable spatial variations. A time and money-consuming experimental program to characterise in detail the properties of humic substances in such areas is usually not feasible, if there is no convincing evidence that humic substances have a strong impact on the environmental system behaviour. Likewise, in the first phase of the performance assessment of future waste repositories, site-specific data are usually scarce and imprecise. Economic constraints require a concentration of efforts on the main features governing the safety of the planned repository. However, decisions on which types of data collection one should spend most time and money must always be made on the basis of incomplete data. A problem-solving strategy concerning the possible impact of metal-humic interactions on the safety of a repository of toxic chemical or radioactive waste is outlined in the following.

V.4.2.1. The “conservative roof” approach for performance assessment

In performance assessment the ultimate goal is not to develop the most realistic model of a system or of certain effects, *e.g.* of humic substances on metal speciation, but to estimate the *maximum negative influence* of the process on a property of the system, such as the safety of a waste disposal site. In other words, we are interested in a *conservative*⁴ *estimate*

⁴ The meaning of the term “conservative” strongly depends on the scenario (the type of physical/chemical system) being considered. In performance assessments, we take a “conservative” estimate to be one that leads to an overestimate of the total concentration of a metal in the liquid phase, leading to a maximum value for the mass being transported. If only the mobile fraction of the humic substances is taken into account, and the total metal concentration in the liquid phase is controlled by either the solubility of a solid phase or by sorption on mineral surfaces, an overestimate of the amount bound to humic substances will lead to an overestimate of the amount in the liquid

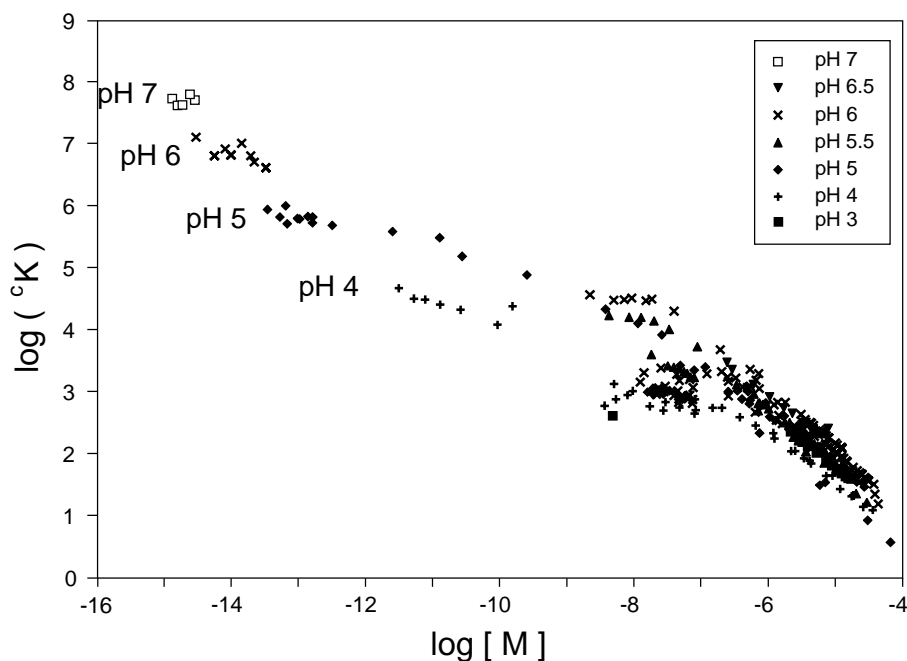
of the influence of humic substances on the speciation of toxic metals or radionuclides. Therefore, it is not necessary that binding models for performance assessment reflect every subtle detail of metal-humic interactions. Even if they are wrong by orders of magnitude, they may still be useful in safety analyses, as long as it can be shown that the models *overestimate* the influence of humic substances on metal ion speciation.

Going back to the example of humic complexation with trivalent lanthanides and actinides, a synopsis of experimental data transformed to a common basis of cK values reveals a consistent picture of the variation of cK with metal concentration and pH (Figure V.4). In the range of low metal loading, cK increases with decreasing free metal concentration and seems to approach constant values at very low metal loading. The effect of pH is quite pronounced in this region (see also Figure V.3), whereas in the range of high metal loading the influence of pH is negligible. If we are interested in a very simple mathematical description of these data, a single site model including a metal-proton exchange reaction would be appropriate (Eq. (V.44)). This model can be calibrated with a minimum number of experimental data: (1) The site complexation capacity, SCC, is derived from data at high metal loading in Figure V.4 by applying Eq. (V.10), and (2) the exchange constant K_{exch} is determined at trace metal concentration (Figure V.3) using Eq. (V.45). In both cases we adjust these parameters to reproduce maximum values rather than mean values of the available experimental data, in order to get conservative estimates. As a result of this procedure, the conservative estimates cover the experimental data like a “roof”. Actually, the expression “the conservative roof” approach was born when for the purpose of visualising Eq. (V.44) a three dimensional plot of the $\log_{10} {}^cK$ surface as function of pH and $\log_{10}[M]$ was created the first time (Figure V.5). All measured data are located at, or somewhat below, the surface of the conservative roof. At trace concentration levels and in the range of high metal loading, the conservative roof is very close to the observed experimental data. In the range of intermediate metal concentration, the simplistic model overestimates the experimental data by up to two orders of magnitude at pH 4 and 5. Hence, a similar overestimation is also expected at higher pH regions of parameter space.

Because the conservative roof approach is intended for use in performance assessment, its main feature is a conservative estimate of the metal-humic binding. Which detailed humic binding model is used to reach this goal is immaterial, as long as it remains simple enough to be “conservatively” calibrated with the (usually few) available experimental

phase, which is conservative. The “conservative roof” approach is based on this scenario. On the other hand, if the total metal content in the liquid phase is limited by the amount available for transport, *i.e.* if its concentration is not solubility-limited and sorption is negligible, the amount of metal-humic binding, or of complexing with any other substances in the liquid phase, will not effect the amount being transported. Likewise, if only the immobile fraction of the humic substances is considered, and the metal concentration is solubility controlled, metal-humic binding will not influence the amount in solution. In both scenarios the term “conservative” is meaningless. By contrast, if the metal concentration is not solubility limited and only the immobile fraction of the humic substances is considered, an increase in metal-humic binding will lower the amount available for transport in the liquid phase. An overestimate of the amount of metal-humic binding in this case will not be conservative.

Figure V.4: A synopsis of experimental data of Eu, Am and Cm complexation with humic and fulvic acids at ionic strength 0.1 M. In the range of low metal loading, $^{\circ}K$ increases with decreasing free metal concentration and seems to approach constant values at very low metal loading. The effect of pH is quite pronounced in this region (see also Figure V.3), whereas in the range of high metal loading the influence of pH is negligible.

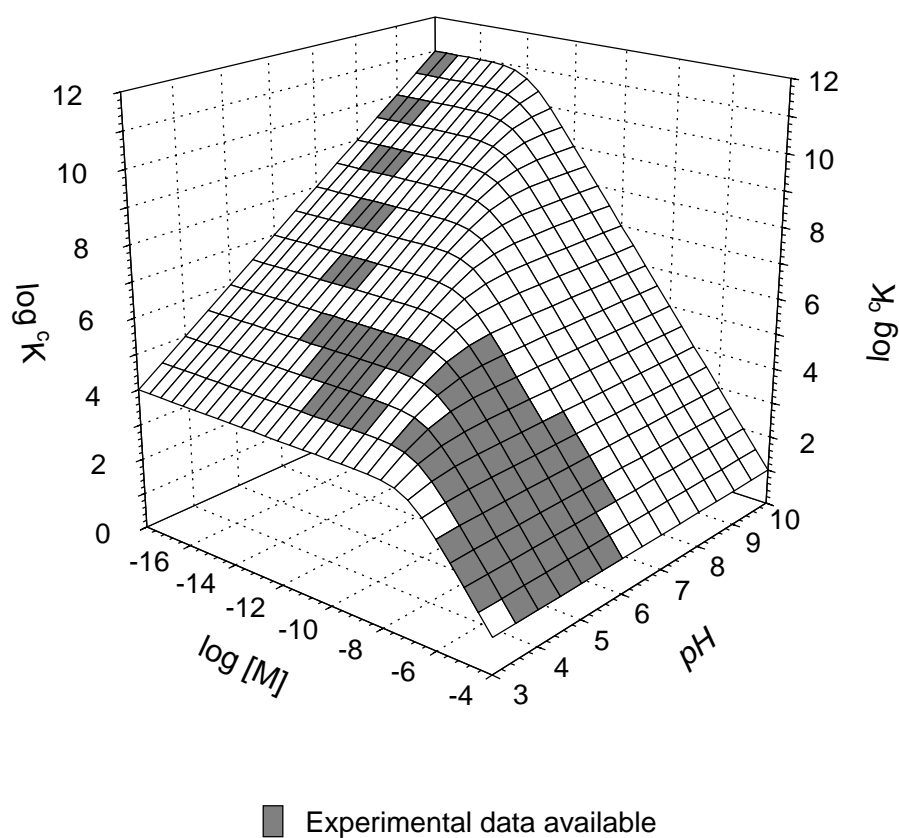


data. The example shown above is a well investigated case. For most other metals of interest experimental data are scarce, especially at trace concentrations and at high pH. For a sound calibration we need some data in the range of high metal loading *and* at trace concentration levels⁵. Calibration at high concentrations alone is not enough, because the resulting model predictions will certainly underestimate humic complexation at trace level (and at neutral to slightly alkaline pH) by several orders of magnitude. This can easily be seen from Figure V.5, if the calibration had been done only with data from the “island” at low pH and high metal loadings!

Speciation calculations using any well-calibrated conservative roof model reveal the maximum effect of humic substances on the speciation of toxic metals or radionuclides. If no significant influence is predicted by the first exploration using a conservative roof

⁵ The calibration procedure proposed for “conservative roof” - type models, using a site complexation capacity obtained for high metal loading and adjusting an exchange constant at trace metal concentration, is inconsistent from the viewpoint of models used as research tools which aim at a deeper understanding of humic binding. However, for the purpose of estimating maximum effects of humic binding in performance assessment any set of parameters is appropriate, as long as it ensures a conservative calibration of the chosen model.

Figure V.5: The “conservative roof” approach for performance assessment. A single site model including a proton-exchange reaction (Eq. (V.44)) is calibrated with the experimental data in Figure V.4. The parameters $\log_{10} K_{\text{exch}} = 4$ and $\log_{10} \text{SCC} = -3$ are adjusted in such a way that Eq. (V.44) reproduces maximum values rather than mean values of the available experimental data. All measured data (dark areas) are located at, or somewhat below, the surface of the conservative roof.



model in the pH and metal ion concentration ranges of interest, humic substances can safely be ignored when describing the properties of the system.

However, if the particular conditions are such that the conservative roof model predicts a significant influence of the humic substances, the situation must be examined further. If enough experimental data are available, a more sophisticated humic binding model may be used, resulting in a more complicated but less conservative roof. In the (usual) case the lack of data can be constrained by a few well designed experiments in this critical region of the parameter space, which subsequently may also lead to a more sophisticated conservative roof model. In both cases, limited experimental effort will identify and constrain the problem, and any decision how to proceed would be based on a sound evaluation of all available information.

Unfortunately, real world systems tend to show much more complicated behaviour than simple laboratory systems. In performance assessment one has to consider *all* relevant features and processes, not just the few thoroughly investigated in laboratory experiments. In the following, we take some cautious steps out of the well illuminated laboratories into the darkness of real world groundwater systems.

V.4.2.2. Competition of other complexes

The interaction of metal ions with humic substances is usually treated within the scope of equilibrium thermodynamics. Therefore, in principle, all other equilibria in the chemical system are expected to influence these interactions. The predicted magnitude of the competitive effects depends not only on equilibrium constants and the chemical composition, but also on the binding model chosen. This model dependence of predicted competitive effects represents a major difference from chemical equilibrium problems comprising only small ligands. The latter problems are usually solved by classic speciation calculations and the uncertainty of the results depends solely on the completeness and accuracy of the set of stability constants used in the calculations. Binding models for humic substances, on the other hand, include a number of assumptions in addition to those of the standard thermodynamic equilibrium model. These additional assumptions, characterising the different binding models, cause a substantial spread in the predicted effects of competition. In extreme cases, as is discussed in the following, one binding model predicts large effects, whereas another model predicts no competition at all.

From the viewpoint of basic research, the discussion of competitive effects could stop here with the rather general statement: "It depends." From the viewpoint of performance assessment, however, the situation is not without promise. Here, it is enough to demonstrate that a certain class of competition reactions may decrease metal-humic interactions in all cases, independent of the binding model, if competition has any influence at all. A conservative binding model may then safely ignore this, if not enough experimental data are available to include the effects in a proper way into the model.

In the following, the main competitive effects are divided into three classes, although all of them are coupled: Direct competition of other cations, competition of other anions with binding sites, and competition of mineral surface sites with organic binding sites. As we

discuss these effects separately, a more and more complex picture of coupled interactions will emerge.

V.4.2.2.1. Competition of other cations like Ca^{2+} and Al^{3+} with toxic metal ions

The most obvious competitive effect is the competition of toxic metal ions with other cations like Ca^{2+} , Mg^{2+} , Fe^{2+} , Fe^{3+} , and Al^{3+} . These cations are major constituents of common groundwaters and they are known to form rather stable aqueous complexes with small organic molecules. Therefore, they have also to be considered as effective competitors for the binding sites of humic substances. The predicted effect of varying the concentrations of these cations on metal ion uptake by humics depends strongly on the binding model chosen. For a single site model, which treats humic substances as similar to small organic ligands, direct competition of, for example, Ca^{2+} with all other metal ions is expected. In groundwaters the concentration of Ca usually exceeds toxic metal concentrations by several orders of magnitude, and an increase in Ca concentration may substantially decrease the uptake of these metal ions by humic substances. If a multiple site model is used, the predicted effect depends on the affinities of the various sites for Ca and other metal ions. In an extreme case, the humic substance may be thought of as a mixture of highly specific organic ligands, some exclusively binding toxic metal ions, others only attracting Ca. Then, the influence of a varying Ca concentration on the uptake of other metal ions may vanish.

The theoretical predictions of competitive effects of cations thus range from very strong to zero. The question now arises, is there any way to obtain more precise predictions? Yes, there is, if we consider chemical systematics, especially linear free energy relationships. For a detailed discussion of linear free energy relationships and other correlations see Chapter III.

Again using the example of trivalent lanthanides and actinides, linear free energy relationships correlating the stability constants of small organic ligands of Eu with Al and Ca reveal a rather consistent picture. The stability constants of Eu and Al organic complexes are found to be of the same order of magnitude. The general conclusion drawn from this observation is that the complexation strength of these two cations is expected to be of comparable magnitude in humic substances as well. We do not expect grossly differing affinities for Eu and Al, even when the nature and stereochemistry of functional groups in humic substances vary. Therefore humic binding models will not only predict direct competition of Eu with Al, but also complexation effects of the same order of magnitude for both cations. This result is experimentally confirmed by a rather detailed study of Eu - Al competitive effects [91BID/GRE]. In contrast to Al, stability constants of Ca organic complexes are always found to be several orders of magnitude smaller than the Eu constants. Hence, we expect a significant competition of Ca only if its concentration exceeds Eu by several orders of magnitude. In the case of multiple site models, the predicted Ca competitive effect may be even weaker than for the limiting case of a single site model. The binding of Eu may be considered in a multiple site model mainly as a

proton exchange reaction with rather strong binding sites of the humic molecule. Ca, however, may not participate in this type of exchange reaction, due to its generally much smaller stability constants. The multiple site model then predicts very different affinities for the two cations and, as a consequence, no competition at all. An experimental study of competitive effects of Ca with trace concentrations of Dy, another rare earth element with similar complexation behaviour to Eu, revealed no influence of Ca on the Dy-humic acid complexation up to a concentration of 0.004 M Ca [95MOU/MOU2], corroborating the validity of our chemical reasoning.

The extent and nature of competition effects will be completely different when considering for instance mercury instead of trivalent lanthanides and actinides. Soft cations like Hg, Pd, Ag, Cd, Tl, Pb are expected to interact with other binding sites of humic substances than hard cations like Ca and Al. Hence, very weak or no competition at all is predicted between these different classes of metal ions by chemical reasoning. For a detailed discussion of qualitative features of complex formations reactions, including the classification of soft and hard metal ions, see Chapter III.

V.4.2.2.2. Competition of other anions like CO_3^{2-} with humic binding sites

In contrast to competition by cations, competition by anions like CO_3^{2-} , F^- , SO_4^{2-} or PO_4^{3-} takes place in an indirect way. The model dependence of this effect is also less obvious than in the case of cations. It is shown in the following that the predicted competition of anions with organic binding sites depends on the type of complexes assumed to be formed in the binding model.

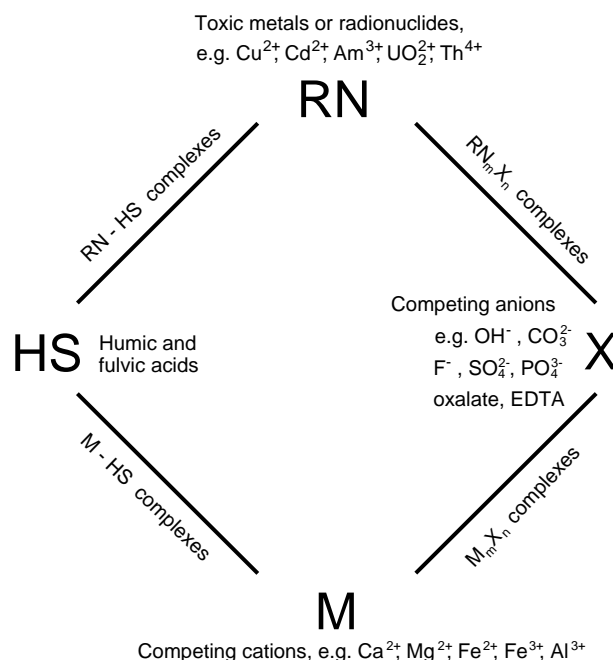
If the cations are assumed to form only binary complexes with humic substances, the competition of anions remains to a large extent in the realm of classic mass action and mass balance equations. For example, at constant toxic metal concentrations, increasing concentrations of anions and, thus, increasing formation of metal-anion complexes, cause decreased metal binding by humic substances.

This effect may be buffered to some extent by a concomitant increase of the complexation of anions with other competing metal ions, which in turn influences the competition of these metal ions for the humic binding sites. The closed circle of mutual interactions of thermodynamic equilibria is shown schematically in Figure V.6.

An additional buffering effect arises from the heterogeneity of the humic binding sites. At trace concentrations of metal ions, an increase in anion concentration decreases the metal loading of humic substances. With decreasing metal loading, the stronger binding sites of the humic substances predominate, which in turn weakens the anion competition. The prediction of this second buffering effect strongly depends on the chosen humic binding model.

If the binding model for humic substances includes mixed or ternary complexes in addition to binary complexes, the predicted influence of anion competition becomes more complicated. The formation of ternary complexes can be envisioned either as the uptake of metal-anion aqueous complexes by humic substances, or as the binding of anions to

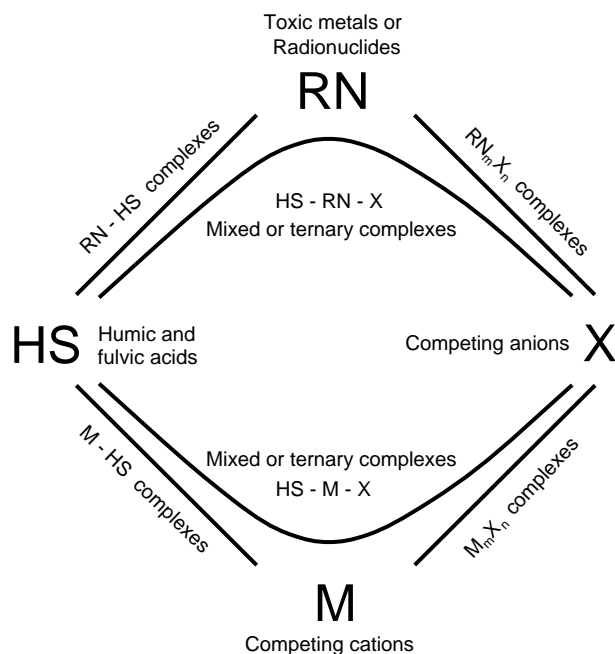
Figure V.6: Schematic representation of competitive effects in metal-humic binding models: The closed circle of competition of other anions with humic binding sites, combined with cation competition. Competing metal-ligand equilibria are indicated as solid lines.



metal cations which are already bound by humic substances. The influence of ternary complexes is schematically shown in Figure V.7 as bent lines, connecting humics, toxic metal ions, and anions, and connecting humics, competing cations, and anions.

Ignoring ternary complexes in modeling natural groundwater systems may lead to significant underestimation of metal-humic complexation. Why? The two most powerful complexing anions in common groundwaters are hydroxide and carbonate. Whereas the pH effect cannot be excluded when studying complexation in aqueous systems, most studies are undertaken in carbonate free environments. If binding models are calibrated with data measured in carbonate free systems, and subsequently applied to groundwater systems with high carbonate concentrations, strong competition of metal-carbonate complexes is predicted. In reality, however, the effect of anion competition may be significantly weaker than predicted due to the formation of ternary metal-carbonate-humic complexes. As a result, the effects of metal-humic complexation are underestimated in the presence of carbonate. The formal inclusion of ternary complexes in humic binding models, the available experimental results and a possible general treatment of these effects [95GLA/HUM] are discussed in Section V.3.2.2.

Figure V.7: Schematic representation of competitive effects in metal-humic binding models: The closed circle of competition of other anions with humic binding sites, combined with cation competition. In addition to Figure V.6, the influence of ternary complexes is shown as bent lines, connecting humics, toxic metal ions, and anions, and connecting humics, competing cations, and anions.

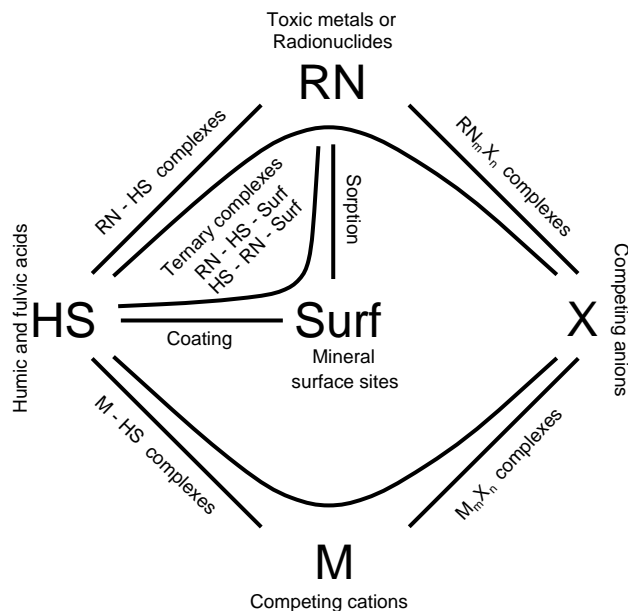


V.4.2.2.3. Competition of mineral surface sites with binding sites

Interactions of metal ions with surface sites, usually summarised as sorption phenomena, are important mechanisms of metal retention in the geologic environment of a repository for toxic chemicals and radioactive waste. Competition of the surface sites with binding sites of humic substances should therefore be discussed in terms of reducing metal ion sorption by complexation with humic substances. In order to emphasise the importance of surface phenomena, the mineral surface sites are placed in the very center of the sketch of metal ion interactions (Figure V.8). On the other hand, as the interaction of humic substances is the topic of our present discussion and not sorption phenomena on mineral surfaces (which are discussed in detail in Chapter VII), we will focus on humic substances and treat surface sites as competitors for humic binding sites.

If interactions of humic substances (HS) with mineral surface sites (Surf) are neglected, then “pure inorganic” sorption remains as competitive effect (Figure V.8). The competing equilibria $RN-HS$ and $RN-Surf$ are shifted towards $RN-Surf$ by increasing the strength of surface interactions and/or increasing area of active mineral surfaces. This type of indirect

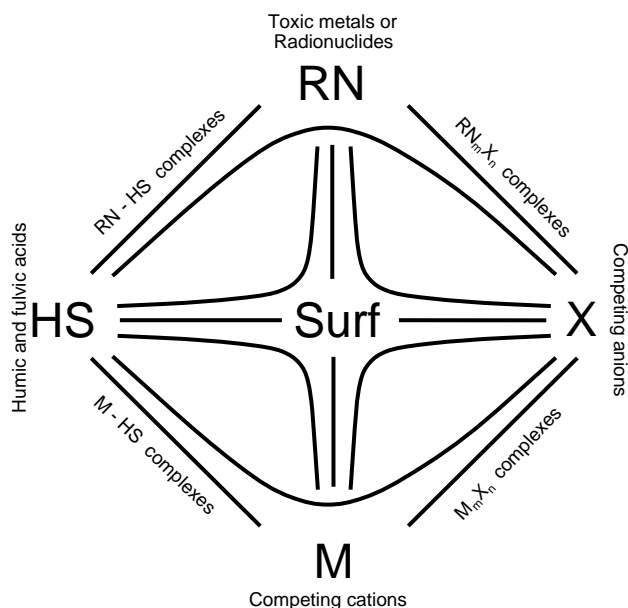
Figure V.8: Schematic representation of competitive effects in metal-humic binding models: Competition of mineral surface sites with humic binding sites. Sorption of toxic metals on surface sites, organic coating of mineral surfaces and the formation of ternary metal - humic - surface complexes is shown.



competition is very similar to the competing effects of anions, as already discussed, if only binary complexes are considered. The resulting binding models, however, are more complex than models dealing with humic substances only. They should include surface complexation and ion exchange to account for interactions of metal ions with humic substances *and* surface interactions at the same time.

If humic substances sorb at surface sites, they may form an organic coating on the mineral surface. This coating may significantly alter the sorption capacity of the immobile phase. In the hypothetical case of “pure” coating, sorption decreases because parts of the active mineral surface sites are not accessible to metal ions any more, due to the organic coating. On the other hand, the coating itself is expected to interact with metal ions in the same way as humic substances in solution, but now forming immobile ternary complexes of the type RN-HS-Surf (Figure V.8). Compared with the scenario of a “pure” organic coating, sorption of metal ions increases again due to the formation of ternary complexes. In addition, a second type of ternary complexes, HS-RN-Surf, may be formed (Figure V.8), where the humic substance is “glued” to mineral surfaces via metal cations forming bridges between humic binding sites and surface sites. This type of ternary complexes can be envisioned as sandwich structures. The net effect of organic coatings and formation of immobile ternary complexes on the sorption of radionuclides is hard to predict. It depends on the ratio of the complexation strengths of radionuclides with organic binding sites and

Figure V.9: Complete sketch of mutual interactions of toxic metals, humic substances, other cations and anions, and mineral surface sites. Straight lines indicate binary interactions, whereas bent lines represent ternary complex formation.



surface sites, and is in addition expected to show a strong pH dependence. If both, the humic acid molecule and the mineral surface are negatively charged, weak interaction is expected due to strong electrostatic repulsion. Strong interaction may only occur within a pH region where the mineral surface is positively charged and the humic molecule still is sufficiently deprotonated. In addition, competing cations and anions further complicate the picture, as shown in our final sketch of competition effects (Figure V.9).

Many of the more complex interactions, schematically shown in the center of Figure V.9, are expected to predominate only within very limited ranges of pH and component concentrations. The most prominent competitive effect, sorption of metal ions by mineral surface sites, may significantly reduce the uptake of these metals by humic substances. An experimental study investigating the uptake of Am by silica colloids in the presence of humic and fulvic acids corroborates this qualitative prediction. This study showed that the humic substances control the cation behaviour in solution leading to a strong decrease of the retention by the inorganic binding sites [95MOU/MOU2].

V.4.2.3. Application of laboratory data in performance assessment

In the following, the major effects influencing metal-humic interactions are summarised from a performance assessment point of view. It is assumed that “average” laboratory data concerning metal-humic binding are used to calibrate the binding models which subsequently are used as assessment tools in a “conservative roof” approach. Plus signs

indicate an increase of metal-humic interaction with respect to binding models calibrated with the “average” laboratory data. If these topics are ignored in humic binding models, the influence of humic substances on metal speciation may be underestimated. Minus signs indicate a decrease of organic interactions and may thus cause an overestimation of humic binding if ignored in the model structure.

- | | | |
|-----|---------------------|---|
| +++ | Metal concentration | Binding models calibrated with standard metal titration data alone tend to grossly underestimate metal-humic interaction when applied to trace metal concentrations in real world assessments. Experimental data at trace concentration level are needed to properly calibrate any humic binding model. |
| +++ | pH effect | Major influence of increasing pH is expected on metal-humic complexation at trace concentration levels of metal ions. In addition to data gathered in the acidic region, experimental data in the neutral and alkaline pH region are needed in order to calibrate humic binding models properly. |
| ++ | Ternary complexes | Formation of ternary complexes consisting of metal ions, humic binding sites, and small anions may increase the influence of humic substances at high concentrations of these anions, compared with predictions of binding models ignoring ternary complexes. Mixed complexes with carbonate may be important in certain groundwaters. Therefore, at least some rough estimates about the possible formation of ternary complexes with carbonate are necessary. |
| − + | Organic coating | Organic coating may reduce the concentration of soluble humic substances and/or may immobilise metal ions by “gluing” them to surfaces. Metal uptake by humic substances in solution, may therefore decrease <i>or</i> increase somewhat. The effects are expected to be limited to certain pH and concentration ranges. They may be neglected as second order effects as long as only the order of magnitude of metal-humic interactions has to be assessed. |

- + Ionic strength Increasing ionic strength in general decreases metal-humic interactions. Most available experimental data refer to an ionic strength of 0.1 M. Binding models calibrated with such data will slightly overestimate metal-humic interactions in more saline waters. Thus, a “conservative roof” approach using binding models which do not explicitly treat ionic strength effects should be calibrated with low ionic strength data. As the ionic strength of common groundwaters rarely drops below 0.01 M, data measured in this range can be used.

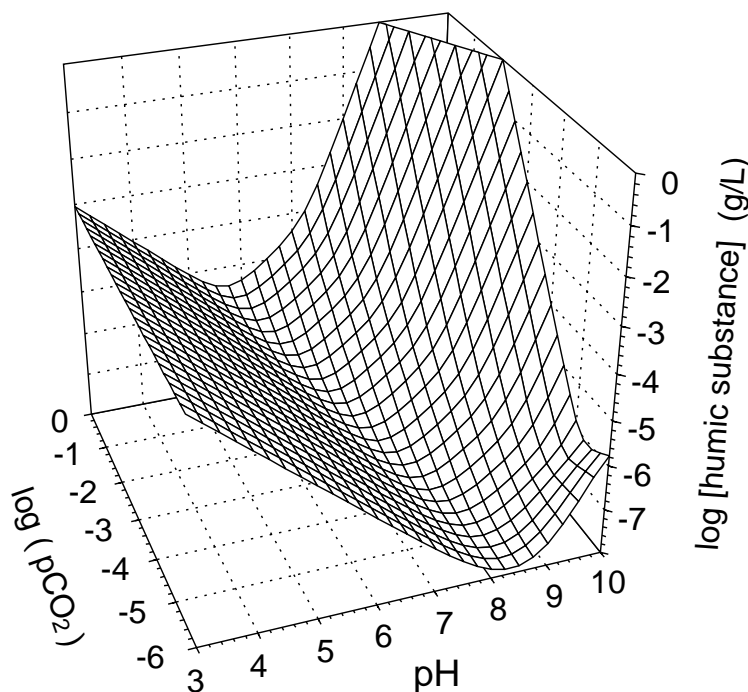
- – Competing anions Complexation of metal ions by inorganic and small organic anions is the realm of NEA TDB reviews. Including this type of competition in humic binding models requires complete and properly reviewed thermodynamic data of small ligands.

- – – Competing cations Competing cations may decrease the influence of humic substances on toxic metal complexation. The predicted effects of cation competition are strongly model dependent. In the absence of reliable experimental data for calibration of humic binding models, cation competition can be neglected for conservative estimates of the influence of humic substances in performance assessment.

- – – Sorption Sorption is the main topic in performance assessment of the behaviour of trace metals in the environment of a repository. Sorption on mineral surface sites may decrease the uptake of metal ions by humic substances. In order to predict effects of metal-humic interactions on sorption, such models have to be included in humic binding models. As long as the two fields of modeling are not coupled, sorption effects can be neglected for conservative estimates of the influence of humic substances in performance assessment.

We conclude our review of humic binding models by presenting some scoping calculations of humic complexation with trivalent lanthanides and actinides, the illustrative example used throughout this chapter.

Figure V.10: Scoping calculations of humic complexation with Eu at trace concentration level. The surface represents the concentration of humic substance (in \log_{10} g/l) necessary to bind 90% of the total dissolved metal by humics. The surface is calculated as a function of pH and p_{CO_2} at ionic strength 0.1 M.



The speciation model of Eu - humic complexation comprises:

- the binary Eu - humic binding represented by the “conservative roof” (Figure V.5), which takes account of the effects of metal concentration and pH,
- a maximum value for the ternary Eu - humic - carbonate complexation constant, represented by K_2 of Eu - carbonate complexes as discussed in Section V.3.2.2 (Eq. (V.21)), and
- the complexation of Eu by hydroxide and carbonate, the major competing anions in groundwater.

The concentration of humic substance (g/l) necessary to complex 90% of the total concentration of Eu is shown in Figure V.10 as a function of pH and p_{CO_2} at $I = 0.1$ M.

At low pH and low p_{CO_2} there is no competition of Eu hydroxide or Eu carbonate complexes. In this range of the pH- p_{CO_2} parameter space the observed increase in complexation strength with increasing pH (Figure V.5) causes a concomitant decrease in

humic substance concentration needed to complex 90% of Eu. Note, that in a region of the parameter space where anion competition and the formation of ternary complexes is negligible, a simple relation between cK and $(HS)_{\text{total}}$ of Eq. (V.1) holds

$$\log_{10}(HS)_{\text{total}} = \log_{10}(n/(100 - n)) - \log_{10} {}^cK \quad (\text{V.69})$$

where n is the percent of total concentration of metal complexed by the ligand, $0 < n < 100$.

The decrease in humic substance concentration with increasing pH proceeds until at $\text{pH} > 8$ and low p_{CO_2} Eu hydroxo complexes act as competitors, or, in the region where both pH and p_{CO_2} increase, the Eu carbonate complexes dominate and Eu hydroxo complexes become minor species. In these ranges a dramatic increase in humic substance concentration is required to maintain 90% Eu - humic complexation.

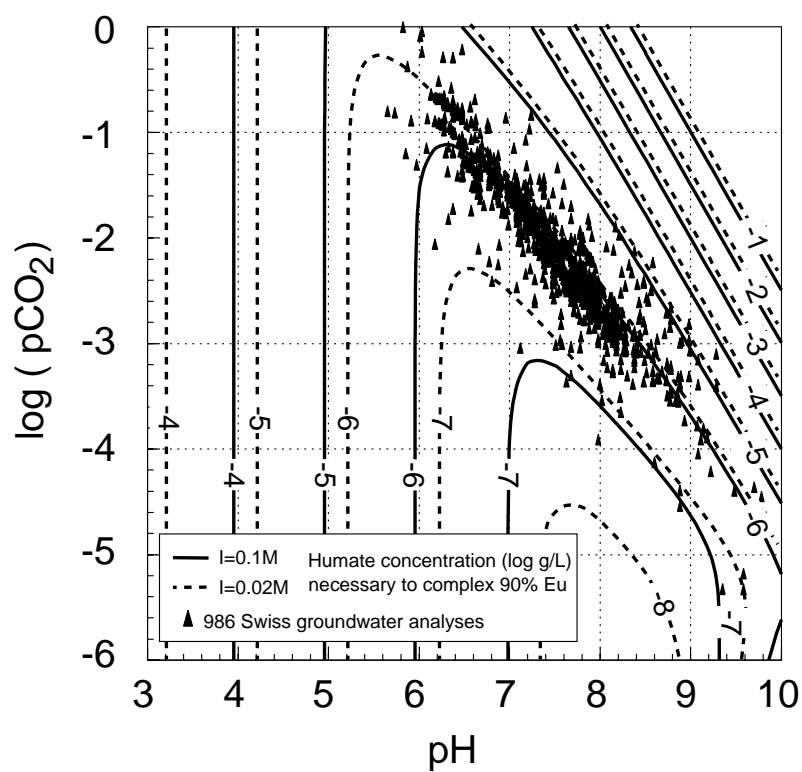
If the three-dimensional surface of Figure V.10 is projected onto the pH- p_{CO_2} plane, contour plots can be drawn, as is shown in Figure V.11. In addition, pH- p_{CO_2} data derived from almost 1000 Swiss groundwater analyses are added. As can be seen in the contour plot, all groundwater data cluster along the iso-concentration line of 10^{-6} g/l humic substance with a maximum spread of \pm one order of magnitude.

Ionic strength variation has a significant influence on the Eu - humic complexation strength. According to Ephraïm, Marinsky and Cramer [89EPH/MAR] and our own experimental results, an increase of one order of magnitude in cK is observed when the ionic strength decreases one order of magnitude. This effect is reflected in a significant shift of the iso-concentration lines in Figure V.11 at low pH. However, ionic strength effects are very small in the pH- p_{CO_2} range of groundwaters, as the concomitant variations of humic and carbonate complexation constants with ionic strength are in the same direction and of the same order of magnitude, resulting in an almost zero net effect.

Competition by other cations is not included in the scoping calculations of Figure V.11. No influence of Ca was observed by Moulin *et al.* [95MOU/MOU2] on the complexation of humic acid with trace concentrations of lanthanides up to a concentration of 0.004 M Ca. Thus, only in Ca-rich groundwaters some (weak) influence of Ca competition on Eu - humic substance complexation is expected. Al is known to exhibit complexation effects of the same order of magnitude as Eu [91BID/GRE], whereas Fe(III) is expected to form much stronger complexes with humic substances than Eu. Both cations therefore may act as powerful competitors to Eu in acidic surface waters at $\text{pH} < 5$. However, in the pH region of groundwaters strong hydrolysis of Al and Fe(III) may prevent both cations from playing any role as competitors to Eu - humic substance complexation.

In summary, our scoping calculations indicate that the complexation of trivalent lanthanides and actinides with humic substance in groundwater can be considered in performance assessments as independent of pH, p_{CO_2} and ionic strength. Competition by other cations is expected to be very weak, and thus, a conservative estimate of humic complexation effects shows that a concentration of 10^{-6} g/l (or 1 ppb) of dissolved humic substance is sufficient to dominate the speciation of trace concentrations of trivalent lanthanides and actinides in groundwater.

Figure V.11: Contour plot of the concentration of humic substance (\log_{10} g/l) necessary to bind 90% of the total dissolved Eu. The solid lines show projections of the \log_{10} [humic substance] levels in Figure V.10 at ionic strength 0.1 M. The dashed lines are the analogous contour lines at ionic strength 0.02 M. The symbols correspond to pH and $p\text{CO}_2$ values of almost one thousand Swiss groundwater analyses.



Chapter VI

Metal Ion Binding by Humic Substances

James H. EPHRAIM
Department of Water and
Environmental Studies
Linköping University
S-581 83 Linköping (Sweden)

Bert ALLARD
Department of Water and
Environmental Studies
Linköping University
S-581 83 Linköping (Sweden)

VI.1. Introduction

Ionic interactions in natural waters are significantly influenced by the presence of natural organic acids which constitute a mixture of different molecules with varying size, containing different functional groups [82STE]. The present methods of extraction are used to divide these natural organic acids into two major categories; hydrophobic and hydrophilic acids. The terms hydrophobic or hydrophilic are defined by adsorption or non adsorption onto XAD-8 amberlite resins, respectively [81THU/MAL, 91MAL, 92PET]. Recent advances have shown that the hydrophobic properties increase with a decrease in pH while their hydrophilic properties increase with an increase in pH [85AIK/MCK, 89EPH/BOR]. Molecular size variations and their correlations with other parameters, *i.e.*, acidity, fluorescence, and turbidity have prompted researchers to postulate that these substances have fractal properties [94OST/MOR, 94SEN]. The solution chemistry of these organic acids, though not well understood, has aroused the interest of many researchers, *e.g.* [70GAM, 80GAM/UND, 80PER/REU, 85MAR, 86EPH/ALE, 92BAR/CAB]. Complicating factors influencing their solution chemistry have been identified as the functional group heterogeneity and the heterogeneity in the molecular size and shape leading to ionic strength effects [86EPH/ALE, 90WIT/RIE, 92TIP/HUR, 93WIT/RIE, 95EPH/PET].

The role that natural organic acids may play in the distribution and mobility of the trace metal ions in surface and ground water systems can be anticipated by examining their interactions with metal ions in the presence and absence of solid/particulates of

geologic origin [93EPH/ALL]. Fulvic and humic acids are normally used to represent natural organic acids in laboratory studies [78SCH, 79PER], as a complement to field studies. These acids which are hydrophobic at lower pH (~ 1) are the predominant species among the natural organic acids which sequester metal ions in solution [94BUR].

In this Chapter, the definition of natural organic acids (with emphasis on humic and fulvic acids), their isolation and characterisation methods, their interaction with metals, their redox properties and the methods of data acquisition and analyses will be presented. Additionally, implications with regard to nuclear waste management and recommendations will be provided.

VI.2. General overview

Humic and fulvic acids are defined as “a class of ubiquitous, biogenic, heterogeneous organic acids which do not belong to a known class of compounds” [82STE]. An intrinsic problem with this definition is the lack of uniqueness. It must be emphasised that the characteristics of any humic or fulvic acid sample depend primarily on the method of isolation/extraction.

These substances contain both Brønsted (proton-donating) and functional groups composed of hydrogen-bonding moieties, *e.g.*, carbohydrates [90PER/GJE]. The genesis of humic substances is envisaged to include processes like microbiological metabolism, mineralization, abiotic oxidation, photochemical processes, adsorption, precipitation and repolymerization [90PER/GJE].

In an attempt to promote inter-laboratory checks and collaboration, the International Humic Substances Society (IHSS) in 1983 adopted a standardized method of isolation/extraction of humic substances [85AIK/MCK]. However, a number of other methods of isolation are also described in the literature. Irrespective of the isolation methods, humic and fulvic acids seem to have certain general characteristics, *i.e.*, the presence of oxygen-containing functional groups, *e.g.*, $-\text{COOH}$, phenolic and enolic $-\text{OH}$, quinones and semi-hydroquinones, nitrogen-containing functional groups, $-\text{RNH}_2$, and sulphur-containing functional groups, $-\text{RSH}$. The presence of these functional groups is responsible for their high affinity for metal ions and other trace components in the environment [82STE].

The concentrations of humic substances in surface and ground waters depend on the concentration of total organic acid, TOC, which may be divided into particulate form and dissolved organic carbon, DOC. The separation of particulates from the dissolved organic carbon has normally been effected using filters with an arbitrary cut-off of 0.45 micron. The DOC in surface waters in the US has an average of $5 \text{ mg C} \cdot \text{l}^{-1}$ ranging from 1.5 to $10 \text{ mg C} \cdot \text{l}^{-1}$ [91MAL] with approximately 50% of humic substances. The DOC in groundwaters have concentrations ranging from 2 to $4 \text{ mg C} \cdot \text{l}^{-1}$. A generalization of these data is that the concentration of humic substances in aquatic environments range from $20 \mu\text{g} \cdot \text{l}^{-1}$ in groundwaters to $30 \text{ mg} \cdot \text{l}^{-1}$ in surface waters [81THU/MAL].

VI.2.1. Isolation and extraction of humic substances

The primary objective of any isolation/extraction procedure is to obtain a sample which is identical to the original material. The isolation is made to facilitate the laboratory studies needed to obtain information about the material and to understand and predict its behaviour in the environment. Various methods of isolation of humic substances in both aquatic and terrestrial environments have been developed to obtain samples that are free from contaminants, mainly metal-ions [81THU/MAL, 83MIL/TUS, 83PLE/JOS, 87GRE/POW, 91MAL, 92PET, 94PET/EPH]. However, there is a school which believes that the samples obtained by the various isolation methods may be chemically different from the non-isolated material. Hence, their studies of natural organic acids have utilised samples which have not been extracted [91MAE/ELE].

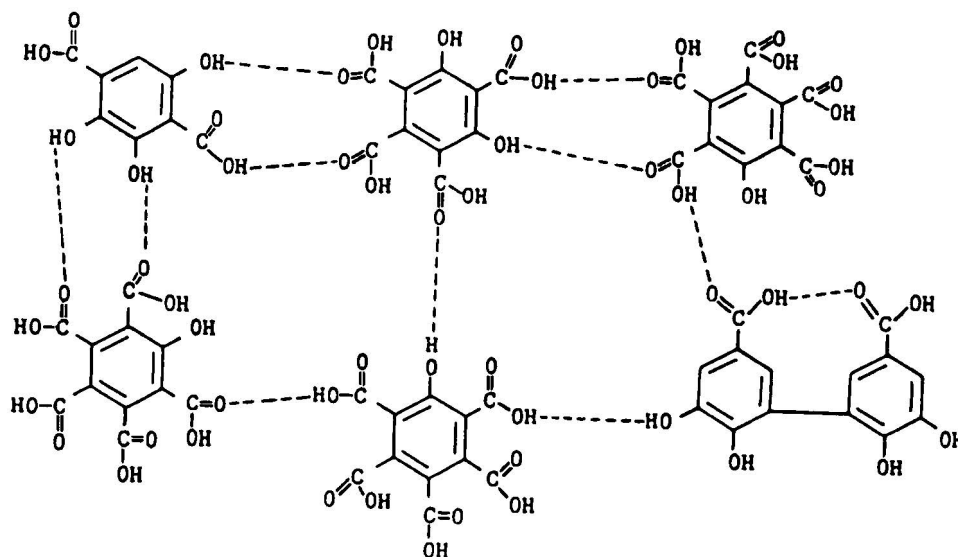
The isolation/extraction procedures are slightly different for material from terrestrial and aquatic environments. In the terrestrial environment, the procedure commonly used is alkali extraction [82STE]. In aquatic systems, the isolation consists of obtaining the hydrophobic and hydrophilic portions of the dissolved organic carbon (DOC) and determining the fractions which are acidic, basic and neutral, respectively. The method adopted by the IHSS, *i.e.*, the XAD-8 method, seems to be widely used by researchers [81THU/MAL]. However, a draw-back of this method is that it requires the addition of HCl to the water samples in order to reduce the pH, to render the fulvic and humic acids hydrophobic (so they can adsorb on XAD-8). Addition of HCl has been avoided in an alternative method where diethylaminoethyl (DEAE) cellulose has been employed to isolate the organic acids at their natural pH, before subsequent adsorption on XAD-8 resins [92PET]. There are arguments as to the similarity of the samples obtained from direct addition of HCl cum XAD-8 adsorption and DEAE cellulose cum XAD-8 adsorption methods. However, comparisons of humic substances extracted from various origins with different methods seem to indicate that these substances have much in common [94PET/EPH]. Another method of isolation of humic substances from aquatic environments involves the successive ultra-filtration of water sample through membranes of varying cutoff sizes, *i.e.*, 100 000, 10 000 and 1 000 daltons ¹ [91PEU/PIH].

VI.2.2. Characterisation methods

Humic and fulvic acids are characterised by using various analytical methods, such as elemental analysis, NMR, FTIR, UV-visible, *etc.* A considerable number of analytical methods have been employed in efforts to obtain a complete structure for fulvic and humic acids. These physicochemical methods also include ultracentrifugation, viscosity, colligative property measurements, light scattering techniques, gel chromatography and electrophoresis [89HAY/MCC]. Despite the advances in the state-of-the-art, structures for humic and fulvic acid have not been obtained. By using information on the reactive functional groups, elemental analysis potentiometric titration results and other chemical analyses [72SCH/KHA] together with known restrictions on the conformation, it is

¹ One "dalton" is one atomic mass unit: conversion factor to grams is 1.66024×10^{-24} .

Figure VI.1: Structure of fulvic acid as proposed by Schnitzer and Kahn. Reprinted with permission from [72SCH/KHA].



possible to deduce reasonable structure models for humic/fulvic acids (see Figure VI.1).

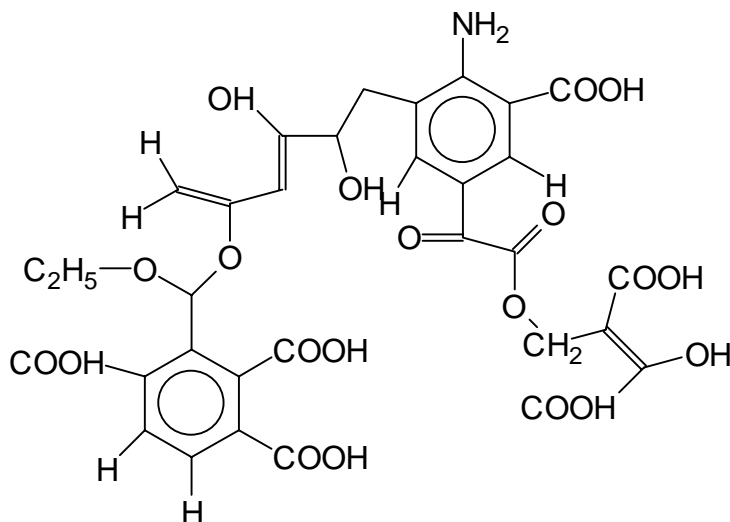
Such an exercise has been performed for an aquatic fulvic acid [89EPH/BOR] and the postulated structure for the fulvic acid shown in Figure VI.2 is not very different from those proposed by earlier researchers [60FLA, 66KON, 72SCH/KHA, 83HAR/BOR]. The extent of aromaticity is much lower, reflecting the origin of the fulvic acid from an aquatic environment.

Isolation of humic substances from aquatic environments normally yield small quantities of material, thus the selection of characterisation method is of vital importance. The criteria for the selection should be the attainment of maximum information through the employment of a minimum amount of sample. In a recent attempt, UV-visible, elemental analysis, total organic acid, potentiometric titrations and molecular weight determinations were considered an appropriate combination for the realisation of this requirement [94PET/EPH]. In such an exercise, it was concluded that fulvic acids extracted from different origins have large similarities.

Information obtained from the application of the various physicochemical analytical methods may be summarised as follows:

1. Humic substances are acidic and their acidity is primarily due to -COOH and phenolic or enolic -OH functional groups [70RAS/KIN, 78SCH, 80PER/REU, 80SAI/HAY]. Numerous attempts have been made to differentiate between the -COOH and -OH groups [82STE]. However, the most important parameter determining their properties in the aquatic environment is the total titratable acidity (which may or may not be a combination of the -COOH and -OH) [70GAM, 72GAM,

Figure VI.2: Hypothetical structure of Bersbo aquatic fulvic acid based on elemental analysis and potentiometric titrations in aqueous and non-aqueous media.



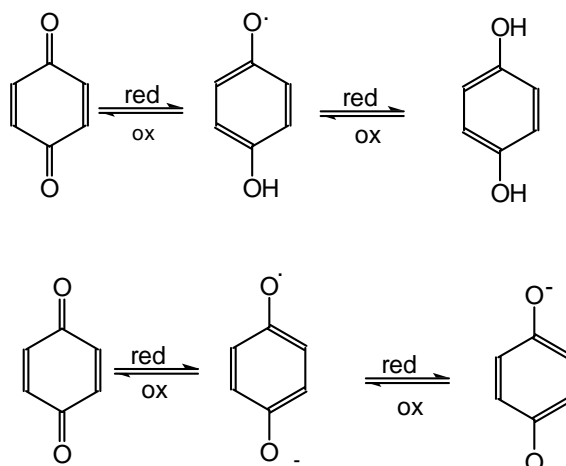
73GAM/SCH, 78PER, 79PER, 80PER/REU, 82GIL/RIL, 82STE, 83PER/LYT]. The titratable acidity is considered to be the value which the humic substance will exhibit under normal environmental conditions [86EPH/ALE]. This does not presuppose that only the titratable acidity will be involved in the complexation with trace metals and other low-molecular weight species. For 14 aquatic fulvic acid samples isolated from a variety of geographical locations (Sweden, Canada, Germany, USA) an average titratable acid capacity of $5.1 \text{ meq} \cdot \text{g}^{-1}$ of sample was obtained [91PET]. The range of acidity was 3.3 to $9.86 \text{ meq} \cdot \text{g}^{-1}$. These results are significantly lower than the corresponding values quoted for soil fulvic acids, where the average is $8.2 \text{ meq} \cdot \text{g}^{-1}$ and the range from 6.4 to $14.2 \text{ meq} \cdot \text{g}^{-1}$ [82STE].

2. Fulvic acids are smaller than typical polyelectrolytes, *e.g.*, poly-metacrylic acid, PMA [67TAN], and heterogeneous with respect to molecular size [69HAN/SCH]. The average molecular weight, M_n , for a number of aquatic fulvic acids is 1153 ± 376 daltons with a range from 660 to 1750 daltons [94PET/EPH]. These molecular weight distributions were determined via the use of gel filtration chromatography, which is normally considered to give higher values than the vapour pressure osmometric measurements [69HAN/SCH, 90MAR/RED]. The average value of M_n (1153 daltons) compares well with other reported values for fulvic acids [82STE, 85AIK/MCK]. The number-average molecular weight, M_n , is expressed as:

$$M_n = \frac{\sum n_i M_i}{\sum n_i}$$

where n_i is the number of molecules with molecular weight M_i . The weight-average

Figure VI.3: One-electron step reactions rationalising the redox properties of humic substances (Adapted from [90SEN]).



molecular weight, M_w , is correspondingly expressed as:

$$M_w = \frac{\sum w_i M_i}{\sum w_i}$$

where w_i is the total weight of molecules with molecular weight M_i . The ratio of M_w/M_n is equal to 1 for monodisperse materials and $M_w/M_n > 1$ for polydisperse substances [72SCH/KHA, 82STE, 94PET/EPH].

VI.2.3. Redox properties of humic substances

Humic substances have been observed to reduce oxidised forms of certain metal ions, examples of which are Fe(III) to Fe(II), Hg(II) to Hg(0), V(V) to V(IV) and also I_2 and I_3^- to I^- [81SKO/WIL, 84WAI/MOR]. From E_H /pH measurements, the following half-cell reaction for a particular fulvic acid was suggested:



with a potential of ~ 0.5 V (*vs.* NHE) [81SKO/WIL]. This potential will differ for different fulvic acid samples. The redox properties of humic substances have been attributed to the presence of phenols, quinones and semi-hydroquinones in the humic molecule and has been rationalised by one-electron redox reaction in solution as shown in Figure VI.3.

The redox properties of humic substances have been studied using EPR, ESR and Mössbauer spectroscopy [77SEN/CHE, 87GOO/CHE]. The oxidation of humic substances is very rapid as indicated by redox titrations with iodine and by photometric detection of the reaction with potassium ferricyanide [91MAT2]. The reaction was found to be complete within 48 hours.

VI.3. Solution chemistry of humic substances

The solution chemistry of these natural organic acids is not fully understood even though considerable advances have been made over the past decade. This short-coming is a consequence of a combination of factors, such as:

- the absence of a unique structure of humic substances,
- the variation in the methods of isolation and extraction,
- the absence of specific analytical methods suitable only for humic substances.

The complex nature of these compounds has made it necessary to develop simplified models to describe them and their chemical properties. The first problem with modelling lies with the manner in which they may be conceptualised. A study of the literature reveals the following examples:

1. Strongly associated aggregates of acids, each of comparatively low molecular weight [86WER].
2. An assemblage of identical “mean fulvic acid” units; a fulvic acid unit is a hypothetical macromolecule that contains one or more distinct classes of acidic functional groups [77SPO/HOL].
3. An oligoelectrolyte (intermediate between simple ions and true polyelectrolytes) composed of impenetrable charged spheres [92BAR/CAB].
4. An assemblage of relatively small amphiphilic moieties which are slightly different but composed of four to five predominant separate acidic sites, with each site characterised by a distribution of acidity constants round an average value [91EPH/RED].

VI.3.1. Proton interactions with humic substances

The concepts enumerated in previous section have led to the development of two major types of models, namely the discrete ligand approach and the continuous distribution approach.

VI.3.1.1. Discrete ligand models

In the discrete ligand approach, the observed protolytic and metal binding behaviour has been attributed to a limited number of predominant sites. Additionally, an electrostatic term has normally been employed to estimate the deviation from ideality in the polyelectrolyte as a result of the change in the electrostatic free energy of the macromolecule caused by group-group interaction accompanying the ionization process. A literature survey reveals that four sites are normally employed to account for the observed acid-base properties [77SPO/HOL, 86EPH/ALE, 88GRE/POW, 89EPH/BOR, 89EPH/BOR2]. However,

a number of researchers have employed three sites [88TIP/BAC, 90TIP/RED, 91FAL]. Five sites [89EPH/BOR] and six sites [85PAX/WED, 91PAX/WED] have also been used to describe the observed potentiometric behaviour of fulvic acids. The absence of a comprehensive method for estimating site-to-site interactions has resulted in their exclusion from the discrete ligand approach. In the school of discrete ligand approach, there exists subtle differences in the method of estimating the electrostatic effects, and the number of sites necessary to describe experimental results. Examples of the discrete ligand models used in the literature are given below.

VI.3.1.1.1. Tipping's model V

Ion binding by humic substances, which is described in terms of complexation at discrete sites, is postulated to be modified by electrostatic attraction and/or repulsion and non-specific binding due to counterion accumulation [92TIP/HUR, 93TIP]. In the model, variations in apparent binding strengths of the major proton-dissociating groups ($-\text{COOH}$, phenolic $-\text{OH}$) are described by using an electrostatic model involving a negative framework and counter-ions. Eight proton-dissociating sites are envisaged and the metal binding is postulated to occur either at a single proton-dissociating site (monodentate) or in a bidentate fashion. Electrostatic corrections are made using the expression e^{2wzZ} , where z is the charge on the cation, Z is the net charge on the humic framework, w is the electrostatic interaction factor obtained from the following:

$$w = P \log_{10} I$$

where I is the ionic strength, and P is an adjustable parameter [93TIP]. Additional counterion concentrations in the diffuse layer of the humic molecule are calculated using Donnan expressions [93MAR] with the volume of the diffuse layer, V_D calculated by:

$$V_D = \left(10^{-3} \frac{4\pi N_A}{3 M_w}\right) \left[\left(r + \frac{1}{K_{\text{DH}}}\right)^3 - r^3 \right]$$

where N_A is Avogadro's number, M_w is the humic molecular weight, r is the radius of the humic molecule, and K_{DH} a Debye-Hückel parameter which depends on the ionic strength and is a measure of the diffuse layer. The humic molecule is considered as a rigid sphere to permit the application of the Debye-Hückel model.

Tipping's model V contains seven adjustable parameters for fitting proton dissociation and two parameters additionally for each cation that can bind at the acid-dissociating sites [92TIP/HUR, 93TIP].

VI.3.1.1.2. The oligoelectrolyte model

In the recent oligoelectrolyte model [92BAR/CAB], humic substances are again represented as impenetrable spheres and the electrostatic effect is calculated using approximations of the nonlinear Poisson-Boltzmann equation. The "local" concentration of metal

ion near the charged polyions, $[M^{z+}]_{\text{loc}}$, is related to the concentration of the metal ion in the bulk solution, $[M^{z+}]$, as follows:

$$[M^{z+}]_{\text{loc}} = \lambda^z [M^{z+}]$$

where the electrostatic factor, λ , is given by:

$$\lambda = \exp\left(\frac{-F\Psi_0}{RT}\right) \quad (\text{VI.1})$$

where Ψ_0 is the electrostatic potential at the surface of the sphere, F is Faraday's constant, R is the universal gas constant and T the absolute temperature. The electrostatic factor can also be interpreted as a ratio of polyion activities when the aqueous components are diffusible into the polymer network, just as in the case of Donnan equilibrium [93MAR]. The model consists of a total of 14 parameters which may be reduced to 9 [92BAR/CAB]. This model was successfully employed to explain pH and copper titration data by considering two copper binding sites and an additional acidic site. The authors claim that the model is simplistic and minimises the number of arbitrary fitting parameters. That much emphasis is placed on just data-fitting is a disadvantage of the model.

VI.3.1.1.3. The Gibbs-Donnan polyelectrolyte two phase model

New advances in the description of proton and metal ion binding by humic substances have been made by the adaptation of an approach originally designed for synthetic polyelectrolytes to humic substances [84MAR/RED, 84MAR/RED2, 85MAR, 88MAR/RED, 93MAR]. The approach which is based on the Gibbs-Donnan equilibrium fits into the discrete model category.

In typical polyelectrolyte solutions, the intrinsic microscopic acid dissociation constant of the repeating functional group HA is defined by:

$$K_a^{\text{intr}} = a_{\text{H}^+}(\text{surf}) \left(\frac{\alpha}{1 - \alpha} \right) \quad (\text{VI.2})$$

where $a_{\text{H}^+}(\text{surf})$ represents the activity of the hydrogen ions at the charged surface of the polyelectrolyte while α , the degree of neutralization, is an experimental quantity. The activity of the hydrogen ion in the bulk solution a_{H^+} , the other experimental quantity, is related to $a_{\text{H}^+}(\text{surf})$ by the Boltzman expression:

$$a_{\text{H}^+}(\text{surf}) = a_{\text{H}^+} e^{-F\Psi/RT} \quad (\text{VI.3})$$

where Ψ is the difference in potential between the charged polymer surface and the bulk of the solution, F is Faraday's constant, R is the universal gas constant and T is the absolute temperature. Incorporation of Eq. (VI.3) into Eq. (VI.2) gives the following equation²:

$$\text{p}K_a^{\text{intr}} = \text{p}K_a^{\text{app}} + (0.434 F\Psi/RT) \quad (\text{VI.4})$$

² In this Chapter the "p" nomenclature is widely used: $\text{p}K$, pH , pM , *etc.*, are symbols for $-\log_{10} K$, $-\log_{10} a_{\text{H}^+}$, $-\log_{10} a_{\text{M}}$, *etc.*

where pK_a^{app} is defined as $\text{pH} - \log_{10}[\alpha/(1 - \alpha)]$.

Thus for typical polyelectrolytes, a plot of pK_a^{app} versus α extrapolated to $\alpha = 0$ (Ψ approaches zero as α approaches zero) for any ionic strength gives the intrinsic constant, pK_a^{intr} . The effect of ionic strength upon such a plot comes from its influence upon the value of Ψ as α is varied. With crosslinked polyelectrolytes (gels), the pH inside the gel is not accessible to direct measurements. Hence, a study of the polyelectrolyte properties of weakly acidic gels has to be based upon the pH of the external solution phase in equilibrium with the gel phase. These properties have been observed to be a sensitive function of the water content of the gel (which depends on the flexibility of its matrix) and the ionic strength of the aqueous medium. At equilibrium, during each step of the potentiometric titration of a weakly acidic polymer gel, HA, in the presence of a simple background electrolyte, MX, the chemical potential, μ , of the *diffusible* components, HX, MX and H₂O are equal in both phases:

$$\begin{aligned}\mu_{\text{HX(aq)}} &= \mu_{\text{HX(gel)}} \\ \mu_{\text{MX(aq)}} &= \mu_{\text{MX(gel)}} \\ \mu_{\text{H}_2\text{O(aq)}} &= \mu_{\text{H}_2\text{O(gel)}}\end{aligned}$$

where “aq” and “gel” identify respectively the aqueous solution and the gel phases. By assuming that the chemical potential in isothermal systems may be divided into two terms, one of which depends only on the composition and the other on pressure, the μ of each component i ($i = \text{HX}, \text{MX}, \text{H}_2\text{O}$) in a solution of ionic strength $I = [\text{MX}]$ and under a pressure p is given by

$$\mu_i(p, I) = \mu_i(p^\circ, I) + (p - p^\circ)V_i \quad (\text{VI.5})$$

where p° is the standard pressure, 1 bar, and V_i is the partial molar volume of component i . V_i might be assumed to be independent of composition and pressure without introduction of significant error. The activity, a_i , of the i^{th} component is defined by

$$\mu_i(p^\circ, I) = \mu_i^\circ(p^\circ) + RT \ln a_i \quad (\text{VI.6})$$

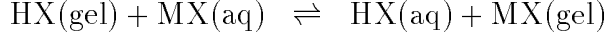
where μ_i is the chemical potential of the i^{th} component in the standard state. Combination of Eqs. (VI.5) and (VI.6) yield the following:

$$\mu_i(p, I) = \mu_i^\circ(p^\circ) + RT \ln a_i + (p - p^\circ)V_i \quad (\text{VI.7})$$

The chemical potentials of MX and HX in each phase are thus given by

$$\begin{aligned}\mu_{\text{HX(aq)}} &= \mu_{\text{HX(aq)}}^\circ + RT \ln a_{\text{HX(aq)}} + (p - p^\circ)V_{\text{HX(aq)}} \\ \mu_{\text{HX(gel)}} &= \mu_{\text{HX(gel)}}^\circ + RT \ln a_{\text{HX(gel)}} + (p - p^\circ)V_{\text{HX(gel)}} \\ \mu_{\text{MX(aq)}} &= \mu_{\text{MX(aq)}}^\circ + RT \ln a_{\text{MX(aq)}} + (p - p^\circ)V_{\text{MX(aq)}} \\ \mu_{\text{MX(gel)}} &= \mu_{\text{MX(gel)}}^\circ + RT \ln a_{\text{MX(gel)}} + (p - p^\circ)V_{\text{MX(gel)}}\end{aligned}$$

For the system described above, the equilibrium expression for the reaction



is

$$\begin{aligned} RT \ln \left[\frac{a_{\text{HX}(\text{aq})} a_{\text{MX}(\text{gel})}}{a_{\text{HX}(\text{gel})} a_{\text{MX}(\text{aq})}} \right] + \Pi (V_{\text{MX}(\text{aq})} - V_{\text{HX}(\text{aq})}) \\ = \mu_{\text{HX}(\text{gel})}^{\circ} + \mu_{\text{MX}(\text{aq})}^{\circ} - \mu_{\text{HX}(\text{aq})}^{\circ} - \mu_{\text{MX}(\text{gel})}^{\circ} \end{aligned} \quad (\text{VI.8})$$

where Π is the osmotic coefficient, which is equal to $(p - p^{\circ})$ as expressed in Eq. (VI.7).

By choosing the same standard state in the gel and solution phases for the reacting components, the sum on the right hand side of Eq. (VI.8) is zero, and assuming that the $\Pi (V_{\text{MX}(\text{aq})} - V_{\text{HX}(\text{aq})})$ term is small enough to neglect, the following expression is obtained:

$$\ln \left[\frac{a_{\text{HX}(\text{aq})} a_{\text{MX}(\text{gel})}}{a_{\text{HX}(\text{gel})} a_{\text{MX}(\text{aq})}} \right] \approx 0$$

By the substitution of the product of single ion activities, this equation may be expressed:

$$\frac{a_{\text{H}^+} a_{\text{X}^-} a_{\text{M}^+ (\text{gel})} a_{\text{X}^- (\text{gel})}}{a_{\text{H}^+ (\text{gel})} a_{\text{X}^- (\text{gel})} a_{\text{M}^+} a_{\text{X}^-}} = 1$$

where cancellation of activities yields the following:

$$\text{pM} - \text{pH} = \text{pM}_{(\text{gel})} - \text{pH}_{(\text{gel})} \quad (\text{VI.9})$$

The value of pM and pH are experimentally measureable or calculable in these systems; the concentration of M^+ in the gel phase, $\text{pM}_{(\text{gel})}$, is also accessible since to preserve electroneutrality in the gel during neutralization with standard base, the concentration of M^+ must be at least equal to the concentration of the deprotonated form of the gel, $[\text{A}^- (\text{gel})]$ (except for the relatively very small quantity of $\text{H}^+ (\text{gel})$ present). The concentration of A^- (the deprotonated form of the gel) is calculable from the stoichiometry of the neutralization reaction and the measured volume, V_g , of the gel,³ while $[\text{MX}(\text{gel})]$ can either be determined experimentally or estimated with the following equation:

$$([\text{MX}(\text{gel})] + [\text{A}^-]) [\text{MX}(\text{gel})] \approx [\text{MX}]^2 \quad (\text{VI.10})$$

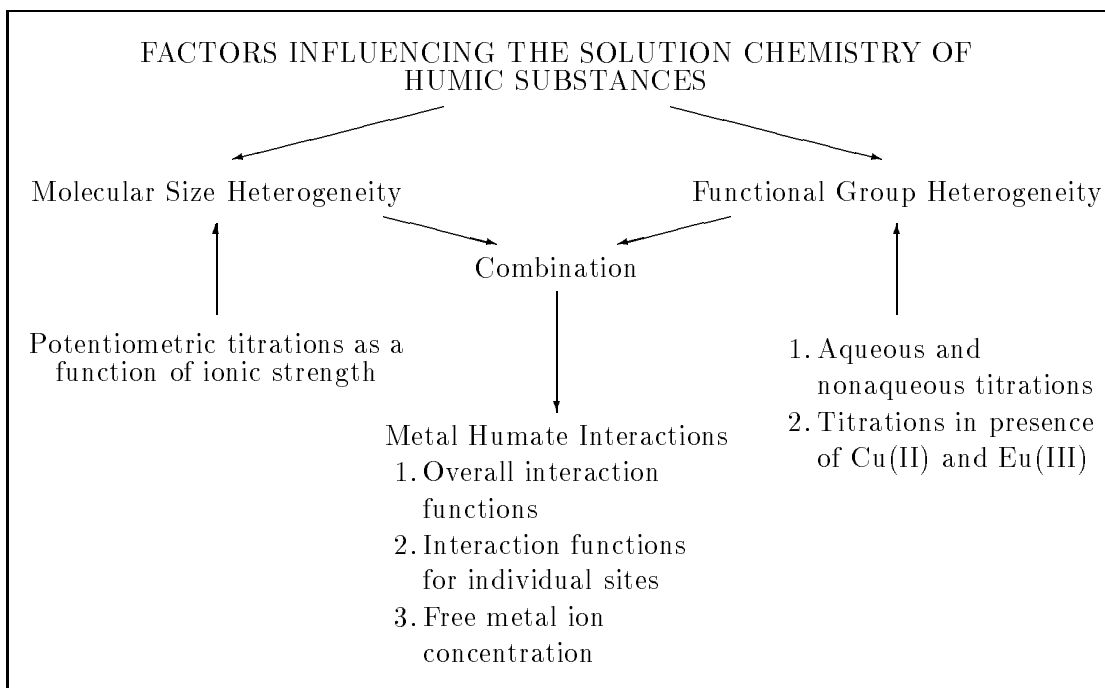
Incorporation of Eq. (VI.9) into the Henderson-Hasselbach equation ($\text{p}K_a = \text{pH} - \log_{10}\{\alpha/(1 - \alpha)\}$) yields:

$$\text{p}K_a^{\text{app}} - \text{p}K_a^{\text{intr}} = \text{pM} - \text{pM}_{(\text{gel})}$$

where $\text{p}K_a^{\text{app}}$ is the negative logarithm of the apparent dissociation constant of the weak acid repeated in the polyelectrolyte and $\text{p}K_a^{\text{intr}}$ corresponds to its intrinsic (thermodynamic) constant. The difference between polyelectrolyte gels and their linear analogs is

³ All concentrations in the gel phase have units of: $\text{mol} \cdot (\text{l of gel})^{-1}$.

Figure VI.4: Stages of the Gibbs-Donnan based program as adapted to metal-humate systems.



due to a difference in charge distribution. The separate well-defined phases of the gel-salt systems are electroneutral, the counterion enriched domain and the solution external to it in the linear analogs are not. The negative charge due to the fractional release of counterions from the polyelectrolyte domain is balanced by the equal positive charge they produce in the aqueous solution phase [88MAR/RED].

An important advantage of the Gibbs-Donnan two phase model derives from the capability it provides for separating the perturbations due to ionic strength effects and functional group heterogeneity [86EPH/ALE, 89EPH/BOR]. Figure VI.4 shows the various stages of the program used in the application of this approach to metal-humate systems [91EPH/RED].

In the literature, humic substances are normally considered as spheres or cylinders [90WIT/RIE, 92BAR/CAB, 92TIP/HUR, 93WIT/RIE, 93WIT/RIE2], but such *a priori* assumptions are avoided in this model. Instead, experimental data (aqueous titrations as a function of ionic strength) are used to obtain insight into the configuration of the humic substances in solution.

In the discrete ligand models, attempts are made to correct for perturbations of the measured concentrations of counterions, *e.g.*, H^+ and M^{z+} , by using the electrostatic term, $\exp(-F\Psi/RT)$. Such electrostatic terms are normally calculated by assuming that the humic substances are spherical to allow the use of the proper form of the Boltz-

man distribution [90WIT/RIE, 92BAR/CAB, 92TIP/HUR, 93WIT/RIE]. However, in the Gibbs-Donnan model, this term which is expressed as a counterion concentration term, is determined experimentally [86EPH/ALE, 89EPH/BOR, 91EPH/RED]. In the adaptation of the Gibbs-Donnan model to humic substances the chemistry of the humic substance as a ligand is emphasized. The stages of the approach are presented in the following paragraphs.

Based on the assumption that humic substances are composed of four to five separate acidic moieties, the potentiometric titrations are interpreted at the ionic strength where separate phase effects are minimal. The steps involved in assigning $pK_{a,i}$ values to the envisaged acidic moieties are presented below:

1. Four to five “average” sites and their respective abundances are estimated from nonaqueous titrations and titrations in presence of increasing amounts of Cu(II) and Eu(III) or La(III).
2. Initial guesses of their $pK_{a,i}$ values are made.
3. The degree of neutralization of each of the envisaged “average” sites, α_i , is computed using the following equation:

$$\alpha_i = \left(1 + 10^{(pK_{a,i} - pH)}\right)^{-1} \quad (\text{VI.11})$$

for the “critical” bulk electrolyte concentration. The “critical” bulk electrolyte concentration is the concentration after which no ionic strength effects are observed on the pK_a vs. degree of neutralization, α curve (determined to be $I = 1.00$ M) [86EPH/ALE].

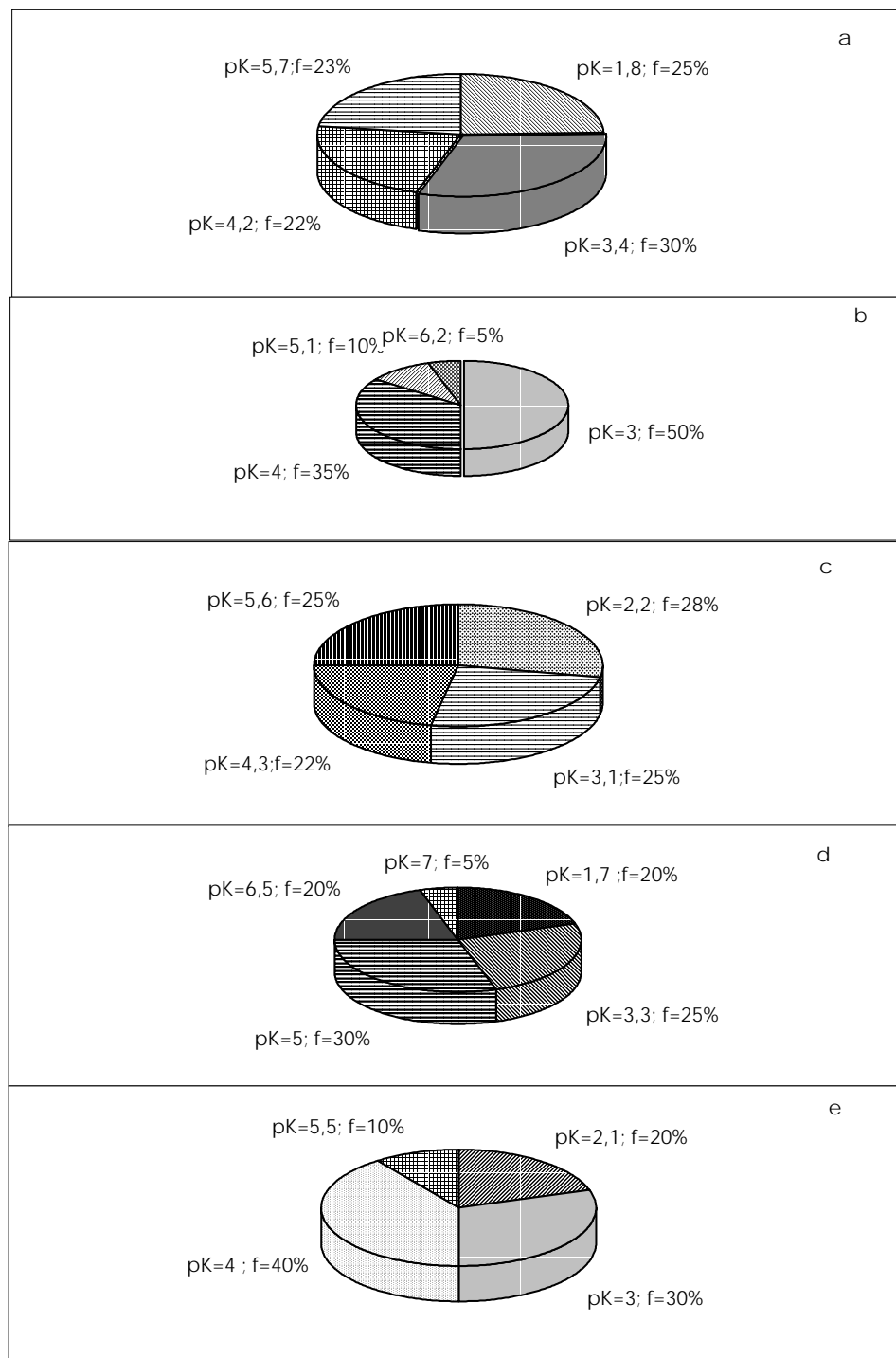
4. Steps 1 and 2 above are changed until the following relationship is achieved:

$$\sum(\alpha_i f_i) \cong \alpha_{\text{computed}} \cong \alpha_{\text{experimental}} \quad (\text{VI.12})$$

or the residual $|\alpha_{\text{computed}} - \alpha_{\text{experimental}}|^2$ reaches a minimum for the set of data points. In Eq. (VI.12), α_i is the degree of ionization for each acid site, f_i is the fraction of the total acid capacity due to the i^{th} site (determined in aqueous titrations), α_{computed} and $\alpha_{\text{experimental}}$ are the overall computed and experimental degree of neutralization, respectively [86EPH/ALE, 89EPH/BOR].

Details of the application of this model to the description of the solution chemistry of humic substances are presented elsewhere [86EPH/ALE, 89EPH/BOR, 95EPH/PET]. Examples of site heterogeneity assignments to a number of fulvic acid samples achieved by the application of the Gibbs-Donnan model are shown in Figure VI.5, where it is apparent that a large fraction of fulvic acids have a pK_a^{app} values under 4.0 suggesting $-\text{COOH}$ functionality which is corroborated by the good agreement between aqueous acid capacity and the $-\text{COOH}$ capacity in non-aqueous titrations [95EPH/PET]. The assignment of site heterogeneity facilitates the design of experimental methods with the aim of elucidating the functionality spectrum in the humic substance molecule [89EPH/BOR2, 92ARS/BOR].

Figure VI.5: Site heterogeneity assignments to a number of fulvic acid (FA) samples, f=percentage of each acid site: *a* = Armadale FA [86EPH/ALE]; *b* = Fanay-Augères FA [94PET/EPH]; *c* = Suwanee River FA [91EPH/RED]; *d* = Bersbo FA [89EPH/BOR]; and *e* = Finnsjön FA [89EPH/BOR2].



VI.3.1.1.4. *An example of the Gibbs-Donnan Approach to Humic Substance Systems*

In all of the models employed to describe proton and metal ion binding to humic substances, the need to make electrostatic corrections to the measured experimental parameters, H^+ , M^{z+} , are of utmost importance. For the proton, this correction term is obtained by the relationships in Eqs. (VI.1), (VI.3), and (VI.4).

The assumption in the Gibbs-Donnan approach is that with subsequent increase in ionic strength, I , the electrostatic contribution to the pK_{app} term decreases until I reaches a “critical value” where further increase in I has no effect on the pK_{app} ($I \geq 1.0$ M). In the Gibbs-Donnan approach, the electrostatic term is designated ΔpK defined as:

$$\Delta pK = pK_{app} - pK_{intr} = (-0.434 F\Psi/RT)$$

An example of the approach as employed to Laurentide fulvic acid [95MAT/EPH] is shown in Figs. VI.6 and VI.7. In Fig. VI.6, the pK_{app} vs. the degree of neutralization is shown for the five different ionic strength ($I = 0.001, 0.01, 0.10, 1.0, 5.0$ M). Note that the curves for $I = 1.0$ and 5.0 M are superimposed indicating that the critical ionic strength has been reached. In Fig. VI.7, the electrostatic term (designated ΔpK) as defined in the above equation, is shown as a function of degree of neutralization for the three ionic strengths, $0.001, 0.01$ and 0.10 M.

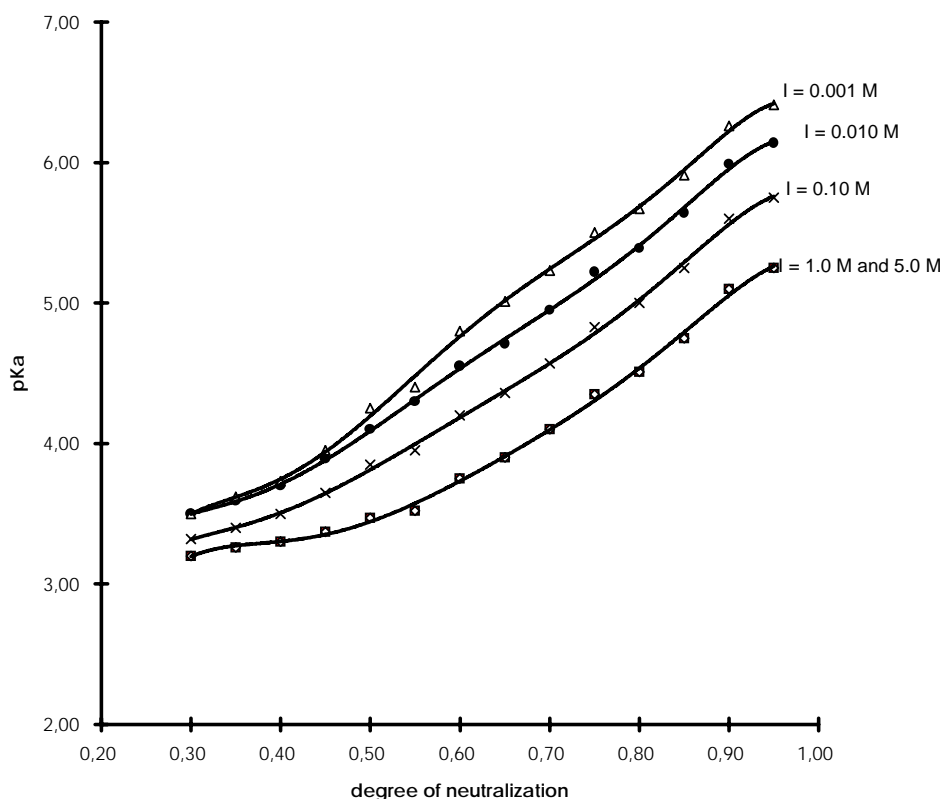
The heterogeneity factor obtained from non-aqueous titrations and titrations in the presence of Cu(II) and La(III)/Eu(III) is thus employed in conjunction with Eqs. (VI.11) and (VI.12) to obtain the predominant acidic moieties in the humic substance. An example of the exercise as applied to the Laurentide fulvic acid [95MAT/EPH] is shown in Table VI.1.

VI.3.1.2. *Continuous distribution models*

In the continuous distribution model, the properties of the various sites are assumed to overlap, thus justifying the use of statistical methods for their estimation. Variations of these models, discussed in Chapter V are presented briefly below.

- *The affinity distribution model* [83SHU/COL, 87BUF/ALT, 90WIT/RIE, 93WIT/RIE, 93WIT/RIE2]. In the application of the continuous distribution model to the acid-base properties of natural organic acids (humic and fulvic acid), the overall acidity is factored into two where a lower pK_a value, normally around 4.2, represents the carboxylic distribution, while a higher pK_a value, normally around 9.1, represents the phenolic distribution [93WIT/RIE, 93WIT/RIE2]. This division yields an equivalent result as in the discrete approach by considering two major acidic sites.
- *The normal distribution model* [83PER/LYT, 87PER/PAR]. The Gaussian distribution model has been employed to distinguish a two ligand mixture from a continuous distribution of ligands [83PER/LYT].

Figure VI.6: Plot of pK_a^{app} versus α (the degree of neutralization) for Laurentide fulvic acid as a function of ionic strength (note: data at $I = 1$ and 5 M are exactly superimposable).



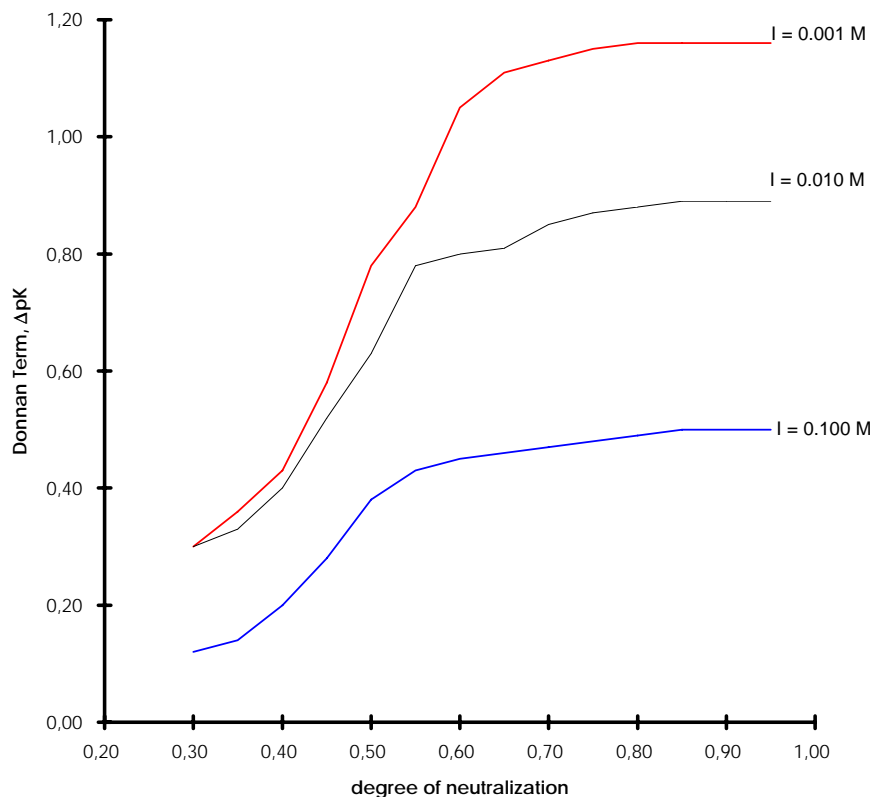
- *The differential equilibrium function model.* A continuous distribution of sites is assumed where the macroscopic binding functions are interpreted in terms of the microscopic binding constants [80GAM/UND, 88ALT/BUF, 88GAM/LAN].

VI.3.1.3. Discrete models versus continuous distribution models

The choice of which model to employ in the description of metal-humate interactions depends on the objective of the data analysis. The discrete ligand approach is easily adapted to experimental data using graphical methods [84FIT/STE] and as such amenable to the prediction of metal-humate interactions by incorporation into existing chemical speciation computer programs, *e.g.*, FITEQL [94HER/WES]. The disadvantages of the discrete ligand model are that the identified ligands may not be representative of the actual binding sites in the humic substance, the difficulty to extend it outside the range of calibration and the tendency to underestimate metal humate interactions at very low metal ion concentration [86DZO/FIS].

Whereas the continuous distribution models probably approach the complexity of nat-

Figure VI.7: Variation of the Donnan potential term, δpK , with the degree of neutralization of Laurentide fulvic acid at three different ionic strengths. The curves have been obtained from the experimental data in Figure VI.6.



ural organic acids, their shortcoming is their inability to describe and predict the sequestering of metal ions. It has been argued that a continuous distribution model serves primarily as a first step towards identifying the most probable distribution of the acidic functionalities in natural organic acids [86DZO/FIS]. In effect, the application of the affinity distribution model [90WIT/RIE, 93WIT/RIE] is intrinsically similar to the discrete model when applied to humic substances [92BAR/CAB, 92TIP/HUR].

VI.3.2. Models for the interaction of metals with humic/fulvic acids

While both the discrete ligand and continuous distribution models recognise the heterogeneous multiligand nature of humic substances, their differences lie in the modelling of the substances and thus their approach of describing their interaction with metal ions [86DZO/FIS].

In situations where very little is known about the nature of humic substances, an “average” approach may be employed. An example of such an “average” approach is presented later in this chapter where the effect of humic substances on the speciation of

Table VI.1: Comparison of experimentally based overall degree of dissociation, $\alpha_{\text{exp}}^{\circ}$, of Laurentide fulvic acid in 1.00 M NaNO_3 with the summation of computed contributions of five different acid sites to overall degree of dissociation, $\alpha_{\text{calc}}^{\circ}$.

Acid Site Identity	$\text{p}K_{a,n}^{\text{int}}$	Acid Site Abundance, A_n	Acid Moiety
1	1.7	0.32	Carboxylic
2	3.0	0.21	Carboxylic
3	4.0	0.204	Carboxylic
4	5.1	0.14	Alcoholic OH
5	6.5	0.126	Alcoholic OH

$\alpha_{\text{calc}}^{\circ} = \sum \alpha_n A_n$							
pH	$\alpha_1 A_1$	$\alpha_2 A_2$	$\alpha_3 A_3$	$\alpha_4 A_4$	$\alpha_5 A_5$	$\alpha_{\text{calc}}^{\circ}$	$\alpha_{\text{exp}}^{\circ}$
3.434	0.314	0.154	0.044	0.003	0.000	0.514	0.511
3.516	0.315	0.161	0.050	0.004	0.000	0.530	0.526
3.607	0.316	0.168	0.059	0.004	0.000	0.548	0.549
3.725	0.317	0.177	0.071	0.006	0.000	0.570	0.570
3.869	0.318	0.185	0.087	0.008	0.000	0.598	0.598
3.953	0.318	0.189	0.097	0.009	0.000	0.613	0.616
4.178	0.319	0.197	0.123	0.015	0.001	0.654	0.657
4.324	0.319	0.201	0.138	0.020	0.001	0.679	0.681
4.725	0.320	0.206	0.172	0.042	0.002	0.741	0.744
5.014	0.320	0.208	0.186	0.063	0.004	0.781	0.783
5.359	0.320	0.209	0.195	0.090	0.009	0.823	0.827
5.833	0.320	0.210	0.201	0.118	0.022	0.871	0.874
6.453	0.320	0.210	0.203	0.134	0.060	0.927	0.924
6.794	0.320	0.210	0.204	0.137	0.084	0.954	0.949

Eu(III) in the environment is anticipated.

In both the discrete ligand and continuous distribution models, a mass-action parameter equivalent to the overall complex formation function, β_{ov} , is calculated as follows:

$$\beta_{\text{ov}} = \frac{\Sigma[\text{M}]_{b,i}}{[\text{M}^{z+}] \gamma_{\text{M}} \exp\left(\frac{-F\Psi}{RT}\right) \Sigma[\text{A}_i^-]} \quad (\text{VI.13})$$

where $\Sigma[\text{M}]_{b,i}$ is the sum of the concentrations of metal bound to all active sites; $[\text{M}^{z+}]$ is the free metal ion concentration; γ_{M} is the single ion activity coefficient of the metal ion under study; $\exp(-F\Psi/RT)$ is the electrostatic term [90WIT/RIE, 92BAR/CAB, 92TIP/HUR, 93WIT/RIE, 93WIT/RIE2] and $\Sigma[\text{A}_i^-]$ is the concentration of the dissociated portion of the fulvic acid molecule [91EPH/RED]. The model for the electrostatic term in the expression for β_{ov} for systems with metal ions has been recently questioned

[92BAR/CAB]. However, for systems with trace quantities of metal ions, *i.e.*, very high ligand to metal ion ration, the choice of the electrostatic term will introduce very small errors.

The overall complex formation function, β_{ov} , is not a thermodynamic quantity describing the various binding patterns to the various complexing sites. However, it can be used to compare, on a macroscopic level, results obtained from different experimental techniques [83TUS/BRE, 89EPH/XU]. Additionally, the overall complex formation function can be used in the three component system, metal ion – inorganic oxide – humic substances, to quantify the influence of humic substances on the adsorption of metal ions on such oxides [89XU/EPH].

VI.3.2.1. Discrete ligand models

This approach considers the humic substance as a heterogeneous multiligand, which could potentially bind metal ions both with and without the release of protons. The extent of proton release is a direct function of the pK_a of the acid and the free energy of complex formation, $\Delta_r G_m^\circ$. The overall equilibria may be described by considering each acid site to bind at most one metal-ion as follows:



This representation implies that at equilibrium, each active site, S_i , forms the “complex” $S_i M$. All these “species” are in equilibrium with each other and their relative concentrations are determined by their respective free energy of complexation, $\Delta_r G_m^\circ(S_i M)$. It is necessary to note that in this model, site-to-site interactions have not been incorporated, not because they do not exist, but rather because there is no method available for their determination. Combination of this bonding model with the acid-base properties as defined by the discrete ligand model [86EPH/MAR, 89EPH/MAR, 90TIP/RED, 92TIP/HUR, 92BAR/CAB] yields the following expression:

$$\left(\frac{\theta_M}{(1 - \theta_M)} \right) \frac{1}{[HA]_{TOT}} = \sum_{i=1}^n \left(\frac{\beta_i f_i}{1 + \frac{[H^+] \exp\left(\frac{-F\Psi}{RT}\right)}{K_i} + \beta_i [M^{z+}]_f \left(\exp\left(\frac{-F\Psi}{RT}\right)\right)^z} \right)$$

where θ_M is the fraction of metal bound, $[HA]_{TOT}$ is the total titratable acid in the system, β_i is the complex formation constant for reaction (VI.14), f_i is the fraction of the i^{th} site, K_i is the acid dissociation constant of the i^{th} site, and $\exp(-F\Psi/RT)$ is the electrostatic term which is obtained from potentiometric titrations of metal-free systems.

The binding of copper by a well characterised aquatic fulvic acid has been successfully described by this model [94EPH/ALL]. Furthermore, the various ways of bonding of Cu(II) in a soil fulvic acid have been suggested recently, following a modification of an earlier algorithm which takes the functional group heterogeneity existent in the fulvic acid [86EPH/MAR, 95MAR/RED] into account. In both cases mentioned above, stability

constants reported for the interaction between Cu(II) and the acid group postulated to be present in the fulvic acid have been employed.

The prediction of proton and metal ion binding to humic substances under different environmental conditions has also been made using with Tipping's model V [92TIP/HUR, 93TIP]. By using two types of acid groups, a good fit is obtained for the binding of copper by fulvic acid.

VI.3.2.2. Continuous distribution models

The Gaussian distribution model has been adapted to take competition between different metal ions into account (MINTEQA2) and employed to describe the binding of Al(III) and Cu(II) by humic substances [94ALL/PER]. An improvement in the model performance is obtained when both carboxylic and phenolic sites are incorporated into the calculations.

The affinity distribution model has also been extensively used to describe metal-humate interactions. A two pK_a model for the competitive binding of metal ions to humic substances [93WIT/RIE2] has been modified to a non-ideal competitive adsorption model (NICA) to describe the binding of H^+ , Cd(II), Cu(II), and Ca(II) to humic substances [95BEN/MIL]. To effect a satisfactory prediction of the experimental results, two classes of acidic functionalities are employed – the first with a median pK_a of 4.60, is assumed to be a carboxylic acid group, while the second with a median pK_a of 9.34, could refer to phenol, alcohol and enol- groups.

VI.3.2.3. Factors affecting the overall complex formation function

The overall complex formation function as expressed by Eq. (VI.13) assumes a 1:1 complex between the metal ion and the humic ligand. This assumption does not take the functional site heterogeneity of the humic substance molecule into consideration [93NOR/EPH, 94EPH/ALL]. The overall complex formation function is affected by ionic strength, pH, temperature, ratio of metal ion to humic substance and experimental method [78BRE/GRA, 79BER/KRA, 80LI/VIC, 83ALB/GIE, 83TUS/BRE, 85GAM/MAR, 87BUF/ALT, 88BUF, 89EPH/XU, 91EPH].

The effect of pH on the overall complex formation function for Eu(III) has been found to be method dependent [91EPH]. For example, while a pH dependence of the overall complex formation function was observed for the Eu(III)-fulvate system studied by the ion exchange distribution method, no such variation was observed using the ultrafiltration technique [91EPH, 93NOR/EPH, 94NOR]. Application of laser-induced fluorescence [91BID/GRE] and laser-induced photoacoustic spectroscopy [93KIM] gave a complex formation function which was not strongly dependent on pH in the range investigated. It must be pointed out that in both studies [91BID/GRE, 93KIM] buffers were employed while the other studies were made in the absence of buffers.

The effect of ionic strength on metal-humate interactions may be illustrated by the ratio of metal bound to free metal for the Eu(III)-fulvate system (Figure VI.8). A higher ratio of metal bound to free metal is obtained at a lower ionic strength (0.01 M NaClO₄) than at

the higher ionic strength (0.10 M NaClO₄). For the Eu–FA system, $\log_{10}([M]_b/[M^{z+}])_{0.01} - \log_{10}([M]_b/[M^{z+}])_{0.1}$ is $\approx 1.5 \log_{10}$ units using the ion exchange distribution technique, while the corresponding difference for the ultrafiltration method is $\approx 0.5 \log_{10}$ units. A theoretical value of $3 \log_{10}$ units difference is expected (as $\log_{10}(0.1/0.01)^3$). The fact that $\Delta \log_{10}([M]_b/[M^{z+}])_{I=0.01-0.1}$ is 1.5 instead of the theoretical value of 3 has been attributed to the small size of the fulvic acid molecule (as compared to typical synthetic polymers) and the functional group heterogeneity existent in the fulvic acid [86EPH/ALE]. However, the values indicate that the ion exchange distribution method yielded values much more sensitive to ionic strength effects, while the results of the ultrafiltration method were less sensitive to such effects [93NOR/EPH]. The discrepancy between these observations may be attributable to the differences in the experimental methods. In the ion exchange distribution method, the reactions involve an exchange of Eu(III) for Na⁺ in the resin. This reaction is strongly influenced by the ionic strength as shown by plots of $\log_{10} D_o$ versus $\log_{10} a_{\text{NaCl}}$. D_o is the distribution coefficient of Eu(III) in absence of fulvic acid, and a_{NaCl} is the activity of the bulk electrolyte [89EPH/MAR]. In the ultrafiltration method, filtration under pressure is effected under conditions where the bulk electrolyte has a retention coefficient of zero for the membrane. Hence, the effect of the ionic strength on the ratio of metal bound to free metal is expected to be minimal since the dependence of free metal determination on the bulk electrolyte concentrations is very small.

VI.3.2.4. Competitive binding of various metal ions to humic substances

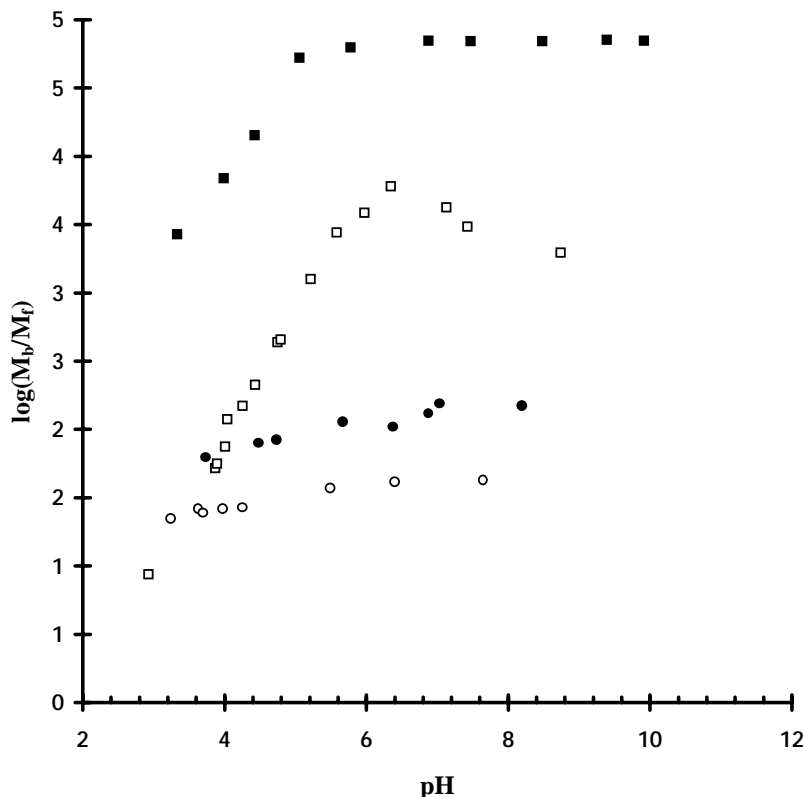
Different metals have different affinities for different ligands [81STU/MOR]. Metals have been classified using their affinity for the first ligand atom of each periodic group (*i.e.*, F, O, N) or with a later member of the group (*e.g.*, I, S, P), *cf.* Chapter III.

A-type metal cations have inert gas type (d^0) electron configuration and are normally visualised as hard spheres whose electron shells are not easily deformed. Examples of such metal cations are H⁺, Li⁺, Na⁺, K⁺, Be²⁺, Mg²⁺, Ca²⁺, Sr²⁺, Al³⁺, Sc³⁺, La³⁺, Si⁴⁺, Ti⁴⁺, Zr⁴⁺, and Th⁴⁺.

B-type metal cations are visualised as “soft spheres” with low electronegativity and high polarizability, *e.g.*, Cu⁺, Ag⁺, Au⁺, Tl⁺, Ga⁺, Zn²⁺, Cd²⁺, Pb²⁺, Sn⁺, Tl³⁺, Au³⁺, In³⁺, and Bi³⁺. While class A-type metal ions prefer ligands having oxygen as donor atoms and F, class B-type metal ions coordinate preferentially with bases containing I, S, or N as donor atom, *cf.* Section III.2.2.4 and Figure III.7 on *p.*86.

The competitive binding of various metal ions to humic substances must recognise the acceptor properties of the metal ion and the functional group heterogeneity in the humic substances [93TIP]. Various experimental evidence suggest that the humic substances have sufficient number of sites to bind different metals simultaneously. For example, in competitive binding studies involving Eu(III) and Sr(II), Eu(III) and Al(III) and Fe(II)/Fe(III) it has been observed that in all instances, the binding of Eu(III) by an aquatic fulvic acid was not significantly affected by Sr(II), Al(III) or Fe(II)/Fe(III) [94NOR]. Copper binding by fulvic acid has also been observed not to be affected by Ca²⁺ [88HER/MOR]. These observations seem to suggest that metal ions need not compete for the same sites

Figure VI.8: Ultrafiltration (UF) and ion-exchange distribution studies (IEDS) of the Eu(III)–FA system ($[FA] = 120 \text{ mg} \cdot \text{l}^{-1}$; $[Eu(III)] = 10^{-11} \text{ M}$). Variations of the fraction metal bound, M_b , to free metal, M_f , with changes in pH as a function of ionic strength. ■ IEDS, $I = 0.01 \text{ M NaClO}_4$; □ IEDS, $I = 0.10 \text{ M NaClO}_4$; ● UF, $I = 0.01 \text{ M NaClO}_4$; ○ UF, $I = 0.10 \text{ M NaClO}_4$.



in the fulvic/humic acid molecule as long as there are enough sites on the humic molecule compared to the total available metal ions.

VI.3.3. Data needs for modelling the role of humic substances

The need for accurate and reliable data in modelling cannot be overemphasised. Estimates of the concentrations of humic substances in soils, surface water and ground water are the first important data required to predict their role in the distribution of trace components [81THU/MAL, 82STE]. After determination of the total concentrations, *e.g.*, as milliequivalent carbon per liter, one must estimate the functional groups concentration. Typically, this is made by acid-base titrations of the humic substances [70GAM, 72GAM, 77ARA/KUM, 83DEM/OME, 86EPH/ALE, 93BON/FIS]. Since environmental conditions span a range of ionic strengths, it is always necessary to perform such titrations as a function of ionic strength and over a range of humic substance concentrations [86EPH/ALE, 89EPH/BOR]. Comparison of potentiometric titrations of surface

and groundwater fulvic acid samples show that the effect of ionic strength on the pK_a^{app} *versus* α (degree of neutralization) curves differ for different fulvic acid samples [94NOR, 94PET/EPH]. Such effects generally depended on the molecular weight of the sample, but for samples with the same molecular weight the ionic strength effects were more pronounced the more polydisperse the sample [94NOR]. The lesson from these observations is that it is not appropriate to calculate electrostatic corrections based on molecular weight alone unless the dispersity in the molecules is included.

Potentiometric titrations of a number of fulvic acids isolated from different origins (12 samples) have been performed at different ionic strengths and compiled (Figure VI.9). The interesting feature of the Figure is the range of the variation of pK_a^{app} *versus* α for all the fulvic acids at three ionic strengths (0.001, 0.010, 0.100 M NaClO₄). At each defined degree of neutralization, the difference between the highest and lowest pK_a^{app} values is ≤ 2 , with the largest difference at lower degrees of dissociation (Figure VI.9). Such data indicate that despite the functional site heterogeneity in the humic substance molecules, some cautious generalizations may be made of their acid-base properties. For example, when modelling the role of humic substances on the distribution of metal ions in the environment, a first approximation could be made by selecting the pK_a^{app} value at 50% dissociation to be $\sim 4.0 \pm 1.0$. Figure VI.9 may be considered as an attempt to determine the upper and lower boundaries of pK_a^{app} *versus* α curves for humic substances under typical environmental conditions.

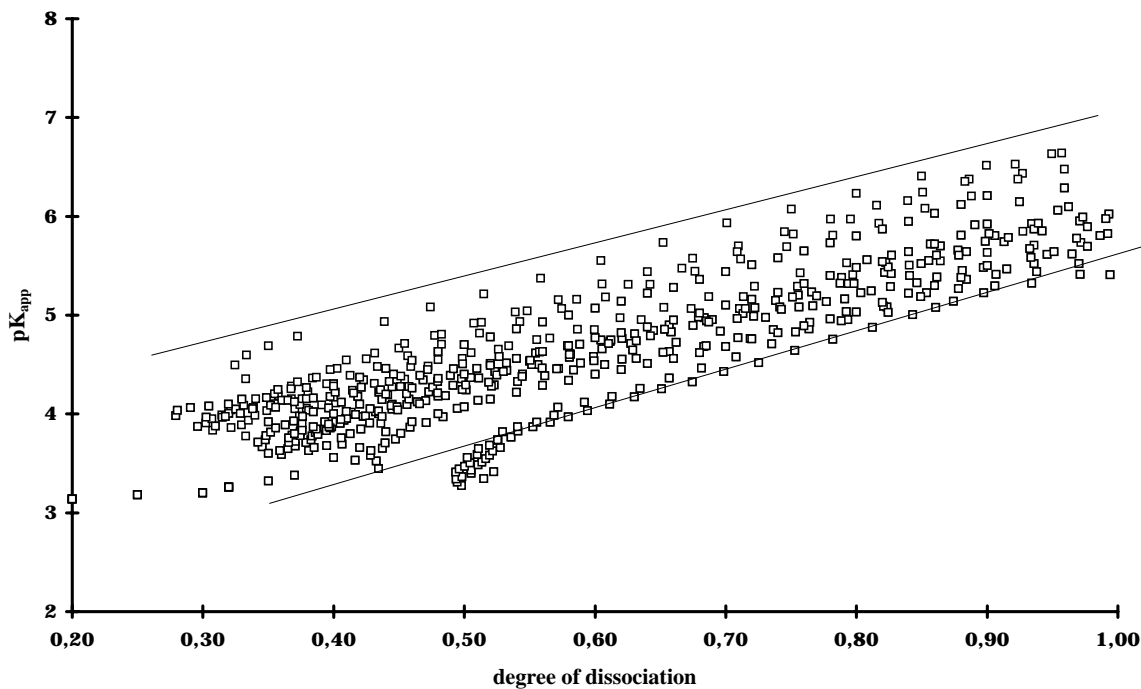
The active functional groups in humic substances may be identified and/or estimated using chemical derivatization techniques [92ARS/BOR] and spectroscopic methods, *e.g.*, FTIR, NMR [78RUG/SCI, 79RUG/INT, 80DER/MOR, 83GIL/WIL, 83HAT/BRE, 84PRE/SCH, 86GIL/WIL]. It is suggested that a combination of derivatization, spectroscopic and potentiometric titration techniques must be made to obtain a comprehensive picture of these substances [89EPH/BOR2].

The methods employed in metal binding studies are based on the determination of the concentrations of the components at equilibrium (free metal, free ligand or metal-ligand complex) without disturbing the equilibrium. Metal-humate studies ought to be conducted with concentrations of both ligand and metal ions which resemble those encountered in the environment. This requirement makes it impossible to use a number of experimental techniques. It has been suggested that metal-humate studies should be made using more than one experimental technique in order to identify the possibility of different reaction “windows” [83CAB/SHU, 83TUS/BRE, 89EPH/XU, 91EPH, 93NOR/EPH]. If two different experimental methods are used to study the same reaction, then the interaction parameters ($\log_{10} \beta_{\text{ov}}$) must be the same within the estimated uncertainty range [85FIS/MOR].

Studies of metal interaction with humic substances must be conducted at more than one ionic strength in order to describe how changes in bulk electrolyte concentrations which may occur in the environment (*e.g.*, saline waters in marine environments) influence the metal-binding [94EPH/ALL].

There is a need to compile potentiometric titration and metal-humate binding data to facilitate the meaningful generalizations which are necessary when modelling metal-ion

Figure VI.9: Acid-base titration curves (pK_a^{app} versus α) for 12 different aquatic fulvic acid samples at different ionic strengths (0.10, 0.01 and 0.001 M NaClO₄). Visualise the curve as providing the upper and lower boundaries for the titration curves for the 12 fulvic acid samples [95EPH/PET].



interactions with organics in the environment.

Efforts to incorporate humic and fulvic acid complexation into existing chemical equilibrium models or speciation codes must begin with the definition of their concentration. In absence of an easily determined molecular weight, concentration determinations have been made using either equivalent per litre ($\text{eq} \cdot \text{l}^{-1}$) or gram per litre ($\text{g} \cdot \text{l}^{-1}$) [91MOU/CAC]. Since most equilibrium constants employed in the speciation codes (FITEQL, PHREEQE) are expressed as $\text{l} \cdot \text{mol}^{-1}$, it would be more convenient to express the parameter describing metal-humate interactions in similar units. Such an option will thus demand that the acid capacities of a large number of humic and fulvic acids be determined (equivalents per gram of humic material) to facilitate the choice of a representative mean value (a function of the origin of the humic substances) [82STE, 94PET/EPH] which can be used to convert the unit $\text{g} \cdot \text{l}^{-1}$ into $\text{eq} \cdot \text{l}^{-1}$. Since protons are the basis for the potentiometric titration measurements, the $\text{eq} \cdot \text{l}^{-1}$ units are the same as the molar units which are usually employed in speciation computer programs. An example of initial estimates that may be made to anticipate the effects of humic/fulvic acids on the speciation of trace metals in the environment is presented in Section VI.4.

VI.3.3.1. Review of studies on interactions between humic substances and metal ions

Metal-humate interactions have been studied for a long time employing various experimental methods. A brief presentation of some of them are given in this Section.

VI.3.3.1.1. Anodic stripping voltammetry

This method which has been used for studying the interaction between humic substances and metals ions (Cd^{2+} , Cu^{2+} and Zn^{2+}) utilises the possibility to determine the free metal ion in the presence of the humic substance [73SHU/WOO, 87BUF/VUI]. The method is based on the fact that the rate of reduction of the free metal ion is very rapid, while the rate of dissociation of the metal-humate complex is much slower. The possible dissociation of the metal-humate complex and/or the humic material is a major disadvantage of this method.

VI.3.3.1.2. Fluorescence spectroscopy

Even though only a small fraction of humic substances exhibit fluorescent properties, the method is employed for studies of metal-humate interactions especially involving paramagnetic transition metal ions such as Cu^{2+} , Fe^{3+} , Fe^{2+} , Co^{2+} , Ni^{2+} and Cr^{3+} [80SAA/WEB, 83RYA/HOL, 90SEN]. Additionally, the fluorescent properties of selected metal ions, *e.g.*, Eu^{3+} , have been utilised in Eu(III)-fulvate system [91BID/GRE].

VI.3.3.1.3. Equilibrium dialysis

The utilisation of membranes of varying sizes to separate free metal ions from the ligand and complex has found considerable use. The drawback of the method is the possible sorption of species onto the surface of the dialysis membrane [81TRU/WEB, 82RAI/WEB, 85CAR].

VI.3.3.1.4. Ion-selective electrodes

The availability of specific electrodes for a number of metal ions has allowed the in situ determination of free metal ion concentrations in metal-humate mixtures. The metal ions for which ion-selective electrodes have been developed include Cu^{2+} , Pb^{2+} , Ca^{2+} and Cd^{2+} [77BUF/GRE, 77STE, 78BRE/GRA, 80GAM/UND, 80SAA/WEB, 83TAK/YOS, 86EPH/MAR, 86FIT/STE, 86TUR/VAR, 87TUR/VAR, 89EPH/XU, 94EPH/ALL]. Recent developments of electrodes for lanthanides and actinides have met with serious drawbacks because of the narrow pH range in which they show Nernstian behaviour. Another disadvantage of these electrodes is the possible poisoning of the electrodes by humic substance coatings of the electroactive membrane of the electrode, leading to serious errors [85FIS/MOR].

VI.3.3.1.5. Ultrafiltration

The separation of species on the basis of their size is employed in the ultrafiltration method where the fulvic acid molecule and the complex are separated from the free metal ion [76SMI, 83STA/BUF, 84BUF/STA, 84STA/BUF, 90EPH/MAR, 91EPH]. Precautions needed for the method include avoiding low-molecular weight fragments filtering through the membrane, and possible dissociation of the metal-humate complex.

VI.3.3.1.6. Gel filtration chromatography

A method generally employed for size evaluation is adapted for metal-humate studies [75MAN/RIL, 77MEA/CRE, 81HIR]. The metal ion concentrations associated with the separated sizes (fractions) are determined, thus allowing a determination of the fractions mostly involved in the binding. Cu^{2+} , Zn^{2+} , Mn^{2+} and their interactions with humic acids have been studied using this method.

VI.3.3.1.7. Solvent extraction

The effect of humic substances on the partition of metal ions in an aqueous and non-aqueous medium is employed to determine formation functions for metal-humate complexes [83TOR, 84TOR/CHO]. Metal ions may be employed both at macro or micro-concentration levels, *i.e.*, 10^{-2} to 10^{-5} M, or 10^{-6} to 10^{-11} M for radioisotopes, *e.g.*, ^{152}Eu , ^{109}Cd , ^{65}Zn , *etc.*

VI.3.3.1.8. Ion exchange distribution

An indirect approach is employed to estimate the ratio of metal bound to free metal [48SCH]. Such an approach has found a useful application in studies involving humic substances and metal ions like Co^{2+} , Zn^{2+} , Eu^{3+} , Cd^{2+} [67SCH/SKI, 72ARD/STE, 72ZUN/GAL, 89EPH/MAR, 91EPH, 93NOR/EPH].

VI.4. Modelling example: speciation of Eu^{3+} in the environment in presence of humic substances and Ca^{2+}

It must be noted that “real” systems do contain other substances in addition to humic substances, *e.g.*, inorganic colloids and particulates, low molecular weight organic and inorganic substances, microorganisms such as fungi and bacteria, *etc.* Since all the models discussed in this chapter are based on laboratory data from binary systems, their application to “real” systems may be questioned. In the models discussed, the interaction between metal ion, humic substances and geologic solids such as FeOOH , alumina, *etc.* has not been considered, and such ternary equilibria are known to influence the distribution and mobility of trace metal ions in the environment. The question then is –

what are the benefits of these models? The clear advantage of the models is that they use accepted “knowledge”, *e.g.*, Debye-Hückel, Boltzman Distribution, Gibbs-Duhem free energy considerations, to describe the solution chemistry of humic substances. In all the models, the important objective has been to adapt these to the humic substance systems and verify how well they may be described and/or predicted. The models provide the “basic knowledge” needed to facilitate the description of real systems.

In the light of the above discussion, our example of the possible effect of humic substances on the distribution and mobility of Eu^{3+} has used an “average” approach. The assumptions and parameters estimates employed are listed below and in Table VI.2.

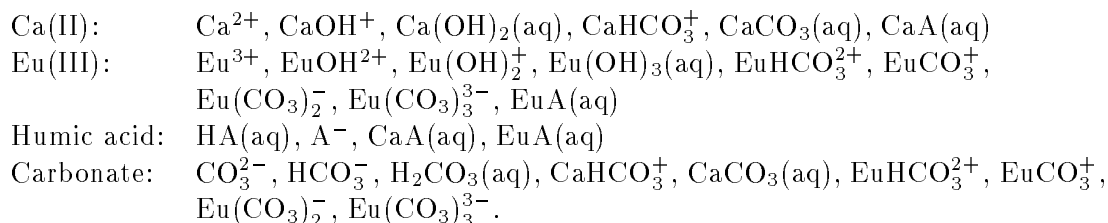
- a) the average acid capacity for humic substances (14 FA samples) = $5.1 \text{ meq} \cdot \text{g}^{-1}$
- b) average $\text{p}K_a^{\alpha=0.5}$ (from composite Figure VI.9) = 4.0
- c) $p\text{CO}_2 = 10^{-3.5} \text{ bar}$.

Depending on the concentrations of the humic substances, three scenarios have been used. In the first, all dissolved organic acid, DOC, in surface water is assumed to be humic substances. This assumption, gives the highest concentration of humic substances. The second scenario designates all the DOC in ground water as humic substances while the third option considers 15% of the DOC in groundwater systems ($1 \text{ mg} \cdot \text{l}^{-1}$) as humic substances.

The concentration in $\text{meq} \cdot \text{l}^{-1}$ is obtained from the concentration in $\text{mg} \cdot \text{l}^{-1}$ multiplied by the average acid capacity of $5.1 \text{ meq} \cdot \text{g}^{-1}$.

Typical concentrations of dissolved organic carbon in (surface) waters is less than or equal to $2 \text{ mg} \cdot \text{l}^{-1}$, while those for groundwater are less than $1 \text{ mg} \cdot \text{l}^{-1}$ [81THU/MAL]. In surface water systems 50% of the DOC is considered to be humic substances, while in the groundwater environments only 15% is humic substances, as determined by their adsorption characteristics on XAD-8 resins. The average concentrations of Ca^{2+} determined in ground and surface water are $10^{-2.9}$ and $10^{-3.8}$ [81STU/MOR, p.551]. The objective of the exercise is to estimate the role of organic acids in the speciation of the trivalent metal ion, *e.g.*, Eu(III) with a concentration of 10^{-8} M in an aquatic system.

The following 20 species, excluding solids, biota and colloids, have been considered in the model calculations:



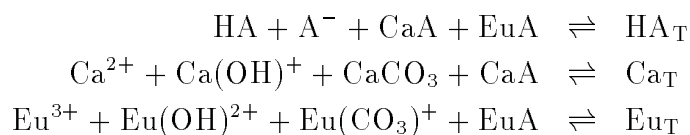
To simplify the situation, only the first hydroxide complexes and the carbonate complexes are considered for Ca(II) and Eu(III). In both surface and ground water environments, it has been assumed that the system may be considered similar to an aqueous

carbonate system open to the atmosphere with constant $\text{CO}_2(\text{g})$ pressure. As a result the CO_3^{2-} concentration may be calculated at each pH using the relationship:

$$[\text{CO}_3^{2-}] = K_1 K_2 K_H \frac{p_{\text{CO}_2}}{[\text{H}^+]^2}$$

where K_1 , and K_2 are the first and second dissociation constants of the acid $\text{H}_2\text{CO}_3(\text{aq})$, K_H is Henry's Law constant and p_{CO_2} is the pressure of CO_2 [81STU/MOR, p.179–182]. The various values employed in this example are: $K_1 = 10^{-6.3}$, $K_2 = 10^{-10.23}$, $K_H = 10^{-1.5}$ and $p_{\text{CO}_2} = 10^{-3.5}$ bar.

The concentrations of the different species were calculated using the material balance for the various components, *i.e.*, Ca(II), Eu(III), humic acid and carbonate, and the charge balance. The material balance considerations for the three major substances, humic substance, HA, calcium, and europium are given in the following equations:



For Ca^{2+} and Eu^{3+} , the following general expression may be used, provided only binary complexes are formed:

$$\text{M}^{z+} = \text{M}_{\text{total}}^{z+} / (1 + \sum \beta_j \text{L}_j)$$

where j is the complex and L_j is the ligand of the complex, M^{z+} is the free metal concentration at equilibrium, $\text{M}_{\text{total}}^{z+}$ is the total amount of metal initially added or present and β_j is the stability constant of the complex.

For the humic material (in this particular example), the following expression holds, provided only binary complexes are formed:

$$\text{A}^- = \text{HA}_\text{T} / (1 + h / K_a^{\text{diss}} + (\beta_{\text{CaA}} \text{Ca}^{2+}) + (\beta_{\text{EuA}} \text{Eu}^{3+}))$$

where HA_T is the total concentration of humic substances, A^- is the concentration of the anion of humic substance, h is the proton concentration, K_a^{diss} is the overall dissociation constant for the humic substance, β_{CaA} is the constant for the calcium complexation by the humic substance, Ca^{2+} is the concentration of calcium ion, β_{EuA} is the constant for the complexation between europium and the humic substance and Eu^{3+} is the concentration of europium ion.

First an overall $\text{p}K_a$ of 4.0 was selected to be representative of the humic substance. The choice of this value was based on the plot of $\text{p}K_a^{\text{app}}$ versus α for a number of aquatic and terrestrial humic substances (Figure VI.9). In addition, it was assumed that Ca^{2+} and Eu^{3+} did not interfere with one another on binding to the organic acid. This assumption is based on results from our laboratory where the interaction of Eu(III) and an aquatic fulvic acid was not influenced by strontium, aluminium or iron [94NOR]. Similar lack

Table VI.2: Concentrations and equilibrium constants used in the calculation of the speciation of Eu(III) in ground and surface waters.

	Surface water	Groundwater	Low conc. of humic substances
[HA]	$2 \text{ mg} \cdot \text{l}^{-1}$	$1 \text{ mg} \cdot \text{l}^{-1}$	$0.15 \text{ mg} \cdot \text{l}^{-1}$
[Eu]	$1.0 \times 10^{-8} \text{ M}$	$1.0 \times 10^{-8} \text{ M}$	$1.0 \times 10^{-8} \text{ M}$
[Ca]	$1.58 \times 10^{-4} \text{ M}$	$1.26 \times 10^{-3} \text{ M}$	$1.58 \times 10^{-4} \text{ M}$

Stability constants:

Species	$\log_{10} \beta$	Reference
CaOH^+	1.3	[83HOG]
$\text{CaCO}_3(\text{aq})$	3.1	[81STU/MOR]
CaA	3.07	[93MAT/EPH]
EuOH^{2+}	6.32	[93KIM]
EuCO_3^+	5.93	[83HOG]
EuA (1)	5.1	[91EPH, 93NOR/EPH]
EuA (2)	$3.84 + 0.74(\text{pH})$	[93NOR/EPH]
EuA (3)	6.5	[93KIM]

of interference has been observed for the interaction of Cu^{2+} and fulvic acid upon the addition of Ca^{2+} [88HER/MOR]. The concentrations under different conditions and the stability constants employed for the various complexes are summarised in Table VI.2.

The calculated percentages of the various species as a function of pH are shown in Figures VI.10, VI.11, VI.12. The various cases studied indicate that the sequestering of Eu(III) in the presence of Ca(II) depends strongly on the value of the equilibrium constant describing the interaction between Eu and HA. A pH-independent $\log_{10} \beta_{\text{EuA}}$ value of 5.10 [93NOR/EPH, 91EPH] gave, for a surface water system where the HA concentration is $2 \text{ mg} \cdot \text{l}^{-1}$, that more than 50% of the Eu(III) was sequestered by the HA in the pH range of 5 to 7 (Figure VI.10). However, at $\text{pH} \geq 8$, the EuCO_3^+ complex becomes the predominant species. An equilibrium constant of $\log_{10} \beta_{\text{CaA}} = 3.07$ was chosen for the interaction between Ca(II) and humic substance [93MAT/EPH]. The speciation diagram shows that the binding of Ca(II) by humic substances is weak and that $\text{CaCO}_3(\text{aq})$ becomes the predominant Ca(II) species after pH of 9.0. At $\text{pH} \leq 9$, Ca^{2+} remains the predominant species.

Figure VI.10: Speciation of Eu(III) in a typical surface water environment. $[HA] = 1.0 \times 10^{-5} \text{ eq} \cdot \text{l}^{-1}$, $\log_{10} \beta(\text{EuA}) = 5.1$.

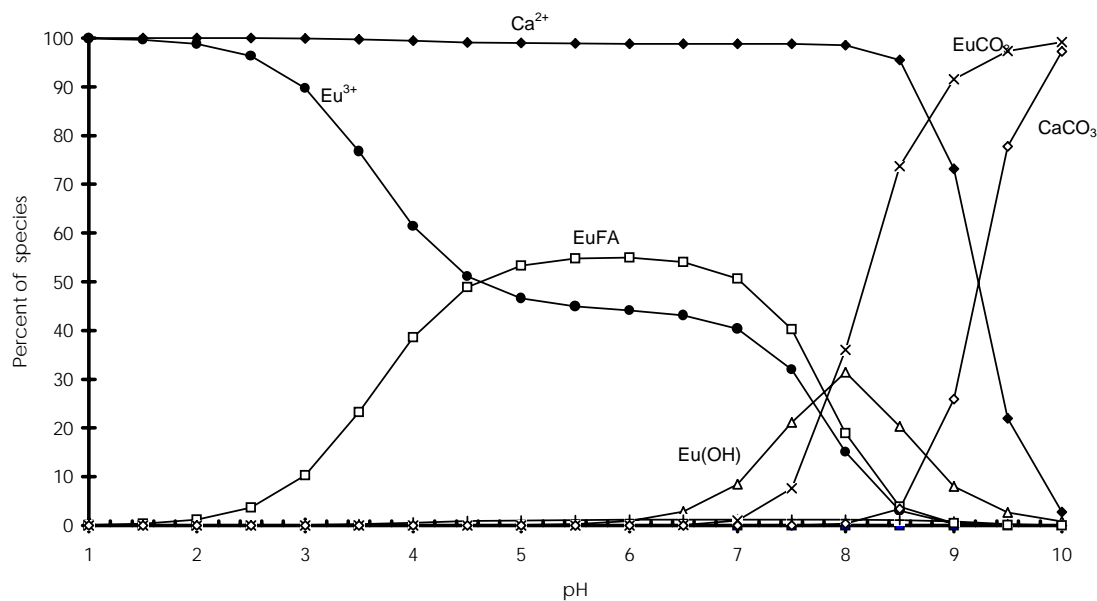


Figure VI.11: Speciation of Eu(III) in a typical surface water environment. $[HA] = 1.0 \times 10^{-5} \text{ eq} \cdot \text{l}^{-1}$, $\log_{10} \beta(\text{EuA}) = (3.04 + 0.74(\text{pH}))$.

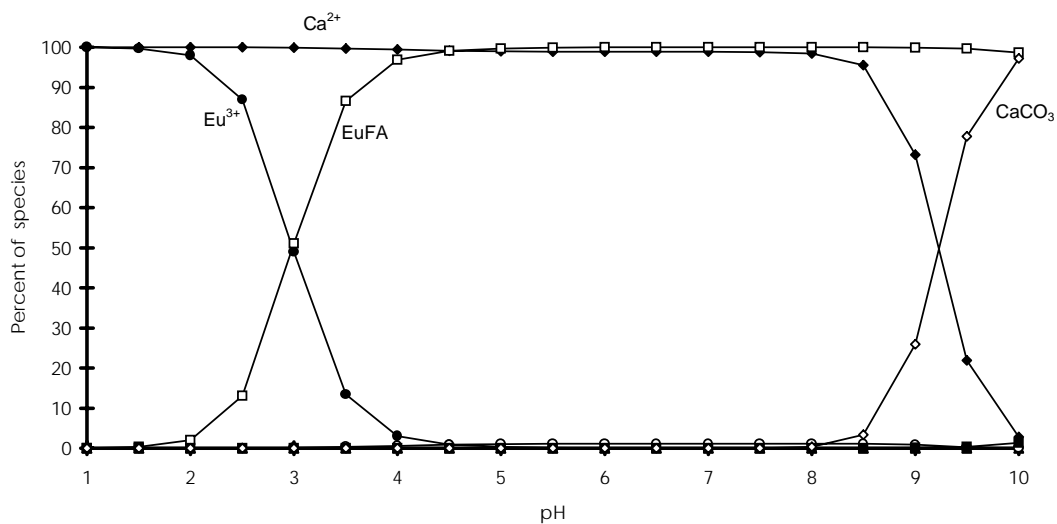
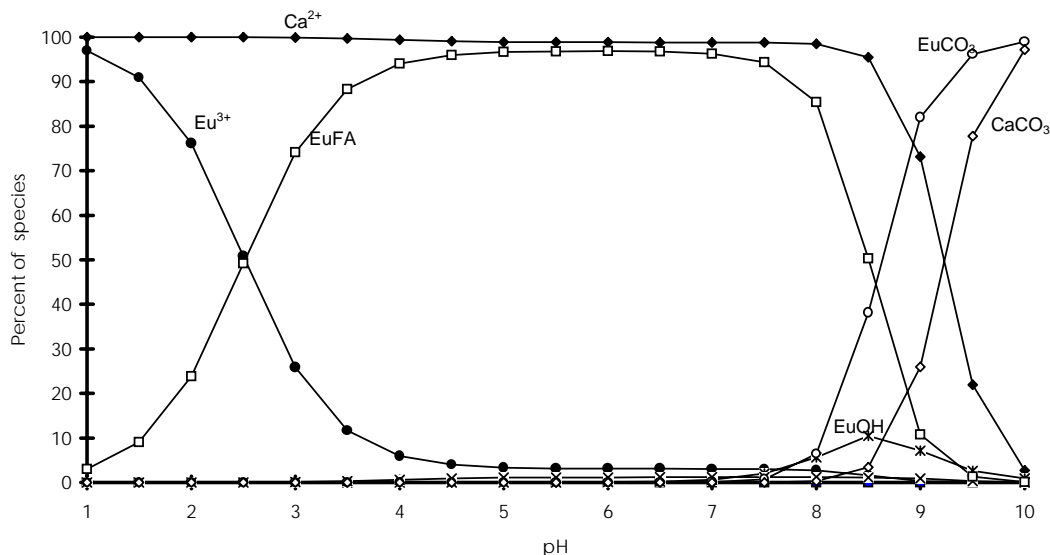


Figure VI.12: Speciation of Eu(III) in a typical surface water environment. $[\text{HA}] = 1.0 \times 10^{-5} \text{ eq} \cdot \text{l}^{-1}$, $\log_{10} \beta(\text{EuA}) = 6.5$.



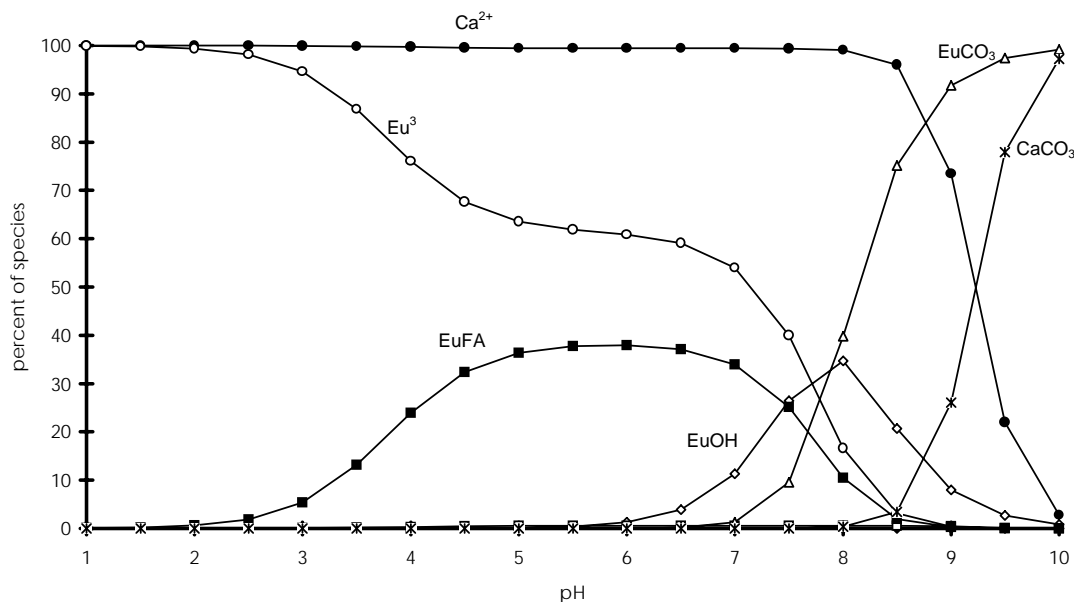
Using a pH dependent value of $\log_{10} \beta_{\text{EuA}}$ obtained from ion exchange distribution studies, [93NOR/EPH] gives a completely different picture (*cf.* Figure VI.11). In this case, the Eu(III) is completely bound by the humic substance at pH values ≥ 4.5 , and EuCO_3^+ is not formed in appreciable amounts. The speciation with respect to Ca(II) is not affected by the change in $\log_{10} \beta_{\text{EuA}}$ because of the assumption of non-interference.

The choice of $\log_{10} \beta_{\text{EuA}}$ is difficult since the literature is swamped with a multitude of different values. A compromise pH-independent value of 6.5 (*cf.* Table VI.2) has been chosen for $\log_{10} \beta_{\text{EuA}}$ [93KIM] and employed in the calculations shown in Figure VI.12. With this value, the $\text{EuA}(\text{aq})$ complex predominates at pH values ≤ 8.5 and the $\text{EuCO}_3(\text{aq})$ complex at pH > 8.5 . The EuOH^{2+} complex reaches a maximum (10%) at pH 8.5 and drops again as the pH increases (Figure VI.12).

In most groundwater systems, the amount of DOC is about 50% of the surface water DOC value, *i.e.*, $1 \text{ mg} \cdot \text{l}^{-1}$. By assuming that the binding characteristics of the DOC are dominated by the characteristics of the humic substances, that the ground water is open to $\text{CO}_2(\text{g})$ at a constant atmospheric pressure as in the surface water system and by employing a pH-independent $\log_{10} \beta_{\text{EuA}}$ of 5.10, we find the results shown in Figure VI.13. At pH values < 7.5 , Eu^{3+} ions predominate. The $\text{EuA}(\text{aq})$ complex formed reaches a maximum of 40% at pH of 5.0, remaining at the same level until pH of 7 and then drops down (Figure VI.13). At pH ≥ 8.0 , the $\text{EuCO}_3(\text{aq})$ complex becomes the predominant species.

Application of the pH-dependent function for the $\log_{10} \beta_{\text{EuA}}$ shows that the $\text{EuA}(\text{aq})$ complex takes over as the predominant species at pH values ≥ 3.5 where all Eu(III) is

Figure VI.13: Speciation of Eu(III) in a typical groundwater environment. $[HA] = 5 \times 10^{-6} \text{ eq} \cdot \text{l}^{-1}$, $\log_{10} \beta(\text{EuA}) = 5.1$.



essentially sequestered by the humic substance (Figure VI.14).

When a $\log_{10} \beta_{\text{EuA}}$ of 6.5 is employed in the exercise, it is observed that the EuA(aq) complex predominates in the pH range of 3 to 8. However, at pH values > 8 , the $\text{EuCO}_3\text{(aq)}$ complex becomes the predominant species (Figure VI.15).

Finally, the situation in which the humic substance will have the smallest effect on the Eu(III) speciation will be considered. This situation will be a typical groundwater environment where not all the $1 \text{ mg} \cdot \text{l}^{-1}$ DOC belong to humic substances but only 15% of the DOC are humic/fulvic acids (*cf.* Section VI.2). The concentration of humic substances thus will be $7.5 \times 10^{-7} \text{ eq} \cdot \text{l}^{-1}$. Employing the lowest $\log_{10} \beta_{\text{EuA}}$ value of 5.10 yields the speciation diagram shown in Figure VI.16. In this figure, it is shown that the EuA(aq) complex constitutes less than 10% of the Eu(III) species in the pH range of 4 to 8. The EuOH^+ complex reaches a maximum (40%) at pH of 8 where the carbonate complex, EuCO_3^+ becomes the predominant species. This picture is however, considerably changed when a $\log_{10} \beta_{\text{EuA}}$ value of 6.5 is employed (Figure VI.17). With this value, the EuA(aq) complex becomes the predominant species in the pH range of 4 to 7.5. The carbonate complex again becomes the predominant species at pH values > 8 . Application of the $\log_{10} \beta_{\text{EuA}}$ as a function of pH even with such low concentrations of HA will indicate that the EuA(aq) complex becomes the predominant species of the Eu(III) speciation (Figure VI.18).

Figure VI.14: Speciation of $\text{Eu}(\text{III})$ in a typical groundwater environment. $[\text{HA}] = 5 \times 10^{-6} \text{ eq} \cdot \text{l}^{-1}$, $\log_{10} \beta(\text{EuA}) = (3.8 + 0.74(\text{pH}))$.

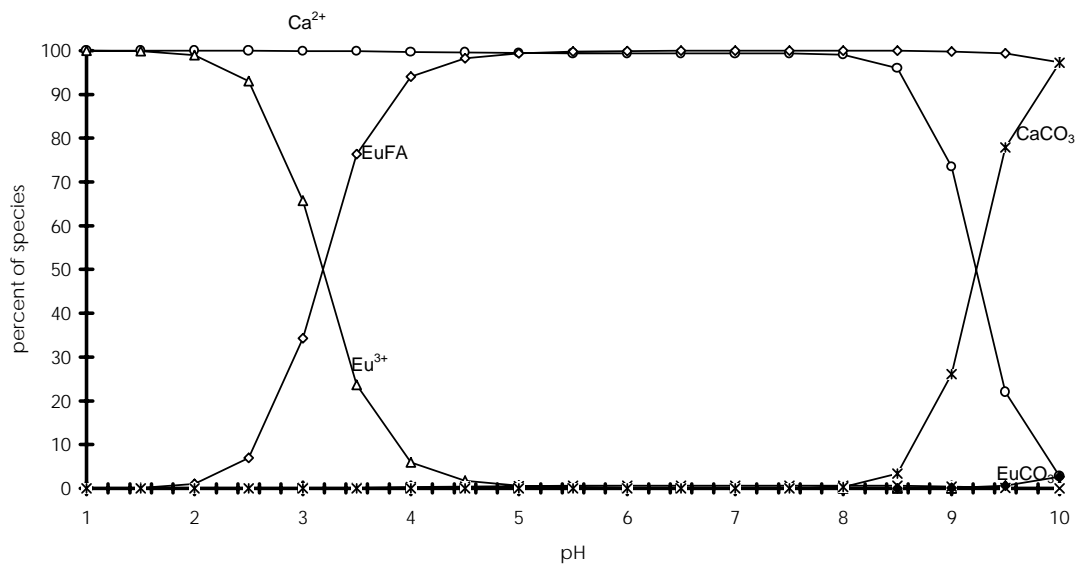


Figure VI.15: Speciation of $\text{Eu}(\text{III})$ in a typical groundwater environment. $[\text{HA}] = 5 \times 10^{-6} \text{ eq} \cdot \text{l}^{-1}$, $\log_{10} \beta(\text{EuA}) = 6.5$.

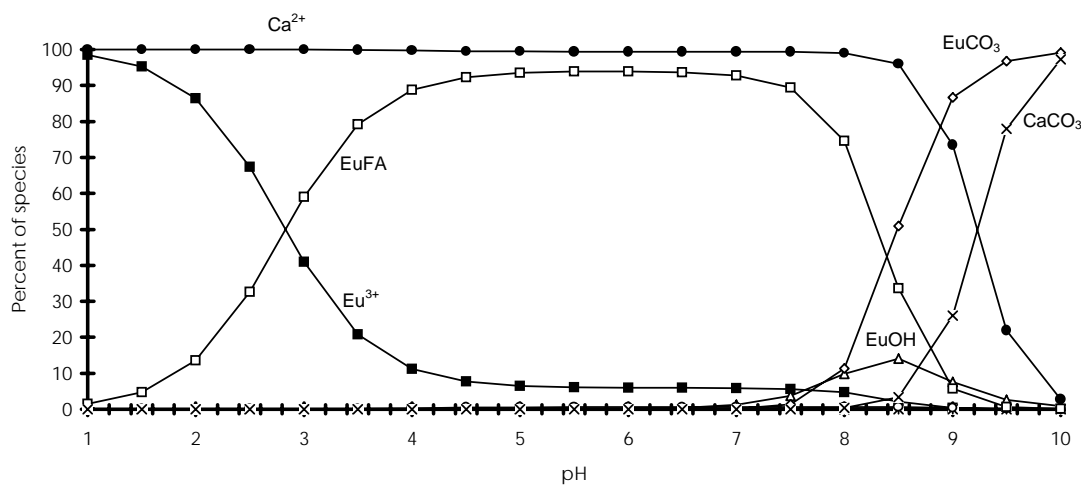


Figure VI.16: Speciation of Eu(III) in an environment with the lowest possible concentration of humic substances. $[HA] = 7.5 \times 10^{-7} \text{ eq} \cdot \text{l}^{-1}$, $\log_{10} \beta(\text{EuA}) = 5.1$.

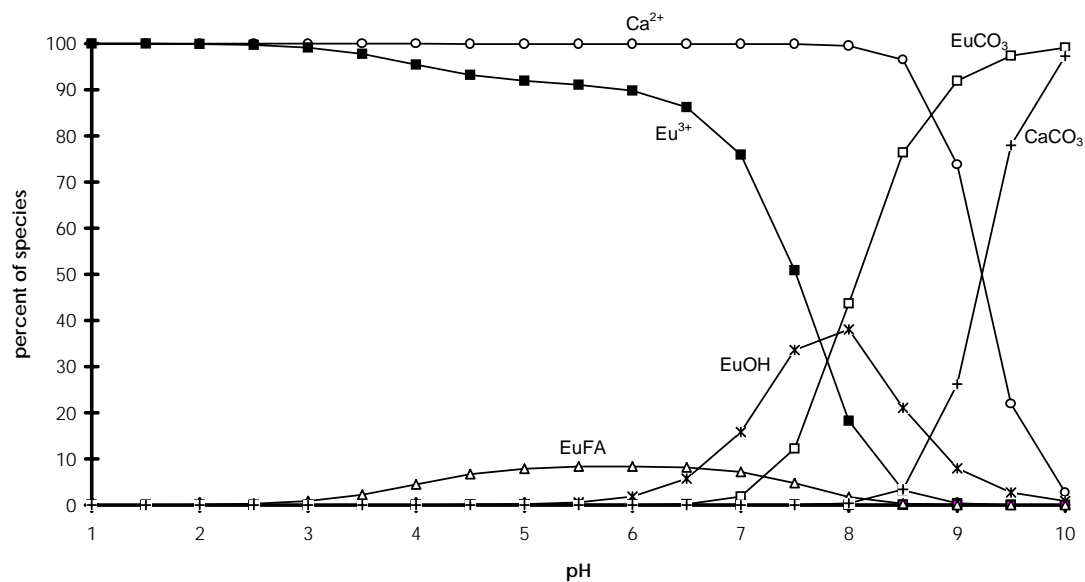


Figure VI.17: Speciation of Eu(III) in an environment with the lowest possible concentration of humic substances. $[HA] = 7.5 \times 10^{-7} \text{ eq} \cdot \text{l}^{-1}$, $\log_{10} \beta(\text{EuA}) = 6.5$.

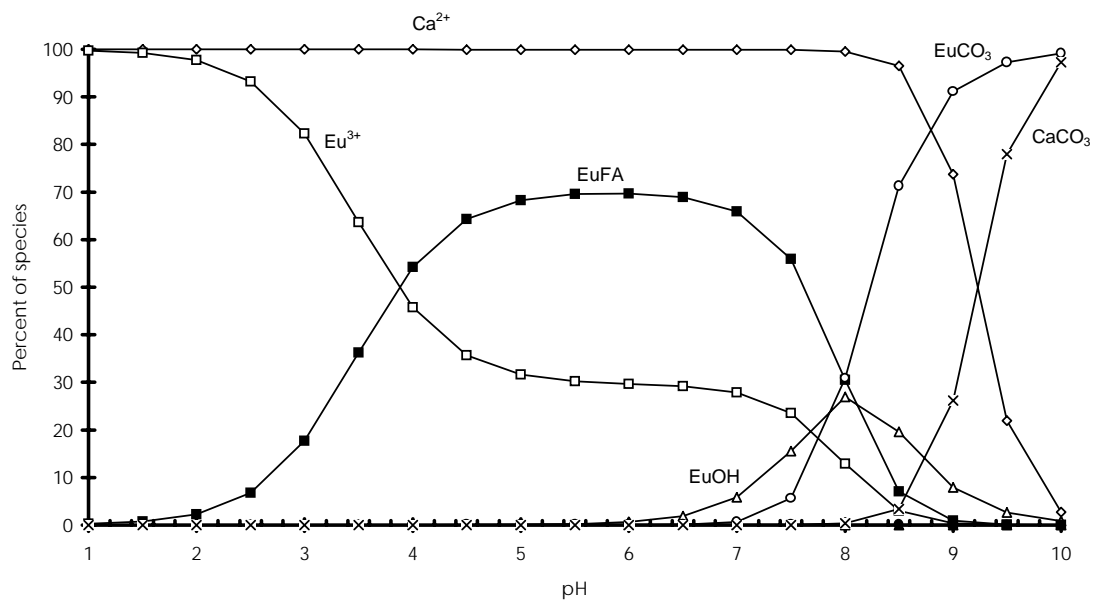
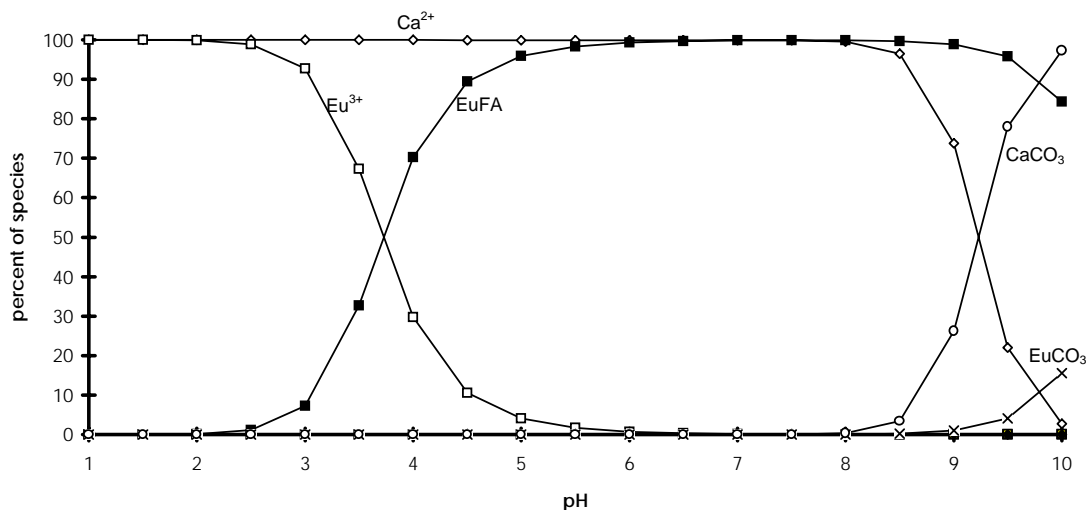


Figure VI.18: Speciation of Eu(III) in an environment with the lowest possible concentration of humic substances. $[HA] = 7.5 \times 10^{-7} \text{ eq} \cdot \text{l}^{-1}$, $\log_{10} \beta(\text{EuA}) = (3.84 + 0.74(\text{pH}))$.



VI.4.1. Relevance of the exercise

This example shows that both in groundwater and surface water environments, the speciation of trace toxic elements may be affected by the organic carbon component. The magnitude of this effect which is directly dependent on the concentrations of the organic matter, will be significant under acidic conditions. Under basic conditions, the carbonate complex (*e.g.*, EuCO_3^+) seems to predominate, especially for groundwater systems where the concentrations of DOC are small ($< 1 \text{ mg} \cdot \text{l}^{-1}$). Addition of the second carbonate and hydrolysis complexes for Eu does not change the picture, *i.e.*, influence of humic substances on the speciation of Eu in the environment. It must, however, be pointed out that the above exercise has been performed without the inclusion of organic acids which are associated with particles and colloids. To obtain a complete picture, one needs to incorporate the interaction of these organic components with inorganic colloids and particulates and microbial species [89XU/EPH, 94KRA/ALL, 94NOR/EPH]. However, it is unlikely that such a model will be particularly helpful for the modelling of “real” systems.

VI.5. Summary

The interaction of metal ions with natural organic acids has been examined by the representation of humic substances as typical natural organic acids. The possible formation pathways of these organic acids especially in aquatic environments has been briefly mentioned and the resultant functionalities which are responsible for their high affinity for metal ions have been considered. The concentrations of these natural organic acids in

the aquatic environments and the isolation and characterisation techniques have been discussed. The lack of information on molecular structure, weight, and configuration has resulted in different model structures for the description of the solution chemical properties of these systems. Two models predominate: the discrete multiligand model and the continuous distribution model. Current advances have shown that the two models actually converge with respect to the functional group heterogeneity in these substances. It was shown with an example that natural organic acids will have significant effect on the distribution of a trace element especially in surface water systems under acidic conditions. Such an effect is dependent on the concentrations of the organic acids, the model employed to estimate the extent of interaction between the metal ion and natural organic acid and the pH of the bulk solution. In groundwater systems open to the atmosphere, the role of humic substances in the speciation of toxic elements is partially reduced due to their small concentrations. The parameters necessary to describe/model the binding of metal ions by humic substances are described in Table VI.3.

Table VI.3: Parameters used in describing/modelling metal ion binding by humic substances.

Parameters	Comments	References
1. Concentration of organic matter in terrestrial and aquatic environments.	In terrestrial environments, units are $\text{g} \cdot \text{C} \cdot \text{g}^{-1}$ soil; in aquatic environment, units are $\text{g} \cdot \text{C} \cdot \text{l}^{-1}$.	[72SCH/KHA], [82STE], [91MAL]
2. Fraction of humic substance in organic matter		
3. Molecular weight of humic material	range from less than 700 to over 200 000 for humic and fulvic acids; humic acids have higher molecular weight than fulvic acid.	[69HAN/SCH], [85AIK/MCK], [89HAY/MCC]
4. Elemental analysis	Major elemental composition - C (55-44%); H (5-3%); O (37-52%); N ($\sim 1\%$); P ($< 1\%$); S ($\sim 1\%$); Cl ($< 1\%$)	[82STE], [85AIK/MCK], [89HAY/MCC]
5. Acid-base characteristics		
Acid capacity	range from 1 to 10 $\text{meq} \cdot \text{g}^{-1}$; fulvic acids generally have higher acid capacity than fulvic acid.	[72GAM], [72SCH/KHA], [82STE], [85AIK/MCK], [86EPH/ALE]
Radius of humic substance molecule	a rigid sphere is normally assumed.	[92BAR/CAB], [92TIP/HUR], [93WIT/RIE]
$\text{p}K_{\text{app}}$ vs. α curve	provides insight into both molecular weight heterogeneity and functional group.	[86EPH/ALE], [89EPH/BOR], [95EPH/PET]
Electrostatic effects	corrects deviation from ideality as a result of group-group interaction accompanying ionization process.	[84MAR/RED], [85GAM/MAR], [86DZO/FIS], [86EPH/ALE], [92BAR/CAB], [92TIP/HUR], [93WIT/RIE]

Table VI.3 (continued)

pK_{intr}	assumed overall intrinsic pK ; does not represent the true nature of humic substances but only used as a crude estimation. Normally, two values are assumed - one for -COOH and the other for -OH.	[84MAR/RED], [84MAR/RED2], [83PLE/JOS]
6. Functional groups		
Functional group heterogeneity	reactivity of humic substances is attributed to the high presence of oxygen-containing functional groups, <i>e.g.</i> -COOH, -OH <i>etc.</i>	[82STE], [85AIK/MCK]
Percentage of predominant acid sites	normally obtained by potentiometric titrations, pyrolysis, derivatization techniques, NMR <i>etc.</i>	[86EPH/ALE], [89EPH/BOR], [89EPH/BOR2], [92ARS/BOR]
pK_a of the sites	these values are normally guesses employed to fit experimental data.	[85PAX/WED], [86EPH/ALE], [92TIP/HUR], [92BAR/CAB]
7. Concentration of total metal ion	values employed in modelling exercise should be close to environmental values.	
8. Concentration of free metal ion	methods employed include anodic stripping voltametry, fluorescence spectroscopy, equilibrium dialysis, ion-selective electrode, ultrafiltration, gel filtration chromatography, solvent extraction, ion exchange distribution.	[72ARD/STE], [75MAN/RIL], [78BRE/GRA], [82STE], [83RYA/HOL], [83TOR], [84TOR/CHO], [89EPH/MAR], [93NOR/EPH]
9. Stability constants of the metal-humate complex	explicit definition of the constants employed is mandated; comparison of values obtained for same metal-humate system using different methods.	[72ARD/STE], [73SHU/WOO], [81HIR], [83TAK/YOS], [94EPH/ALL]

Chapter VII

Aqueous Speciation at the Interface Between Geological Solids and Groundwater

Steven A. BANWART
Dept. Civil & Environmental Engineering
University of Bradford
Bradford, W. Yorkshire BD7 1DP (United Kingdom)

VII.1. Introduction

The mobility, reactivity and bioavailability of pollutants within the hydrologic cycle is critically dependent on the aqueous speciation controlling their solubility and adsorption behaviour. In soils and aquifers, the geological medium is in intimate contact with sub-surface water, and provides a dominant reaction partner for the chemical transformation and immobilisation of solutes. Assessment of pollution risk to the biosphere, design of sub-surface waste containment facilities and evaluation of remediation strategies for contaminated land and groundwater demand that the partitioning of contaminants between water and immobile solid phases is understood.

This chapter intends to provide a conceptual framework for understanding the interfacial forces at work in adsorption reactions. Quantitative treatment of these reactions stems from considering aqueous surface speciation at the solid-water interface, and applying mass balances and thermodynamic mass action laws that are analogous to those used for modelling speciation in solution (*cf.* Chapter 9 in [96STU/MOR]). Thermodynamic data for such surface complexation reactions are compiled for hydrous ferric oxide surfaces [90DZO/MOR], and can be estimated from analogous complexation reactions between dissolved metals and ligands [87SCH/STU].

Modelling of surface speciation can predict the trends in adsorption behaviour with mas-

ter variables such as pH and redox status. The complexity of natural systems can make quantitative prediction of solute adsorption and retardation in the field very uncertain. However, application of sound thermodynamic principles to adsorption reactions provides a modelling framework that is theoretically rigorous, and that allows a sound mathematical formulation of even very complex adsorption reactions. This chapter outlines the theoretical principles involved, and develops the necessary mathematical framework. The tutorial case studies presented can be calculated by hand, and do not require knowledge of specialised computer codes for geochemical modelling.

VII.2. Theoretical background

VII.2.1. Intermolecular forces at the solid-solution interface

Adsorption of dilute solutes onto immobile geologic solids is a key process for retarding the movement of solutes with groundwater flow. The imbalance of forces at phase boundaries drives such adsorption reactions. Ions in an aqueous electrolyte will migrate to charged surfaces such as clay minerals. Non-polar solutes such as hydrocarbons will displace water molecules at a non-polar surface such as sedimentary carbon. Dissolved metal ions and ligands will respectively bind to functional groups and metal centres on organic or mineral surfaces, analogous to hydrolysis and complexation reactions in solution.

Figure VII.1 illustrates such reactions at the solid-water interface. In seeking a free energy minimum, aqueous surface species will respond to three types of intermolecular forces [87WES]:

- inner-sphere chemical co-ordination bonding (surface complexation),
- electrical charge interactions (ion-exchange),
- solvation energies (hydrophobic adsorption).

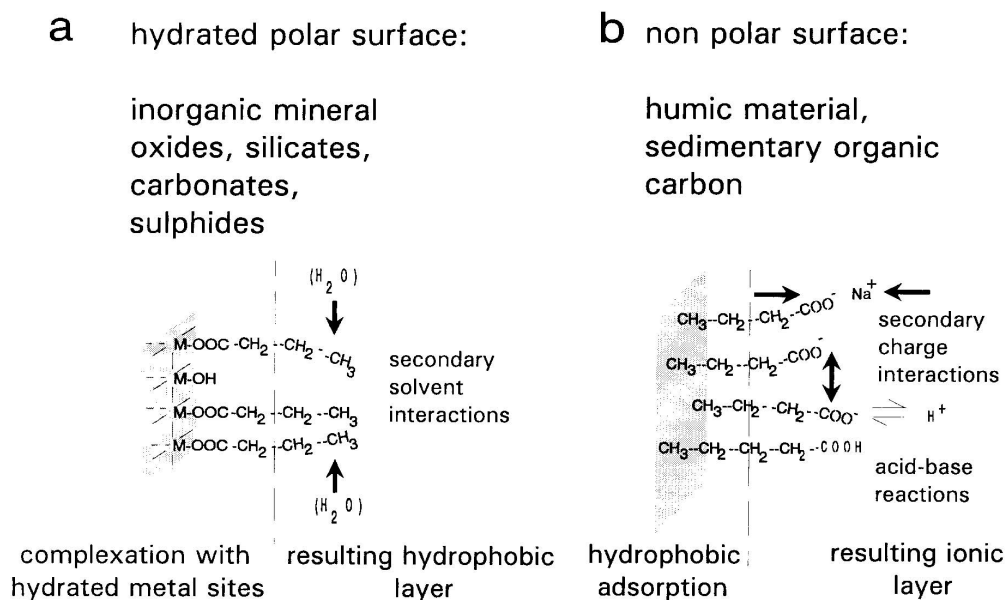
Formal application of the law of mass action, combined with mass balances for aqueous species, provides mathematical descriptions of adsorption reactions. The free energy of formation for the adsorbed species may depend on contributions from all three types of intermolecular forces.

VII.2.2. Mass balances for adsorbing substances: The concept of surface excess

Adsorption is a chemical process that accumulates dilute solutes, from the bulk aqueous phase, at phase interfaces. Chemical reactions that cause contaminants to be removed from the groundwater onto mineral or organic surfaces are of particular interest in contaminant hydrogeology.

The mass balance for adsorbing substances is defined by the concept of surface excess. On a volume basis, the concentration of a dilute solute $C_{(aq)}$ ($\text{mol} \cdot \text{l}^{-1}$) is defined as the mol of the solute in a fixed volume of the solution. The surface excess is the additional amount of solute ($\text{mol} \cdot \text{m}^{-2}$) in the system when a fixed amount of reactive surface (m^2) is

Figure VII.1: Adsorption reactions depend on the chemical nature of the adsorbing solute (adsorbate) and of the solid surface (adsorbent). The adsorption of an ionisable organic compound is represented here by an aliphatic carboxylic acid adsorbed on (a) polar and (b) non-polar surfaces. Short-range chemical bonding effects and longer-range electrostatic and solvation interactions contribute to the free energy of the adsorption reaction. In (a) chemical bonds are formed between functional groups on the organic compound and metal sites on the polar surface. In (b) the non-polar methyl groups of the adsorbate are driven to the solid surface because of the high solvation energy required to keep the compound in solution. The primary adsorption reaction leads, in both cases, to secondary layers with characteristics very different from the original surface; reprinted with permission from [94BAN].



present and in equilibrium with a solution of the same aqueous concentration, $C_{(aq)}$ (see for example [81JAY/PAR]).

The surface excess can be determined experimentally by preparing a standard solution of the adsorbing compound, then contacting the solution with a solid phase. If the system is then slowly titrated (so that equilibrium is always maintained) with a solution of the adsorbing compound, the amount added to bring the aqueous concentration back to that of the original standard solution is the surface excess.

Eq. (VII.1) defines this mass balance. The amount of substance adsorbed is equal to the difference between the total amount added to the system and the amount in solution. C_T is the total concentration of the substance, $C_{(aq)}$ is the dissolved concentration and $C_{(sur)}$ is the adsorbed concentration. The surface excess is expressed as adsorption density, Γ ($\text{mol} \cdot \text{m}^{-2}$). In contaminant hydrogeology, useful conventions defining the amount adsorbed include the partitioned concentration, s ($\text{mol} \cdot \text{kg}^{-1}$ (solid)), and the fractional adsorption density, Θ (fraction of monolayer coverage).

Eqs. (VII.2) – (VII.4) define the relationship between these variables where Γ_T ($\text{mol} \cdot \text{m}^{-2}$) is the maximum adsorption density at monolayer coverage, ρ_b ($\text{kg} \cdot \text{l}^{-1}$) is the dry bulk density of a geological medium with pore spaces, ε is the porosity (units-less: (l solution)/(l geologic medium)), and a ($\text{m}^2 \cdot \text{kg}^{-1}$) is the specific surface area of the solid phase. The dimensionless distribution coefficient K_d is defined as the ratio between adsorbed concentration and solution concentration (Eq. (VII.5)). An additional variable important to reactions in water-saturated soils and aquifers is the solid-to-solution ratio ($\text{kg} \cdot \text{l}^{-1}$), $\mathcal{S} = \rho_b \varepsilon^{-1}$, determined from bulk density and porosity.

$$C_{(sur)} = C_T - C_{(aq)} \quad (\text{mol} \cdot \text{l}^{-1}) \quad (\text{VII.1})$$

$$\Gamma = C_{(sur)} \varepsilon \rho_b^{-1} a^{-1} \quad (\text{mol} \cdot \text{m}^{-2}) \quad (\text{VII.2})$$

$$s = C_{(sur)} \varepsilon \rho_b^{-1} \quad (\text{mol} \cdot \text{kg}^{-1}(\text{solid})) \quad (\text{VII.3})$$

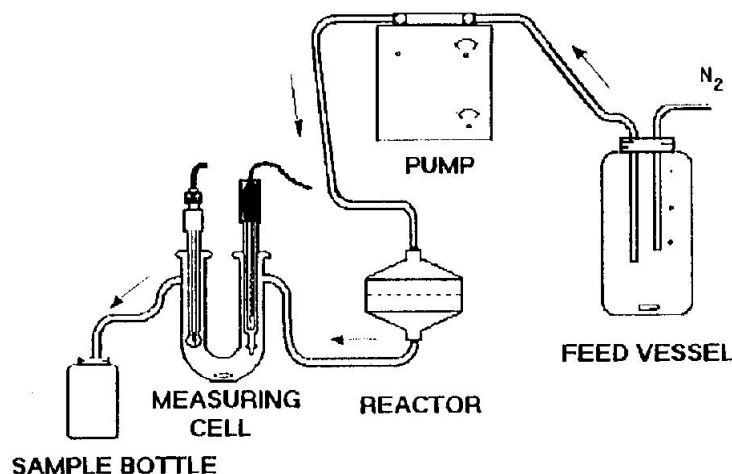
$$\Theta = \Gamma / (\Gamma_T) \quad (\text{dimensionless}) \quad (\text{VII.4})$$

$$K_d = C_{(sur)} / C_{(aq)} \quad (\text{dimensionless}) \quad (\text{VII.5})$$

In practice, the surface excess is usually determined by mixing particles of the solid with a standard solution of the adsorbing substance, or passing the standard solution through a fixed-bed or column containing the solid phase as a porous medium. The amount of the solute remaining, after equilibrium has been reached with the solid, is determined analytically. Wet chemical techniques such as spectrophotometry are often disturbed by the presence of the solid phase which must first be separated from the mixture by filtration or centrifugation.

Figure VII.2 shows a schematic drawing of a thin-film continuous-flow reactor [91BRU/CAS], where the reactive phase is held on a membrane filter across which re-

Figure VII.2: Schematic diagram of a flow-through reactor system used to study adsorption on mineral surfaces. A thin packed-bed of mineral powder is placed on a membrane filter in the reactor. A feed solution containing the adsorbate is pumped through the reactor. Outflow concentrations indicate if adsorption takes places. A delayed breakthrough of adsorbate, compared to a non-adsorbing tracer, indicates loss of adsorbate from solution. The mass difference between the total amount of adsorbate pumped into the reactor, and the total amount leaving the reactor, gives the adsorbed amount (see Figure VII.3). Ion-selective electrodes or other probes can be used with automatic data loggers to monitor reactor effluent continuously; reprinted with permission from [96MAL/BAN].

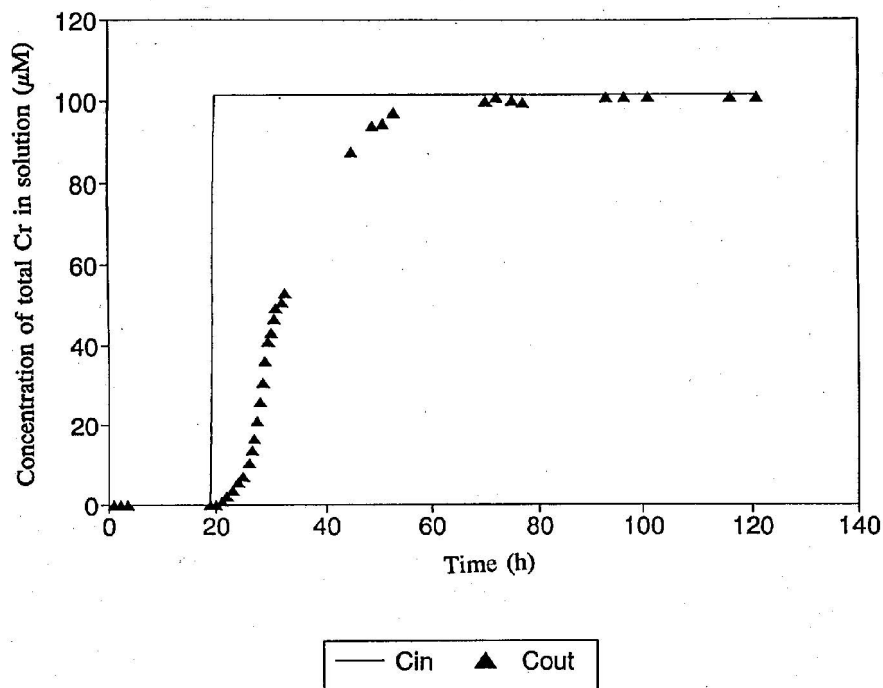


acting solutions are pumped. Figure VII.3 shows the accumulation of chromate from solutions which have been pumped through such a reactor [96DEN/STJ]. Comparing the breakthrough of chromate with a non-adsorbing tracer (Na^+) shows a significant retardation of Cr due to adsorption on the mineral in the reactor. Figure VII.4 shows the surface excess, calculated from the difference in inflow and outflow concentrations as a function of time during the experiments. Results are plotted for experiments with three different inflowing standard solutions of chromate. In each experiment, the adsorption density reaches a constant value with time. This value depends on the concentration of chromate in the inflowing standard solution. The relation between chromate adsorption density and chromate ion activity in solution can be described by a mathematical model of chromate adsorption equilibrium; an adsorption isotherm. The following sections present the necessary theoretical concepts, and then develop them into adsorption isotherms.

VII.2.3. Stoichiometric adsorption reactions and the thermodynamic law of mass action

The stoichiometric reaction for adsorption of chromate on goethite is described as a ligand exchange reaction where chromate ion displaces water at hydrated iron sites (represented by the notation $>\text{FeOH}_2^+$) on the mineral (Eq. (VII.6)). Eq. (VII.7) defines the corre-

Figure VII.3: Breakthrough of total dissolved Cr with time for Cr(VI) adsorption on iron oxide, using the flow-through reactor shown in Figure VII.2. At 20 hours, a solution containing NaHCrO_4 is pumped into the reactor. The delayed breakthrough of Cr, compared with Na, in the reactor effluent indicates adsorption of Cr on the mineral ($\text{pH} = 5$, $I = 0.5 \text{ M NaClO}_4$, 0.11 g FeOOH ; reprinted with permission from [96DEN/STJ]).



sponding thermodynamic mass law in terms of molar activities ($\text{mol} \cdot \text{l}^{-1}$), denoted by curved brackets, of reactants and products. For reaction of dilute solutes, the activity of water approaches unity and is neglected in the mass law. The superscript “s” on the formation constant is used to note the formation of a surface complex. Eq. (VII.8) is analogous to Eq. (VII.7) but written in terms of molar concentration and activity coefficients.

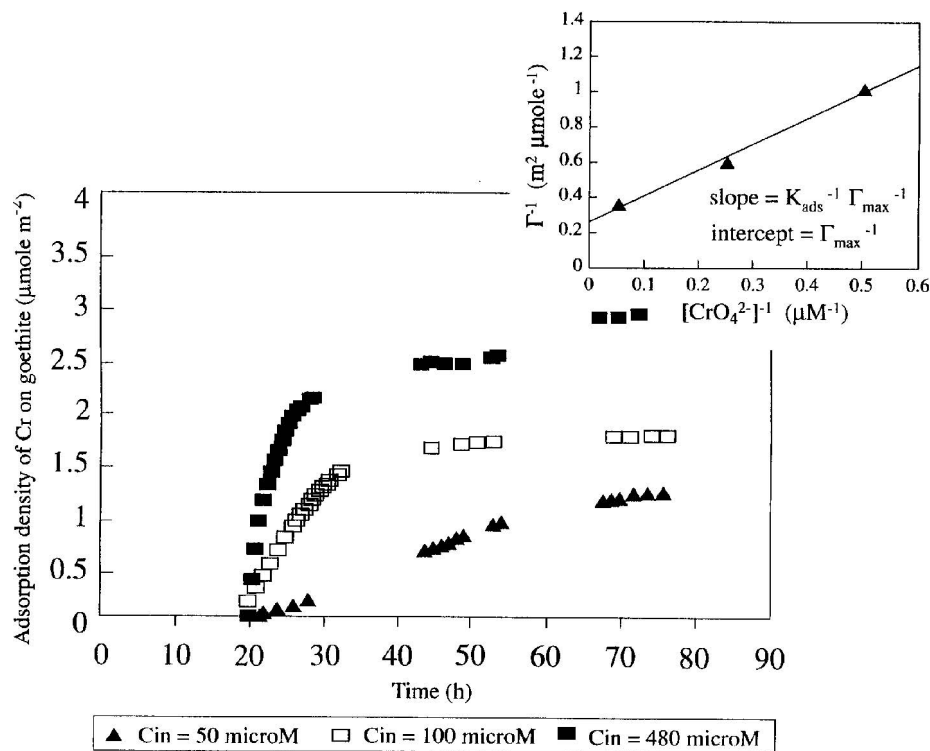


$$\beta_1^s = \frac{\{>\text{FeCrO}_4^-\}}{\{>\text{FeOH}_2^+\}\{\text{CrO}_4^{2-}\}} \quad (\text{VII.7})$$

$$\beta_1^s = \frac{\gamma_{\text{FeCr}}[>\text{FeCrO}_4^-]}{\gamma_{\text{Fe}}[>\text{FeOH}_2^+]\gamma_{\text{Cr}}[\text{CrO}_4^{2-}]} \quad (\text{VII.8})$$

$$\beta_1'^s = \frac{\gamma_{\text{Fe}}\gamma_{\text{Cr}}}{\gamma_{\text{FeCr}}} \beta_1^s = \frac{[>\text{FeCrO}_4^-]}{[>\text{FeOH}_2^+][\text{CrO}_4^{2-}]} \quad (\text{VII.9})$$

Figure VII.4: Surface excess of Cr on colloidal goethite, calculated by mass balance from Cr breakthrough curves for three different feed solution concentrations: $[\text{Cr(VI)}]_{\text{in}} = 50, 100$ and $480 \mu\text{M}$. Insert: the adsorption isotherm obtained by plotting the reciprocal of surface excess against the reciprocal of chromate ion concentration in solution (see text; $\text{pH} = 5$, $I = 0.5 \text{ M NaClO}_4$, 0.11 g FeOOH ; reprinted with permission from [96DEN/STJ]).



Eq. (VII.9) defines the conditional formation constant β_1^s , where the corresponding mass law can be written solely in terms of molar concentrations. Chemical activity can be expressed as the product of molar concentration and an activity coefficient γ_i for each species i . Activity coefficients correct molar concentrations to molar activities for non-idealities introduced by interactions between charged species, both on the surface and in solution, and take the value of unity at the reference state. For surface species, the reference state is the uncharged surface. For dissolved species, the reference state is a hypothetical condition: an ideal solution of unit molality in which the activity of the solute is unity (the dissolved species thus has the properties it would have at infinite dilution). Because the singly protonated surface site, $>\text{FeOH}_2^+$, has a formal charge of +1, the reference state of zero charge is represented by the deprotonated site, $>\text{FeOH}$.

VII.2.4. Combining mass balances and thermodynamic mass laws: The adsorption isotherm

Eq. (VII.9) can be combined with the mass balance for surface sites (Eq. (VII.10)) written in terms of molar concentration.

$$\Gamma_T a \rho_b \varepsilon^{-1} = [> \text{FeOH}_2^+] + [> \text{FeCrO}_4^-] \quad (\text{VII.10})$$

Combining Eqs. (VII.9) and (VII.10) by eliminating the term $[> \text{FeOH}_2^+]$ and solving the resulting expression for $[> \text{FeCrO}_4^-]$ gives a mathematical expression relating the surface excess of chromate (Γ_{Cr}) to the chromate ion concentration in solution; *i.e.*, the chromate adsorption isotherm (Eq. (VII.11)).

$$\Gamma_{\text{Cr}} a \rho_b \varepsilon^{-1} = \frac{\beta_1'^s \Gamma_T a \rho_b \varepsilon^{-1} [\text{CrO}_4^{2-}]}{1 + \beta_1'^s [\text{CrO}_4^{2-}]} \quad (\text{VII.11})$$

Dividing Eq. (VII.10) by $(a \rho_b \varepsilon^{-1})$, and taking the reciprocal of both sides, yields a linear expression (Eq. (VII.12)) with slope $(\beta_1'^s \Gamma_T)^{-1}$ and intercept $(\Gamma_T)^{-1}$.

$$(\Gamma_{\text{Cr}})^{-1} = (\beta_1'^s \Gamma_T)^{-1} [\text{CrO}_4^{2-}]^{-1} + (\Gamma_T)^{-1} \quad (\text{VII.12})$$

The inset to Figure VII.4 shows $(\Gamma_{\text{Cr}})^{-1}$, plotted against $[\text{CrO}_4^{2-}]^{-1}$. The three data points fall on a straight line, and values of $\Gamma_T = 3.7 \times 10^{-6} \text{ mol} \cdot \text{m}^{-2}$ and $\beta_1'^s = 1.9 \times 10^{-5} \text{ M}^{-1}$ are estimated from linear regression of the data. The Gibbs' free energy of formation for the surface species $> \text{FeCrO}_4^-$ can thus be estimated if $\beta_1'^s$ has been determined under conditions approaching the standard states of infinite dilution and zero surface charge, or if the activity coefficients are known (Eq. (VII.13)).

$$\Delta_r G_m = -RT \ln(\beta_1'^s) \quad (\text{VII.13})$$

VII.2.4.1. The Langmuir adsorption isotherm

Dividing Eq. (VII.11) by $(a \Gamma_T)$ and re-arranging yields a standard form of the Langmuir isotherm (Eq. (VII.14)), where the ratio of surface sites occupied by chromate, to those unoccupied, is proportional to the solution concentration of the adsorbing species. For chromate adsorption on iron oxide, the adsorption intensity constant, K , is defined by the conditional surface complexation constant, $\beta_1'^s$, and the aqueous concentration of adsorbate, $C_{(\text{aq})}$, is $[\text{CrO}_4^{2-}]$. This isotherm results from a model of a single adsorbate on a single adsorbent with a finite number of adsorption sites, all with an equal free energy of adsorption at a fixed temperature.

$$\frac{\Theta}{(1 - \Theta)} = K C_{(\text{aq})} \quad (\text{VII.14})$$

These assumptions are inherent in our treatment of chromate adsorption as formation of a single surface species with a fixed number of sites for complex formation at the iron oxide surface. The isotherm is widely used in surface science and has been applied to solid-gas and liquid-gas interfaces as well as to many types of solid-liquid phase interfaces.

VII.2.4.2. A linear adsorption isotherm: The distribution coefficient

Inspection of Eq. (VII.14) shows that a consequence of the Langmuir isotherm is that for low surface concentration of adsorbate, $\Theta \ll 1$, the surface density is predicted to be proportional to the solution concentration, $\Theta = K C_{(\text{aq})}$. Inspection of Eq. (VII.11) shows that low adsorption density and linear adsorption are likewise predicted for low concentrations of chromate ion ($\beta_1'^s [\text{CrO}_4^{2-}] \ll 1$). This means that for trace concentrations of chromate, its adsorption can be adequately modelled by a simple K_d expression (Eq. (VII.15)), where $C_{(\text{sur})} = [>\text{FeCrO}_4^-]$, $C_{(\text{aq})} = [\text{CrO}_4^{2-}]$, and $K_d = (\beta_1'^s \Gamma_T a \mathcal{S})$

$$C_{(\text{sur})} = K_d C_{(\text{aq})} \quad (\text{VII.15})$$

VII.2.5. The influence of solution speciation on adsorption

The stoichiometric reaction for Cr(VI) adsorption on iron oxide is written in terms of the chromate ion concentration. The adsorption reaction corresponds to formation of unique surface chemical species with a specific Gibbs' free energy. The free energy of reaction in turn depends on the free energy of the aqueous species chosen as the Cr component for the adsorption reaction; solution speciation must be considered when modelling adsorption.

Wet chemical analytical techniques often determine the total concentration of an element in solution. We represent this by the notation $\sum[\text{H}_2\text{CrO}_4]$ for chromium, indicating the sum of concentration for all chromium(VI) species in solution. Eqs. (VII.16) and (VII.17) are the stoichiometric reactions for formation of hydrogen-chromate and chromate ion, respectively. The conditional thermodynamic constants have been adjusted for changes in chemical activity due to ionic strength effects using the Davies' equation (*p.103* in [96STU/MOR]).



$$\log_{10} K_1'(\text{VII.16}, 25^\circ\text{C}, 0.5 \text{ M NaClO}_4) = 0.7$$

$$\log_{10} K_2'(\text{VII.17}, 25^\circ\text{C}, 0.5 \text{ M NaClO}_4) = -5.8$$

For the experiments shown above, carried out at pH 5, the concentration of the species H_2CrO_4 is negligible for $\text{pH} \gg \text{p}K_1' = -0.7^\dagger$

$$\begin{aligned} \sum[\text{H}_2\text{CrO}_4] &= [\text{H}_2\text{CrO}_4] + [\text{HCrO}_4^-] + [\text{CrO}_4^{2-}] \\ &\approx [\text{HCrO}_4^-] + [\text{CrO}_4^{2-}] \end{aligned} \quad (\text{VII.18})$$

The distribution of dissolved species is thus defined by Eqs. (VII.19) and (VII.20), and depends strongly on pH.

$$\alpha_1 = \frac{[\text{HCrO}_4^-]}{\sum[\text{H}_2\text{CrO}_4]} = \frac{[\text{H}^+]}{K_2' + [\text{H}^+]} \quad (\text{VII.19})$$

[†] In this Chapter the “p” nomenclature is sometimes used: $\text{p}K$, pH , pM , *etc.*, are symbols for $-\log_{10} K$, $-\log_{10} a_{\text{H}^+}$, $-\log_{10} a_{\text{M}}$, *etc.*

$$\alpha_2 = \frac{[\text{CrO}_4^{2-}]}{\sum [\text{H}_2\text{CrO}_4]} = \frac{K'_2}{K'_2 + [\text{H}^+]} \quad (\text{VII.20})$$

The chromate ion concentrations plotted in Figure VII.4, and used to estimate β_1^s and Γ_T can thus be calculated for pH 5 from the total analytical concentration of Cr(VI) in solution, and Eq. (VII.20): $[\text{CrO}_4^{2-}] = (\sum [\text{H}_2\text{CrO}_4] K'_2) / (K'_2 + [\text{H}^+])$.

Analogous to solution species, many mineral and organic surfaces undergo protonation and deprotonation reactions. Potentiometric titration of aqueous suspensions of colloidal goethite ($\alpha\text{-FeOOH}$) show that proton adsorption and desorption corresponds to the following stoichiometric reactions, [90LOE/SJO]:



$$\log_{10} K'_1(\text{VII.21}, 25^\circ\text{C}, 0.5 \text{ M NaClO}_4) = -7.47$$

$$\log_{10} K'_2(\text{VII.22}, 25^\circ\text{C}, 0.5 \text{ M NaClO}_4) = -9.51$$

The isotherm for chromate adsorption (Eq. (VII.11)) thus corresponds to neglecting the species $>\text{FeOH}$ and $>\text{FeO}^-$ in the mass balance for surface sites (Eq. (VII.10)). This assumption is valid for pH values well below the first and second acidity constant for the goethite surface; $\text{pH} \ll \text{p}K_1^s$ and $\text{pH} \ll \text{p}K_2^s$. This assumption holds for the case here; $\text{pH} = 5$, $\text{p}K_1 = 7.47$, $\text{p}K_2 = 9.51$.

VII.3. Surface complexation

The example of chromate adsorption in the previous section provides a case study of adsorption by formation of ionic complexes at the mineral-water interface. The boundary of a solid phase at the mineral-water interface leaves surface sites with unsaturated coordination bonds. These bonds seek co-ordination partners from solution, *i.e.*, chemisorption of water, protons or hydroxide ions, forming surface complexes of variable charge.

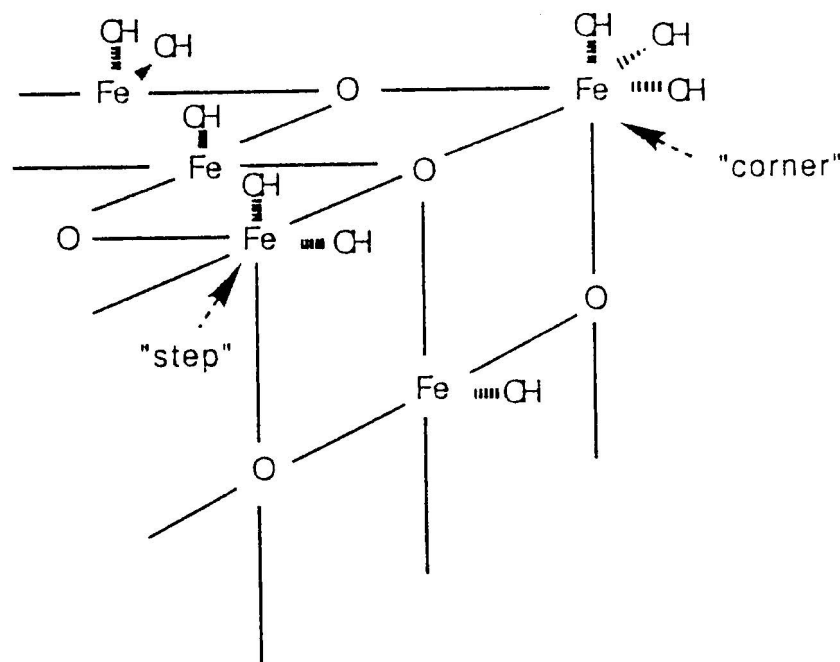
VII.3.1. Chemisorption of water: Formation of variable charged surfaces

Figure VII.5 represents a highly simplified picture of the surface of an iron oxide mineral at the solid-solution interface. Chemisorption from solution results in surface aquo complexes that undergo further co-ordination reactions in response to changes in the chemical activities of solutes; for example changes in pH. Surface charge derives from protonation/deprotonation of functional groups. Surface charge can be further modified by adsorbing charged ionic species from solution.

VII.3.2. Adsorption of ligands and metals at the hydrated surface

Chemisorbed water can be exchanged for ligands in solution. Oxy-hydroxy groups on metal carbonates and phosphates, and di-sulfide groups on sulfide minerals, can be exchanged for water. Ligands remaining on the surface, or which re-adsorb, can likewise

Figure VII.5: Hydroxide ions chemically bound to terminal Fe(III) sites on the surface of iron oxide. These groups can protonate, de-protonate, undergo ligand exchange with dissolved species or bind metal ions through formation of surface hydrolysis species. Such reactions for metal-oxide, -sulphide, -carbonate and -phosphate surfaces, and organic surfaces are listed in Table VII.1.



undergo acid-base reactions, and bind metal ions from solution. For example, metal ions display a chemical affinity for surface hydroxy groups, as they do for hydroxide ions in solution. Metals will therefore adsorb by forming surface hydrolysis complexes. Table VII.1 shows types of surface functional groups, and the changes in surface charge that result from co-ordination reactions with ligands and metals at the surface.

The general notation for surface functional groups at the solid-water interface is given by $>\text{SOH}$, where S represents the central cation of a hydroxy or oxy-hydroxy complex. Based on Table VII.1, some examples for $>\text{SOH}$ are: hydroxylated $>\text{AlOH}$ sites on aluminium oxides or aluminosilicate minerals, hydroxyl groups bound to sulfide minerals ($>\text{SMOH}^-$), $>(\text{PO}_3)\text{OH}$ groups on metal phosphates, $>(\text{CO}_2)\text{OH}$ groups on metal carbonates, carboxyl groups, $>(\text{CO})\text{OH}$ on organic surfaces (after Charlet [94CHA]).

Table VII.1: Functional groups at the solid-water interface

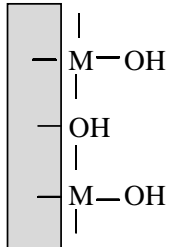
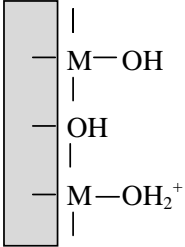
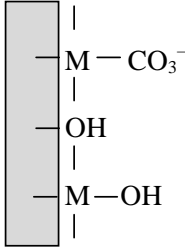
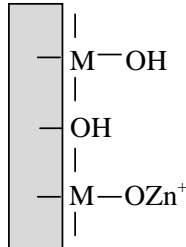
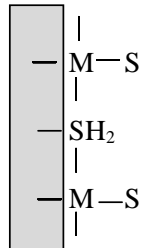
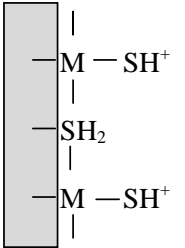
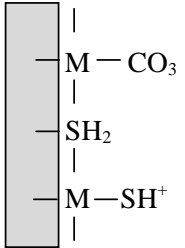
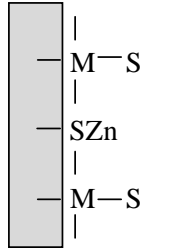
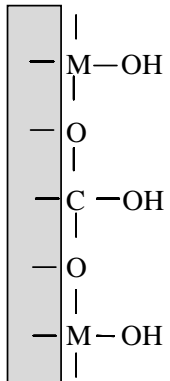
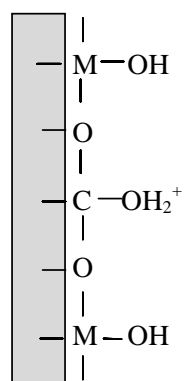
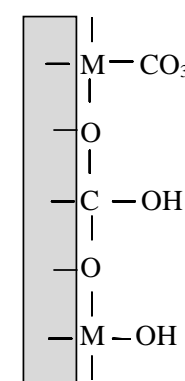
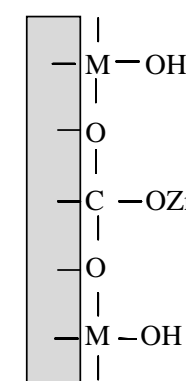
UNCHARGED SURFACE	PROTONATION	LIGAND EXCHANGE	METAL COMPLEXATION
$>\text{SOH}$	$>\text{SOH} + \text{H}^+ = >\text{SOH}_2^+$	$>\text{SOH} + \text{CO}_3^{2-} = >\text{SCO}_3^- + \text{OH}^-$	$>\text{SOH} + \text{Zn}^{2+} = >\text{SOZn}^+ + \text{H}^+$
 <p>METAL OXIDE</p>			
 <p>METAL SULFIDE</p>	 <p>see [91ROE/SJO]</p>		
 <p>METAL CARBONATE</p>			

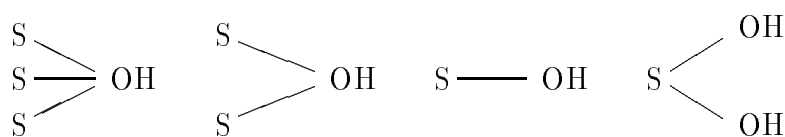
Table VII.1 (continued)

UNCHARGED SURFACE	PROTONATION	LIGAND EXCHANGE	METAL COMPLEXATION
$>\text{SOH}$	$>\text{SOH} + \text{H}^+ = >\text{SOH}_2^+$	$>\text{SOH} + \text{CO}_3^{2-} = >\text{SCO}_3^- + \text{OH}^-$	$>\text{SOH} + \text{Zn}^{2+} = >\text{SOZn}^+ + \text{H}^+$
<p>METAL PHOSPHATE</p>			
<p>ORGANIC SURFACE</p>	<p>deprotonation: $>\text{SOH} = >\text{SO}^- + \text{H}^+$</p>	<p>Organic functional groups are assumed to be irreversibly bound to the organic matrix, analogous to synthetic organic chelating resins, and do not undergo reversible ligand exchange with solution species.</p>	

Table VII.2 compares the general framework for co-ordination reactions in solution and at solid-water interfaces. This framework provides consistent notation for:

- writing stoichiometric reactions,
- formulation of the corresponding thermodynamic mass action laws, and
- definition of important conservative parameters.

It is important to note that the picture of the hydrated mineral surface represented by the reactions in Table VII.2 is very much simplified. For example, the surface of even a very simple hydrous oxide mineral is not uniform. It contains a variety of hydroxyl groups that are neither structurally nor chemically equivalent, [89HIE/RIE]:



The simple surface complexation models presented in Table VII.2 are only qualitatively correct at the microscopic level, even though a good quantitative description of titration data, adsorption isotherms and surface charge changes with pH are obtained. Surface complexation models thus reflect the average stoichiometry and intensity of surface chemical reactions at macroscopic level, in the statistical sense of a mean field. The heterogeneity at microscopic level is confirmed by results from surface spectroscopic studies (see review by Charlet [94CHA]). Such results are critical to understanding the limits of applicability for the simple one site model presented here.

VII.3.3. The pH dependence of adsorption

Because water is the solute and a dominant reaction partner, protons and hydroxide ions, respectively, compete with metals and ligands for co-ordination partners on the surface and in solution. Table VII.3 summarises an example that compares the pH dependence of adsorption for Cr^{3+} and CrO_4^{2-} on iron oxide. The results plotted in Figure VII.6a show that Cr^{3+} adsorption increases with increasing pH. The adsorption edge, the pH where surface concentration of Cr^{3+} starts to increase sharply, occurs at a relatively low pH. This behaviour is explained by the tendency of tri-valent aquo ions to hydrolyse at low pH. In the presence of iron oxide, Cr^{3+} forms surface complexes, binding to OH groups on the surface.

Eqs. (VII.25) and (VII.26) illustrate the tendency of metal ions to form complexes with OH groups either on the surface or in solution. The dash between the oxygen and hydrogen

Table VII.2: Stoichiometry, thermodynamic laws of mass action and capacity factors for solution and surface coordination reactions.

SOLUTION COORDINATION REACTIONS:	
Stoichiometric reaction:	Thermodynamic mass action law:
Protonation of a ligand: $r \text{H}^+ + \text{L}^{p-} \rightleftharpoons \text{H}_r\text{L}^{r-p}$	$\beta_{1,r} = [\text{H}_r\text{L}^{r-p}] / ([\text{H}^+]^r [\text{L}^{p-}])$
Hydrolysis of a metal ion: $\text{M}^{n+} + q \text{H}_2\text{O}(l) \rightleftharpoons \text{M}(\text{OH})_q^{n-q} + q \text{H}^+$	${}^*\beta_q = [\text{M}(\text{OH})_q^{n-q}] [\text{H}^+]^q / [\text{M}^{n+}]$
Formation of metal ion complexes: $\text{M}^{n+} + qr \text{H}^+ + q \text{L}^{p-} \rightleftharpoons \text{M}(\text{H}_r\text{L})_q^{n+q(r-p)}$	$\beta_q = [\text{M}(\text{H}_r\text{L})_q^{n+q(r-p)}] / ([\text{M}^{n+}] [\text{H}^+]^{qr} [\text{L}^{p-}]^q)$
Conservative parameters:	
<p>Total metal concentration (j different ligands, L; all q):</p> $\begin{aligned} \text{M}_T &= [\text{M}^{n+}] + \sum_j \sum_q [\text{M}(\text{H}_r\text{L})_q^{n+q(r-p)}] + \sum_q [\text{M}(\text{OH})_q^{n-q}] \\ &= [\text{M}^{n+}] \left(1 + \sum_j \sum_q \beta_q [\text{H}^+]^{qr} [\text{L}^{p-}]^q + \sum_q {}^*\beta_q [\text{H}^+]^{-q} \right) \end{aligned}$ <p>Total ligand concentration (i different metals, M; all r and q):</p> $\begin{aligned} \text{L}_T &= [\text{L}^{p-}] + \sum_r [\text{H}_r\text{L}^{r-p}] + \sum_i \sum_q \sum_r q [\text{M}(\text{H}_r\text{L})_q^{n+q(r-p)}] \\ \text{for the formation of 1:1 complexes } q = 1: \\ &= [\text{L}^{p-}] \left(1 + \sum_r \beta_{1,r} [\text{H}^+]^r + \sum_i \sum_q \sum_r \beta_q [\text{H}^+]^{qr} [\text{M}^{n+}] \right) \end{aligned}$ <p>Proton binding capacity (j different ligands, L):</p> $\text{C}_T = \sum_j p \text{L}_T$ <p>Total acidity with reference to H_2O, M^{n+}, L^{p-} (i different metals, j different ligands; all r and q):</p> $\begin{aligned} \text{H}_T &= [\text{H}^+] + \sum_j \sum_r r [\text{H}_r\text{L}^{r-p}] + \sum_i \sum_j \sum_r r q [\text{M}(\text{H}_r\text{L})_q^{n+q(r-p)}] \\ &\quad - \sum_i \sum_q q [\text{M}(\text{OH})_q^{n-q}] - [\text{OH}^-] \end{aligned}$	

Table VII.2 (continued)

SURFACE COORDINATION REACTIONS:	
Stoichiometric reaction:	Thermodynamic mass action law:
Protonation/deprotonation of sites:	
$>\text{SOH} + \text{H}^+ \rightleftharpoons >\text{SOH}_2^+$	$K_{\text{surf},1,2} = [>\text{SOH}_2^+] / ([>\text{SOH}] [\text{H}^+])$
$>\text{SOH} \rightleftharpoons >\text{SO}^- + \text{H}^+$	$(K_{\text{surf},1,1})^{-1} = [>\text{SO}^-] [\text{H}^+] / [>\text{SOH}]$
Metal ion adsorption:	
$>\text{SOH} + m \text{M}^{n+} \rightleftharpoons >\text{SOM}_m^{nm-1} + \text{H}^+$	${}^*\beta_{\text{surf},1,m} = [>\text{SOM}_m^{nm-1}] [\text{H}^+] / ([>\text{SOH}] [\text{M}^{n+}]^m)$
Ligand adsorption:	
$>\text{SOH} + (qr + 1) \text{H}^+ + q \text{L}^{p-} \rightleftharpoons >\text{S}(\text{H}_r\text{L})_q^{q(r-p)+1} + \text{H}_2\text{O}(\text{l})$	$\beta_{\text{surf},1,q} = [>\text{S}(\text{H}_r\text{L})_q^{q(r-p)+1}] / ([>\text{SOH}] [\text{H}^+]^{(qr+1)} [\text{L}^{p-}]^q)$
Conservative parameters:	
Total adsorbed metal concentration (i different metals):	
$\text{M}_T^{\text{surf}} = \sum_m m [>\text{SOM}_m^{nm-1}]$ $= \sum_m m ([\text{M}^{n+}] {}^*\beta_{\text{surf},1,m} [>\text{SOH}] [\text{H}^+]^{-1})$ for the formation of 1:1 complexes, $m = 1$: $\text{M}_T^{\text{surf}} = [\text{M}^{n+}] \sum_m {}^*\beta_{\text{surf},1,m} [>\text{SOH}] [\text{H}^+]^{-1}$	
Total adsorbed ligand concentration:	
$\text{L}_T^{\text{surf}} = \sum_r \sum_q q [>\text{S}(\text{H}_r\text{L})_q^{q(r-p)+1}]$ $= \sum_r \sum_q q \beta_{\text{surf},1,q} [>\text{SOH}] [\text{H}^+]^{(qr+1)} [\text{L}^{p-}]^q$	
Total surface acidity (i different metals, j different ligands):	
$\text{H}_T^{\text{surf}} = [>\text{SOH}_2^+] + \sum_j \sum_r \sum_q q [>\text{S}(\text{H}_r\text{L})_q^{q(r-p)+1}]$ $- \sum_i \sum_m m [>\text{SOM}_m^{nm-1}] - [>\text{SO}^-]$	
Total surface charge (i different metals, j different ligands):	
$\text{Q}_T^{\text{surf}} = [>\text{SOH}_2^+] + \sum_j \sum_r \sum_q (q(r-p) + 1) [>\text{S}(\text{H}_r\text{L})_q^{q(r-p)+1}]$ $+ \sum_i \sum_m (nm - 1) [>\text{SOM}_m^{nm-1}] - [>\text{SO}^-]$	

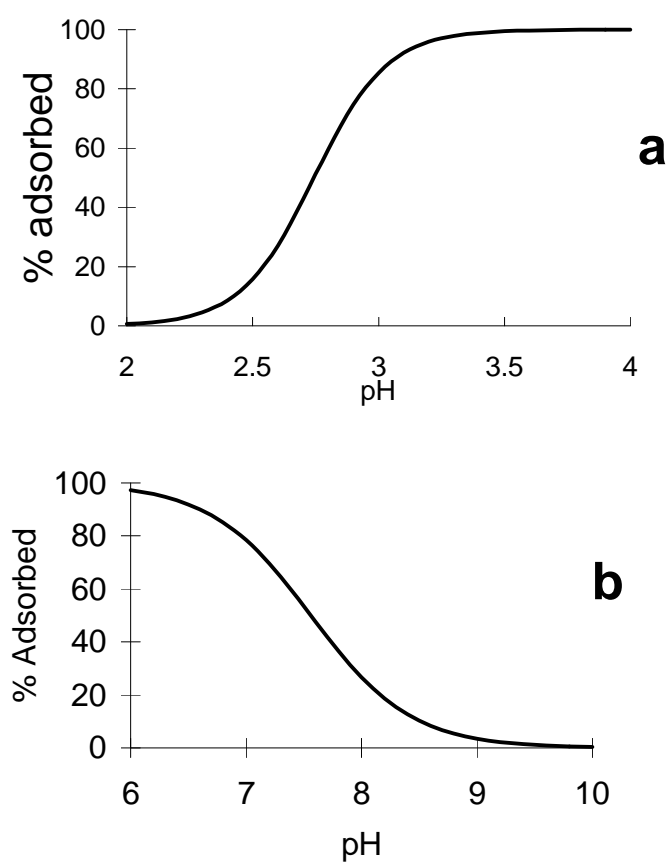
Table VII.3: Cr^{3+} and CrO_4^{2-} adsorption on iron hydroxide

Cr^{3+} ADSORPTION:			
Stoichiometric Model:		$\log_{10} K$	Reference
$>\text{FeOH} + \text{Cr}^{3+} + \text{H}_2\text{O(l)} \rightleftharpoons >\text{FeOCrOH}^+ + 2 \text{H}^+$		2.06	[90DZO/MOR]
$>\text{FeOH}_2^+ \rightleftharpoons >\text{FeOH} + \text{H}^+$		-7.29	[90DZO/MOR]
$>\text{FeOH}_2^+ + \text{Cr}^{3+} + \text{H}_2\text{O(l)} \rightleftharpoons >\text{FeOCrOH}^+ + 3 \text{H}^+ \quad (\text{VII.23})$		-5.23	
Thermodynamic Law of Mass Action:			
$^*\beta_{\text{surf}}(\text{VII.23}) = [>\text{FeOCrOH}^+] [\text{H}^+]^3 / ([>\text{FeOH}_2^+] [\text{Cr}^{3+}]), \quad \log_{10} ^*\beta_{\text{surf}}(\text{VII.23}) = -5.23$			
Mass Balances:			
Chromium:	$\text{Cr}_T = [\text{Cr}^{3+}] + [>\text{FeOCrOH}^+]$		
Iron Hydroxide:	$\text{Fe}_T = [>\text{FeOH}_2^+] + [>\text{FeOH}] + [>\text{FeO}^-] + [>\text{FeOCrOH}^+]$		
Assumptions:			
1. Surface sites are protonated at low pH:	$[>\text{FeOH}], [>\text{FeO}^-] \ll [>\text{FeOH}_2^+]$		
2. Chromium in trace concentrations:	$[\text{Cr}^{3+}], [>\text{FeOCrOH}^+] \ll [>\text{FeOH}_2^+]$		
Adsorption Model from combining mass action law, mass balances and assumptions:			
$[>\text{FeOCrOH}^+] = ^*\beta_{\text{surf}}(\text{VII.23}) \text{Cr}_T / ([\text{H}^+]^3 + ^*\beta_{\text{surf}}(\text{VII.23}) \text{Fe}_T)$			

Table VII.3 (continued)

CrO ₄ ²⁻ ADSORPTION:			
Stoichiometric Reactions:		log ₁₀ <i>K</i>	Reference
$\begin{aligned} >\text{FeOH} + \text{CrO}_4^{2-} + \text{H}^+ &\rightleftharpoons >\text{FeCrO}_4^- + \text{H}_2\text{O(l)} & \text{(VII.24)} \\ >\text{FeOH}_2^+ &\rightleftharpoons >\text{FeOH} + \text{H}^+ \\ >\text{FeOH} &\rightleftharpoons >\text{FeO}^- + \text{H}^+ \\ \text{CrO}_4^{2-} + \text{H}^+ &\rightleftharpoons \text{HCrO}_4^- \\ \text{HCrO}_4^- + \text{H}^+ &\rightleftharpoons \text{H}_2\text{CrO}_4(\text{aq}) \end{aligned}$		10.85 -7.29 -8.93 5.8 -0.7	[90DZO/MOR] [90DZO/MOR] [90DZO/MOR] [96DEN/STJ] [96DEN/STJ]
Thermodynamic Laws of Mass Action:			
$\begin{aligned} \beta_{\text{surf}}(\text{VII.24}) &= [>\text{FeCrO}_4^-] / \left([>\text{FeOH}] [\text{CrO}_4^{2-}] [\text{H}^+] \right) \\ (\text{K}_{\text{surf},1,2})^{-1} &= [>\text{FeOH}] [\text{H}^+] / [>\text{FeOH}_2^+] \\ \text{K}_{\text{surf},1,1} &= [>\text{FeO}^-] [\text{H}^+] / [>\text{FeOH}] \\ \text{K}_{1,1} &= [\text{HCrO}_4^-] / \left([\text{CrO}_4^{2-}] [\text{H}^+] \right) \\ \text{K}_{1,2} &= [\text{H}_2\text{CrO}_4(\text{aq})] / \left([\text{HCrO}_4^-] [\text{H}^+] \right) \end{aligned}$			
Mass Balances:			
Chromium:	$\text{Cr}_T = [\text{H}_2\text{CrO}_4] + [\text{HCrO}_4^-] + [\text{CrO}_4^{2-}] + [>\text{FeCrO}_4^-]$		
Iron Hydroxide:	$\text{Fe}_T = [>\text{FeOH}_2^+] + [>\text{FeOH}] + [>\text{FeO}^-] + [>\text{FeCrO}_4^-]$		
Assumptions:			
<div> 1. Unoccupied surface sites singly protonated: $[>\text{FeOH}_2^+], [>\text{FeO}^-] \ll [>\text{FeOH}]$ </div> <div> 2. Chromium in trace concentrations: $[\text{CrO}_4^{2-}], [>\text{FeCrO}_4^-] \ll [>\text{FeOH}]$ </div> <div> 3. Dissolved chromate as chromate anion: $[\text{H}_2\text{CrO}_4], [\text{HCrO}_4^-] \ll [\text{CrO}_4^{2-}]$ </div>			
Adsorption Model from combining mass action law, mass balances and assumptions:			
$[>\text{FeCrO}_4^-] = \beta_{\text{surf}}(\text{VII.24}) \text{Fe}_T [\text{H}^+] \text{Cr}_T / (1 + \beta_{\text{surf}}(\text{VII.24}) \text{Fe}_T [\text{H}^+])$			

Figure VII.6: The pH dependence of (a) Cr^{3+} and (b) CrO_4^{2-} adsorption on iron oxide, calculated by the model given in Table VII.3. These results demonstrate the important role of pH and redox state as master variables for adsorption reactions.



atoms emphasises the hydrolysis reaction as a tendency for metal ions to displace protons as co-ordination partners for hydroxide ions (after Schindler and Stumm, [87SCH/STU]).

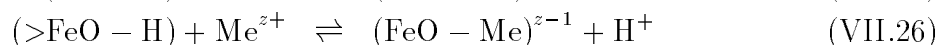


Figure VII.6b shows that the adsorbed concentration of CrO_4^{2-} decreases with increasing pH. In this case, the surface metal sites act as co-ordination partners for the chromate ligand. Hydroxide ions begin to effectively compete for surface sites as pH goes up; *i.e.*, hydroxide displaces chromate from the surface.

For either cations or anions, the pH dependence of adsorption results from chemical speciation, and the relative free energy of reaction of the surface and solution complexes. Formation of surface complexes is different to ion exchange reactions. In the case of surface complexation, ions are bound directly to metal centers and ligand functional groups on the surface. Ion exchange results from excess surface charge that is balanced by a mobile, diffuse ion swarm in the electrical double layer (see Section VII.3.6). The excess charge can, however, result from surface complexation reactions that form charged species at the surface.

VII.3.4. Competitive adsorption

Major groundwater ions that are present at total concentrations that approach the available adsorption capacity (total site concentration) will compete for available adsorption sites. Adsorption competition between sulphate, hydrogen carbonate and carbonate ions on iron hydroxide is summarised in Table VII.4. Figure VII.7a shows the effect of increasing groundwater p_{CO_2} to form surface Fe-carbonate complexes at near-neutral pH. For an open system in equilibrium with the atmosphere ($p_{\text{CO}_2} = 10^{-3.5}$ atm), surface carbonate species dominate the surface.

Figure VII.7b shows that sulphate, which forms less stable iron complexes than carbonate, is a minor species on the surface, with adsorption highest at low p_{CO_2} . If p_{CO_2} is increased, *i.e.* respiration of organic carbon in an aquifer with slow diffusion of the resulting $\text{CO}_2(\text{g})$ to the atmosphere, initially adsorbed sulphate will be driven off the mineral surface due to preferential formation of the more stable surface carbonate complexes.

This predicts that increasing bicarbonate concentrations at near-neutral pH could lead to increasing sulphate concentrations in the groundwater, as recently discussed by Bruton and Viani [97BRU/VIA] for the shallow bedrock environment at the Äspö Hard Rock Laboratory. Table VII.4 compares sulphate adsorption before and after an increase in p_{CO_2} , and provides an order-of-magnitude estimate of the total adsorption capacity for the fracture minerals based on this adsorption model.

These calculations demonstrate the potential for adsorption reactions to influence major ion chemistry in groundwaters, as well as the partitioning of trace elements. Adsorption of trace elements will be affected less by adsorption competition because their concentration, by definition, will often be far less than that of available adsorption sites. In this case,

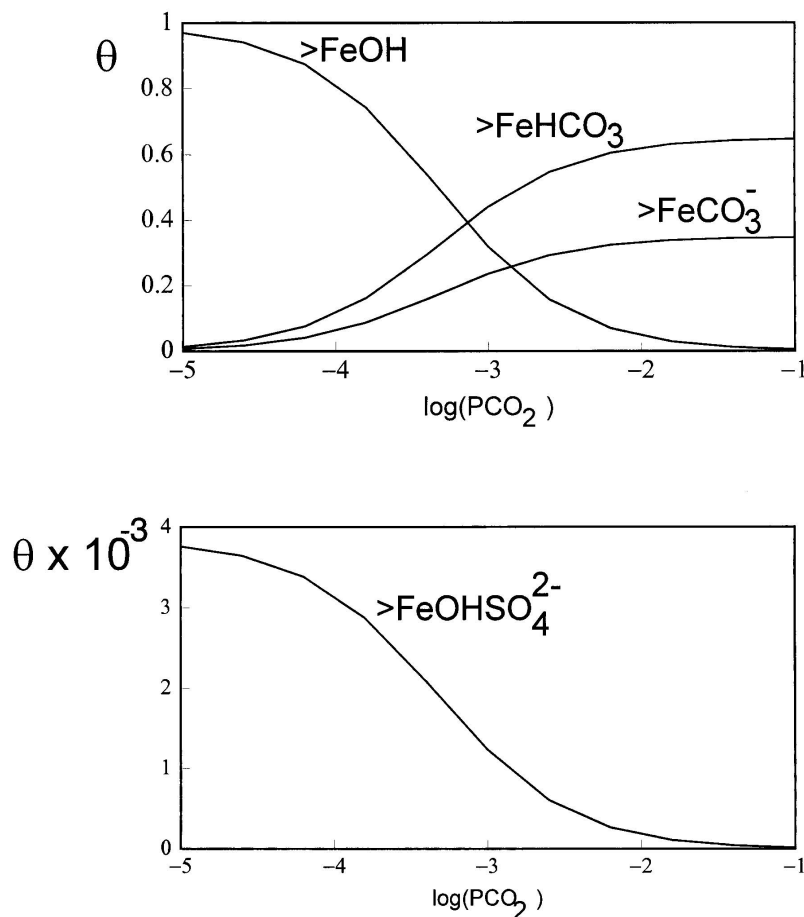
Table VII.4: Adsorption competition between sulfate and carbonate ions.

Stoichiometric Reactions:		$\log_{10} K$	Reference
$>\text{FeOH} + \text{H}^+ + \text{CO}_3^{2-} \rightleftharpoons >\text{FeCO}_3^- + \text{H}_2\text{O}$		12.71	[90DZO/MOR]
$\text{H}_2\text{O} + \text{CO}_2(\text{g}) \rightleftharpoons \text{CO}_3^{2-} + 2\text{H}^+$		-17.64	[92BRU/STU]
$>\text{FeOH} + \text{CO}_2(\text{g}) \rightleftharpoons >\text{FeCO}_3^- + \text{H}^+$	(VII.27)	-4.93	
$>\text{FeOH} + 2\text{H}^+ + \text{CO}_3^{2-} \rightleftharpoons >\text{FeHCO}_3 + \text{H}_2\text{O}$		20.78	[90DZO/MOR]
$\text{H}_2\text{O} + \text{CO}_2(\text{g}) \rightleftharpoons \text{CO}_3^{2-} + 2\text{H}^+$		-17.64	[92BRU/STU]
$>\text{FeOH} + \text{CO}_2(\text{g}) \rightleftharpoons >\text{FeHCO}_3$	(VII.28)	3.14	
$>\text{FeOH} + \text{SO}_4^{2-} \rightleftharpoons >\text{FeOHSO}_4^{2-}$	(VII.29)	0.79	[90DZO/MOR]
$>\text{FeOH} + \text{SO}_4^{2-} + \text{H}^+ \rightleftharpoons >\text{FeSO}_4^- + \text{H}_2\text{O}$	(VII.30)	7.78	[90DZO/MOR]
$>\text{FeOH}_2^+ \rightleftharpoons >\text{FeOH} + \text{H}^+$		-7.29	[90DZO/MOR]
$>\text{FeOH} \rightleftharpoons >\text{FeO}^- + \text{H}^+$		-8.93	[90DZO/MOR]
Thermodynamic Laws of Mass Action:			
$\beta_{\text{surf}}(\text{VII.27}) = [>\text{FeCO}_3^-] [\text{H}^+] ([>\text{FeOH}] p_{\text{CO}_2})^{-1}$			
$\beta_{\text{surf}}(\text{VII.28}) = [>\text{FeHCO}_3] ([>\text{FeOH}] p_{\text{CO}_2})^{-1}$			
$\beta_{\text{surf}}(\text{VII.29}) = [>\text{FeOHSO}_4^{2-}] ([>\text{FeOH}] [\text{SO}_4^{2-}])^{-1}$			
$\beta_{\text{surf}}(\text{VII.30}) = [>\text{FeSO}_4^-] ([\text{H}^+] [>\text{FeOH}] [\text{SO}_4^{2-}])^{-1}$			
$(K_{\text{surf},1,2})^{-1} = [>\text{FeOH}] [\text{H}^+] [>\text{FeOH}_2^+]^{-1}$			
$K_{\text{surf},1,1} = [>\text{FeO}^-] [\text{H}^+] [>\text{FeOH}]^{-1}$			
Mass Balances:			
Sulfate:	$S_T = [\text{SO}_4^{2-}] + [>\text{FeOHSO}_4^{2-}] + [>\text{FeSO}_4^-]$		
Carbon:	$C_T = [>\text{FeCO}_3^-] + [>\text{FeHCO}_3] + [\text{HCO}_3^-] + [\text{CO}_3^{2-}]$		
Iron Hydroxide:	$\text{Fe}_T = [>\text{FeOHSO}_4^{2-}] + [>\text{FeSO}_4^-] + [>\text{FeCO}_3^-] + [>\text{FeHCO}_3] + [>\text{FeOH}_2^+] + [>\text{FeOH}] + [>\text{FeO}^-]$		

Table VII.4 (continued)

<p>Assumption for neglecting minor species at $7.5 < \text{pH} < 8$:</p> $[>\text{FeSO}_4^-], [>\text{FeOH}_2^+], [>\text{FeO}^-] \ll [\text{FeOH}], [>\text{FeOHSO}_4^{2-}], [>\text{FeCO}_3^-], [>\text{FeHCO}_3]$													
<p>Adsorption Model by combining mass action laws, mass balances and assumptions:</p> $[>\text{FeCO}_3^-] = \beta_{\text{surf}}(\text{VII.27}) p_{\text{CO}_2} \text{Fe}_T / ([\text{H}^+] + \beta_{\text{surf}}(\text{VII.27}) p_{\text{CO}_2} + \beta_{\text{surf}}(\text{VII.28}) p_{\text{CO}_2} + \beta_{\text{surf}}(\text{VII.29}) [\text{SO}_4^{2-}] [\text{H}^+])$ $[>\text{FeHCO}_3] = \beta_{\text{surf}}(\text{VII.28}) p_{\text{CO}_2} \text{Fe}_T / ([\text{H}^+] + \beta_{\text{surf}}(\text{VII.27}) p_{\text{CO}_2} + \beta_{\text{surf}}(\text{VII.28}) p_{\text{CO}_2} + \beta_{\text{surf}}(\text{VII.29}) [\text{SO}_4^{2-}] [\text{H}^+])$ $[>\text{FeOHSO}_4^{2-}] = \beta_{\text{surf}}(\text{VII.29}) [\text{SO}_4^{2-}] [\text{H}^+] \text{Fe}_T / ([\text{H}^+] + \beta_{\text{surf}}(\text{VII.27}) p_{\text{CO}_2} + \beta_{\text{surf}}(\text{VII.28}) p_{\text{CO}_2} + \beta_{\text{surf}}(\text{VII.29}) [\text{SO}_4^{2-}] [\text{H}^+])$ $[>\text{FeOH}] = [\text{H}^+] \text{Fe}_T / ([\text{H}^+] + \beta_{\text{surf}}(\text{VII.27}) p_{\text{CO}_2} + \beta_{\text{surf}}(\text{VII.28}) p_{\text{CO}_2} + \beta_{\text{surf}}(\text{VII.29}) [\text{SO}_4^{2-}] [\text{H}^+])$													
<p>Case study (from Ref. [96BAN/TUL]):</p> <table> <tr> <th>Initial groundwater:</th><th>Final groundwater:</th></tr> <tr> <td>$I = 0.2 \text{ M}$</td><td>$I = 0.05 \text{ M}$</td></tr> <tr> <td>$\text{pH} = 7.5$</td><td>$\text{pH} = 7.8$</td></tr> <tr> <td>$[\text{SO}_4^{2-}] = 6.25 \times 10^{-4} \text{ M}$</td><td>$[\text{SO}_4^{2-}] = 1.4 \times 10^{-3} \text{ M}$</td></tr> <tr> <td>for $p_{\text{CO}_2} < 10^{-5} \text{ atm}$</td><td>for $p_{\text{CO}_2} > 10^{-2} \text{ atm}$</td></tr> <tr> <td>$[>\text{FeOHSO}_4^{2-}]/\text{Fe}_T = 3.75 \times 10^{-3}$</td><td>$[>\text{FeOHSO}_4^{2-}]/\text{Fe}_T \approx 0$</td></tr> </table>		Initial groundwater:	Final groundwater:	$I = 0.2 \text{ M}$	$I = 0.05 \text{ M}$	$\text{pH} = 7.5$	$\text{pH} = 7.8$	$[\text{SO}_4^{2-}] = 6.25 \times 10^{-4} \text{ M}$	$[\text{SO}_4^{2-}] = 1.4 \times 10^{-3} \text{ M}$	for $p_{\text{CO}_2} < 10^{-5} \text{ atm}$	for $p_{\text{CO}_2} > 10^{-2} \text{ atm}$	$[>\text{FeOHSO}_4^{2-}]/\text{Fe}_T = 3.75 \times 10^{-3}$	$[>\text{FeOHSO}_4^{2-}]/\text{Fe}_T \approx 0$
Initial groundwater:	Final groundwater:												
$I = 0.2 \text{ M}$	$I = 0.05 \text{ M}$												
$\text{pH} = 7.5$	$\text{pH} = 7.8$												
$[\text{SO}_4^{2-}] = 6.25 \times 10^{-4} \text{ M}$	$[\text{SO}_4^{2-}] = 1.4 \times 10^{-3} \text{ M}$												
for $p_{\text{CO}_2} < 10^{-5} \text{ atm}$	for $p_{\text{CO}_2} > 10^{-2} \text{ atm}$												
$[>\text{FeOHSO}_4^{2-}]/\text{Fe}_T = 3.75 \times 10^{-3}$	$[>\text{FeOHSO}_4^{2-}]/\text{Fe}_T \approx 0$												
<p>Change in SO_4^{2-} adsorption with p_{CO_2} (see Figure VII.7):</p> <p>Change in solution sulfate concentration, $\Delta[\text{SO}_4^{2-}] = 7.75 \times 10^{-4} \text{ M}$</p> <p>Change in fractional sulfate coverage, $\Delta\Theta = 3.75 \times 10^{-3}$</p> <p>Corresponding adsorption capacity, $C_T = \Delta[\text{SO}_4^{2-}]/\Delta\Theta = 0.2 \text{ M}$</p>													

Figure VII.7: The dependence of surface carbonate (top) and sulphate (bottom) species on $p\text{CO}_2$ calculated for near-neutral pH by the model presented in Table VII.4. Increasing $p\text{CO}_2$ favours the formation of surface carbonate species, and causes the weakly bound sulphate to be displaced from the mineral surface.



trace metal partitioning will be influenced much more strongly by competition between their binding by surface sites and solution ligands, and the effect of pH as presented in Figure VII.6.

VII.3.5. Non-ideal behaviour: Activity corrections for surface coverage

It is experimentally observed, notably for metal oxides, that under conditions of fixed temperature, pressure and ionic strength, that resulting conditional thermodynamic constants for surface complexation reactions vary with surface coverage of adsorbate. The reference state for the activity of surface species is defined as the uncharged surface for the two component system, solid-water, represented by the species $>\text{S-OH}$ (see Table VII.1). The variation in conditional constants with surface coverage

often fits the empirical relation described by Eq. (VII.31) [87SCH/STU]. $\beta'^s(\Theta)$ is the conditional value of the constant, β'^s , evaluated at surface coverage, Θ . Linear extrapolation of a plot of $\log_{10} \beta'^s(\Theta)$ against Θ , to the intercept at $\Theta = 0$ gives the conditional constant, β'^s , at the reference zero-charge state for the surface.

$$\beta'^s(\Theta) = \beta'^s e^{-\mathcal{A}\Theta} \quad (\text{VII.31})$$

The term $e^{-\mathcal{A}\Theta}$ thus is an empirical activity correction factor.

Defining β'^s in terms of the Langmuir adsorption isotherm (Eq. (VII.14)), and rearranging Eq. (VII.31), yields the Frumkin-Fowler-Guggenheim (FFG) isotherm (Equation (VII.32), where $b = \mathcal{A}/2$).

$$\frac{\Theta}{(1 - \Theta)} e^{-2b} = \beta'^s C_{(\text{aq})} \quad (\text{VII.32})$$

Whereas the Langmuir adsorption isotherm assumes ideal behaviour, with constant adsorption intensity for all sites up to mono-layer coverage, the FFG isotherm is derived by considering lateral interactions between adsorbed species [88ULR/STU]. These interactions can reflect contributions from chemical, electrostatic and solvation energies. This correction for non-ideal behaviour is analogous to the calculation of activity coefficients for solutes.

The Freundlich Isotherm Eq. (VII.33) is an empirical relationship that often predicts trends in surface concentration with changes in solution concentration.

$$\Gamma = K C_{(\text{aq})}^{1/m} \quad (\text{VII.33})$$

It derives from consideration of a heterogeneous surface where the adsorption intensity of the sites is defined by an exponential distribution [90ADA]. K and $1/m$ are empirical parameters fitted to a log-log plot of the data. Unlike the Langmuir isotherm, where the adsorption intensity is constant and there is a fixed number of adsorption sites, the Freundlich equation does not collapse to a linear isotherm at low solution concentrations of the adsorbate, and does not reach a defined maximum at high concentrations.

Schindler and Stumm [87SCH/STU], point out that current understanding of factors resulting in non-ideal adsorption behaviour is poor. Changes in adsorption intensity with surface coverage of charged species is often attributed to an electrostatic energy contribution to the total adsorption energy (Eq. (VII.34)). This contribution corresponds to the Coulombic energy required to move ions from the electrically-neutral solution bulk to the charged surface. The Coulombic energy is defined by Eq. (VII.35) where z is the charge of the adsorbing ion, F is Faraday's constant ($96,490 \text{ C} \cdot \text{mol}^{-1}$) and Ψ is the potential difference between the surface, Ψ_0 and the bulk of the solution, Ψ_∞ . Because of the electroneutrality condition in the solution bulk ($\Psi_\infty = 0$), Ψ is identically equal to the surface potential. It is not possible to determine Ψ_0 experimentally.

$$\Delta_{\text{ads.}} G_{\text{m}} = \Delta_{\text{chem.}} G_{\text{m}} + \Delta_{\text{coul.}} G_{\text{m}} \quad (\text{J} \cdot \text{mol}^{-1}) \quad (\text{VII.34})$$

$$\Delta_{\text{coul.}} G_{\text{m}} = z F \Psi \quad (\text{J} \cdot \text{mol}^{-1}) \quad (\text{VII.35})$$

The constant capacitance model calculates the surface potential from the surface charge assuming a linear capacitance relationship (Eq. (VII.36)), where σ is the charge density ($\text{C} \cdot \text{m}^{-2}$) and κ is the specific capacitance ($\text{F} \cdot \text{m}^{-2}$). The Coulombic energy term can thus be related to the surface concentration (Γ) of an adsorbing ion with charge z by Eq. (VII.37) where surface charge density is measured as surface excess of charged ions, Γ ($\text{mol} \cdot \text{m}^{-2}$), and then converted by $\sigma = F\Gamma$ ($\text{C} \cdot \text{m}^{-2}$). Substituting Eq. (VII.34) into Eq. (VII.13) and taking the antilogarithm yields Eq. (VII.38) where K_{ads} reflects the adsorption intensity, and K_{chemical} corresponds to the contribution of $\Delta_{\text{chem}}G_{\text{m}}$ to the adsorption intensity.

$$\Psi = \sigma/\kappa = \Gamma zF/\kappa \quad (\text{V}) \quad (\text{VII.36})$$

$$\Delta_{\text{coul}}G_{\text{m}} = \frac{\Gamma(zF)^2}{\kappa} \quad (\text{J} \cdot \text{mol}^{-1}) \quad (\text{VII.37})$$

$$K_{\text{ads}} = K_{\text{chemical}} \exp\left(\frac{-\Gamma(zF)^2}{RT\kappa}\right) \quad (\text{VII.38})$$

Eq. (VII.38) corresponds to the empirical relation for the dependence of adsorption intensity on surface coverage (Eq. (VII.31)), where $\mathcal{A} = \Gamma_{\text{T}}(zF)^2/(RT\kappa a\mathcal{S})$. Other physical-chemical models for surface potential have been used, but their description is beyond the scope of this chapter. The reader is referred to Schindler and Stumm [87SCH/STU] and included references.

Three possible causes of non-ideal adsorption behaviour can now be outlined. [87SCH/STU]:

- a heterogeneous surface with a distribution of adsorption intensities,
- lateral interactions between adsorbed species, and
- electrostatic and solvation effects for adsorption of ions on a charged surface.

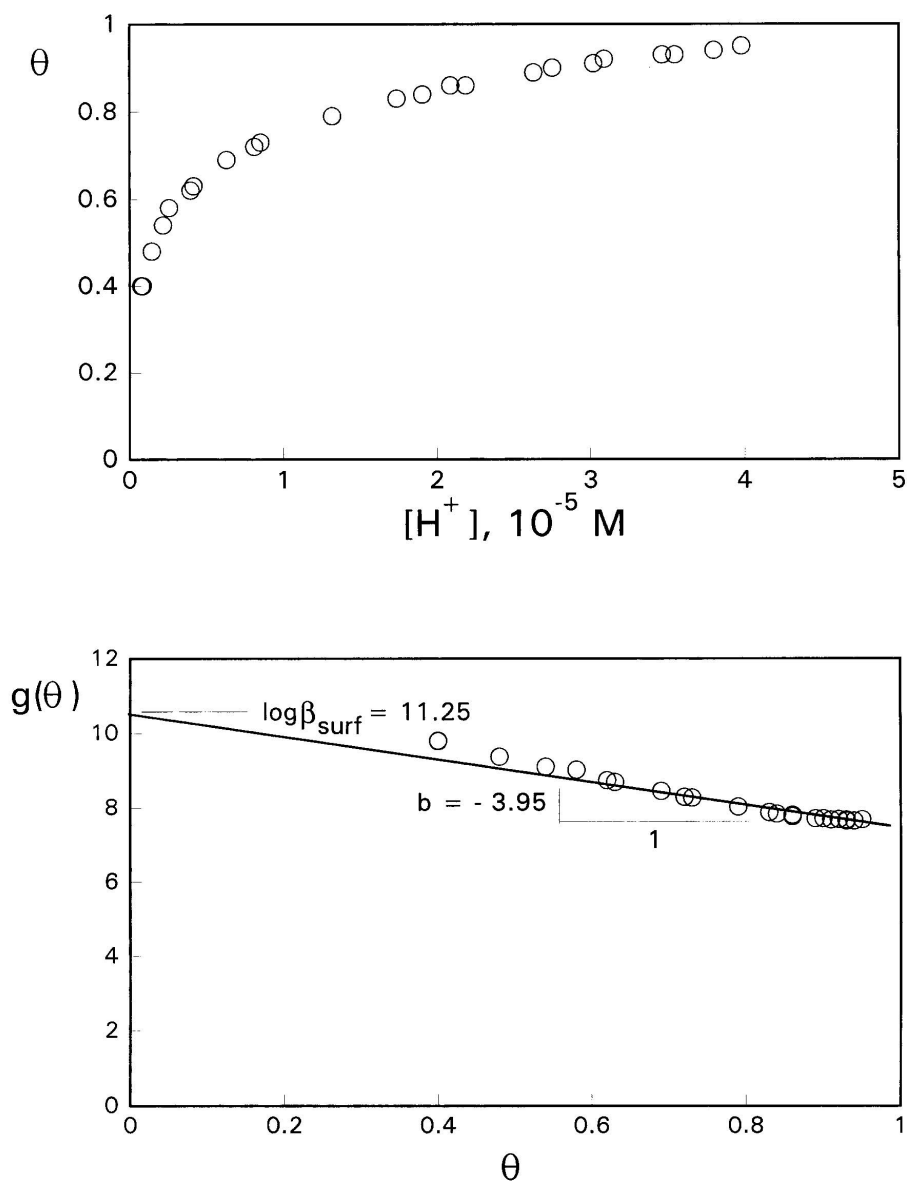
Table VII.5 (data from Gustafsson, [94GUS]) summarises an adsorption model of sulphate exchange for hydroxide ions on whole soil, based on non-ideal adsorption behaviour, and observing the empirical dependence of adsorption intensity with surface coverage. As outlined above, this mathematical model for adsorption is a result of considering either lateral interactions between adsorbate species, or coulombic energy contributions to the adsorption intensity.

Figure VII.8a shows a plot of the data referred to in Table VII.5. The smooth dependence between surface coverage and proton concentration can easily be linearised by a semi-logarithmic plot of Θ *vs.* pH [94GUS]. The model presented in Table VII.5 provides a thermodynamic description of the reaction. Figure VII.8b shows the linear relation provided by the thermodynamic model, and the line obtained by using a best fit procedure to estimate the adsorption intensity parameter at the reference state for the surface, β_1^{rs} ,

Table VII.5: Non-ideal behaviour for sulphate adsorption on soil. The data were obtained from values plotted in Ref. [94GUS], where Gustafsson demonstrated that the empirical relationship shown in Figure VII.8 is linearized on a semi-logarithmic plot of Θ *versus* 2pH .

<p>Stoichiometric Reaction:</p> $2 \text{>SOH} + \text{SO}_4^{2-} + 2 \text{H}^+ \rightleftharpoons \text{>S}_2\text{SO}_4 + 2 \text{H}_2\text{O(l)}$
<p>Thermodynamic Mass Action Law:</p> $\beta_{\text{surf},1,1} = [\text{>S}_2\text{SO}_4] \left([\text{>SOH}]^2 [\text{H}^+]^2 [\text{SO}_4^{2-}] \right)^{-1}$
<p>Mass Balance (let one adsorption site be defined as $\frac{1}{2} \text{>FeOH}$):</p> $S_T = [2 \text{>SOH}] + [\text{>S}_2\text{SO}_4]$
<p>Adsorption Model, where $e^{b\Theta}$ reflects change in adsorption intensity with surface coverage (see text):</p> $\Theta / (1 - \Theta) = e^{b\Theta} \beta_{\text{surf},1,1} [\text{H}^+]^2 [\text{SO}_4^{2-}]$
<p>Linearized Form of Adsorption Model:</p> $g(\Theta) = \log_{10} \beta_{\text{surf},1,1} + b\Theta$ <p>where $g(\Theta) = \log_{10} (\Theta / (1 - \Theta)) + 2 \text{pH} - \log_{10} [\text{SO}_4^{2-}]$. Plotting $g(\Theta)$ <i>vs.</i> Θ for a data set of Θ measured at known values of pH and $[\text{SO}_4^{2-}]$ allows a linear regression of the data to obtain $\log_{10} \beta_{\text{surf},1,1}$ as the intercept, and b as the slope, see Figure VII.8a.</p>
<p>Constants Fitted by Linear Regression (Figure VII.8, uncertainties = 3σ):</p> $\log_{10} \beta_{\text{surf},1,1} = 11.2 \pm 0.3$ $b = -3.9 \pm 0.4$

Figure VII.8: An empirical relationship showing the amount of surface-bound sulphate corresponding to dissolved proton concentration for a number of Swedish soils is shown in the upper diagram (from [94GUS]). The bottom graph shows the determination of the conditional stability constant for: $2 >\text{SOH} + \text{SO}_4^{2-} + 2 \text{H}^+ \rightleftharpoons >\text{S}_2\text{SO}_4 + 2 \text{H}_2\text{O}(\text{l})$ (see equations in Table VII.5). The slope of the line reflects the degree to which the conditional constant is affected by surface coverage. This dependence is conceptually similar to using activity coefficients in order to account for the effects of ionic strength on the stability of solution complexes.



and the empirical coefficient, \mathcal{A} , used in Eq. (VII.31) to correct the activity of adsorbed sulphate for surface coverage.

It is reasonable to assume that for adsorption in a complex matrix such as soil, surface heterogeneity will result from a wide distribution of sites (organic material, clay minerals, calcite, iron oxides, organic coatings and mineral precipitates on these surfaces) having different free energies of adsorption for sulphate. Electrostatic effects and lateral interactions between adsorbed ions may play a role as well. This example demonstrates that adsorption behaviour in a complex system can be modelled with relatively simple mathematical tools. The fundamental principle underlying this approach is, however, formal application of the thermodynamic law of mass action using a simple stoichiometric reaction model for the interaction between unoccupied surface sites and the adsorbing solute. Non-idealities are accounted for by using an empirical activity coefficient for the surface species.

VII.3.6. Charged surfaces and ion exchange

VII.3.6.1. Origins of surface charge

The aquated surfaces of solid phases acquire charge in three ways (Figure VII.9):

- Adsorption of solution species (generally, but not necessarily charged) which create surface charge upon adsorption,
- lattice imperfections in crystalline solids including ion vacancies and isomorphic substitution by charge-excess or charge-deficient ions.
- structural incorporation or hydrophobic adsorption of organic polymers with ionic functional groups that act as strong or weak acids and bases.

Eq. (VII.39) defines the net surface charge density (σ) with units $\text{C} \cdot \text{m}^{-2}$.

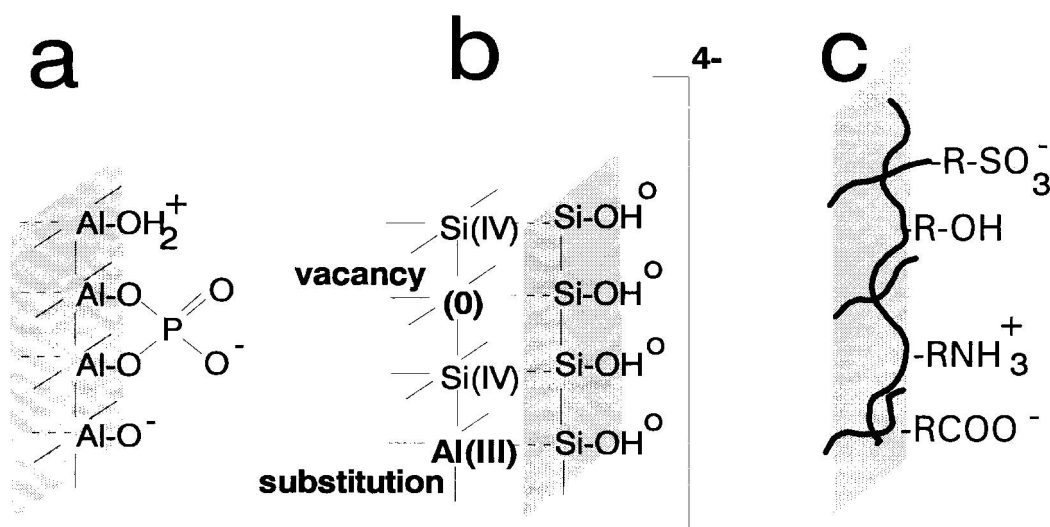
$$\sigma = \sigma_0 + \sigma_{\text{H}} + \sigma_{\text{s}} \quad (\text{VII.39})$$

σ_0 is the permanent structural charge, σ_{H} is the charge due to protons in the absence of other charged species and σ_{s} is charge density due to adsorption of all other species which create surface charge; M^{n+} , L^{p-} . Based on the concepts outlined in Table VII.2, Eqs. (VII.40) and (VII.41) relate charge density to the adsorption density of charged surface complexes. Faraday's constant ($F = 96,490 \text{ C} \cdot \text{mol}^{-1}$) converts mol of adsorbed ions to the equivalent amount of charge. The terms nm^{-1} and $q(r - p + 1)$ are the charges on surface complexes formed by metal and ligand adsorption, respectively (see Table VII.2).

$$\sigma_{\text{H}} = F\varepsilon\rho_{\text{b}}^{-1}a^{-1} \left([>\text{SOH}_2^+] - [>\text{SO}^-] \right) \quad (\text{VII.40})$$

$$\begin{aligned} \sigma_{\text{s}} = F\varepsilon\rho_{\text{b}}^{-1}a^{-1} & \left(\sum_i \sum_m (nm^{-1}) [>\text{SOH}_m] \right. \\ & \left. - \sum_j \sum_q \sum_r (q(r - p) + 1) [>\text{SH}_r\text{L}_q] \right) \end{aligned} \quad (\text{VII.41})$$

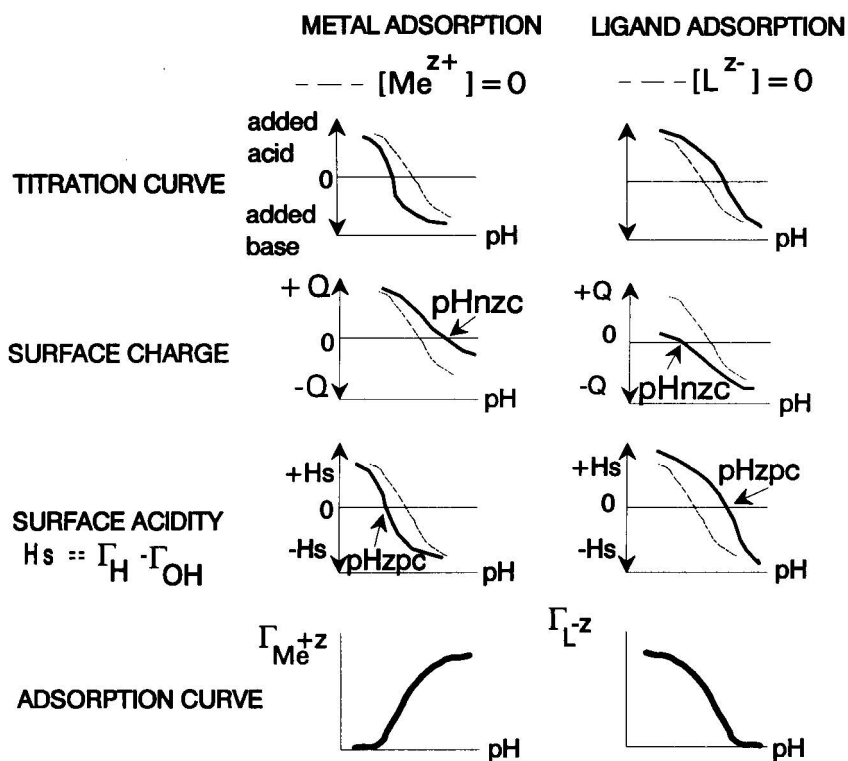
Figure VII.9: The origins of surface charge. These diagrams are not structural formulas, but generalised illustrations of the origins of surface charge. In each diagram, the bulk phase is to the left of the shaded “surface”; aqueous solution is to the right. (a) Adsorption and desorption of charge-determining-ions at an aluminium oxide surface results in a variable-charge surface. (b) Structural vacancies, or substitutions by charge-deficient network cations in the bulk of silicate minerals (such as clays), results in net negative charge. The Si(IV) atom that is missing from the vacant site leads to a net charge deficiency of 4− for the structural group that is shown. (c) Structural incorporation or adsorbed organic polymer units have ionisable functional groups that acquire charge through protonation, deprotonation or complexation reactions with solutes; reprinted with permission from [94BAN].



In the absence of permanent structural charge or charged surface complexes other than those involving adsorption or desorption of protons, the pH at which the surface has net zero charge (pH_{nzc}) is the same as the pH of the zero proton condition (pH_{zpc}); *i.e.*, no net adsorption/desorption of protons corresponds to zero net surface charge. Adsorption of cations as charge-determining species at the pH_{zpc} , will add charge and displace protons according to the reactions listed in Table VII.2. pH would then have to increase further, in order for additional protons to desorb sufficiently, to restore the zero charge condition. pH would have to decrease, to cause enough protons to re-adsorb, in order to restore the zero proton condition.

Adsorption of anions at the pH_{zpc} will remove charge and add protons at the surface (see Table VII.1). In this case, the pH would have to decrease in order for protons to adsorb sufficiently to restore the zero charge condition. The pH would have to increase in order to restore the zero proton condition. Figure VII.10 shows trends in surface charge and surface acidity during titration of the surface with solutes that form charged surface complexes.

Figure VII.10: Qualitative diagrams for titration of hydroxyl groups at mineral surfaces; from [94BAN]. Surface charge is the density of charge equivalents due to adsorbed ions (Q , $\text{mol} \cdot \text{m}^{-2}$). Surface acidity defines the net gain or loss of adsorbed protons with respect to the zero proton condition (Γ_{H} , Γ_{OH} , $\text{mol} \cdot \text{m}^{-2}$). In the absence of charge-determining-species other than protons and hydroxide ions, the pH of zero net charge (pH_{znc}) equals the pH of zero proton condition (pH_{zpc}). Cation adsorption increases surface charge and displaces protons, causing decreasing surface acidity. Anion adsorption decreases surface charge and displaces hydroxide ions, causing an increase in surface acidity (based on [96STU/MOR], *p*.561; reprinted with permission from [94BAN]).



VII.3.6.2. *The electrical double layer*

Charged surfaces in contact with electrolyte solutions achieve charge neutrality by diffusion of solution counter-ions to the charged surface. Figure VII.11 represents the structure of the charged surface and the resulting electrical double layer. Table VII.6 summarises the Gouy-Chapman diffuse layer model for relating surface charge, σ , to surface potential, Ψ_0 . This differs from the constant capacitance model in that the specific capacitance changes with the double-layer thickness. Models for relating surface charge and surface potential have been previously summarised and discussed by Westall and Hohl [80WES/HOH].

VII.3.6.3. *Ion exchange reactions*

Counter-ions within the diffuse layer are mobile and thus free to exchange with ions of the bulk electrolyte. The Gouy-Chapman model predicts the distribution of exchangeable ions at an idealised charged surface, and the dependence on counter ion charge and ionic strength (Figure VII.11). The distribution of charges within the interfacial region of real systems is complex. Exchangeable ions and hydration water diffuse into clay mineral interlayers. The degree of hydration is not generally known and the activity of water may depart from unity. Lateral interactions occur between exchangeable species in the double layer, and also between exchangeable species and charged surface complexes. Högfeldt [93HOG] and Marinsky [93MAR] respectively review their empirical and theoretical models for non-ideal behaviour of the exchanger surface.

The ionic composition of the double layer will reflect the chemical activity of the counter-ions in the bulk electrolyte. If it is assumed that the activity of exchangeable species in the double layer remains approximately constant for small changes in the chemical composition of the double layer, then conditional equilibrium constants can be defined. These constants can be experimentally assessed for conditions of known solution and double layer composition, and fixed temperature and pressure. The total charge in the double layer will reflect the net surface charge arising from the contributions outlined in Section VII.3.6.1. Variations in total double layer charge will therefore be restricted to an order-of-magnitude for changes in surface coverage of charge-determining species of between approximately 10% and 90% of the total sites.

Applying the thermodynamic law of mass action provides an empirical description of ion exchange reactions in complex natural systems. Soils or rock fracture fillings, for example, will consist of a highly heterogeneous mixture of mineral and organic surfaces. In spite of these complexities, formal application of thermodynamic mass action laws can predict trends in ion-exchange behaviour and provide estimates of ion-exchange capacities.

Table VII.7 summarises a quantitative application of thermodynamics to ion-exchange behaviour in a hydraulically-conductive fracture which contains clay minerals as fracture-fillings. The case study demonstrates the role of groundwater dilution on ion-exchange behaviour. During construction of the Äspö Hard Rock Laboratory in Sweden, saline groundwater in a conductive fracture zone was extensively diluted by increased recharge. In Figure VII.12, the trend in Na^+ and Ca^{2+} ion concentrations in the groundwater can-

Table VII.6: The relationship between surface charge and electrical double-layer potential.

<p>1. Gouy-Chapman diffuse layer model:</p> $\sigma = (8 \times 10^3 RT \varepsilon \varepsilon_0 C)^{1/2} \sinh \left(\frac{Z \Psi_0 F}{2RT} \right)$ <p>where:</p> <p>σ is the surface charge density, $\text{C} \cdot \text{m}^{-2}$</p> <p>$\Psi_0$ is the surface potential, V</p> <p>R is the molar gas constant, $8.314 \text{ J} \cdot \text{K}^{-1} \cdot \text{mol}^{-1}$</p> <p>$\varepsilon$ is the dielectric constant of water, dimensionless</p> <p>ε_0 is the permittivity of vacuum, $8.854 \times 10^{-12} \text{ C} \cdot \text{V}^{-1} \cdot \text{m}^{-1}$</p> <p>$F$ is the Faraday's constant, $96\,485 \text{ C} \cdot \text{mol}^{-1}$</p> <p>$T$ is the temperature, K</p> <p>C is the molar concentration of a 1:1 electrolyte, $\text{mol} \cdot \text{l}^{-1}$</p> <p>$Z$ is valent charge on 1:1 electrolyte</p>
<p>2. Double layer thickness (in units of m): $\delta = 1/\kappa$</p> $\kappa^2 = (2 \times 10^3 F^2 I) / (\varepsilon \varepsilon_0 RT)$ <p>where: $I = \frac{1}{2} \sum_i (Z_i^2 C_i)$ is the ionic strength, $\text{mol} \cdot \text{l}^{-1}$, and C_i is the concentration of an ion of the background electrolyte.</p>
<p>3. Approximations valid for $\Psi_0 < 25 \text{ mV}$:</p> $\sigma = \varepsilon \varepsilon_0 \kappa \Psi_0$ $\Psi = \Psi_0 e^{-\kappa \delta}$ <p>At 25°C, $\varepsilon = 78.5$, and the charge density - potential relationship simplifies further to:</p> $\sigma = 2.3 \sqrt{I} \Psi_0$

Figure VII.11: The relation between interfacial charge and potential distribution through the electrical double-layer. (a) The interfacial region is conceptually divided into two layers: a layer of fixed charge and a diffuse layer of mobile counter ions. (b) The potential in the diffuse layer decreases with distance away from surface. The double layer thickness depends on the bulk electrolyte composition and the surface charge. (c) The double layer potential and thickness decrease with increasing charge ($Z = 1, 2, 3$) of a 10^{-3} M 1:1 electrolyte. (d) The double-layer potential and thickness decrease with increasing concentration of a 1:1 electrolyte with monovalent charge; $Z = 1$. Calculations are based on the equations given in Table VII.6, assuming a fixed surface charge density of 10^{-8} eq \cdot m $^{-2}$, which corresponds to low charge density for mineral surfaces; about 1% surface coverage by monovalent surface species on silica; reprinted with permission from [94BAN].

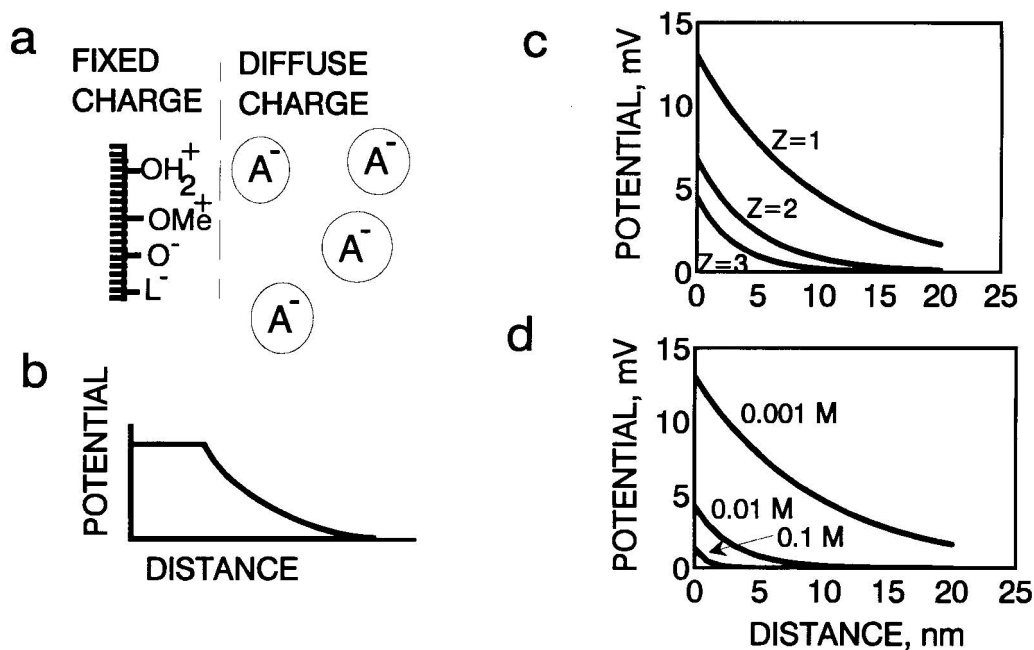


Figure VII.12: The ratio of sodium and calcium activity in solution ($\text{mol} \cdot \text{l}^{-1}$), plotted according to the thermodynamic mass law given in Table VII.7. The data correspond to a wide range of deep groundwater dilutions observed during construction, and the resulting enhanced recharge, of the Äspö Hard Rock Laboratory. The filled squares are field observations, the open circles represent ion ratios assuming dilution of saline groundwater without ion-exchange. The steep transition in the ion ratio upon dilution is due to ion-exchange. The dashed horizontal line corresponds to the ionic composition of the original saline groundwater at the site. Sodium and calcium ions dominate the contribution of cations to the charge balance of the groundwater, and are used to determine the degree of dilution. Because sulphate and bicarbonate ions provide dominant contributions to the charge balance in dilute water, Cl^- is unreliable as a conservative tracer for groundwater dilution over the range of dilution observed.

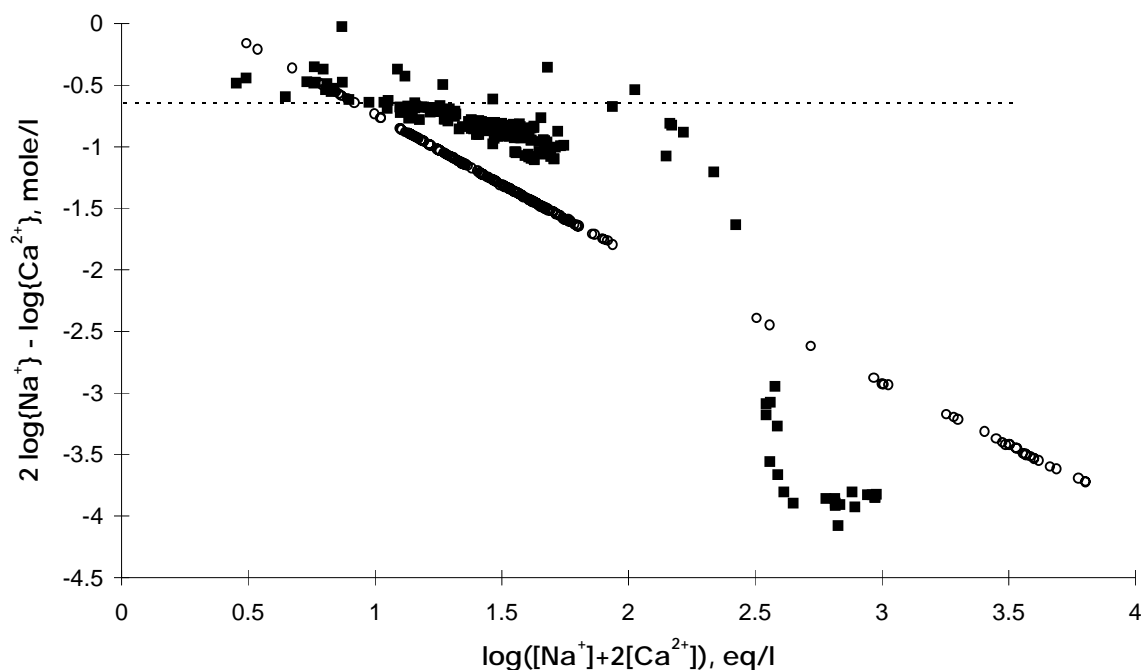
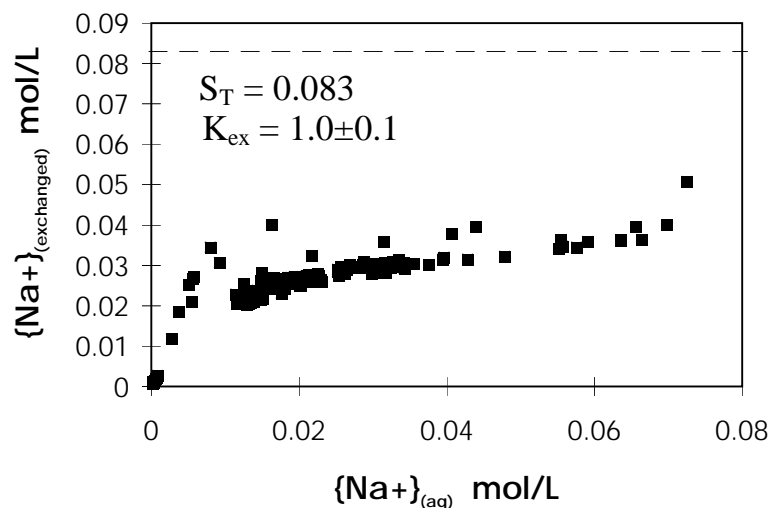


Table VII.7: Ion-exchange equilibria during dilution of saline groundwaters. See Ref. [94VIA/BRU].

<p>Stoichiometric Reaction:</p> $2 \text{NaR} + \text{Ca}^{2+} \rightleftharpoons \text{CaR} + 2 \text{Na}^+ \quad \log_{10} K_{\text{ex}} = 0.98, \text{ [94VIA/BRU]}$ <p>where “NaR” and “CaR” are the Na^+ and Ca^{2+} ions in the ion-exchanger, respectively.</p>
<p>Thermodynamic Mass Action Law:</p> $K_{\text{ex}} = \frac{f_{\text{CaR}} X_{\text{CaR}}}{(f_{\text{NaR}} X_{\text{NaR}})^2} \frac{\{\text{Na}^+\}^2}{\{\text{Ca}^{2+}\}}$ <p>where:</p> <p>$X_{\text{CaR}} = 2 [\text{Ca}^{2+}]_{\text{ex}} / S_{\text{T}}$, molar fraction of Ca in the ion-exchanger $X_{\text{NaR}} = [\text{Na}^+]_{\text{ex}} / S_{\text{T}}$, molar fraction of Na in the ion-exchanger S_{T} = ion-exchange capacity f_{CaR} = activity coefficient for Ca^{2+} in ion-exchanger f_{NaR} = activity coefficient for Na^+ in ion-exchanger</p>
<p>Mass Balance:</p> <p>1. Surface sites: $1 = X_{\text{NaR}} + X_{\text{CaR}}$</p> <p>2. Total Na^+: $X_{\text{NaR}} = (S_{\text{T}} X_{\text{NaR}_0} + x[\text{Na}^+]_0 - [\text{Na}^+]) / S_{\text{T}}$</p> <p>where: $[\text{Na}^+]_0$ = initial sodium ion aqueous concentration X_{NaR_0} = ion-exchanger Na^+ molar fraction in equilibrium with $[\text{Na}^+]_0$ before dilution $[\text{Na}^+]$ = sodium ion concentration after dilution X_{NaR} = ion-exchanger Na^+ molar fraction in equilibrium with diluted groundwater</p>
<p>Adsorption Model:</p> <p>Obtained by simultaneous solution of the thermodynamic mass action law and mass balances 1 and 2 with unknowns X_{NaR}, X_{CaR} and S_{T}, and assuming $f_{\text{NaR}} = f_{\text{CaR}} = 1$.</p>
<p>Fitted constants, <i>cf.</i> Figure VII.13:</p> $K_{\text{ex}} = 1.0 \pm 0.1$ $S_{\text{T}} = 0.083 \text{ mol} \cdot \text{l}^{-1}$

Figure VII.13: Thermodynamic modelling of the sodium and calcium ion-exchange reaction during groundwater dilution at the Äspö Hard Rock Laboratory, Sweden, yields the following plot of surface Na^+ concentration *vs.* solution Na^+ activity (see equations in Table VII.7). Although the ratio of $[\text{Na}^+]/[\text{Ca}^{2+}]$ remains fairly constant at the site, dilution eventually favours the divalent ion on the exchanger surface, and causes Na^+ to be displaced. This transition is observed for these waters at around 0.01 M Na^+ .



not be understood as a result of pure dilution, but indicates two different ion-exchange regions with a sharp transition between them. Figure VII.13 shows the sodium ion-exchange isotherm obtained from the thermodynamic model given in Table VII.7. The sharp transition in ion ratios observed in the groundwater, results from the sharp decrease in selectivity of the ion-exchange surfaces for Na^+ upon dilution below $[\text{Na}^+] = 0.01$ M. This decrease in selectivity for monovalent ions upon dilution is well-known for ion-exchange behaviour (*cf.* [94BAN]).

VII.3.7. Thermodynamic descriptions of complex adsorption systems

There is often little detailed information on contaminant adsorption behaviour in complex systems such as soils or granite fractures filled with a variety of secondary minerals. How might one gain some understanding without investing enormous amounts of time and money on detailed experimental investigations?

The thermodynamic mass action laws and mass balances described in Table VII.2 can be implemented in geochemical codes that calculate aqueous speciation, thus including adsorption as surface complexation. If the electrostatic interaction of charged surfaces with ions is considered, a mathematical model of the electrical double-layer must be included. There are several different approaches that have been previously reviewed and compared by Westall and Hohl [80WES/HOH].

In the absence of detailed thermodynamic information for adsorption reactions, how

might one estimate surface speciation? For adsorption on inorganic surfaces, the data compilation of Dzombak and Morel [90DZO/MOR] allows modelling of adsorption on hydrous ferrous oxide as an analogue for adsorption on other oxide minerals. Schindler and Stumm [87SCH/STU] demonstrate that thermodynamic data for hydrolysis in solution and trace metal adsorption on mineral surfaces correlate relatively well. The authors also demonstrate that for ligands, the tendency to form solution complexes with Fe^{3+} or Al^{3+} correlates with the relative tendency of such ligands to adsorb onto Fe- and Al-oxides.

The relative tendency for ligands and metals to adsorb through surface complexation reactions is thus reflected in the data for adsorption on hydrous ferrous oxide, compiled by Dzombak and Morel [90DZO/MOR], and in the extensive compilations of thermodynamic data for complexation in solution (*cf.* Chapter I, *p.*19). Application of such data to calculation of surface speciation and thus adsorption for complex systems will not necessarily provide a quantitative prediction of adsorption behaviour, but can indicate expected trends in adsorption with master variables such as pH, redox state of the sorbent, ionic strength.

VII.4. Surface precipitation

VII.4.1. *The transition from adsorption to surface precipitation*

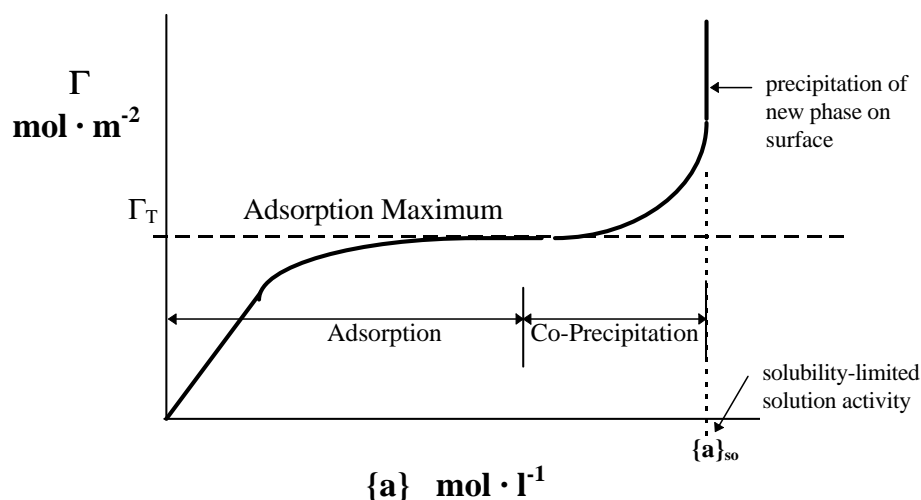
If a solid solution or new phase is formed at the mineral-water interface, the dependence of surface excess on solute activity changes dramatically from that predicted by adsorption equilibrium. Figure VII.14 shows the relationship between surface excess and solute activity for transition between adsorption equilibrium, formation of a solid solution, and finally transition to a new surface phase.

Adsorption equilibrium is characterised by surface coverage augmenting with increasing solute activity. The adsorption maximum corresponds to formation of a mono-layer; *i.e.*, all available adsorption sites are filled.

A further increase in solute activity is then associated with formation of a surface co-precipitate where the solute is not only adsorbed onto surface sites, but forms a solid-solution, or a separate phase, by structural incorporation into the underlying mineral.

For formation of a solid solution, the activity of the minor component contributed by the adsorbate is approximately equal to its molar fraction. The adsorption density, and thus molar fraction, of the adsorbate increases with increasing solute activity in solution. If the molar fraction of the component contributed by the adsorbate becomes dominating, its activity may approach unity. This limiting case results in a fixed solute activity in solution, dictated by solubility equilibrium with the new surface precipitate. Alternatively, direct formation of a new solid phase by the adsorbate may occur. As the new phase grows, it will eventually cover the entire surface of the original mineral. In this case, the solute activity will be fixed by the solubility of the new phase.

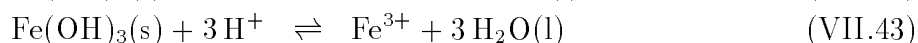
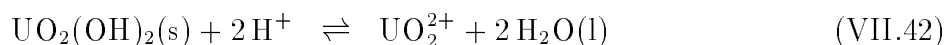
Figure VII.14: A conceptual isotherm describing the transition between adsorption equilibrium and surface-precipitation equilibrium at the mineral-water interface. The relationship between surface excess and solute activity changes dramatically across the transition region. For adsorption equilibrium, surface activity depends on solute activity, until surface excess approaches the adsorption maximum corresponding to mono-layer coverage, where surface excess becomes independent of solution activity. Higher solute activities are associated with formation of a new surface phase. Establishment of solubility equilibrium with the new phases is associated with a fixed solution activity that is independent of surface excess, and depends only on the activity of the new solid phase.



VII.4.2. The conditional solubility constant for surface precipitation/co-precipitation

A relatively simple thermodynamic approach can be used to calculate surface-precipitation. Bruno *et al.* [95BRU/PAB] recently described the co-precipitation of uranium(VI) onto iron hydroxide using this method. The solubility of the individual end-member oxide phases present can be manipulated to provide a conditional solubility constant for the trace element phase that is formed as U(VI) precipitates onto the iron hydroxide.

The solubility equilibrium of iron hydroxide and uranium oxide are defined according to the following stoichiometric equations and corresponding thermodynamic mass laws where the activity of water is assumed unity.



$$K_{\text{so(Fe)}} = \frac{[\text{Fe}^{3+}]}{[\text{H}^+]^3 \{\text{Fe}(\text{OH})_3(\text{s})\}} \quad (\text{VII.44})$$

$$K_{\text{so(U)}} = \frac{[\text{UO}_2^{2+}]}{[\text{H}^+]^2 \{\text{UO}_2(\text{OH})_2(\text{s})\}} \quad (\text{VII.45})$$

If the minerals are treated as ideal solid solutions, then the activity of the uranium oxide component can be approximated by its molar fraction (Eq. (VII.46)). The conditional solubility constant for uranium, $K_{\text{so(U)}}^*$, which will depend on the molar fraction of uranium oxide in the host iron oxide, is described by Equation (VII.47).

$$\{\text{UO}_2(\text{OH})_2(\text{s})\} = X \quad (\text{VII.46})$$

$$K_{\text{so(U)}}^* = K_{\text{so(U)}} \cdot X = [\text{UO}_2^{2+}]/[\text{H}^+]^2 \quad (\text{VII.47})$$

The important conclusions from this simple approach to modelling surface precipitation/co-precipitation of uranium as a trace metal are:

- The conditional solubility of uranium(VI) can be estimated from existing thermodynamic data.
- X will be several orders-of-magnitude less than 1, since uranium is a trace element and will only be associated in minute quantities with the $\text{Fe}(\text{OH})_3(\text{s})$.
- therefore, for $X \ll 1$, the dissolved concentration of uranyl ion $[\text{UO}_2^{2+}]$ will be much lower than if in equilibrium with the pure uranium phase.

Bruno *et al.* [95BRU/PAB] demonstrate that this approach successfully explains the concentrations of dissolved uranium in laboratory experiments and some natural waters. The authors point out that very similar solute activities are predicted by surface complexation modelling; *i.e.*, assuming only adsorption without surface precipitation. Although no distinction between adsorption mechanism or surface structure can be made on the basis of thermodynamic information, one advantage of the conditional solubility constant approach is the simplicity of this two-parameter model. $K_{\text{so(U)}}$ is available from tabulated thermodynamic data and X can be experimentally determined by analysing the uranium content of iron hydroxide phases.

VII.5. Implications for contaminant hydrogeology

VII.5.1. Reversible partitioning of contaminants

Partitioning between the mobile aqueous phases and immobile solids is an important process that must be understood in assessing the risk posed by subsurface contaminants. Although this chapter focuses on the thermodynamic description of reversible adsorption reactions, a key area of current research is the reversibility and kinetics of adsorption/desorption reactions. This has been recently summarised and discussed by Charlet [94CHA], and has profound implications for contaminant transport in the subsurface.

Table VII.8 presents two models for the retardation of adsorbing contaminants. In the first case, adsorption is controlled by reversible reactions where the ratio of total adsorbate on the solid phase(s) to that in solution can be modelled using thermodynamic descriptions of the adsorption reactions, as presented in the examples above. The general approach to describing solution and surface complexation reactions in Table VII.2 can be used to define a conditional K_d value that describes the partitioning as in Eq. (VII.5). Table VII.8 shows the general form of the distribution coefficient, K_d (based on [94SIG/XUE]).

Inspection of the equation defining K_d in Table VII.8 shows that it depends on the conditional thermodynamic constants $^*\beta_{1,1}^s$, β_q , $^*\beta_q$ which in turn depend on temperature, pressure and ionic strength. The K_d value depends on $[H^+]$, thus pH. It also depends on the concentration of the adsorbent species, $[>SOH]$, which depends in turn on chemical speciation. $[>SOH]$ may be taken as the total concentration of surface sites for adsorption of trace elements at the conditions of pH and ionic composition of the groundwater where $>SOH$ predominates; *i.e.*, in the notation in Table VII.2, $[S] \gg [SM_m]$, $[S(H_rL)_q]$, $[S^+]$, $[S^-]$. Under these conditions, the concentration of available adsorption sites approaches the adsorption capacity $[S]_T = \Gamma_T a \rho_b \varepsilon^{-1}$.

It is also important to note that the molar concentration of surface sites $[S]$ ($\text{mol} \cdot \text{l}^{-1}$), depends not only on the surface concentration of sites Γ_{SOH} ($\text{mol} \cdot \text{m}^{-2}$), but also on the physical parameters controlling the specific surface area and solid-solution ratio; ρ_b, ε, a . This model for K_d demonstrates that the partitioning of contaminants in the subsurface depends not only on the intensity parameters of the contaminant-groundwater chemical system, but also on the physical properties of the geological medium. Because these properties are known to vary spatially, the partitioning of contaminants can be expected to exhibit an associated spatial heterogeneity.

Table VII.8 explicitly presents the expression for K_d so that all terms reflecting physical-chemical properties of the geological medium are collected together and written separately; $\Gamma_{SOH} a \rho_b \varepsilon^{-1}$. If relatively good thermodynamic data exist, then the term containing the chemical intensity parameters and pH, $(\sum_k ^*\beta_{\text{surf},1,1} [H^+]^{-1}) / (1 + \sum_j \sum_q \beta_q [H^+]^{qr} [L^{p-}]^q + \sum_q ^*\beta_q [H^+]^{-q})$, can be calculated independently. For a single geological medium with specified physical-chemical properties, these properties will be the same when calculating K_d values for any adsorbing species. If the term containing the chemical intensity parameters is reliable, at least the relative values for conditional K_d values can be compared. This may be useful even if considerable uncertainty may exist for the parameters in the term: $\Gamma_{SOH} a \rho_b \varepsilon^{-1}$.

The role of adsorption in trace metal transport in the sub-surface can be qualitatively discussed by considering the limiting case where the conditional partitioning coefficient is constant along a groundwater flow path. This would be the case only if the variables that affect K_d were constant. In real systems, this is usually not the case. The relative concentration of sorbent sites $[S]$ can vary extensively due to the physical and chemical heterogeneity of the geological media; *i.e.*, pH, redox status, major ion concentrations, mineralogy, organic carbon content, porosity, bulk density etc., change along the flow path. In addition, if the contaminant is present in concentrations that approach the concentration of available adsorption sites, the values for $[S]$ that influence K_d will change

Table VII.8: Comparison of reversible and irreversible adsorption effects on contaminant retardation.

<p>For adsorption of dissolved metal ions by formation of 1:1 surface complexes:</p> $K_d = \frac{C_{(sur)}}{C_{(aq)}} = \frac{\sum_k {}^*\beta_{surf,1,1} [>SOH][H^+]^{-1}}{1 + \sum_j \sum_q \beta_q [H^+]^{qr} [L^{p-}]^q + \sum_q {}^*\beta_q [H^+]^{-q}}$ <p>where: $[>SOH] = \Gamma_{SOH} a \rho_b \varepsilon^{-1}$</p> <p>$[>SOH]$ refers to the concentration of free adsorption sites for a particular surface, k, and will be different for each surface present depending on the mineralogy and organic carbon content of the geological media. For surfaces where $>SOH$ dominates, and for adsorption of only trace concentrations of a contaminant, $[>SOH]$ approaches the total adsorption capacity. Converting surface excess (Γ_{SOH} ($\text{mol} \cdot \text{m}^{-2}$)) to molar concentration ($[>SOH]$, $\text{mol} \cdot \text{l}^{-1}$) requires physical information about the geological medium; bulk density, specific surface area and porosity.</p>
<p>Retardation factor for linear adsorption equilibrium with constant K_d:</p> <p>v is the average velocity of groundwater flow v_c is the average velocity of contaminant movement</p> $R = v/v_c = 1 + K_d$ $K_d = \Gamma_{SOH} a \rho_b \varepsilon^{-1} \left(\frac{\sum_k {}^*\beta_{surf,1,1} [H^+]^{-1}}{1 + \sum_j \sum_q \beta_q [H^+]^{qr} [L^{p-}]^q + \sum_q {}^*\beta_q [H^+]^{-q}} \right)$
<p>Retardation factor for irrevesible adsorption:</p> $R = v/v_c = [S]_T / C_{(aq)}$ <p>where: $[S]_T = \Gamma_T a \rho_b \varepsilon^{-1}$</p>

as adsorption or desorption occurs.

The model of a constant K_d thus refers to adsorption of a trace contaminant. Hence the concentration of free adsorption sites and free ligand concentrations are much greater than the contaminant concentrations, and do not change appreciably upon adsorption, desorption or complexation of the contaminant. In addition, this model assumes that the geological medium and groundwater composition along the flow path do not vary significantly.

In this case, the mean velocity of groundwater movement, compared with that of the contaminant, is the retardation factor R , where $R = 1 + K_d$. Derivation of R , and the limitations to this concept are discussed in detail by Appelo and Postma (*pp.* 339-349 in [93APP/POS]).

VII.5.2. Irreversible adsorption

The free energy of a surface species may change irreversibly if the solid phase is metastable. An example is the aging of freshly precipitated hydrous ferric oxide. Slow dehydration reactions convert the initially amorphous $\text{Fe}(\text{OH})_3(\text{s})$ into crystalline $\text{FeOOH}(\text{s})$. During this slow transformation, surface reactions that go to completion relatively rapidly remain in quasi-equilibrium with the aqueous solution. However, as surface sites undergo structural rearrangement during this process, adsorbed species such as metal ions may be incorporated into the crystal structure.

This transformation, although relatively slow compared to adsorption, may take place over time scales that are short compared to the time scale of modelling interest (perhaps years, decades, centuries or millennia depending on the contaminant and risk being addressed). A reasonable approximation to a kinetic description of the process is that of instantaneous reaction. If the solubility of the phase formed maintains much lower contaminant ion activity in solution than the initial adsorption equilibrium, then the uptake may be approximated as irreversible adsorption. This approximation assumes that once an ion is adsorbed, it remains permanently associated with the solid phase.

Under the assumption of instantaneous, irreversible adsorption, factors that control the relative rates of transport for water and contaminants are the adsorption capacity and the aqueous concentration of the contaminant species. Again, the ratio of total adsorption sites to volume or mass of groundwater depends on the physical characteristics of the geological medium. Contaminant released from a source will be instantaneously removed locally until the local adsorption capacity is filled. A contaminant front will thus move at a rate that is less than that of groundwater flow.

The effect of retardation for reversible adsorption is the time needed to “fill up” adsorption sites until the instantaneous equilibrium between the surface and the solution achieves a solution concentration that is equal to the upstream plume concentration. In the case of instantaneous, irreversible adsorption, the contaminant will “fill up” the total adsorption capacity available regardless of the concentration in solution or on the surface. Irreversible adsorption thus presents an upper limit for retardation by adsorption. It can exhibit a much longer time for contaminant breakthrough downstream of a source, than

that estimated from the K_d value.

VII.5.3. Coupling geochemistry and hydrogeology

Assessment of chemical risk due to subsurface contaminants, and the cost of subsurface waste disposal or remediation, depends critically on models that predict contaminant breakthrough times and concentrations to specific targets; drinking water wells, surface water bodies, geographical boundaries to a contaminated site. It is important to distinguish between reversible and irreversible adsorption processes. For adsorption equilibrium, detailed chemical modelling of aqueous speciation can provide conditional K_d values that are based on rigorous chemical thermodynamic principles. However, it may be difficult to convert this chemical information into meaningful predictions of contaminant breakthrough along a specific streamline without also knowing the spatial distribution and variability of the physical properties; *i.e.*, distribution of:

- minerals with different surface chemical properties,
- pore volume containing solutes, and
- particle sizes with different specific surface areas.

For systems where contaminant partitioning is dominated by chemical equilibria, a rigorous approach to surface and solution speciation will provide a reliable description of contaminant chemistry. The main problem is the spatial heterogeneity of geological media. If a rigorous chemical approach to contaminant partitioning is used, discrepancies between observed and modelled contaminant behaviour should be more reliably assigned to uncertainty and variability in the physical characteristics of the system.

Chapter VIII

Systematization and Estimation of Thermochemical Data on Silicates

Surendra SAXENA
Theoretical Geochemistry
Institute of Earth Sciences
University of Uppsala
Norbyvägen 18 B
S-752 36 Uppsala (Sweden)

VIII.1. Introduction

Thermodynamic modelling of phase equilibrium and kinetics in industrially useful chemical systems has become an integral part of process developmental research. Computer programs such as THERMOCALC [85SUN/JAN] and ChemSage [92ERI/HAC] can be used with available thermodynamic data bases to calculate phase equilibrium relations in fairly complex multicomponent systems over wide ranges of pressure and temperatures. The problem in using such model calculations in practical applications, therefore, lies mainly in obtaining an internally consistent systematized thermodynamic data base for a given chemical system. We are generally concerned with modelling of phase equilibrium relations in an entire chemical system. Therefore the errors of data for an individual phase is of less interest than the overall fit of that value with the data on other phases in the system in reproducing experimental phase equilibrium results. As an example consider the system $\text{MgO-SiO}_2\text{-H}_2\text{O}$. The possible stable phases at low pressure and temperature are periclase ($\text{MgO}(\text{cr})$), water/steam/fluid (H_2O), quartz ($\text{SiO}_2(\text{cr})$), brucite ($\text{MgO}_2\text{H}_2(\text{cr})$), talc ($\text{Mg}_3\text{Si}_4\text{O}_{12}\text{H}_2(\text{cr})$), anthophyllite ($\text{Mg}_7\text{Si}_8\text{O}_{24}\text{H}_2(\text{cr})$), chrysotile ($\text{Mg}_3\text{Si}_2\text{O}_7\text{H}_2(\text{cr})$), antigorite ($\text{Mg}_{48}\text{Si}_{34}\text{O}_{147}\text{H}_{62}(\text{cr})$), forsterite ($\text{Mg}_2\text{SiO}_4(\text{cr})$) and enstatite ($\text{MgSiO}_3(\text{cr})$). In literature one encounters ranges of calorimetrically determined enthalpy data for each of these phases; the question of how

the data should be used in modelling of a chemical process in this system is not easy to answer unless one assumes a specific goal for such modelling. The results of a phase equilibrium calculation would then depend on the choice of a data set. A good yard-stick for an industrial process evaluation may be that the data base permits the simulation of phase equilibrium experimental results. We may then systematize the available data internally for a given chemical system by adjusting the calorimetric data, as far as possible within the listed uncertainties, to fit a set of well-reversed phase equilibrium experimental results (a reversed experiment is where the products are allowed to react to form the starting reactants by reversing either the pressure or temperature to a lower value). Such a standard of reference may not be quite satisfying to a calorimetrist but if one introduces structural-chemical and other theoretical constraints in the optimization procedure, one may obtain reliable data both collectively and on individual species. This type of systematized data base should be considered as an essential part of any thermodynamic calculation. This brings us to the second part of this chapter, which is purported to be the major theme here. What if there are other stable phases in the system of interest for which there is no calorimetric data? One way, of course, would be to use the phase equilibrium data if available and determine the unknown data on one or more phases, from the phase equilibrium experiments and with the known data on other phases. Several data bases which are built using optimization techniques relating the phase equilibrium data and the calorimetric data are currently available [88BER, 90HOL/POW, 93SAX/CHA]. In absence of any phase equilibrium data, we must use models such as that of Gibbs [82GIB] to understand the regularities in the energetic behavior of various bond-linkages in groups of ions or use the semi-empirical methods using molecular dynamics [94BEL] to simulate individual properties of a crystal under different physical conditions. In this chapter, we limit ourselves to describing certain empirical methods which result from attempts to find a correlation between energy properties and certain measurable parameters of a crystal. The method is similar to that of calculating bond energies for simple molecules and then summing up the bond energies to obtain the enthalpy of a given solid. For example, one may use the Born-Haber-Fayans thermochemical cycle to calculate the lattice energy from the available energy data on the constituting ions (for a mineralogical example, see Ottonello *et al.* [92OTT/DEL]). For a series of multicomponent complex structures, the individual bond energies are not easily calculated and one must attempt to find crystal-chemical regularities in the available thermochemical data. Such correlations may involve detail crystal-structural information on the size and orientation of every type of bond in the crystal (*e.g.*, [92OTT/DEL]) needed for a precise description of the bond energies or it may be an attempt to generalize some prominent structural features such as the cation coordination polyhedral volumes. In the latter case, which is the subject of this chapter, we must sacrifice some precision for the sake of simplicity and for including a large class of solids for which detail structural data are not available.

This chapter is divided in two parts. The first part describes the data base systematization and the second part deals with estimation of enthalpy and entropy for solids.

VIII.2. A systematized data base

The data base adopted in this study is evaluated by considering all the available information in a system of oxides and silicates. Saxena *et al.* [93SAX/CHA] critically evaluated the available data and obtained an internally consistent set of thermochemical and thermophysical data. An internally consistent data set is one which permits the computation of phase equilibrium relations as established through experimental studies and is at the same time compatible with calorimetric and other measurements of thermophysical properties of the phases. Generating such a data base is complicated by the large uncertainties associated with the high pressure phase equilibrium studies, both because of the errors in pressure and temperature calibration and because many experiments may be for unreversed reactions. If a thermochemical data set produces calculated results which are reasonably consistent with experimental work, it can be used for computing possible phase equilibrium relations over a wide range of pressure, temperature and composition conditions. Such predictions are useful in planning future phase equilibrium experiments, which may then be used to better constrain the preliminary data base. Conversely, if the attempt to create a data base exposes major inconsistencies, experiments to resolve these discrepancies would be important.

Various techniques may be adopted in the systematization, depending upon the complexity of a problem, to construct an internally consistent data base. Typically one finds the following:

- i) Phases with well determined calorimetric data, *e.g.*, MgO(cr).
- ii) Phases whose thermochemical properties have been measured calorimetrically by different workers with different results, *e.g.*, enstatite, forsterite.
- iii) Phases whose thermochemical properties are not available, but experimental reversals, including data on distribution of major elements between coexisting phases, are available, *e.g.*, ferrosilite.
- iv) Phases for which neither calorimetric nor experimental data are available.

In the first case, the calorimetric data are accepted as they are and the phases are used as a foundation for the data base. In the second and third cases, a method of optimization is adopted to find the best set of data which reproduces the experimental phase equilibrium data within their uncertainty limits. In the fourth case, an estimate based on theoretical considerations is made; this is described in part 2 of this Chapter.

VIII.2.1. Thermodynamics

VIII.2.1.1. Temperature dependence of the Gibbs free energy

The change in Gibbs free energy ($\Delta_r G_m^\circ$) as a function of temperature (T) and pressure (p) can be obtained from the relations:

$$\left(\frac{\partial^2 \Delta_r G_m^\circ}{\partial T^2} \right)_p = - \frac{\Delta_r C_{p,m}^\circ(T)}{T} \quad (\text{VIII.1})$$

and

$$\left(\frac{\partial \Delta_r G_m^\circ}{\partial p} \right)_T = \Delta_r V_m^\circ(p, T) \quad (\text{VIII.2})$$

where $\Delta_r C_{p,m}^\circ(T)$ is heat capacity change at constant p and at a temperature T and $\Delta_r V_m^\circ(p, T)$ is the molar volume change at a temperature T and a pressure p . The free energy of a reaction is given by

$$\Delta_r G_m^\circ(p, T) = \Delta_r H_m^\circ(T) - T \Delta_r S_m^\circ(T) + \int_1^p \Delta_r V_m^\circ(p, T) dp \quad (\text{VIII.3})$$

where $\Delta_r H_m^\circ(T)$ and $\Delta_r S_m^\circ(T)$ are the standard enthalpy and entropy of a reaction, respectively, at temperature T and 1 bar. They are given by

$$\Delta_r H_m^\circ(T) = \Delta_r H_m^\circ(298) + \int_{298}^T \Delta_r C_{p,m}^\circ dT \quad (\text{VIII.4})$$

and

$$\Delta_r S_m^\circ(T) = \Delta_r S_m^\circ(298) + \int_{298}^T \frac{\Delta_r C_{p,m}^\circ}{T} dT \quad (\text{VIII.5})$$

where $\Delta_r H_m^\circ(298)$ and $\Delta_r S_m^\circ(298)$ are the standard enthalpy and entropy of reaction at 298.15 K, $\Delta_r C_{p,m}^\circ$ is the heat capacity difference between products and reactants, and $\Delta_r V_m^\circ(p, T)$ is the volume change for the reaction.

The extrapolation of the temperature dependence of the Gibbs free energy of a solid or a liquid phase to high temperature is thus complicated by the nature of the heat capacity, C_p .

VIII.2.1.2. Heat capacity at high temperature

a) The general relations

In general, C_p for a solid can be expressed as

$$C_p = C_V + \alpha^2 V K_T T + C_p' \quad (\text{VIII.6})$$

where C_V is the heat capacity of a crystal at constant volume, α is the coefficient of thermal expansion, V is the molar volume, and K_T is the isothermal bulk modulus, all at temperature T . C'_p is the contribution from cation disordering and anharmonicity (other than those incorporated in the $\alpha^2 V K_T T$ term).

The Einstein's and Debye's approximations for heat capacities are well known (see review in [79KIE]). Equations for the temperature dependence of C_V are based on the assumption that atoms behave as harmonic oscillators in a crystal lattice. Kieffer's [79KIE] review on the applicability of the Debye theory of lattice vibrations shows that heat capacities of silicates show large deviations from the behavior expected from the theory. The isobaric thermal expansion α_p and isothermal compressibility β_T , respectively, are given by:

$$\alpha_p = \frac{1}{\Delta_r V_m^\circ(p, T)} \left(\frac{\partial \Delta_r V_m^\circ(p, T)}{\partial T} \right)_p \quad (\text{VIII.7})$$

$$\beta_T = -\frac{1}{\Delta_r V_m^\circ(p, T)} \left(\frac{\partial \Delta_r V_m^\circ(p, T)}{\partial p} \right)_T \quad (\text{VIII.8})$$

The inverse of β_T is the bulk modulus K_T . It is experimentally convenient to measure the heat capacity of solids at constant pressure (C_p) rather than at constant volume (C_V). Many different polynomial equations have been used for fitting the measured C_p data [88SAX, 89SAX/ZHA]. We use the following equations:

$$C_V = c_0 + c_1 T + c_2 T^{-1} + c_3 T^{-2} + \dots \quad (\text{VIII.9})$$

$$\alpha_p = a_0 + a_1 T + a_2 T^{-1} + a_3 T^{-2} + \dots \quad (\text{VIII.10})$$

$$K_T = 1/(\beta_0 + \beta_1 T + \beta_2 T^2 + \beta_3 T^3 + \dots) \quad (\text{VIII.11})$$

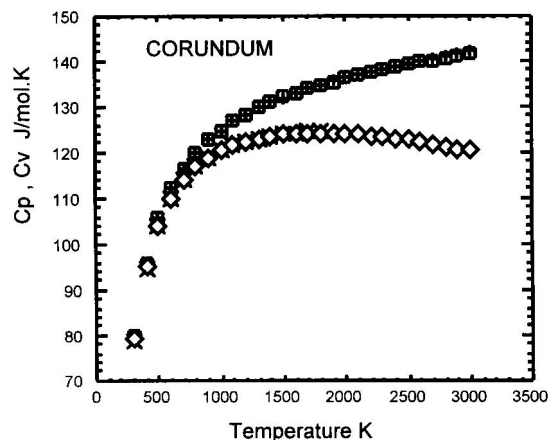
where c_i are the coefficients of the heat capacity equation, a_i the coefficients in the expansion for isobaric thermal expansion, and β_i the coefficients of compressibility.

The choice of a suitable polynomial expression for C_V is difficult. For a Debye solid, the low-temperature limit is given by the "Debye T^3 " law ($C_V = A [T/\theta^3]$) where A is a constant and θ is the Debye temperature. At high temperature C_V for a Debye solid will approach the $3nR$ limit (where n = number of atoms, R = gas constant). In a non-Debye solid the departure from this limit must be considered. Saxena *et al.* [93SAX/CHA] used the Kieffer model to calculate C_V to temperatures of about 1000 K. An example of this type of systematization is shown in Figure VIII.1 [93SAX/CHA]. Saxena *et al.* used the data on corundum as an example to show how the choice of the form of an equation affects the extrapolated data. Eq. (VIII.10) may be used with two or more of the four constants a_0 , a_1 , a_2 and a_3 for thermal expansion. Saxena *et al.* showed that the equation with two constants (straight line, not shown) will not fit the experimental data as well as the equation with three or four constants. Similarly the three constant equation provides us with a superior fit to the experimental data on compressibility. The C_p data are fitted with the general 5 constant expressions used in this study:

$$C_p = a + bT + cT^{-2} + eT^{-3} + gT^{-1}, \quad (\text{VIII.12})$$

$$C_p = a + b \ln T + cT^{-1} + dT^{-2} + eT^{-3} \quad (\text{VIII.13})$$

Figure VIII.1: The experimental data and extrapolations on C_p and C_V of corundum. Squares: C_p data of Richet and Fiquet [91RIC/FIQ] and extrapolation by Eq. (VIII.13); plusses: C_p data of Richet and Fiquet [91RIC/FIQ] and extrapolation by Eq. (VIII.12); crosses: experimental C_V from available C_p , α_p and K_T (Anderson *et al.* [91AND/ISA]); diamonds: calculated C_V data from the extrapolated data on C_p , α_p and K_T .



Eq. (VIII.13) is from Richet and Fiquet [91RIC/FIQ]. Both expressions produced a perfect fit of the experimental data. There is also no significant difference between the extrapolated data to 3000 K.

In this work, the C_p is formulated by taking into account the important role of the $\alpha^2 V K_T T$ term and, therefore, links the measured heat capacity with the measured physical properties of solids at high temperature. This provides an additional constraint for evaluating an internally consistent thermochemical and thermophysical data set based on data from the calorimetric measurements, from the experimental phase equilibria and from the measurements of solid physical properties.

Eq. (VIII.12) is used in assessing and refitting the C_p data. Such assessed data are presented with a flexible C_p formulation adopted at many centers (*e.g.*, A.D. Pelton with the F*A*C*T system at Ecole Polytechnique, Montreal, or B. Sundman with THERMOCALC at the Royal Institute of Technology (KTH) at Stockholm) working with large data bases. The formulation is:

$$C_p = a + bT + cT^{-2} + dT^2 + eT^{-3} + fT^{-0.5} + gT^{-1} \quad (\text{VIII.14})$$

b) Estimation of C_V

The measured heat capacities of minerals show strong deviations from Debye-like calorimetric behavior at all temperatures. The deviations increase with the complexity of the structure. The Debye model does not account for the measured calorimetric properties

of minerals because it does not allow for the details of the vibrational spectra. Kieffer [79KIE, 79KIE2, 79KIE3, 80KIE] has developed a model based on lattice dynamics that allows calculation of heat capacity at constant volume from vibration spectra and acoustic velocities. Kieffer [79KIE3, 80KIE] calculated heat capacities of many minerals with the use of the model. The model generally yields good estimates of the heat capacity. With more experimental data, a set of related models has been developed with small differences in band assignments, partitioning of modes into optic continua and Einstein oscillators, and dispersion relations for each phase such that these models are consistent with the observed spectra, acoustic velocities and constraints of crystallographic symmetry. The results show that the calculated heat capacities are insensitive to the details of modelling. Kieffer [79KIE3] pointed out that the model has different accuracies in different temperature ranges: for C_V , ± 30 -50% below 50 K, $\pm 4\%$ at 298 K and $\pm 1\%$ at 700 K. Kieffer's model demonstrates that the heat capacities of minerals at the temperature range from 300 to 1000 K are relatively sensitive to the distribution of optic modes; the insufficient vibrational parameters clearly constitute a weak point of the modelling. Saxena *et al.* [93SAX/CHA] took the lower and upper cutoff frequencies, w_l , w_u , of the optic continuum as calculation parameters based on the spectroscopic data to put some bounds on the thermodynamic C_p data over the temperature range of 200-400 K. The upper limit of the applicability of Kieffer's model was taken somewhat generously as 1000 K by Saxena *et al.* [93SAX/CHA]. Kieffer's model does not include the effect of thermal expansion (p.43. in [79KIE3]).

VIII.2.2. The regression technique

Many techniques of curve fitting have been suggested by different workers such as Haas and Fisher's [76HAA/FIS] regression analysis method and the linear and mathematical programming methods of Gordon [73GOR], Halbach and Chatterjee [82HAL/CHA], Berman *et al.* [86BER/ENG], Day and Kumin [80DAY/KUM], *etc.* In some cases, thermochemical data for phases are not available. In such cases, they are calculated from equilibrium data involving the phase. When data for only one phase in a reaction are unknown, it is calculated as follows. The change in free energy of a reaction

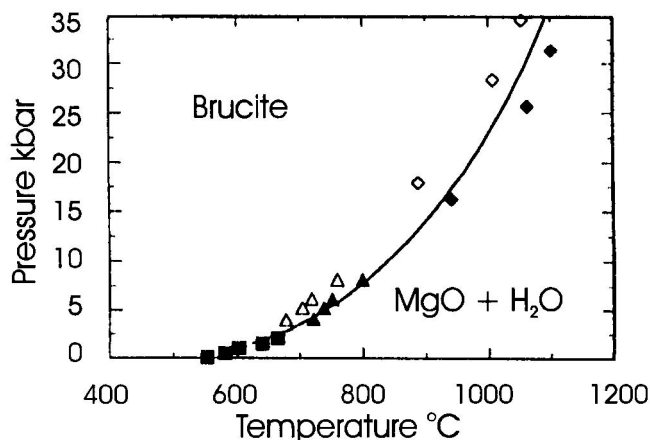


at equilibrium is zero and can be written as

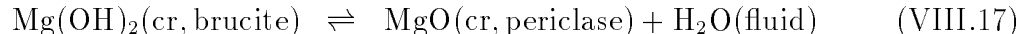
$$\Delta_r G_m^\circ = \Delta_f G_m^\circ(C) + \Delta_f G_m^\circ(D) - \Delta_f G_m^\circ(A) - \Delta_f G_m^\circ(B) = 0 \quad (\text{VIII.16})$$

where $\Delta_f G_m^\circ(A)$ is the free energy of formation of phase A, *etc.* If $\Delta_f G_m^\circ(C)$ is unknown, it is easily calculated from Eq. (VIII.16). If several equilibrium pressures and temperatures are known for reaction (VIII.15), $\Delta_f G_m^\circ(C)$ is regressed according to Eq. (VIII.16) and enthalpy, entropy and heat capacity functions for phase "C" are obtained. In many cases, one or two quantities among $\Delta_f H_m^\circ(C)$, $S_m^\circ(C)$, and $C_{p,m}^\circ(C)$ are known from calorimetry.

Figure VIII.2: Comparison of phase equilibrium computations with experimental data of the reaction $\text{Mg}(\text{OH})_2(\text{cr, brucite}) \rightleftharpoons \text{MgO}(\text{cr, periclase}) + \text{H}_2\text{O}(\text{fluid})$: triangles, Schramke *et al.* [82SCH/KER]; diamonds, Irving *et al.* [77IRV/HUA]; squares, Barnes and Ernst [63BAR/ERN]. From Saxena *et al.* [93SAX/CHA]. The open and solid symbols represent reversal brackets within which the equilibrium pressure and temperature may be found.



This makes the regression procedure much simpler. An example of the above technique may be illustrated with the reaction:



If we assume that the data on brucite is not available or is uncertain, one may determine the data from the phase equilibrium curve shown in Figure VIII.2.

The data set obtained is finally tested in a multiphase-multicomponent environment for global consistency. This is done by the method of minimization of total Gibbs free energy of an assemblage as discussed before.

VIII.2.3. The optimization technique

An internally consistent data base is constructed by considering all the experimentally determined data and theoretically or empirically extrapolated values for the system under consideration. These include phase equilibrium data, calorimetric and volume data and values extrapolated by theoretical methods such as that of heat capacity. Thermodynamic relationships described above link these data together and constrain it as a set. Evaluation of thermodynamic properties of a phase by refinement involves a large number of data. A standard optimization technique may be used to solve this problem.

The problem of minimizing the difference (*e.g.*, chi-square) between predictions from a theoretical form of an expression and the experimental data has been commonly solved in geochemical literature through regression analyses which use the middle points of the error

bars. Recently, however, the linear and non-linear programming techniques have been popularly used to perform optimization procedures to obtain thermodynamic consistency of the optimized parameters with all valid experimental data (*e.g.*, Halbach and Chatterjee [82HAL/CHA], Berman *et al.* [86BER/ENG]). Recently Chatterjee *et al.* [94CHA/MIL] used a method based on Bayes estimation technique.

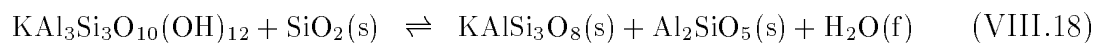
Today, many optimization or minimization routines are available (*e.g.*, in Numerical Recipes, [87PRE/FLA]). Saxena *et al.* [93SAX/CHA] used the method based on the minimizing subroutines (MINUIT) as discussed by James and Roots [75JAM/ROO].

The regression may take the form of minimizing a chi-square function built from several different types of data. For example, we may define a function for $\Delta_r G_m^\circ$ of a heterogeneous reaction in which there are subfunctions corresponding to thermochemical and thermo-physical properties of individual phases of the reaction. A typical problem may consist of minimizing the $\Delta_r G_m^\circ$ of a reaction with experimentally determined brackets for equilibrium pressures and temperatures and with some known and unknown thermodynamic properties of the reacting phases. To demonstrate how the method works, the following example has been chosen [93SAX/CHA]:

Example

Goal: The assessment of thermodynamic properties of muscovite, Al_2SiO_5 polymorphs (structurally different species andalusite, sillimanite and kyanite), KAlSi_3O_8 polymorphs (microcline, orthoclase and sanidine) SiO_2 polymorphs and corundum.

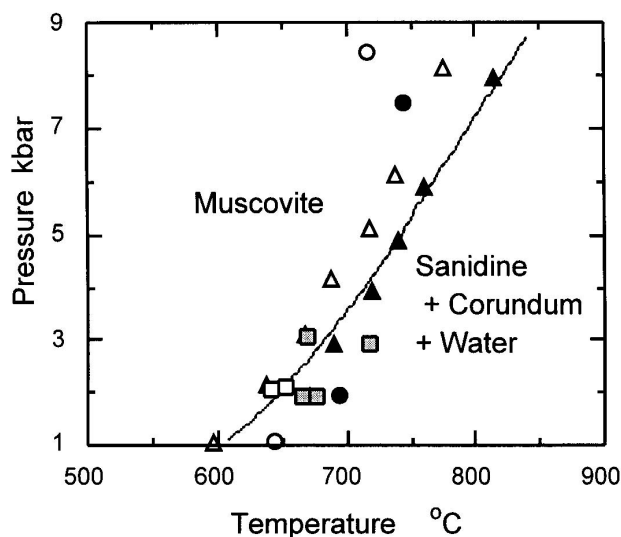
The problem: We want to obtain a data set which permits the calculation of phase equilibrium relations consistent with the available experimental data; ideally such a data set would also contain individual values of thermodynamic parameters which remain within the errors of the measured calorimetric and other physical data. This is a case of multireaction optimization. The reactions (with polymorphs of $\text{Al}_2\text{Si}_2\text{O}_5$: andalusite, sillimanite, kyanite) can be considered as:



Muscovite Quartz Sanidine

The available data: To obtain an internally systemized data base for this system, we use both the available calorimetric data on the phases as well as the experimental phase equilibrium data described below. The available calorimetric data were reviewed by Robie *et al.* [84ROB/HEM3]. Such data are then to be modified with the help of the phase equilibrium data, *e.g.*, on muscovite breakdown reactions (Figures VIII.3, VIII.4 and VIII.5). Experimental work has been done on the reactions (VIII.18) by Velde [66VEL], Chatterjee and Johannes [74CHA/JOH], Evans [65EVA], Althaus *et al.* [70ALT/KAR] and Day [73DAY]. Experimental information is also available on the stability of sanidine and muscovite. Krupka *et al.* [79KRU/ROB] attempted to calculate the enthalpy and free energy of muscovite from the experimental data of Chatterjee and Johannes [74CHA/JOH] on

Figure VIII.3: Comparison of phase equilibrium computations with experimental data of the reaction $\text{KAl}_3\text{Si}_3\text{O}_{10}(\text{OH})_{12}(\text{cr, muscovite}) \rightleftharpoons \text{KAlSi}_3\text{O}_8(\text{cr, sanidine}) + \text{Al}_2\text{O}_3(\text{cr, corundum}) + \text{H}_2\text{O}(\text{fluid})$: circles, Velde [66VEL]; triangles, Chatterjee and Johannes [74CHA/JOH]; squares, Evans [65EVA]. From Saxena *et al.* [93SAX/CHA].



the above reactions. Their calculations were based on the fugacity values of steam from Chatterjee and Johannes [74CHA/JOH] and Fisher and Zen [71FIS/ZEN] and the heat capacity data on muscovite determined by them and the unpublished data on sanidine listed in Robie *et al.* [78ROB/HEM]. Saxena *et al.* [93SAX/CHA] used the more general equation for water fugacity of Saxena and Fei [87SAX/FEI, 87SAX/FEI2] and the published heat capacity data on sanidine by Hemingway *et al.* [81HEM/KRU]. The enthalpy of sanidine is from Robie *et al.* [78ROB/HEM]. The optimized entropy of sanidine is found to be $7.09 \text{ J} \cdot \text{K}^{-1} \cdot \text{mol}^{-1}$ higher than that determined by Openshaw *et al.* [76OPE/HEM]. This amount can be considered as the disorder entropy of sanidine. Sanidine shows an Al/Si disorder and since, at very low temperatures, the heat capacity is not well characterized, this treatment is reasonable. However, it should be kept in mind that the zero-point Al/Si disorder entropy of muscovite is also unknown. The thermal expansion of muscovite is also optimized from a combination of the phase equilibrium and heat capacity data.

Results: The resulting data are included in Table VIII.1. Calculated curves for reactions (for sillimanite and andalusite) along with the experimental data are shown respectively in Figures VIII.3, VIII.4 and VIII.5.

The example discussed above is one of several subsystems in the general system Na-K-Al-Fe-Mg-Ca-C-H-O for which data have been assessed to be compatible as far as possible

Figure VIII.4: Comparison of phase equilibrium computations with experimental data of the reaction $\text{KAl}_3\text{Si}_3\text{O}_{10}(\text{OH})_{12}(\text{cr, muscovite}) + \text{SiO}_2(\text{cr, quartz}) \rightleftharpoons \text{KAlSi}_3\text{O}_8(\text{cr, sanidine}) + \text{Al}_2\text{SiO}_5(\text{cr, sillimanite}) + \text{H}_2\text{O}(\text{fluid})$: circles, Day [73DAY]; triangles, Chatterjee and Johannes [74CHA/JOH]; squares, Evans [65EVA]; diamonds, Althaus *et al.* [70ALT/KAR]. From Saxena *et al.* [93SAX/CHA].

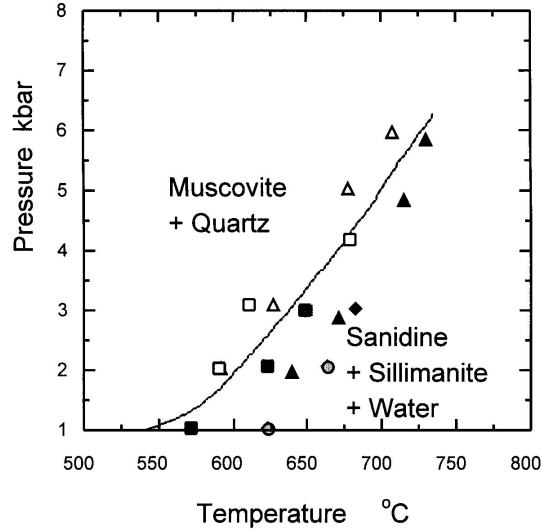
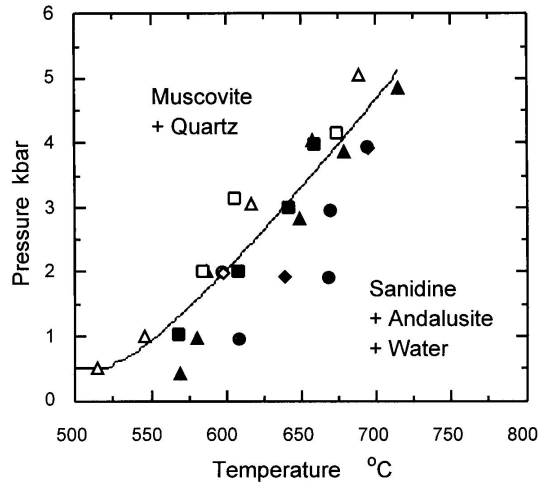


Figure VIII.5: Comparison of phase equilibrium computations with experimental data of the reaction $\text{KAl}_3\text{Si}_3\text{O}_{10}(\text{OH})_{12}(\text{cr, muscovite}) + \text{SiO}_2(\text{cr, quartz}) \rightleftharpoons \text{KAlSi}_3\text{O}_8(\text{cr, sanidine}) + \text{Al}_2\text{SiO}_5(\text{cr, andalusite}) + \text{H}_2\text{O}(\text{fluid})$: circles, Althaus *et al.* [70ALT/KAR]; triangles, Chatterjee and Johannes [74CHA/JOH]; squares, Evans [65EVA]; diamonds, Kerrick [72KER]. From Saxena *et al.* [93SAX/CHA].



with all types of measured data and experimental phase equilibrium studies.

VIII.2.4. Data base

The data on several phases are extracted from Saxena *et al.* [93SAX/CHA] and Holland and Powell [90HOL/POW] and are presented later in Table VIII.1. These data are to be regarded as internally consistent, *i.e.*, they follow the principles discussed above and reproduce most of the available experimental phase equilibrium data.

VIII.3. Estimation of enthalpy of silicates

VIII.3.1. Principles underlying empirical correlation

The most important data on solid substances for estimating the thermodynamic properties is the information on crystal structures; the more information we have, the more sophisticated the modelling can be. The models based on the quantum-mechanical interatomic potentials require quantitative data on all geometric parameters of the crystal (*e.g.*, Gibbs [82GIB]). Models based on statistical correlations between the chemical compositions and energy could range in sophistication from that of Ottonello [87OTT] to the basically simple model of Tardy and coworkers (*e.g.*, Tardy and Garrels [77TAR/GAR]). The art of this type of study is to find certain common energy parameters for a component, which may be real or fictive, in structurally analogous compounds. Tardy and Garrels [77TAR/GAR] do this by using the Gibbs free energy of formation of an aqueous ion and determining an empirical parameter for the other cation from a difference between the Gibbs free energy of formation of the compound from oxides and that of the aqueous ion. A somewhat more rigorous approach than that of Tardy in searching for transferable potentials is that suggested by Hazen [88HAZ] and used by Robinson and Haas [83ROB/HAA] and Chermak and Rimstidt [89CHE/RIM]. Robinson and Haas use the common geometry of the coordination polyhedra, which tend to remain similar over symmetry classes. Some possible alternative methods are discussed by Karpov and Kashik [68KAR/KAS], Eugster and Chou [73EUG/CHO], Nriagu [75NRI] and Chen [75CHE].

Before we get too involved with the description of the empirical methods, it must be emphasized as done by Hazen [88HAZ] that such relationships ‘should be viewed as valuable “yard-sticks” against which the behavior of minerals may be compared, rather than rigid “laws” to which minerals are expected to conform’.

VIII.3.2. Tardy’s method

Tardy and Garrels [77TAR/GAR] found that for the structurally analogous compounds, *e.g.*, meta- or ortho-silicates, the Gibbs free energy of formation of a silicate from its component oxides ($\Delta_{\text{ox}}G$) may be considered to vary linearly with a characteristic property of a constituent cation.

For example, the $\Delta_{\text{ox}}G$ for several metasilicates could vary linearly with the radii of the constituent cations. Tardy used the Gibbs free energy of the constituent aqueous ion.

Table VIII.1: A thermochemical data base on silicates Standard state enthalpy of formation from elements and molar entropy at 298.15 K. The data are a combination of the assessments by Saxena *et al.* [93SAX/CHA] and by Holland and Powell [90HOL/POW] who have also discussed the errors of statistical fits. Although the data bases are separately assessed, there is apparently little conflict in the two sets. For each compound, the table lists the enthalpy $\Delta_f H_m^\circ$ ($\text{kJ} \cdot \text{mol}^{-1}$), the entropy S_m° ($\text{J} \cdot \text{K}^{-1} \cdot \text{mol}^{-1}$), the T range, the standard enthalpy of transformation ($\text{kJ} \cdot \text{mol}^{-1}$), and the temperature function $C_p^\circ(T) = a + bT + cT^2 + dT^{-2} + eT^{-3} + gT^{-0.5} + hT^{-1}$.

FeAl₂O₄ HERCYNITE							
-1958.2	113.500						
4000.0							
$1.7572 \cdot 10^2$	$2.22 \cdot 10^{-2}$	0	$8.1615 \cdot 10^6$	$-1.7335 \cdot 10^9$	0	$-2.4517 \cdot 10^4$	
Ca₂Al₂SiO₇ GEHLENITE							
-3977.9	204.350						
4000.0							
$3.4154 \cdot 10^2$	$3.795 \cdot 10^{-3}$	0	$-7.663 \cdot 10^5$	$4.074 \cdot 10^8$	0	$-4.037 \cdot 10^4$	
MgCa₂SiO₇ AKERMANITE							
-3867.5	208.200						
4000.0							
$3.4884 \cdot 10^2$	$6.274 \cdot 10^{-3}$	0	$9.515 \cdot 10^6$	$-8.781 \cdot 10^8$	0	$-6.539 \cdot 10^4$	
Fe₂SiO₄ FAYALITE							
-1478.170	151.000						
4000.0							
$2.089 \cdot 10^2$	$8.064 \cdot 10^{-3}$	0	$5.894 \cdot 10^6$	$-7.882 \cdot 10^8$	0	$-3.466 \cdot 10^4$	
CaMgSiO₄ MONTICELLITE							
-2246.3	112.050						
4000.0							
$1.87612 \cdot 10^2$	$7.99 \cdot 10^{-3}$	0	$1.9283 \cdot 10^6$	$-3.6248 \cdot 10^8$	0	$-2.2822 \cdot 10^4$	
FeSiO₃ ORTHOFERROSILITE							
-1193.45	95.900						
4000.0							
$1.096 \cdot 10^2$	$1.388 \cdot 10^{-2}$	0	$-9.116 \cdot 10^6$	$1.033 \cdot 10^9$	0	$1.098 \cdot 10^4$	
CaMgSi₂O₆ CLINODIOPSIDE							
-1600.91	71.550						
4000.0							
$1.21665 \cdot 10^2$	$8.14 \cdot 10^{-3}$	0	$-6.8095 \cdot 10^6$	$9.384 \cdot 10^8$	0	$1.2772 \cdot 10^2$	
CaFeSi₂O₆ CLINOHEDENBERGITE							
-1419.41	85.145						
4000.0							
$1.5465 \cdot 10^2$	$7.025 \cdot 10^{-3}$	0	$1.5395 \cdot 10^7$	$-2.393 \cdot 10^9$	0	$-4.661 \cdot 10^4$	
NaAlSi₂O₆ JADEITE							
-3029.87	134.720						
4000.0							
$1.9337 \cdot 10^2$	$3.408 \cdot 10^{-2}$	0	$-3.0733 \cdot 10^7$	$4.1913 \cdot 10^9$	0	$4.2914 \cdot 10^4$	

These values have been selected by the Author and not by the NEA.

Table VIII.1 (continued)

Fe₃Al₂Si₃O₁₂ ALMANDINE							
-5276.337	336.300						
4000.0							
$7.13 \cdot 10^2$	$-8.85 \cdot 10^{-2}$	$1.56 \cdot 10^{-5}$	$1.458 \cdot 10^7$	0	0	$-1.496 \cdot 10^5$	
Mg₃Al₂Si₃O₁₂ PYROPE							
-6291.54	266.270						
4000.0							
$4.768 \cdot 10^2$	$3.167 \cdot 10^{-2}$	0	$-2.12 \cdot 10^7$	$2.168 \cdot 10^9$	0	$-1.17 \cdot 10^3$	
Ca₃Al₂Si₃O₁₂ GROSSULAR							
-6634.308	256.118						
4000.0							
$5.426 \cdot 10^2$	$1.294 \cdot 10^{-2}$	0	$-3.186 \cdot 10^6$	$2.777 \cdot 10^8$	0	$-5.602 \cdot 10^4$	
Ca₃Fe₂Si₃O₁₂ ANDRADITE							
-5769.999	316.350						
4000.0							
$8.0924 \cdot 10^2$	$-7.0251 \cdot 10^{-2}$	0	$-6.789 \cdot 10^5$	0	$-7.403 \cdot 10^3$	0	
CaAl₂Si₂O₈ ANORTHITE							
-4232.5	203.000						
4000.0							
$2.909 \cdot 10^2$	$2.76 \cdot 10^{-2}$	0	$-3.408 \cdot 10^7$	$5.218 \cdot 10^9$	0	$2.9625 \cdot 10^4$	
NaAlSi₃O₈ ALBITE							
-3929.86	221.800						
4000.0							
$3.0974 \cdot 10^2$	$1.527 \cdot 10^{-2}$	0	$-2.616 \cdot 10^7$	$4.1092 \cdot 10^9$	0	$8.8361 \cdot 10^3$	
CaSiO₃ WOLLASTONITE							
-1632.00	82.028						
4000.0							
$1.3958 \cdot 10^2$	$2.36 \cdot 10^{-3}$	0	$1.4012 \cdot 10^6$	$-2.1722 \cdot 10^8$	0	$-1.8547 \cdot 10^4$	
Al₂O₃ CORUNDUM							
-1675.711	50.917						
4000.0							
$1.226 \cdot 10^2$	$7.031 \cdot 10^{-3}$	0	$-5.583 \cdot 10^6$	$5.707 \cdot 10^8$	0	$-1.414 \cdot 10^3$	
Al₂SiO₅ SILLIMANITE							
-2587.77	95.790						
4000.0							
$1.8387 \cdot 10^2$	$1.815 \cdot 10^{-2}$	0	$-1.236 \cdot 10^7$	$1.6024 \cdot 10^9$	0	$3.2052 \cdot 10^3$	
Al₂SiO₅ KYANITE							
-2596.2	82.300						
4000.0							
$2.2354 \cdot 10^2$	$2.645 \cdot 10^{-3}$	0	$-4.149 \cdot 10^6$	$7.601 \cdot 10^8$	0	$-2.524 \cdot 10^4$	
Al₂SiO₅ ANDALUSITE							
-2591.7	91.420						
4000.0							
$2.217 \cdot 10^2$	$2.581 \cdot 10^{-3}$	0	$-2.559 \cdot 10^6$	$4.899 \cdot 10^8$	0	$-2.669 \cdot 10^4$	

These values have been selected by the Author and not by the NEA.

Table VIII.1 (continued)

Mg₂Al₄Si₅O₁₈ CORDIERITE							
-9164.869	411.000						
4000.0							
$7.6548 \cdot 10^2$	$-1.9181 \cdot 10^{-2}$	0	$5.7814 \cdot 10^6$	$-5.4662 \cdot 10^8$	0	$-8.8644 \cdot 10^4$	
Fe₂Al₄Si₅O₁₈ FERROCORDIERITE							
-8446.904	471.121						
4000.0							
$1.08564 \cdot 10^3$	$-3.7262 \cdot 10^{-1}$	0	$1.3161 \cdot 10^7$	$-1.2848 \cdot 10^{10}$	0	$-7.0756 \cdot 10^4$	
FeO WUSTITE (Stoichiometric)							
-267.27	57.590						
4000.0							
$-1.667 \cdot 10^1$	$5.6696 \cdot 10^{-2}$	$-1.0801 \cdot 10^{-5}$	$-5.3269 \cdot 10^6$	0	0	$3.2403 \cdot 10^4$	
Fe₃O₄ MAGNETITE							
-1115.548	150.640						
848.0	1.564						
$7.3372 \cdot 10^1$	$2.2668 \cdot 10^{-1}$	0	$9.536 \cdot 10^5$	$6.988 \cdot 10^6$	0	$1.5476 \cdot 10^2$	
1300.0	0						
$-1.1312 \cdot 10^1$	$9.804 \cdot 10^{-2}$	0	$1.2456 \cdot 10^8$	$7.444 \cdot 10^7$	0	$1.5336 \cdot 10^3$	
4000.0							
$3.47248 \cdot 10^2$	$6.328 \cdot 10^{-2}$	0	$7.896 \cdot 10^7$	$3.5584 \cdot 10^{11}$	0	$-5.792 \cdot 10^5$	
Fe₂O₃ HEMATITE							
-824.782	87.400						
956.0	670.00						
$7.974 \cdot 10^1$	$9.288 \cdot 10^{-2}$	0	$-3.284 \cdot 10^6$	$2.804 \cdot 10^8$	0	$7.15 \cdot 10^3$	
1250.0	0.00						
$-1.3983 \cdot 10^2$	$1.449 \cdot 10^{-1}$	0	$1.5648 \cdot 10^8$	$-1.4568 \cdot 10^7$	0	$-3.516 \cdot 10^2$	
4000.0							
$3.948 \cdot 10^2$	$8.646 \cdot 10^{-2}$	0	$1.2394 \cdot 10^8$	$4.808 \cdot 10^{11}$	0	$-8.654 \cdot 10^5$	
KAlSi₃O₈ SANIDINE							
-3959.56	239.990						
4000.0							
$3.2527 \cdot 10^2$	$8.37 \cdot 10^{-3}$	0	$-2.1373 \cdot 10^7$	$3.4796 \cdot 10^9$	0	$-4.3104 \cdot 10^3$	
C GRAPHITE							
0.00	5.742						
4000.0							
$2.7797 \cdot 10^1$	$4.583 \cdot 10^{-4}$	0	$4.475520 \cdot 10^5$	0	$-7.39242 \cdot 10^3$	0	
KFe₃AlSi₃O₁₀(OH)₂ ANNITE							
-5125.500	440.910						
4000.0							
$6.265 \cdot 10^2$	$6.263 \cdot 10^{-2}$	0	$1.3276 \cdot 10^7$	$-7.947 \cdot 10^8$	0	$-1.167 \cdot 10^5$	
KMg₃AlSi₃O₁₀(OH)₂ PHLOGOPITE							
-6203.900	334.600						
4000.0							
$5.5442 \cdot 10^2$	$2.7835 \cdot 10^{-2}$	0	$-1.6458 \cdot 10^6$	$-1.0629 \cdot 10^8$	0	$-5.5447 \cdot 10^4$	
Mg₂Al₄Si₅O₁₈.H₂O HYDROUS CORDIERITE							
-9430.3186	275.904						
4000.0							
$7.6548 \cdot 10^2$	$-1.9181 \cdot 10^{-2}$	0	$5.7814 \cdot 10^6$	$-5.4662 \cdot 10^8$	0	$-8.8644 \cdot 10^4$	

These values have been selected by the Author and not by the NEA.

Table VIII.1 (continued)

Mg(OH)₂ BRUCITE							
-925.5	64.400						
4000.0							
$1.0301 \cdot 10^2$	$1.6533 \cdot 10^{-2}$	0	$-2.7462 \cdot 10^6$	$-1.365 \cdot 10^2$	0	$-1.141 \cdot 10^2$	
KAl₃Si₃O₁₀(OH)₂ MUSCOVITE							
-5976.3	306.400						
4000.0							
$4.626 \cdot 10^2$	$6.598 \cdot 10^{-2}$	0	$-3.3374 \cdot 10^7$	$4.7388 \cdot 10^9$	0	$1.2027 \cdot 10^4$	
Mg₄₈Si₃₄O₈₅(OH)₆₂ ANTIGORITE							
-71377.0	3672.800						
4000.0							
$7.7014 \cdot 10^3$	$2.091 \cdot 10^{-1}$	0	$-3.8256 \cdot 10^7$	$1.144 \cdot 10^{10}$	0	$-9.9281 \cdot 10^5$	
NaAl₃Si₃O₁₀(OH)₂ PARAGONITE							
-5951.0	277.100						
4000.0							
$5.02209 \cdot 10^2$	$3.2215 \cdot 10^{-2}$	0	$-1.9623 \cdot 10^7$	$2.6177 \cdot 10^9$	0	$-2.1204 \cdot 10^4$	
Mg₇Si₈O₂₂(OH)₂ CUMMINGTONITE							
-12217.1	483.056						
4000.0							
$6.71461 \cdot 10^2$	$4.9935 \cdot 10^{-2}$	0	$-2.6698 \cdot 10^7$	$-2.4368 \cdot 10^9$	0	$4.0199 \cdot 10^4$	
Fe₇Si₈O₂₂(OH)₂ GRUNERITE							
-9631.5	714.600						
4000.0							
$1.1377 \cdot 10^3$	$2.4812 \cdot 10^{-1}$	0	$1.5574 \cdot 10^8$	$-2.399 \cdot 10^{10}$	0	$-4.0674 \cdot 10^5$	
Mg₇Si₈O₂₂(OH)₂ ANTHOPHYLLITE							
-12071.032	535.190						
4000.0							
$1.1287 \cdot 10^3$	$3.886 \cdot 10^{-2}$	0	$5.043 \cdot 10^6$	$-7.642 \cdot 10^8$	0	$-1.51 \cdot 10^5$	
Mg₃Si₄O₁₀(OH)₂ TALC							
-5900.5	260.180						
4000.0							
$5.5848 \cdot 10^2$	$2.072 \cdot 10^{-2}$	0	$8.122 \cdot 10^6$	$-1.324 \cdot 10^9$	0	$-8.489 \cdot 10^4$	
Mg₃Si₂O₅(OH)₄ CHRYSOTILE							
-4363.0	219.820						
4000.0							
$5.0768 \cdot 10^2$	$2.8294 \cdot 10^{-2}$	0	$1.0798 \cdot 10^7$	$-8.4309 \cdot 10^8$	0	$-9.7731 \cdot 10^4$	
FeTiO₃ ILMENITE							
-1235.35	106.350						
4000.0							
$1.5456 \cdot 10^2$	$2.292 \cdot 10^{-3}$	0	$3.385 \cdot 10^6$	$-4.066 \cdot 10^8$	0	$-2.348 \cdot 10^4$	
TiO₂ RUTILE							
-944.75	50.290						
4000.0							
$7.359 \cdot 10^1$	$1.0063 \cdot 10^{-2}$	$-1.7085 \cdot 10^{-6}$	$6.042 \cdot 10^5$	0	0	$-8.353 \cdot 10^3$	

These values have been selected by the Author and not by the NEA.

Table VIII.1 (continued)

CaCO₃ CALCITE							
–1206.0	91.700						
4000.0							
$1.3997 \cdot 10^2$	$3.525 \cdot 10^{-3}$	$1.7936 \cdot 10^{-6}$	$1.5067 \cdot 10^6$	0	0	$-2.183 \cdot 10^4$	
MgCO₃ MAGNESITE							
–1106.0	69.000						
4000.0							
$1.2359 \cdot 10^2$	$2.0986 \cdot 10^{-2}$	$2.7041 \cdot 10^{-6}$	$7.122 \cdot 10^5$	0	0	$-1.8114 \cdot 10^4$	
CaMgC₂O₆ DOLOMITE							
–2325.72	155.200						
4000.0							
$2.738 \cdot 10^2$	$1.3125 \cdot 10^{-2}$	$8.0432 \cdot 10^{-6}$	$2.8653 \cdot 10^6$	0	0	$-4.5578 \cdot 10^4$	
CaO							
–634.26	38.100						
4000.0							
$5.425 \cdot 10^1$	$1.215 \cdot 10^{-3}$	0	$3.01 \cdot 10^5$	$-5.95 \cdot 10^7$	0	$-3.66 \cdot 10^3$	
Al₂Si₄O₁₀(OH)₂ PYROPHYLLITE							
–5640.96	239.400						
4000.0							
$4.43088 \cdot 10^2$	$3.909830 \cdot 10^{-2}$	0	$-3.620490 \cdot 10^7$	$4.869440 \cdot 10^9$	0	$1.812120 \cdot 10^4$	
Ca₂Mg₅Si₈O₂₂(OH)₂ TREMOLITE							
–12313.6	550.000						
4000.0							
$1.04075 \cdot 10^3$	$6.9 \cdot 10^{-2}$	0	$-3.2361 \cdot 10^7$	$5.0535 \cdot 10^9$	0	$-6.9176 \cdot 10^4$	
Na₂Mg₃Al₂Si₈O₂₂(OH)₂ GLAUCOPHANE							
–11954.1	535.000						
4000.0							
$1.0694 \cdot 10^3$	$2.932 \cdot 10^{-2}$	0	$-7.302 \cdot 10^6$	$7.04 \cdot 10^8$	0	$-1.1371 \cdot 10^5$	
KAlSiO₄ KALSILIT							
–2114.5	134.000						
4000.0							
$2.42 \cdot 10^2$	$-4.482 \cdot 10^{-3}$	0	$-8.958 \cdot 10^5$	0	$-1.9358 \cdot 10^3$	0	
Ca₄CO₃Si₆Al₆O₂₄ MEIONITE							
–13871.25	720.000						
4000.0							
$1.316 \cdot 10^3$	$6.499 \cdot 10^{-2}$	0	$-8.963 \cdot 10^6$	0	$-8.932 \cdot 10^3$	0	
Ca₄Si₂O₈.CaCO₃ SPURRITE							
–5840.2	330.000						
4000.0							
$6.1409998 \cdot 10^2$	$-3.508 \cdot 10^{-3}$	0	$-2.4931 \cdot 10^6$	0	$-4.168 \cdot 10^3$	0	
Al₂Si₂O₅(OH)₄ KAOLINITE							
–4120.6	203.050						
4000.0							
$5.89486 \cdot 10^2$	$-1.9893 \cdot 10^{-2}$	0	$2.84 \cdot 10^3$	0	$-5.8351 \cdot 10^3$	0	

These values have been selected by the Author and not by the NEA.

Table VIII.1 (continued)

MgAl₂O₄ SPINEL							
-2305.45644	82.896						
4000.0							
$2.0785 \cdot 10^2$	$4.49 \cdot 10^{-3}$	0	$6.7109 \cdot 10^6$	$-9.5984 \cdot 10^8$	0	$-3.9681 \cdot 10^4$	
KAlSi₃O₈ KSPAR							
-3969.62	214.000						
4000.0							
$4.4879999 \cdot 10^2$	$-1.0075 \cdot 10^{-2}$	0	$-1.0073 \cdot 10^6$	0	$-3.9731 \cdot 10^3$	0	
CaAl₂Si₂O₇(OH)₂·H₂O LAWSONITE							
-4868.07	230.000						
4000.0							
$9.5009998 \cdot 10^2$	$-1.1321 \cdot 10^{-1}$	0	$6.6456 \cdot 10^6$	0	$-1.2318 \cdot 10^4$	0	
FeCO₃							
-761.180	95.500						
4000.0							
$2.5739999 \cdot 10^2$	$-4.62 \cdot 10^{-2}$	0	$1.523 \cdot 10^6$	0	$-3.0819 \cdot 10^3$	0	
MgAl₂Si₂O₆(OH)₄ MGCARPHOLITE							
-4794.81	194.000						
4000.0							
$6.6779999 \cdot 10^2$	$-1.2559 \cdot 10^{-2}$	0	$-1.1671 \cdot 10^6$	0	$-6.44 \cdot 10^3$	0	
MgAl₂SiO₅(OH)₂ MGCHLORITOID							
-3557.95	132.000						
4000.0							
$4.6439999 \cdot 10^2$	$-1.2654 \cdot 10^{-2}$	0	$-1.1472 \cdot 10^6$	0	$-4.341 \cdot 10^3$	0	
Mg₄Al₁₈Si₇·5O₄₈H₄ MGSTAUROLITE							
-25118.49	890.000						
4000.0							
$2.8205 \cdot 10^3$	$-5.9366 \cdot 10^{-2}$	0	$-1.3774 \cdot 10^7$	0	$-2.4126 \cdot 10^4$	0	
NaAlSiO₄ NEPHELINE							
-2105.44	123.000						
4000.0							
$2.7270001 \cdot 10^2$	$-1.2398 \cdot 10^{-2}$	0	0	0	$-2.7631 \cdot 10^3$	0	
Ca₂Al₂Si₃O₁₀(OH)₂ PREHNITE							
-6199.86	292.800						
4000.0							
$7.2490002 \cdot 10^2$	$-1.3865 \cdot 10^{-2}$	0	$-2.059 \cdot 10^6$	0	$-6.3239 \cdot 10^3$	0	
Ca₃Si₂O₇ RANKINITE							
-3721.07	197.200						
4000.0							
$6.7229999 \cdot 10^2$	$-2.893 \cdot 10^{-3}$	0	$-2.4624 \cdot 10^6$	0	$-2.1813 \cdot 10^3$	0	
CaTiO₃ SPHENE							
-2596.48	129.200						
4000.0							
$1.767 \cdot 10^2$	$2.3852 \cdot 10^{-2}$	0	$-3.9905 \cdot 10^6$	0	0	0	

These values have been selected by the Author and not by the NEA.

Table VIII.1 (continued)

NaFeSi₂O₆ ACMITE							
-2584.42	170.600						
4000.0							
$3.5020001 \cdot 10^2$	$4.154 \cdot 10^{-3}$	0	$-4.53 \cdot 10^5$	0	$-3.0229 \cdot 10^3$	0	
Mg₄Al₄Si₂O₁₀(OH)₈ AMESITE							
-9046.04	400.000						
4000.0							
$1.177 \cdot 10^3$	$9.041 \cdot 10^{-3}$	0	$-7.4587 \cdot 10^6$	0	$-1.0053 \cdot 10^4$	0	
KMgAlSi₄O₁₀(OH)₂ CELADONITE							
-5834.27	297.000						
4000.0							
$7.4119995 \cdot 10^2$	$-1.8748 \cdot 10^{-2}$	0	$-2.3688 \cdot 10^6$	0	$-6.6169 \cdot 10^3$	0	
Fe₅Al₂Si₃O₁₀(OH)₈ DAPHNITE							
-7148.44	559.000						
4000.0							
$1.2374 \cdot 10^3$	$1.3594 \cdot 10^{-2}$	0	$-3.743 \cdot 10^6$	0	$-1.125 \cdot 10^4$	0	
Fe₁₈Si₁₂O₄₀(OH)₁₀ DEERITE							
-18344.32	1650.000						
4000.0							
$3.1644001 \cdot 10^3$	$-2.7883 \cdot 10^{-2}$	0	$-5.0391 \cdot 10^6$	0	$-2.6721 \cdot 10^4$	0	
KMg₂Al₃Si₂O₁₀(OH)₂ EASTONITE							
-6336.56	315.000						
4000.0							
$7.855 \cdot 10^2$	$-3.8031 \cdot 10^{-2}$	0	$-2.1303 \cdot 10^6$	0	$-6.8937 \cdot 10^3$	0	
NaCa₂Mg₅Si₇AlO₂₂(OH)₂ EDENITE							
-12580.53	599.000						
4000.0							
$1.2649 \cdot 10^3$	$2.409 \cdot 10^{-2}$	0	$-1.256 \cdot 10^7$	0	$-7.704 \cdot 10^3$	0	
Fe₄Al₄Si₂O₁₀(OH)₈ FE-AMESITE							
-7629.39	513.000						
4000.0							
$1.2375 \cdot 10^3$	$1.181 \cdot 10^{-2}$	0	$-4.4173 \cdot 10^6$	0	$-1.13 \cdot 10^4$	0	
Fe₇Si₈O₂₂(OH)₂ FE-ANTHOPHYLLITE							
-9625.86	729.000						
4000.0							
$1.3831 \cdot 10^3$	$3.0669 \cdot 10^{-2}$	0	$-4.2247 \cdot 10^6$	0	$-1.1258 \cdot 10^4$	0	
FeAl₂Si₂O₆(OH)₄ FE-CARPHOLITE							
-4438.98	223.000						
4000.0							
$6.7479999 \cdot 10^2$	$-1.0092 \cdot 10^{-2}$	0	$-7.158 \cdot 10^5$	0	$-6.5545 \cdot 10^3$	0	
KFeAlSi₄O₁₀(OH)₂ FE-CELADONITE							
-5484.96	328.000						
4000.0							
$7.5629999 \cdot 10^2$	$-1.9147 \cdot 10^{-2}$	0	$-1.5861 \cdot 10^6$	0	$-6.9287 \cdot 10^3$	0	

These values have been selected by the Author and not by the NEA.

Table VIII.1 (continued)

Na₂Fe₃Al₂Si₈O₂₂(OH)₂ FE-GLAUCOPHANE							
-10901.1	624.000						
4000.0							
$1.7629 \cdot 10^3$	$-1.1899 \cdot 10^{-1}$	0	$9.4237 \cdot 10^6$	0	$-2.0207 \cdot 10^4$	0	
Ca₂Fe₄Al₂Si₇O₂₂(OH)₂ FE-HORNBLENDE							
-10999.97	690.000						
4000.0							
$1.29 \cdot 10^3$	$2.8209 \cdot 10^{-2}$	0	$-9.0319 \cdot 10^6$	0	$-8.9971 \cdot 10^3$	0	
Fe₄Al₁₈Si_{7.5}O₄₈H₄ FE-STAUROLITE							
-23745.11	1030.000						
4000.0							
$2.88 \cdot 10^3$	$-5.6595 \cdot 10^{-2}$	0	$-1.0642 \cdot 10^7$	0	$-2.5373 \cdot 10^4$	0	
Fe₃Si₄O₁₀(OH)₂ FE-TALC							
-4861.02	358.000						
4000.0							
$5.7970001 \cdot 10^2$	$3.9494 \cdot 10^{-2}$	0	$-6.4593 \cdot 10^6$	0	$-3.0881 \cdot 10^3$	0	
Ca₂Fe₅Si₈O₂₂(OH)₂ FE-TREMOLITE							
-10527.1	705.000						
4000.0							
$1.29 \cdot 10^3$	$2.9991 \cdot 10^{-2}$	0	$-8.4475 \cdot 10^6$	0	$-8.947 \cdot 10^3$	0	
Na₂Mg₃Al₂Si₈O₂₂(OH)₂ MG-RIEBECKITE							
-11087.79	602.000						
4000.0							
$1.7015 \cdot 10^3$	$-1.1565 \cdot 10^{-1}$	0	$7.0216 \cdot 10^6$	0	$-1.8534 \cdot 10^4$	0	
NaCa₂Mg₄Al₃Si₆O₂₂(OH)₂ PARGASITE							
-12719.83	591.000						
4000.0							
$1.2802 \cdot 10^3$	$2.2997 \cdot 10^{-2}$	0	$-1.236 \cdot 10^7$	0	$-8.0658 \cdot 10^3$	0	
KFe₂Al₃Si₂O₁₀(OH)₂ SIDEROPHYLLITE							
-5628.27	375.000						
4000.0							
$8.1579999 \cdot 10^2$	$-3.6645 \cdot 10^{-2}$	0	$-5.645 \cdot 10^5$	0	$-7.5171 \cdot 10^3$	0	
Ca₂Al₃Si₃O₁₂(OH) ZOISITITE							
-6899.0	294.000						
4000.0							
$6.975 \cdot 10^2$	$1.3263 \cdot 10^{-2}$	0	$-3.7941 \cdot 10^6$	0	$-5.3179 \cdot 10^3$	0	
Mg₅Al₂Si₃O₁₀(OH)₈ CLINOCHLORE							
-8928.25	421.000						
4000.0							
$1.1618 \cdot 10^3$	$1.0133 \cdot 10^{-2}$	0	$-7.6573 \cdot 10^6$	0	$-9.6909 \cdot 10^3$	0	
CaCO₃ ARAGONITE							
-1208.16	88.000						
4000.0							
$8.4200005 \cdot 10^1$	$4.2844 \cdot 10^{-2}$	0	$-1.3975 \cdot 10^6$	0	0	0	

These values have been selected by the Author and not by the NEA.

Table VIII.1 (continued)

CaAl₄Si₂O₁₀(OH)₂ MARGARITE							
-6244.64	265.000						
4000.0							
$7.4440002 \cdot 10^2$	$-1.68 \cdot 10^{-2}$	0	$-2.0744 \cdot 10^6$	0	$-6.7832 \cdot 10^3$	0	
Ca₃MgSi₂O₈ MERWINITE							
-4537.32	252.200						
4000.0							
$4.4160001 \cdot 10^2$	$2.228 \cdot 10^{-3}$	0	$-2.0029 \cdot 10^6$	0	$-2.8882 \cdot 10^3$	0	
Ca₂FeAl₂Si₃O₁₂(OH) EPIDOTE							
-6462.05	326.000						
4000.0							
$6.9790002 \cdot 10^2$	$-9.993 \cdot 10^{-3}$	0	$-5.1053 \cdot 10^6$	0	$-4.7101 \cdot 10^3$	0	
FeAl₂SiO₅(OH)₂ FECHLORITOID							
-3211.38	162.000						
4000.0							
$4.8460001 \cdot 10^2$	$-1.3808 \cdot 10^{-2}$	0	$-1.989 \cdot 10^5$	0	$-4.7622 \cdot 10^3$	0	
FeCaC₂O₆ FEDOLOMITE							
-1969.3	185.600						
4000.0							
$4.4209998 \cdot 10^2$	$-4.743 \cdot 10^{-2}$	0	$2.037 \cdot 10^6$	0	$-4.931 \cdot 10^3$	0	
Ca₂Mg₄Al₂Si₇O₂₂(OH)₂ HORNBLLENDE							
-12420.29	551.000						
4000.0							
$1.2296 \cdot 10^3$	$2.5438 \cdot 10^{-2}$	0	$-1.2164 \cdot 10^7$	0	$-7.7503 \cdot 10^3$	0	
KAlSi₂O₆ LEUCITE							
-3020.72	202.200						
4000.0							
$3.6979999 \cdot 10^2$	$-1.6332 \cdot 10^{-2}$	0	$6.847 \cdot 10^5$	0	$-3.6831 \cdot 10^3$	0	
SiO₂ QUARTZ							
-910.7	41.500						
848.0	844.00						
$8.11447 \cdot 10^1$	$1.828 \cdot 10^{-2}$	$5.4058 \cdot 10^{-6}$	$-1.809860 \cdot 10^5$	0	$-6.984580 \cdot 10^2$	0	
4000.0							
$7.8812 \cdot 10^1$	$1.205 \cdot 10^{-3}$	0	$1.731 \cdot 10^6$	$1.202 \cdot 10^8$	0	$-1.213 \cdot 10^4$	
MgO PERICLASE							
-601.49	26.940						
4000.0							
$4.549 \cdot 10^1$	$4.773 \cdot 10^{-3}$	0	$-2.16 \cdot 10^6$	$1.744 \cdot 10^8$	0	$2.411 \cdot 10^3$	
MgSiO₃ CLINOENSTATITE-LOW							
-1548.71511	63.230						
4000.0							
$1.3807968 \cdot 10^2$	$8.708750 \cdot 10^{-3}$	$-1.352318 \cdot 10^{-6}$	$4.059147 \cdot 10^5$	0	0	$-1.8888 \cdot 10^4$	
MgSiO₃ ORTHOENSTATITE							
-1546.29	66.270						
4000.0							
$1.4445 \cdot 10^2$	$1.882 \cdot 10^{-3}$	0	$-1.35 \cdot 10^6$	$4.612 \cdot 10^8$	0	$-1.938 \cdot 10^4$	

These values have been selected by the Author and not by the NEA.

Table VIII.2: Results of regressed data on lattice energy and fictive polyhedral parameters for 41 silicates for which internally systematized data are available as discussed in the previous section of this chapter. To obtain the simulated value add the error of fit (last column) to $\Delta_f H_m^\circ$. $\Delta_L H_m$ represents the lattice enthalpy (see text for calculation, Section VIII.3.3.2, *p.*316) which is regressed with the polyhedral energies. The regressions are given in Table VIII.3. Full oxygen is shown in the chemical formula of the hydrous compounds for convenience but it is not used as a parameter in the calculations. The following structural abbreviations have been used below: Ol, olivine; Px, pyroxene; Gr, grossular (garnet); Alm, almandine (garnet); Tlc, talc; Amp, amphibole; An, anorthite; Kao, kaolinite; Gar, garnet. All data in $\text{kJ} \cdot \text{mol}^{-1}$.

Phase	$-\Delta_L H_m$	$-\Delta_f H_m^\circ$	Error
Forsterite $\text{Mg}(\text{M1-Ol})\text{Mg}(\text{M2-Ol})\text{SiO}_4$	20900.42	2175.72	-1.58
alfa-Ca-Olivine $\text{Ca}(\text{M1-Ol})\text{Ca}(\text{M2-Ol})\text{SiO}_4$	20198.10	2318.02	-0.20
Fayalite $\text{Fe}(\text{M1-Ol})\text{Fe}(\text{M2-Ol})\text{SiO}_4$	21190.31	1477.02	1.01
Monticellite $\text{Mg}(\text{M1-Ol})\text{Ca}(\text{M2-Ol})\text{SiO}_4$	20549.58	2246.62	-0.33
Pyrope $\text{Mg}(\text{Ol-M1})_3\text{Al}(6)_2\text{Si}_3\text{O}_{12}$	66391.37	6294.37	-2.83
Orthoenstatite $\text{Mg}(\text{M1-Px})\text{Mg}(\text{M2-Px})\text{Si}_2\text{O}_6$	34047.13	3095.45	-2.87
Orthoferrosilite $\text{Fe}(\text{M1-Px})\text{Fe}(\text{M2-Px})\text{Si}_2\text{O}_6$	34327.45	2389.35	-2.45
Diopside $\text{Mg}(\text{M1-Px})\text{Ca}(\text{M2-Px})\text{Si}_2\text{O}_6$	33733.37	3206.75	-4.93
Wollastonite $\text{Ca}(\text{M2-Px})_2\text{Si}_2\text{O}_6$	33372.55	3264.05	-0.05

Table VIII.2 (continued)

Phase	$-\Delta_L H_m$	$-\Delta_f H_m^\circ$	Error
Hedenbergite $\text{Ca}(\text{M2-Px})\text{Fe}(\text{M1-Px})\text{Si}_2\text{O}_6$	33863.37	2835.05	3.77
Jadeite $\text{NaAl}(6)\text{Al}(4)\text{Si}_2\text{O}_6$	35381.42	3029.55	0.32
Albite $\text{NaAl}(4)\text{Si}_3\text{O}_8$	48509.68	3929.57	0.28
Sanidine $\text{KAl}(4)\text{Si}_3\text{O}_8$	48412.39	3929.57	-0.01
Grossular $\text{Ca}(\text{Gr})_3\text{Al}_2(6)\text{Si}_3\text{O}_{12}$	65465.33	6634.87	-0.37
Almandine $\text{Fe}(\text{Alm})_3\text{Al}_2(6)\text{Si}_3\text{O}_{12}$	66855.16	5276.77	-0.44
Quartz SiO_2	13139.00	912.72	-2.00
Akermanite $\text{Mg}(\text{M2-Ol})\text{Ca}(\text{M2-Ol})_2\text{Si}_2\text{O}_7$	37225.05	3865.25	2.25
Gehlenite $\text{Ca}(\text{M2-Ol})_2\text{Al}(4)\text{Al}(6)\text{SiO}_7$	35526.18	3980.02	-2.12
Cordierite $\text{Mg}(\text{M1-Ol})\text{Mg}(\text{M2-Ol})\text{Al}(6)_4\text{Si}_5\text{O}_{18}$	104147.40	9171.02	1.00
Fe-cordierite $\text{Fe}(\text{M1-Ol})\text{Fe}(\text{M2-Ol})\text{Al}(6)_4\text{Si}_5\text{O}_{18}$	104431.98	8472.32	-1.72
Muscovite $\text{KAl}(4)\text{Al}(6)_{1.334}\text{Si}_3\text{Al}(\text{O}_3\text{H}_3)_{0.666}\text{O}_{10}$	68101.13	5981.76	-2.39
Phlogopite $\text{KMg}(\text{M1-Px})_2\text{Al}(4)\text{Si}_3\text{Mg}(\text{O}_2\text{H}_2)\text{O}_{10}$	64407.72	6202.57	1.32

Table VIII.2 (continued)

Phase	$-\Delta_L H_m$	$-\Delta_f H_m^\circ$	Error
Annite KFe(M1-Px) ₂ Al(4)Si ₃ Mg(O ₂ H ₂)O ₁₀	64808.325	5125.50	0.00
Paragonite NaAl(4)Al(6) _{1.334} Si ₃ Al(O ₃ H ₃) _{0.666} O ₁₀	68198.13	5981.76	-2.39
Talc Mg(Tlc)Mg(M1-Px)Si ₄ Mg(O ₂ H ₂)O ₁₀	68534.60	5901.90	-1.40
Anthophyllite Mg(Tlc) ₂ Mg(M1-Px) ₂ Mg(M2-Px) ₂ Si ₈ Mg(O ₂ H ₂)O ₂₂	136614.23	12070.80	0.23
Chrysotile Mg(Tlc)Mg(O ₂ H ₂) ₂ Si ₂ O ₅	46514.55	4363.45	-0.45
Tremolite Ca(Amp) ₂ Mg(Tlc) ₂ Mg(M1-Px) ₂ Si ₈ Mg(O ₂ H ₂)O ₂₂	136010.80	12314.40	-0.80
Pyrophyllite Al(6) _{1.334} Si ₄ Al(O ₃ H ₃ -Kao) _{0.666} O ₁₀	72196.06	5639.15	4.88
Kaolinite Al(6) _{0.666} Si ₂ Al(O ₃ H ₃ -Kao) _{1.334} O ₅	50206.15	4133.40	-2.87
Tschermak Ca(M2-Px)Al(4)Al(6)SiO ₆	32019.00	3298.02	-1.30
Zoisite Ca(M2-Ol) ₂ Al(6) _{2.667} Si ₃ Al(O ₃ H ₃ -Zo) _{0.333} O ₁₂	71724.82	6900.88	-0.34
Anorthite Ca(An)Al(4) ₂ Si ₂ O ₈	45183.00	4233.45	-1.00
Margarite Al(4) ₂ Al(6) _{1.334} Si ₂ Al(O ₃ H ₃) _{0.666} O ₁₀	64837.19	6246.23	1.48
Analcime NaAl(4)Si ₂ O ₆ H ₂ O	39635.35	3317.15	-7.35

Table VIII.2 (continued)

Phase	$-\Delta_L H_m$	$-\Delta_f H_m^\circ$	Error
Lawsonite $\text{Ca}(\text{M2-ol})\text{Al}(4)\text{Al}(6)_{0.334}\text{Si}_2\text{Al}(\text{O}_3\text{H}_3)_{0.666}\text{O}_7\text{H}_2\text{O}$	53762.45	5767.13	-0.16
Laumontite $\text{Al}(4)\text{Al}(6)\text{Si}_4\text{Ca}(\text{An})\text{O}_{12}4\text{H}_2\text{O}$	88580.30	7276.80	0.40
Acmite $\text{NaFe}^{3+}\text{Si}_2\text{O}_6$	35166.97	2584.35	0.07
Grunerite $\text{Fe}(\text{M1-Px})_2\text{Fe}(\text{M2-Px})_2\text{Fe}(\text{O}_2\text{H}_2)\text{Si}_8\text{O}_{22}$	137608.20	9613.90	0.10
Glaucophane $\text{Na}(\text{Amp})_2\text{Mg}(\text{M1-Px})_2\text{Al}(6)_2\text{Mg}(\text{O}_2\text{H}_2)\text{Si}_8\text{O}_{24}$	139291.30	11953.00	1.10
Andradite $\text{Ca}(\text{Gr})_3\text{Fe}^{3+}(\text{Gar})_2\text{Si}_3\text{O}_{12}$	65060.83	5769.99	0.21

Thus we have

$$\begin{aligned}\Delta_{\text{ox}}G^\circ(\text{meta-silicate}) &= -\frac{2}{3}(-E_{\text{cation}} + 188.28) \text{ (kJ} \cdot \text{mol}^{-1}) \\ \Delta_{\text{ox}}G^\circ(\text{ortho-silicate}) &= -\frac{4}{4}(-E_{\text{cation}} + 188.28) \text{ (kJ} \cdot \text{mol}^{-1})\end{aligned}$$

where E_{cation} is a characteristic energy associated with the divalent cation. For example for Mg^{2+} , Ca^{2+} and Fe^{2+} , the energies are 114.18, 51.2 and 159.2 kJ/cation respectively.

Unfortunately Tardy and Garrels used unsystematized literature data, which is not assessed for compatibility with phase equilibrium relations. If one uses a systematized data base such as that of Holland and Powell [90HOL/POW] or Berman [88BER], one is likely to get quite different results. Tardy and Garrels also let their characteristic cation property adjust to whichever of the several available data that best fitted a straight line regression. It can be easily demonstrated that if one uses a systematized data base and attempts to use a simple two variable fit, the errors in the predicted data are quite significant. The reason is not difficult to understand; the same cation in silicate structures may occupy different coordination polyhedra and a single energy value could only be an

average of the various energy values pertaining to various structural sites. Despite the lack of rigor, Tardy's method does provide fair to rough estimates of the thermodynamic data for a large class of solids and may be used with caution if there is a need for such data. The method is explained in several studies [77TAR/GAR, 78TAR]. Tardy and coworkers [74TAR/GAR, 92TAR/DUP] have also worked extensively with estimating the data for clay minerals.

VIII.3.3. The polyhedral approach

Robinson and Haas [83ROB/HAA] worked with fictive structural components of silicates such as MgO-4, MgO-6 or MgO-8, where the numbers represent coordination geometries. The component energies were obtained from experimental calorimetric data on several silicates. Hazen [88HAZ] discussed the justification for the polyhedral approach which depends on the fundamental assumptions that *a*) silicate structures are built from distinct polyhedral units (*e.g.*, SiO₄ tetrahedra, MgO-6 octahedra) which have similar energies in all structures; and *b*) there exists a summation method which permits the proportional addition of the energies of the polyhedral units to obtain the crystal energy.

VIII.3.3.1. Chermak-Rimstidt method

Karpov and Kashik [68KAR/KAS] had first used a multiple linear regression technique to estimate the energy contributions of 36 different oxides. Chermak and Rimstidt [89CHE/RIM] considered the inclusion of hydroxide components. They determined the fictive enthalpies of several components by using a thermodynamic data set on 29 minerals. The advantages of this approach are:

1. The thermodynamic data used for modelling were based on calorimetric and high-temperature phase equilibrium measurements rather than on the hard-to-determine solubility measurements (*e.g.*, in Tardy's method).
2. The approach is based on the polyhedral building blocks [88HAZ].
3. The method is simple requiring only the chemical composition of the minerals and the coordination of the polyhedral components.
4. A fairly large data set is used (29 minerals) for calibration.

a) Componental Gibbs free energy

The following component data ($\text{kJ} \cdot \text{mol}^{-1}$) are to be used for Gibbs free energy:

4- Al_2O_3	-1631.32	(13.3)
6- Al_2O_3	-1594.52	(15.3)
6- $\text{Al}(\text{OH})_3$	-1181.62	(13.2)
SiO_2	-853.95	(4.6)
6- MgO	-628.86	(10.6)
6- $\text{Mg}(\text{OH})_2$	-851.86	(10.2)
6- CaO	-669.13	(5.9)
8- CaO	-710.08	(7.2)
6-8- Na_2O	-672.5	(26.0)
8-12- K_2O	-722.94	(27.4)
H_2O	-239.91	(5.7)
6- FeO	-266.29	(6.8)
6- $\text{Fe}(\text{OH})_2$	-542.04	(24.6)
6- Fe_2O_3	-776.07	(33.0)

(the first one or two numbers represent the coordination number, the individual errors are given in parenthesis).

b) Rules of determination

1. Determine chemical composition.
2. Determine the coordination of the cation components based on known structures.
 - a) For Ca-bearing zeolite minerals with an unknown coordination number, use 8- CaO .
 - b) For 1:1 phyllosilicates, distribute the octahedral cations as 0.6666 hydroxide and 0.3333 oxide. For 2:1 phyllosilicates, do the reverse.
 - c) For chlorites, distribute cations into the interlayer in the order $\text{Al}^{3+} > \text{Fe}^{2+} \geq \text{Mg}^{2+} > \text{Fe}^{3+}$ until the interlayer OH totals 8. The remaining cations go to octahedral sites as in 2.b.
3. Determine the number of polyhedra, n , of each component in the formula unit.
4. Multiply n by the component Gibbs free energy and sum up. The interlayer thermodynamic contribution for chlorites is then calculated by multiplying the Gibbs free energy of the free oxide or hydroxide (from thermodynamic data tables) by the corresponding values of n determined in 2.c.

c) *An example: Estimation of the $\Delta_f G_m^\circ$ for illite*

1. Chemical formula $K_{0.75} (Al_{1.75} Mg_{0.25}) Si_{3.5} Al_{0.5} O_{10} (OH)_2 (cr)$.
2. In the structure, the polyhedra are 4- Al_2O_3 , 6- Al_2O_3 , 6- $Al(OH)_3$, SiO_2 , 6-MgO, 6-Mg(OH)₂, 8-12- K_2O .
3. The numbers are 0.25 (4- Al_2O_3), 0.5833 (6- Al_2O_3), 0.5833 (6- $Al(OH)_3$), 3.5 (SiO_2), 0.1666 (6-MgO), 0.08333 (6-Mg(OH)₂), 0.3750 (8-12- K_2O).
4. We now simply multiply the corresponding numbers with the appropriate componental free energy and the sum is the Gibbs free energy of formation of illite from elements. The total is $-5463.0 \text{ kJ} \cdot \text{mol}^{-1}$.

The Chermak-Rimstidt method is simple and seems to work well particularly for hydrous minerals. As expected, there are some serious problems. For example, the method is not good for many important silicates such as lawsonite, jadeite, talc, kaolinite, fayalite and forsterite with errors of -29.0 , -20.9 , -10.3 , 11.1 , 12.7 and $55.37 \text{ kJ} \cdot \text{mol}^{-1}$, respectively.

VIII.3.3.2. A new polyhedral method

The method being presented here is in principle based on Hazen's polyhedral method. Many silicates consist of cation crystallographic sites with different coordination numbers. For example, the pyroxene structure contains single chains of tetrahedrally coordinated Si^{4+} which are laterally linked through octahedrally coordinated cations (Fe^{2+} , Mg^{2+} and Ca^{2+}); there may be one or more of these octahedrally coordinated sites. For example in pyroxenes (Figure VIII.6), there is a regular octahedron called the M1 site and a distorted octahedron called M2 site. We attempt to characterize energetically as many polyhedral units as possible. For this purpose, we need thermodynamic data that are internally systematized and are consistent with most experimental phase equilibrium data. Some data bases do satisfy these criteria [88BER, 90HOL/POW, 93SAX/CHA]. If we can determine the energy of several polyhedral units, we may be able to recognize certain regularities related to measurable polyhedral properties such as polyhedral volumes and their deviations from a regular symmetry. To estimate the enthalpy of a crystal with any degree of precision, we would need to know the structure of the phase including the distribution of cations over various crystallographic sites. For solid solutions, we will need additional information on mixing energies.

Table VIII.2 shows the enthalpy data $\Delta_f H_m^\circ$ of 41 silicates from Table VIII.1 (Saxena *et al.* [93SAX/CHA] or Holland and Powell [90HOL/POW]). These compounds have been chosen because of the structural information available on coordination polyhedra. The enthalpy of formation from elements in their standard state (298.15 K at 1 bar) has been converted to lattice enthalpy ($\Delta_L H_m$). For example for enstatite, we have:

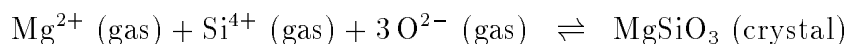
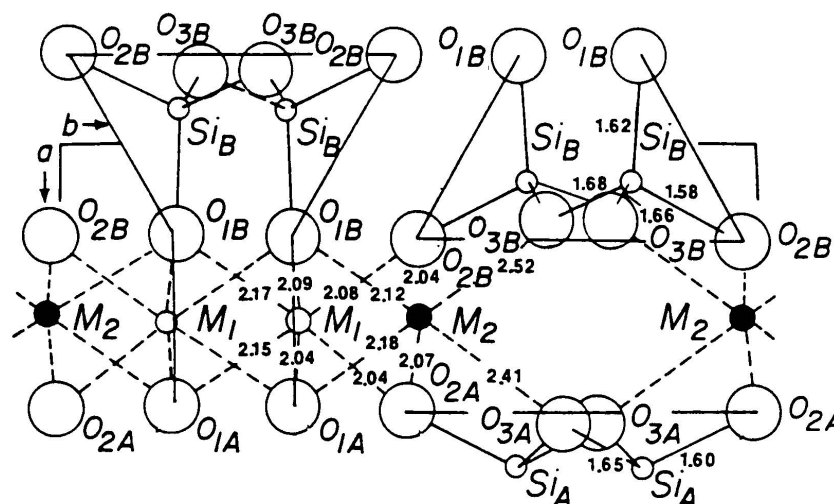


Figure VIII.6: The pyroxene structure showing the silicon tetrahedral chain and the M1 and M2 octahedra; the regular M1 site is principally occupied by Mg^{2+} and Fe^{2+} and the distorted M2 site by Ca^{2+} and Fe^{2+} . Data from Ghose [65GHO].



The $\Delta_L H_m$ is then the difference between the enthalpies of the crystal and the gaseous species. Such data are shown in Table VIII.2. The enthalpies of the gaseous ions are (kJ/cation): H^+ 1537, Na^+ 611, Mg^{2+} 2349, Al^{3+} 5484, K^+ 514, Fe^{2+} 2842, Fe^{3+} 5715, Ca^{2+} 1926 and Si^{4+} 10428.3. For O^{2-} the data are not available and we use 900 kJ which gives the least error in the regression. The $\Delta_f H_m^\circ$ is the enthalpy of formation as reported in Saxena *et al.* [93SAX/CHA] or Holland and Powell [90HOL/POW] except for kaolinite (Hemley *et al.* [80HEM/MON]).

The regressed polyhedral coefficients are shown in Table VIII.3. There are 32 such coefficients (Mg-pyroxene is the same as for M1-pyroxene) based on the enthalpy data of 41 silicates. The increased number of coefficients has led to substantial reduction in errors of fitting. No individual errors in the coefficients are calculated because these depend on the errors in the thermochemical data used. In the systematized data set used here, individual errors of enthalpy data are not useful (see [93SAX/CHA]). Table VIII.2 shows how the various cations are distributed among the polyhedra. For most substances, the distribution is standard (*e.g.*, for forsterite Mg in M1 and M2 site and Si in Si-site); for some others the distribution must be modified to fit to the thermochemical data. These are discussed below:

- CaSiO_3 (Wollastonite): Ca is in irregular octahedral coordination. Both M1 and M2 sites are regarded as equivalent to the M2 site in pyroxene.
- $\text{MgCa}_2\text{Si}_2\text{O}_7$ (Aikmanite): There appears to be a reasonably good fit to enthalpy data if the olivine M2 coordination is chosen both for Ca and Mg.

- $\text{Ca}_2\text{Al}_2\text{SiO}_7$ (Gehlenite): Same as above.
- $\text{Mg}_2\text{Al}_4\text{Si}_5\text{O}_{18}$ (Cordierite): The octahedral sites are regarded as comparable to those of olivine.
- $\text{KAl}_3\text{Si}_3\text{O}_{10}(\text{OH})_{12}$ (Muscovite): The octahedral Al is divided between 1.334 of Al-6 and 0.666 of Al(OH)₃. The choice of decimal rounding is important and the numbers must be as written.
- $\text{KMg}_3\text{AlSi}_3\text{O}_{10}(\text{OH})_{12}$ (Phlogopite): Two Mg are assigned to the pyroxene M1 site and one Mg to Mg(OH)₂.
- Talc: The best fit to the data on talc is obtained by assigning one Mg to pyroxene M1, one to Mg(OH)₂ and by assigning the third Mg to a talc site typical to the talc structure.
- Non-aluminous amphiboles: For $\text{Mg}_7\text{Si}_8(\text{OH})_{24}$ (anthophyllite) the seven Mg ions are distributed as MgTlc:Mg(M1-Px):Mg(M2-Px):Mg(OH)₂ = 2:2:2:1. In general, the procedure requires that all necessary Mg is assigned to (OH) and then the remaining cations are distributed equally among the three sites. If Ca or Na is present, the M2-Px site is replaced with either the Ca-Amp (Amp=amphibole) or Na-Amp site. Note that the two M1-Px sites should have two Mg or Fe ions before the Mg- or Fe-Tlc site is filled.

The remaining assignments are obvious and done by comparison with the mineral closest in coordination behavior.

Examples of application:

Some calculated results are shown in Table VIII.4. The lattice enthalpy componental contributions in hornblende may be calculated as follows:

$$\begin{aligned}\text{Ca(Amp)} &= 2 \times (-3555.8) \\ \text{MgTlc} &= 1 \times (-3889.2) \\ \text{Mg(M1-Px)} &= 2 \times (-3911.4) \\ \text{Al-4} &= 1 \times (-7653.4) \\ \text{Al-6} &= 1 \times (-7670.1) \\ \text{Si} &= 7 \times (-13141.0) \\ \text{Mg(O}_2\text{H}_2) &= 1 \times (-8172.1) \\ \text{Total} &= -134306.2 \text{ kJ} \cdot \text{mol}^{-1}\end{aligned}$$

Table VIII.3: Regressed lattice enthalpy of the polyhedral units ($\text{kJ} \cdot (\text{mol unit})^{-1}$).

Polyhedral	Ca ²⁺	Mg ²⁺	Fe ²⁺	Al ³⁺	Fe ³⁺	Na ⁺	K ⁺	Si ⁴⁺	H ₂ O
Type									
Garnet	-3567.5	-3911.4	-4030.8		-7467.5				
Olivine M1	-3525.4	-3884.3	-4028.9						
Olivine M2	-3531.9	-3877.3	-4019.4						
Pyroxene M1		-3911.4	-4032.3		-7455.4				
Pyroxene M2	-3545.3	-3857.9	-4015.6			-1429.3			
Amphibole	-3555.8					-1414.0			
Feldspar	-3595.2					-1433.3	-1336.6		
Talc		-3889.2	-4026.84						
4-coord				-7653.4				-13141.0	
6-coord				-7670.1					
Kaol				-14107.0					
(O ₃ H ₃)				-14203.0					
Zoisite				-14361.0					
Analcime									-4273
(O ₂ H ₂)		-8172.1	-8330.725						

$$\begin{aligned}
 \Delta H (\text{gas ions}) &= 2 \times 1926 + 2349 + 2 \times 2349 + 5484.0 + 5484.0 + 7 \times 10428.3 \\
 &\quad + 2349 + 2 \times 1537 + 24 \times 900.0 \\
 &= 121888.1 \text{ kJ} \cdot \text{mol}^{-1} \\
 \Delta_f H_m^\circ &= -134306.2 + 121888.1 = -12418.1 \text{ kJ} \cdot \text{mol}^{-1}
 \end{aligned}$$

Table VIII.4 shows that for some phases, *e.g.*, Fe-talc or greenalite, the estimation is not good. The same appears to be the case for high (OH) content minerals such as amesite ($\text{Mg}_4\text{Al}_3\text{Si}_2\text{O}_{10}(\text{OH})_8$) or clinocllore (Table VIII.4). For amesite, one octahedral Mg is replaced by one octahedral Al. If this is the replacement for the $\text{Mg}(\text{OH})_2$ component, we should use $\text{Mg}(\text{M1-Px})\text{Mg}(\text{Tlc})\text{Al}(4)_2\text{Al}(6)_{0.666}\text{Al}(\text{O}_3\text{H}_3)_{1.334}\text{Mg}(\text{O}_2\text{H}_2)_2$ for which the calculated enthalpy is -9100.26 as compared to $-9046.04 \text{ kJ} \cdot \text{mol}^{-1}$ [90HOL/POW]. We encounter similar problems with kerolite for which Chermak and Rimstidt get a good value but then their data on laumontite and lawsonite, which are used here, are different by 11.5 and 29.1 $\text{kJ} \cdot \text{mol}^{-1}$, respectively.

Table VIII.4: Some estimated results ($\text{kJ} \cdot \text{mol}^{-1}$). The second column shows the calculated value; the third column shows the assessed data from Table VIII.1. Data on enthalpy from Holland and Powell [90HOL/POW] except for greenalite [83MIY/KLE]).

Phase	$-\Delta_L H_m$	$-\Delta_f H_m^\circ$	Error
Hornblende $\text{Ca}(\text{Amp})_2\text{Mg}(\text{Tlc})\text{Mg}(\text{M1-Px})_2\text{Al}(4)\text{Al}(6)\text{Si}_7\text{Mg}(\text{O}_2\text{H}_2)\text{O}_{24}$	12418.1	12420.29	2.19
Edenite $\text{Na}(\text{Amp})\text{Ca}(\text{Amp})_2\text{Mg}(\text{M1-Px})_2\text{Al}(4)\text{Mg}(\text{Tlc})_2\text{Si}_7\text{Mg}(\text{O}_2\text{H}_2)\text{O}_{24}$	12574.1	12580.53	6.43
Prehnite $\text{Ca}(\text{M2-Px})\text{Ca}(\text{Amp})\text{Al}(4)\text{Al}(6)_{0.334}\text{Si}_3\text{Al}(\text{O}_3\text{H}_3)_{0.666}\text{O}_{12}$	6202.86	6199.86	-3.0
Kalsilite $\text{KAl}(4)\text{SiO}_4$	2104.13	2114.50	10.37
Nepheline $\text{NaAl}(4)\text{SiO}_4$	2104.12	2105.44	1.32
Leucite $\text{KAl}(4)\text{Si}_2\text{O}_6$	3016.82	3020.72	3.9
Clinochlore $\text{Mg}(\text{M1-Px})\text{Al}(4)\text{Al}(6)_{0.334}\text{Si}_3\text{Mg}(\text{O}_2\text{H}_2)_3\text{Mg}(\text{Tlc})\text{Al}(\text{O}_3\text{H}_3)_{0.666}\text{O}_{18}$	8914.0	8922.66	8.66
Fe-talc $\text{Fe}(\text{M1-Px})\text{Fe}(\text{O}_2\text{H}_2)\text{Fe}(\text{Tlc})\text{Si}_4\text{O}_{10}$	4840.77	4816.02	-24.75
Greenalite $\text{Fe}(\text{Tlc})\text{Fe}(\text{O}_2\text{H}_2)_2\text{Si}_2\text{O}_5$	3378.5	3339.75	-38.75

VIII.4. Estimation of entropy

Methods of estimation of entropy were recently reviewed by Holland [89HOL]. Fyfe *et al.* [58FYF/TUR] used entropies of simple oxides to estimate entropies of complex oxides and silicates. Their equation may be represented as:

$$S_{m,j}^\circ = n_i S_{m,i}^\circ + k (V_{m,j}^\circ - n_i V_{m,i}^\circ) \quad (\text{VIII.19})$$

where $S_{m,j}^\circ$ is the entropy to be determined of phase j , $V_{m,j}^\circ$ is the molar volume of phase j and the component oxide values are given by the subscript i . Holland [89HOL] reviewed the relationship between entropy and volume; he emphasized the reduction in bond stiffnesses and lowering of their vibrational frequencies with increasing cell volume. Since entropy and other thermodynamic properties are functions of the average vibrational spectrum, the molar volume should reflect the overall bonding state of the crystal. Holland [89HOL] also found that the consideration of cation coordination led to a significantly improved relationship between molar volumes and entropies of a number of substances.

Table VIII.5: Data for use with Holland's entropy model. The numbers after the dash refer to the coordination type. The H₂O-a and H₂O-b are to be used with micas and chlorites respectively. K₂O-a and K₂O-b are for feldspars/feldspathoids and micas respectively. All data in J · K⁻¹ · mol⁻¹.

Component	$S_m^\circ - V_m^\circ$	\pm
SiO ₂ -4	17.45	0.38
Al ₂ O ₃ -6	22.60	0.84
Al ₂ O ₃ -4	28.89	1.06
MgO-6	15.75	0.53
MgO-gt	26.06	0.88
CaO-6	21.94	0.80
CaO-8	27.37	0.84
CaO-8,10	34.37	0.70
CaO-gt	17.86	0.67
FeO-4,8	30.78	0.83
FeO-gt	36.50	0.67
MnO-6	33.41	1.20
TiO ₂ -6	32.63	1.54
Fe ₂ O ₃ -6	50.24	1.60
Na ₂ O-8	56.32	3.67
Na ₂ O-9,12	79.49	3.12
K ₂ O-a	79.55	3.53
K ₂ O-b	87.96	3.03
H ₂ O-a	15.71	0.91
H ₂ O-b	7.44	0.87

His results show that the value of k in the Eq. (VIII.19) is close to unity which reduces (VIII.19) to

$$S_{m,j}^\circ = V_{m,j}^\circ + n_i S'_{m,i} \quad (\text{VIII.20})$$

where $S'_{m,i}$ is $(S_{m,i}^\circ - V_{m,i}^\circ)$. Table VIII.5 gives the data for Eq. (VIII.20).

VIII.4.1. Example of a calculation

An example of Holland's [89HOL] method of calculating the entropy of a Mn-carpholite (MnAl₂Si₂O₆(OH)₂) is given below. The molar volume for the phase is 108.2 cm³ · mol⁻¹. All Al is octahedral and assuming that H₂O is like in the trioctahedral micas, we have:

$$\begin{aligned} S_m^\circ(\text{carpholite}) = & V_m^\circ(\text{carpholite}) + (S_m^\circ - V_m^\circ)_{\text{MnO}} + (S_m^\circ - V_m^\circ)_{\text{Al}_2\text{O}_3-6} \\ & + 2(S_m^\circ - V_m^\circ)_{\text{SiO}_2} + 2(S_m^\circ - V_m^\circ)_{\text{H}_2\text{O-b}} \end{aligned}$$

$$\begin{aligned}
 &= 108.2 + 33.41 + 22.60 + 2(17.45) + 2(7.44) \\
 &= 214.7 \text{ kJ} \cdot \text{mol}^{-1} + (\text{magnetic term})
 \end{aligned}$$

The last term in the equation is for magnetic order-disorder transformation in solids containing transition metals. This transformation is temperature dependent and varies in magnitude for different species. Holland added a simplified term $R \ln(2s+1)$ where s is the spin quantum number. Thus for Fe^{2+} with s as 2 the magnetic term is $13.4 \text{ J} \cdot \text{K}^{-1} \cdot \text{atom}^{-1}$; for Mn^{2+} , s is $5/2$ and the addition is $14.9 \text{ J} \cdot \text{K}^{-1} \cdot \text{atom}^{-1}$. If the data on molar volume is not available, it is possible to use the method proposed by Robinson and Haas [83ROB/HAA].

VIII.5. Estimation of heat capacities of solids

The method of a simple summation of the heat capacities of the component oxides for a silicate yields a value that may be generally within 5% of the measured value (*e.g.*, for MgSiO_3 , the measured C_p at 298 K is 82.2, for MgO 37.3 and for quartz 44.6 $\text{J} \cdot \text{K}^{-1} \cdot \text{mol}^{-1}$; the latter two sum up to 81.9). A greater precision may be achieved if one uses the polyhedral methods as worked out by Robinson and Haas [83ROB/HAA] or by Berman and Brown [85BER/BRO2]. The latter authors used a large number of silicates to obtain the regression coefficients listed in Table VIII.6. These coefficients may be used to estimate the heat capacity of a solid (assuming no lambda transitions). The data are to be used with the equation:

$$C_p = n_i C_i \quad (\text{VIII.21})$$

where n_i and C_i are number of moles and the regressed C_p function (VIII.22) given by

$$C_p = a + cT^{-2} + eT^{-3} + fT^{-0.5} \quad (\text{VIII.22})$$

The coefficients in (VIII.21) are comparable to those of Eq. (VIII.14). The authors have also provided to account for the lambda transition heat capacities with a separate term (not given here). This method has the advantage over the Robinson and Haas [83ROB/HAA] method that a knowledge of cation coordination is not necessary.

VIII.6. Conclusions

The use of assessed data bases in thermodynamic calculations is essential. Today, we have many more methods of studying the properties of a solid than in the past when calorimetry was the only reliable technique. Although it is difficult to assign definite errors to the assessed data on an individual phase, the overall reliability may be judged by the applicability of the data to all available phase equilibrium data in a given system.

There does not appear to be an entirely satisfactory empirical method available which could let us use a simple summation of polyhedral contributions of energy and obtain the enthalpy of a given silicate. However, it seems quite possible that with a sufficiently

Table VIII.6: Coefficients for calculating the heat capacity of a solid [85BER/BRO2].

Component	K_0	$K_1 \times 10^{-2}$	$k_2 \times 10^{-5}$	$k_3 \times 10^{-7}$
Na ₂ O	95.148	0.00	-51.0405	83.3648
K ₂ O	105.140	-5.7735	0.00	0.00
CaO	60.395	-2.3629	0.00	-9.3493
MgO	58.196	-1.6114	-14.0458	11.2673
FeO	77.036	-5.8471	0.00	0.5558
Fe ₂ O ₃	168.211	-9.7572	0.00	-17.3034
TiO ₂	85.059	-2.2072	-22.5138	22.4979
SiO ₂	87.781	-5.0259	-25.2856	36.3707
Al ₂ O ₃	155.39	-8.5229	-46.9130	64.0084
H ₂ O (Structural)	106.330	-12.4322	0.0	9.0628
H ₂ O (zeolitic)	87.617	-7.5814	0.0	0.5291
CO ₂	119.626	-15.0627	0.0	17.3869

enlarged systematized and internally consistent thermodynamic data base, we may be able to determine the fictive componental polyhedral contributions whose linear combination could fit the enthalpy data closely; this would be particularly true for the estimation of entropy and heat capacities. In this regard, we can already rely on the methods proposed by Holland [89HOL] for entropy and by Berman and Brown [85BER/BRO2] for heat capacity. The estimation of enthalpy remains a formidable task and the two methods adopted here, the one by Cermak and Rimstidt and the other a new method first being reported here, could be used with great caution. The latter method can be simply extended to include other components if reliable data are available.

Chapter IX

Estimations of Medium Effects on Thermodynamic Data [†]

Ingmar GRENTHE
Department of Inorganic Chemistry
Royal Institute of Technology
S-100 44 Stockholm (Sweden)

Andrey V. PLYASUNOV ¹
Department of Inorganic Chemistry
Royal Institute of Technology
S-100 44 Stockholm (Sweden)

Kastriot SPAHIU
Swedish Nuclear Fuel
& Waste Management Co.
Box 5864
S-102 40 Stockholm (Sweden)

IX.1. Introduction

This chapter describes methods for the estimation of deviations from ideality, *e.g.*, the activity coefficients of reactants and products (usually ions) of chemical reactions in solution, usually complex formation, redox and acid/base equilibria. The typical feature of these reactions is that they involve *strong* interactions between the components of the system, where often many different species (complexes) are present simultaneously in comparable concentrations. This is a situation that is very different from mixtures of strong electrolytes, and these differences will be reflected in the methods used to describe the deviations from ideality.

[†] This Chapter originates from an internal NEA technical report (TDB-2), and from Appendices B in the published NEA reviews on the thermochemistry of uranium and americium [92GRE/FUG, 95SIL/BID]. However, the text has undergone a complete revision and it has been substantially expanded.

¹ Permanent address: Institute of Experimental Mineralogy of the Russian Academy of Sciences, Chernogolovka, Moscow District, 142432, Russia.

Compilations of thermodynamic data *always* contain information referring to *standard state conditions*, defined according to IUPAC [82LAF] in Chapter II, Section II.3.1. Users of thermodynamic data must therefore recalculate these data to the conditions present in the system they are studying. Thermodynamics in combination with physico-chemical theories provides the framework for such calculations and we will briefly review the theories on which these methods are based, and their relative merits. We will discuss two types of calculations:

- Those using equilibrium constant data determined in the laboratory, usually in an ionic medium, to determine the corresponding constant at zero ionic strength (the usual standard state in compilations of thermodynamic data). However, there is no “standard” ionic medium, or ionic strength, preferred in the experimental determinations of equilibrium constants. Hence, there is a need to recalculate the data to a common standard state in order to allow a comparison of them. The standard state preferred in compilations of thermodynamic data is the infinite dilute solution, with pure water as the solvent. The experimental data are usually available at a *few* ionic strengths, typically from 0.1 up to 4 mol · kg⁻¹.
- Those using tabulated standard state data to calculate equilibrium constants and properties of single strong electrolytes and their mixtures over a *large* ionic strength range.

An important aspect of activity coefficient estimations is related to the possibility of *measuring* precise thermodynamic data in the laboratory, particularly data for complex formation and other reactions involving ionic species in solution. In order to deduce the stoichiometry and equilibrium constants in such systems, it is always necessary to vary the concentrations of reactants and products over fairly large concentration ranges under conditions where the activity coefficients of the species are either *known*, or *constant*. Only in this way is it possible to use the mass balance equations for the various components, together with the measurement of one or more free concentrations to obtain the information desired [61ROS/ROS, 90BEC/NAG]. Activity coefficients may be estimated at very low total concentrations of reactants/products (where they approach unity). However, under these conditions it is not possible to perform the variation in concentrations required to establish a proper chemical model.

The activity coefficient of a species *i*, denoted γ_i , in an electrolyte mixture composed of different ionic species depends on the concentrations of all these species and their chemical characteristics (*e.g.*, size and charge), on temperature, pressure and solvent properties. If one component of the electrolyte mixture is present in a much larger concentration than the others, this component will determine the activity coefficients of the minor components, which are then called “trace” activity coefficients.

For this reason most experimental studies of solution chemical equilibria are performed in the presence of an ionic medium, using an *inert* electrolyte (a strong electrolyte, usually NaClO₄), the ions of which do not react with the reactants/products of the reactions studied. The concentration of inert electrolyte is usually 10 - 100 times larger than the

concentration of the reactants. More details about the use of the ionic medium method may be found in [53BIE/SIL, 61ROS/ROS, Chapter 1, 90BEC/NAG, Chapter 2]. By using an ionic medium one ensures that the (trace) activity coefficients of reactants and products are nearly constant over a *large* concentration range, and that activities and concentrations are proportional to one another. It is customary to define the proportionality constant as unity in the ionic medium used. This is equivalent to assuming that the activity coefficients of reactants and products approach unity when their concentrations are much lower than the total concentration of the ionic medium. The most important difference between the ionic medium solvent and the pure water solvent is that the concentration range where the activity coefficients are constant is *much larger* in the former case.

The equilibrium constants deduced from measurements in ionic media are *conditional* equilibrium constants, because the activity coefficients may be *defined* as unity in *any* ionic medium. In order to compare the magnitude of equilibrium constants obtained in *different* ionic media it is necessary to have a method for estimating activity coefficients of ionic species in mixed electrolyte systems by using *one common* standard state. The “infinite dilution” state is the one generally used. This will also be the standard state in the following discussion.

IX.2. On the estimation of activity coefficients in electrolyte systems

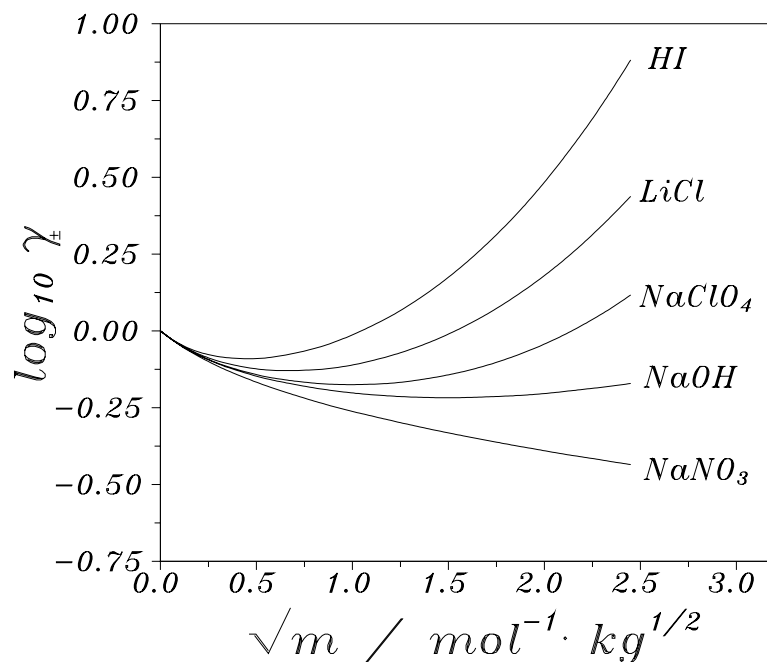
Ionic solutions depart strongly from ideality due to the long-range electrostatic interactions. The interaction energy between neutral molecules falls off as r^{-6} , while Coulomb interactions between ions falls off as r^{-1} (r is the distance between the interacting particles).

In most cases it is experimentally straightforward to measure deviations from ideality in pure electrolyte and other systems [58HAR/OWE, Chapters 9 and 10, 59ROB/STO, 90ATK, Chapter 10]. The interpretation of these deviations in terms of theoretical models, is less simple. There exists a number of alternative semi-empirical methods for the estimation of activity coefficients, each with its own advantages and draw-backs. The following figure shows the variation of the mean-activity coefficient for some 1:1 electrolytes as a function of the square-root of the ionic strength I_m ($I_m = \frac{1}{2} \sum m_i Z_i^2$, where m_i and Z_i stand for molality and charge of species i).

There are four main observations to be made:

- There are large changes in the mean activity coefficients with concentration.
- The slopes of $\log_{10} \gamma_{\pm}$ vs. $\sqrt{I_m}$ are identical within the experimental error at very low ionic strengths for a particular valence type. Any theory must be able to explain this limiting behavior.
- The variations are not the same for different electrolytes. Any theory must be able to describe their individual characteristics.

Figure IX.1: The variation of $\log_{10} \gamma_{\pm}$ for some 1:1 electrolytes as a function of the square-root of the ionic strength at 298.15 K and 1 atm. The source of $\log_{10} \gamma_{\pm}$ is Ref. [91PIT].



- At intermediate high ionic strengths $\log_{10} \gamma_{\pm}$ is a linear function of the ionic strength over fairly large molality ranges, *cf.* Figure IX.2.

All electrolyte models are based on microscopic physico-chemical descriptions of the interactions between dissolved ions, and sometimes the interactions between ions and solvent. The reader should be aware that a self-consistent theory of ionic solutions is still to be awaited. Until such a theory is available we have to rely on *provisional* models. The ones described in this chapter are all based on the Debye-Hückel theory [90ATK, Chapter 10] and extensions thereof.

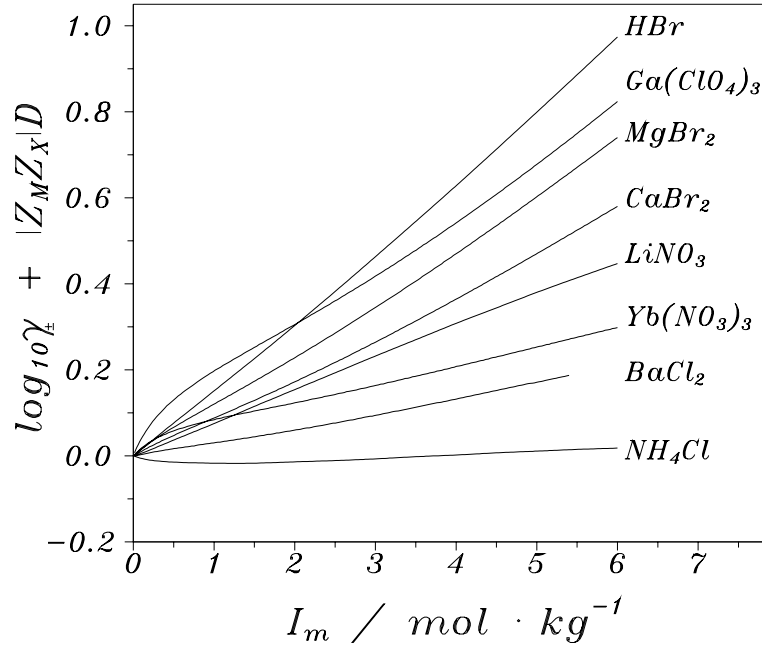
The classical Debye-Hückel model takes only into account electrostatic interactions between ions of opposite charge, and is able to give a quantitative description of the variation of $\log_{10} \gamma_{\pm}$ *vs.* $\sqrt{I_m}$, as the ionic strength approaches zero.

The Debye-Hückel limiting law is

$$\log_{10} \gamma_{\pm} = -|Z_M Z_X| A \sqrt{I_m} \quad (\text{IX.1})$$

where Z_M and Z_X are the ionic charges for the particular electrolyte, I_m the ionic strength, and A a constant with the value $0.5100 \text{ mol}^{-1/2} \cdot \text{kg}^{1/2}$ at 298.15 K and 1 atm [90ARC/WAN]. γ_{\pm} is used here for the molal mean-activity coefficient. The range of validity of the limiting law varies with the electrolyte, typically up to $I_m = 0.01 \text{ mol} \cdot \text{kg}^{-1}$ for 1:1 electrolytes, and 0.001 for 3:1 electrolytes. Various empirical attempts to “extend” the

Figure IX.2: The variation of function $[\log_{10} \gamma_{\pm} + |Z_M Z_X|D]$ vs. ionic strength for a number of electrolytes at 298.15 K and 1 atm. The source of $\log_{10} \gamma_{\pm}$ is Ref. [91PIT].



range of application of the Debye-Hückel limiting law have been made, typically to ionic strengths of about $0.03 \text{ mol} \cdot \text{kg}^{-1}$ for 1:1 electrolytes, by the introduction of an electrolyte dependent “effective” diameter of the hydrated ions, which results in a Debye-Hückel term of the type:

$$D = \frac{A\sqrt{I_m}}{1 + Ba_{MX}\sqrt{I_m}} \quad (\text{IX.2})$$

where a_{MX} stands for an “effective” distance, and B is a Debye-Hückel parameter, defined by temperature, pressure (the density of pure water), and the dielectric constant of water, (see [81HEL/KIR] for further details). In order to extend the equations for activity coefficient estimations to higher ionic strength, and to take the individual characteristics of different electrolytes into account, various techniques have been used:

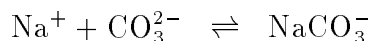
- Non-electrostatic short range interactions, with terms proportional to the concentration of ions or to the ionic strength are included in addition to the Debye-Hückel term. In Figure IX.2 we have illustrated the deviations from the simple Debye-Hückel theory by plotting $[\log_{10} \gamma_{\pm} + |Z_M Z_X|D]$ vs. I_m , where D has been calculated using Eq. (IX.2) with $Ba_{MX} = 1.5$.

The best known of this type of models is the Davies’ equation, which describes the

activity coefficient of an ion i of charge Z_i at 298.15 K with the expression:

$$\log_{10} \gamma_i = -0.5100 Z_i^2 \left(\frac{\sqrt{I_m}}{1 + \sqrt{I_m}} - 0.3 I_m \right) \quad (\text{IX.3})$$

Davies' equation has a formal similarity to the specific ion interaction equations described in the following text, but has no theoretical foundation. It is often found to work fairly well up to ionic strengths of 0.1 mol·kg⁻¹. Davies' equation takes only the charge of the ions into account, not their individual characteristics. In order to account for these the concept of *ionic pairing* is introduced, where deviations between measured values of mean-activity coefficients and those calculated using Eq. (IX.3) are *assumed* to be due to complex formation reactions, *e.g.*, of the type:



which are described by equilibrium constants.

Ion association models use the same extended Debye-Hückel expression to describe the electrostatic interactions between all electrolytes, while the electrolyte specific characteristics are described using ion-pair formation between ions of opposite charge. The equations used vary in complexity from Davies' equation, to the equations developed by Helgeson *et al.* [81HEL/KIR]. Davies' equation is used in some codes for the calculation of thermodynamic properties in geochemical systems, but its use at moderate, or high ionic strengths for the calculation of activity coefficients of species in trace concentrations is not recommended [84HAR/MOL].

- The individual characteristics of electrolytes may also be described using *specific ion interaction models*. These semiempirical models contain a number of parameters which have a theoretical basis, but must be determined from the experimental data. The precision of the description *e.g.*, of mean-activity coefficient data, increases with the number of model parameters. These models often describe the activity coefficients and their temperature and pressure derivatives fairly well, especially in binary systems (*vide infra* Section IX.9, p.397).

Specific ion interaction models also use a Debye-Hückel term for the description of long range electrostatic forces and a virial series expansion in powers of the molality of the electrolyte(s) to model short-range interactions [91PIT], with specific interaction terms for each type of pair, or triple interaction.

In the following sections we will outline the basic features of the most important specific ion interaction models, always with the emphasis on their use for the modelling of complex geochemical systems at moderate temperatures and pressures. These models allow the user to:

- extend the equations describing the activity coefficient variations in simple electrolyte systems to more complex systems with many components;

- use “single-ion” activity coefficients, provided that comparisons with experimental data are always made on electroneutral combinations of ions.

This chapter is intended to provide a rationale for the selection and use of models for the estimate of the ionic medium/ionic strength dependence of thermodynamic quantities in (multi)electrolyte media. All such methods have a common theoretical basis in the Debye-Hückel theory, which is then extended to include various non-electrostatic interactions. These take the form of phenomenological parameters which have to be determined from experimental data. The various models differ mainly in the number of parameters they contain, and this will influence their predictive capacity. We will concentrate on the Pitzer and the Brønsted-Guggenheim-Scatchard (SIT) models. The main part of the discussion refers to chemical equilibria in ionic medium systems, where the reactants/products are present in low concentration, compared to that of the medium.

The Pitzer method has mainly been applied to strong electrolyte systems, both single and mixtures at high concentrations, while the SIT model has been used by solution coordination chemists for the description of the ionic medium/ionic strength dependence of concentration equilibrium constants. There is some overlap, but fairly small, between these two areas. In order to use all solution chemical information in an efficient way, it is necessary to have a common method for estimating deviations from ideality. Such a method should be based on the most developed theoretical framework, *i.e.*, the Pitzer model. However, when treating equilibrium constant data in this way, it is often necessary to make a number of approximations, or use procedures for estimating unknown interaction coefficients.

By using a number of examples we will demonstrate the characteristics of the models, and how their predictive capacity is influenced by the model parameters and their uncertainty. We will also describe methods to transform interaction coefficients between the two model structures, and to estimate unknown parameters.

IX.3. The Brønsted-Guggenheim-Scatchard model (SIT) [†]

The Debye-Hückel term, which is the dominant term in the expression for the activity coefficients in dilute solutions, accounts for electrostatic, long-range interactions. At higher concentrations short-range, non-electrostatic interactions have to be taken into account as well. This is usually done by adding terms to the Debye-Hückel expression as outlined by Brønsted [22BRO, 22BRO2] and elaborated by Guggenheim [35GUG, 66GUG] and Scatchard [36SCA]. This approach was successfully used by different groups of solution coordination chemists, mainly for the description of the concentration dependence of complex formation equilibria, including the determination of equilibrium constants for

[†] Note by the Editors: The abbreviation “SIT” stands for **S**pecific **I**on **I**nteraction **T**heory. Although the name is misleading, the use of this abbreviation is continued because of its wide use in the literature (it apparently originates from Ref. [82BIE/BRU]; see also Refs. [89RIG/ROB, 92CAP/VIT, 92CHO/DU, 94ERT/MOH, 94FAN/KIM, 95CAP/VIT, 95NEC/FAN], *etc.*).

reactions at infinite dilution [75BIE, 80CIA, 92GRE/FUG]. The two basic assumptions in the Brønsted-Guggenheim-Scatchard model are described below.

Assumption 1:

The activity coefficient γ_i of an ion of charge Z_i in a solution of ionic strength is equal to:

$$\ln \gamma_i = -\frac{Z_i^2 A_\gamma \sqrt{I_m}}{1 + 1.5 \sqrt{I_m}} + \sum_k \varepsilon_\gamma(i, k) m_k \quad (\text{IX.4})$$

or

$$\begin{aligned} \log_{10} \gamma_i &= -\frac{Z_i^2 A \sqrt{I_m}}{1 + 1.5 \sqrt{I_m}} + \sum_k \varepsilon(i, k) m_k \\ &= -Z_i^2 D + \sum_k \varepsilon(i, k) m_k \end{aligned} \quad (\text{IX.5})$$

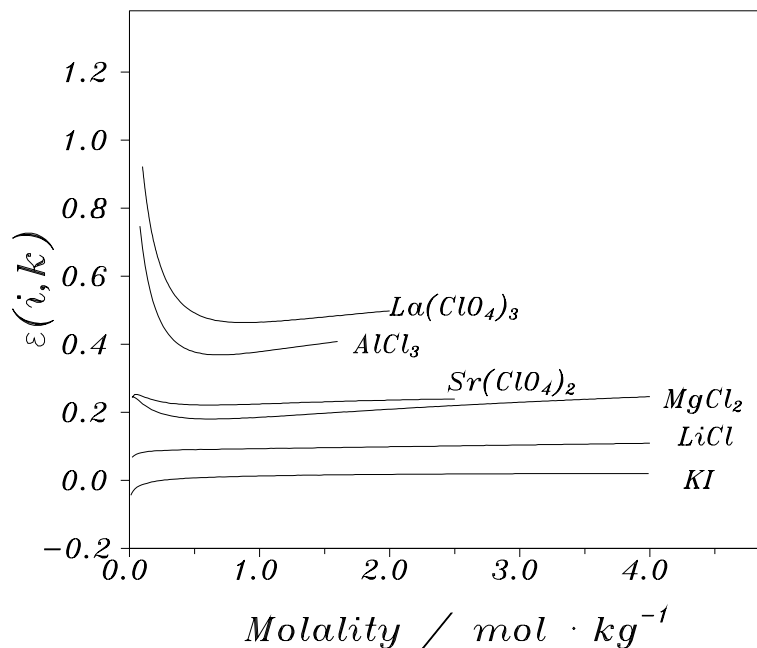
where D is a particular form of Debye-Hückel term used in the SIT model. A_γ and A are the limiting Debye-Hückel law slopes for the natural and decadic logarithm of the activity coefficient ($A_\gamma = \ln(10)A$), and $\varepsilon(i, k)$ (or $\varepsilon_\gamma(i, k) = \ln(10)\varepsilon(i, k)$) is an aqueous species interaction coefficient, which describes the specific short-range interactions between aqueous species i and k . Values of $\varepsilon(i, k)$ are given in Tables IX.1 and IX.2 (*p.*335) and Figures IX.6 to IX.12.

In the simplest approximation the ion interaction coefficients are considered to be concentration independent. The summation extends over all species k , with molality m_k , present in solution. The value of $1.5 \text{ kg}^{1/2} \cdot \text{mol}^{-1/2}$ in the denominator of the Eqs. (IX.4), (IX.5) is an empirical value of the product $a_j B$ in the Debye-Hückel term (where a_j is an “effective” ion diameter and B is a constant determined by the temperature and the physical properties of pure water, *cf.* *p.*329). The value 1.5 was proposed by Scatchard [76SCA] in order to minimise the ionic strength dependence of $\varepsilon(i, k)$ for a number of electrolytes at 298.15 K, *cf.* Figure IX.3.

It should be mentioned that a small change in the proposed value ($1.5 \text{ kg}^{1/2} \cdot \text{mol}^{-1/2}$) has very little influence on the quality of the fit of experimental mean-activity coefficients data, presumably due to correlation between $a_j B$ and the fitted value of $\varepsilon(i, k)$. A constant value of $a_j B$ for all ionic species simplifies the modelling of both binary and multicomponent aqueous electrolyte systems and makes it easy to give a consistent description of mean activity coefficients both in binary and multicomponent solutions [59ROB/STO, *p.*435–441].

The model assumption that the SIT interaction coefficients $\varepsilon(i, k)$ are concentration independent is an oversimplification. There is both theoretical and experimental evidence [91PIT] that they vary at lower molality, *cf.* Figure IX.3. At high molality the value of $\varepsilon(i, k)$ becomes nearly constant. In principle, it is possible to consider the SIT coefficient to be dependent on concentration, but in this case all required thermodynamic transformations become complex. In the simplest SIT model one does not take this concentration

Figure IX.3: The concentration dependence of the SIT coefficient for a number of electrolytes at 298.15 K and 1 atm. The source of $\log_{10} \gamma_{\pm}$ is Ref. [91PIT]. The units of ε are $\text{kg} \cdot \text{mol}^{-1}$.



dependence into account. If the available experimental data permit the determination of more than one interaction parameter the reader is advised to use the Pitzer approach. One should also observe that the variations of $\varepsilon(i, k)$ are largest at low molalities where the second term makes only a small contribution to the total value of the activity coefficient, *cf.* Eq. (IX.4).

Note. This assumption results in the identity $\varepsilon(i, k) \equiv \varepsilon(k, i)$, *i.e.*, $\log_{10} \gamma_+ \equiv \log_{10} \gamma_-$ for all strong n:n electrolytes. In the framework of other models these single ion activities could be assumed to be rather different from one another, *cf.* [70BAT/STA].

Assumption 2:

The ion interaction coefficients $\varepsilon(i, k)$ are zero for ions of the same charge sign, according to the Brønsted principle of specific ion interaction [22BRO, 22BRO2]. The rationale behind this is straightforward: the ions of the same charge sign are far from one another due to electrostatic repulsion. Hence, short-range forces between them are small. The ions of opposite charge are close to one other, and they are therefore strongly affected by the short-range forces, which are specific for each pair of co-ions. It is known that the Brønsted principle is not fully in agreement with the best experimental data, but these deviations are usually small (often < 0.01 - 0.02 in the values of the osmotic coefficient Φ or

$\ln \gamma_{\pm}$ [91PIT]). Thus, Assumption 2 (the Brønsted principle of specific ion interaction) is a good approximation with a sound theoretical basis. In order to compare the SIT model with experimental data, one must combine Eq. (IX.4) or (IX.5) for single ion activity coefficients to a measurable quantity, mean-activity coefficients, osmotic coefficients, or equilibrium constants. In [92GRE/FUG] it was assumed that the interaction coefficients for uncharged species were zero. There is no problem (and it is more correct) with including possible interactions between uncharged and ionic species in the SIT model.

For uncharged solutes the SIT model is reduced to one term, which is equivalent to the Setchenow equation [52LON/MCD, 58HAR/OWE], which assumes a linear dependence of $\ln \gamma^{\circ}$ on electrolyte concentration (where γ° is the activity coefficient of the uncharged molecule in an aqueous electrolyte solution). The Setchenow equation has been shown [52LON/MCD, 58HAR/OWE] to be a good approximation for the concentration dependence of the solubility of many gases (N_2O , C_2H_4 , CO_2 , O_2 , *etc.*), liquids (phenol, ethyl acetate, *etc.*), complexes (CdX_2 , $\text{X} = \text{Cl}^-$, Br^- , I^-) and solids (*e.g.*, SiO_2), in electrolyte solutions (“salting-in” or “salting-out” effects). Hence, the SIT equation has the potential to describe the activity coefficients and related properties of neutral species. SIT parameters for the interaction between ions and uncharged species can only be determined for electroneutral combinations of ions and uncharged species. To handle this problem Pitzer [91PIT, p.93] proposed to define an arbitrary zero point for the interaction between single ions and neutral molecules, and suggested that the interactions between H^+ and neutral molecules be defined as zero. Other single-ion neutral molecule interactions may then be calculated from experimental data. A number of SIT interaction coefficients for neutral species — electroneutral combination of ions have been tabulated by Ciavatta [90CIA]: $\varepsilon(\text{CdCl}_2^0, \text{Na}^+ + \text{ClO}_4^-) = (0.15 \pm 0.02)$; $\varepsilon(\text{CdCl}_2^0, \text{Li}^+ + \text{ClO}_4^-) = (0.23 \pm 0.05)$; $\varepsilon(\text{CdI}_2^0, \text{Na}^+ + \text{ClO}_4^-) = (0.25 \pm 0.05)$; $\varepsilon(\text{Hg}(\text{OH})_2^0, \text{Na}^+ + \text{ClO}_4^-) = (0.06 \pm 0.05)$; $\varepsilon(\text{HgCl}_2^0, \text{Na}^+ + \text{ClO}_4^-) = (0.06 \pm 0.03)$; $\varepsilon(\text{PbCl}_2^0, \text{Li}^+ + \text{ClO}_4^-) = (0.13 \pm 0.02)$, where all values are given in units of $\text{kg} \cdot \text{mol}^{-1}$.

Interactions between uncharged species may be far from negligible due to a so-called “self-interaction” contribution. Robinson and Stokes [59ROB/STO] give evidence that the activity coefficients of sucrose and glycerol are larger than 1 in an aqueous solution; other examples are given by Long and McDevit [52LON/MCD]. Interactions of this type may also be described using the SIT model, *e.g.*, the activity coefficients of the non-electrolytes mentioned above are reproduced better than 0.001 \log_{10} unit in $\log_{10} \gamma$ up to 3 $\text{mol} \cdot \text{kg}^{-1}$ by using the self-interaction coefficients 0.08 for sucrose ($\varepsilon(\text{sucrose}, \text{sucrose}) = 0.08$) and 0.01 for glycerol ($\varepsilon(\text{glycerol}, \text{glycerol}) = 0.01$). However, the deviations from ideality in aqueous solutions of non-electrolytes are in general small.

Table IX.1: Ion interaction coefficients $\varepsilon_{j,k}$ ($\text{kg} \cdot \text{mol}^{-1}$) at 25°C and 1 bar for cations j with $k = \text{Cl}^-$, ClO_4^- and NO_3^- , taken from Ciavatta [80CIA] unless indicated otherwise. The uncertainties represent the 95% confidence level, most of them were estimated by Ciavatta [88CIA]. Care should be taken when using the coefficients $\varepsilon_{(\text{M}^{n+}, \text{Cl}^-)}$ and $\varepsilon_{(\text{M}^{n+}, \text{NO}_3^-)}$ reported by Ciavatta [80CIA], which were evaluated without taking chloride and nitrate complexation into account.

$j \quad k \rightarrow$ \downarrow	Cl^-	ClO_4^-	NO_3^-
H^+	0.12 ± 0.01	0.14 ± 0.02	0.07 ± 0.01
NH_4^+	-0.01 ± 0.01	-0.08 ± 0.04	-0.06 ± 0.03
H_2gly^+	-0.06 ± 0.02		
Tl^+		-0.21 ± 0.06	
ZnHCO_3^+	$0.2^{(h)}$		
CdCl^+		0.25 ± 0.02	
CdI^+		0.27 ± 0.02	
CdSCN^+		0.31 ± 0.02	
HgCl^+		0.19 ± 0.02	
Cu^+		0.11 ± 0.01	
Ag^+		0.00 ± 0.01	-0.12 ± 0.05
YCO_3^+		$0.17 \pm 0.04^{(d)}$	
UO_2^+		$0.26 \pm 0.03^{(c)}$	
UO_2OH^+		$-0.06 \pm 3.7^{(c)}$	$0.51 \pm 1.4^{(c)}$
$(\text{UO}_2)_3(\text{OH})_5^+$	$0.81 \pm 0.17^{(c)}$	$0.45 \pm 0.15^{(c)}$	$0.41 \pm 0.22^{(c)}$
UF_3^+	$0.1 \pm 0.1^{(f)}$	$0.1 \pm 0.1^{(f)}$	
UO_2F^+	$0.04 \pm 0.07^{(b)}$	$0.29 \pm 0.05^{(c)}$	
UO_2Cl^+		$0.33 \pm 0.04^{(c)}$	
$\text{UO}_2\text{ClO}_3^+$		$0.33 \pm 0.04^{(f)}$	
UO_2Br^+		$0.24 \pm 0.04^{(f)}$	
$\text{UO}_2\text{BrO}_3^+$		$0.33 \pm 0.04^{(f)}$	
UO_2IO_3^+		$0.33 \pm 0.04^{(f)}$	
UO_2N_3^+		$0.3 \pm 0.1^{(f)}$	
UO_2NO_3^+		$0.33 \pm 0.04^{(f)}$	
UO_2SCN^+		$0.22 \pm 0.04^{(f)}$	
NpO_2^+		$0.25 \pm 0.05^{(b)}$	
PuO_2^+		$0.17 \pm 0.05^{(b)}$	
$\text{Am}(\text{OH})_2^+$		$0.17 \pm 0.04^{(j)}$	
AmF_2^+		$0.17 \pm 0.04^{(j)}$	

Table IX.1 (continued)

$j \quad k \rightarrow$ \downarrow	Cl^-	ClO_4^-	NO_3^-
AmSO_4^+ AmCO_3^+		$0.22 \pm 0.08^{(k)}$ $0.17 \pm 0.04^{(j)}$	
AlOH^{2+} $\text{Al}_2\text{CO}_3(\text{OH})_2^{2+}$	$0.09^{(a)}$ $0.26^{(a)}$	$0.31^{(a)}$	
Pb^{2+} Zn^{2+}		0.15 ± 0.02 0.33 ± 0.03	-0.20 ± 0.12 0.16 ± 0.02
ZnCO_3^{2+} Cd^{2+}	$0.35 \pm 0.05^{(h)}$		0.09 ± 0.02
Hg^{2+} Hg_2^{2+}		0.34 ± 0.03 0.09 ± 0.02	-0.1 ± 0.1 -0.2 ± 0.1
Cu^{2+} Ni^{2+}	0.08 ± 0.01 0.17 ± 0.02	0.32 ± 0.02	0.11 ± 0.01
Co^{2+} FeOH^{2+}	0.16 ± 0.02	0.34 ± 0.03 $0.38^{(d)}$	0.14 ± 0.01
FeSCN^{2+} Mn^{2+}		$0.45^{(d)}$	
YHCO_3^{2+} UO_2^{2+}	0.13 ± 0.01	$0.39 \pm 0.04^{(d)}$	
$(\text{UO}_2)_2(\text{OH})_2^{2+}$ $(\text{UO}_2)_3(\text{OH})_4^{2+}$	$0.21 \pm 0.02^{(i)}$ $0.69 \pm 0.07^{(c)}$ $0.50 \pm 0.18^{(c)}$	0.46 ± 0.03 $0.57 \pm 0.07^{(c)}$ $0.89 \pm 0.23^{(c)}$	$0.24 \pm 0.03^{(i)}$ $0.49 \pm 0.09^{(c)}$ $0.72 \pm 1.0^{(c)}$
UF_2^{2+} USO_4^{2+}		$0.3 \pm 0.1^{(f)}$ $0.3 \pm 0.1^{(f)}$	
$\text{U}(\text{NO}_3)_2^{2+}$ AmOH^{2+}		$0.49 \pm 0.14^{(g)}$ $0.39 \pm 0.04^{(j)}$	
AmF^{2+} AmCl^{2+}		$0.39 \pm 0.04^{(j)}$ $0.39 \pm 0.04^{(j)}$	
AmN_3^{2+} AmNO_2^{2+}		$0.39 \pm 0.04^{(j)}$ $0.39 \pm 0.04^{(j)}$	
AmNO_3^{2+} $\text{AmH}_2\text{PO}_4^{2+}$		$0.39 \pm 0.04^{(j)}$ $0.39 \pm 0.04^{(j)}$	
AmSCN^{2+} Mg^{2+}		$0.39 \pm 0.04^{(j)}$	
Ca^{2+} Ba^{2+}	0.19 ± 0.02 0.14 ± 0.01 0.07 ± 0.01	0.33 ± 0.03 0.27 ± 0.03 0.15 ± 0.02	0.17 ± 0.01 0.02 ± 0.01 -0.28 ± 0.03

Table IX.1 (continued)

$j \quad k \rightarrow$ \downarrow	Cl^-	ClO_4^-	NO_3^-
Al^{3+}	0.33 ± 0.02		
Fe^{3+}		0.56 ± 0.03	0.42 ± 0.08
Cr^{3+}	0.30 ± 0.03		0.27 ± 0.02
La^{3+}	0.22 ± 0.02	0.47 ± 0.03	
$\text{La}^{3+} \rightarrow \text{Lu}^{3+}$		$0.47 \rightarrow 0.52^{(d)}$	
UOH^{3+}		$0.48 \pm 0.08^{(g)}$	
UF^{3+}		$0.48 \pm 0.08^{(f)}$	
UCI^{3+}		$0.59 \pm 0.10^{(g)}$	
UBr^{3+}		$0.52 \pm 0.10^{(f)}$	
UI^{3+}		$0.55 \pm 0.10^{(f)}$	
UNO_3^{3+}		$0.62 \pm 0.08^{(g)}$	
Am^{3+}		$0.49 \pm 0.03^{(j)}$	
$\text{Be}_2\text{OH}^{3+}$		$0.50 \pm 0.05^{(e)}$	
$\text{Be}_3(\text{OH})_3^{3+}$	$0.30 \pm 0.05^{(e)}$	$0.51 \pm 0.05^{(e)}$	$0.29 \pm 0.05^{(e)}$
$\text{Al}_3\text{CO}_3(\text{OH})_4^{4+}$	$0.41^{(a)}$		
$\text{Fe}_2(\text{OH})_2^{4+}$		$0.82^{(d)}$	
$\text{Y}_2\text{CO}_3^{4+}$		$0.80 \pm 0.04^{(d)}$	
Pu^{4+}		$1.03 \pm 0.05^{(b)}$	
Np^{4+}		$0.82 \pm 0.05^{(b)}$	
U^{4+}		$0.76 \pm 0.06^{(f)}$	
Th^{4+}	0.25 ± 0.03		0.11 ± 0.02
$\text{Al}_3(\text{OH})_4^{5+}$	$0.66^{(a)}$	$1.30^{(a)}$	

Table IX.1 (continued)

Footnotes:

- (a) Taken from Hedlund [88HED].
- (b) Taken from Riglet, Robouch and Vitorge [89RIG/ROB], where the following assumptions were made : $\varepsilon_{(\text{Np}^{3+}, \text{ClO}_4^-)} \approx \varepsilon_{(\text{Pu}^{3+}, \text{ClO}_4^-)} = 0.49 \text{ kg} \cdot \text{mol}^{-1}$ as for other $(\text{M}^{3+}, \text{ClO}_4^-)$ interactions, and $\varepsilon_{(\text{NpO}_2^{2+}, \text{ClO}_4^-)} \approx \varepsilon_{(\text{PuO}_2^{2+}, \text{ClO}_4^-)} \approx \varepsilon_{(\text{UO}_2^{2+}, \text{ClO}_4^-)} = 0.46 \text{ kg} \cdot \text{mol}^{-1}$.
- (c) Evaluated in the NEA-TDB review on uranium thermodynamics [92GRE/FUG], using $\varepsilon_{(\text{UO}_2^{2+}, \text{X})} = (0.46 \pm 0.03) \text{ kg} \cdot \text{mol}^{-1}$, where $\text{X} = \text{Cl}^-$, ClO_4^- and NO_3^- .
- (d) Taken from Spahiu [83SPA].
- (e) Taken from Bruno [86BRU], where the following assumptions were made: $\varepsilon_{(\text{Be}^{2+}, \text{ClO}_4^-)} = 0.30 \text{ kg} \cdot \text{mol}^{-1}$ as for other $\varepsilon_{(\text{M}^{2+}, \text{ClO}_4^-)}$, $\varepsilon_{(\text{Be}^{2+}, \text{Cl}^-)} = 0.17 \text{ kg} \cdot \text{mol}^{-1}$ as for other $\varepsilon_{(\text{M}^{2+}, \text{Cl}^-)}$, and $\varepsilon_{(\text{Be}^{2+}, \text{NO}_3^-)} = 0.17 \text{ kg} \cdot \text{mol}^{-1}$ as for other $\varepsilon_{(\text{M}^{2+}, \text{NO}_3^-)}$.
- (f) Estimated in the NEA-TDB review on uranium thermodynamics [92GRE/FUG].
- (g) Evaluated in the NEA-TDB review on uranium thermodynamics [92GRE/FUG] using $\varepsilon_{(\text{U}^{4+}, \text{ClO}_4^-)} = (0.76 \pm 0.06) \text{ kg} \cdot \text{mol}^{-1}$.
- (h) Taken from Ferri *et al.* [85FER/GRE].
- (i) It is recalled that these coefficients were not used in the NEA-TDB review on uranium thermodynamics [92GRE/FUG] because they were evaluated by Ciavatta [80CIA] without taking chloride and nitrate complexation into account. Instead, Grenthe *et al.* used $\varepsilon_{(\text{UO}_2^{2+}, \text{X})} = (0.46 \pm 0.03) \text{ kg} \cdot \text{mol}^{-1}$, for $\text{X} = \text{Cl}^-$, ClO_4^- and NO_3^- .
- (k) Estimated in the NEA-TDB review on americium thermodynamics [95SIL/BID].
- (k) Evaluated in the NEA-TDB review on americium thermodynamics [95SIL/BID].

Table IX.2: Ion interaction coefficients $\varepsilon_{j,k}$ ($\text{kg} \cdot \text{mol}^{-1}$) at 25°C and 1 bar for anions j with $k = \text{Li}^+, \text{Na}^+$ and K^+ , taken from Ciavatta [80CIA] unless indicated otherwise. The uncertainties represent the 95% confidence level, most of them were estimated by Ciavatta [88CIA].

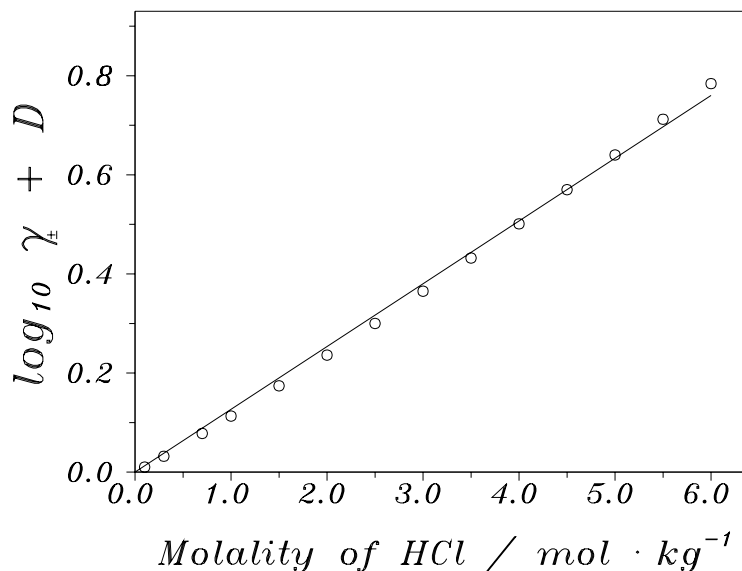
$j \quad k \rightarrow$ \downarrow	Li^+	Na^+	K^+
OH^-	-0.02 ± 0.03	0.04 ± 0.01	0.09 ± 0.01
F^-		$0.02 \pm 0.02^{(a)}$	0.03 ± 0.02
HF_2^-		$-0.11 \pm 0.06^{(a)}$	
Cl^-	0.10 ± 0.01	0.03 ± 0.01	0.00 ± 0.01
ClO_3^-		-0.01 ± 0.02	
ClO_4^-	0.15 ± 0.01	0.01 ± 0.01	
Br^-	0.13 ± 0.02	0.05 ± 0.01	0.01 ± 0.02
BrO_3^-		-0.06 ± 0.02	
I^-	0.16 ± 0.01	0.08 ± 0.02	0.02 ± 0.01
IO_3^-		$-0.06 \pm 0.02^{(b)}$	
HSO_4^-		-0.01 ± 0.02	
N_3^-		$0.0 \pm 0.1^{(b)}$	
NO_2^-	0.06 ± 0.04	0.00 ± 0.02	-0.04 ± 0.02
NO_3^-	0.08 ± 0.01	-0.04 ± 0.03	-0.11 ± 0.04
H_2PO_4^-		-0.08 ± 0.04	-0.14 ± 0.04
HCO_3^-		$0.00 \pm 0.02^{(c)}$	
SCN^-		0.05 ± 0.01	-0.01 ± 0.01
HCOO^-		0.03 ± 0.01	
CH_3COO^-	0.05 ± 0.01	0.08 ± 0.01	0.09 ± 0.01
$\text{SiO}(\text{OH})_3^-$		$-0.08 \pm 0.03^{(a)}$	
$\text{Si}_2\text{O}_2(\text{OH})_5^-$		$-0.08 \pm 0.04^{(b)}$	
$\text{B}(\text{OH})_4^-$		-0.07 ± 0.05	
$\text{UO}_2(\text{OH})_3^-$		$-0.09 \pm 0.05^{(b)}$	
UO_2F_3^-		$0.00 \pm 0.05^{(b)}$	
$\text{UO}_2(\text{N}_3)_3^-$		$0.0 \pm 0.1^{(b)}$	
$(\text{UO}_2)_2\text{CO}_3(\text{OH})_3^-$		$0.00 \pm 0.05^{(b,d)}$	
$\text{Am}(\text{SO}_4)_2^-$		$-0.05 \pm 0.05^{(e)}$	
$\text{Am}(\text{CO}_3)_2^-$		$-0.05 \pm 0.05^{(e)}$	
SO_3^{2-}		-0.08 ± 0.05	
SO_4^{2-}	-0.03 ± 0.04	-0.12 ± 0.06	-0.06 ± 0.02

Table IX.2 (continued)

$j \quad k \rightarrow$ \downarrow	Li^+	Na^+	K^+
$\text{S}_2\text{O}_3^{2-}$		-0.08 ± 0.05	
HPO_4^{2-}		-0.15 ± 0.06	-0.10 ± 0.06
CO_3^{2-}		$-0.08 \pm 0.03^{(c)}$	0.02 ± 0.01
$\text{SiO}_2(\text{OH})_2^{2-}$		$-0.10 \pm 0.07^{(a)}$	
$\text{Si}_2\text{O}_3(\text{OH})_4^{2-}$		$-0.15 \pm 0.06^{(b)}$	
CrO_4^{2-}		-0.06 ± 0.04	-0.08 ± 0.04
$\text{UO}_2\text{F}_4^{2-}$		$-0.08 \pm 0.06^{(b)}$	
$\text{UO}_2(\text{SO}_4)_2^{2-}$		$-0.12 \pm 0.06^{(b)}$	
$\text{UO}_2(\text{N}_3)_4^{2-}$		$-0.1 \pm 0.1^{(b)}$	
$\text{UO}_2(\text{CO}_3)_2^{2-}$		$-0.02 \pm 0.09^{(d)}$	
PO_4^{3-}		-0.25 ± 0.03	-0.09 ± 0.02
$\text{Si}_3\text{O}_6(\text{OH})_3^{3-}$		$-0.25 \pm 0.03^{(b)}$	
$\text{Si}_3\text{O}_5(\text{OH})_5^{3-}$		$-0.25 \pm 0.03^{(b)}$	
$\text{Si}_4\text{O}_7(\text{OH})_5^{3-}$		$-0.25 \pm 0.03^{(b)}$	
$\text{Am}(\text{CO}_3)_3^{3-}$		$-0.15 \pm 0.05^{(e)}$	
$\text{P}_2\text{O}_7^{4-}$		-0.26 ± 0.05	-0.15 ± 0.05
$\text{Fe}(\text{CN})_6^{4-}$			-0.17 ± 0.03
$\text{U}(\text{CO}_3)_4^{4-}$		$-0.09 \pm 0.10^{(b,d)}$	
$\text{UO}_2(\text{CO}_3)_3^{4-}$		$-0.01 \pm 0.11^{(d)}$	
$\text{UO}_2(\text{CO}_3)_3^{5-}$		$-0.62 \pm 0.15^{(d)}$	
$\text{U}(\text{CO}_3)_5^{6-}$		$-0.30 \pm 0.15^{(d)}$	
$(\text{UO}_2)_3(\text{CO}_3)_6^{6-}$		$0.37 \pm 0.11^{(d)}$	

- (a) Evaluated in the NEA-TDB review on uranium thermodynamics [92GRE/FUG].
(b) Estimated in the NEA-TDB review on uranium thermodynamics [92GRE/FUG].
(c) From [80CIA]. These values differ from those reported in the NEA-TDB uranium review [92GRE/FUG]. See the discussion in Appendix D of the NEA-TDB review on americium thermodynamics [95SIL/BID].
(d) See the discussion in Appendix D of the NEA-TDB review on americium thermodynamics [95SIL/BID].
(e) Estimated in the NEA-TDB review on americium thermodynamics [95SIL/BID].

Figure IX.4: The determination of the SIT coefficient from the mean activity coefficients for HCl at 298.15 K and 1 atm from [59ROB/STO].



IX.3.1. Determination of ion interaction coefficients

Example 1:

Figure IX.4 illustrates both the method used to obtain ion interaction coefficients from mean-activity coefficient data, and the precision of the SIT method in single electrolyte systems. The mean activity coefficient γ_{\pm} (HCl) is equal to:

$$\begin{aligned} 2 \log_{10} \gamma_{\pm, \text{HCl}} &= \log_{10} \gamma_{+, \text{H}^+} + \log_{10} \gamma_{-, \text{Cl}^-} \\ &= -D + \varepsilon(\text{H}^+, \text{Cl}^-) m_{\text{Cl}^-} - D + \varepsilon(\text{Cl}^-, \text{H}^+) m_{\text{H}^+} \end{aligned}$$

or

$$\log_{10} \gamma_{\pm, \text{HCl}} = -D + \varepsilon(\text{H}^+, \text{Cl}^-) m_{\text{HCl}}$$

By plotting $[\log_{10} \gamma_{\pm, \text{HCl}} + D]$ vs. m_{HCl} a straight line with the slope $\varepsilon(\text{H}^+, \text{Cl}^-)$ is obtained. The degree of linearity should in itself indicate the range of validity of the specific ion interaction approach. Osmotic coefficient data can be treated in an analogous way.

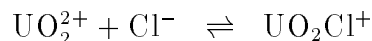
Example 2:

Figure IX.5 illustrates the modelling of equilibrium constant data obtained at different

Table IX.3: Equilibrium constants for $\text{UO}_2^{2+} + \text{Cl}^- \rightleftharpoons \text{UO}_2\text{Cl}^+$

I_m (mol · kg ⁻¹)	$\log_{10} \beta_1$	$\log_{10} \beta_1 + 4D$
0.10	-0.174 ± 0.10	0.264 ± 0.10
0.20	-0.254 ± 0.10	0.292 ± 0.10
0.26	-0.357 ± 0.04	0.230 ± 0.04
0.31	-0.397 ± 0.04	0.220 ± 0.04
0.41	-0.420 ± 0.04	0.246 ± 0.04
0.51	-0.331 ± 0.10	0.371 ± 0.10
0.57	-0.432 ± 0.04	0.288 ± 0.04
0.67	-0.354 ± 0.04	0.395 ± 0.04
0.89	-0.438 ± 0.04	0.357 ± 0.04
1.05	-0.331 ± 0.10	0.491 ± 0.10
1.05	-0.298 ± 0.26	0.525 ± 0.26
1.61	-0.272 ± 0.10	0.618 ± 0.10
2.21	-0.193 ± 0.10	0.744 ± 0.10
2.21	-0.163 ± 0.10	0.774 ± 0.10
2.82	-0.021 ± 0.10	0.860 ± 0.10
3.50	-0.021 ± 0.10	0.974 ± 0.10

ionic strengths for the formation of UO_2Cl^+ , according to $\text{UO}_2^{2+} + \text{Cl}^- \rightleftharpoons \text{UO}_2\text{Cl}^+$. For the reaction



the following formula is deduced for the extrapolation to $I = 0$:

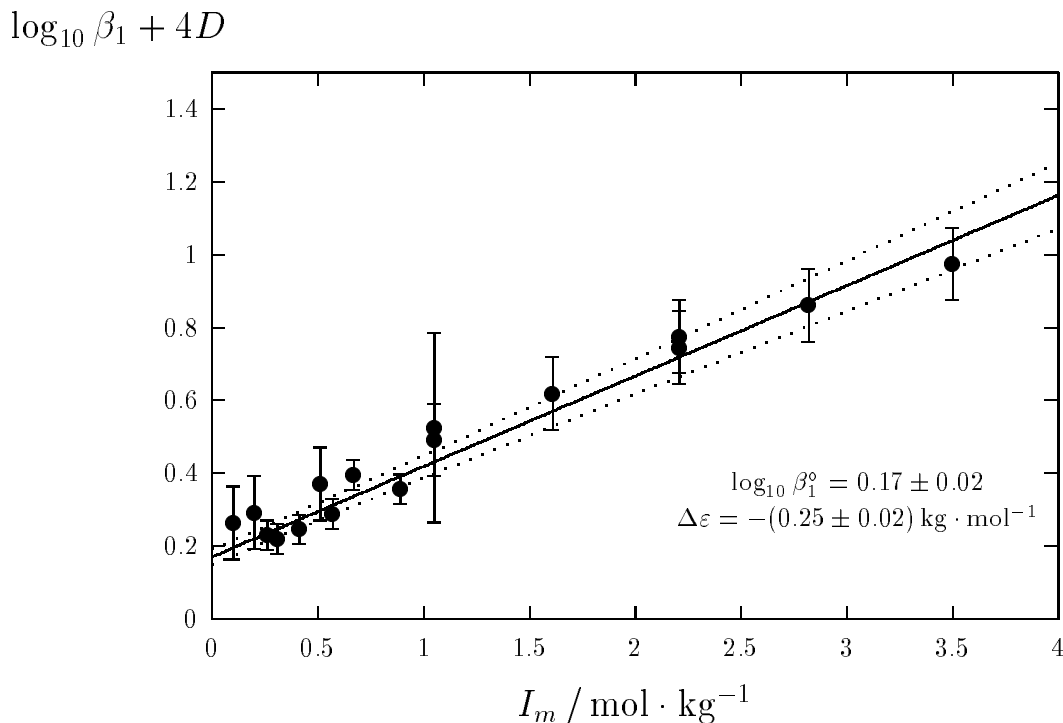
$$\log_{10} \beta_1 + 4D = \log_{10} \beta_1^\circ - \Delta\varepsilon I_m$$

where $\Delta\varepsilon = \varepsilon(\text{UO}_2\text{Cl}^+, \text{ClO}_4^-) - \varepsilon(\text{UO}_2^{2+}, \text{ClO}_4^-) - \varepsilon(\text{Na}^+, \text{Cl}^-)$.

Equilibrium constants (the source of the data is [92GRE/FUG]) for this reaction with assigned uncertainties, corrected to 298.15 K where necessary, and recalculated into molality units, are given in Table IX.3.

From the linear regression the following results are obtained: $\log_{10} \beta_1^\circ = 0.17 \pm 0.02$, $\Delta\varepsilon = -(0.25 \pm 0.02) \text{ kg} \cdot \text{mol}^{-1}$. The experimental data are depicted in Figure IX.5, where the area between the dotted lines represents the uncertainty range that is obtained by using the results in $\log_{10} \beta_1^\circ$ and $\Delta\varepsilon$ and correcting back to $I \neq 0$. $\Delta\varepsilon \approx \varepsilon(\text{UO}_2\text{Cl}^+, \text{ClO}_4^-) - \varepsilon(\text{UO}_2^{2+}, \text{ClO}_4^-) - \varepsilon(\text{Na}^+, \text{ClO}_4^-)$ only if at most 10% of the ClO_4^- ionic medium is replaced by Cl^- . (The example refers to a system with *weak* complex formation. In such systems it is difficult to distinguish between complex formation and specific

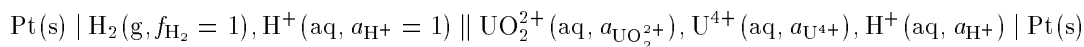
Figure IX.5: Plot of $[\log_{10} \beta_1 + 4D]$ vs. I_m for the reaction $\text{UO}_2^{2+} + \text{Cl}^- \rightleftharpoons \text{UO}_2\text{Cl}^+$ at 298.15 K and 1 atm. The straight line shows the result of the weighted linear regression, and the dotted lines represent the uncertainty range.



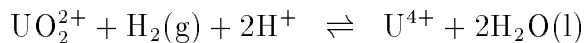
ion interaction of the type used *e.g.*, in the Pitzer model, *vide infra* p.352. Spectroscopic evidence [92GRE/FUG, p.193–194] indicates that chloride *complexes* are formed in this system).

Example 3:

When using the specific interaction theory, the relationship between the redox potential of the couple $\text{UO}_2^{2+}/\text{U}^{4+}$ in a medium of ionic strength I_m and the corresponding quantity at $I = 0$ should be calculated in the following way. The reaction in the galvanic cell



is



For this reaction

$$\log_{10} K^\circ = \log_{10} \frac{a_{\text{U}^{4+}} \times a_{\text{H}_2\text{O}}^2}{a_{\text{UO}_2^{2+}} \times a_{\text{H}^+}^2 \times f_{\text{H}_2}}$$

$$= \log_{10} K + \log_{10} \gamma_{\text{U}^{4+}} - \log_{10} \gamma_{\text{UO}_2^{2+}} - 2 \log_{10} \gamma_{\text{H}^+} - \log_{10} \gamma_{f, \text{H}_2} \\ + 2 \log_{10} a_{\text{H}_2\text{O}}$$

At reasonably low partial pressure of $\text{H}_2(\text{g})$ $f_{\text{H}_2} \approx p_{\text{H}_2}$, and on the basis of the SIT model:

$$\begin{aligned} \log_{10} \gamma_{\text{U}^{4+}} &= -16D + \varepsilon(\text{U}^{4+}, \text{ClO}_4^-) m_{\text{ClO}_4^-} \\ \log_{10} \gamma_{\text{UO}_2^{2+}} &= -4D + \varepsilon(\text{UO}_2^{2+}, \text{ClO}_4^-) m_{\text{ClO}_4^-} \\ \log_{10} \gamma_{\text{H}^+} &= -D + \varepsilon(\text{H}^+, \text{ClO}_4^-) m_{\text{ClO}_4^-} \end{aligned}$$

Hence,

$$\begin{aligned} \log_{10} K^\circ &= \log_{10} K - 10D + \left(\varepsilon(\text{U}^{4+}, \text{ClO}_4^-) - \varepsilon(\text{UO}_2^{2+}, \text{ClO}_4^-) \right. \\ &\quad \left. - 2\varepsilon(\text{H}^+, \text{ClO}_4^-) \right) m_{\text{ClO}_4^-} + 2 \log_{10} a_{\text{H}_2\text{O}} \end{aligned}$$

The relationship between the equilibrium constant and the redox potential is

$$\ln K = \frac{nF}{RT} E$$

where E is the redox potential in the particular ion medium, n is the number of transferred electrons in the reaction considered. Combining and rearranging the required equation then leads to

$$E - 10D \left(\frac{RT \ln(10)}{nF} \right) = E^\circ - \Delta\varepsilon m_{\text{ClO}_4^-} \left(\frac{RT \ln(10)}{nF} \right)$$

For $n = 2$ in the present example and $T = 298.15$ K, this equation becomes

$$E[\text{mV}] - 295.8 D = E^\circ[\text{mV}] - 29.58 \Delta\varepsilon m_{\text{ClO}_4^-}$$

where

$$\Delta\varepsilon = \varepsilon(\text{U}^{4+}, \text{ClO}_4^-) - \varepsilon(\text{UO}_2^{2+}, \text{ClO}_4^-) - 2\varepsilon(\text{H}^+, \text{ClO}_4^-)$$

The same procedure can be followed when using the Pitzer equations.

The following can be used as auxiliary sources of information on the SIT coefficients: a) the experimental data on mean activity coefficients of the electrolyte of interest in its mixture with other electrolytes; b) solubility data in ternary systems with a common ion, where the thermodynamic information (activity product and the SIT coefficient) is available for one component.

IX.4. Other equations, approximately equivalent with the SIT model

Vasil'ev [62VAS] seems to be the first to systematically use an equation of type (IX.4) to extrapolate equilibrium constant data to zero ionic strength. The Vasil'ev equation for the single-ion activity coefficient has the following form:

$$\log_{10} \gamma_i = -\frac{AZ_i^2 \sqrt{I_m}}{1 + 4.9B\sqrt{I_m}} + bI_m \quad (\text{IX.6})$$

where the numerical factor 4.9 is used as a constant value of the “effective” diameter for all ions (in Å). At 298.15 K and 1 atm the value of the Debye-Hückel parameter $B = 0.3283 \cdot 10^8 \text{ kg}^{1/2} \cdot \text{mol}^{-1/2} \cdot \text{cm}^{-1} = 0.3283 \text{ kg}^{1/2} \cdot \text{mol}^{-1/2} \cdot \text{Å}^{-1}$, *i.e.*, the value of product $4.9B = 1.6 \text{ kg}^{1/2} \cdot \text{mol}^{-1/2}$ as compared with 1.5 accepted in the SIT model. As far as we know, the value of the parameter b in the Vasil'ev equation was considered to be a purely empirical constant, the value of which had to be determined separately in each medium by experiments (in contrast to the SIT, where it was assumed that the values of the specific interaction coefficients for pairs of ions could also be evaluated from independent sources of thermodynamic information, if available).

Pitzer and Brewer [61LEW/RAN] have suggested the following equation, similar to the SIT equation (the well known Guggenheim equation):

$$\log_{10} \gamma_i = \frac{-Z_i^2 A \sqrt{I_m}}{1 + \sqrt{I_m}} + \sum_j B(i, j) m_j \quad (\text{IX.7})$$

where the summation over j covers all anions in the case where i is a cation and vice versa. Tables of $B(i, j)$ are given by Pitzer and Brewer and by Baes and Mesmer [76BAE/MES]. The Debye-Hückel term is different from that used in our version of the SIT model. The Pitzer and Brewer equation has been used by Baes and Mesmer in their monograph on the hydrolysis of cations [76BAE/MES].

The interaction coefficients and the value of $a_j B$ are correlated with one another, and it is important to use the interaction coefficients only with the model used to determine them. The equations of Vasil'ev, Pitzer and Brewer and the SIT are all essentially equivalent *for the extrapolation of laboratory data obtained in different ionic media* ($I < 3\text{-}4 \text{ mol} \cdot \text{kg}^{-1}$) *to infinite dilution*.

In 1973 Bromley [73BRO], using a trial and error method, proposed the following empirical equation for mean-activity coefficients

$$\log_{10} \gamma_{\pm} = -\frac{A|Z_M Z_X| \sqrt{I_m}}{1 + \sqrt{I_m}} + \frac{(0.06 + 0.6 B)|Z_M Z_X| I_m}{\left(1 + \frac{1.5 I_m}{|Z_M Z_X|}\right)^2} + B I_m \quad (\text{IX.8})$$

As one can see, the Bromley equation can be considered an empirical extension of the Pitzer-Brewer or the SIT equations. However, the complication resulting from the addition of the second term results only in a very slight improvement of the fitting of $\log_{10} \gamma_{\pm}$ for strong electrolytes, *cf.* [86COE], where it was shown that the Bromley and the SIT

equations give practically the same descriptions of the concentration dependence of equilibrium constants, and almost identical values of $\log_{10} K^\circ$ at infinite dilution, for some two-phase equilibria.

Helgeson *et al.* [81HEL/KIR] have proposed a rather sophisticated semiempirical model involving ion hydration to describe the temperature and pressure dependence of both standard state and excess properties of aqueous ions and electrolytes. The Helgeson model postulates the following equation (with some simplifications) for the mean-activity coefficient of a completely dissociated binary electrolyte, consisting of ν_M cations and ν_X anions per formula unit, with ion charges Z_M and Z_X respectively:

$$\log_{10} \gamma_{\pm} = -\frac{A|Z_M Z_X| \sqrt{I_m}}{1 + a_j B \sqrt{I_m}} - \log_{10}(1 + 0.0180153 m^*) + b_\gamma I_m \quad (\text{IX.9})$$

where b_γ is

$$b_\gamma = \frac{(b_{MX}^0 + 2 \nu_M \nu_X b_{MX}^1)}{\nu}$$

and $\nu = \nu_M + \nu_X$; a_j , as earlier, is an “effective” ion diameter (particular for each ion or electrolyte); B is the Debye-Hückel parameter; the term $-\log_{10}(1 + 0.0180153 m^*)$ is the mole fraction to molality conversion factor; m^* stands for the sum of the ionic molalities of all species in solution; the parameter b_{MX}^0 is a constant at constant temperature for each particular ion (electrolyte); b_{MX}^1 is a short-range interaction parameter due to specific cation-anion (or ion-neutral) interactions. The parameters b_γ are tabulated [81HEL/KIR] for many single electrolytes and ion combinations ([81HEL/KIR], Table 5, 6 there), but not for complex ions. Hence, the Helgeson equation is actually a one-parameter equation. The maximum error between measured and calculated mean-activity coefficients is within 3-4% in a limited ionic strength range (up to 2-6 mol · kg⁻¹), but may increase up to 20% at ionic strengths 10-12 mol · kg⁻¹ (Tables 5 and 6 in [81HEL/KIR]). This is essentially the same accuracy as for the SIT model. However, the validity of the assumptions on which the Helgeson model are based is not quite clear, *e.g.*, the approximation used for the concentration dependence of the dielectric constant of an aqueous solution. An obvious drawback of this model is the need to use different values of the size parameter a_j , for different ions and electrolytes, which makes it difficult to extend the model to multicomponent solutions. For instance (see [59ROB/STO], p.435) in a mixture of two 1-1 electrolytes B and C the following cross-differential relation must be obeyed:

$$\left(\frac{\partial \ln \gamma_B}{\partial m_C} \right)_{m_B} = \left(\frac{\partial \ln \gamma_C}{\partial m_B} \right)_{m_C}$$

and it is impossible to satisfy this equation using different values of the parameter a_j for each electrolyte. In order to circumvent this problem Helgeson *et al.* proposed that the average of the a_j values (see Eq. (124) in [81HEL/KIR]) should be used. However, this is not a strict solution of the problem, although the error introduced is usually less than

10% in the value of the mean-activity coefficient of a certain electrolyte in a mixture with other electrolytes (see [81HEL/KIR], p.1346–1347).

This short survey of the equations proposed for the description of concentration dependence of equilibrium constants in aqueous solutions is rather subjective and incomplete. Many other equations for these purposes have been proposed in literature; see, for instance, [90BEC/NAG]. However, most of them are based on the following equation for mean activity coefficients

$$\log_{10} \gamma_{\pm} = -\frac{A|Z_M Z_X| \sqrt{I_m}}{1 + a_j B \sqrt{I_m}} + C I_m + D I_m^{3/2} + E I_m^2 + \dots$$

and merely use different number of terms in an ionic strength expansion and different values of the $a_j B$ product. We do not recommend procedures that consider $a_j B$ as a fitting parameter, even though this leads to a “better” description of the ionic strength dependence of the equilibrium constants [94AND/KHO] in one particular ionic medium. These fitting parameters cannot be used for predictions in other ionic media.

IX.5. On the magnitude of the specific ion interaction coefficients

From the previous text it is obvious that in order to model the p , T , and ionic strength/medium dependence of chemical equilibria in aqueous electrolyte systems, not only do we need a proper model to describe deviations from ideality, but also a number of empirical parameters. An important point for the application of these models is the ability to *estimate* either interaction parameters for which no experimental information is available, or[†] $\Delta\varepsilon$ for reactions. Interaction coefficients for a large number of strong electrolytes, and some complexes, have been listed in Tables IX.1 and IX.2. In the following figures we demonstrate possible internal correlations between these data, and also correlations with size and charge parameters.

Figures IX.6, IX.7, IX.8 and IX.9 shows correlations between the interaction coefficients in chloride and perchlorate media for ions of various charge types. These correlations are useful for the estimation of unknown interaction parameters, provided that information in one system is available.

IX.5.1. Correlations among specific ion interaction parameters for cations

The specific ion interaction coefficients are known for many cations; they may also be estimated by using correlations where experimental data are lacking. Figs. IX.10 to IX.12, show correlations between $\varepsilon(i, j)$ and the ion potential Z/r for various cations, Z and r are the charge and crystallographic ionic radius of the cation, respectively. The scatter indicates that unknown interaction coefficients for cations of charge +3, or less,

[†] $\Delta\varepsilon = \sum_i \nu_i \varepsilon(i, Y)$, where the summation is taken over all species i in the reaction, and Y stands for the cation of the ionic medium electrolyte if i is an anion, but Y stands for the ionic medium anion if i is a cation. The reaction stoichiometric coefficients, ν_i , are positive for products and negative for reactants, cf. Eq. (II.4).

Figure IX.6: The correlations between interaction coefficients in chloride and perchlorate media for monovalent cations. The units of ε are $\text{kg} \cdot \text{mol}^{-1}$.

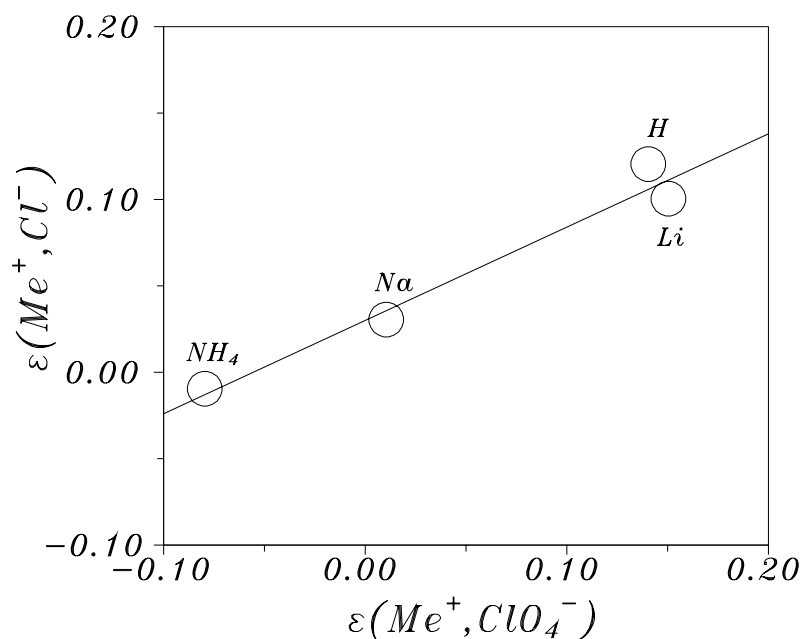


Figure IX.7: The correlations between interaction coefficients in chloride and nitrate media for monovalent cations. The units of ε are $\text{kg} \cdot \text{mol}^{-1}$.

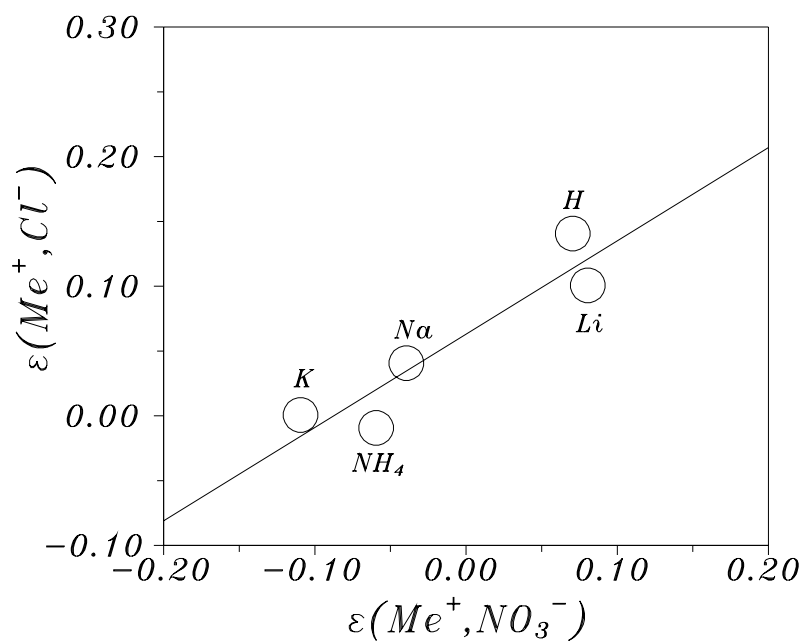


Figure IX.8: The correlations between interaction coefficients in chloride and perchlorate media for divalent cations. The units of ε are $\text{kg} \cdot \text{mol}^{-1}$.

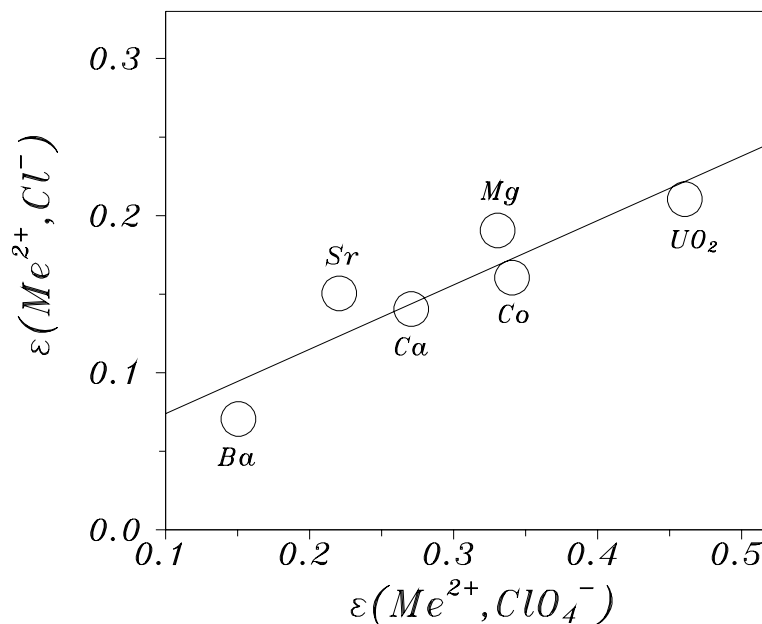


Figure IX.9: The correlations between interaction coefficients in chloride and nitrate media for trivalent cations. The units of ε are $\text{kg} \cdot \text{mol}^{-1}$.

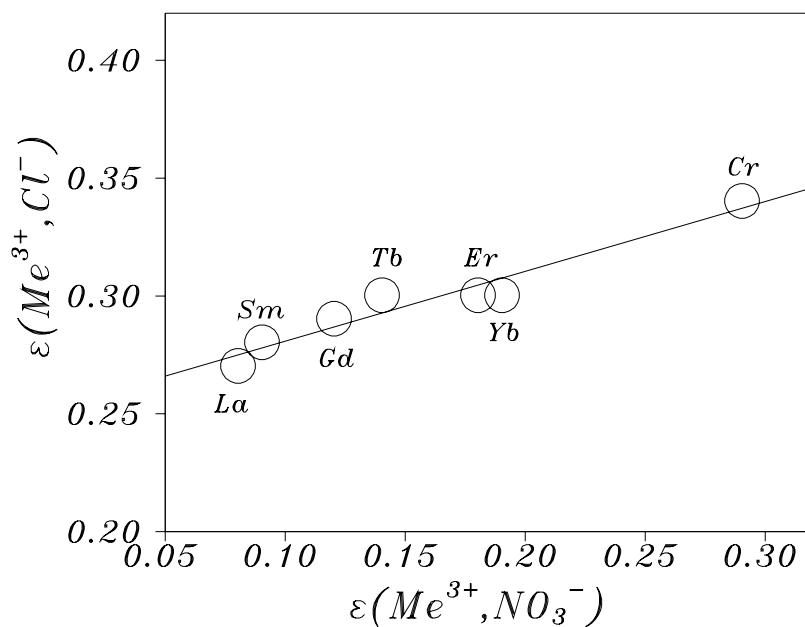
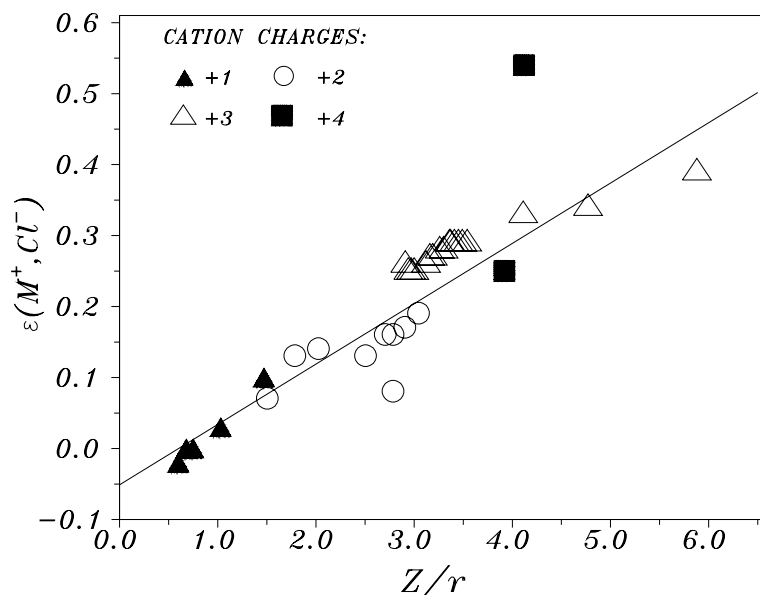


Figure IX.10: The correlations between interaction coefficients and the ion potential Z/r (Z and r stand for the charge and crystallographic ionic radius in Å, respectively) for various cations in chloride media. The units of ε are $\text{kg} \cdot \text{mol}^{-1}$.



may be estimated with an accuracy of about $0.05 \text{ kg} \cdot \text{mol}^{-1}$. The interaction coefficients for several tetravalent actinide ions have been determined experimentally and do not have to be estimated. Unhydrolysed M^{4+} ions are in general not present in aqueous systems because of very strong hydrolysis, with the exceptions of Zr^{4+} , Hf^{4+} and tetravalent actinides which are present in strongly acid ($> 2 \text{ M}$) solution.

IX.5.2. Correlations among specific ion interaction parameters for complexes

The following general observations might be useful:

- Complexes of high positive charge tend to have interaction parameters close to those for simple cations of the same charge, *cf.* Table IX.1.
- Complexes with a large negative charge frequently have negative interaction parameters with M^+ ions; this may be a result of ion pairing.

Ciavatta [90CIA] has proposed the following method to estimate values of ε for the complexes ML and ML_2 in an ionic medium NX :

$$\begin{aligned}\varepsilon(ML, N \text{ or } X) &\approx \frac{\varepsilon(M, X) + \varepsilon(L, N)}{2} \\ \varepsilon(ML_2, N \text{ or } X) &\approx \frac{\varepsilon(M, X) + 2\varepsilon(L, N)}{3}\end{aligned}$$

Figure IX.11: The correlations between interaction coefficients and the ion potential Z/r (Z and r stand for the charge and crystallographic ionic radius in Å, respectively) for various cations in perchlorate media. The units of ε are $\text{kg} \cdot \text{mol}^{-1}$.

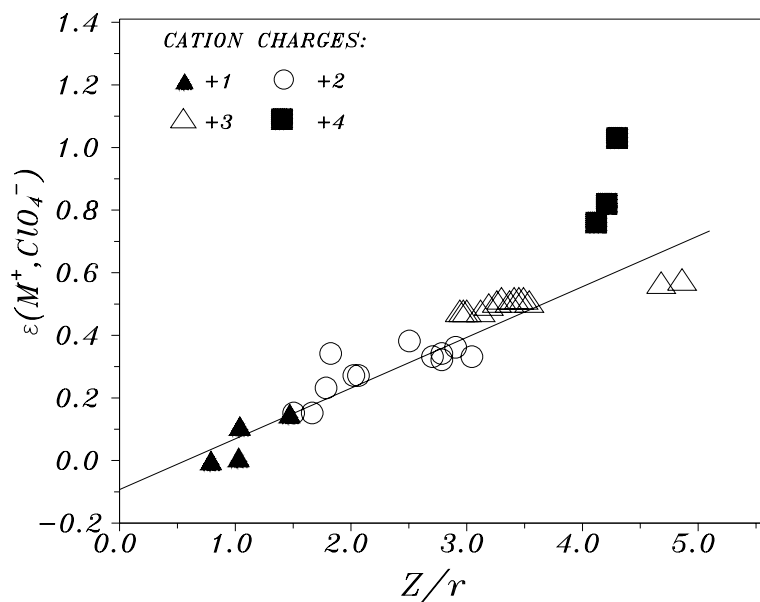
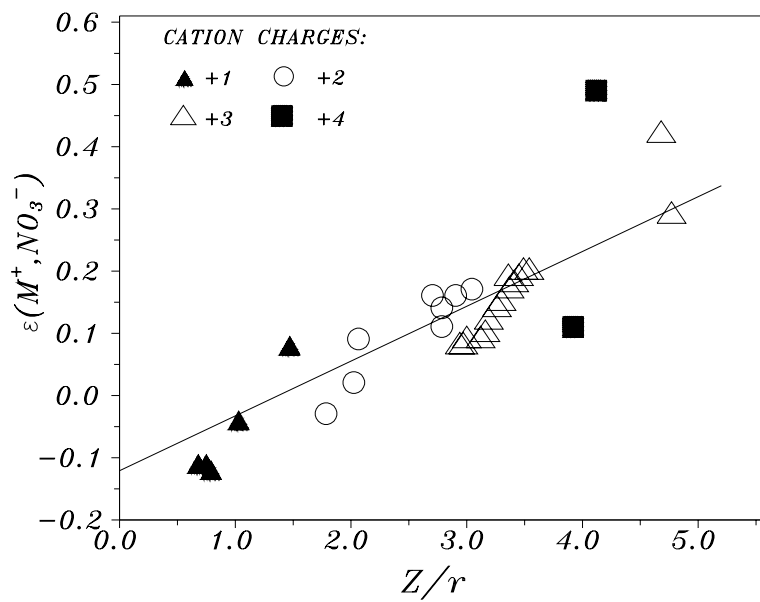


Figure IX.12: The correlations between interaction coefficients and the ion potential Z/r (Z and r stand for the charge and crystallographic ionic radius, respectively) for various cations in nitrate media. The units of ε are $\text{kg} \cdot \text{mol}^{-1}$.



The average deviations between the estimates based on the equations above and the experimental values was $\pm 0.05 \text{ kg} \cdot \text{mol}^{-1}$. However, it is difficult to know how general this estimation method is, because of the few examples.

IX.5.3. Correlations between $\Delta\varepsilon$ -values for chemical reactions

Reactions that involve ions of the same charge type have approximately the same values of $\Delta\varepsilon$, and the uncertainty in this estimation is in general equal to, or better than $\pm(0.05 \text{ to } 0.1) \text{ kg} \cdot \text{mol}^{-1}$.

IX.6. The Pitzer equations

The Pitzer model in its original form describes the thermodynamics of electrolyte mixtures where ionic pairing and complex formation are relatively weak. The physical theory on which the Pitzer model is based takes more interactions between the dissolved species into account than the simpler models. This is essential when describing thermodynamic properties in mixed electrolyte systems at high ionic strength. However, this requires a large number of empirical parameters, which must be obtained from experimental data. Many such parameters for various strong electrolytes have been determined, and they can be used to deduce interaction parameters for complexes by using experimental equilibrium constants at high ionic strength and extrapolated values of these constants at zero ionic strength. There is only a marginal gain to use the Pitzer equations when modelling the thermodynamics of complex formation and similar equilibrium reactions at fairly low ionic strengths, up to $3\text{-}4 \text{ mol} \cdot \text{kg}^{-1}$. The real advantage is apparent in mixtures of electrolytes at high ionic strength.

The following text is only intended to provide the reader with a brief outline of the Pitzer method. The notation is the same as used by Pitzer, *e.g.*, in [91PIT]. Pitzer's approach is based on physical models of the interactions in multicomponent ionic systems. Applying relations based on statistical thermodynamics, and using a number of reasonable simplifications/assumptions [73PIT, 91PIT], he proposed an analytical form of a virial type equation for the excess Gibbs energy for the system water + an electroneutral mixture of aqueous ionic species. For the solution of a single electrolyte MX, the mean-activity coefficient may be expressed by Eq. (IX.10)

$$\ln \gamma_{\text{MX}} = |Z_{\text{M}}Z_{\text{X}}| f^{\gamma} + m \frac{(2\nu_{\text{M}}\nu_{\text{X}})}{\nu} B_{\text{MX}}^{\gamma} + m^2 \left(\frac{2(\nu_{\text{M}}\nu_{\text{X}})^{3/2}}{\nu} \right) C_{\text{MX}}^{\gamma} \quad (\text{IX.10})$$

and the corresponding equation for the osmotic coefficient by

$$\Phi - 1 = |Z_{\text{M}}Z_{\text{X}}| f^{\Phi} + m \frac{(2\nu_{\text{M}}\nu_{\text{X}})}{\nu} B_{\text{MX}}^{\Phi} + m^2 \left(\frac{2(\nu_{\text{M}}\nu_{\text{X}})^{3/2}}{\nu} \right) C_{\text{MX}}^{\Phi} \quad (\text{IX.11})$$

where ν_{M} and ν_{X} are the number of M and X ions in the formula unit, Z_{M} and Z_{X} their

charges, m is the molality of the solution and $\nu = \nu_M + \nu_X$,

$$f^\gamma = -A_\Phi \left(\frac{\sqrt{I_m}}{1 + b\sqrt{I_m}} + \frac{2}{b} \ln(1 + b\sqrt{I_m}) \right) \quad (\text{IX.12})$$

$$B_{MX}^\gamma = 2\beta_{MX}^{(0)} + \frac{2\beta_{MX}^{(1)}}{\alpha^2 I_m} \left(1 - (1 + \alpha\sqrt{I_m} - \frac{\alpha^2 I_m}{2}) e^{-\alpha\sqrt{I_m}} \right) \quad (\text{IX.13})$$

$$C_{MX}^\gamma = \frac{3}{2} C_{MX}^\Phi \quad (\text{IX.14})$$

$$f^\Phi = -A_\Phi \frac{\sqrt{I_m}}{1 + b\sqrt{I_m}} \quad (\text{IX.15})$$

$$B_{MX}^\Phi = \beta_{MX}^{(0)} + \beta_{MX}^{(1)} e^{-\alpha\sqrt{I_m}} \quad (\text{IX.16})$$

f^γ and f^Φ are the forms of the Debye-Hückel term in the Pitzer model for mean activity coefficient and osmotic coefficients respectively; $A_\Phi = 0.3915 \text{ kg}^{1/2} \cdot \text{mol}^{-1/2}$ at 298.15 K and 1 atm is the Debye-Hückel parameter for the osmotic coefficient, note that $A_\Phi = A_\gamma/3$; b and α are fixed parameters ($b = 1.2 \text{ kg}^{1/2} \cdot \text{mol}^{-1/2}$; $\alpha = 2.0 \text{ kg}^{1/2} \cdot \text{mol}^{-1/2}$ for all electrolytes, except the 2-2-charge type). In the case of 2-2 electrolytes Pitzer adds an additional virial term. The Pitzer equations have been extended to cover electrolyte mixtures by including terms allowing for the interaction of ions of the same charge sign and for triplet interactions. This extension results in the following equation for the concentration dependence of the activity coefficient of a cation M (the corresponding equation for an anion L is obtained by interchanging L for M, a for c , and c for a throughout) in a mixed solution containing a number of different ions and neutral species (in the simplified form without the third virial terms for neutral species [91PIT, Eq. 63]):

$$\begin{aligned} \ln \gamma_M = & Z_M^2 F + \sum_a m_a (2B_{Ma} + \mathcal{Z}C_{Ma}) + \sum_c m_c \left(2\phi_{Mc} + \sum_a m_a \psi_{Mca} \right) \\ & + \sum_a \sum_{a'} m_a m_{a'} \psi_{Maa'} + |Z_M| \sum_c \sum_a m_c m_a C_{ca} \\ & + 2 \sum_n m_n \lambda_{nM} \end{aligned} \quad (\text{IX.17})$$

The subscripts c and a refer to cations and anions in general, n denotes neutral species; Z_M is the charge of a specific cation; ϕ_{Mc} is the second virial coefficient arising from binary interaction between a specific cation and the other cations; λ_{nM} is the second virial coefficient representing the interactions between a specific cation and neutral species; ψ_{ijk} is the third virial coefficient representing triple interactions between ions i , j , and k (where i and j are different anions, k is a cation; when i and j are different cations, k is

an anion). The parameters ψ and λ are assumed to be independent of the ionic strength. The quantity F includes the Debye-Hückel and other terms as follows:

$$F = f^\gamma + \sum_c \sum_a m_c m_a B'_{ac} + \sum_c \sum_{c'} m_c m_{c'} \phi'_{cc'} + \sum_a \sum_{a'} m_a m_{a'} \phi'_{aa'} \quad (\text{IX.18})$$

ϕ' and B' are the ionic strength derivatives of ϕ and B respectively (see below), and

$$\mathcal{Z} = \sum_i m_i |Z_i| \quad (\text{IX.19})$$

The ionic strength dependence of B_{Ma} is the following:

$$\begin{aligned} B_{Ma} &= \beta_{Ma}^{(0)} + \frac{2\beta_{Ma}^{(1)}}{\alpha^2 I_m} \left[1 - \left(1 + \alpha\sqrt{I_m} \right) e^{-\alpha\sqrt{I_m}} \right] \\ &= \beta_{Ma}^{(0)} + \beta_{Ma}^{(1)} g(I_m) \end{aligned} \quad (\text{IX.20})$$

and

$$\begin{aligned} B'_{Ma} &= -\frac{2\beta_{Ma}^{(1)}}{\alpha^2 I_m^2} \left[1 - \left(1 + \alpha\sqrt{I_m} + \frac{1}{2}\alpha^2 I_m \right) e^{-\alpha\sqrt{I_m}} \right] \\ &= \beta_{Ma}^{(1)} \frac{g'(I_m)}{I_m} \end{aligned} \quad (\text{IX.21})$$

where the functions g and g' are defined as:

$$g(I_m) = \frac{2}{\alpha^2 I_m} \left[1 - \left(1 + \alpha\sqrt{I_m} \right) e^{-\alpha\sqrt{I_m}} \right] \quad (\text{IX.22})$$

$$g'(I_m) = -\frac{2}{\alpha^2 I_m} \left[1 - \left(1 + \alpha\sqrt{I_m} + \frac{1}{2}\alpha^2 I_m \right) e^{-\alpha\sqrt{I_m}} \right] \quad (\text{IX.23})$$

C_{ca} is defined as follows:

$$C_{ca} = \frac{C_{ca}^\Phi}{2|Z_c Z_a|^{1/2}} \quad (\text{IX.24})$$

The virial coefficient ϕ_{ij} has the following form

$$\phi_{ij} = \theta_{ij} + {}^E\theta_{ij}(I_m) \quad (\text{IX.25})$$

where ${}^E\theta_{ij}(I_m)$ is a function of the ionic strength only, it is zero except for unsymmetrical mixing of ions of the same sign, *i.e.*, when the charges on i and j are different, but have the same sign (numerical values of this term are given by theory and several equations have been proposed that accurately represent the results obtained by numerical integration [91PIT]).

Therefore, in order to calculate the activity coefficients for ions the following parameters are needed: $\beta^{(0)}$, $\beta^{(1)}$, C^Φ for each anion-cation pair; θ_{ij} for each unlike cation-cation or anion-anion pair; ψ for each triple ion interaction where the ions are not all of the same sign, and λ for ion-neutral pairs. We should notice that, for the case of interactions between cations and anions with charges 2 or higher, it is preferable to use an additional parameter $\beta^{(2)}$ (which is strongly correlated with the association constant for these ions). In some cases triple ion-ion-neutral interactions also have to be taken into account. The full set of the Pitzer parameters is available for many single electrolytes and electrolytes mixtures [91PIT], but only in very few cases for complexes.

The activity coefficient of a neutral species N is described by the following equation in the Pitzer approach, which is consistent with the traditional Setchenov equation:

$$\ln \gamma_N = 2 \left(\sum_c m_c \lambda_{Nc} + \sum_a m_a \lambda_{Na} + \sum_n m_n \lambda_{Nn} \right) \quad (\text{IX.26})$$

The individual values of neutral-ion interaction coefficients cannot be determined in any experiment, but only values of electrically neutral combinations. In order to handle the problem of estimation of neutral-ion interaction coefficients Pitzer proposed to set all ion-neutral parameters involving H^+ to zero, whereupon the other ion-neutral parameters are determined.

IX.7. Comparison of the SIT and the Pitzer models for the description of concentration dependence of equilibrium constants of complex formation reactions in ionic media

The Brønsted-Guggenheim-Scatchard specific ion interaction model can be considered as a simplified form of the Pitzer ion interaction approach, neglecting triple interactions (which are important only in very concentrated solutions) and the interactions between the ions of the same signs (they are typically small). We have already pointed out that the Pitzer model offers a much more precise description of deviations from ideality in mixtures of strong electrolytes at high ionic strength, than the SIT, provided that the necessary interaction coefficients are available. Many users of the Pitzer formalism interpret experimental data (for instance, mean activity coefficients of electrolytes in electrolyte mixtures) without explicit consideration of complex formation, because this many-parameter model is able to reproduce the measured quantities with high precision without complications of this kind. There is no unambiguous *thermodynamic* method to distinguish between complex formation/ion-pairing and other types of short-range interactions between species in

solution when the extent of complex formation is small or moderate. Most solution coordination chemists are aware of the ambiguity which this may cause in systems where *weak* complexes are formed (these are also the systems where large variations in the concentrations of the reactants are necessary in order to detect the effects of “complex” formation), and require additional non-thermodynamic evidence for the formation of complexes, such as spectroscopic (uv/vis, NMR), or kinetic information [61ROS/ROS]). It is up to the modeller to decide if he/she wishes to describe weak interactions between ions in terms of complex formation, or by Pitzer type of ion interactions. However, it is important not to mix the two systems, for instance, to use the Pitzer set of parameters for systems containing both Mg^{2+} and SO_4^{2-} as components, together with an experimental value of $\log_{10} K$ for the reaction $\text{Mg}^{2+} + \text{SO}_4^{2-} \rightleftharpoons \text{MgSO}_4(\text{aq})$.

The Pitzer equations have been used to describe the concentration dependence of stoichiometric equilibrium constants for protolytic equilibria involving weak acids and bases where the chemical speciation is known. In these systems most of the parameters needed can be obtained from activity coefficient measurements of pure solutions of electrolytes, or the corresponding mixtures. Information of this type is rarely available for complex formation reactions. However, the data for complexes can be introduced into the Pitzer-type databases, provided that information of *concentration* equilibrium constants are available. In equilibrium analysis, where the studies are carried out in the presence of an inert electrolyte (ionic medium salt NX) and small (“trace”) concentrations of reactants/products, only the terms involving m_{NX} have to be considered in the equations for the activity coefficients of reactants/products, while those involving molalities of “trace” components can be neglected. For a chemical reaction in the general form



we therefore have

$$\begin{aligned} \ln K^\circ &= \sum_i \nu_i \ln m_i + \sum_i \nu_i \ln \gamma_i + r \ln a_{\text{H}_2\text{O}} \\ &= \ln K + \sum_i \nu_i \ln \gamma_i + r \ln a_{\text{H}_2\text{O}} \end{aligned} \quad (\text{IX.28})$$

where the index i denotes a particular reactant/product, r stands for the number of moles of water participating in the reaction. A correction for water activity can easily be made using the available values of the osmotic coefficients for the ionic medium electrolyte. At trace concentrations of the reaction participants, the Pitzer model results in the following analytical equation for the reaction (IX.27) in the ionic medium NX (an 1-1 electrolyte)

$$\begin{aligned} \ln K^\circ &= \ln K + r \ln a_{\text{H}_2\text{O}} + \sum_i \nu_i Z_i^2 \left(f^\gamma + m^2 B'_{\text{NX}} \right) + 2m \sum_i \nu_i B_{ij} + 2m^2 \sum_i \nu_i C_{ij} \\ &\quad + 2m \sum_i \nu_i \phi_{ii'} + m^2 \sum_i \psi_{ii'j} + m^2 \sum_i \nu_i |Z_i| C_{\text{NX}} \end{aligned} \quad (\text{IX.29})$$

where the index i refers to the reaction participants, i' and j stand for the ionic medium ions, having the same and opposite charge sign respectively, to the species i , and m is the molality of the ionic medium electrolyte NX.

The corresponding analytical statement for the concentration dependence of $\log_{10} K$ for the reaction (IX.27) at trace concentrations of reactants/products in a NX electrolyte medium using the SIT equation is:

$$\begin{aligned} \log_{10} K^\circ &= \log_{10} K + r \log_{10} a_{\text{H}_2\text{O}} \\ &\quad - D \sum_i \nu_i Z_i^2 + m \sum_i \nu_i \varepsilon(i, j) \end{aligned} \quad (\text{IX.30})$$

where D is the Debye-Hückel term, defined in Eq. (IX.5); index i refers to a reactant/product, j stands either for an ionic medium ion with charge sign opposite to that of i , or for a neutral species, and m is the molality of the ionic medium electrolyte NX.

Example 4:

The first example of an application of both the Pitzer and the SIT methods describes the concentration dependence of the equilibrium constant for the reaction $\text{CO}_2(\text{aq}) + \text{H}_2\text{O}(\text{l}) \rightleftharpoons \text{H}^+ + \text{HCO}_3^-$ in a NaCl medium. In accordance with Eq. (IX.28) we have:

$$\ln K^\circ = \ln K + \ln \gamma_{\text{H}^+} + \ln \gamma_{\text{HCO}_3^-} - \ln \gamma_{\text{CO}_2(\text{aq})} - \ln a_{\text{H}_2\text{O}}$$

The Pitzer approach gives the following statements for the activity coefficients of the reaction participants at trace concentrations in the NaCl medium:

$$\begin{aligned} \ln \gamma_{\text{H}^+} &= F + m_{\text{Cl}}(2B_{\text{H,Cl}} + 2m_{\text{Cl}}C_{\text{H,Cl}}) + m_{\text{Na}}(2\phi_{\text{H,Na}} + m_{\text{Cl}}\psi_{\text{H,Na,Cl}}) \\ &\quad + m_{\text{Na}}m_{\text{Cl}}C_{\text{Na,Cl}} \end{aligned}$$

$$\begin{aligned} \ln \gamma_{\text{HCO}_3^-} &= F + m_{\text{Na}}(2B_{\text{Na,HCO}_3} + 2m_{\text{Na}}C_{\text{Na,HCO}_3} + m_{\text{Cl}}(2\phi_{\text{Cl,HCO}_3} \\ &\quad + m_{\text{Na}}\psi_{\text{Na,Cl,HCO}_3}) + m_{\text{Na}}m_{\text{Cl}}C_{\text{Na,Cl}} \end{aligned}$$

where

$$F = -A_\Phi \left[\frac{\sqrt{I_m}}{1 + b\sqrt{I_m}} + \frac{2}{b} \ln \left(1 + b\sqrt{I_m} \right) \right] + m_{\text{Na}}m_{\text{Cl}}B'_{\text{Na,Cl}}$$

The ionic strength dependence of $B_{\text{H,Cl}}$ and $B_{\text{Na,HCO}_3}$ is given by Eq. (IX.20), the ionic strength dependence of $B'_{\text{Na,Cl}}$ by Eq. (IX.21), and the relation between $C_{\text{M,X}}$ and the tabulated Pitzer parameter $C_{\text{M,X}}^\Phi$ is given by Eq. (IX.24).

As all components are at trace concentrations, except NaCl, the correction for water activity can be made using the values of the osmotic coefficients of pure sodium chloride solutions from the available tabulation [59ROB/STO], or calculated on the basis of the Pitzer approach, keeping in mind the usual relation between water activity and the osmotic coefficient Φ of an electrolyte:

$$\ln a_{\text{H}_2\text{O}} = -\frac{\Phi \nu m}{1000} M_{\text{w}}$$

where M_{w} is the molar mass of water ($18.0153 \text{ g} \cdot \text{mol}^{-1}$) and $\nu = 2$.

The expression for the activity coefficient of $\text{CO}_2(\text{aq})$ is given by Eq. (IX.26) as

$$\ln \gamma_{\text{CO}_2(\text{aq})} = 2(\lambda_{\text{CO}_2, \text{Na}} + \lambda_{\text{CO}_2, \text{Cl}})$$

The required values of all the relevant Pitzer parameters for the system $\text{Na}^+ - \text{Cl}^- - \text{H}^+ - \text{HCO}_3^-$ are available in literature from the regression analysis of potentiometric and solubility data [84HAR/MOL, 91PIT]:

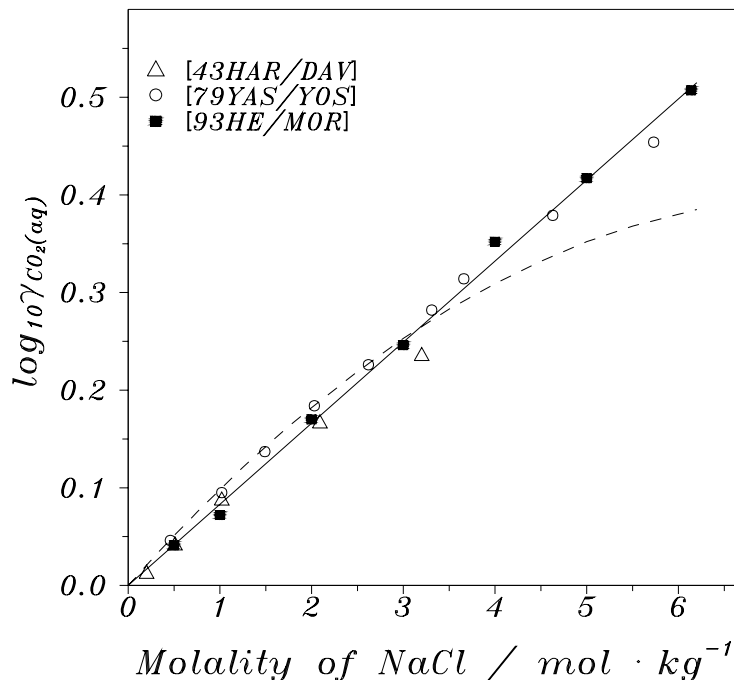
$$\begin{array}{lll} \beta_{\text{H,Cl}}^{(o)} = 0.1775, & \beta_{\text{H,Cl}}^{(1)} = 0.2945, & C_{\text{H,Cl}}^{\Phi} = 0.00080, \\ \beta_{\text{Na,Cl}}^{(o)} = 0.0765, & \beta_{\text{Na,Cl}}^{(1)} = 0.2664, & C_{\text{Na,Cl}}^{\Phi} = 0.00127, \\ \beta_{\text{Na,HCO}_3}^{(o)} = 0.0277, & \beta_{\text{Na,HCO}_3}^{(1)} = 0.0411, & C_{\text{Na,HCO}_3}^{\Phi} = 0.0, \\ \theta_{\text{H,Na}} = 0.036, & \theta_{\text{Cl,HCO}_3} = 0.03, & \\ \psi_{\text{H,Na,Cl}} = -0.004, & \psi_{\text{Na,Cl,HCO}_3} = -0.015. & \end{array}$$

The values of neutral-ion interaction coefficients involving $\text{CO}_2(\text{aq})$ are given in [91PIT]: $\lambda_{\text{CO}_2, \text{Na}} = 0.100$, $\lambda_{\text{CO}_2, \text{Cl}} = 0.005$. However, after recommendation of these values a new study on the solubility of CO_2 in NaCl solutions [93HE/MOR] was published. Hence, we determined the sum $\lambda_{\text{CO}_2, \text{Na}} + \lambda_{\text{CO}_2, \text{Cl}} = 0.096$ from all available consistent data on the solubility of CO_2 in sodium chloride solutions [43HAR/DAV, 79YAS/YOS, 93HE/MOR], see Figure IX.13.

The value of K° was taken from the CODATA [89COX/WAG] recommendation, $\ln K^\circ = -14.624 \pm 0.010$ or $\log_{10} K^\circ = -6.351 \pm 0.004$.

The calculated values of $\log_{10} K$ for the reaction $\text{H}_2\text{O}(\text{l}) + \text{CO}_2(\text{aq}) \rightleftharpoons \text{H}^+ + \text{HCO}_3^-$ using the Pitzer approach (solid lines) are compared with the experimental ones (different symbols) in Figure IX.14. Some experimental data have been reported as $\log_{10} K$ for the reaction $\text{H}_2\text{O}(\text{l}) + \text{CO}_2(\text{g}) \rightleftharpoons \text{H}^+ + \text{HCO}_3^-$. By combining these values with the Henry's law constant for CO_2 from the CODATA recommendation and the value for the activity coefficient of $\text{CO}_2(\text{aq})$ in sodium chloride solutions given above, we obtain a second set of equilibrium constants for the reaction discussed. We should notice that Thurmond and Millero [82THU/MIL] have used a quite different equation for the concentration dependence of the activity coefficient of $\text{CO}_2(\text{aq})$, namely $\ln \gamma_{\text{CO}_2} = 0.242 m - 0.0106 m^2$ for the interpretation of their potentiometric data. This equation gives a poor fit of $\log_{10} \gamma_{\text{CO}_2}$ data above 3 m NaCl; see Figure IX.13. Therefore, the equilibrium constants from [82THU/MIL] were corrected using the more accurate values of the activity coefficient of $\text{CO}_2(\text{aq})$ in NaCl solutions.

Figure IX.13: The concentration dependence of $\log_{10} \gamma$ of $\text{CO}_2(\text{aq})$ in NaCl solutions at 298.15 K and 1 atm. The symbols are the experimental data, the solid line - the regression using the sum $\lambda_{\text{CO}_2, \text{Na}} + \lambda_{\text{CO}_2, \text{Cl}} = 0.096$ (see text), the dashed line - the approximation used in [82THU/MIL].



Many experimental values of $\log_{10} K$ refer to the molar concentration scale and they have to be converted to the molality scale. The concentrations were converted using the following relationship

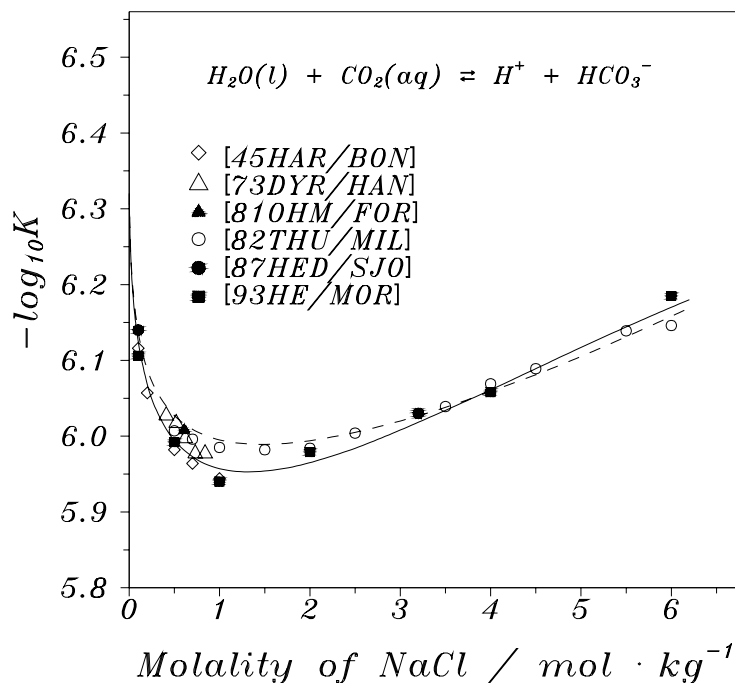
$$m_i = \frac{1000C_i}{1000\rho - C_iM}$$

where C_i and m_i stand for molarity and molality of the dissolved substance i , ρ is the density of the solution and M is the molar mass of the solute; see also Section II.2. The densities of electrolyte solutions are available in the compilation [85SOH/NOV]. The relation between equilibrium constants expressed in molarity (K_c) or molality units (K_m) is

$$\log_{10} K_m = \log_{10} K_c + \sum \nu \log_{10} \frac{m}{C}$$

where $\sum \nu$ is here the sum of the stoichiometric coefficients for the reaction, m and C stand for molality and molarity of the ionic medium (for the reactions studied at trace concentrations of the reaction participants). We will always use the molality concentration scale and therefore the notation $\ln K$ and $\log_{10} K$ instead of $\ln K_m$ and $\log_{10} K_m$.

Figure IX.14: The comparison of the experimental (different symbols) and calculated values of $\log_{10} K$ using the Pitzer approach (solid line) and the SIT model (dashed line) for the reaction $\text{H}_2\text{O}(\text{l}) + \text{CO}_2(\text{aq}) \rightleftharpoons \text{H}^+ + \text{HCO}_3^-$ in NaCl solutions at 298.15 K and 1 atm.



From the SIT model we obtain the following statements for the activity coefficients of H^+ , HCO_3^- and $\text{CO}_2(\text{aq})$ at their trace concentrations in NaCl ionic medium:

$$\begin{aligned} \log_{10} \gamma_{\text{H}^+} &= -\frac{A\sqrt{T_m}}{1 + 1.5\sqrt{T_m}} + \varepsilon(\text{H}^+, \text{Cl}^-)m_{\text{Cl}^-} \\ \log_{10} \gamma_{\text{HCO}_3^-} &= -\frac{A\sqrt{T_m}}{1 + 1.5\sqrt{T_m}} + \varepsilon(\text{Na}^+, \text{HCO}_3^-)m_{\text{Na}^+} \\ \log_{10} \gamma_{\text{CO}_2(\text{aq})} &= \varepsilon(\text{CO}_2(\text{aq}), \text{Na}^+)m_{\text{Na}^+} + \varepsilon(\text{CO}_2(\text{aq}), \text{Cl}^-)m_{\text{Cl}^-} \\ &= \varepsilon(\text{CO}_2(\text{aq}), \text{Na}^+ + \text{Cl}^-)m_{\text{NaCl}} \end{aligned}$$

The required interaction coefficient for the H^+ and the Cl^- ion combination was taken from [92GRE/FUG]: $\varepsilon(\text{H}^+, \text{Cl}^-) = 0.12 \pm 0.01 \text{ kg} \cdot \text{mol}^{-1}$, and the value of $\varepsilon(\text{Na}^+, \text{HCO}_3^-) = 0.00 \pm 0.01 \text{ kg} \cdot \text{mol}^{-1}$ was determined by minimisation of the deviations of calculated and experimental $\log_{10} K$ data. In reference [92GRE/FUG] a somewhat different value -0.02 ± 0.02 was used. This was modified in [95SIL/BID] and agrees with the value reported by Ciavatta [80CIA]. The value of

$\varepsilon(\text{CO}_2(\text{aq}), \text{Na}^+) + \varepsilon(\text{CO}_2(\text{aq}), \text{Cl}^-) = 0.083 \text{ kg} \cdot \text{mol}^{-1}$ was calculated from the corresponding sum $\lambda_{\text{CO}_2, \text{Na}} + \lambda_{\text{CO}_2, \text{Cl}}$ values using the relationship $\varepsilon(n, i) = 2\lambda_{(n, i)} / \ln(10)$. In [92GRE/FUG] this value was assumed to be zero. The values of $\log_{10} K$ calculated from the SIT model are shown in Figure IX.14 by the dashed line.

As one can see, the Pitzer model provides better agreement with the experimental data than the less-parameterised SIT model. Nevertheless, the maximal deviation between the two curves is less than $0.04 \log_{10}$ unit, which is close to expected accuracy of the experimental data, $\pm 0.03 \log_{10}$ units.

An analogous procedure can be used for the description of the concentration dependence of the second dissociation constant of carbonic acid in a NaCl medium, $\text{HCO}_3^- \rightleftharpoons \text{H}^+ + \text{CO}_3^{2-}$. For this reaction we write

$$\ln K^\circ = \ln K + \ln \gamma_{\text{H}^+} + \ln \gamma_{\text{CO}_3^{2-}} - \ln \gamma_{\text{HCO}_3^-}$$

The analytical equations for the activity coefficients of H^+ and HCO_3^- at trace concentrations in the NaCl ionic medium based on the Pitzer approach are given above, and for the activity coefficient of CO_3^{2-} one can write in accordance with Eq. (IX.17)

$$\begin{aligned} \ln \gamma_{\text{CO}_3^{2-}} = & 4F + m_{\text{Na}}(2B_{\text{Na}, \text{CO}_3} + 2m_{\text{Na}} C_{\text{Na}, \text{CO}_3}) \\ & + m_{\text{Cl}}(2\phi_{\text{Cl}, \text{CO}_3} + m_{\text{Na}} \psi_{\text{Na}, \text{Cl}, \text{CO}_3}) + 2m_{\text{Na}} m_{\text{Cl}} C_{\text{Na}, \text{Cl}} \end{aligned}$$

As the charges of CO_3^{2-} and Cl^- co-ions differ, the interaction parameter $\phi_{\text{Cl}, \text{CO}_3}$ should be considered to be ionic strength dependent, $\phi_{\text{Cl}, \text{CO}_3} = \theta_{\text{Cl}, \text{CO}_3} + {}^E\theta_{\text{Cl}, \text{CO}_3}(I)$. The values of the term ${}^E\theta_{\text{Cl}, \text{CO}_3}(I)$ at different ionic strength can be obtained numerically, as described in [91PIT], Appendix B. The values of the Pitzer parameters used have been taken from the literature [84HAR/MOL, 91PIT]:

$$\begin{aligned} \beta_{\text{Na}, \text{CO}_3}^{(0)} = 0.0399, \quad \beta_{\text{Na}, \text{CO}_3}^{(1)} = 1.389, \quad C_{\text{Na}, \text{CO}_3}^\Phi = 0.0044, \\ \theta_{\text{Cl}, \text{CO}_3} = -0.02, \quad \psi_{\text{Na}, \text{Cl}, \text{CO}_3} = 0.0085. \end{aligned}$$

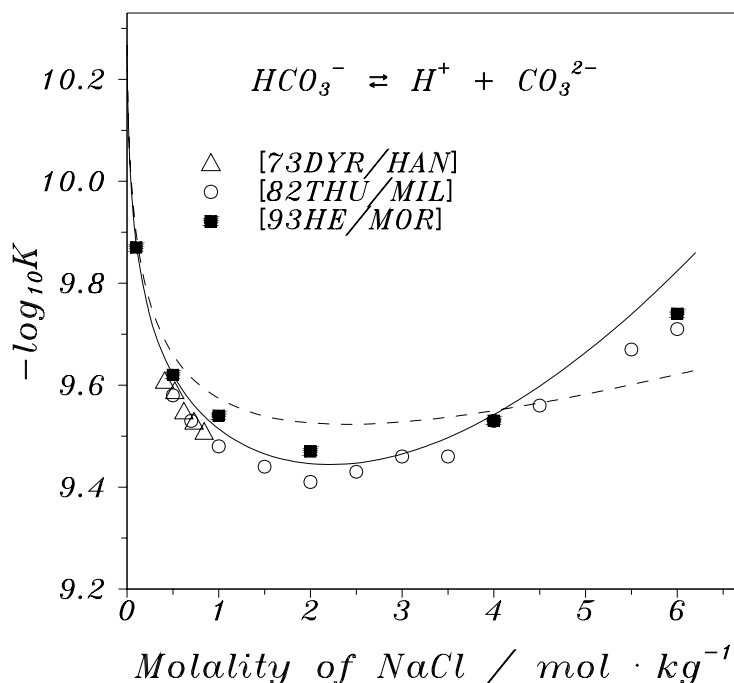
The value of K° for the second dissociation constant for CO_2 was taken from the CODATA [89COX/WAG] recommendation, $\ln K^\circ = -23.79 \pm 0.16$ or $\log_{10} K^\circ = -10.33 \pm 0.07$.

The calculated values of $\log_{10} K$ for the reaction $\text{HCO}_3^- \rightleftharpoons \text{H}^+ + \text{CO}_3^{2-}$, using the Pitzer approach (solid lines) are compared with experimental ones (different symbols) in Figure IX.15. We should note that the experimental values of $\log_{10} K$ in the NaCl medium have not been considered in the evaluation of the Pitzer parameters for the ion combinations in the system $\text{Na}^+ - \text{Cl}^- - \text{HCO}_3^- - \text{CO}_3^{2-} - \text{H}^+$. Probably, a small change in the numerical values of mixing terms might improve the quality of reproduction of experimental data on the basis of the Pitzer model at high concentrations of NaCl.

Using the SIT model we obtain the following equation for the activity coefficients of CO_3^{2-} at trace concentrations in NaCl ionic medium:

$$\log_{10} \gamma_{\text{CO}_3^{2-}} = -\frac{4A\sqrt{I_m}}{1 + 1.5\sqrt{I_m}} + \varepsilon(\text{Na}^+, \text{CO}_3^{2-})m_{\text{Na}^+}$$

Figure IX.15: The comparison of the experimental (different symbols) and calculated values of $\log_{10} K$ using the Pitzer approach (solid line) and the SIT model (dashed line) for the reaction $\text{HCO}_3^- \rightleftharpoons \text{H}^+ + \text{CO}_3^{2-}$ in NaCl solutions at 298.15 K and 1 atm.



The corresponding equations for the activity coefficients of H^+ and HCO_3^- have been given previously. The value of the interaction coefficient for Na^+ and CO_3^{2-} ion combination, $\varepsilon(\text{Na}^+, \text{CO}_3^{2-})$, was estimated from the experimental values of $\log_{10} K$ for the reaction and the SIT interaction coefficients $\varepsilon(\text{H}^+, \text{Cl}^-)$ and $\varepsilon(\text{Na}^+, \text{HCO}_3^-)$, and found to be $-(0.06 \pm 0.02) \text{ kg} \cdot \text{mol}^{-1}$. The values of $\log_{10} K$ for the reaction, calculated with the SIT, are shown by the dashed line in Figure IX.15.

The Pitzer model provides a better reproduction of the experimental values of $\log_{10} K$ as compared to the SIT model, especially taking into account that the experimental data have not been considered in the evaluation of the Pitzer parameters in [82PEI/PIT, 84HAR/MOL]. However, the accuracy of the SIT model is better than $\pm 0.10 \log_{10}$ unit, which is satisfactory in many cases. In order to better understand the “price” for the higher accuracy in the Pitzer model we turn to Example 5.

Example 5:

This example discusses the dissociation constants of carbonic acid in a NaClO_4 ionic medium at 298.15 K and 1 atm.

The equations in this case are identical with those used for the NaCl medium, sub-

stituting Cl^- for ClO_4^- . The difference is that for the first dissociation constant the experimental data refer to the reaction $\text{CO}_2(\text{g}) + \text{H}_2\text{O}(\text{l}) \rightleftharpoons \text{H}^+ + \text{HCO}_3^-$. The CODATA [89COX/WAG] recommended value of K° for this reaction is $\ln K^\circ = -18.001 \pm 0.008$ or $\log_{10} K^\circ = -7.818 \pm 0.004$.

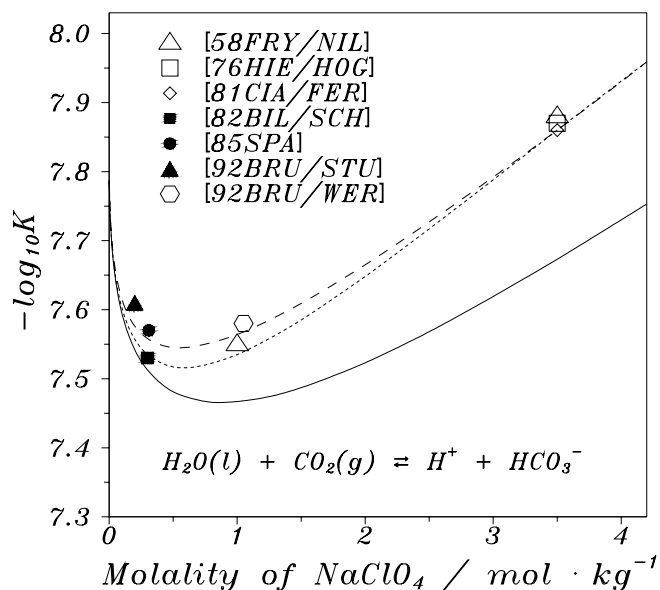
All the SIT parameters needed are available for the ion combinations in this system, $\varepsilon(\text{H}^+, \text{ClO}_4^-) = 0.14 \pm 0.02$, $\varepsilon(\text{Na}^+, \text{HCO}_3^-) = 0.00 \pm 0.02$, and $\varepsilon(\text{Na}^+, \text{CO}_3^{2-}) = -0.08 \pm 0.03$ (all in units of $\text{kg} \cdot \text{mol}^{-1}$), *c.f.* Tables IX.1 and IX.2. Hence, the values of $\log_{10} K$ for the first and the second dissociation constants for carbonic acid in NaClO_4 medium may be predicted. The predicted and experimental values of $\log_{10} K$ for the two reactions are shown in Figures IX.16 and IX.17 by dashed lines. As one can see, the SIT model predicts the values of $\log_{10} K$ in NaClO_4 medium surprisingly well. Indeed, the values of $\log_{10} K$ for the first dissociation constant of carbonic acid are reproduced practically within the expected experimental uncertainty, ± 0.03 ; the deviations between experimental and predicted values of $\log_{10} K$ for the second dissociation constant are less than ± 0.1 . The agreement between experimental and calculated values of $\log_{10} K$ for both reactions in the NaClO_4 medium is better than in the NaCl medium, where the values of the SIT interaction coefficients $\varepsilon(\text{Na}^+, \text{HCO}_3^-)$ and $\varepsilon(\text{Na}^+, \text{CO}_3^{2-})$ were determined. This better agreement in sodium perchlorate is fortuitous. Nevertheless, our experience shows that, in general, the less-parametrised SIT model gives quite reasonable estimations of equilibrium constants in different media, provided that the necessary interaction coefficients are known.

For the Pitzer model the values of mixing parameters are not available in literature for all the interactions in the system $\text{Na}^+ - \text{H}^+ - \text{ClO}_4^- - \text{HCO}_3^- - \text{CO}_3^{2-}$. The known values are listed below [91PIT]:

$$\begin{array}{lll}
 \beta_{\text{H},\text{ClO}_4}^{(0)} = 0.1747, & \beta_{\text{H},\text{ClO}_4}^{(1)} = 0.2931, & C_{\text{H},\text{ClO}_4}^\Phi = 0.00819, \\
 \beta_{\text{Na},\text{ClO}_4}^{(0)} = 0.0554, & \beta_{\text{Na},\text{ClO}_4}^{(1)} = 0.2755, & C_{\text{Na},\text{ClO}_4}^\Phi = -0.00118, \\
 \beta_{\text{Na},\text{CO}_3}^{(0)} = 0.0399, & \beta_{\text{Na},\text{CO}_3}^{(1)} = 1.389, & C_{\text{Na},\text{CO}_3}^\Phi = 0.0044, \\
 \beta_{\text{Na},\text{HCO}_3}^{(0)} = 0.0277, & \beta_{\text{Na},\text{HCO}_3}^{(1)} = 0.0411, & C_{\text{Na},\text{HCO}_3}^\Phi = 0.0, \\
 \theta_{\text{H},\text{Na}} = 0.036, & \theta_{\text{ClO}_4,\text{HCO}_3} = \text{unknown} & \\
 \psi_{\text{H},\text{Na},\text{ClO}_4} = -0.016, & \psi_{\text{Na},\text{ClO}_4,\text{HCO}_3} = \text{unknown} & \\
 \theta_{\text{ClO}_4,\text{CO}_3} = \text{unknown}, & \psi_{\text{Na},\text{ClO}_4,\text{CO}_3} = \text{unknown} &
 \end{array}$$

In Figures IX.16 and IX.17 the values of $\log_{10} K$ for the first and second dissociation constants of carbonic acid are calculated from the Pitzer model with the available parameters (solid lines). The difference between the experimental and calculated values (with only the two known mixing parameters reported in the literature) is appreciable, especially for the first dissociation constant. These examples show the accuracy to expect from the Pitzer type of calculations when some mixing parameters are not available. The procedure recommended to improve the performance of the Pitzer model is to estimate the remaining mixing parameters from the differences between the calculated and experimental values of the constants. This resulted in the following values: $\theta_{\text{ClO}_4,\text{HCO}_3} = 0.07$, $\theta_{\text{ClO}_4,\text{CO}_3} = 0.07$, $\psi_{\text{Na},\text{ClO}_4,\text{HCO}_3} = -0.015$, $\psi_{\text{Na},\text{ClO}_4,\text{CO}_3} = 0$. These estimations are only

Figure IX.16: Comparison of the experimental (different symbols) values of $\log_{10} K$ and the predicted values of $\log_{10} K$ using the Pitzer approach for the reaction $\text{H}_2\text{O}(\text{l}) + \text{CO}_2(\text{g}) \rightleftharpoons \text{H}^+ + \text{HCO}_3^-$ in NaClO_4 solutions at 298.15 K and 1 atm. The solid line has been calculated using literature values for the mixing terms, the dashed line refers to the SIT model. The dotted line represents the calculation based on the Pitzer model with estimated values of the required mixing terms (see text).

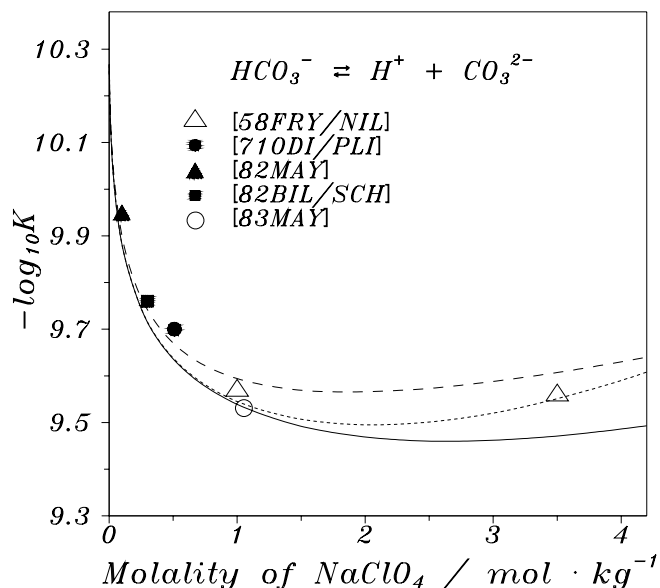


preliminary; many more determinations, preferably of better quality, are needed to get reliable values for these parameters. The values of $\log_{10} K$ for both reactions calculated using all Pitzer's parameters are shown in Figures IX.16 and IX.17 by dotted lines. As expected, the additional parameters strongly improve the performance of the Pitzer model.

These examples demonstrate the difference between the two models considered:

- The SIT uses the minimal number of regression parameters. The deviations between experimental and fitted values of $\log_{10} K$ are usually within ± 0.05 - $0.10 \log_{10}$ unit. Such deviations are expected, because the uncertainty of the values of mean activity coefficients, $\log_{10} \gamma_{\pm}$ for strong 1-1, 2-1, 3-1 electrolytes is usually within 0.02 - $0.05 \log_{10}$ units, when calculated from this model. This allows a reasonable extrapolation of $\log_{10} K$ values in different ionic media, if the required SIT interaction coefficients are known. Hence, using the data from the sodium chloride medium, we could predict the values of equilibrium constants for the same reactions in solutions of sodium perchlorate, practically with the same accuracy as in the NaCl medium. The accuracy of the SIT model does not permit the reproduction of the concentration dependence of the more precise data, to which the dissociation constants of carbonic acid belongs. The number of such examples is limited to the relatively simple chemical systems which can be studied without

Figure IX.17: Comparison of the experimental (different symbols) and the predicted values of $\log_{10} K$ using the Pitzer approach with the available data from the literature values of the mixing terms (solid line) and the SIT model (dashed line) for the reaction $\text{HCO}_3^- \rightleftharpoons \text{H}^+ + \text{CO}_3^{2-}$ in NaClO_4 solutions at 298.15 K and 1 atm. The dotted line represents the calculation based on the Pitzer model with estimated values of the required mixing terms (see text).



serious experimental difficulties, where the speciation is known, the number of complexes formed is limited, and where it is possible to find the conditions under which the studied complex is the main species in solution, etc. The precision and accuracy of experimental equilibrium constants for metal — ligand systems is in general much smaller than that of simple protolytes, like carbonic acid. This issue will be considered in the following Section.

- The Pitzer model, which was developed for the description of the concentration dependence of very accurate activity coefficient and osmotic coefficient data, is able to reproduce the precise values of $\log_{10} K$ practically within experimental accuracy, provided that the numerical values of all the relevant parameters are available. If the values of a number of parameters are unknown, the quality of the data reproduction and the predictions are much poorer and comparable with the accuracy of the SIT approach. The large number of parameters in the Pitzer model and their strong interrelations and correlations makes it difficult to use this model in systems where complex formation takes place, especially if some parameters have to be determined from concentration equilibrium constant data. By using a large number of fitting parameters in the Pitzer model it is possible to describe very precise emf or isopiestic data for many ternary systems, *e.g.*, $\text{MeCl}_2\text{-HCl-H}_2\text{O}$ without consid-

eration of complex formation at all, provided that the extent of complex formation is not large. However, for a solution coordination chemist it is essential to have correct information about the constitution of the complexes formed, because this determines important properties of a metal in solution such as chemical reactivity, toxicity, adsorption etc. The real speciation is important in many technological processes, for instance, the formation of negatively charged chloride complexes of cobalt in concentrated chloride solutions is used for the separation of nickel and cobalt. Progress in the understanding of chemical processes in solutions requires knowledge of their chemistry, *i.e.*, their real speciation ! Therefore, one must not use an extensively parametrized Pitzer model as a “substitution” for knowledge of the detailed chemistry, even if this model is excellent for describing the thermodynamic observations. However, it is desirable to extend the Pitzer formalism to all types of complex formation reactions and to obtain experimental values of the required Pitzer parameters for complexes. Such determinations must be based on experimental concentration equilibrium constants in different ionic media, which require an extensive experimental effort, even though a very large amount of stability constants for complex species have already been accumulated during the past 100 years [64SIL/MAR, 71SIL/MAR, 82HOG]. The problems will be described and discussed in the following section.

IX.7.1. The determination of the Pitzer and the SIT parameters from the $\log_{10} K$ data

Our primary goal is the description of the concentration dependence of equilibrium constants, since most data on the thermodynamics of complex formation reactions are reported in this way. The existing $\log_{10} K$ data have the following characteristics:

- The equilibrium constants have, as a rule, been obtained in a constant ionic medium. As discussed in the Introduction (*p.*325), the use of high concentrations of supporting electrolyte is a convenient and widely accepted method to establish a unique chemical model of a system under study. The $\log_{10} K$ data are not equally distributed on the ionic strength/concentration scale. Usually the experimentally covered interval is between 0.1 and 4 mol · kg⁻¹. The high molality of the ionic medium as compared to the concentrations of reactants/products ensures nearly constant values of the activity coefficients of the reaction participants even for reasonable variations of the total concentrations of reactants/ products.

Note. When equilibrium constants are determined using the emf-technique one must know or estimate liquid-junction potentials. However, by using a constant ionic medium the variations of the liquid-junction potential with the composition of the system are small.

- Relatively few experimental determinations, often less than 10 data points, are reported in the literature for a particular reaction in a particular ionic medium.

- The accuracy of the $\log_{10} K$ data is often much smaller than the precision of individual measurements, a fact which deserves a separate comment.

One has to distinguish between the reproducibility of the determination of the constant for given experimental conditions, with a particular experimental method, and an accepted chemical model and the accuracy of $\log_{10} K$. As stated in [90BEC/NAG, p.280] “the true error in the stability constants can be estimated with a high degree of certainty only through the comparison of constants obtained with methods differing in basic principles, or of constants obtained in independent laboratories”, and “agreement within $\pm 0.05 \log_{10}$ unit is classified as very good agreement, even in systems that can be studied experimentally without difficulty”. This means that the $\log_{10} K$ data are 20-100 times less accurate than the values of mean activity coefficients or osmotic coefficients, which often have an accuracy better than 0.5 per cent. This important fact should be kept in mind when discussing the determination of the Pitzer parameters for a reaction from the $\log_{10} K$ values.

The analytical statement for the concentration dependence of the equilibrium constant for a general chemical reaction

$$\sum_i \nu_i Q_i + r \text{H}_2\text{O}(l) = 0 \quad (\text{IX.27})$$

for the Pitzer model is given by Eq. (IX.29), which is valid for constant ionic medium NX, where NX is an 1-1 electrolyte, and for the trace concentrations of the reaction participants. For the purposes of a regression it is convenient to rewrite this equation as follows

$$\begin{aligned} \ln K^\circ &= \ln K + r \ln a_{\text{H}_2\text{O}} + \Delta(Z^2) \left(f^\gamma + m^2 B'_{\text{NX}} \right) + m^2 \Delta|Z| C_{\text{NX}} + 2m X_1 \\ &\quad + 2m g(I_m) X_2 + 2m^2 X_3 \end{aligned} \quad (\text{IX.31})$$

where m stands for the molality of the supporting NX electrolyte, and

$$\begin{aligned} \Delta(Z^2) &= \sum_i \nu_i Z_i^2 \\ \Delta|Z| &= \sum_i \nu_i |Z_i| \\ X_1 &= \Delta\beta^{(0)} + \Delta\phi = \sum_i \nu_i \beta_{ij}^{(0)} + \sum_i \nu_i \phi_{ii'} \\ X_2 &= \Delta\beta^{(1)} = \sum_i \nu_i \beta_{ij}^{(1)} \\ X_3 &= \Delta C + \frac{1}{2} \Delta\psi = \sum_i \nu_i C_{ij} + \frac{1}{2} \sum_i \nu_i \psi_{ii'} \end{aligned}$$

and $g(I_m)$ is defined in Eq. (IX.22).

Eq. (IX.31) is the general equation to be used if we want to determine $\log_{10} K^\circ$ and the sum of the Pitzer parameters for reactants and products from experimental equilibrium constants at different ionic strengths. The second, third and fourth terms on the right hand side of Eq. (IX.31) can be calculated from the known Pitzer parameters for the ionic medium NX. The equation shows that the coefficients for the other terms in m and m^2 contain $\Delta\beta^{(0)}$ and $\Delta\phi$, and ΔC and $\Delta\psi$, respectively. Hence, it is not possible to obtain the individual Pitzer parameters $\Delta\beta^{(0)}$ and ΔC from this equation alone. Pitzer [79PIT] points out, that in most cases the mixing parameters are small and may be neglected, hence, $X_1 = \Delta\beta^{(0)}$ and $X_3 = \Delta C$ is a reasonable approximation. The main difficulty is still to determine the parameters X_1 , X_2 , X_3 (as well as $\ln K^\circ$) from a limited number of experimental concentration constants, $\log_{10} K$, which rarely have a high accuracy, as indicated by the previous discussion. In order to use the Pitzer equations in systems where complex formation takes place, it therefore seems necessary to make some simplifications. A check of the typical values of C^Φ from [91PIT] showed that the contribution of ΔC is significant only at high ionic strength, typically above $5\text{-}6 \text{ mol} \cdot \text{kg}^{-1}$, and that this term could be neglected at lower ionic strengths. Another simplification was proposed by Millero [83MIL2], who assumed the value $\beta^{(1)} = 0$ for complexes. The validity of these two simplifications will be checked below.

The corresponding analytical statement for the concentration dependence of $\log_{10} K$ for the reaction (IX.27) at trace concentrations of reactants/products in a NX electrolyte medium using the SIT equation is given by Eq. (IX.30), and can be rewritten as follows:

$$\log_{10} K^\circ = \log_{10} K + r \log_{10} a_{\text{H}_2\text{O}} - \Delta(Z^2)D + m \Delta\varepsilon \quad (\text{IX.32})$$

where D is the Debye-Hückel term, defined in Eq. (IX.5); m stands for the molality of the ionic medium, the 1-1 electrolyte NX, and

$$\begin{aligned} \Delta(Z^2) &= \sum_i \nu_i Z_i^2 \\ \Delta\varepsilon &= \sum_i \nu_i \varepsilon(i, j) \end{aligned}$$

see Eq. (IX.30) for further explanations. After correction for the water activity and the Debye-Hückel contribution, the SIT equation becomes a simple linear function of the molality of the ionic medium.

We will use the literature data of $\log_{10} K$ for some selected reactions for the parametrization of both the models discussed. The main questions are:

- The reliability of $\log_{10} K^\circ$ (*i.e.*, the thermodynamic constants) obtained by a regression. Therefore, we use the experimental data for the reactions, for which CODATA recommendations [89COX/WAG] are available; see Examples 6 and 7. For the reactions selected, the $\log_{10} K$ data from solutions of high ionic strength have not been considered when making the CODATA recommendations.
- The typical uncertainty in the fitting parameters, which is decisive for the possibility to determine the Pitzer or the SIT concentration parameters from a limited number of experimental points of limited accuracy.

Table IX.4: Equilibrium constants for the dissociation of water in KCl solutions at 298.15 K.

$\frac{m \text{ KCl}}{\text{mol kg}^{-1}}$	$-\log_{10} K(m)$	$-\log_{10} K(m) + \log_{10} a_w$
4.82	14.27 ± 0.10	14.20 ± 0.10
4.22	14.24 ± 0.10	14.18 ± 0.10
3.31	14.08 ± 0.05	14.03 ± 0.05
3.31	14.09 ± 0.05	14.04 ± 0.05
3.30	14.08 ± 0.05	14.03 ± 0.05
2.13	13.90 ± 0.05	13.87 ± 0.05
2.13	13.91 ± 0.05	13.88 ± 0.05
2.13	13.90 ± 0.05	13.87 ± 0.05
1.03	13.77 ± 0.05	13.76 ± 0.05
1.03	13.93 ± 0.10	13.92 ± 0.10
1.03	13.90 ± 0.10	13.89 ± 0.10
0.51	13.75 ± 0.05	13.74 ± 0.05
0.10	13.78 ± 0.05	13.78 ± 0.05

For the regression we use the weighted general linear regression method as outlined in [65SHC]. The weight ω of an experimental point was defined as $\omega = 1/\delta^2$, where δ is an estimated uncertainty of $\log_{10} K$ value.

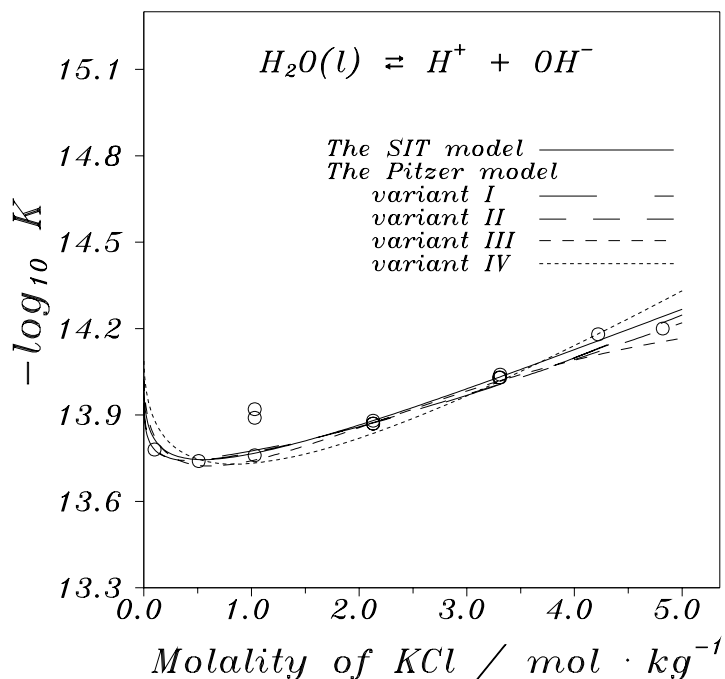
Example 6:

This example is a simple chemical reaction, $\text{H}_2\text{O}(\text{l}) \rightleftharpoons \text{H}^+ + \text{OH}^-$ where precise experimental data in KCl media at 298.15 K are available. After recalculating the experimental data of $\log_{10} K$, quoted from the “Stability constants” compilations [64SIL/MAR, 71SIL/MAR, 82HOG], to molality units and correcting for the water activity $\log_{10} a_w$ the values given in Table IX.4 were obtained.

The results of the regression are presented in Table IX.5 and in Figure IX.18. The following methods to estimate the Pitzer parameters are discussed:

- I. the determination of the whole set of parameters $\log_{10} K^\circ$, X_1 , X_2 , X_3 ;
- II. the determination of $\log_{10} K^\circ$, X_1 , X_2 , *i.e.*, neglecting the contribution of all ternary interactions;
- III. the determination of $\log_{10} K^\circ$, X_1 , X_3 , *i.e.*, assuming $\beta^{(1)} = 0$ for all reaction participants as suggested in [83MIL2];
- IV. the determination of $\log_{10} K^\circ$, X_1 , *i.e.*, using the smallest possible number of parameters in the Pitzer model.

Figure IX.18: The parametrization of the SIT and different variants of the Pitzer models (see text for details) for the reaction $\text{H}_2\text{O}(l) \rightleftharpoons \text{H}^+ + \text{OH}^-$ in KCl medium at 298.15 K and 1 atm.



The symbol (0) in Table IX.5 means that this parameter was set equal to zero in the data fitting. All uncertainties are given as $\pm 3\sigma$, where σ is the mean square error of an unknown [65SHC]. “True” values of the parameters X_1 - X_3 were calculated from tabulated values of $\beta^{(0)}$, $\beta^{(1)}$, and C for KOH and HCl, as well from ϕ and ψ for binary and ternary ions interactions, between H^+ , K^+ and OH^- , Cl^- ; H^+ , K^+ , Cl^- , and OH^- ; Cl^- , K^+ respectively [91PIT]. In accordance with Eq. (IX.31)

$$\begin{aligned} X_1 &= \Delta\beta^{(0)} + \Delta\phi \\ &= \beta_{\text{H,Cl}}^{(0)} + \beta_{\text{K,OH}}^{(0)} + \theta_{\text{H,K}} + \theta_{\text{Cl,OH}} \\ &= 0.1775 + 0.1298 + 0.005 - 0.050 \\ &= 0.262, \end{aligned}$$

$$\begin{aligned} X_2 &= \Delta\beta^{(1)} \\ &= \beta_{\text{H,Cl}}^{(1)} + \beta_{\text{K,OH}}^{(1)} \\ &= 0.295 + 0.320 \\ &= 0.615, \end{aligned}$$

Table IX.5: Regression results of data in Table IX.4 following procedures described in the text. The data in italics have been obtained by omitting three experimental determinations that may be in error.

The parameters of the SIT and the Pitzer (variants I-IV) models						
Parameter	SIT	I	II	III	IV	Accepted values
$-\log_{10} K^\circ$	14.02 ± 0.06 <i>14.00 ± 0.02</i>	13.96 ± 0.15 <i>13.98 ± 0.05</i>	13.97 ± 0.11 <i>13.97 ± 0.04</i>	14.05 ± 0.10 <i>14.04 ± 0.05</i>	14.12 ± 0.10 <i>14.10 ± 0.08</i>	14.001 ± 0.014
X_1^*	0.155 ± 0.027 <i>0.160 ± 0.009</i>	0.16 ± 0.33 <i>0.26 ± 0.12</i>	0.21 ± 0.06 <i>0.22 ± 0.02</i>	0.41 ± 0.12 <i>0.40 ± 0.05</i>	0.292 ± 0.045 <i>0.299 ± 0.036</i>	0.262
X_2		1.22 ± 1.56 <i>0.73 ± 0.55</i>	1.00 ± 0.68 <i>0.90 ± 0.24</i>	(0)	(0)	0.615
X_3		0.01 ± 0.27 <i>-0.01 ± 0.10</i>	(0)	-0.03 ± 0.03 <i>-0.03 ± 0.01</i>	(0)	-0.005

* in the case of the SIT model $X_1 = \Delta\epsilon$.

$$\begin{aligned}
 X_3 &= \Delta C + 1/2\Delta\psi \\
 &= C_{\text{H,Cl}} + C_{\text{K,OH}} + \frac{1}{2}\psi_{\text{H,K,Cl}} + \frac{1}{2}\psi_{\text{K,Cl,OH}} \\
 &= \frac{1}{2}C_{\text{H,Cl}}^\Phi + \frac{1}{2}C_{\text{K,OH}}^\Phi + \frac{1}{2}\psi_{\text{H,K,Cl}} + \frac{1}{2}\psi_{\text{K,Cl,OH}} \\
 &= 0.5 \times 0.0008 + 0.5 \times 0.0041 - 0.5 \times 0.007 - 0.5 \times 0.008 \\
 &= -0.0050.
 \end{aligned}$$

The “correct” value of $\log_{10} K^\circ$ was assumed to be that recommended by CODATA [89COX/WAG].

In addition, we tested the possibility of determining the values of the Pitzer parameters for the data set, using the CODATA value of $\log_{10} K^\circ$ as a fixed parameter, and obtained $X_1 = 0.22 \pm 0.25$, $X_2 = 0.85 \pm 0.85$, and $X_3 = 0.001 \pm 0.039$. The parameter X_3 is very uncertain and we therefore also tested a refinement involving only X_1 and X_2 and obtained 0.216 ± 0.051 and 0.86 ± 0.33 , respectively. The second model is in fair

agreement with the “accepted” values. By using Eq. (IX.34) in *p.*383 and the average value $X_2/\Delta(Z^2) = 0.337 \pm 0.014$ from Table IX.9, *p.*384, we obtain $X_2 = 0.74 \pm 0.03$ in good agreement with the “accepted” value 0.62.

We also determined the value of $\log_{10} K^\circ$ from the experimental values of $\log_{10} K$ using the “accepted” values of the Pitzer coefficients. Of 13 experimental values, 10 lie in the interval -14.00 ± 0.03 , and only two values (at $1.03 \text{ mol} \cdot \text{kg}^{-1}$) show a large systematic error, with values of $\log_{10} K^\circ$ equal to -14.17 and -14.14 , respectively. This indicates that the real accuracy of most of these data is within $\pm 0.03 \log_{10}$ units. However, two experimental determinations should be classified as discrepant. When these values are excluded from the data set, one obtains a significant reduction in the uncertainty of the estimated parameters, and much better agreement with the “accepted” values (including the CODATA value for $\log_{10} K^\circ$); these data are shown in italics. A problem facing the evaluators of published thermodynamic data is the lack of all needed experimental details and often primary experimental data (*e.g.*, emf, solubility or absorption data) in the original publication. This makes it very difficult to detect data that are flawed. The consequences are obvious from Example 6 !

The reduced versions of the Pitzer equation (variants II-IV) are much less sensitive for erroneous data, presumably due to the smaller number of fitting parameters. However, there is a noticeable increase in the estimated uncertainty. This example indicates that the uncertainty in Pitzer parameters determined from equilibrium constants are likely to be fairly large (of the same magnitude as the X_i) even in cases where $\log_{10} K^\circ$ is assumed to be known; the determination is also strongly affected by even a small number of erroneous experimental data.

Example 7:

This example refers to the determination of $\log_{10} K^\circ$ and the Pitzer or the SIT parameters from the experimental values of $\log_{10} K$ for the first protonation constant of the sulphate ion $\text{H}^+ + \text{SO}_4^{2-} \rightleftharpoons \text{HSO}_4^-$ studied in NaClO_4 medium. Only the results obtained from a potentiometric method have been used. The experimental data, quoted from “Stability Constants” compilations [64SIL/MAR, 71SIL/MAR, 82HOG] and from more recent work [77SAP/PAT] recalculated into molality units and to 298.15 K where necessary, are given in Table IX.6.

For this reaction one has to take into account the ionic strength dependence of the electrostatic unsymmetrical mixing term ${}^E\theta_{\text{ClO}_4, \text{SO}_4}(I_m)$. This was made as recommended in [91PIT], Appendix B. The results of the regression are given in Table IX.7 and in Figure IX.19. The same models for the estimation of the Pitzer parameters as in Example 6 are discussed:

- I. with determinations of the whole set of parameters $\log_{10} K^\circ$, X_1 , X_2 , X_3 ; and simplified variants:
- II. with determinations $\log_{10} K^\circ$, X_1 , X_2 ;

Table IX.6: Equilibrium constants for reaction $\text{H}^+ + \text{SO}_4^{2-} \rightleftharpoons \text{HSO}_4^-$ in NaClO_4 solutions.

$m \text{ NaClO}_4$	$\log_{10} K(m)$	$m \text{ NaClO}_4$	$\log_{10} K(m)$
3.50	0.82 ± 0.20	1.05	1.00 ± 0.15
3.06	1.08 ± 0.10	1.05	1.10 ± 0.10
2.21	1.04 ± 0.10	1.05	1.20 ± 0.10
2.21	0.95 ± 0.10	1.05	1.14 ± 0.10
2.21	1.01 ± 0.10	0.78	1.23 ± 0.10
2.08	1.12 ± 0.10	0.51	1.25 ± 0.10
1.65	1.10 ± 0.10	0.51	1.30 ± 0.10
1.62	1.18 ± 0.10	0.25	1.43 ± 0.10
1.05	1.13 ± 0.10	0.10	1.59 ± 0.10

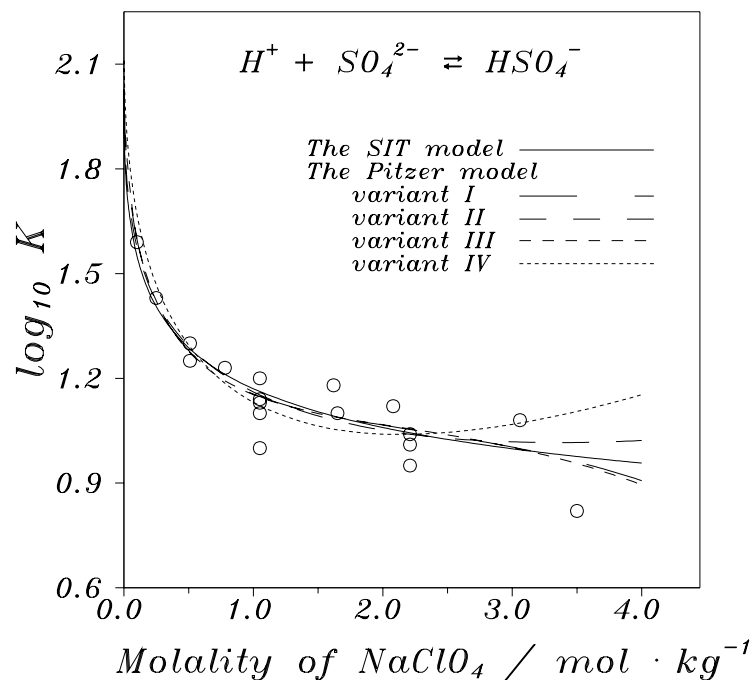
 Figure IX.19: The parametrization of the SIT and different variants of the Pitzer models (see text for details) for the reaction $\text{H}^+ + \text{SO}_4^{2-} \rightleftharpoons \text{HSO}_4^-$ in NaClO_4 medium at 298.15 K and 1 atm.


Table IX.7: Regression results for data in Table IX.6 following the procedure indicated in the text.

The SIT model	The Pitzer model, the values of parameters in variants I-IV					
	Parameter	I	II	III	IV	Accepted values
$\log_{10} K^\circ = 1.989 \pm 0.084$	$\log_{10} K^\circ$	2.10 ± 0.27	2.04 ± 0.20	2.13 ± 0.13	2.23 ± 0.11	1.987 ± 0.009
$\Delta\varepsilon = (0.003 \pm 0.051) \text{ kg} \cdot \text{mol}^{-1}$	X_1	-0.45 ± 0.88	-0.19 ± 0.16	-0.56 ± 0.21	-0.34 ± 0.08	-0.15 ± 0.05
	X_2	-0.46 ± 3.40	-1.39 ± 1.34	(0)	(0)	-0.995
	X_3	0.05 ± 1.02	(0)	0.07 ± 0.07	(0)	-0.006 ± 0.010

III. $\log_{10} K^\circ$, X_1 , X_3 ;

IV. $\log_{10} K^\circ$, X_1 .

All uncertainties are given as 3σ . “Accepted” values of the parameters were calculated only from the values of $\beta^{(0)}$, $\beta^{(1)}$, C for NaHSO_4 , Na_2SO_4 , and HClO_4 [91PIT]. The parameters for binary and ternary interactions of ClO_4^- with HSO_4^- and SO_4^{2-} are unknown, but the possible effect of neglecting them is probably within the proposed uncertainties of the “accepted” values. The “accepted” value of $\log_{10} K^\circ$ was chosen to be the CODATA [89COX/WAG] recommendation.

The two examples discussed refer to very simple acid-base equilibria, which can be studied without major experimental difficulties. In addition, a large number of experimental determinations have been reported for each of these reactions, 13 for the first and 18 for the second. In both cases the experimental determinations have also been carried out at relatively low ionic strength, $0.10 \text{ mol} \cdot \text{kg}^{-1}$, that facilitates the regression analysis.

The examples considered allow us to conclude that the simple one-parameter SIT model reproduces the experimental data very well. It also results in a reliable determination of $\log_{10} K^\circ$ with small uncertainties in the parameters evaluated (for both reactions the values of $\log_{10} K^\circ$ are in excellent agreement with the CODATA recommendations). The

problems encountered when using the Pitzer model are clearly demonstrated in both examples. All refinement models allow a precise data interpolation; however, the estimates of $\log_{10} K^\circ$ and the values of the coefficients X_i differ fairly much. Determination of the complete set of constants results in very large uncertainties (variant I). Of the other models only II which includes X_1 ($\approx \Delta\beta^{(0)}$) and X_2 ($\Delta\beta^{(1)}$) can be recommended, provided that the ionic strength is not too high (the estimation of X_3 ($\approx \Delta C$) seems only to be possible if reliable values of $\log_{10} K$ are available at ionic strengths above 6-8 mol·kg⁻¹). The value of X_2 estimated using Eq. (IX.34) in p.383 is equal to $X_2 = -1.35 \pm 0.06$ in fair agreement with the “true” value in Table IX.7. The models III (assuming $X_2 = \Delta\beta^{(1)} = 0$) and IV give unreliable estimations of the parameters and should be avoided.

Model IV (with the determination of $\log_{10} K^\circ$ and $X_1 \approx \Delta\beta^{(0)}$) deserves a more detailed discussion due to its formal similarity to the SIT model. The single-ion activity coefficient for an ion, i , in the SIT model is:

$$\ln \gamma_i = \text{DH-term} + \sum_j \varepsilon_\gamma(i, j) m_j$$

while the corresponding quantity for a metal ion, M, using the simplified one-parameter Pitzer equation is:

$$\ln \gamma_M = \text{DH-term} + 2 \sum_a \beta_{Ma}^{(0)} m_a$$

where “DH-term” denotes the Debye-Hückel term. Formally, both expressions are equivalent. However, the two models use quite different forms of the Debye-Hückel terms. The electrostatic contribution to the activity coefficient of an ion in the Pitzer theory is larger than in the SIT model and has a quite different concentration dependence, see Figure IX.20.

It is important to observe that, in the Pitzer theory, the short-range contributions cannot be represented by a linear function of the concentration. To illustrate this point, we have plotted[†] $Y = \beta^{(0)} + (\beta^{(1)}/\alpha^2 I_m)[1 - (1 + \alpha\sqrt{I_m} - \alpha^2 I_m/2) \exp(-\alpha\sqrt{I_m})]$ versus concentration for 1-1 (curve **a** in Figure IX.21) and 2-1 electrolytes (curve labeled **b**), using rather typical values of $\beta^{(0)}$ and $\beta^{(1)}$, (0.10 and 0.25) and (0.40 and 1.7), respectively, for 1-1 and 2-1 electrolytes. From these curves it is obvious that the approximation of a constant value of Y results in an erroneous estimation of both $\log_{10} K^\circ$ and $\beta^{(0)}$.

As a matter of fact, the introduction in explicit form of an ionic strength dependence of the parameter for binary interactions was one of the principal innovations in the Pitzer equations, see [73PIT, 91PIT]. The problem is even more obvious if one compares the quality of reproducing experimental data of γ_\pm for some chlorides at 298.15 K in a limited ionic strength range (0-3 mol·kg⁻¹) using the SIT and the reduced Pitzer equation with only the $\beta^{(0)}$ term. In Figure IX.22 we have plotted the experimental (full drawn lines) and fitted values of mean activity coefficients of NaCl, MgCl₂, and NdCl₃ by using the SIT model (dashed lines) and the reduced Pitzer model (dotted lines). Two points should be noted:

[†] $\alpha = 2.0 \text{ kg}^{1/2} \cdot \text{mol}^{-1/2}$ for all three electrolytes, cf. p.353.

Figure IX.20: The relative contributions of the Debye-Hückel term to $\ln \gamma_{\pm}$ for the SIT and the Pitzer models at 298.15 K and 1 atm.

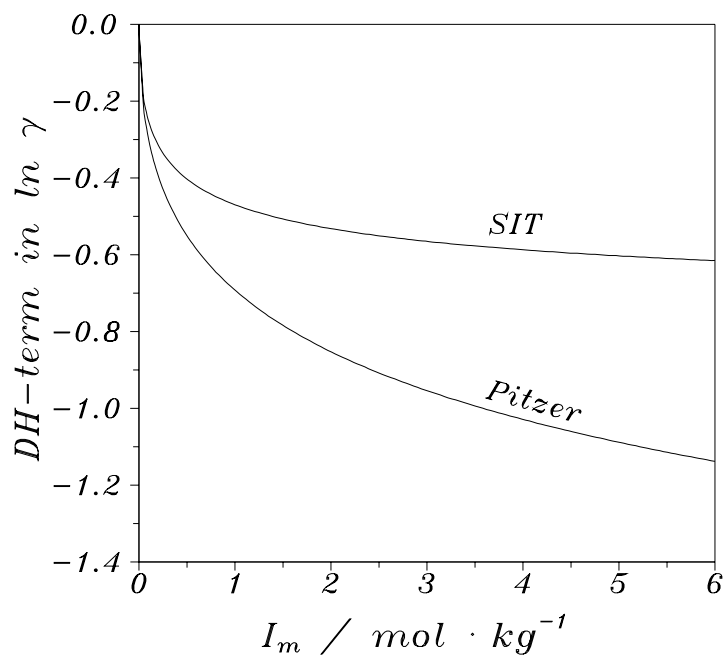


Figure IX.21: The concentration dependence of function $Y = \beta^{(0)} + (\beta^{(1)}/\alpha^2 I_m)[1 - (1 + \alpha\sqrt{I_m} - \alpha^2 I_m/2) \exp(-\alpha\sqrt{I_m})]$ for the typical 1-1 (curve labeled as **a**) and 2-1 electrolytes (curve labeled as **b**) at 298.15 K and 1 atm.

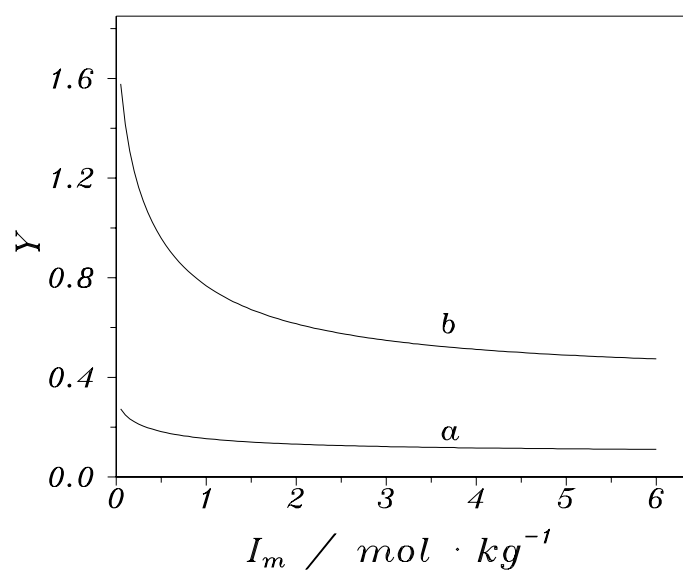
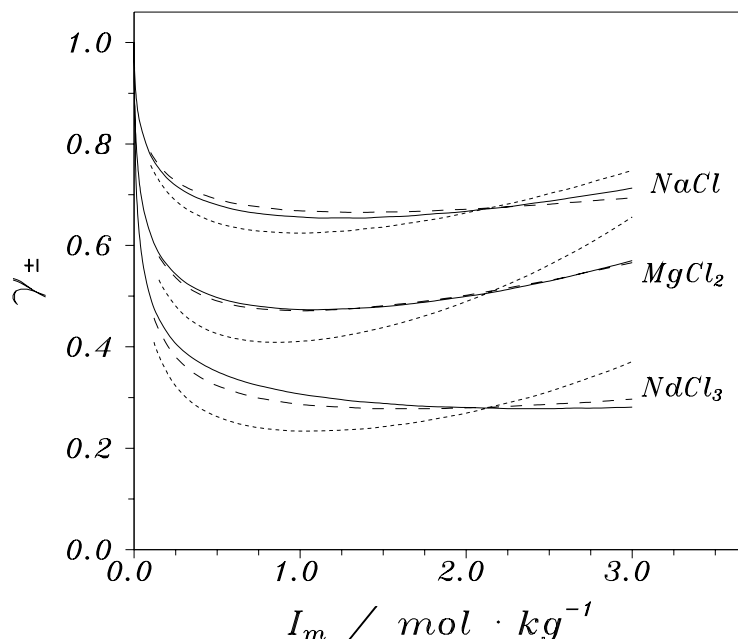


Figure IX.22: The comparison of the quality of the reproduction of experimental data of mean activity coefficients for different electrolytes (solid lines) at 298.15 K using the SIT model (dashed lines) and the Pitzer model containing only the $\beta^{(0)}$ term (dotted lines).



- The obtained values of $\beta^{(0)}$ always differ from the “true” ones. For instance, for NaCl the obtained value of $\beta^{(0)}$ is equal to 0.110 as compared with 0.0765 from [91PIT]; for MgCl₂ the value $\beta^{(0)} = 0.557$ as compared with “true” value 0.352; for NdCl₃ $\beta^{(0)} = 1.247$ as compared with 0.586. The noticeable increase in the value of $\beta^{(0)}$ obtained in this way is an inevitable consequence of neglecting the contribution of the $\beta^{(1)}$ term. The higher the valence type of the electrolyte, the larger the error introduced in the $\beta^{(0)}$ value;
- The accuracy of data reproduction is much poorer when using the one-parameter Pitzer model than in the one-parameter SIT model. We may compare the mean and maximum errors (defined as $(1 - \gamma_{\text{calc}}/\gamma_{\text{exp}})$) using both approaches: for NaCl they are 3.3 and 5.3%, in the reduced Pitzer model, and 1.4 and 2.7% in the SIT model; for MgCl₂ the corresponding numbers are 9.3 and 15% in the reduced Pitzer model and 0.6 and 1.3% in the SIT; for NdCl₃ 17 and 32% in the reduced Pitzer model, and 4.4 and 8% in the SIT model.

This comparison of the mean activity coefficient data (which are supposed to be very precise) by means of the one-parameter Pitzer and SIT models clearly demonstrates the problems of reducing the number of parameters in the Pitzer approach: neglect of the contribution of the $\beta^{(1)}$ term in the Pitzer model results in a significant loss of accuracy

in the data reproduction (as compared with the SIT model) and a wrong estimate of the $\beta^{(0)}$ term. Hence, *the Pitzer equation in general has to be used with both the $\beta^{(0)}$ and $\beta^{(1)}$ terms.* Returning to the concentration dependence of complex formation reactions, we emphasise that in order to determine both X_1 and X_2 , it is necessary to have precise data on $\log_{10} K$ at rather low ionic strengths, less than $0.5 \text{ mol} \cdot \text{kg}^{-1}$, where the relative contribution of $\beta^{(1)}$ is largest. The difficulty to determine $\beta^{(1)}$ is most pronounced for reactions where the ions have a charge ± 1 , for which the uncertainty in $\log_{10} K$ must be far less than ± 0.05 in order to determine both parameters. The determination of the Pitzer parameters for complexes is an important, but far from simple task. In systems with few experimental data, one is forced to use approximations when determining $\log_{10} K^\circ$ and the Pitzer parameters. We recommend the correlation methods described below in Sections IX.8 and IX.8.1, which are to be preferred to simplistic “procedures” such as: “If the data are restricted, just limit the number of parameters used in the Pitzer model”.

IX.8. The relationship between the SIT $\varepsilon(i, j)$ and the Pitzer $\beta_{ij}^{(0)}$ and $\beta_{ij}^{(1)}$ parameters for mean-activity coefficients

The previous sections indicate some difficulties that may be encountered when using the Pitzer model for the description of the concentration dependence of equilibrium constants in electrolyte systems of high ionic strength. The problem is the lack of experimental Pitzer parameters for complexes, while they are often available for the reactants if these are metal ions and simple ionic ligands. This means that the activity coefficients of these species can be calculated even in rather complicated systems, like mixtures of strong electrolytes. A modeller might then wish to combine known information for the strong electrolyte mixture with experimental information on equilibrium constants for trace components using the Pitzer formalism. In order to do this it will be necessary to make approximations, and some of these will be discussed in the following two sections.

An analysis of the values of $\beta^{(1)}$ at 298.15 K from the available compilation [91PIT] shows that there is a correlation between the values of $\beta^{(1)}$ and the charge type of the electrolyte: for most 1-1 electrolytes the values of the $\beta^{(1)}$ parameter fall in a range 0.20 ± 0.20 ; for most 2-1 electrolytes in the range 1.4 ± 0.6 and for most 3-1 electrolytes in the range 5.2 ± 1.2 . These averages may then be used as “fixed” values of $\beta^{(1)}$ in the Pitzer equations, thus reducing the number of unknown parameters. A better estimate of $\beta^{(1)}$ is obtained by using the following simple relationship between the Pitzer parameters $\beta^{(0)}$ and $\beta^{(1)}$ and the ε_γ parameters, which is valid when the term with C_{MX}^Φ may be neglected. The Pitzer equation for the mean-activity coefficient is then equal to:

$$\ln \gamma_{\pm} = -|Z_M Z_X| A_\Phi \left[\frac{\sqrt{I_m}}{1 + b\sqrt{I_m}} + \frac{2}{b} \ln \left(1 + b\sqrt{I_m} \right) \right] + m \frac{2\nu_M \nu_X}{\nu} \left(2\beta^{(0)} + 2\beta^{(1)} X \right)$$

where

$$X = \frac{1}{\alpha^2 I_m} \left[1 - \left(1 + \alpha\sqrt{I_m} - \frac{1}{2}\alpha^2 I_m \right) e^{-\alpha\sqrt{I_m}} \right]$$

Table IX.8: Quantitative relationship between the Pitzer parameters $\beta^{(0)}$ and $\beta^{(1)}$ and the SIT ε_γ parameters for different ion combinations at 298.15 K.

Ion combination	$\left(\beta^{(0)} - \varepsilon_\gamma/2\right)$	$\beta^{(1)}$
M^+, X^-	0.035	$0.34 \approx 0.3$
M^{2+}, X^- and M^+, X^{2-}	0.150	$1.56 \approx 1.6$
M^{3+}, X^- and M^+, X^{3-}	0.366	$4.29 \approx 4.3$
M^{4+}, X^- and M^+, X^{4-}	0.754	$8.89 \approx 8.9$

From the SIT model we have (taking into account that $A_\gamma = 3A_\Phi$)

$$\ln \gamma_\pm = -\frac{3A_\Phi |Z_M Z_X| \sqrt{I_m}}{1 + 1.5\sqrt{I_m}} + \frac{2\nu_M \nu_X}{\nu} \varepsilon_\gamma m$$

After elementary transformations we obtain

$$\begin{aligned} Y &= -\frac{A_\Phi |Z_M Z_X| \nu}{4\nu_M \nu_X m} \left[\frac{3\sqrt{I_m}}{1 + 1.5\sqrt{I_m}} - \frac{\sqrt{I_m}}{1 + b\sqrt{I_m}} - \frac{2}{b} \ln \left(1 + b\sqrt{I_m} \right) \right] \\ &= \left(\beta^{(0)} - \frac{\varepsilon_\gamma}{2} \right) + \beta^{(1)} X \end{aligned} \quad (\text{IX.33})$$

The values of X and Y can be easily calculated, and Y should be a linear function of X with the intercept $(\beta^{(0)} - \varepsilon_\gamma/2)$ and the slope $\beta^{(1)}$. The quality of linearity is the criterion of the compatibility of the Pitzer and the SIT models. Figures IX.23, IX.24 and IX.25 show plots of Y vs. X for different M^{Z+} and X^{Z-} combinations. The linearity is good, showing that the SIT model is approximately equivalent to a simplified Pitzer model (without the C_{MX}^Φ term) and results in a constant value of the $\beta^{(1)}$ parameter for each charge type. Table IX.8 summarises the relationships between the two sets of parameters.

Note: Usually the values of $\varepsilon(i, j)$, not $\varepsilon_\gamma(i, j)$ are tabulated, and the relationship between them is: $\varepsilon(i, j) = \varepsilon_\gamma(i, j)/\ln(10)$.

The values of the parameter $\beta^{(1)}$ are in reasonable good agreement with the values tabulated for individual electrolytes (see above). Using these values one obtains approximately the same accuracy of the reproduction of γ_\pm values with both models. This approximation allows a good estimate of the $\beta^{(1)}$ parameter for different ion combinations. For a more detailed discussion of the concentration dependence of the second virial coefficient for solutes, see the discussions in [73PIT, 91PIT]. In principle, the same procedure may be used to estimate the temperature dependence of the $\beta^{(1)}$ parameter, because the temperature

Figure IX.23: The determination of quantitative relationship between the parameter ε_γ in the SIT model and the parameters $\beta^{(0)}$ and $\beta^{(1)}$ in the Pitzer model for the case of 1-1 completely dissociated electrolytes at 298.15 K and 1 atm. X and Y are defined in the text. The circles denote data which have been calculated from Eq. (IX.33).

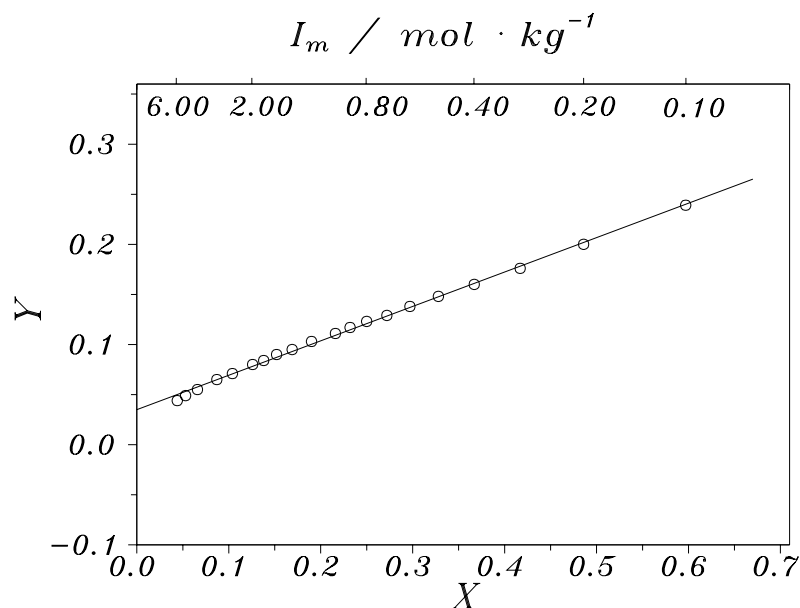


Figure IX.24: The determination of quantitative relationship between the parameter ε_γ in the SIT model and the parameters $\beta^{(0)}$ and $\beta^{(1)}$ in the Pitzer model for the case of 2-1 or 1-2 completely dissociated electrolytes at 298.15 K and 1 atm. X and Y are defined in the text.

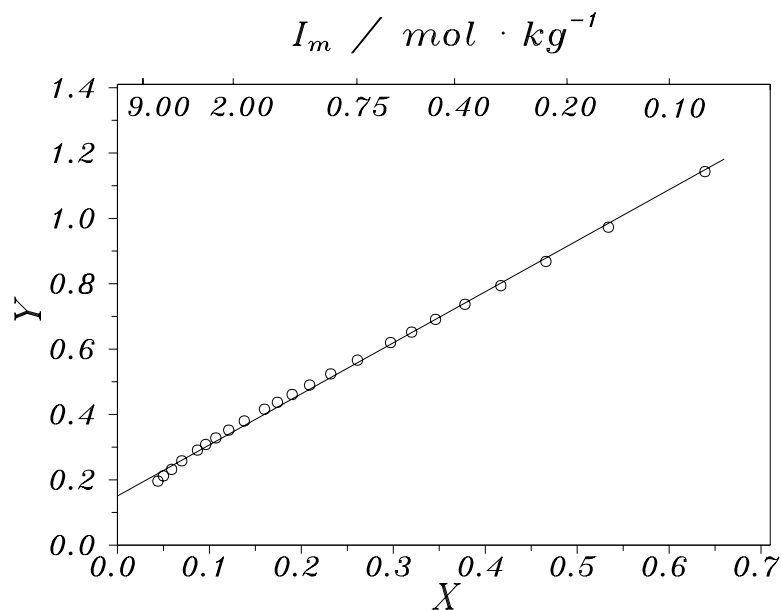
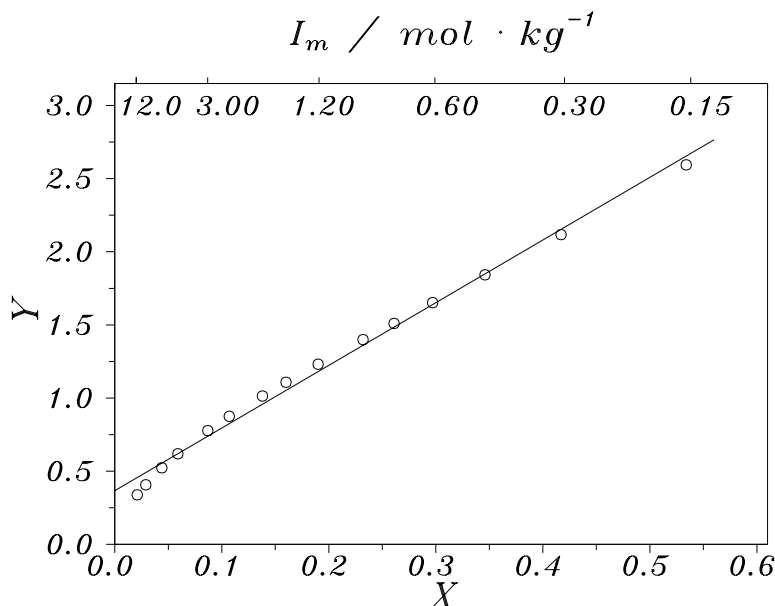


Figure IX.25: The determination of quantitative relationship between the parameter ε_γ in the SIT model and the parameters $\beta^{(0)}$ and $\beta^{(1)}$ in the Pitzer model for the case of 3-1 or 1-3 completely dissociated electrolytes at 298.15 K and 1 atm. X and Y are defined in the text.



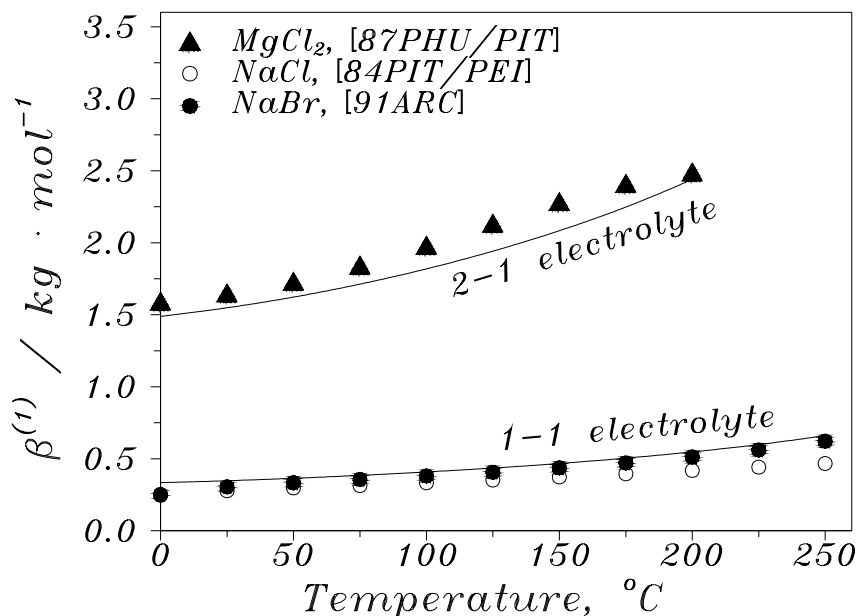
dependence of A_Φ is well known [90ARC/WAN], provided the value of numerical factor 1.5 used in the SIT model is temperature independent. In Figure IX.26 we have plotted the calculated values of $\beta^{(1)}$ for 1-1 and 2-1 electrolytes *versus* temperature, at saturated water vapor pressure (solid lines) and compared them with “experimental” values for NaCl, NaBr, and MgCl₂ from available compilations. The semiquantitative agreement is obvious.

The previous relationships between the SIT and the Pitzer parameters may be used to convert the $\varepsilon(i, j)$ values for the SIT model into $\beta_{ij}^{(0)}$ and $\beta_{ij}^{(1)}$ values of the Pitzer approach, and vice versa. A similar relationship may also be obtained between $\Delta\varepsilon$ and $\Delta\beta^{(0)}$ and $\Delta\beta^{(1)}$ for reactions. It is more convenient to estimate the Pitzer parameters X_1 and X_2 directly from the experimental values of $\Delta\varepsilon$ than to use estimates of all the individual $\beta_{ij}^{(0)}$ and $\beta_{ij}^{(1)}$ values for the reactants/products.

Example 8:

Let us consider the estimation of the Pitzer parameters for the interaction Fe³⁺-ClO₄⁻. In [92GRE/FUG] the value of the SIT interaction coefficient $\varepsilon(\text{Fe}^{3+}, \text{ClO}_4^-) = (0.56 \pm 0.03) \text{ kg} \cdot \text{mol}^{-1}$ is given, as estimated from the available information by Biedermann [75BIE]. Using the correlation proposed above one may *estimate* the Pitzer parameters Fe³⁺-ClO₄⁻ as follows: $\beta^{(0)} = \varepsilon_\gamma/2 + 0.366 = (0.56 \pm 0.03) \times \ln(10)/2 + 0.366 = (1.01 \pm$

Figure IX.26: The comparison of “predicted” (see text for details) and “experimental” values of the $\beta^{(1)}$ parameter as a function of temperature at saturated water vapor pressure.



0.04) $\text{kg} \cdot \text{mol}^{-1}$; $\beta^{(1)} = 4.3 \text{ kg} \cdot \text{mol}^{-1}$.

Example 9:

Let us consider the estimation of the Pitzer parameters for the interaction Bi^{3+} - ClO_4^- . Only a few sets of measurements are available in literature. For the reaction $\text{BiOCl}(\text{cr}) + 2\text{H}^+ \rightleftharpoons \text{Bi}^{3+} + \text{Cl}^- + \text{H}_2\text{O}(\text{l})$ the values of $\log_{10} K$ have been obtained by Ahrlund and Grenthe [57AHR/GRE] from solubility and potentiometric measurements in mixture 1 M HClO_4 + 1 M NaClO_4 and by Vasil'ev and Grechikhina [67VAS/GRE] from solubility measurements in HClO_4 solutions of concentrations 0.5-2.0 M. Using the SIT model to treat these data one obtains the following estimations of the SIT interaction coefficient $\varepsilon(\text{Bi}^{3+}, \text{ClO}_4^-) = (0.47 \pm 0.12) \text{ kg} \cdot \text{mol}^{-1}$. For the reaction $\text{BiOBr}(\text{cr}) + 2\text{H}^+ \rightleftharpoons \text{Bi}^{3+} + \text{Br}^- + \text{H}_2\text{O}(\text{l})$ the values of $\log_{10} K$ have been reported by Ahrlund and Grenthe [57AHR/GRE] and by Fedorov *et al.* [71FED/KAL] from the solubility of $\text{BiOBr}(\text{cr})$ in HClO_4 - LiClO_4 mixtures of different constant ionic strengths between 0.5 and 4 M. The SIT results in the value of $\varepsilon(\text{Bi}^{3+}, \text{ClO}_4^-) = (0.59 \pm 0.07) \text{ kg} \cdot \text{mol}^{-1}$. Vasil'ev and Grechikhina [67VAS/GRE2] have measured the solubility of $\text{BiONO}_3(\text{cr})$ in HClO_4 solutions of concentrations between 0.30 and 1.35 M and obtained the values of solubility product of the solid phase after a correction for the formation of nitrate complexes of Bi(III). From these data the value of $\varepsilon(\text{Bi}^{3+}, \text{ClO}_4^-)$ was estimated to be

0.59 ± 0.07 . These examples illustrate typical uncertainties in the estimation of interaction coefficients from a small number of data from different laboratories. The mean value $\varepsilon(\text{Bi}^{3+}, \text{ClO}_4^-) = (0.54 \pm 0.07) \text{ kg} \cdot \text{mol}^{-1}$, is in reasonable agreement with the corresponding quantities for the lanthanoids, which have the charge 3 and very similar ionic radii. Using the correlation proposed above we obtain for the $\text{Bi}^{3+}\text{-ClO}_4^-$ interaction the following preliminary values of the Pitzer parameters: $\beta^{(0)} = (0.99 \pm 0.08) \text{ kg} \cdot \text{mol}^{-1}$; $\beta^{(1)} = 4.3 \text{ kg} \cdot \text{mol}^{-1}$.

IX.8.1. The relationship between the $\Delta\varepsilon$ values in the SIT model and the $\Delta\beta^{(0)}$ and $\Delta\beta^{(1)}$ values in the Pitzer models for complex formation reactions at “trace” concentrations of reactants/products

By neglecting the contribution of all the ternary interactions, and excluding higher order electrostatic unsymmetrical mixing terms in the Pitzer equation we can write the following statement for the ionic medium dependence of $\ln K$:

$$\begin{aligned} \ln K^\circ &= \ln K - \Delta(Z^2) A_\Phi \left[\frac{\sqrt{I_m}}{1 + b\sqrt{I_m}} + \frac{2}{b} \ln \left(1 + b\sqrt{I_m} \right) \right] \\ &\quad + \Delta(Z^2) m^2 B'_{\text{NX}} + 2mX_1 + 2m g(I_m) X_2 \end{aligned}$$

See Eq. (IX.31) for explanations. The consequences of excluding the higher order electrostatic unsymmetrical mixing terms will be discussed later. The corresponding analytical statement for the concentration dependence of $\ln K$ using the SIT formalism is:

$$\ln K^\circ = \ln K - \Delta(Z^2) \frac{3A_\Phi \sqrt{I_m}}{1 + 1.5\sqrt{I_m}} + m\Delta\varepsilon_\gamma$$

See Eq. (IX.32) for the explanation of abbreviations. Note again that $A_\gamma = 3A_\Phi$ and $\Delta\varepsilon = \Delta\varepsilon_\gamma / \ln(10)$. After elementary transformations we obtain:

$$\begin{aligned} Y &= \left\{ A_\Phi \left[\frac{\sqrt{I_m}}{1 + b\sqrt{I_m}} + \frac{2}{b} \ln \left(1 + b\sqrt{I_m} \right) - \frac{3\sqrt{I_m}}{1 + 1.5\sqrt{I_m}} \right] - m^2 B'_{\text{NX}} \right\} / 2m \\ &= \frac{1}{\Delta(Z^2)} \left(X_1 - \frac{\Delta\varepsilon_\gamma}{2} \right) + \frac{X_2}{\Delta(Z^2)} g(I_m) \end{aligned} \quad (\text{IX.34})$$

i.e., Y is a linear function of $g(I_m)$, where the slope is $X_2/\Delta(Z^2)$ and the intercept $(X_1 - \Delta\varepsilon_\gamma/2)/\Delta(Z^2)$. In order to calculate the values of Y one has to know the Debye-Hückel parameter A_Φ and B'_{NX} , *i.e.*, $\beta^{(1)}$ for the 1-1 ionic medium electrolyte, these data are available. The values of $g(I_m)$ are obtained from the ionic strength of the solution. The quality of the linearity will be a criterion of the compatibility of the SIT model and the simplified Pitzer equation. In Figure IX.27 we have plotted the values of Y calculated for reactions in some common 1-1 ionic media. The linearity is good for

Figure IX.27: The determination of relationship between the SIT parameter $\Delta\epsilon$ and the Pitzer parameters $\Delta\beta^{(0)}$ and $\Delta\beta^{(1)}$ for reactions studied in solutions of different 1-1 ionic medium electrolytes at 298.15 K and 1 atm (see text for details). The symbols are calculated values of Y versus $g(I_m)$ using Eq. (IX.34) for the different ionic media.

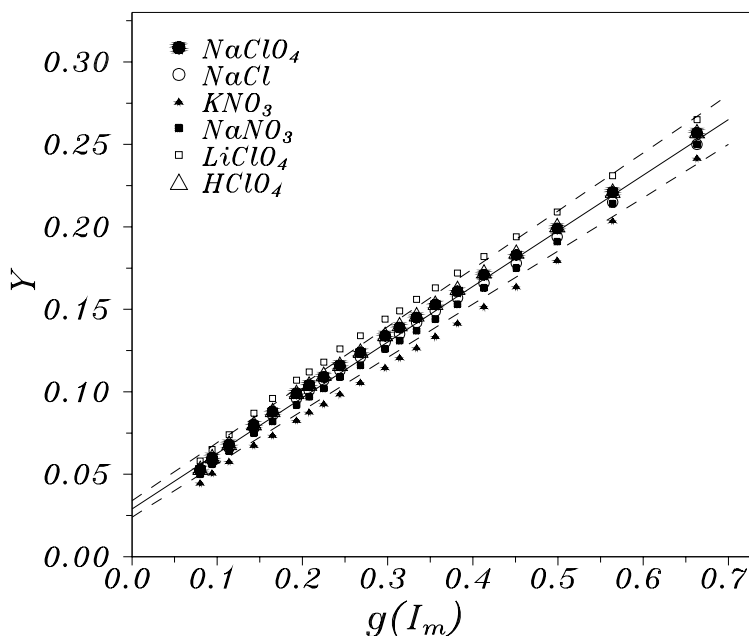


Table IX.9: Relation between the Pitzer and the SIT parameters for the complex formation reaction studied in different 1-1 supporting electrolytes at 298.15 K.

1-1 electrolyte	$(X_1 - \Delta\epsilon_\gamma/2)/\Delta(Z^2)$	$X_2/\Delta(Z^2)$
NaClO ₄	0.031	0.340
LiClO ₄	0.038	0.348
HClO ₄	0.032	0.342
NaNO ₃	0.026	0.334
KNO ₃	0.019	0.327
NaCl	0.030	0.332
All data	0.029 ± 0.005	0.337 ± 0.014

all electrolytes considered. The optimal values of the parameters $(X_1 - \Delta\varepsilon_\gamma/2)/\Delta(Z^2)$ and $X_2/\Delta(Z^2)$ can be determined for each electrolyte (see Table IX.9). However, the parameters, especially the slope of the line, which is related to $X_2/\Delta Z^2$ or $\Delta\beta^{(1)}$ for the reaction (see Table IX.9) do not vary much with the nature of electrolyte. Hence we can use all the data to determine *one* unique set of parameters, (see the last line of Table IX.9 where the uncertainties are given as 3σ). Because of the difficulty of making an accurate determination of $\Delta\beta^{(1)}$ using regression analysis of $\log_{10} K$ data, *cf.* Examples 6 and 7, we suggest that an alternative is to use the proposed correlation to estimate $\Delta\beta^{(1)}$ (and $\beta^{(1)}$ for complex species if these values for single ions are available already). For instance, for the Example 6 one estimates the value of $X_2 = (0.337 \pm 0.14) \times \Delta(Z^2) = (0.337 \pm 0.014) \times 2 = 0.67 \pm 0.03$, which is rather close to the “true” $X_2 = 0.62$ (the most reliable estimation using regression of the data set without erroneous points gives 0.90 ± 0.24 ; see Table IX.5 in Example 6). For the Example 7 the estimated value using the proposed correlation is $X_2 = (0.337 \pm 0.014) \times \Delta(Z^2) = (0.337 \pm 0.014) \times (-4) = -1.35 \pm 0.06$. This result is only in fair agreement with the “true” $X_2 = -1.00$. However, the value from the regression has very large uncertainties, $X_2 = -1.39 \pm 1.34$ from Table IX.7 in Example 7.

The analysis must be modified for the case of reactions where $\Delta(Z^2) = 0$. It is possible to show that in this case the following relationship is valid at any molality:

$$\left(X_1 - \frac{\Delta\varepsilon_\gamma}{2}\right) + X_2 g(I_m) = 0$$

Because the first term is constant, and $g(I_m)$ is a monotone function of the ionic strength, this equality is only possible if $(X_1 - \Delta\varepsilon_\gamma/2)$ and X_2 both are equal to zero.

The relationship discussed was obtained by neglecting the contribution of the terms for higher order electrostatic unsymmetrical mixing. By including these terms the slope of the function Y is changed somewhat, particularly for ions of charge 3, or higher. However, for this type of reactions the problem to determine the contributions of the $\beta^{(0)}$ and $\beta^{(1)}$ terms is not severe, because of the large absolute values of $\beta^{(1)}$ for interactions involving ions of high charges. We therefore suggest that the correlation between $\Delta(Z^2)$ and $\Delta\beta^{(1)}$ should only be used for reactions involving ions with absolute charges ± 1 and ± 2 .

Summing up the discussion about the determination of the Pitzer parameters for a reaction from $\log_{10} K$ data, we conclude that this, as a rule, is an ill-conditioned problem. To obtain reasonable estimates of the parameters in the Pitzer model from few experimental data of limited accuracy, one has to use some simplifications. From our experience, the existing $\log_{10} K$ data rarely permit the determination of more than one interaction parameter. Therefore, we suggest the following strategy when using the $\log_{10} K$ data in solutions of an 1:1 ionic medium:

- Step 1, use the SIT equation to obtain $\log_{10} K^\circ$ and $\Delta\varepsilon$.
- Step 2, if the reaction involves ions with charges 1 and 2, then use the $\Delta(Z^2)$ value for the reaction to estimate the values of X_1 and X_2 for the reaction. This estimate

of X_1 is preliminary, a more accurate value is then determined in a new regression using $\log_{10} K^\circ$ from step 1 and X_2 determined from $\Delta\varepsilon$ as fixed parameters. For reactions involving ions with charges 3 and higher it is sufficient to use only $\log_{10} K^\circ$ from step 1 as a fixed parameter and then determine X_1 and X_2 in the regression.

If the values of the Pitzer parameters for single ion reactants/products are known, one can proceed to determine the corresponding coefficients for the complexes in the following way:

- Use the SIT equation to obtain $\log_{10} K^\circ$ for the reaction.
- Use the Pitzer interaction coefficients for single ions, the known values of binary and ternary mixing terms for interactions involving single ion reactants/products and the ions of the ionic medium, and $\log_{10} K^\circ$ value as fixed parameters in the regression analysis to obtain $\beta^{(0)}$ and $\beta^{(1)}$ for the complexes. If the charge of the complexes does not exceed 2, estimate X_2 from the $\Delta(Z^2)$ value for the reaction, followed by the calculation of $\beta^{(1)}$ for the complex species. Then use the regression analysis to obtain $\beta^{(0)}$ for the complex using $\log_{10} K^\circ$ and X_2 as fixed parameters.

All terms, including $m^2\Delta|Z|C_{\text{NX}}$ (see Eq. (IX.31)) and higher order electrostatic unsymmetrical mixing terms, should be taken into account in the regression procedure.

Example 10:

The reaction $\text{Cd}^{2+} + \text{NO}_2^- \rightleftharpoons \text{CdNO}_2^+$ has been studied in NaClO_4 ionic media. The experimental results, quoted from “Stability Constants” [64SIL/MAR, 71SIL/MAR, 82HOG], recalculated into molality units, are given in Table IX.10. The total number of experimental points is only 7, their real accuracy can be estimated to be $\pm 0.1 \log_{10}$ units based on comparison of the values from 5 different laboratories, using different experimental methods (potentiometry, spectrophotometry, polarography). The experimentally covered range of ionic medium concentrations is 1.0-3.5 mol · kg⁻¹.

Using the SIT model one obtains the following results: $\log_{10} K^\circ = 2.43 \pm 0.33$, $\Delta\varepsilon = -0.13 \pm 0.13 \text{ kg} \cdot \text{mol}^{-1}$. All errors are here given as 3σ .

The Pitzer parameters for the ion combinations $\text{Cd}^{2+}\text{-ClO}_4^-$ and $\text{Na}^+\text{-NO}_2^-$ were taken from the literature: $\beta_{\text{Cd,ClO}_4}^{(0)} = 0.3899$, $\beta_{\text{Cd,ClO}_4}^{(1)} = 1.996$, $C_{\text{Cd,ClO}_4}^\Phi = 0.0208$ [88KIM/FRE], $\beta_{\text{Na,NO}_2}^{(0)} = 0.0641$, $\beta_{\text{Na,NO}_2}^{(1)} = 0.1015$, $C^\Phi = -0.0049$ [91PIT]. No values of binary and ternary mixing terms for these ion combinations are available, so they were assumed to be zero. The task is to determine the values of the Pitzer parameters for the $\text{CdNO}_2^+\text{-ClO}_4^-$ interaction, $\beta_{\text{CdNO}_2,\text{ClO}_4}^{(0)}$ and $\beta_{\text{CdNO}_2,\text{ClO}_4}^{(1)}$, and $\log_{10} K^\circ$ using a regression analysis.

First we used the regression in an attempt to determine all the required parameters from the existing $\log_{10} K$ data set. The results are: $\log_{10} K^\circ = 2.3 \pm 3.0$, $\beta_{\text{CdNO}_2,\text{ClO}_4}^{(0)} = 0.21 \pm 0.82$, $\beta_{\text{CdNO}_2,\text{ClO}_4}^{(1)} = -0.2 \pm 13.6$. All uncertainties are given here as 3σ . These very large uncertainties are typical when making a data evaluation using a Pitzer model from

Table IX.10: Equilibrium constants for reaction $\text{Cd}^{2+} + \text{NO}_2^- \rightleftharpoons \text{CdNO}_2^+$ in NaClO_4 solutions at 298.15 K.

$\frac{m}{\text{mol}\cdot\text{kg}^{-1}} \text{NaClO}_4$	$\log_{10} K$
1.05	1.68 ± 0.10
1.05	1.80 ± 0.10
2.21	1.74 ± 0.10
2.80	1.91 ± 0.10
2.80	1.74 ± 0.10
3.50	1.99 ± 0.10
3.50	1.73 ± 0.10

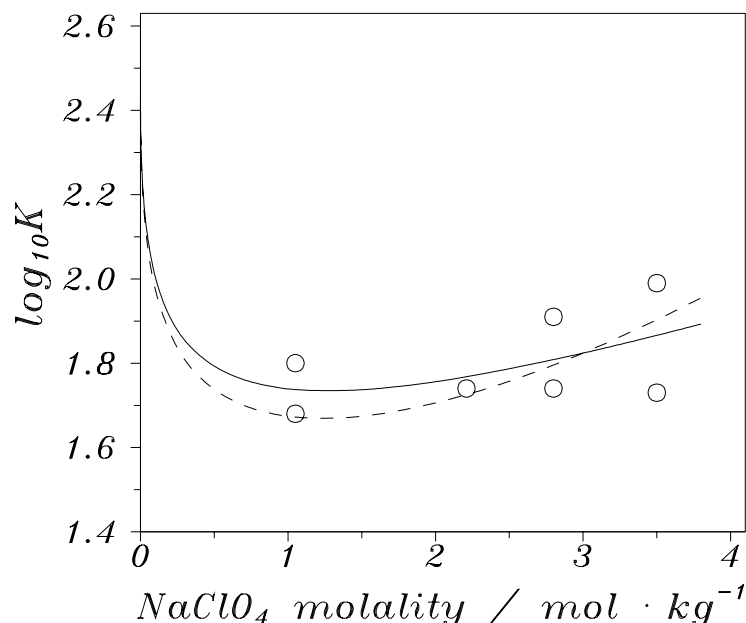
a limited number of experimental points of low accuracy. It is obvious that the data do not allow an accurate determination of the parameters. Therefore, we used the regression with a fixed value of $\log_{10} K^\circ$ as it was obtained in the SIT-type of data treatment, *i.e.*, $\log_{10} K^\circ = 2.43 \pm 0.33$. The resulting Pitzer parameters are: $\beta_{\text{CdNO}_2, \text{ClO}_4}^{(0)} = 0.19 \pm 0.23$, $\beta_{\text{CdNO}_2, \text{ClO}_4}^{(1)} = 0.2 \pm 1.5$ (3σ). Finally, we used the procedure recommended above. As the reaction under consideration involves only ions with the charges 1 and 2, we can estimate the value of $X_2 = \Delta\beta^{(1)}$ from $\Delta(Z^2) = -4$ and obtain $X_2 = (0.337 \pm 0.014) \times \Delta(Z^2) \approx -1.35$. As the values of $\beta^{(1)}$ for the single ions are available, we can estimate the value of the Pitzer parameter $\beta_{\text{CdNO}_2, \text{ClO}_4}^{(1)} = -1.35 + 1.996 + 0.102 \approx 0.75$. This value seems to be rather high for 1-1 ions but it does not contradict the estimate 0.2 ± 1.5 , obtained above. Using $\log_{10} K^\circ$ and $\beta_{\text{CdNO}_2, \text{ClO}_4}^{(1)} = 0.75$ as fixed parameters, we obtained from the regression $\beta_{\text{CdNO}_2, \text{ClO}_4}^{(0)} = 0.11 \pm 0.05$ (3σ). This quantity can also be estimated from the correlation between $\Delta\varepsilon$ and X_1 for the reaction, $(X_1 - \Delta\varepsilon_\gamma/2)/\Delta(Z^2) = (0.029 \pm 0.005)$. We find: $X_1 = (-4) \times [(0.029 \pm 0.005) + \ln(10) \times (-0.13 \pm 0.13)/2] \approx -0.27 \pm 0.15$. For this reaction $X_1 = \beta_{\text{CdNO}_2, \text{ClO}_4}^{(0)} - \beta_{\text{Cd}, \text{ClO}_4}^{(0)} - \beta_{\text{Na}, \text{NO}_2}^{(0)}$, hence, the estimated value from the correlation is $\beta_{\text{CdNO}_2, \text{ClO}_4}^{(0)} \approx -0.27 \pm 0.15 + 0.39 + 0.06 = 0.18 \pm 0.15$, which is rather close to $\beta_{\text{CdNO}_2, \text{ClO}_4}^{(0)} = 0.11 \pm 0.05$. We recommend the use of the regression procedure to get more accurate values of the $\beta^{(0)}$ parameters.

The experimental $\log_{10} K$ data and those obtained using the SIT (solid line) and the simplified Pitzer (dashed line) models are shown in Figure IX.28.

Example 11:

The reaction $\text{Fe}^{3+} + \text{Cl}^- \rightleftharpoons \text{FeCl}^{2+}$ has been studied in $\text{HClO}_4/\text{NaClO}_4$ media over a

Figure IX.28: The comparison of the experimental (circles) and the calculated values of the $\log_{10} K$ obtained using the SIT (solid line) and the simplified Pitzer (dashed line) models for the reaction $\text{Cd}^{2+} + \text{NO}_2^- \rightleftharpoons \text{CdNO}_2^+$ in NaClO_4 solutions at 298.15 K and 1 atm (see text for details).



wide concentration range. The experimental results in pure HClO_4 , quoted from “Stability Constants” [64SIL/MAR, 71SIL/MAR, 82HOG], recalculated to molality units and to 298.15 K where necessary, are given in Table IX.11. The results obtained at ionic strength above 6 M ($8.13 \text{ mol} \cdot \text{kg}^{-1}$) HClO_4 have not been included in the Table.

The example considered is exceptional: in all there are 25 experimental $\log_{10} K$ values from 9 independent laboratories, obtained using spectrophotometric, potentiometric or distribution methods. All the data are in good agreement with each other, and the estimated uncertainties of the experimental $\log_{10} K$ points seem to be within ± 0.05 - $0.08 \log_{10}$ units. Using the SIT-type of data treatment the following values of the parameters have been obtained by the least-square method: $\log_{10} K^\circ = 1.55 \pm 0.10$, $\Delta\epsilon = -0.241 \pm 0.023 \text{ kg} \cdot \text{mol}^{-1}$ (all errors are given as 3σ). The results of the regression in comparison with the experimental data are shown in Figure IX.29 (solid line).

Accurate values of the Pitzer parameters for the Fe^{3+} - ClO_4^- interaction are unknown (only preliminary estimations can be made, see Example 8). Hence, we can only determine the Pitzer parameters for the reaction. First we tried to determine all the relevant parameters ($\log_{10} K^\circ$, X_1 , X_2 , X_3) from the regression; the obtained results are: $\log_{10} K^\circ = 1.66 \pm 0.38$, $X_1 = -0.62 \pm 0.27$, $X_2 = -3.64 \pm 2.36$, $X_3 = +0.01 \pm 0.10$; the errors are given as 3σ . Although there are a large number of experimental points (25) of good accuracy ($< 0.08 \log_{10}$ unit), the result of the regression is very uncertain. Another point to

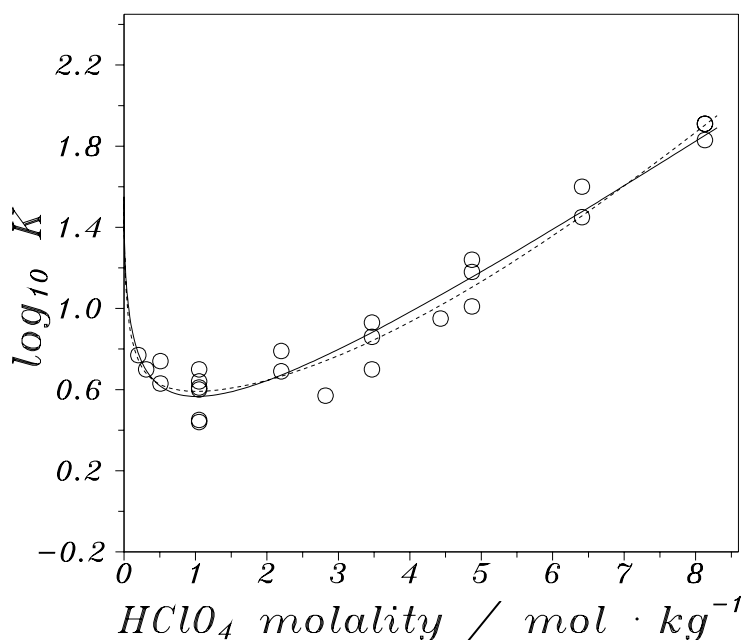
Table IX.11: Equilibrium constants for reaction $\text{Fe}^{3+} + \text{Cl}^- \rightleftharpoons \text{FeCl}^{2+}$ in HClO_4 solutions.

$\frac{m}{\text{mol} \cdot \text{kg}^{-1}}$	$\log_{10} K(m)$	$\frac{m}{\text{mol} \cdot \text{kg}^{-1}}$	$\log_{10} K(m)$
0.20	0.77	3.47	0.70
0.31	0.70	3.47	0.86
0.51	0.63	3.47	0.93
0.51	0.74	4.43	0.95
1.05	0.60	4.87	1.01
1.05	0.70	4.87	1.24
1.05	0.64	4.87	1.18
1.05	0.61	6.41	1.60
1.05	0.44	6.41	1.45
1.05	0.45	8.13	1.83
2.20	0.79	8.13	1.91
2.20	0.69	8.13	1.91
2.82	0.57		

be noticed is that despite the large range of HClO_4 concentrations covered in experiments ($0.2\text{--}8 \text{ mol} \cdot \text{kg}^{-1}$), the X_3 parameter is statistically insignificant. In a second attempt we tried to determine all parameters, except X_3 and obtained $\log_{10} K^\circ = 1.60 \pm 0.27$, $X_1 = -0.56 \pm 0.05$, $X_2 = -4.14 \pm 1.14$. Finally we applied the procedure discussed in the previous examples for the determination of the Pitzer parameters for the reaction using the value of $\log_{10} K^\circ$, obtained from the SIT-type of data treatment as a fixed parameter. The parameters X_1 and X_2 were then determined by regression. The final set of the Pitzer parameters is: $X_1 = -0.55 \pm 0.04$, $X_2 = -4.34 \pm 0.40$. The result of the simplified Pitzer-type of regression is shown in comparison with experimental data in Figure IX.29 (dashed line). This example shows that the contribution of ternary terms (X_3) are relatively small in this case, and can be neglected even at very high ionic medium concentrations.

It is interesting to test the ability of the SIT and the Pitzer model (with the simplifications outlined above) to predict the $\log_{10} K$ for the reaction $\text{Fe}^{3+} + \text{Cl}^- \rightleftharpoons \text{FeCl}^{2+}$ in different perchlorate media. The concentration quotient ($\log_{10} K$) is a function of the ionic medium composition, as indicated by the experimental data in $(\text{Na,H})\text{ClO}_4$ mixtures as given in [63HEI/CLE]. We have used both the SIT and the Pitzer models, to predict the changes of the equilibrium constant as a function of the composition of the ionic medium. Using the SIT model we obtain the following statement for $\log_{10} K$ of the reaction in a medium of constant total ionic strength and constant total perchlorate-ion concentration,

Figure IX.29: The comparison of experimental (circles) and calculated values of $\log_{10} K$ for the reaction $\text{Fe}^{3+} + \text{Cl}^- \rightleftharpoons \text{FeCl}^{2+}$ in HClO_4 medium at 298.15 K and 1 atm (see text for details) using the SIT (solid line) or the simplified Pitzer (dashed line).



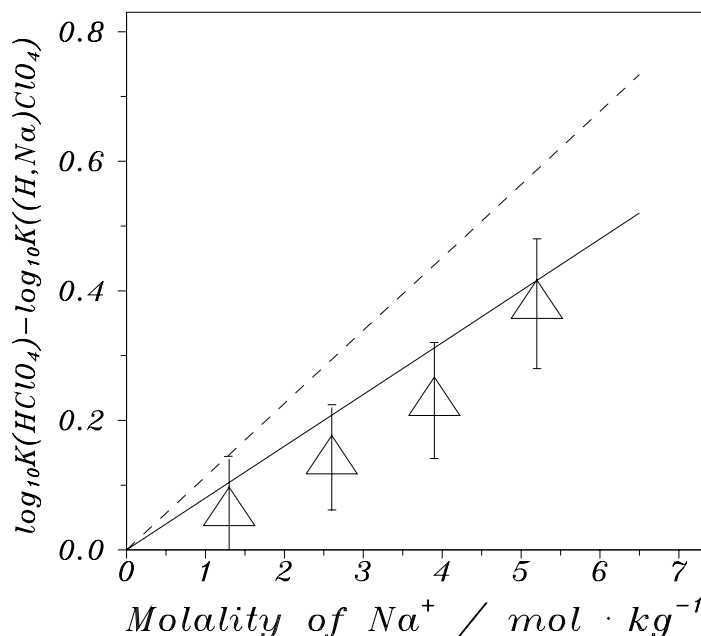
but with varying H^+ and Na^+ concentrations:

$$\log_{10} K_{(\text{HClO}_4)} - \log_{10} K_{((\text{Na},\text{H})\text{ClO}_4)} = [\varepsilon(\text{H}^+, \text{Cl}^-) - \varepsilon(\text{Na}^+, \text{Cl}^-)] m_{\text{Na}^+}$$

This simple relation is consistent with Harned's rule [58HAR/OWE], which postulates a linear dependence of the logarithm of the activity coefficient of a solute on the molality of the second electrolyte in mixtures of constant total ionic strength. The calculated values of the difference in $\log_{10} K$ when replacing H^+ for Na^+ at constant ionic strength $6.5 \text{ mol} \cdot \text{kg}^{-1}$ are shown in Figure IX.30 (the solid line) in comparison with the experimental values (the triangles, with uncertainty estimates) from [63HEI/CLE]. The following SIT interaction coefficients were used: $\varepsilon(\text{H}^+, \text{Cl}^-) = 0.12 \pm 0.01 \text{ kg} \cdot \text{mol}^{-1}$, $\varepsilon(\text{Na}^+, \text{Cl}^-) = 0.04 \pm 0.01 \text{ kg} \cdot \text{mol}^{-1}$. The quantitative agreement between experimental and predicted data is apparent in Figure IX.30.

On the basis of the Pitzer model the following equation is obtained (neglecting the ternary interaction parameters for the reaction participants):

Figure IX.30: The comparison of the experimental and predicted values of the difference in $\log_{10} K$ values for the reaction $\text{Fe}^{3+} + \text{Cl}^- \rightleftharpoons \text{FeCl}^{2+}$ in pure HClO_4 and mixed HClO_4 - NaClO_4 media at 298.15 K and 1 atm. Triangles are the experimental results from [63HEI/CLE]; the solid line - the prediction based on the SIT model; the dashed line - the prediction based on the Pitzer model.



$$\begin{aligned}
 \ln K_{(\text{HClO}_4)} - \ln K_{((\text{H,Na})\text{ClO}_4)} &= \Delta(Z^2)m_{\text{Na}}m \left(B'_{\text{Na,ClO}_4} - B'_{\text{H,ClO}_4} \right) \\
 &+ \Delta|Z|m_{\text{Na}}m \left(C_{\text{Na,ClO}_4} - C_{\text{H,ClO}_4} \right) \\
 &- 2m_{\text{Na}}m \left[\beta_{\text{Na,Cl}}^{(0)} - \beta_{\text{H,Cl}}^{(0)} \left(\beta_{\text{Na,Cl}}^{(1)} - \beta_{\text{H,Cl}}^{(1)} \right) g(I_m) \right] \\
 &+ 2m_{\text{Na}} \left(\phi_{\text{Fe,H}} - \phi_{\text{Fe,Na}} - \phi_{\text{FeCl,H}} - \phi_{\text{FeCl,Na}} \right)
 \end{aligned}$$

where m refers to the total molality of the ionic medium (or perchlorate ion concentration), m_{Na} stands for the molality of Na^+ in mixture. The numerical values of binary mixing terms for the interactions Fe^{3+} - H^+ , Fe^{3+} - Na^+ , FeCl^{2+} - Na^+ , FeCl^{2+} - H^+ are unknown. The numerical values of the other relevant Pitzer parameters were taken from [91PIT]. The calculated differences in $\log_{10} K$ from this equation are also shown in Figure IX.30 by a dashed line. The agreement is qualitative, due to lack of all parameters needed in the model. This situation is not unusual, if not all the needed parameters of the Pitzer model are available, then the accuracy of predictions of $\log_{10} K$ data using this approach may be no better than those obtained from the simpler SIT model. By fitting the unknown interaction parameters to the data one will obtain a much better agreement with the Pitzer model. This requires many additional experiments of high precision.

Example 12:

The example refers to the reaction $\text{Cd}^{2+} + \text{Cl}^- \rightleftharpoons \text{CdCl}^+$, studied in different perchlorate media. The experimental results, quoted from “Stability constants” compilations [64SIL/MAR, 71SIL/MAR, 82HOG] and more recent studies [75FED/CHE, 75KUT/LES, 83GRA/SJO, 84PRO/EIN, 85PRO/BEL], and recalculated into molality units and to 298.15 K where necessary, are given in Table IX.12. Only data in NaClO_4 , LiClO_4 and $\text{Mg}(\text{ClO}_4)_2$ media, where most of the experimental determinations have been made, are included.

The data have been obtained in different laboratories using different experimental methods and different perchlorate media. How can we check the compatibility of the different sets of data ?

Using the SIT-type of data treatment, we obtain the following statement for the reaction in perchlorate media

$$\begin{aligned} \log_{10} K^\circ &= \log_{10} K + 4D + \varepsilon(\text{CdCl}^+, \text{ClO}_4^-)m_{\text{ClO}_4^-} - \varepsilon(\text{Cd}^{2+}, \text{ClO}_4^-)m_{\text{ClO}_4^-} \\ &\quad - \varepsilon(\text{N}^{n+}, \text{Cl}^-)m_{\text{N}^{n+}} \end{aligned}$$

Only the terms $\log_{10} K^\circ$ and $\varepsilon(\text{CdCl}^+, \text{ClO}_4^-)$ are unknown (we have not used the value of $\varepsilon(\text{CdCl}^+, \text{ClO}_4^-)$ proposed by Ciavatta [80CIA] because this is based on a smaller data set). It is convenient to define a function Y as follows

$$\begin{aligned} Y &= \log_{10} K + 4D - \varepsilon(\text{Cd}^{2+}, \text{ClO}_4^-)m_{\text{ClO}_4^-} - \varepsilon(\text{N}^{n+}, \text{Cl}^-)m_{\text{N}^{n+}} \\ &= \log_{10} K^\circ - \varepsilon(\text{CdCl}^+, \text{ClO}_4^-)m_{\text{ClO}_4^-} \end{aligned}$$

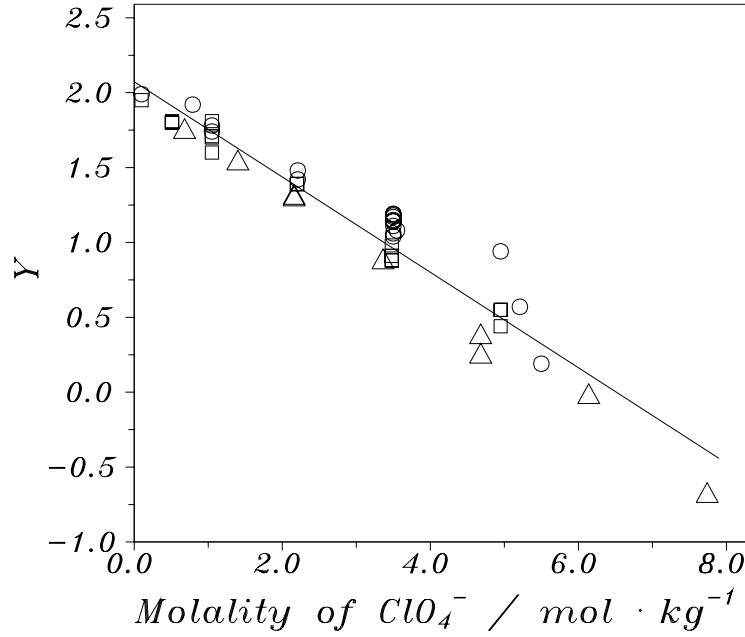
According to this equation, the function Y must be represented by a straight line with a slope equal to $-\varepsilon(\text{CdCl}^+, \text{ClO}_4^-)$ and an intercept equal to $\log_{10} K^\circ$. In Figure IX.31 we have plotted the values of Y calculated from $\log_{10} K$ in different perchlorate media using auxiliary SIT coefficients $\varepsilon(\text{Cd}^{2+}, \text{ClO}_4^-) = (0.34 \pm 0.04) \text{ kg} \cdot \text{mol}^{-1}$, $\varepsilon(\text{Na}^+, \text{Cl}^-) = (0.04 \pm 0.01) \text{ kg} \cdot \text{mol}^{-1}$, $\varepsilon(\text{Li}^+, \text{Cl}^-) = (0.10 \pm 0.01) \text{ kg} \cdot \text{mol}^{-1}$, $\varepsilon(\text{Mg}^{2+}, \text{Cl}^-) = (0.19 \pm 0.02) \text{ kg} \cdot \text{mol}^{-1}$. All values of Y have been treated together. The results of the least-square regression are: $\log_{10} K^\circ = 2.07 \pm 0.11$, $\varepsilon(\text{CdCl}^+, \text{ClO}_4^-) = (0.318 \pm 0.033) \text{ kg} \cdot \text{mol}^{-1}$, the errors are given as 3σ . This value differs from the one reported by Ciavatta [80CIA], namely $\varepsilon(\text{CdCl}^+, \text{ClO}_4^-) = 0.25 \pm 0.02$, which was based on data for NaClO_4 solutions only. In the majority of cases the deviations between the “experimental” and calculated values of Y do not exceed $0.2 \log_{10}$ units, which is consistent with the estimated uncertainty in the experimental $\log_{10} K$ values. This means that the data obtained in different perchlorate media are consistent. This result indicates that the specific effects of the ionic media, which are not taken into account in the SIT approximation (triple ion-ion interactions, mixing terms, *etc.*) are expected to be of the same order of magnitude as the estimated accuracy of $\log_{10} K$ data. Hence, they are not statistically significant, and their determination requires much more accurate $\log_{10} K$ data.

The data treatment based on the Pitzer approach is discussed, taking into account only the binary interaction terms for the complex CdCl^+ . The equation for the concentration

Table IX.12: Equilibrium constants for reaction $\text{Cd}^{2+} + \text{Cl}^- \rightleftharpoons \text{CdCl}^+$ in NaClO_4 , LiClO_4 and $\text{Mg}(\text{ClO}_4)_2$ media.

Medium	m (mol · kg ⁻¹)	$\log_{10} K(m)$	Medium	m (mol · kg ⁻¹)	$\log_{10} K(m)$
NaClO_4	0.10	1.59	NaClO_4	3.50	1.51
	0.79	1.44		3.50	1.39
	1.05	1.32		3.50	1.50
	1.05	1.36		3.50	1.44
	2.21	1.38		3.50	1.52
	2.21	1.32		3.50	1.48
	3.50	1.52		3.55	1.42
	3.50	1.37		4.95	1.77
	3.50	1.47		5.21	1.50
	3.50	1.47		5.50	1.22
LiClO_4	0.10	1.45	LiClO_4	2.20	1.42
	0.51	1.32		2.20	1.42
	0.51	1.33		3.48	1.41
	0.51	1.32		3.48	1.44
	0.51	1.32		3.48	1.51
	1.05	1.35		3.48	1.41
	1.05	1.35		3.48	1.44
	1.05	1.24		4.91	1.68
	1.05	1.34		4.91	1.57
	2.20	1.42		4.91	1.68
	2.20	1.42			
$\text{Mg}(\text{ClO}_4)_2$	0.34	1.24	$\text{Mg}(\text{ClO}_4)_2$	2.34	1.21
	0.70	1.23		2.34	1.34
	1.08	1.27		3.07	1.55
	1.08	1.26		3.87	1.56
	1.68	1.30			

Figure IX.31: The values of function Y (see text for details) calculated from the $\log_{10} K$ data for the reaction $\text{Cd}^{2+} + \text{Cl}^- \rightleftharpoons \text{CdCl}^+$ in NaClO_4 (circles), LiClO_4 (squares) and $\text{Mg}(\text{ClO}_4)_2$ (triangles) media at 298.15 K and 1 atm based on the SIT model.



dependence of $\log_{10} K$ for the reaction is

$$\ln K^\circ = \ln K + \ln \gamma_{\text{CdCl}^+} - \ln \gamma_{\text{Cd}^{2+}} - \ln \gamma_{\text{Cl}^-}$$

The equations for the concentration dependence of the activity coefficient of Cd^{2+} , Cl^- , CdCl^+ in perchlorate media $\text{M}^{n+}(\text{ClO}_4)_n$ are given below:

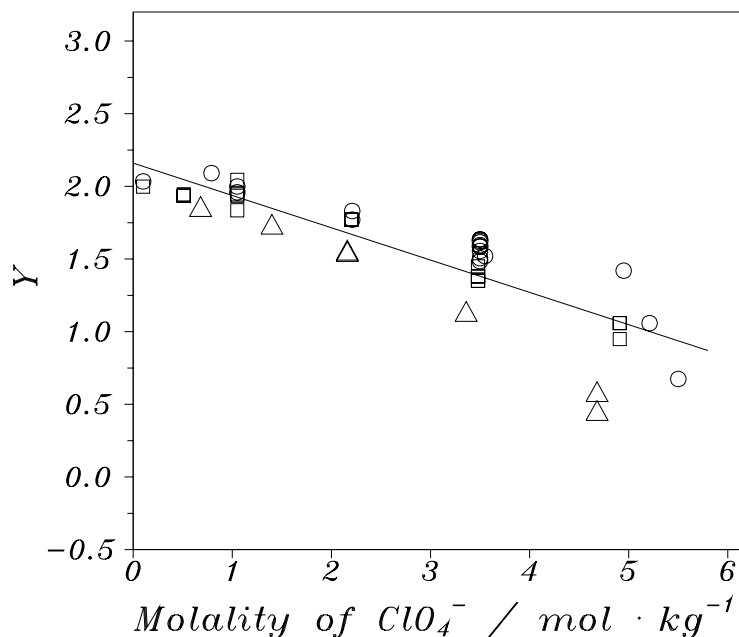
$$\begin{aligned} \ln \gamma_{\text{Cd}^{2+}} = & f^\gamma + m n \left[2\beta_{\text{Cd},\text{ClO}_4}^{(0)} + 2\beta_{\text{Cd},\text{ClO}_4}^{(1)} g(I_m) \right] + 2m^2 n^2 C_{\text{Cd},\text{ClO}_4} \\ & + 2m \phi_{\text{Cd},\text{M}} + m^2 n \psi_{\text{Cd},\text{M},\text{ClO}_4} + 2m^2 n C_{\text{M},\text{ClO}_4} \end{aligned}$$

$$\begin{aligned} \ln \gamma_{\text{Cl}^-} = & f^\gamma + m \left[2\beta_{\text{M},\text{Cl}}^{(0)} + 2\beta_{\text{M},\text{Cl}}^{(1)} g(I_m) \right] + 2m^2 n C_{\text{M},\text{Cl}} \\ & + 2m n \phi_{\text{Cl},\text{ClO}_4} + m^2 n \psi_{\text{Cl},\text{ClO}_4,\text{M}} + m^2 n C_{\text{M},\text{ClO}_4} \end{aligned}$$

$$\begin{aligned} \ln \gamma_{\text{CdCl}^+} = & f^\gamma + m n \left[2\beta_{\text{CdCl},\text{ClO}_4}^{(0)} + 2\beta_{\text{CdCl},\text{ClO}_4}^{(1)} g(I_m) \right] \\ & + 2m \phi_{\text{CdCl},\text{M}} + m^2 n C_{\text{M},\text{ClO}_4} \end{aligned}$$

where n reflects the charge type of the ionic medium ($n = 1$ for NaClO_4 and LiClO_4 , $n = 2$ for $\text{Mg}(\text{ClO}_4)_2$), m is the molality of the ionic medium, all other symbols have been defined before. The binary mixing parameter $\phi_{\text{Cd},\text{M}}$ is ionic strength dependent if $\text{M} = \text{Na}$

Figure IX.32: The values of function Y (see text for details) calculated from the $\log_{10} K$ data for the reaction $\text{Cd}^{2+} + \text{Cl}^- \rightleftharpoons \text{CdCl}^+$ in NaClO_4 (circles), LiClO_4 (squares) and $\text{Mg}(\text{ClO}_4)_2$ (triangles) media at 298.15 K and 1 atm based on the Pitzer model.



or Li, and $\phi_{\text{CdCl},\text{M}}$ if $\text{M} = \text{Mg}$. For further simplification the parameter $\beta_{\text{CdCl},\text{ClO}_4}^{(1)} = 0.9$ was estimated from the $\Delta(Z^2)$ value for the reaction and known values of the $\beta^{(1)}$ for other reaction participants in NaClO_4 and LiClO_4 media (note that the proposed correlation between $\Delta(Z^2)$ and $X_2 = \Delta\beta^{(1)}$ is valid only for the supporting electrolyte of 1-1 type). Now we can define the function Y

$$\begin{aligned} Y &= \log_{10} K - [\ln \gamma_{\text{Cd}^{2+}} + \ln \gamma_{\text{Cl}^-} - f^\gamma - 2m n \beta_{\text{CdCl},\text{ClO}_4} g(I_m) \\ &\quad - m^2 n C_{\text{M},\text{ClO}_4}] / \ln(10) \\ &= \log_{10} K^\circ - 2m n \left[\beta_{\text{CdCl},\text{ClO}_4}^{(0)} + \frac{1}{n} \phi_{\text{CdCl},\text{M}} \right] / \ln(10) \end{aligned}$$

The function Y calculated from $\log_{10} K$ data in different perchlorate media is shown in Figure IX.32, the values of the $\beta^{(0)}$ and $\beta^{(1)}$ for $\text{Cd}^{2+}\text{-ClO}_4^-$ interaction are taken from [88KIM/FRE], and other Pitzer parameters are quoted from [91PIT]. Neither the relevant binary mixing parameters $\phi_{\text{Cd,Li}}$, $\phi_{\text{Cd,Na}}$, $\phi_{\text{Cd,Mg}}$, $\phi_{\text{Cl,ClO}_4}$, nor the ternary mixing parameter are available. As the Pitzer parameters reported are valid up to ionic strength 6 $\text{mol} \cdot \text{kg}^{-1}$, only the results obtained at lower ionic strength were considered. As expected, the data scatter considerably, and the Y values referring to the $\text{Mg}(\text{ClO}_4)_2$ ionic

medium, shown by triangles, deviate from the points in LiClO_4 (squares) and NaClO_4 (circles) media. There are several possible explanations for these deviations, *e.g.*, the contribution from the $\phi_{\text{Cd,M}}$ and $\phi_{\text{CdCl,M}}$ terms. This issue cannot be resolved due to lack of experimental values of $\phi_{\text{Cd,M}}$. Nevertheless, we used the linear regression of all the data to obtain $\log_{10} K^\circ = 2.16 \pm 0.17$ as intercept and -0.25 ± 0.06 as the slope of the resulting linear plot (see Figure IX.32). The value of $\log_{10} K^\circ$ is, within the estimated uncertainty, in agreement with the value from the SIT-type of data treatment.

Before using experimental concentration equilibrium constants for the determination of $\log_{10} K^\circ$ and the various interaction parameters one must be aware of the following:

- The experimental concentration constants have been determined on the assumption that the activity coefficients of reactants/products are constant at a constant ionic strength. This may not be the case if a sufficiently large part of the ionic medium has been replaced by the reactants/products. As a result one may have introduced a systematic error in the equilibrium constants, but rarely with the chemical model. These errors will then be propagated in the determination of $\log_{10} K^\circ$ and the interaction parameters. The magnitude of the systematic error will be ionic strength dependent.
- The presence of other types of systematic errors, related to the method of investigation, are difficult to spot unless different experimental methods are used.

These factors result in an accuracy of most published equilibrium constants that is much lower than the claimed uncertainty of the results, which in general describe the precision of the experiment. With this in mind, one will often find that even the SIT model provides reasonably good estimates of the concentration/ionic medium dependence of most equilibrium constants, especially for complex systems such as the ones encountered in nature. We can conclude that the simple SIT approach, which uses only one parameter for each ion-counter ion, ion-neutral, and neutral-neutral interaction, results in a reliable value of the equilibrium constant at infinite dilution, and an adequate reproduction of $\log_{10} K$ data for complex formation equilibria as a function of both the ionic strength and the ionic composition of the medium. The “intrinsic error” in the SIT model, due to the approximations used is less than 5-10 per cent for the mean activity coefficients of completely dissociated electrolytes, even at ionic strengths as high as $6\text{-}10 \text{ mol} \cdot \text{kg}^{-1}$. Hence, the expected “intrinsic” error (which will depend on the number of reactants/products in the equilibrium expression) in the reproduction of the $\log_{10} K$ data is less than $0.10 \log_{10}$ units for reactions involving two reactants and one product. The agreement of the experimental $\log_{10} K$ data obtained in independent laboratories using different methods is seldom better than $0.1 (\log_{10}\text{-unit})$, for complex formation reactions. As discussed by Beck and Nagypal [90BEC/NAG], the errors claimed by authors usually reflect the reproducibility of $\log_{10} K$ values from the experimental data set for the particular experimental method used, and the particular chemical model of the system under study.

IX.9. The use of the SIT at elevated temperatures

In order to describe the concentration behavior of $\log_{10} K$ at elevated temperatures and pressures it is necessary to have information on the temperature and pressure dependence of the interaction parameters (either the Pitzer, or the SIT parameters). The equations involving temperature and pressure derivatives of the chemical potential of the solute on the basis of the Pitzer model are published [91PIT]. Below we give the corresponding equations for the SIT model.

IX.9.1. Osmotic coefficient

The following formulae are all based on the application of standard thermodynamic relations to the SIT expression for the activity coefficient (Eq. (IX.4)) of the dissolved species in an aqueous system. The reader is referred to [58HAR/OWE, 61LEW/RAN] for additional details.

The mean activity coefficient of single electrolytes is equal to

$$\ln \gamma_{\pm} = -\frac{A_{\gamma}|Z_+Z_-|\sqrt{I_m}}{t} + \frac{2\nu_+\nu_-}{\nu} \varepsilon_{\gamma} m \quad (\text{IX.35})$$

where

$$I_m = \frac{m}{2} (\nu_+ Z_+^2 + \nu_- Z_-^2)$$

$$t = 1 + 1.5\sqrt{I_m} \quad (\text{IX.36})$$

all other symbols have been explained before.

Using the definition of the osmotic coefficient Φ for a single electrolyte [58HAR/OWE] we obtain:

$$\Phi = 1 - \frac{A_{\gamma}|Z_+Z_-|}{1.5^3 I_m} \left(t - 2 \ln t - \frac{1}{t} \right) + \frac{\nu_+\nu_-}{\nu} \varepsilon_{\gamma} m \quad (\text{IX.37})$$

Equilibria involving $\text{H}_2\text{O}(l)$ as a reactant or product require a correction for the activity of water, $a_{\text{H}_2\text{O}}$. In an electrolyte mixture this can be calculated from Φ , by using Eqs. (IX.33), (IX.35), or from the experimentally determined osmotic coefficient of the mixture :

$$\ln a_{\text{H}_2\text{O}} = -\frac{\Phi \sum_k m_k}{55.5084} \quad (\text{IX.38})$$

The summation extends over all solutes k with molality m_k present in the solution. The SIT model, with the analytical statement for the activity coefficients for the dissolved species (ions and neutral species), can be used to obtain an analytical statement for the osmotic coefficients of the solution. The deduction which uses the Gibbs-Duhem equation is straightforward and results in the following expression (the subscripts c and a refer

to cations and anions in general, n_i and n_j denote the different kinds of neutral species, subscript k refer to any species):

$$\begin{aligned} \Phi - 1 = & -\frac{2A_\gamma}{1.5^3} \frac{\left(t - 2 \ln t - \frac{1}{t}\right)}{\sum_k m_k} + \frac{1}{\sum_k m_k} \left[\sum_c \sum_a \varepsilon_\gamma(c, a) m_a m_c \right. \\ & + \sum_c \sum_n \varepsilon_\gamma(c, n) m_c m_n + \sum_a \sum_n \varepsilon_\gamma(a, n) m_a m_n \\ & \left. + \frac{1}{2} \sum_{n_i} \sum_{n_j} \varepsilon_\gamma(n_i, n_j) m_{n_i} m_{n_j} \right] \end{aligned} \quad (\text{IX.39})$$

If no uncharged species are present the last three terms are zero and the expression for the osmotic coefficient is then very close to the expression given by Pitzer and Brewer [61LEW/RAN, their Eq. (23-39)].

IX.9.2. The analytical statements for partial and apparent molar properties of single electrolytes on the basis of the SIT model

The equation presented below have been derived using the approximation that the quantity $a_j B = 1.5$ is independent of temperature and pressure.

1. The relative partial molar enthalpy is defined as [58HAR/OWE]:

$$L_2 = H_2 - H_2^\circ = -\nu RT^2 \left(\frac{\partial \ln \gamma_\pm}{\partial T} \right)_P \quad (\text{IX.40})$$

where H_2 and H_2° are the partial molar enthalpies in a given solution and at infinite dilution, respectively. Only the relative value, L_2 , can be determined from experimental measurements. We have:

$$L_2 = \frac{3}{4} \nu \frac{A_L |Z_+ Z_-| \sqrt{I_m}}{t} - 2 \nu_+ \nu_- RT^2 \varepsilon_L m \quad (\text{IX.41})$$

where

$$\varepsilon_L = \left(\frac{\partial \varepsilon_\gamma}{\partial T} \right)_P \quad (\text{IX.42})$$

A_L is a Debye-Hückel slope defined in Section IX.9.3. Using the general relation between partial and apparent properties

$$\Xi_2 = \frac{\partial}{\partial n_2} \left({}^\phi \Xi n_2 \right)_{p,T} \quad (\text{IX.43})$$

where Ξ and ${}^\phi\Xi$ are partial and apparent properties respectively, and n_2 the solute concentration, we obtain the analytical statement for the concentration dependence of the relative apparent molar enthalpy ${}^\phi L$:

$$\begin{aligned} {}^\phi L &= \frac{3}{4} \nu \frac{A_L |Z_+ Z_-|}{1.5^3 I_m} (t^2 - 4t + 2 \ln t + 3) \\ &\quad - \nu_+ \nu_- RT^2 \varepsilon_L m \end{aligned} \quad (\text{IX.44})$$

2. The partial molar volume is defined as [58HAR/OWE]:

$$V_2 - V_2^\circ = \nu RT \left(\frac{\partial \ln \gamma_\pm}{\partial p} \right)_T \quad (\text{IX.45})$$

where V_2 and V_2° are partial molar volumes in a given solution and at infinite dilution, respectively. We have

$$V_2 - V_2^\circ = \frac{3}{4} \nu \frac{A_V |Z_+ Z_-| \sqrt{I_m}}{t} + 2 \nu_+ \nu_- RT \varepsilon_V m \quad (\text{IX.46})$$

where

$$\varepsilon_V = \left(\frac{\partial \varepsilon_\gamma}{\partial p} \right)_T \quad (\text{IX.47})$$

and we obtain the analytical statement for the concentration dependence of the apparent molar volume ${}^\phi V$

$$\begin{aligned} {}^\phi V - V_2^\circ &= \frac{3}{4} \nu \frac{A_V |Z_+ Z_-|}{1.5^3 I_m} (t^2 - 4t + 2 \ln t + 3) \\ &\quad + \nu_+ \nu_- RT \varepsilon_V m \end{aligned} \quad (\text{IX.48})$$

A_V is a Debye-Hückel slope defined in Section IX.9.3.

3. By definition [58HAR/OWE]

$$Cp_2 - Cp_2^\circ = \left(\frac{\partial L_2}{\partial T} \right)_P \quad (\text{IX.49})$$

where Cp_2 and Cp_2° are partial molar heat capacities in a given solution and at infinite dilution, respectively. Hence

$$Cp_2 - Cp_2^\circ = \frac{3}{4} \nu \frac{A_J |Z_+ Z_-| \sqrt{I_m}}{t} - 2 \nu_+ \nu_- RT^2 \varepsilon_J m \quad (\text{IX.50})$$

where

$$\varepsilon_J = \frac{2\varepsilon_L}{T} + \left(\frac{\partial\varepsilon_L}{\partial T}\right)_P = \frac{2}{T} \left(\frac{\partial\varepsilon_\gamma}{\partial T}\right)_P + \left(\frac{\partial^2\varepsilon_\gamma}{\partial T^2}\right)_P \quad (\text{IX.51})$$

The analytical statement for the concentration dependence of the molar apparent heat capacity ${}^\phi J$ (A_J is a Debye-Hückel slope, *cf.* Section IX.9.3) is:

$$\begin{aligned} {}^\phi J - Cp_2^\circ &= \frac{3}{4} \nu \frac{A_J |Z_+ Z_-|}{1.5^3 I_m} (t^2 - 4t + 2 \ln t + 3) \\ &\quad - \nu_+ \nu_- RT^2 \varepsilon_J m \end{aligned} \quad (\text{IX.52})$$

4. For the partial molar isothermal compressibility k_2 we use the definition

$$k_2 = \left(\frac{\partial V_2}{\partial p}\right)_T \quad (\text{IX.53})$$

Hence

$$k_2 - k_2^\circ = \frac{3}{4} \nu \frac{A_k |Z_+ Z_-| \sqrt{I_m}}{t} + 2 \nu_+ \nu_- RT \varepsilon_k m \quad (\text{IX.54})$$

where k_2° is the partial molar isothermal compressibility at infinite dilution, and

$$\varepsilon_k = \left(\frac{\partial\varepsilon_\nu}{\partial p}\right)_T = \left(\frac{\partial^2\varepsilon_\gamma}{\partial p^2}\right)_T \quad (\text{IX.55})$$

A_k is the Debye-Hückel limiting slope defined in Section IX.9.3. The concentration dependence of the apparent molar isothermal compressibility ${}^\phi k$ is given by

$$\begin{aligned} {}^\phi k - k_2^\circ &= \frac{3}{4} \nu \frac{A_k |Z_+ Z_-|}{1.5^3 I_m} (t^2 - 4t + 2 \ln t + 3) \\ &\quad + \nu_+ \nu_- RT \varepsilon_k m \end{aligned} \quad (\text{IX.56})$$

With the model assumptions made, we obtain very simple analytical expressions for the concentration dependence of partial and apparent molar properties of aqueous electrolytes as compared to more parametrized versions of extended Debye-Hückel equations (*e.g.*, Helgeson *et al.* [81HEL/KIR]).

IX.9.3. The Debye-Hückel limiting law slopes

We use the following definitions of the Debye-Hückel limiting law slopes [79BRA/PIT, 84ANA/ATK]:

For activity and osmotic coefficients:

$$A_\gamma = \frac{(2\pi N)^{1/2}}{(1000)^{1/2}} \frac{e^3}{k^{3/2}} \frac{\rho^{1/2}}{(\epsilon T)^{3/2}} \quad (\text{IX.57})$$

$$A_\Phi = \frac{A_\gamma}{3} \quad (\text{IX.58})$$

where N is the Avogadro number, e stands for absolute electronic charge, ϵ is here the dielectric constant of water, ρ is the pure water density, k is Boltzman constant, T is absolute temperature, K .

For partial and apparent molar relative enthalpies:

$$A_L = 4RT^2 \left(\frac{\partial A_\Phi}{\partial T} \right)_P = -2A_\gamma RT \left(1 + \frac{T}{\epsilon} \left(\frac{\partial \epsilon}{\partial T} \right)_P + \frac{T\alpha}{3} \right) \quad (\text{IX.59})$$

where R is gas constant, α is expansivity of pure water ($\alpha = (\partial \ln V / \partial T)_P$).

For partial and apparent molar volumes:

$$A_V = -4RT \left(\frac{\partial A_\Phi}{\partial p} \right)_T = 2A_\gamma RT \left(\frac{1}{\epsilon} \left(\frac{\partial \epsilon}{\partial p} \right)_T - \frac{\beta}{3} \right) \quad (\text{IX.60})$$

where β is compressibility of pure water ($\beta = -(\partial \ln V / \partial p)_T$).

For partial and apparent molar heat capacities:

$$\begin{aligned} A_J = \left(\frac{\partial A_H}{\partial T} \right)_P &= -2A_\gamma RT^2 \left(\frac{1}{\epsilon} \left(\frac{\partial^2 \epsilon}{\partial T^2} \right)_P - \frac{1}{\epsilon^2} \left(\frac{\partial \epsilon}{\partial T} \right)_P^2 - \frac{1}{T^2} + \frac{1}{3} \left(\frac{\partial \alpha}{\partial T} \right)_P \right) \\ &+ \frac{2A_L}{T} + \frac{3A_L^2}{4A_\gamma RT^2} \end{aligned} \quad (\text{IX.61})$$

For partial and apparent isothermal molar compressibilities:

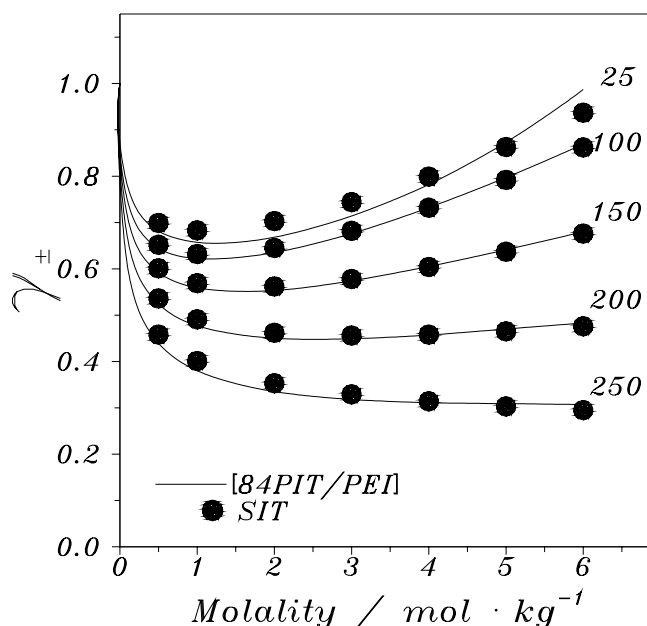
$$\begin{aligned} A_k = \left(\frac{\partial A_V}{\partial p} \right)_T &= 2A_\gamma RT \left(\frac{1}{\epsilon} \left(\frac{\partial^2 \epsilon}{\partial p^2} \right)_T - \frac{1}{\epsilon^2} \left(\frac{\partial \epsilon}{\partial p} \right)_T^2 - \frac{1}{3} \left(\frac{\partial \beta}{\partial p} \right)_T \right) \\ &- \frac{A_V}{2} \left(\frac{3}{\epsilon} \left(\frac{\partial \epsilon}{\partial p} \right)_T - \beta \right) \end{aligned} \quad (\text{IX.62})$$

When calculating the Debye-Hückel limiting law slopes we use the Haar-Gallagher-Kell equation of state for pure water [84KES/SEN] and the Archer-Wang [90ARC/WAN] equation for the dielectric constant of pure water.

Example 13:

The equations given above have been used to correlate the experimental data on activity coefficients, relative apparent molar enthalpies, apparent molar heat capacities and apparent molar volumes for NaCl at different temperatures at saturated water vapor pressure.

Figure IX.33: Comparison of experimental (solid line) and smoothed values of activity coefficients of aqueous NaCl solutions at saturated water vapor pressure on the basis of the SIT model. The numbers adjacent to the curves are Celsius temperatures.



See Figures IX.33, IX.34, IX.35 and IX.36 where the recent precise experimental data are shown by full-drawn lines and the values obtained from the SIT model are shown by the filled circles.

The accuracy of the fitting of the experimental data using the SIT model is far less than that obtained by using the three-parameter Pitzer model, which describes the thermodynamic properties of electrolyte solutions practically within the experimental errors in most cases. The one-parameter SIT approach should not be used for the treatment of experimental thermochemical data and data at different pressure, when information on the Pitzer parameters for the system is available. Nevertheless, the following points should be noticed:

- The SIT model provides a reasonably good description of data on the activity coefficients, relative apparent molar enthalpies, apparent molar heat capacities and apparent molar volumes of the NaCl aqueous solutions both at 298.15 K and elevated temperatures;
- The SIT model works better at temperatures above 298.15 K, both for other 1-1 and 2-1 electrolytes, indicating that the “intrinsic” error of the model decreases with increasing temperature. Hence, we recommend the use of this approach for the description of the concentration dependence of the equilibrium constants at elevated temperatures, *cf.* Example 14.

Figure IX.34: Comparison of experimental (solid line) and smoothed values of relative apparent molar enthalpies, ϕ_L , of aqueous NaCl solutions at saturated water vapor pressure on the basis of the SIT model. The numbers adjacent to the curves are Celsius temperatures.

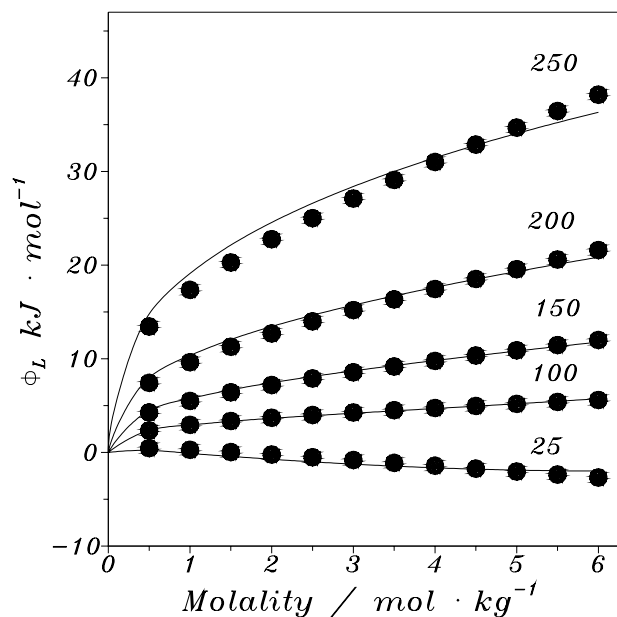


Figure IX.35: Comparison of experimental (solid line) and smoothed values of apparent molar volumes of aqueous NaCl solutions at saturated water vapor pressure on the basis of the SIT model. The numbers adjacent to the curves are Celsius temperatures.

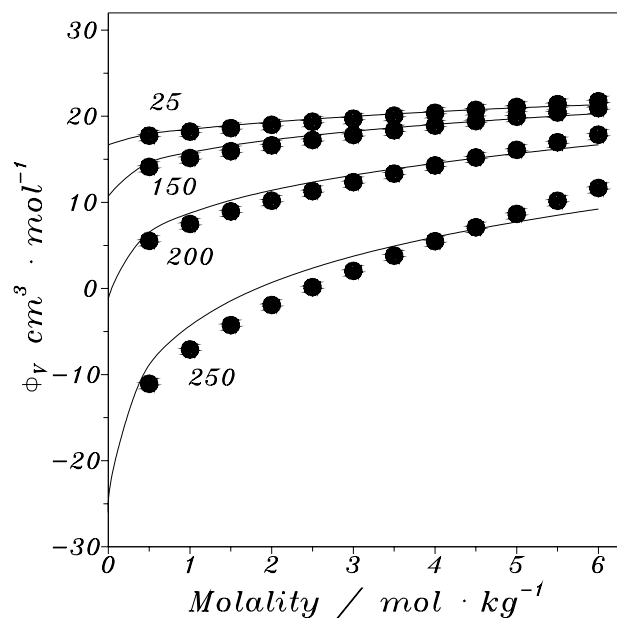
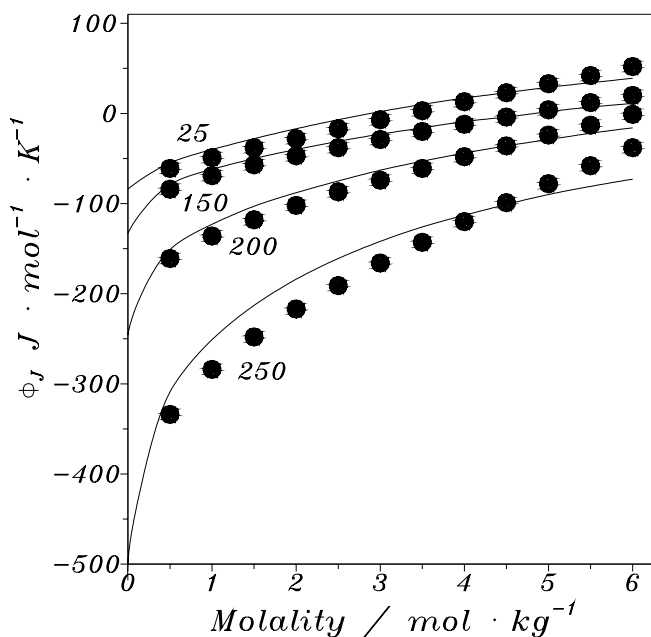
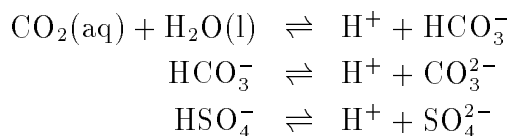


Figure IX.36: Comparison of experimental (solid line) and smoothed values of the apparent molar heat capacities of aqueous NaCl solutions at saturated water vapor pressure on the basis of the SIT model. The numbers adjacent to the curves are Celsius temperatures.



Example 14:

The main field of application of the SIT approach is the description of the ionic strength/ionic medium dependence of complex formation reactions. It was repeatedly shown [80CIA, 92GRE/FUG] that the SIT model results in fair reproduction of experimental results and a correct estimation of $\log_{10} K^\circ$ for data at 298.15 K. In this example we will check the applicability of this model to data obtained at elevated temperatures. The equilibrium constants for the following reactions have been studied experimentally by potentiometric method at different temperatures in NaCl ionic media [82PAT/SLO, 84PAT/BUS, 90DIC/WES]:



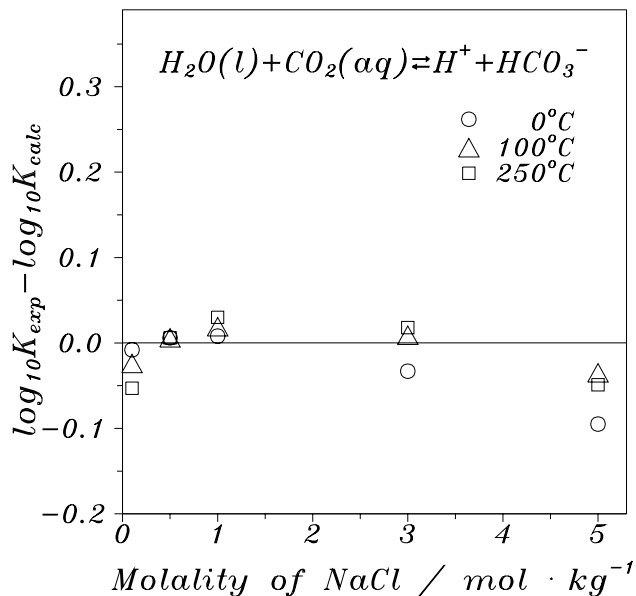
A comparison between experimental data and those fitted using the SIT model are shown in Figures IX.37, IX.38, IX.39 and in Table IX.13. When using the SIT model we have assumed that

- A is a temperature- and pressure-dependent function, *cf.* Eq. IX.57.
- The numerical factor 1.5 is independent of temperature.

Table IX.13: Test of the SIT approach for some reactions at elevated temperatures in NaCl media ($\log_{10} K_{\text{exp}}^{\circ}$ is the value from the original publications). The results at 300°C are shown in parenthesis, because these data may be affected by a partial association of the ionic medium.

$t(^{\circ}\text{C})$	$[-\log_{10} K_{\text{exp}}^{\circ} \pm 3\sigma]$	$[-\log_{10} K_{\text{calc}}^{\circ} \pm 3\sigma]$	$[\log_{10} K_{\text{exp}}^{\circ} - \log_{10} K_{\text{calc}}^{\circ}]$	$\Delta\varepsilon \pm 3\sigma$ ($\text{kg} \cdot \text{mol}^{-1}$)
Reaction: $\text{CO}_2(\text{aq}) + \text{H}_2\text{O}(\text{l}) \rightleftharpoons \text{H}^+ + \text{HCO}_3^-$ [82PAT/SLO]				
0	6.569 ± 0.007	6.549 ± 0.021	-0.020 ± 0.022	0.002 ± 0.033
25	6.349 ± 0.005	6.327 ± 0.024	-0.022 ± 0.025	0.011 ± 0.036
50	6.279 ± 0.005	6.251 ± 0.030	-0.028 ± 0.031	0.039 ± 0.036
100	6.397 ± 0.012	6.351 ± 0.042	-0.046 ± 0.044	0.036 ± 0.024
150	6.721 ± 0.018	6.658 ± 0.054	-0.063 ± 0.057	-0.001 ± 0.024
200	7.189 ± 0.023	7.112 ± 0.063	-0.077 ± 0.067	-0.062 ± 0.027
250	7.783 ± 0.027	7.685 ± 0.078	-0.098 ± 0.083	-0.146 ± 0.039
300	8.498 ± 0.060	(8.348 ± 0.120)	(-0.150 ± 0.134)	(-0.252 ± 0.051)
Reaction: $\text{HCO}_3^- \rightleftharpoons \text{H}^+ + \text{CO}_3^{2-}$ [84PAT/BUS]				
0	10.627 ± 0.005	10.585 ± 0.042	-0.042 ± 0.042	0.073 ± 0.057
25	10.337 ± 0.003	10.288 ± 0.054	-0.049 ± 0.054	0.061 ± 0.039
50	10.180 ± 0.004	10.127 ± 0.057	-0.053 ± 0.057	0.041 ± 0.045
100	10.120 ± 0.017	10.032 ± 0.084	-0.088 ± 0.086	0.008 ± 0.057
150	10.255 ± 0.039	10.120 ± 0.114	-0.135 ± 0.120	-0.015 ± 0.048
200	10.491 ± 0.056	10.317 ± 0.144	-0.174 ± 0.155	-0.047 ± 0.051
250	10.777 ± 0.073	10.560 ± 0.171	-0.217 ± 0.186	-0.095 ± 0.072
Reaction: $\text{HSO}_4^- \rightleftharpoons \text{H}^+ + \text{SO}_4^{2-}$ [90DIC/WES]				
0	1.659 ± 0.030	1.565 ± 0.078	-0.094 ± 0.084	0.046 ± 0.030
25	1.964 ± 0.018	1.876 ± 0.075	-0.088 ± 0.077	0.032 ± 0.030
50	2.316 ± 0.012	2.227 ± 0.069	-0.089 ± 0.070	0.020 ± 0.030
100	3.061 ± 0.008	2.960 ± 0.066	-0.101 ± 0.067	-0.003 ± 0.027
150	3.809 ± 0.007	3.691 ± 0.072	-0.118 ± 0.073	-0.032 ± 0.030
200	4.561 ± 0.008	4.419 ± 0.099	-0.142 ± 0.100	-0.070 ± 0.039
250	5.355 ± 0.012	5.187 ± 0.141	-0.168 ± 0.142	-0.124 ± 0.063

Figure IX.37: The differences ($\log_{10} K_{\text{exp}} - \log_{10} K_{\text{calc}}$) between experimental and calculated values of $\log_{10} K$ using the SIT model as a function of the molality of the ionic medium (NaCl) and temperatures (at saturated water vapor pressure) for the reaction $\text{CO}_2(\text{aq}) + \text{H}_2\text{O}(\text{l}) \rightleftharpoons \text{H}^+ + \text{HCO}_3^-$ [82PAT/SLO].



- $\Delta\varepsilon$ is a temperature- and pressure-dependent parameter.

One can conclude that it is possible to describe the concentration dependence of the equilibrium constants at temperatures up to 250°C (saturation water vapor pressure) in fairly good agreement with experimental data (in almost all cases the difference between experimental and calculated data do not exceed 0.05-0.08 \log_{10} units up to the ionic strength 5 mol · kg⁻¹). The values of $\log_{10} K^\circ$ (*i.e.*, at infinite dilution) agree almost within the obtained uncertainties with the estimates based on more complicated models containing 2-3 fitting parameters. However, the values of $\log_{10} K^\circ$ obtained using the SIT are systematically slightly higher than the values reported in the original publications. This is due to the fact that $\log_{10} K^\circ$ value depends somewhat on the extrapolation method used. However, these variations are small.

IX.10. The concentration dependence of heats of reactions

The enthalpy of reaction, $\Delta_r H_m$, is another characteristic of importance for complex formation reactions. All problems, which were discussed for the description of the concentration dependence of $\log_{10} K$ are relevant also for $\Delta_r H_m$ data. Determinations of standard heats of reactions in aqueous solutions (*i.e.*, at infinite dilution) in general in-

Figure IX.38: The differences ($\log_{10} K_{\text{exp}} - \log_{10} K_{\text{calc}}$) between experimental and calculated values of $\log_{10} K$ using the SIT model as a function of the molality of the ionic medium (NaCl) and temperatures (at saturated water vapor pressure) for the reaction $\text{HCO}_3^- \rightleftharpoons \text{H}^+ + \text{CO}_3^{2-}$ [84PAT/BUS].

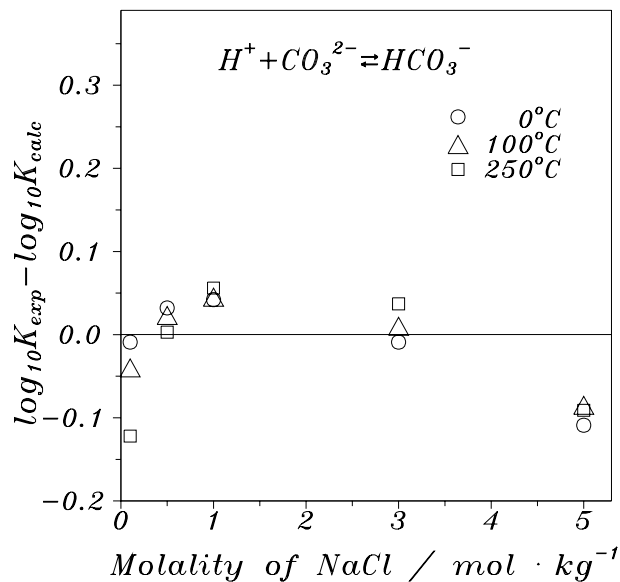
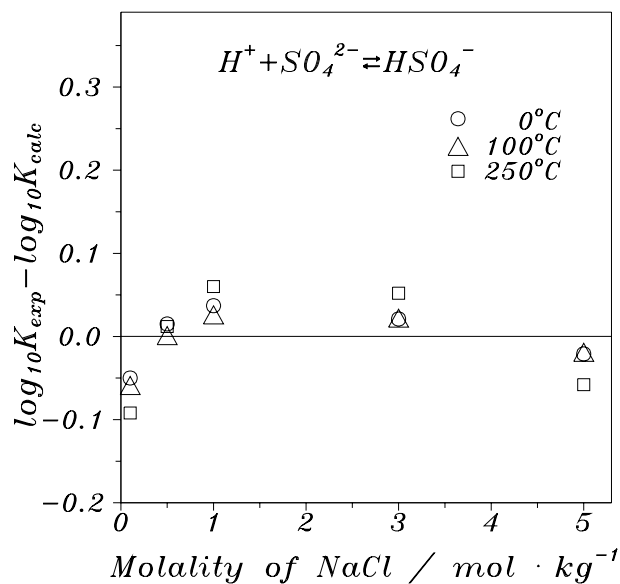


Figure IX.39: The differences ($\log_{10} K_{\text{exp}} - \log_{10} K_{\text{calc}}$) between experimental and calculated values of $\log_{10} K$ using the SIT model as a function of the molality of the ionic medium (NaCl) and temperatures (at saturated water vapor pressure) for the reaction $\text{HSO}_4^- \rightleftharpoons \text{H}^+ + \text{SO}_4^{2-}$ [90DIC/WES].



volve the determinations of heats of reactions at finite concentrations and the relevant heats of mixing and dilution of the components. Typical examples are the papers of Berg and Vanderzee [75BER/VAN, 75BER/VAN2], where the value of the standard enthalpy of formation of aqueous zinc ion was calculated from the enthalpies of solution of $\text{ZnO}(\text{cr})$ in HClO_4 solutions, the enthalpy of dilution of $\text{Zn}(\text{ClO}_4)_2(\text{aq})$ and the enthalpy of mixing of $\text{Zn}(\text{ClO}_4)_2(\text{aq})$ and $\text{HClO}_4(\text{aq})$ solutions. There are many examples in the literature where only the enthalpies of reaction at finite concentrations, often in solution with a large excess of ionic medium electrolyte, have been measured experimentally. These data have then been extrapolated to infinite dilution by using some empirical or semi-empirical methods, for instance, assuming that the thermochemical quantities follow a simple square root dependence of the ionic strength of the solution, *etc.* The use of such methods may result in a loss of accuracy of the value at infinite dilution, as compared to the accuracy of the experimental data, and were abandoned a long time ago for the determination of $\log_{10} K^\circ$. A clear and unambiguous discussion of the problem to describe the concentration dependence of $\Delta_r H_m$ and to determine $\Delta_r H_m^\circ$ for complex formation reactions is still absent (or we are not aware of it).

As discussed in Section IX.7 for a chemical reaction in the general form

$$\sum_i \nu_i Q_i + r \text{H}_2\text{O}(\text{l}) = 0 \quad (\text{IX.27})$$

the equation for the concentration dependence of $\ln K$ is given as follows:

$$\ln K^\circ = \ln K + \sum_i \nu_i \ln \gamma_i + r \ln a_{\text{H}_2\text{O}} \quad (\text{IX.28})$$

Using the known thermodynamic relations and definitions

$$\Delta_r H_m = RT^2 \left(\frac{\partial \ln K}{\partial T} \right)_p \quad (\text{IX.63})$$

$$L_1 = -RT^2 \left(\frac{\partial \ln a_{\text{H}_2\text{O}}}{\partial T} \right)_{p,m} \quad (\text{IX.64})$$

$$L_{2,i} = -RT^2 \left(\frac{\partial \ln \gamma_i}{\partial T} \right)_{p,m_i} \quad (\text{IX.65})$$

where L_1 and $L_{2,i}$ stand for the relative partial molar enthalpies of water and solute i respectively, one obtains the following basic equation for the concentration dependence of the enthalpy of reaction:

$$\Delta_r H_m^\circ = \Delta_r H_m - \sum_i \nu_i L_{2,i} - r L_1 \quad (\text{IX.66})$$

Values of the relative partial molar enthalpy of water, L_1 , in solutions of some common electrolytes are given in Table IX.14.

Table IX.14: Values of the relative partial molar enthalpy of water, L_1 , in solutions of some common electrolytes [91PIT]. The values in parenthesis are short range extrapolations.

$\frac{m}{(\text{mol} \cdot \text{kg}^{-1})}$	$L_1 / (\text{kJ} \cdot \text{mol}^{-1})$					
	HCl	HBr	HClO ₄	LiCl	LiClO ₄	NaCl
0.50	−0.005	−0.004	0.003	−0.004	−0.002	0.002
1.00	−0.017	−0.013	0.009	−0.012	−0.007	0.011
1.50	−0.037	−0.028	0.015	−0.025	−0.014	0.024
2.00	−0.064	−0.050	0.021	−0.043	−0.027	0.039
2.50	−0.101	−0.079	0.022	−0.067	−0.045	0.056
3.00	−0.148	−0.117	0.017	−0.099	−0.071	0.071
3.50	−0.206	−0.164	0.004	−0.139	−0.106	0.083
4.00	−0.278	−0.223	−0.019	−0.187	−0.152	0.089
4.50	−0.364	−0.293	−0.054	−0.245		0.088
5.00		−0.377	−0.105	−0.313		0.077
5.50		−0.474	−0.173	−0.393		0.054
6.00		−0.587	−0.260	−0.484		0.018
$\frac{m}{(\text{mol} \cdot \text{kg}^{-1})}$	NaBr	NaNO ₃	NaClO ₄	NaOH	KCl	KNO ₃
0.50	0.003	0.008	0.008	0.001	0.002	0.010
1.00	0.014	0.027	0.030	0.006	0.010	0.031
1.50	0.030	0.052	0.062	0.012	0.022	0.068
2.00	0.050	0.080	0.099	0.016	0.039	0.128
2.50	0.073	(0.10)	0.140	0.014	0.058	(0.22)
3.00	0.095		0.181	0.002	0.080	
3.50	0.117		0.219	−0.023	0.103	
4.00	0.136		0.251	−0.066	0.126	
4.50	0.149		0.275	(−0.13)	0.149	
5.00	0.156		0.286			
5.50	0.155		0.281			
6.00	0.143		0.259			

The particular analytical form of the equation will depend on the model used to describe the activity coefficients. Most complex formation reactions have been studied at trace concentrations of the reactants/products in a large excess of supporting electrolytes. In the following sections we will describe two equations based on the Pitzer and the SIT models that could be used for the description of the concentration dependence of the $\Delta_r H_m$ for such reactions.

IX.10.1. The calculation of the standard enthalpy of reaction from experimental $\Delta_r H_m$ data using the Pitzer equation

Using the Pitzer equations the following statement is obtained for the relative partial molar enthalpy of a cation M present at trace concentration in a solution of a “supporting” electrolyte NX (see Eqs. (IX.12), (IX.17-IX.21), (IX.59), (IX.65)):

$$\begin{aligned}
 L_{2,M} = & \frac{Z_M^2 A_L}{4} \left[\frac{\sqrt{I_m}}{1 + b\sqrt{I_m}} + \frac{2}{b} \ln \left(1 + b\sqrt{I_m} \right) \right] \\
 & - RT^2 Z_M^2 m_N m_X \beta_{NX}^{(1)L} \frac{g'(I_m)}{I_m} \\
 & - 2RT^2 m_X \left[\beta_{MX}^{(0)L} + \beta_{MX}^{(1)L} g(I_m) \right] \\
 & - RT^2 m_N \left[2 \left(\frac{\partial \phi_{MN}}{\partial T} \right)_p + m_X \left(\frac{\partial \psi_{MNX}}{\partial T} \right)_p \right] \\
 & - RT^2 m_X (m_N Z_N + m_X Z_X) C_{MX}^L - RT^2 Z_M m_N m_X C_{NX}^L
 \end{aligned} \tag{IX.67}$$

where A_L is the Debye-Hückel parameter for the enthalpy (at 25°C and 1 atm $A_L = 1.986 \text{ kJ} \cdot \text{kg}^{1/2} \cdot \text{mol}^{-3/2}$ [91PIT]); Z_M , Z_N , Z_X stand for the charges of M, N, and X respectively; g and g' are defined in Eqs. (IX.22) and (IX.23) in p.354; and the parameters $\beta^{(0)L}$, $\beta^{(1)L}$, C^L are defined as

$$\beta^{(0)L} = \left(\frac{\partial \beta^{(0)}}{\partial T} \right)_p ; \quad \beta^{(1)L} = \left(\frac{\partial \beta^{(1)}}{\partial T} \right)_p ; \quad C^L = \left(\frac{\partial C}{\partial T} \right)_p$$

where $\beta^{(0)}$, $\beta^{(1)}$ and C are the parameters for the osmotic and activity coefficients in the Pitzer model. The corresponding expression for the relative partial molar enthalpy of an anion Y is obtained by changing the subscript M for Y and the subscript X for N.

For the relative partial molar enthalpy of water in solution of NX electrolyte, the following equation is obtained:

$$L_1 = \frac{M_w}{1000} \left[-\frac{A_L}{2} \frac{I_m^{3/2}}{(1 + b\sqrt{I_m})} + 2RT^2 \nu_M \nu_X m^2 \left(\beta_{NX}^{(0)L} + \beta_{NX}^{(1)L} e^{-\alpha\sqrt{I_m}} \right. \right. \\ \left. \left. + 2\nu_N Z_N m C_{NX}^L \right) \right] \quad (\text{IX.68})$$

where M_w is the molar mass of water; ν_N and ν_X are the number of N and X in the electrolyte NX.

The Pitzer approach gives the following equation for the concentration dependence of the enthalpy of the reaction studied at trace concentrations of the reactants/products in solution with a large excess of a 1-1 electrolyte ionic medium:

$$\Delta_r H_m - rL_1 = \Delta_r H_m^\circ + \frac{\Delta(Z^2)A_L}{4} \left[\frac{\sqrt{I_m}}{1 + b\sqrt{I_m}} + \frac{2}{b} \ln(1 + b\sqrt{I_m}) \right] \\ - RT^2 \Delta(Z^2)m^2 \beta_{NX}^{(1)L} \frac{g'(I_m)}{I_m} - RT^2 m^2 \Delta|Z| C_{NX}^L \\ - 2RT^2 m \Delta\beta^{(0)L} - 2RT^2 m \Delta \left(\frac{\partial\phi}{\partial T} \right)_p - 2RT^2 m \Delta\beta^{(1)L} g(I_m) \\ - 2RT^2 m^2 \Delta C^L - RT^2 m^2 \Delta \left(\frac{\partial\psi}{\partial T} \right)_p \quad (\text{IX.69})$$

where

$$\Delta(Z^2) = \sum_i \nu_i Z_i^2 ; \quad \Delta|Z| = \sum_i \nu_i |Z_i| ; \\ \Delta\beta^{(0)L} = \sum_i \nu_i \beta_{ij}^{(0)L} ; \quad \Delta\beta^{(1)L} = \sum_i \nu_i \beta_{ij}^{(1)L} ; \quad \Delta C^L = \sum_i \nu_i C_{ij}^L ; \\ \Delta \left(\frac{\partial\phi}{\partial T} \right)_p = \sum_i \nu_i \left(\frac{\partial\phi_{ij}}{\partial T} \right)_p ; \quad \Delta \left(\frac{\partial\psi}{\partial T} \right)_p = \sum_i \nu_i \left(\frac{\partial\psi_{i'j}}{\partial T} \right)_p$$

Here subscript i refers to reaction participants, i' and j stand for the ionic medium ions, having the same and opposite charge sign respectively, to the species i , and m denotes the molality of the ionic medium 1-1 electrolyte, NX. The Pitzer parameters $\beta^{(0)L}$, $\beta^{(1)L}$, C_L are tabulated for many electrolytes [91PIT]. However, the information on the temperature derivatives of the mixing terms $(\partial\phi/\partial T)_p$ and $(\partial\psi/\partial T)_p$ is scarce due to the small number of studies of the enthalpy of mixing of electrolyte solutions that have been analysed with this method. We did not include the analytical expression of the contribution of rL_1 term in order not to complicate the resulting equation. From a practical point of view it is

more convenient to correct the experimental values of $\Delta_r H_m$ with the contribution from the term rL_1 , when necessary, using the values of the relative partial molar enthalpies of water in electrolyte solutions from the thermochemical tables or calculating them using the Pitzer model.

IX.10.2. The calculation of the standard enthalpy of a reaction from experimental $\Delta_r H_m$ data using the SIT model

The corresponding equations for the concentration dependence of the relative partial molar enthalpy of cation M present at trace concentration in an ionic medium electrolyte NX and for relative partial molar enthalpy of water (L_1) are given below (considering the numerical factor $1.5 \text{ kg}^{1/2} \cdot \text{mol}^{-1/2}$ to be a constant, independent of temperature)

$$\begin{aligned} L_{2,M} &= -RT^2 \left(\frac{\partial \ln \gamma_M}{\partial T} \right)_{p,m_j} \\ &= \frac{3}{4} \frac{A_L Z_i^2 \sqrt{I_m}}{1 + 1.5\sqrt{I_m}} - RT^2 \varepsilon_L(M, X) m_X \end{aligned} \quad (\text{IX.70})$$

$$L_1 = \frac{M_w}{1000} \left[-\frac{3}{2} \frac{A_L}{1.5^3} \left(t - 2 \ln t - \frac{1}{t} \right) + RT^2 \nu_N Z_N m^2 \varepsilon_L(N, X) \right] \quad (\text{IX.71})$$

where $t = 1 + 1.5\sqrt{I_m}$ was defined before.

The concentration dependence of the heat of reaction studied at trace concentrations of reactants/products in a solution with a large excess of an 1-1 ionic medium is then equal to:

$$\Delta_r H_m - rL_1 = \Delta_r H_m^\circ + \frac{3}{4} \frac{A_L \Delta(Z^2) \sqrt{I_m}}{1 + 1.5\sqrt{I_m}} - RT^2 m \Delta \varepsilon_L \quad (\text{IX.72})$$

where

$$\Delta \varepsilon_L = \sum_i \nu_i \varepsilon_L(i, j)$$

here subscript i refers to a reaction participant and j to the counter-ion of the ionic medium.

Example 15:

This example refers to the determination of the $\Delta_r H_m^\circ$ value for the reaction $\text{Mg}(\text{cr}) + 2\text{H}^+ \rightleftharpoons \text{Mg}^{2+} + \text{H}_2(\text{g})$, which is equal to the standard enthalpy of formation of the magnesium ion. In 1943 Shomate and Huffman [43SHO/HUF] measured the enthalpy of reaction of very pure magnesium metal in $1.02 \text{ mol} \cdot \text{kg}^{-1}$ HCl at 298.15 K and obtained the value of $\Delta_r H_m = -465.48 \pm 0.17 \text{ kJ} \cdot \text{mol}^{-1}$ (as recalculated by Morss and Williams

[83MOR/WIL] using a more accurate value of the molar mass of Mg). This measurement has been accepted as a standard for metal-dissolution calorimetry and has been confirmed many times (see [83MOR/WIL]).

For this reaction we obtain

$$\Delta_r H_m^\circ = \Delta_r H_m - L_{2,\text{Mg}^{2+}} + 2L_{2,\text{H}^+}$$

The corresponding statements for the relative partial molar enthalpies of this reaction participants in a solution with a large excess of HCl based on the Pitzer model are given as follows

$$\begin{aligned} L_{2,\text{Mg}} &= A_L \left[\frac{\sqrt{I_m}}{1 + b\sqrt{I_m}} + \frac{2}{b} \ln \left(1 + b\sqrt{I_m} \right) \right] - 4RT^2 m^2 \beta_{\text{H,Cl}}^{(1)L} \frac{g'(I_m)}{I_m} \\ &\quad - 2RT^2 m \left[\beta_{\text{Mg,Cl}}^{(0)L} + \beta_{\text{Mg,Cl}}^{(1)L} g(I_m) \right] \\ &\quad - RT^2 m \left[2 \left(\frac{\partial \phi_{\text{Mg,H}}}{\partial T} \right)_p + m \left(\frac{\partial \psi_{\text{Mg,H,Cl}}}{\partial T} \right)_p \right] \\ &\quad - 2RT^2 m^2 C_{\text{Mg,Cl}}^L - 2RT^2 m^2 C_{\text{H,Cl}}^L \\ L_{2,\text{H}} &= \frac{A_L}{4} \left[\frac{\sqrt{I_m}}{1 + b\sqrt{I_m}} + \frac{2}{b} \ln \left(1 + b\sqrt{I_m} \right) \right] - 2RT^2 m \beta_{\text{H,Cl}}^{(0)L} \\ &\quad - 2RT^2 m \frac{\beta_{\text{H,Cl}}^{(1)L}}{\alpha^2 I_m} \left[1 - \left(1 + \alpha\sqrt{I_m} - \frac{\alpha^2 I_m}{2} \right) e^{-\alpha\sqrt{I_m}} \right] - 3RT^2 m^2 C_{\text{H,Cl}}^L \end{aligned}$$

where m stands for the molality of HCl. The required values of the Pitzer parameters for the HCl and MgCl_2 electrolytes are available from the compilation [91PIT]:

$$\begin{aligned} \beta_{\text{H,Cl}}^{(0)L} &= -3.081 \times 10^{-4} \text{ kg} \cdot \text{mol}^{-1} \cdot \text{K}^{-1}, \quad \beta_{\text{H,Cl}}^{(1)L} = 1.419 \times 10^{-4} \text{ kg} \cdot \text{mol}^{-1} \cdot \text{K}^{-1}, \\ C_{\text{H,Cl}}^L &= -3.107 \times 10^{-5} \text{ kg}^2 \cdot \text{mol}^{-2} \cdot \text{K}^{-1}, \\ \beta_{\text{Mg,Cl}}^{(0)L} &= -1.94 \times 10^{-4} \text{ kg} \cdot \text{mol}^{-1} \cdot \text{K}^{-1}, \quad \beta_{\text{Mg,Cl}}^{(1)L} = 2.78 \times 10^{-3} \text{ kg} \cdot \text{mol}^{-1} \cdot \text{K}^{-1}, \\ C_{\text{Mg,Cl}}^L &= -5.8 \times 10^{-5} \text{ kg}^2 \cdot \text{mol}^{-2} \cdot \text{K}^{-1}. \end{aligned}$$

The temperature derivatives of the mixing terms $(\partial \phi_{\text{Mg,H}}/\partial T)_p$ and $(\partial \psi_{\text{Mg,H,Cl}}/\partial T)_p$ are not given in the literature due to lack of the experimental determinations of the enthalpy of mixing HCl and MgCl_2 solutions. Only rough estimations can be made from the potentiometric determinations of the mean activity coefficients of HCl in its mixtures with alkali earth halides at different temperatures [86ROY/GIB, 90ROY/RIC, *etc.*]: $(\partial \phi_{\text{Mg,H}}/\partial T)_p = (-8 \pm 4) \times 10^{-4} \text{ kg} \cdot \text{mol}^{-1} \cdot \text{K}^{-1}$ and $(\partial \psi_{\text{Mg,H,Cl}}/\partial T)_p = (5 \pm 5) \times 10^{-4} \text{ kg}^2 \cdot \text{mol}^{-2} \cdot \text{K}^{-1}$,

using the reported sets of ϕ and ψ values without consideration of the higher order electrostatic terms. We did not take into account the contribution of the unsymmetrical mixing terms. As pointed out by Pitzer [83PIT] the effect of the higher order electrostatic term is non-linear with the ionic strength only at low concentrations and can be omitted for simplicity.

The calculated values are $L_{2,H} = 1.37 \text{ kJ} \cdot \text{mol}^{-1}$ and $L_{2,Mg} = 3.62 \pm 0.25 \text{ kJ} \cdot \text{mol}^{-1}$, where the error is due to uncertainty in the contributions of the mixing terms. Therefore, $\Delta_r H_m^\circ = \Delta_f H^\circ(\text{Mg}^{2+}, 298.15 \text{ K}) = \Delta_r H_m - L_{2,Mg} + 2L_{2,H} = (-465.48 \pm 0.17) - (3.62 \pm 0.25) + 2 \times 1.37 = -466.36 \pm 0.30 \text{ kJ} \cdot \text{mol}^{-1}$.

Using the SIT model, we obtain the following equations for the relative partial molar enthalpies of the reaction participants:

$$L_{2,Mg^{2+}} = 3 \frac{A_L \sqrt{I_m}}{1 + 1.5 \sqrt{I_m}} - RT^2 \varepsilon_L(\text{Mg}^{2+}, \text{Cl}^-)m$$

$$L_{2,H^+} = \frac{3}{4} \frac{A_L \sqrt{I_m}}{1 + 1.5 \sqrt{I_m}} - RT^2 \varepsilon_L(\text{H}^+, \text{Cl}^-)m$$

where m stands for the molality of HCl. The values of the SIT interaction coefficients can be evaluated from the available [91PIT] data on the heats of dilution of MgCl_2 and HCl: $\varepsilon_L(\text{Mg}^{2+}, \text{Cl}^-) = (-1.2 \pm 0.2) \times 10^{-3} \text{ kg} \cdot \text{mol}^{-1} \cdot \text{K}^{-1}$, $\varepsilon_L(\text{H}^+, \text{Cl}^-) = (-1.0 \pm 0.1) \times 10^{-3} \text{ kg} \cdot \text{mol}^{-1} \cdot \text{K}^{-1}$. The calculated results are: $L_{2,H} = 1.35 \pm 0.16 \text{ kJ} \cdot \text{mol}^{-1}$ and $L_{2,Mg} = 3.30 \pm 0.30 \text{ kJ} \cdot \text{mol}^{-1}$ (the uncertainties have been doubled to take the neglect of specific mixing effects in the SIT model into account). Hence, $\Delta_r H_m^\circ = \Delta_f H^\circ(\text{Mg}^{2+}, 298.15 \text{ K}) = (-465.48 \pm 0.17) - (3.30 \pm 0.30) + 2 \times (1.35 \pm 0.16) = -466.08 \pm 0.41 \text{ kJ} \cdot \text{mol}^{-1}$.

Both of the values, $-466.36 \pm 0.30 \text{ kJ} \cdot \text{mol}^{-1}$ from the Pitzer model and $-466.08 \pm 0.41 \text{ kJ} \cdot \text{mol}^{-1}$ from the SIT model can be compared with the CODATA [89COX/WAG] recommended value $-467.0 \pm 0.6 \text{ kJ} \cdot \text{mol}^{-1}$, which is based on different experimental sets varying from -465.3 ± 1.0 to $-468.86 \pm 0.80 \text{ kJ} \cdot \text{mol}^{-1}$. These values of the enthalpy of formation of the magnesium ion were obtained from a number of different thermochemical cycles. In most cases the values of $\Delta_r H_m^\circ$ deduced by the authors of the original works were quoted in [89COX/WAG] without critical discussion of the extrapolation procedures employed, although this might be an additional reason for the discrepancies between the reported values of the enthalpy changes at infinite dilution. For instance, the extrapolation equation widely used by Vasil'ev with coworkers [67VAS, 78VAS/YAS2] is actually based on the assumption $H_{2,m} = H_2^\circ + \phi L$ (see Eq. (5) in [78VAS/YAS2]), where $H_{2,m}$ is the enthalpy of a species in a solution of finite concentration, H_2° stands for the enthalpy of the species at infinite dilution, ϕL is the relative apparent molar enthalpy. This relation is in contradiction to the strict thermodynamic relation $H_{2,m} = H_2^\circ + L_2$, which follows from the definition of the relative partial molar enthalpy of the species of the solution (see Eq. (IX.40)). The relative apparent molar enthalpy is not a characteristic of the solute, in fact it is the characteristic of the system, which follows from the following relation [58HAR/OWE]

$$L = n_1 L_1 + n_2 L_2 = n_2 \cdot \phi L$$

where L is the relative enthalpy of the solution, n_1 and n_2 stand for the concentrations of water and solute, respectively. Hence, the extrapolation equation used by Vasil'ev and coworkers seems to be based on erroneous assumptions, and the numerous results of $\Delta_r H_m^\circ$ obtained using this equation should be revised; a discussion is given in [96PLY/GRE].

Example 16:

The previous example referred to a situation where very accurate data for $\Delta_r H_m$ in an ionic medium was available, but where the $\Delta_r H_m^\circ$ value from the CODATA recommendation had a rather large uncertainty. In this example we will discuss the dissociation of water in NaCl media, where the $\Delta_r H_m^\circ = 55.82 \pm 0.06 \text{ kJ} \cdot \text{mol}^{-1}$ [89COX/WAG] is known with very high precision, but where individual experimental results might be subject to undiscovered experimental errors.

A number of sets of $\Delta_r H_m$ data for the reaction $\text{H}_2\text{O}(l) \rightleftharpoons \text{H}^+ + \text{OH}^-$ in NaCl ionic media have been reported in the literature at 298.15 K: Harned and Mannweiler [35HAR/MAN] have obtained the $\Delta_r H_m$ values at different NaCl concentrations from the temperature dependence of the very accurate $\log_{10} K$ data in the temperature range 0-60°C; Lobanov and Vasil'ev [69LOB/VAS] have made calorimetric determinations of the corresponding quantities; Busey and Mesmer [78BUS/MES] have tabulated the $\Delta_r H_m$ values consistent with $\log_{10} K$ data at different temperatures; Maeda [86MAE] has reported the calorimetric results. These values of the enthalpy changes, corrected for the values of the relative partial molar enthalpies of water in NaCl solutions, are given in Table IX.15.

For this reaction one obtains

$$\Delta_r H_m^\circ = \Delta_r H_m + L_1 - L_{2,\text{H}} - L_{2,\text{OH}}$$

The Pitzer model results on the following equations for the relative partial molar enthalpies of the reaction participants:

$$\begin{aligned} L_{2,\text{H}} = & \frac{A_L}{4} \left[\frac{\sqrt{I_m}}{1 + b\sqrt{I_m}} + \frac{2}{b} \ln \left(1 + b\sqrt{I_m} \right) \right] - RT^2 m^2 \beta_{\text{Na,Cl}}^{(1)L} \frac{g'(I_m)}{I_m} \\ & - 2RT^2 m \left[\beta_{\text{H,Cl}}^{(0)L} + \beta_{\text{H,Cl}}^{(1)L} g(I_m) \right] \\ & - RT^2 m \left[2 \left(\frac{\partial \phi_{\text{H,Na}}}{\partial T} \right)_p + m \left(\frac{\partial \psi_{\text{H,Na,Cl}}}{\partial T} \right)_p \right] \\ & - 2RT^2 m^2 C_{\text{H,Cl}}^L - RT^2 m^2 C_{\text{Na,Cl}}^L \end{aligned}$$

$$\begin{aligned}
 L_{2,\text{OH}} = & \frac{A_L}{4} \left[\frac{\sqrt{I_m}}{1 + b\sqrt{I_m}} + \frac{2}{b} \ln \left(1 + b\sqrt{I_m} \right) \right] - RT^2 m^2 \beta_{\text{Na,Cl}}^{(1)L} \frac{g'(I_m)}{I_m} \\
 & - 2RT^2 m \left[\beta_{\text{Na,OH}}^{(0)L} + \beta_{\text{Na,OH}}^{(1)L} g(I_m) \right] \\
 & - RT^2 m \left[2 \left(\frac{\partial \phi_{\text{OH,Cl}}}{\partial T} \right)_p + m \left(\frac{\partial \psi_{\text{OH,Na,Cl}}}{\partial T} \right)_p \right] \\
 & - 2RT^2 m^2 C_{\text{Na,OH}}^L - RT^2 m^2 C_{\text{Na,Cl}}^L
 \end{aligned}$$

The Pitzer parameters are available [91PIT] for the single electrolytes NaOH, HCl and NaOH (the dimensions are $\text{kg} \cdot \text{mol}^{-1} \cdot \text{K}^{-1}$ for the $\beta^{(0)L}$ and $\beta^{(1)L}$, $\text{kg}^2 \cdot \text{mol}^{-2} \cdot \text{K}^{-1}$ for the C^L):

$$\begin{aligned}
 \beta_{\text{H,Cl}}^{(0)L} &= -3.081 \times 10^{-4}, & \beta_{\text{H,Cl}}^{(1)L} &= 1.419 \times 10^{-4}, & C_{\text{H,Cl}}^L &= -3.107 \times 10^{-5}, \\
 \beta_{\text{Na,OH}}^{(0)L} &= 7.00 \times 10^{-4}, & \beta_{\text{Na,OH}}^{(1)L} &= 1.34 \times 10^{-4}, & C_{\text{Na,OH}}^L &= -9.47 \times 10^{-5}, \\
 \beta_{\text{Na,Cl}}^{(0)L} &= 7.159 \times 10^{-4}, & \beta_{\text{Na,Cl}}^{(1)L} &= 7.005 \times 10^{-4}, & C_{\text{Na,Cl}}^L &= -5.27 \times 10^{-5}.
 \end{aligned}$$

The parameters for the NaOH solutions are valid up to concentration $4.2 \text{ mol} \cdot \text{kg}^{-1}$, those for the HCl solutions up to $4.5 \text{ mol} \cdot \text{kg}^{-1}$. The temperature derivatives of the mixing terms $(\partial \phi_{\text{H,Na}}/\partial T)_p$, $(\partial \psi_{\text{H,Na,Cl}}/\partial T)_p$, $(\partial \phi_{\text{Cl,OH}}/\partial T)_p$, $(\partial \psi_{\text{Cl,OH,Na}}/\partial T)_p$ are not known. We assume that the sum of the terms $(\partial \phi_{\text{H,Na}}/\partial T)_p + (\partial \phi_{\text{Cl,OH}}/\partial T)_p$ is less than $\pm 2 \times 10^{-4}$, and that the sum of the terms $(\partial \psi_{\text{H,Na,Cl}}/\partial T)_p + (\partial \psi_{\text{Cl,OH,Na}}/\partial T)_p$ is less than $\pm 3 \times 10^{-5}$ based on the available information on the temperature dependence of the mixing terms in some binary systems [90HOL/MES]. Using the equations given above we have calculated the values of the sum of the $L_{2,\text{H}} + L_{2,\text{OH}}$ at different NaCl concentrations, considering the possible contribution of the mixing terms as an estimate of the uncertainty of the derived sum. The value of $\Delta_r H_m^\circ$ obtained from the experimental enthalpy changes are given in Table IX.15, the errors quoted are the square root of the sum of the squares of the uncertainty of experimental determinations and the estimated uncertainty of the sum of $L_{2,\text{H}} + L_{2,\text{OH}}$.

From the SIT model we obtain for the relative partial molar enthalpies of H^+ and OH^- in NaCl solutions:

$$\begin{aligned}
 L_{2,\text{H}^+} &= \frac{3}{4} \frac{A_L \sqrt{I_m}}{1 + 1.5\sqrt{I_m}} - RT^2 \varepsilon_L(\text{H}^+, \text{Cl}^-) m \\
 L_{2,\text{OH}^-} &= \frac{3}{4} \frac{A_L \sqrt{I_m}}{1 + 1.5\sqrt{I_m}} - RT^2 \varepsilon_L(\text{Na}^+, \text{OH}^-) m
 \end{aligned}$$

The values of the SIT interaction coefficients are obtained from the enthalpy of dilution data for HCl and NaOH solutions: $\varepsilon_L(\text{H}^+, \text{Cl}^-) = (-1.0 \pm 0.1) \times 10^{-1} \text{ kg} \cdot \text{mol}^{-1} \cdot \text{K}^{-1}$,

$\varepsilon_L(\text{Na}^+, \text{OH}^-) = (0.5 \pm 0.2) \times 10^{-3} \text{ kg} \cdot \text{mol}^{-1} \cdot \text{K}^{-1}$. These values were used to calculate the sum of the relative partial molar enthalpies of H^+ and OH^- in NaCl solutions and to obtain the values of $\Delta_r H_m^\circ$ from the experimental enthalpy changes (see Table IX.15). When estimating the possible error in the $\Delta_r H_m^\circ$, the uncertainty in the correction was doubled, to account for the specific mixing effects which are ignored in this model.

The values of the sum $L_{2,\text{H}} + L_{2,\text{OH}}$ calculated from the Pitzer and the SIT models, are in satisfactory agreement with one another only at concentrations of NaCl less than $3\text{--}3.5 \text{ mol} \cdot \text{kg}^{-1}$, where the difference between them is less than $1 \text{ kJ} \cdot \text{mol}^{-1}$, with an expected uncertainty within $1.0\text{--}1.2 \text{ kJ} \cdot \text{mol}^{-1}$. In this concentration range the experimental values of $\Delta_r H_m$, reported in the different studies, are in acceptable agreement with one another. The values of the enthalpy change at infinite dilution, $\Delta_r H_m^\circ$, calculated based on either the Pitzer or the SIT approaches are also in excellent agreement (within the expected uncertainties of the calculations) with the CODATA recommendation. The analysis of the results at higher NaCl concentrations is ambiguous: the Pitzer and the SIT models result in quite different values of the sum of the relative partial molar enthalpies of the H^+ and OH^- ions, and the differences exceed the expected uncertainty of the calculated values. One also obtains different values of $\Delta_r H_m^\circ$ from the same experimental data at high NaCl concentrations, using the two models. The reasons can be the approximate character of the postulates used in the SIT approach and a larger than expected contribution of the mixing terms in the Pitzer model. This ambiguity cannot be resolved due to lack of the experimental determinations of the enthalpy of mixing for the NaCl-NaOH aqueous mixtures. The example indicates that the Pitzer model gives a precise description of the ionic strength/medium dependence of the enthalpy of reaction even at high concentrations, provided that all the relevant Pitzer parameters for the reaction participants are known. Unfortunately, the data on the temperature derivative of the mixing parameters for the Pitzer models are scarce, and the omission of these terms in a “reduced” Pitzer model at high concentrations may result in errors, which are comparable with those of the SIT model at these concentrations. We recommend to use the Pitzer and SIT models only for the $\Delta_r H_m$ data in the limited ionic strength range up to $3\text{--}4 \text{ mol} \cdot \text{kg}^{-1}$.

IX.10.3. The extrapolation equations for the determination of the standard enthalpy of reaction from the experimental $\Delta_r H_m$ data based on the Pitzer and the SIT models

The previous discussion was made for a reaction, where the Pitzer or the SIT parameters are known for the reaction participants in the ionic medium. However, these parameters are in general only known for the single ion combinations, and not for complexes. When discussing the experimental results for the enthalpy change of complex formation reactions using the Pitzer model it is convenient to write Eq. (IX.69) as follows (as before, this equation is valid only for the case of reactions studied at trace concentrations of the

Table IX.15: The results of the calculation of the $\Delta_r H_m^\circ$ value for the reaction $\text{H}_2\text{O}(l) \rightleftharpoons \text{H}^+ + \text{OH}^-$ in NaCl medium at 298.15 K from the heat effects at finite concentrations based on the Pitzer and the SIT model. The uncertainties of the experimental results are quoted from the original studies, the uncertainties of the calculated values of $\Delta_r H_m^\circ$ result from both of the claimed error in the experimental data and the error of the correction terms. The CODATA recommended value for the reaction of water dissociation is $\Delta_r H_m^\circ = 55.82 \pm 0.06 \text{ kJ} \cdot \text{mol}^{-1}$ [89COX/WAG].

Reference	m NaCl ($\text{mol} \cdot \text{kg}^{-1}$)	$\Delta_r H_m + L_1$ ($\text{kJ} \cdot \text{mol}^{-1}$)	The calculated value of $\Delta_r H_m^\circ$, $\text{kJ} \cdot \text{mol}^{-1}$	
			The Pitzer model	The SIT model
[35HAR/MAN]	0.51	57.17 ± 0.3^a	55.99 ± 0.34	55.95 ± 0.34
	1.01	57.55 ± 0.3	56.06 ± 0.44	55.98 ± 0.45
	2.01	58.08 ± 0.3	55.89 ± 0.74	55.99 ± 0.75
	3.01	58.49 ± 0.3	55.25 ± 1.13	55.94 ± 1.03
[69LOB/VAS]	0.51	57.24 ± 0.13	56.06 ± 0.21	56.03 ± 0.21
	1.02	57.50 ± 0.16	56.00 ± 0.36	55.93 ± 0.38
	2.09	57.99 ± 0.10	55.73 ± 0.69	55.85 ± 0.70
	3.20	58.49 ± 0.11	55.00 ± 1.18	55.86 ± 1.07
[78BUS/MES]	0.50	57.12 ± 0.19	55.94 ± 0.24	55.91 ± 0.23
	1.00	57.41 ± 0.23	55.92 ± 0.39	55.85 ± 0.47
	3.00	57.93 ± 0.71	54.70 ± 1.30	55.39 ± 1.22
	5.00	58.15 ± 1.17	$(51.46 \pm 2.34)^b$	54.77 ± 2.02
[86MAE]	4.37	60.29 ± 0.30	54.89 ± 1.74	57.17 ± 1.47
	5.61	62.45 ± 0.30	$(54.32 \pm 2.38)^b$	58.83 ± 1.87

^a Our estimation of the uncertainty of the data from [35HAR/MAN];

^b The concentration exceeds the range of applicability of the Pitzer parameters for the HCl and NaOH electrolytes.

reaction participants in solutions with a large excess of supporting 1-1 electrolyte):

$$\begin{aligned}
 \Delta_r H_m^\circ &= \Delta_r H_m - r L_1 - \frac{\Delta(Z^2) A_L}{4} \left[\frac{\sqrt{I_m}}{1 + b\sqrt{I_m}} + \frac{2}{b} \ln \left(1 + b\sqrt{I_m} \right) \right] \\
 &\quad + RT^2 \Delta(Z^2) m^2 \beta_{\text{NX}}^{(1)L} \frac{g'(I_m)}{I_m} + RT^2 m^2 \Delta|Z| C_{\text{NX}}^L + 2RT^2 m X_1 \\
 &\quad + 2RT^2 m X_2 g(I_m) + 2RT^2 m^2 X_3
 \end{aligned} \tag{IX.73}$$

where

$$\begin{aligned}
 X_1 &= \Delta\beta^{(0)L} + \Delta \left(\frac{\partial\phi}{\partial T} \right)_p = \sum_i \nu_i \beta_{ij}^{(0)L} + \sum_i \nu_i \left(\frac{\partial\phi_{ij}}{\partial T} \right)_p \\
 X_2 &= \Delta\beta^{(1)L} = \sum_i \nu_i \beta_{ij}^{(1)L} \\
 X_3 &= \Delta C^L + \frac{1}{2} \Delta \left(\frac{\partial\psi}{\partial T} \right)_p = \sum_i \nu_i C_{ij}^L + \frac{1}{2} \sum_i \nu_i \left(\frac{\partial\psi_{ij}}{\partial T} \right)_p
 \end{aligned}$$

the notation has been defined before (see Eq. (IX.69)). As practically all experimental determinations of the enthalpy changes for the complex formation reactions have been studied at relatively high concentration of the ionic medium electrolytes, there is no reason to take into account the contribution of higher order electrostatic terms for the reaction participants, because this contribution is approximately linear with the concentration [83PIT] and therefore is accounted for mainly in the term X_1 .

The corresponding extrapolation equation for the SIT model is given by Eq. (IX.72).

Example 17:

In order to test the equations for the description of the concentration dependence of $\Delta_r H_m$ and the determination of $\Delta_r H_m^\circ$ at infinite dilution, we have used data for the reaction $\text{H}_2\text{O}(l) \rightleftharpoons \text{H}^+ + \text{OH}^-$ in NaClO_4 ionic medium. For this reaction the value of $\Delta_r H_m^\circ$ is recommended by CODATA [89COX/WAG]. The experimental calorimetric data in NaClO_4 medium at 25°C have been obtained in three laboratories by Arnek and Kakolowicz [67ARN/KAK] at 3.50 mol · kg⁻¹, Lobanov and Vasil'ev [69LOB/VAS] at 0.51-3.50 mol · kg⁻¹, and Maeda [86MAE] at 3.50 and 4.95 mol · kg⁻¹. The results at the same ionic medium concentration, 3.50 mol · kg⁻¹, agree within ± 0.25 kJ · mol⁻¹.

The experimental results on $\Delta_r H_m$ corrected for the value of L_1 are given in Table IX.16.

We used the weighted linear least-square method to obtain the regression parameters for both the Pitzer and the Brønsted-Guggenheim-Scatchard models. The regression analysis was made by using the uncertainty estimates in $\Delta_r H_m$, equal to ± 0.3 kJ · mol⁻¹. The point at highest molality, 4.95 mol · kg⁻¹, was not used in the regression, because as discussed

Table IX.16: The results of the experimental determinations of the $\Delta_r H_m$ for the reaction $\text{H}_2\text{O}(\text{l}) \rightleftharpoons \text{H}^+ + \text{OH}^-$ in NaClO_4 medium. The uncertainties are given as claimed by the authors.

Reference	m (NaClO_4) ($\text{mol} \cdot \text{kg}^{-1}$)	$\Delta_r H_m + L_1$ ($\text{kJ} \cdot \text{mol}^{-1}$)
[67ARN/KAK]	3.50	54.82 ± 0.13
[69LOB/VAS]	0.51	56.49 ± 0.27
	1.05	56.14 ± 0.07
	2.20	55.64 ± 0.09
	3.50	55.07 ± 0.09
[86MAE]	3.50	55.02 ± 0.30
	4.95	56.09 ± 0.30

in the previous example, the concentration range used should not exceed $4 \text{ mol} \cdot \text{kg}^{-1}$ (this point also deviates from the general trend of the $\Delta_r H_m$ values). The results of the regression are given in Table IX.17 and shown in Figure IX.40.

For the case of the Pitzer equation we tested 3 models:

- with the determination of all the relevant parameters,
- neglecting the contribution of the X_3 term, *i.e.*, all the ternary interactions,
- neglecting the contribution of the X_2 and X_3 terms, *i.e.*, neglecting the all ternary interactions and the ionic strength dependence of the second virial coefficients.

The value of the Pitzer terms can only be predicted for X_2 : $X_2 = \beta_{\text{Na,OH}}^{(1)L} + \beta_{\text{H,ClO}_4}^{(1)L} = 1.34 \times 10^{-4} + 19.31 \times 10^{-4} \approx 2.1 \times 10^{-3} \text{ kg} \cdot \text{mol}^{-1} \cdot \text{K}^{-1}$. As the temperature derivatives of the mixing terms are not available, we can only estimate the values of the parameters X_1 and X_3 : $X_1 \approx \beta_{\text{Na,OH}}^{(0)L} + \beta_{\text{H,ClO}_4}^{(0)L} = 7.00 \times 10^{-4} + 4.905 \times 10^{-4} \approx 1.19 \times 10^{-3} \text{ kg} \cdot \text{mol}^{-1} \cdot \text{K}^{-1}$, $X_3 \approx C_{\text{Na,OH}}^L + C_{\text{H,ClO}_4}^L = -9.47 \times 10^{-5} - 5.89 \times 10^{-5} \approx -1.5 \times 10^{-4} \text{ kg}^2 \cdot \text{mol}^{-2} \cdot \text{K}^{-1}$. As in Examples 5 and 6 where we attempted to determine the Pitzer terms for a $\log_{10} K$ regression, we also obtain in this case very large uncertainties in the estimated values of the fitting parameters. By neglecting the contribution of the ternary terms we obtain more precise estimates of the unknowns. Even so, the error in the X_2 term exceeds the magnitude of this term. However, the contribution of this term affects the value of

Table IX.17: The results of the least square determination of unknowns in fitting equations for the reaction $\text{H}_2\text{O}(\text{l}) \rightleftharpoons \text{H}^+ + \text{OH}^-$ in NaClO_4 medium. All the errors are given as 3σ . The concentration units: for X_1 , X_2 , $\Delta\varepsilon_L$ - $\text{kg} \cdot \text{mol}^{-1} \cdot \text{K}^{-1}$, for X_3 - $\text{kg}^2 \cdot \text{mol}^{-2} \cdot \text{K}^{-1}$.

Fitting equation	$\Delta_r H_m^\circ$ $\text{kJ} \cdot \text{mol}^{-1}$	Concentration parameters	The mean square error per unit $\sigma_o^{(a)}$
Pitzer ^(b)	55.50 ± 0.32	$X_1 = (1.11 \pm 0.08) \times 10^{-3}$	0.406
Pitzer ^(c)	55.88 ± 1.40	$X_1 = (1.02 \pm 0.31) \times 10^{-3}$ $X_2 = (1.3 \pm 4.4) \times 10^{-3}$	0.419
Pitzer	57.30 ± 5.38	$X_1 = (-0.5 \pm 5.5) \times 10^{-3}$ $X_2 = (9.1 \pm 29.0) \times 10^{-3}$ $X_3 = (2.3 \pm 9.3) \times 10^{-4}$	0.450
SIT	55.70 ± 0.35	$\Delta\varepsilon_L = (0.85 \pm 0.16) \times 10^{-3}$	0.425
CODATA	55.82 ± 0.06		

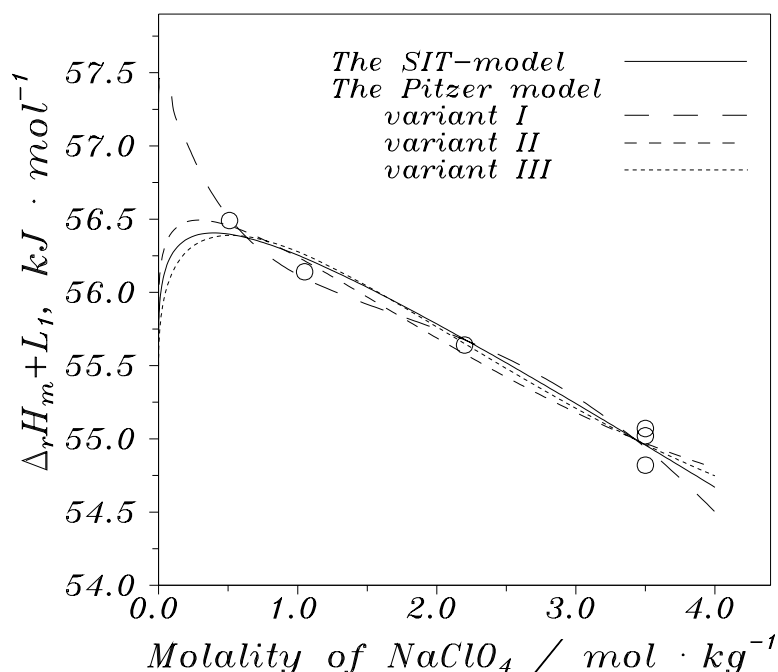
- (a) the mean square error per unit weight σ_o is defined as $\sigma_o^2 = \sum w(\Delta_r H_m - \Delta_r H_{m,\text{calc}})^2 / (n - m)$, where w is the weighting factor determined as the reciprocal square of the estimated uncertainty in $\Delta_r H_m$ value; $\Delta_r H_{m,\text{calc}}$ is the value of the heat of reaction calculated using the obtained regression parameters; n is the number of experimental data; m is the number of variables;
- (b) neglecting the contribution of X_2 and X_3 terms;
- (c) neglecting the contribution of X_3 term.

the enthalpy change at infinite dilution. The application of the Pitzer equation both for the description of the concentration dependence of heats of reaction, and of $\log_{10} K$ data is an ill-conditioned task. The main problem is the reliable estimation of the $\Delta\beta^{(1)L}$ parameter, which determines the concentration dependence of the second virial coefficient in the Pitzer approach and, therefore, has a substantial influence on the estimated value of $\Delta_r H_m^\circ$ for the reaction. However, the determination of $\Delta\beta^{(1)L}$ parameter requires precise experimental data at low ionic strengths, where the relative contribution of this parameter to the value of ΔB^L is most pronounced.

The SIT model results in a reliable value of the $\Delta_r H_m^\circ$ term, and the value $\Delta\varepsilon_L = (0.85 \pm 0.16) \times 10^{-3} \text{ kg} \cdot \text{mol}^{-1} \cdot \text{K}^{-1}$ obtained by the regression is consistent with the estimate based on the parameters $\varepsilon_L(\text{H}^+, \text{ClO}_4^-)$ and $\varepsilon_L(\text{Na}^+, \text{OH}^-)$, obtained from the enthalpies of dilution of the corresponding electrolytes: $\Delta\varepsilon_L = \varepsilon_L(\text{H}^+, \text{ClO}_4^-) + \varepsilon_L(\text{Na}^+, \text{OH}^-) = (0.9 \pm 0.2) \times 10^{-3} + (0.5 \pm 0.2) \times 10^{-3} = (1.4 \pm 0.3) \times 10^{-3} \text{ kg} \cdot \text{mol}^{-1} \cdot \text{K}^{-1}$.

It should be kept in mind that the omission of the parameter $\Delta\beta^{(1)L}$ may be essential

Figure IX.40: The parametrization of the SIT and different variants of the Pitzer models (see text for details) from the experimental values of $\Delta_r H_m$ for the reaction $\text{H}_2\text{O}(\text{l}) \rightleftharpoons \text{H}^+ + \text{OH}^-$ in NaClO_4 medium at 298.15 K and 1 atm.



for the accuracy of the $\Delta_r H_m^\circ$ determination. The Pitzer equation with only the $\Delta\beta^{(0)L}$ is not analogous to the SIT equation (see previous discussion of the simplified one-parameter Pitzer and the SIT model IV in Examples 6 and 7). The choice between the Pitzer and the SIT models must be based on the number of data available, the ionic strength range used and the precision of the experimental results. In our experience, the existing data on heats of complex formation reactions do not allow the use of extrapolation equations more complex than the linear expression used here. In principle, one could try to estimate the values of the Pitzer parameter $\beta^{(1)L}$ using a procedure like the one employed to estimate the $\beta^{(1)}$ parameters. This can be done by comparison of the analytical equations for the relative partial molar enthalpies based on the SIT and the simplified (without C^L term) Pitzer approaches. However, an analysis of the typical values of the C^L parameters for the different electrolytes from the available compilation [91PIT] showed that in general the contribution of the C^L term cannot be neglected even at moderate ($1\text{--}2 \text{ mol} \cdot \text{kg}^{-1}$) ionic strengths.

Example 18:

Another example of the use of the Pitzer and the SIT model to obtain the value of $\Delta_r H_m^\circ$ for a complex formation equilibrium is the determination of $\Delta_r H_m^\circ$ for the reaction

Table IX.18: The experimental values of the enthalpy change for the reaction $\text{Hg}^{2+} + \text{Cl}^- \rightleftharpoons \text{HgCl}^+$ in NaClO_4 ionic medium at 298.15 K, with our estimations of the uncertainties.

Reference	m (NaClO_4) ($\text{mol} \cdot \text{kg}^{-1}$)	$\Delta_r H_m$ ($\text{kJ} \cdot \text{mol}^{-1}$)
[64CHR/IZA]	0.51	-23.0 ± 1.0
[65ARN]	3.50	-24.2 ± 1.0
[75CIA/GRI]	1.05	-23.2 ± 0.5
[80VAS/KOZ]	0.51	-23.64 ± 0.5
	1.05	-24.35 ± 0.5
	2.20	-24.60 ± 0.5

$\text{Hg}^{2+} + \text{Cl}^- \rightleftharpoons \text{HgCl}^+$ at 298.15 K. There are a number of experimental calorimetric determinations of the enthalpies of this reaction in NaClO_4 medium [64CHR/IZA, 65ARN, 75CIA/GRI, 80VAS/KOZ], see Table IX.18.

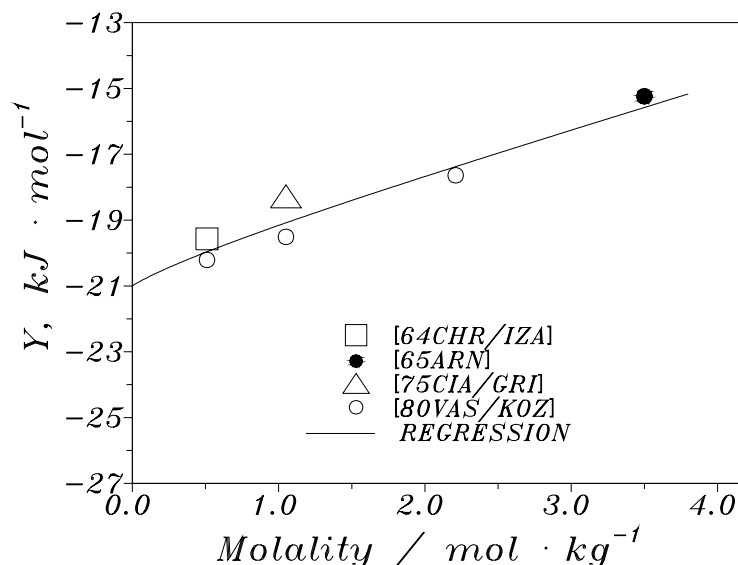
We should notice that the example considered is exceptional in the sense that we have experimental results from 4 independent laboratories, which are in good agreement with one another.

We used the simplified Pitzer-type of the regression neglecting the contribution of the X_3 term. For this reaction $\Delta(Z^2) = -4$, $\Delta|Z| = -2$. The function to be fitted is given by

$$\begin{aligned}
 Y &= \Delta_r H_m + A_L \left[\frac{\sqrt{I_m}}{1 + b\sqrt{I_m}} + \frac{2}{b} \ln \left(1 + b\sqrt{I_m} \right) \right] \\
 &\quad - 4RT^2 m^2 \beta_{\text{Na,ClO}_4}^{(1)L} \frac{g'(I_m)}{I_m} - 2RT^2 m^2 C_{\text{Na,ClO}_4}^L \\
 &= \Delta_r H_m^\circ - 2RT^2 m X_1 + 2RT^2 m X_2 g(I_m)
 \end{aligned}$$

In Figure IX.41 we plotted the function Y *versus* the concentration of the supporting electrolyte. The parameters $\Delta_r H_m^\circ$ and X_2 depend on the relative contribution of the term $g(I_m)$, which is maximal at low concentrations. However, the existing data cannot define this function with any reliability, which results in very large uncertainties in the fitting parameters values: $\Delta_r H_m^\circ = -21.0 \pm 6.5 \text{ kJ} \cdot \text{mol}^{-1}$, $X_1 = (-9.0 \pm 20.6) \times 10^{-3} \text{ kg} \cdot \text{mol}^{-1} \cdot \text{K}^{-1}$, $X_2 = (1.2 \pm 20.0) \times 10^{-3} \text{ kg} \cdot \text{mol}^{-1} \cdot \text{K}^{-1}$. All errors are given as 3σ .

Figure IX.41: The concentration dependence of the fitting function Y (see text for details) for the reaction $\text{Hg}^{2+} + \text{Cl}^- \rightleftharpoons \text{HgCl}^+$ in NaClO_4 solutions at 298.15 K and 1 atm based on the Pitzer model.



Based on the SIT model, one can define the fitting function Y as follows

$$Y = \Delta_r H_m^\circ + \frac{3A_L \sqrt{I_m}}{1 + 1.5\sqrt{I_m}} = \Delta_r H_m^\circ - RT^2 m \Delta \varepsilon_L$$

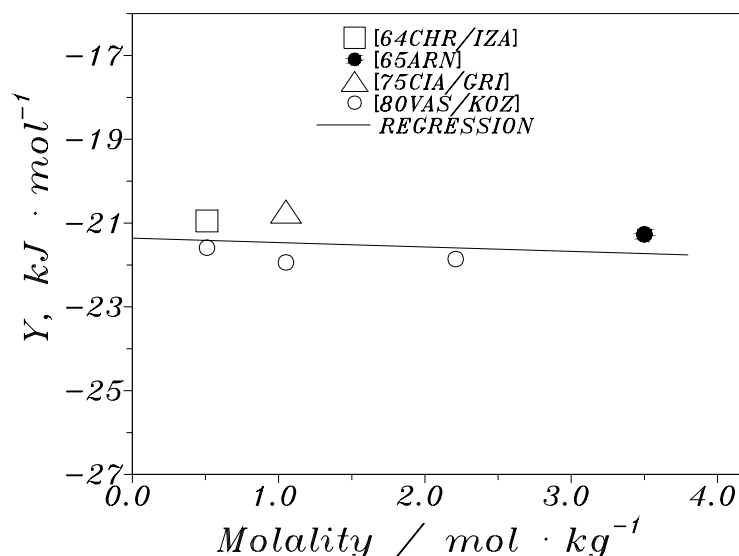
where $\Delta_r H_m^\circ$ and the $\Delta \varepsilon_L$ can be determined using the weighted linear regression procedure. Figure IX.42 shows that the agreement between the experimental data and the model function, and the deviations from the linear dependence are within the estimated uncertainty of experimental values (± 0.5 - 1.0 kJ · mol⁻¹). The results are: $\Delta_r H_m^\circ = -21.36 \pm 1.26$ kJ · mol⁻¹, $\Delta \varepsilon_L = (0.14 \pm 1.12) \times 10^{-3}$ kg · mol⁻¹ · K⁻¹. This value of $\Delta_r H_m^\circ$ can be compared with the reported literature estimates: -20.1 ± 2.1 [61MAL/PAR] and -22.3 ± 0.35 kJ · mol⁻¹ [80VAS/KOZ].

IX.11. Conclusions

Our findings may be summarised as follows:

- The more extensively parametrized Pitzer model allows the most precise modelling of mean-activity coefficient data and equilibrium constants, *provided that all interaction parameters are known*. If some parameters are missing (*e.g.* for ternary interactions between the “strong electrolyte” reactants, or interaction parameters for complexes) they have to be determined experimentally or to be *estimated*, otherwise there may be a substantial loss of accuracy.

Figure IX.42: The concentration dependence of the fitting function Y (see text for details) for the reaction $\text{Hg}^{2+} + \text{Cl}^- \rightleftharpoons \text{HgCl}^+$ in NaClO_4 solutions at 298.15 K and 1 atm based on the SIT model.



- Estimations of missing Pitzer parameters must be made from thermodynamic data obtained in media of different composition. The estimate of parameters for complex formation reactions and other equilibria is a particular case. They are based on concentration equilibrium constants determined in different ionic media/ionic strength, and we have demonstrated that it is difficult, or impossible, to make precise estimates from such data using the complete Pitzer formalism. Approximations are necessary, and this will reduce the precision of the model.
- In the different examples we have demonstrated how different model assumptions will influence both the precision in the parameter estimates and the description of the concentration/ionic strength dependence of the experimental data.
- The SIT model is inherently less precise than the Pitzer model, because it contains fewer parameters. Hence, the precision in the description of mean-activity coefficient data in systems of strong electrolytes is much lower than for the Pitzer model. As indicated above, it is in general necessary to make approximations in the complete Pitzer model, when describing complex formation reactions. For these cases, we have shown that the less parametrized SIT model is in good agreement with the Pitzer model in the concentration range 0.1-4 mol · kg⁻¹.
- The Pitzer and SIT models are equivalent for the intercomparison of equilibrium constants determined in ionic media. The structure of the Pitzer formalism makes it more suitable for recalculation of tabulated equilibrium constants to concentration

constants valid for media containing different strong electrolytes and/or of very high ionic strength, *e.g.* in salt brines.

Both models are internally consistent and the same formalism may also be used to describe the concentration dependence of other thermodynamic quantities, such as enthalpies of reaction, partial molar heat capacities, partial molar volumes, *etc.*

From the structure of the models follows that their range of validity varies with the chemical system studied. The information we have provided should enable the user of these models to make estimates of the precision to be expected from them, and to make a sensitivity analysis of how various assumptions affect the modelling of the system.

The Pitzer model is included in many computer codes and a user of thermodynamic data for complex formation reactions may therefore wish to use this formalism rather than the SIT model. One may then re-evaluate existing equilibrium constant data to deduce the required Pitzer parameters (very few such analyses have been reported in the literature). We have proposed the transformation of existing SIT interaction parameters into a set of Pitzer parameters using correlations established in Sections IX.7.1 and IX.8, as an alternative. However, this requires approximations in the Pitzer model, as indicated above.

When modelling *e.g.* the speciation of trace elements in the systems encountered in nature, one invariably has to make approximations of various kinds. The most important information for the model is the identification of the key chemical reactions, and this can nearly always be achieved, even if the relevant equilibrium constants are known no better than within 0.2-0.3 logarithmic units. The uncertainty expected from both the Pitzer and the SIT models is smaller than this.

Finally, the relative merits of different models may give rise to controversy among the users. Let us remind the reader that *no* model can give a “complete” description of a system, or a process. A model is designed to achieve a “practical” purpose, a “partial” description of a more complex phenomenon. It is up to the user to decide if a particular model is useful, or not, for his/her purpose ! In this chapter we have tried to make a description/discussion of the advantages/draw-backs of two such models.

Chapter X

Temperature Corrections to Thermodynamic data and Enthalpy Calculations [†]

Ignasi PUIGDOMENECH ¹
OECD Nuclear Energy Agency
Le Seine – Saint Germain
12, boulevard des Iles
F-92130 Issy-les-Moulineaux (France)

Joseph A. RARD
Geosciences and Environmental Technologies
Environmental Programs Directorate
Lawrence Livermore National Laboratory
Livermore, California 94550 (USA)

Andrey V. PLYASUNOV ²
Department of Inorganic Chemistry
Royal Institute of Technology
S-100 44 Stockholm (Sweden)

Ingmar GRENTHE
Department of Inorganic Chemistry
Royal Institute of Technology
S-100 44 Stockholm (Sweden)

X.1. Introduction

Recalculation of chemical equilibrium data from the reference temperature of 298.15 K (25.00°C) to any desired temperature is made by using the relationships provided by thermodynamics. The procedures are straight-forward provided that information is available for $\Delta_r H_m^\circ$ or $\Delta_r S_m^\circ$ at the reference temperature and for their temperature dependencies. Complete information of this kind is rarely available for formation reactions of chemical complexes in aqueous solution and it is therefore necessary to rely on approximation methods of various kinds. These methods will be described in some detail in this chapter.

[†] A substantial portion of this Chapter originates from an internal NEA technical report (TDB-4).

¹ Permanent address: Department of Inorganic Chemistry, Royal Institute of Technology, S-100 44 Stockholm, Sweden.

² Permanent address: Institute of Experimental Mineralogy, Chernogolovka, Moscow District, 142432 Russia.

Experimental thermodynamic information about the chemical species (chemical speciation) in a particular system forms the basis of thermodynamic databases. However, experiments only provide information about the species that are present in noticeable amounts in the laboratory systems (and thus are detectable in the experiments). A complication in the modelling of the properties of systems at different temperatures is the possibility of a change in speciation with temperature, since even a temperature change as small as from 298 to 323 K may result in the appearance of new species [76BAE/MES, 87CIA/IUL]. The modelling in such situations can only be made using the general principles of chemistry as outlined in Chapter III. One may also have to make experimental determinations in situations where one is reasonably confident that a change in speciation is of critical importance for the understanding of the system at higher temperatures.

There are some general considerations that can be used as guidelines:

- The dielectric constant of liquid water decreases strongly with increasing temperature (*cf.* Figure X.2 on *p.*438), hence, complexes of low or zero charge are favoured at higher temperatures.
- Hydrolysis of metal ions increases with increasing temperature, in keeping with the general increase of acidity of water with increasing temperature.
- The relative amounts of polynuclear complexes and other complexes with high charges decrease with increasing temperature [94PLY/GRE]. This effect can be correlated with the decrease in the dielectric constant of the solvent water with increasing temperature (*cf.* Figure X.2). Even surprisingly simple electrostatic models are able to describe this feature with fair accuracy. In the final section of this chapter we will describe the characteristic features of one such model and its predictive properties.

Thermodynamic data may also need to be corrected for ionic strength effects both at 298.15 K and at other temperatures. This is not a straight-forward problem at $T \neq 298.15$ K as discussed in Chapter IX.

As will be seen from the following text the approximation methods used to describe the temperature dependencies of chemical equilibria rely heavily on simple electrostatic models which treat the participating ionic species as point-charges and the solvent as a homogeneous dielectric continuum; both assumptions are oversimplifications.

The extrapolation of experimental values of $\Delta_r G_m^\circ(T)$ (or, conversely, equilibrium constants) to a reference temperature, generally 298.15 K, is usually done by using various modifications of the so-called second- and third-law methods. The third-law extrapolations require free energy functions and are generally the preferred method of calculation when long temperature extrapolations are required, particularly where the reactants and products are pure phases for which experimental heat capacities or relative enthalpies are available or can be accurately estimated. That is, third-law extrapolations should generally be used for equilibria between different phases at high temperatures. When

extrapolations over relatively small temperature ranges are made, then second-law extrapolations can be used for accurate calculations, but this method requires experimental or estimated heat capacities around the temperature of interest. Second-law extrapolations should generally be used for aqueous equilibria.

X.2. Second-law extrapolations

The standard molar Gibbs energy change for a reaction at any given temperature is given by

$$\Delta_r G_m^\circ = \Delta_r H_m^\circ - T \Delta_r S_m^\circ, \quad (\text{X.1})$$

and the temperature dependence of the Gibbs energy is:

$$\left(\frac{\partial \Delta_r G_m^\circ}{\partial T} \right)_p = -\Delta_r S_m^\circ.$$

The *Gibbs-Helmholtz equation* is:

$$\left(\frac{\partial \Delta_r G_m^\circ / T}{\partial T} \right)_p = \frac{-\Delta_r H_m^\circ(T)}{T^2}, \quad (\text{X.2})$$

which has the integrated form[†]:

$$\int_{T_0}^T d \left(\frac{\Delta_r G_m^\circ(T)}{T} \right) = - \int_{T_0}^T \left(\frac{\Delta_r H_m^\circ(T)}{T^2} \right) dT. \quad (\text{X.3})$$

From the integration of this equation, and from using the temperature derivatives of the enthalpy and entropy,

$$\left(\frac{\partial \Delta_r H_m^\circ}{\partial T} \right)_p = \Delta_r C_{p,m}^\circ, \quad (\text{X.4})$$

$$\left(\frac{\partial \Delta_r S_m^\circ}{\partial T} \right)_p = \frac{\Delta_r C_{p,m}^\circ}{T}, \quad (\text{X.5})$$

it is possible to write the temperature dependence of the Gibbs energy as a function of the entropy at the reference temperature ($T_0 = 298.15$ K), as well as the heat capacity function. It is, however, also possible [86NOR/MUN, Eq. (4-14)] and simpler to use Eqs. (X.1), (X.4) and (X.5) to write

$$\begin{aligned} \Delta_r G_m^\circ(T) = & \Delta_r H_m^\circ(T_0) + \int_{T_0}^T \Delta_r C_{p,m}^\circ dT \\ & - T \left(\Delta_r S_m^\circ(T_0) + \int_{T_0}^T \frac{\Delta_r C_{p,m}^\circ}{T} dT \right). \end{aligned}$$

[†] T_0 stands for the reference temperature ($= 298.15$ K).

This equation is usually recast in terms of only one thermodynamic function other than Gibbs energy and heat capacity, *e.g.*, if the choice is entropy,

$$\begin{aligned}\Delta_r G_m^\circ(T) &= \Delta_r G_m^\circ(T_0) - (T - T_0)\Delta_r S_m^\circ(T_0) \\ &\quad + \int_{T_0}^T \Delta_r C_{p,m}^\circ dT - T \int_{T_0}^T \frac{\Delta_r C_{p,m}^\circ}{T} dT.\end{aligned}\quad (\text{X.6})$$

Alternatively, one may write the temperature dependence of the equilibrium constant as a function of the standard enthalpy and the standard heat capacity,

$$\begin{aligned}\log_{10} K^\circ(T) &= \log_{10} K^\circ(T_0) - \frac{\Delta_r H_m^\circ(T_0)}{R \ln(10)} \left(\frac{1}{T} - \frac{1}{T_0} \right) \\ &\quad - \frac{1}{RT \ln(10)} \int_{T_0}^T \Delta_r C_{p,m}^\circ dT + \frac{1}{R \ln(10)} \int_{T_0}^T \frac{\Delta_r C_{p,m}^\circ}{T} dT,\end{aligned}\quad (\text{X.7})$$

where R is the gas constant ($8.31451 \text{ J} \cdot \text{K}^{-1} \cdot \text{mol}^{-1}$). Either Eq. (X.6) or (X.7) may be used to calculate equilibrium constants at a temperature T if:

1. the equilibrium constant at 298.15 K is known;
2. the temperature dependence of $\Delta_r C_{p,m}^\circ$ is known, or the temperature interval is small enough that $\Delta_r C_{p,m}^\circ$ can be assumed to be constant;
3. either $\Delta_r H_m^\circ(T_0)$ or $\Delta_r S_m^\circ(T_0)$ are known.

Unfortunately, experimentally derived heat capacity data have not been measured for most aqueous species and for many solid phases. Therefore, in order to use Eqs. (X.6) or (X.7), one will have to make either approximations (as discussed below) or estimations (*cf.* Section X.4).

If the reaction of interest involves only species for which the pertinent coefficients in the following equation for the heat capacity[†]

$$\begin{aligned}C_{p,m}^\circ(T) &= a + bT + cT^2 + jT^3 + dT^{-1} + eT^{-2} + kT^{-3} \\ &\quad + f \ln T + gT \ln T + h\sqrt{T} + i \frac{1}{\sqrt{T}}\end{aligned}\quad (\text{X.8})$$

[†] This equation is used as a general form for the temperature dependency of the heat capacity in temperature intervals that do not involve any phase transition. For any specific system, only a few of these coefficients will be required (frequently a , b and e). Some of these terms should obviously not be used if the heat capacity equation is required to be valid as $T \rightarrow 0$, since they become infinite at that limit.

are available (which is seldom the case), then the approximation methods given below are not needed, and the integrals in Eqs. (X.6) and (X.7) can be performed analytically and will take the following form:

$$\begin{aligned}
 \int_{T_0}^T \Delta_r C_{p,m}^\circ dT &= \Delta a (T - T_0) + \frac{\Delta b}{2} (T^2 - T_0^2) \\
 &+ \frac{\Delta c}{3} (T^3 - T_0^3) + \frac{\Delta j}{4} (T^4 - T_0^4) + \Delta d \ln \left(\frac{T}{T_0} \right) \\
 &- \Delta e \left(\frac{1}{T} - \frac{1}{T_0} \right) - \frac{\Delta k}{2} (T^{-2} - T_0^{-2}) \\
 &- \Delta f [T (1 - \ln T) - T_0 (1 - \ln T_0)] \\
 &- \frac{\Delta g}{2} [T^2 (0.5 - \ln T) - T_0^2 (0.5 - \ln T_0)] \\
 &+ \frac{2\Delta h}{3} (T^{3/2} - T_0^{3/2}) + 2\Delta i \left(\sqrt{T} - \sqrt{T_0} \right), \quad (X.9)
 \end{aligned}$$

$$\begin{aligned}
 \int_{T_0}^T \frac{\Delta_r C_{p,m}^\circ}{T} dT &= \Delta a \ln \left(\frac{T}{T_0} \right) + \Delta b (T - T_0) \\
 &+ \frac{\Delta c}{2} (T^2 - T_0^2) + \frac{\Delta j}{3} (T^3 - T_0^3) \\
 &- \Delta d \left(\frac{1}{T} - \frac{1}{T_0} \right) - \frac{\Delta e}{2} (T^{-2} - T_0^{-2}) \\
 &- \frac{\Delta k}{3} (T^{-3} - T_0^{-3}) + \frac{\Delta f}{2} [(\ln T)^2 - (\ln T_0)^2] \\
 &- \Delta g [T (1 - \ln T) - T_0 (1 - \ln T_0)] \\
 &+ 2\Delta h \left(\sqrt{T} - \sqrt{T_0} \right) - 2\Delta i \left(\frac{1}{\sqrt{T}} - \frac{1}{\sqrt{T_0}} \right), \quad (X.10)
 \end{aligned}$$

where Δa , Δb , Δc ,... are the changes in the parameters a , b , c ,... of Eq. (X.8) with the reaction, *i.e.*,

$$\Delta a = \sum_i \nu_i a_i,$$

etc., and where ν_i are the stoichiometric coefficients of the species i of the reaction.

If equilibrium constants are known at several temperatures, the parameters of Eq. (X.7) (together with Eqs. (X.9) and (X.10)) can be evaluated from the experimental data by a least-squares procedure.

It is sometimes convenient to use “apparent” standard partial molar Gibbs energies and enthalpies, *cf.* Refs. [74HEL/KIR, 78HEL/DEL, 80TRE/LEB] defined as

$$\Delta_a G_m^\circ(i, T) = \Delta_f G_m^\circ(i, T_0) + (G_m^\circ(i, T) - G_m^\circ(i, T_0)) \quad (X.11)$$

and

$$\Delta_a H_m^\circ(i, T) = \Delta_f H_m^\circ(i, T_0) + \int_{T_0}^T C_{p,m}^\circ(i, T) dT. \quad (X.12)$$

Using the relationship

$$S_{\text{m}}^{\circ}(i, T) = S_{\text{m}}^{\circ}(i, T_0) + \int_{T_0}^T \frac{C_{p,\text{m}}^{\circ}(i, T)}{T} dT, \quad (\text{X.13})$$

it is possible to rewrite Eq. (X.6),

$$\Delta_{\text{r}}G_{\text{m}}^{\circ}(T) = \sum_i \nu_i \Delta_{\text{a}}H_{\text{m}}^{\circ}(i, T) - T \sum_i \nu_i S_{\text{m}}^{\circ}(i, T) \quad (\text{X.14})$$

$$= \sum_i \nu_i \Delta_{\text{a}}G_{\text{m}}^{\circ}(i, T) \quad (\text{X.15})$$

$$= \sum_i \nu_i \left(\Delta_{\text{f}}G_{\text{m}}^{\circ}(i, T_0) - (T - T_0)S_{\text{m}}^{\circ}(i, T_0) + \int_{T_0}^T C_{p,\text{m}}^{\circ}(i, T) dT - T \int_{T_0}^T \frac{C_{p,\text{m}}^{\circ}(i, T)}{T} dT \right). \quad (\text{X.16})$$

If the heat capacity is expressed according to Eq. (X.8), the integrals in Eq. (X.16) have the same form as Eqs. (X.9) and (X.10) except that in Eqs. (X.9) and (X.10), $\Delta_{\text{r}}C_{p,\text{m}}^{\circ}$, Δa , Δb , Δc , *etc.*, must be substituted for $C_{p,\text{m}}^{\circ}$, a , b , c , *etc.*

Eqs. (X.12) through (X.16) are especially useful when the assumption is made that for some of the reactants (or products) the heat capacity does not vary with temperature, whereas for the rest of the reactants (or products) Eq. (X.8) applies.

X.2.1. The hydrogen ion convention

The hydrogen ion convention states that the conventional standard partial molar Gibbs energy of formation, entropy and heat capacity of H^+ are all set equal to zero at all temperatures. This allows values to be assigned for the thermodynamic properties of each ionic species participating in a reaction. Therefore, it is possible to write

$$\Delta_{\text{r}}G_{\text{m}}^{\circ}(T) = \sum_i \nu_i G_{\text{m}}^{\circ}(i, T), \quad (\text{X.17})$$

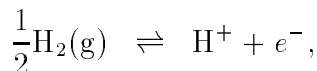
where $G_{\text{m}}^{\circ}(i, T)$ is the resulting standard state Gibbs energy of ion i based on the hydrogen ion convention.

As just stated, the hydrogen ion convention involves the arbitrary assignment of the standard ionic entropy of the aqueous hydrogen ion as being equal to zero at all temperatures, *i.e.*, $S_{\text{m}}^{\circ}(\text{H}^+, \text{aq}, T) = 0$. Another assumption of this convention is that the standard partial molar Gibbs energy of formation of the hydrogen ion is equal to zero at all temperatures, $\Delta_{\text{f}}G_{\text{m}}^{\circ}(\text{H}^+, \text{aq}, T) = 0$. However, the entropy of formation of an ion is equal to the temperature derivative of its Gibbs energy of formation:

$$\left(\frac{\partial \Delta_{\text{f}}G_{\text{m}}^{\circ}(i, T)}{\partial T} \right)_p = -\Delta_{\text{f}}S_{\text{m}}^{\circ}(i, T).$$

Thus the assumption that $\Delta_f G_m^\circ(\text{H}^+, \text{aq}, T) = 0$ also implies that $\Delta_f S_m^\circ(\text{H}^+, \text{aq}, T) = 0$, and according to Eq. (X.1) it also implies that $\Delta_f H_m^\circ(\text{H}^+, \text{aq}, T) = 0$.

The reaction for formation of the aqueous hydrogen ion is



for which the entropy of formation is given by

$$\begin{aligned}\Delta_f S_m^\circ(T) &= \Delta_f S_m^\circ(\text{H}^+, \text{aq}, T) \\ &= S_m^\circ(\text{H}^+, \text{aq}, T) + S_m^\circ(e^-, T) - \frac{1}{2}S_m^\circ(\text{H}_2, \text{g}, T)\end{aligned}$$

In this case the standard partial molar entropy of formation of the hydrogen ion is identical to the entropy of reaction. However, the standard partial molar entropy of formation of the hydrogen ion and its standard partial molar ionic entropy are both set equal to zero in the hydrogen ion convention, $\Delta_f S_m^\circ(\text{H}^+, \text{aq}, T) = S_m^\circ(\text{H}^+, \text{aq}, T) = 0$. Consequently, to remain consistent with the standard entropy of $\text{H}_2(\text{g})$, the “aqueous electron” must be assigned an effective molar entropy of

$$S_m^\circ(e^-, T) = \frac{1}{2}S_m^\circ(\text{H}_2, \text{g}, T)$$

At 298.15 K, the CODATA key values [89COX/WAG] at 1 bar pressure yield

$$S_m^\circ(e^-, T_0) = (65.340 \pm 0.001_5) \text{ J} \cdot \text{K}^{-1} \cdot \text{mol}^{-1}.$$

This value must be included when the entropy of an ionic species is being calculated from the entropies of the elements from which it is formed.

As an example, the ionic entropy of the divalent calcium ion will be calculated at 298.15 K from its entropy of formation. The formation reaction is



and the corresponding entropy of formation is given by

$$\begin{aligned}\Delta_f S_m^\circ(\text{Ca}^{2+}, \text{aq}, 298.15 \text{ K}) &= S_m^\circ(\text{Ca}^{2+}, \text{aq}, 298.15 \text{ K}) + 2S_m^\circ(e^-, 298.15 \text{ K}) \\ &\quad - S_m^\circ(\text{Ca}, \text{cr}, 298.15 \text{ K})\end{aligned}$$

The entropy of formation of the calcium ion can be calculated from its standard Gibbs free energy of formation and the enthalpy of formation as given in the CODATA tables to yield $\Delta_f S_m^\circ(\text{Ca}^{2+}, \text{aq}, 298.15 \text{ K}) = (32.9 \pm 5.0) \text{ J} \cdot \text{K}^{-1} \cdot \text{mol}^{-1}$. Then,

$$\begin{aligned}S_m^\circ(\text{Ca}^{2+}, \text{aq}, 298.15 \text{ K}) &= S_m^\circ(\text{Ca}, \text{cr}, 298.15 \text{ K}) - 2S_m^\circ(e^-, 298.15 \text{ K}) \\ &\quad + \Delta_f S_m^\circ(\text{Ca}^{2+}, \text{aq}, 298.15 \text{ K}) \\ &= (41.6 \pm 0.4) - 2(65.340 \pm 0.001_5) + (32.9 \pm 5.0) \\ &= -(56.2 \pm 5.0) \text{ J} \cdot \text{K}^{-1} \cdot \text{mol}^{-1} \dagger\end{aligned}$$

† This calculated value of $S_m^\circ(\text{Ca}^{2+}, \text{aq}, 298.15 \text{ K})$ is identical to that given in the CODATA tables, whereas the uncertainties are quite different. This arises because the calculations involved different thermodynamic cycles.

X.2.2. Approximations

For many chemical reactions there is a lack of heat capacity functions for all or some of the species involved, and therefore approximations (as described in this section) or estimations (*cf.* Section X.4) must be made in order to use Eqs. (X.6), (X.7) or (X.16). The method of choice will depend on the type of chemical reaction being considered.

X.2.2.1. Constant enthalpy of reaction

The simplest assumption to be made is that the heat capacity change of reaction is zero at all temperatures (*i.e.*, the standard molar enthalpy of reaction does not vary with temperature, *cf.* Eqs. (X.4) and (X.5)). In that case, Eq. (X.7) reduces to the integrated van't Hoff expression[†]

$$\log_{10} K^\circ(T) = \log_{10} K^\circ(T_0) + \frac{\Delta_r H_m^\circ(T_0)}{R \ln(10)} \left(\frac{1}{T_0} - \frac{1}{T} \right). \quad (\text{X.18})$$

For a temperature range $(T - T_0)$ equal or less than ± 10 K, the error introduced in $\log_{10} K^\circ(T)$ by this simplification will, in most cases, be well within its uncertainty limits.

Eq. (X.18) is applicable to chemical reactions in a single phase or a multiphase system at constant total pressure provided no further constraint is placed upon the system. For certain other cases, for example when the temperature dependence of a solubility product is being studied, the system is constrained to fall on the saturated solution curve, and Eq. (X.18) must be modified. See Section X.2.3.

X.2.2.2. Constant heat capacity of reaction

Another approach, which is often used in conjunction with Eq. (X.7) when the extrapolation extends over a temperature range larger than about 20 K, is to assume that the heat capacity of the reaction does not vary with temperature. In that case Eq. (X.7) becomes

$$\begin{aligned} \log_{10} K^\circ(T) = \log_{10} K^\circ(T_0) + \frac{\Delta_r H_m^\circ(T_0)}{R \ln(10)} \left(\frac{1}{T_0} - \frac{1}{T} \right) \\ + \frac{\Delta_r C_{p,m}^\circ}{R \ln(10)} [(T_0/T) - 1 + \ln(T/T_0)], \end{aligned} \quad (\text{X.19})$$

where, as mentioned earlier, the reference temperature is $T_0 = 298.15$ K.

[†] By combining Eq. (X.2) and the relation $\Delta_r G_m^\circ(T) = -RT \ln K^\circ(T)$, it is possible to obtain, for a given constant pressure p :

$$\frac{d \ln K_p^\circ(T)}{dT} = \frac{\Delta_r H_m^\circ(T)}{RT^2}$$

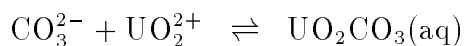
which is called the *van't Hoff equation*.

Using Eq. (X.1) it is possible to rewrite this expression as follows (compare also with Eqs. (X.6) and (X.7)):

$$\begin{aligned}\Delta_r G_m^\circ(T) &= \Delta_r G_m^\circ(T_0) - (T - T_0)\Delta_r S_m^\circ(T_0) \\ &\quad + \Delta_r C_{p,m}^\circ [T - T_0 - T \ln(T/T_0)].\end{aligned}\quad (\text{X.20})$$

Use of Eqs. (X.19) or (X.20) to represent values of $\log_{10} K(T)$ will give enthalpies of reaction which are more reliable than those obtained assuming a “constant enthalpy of reaction”, Eq. (X.18), but the $\Delta_r C_{p,m}^\circ(T_0)$ values obtained will be imprecise [67HEL]. For most reactions the assumption made in Eqs. (X.19) and (X.20) will be appropriate for temperatures in the range 273 to 473 K.

As an example, Eq. (X.19) can be used to fit the high-temperature equilibrium constants reported by [72SER/NIK] for the reaction



which will be evaluated below as an isoelectric reaction. The resulting values are $\log_{10} K(T_0) = (9.90 \pm 0.07)$, $\Delta_r H_m^\circ(T_0) = -(1.8 \pm 3.4) \text{ kJ} \cdot \text{mol}^{-1}$, and $\Delta_r C_{p,m}^\circ(T_0) = (551 \pm 31) \text{ J} \cdot \text{K}^{-1} \cdot \text{mol}^{-1}$. If the equilibrium constant at 298.15 K is not a fitting parameter, but instead is set equal to the recommended value of $\log_{10} K^\circ(T_0) = (9.68 \pm 0.04)$ [92GRE/FUG], the following results are obtained: $\Delta_r H_m^\circ(T_0) = (6 \pm 6) \text{ kJ} \cdot \text{mol}^{-1}$, and $\Delta_r C_{p,m}^\circ(T_0) = (499 \pm 74) \text{ J} \cdot \text{K}^{-1} \cdot \text{mol}^{-1}$.

A comparison between the results from Eq. (X.19) (using both sets of fitted parameters) and the experimental data is shown in Figure X.1.

The reaction enthalpy is found in this case to be zero within the experimental error. The entropy of reaction is given (*cf.* Eq. (X.1)) by

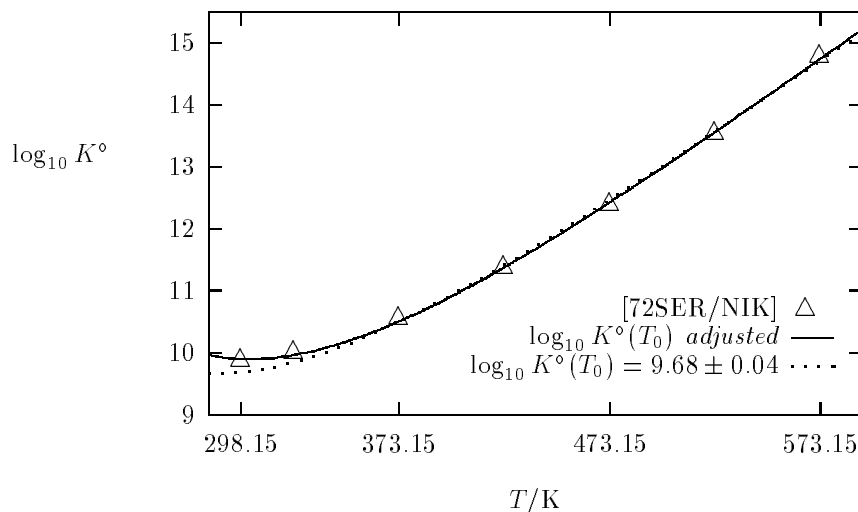
$$\begin{aligned}\Delta_r S_m^\circ(T_0) &= \frac{\Delta_r H_m^\circ(T_0)}{T_0} + \ln(10)R \log_{10} K^\circ(T_0) \\ \sigma^2(\Delta_r S_m^\circ) &= 1.125 \times 10^{-5} \sigma^2(\Delta_r H_m^\circ) + 366.5 \sigma^2(\log_{10} K^\circ),\end{aligned}$$

which gives $\Delta_r S_m^\circ(T_0) = (183 \pm 12) \text{ J} \cdot \text{K}^{-1} \cdot \text{mol}^{-1}$ (when the equilibrium constant at 298.15 K is also fitted to Eq. (X.19)) or which gives $\Delta_r S_m^\circ(T_0) = (206 \pm 22) \text{ J} \cdot \text{K}^{-1} \cdot \text{mol}^{-1}$ (with $\log_{10} K^\circ(T_0)$ fixed at 9.68).

Eqs. (X.19) and (X.20) are useful to calculate higher temperature equilibrium constants when average heat capacities for aqueous ions have been determined experimentally or estimated (*cf.* Section X.4.1.2).

Alternatively, partial molar heat capacities at 298.15 K are sometimes considered to be constant with temperature. This assumption is based on the fact that although values for ionic heat capacities generally increase with temperature, they usually also have a maximum around 325 to 375 K and then begin to decrease (see for example Figure 4 in Ref. [82PAT/SLO] and Figures 103 to 106 in Ref. [81HEL/KIR]). Therefore setting $C_{p,m}^\circ(T) \approx C_{p,m}^\circ(T_0)$ may be a valid simplification in the temperature range between 273 and 373 to 423 K depending on the nature of the reaction [67HEL]. However, using the

Figure X.1: Equilibrium constants from [72SER/NIK] for Reaction (X.27): $\text{CO}_3^{2-} + \text{UO}_2^{2+} \rightleftharpoons \text{UO}_2\text{CO}_3(\text{aq})$, compared with the two different least squares fits to the “constant $\Delta_r C_{p,m}^\circ$ ” equation, Eq. (X.19), described in the text.



heat capacity at the average temperature $C_{p,m}^\circ(\frac{T+T_0}{2})$ may be an even better approximation over some temperature intervals.

Partial molar heat capacities at 298.15 K for ions in aqueous solutions may be estimated from ionic entropies as discussed later, with some of the equations given in Refs. [64CRI/COB2, 81HEL/KIR, 88SHO/HEL].

Once heat capacities have been estimated, they can then be used as follows [69HEL]:

- If the chemical reaction involves only aqueous ionic species, then the average heat capacities may be combined into a single average heat capacity of reaction, and Eqs. (X.19) or (X.20) can be used. This method is used for example in Ref. [80LEM/TRE].
- If the chemical reaction includes phases for which heat capacity functions are available (*i.e.*, expressions compatible with Eq. (X.8)), it is convenient to use Eq. (X.14),

$$\Delta_r G_m^\circ(T) = \sum_i \nu_i \Delta_a H_m^\circ(i, T) - T \left(\sum_i \nu_i S_m^\circ(i, T) \right), \quad (\text{X.14})$$

together with the following equations [69HEL] for the aqueous species (which are to be used instead of Eqs. (X.12) and (X.13)):

$$\Delta_a H_m^\circ(i, T) = \Delta_f H_m^\circ(i, T_0) + C_{p,m}^\circ|_{T_0}^T(i) (T - T_0) \quad (\text{X.21})$$

Table X.1: Temperature contributions in Eq. (X.20).

$t(^{\circ}\text{C})$	$T(\text{K})$	$\Delta T = T - T_0$ (K)	$T \ln(T/T_0)$ (K)	$\Delta T - T \ln(T/T_0)$ (K)
0.00	273.15	-25.0	-23.92	1.08
15.00	288.15	-10.0	-9.83	0.17
20.00	293.15	-5.0	-4.96	0.04
25.00	298.15	0.0	0.0	0.0
30.00	303.15	5.0	5.04	-0.04
35.00	308.15	10.0	10.17	-0.17
50.00	323.15	25.0	26.02	-1.02
100.00	373.15	75.0	83.73	-8.73
200.00	473.15	175.0	218.5	-43.5

$$S_{\text{m}}^{\circ}(i, T) = S_{\text{m}}^{\circ}(i, T_0) + C_{p,\text{m}}^{\circ}|_{T_0}^T(i) \ln(T/T_0), \quad (\text{X.22})$$

while for the non-ionic species Eqs. (X.12) and (X.13) can be used, for which (as mentioned earlier) the integrals take the form of expressions like Eqs. (X.9) and (X.10) except that one must substitute $\Delta_{\text{r}}C_{p,\text{m}}^{\circ}$, Δa , Δb , ..., *etc.*, for $C_{p,\text{m}}^{\circ}$, a , b , c , ..., *etc.*

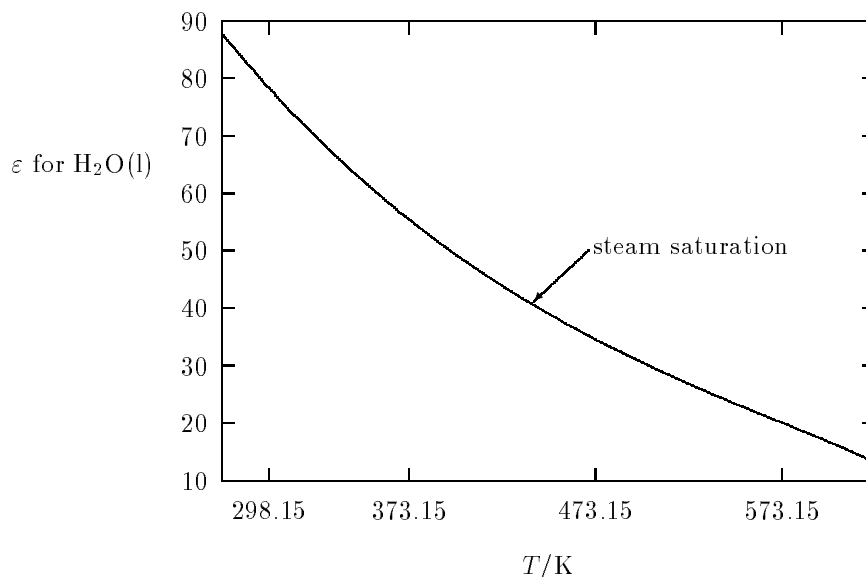
It may be interesting to note that, if $\Delta_{\text{r}}S_{\text{m}}^{\circ}$ and $\Delta_{\text{r}}C_{p,\text{m}}^{\circ}$ are comparable in magnitude, the term in Eq. (X.20) with $\Delta_{\text{r}}C_{p,\text{m}}^{\circ}$ becomes small compared to $\Delta_{\text{r}}S_{\text{m}}^{\circ}\Delta T$ over short temperature ranges, as shown in Table X.1.

In many cases, the $\Delta_{\text{r}}C_{p,\text{m}}^{\circ}$ term can be neglected as it is probably smaller than the error in the estimates of $\Delta_{\text{r}}S_{\text{m}}^{\circ}$. This amounts to the assumption that $\Delta_{\text{r}}C_{p,\text{m}}^{\circ} = 0$ and, thus, $\Delta_{\text{r}}H_{\text{m}}^{\circ}$ and $\Delta_{\text{r}}S_{\text{m}}^{\circ}$ each have the same values for the reaction at any two different temperatures (Eq. (X.18)). This may be a good approximation for small temperature ranges.

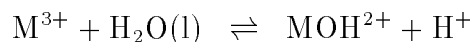
X.2.2.3. Isoelectric and isocoulombic reactions

For a reaction involving aqueous ionic species (but without oxidation/reduction), the enthalpy of reaction may be divided conceptually into two contributions: electrostatic and non-electrostatic. The main part of the enthalpy of reaction is due to the electrostatic interactions between the ionic species participating in the reaction, and between these ionic species and the solvent. Figure X.2 shows that the dielectric constant of water decreases significantly with temperature, reaching values which at $T > 473$ K are similar to those of some organic solvents (acetone, ethanol, *etc.*) at room temperature. Because of this temperature dependence of the dielectric properties of water, electrostatic interactions will bring the largest contribution to the heat capacity of reaction [38GUR, 88SHO/HEL].

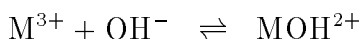
Figure X.2: Temperature dependence for the static dielectric constant of water calculated according to the equation of Bradley and Pitzer [79BRA/PIT] at the standard pressure (1 bar) for $T < 373\text{ K}$ and at the steam saturated pressure [69KEE/KEY, Eq. (17) in their Appendix] at $T \geq 373\text{ K}$.



“Isoelectric” reactions are defined as reactions in which **a)** the total amount of positive charges among the reactants equals the sum of positive charges among the products, and **b)** the same applies for negative charges among reactants and products. For example*:



is an isoelectric reaction, while



is not.

In isoelectric reactions the electrostatic contributions to the temperature dependence will balance out to a large extent, and the heat capacities of reactions will be small and can be assumed constant with temperature. For these reactions, the “constant enthalpy of reaction”, Eq. (X.18), is generally a reliable approximation over a fairly large temperature interval (up to $T \leq 473\text{ K}$). Furthermore, the “constant heat capacity of reaction” approximation, Eq. (X.19), is generally reliable up to $T \leq 623\text{ K}$.

* “M”, “R” and “AN” are used as general abbreviations for metal, rare earth (lanthanide), and actinide respectively.

All ionic species participating in isoelectric reactions often (but not necessarily) have the same sign in the electrical charges [81BAE/MES], *i.e.*, either all charged species have positive or all have negative charges.

The term “isocoulombic” [80LIN, 85JAC/HEL] is used for isoelectric aqueous reactions in which the magnitude of the electrical charge of each individual ionic species also is balanced between reactants and products, for example



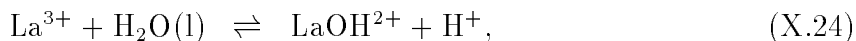
For this kind of reaction, $\Delta_r C_{p,m}^\circ \approx 0$ and thus Eq. (X.18) becomes an even better approximation of the experimental data. It should be noted that there is also an approximate cancellation of activity coefficients in the expression for the equilibrium constant of this reaction.

It is possible to estimate the solvation contribution to the absolute[†] standard partial molar ionic heat capacity with a continuum electrostatic model. For example, using the Born equation [74HEL/KIR, their Eqs. (59), (61) and (66), 88SHO/HEL, their Eq. (30), 88TAN/HEL, their Appendix D],

$$\begin{aligned} C_{p,m,s}^{\circ,\text{abs}}(i, T) &= \frac{z_i^2}{r_{\text{eff},i}} \frac{N_A e^2}{8\pi\epsilon_o} T \frac{1}{\epsilon} \left[\left(\frac{\partial^2 \ln \epsilon}{\partial T^2} \right)_p - \left(\frac{\partial \ln \epsilon}{\partial T} \right)_p^2 \right] \\ &= \frac{z_i^2}{r_{\text{eff},i}} \frac{N_A e^2}{8\pi\epsilon_o} T X(T) \end{aligned} \quad (\text{X.23})$$

where the subscript “s” stands for solvation, and where $(N_A e^2 / (8\pi\epsilon_o)) = 6.947 \times 10^{-5} \text{ m} \cdot \text{J} \cdot \text{mol}^{-1}$; $X(T)$ is a temperature function of the solvent’s dielectric constant which at 298.15 K is equal to $-3.09 \times 10^{-7} \text{ K}^{-2}$ [88TAN/HEL, Table H-1]; and r_{eff} (units m) is the effective electrostatic radius, which at $T < 423 \text{ K}$ is equal to the crystallographic radius to which is added an empirical valence-dependent constant (equal to $z_i \times 0.94 \times 10^{-10} \text{ m}$ for cations and zero for anions [88TAN/HEL, their Eq. (21)]).

The first hydrolysis step of the lanthanum(III) ion will be used as an example. The reaction may be written either as an isoelectric reaction,



or as a complexation reaction involving the hydroxide ion,



The solvation contribution, $\Delta_r C_{p,m,s}^\circ$ (in $\text{J} \cdot \text{K}^{-1} \cdot \text{mol}^{-1}$), to the heat capacity for the isoelectric Reaction (X.24) is, according to Eq. (X.23),

$$\begin{aligned} \Delta_r C_{p,m,s}^\circ(\text{X.24}, T_0) &= \frac{N_A e^2}{8\pi\epsilon_o} T_0 X(T_0) \left(\frac{4}{3.02 \times 10^{-10}} + \frac{1}{3.082 \times 10^{-10}} - \frac{9}{3.96 \times 10^{-10}} \right) \\ &= 39.9 \text{ J} \cdot \text{K}^{-1} \cdot \text{mol}^{-1}, \end{aligned}$$

[†] “Absolute” ionic standard partial molar thermodynamic values are defined in Section X.4.1.2.1, p.478.

where the crystallographic and effective radii for LaOH^{2+} were taken equal to that of La^{3+} ($r_i = 1.14 \times 10^{-10}$ m, given in [88SHO/HEL, Table 1]), and the effective radius for H^+ was taken from [88TAN/HEL, their Table 3]. The heat capacity change for Reaction (X.24) would then be estimated as

$$\begin{aligned}\Delta_r C_{p,m}^\circ(\text{X.24}, T_0) &\approx \Delta_r C_{p,m,s}^\circ(\text{X.24}, T_0) - C_{p,m}^\circ(\text{H}_2\text{O}, l, T_0) \\ &\approx -30.0 \text{ J} \cdot \text{K}^{-1} \cdot \text{mol}^{-1}.\end{aligned}$$

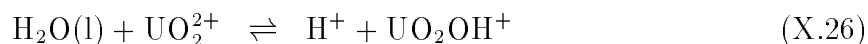
For Reaction (X.25) the ionic radius for OH^- given in [88TAN/HEL, their Table 3] results in a solvent contribution of

$$\begin{aligned}\Delta_r C_{p,m,s}^\circ(\text{X.25}, T_0) &= \frac{N_A e^2}{8\pi \epsilon_0} T_0 X(T_0) \left(\frac{4}{3.02 \times 10^{-10}} - \frac{9}{3.96 \times 10^{-10}} - \frac{1}{1.40 \times 10^{-10}} \right) \\ &= 106.4 \text{ J} \cdot \text{K}^{-1} \cdot \text{mol}^{-1},\end{aligned}$$

and the heat capacity change for Reaction (X.25) is therefore estimated to be $\approx 106.4 \text{ J} \cdot \text{K}^{-1} \cdot \text{mol}^{-1}$. In this case the value of the estimated heat capacity change for Reaction (X.24) is about one third of that for Reaction (X.25). Similar results are obtained for the first hydrolysis step of a divalent cation like Fe^{2+} , or for a tetravalent cation like U^{4+} .

Although the examples given above only take into account solvation contributions to the heat capacity of reaction (furthermore estimated with an oversimplified electrostatic model), they support the assertion that the approximation $\Delta_r C_{p,m}^\circ \approx \text{const.}$ is more appropriate for isoelectric reactions than for most other types of reactions. However, for isocoulombic reactions $\Delta_r C_{p,m}^\circ$ may be even closer to zero.

Many hydrolysis equilibria are isoelectric [88RUA]. As an example, the data reported by Nikolaeva [76NIK] (in the temperature range 298 to 473 K) for the reaction



are plotted in Figure X.3. The values of $\log_{10} K^\circ$ are essentially a linear function of T^{-1} in this temperature interval, indicating that $\Delta_r C_{p,m}^\circ$ is small. Other examples with linear or nearly-linear regions for acid-base equilibria are given by Lindsay [80LIN], Cobble *et al.* [82COB/MUR, pp.4-11 to 4-15] and by Mesmer *et al.* [88MES/MAR, 91MES/PAL].

If a reaction of interest is neither isocoulombic nor isoelectric, it may be converted into an isocoulombic or isoelectric reaction by combination with an appropriate reaction for which accurate high-temperature equilibrium constants are known. This approach has been widely used, *e.g.*, [81BAE/MES, 83PHI/SIL, 85JAC/HEL, 88RUA, 89IZA/CHR, 89IZA/CHR2, 90OSC/GIL, 90OSC/IZA, 92IZA/OSC, 93CHE/GIL, 93CHE/GIL2, 93GIL/OSC].

The data by Piroshkov and Nikolaeva [76PIR/NIK] and by Sergeyeva *et al.* [72SER/NIK] in the temperature range 298 to 523 K for the equilibrium

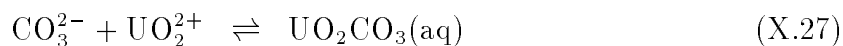


Figure X.3: Equilibrium constants from [76NIK] for Reaction (X.26), $\text{H}_2\text{O}(\text{l}) + \text{UO}_2^{2+} \rightleftharpoons \text{H}^+ + \text{UO}_2\text{OH}^+$ (\diamond), compared with results from the “constant $\Delta_r H_m^\circ$ ” equation, Eq. (X.18), using $\log_{10} K^\circ(T_0) = -(5.157 \pm 0.005)$ and $\Delta_r H_m^\circ = (+50.4 \pm 0.1) \text{ kJ} \cdot \text{mol}^{-1}$ (solid line).

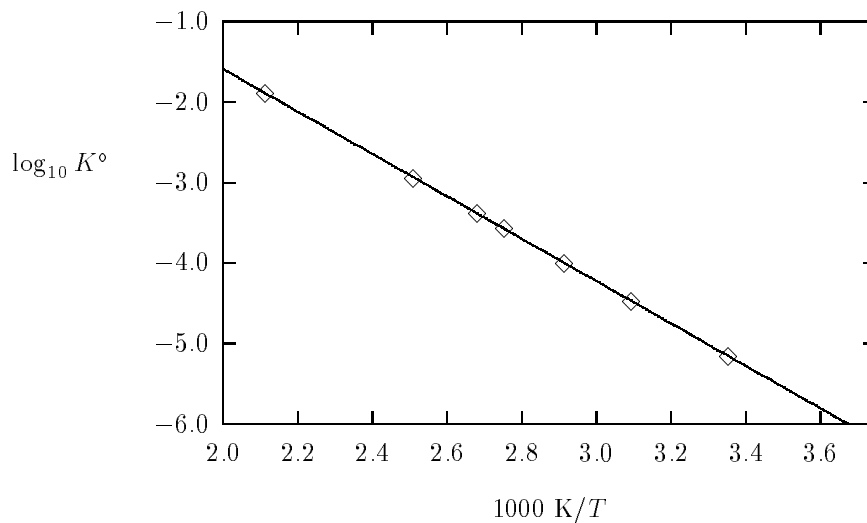
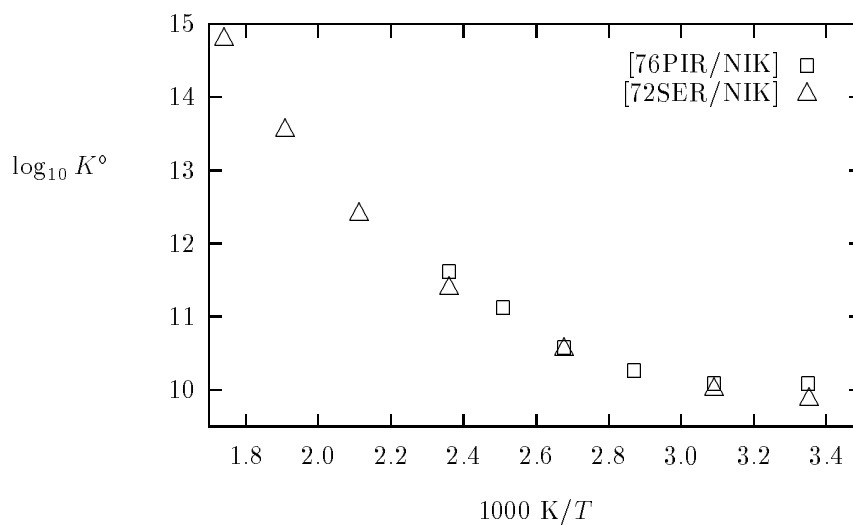
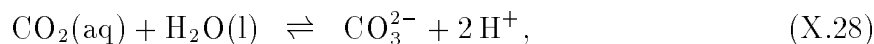


Figure X.4: Equilibrium constants from [72SER/NIK, 76PIR/NIK] for Reaction (X.27): $\text{CO}_3^{2-} + \text{UO}_2^{2+} \rightleftharpoons \text{UO}_2\text{CO}_3(\text{aq})$.



are used as an example.

It is readily seen in Figure X.4 that Eq. (X.18) cannot be used directly to describe the experimental data since $\log_{10} K_{\text{eq}}$ is not linear in T^{-1} . However, it is possible to combine Eq. (X.27) with Eq. (X.28),



to obtain the isoelectric reaction



This example is used in two ways. Firstly, a discussion of the procedure to be taken to extrapolate high-temperature data to 298.15 K will be given, and secondly, a description will be presented of how Reactions (X.27) to (X.29) may be used together with Eq. (X.18) to calculate equilibrium constants at high temperatures.

X.2.2.3.1. Correlation of high-temperature equilibrium constants

In order to make a temperature extrapolation of the $\log_{10} K^\circ(T)$ data like those available from Refs. [76PIR/NIK, 72SER/NIK] for Reaction (X.27), one adds the well-known $\log_{10} K^\circ(\text{X.28}, T)$ to $\log_{10} K^\circ(\text{X.27}, T)$. The values of $\log_{10} K^\circ(\text{X.28}, T)$ may be obtained from Table 5 in Ref. [82PAT/SLO] and Table IV of Ref. [84PAT/BUS], *cf.* Table X.2. This converts the reaction to an isoelectric form.

The values of the last row of Table X.2 are added to the $\log_{10} K^\circ(T)$ for Reaction (X.27) reported in Refs. [72SER/NIK, 76PIR/NIK]. The resulting values are plotted in Figure X.5. It can be seen that the isoelectric approach ($\Delta_r C_{p,m}^\circ \approx 0$) can be used successfully to describe the experimental data using Eq. (X.18), with $\log_{10} K^\circ(T_0) = -(6.72 \pm 0.11)$, and $\Delta_r H_m^\circ = (23.7 \pm 2.7) \text{ kJ} \cdot \text{mol}^{-1}$.

For data of higher quality, over larger temperature intervals, the “constant heat capacity of reaction” approximation, Eq. (X.19), should be used instead to obtain more reliable thermodynamic values at the reference temperature.

X.2.2.3.2. Extrapolation of 298.15 K data to higher temperatures

The following selected values for Reaction (X.27) are reported in Table III.2 of [92GRE/FUG]: $\log_{10} K^\circ(\text{X.27}, 298.15 \text{ K}) = (9.68 \pm 0.04)$, $\Delta_r H_m^\circ(\text{X.27}, 298.15 \text{ K}) = (5 \pm 2) \text{ kJ} \cdot \text{mol}^{-1}$. From the data for auxiliary compounds, the following results are obtained for Reaction (X.28) at 298.15 K: $\log_{10} K^\circ(\text{X.28}, 298.15 \text{ K}) = -(16.68 \pm 0.03)$ and $\Delta_r H_m^\circ(\text{X.28}, 298.15 \text{ K}) = (23.86 \pm 0.26) \text{ kJ} \cdot \text{mol}^{-1}$. Therefore, the following values are found: $\log_{10} K^\circ(\text{X.29}, 298.15 \text{ K}) = -(7.00 \pm 0.05)$ and $\Delta_r H_m^\circ(\text{X.29}, 298.15 \text{ K}) = (28.9 \pm 2.0) \text{ kJ} \cdot \text{mol}^{-1}$. Eq. (X.18) is now used to extrapolate the equilibrium constant of Reaction (X.29) to higher temperatures. Once this is done, it is possible to obtain the equilibrium constants of Reaction (X.27) at higher temperatures by subtracting the values

Figure X.5: Equilibrium constants for Reaction (X.29): $\text{UO}_2^{2+} + \text{CO}_2(\text{aq}) + \text{H}_2\text{O}(\text{l}) \rightleftharpoons \text{UO}_2\text{CO}_3(\text{aq}) + 2\text{H}^+$ (obtained by combining results from Refs. [76PIR/NIK, 72SER/NIK] for Reaction (X.27) with the values in the last row of Table X.2). The line represents a least squares fit to the “constant $\Delta_r H_m^\circ$ ” equation, Eq. (X.18).

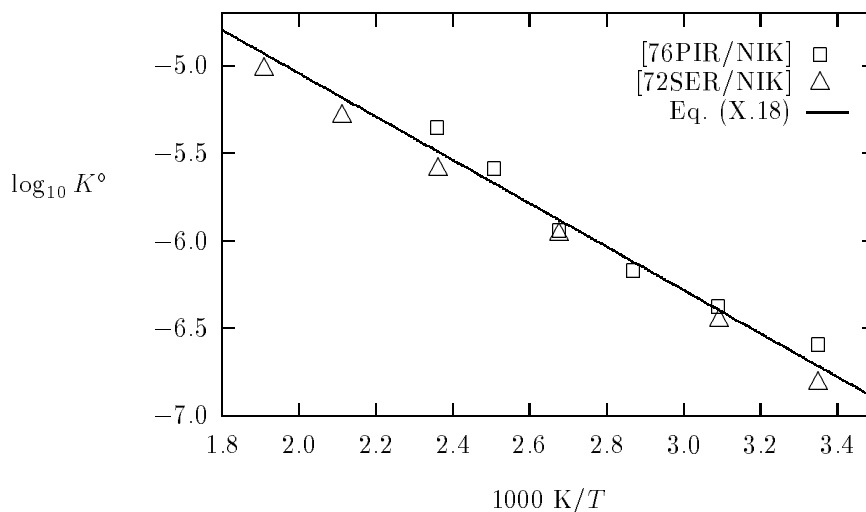


Figure X.6: Equilibrium constants for the reaction $\text{CO}_3^{2-} + \text{UO}_2^{2+} \rightleftharpoons \text{UO}_2\text{CO}_3(\text{aq})$ from Refs. [72SER/NIK, 76PIR/NIK] compared with values obtained with the isoelectric procedure described in the text.

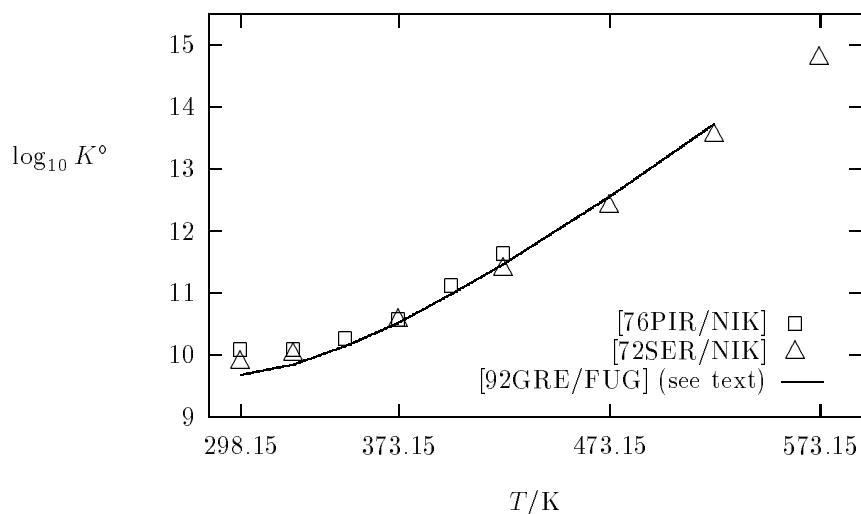


Table X.2: Experimental equilibrium constants^(a) for the ionisation of carbonic acid from Refs. [82PAT/SLO] and [84PAT/BUS].

$\log_{10} K^\circ$							
25°C (298.15 K)	50°C (323.15 K)	75°C (348.15 K)	100°C (373.15 K)	125°C (398.15 K)	150°C (423.15 K)	200°C (473.15 K)	250°C (523.15 K)
$\text{HCO}_3^- \rightleftharpoons \text{H}^+ + \text{CO}_3^{2-}$:							
-10.337	-10.180	-10.117	-10.120	-10.171	-10.255	-10.491	-10.777
$\text{CO}_2(\text{aq}) + \text{H}_2\text{O}(\text{l}) \rightleftharpoons \text{HCO}_3^- + \text{H}^+$:							
-6.349	-6.279	-6.305	-6.397	-6.539	-6.721	-7.189	-7.783
$\text{CO}_2(\text{aq}) + \text{H}_2\text{O}(\text{l}) \rightleftharpoons \text{CO}_3^{2-} + 2 \text{H}^+$:							
-16.686	-16.459	-16.422	-16.517	-16.710	-16.976	-17.680	-18.560

^(a) Values at infinite dilution as extrapolated by the authors.

for Reaction (X.28) at the same temperature (*cf.* Table X.2). The results are shown in Figure X.6, compared with the available literature data for Reaction (X.27).

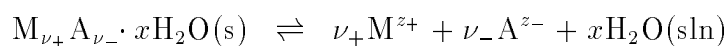
The practical importance of this method is the fact that the approximation $\Delta_r C_{p,m}^\circ(\text{X.29}, 298.15 \text{ K}) = 0$ can be used. The values of the individual standard partial molar heat capacities of the reacting species are thus not required. For neutral complexes or molecular solutes this is very important because the available methods to estimate their standard partial molar heat capacities are less well developed than for electrolytes.

However, if a value of $\Delta_r C_{p,m}^\circ(298.15 \text{ K})$ is available, more accurate predictions of equilibrium constants at higher temperatures are obtained by using the “constant heat capacity of reaction” approximation, Eq. (X.19). The assumption $\Delta_r C_{p,m}^\circ(298.15 \text{ K}) = 0$ should only be used if heat capacities cannot be estimated.

The isoelectric method is, however, limited to reactions that are either isoelectric in themselves, or which can be converted to such reactions. For reactions including species with electrical charges greater than ± 2 this is certainly a problem, because it is less probable that literature data can be found for an additional reaction which may be combined to obtain an isoelectric reaction (in the same way as Reaction (X.28) was used above).

X.2.3. Calculation of the enthalpy of solution from temperature dependence of solubility

Consider the dissolution of a hydrated salt to form a saturated solution,



for which the thermodynamic solubility product is given by:

$$K_s^\circ(T) = \nu_+^{\nu_+} \nu_-^{\nu_-} m_s^\nu \gamma_\pm^\nu a_w^x.$$

Here a_w is the activity of water in a saturated solution; γ_\pm the mean molal activity coefficient of the solute for a saturated solution; $\nu = \nu_+ + \nu_-$; z_+ and z_- the charges on the cation and anion, respectively; and m_s is the molality of the saturated solution.

The starting point for our calculations in the differential form of the van't Hoff equation (*cf.* Section X.2.2.1, footnote on p.434):

$$\frac{d \ln K_s^\circ(T)}{dT} = \frac{\Delta_{\text{sol}} H_m^\circ}{RT^2},$$

where $\Delta_{\text{sol}} H_m^\circ$ is the enthalpy change that occurs when one mole of the hydrated solid is dissolved to form an infinitely dilute solution. Taking this derivative gives

$$\frac{d \ln K_s^\circ}{dT} = \nu \frac{d \ln m_s}{dT} + \nu \frac{d \ln \gamma_\pm}{dT} + x \frac{d \ln a_w}{dT},$$

where these derivatives are constrained to fall along the saturated solution molality curve at a constant pressure greater than or equal to the saturation vapour pressure of the saturated solution at the highest temperature considered. (At temperatures below about 500 K, the differences between values of these derivatives taken at constant pressure and those taken at the saturation vapour pressure of the solution will be insignificant compared to experimental error).

Since γ_\pm and a_w are being constrained to fall along the saturated solution molality curve, they are functions of both saturation molality and of temperature. Thus,

$$\frac{d \ln \gamma_\pm}{dT} = \left(\frac{\partial \ln \gamma_\pm}{\partial T} \right)_{m_s, p} + \left(\frac{\partial \ln \gamma_\pm}{\partial m_s} \right)_{T, p} \left(\frac{dm_s}{dT} \right)$$

and:

$$\frac{d \ln a_w}{dT} = \left(\frac{\partial \ln a_w}{\partial T} \right)_{m_s, p} + \left(\frac{\partial \ln a_w}{\partial m_s} \right)_{T, p} \left(\frac{dm_s}{dT} \right).$$

Combining the last four equations, and using the relationship

$$\frac{d \ln m_s}{dT} = \left(\frac{dm_s}{dT} \right) \left(\frac{1}{m_s} \right)$$

then gives:

$$\begin{aligned} \Delta_{\text{sol}} H_m^\circ &= RT^2 \frac{d \ln K_s^\circ(T)}{dT} \\ &= RT^2 \left\{ \left[\frac{\nu}{m_s} + \nu \left(\frac{\partial \ln \gamma_\pm}{\partial m_s} \right)_{T, p} + x \left(\frac{\partial \ln a_w}{\partial m_s} \right)_{T, p} \right] \left(\frac{dm_s}{dT} \right) \right. \\ &\quad \left. + \left[\nu \left(\frac{\partial \ln \gamma_\pm}{\partial T} \right)_{m_s, p} + x \left(\frac{\partial \ln a_w}{\partial T} \right)_{m_s, p} \right] \right\}. \end{aligned}$$

The last term can be recast using well known expressions for these temperature derivatives:

$$\nu \left(\frac{\partial \ln \gamma_{\pm}}{\partial T} \right)_{m_s, p} + x \left(\frac{\partial \ln a_w}{\partial T} \right)_{m_s, p} = -\frac{1}{RT^2} (\nu L_2 + x L_1)$$

where L_2 and L_1 are the relative partial molar enthalpies of solute and solvent in the saturated solution, respectively, relative to infinite dilution[†]. The enthalpy of solution to form a saturated solution is related to the enthalpy of solution to form an infinitely dilute solution by:

$$\Delta_{\text{sol}} H_m(\text{sat}) = \Delta_{\text{sol}} H_m^{\circ} + (\nu L_2 + x L_1).$$

One additional simplification can be made. The Gibbs-Duhem equation for a binary solution can be cast into the form:

$$\left(\frac{\partial \ln a_w}{\partial m_s} \right)_{T, p} = - \left(\frac{m_s}{n_w} \right) \left(\frac{\partial \ln a_2}{\partial m_s} \right)_{T, p}$$

where a_2 is the activity of the solute in the saturated solution, and n_w is the number of moles of water in 1 kg of water. Taking this derivative yields:

$$\left(\frac{\partial \ln a_2}{\partial m_s} \right)_{T, p} = \nu \left(\frac{\partial \ln \gamma_{\pm}}{\partial m_s} \right)_{T, p} + \frac{\nu}{m_s}.$$

The final expression for the enthalpy of solution then becomes:

$$\Delta_{\text{sol}} H_m(\text{sat}) = \nu RT^2 \left(1 - \frac{x m_s}{n_w} \right) \left[\frac{1}{m_s} + \left(\frac{\partial \ln \gamma_{\pm}}{\partial m_s} \right)_{T, p} \right] \left(\frac{dm_s}{dT} \right).$$

[†] L_1 and L_2 denote the excess (relative to the standard state of infinite dilution) or relative partial molar enthalpy of the solvent (water) and the solute, respectively. The total enthalpy of a solution is expressed as a function of its composition and the partial molar enthalpies of its constituents:

$$H(\text{solution}) = n_1 H_1 + n_2 H_2$$

where n_i and H_i are the amount and the partial molar enthalpy of a substance. The *excess* enthalpy is then

$$H(\text{solution}) - n_1 H_1^{\circ} - n_2 H_2^{\circ} = L = n_1 L_1 + n_2 L_2$$

and $L_i = H_i - H_i^{\circ}$. These relative partial molar enthalpies are related to the activities of the solute and solvent as follows:

$$L_1 = -RT^2 \left(\frac{\partial \ln a_w}{\partial T} \right)_{p, m}, \quad \text{and} \quad L_2 = -\nu RT^2 \left(\frac{\partial \ln \gamma_{\pm}}{\partial T} \right)_{p, m}.$$

Values of L_i are usually calculated from experimental measurements of enthalpies of either solution or dilution.

By setting $\nu = 1$, this equation also becomes valid for a non-electrolyte, and by setting $x = 0$, for a solid anhydrous electrolyte or non-electrolyte.

We note that the temperature dependence of solubilities (*i.e.*, of m_s) gives $\Delta_{\text{sol}}H_m$ for the formation of a saturated solution and not for an infinitely dilute solution as is generally (and erroneously) assumed. These two types of solution enthalpies will differ very little for sparingly soluble solutes, but their differences can be substantial for more soluble electrolytes. Some numerical calculations of $\Delta_{\text{sol}}H_m(\text{sat})$ were given by Williamson [44WIL] and Brice [83BRI]. Williamson also gave the first systematic presentation of solubility equations for hydrated and non-hydrated electrolytes and non-electrolytes.

X.2.4. Alternative heat capacity expressions for aqueous species

As an alternative to the general heat capacity temperature function given in Eq. (X.8), Clarke and Glew [66CLA/GLE] proposed a Taylor series expansion for the temperature dependence of the heat capacity. This approach was used subsequently by Phillips and Silvester [84PHI/SIL]. Clarke and Glew's equations do not offer any special advantage over Eq. (X.8), and the Taylor series expansion requires more parameters than models described below, which are based either on the density of the solvent, or on the Born equation. However, as pointed out by Clarke and Glew, it is not justifiable to set lower order temperature derivatives equal to zero in these expansions while retaining higher order ones (*e.g.*, do not set $c = 0$ in Eq. (X.8) if the jT^3 term is retained).

Electrostatic models can be used to predict electrolyte behaviour at high temperatures with a lesser number of parameters. The model that is perhaps most widely used among geochemists is that of Helgeson and co-workers (*e.g.*, [88SHO/HEL]). Some of their equations are presented below.

X.2.4.1. DQUANT Equation

The DQUANT equation was proposed by Helgeson [67HEL] and it is of historical interest because it has been used by several researchers, for example by Haas and Fisher [76HAA/FIS], Helgeson's group [85JAC/HEL], Smith, Popp and Norman [86SMI/POP], *etc.*, although the authors of Refs. [76HAA/FIS, 86SMI/POP] used additional terms for the non-electrostatic contributions to the heat capacity. Furthermore, the EQ3/6 geochemical computer program package [88JAC/WOL] uses the DQUANT equation to calculate high-temperature equilibrium constants of dissociation for neutral inorganic complexes.

The name of "DQUANT" appears to have its origin in the name of a computer program which was used earlier at the Laboratory of Theoretical Geochemistry, University of California, Berkeley.

Assuming that the temperature dependence of the heat capacity change of a dissociation reaction is proportional to the temperature dependence of the electrostatic contribution, Helgeson [67HEL, his Eqs. (21) and (22)] obtained the expression

$$\log_{10} K^\circ(T) = \frac{\Delta_r S_m^\circ(T_0)}{\ln(10)RT} \left\{ T_0 - \frac{\theta}{\omega} \left[1 - \exp \left(\exp(b + aT) - c + \frac{T - T_0}{\theta} \right) \right] \right\} - \frac{\Delta_r H_m^\circ(T_0)}{\ln(10)RT}, \quad (\text{X.30})$$

which is consistent with the following expressions for the heat capacity change of the dissociation reaction and the dielectric constant (relative permittivity) for water:

$$\begin{aligned} \Delta_r C_{p,m}^\circ(T) &= \frac{T \Delta_r S_m^\circ(T_0)}{\omega \theta} \exp \left(\exp(b + aT) - c + \frac{T - T_0}{\theta} \right) \times \\ &\quad \left[[1 + \phi \exp(b + aT)]^2 + \phi^2 \exp(b + aT) \right] \\ \varepsilon(T) &= \varepsilon_0 \exp \left(- \exp(b + aT) - \frac{T}{\theta} \right), \end{aligned} \quad (\text{X.31})$$

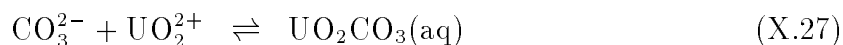
where $\varepsilon_0 = 305.7$, $b = -12.741$, $a = 0.01875 \text{ K}^{-1}$, $\theta = 219 \text{ K}$, $c = \exp(b + aT_0) = 7.84 \times 10^{-4}$, $\omega = (1 + ac\theta) = 1.00322$ and $\phi = a\theta = 4.106$.

It should be noted that Eqs. (X.30) and (X.31) have been superseded by subsequent models of Helgeson and co-workers, described in next Section, which generally yield more reliable model fits.

Helgeson [67HEL, 69HEL] claimed agreement of Eq. (X.30) with experimental values for most reactions in the temperature range 273 to 423 or to 523 K, with the upper temperature limit depending on the reaction. The errors at 473 K were of the order of 1 to 9 % of $\log_{10} K^\circ(T)$ [67HEL, p.3131] but increased with temperature. Note, however, that for some dissociation reactions whose $\Delta_r H_m^\circ(T_0)$ and $\Delta_r S_m^\circ(T_0)$, and/or the heat capacity of dissociation are positive, the use of Eqs. (X.30) and (X.31) is not recommended [67HEL, pp.3131–3132].

Eq. (X.30) is of interest because it does not require any knowledge of the heat capacity change of a reaction. For neutral inorganic species in aqueous solution, except for a few simple dissolved gases, there are no known methods to estimate the standard molar heat capacities. Therefore, Eq. (X.30) is of special interest to estimate high-temperature equilibrium constants for dissociation of neutral species.

As an example, Figure X.7 compares experimental results [72SER/NIK] for Reaction (X.27)

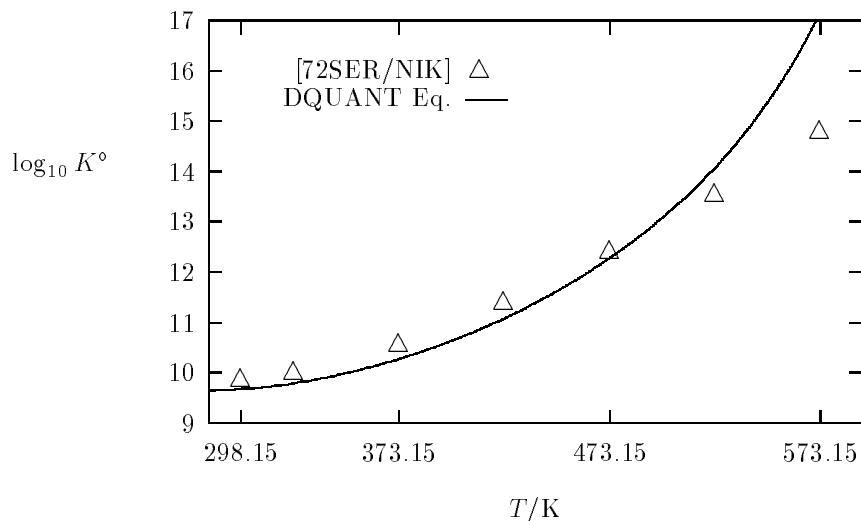


with calculated values of $\log_{10} K^\circ(T)$ using Eq. (X.30) and selected reaction parameters from [92GRE/FUG].

X.2.4.2. The revised Helgeson–Kirkham–Flowers model

The electrostatic heat capacity model used by Helgeson *et al.*, which was briefly described in Section X.2.2.3, has evolved into a set of equations of state for the standard partial molar

Figure X.7: Comparison of equilibrium constants from [72SER/NIK] for Reaction (X.27), $\text{CO}_3^{2-} + \text{UO}_2^{2+} \rightleftharpoons \text{UO}_2\text{CO}_3(\text{aq})$, with calculated values using the DQUANT equation, Eq. (X.30), and the following selected reaction values [92GRE/FUG]: $\log_{10} K(T_0) = (9.68 \pm 0.04)$, and $\Delta_r S_m^\circ(T_0) = (202.1 \pm 6.8) \text{ J} \cdot \text{K}^{-1} \cdot \text{mol}^{-1}$.



properties of aqueous species [88TAN/HEL, 88SHO/HEL, 89SHO/HEL, 89SHO/HEL2]. These equations of state, which constitute the “Revised Helgeson-Kirkham-Flowers” model (“Revised HKF” model), allow predictions to be made to 1273 K and to 5 kbar. Neither this equation nor the DQUANT equation are expected to be reliable near the critical “point” of water, 641.7 K and 220.7 bar [83LEV/KAM, 84HAA/GAL, 89SAU/WAG].

According to this model, the standard partial molar heat capacity for an aqueous ion i is given by

$$C_{p,m}^\circ(i) = c_1 + \frac{c_2}{(T - 228)^2} - \left(\frac{2T}{(T - 228)^3} \right) \left[a_3(p - p^\circ) + a_4 \ln \left(\frac{2600 + p}{2600 + p^\circ} \right) \right] + \omega TX + 2TY \left(\frac{\partial \omega}{\partial T} \right)_p - T \left(\frac{1}{\varepsilon} - 1 \right) \left(\frac{\partial^2 \omega}{\partial T^2} \right)_p,$$

where $p^\circ = 1$ bar is the standard state pressure, the pressure p has units of bar, ε is the dielectric constant (relative permittivity) of $\text{H}_2\text{O}(\text{l})$ which is temperature and pressure dependent (see for example Figure X.2, or [74HEL/KIR, Table 39]), c_1 , c_2 , a_3 and a_4 are temperature and pressure independent parameters and are specific to each ion i , and X , Y and ω are temperature and pressure dependent functions (*cf.* our Eq. (X.23) for X , Eq. (X.33) below for ω , and Ref. [88SHO/HEL, Eq. (28)] for Y), which were tabulated by Tanger and Helgeson [88TAN/HEL]. Equations for the partial derivatives of ω with regard to temperature and pressure are also given there [88TAN/HEL, Appendix B].

Pressure effects will be neglected here for the following reasons. The saturated pressure of steam at 573 K is 85.8 bar [74HEL/KIR, Table 38]. The effect that this pressure will have on equilibrium constants will depend on the reactants and products involved and on the partial molar volume change of reaction. For example, the effect that a pressure of 85.8 bar has on the chemical potential of $\text{H}_2\text{O}(\text{l})$ is about $0.15 \text{ kJ} \cdot \text{mol}^{-1}$ [81STU/MOR], which at 573 K would change an equilibrium constant involving one water molecule by $0.014 \log_{10}$ units. This may be accounted for if the “apparent” Gibbs energy of $\text{H}_2\text{O}(\text{l})$ as calculated from Table III-5 of Ref. [89COX/WAG] (see also Eqs. (X.11) and (X.15)) is used in the calculations of the temperature effects on equilibrium constants. In general, the pressure effect on an equilibrium constant may be estimated assuming that the molar volume of reaction is independent of pressure [69HEL, *p*.742, 81STU/MOR, *pp*.73–78]:

$$\log_{10} K^\circ(p) = \log_{10} K^\circ(p_0) - \frac{\Delta_r V_m^\circ(p-1)}{RT 10^{-2} \ln(10)}.$$

For a partial molar volume change of reaction of $0.1 \text{ dm}^3 \cdot \text{mol}^{-1}$, this equation estimates the pressure effect, at 573 K and 85.8 bar, as -0.077 on $\log_{10} K^\circ$.

Since the major temperature range of interest for the modelling of aqueous systems is 273 to 573 K, and in order to simplify the equations of the “Revised HKF” model, pressure effects on temperature corrections will be neglected here. The reader interested in even higher temperatures (and therefore higher pressures) is referred to the original publications [88TAN/HEL, 88SHO/HEL, 89SHO/HEL, 89SHO/HEL2, 97SHO/SAS, 97SVE/SHO].

By neglecting the pressure effects, the following equation is obtained. The apparent standard partial molar Gibbs energy of an aqueous ion i , *cf.* Eqs. (X.11) and (X.16), is given by the expression

$$\begin{aligned} \Delta_a G_m^\circ(i, T) = & \Delta_f G_m^\circ(i, T_0) - S_m^\circ(i, T_0)(T - T_0) - c_1 \left[T_0 - T + T \ln \left(\frac{T}{T_0} \right) \right] \\ & - c_2 \left[\left(\frac{1}{T - 228} - \frac{1}{T_0 - 228} \right) \left(\frac{228 - T}{228} \right) \right. \\ & \quad \left. - \frac{T}{(228)^2} \ln \left\{ \frac{T_0(T - 228)}{T(T_0 - 228)} \right\} \right] \\ & + \omega(T) \left(\frac{1}{\varepsilon} - 1 \right) - \omega(T_0) \left(\frac{1}{\varepsilon_0} - 1 \right) \\ & + (T - T_0)\omega(T_0)Y(T_0), \end{aligned} \quad (\text{X.32})$$

where c_1 and c_2 are the non-solvation parameters specific to each aqueous ion; the dielectric constant (relative permittivity) of $\text{H}_2\text{O}(\text{l})$, ε , is temperature and pressure dependent [74HEL/KIR, Table 39] (at 298.15 K and 1 bar $\varepsilon_0 = 78.4$, *cf.* Table X.4); and $Y(T_0)$ has the value $-5.81 \times 10^{-5} \text{ K}^{-1}$ [88TAN/HEL, Table H-4].

The temperature (and pressure) dependent function $\omega(T)$ is defined for ionic aqueous species as [88TAN/HEL, Eq. (B-9)]:

$$\omega(i, T) = \frac{N_A e^2}{8\pi\epsilon_0} \left(\frac{z_i^2}{r_i + |z_i|(k_z + g(T))} - \frac{z_i}{3.082 \times 10^{-10} + g(T)} \right), \quad (\text{X.33})$$

where $(N_A e^2 / (8\pi \epsilon_0))$ is equal to $6.9466 \times 10^{-5} \text{ m} \cdot \text{J} \cdot \text{mol}^{-1}$, r_i is the crystallographic ionic radius, k_z is a charge dependent constant (equal to zero for anions and $0.94 \times 10^{-10} \text{ m}$ for cations), and $g(T)$ is a non salt-specific function which accounts for the dependence of the effective electrostatic ionic radius on temperature and pressure (at the steam saturated pressure, g is zero for $T < 448 \text{ K}$ [88TAN/HEL, Table H-8, 92SHO/OEL, Table 5]). As Eq. (X.33) shows, the Revised HKF model uses an effective radius for the electrostatic interactions between the dissolved species and the solvent:

$$r_{\text{eff},i}(T) = r_i + |z_i|(k_z + g(T)). \quad (\text{X.34})$$

For neutral species, the model function ω , *cf.* Eq. (X.33), is assumed to be independent of temperature and pressure, and thus becomes a model parameter. Correlations at 298.15 K with standard partial molar entropies [89SHO/HEL2, their Eqs. (44) and (45)] give for volatile neutral non-polar aqueous species (noble and diatomic elemental gases)

$$\omega(i) = -1514.4 S_m^\circ(i, T_0),$$

and for neutral polar aqueous species ($\text{H}_2\text{S}(\text{aq})$, $\text{CO}_2(\text{aq})$, $\text{SiO}_2(\text{aq})$, *etc.*)

$$\omega(i) = 1.422 \times 10^5 - 1514.4 S_m^\circ(i, T_0), \quad (\text{X.35})$$

where ω is in units of $\text{J} \cdot \text{mol}^{-1}$.

The c_1 and c_2 parameters for Eq. (X.32) of this model are temperature and pressure independent, and are correlated at 298.15 K with the standard partial molar ionic heat capacity as follows [88SHO/HEL, Eqs. (29), (31), (35) and (89); 88TAN/HEL, *p.*36, Eqs. (19), (24), (28c), and (48)]:

$$\begin{aligned} c_2 &= -1.26968 \times 10^5 + 2037 C_{p,m}^\circ(i, T_0) \\ c_1 &= C_{p,m}^\circ(i, T_0) - c_2 \left(\frac{1}{T_0 - 228} \right)^2 + 9.213 \times 10^{-5} \omega(i, T_0), \end{aligned}$$

where c_1 and c_2 are in units of $\text{J} \cdot \text{K}^{-1} \cdot \text{mol}^{-1}$ and $\text{J} \cdot \text{K} \cdot \text{mol}^{-1}$ respectively.

The crystallographic ionic radius, r_i , in Eq. (X.33) is correlated to the standard partial molar ionic entropy [88SHO/HEL, Eq. (58)],

$$r_i = \frac{-458.8 \times 10^{-10} z_i^2}{S_m^\circ(i, T_0) - a_z} - |z_i| k_z, \quad (\text{X.36})$$

where a_z is a charge dependent regression constant (equal to 301, 590 and 883 $\text{J} \cdot \text{K}^{-1} \cdot \text{mol}^{-1}$ for mono-, di- and trivalent ions, respectively, and $a_z = 299.2|z_i|$ for cations or anions with $z_i > 3$ [88SHO/HEL, Eq. (56)]).

If the chemical reaction only involves aqueous species, the calculations can be done with Eqs. (X.15) and (X.32). If the chemical reaction includes phases for which heat capacity functions (of type Eq. (X.8)) are available (*e.g.*, solid phases or $\text{H}_2\text{O}(\text{l})$), it is convenient to use Eq. (X.32) for aqueous species, and Eqs. (X.12) and (X.13) for the solid phases.

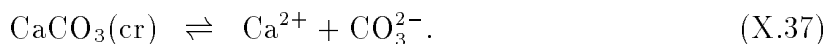
As mentioned earlier, the integrals in Eqs. (X.12) and (X.13) may have expressions like Eqs. (X.9) and (X.10), except that one must disregard the delta signs on the right hand side of Eqs. (X.9) and (X.10). For water, the apparent Gibbs energy should be calculated from values given in the CODATA tables [89COX/WAG].

In order to avoid computational errors, it is advantageous to use a computer program to do the calculations described here. The computer program SUPCRT is available from Helgeson's laboratory at Berkeley [92JOH/OEL] and on the GEOPIG home page (<http://zonvark.wustl.edu/geopig>). That program also includes a mineral and aqueous species data base.

As it stands, Eq. (X.32) contains five parameters for each aqueous species (standard partial molar ionic entropy and standard Gibbs energy of formation, as well as c_1 , c_2 , and r_i). When Eqs. (X.35) and (X.36) are included in the model, only three parameters remain in Eq. (X.32): the standard partial molar entropy, the standard partial molar Gibbs energy of formation, and the standard partial molar heat capacity.*

Tremaine, Sway and Barbero [86TRE/SWA] and Apps and Neil [90APP/NEI] have reanalysed some experimental data using the Helgeson-Kirkham-Flowers equations.

As an example of the application of Eq. (X.32) to predict high-temperature equilibrium constants, the calcite dissolution reaction is used:

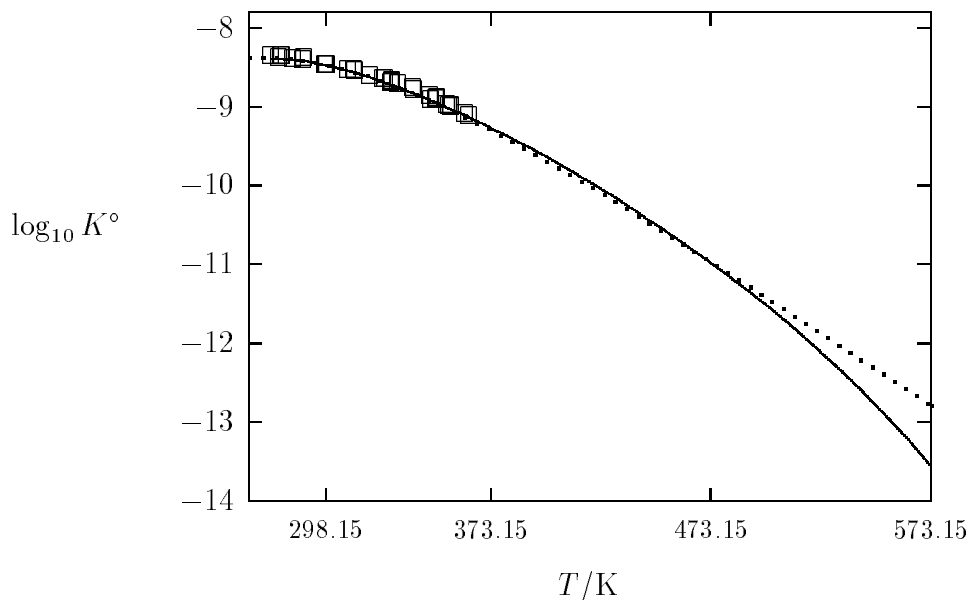


The data for the aqueous ions are taken from CODATA [89COX/WAG] except for the standard partial molar ionic heat capacities which are not given in the CODATA publication, and are taken instead from Ref. [76DES/VIS]. For calcite, the value for the entropy and the heat capacity function of CODATA [87GAR/PAR] are used, whereas the standard Gibbs energy of formation is adjusted to $-1129.1 \text{ kJ} \cdot \text{mol}^{-1}$ in order to force the logarithm of the equilibrium constant at 298.15 K to be $\log_{10} K^\circ(\text{X.37}) = -8.480$ as recommended by Plummer and Busenberg [82PLU/BUS]. The predicted temperature dependence of the equilibrium constant for calcite dissolution is shown in Figure X.8, together with experimental values from Ref. [82PLU/BUS]. Large differences in calculated values are in general obtained at $T \geq 423 \text{ K}$ between the "constant $\Delta_r C_{p,m}^\circ$ " equation, Eq. (X.19), and the simplified revised HKF model, Eq. (X.32) and Eqs. (X.35) to (X.36).

The fitting capabilities of the revised Helgeson, Kirkham and Flowers model are very high, because of the large number of parameters for each dissolved species. With the simplification introduced by Eqs. (X.35) and (X.36), the number of parameters is reduced, but still one must avoid overfitting experimental data. Only good quality data in a broad temperature range should be used to determine the model parameters. This is due to the fact that ionic heat capacities generally show gentle maxima at about 325 to 375 K, and have a steep decrease as the temperature approaches the critical temperature of water ($\sim 647.1 \text{ K}$) [83LEV/KAM, 84HAA/GAL, 89SAU/WAG]. The heat capacities for ions are

* Note added in press: Sverjensky, Shock and Helgeson [97SVE/SHO] have recently published several examples of this technique. Furthermore they present several correlation strategies to estimate thermodynamic properties of aqueous complexes (mostly inorganic).

Figure X.8: Comparison of experimental equilibrium constants for calcite dissolution [82PLU/BUS], Reaction (X.37), with those predicted with the simplified “Revised Helgeson-Kirkham-Flowers model” described in the text (continuous line). The predictions with the “constant $\Delta_r C_{p,m}^\circ$ ” equation, Eq. (X.19), using $\Delta_r S_m^\circ = -198 \text{ J} \cdot \text{K}^{-1} \cdot \text{mol}^{-1}$ and $\Delta_r C_{p,m}^\circ = -377 \text{ J} \cdot \text{K}^{-1} \cdot \text{mol}^{-1}$ are shown as a dotted line.



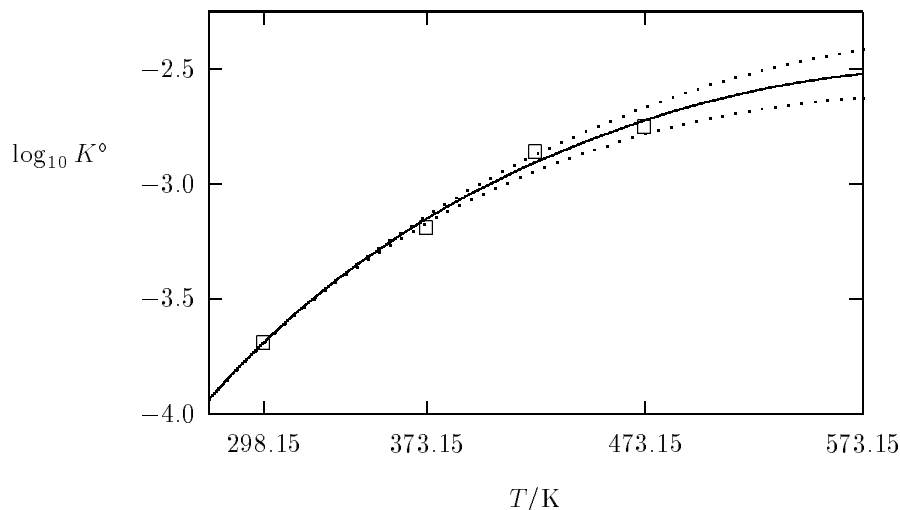
usually not determined reliably by a least-squares representation of equilibrium constants in the range 273 to 423 K.

As an example of the uncertainties that might be found in fitting S_m° or $C_{p,m}^\circ$ to experimental values of equilibrium constants, the data on the solubility of zincite are used. The equilibrium constants for the reaction



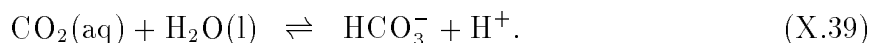
are taken from Khodakovskiy and Yelkin [75KHO/YEL, their Table 3]. For zincite, the standard entropy and the heat capacity function are taken from Kubaschewski *et al.* [93KUB/ALC] and the standard Gibbs energy of formation from the US NBS tables [82WAG/EVA]. For ZnOH^+ , the standard ionic partial molar Gibbs energy is set to the value required for achieving an equilibrium constant at 298.15 K of $\log_{10} K^\circ = -3.69$, which is the value recommended in Ref. [75KHO/YEL]. A least-squares fit to the simplified “Revised HKF model” on the four experimental values of $\log_{10} K^\circ$ (X.38) yields $S_m^\circ(\text{ZnOH}^+, \text{aq}, T_0) = (24 \pm 17) \text{ J} \cdot \text{K}^{-1} \cdot \text{mol}^{-1}$ and $C_{p,m}^\circ(\text{ZnOH}^+, \text{aq}, T_0) = (44 \pm 102) \text{ J} \cdot \text{K}^{-1} \cdot \text{mol}^{-1}$ and is shown in Figure X.9. The large uncertainties are due to the correlation between $S_m^\circ(T_0)$ and $C_{p,m}^\circ(T_0)$. A more precise value of $C_{p,m}^\circ(T_0)$ is obtained by a least-squares fit if the value of $S_m^\circ(\text{ZnOH}^+, \text{aq}, T_0)$ is fixed to $24 \text{ J} \cdot \text{K}^{-1} \cdot \text{mol}^{-1}$ (the value obtained above), namely $C_{p,m}^\circ(\text{ZnOH}^+, \text{aq}, T_0) = (41 \pm 16) \text{ J} \cdot \text{K}^{-1} \cdot \text{mol}^{-1}$. Figure X.9

Figure X.9: Comparison of experimental equilibrium constants [75KHO/YEL] for Reaction (X.38), $\text{ZnO}(\text{cr}) + \text{H}^+ \rightleftharpoons \text{ZnOH}^+$, with a least-squares fit to the simplified “Revised HKF model”. The dotted lines reflect the effect of an uncertainty of $\pm 16 \text{ J} \cdot \text{K}^{-1} \cdot \text{mol}^{-1}$ in $C_{p,m}^\circ(\text{ZnOH}^+, \text{aq}, T_0)$.



shows that data at higher temperatures are needed in order to constrain the least-squares fits sufficiently to obtain unambiguous thermodynamic parameters for ZnOH^+ .

An example where experimental data up to 573 K are available [82PAT/SLO] is the reaction



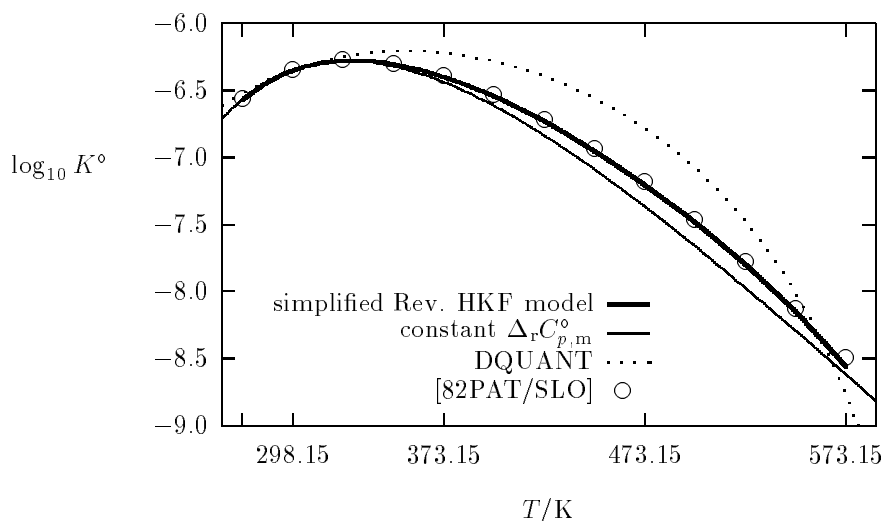
The thermodynamic data are taken from CODATA [89COX/WAG], except for the standard partial molar heat capacities of the bicarbonate ion, which is taken from Ref. [76DES/VIS], and of $\text{CO}_2(\text{aq})$, which is fitted by least-squares to the experimental equilibrium constants of [82PAT/SLO]. The calculation yields $C_{p,m}^\circ(\text{CO}_2, \text{aq}, T_0) = (208.5 \pm 2.2) \text{ J} \cdot \text{K}^{-1} \cdot \text{mol}^{-1}$, and the model results are shown in Figure X.10. For comparison, results obtained with the DQUANT expression, Eq. (X.30), and the “constant $\Delta_r C_{p,m}^\circ$ ” Eq. (X.19), with a heat capacity of reaction of $-334 \text{ J} \cdot \text{K}^{-1} \cdot \text{mol}^{-1}$, are also displayed. The approximation expressed by the DQUANT equation, Eq. (X.30), resulted in errors of up to ± 0.3 in $\log_{10} K^\circ(T)$.

A better fit of the data could be achieved by using the isocoulombic reaction:



and the “constant $\Delta_r C_{p,m}^\circ$ ” approximation, Eq. (X.19). Reaction (X.39) has been used for illustrative purposes only.

Figure X.10: Comparison of experimental equilibrium constants for the hydrolysis of $\text{CO}_2(\text{aq})$ [82PAT/SLO], Reaction (X.39), with those obtained from fitting $C_{p,m}^\circ(\text{CO}_2, \text{aq}, T_0)$ with the simplified “Revised HKF model”. Results obtained using the DQUANT equation, Eq. (X.30), and the “constant $\Delta_r C_{p,m}^\circ$ ” equation, Eq. (X.19) (with $\Delta_r H_m^\circ(T_0) = 9.16 \text{ kJ} \cdot \text{mol}^{-1}$, $\Delta_r S_m^\circ(T_0) = -90.91 \text{ J} \cdot \text{K}^{-1} \cdot \text{mol}^{-1}$, and $\Delta_r C_{p,m}^\circ = -334 \text{ J} \cdot \text{K}^{-1} \cdot \text{mol}^{-1}$), are also displayed for comparison.



X.2.4.3. The Ryzhenko–Bryzgalin model

Ryzhenko and Bryzgalin [81RYZ, 82BRY/RAF, 91RYZ/BRY] and Bryzgalin [86BRY, 89BRY] describe the temperature dependence of mononuclear complex formation reactions using a simple electrostatic model where the Gibbs energy of reaction $\Delta_r G_m^\circ(T, p)$ is described as a sum of two contributions (an idea first proposed in detail by Gurney [53GUR, Chapter 7]):

$$\Delta_r G_m^\circ(T, p) = \Delta_r G_{m,\text{nonel}}^\circ + \Delta_r G_{m,\text{electr}}^\circ(T, p) \quad (\text{X.40})$$

where $\Delta_r G_{m,\text{nonel}}^\circ$ is a temperature and pressure independent non-electrostatic contribution to the Gibbs energy, and $\Delta_r G_{m,\text{electr}}^\circ(T, p)$ is a temperature and pressure dependent electrostatic contribution given by the following Coulomb-type equation:

$$\Delta_r G_{m,\text{electr}}^\circ(T, p) = -\frac{|Z_c Z_a|_{\text{eff}} N_A e^2}{r_{\text{eff}}} \frac{1}{4\pi \epsilon_0 \epsilon(T, p)} \quad (\text{X.41})$$

where e is the elementary charge and N_A is the Avogadro constant ($N_A e^2 / (4\pi \epsilon_0) = 1.38935 \times 10^{-4} \text{ m} \cdot \text{J} \cdot \text{mol}^{-1}$, *cf.* Table II.6); $\epsilon(T, p)$ is the relative permittivity of the solvent (in this case the dielectric constant of water); r_{eff} is an effective bond distance,

Table X.3: Polarisabilities of ions in aqueous solutions from Ref. [66NIK, *p.*385] (also reported in [85RYZ/SHA, 87RYZ/BRY]). We note however that there are inconsistencies between the values listed in this table and the data found in Refs. [40RIC, 50SYR/DYA], apparently because the latter two references contain electronic ionic polarisabilities of ions either in vacuo or in crystal lattices.

Anion	$\alpha \times 10^{30}$ (m ³)	Cation	$\alpha \times 10^{30}$ (m ³)	Cation	$\alpha \times 10^{30}$ (m ³)
OH ⁻	2.04	H ⁺	-0.21	Zn ²⁺	0.24
F ⁻	1.03	Li ⁺	-0.13	Cd ²⁺	0.92
Cl ⁻	3.59	Na ⁺	0.08	Hg ²⁺	2.22
Br ⁻	5.02	K ⁺	0.90	Mn ²⁺	0.55
I ⁻	3.62	Rb ⁺	1.50	Mn ³⁺	0.0
CN ⁻	3.30	Cs ⁺	2.59	Mn ⁴⁺	0.0
NO ₃ ⁻	4.37	Mg ²⁺	-0.71	Fe ²⁺	0.48
HCOO ⁻	3.92	Ca ²⁺	0.28	Fe ³⁺	1.13
SiO ₄ ⁴⁻	5.30	Sr ²⁺	0.75	Co ²⁺	0.51
SO ₄ ²⁻	5.83	Ba ²⁺	1.73	Ni ²⁺	0.30
CO ₃ ²⁻	4.81	Pb ²⁺	3.48	Al ³⁺	-1.00
CrO ₄ ²⁻	10.62	Cu ²⁺	0.15	Y ³⁺	0.0
				La ³⁺	0.0

which in most cases is approximately equal to the sum of radii of the central ion and ligand, and it is independent of the total number of ligands in the complex; $|Z_c Z_a|_{\text{eff}}$ is an “effective charge”, which is a function of the formal charges of the anion and the cation (Z_a and Z_c , respectively), and of the number of ligands and geometry of the complex. The model can only be applied to monodentate ligands, but protonation equilibria for polybasic acids can be described by considering complexes where the central ion is the anion, and the ligands are protons [87RYZ/BRY].

Bryzgalin and Rafal’skiy [82BRY/RAF] give the following equation to calculate $|Z_c Z_a|_{\text{eff}}$ for a number of different coordination geometries:

$$|Z_c Z_a|_{\text{eff}} = |Z_c Z_a|L - QZ_a^2 + \frac{\alpha_a Z_c^2 L}{2r_{\text{eff}}^3} - \frac{(\alpha_a Z_c)^2 Q}{2r_{\text{eff}}^6} \quad (\text{X.42})$$

where L is the total number of ligands in the mononuclear complex; Q is a stereochemical factor, $Q = (3L^2 - 5L + 2)/8$; and α_a is the polarisability of the ligand (*cf.* Table X.3). The first term on the right hand side of Eq. (X.42) takes into account the attraction between the central ion and each of the ligands; the second term includes mutual repulsions between

ligands; the third term deals with the attractive interactions between the central ion and the induced dipoles in the ligands; and the last term considers the mutual repulsion among the dipoles induced in the ligands [82BRY/RAF]. For 1:1 complexes $L = 1$, $Q = 0$, and the last term of Eq. (X.42) is modified so that the effective charge is instead given by [83BRY]:

$$|Z_c Z_a|_{\text{eff}} = |Z_c Z_a| + \frac{\alpha_a Z_c^2}{2 r_{\text{eff}}^3} + \frac{\alpha_c Z_a^2}{2 r_{\text{eff}}^3} \quad (\text{X.43})$$

where α_c is the polarisability of the central ion (*cf.* Table X.3).

Electrostatic models are based on incompressible spherical ions. The thermodynamic values obtained by such models require the conversion from the molar volume of the ideal gas to that of a solution at $1 \text{ mol} \cdot (\text{kg H}_2\text{O})^{-1}$. This correction is adsorbed by adjustable parameters in the Helgeson-Kirkham-Flowers model which is described in Section X.2.4.2.

The Ryzhenko-Bryzgalin model yields thermodynamic data in volumetric concentration units [69PRU], *i.e.*, on the molar concentration scale. The conversion of equilibrium constants from molar to molal units is straightforward, *cf.* Eq. (II.43) on page 56, where the factor for the conversion of molality to molarity, ρ , at infinite dilution becomes equal to the density of $\text{H}_2\text{O}(\text{l})$, $\rho(T, p)$ in $\text{kg} \cdot \text{dm}^{-3}$, and (at infinite dilution) this conversion factor is ≈ 1 at $T < 323 \text{ K}$. Taking this units conversion into account, it is possible to obtain, from Eqs. (X.40) to (X.43), an expression for the formation equilibrium constants of mononuclear complexes:

$$\begin{aligned} \log_{10} K^\circ(T, p) &= \frac{T_0}{T} \log_{10} K^\circ(T_0, p^\circ) \\ &+ \frac{|Z_a Z_c|_{\text{eff}}}{r_{\text{eff}}} \frac{N_A e^2}{4\pi \epsilon_0 R T \ln(10)} \left(\frac{1}{\epsilon(T, p)} - \frac{1}{\epsilon(T_0, p^\circ)} \right) \\ &- \sum_i \nu_i \log_{10} \rho(T, p) \end{aligned} \quad (\text{X.44})$$

provided that r_{eff} is assumed to be independent of temperature and pressure. In this equation it is seen that the model requires only two parameters: the equilibrium constant at one temperature and an effective bond distance r_{eff} .

For the standard partial molar entropy of a reaction involving the formation of mononuclear complexes the following expression is obtained:

$$\begin{aligned} \Delta_r S_m^\circ(T, p) &= - \left(\frac{\partial \Delta_r G_m^\circ}{\partial T} \right)_p \\ &= - \frac{|Z_c Z_a|_{\text{eff}}}{r_{\text{eff}}} \frac{N_A e^2}{4\pi \epsilon_0 \epsilon(T, p)^2} \left(\frac{\partial \epsilon(T, p)}{\partial T} \right)_p - \sum_i \nu_i R \ln \rho(T, p) \\ &+ \sum_i \nu_i R T \alpha_T(T, p) \end{aligned} \quad (\text{X.45})$$

where $\alpha_T(T, p) = (1/V_m^\circ) (\partial V_m^\circ / \partial T)_p = -(1/\rho) (\partial \rho / \partial T)_p = -(\partial \ln \rho / \partial T)_p$ is the coefficient of thermal expansion of water, *cf.* Table X.4 (here V_m° represents the molar volume

of pure liquid water in $\text{cm}^3 \cdot \text{mol}^{-1}$, $V_m^\circ(T, p) = 18.0153/\rho(T, p)$). At 298.15 K, and 1 bar the contribution of the second term is negligible, and one can then write:

$$\Delta_r S_m^\circ(T_0, p^\circ) \approx \left(81.4 \times 10^{-10} \frac{|Z_c Z_a|_{\text{eff}}}{r_{\text{eff}}} + 0.64 \sum_i \nu_i \right) \text{ J} \cdot \text{K}^{-1} \cdot \text{mol}^{-1} \quad (\text{X.46})$$

where r_{eff} is in units of m. Similarly, for the standard partial molar heat capacity of a reaction involving the formation of mononuclear complexes the following equation is obtained:

$$\begin{aligned} \Delta_r C_{p,m}^\circ(T, p) &= T \left(\frac{\partial \Delta_r S_m^\circ}{\partial T} \right)_p \\ &= -T \frac{|Z_a Z_c|_{\text{eff}}}{r_{\text{eff}}} \frac{N_A e^2}{4\pi \epsilon_o \epsilon(T, p)^2} \left(\left(\frac{\partial^2 \epsilon(T, p)}{\partial T^2} \right)_p - \frac{2}{\epsilon(T, p)} \left(\frac{\partial \epsilon(T, p)}{\partial T} \right)_p^2 \right) \\ &\quad + 2 \sum_i \nu_i R T \alpha_T(T, p) + \sum_i \nu_i R T^2 \left(\frac{\partial \alpha_T(T, p)}{\partial T} \right)_p \end{aligned} \quad (\text{X.47})$$

At 298.15 K and 1 bar the contribution of the second term is negligible and the following equation can be used:

$$\Delta_r C_{p,m}^\circ(T_0, p^\circ) \approx \left(115 \times 10^{-10} \frac{|Z_c Z_a|_{\text{eff}}}{r_{\text{eff}}} + 7.1 \sum_i \nu_i \right) \text{ J} \cdot \text{K}^{-1} \cdot \text{mol}^{-1} \quad (\text{X.48})$$

The uncertainty in this expression is $\sim 20\%$ (as estimated from the uncertainty in the derivatives $(\partial \epsilon / \partial T)_p$ and $(\partial^2 \epsilon / \partial T^2)_p$). The expression for the standard partial molar volume of a reaction involving the formation of mononuclear complexes is:

$$\begin{aligned} \Delta_r V_m^\circ(T, p) &= \left(\frac{\partial \Delta_r G_m^\circ}{\partial p} \right)_T \\ &= \frac{|Z_c Z_a|_{\text{eff}}}{r_{\text{eff}}} \frac{N_A e^2}{4\pi \epsilon_o \epsilon(T, p)^2} \left(\frac{\partial \epsilon(T, p)}{\partial p} \right)_T + \sum_i \nu_i R T k_T \end{aligned} \quad (\text{X.49})$$

where $k_T(T, p) = -(1/V_m^\circ) (\partial V_m^\circ / \partial p)_T = (\partial \ln \rho / \partial p)_T$ is the coefficient of isothermal compressibility of pure water. At 298.15 K and 1 bar the following equation may be used:

$$\Delta_r V_m^\circ(T_0, p^\circ) \approx \left(8.23 \times 10^{-10} \frac{|Z_c Z_a|_{\text{eff}}}{r_{\text{eff}}} + 1.1 \sum_i \nu_i \right) \text{ cm}^3 \cdot \text{mol}^{-1}$$

The uncertainty in $\Delta_r V_m^\circ(T_0, p^\circ)$ should be $\sim 10\%$ (from the estimated uncertainty in $(\partial \epsilon / \partial p)_T$).

The values of the temperature and pressure derivatives of the dielectric constant of water, which are needed in Eqs. (X.45) to (X.49), can be calculated from the equations of Refs. [91JOH/NOR, 92SHO/OEL], or from the equations of Archer and Wang [90ARC/WAN] together with an equation of state for water to calculate the density of liquid water, $\rho(T, p)$ (such equations of state may be found for example in Refs. [84HAA/GAL, 84KES/SEN, 89SAU/WAG, 93WAG/PRU]). All the data needed to use the Ryzhenko-Bryzgalin model for aqueous solutions from 273.15 K to 573.15 K are given in Table X.4.

The Ryzhenko-Bryzgalin model considers thermodynamic quantities at zero ionic strength, hence it is in general necessary to recalculate the experimental data to $I = 0$. This can be done, for example, by using the specific ion interaction theory as described in Chapter IX.

As mentioned above, the Ryzhenko-Bryzgalin model is a two parameter model, requiring only $K(T_0, p^\circ)$ and r_{eff} . If the value of $\Delta_r S_m^\circ$ for the reaction is known at 298.15 K (or may be estimated, *cf.* Section X.4.2.2, *p.*485), the required value of the distance parameter r_{eff} may be calculated with Eq. (X.46). However, in general it is possible to estimate the “distance” parameter r_{eff} from the sum of crystallographic radii of the central ion and the ligand. This allows the calculation of preliminary values of $\log_{10} K^\circ(T, p)$, even when all thermodynamic properties of reaction are lacking except for $\log_{10} K^\circ(T_0, p^\circ)$.

X.2.4.3.1. Example: the mononuclear $\text{Al}^{3+}-\text{OH}^-$ system

This section describes the procedure used and indicates the accuracy of the method. Further details on this example are given in Ref. [94PLY/GRE].

In the system $\text{Al}^{3+}-\text{OH}^-$ the following mononuclear complexes have been established [76BAE/MES]: Al^{3+} , AlOH^{2+} , $\text{Al}(\text{OH})_2^+$, $\text{Al}(\text{OH})_3(\text{aq})$, and $\text{Al}(\text{OH})_4^-$. Standard values of the equilibrium constants of formation of these complexes, $\log_{10} \beta_i^\circ$, at 298.15 K have been selected by Plyasunov and Grenthe [94PLY/GRE] from recent literature studies: (9.04 ± 0.03) , (17.44 ± 0.19) , (25.50 ± 0.50) and (33.10 ± 0.06) for $i = 1$ to 4, respectively. The second step is to find r_{eff} for this system. Several estimations of this parameter are given in [94PLY/GRE]. Preliminary calculations readily show that a reasonable agreement with the available experimental data can be achieved with $r_{\text{eff}} = (2.10 \pm 0.05) \times 10^{-10}$ m. The results obtained with Eq. (X.44) are compared with the literature equilibrium constants for the first and last hydrolysis steps (for which more accurate data have been obtained experimentally) in Figures X.11 and X.12. In addition, calculated and experimental equilibrium constants for the step-wise reaction:



are compared in Figure X.13.

The calculations indicate that the simple electrostatic model of Ryzhenko and Bryzgalin is able to describe at least semiquantitatively the temperature dependence of the formation constants for the mononuclear hydroxy complexes of aluminium up to 473 or

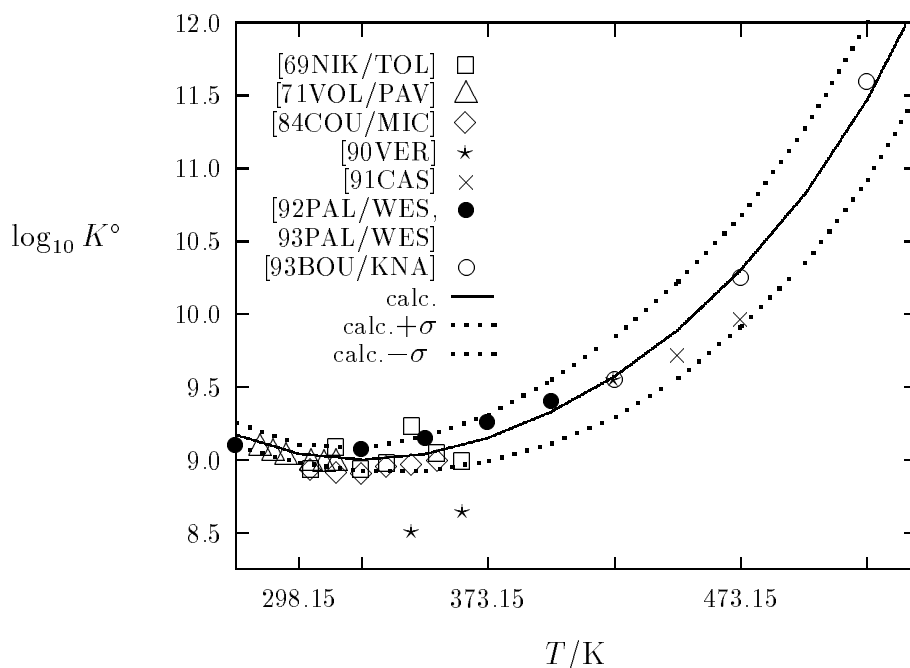
Table X.4: Temperature and pressure variation of the density and dielectric constant (relative permittivity) of liquid water at the standard pressure ($p^\circ = 1$ bar) for $T \leq 373.15$ K and at the vapour saturation pressure at $T > 373.15$ K, as well as some other properties of liquid water at the reference temperature, T_0 , and at the standard pressure, p° , namely: the coefficient of thermal expansion and its temperature derivative, the coefficient of isothermal compressibility, the first and second temperature derivatives and the pressure derivative of the dielectric constant. These values have been calculated with the equation of state of Kestin *et al.* [84KES/SEN] and the equation of Archer and Wang [90ARC/WAN] for the dielectric constant of water.

t (°C)	T (K)	p (bar)	ρ (g · cm ⁻³)	ε
0.00	273.15	1.000	0.9998	87.90
25.00	298.15	1.000	0.9970	78.38
50.00	323.15	1.000	0.9880	69.88
75.00	348.15	1.000	0.9749	62.29
100.00	373.15	1.013	0.9584	55.52
125.00	398.15	2.32	0.9391	49.47
150.00	423.15	4.76	0.9171	44.06
175.00	448.15	8.92	0.8923	39.19
200.00	473.15	15.5	0.8647	34.77
225.00	498.15	25.5	0.8339	30.73
250.00	523.15	39.8	0.7991	26.99
275.00	548.15	59.4	0.7592	23.47
300.00	573.15	85.8	0.7124	20.09

Values at $T_0 = 298.15$ K and $p^\circ = 1$ bar:

$$\begin{aligned}
 \alpha_T &= 2.594 \times 10^{-4} \text{ K}^{-1} \\
 (\partial \alpha_T / \partial T)_{p^\circ} &= 9.56 \times 10^{-6} \text{ K}^{-2} \\
 k_T &= 4.522 \times 10^{-5} \text{ bar}^{-1} \\
 (\partial \varepsilon / \partial T)_{p^\circ} &= -3.60 \times 10^{-1} \text{ K}^{-1} \\
 (\partial^2 \varepsilon / \partial T^2)_{p^\circ} &= 1.60 \times 10^{-3} \text{ K}^{-2} \\
 (\partial \varepsilon / \partial p)_{T_0} &= 3.64 \times 10^{-3} \text{ bar}^{-1}
 \end{aligned}$$

Figure X.11: Comparison of experimental equilibrium constants for the reaction of formation of AlOH^{2+} with those obtained on the basis of the Ryzhenko-Bryzgalin model. Adapted from Ref. [94PLY/GRE].



523 K using the values of stability constants at 298.15 K with only one fitting parameter, r_{eff} , which has *the same value for all mononuclear complexes formed in the system*. At higher temperatures the calculated values of K° differ systematically from the equilibrium constants determined experimentally.

The model is put to a more rigorous test by trying to predict $\Delta_r S_m^\circ$, $\Delta_r C_{p,m}^\circ$ and $\Delta_r V_m^\circ$, for the formation reactions, with Eqs. (X.45) to (X.49), and the same size parameter as above ($r_{\text{eff}} = (2.10 \pm 0.05) \times 10^{-10}$ m). Precise experimental values for $\Delta_r S_m^\circ$, $\Delta_r C_{p,m}^\circ$ and $\Delta_r V_m^\circ$ at 298.15 K and 1 bar are only available for one of the aluminium hydrolysis reactions:

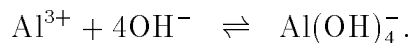


Table X.5 shows that the calculated values of $\Delta_r S_m^\circ$, $\Delta_r C_{p,m}^\circ$ and $\Delta_r V_m^\circ$ are only in qualitative agreement with the experimental determinations. This reflects the limitations of this simple electrostatic model, for example the assumption that $\Delta_r G_{m,\text{nonel}}^\circ$ is independent of T and p . More sophisticated models, *e.g.*, the revised Helgeson-Kirkham-Flowers model, consider the non-electrostatic term to be a function of temperature and pressure.

It should be noted that in order to improve the predictive capabilities of this simple electrostatic model, Ryzhenko [81RYZ] suggested the following empirical temperature and

Figure X.12: Comparison of experimental equilibrium constants for the reaction of formation of $\text{Al}(\text{OH})_4^-$ from Al^{3+} and OH^- with those obtained on the basis of the Ryzhenko-Bryzgalin model. See Figure X.11 for symbols. Adapted from Ref. [94PLY/GRE].

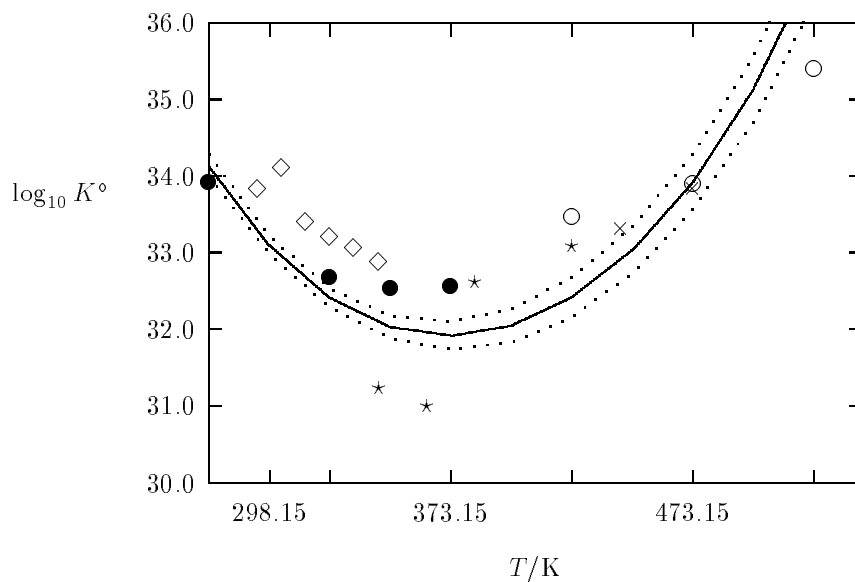


Figure X.13: Comparison of experimental equilibrium constants for the reaction $\text{AlOH}^{2+} + 3\text{OH}^- \rightleftharpoons \text{Al}(\text{OH})_4^-$ with those obtained on the basis of the Ryzhenko-Bryzgalin model. See Figure X.11 for symbols. Adapted from Ref. [94PLY/GRE].

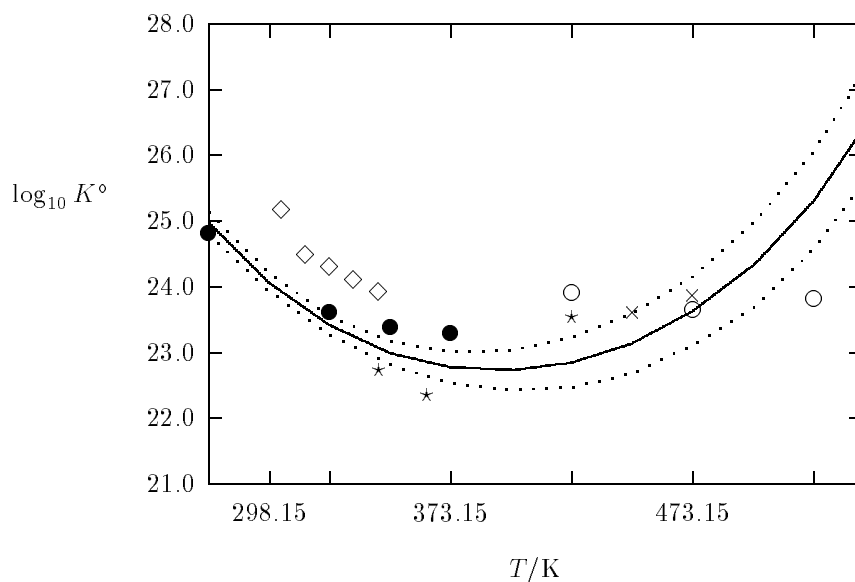


Table X.5: The calculated and experimental values of $\Delta_r S_m^\circ$, $\Delta_r C_{p,m}^\circ$ and $\Delta_r V_m^\circ$ for reaction $\text{Al}^{3+} + 4\text{OH}^- \rightleftharpoons \text{Al}(\text{OH})_4^-$ at 298.15 K and 1 bar. Adapted with revisions from Ref. [94PLY/GRE]. The experimental values were derived in Ref. [94PLY/GRE] from experimental results presented in the literature sources.

Property	Calculated value	Experimental value	Literature source
$\Delta_r S_m^\circ$ ($\text{J} \cdot \text{K}^{-1} \cdot \text{mol}^{-1}$)	$435 \pm 17^{(a)}$	501 ± 9.1 470.1 ± 14	[92PAL/WES] [91CHE/XU, 89COX/WAG]
$\Delta_r C_{p,m}^\circ$ ($\text{J} \cdot \text{K}^{-1} \cdot \text{mol}^{-1}$)	$660 \pm 30^{(a)}$	790 784 829 ± 37	[88HOV/HEP] [92PAL/WES] [92PAL/WES]
$\Delta_r V_m^\circ$ ($\text{cm}^3 \cdot \text{mol}^{-1}$)	$45 \pm 3^{(b)}$	108	[88HOV/HEP]

(a) The \pm term is based on the uncertainty in r_{eff} .

(b) The \pm term has been estimated from the uncertainty in $(\partial \varepsilon / \partial p)_T$, *cf.* Eq. (X.49).

pressure dependence of r_{eff} :

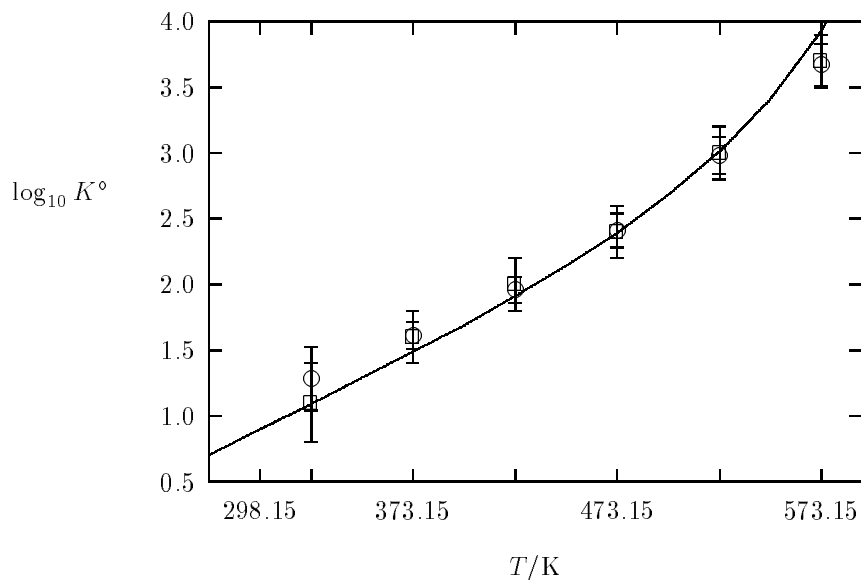
$$r_{\text{eff}}(T, p) = r_{\text{eff}}(T_0, p^\circ) \left(\frac{V_m^\circ(\text{H}_2\text{O}, 1, T, p)}{V_m^\circ(\text{H}_2\text{O}, 1, T_0, p^\circ)} \right)^{1/3} \quad (\text{X.50})$$

where values for the molar volume of pure water are needed both at the T and p of interest, and at the reference temperature $T_0 = 298.15 \text{ K}$ and the standard pressure $p^\circ = 1 \text{ bar}$. In later publications Ryzhenko and Bryzgalin [85RYZ/BRY, 86BRY, 87RYZ/BRY, 89BRY] used a somewhat different function:

$$r_{\text{eff}}(T, p) = r_{\text{eff}}(T_0, p^\circ) \left(\frac{\rho(T_0, p^\circ)}{\rho(T, p)} \right)^{\rho(T, p)/5} \quad (\text{X.51})$$

Eqs. (X.50) and (X.51) are perhaps indirect attempts to take into account both differences in concentration units (molar to molal, as discussed above) as well as physical phenomena occurring when the molar volume of water increases. Eqs. (X.50) and (X.51) predict a gradual *increase* of r_{eff} with temperature, typically in the range $(0.2 \text{ to } 0.6) \times 10^{-10} \text{ m}$ at 573 K. It should be noted that in the revised Helgeson-Kirkham-Flowers model, *cf.* Eq. (X.34), the effective radius *decreases* with temperature because the function $g(T)$ has negative values [88TAN/HEL, Table H-8, 92SHO/OEL, Table 5]. From Eqs. (X.42) and (X.43) it follows that if r_{eff} is temperature and pressure dependent, then $|Z_c Z_a|_{\text{eff}}$ will also be a function of T and p , and Eqs. (X.44) and (X.45), *etc.*, must be rewritten accordingly.

Figure X.14: Comparison of experimental equilibrium constants (squares: [88PAL/DRU], circles: [93PAL/HYD]) for reaction: $\text{Fe}^{2+} + \text{CH}_3\text{COO}^- \rightleftharpoons \text{FeCH}_3\text{COO}^+$ with those obtained on the basis of the Ryzhenko-Bryzgalin model.

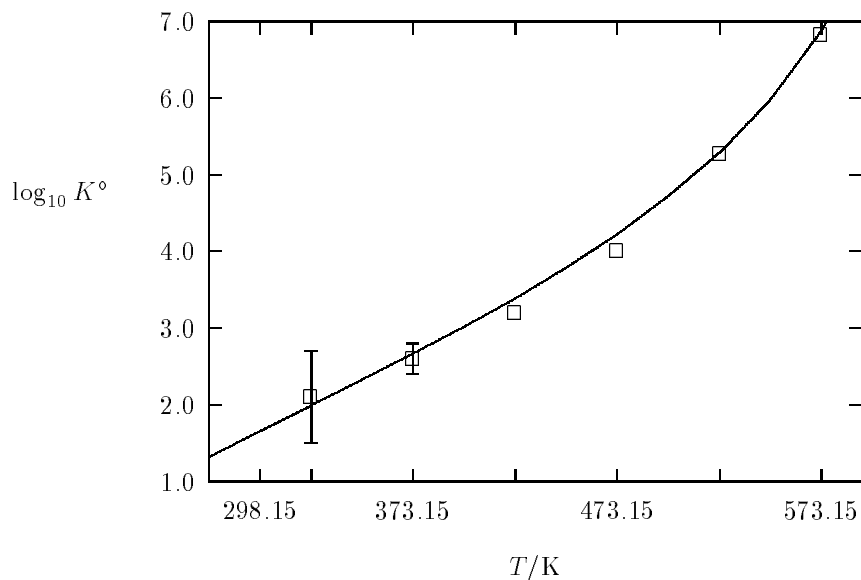


See, for example, Ref. [94PLY/GRE] for r_{eff} given by Eq. (X.50). Nevertheless, in both the Ryzhenko-Bryzgalin and in the revised Helgeson-Kirkham-Flowers models the effects of the variation in r_{eff} with increasing temperature are essentially negligible at $T \leq 473$ K. For simplicity, the examples in this chapter have been worked out with Eqs. (X.44) to (X.49), that is, assuming that r_{eff} is independent of temperature and pressure. Plyasunov and Grenthe [94PLY/GRE] presented the results of the Ryzhenko-Bryzgalin model on the Al(III)-OH^- system using Eq. (X.50) to describe the T and p dependence of r_{eff} .

X.2.4.3.2. Example: the stability of acetate complexes of Fe^{2+}

Palmer *et al.* [88PAL/DRU, 93PAL/HYD] have used a potentiometric method to study the stability of acetate complexes of Fe(II) in aqueous solutions at temperatures between 323 and 568 K (at steam saturated pressures above 373 K). Palmer and co-workers obtained equilibrium constants for the formation of $\text{FeCH}_3\text{COO}^+$ and $\text{Fe}(\text{CH}_3\text{COO})_2(\text{aq})$, and observed indications of the presence of $\text{Fe}(\text{CH}_3\text{COO})_3^-$ at high concentrations of acetate. The experimental equilibrium constants [88PAL/DRU, 93PAL/HYD] are compared in Figures X.14 and X.15 with those obtained with the Ryzhenko-Bryzgalin model using $r_{\text{eff}} = 2.6 \times 10^{-10}$ m and a polarisability of zero for the acetate ion.

Figure X.15: Comparison of experimental equilibrium constants [88PAL/DRU] for reaction: $\text{Fe}^{2+} + 2\text{CH}_3\text{COO}^- \rightleftharpoons \text{Fe}(\text{CH}_3\text{COO})_2(\text{aq})$ with those obtained on the basis of the Ryzhenko-Bryzgalin model.



X.2.4.4. The density or “complete equilibrium constant” model

The density model is based on the experimental observation that in aqueous systems the logarithm of the equilibrium constants of many reactions at isothermal conditions are linear functions of the logarithm of the density of the solvent over large p and T ranges [56FRA, 61FRA]. The theoretical basis for this has been discussed by many authors, and a comprehensive review of the literature is given by Anderson *et al.* [91AND/CAS]. The conclusion from these discussions is that the origin of the linear relationship is unknown, *cf.* [91AND/CAS, pp.1772–1773]. The model postulates a direct proportionality between $\log_{10} K^\circ(T, p)$, for reactions involving aqueous species, and $\log_{10} \rho(T, p)$, where $\rho(T, p)$ is the density of pure water. This proportionality was discovered by Franck [56FRA, 61FRA] during his conductimetric investigations of the electrolytic properties of KCl and other electrolytes at temperatures between 573 to 1073 K at a wide range of pressures. Later, Marshal [70MAR, 72MAR] confirmed this observation and formulated the concept of “complete equilibrium constant” on the basis of determinations of dissociation constants of many salts and acids at temperatures above 673 K. This concept is outlined by the following relation:

$$\log_{10} K^\circ(T, p) = \log_{10} K'(T) + k(T) \log_{10} \rho(T, p) \quad (\text{X.52})$$

where $K^\circ(T, p)$ stands for the conventional equilibrium constant in molar concentration units, which depends both on temperature and pressure; $K'(T)$ is the “complete equi-

librium constant”, which is assumed to depend on temperature only; $k(T)$ is a function which Marshall [70MAR, 72MAR] considered to represent the change in hydration numbers between the products and the reactants; and $\rho(T, p)$ is the density of pure water. It must be pointed out that Eq. (X.52) has *no* rigorous thermodynamic basis. However, it provides a remarkably good correlation, valid over a very wide range of state parameters. It describes the dissociation constants for HCl [84FRA/MAR], HBr [68QUI/MAR2], NaCl [68QUI/MAR], NaBr [68QUI/MAR3], NaI [69DUN/MAR] and NH_4OH [68QUI/MAR4] in the temperature range 673 to 973-1073 K and a water density of 0.3 or 0.4 to 0.8 $\text{g} \cdot \text{cm}^{-3}$, as well as the pressure dependence of $\log_{10} K^\circ(T, p)$ for the dissociation of a number of electrolytes up to 4 kbar at room temperature [72MAR], *etc.* Eq. (X.52) also describes the thermodynamic solubility product for salts, for instance, that of $\text{CaSO}_4(\text{s})$ at temperatures between 373 and 573 K, and pressures up to 1000 bar [72MAR].

The following type of equation was used by Marshall and Franck [81MAR/FRA] to describe the molal ion product of water as a function of p and T , and the same expression can also be used for other chemical equilibria:

$$\begin{aligned} \log_{10} K^\circ(T, p) = & \left(A + \frac{B}{T} + \frac{C}{T^2} + \frac{D}{T^3} \right) \\ & + \left(E + \frac{F}{T} + \frac{G}{T^2} \right) \log_{10} \rho(T, p) \end{aligned} \quad (\text{X.53})$$

Eq. (X.53) is a formulation issued by the International Association for the Properties of Steam [81MAR/FRA] which describes the dissociation constant of pure water up to 1273 K and 10 kbar, practically within the experimental uncertainties in the whole T - p range (at least at densities above $\sim 0.3 \text{ g} \cdot \text{cm}^{-3}$).

The density model is a useful empirical generalization of a large number of experimental data on the thermodynamic behaviour of solutes at high temperatures and pressures.

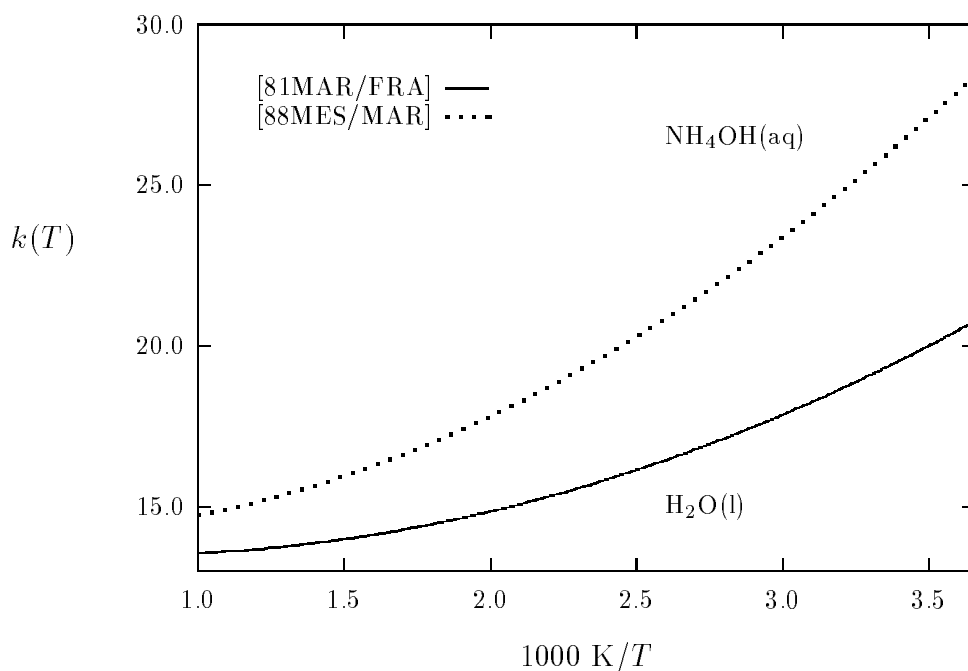
The full set of coefficients of Eq. (X.53) can be determined only if experimental data on $\log_{10} K^\circ(T, p)$ are available in a wide range of temperature and pressure (or solvent density). Anderson *et al.* [91AND/CAS] cited Mesmer for the use of a simplified form of Eq. (X.53):

$$\ln K^\circ(T, p) = a_1 + \frac{a_2}{T} + \frac{a_3}{T} \ln \rho(T, p) \quad (\text{X.54})$$

where a_1 , a_2 , and a_3 are independent of T and p . This equation is very useful for correlations up to 400 or 553 K depending on the system. Standard thermodynamic relationships allow the derivation of the parameters a_1 , a_2 , and a_3 as follows [91AND/CAS]:

$$\begin{aligned} a_1 &= \ln K^\circ(T_0, p^\circ) + \frac{\Delta_r H_m^\circ(T_0, p^\circ)}{RT_0} - \frac{\Delta_r C_{p,m}^\circ(T_0, p^\circ) \alpha_T(T_0, p^\circ)}{RT_0 (\partial \alpha_T / \partial T)_{p^\circ}} \\ a_2 &= -\frac{\Delta_r H_m^\circ(T_0, p^\circ)}{R} + \frac{(T_0 \alpha_T(T_0, p^\circ) + \ln \rho(T_0, p^\circ)) \Delta_r C_{p,m}^\circ(T_0, p^\circ)}{RT_0 (\partial \alpha_T / \partial T)_{p^\circ}} \\ a_3 &= -\frac{\Delta_r C_{p,m}^\circ(T_0, p^\circ)}{RT_0 (\partial \alpha_T / \partial T)_{p^\circ}} = -\frac{\Delta_r V_m^\circ(T_0, p^\circ)}{Rk_T(T_0, p^\circ)} \end{aligned}$$

Figure X.16: The temperature dependence of parameter $k(T)$ of Eq. (X.52) between 273.15 and 1000 K, from experimental studies on the dissociation equilibria of $\text{H}_2\text{O}(\text{l})$ [81MAR/FRA] and $\text{NH}_4\text{OH}(\text{aq})$ [88MES/MAR].

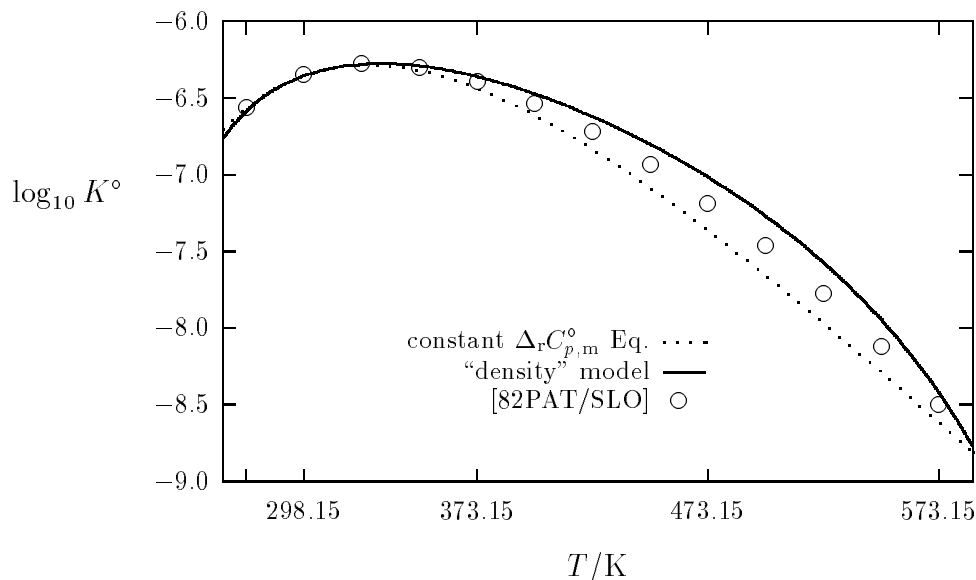


where α_T and k_T are the coefficient of thermal expansion of water and the coefficient of isothermal compressibility of water, respectively, and the subscript “ p° ” in the derivative $(\partial\alpha_T/\partial T)_{p^\circ}$ indicates that the derivative is taken at T_0 and p° . The values for α_T , k_T , and $(\partial\alpha_T/\partial T)_{p^\circ}$ needed to calculate a_1 , a_2 , and a_3 are given in Table X.4. Values for the density of water, ρ , which are needed in Eq. (X.54), may be calculated at the steam saturated pressure and for any temperature below the critical point with the equation given by Wagner and Pruss [93WAG/PRU].

A comparison of Eqs. (X.52) and Eq. (X.54) shows that the latter equation assumes the simplest possible temperature dependence for $\log_{10} K'(T)$ and a simple T^{-1} dependence of $k(T)$. This simplification reduces the temperature range of applicability of Eq. (X.54), because the true temperature dependence of $k(T)$ might be more complicated, for example as in Eq. (X.53). Among the most reliable expressions available for $k(T)$ are those for the dissociation of H_2O and NH_4OH . These expressions are shown in Figure X.16, which shows that $k(T)$ can be considered to be approximately linear functions of T^{-1} only up to about 550 K. Anderson *et al.* [91AND/CAS] estimated the upper temperature limit of applicability of Eq. (X.54) to be ~ 573 K.

An important feature of the “density” model in the Anderson-Castet-Schott-Mesmer modification [91AND/CAS] is the possibility of using experimentally determined thermodynamic quantities like $\Delta_r H_m^\circ(T_0, p^\circ)$, $\Delta_r C_{p,m}^\circ(T_0, p^\circ)$ (or alternatively $\Delta_r S_m^\circ(T_0, p^\circ)$,

Figure X.17: Comparison of experimental equilibrium constant for the reaction $\text{CO}_2(\text{aq}) + \text{H}_2\text{O}(\text{l}) \rightleftharpoons \text{HCO}_3^- + \text{H}^+$ [82PAT/SLO] with those calculated on the basis of the “density” model and the constant $\Delta_r C_{p,m}^\circ$ method. See Eq. (X.19) (Section X.2.2.2) and Figure X.10.



$\Delta_r V_m^\circ(T_0, p^\circ)$, *etc.*) together with the value of $\log_{10} K^\circ(T_0, p^\circ)$ to *predict* values of $\log_{10} K^\circ(T, p)$. This calculation also requires the numerical values of $\rho(T, p)$, $\alpha_T(T_0, p^\circ)$, $k_T(T_0, p^\circ)$ and $(\partial\alpha_T/\partial T)_{p^\circ}$ for pure water at saturation water vapour pressure, which are well known. All the data needed to use the “density” model of Anderson *et al.* [91AND/CAS] are given in Table X.4, *p.* 460.

Unlike the electrostatic model of Ryzhenko and Bryzgalin, which is valid only for formation (or dissociation) reactions involving exclusively aqueous species, the “density” model can be used for any reaction involving aqueous species, including reactions where solid phases participate (see [91AND/CAS] for further details), and the “density” model appears to be as general as the revised Helgeson-Kirkham-Flowers model described in Section X.2.4.2. However, relatively fewer aqueous systems have been analysed with the “density” model.

We will demonstrate the accuracy of the method by using experimental data for the first deprotonation constant of $\text{CO}_2(\text{aq})$ from [82PAT/SLO], *cf.* Figure X.10.

From the experimental values at 298.15 K and 1 bar ($\log_{10} K^\circ(T_0, p^\circ) = -6.349 \pm 0.005$, $\Delta_r H_m^\circ(T_0, p^\circ) = (9.16 \pm 0.12) \text{ kJ} \cdot \text{mol}^{-1}$, $\Delta_r C_{p,m}^\circ(T_0, p^\circ) = -(338 \pm 27) \text{ J} \cdot \text{K}^{-1} \cdot \text{mol}^{-1}$) we obtain the following values of the parameters a_1 to a_3 in Eq. (X.54): $a_1 = -7.274$, $a_2 = -2149.2 \text{ K}$, $a_3 = 14078 \text{ K}$. The calculated values of $\log_{10} K^\circ$ (the solid curve) and the experimental values are shown in Figure X.17. The maximal deviations are ~ 0.2 logarithmic units at 473 - 548 K.

X.3. Third-law method

The second-law method of extrapolation described in previous sections is frequently used, and it is well suited for extrapolation of Gibbs energy data when only a small temperature interval is involved. However, if a temperature extrapolation over a large temperature range is required, and the original Gibbs energy data are for a restricted temperature interval, then the second-law extrapolation method can be very sensitive to extrapolation errors. This arises because the integral on the right hand side of Eq. (X.3) depends on $\Delta_r H_m^\circ(T)$. For experimental Gibbs energy data over a short temperature range, the derived values $\Delta_r H_m^\circ(T)$ and $\Delta_r S_m^\circ(T)$ can be very inaccurate (even if $\Delta_r G_m^\circ(T)$ is fairly accurately known) since they depend on the intercept and slope of

$$\Delta_r G_m^\circ(T) = \Delta_r H_m^\circ(T) - T \Delta_r S_m^\circ(T). \quad (\text{X.1})$$

This issue has been discussed in many textbooks. For example, according to the revised version of Lewis and Randall's *Thermodynamics* [61LEW/RAN, p.178]: "Often temperature-dependent errors are difficult to eliminate from the equilibrium measurements, and while the resulting equilibrium constants or free energies of reaction are approximately correct, the temperature coefficient and the corresponding heat of reaction from the second law ... may be greatly in error. The third-law method will also yield the heat of reaction when ΔF° values have been determined over too small a temperature interval to determine the temperature coefficient accurately".

The preferred method to obtain $\Delta_f H_m^\circ(T_0)$ of a compound or ion is by direct use of calorimetric measurements[†]. For example, both Ca(cr) and CaO(cr) readily dissolve in aqueous solutions of strong mineral acids, and these $\Delta_{\text{sol}} H_m^\circ$ values can be combined to yield $\Delta_f H_m^\circ(\text{CaO, cr}, T_0)$. However, for some systems this type of measurement is not possible. That approach cannot be used for Tc(cr) and TcO₂(cr), Ru(cr) and RuO₂(cr), Pd(cr) and PdO(cr), *etc.*, and other oxides which are only very slightly soluble in aqueous solutions of mineral acids, and where the metals are even less reactive. Direct combustion of the metal with O₂(g) under pressure can sometimes be used instead to yield direct calorimetric values of $\Delta_f H_m^\circ(T_0)$, but the desired oxide is not always obtained or the reaction may be incomplete or yield more than one product. Combustion of Tc(cr) yields mainly Tc₂O₇(cr), for example, so it will not yield data for TcO₂(cr).

An alternative way of obtaining thermodynamic data is by use of Gibbs energy measurements at very high temperatures. For example, a reaction such as



can be studied by means of oxygen decomposition pressure measurements or solid state emf measurements. (This reaction does not occur for some metal-oxide systems, *e.g.*, in the case of TcO₂(cr), since it sublimes rather than decomposes at high temperatures.) In many cases it may be necessary to use temperatures of 1000 K or higher to obtain a

[†] T_0 stands for the reference temperature (= 298.15 K).

significant vapour pressure of oxygen from decomposition of a MO_2 , and 700 to 800 K or higher to obtain sufficient solid state diffusion required for a solid state emf measurement. A third-law extrapolation of such $\Delta_r G_m^\circ(T)$ data to 298.15 K will, in general, be much more reliable than direct use of the second-law method.

The third-law method makes use of the free energy functions for reactants and products

$$\frac{G_m^\circ(T) - H_m^\circ(T_0)}{T},$$

which have much smaller variations with temperature than $G_m^\circ(T)$. Thus, this method can generally be used for numerical or graphical interpolations or extrapolations with a higher degree of precision than direct calculations with either $G_m^\circ(T)$ or $H_m^\circ(T)$.

The third-law method equation can be written in the general form

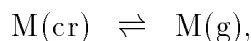
$$\begin{aligned} \Delta_r \left(\frac{G_m^\circ(T) - H_m^\circ(T_0)}{T} \right) &= \sum_{\text{products}} \left(\frac{G_m^\circ(T) - H_m^\circ(T_0)}{T} \right) \\ &\quad - \sum_{\text{reactants}} \left(\frac{G_m^\circ(T) - H_m^\circ(T_0)}{T} \right) \\ &= \frac{\Delta_r G_m^\circ(T)}{T} - \frac{\Delta_r H_m^\circ(T_0)}{T}. \end{aligned} \quad (\text{X.55})$$

For this equation to be used the value of $\Delta_r G_m^\circ(T)$ must be known from low-temperature calorimetric data or from high-temperature Gibbs energy measurements, and the value of $\Delta_r H_m^\circ(T_0)$ needs to be obtained. Once $\Delta_r H_m^\circ(T_0)$ has been determined, it can be used to derive $\Delta_f H_m^\circ(T_0)$ of one of the reactants or products. Two different cases will now be considered.

X.3.1. Evaluation from high and low-temperature calorimetric data

If both low-temperature (heat capacity) and high-temperature (relative enthalpies as from drop calorimetry) thermal data are available, then the calculation of $\Delta_r H_m^\circ(T_0)$ is straightforward. The middle terms of Eq. (X.55), $\frac{G_m^\circ(T) - H_m^\circ(T_0)}{T}$, are then known, and they can be combined with each experimental $\Delta_r G_m^\circ(T)$ point at each temperature to yield a value of $\Delta_r H_m^\circ(T_0)$. If there is no drift in the calculated values of $\Delta_r H_m^\circ(T_0)$ within the temperature range over which $\Delta_r G_m^\circ(T)$ was measured, then the thermodynamic data are internally consistent and the average of these $\Delta_r H_m^\circ(T_0)$ should be reliable. We now give a specific example of this type of calculation.

Consider the simple case of the calculation of $\Delta_{\text{sub}} H_m^\circ(T_0)$ from high-temperature sublimation data of a pure metal to form its monoatomic vapour. The reaction is thus



and $\Delta_r G_m^\circ(T)$ becomes $\Delta_{\text{sub}} G_m^\circ(T)$. For the solid phase

$$G_m(\text{cr}, T) = G_m^\circ(\text{cr}, T),$$

and for the vapour phase

$$G_m(g, T) = G_m^\circ(g, T) + RT \ln f,$$

where f is the fugacity of $M(g)$. Vapour pressures of metals are generally quite low at temperatures used for sublimation measurements, so the fugacity can be equated to the vapour pressure

$$G_m(g, T) = G_m^\circ(g, T) + RT \ln p.$$

For the sublimation process,

$$\begin{aligned} \Delta_{\text{sub}} G_m(T) &= G_m(g, T) - G_m(\text{cr}, T) \\ &= G_m^\circ(g, T) + RT \ln p - G_m^\circ(\text{cr}, T) \\ &= [G_m^\circ(g, T) - G_m^\circ(\text{cr}, T)] + RT \ln p \\ &= \Delta_{\text{sub}} G_m^\circ(T) + RT \ln p. \end{aligned}$$

Vapour pressure measurements are measurements of an equilibrium property, so $\Delta_{\text{sub}} G_m(T) = 0$ at each T . Thus for a closed system,

$$\begin{aligned} \Delta_{\text{sub}} G_m^\circ(T) &= G_m^\circ(g, T) - G_m^\circ(\text{cr}, T) \\ &= -RT \ln p. \end{aligned}$$

For this case, the third-law extrapolation Eq. (X.55) becomes

$$\begin{aligned} \Delta_{\text{sub}} H_m^\circ(T_0) &= T \left(\frac{G_m^\circ(\text{cr}, T) - H_m^\circ(\text{cr}, T_0)}{T} - \frac{G_m^\circ(g, T) - H_m^\circ(g, T_0)}{T} \right) \\ &\quad - RT \ln p. \end{aligned}$$

The T values were not cancelled in the first term of the right hand side of this equation, since free energy functions will be used to interpolate thermal data.

As a numerical example, we will reanalyse ruthenium vapour pressure measurements reported by Carrera *et al.* [64CAR/WAL]. They were measured from 1932 to 2377 K by use of weight loss recorded with a microbalance (Langmuir method). Values of $[G_m^\circ(T) - H_m^\circ(T_0)]$ both for $\text{Ru}(\text{cr})$ and $\text{Ru}(g)$ are taken from Hultgren *et al.* [73HUL/DES]; thermodynamic properties for the vapour phase in that report were obtained from statistical thermodynamic calculations. Values of $[G_m^\circ(\text{cr}, T) - H_m^\circ(\text{cr}, T_0)]$, $[G_m^\circ(g, T) - H_m^\circ(g, T_0)]$ and \sum/T are summarised in Table X.6. Here \sum denotes

$$\sum = [G_m^\circ(\text{cr}, T) - H_m^\circ(\text{cr}, T_0)] - [G_m^\circ(g, T) - H_m^\circ(g, T_0)].$$

Carrera *et al.* [64CAR/WAL] reported a large number of vapour pressures, but we will reanalyse only a few representative values. The results of these calculations are given in Table X.7; pressures in atm are converted to bar, and values of \sum/T at each temperature T are obtained graphically from a plot of \sum/T against T . There is no trend in the calculated

Table X.6: Free energy functions needed for the evaluation of sublimation data of ruthenium. From Ref. [73HUL/DES].

T (K)	$G_m^\circ(\text{cr}, T) - H_m^\circ(\text{cr}, T_0)$ (kJ · mol ⁻¹)	$G_m^\circ(\text{g}, T) - H_m^\circ(\text{g}, T_0)$ (kJ · mol ⁻¹)	Σ/T (kJ · K ⁻¹ · mol ⁻¹)
1800	-96.32	-377.61	0.15627
2000	-112.20	-424.13	0.15597
2200	-128.81	-471.19	0.15563
2400	-146.14	-518.77	0.15526

Table X.7: Ruthenium vapour pressure data [64CAR/WAL] and standard sublimation enthalpies calculated with the third-law extrapolation method.

T (K)	p (bar)	$-R \ln p$ (kJ · K ⁻¹ · mol ⁻¹)	Σ/T (kJ · K ⁻¹ · mol ⁻¹)	$\Delta_{\text{sub}}H_m^\circ(T_0)$ (kJ · mol ⁻¹)
1940	3.59×10^{-10}	0.18082	0.15607	653.6
2023	2.72×10^{-9}	0.16398	0.15593	647.2
2107	9.82×10^{-9}	0.15331	0.15580	651.3
2199	5.83×10^{-8}	0.13850	0.15563	646.8
2324	2.75×10^{-7}	0.12560	0.15540	653.0

values of $\Delta_{\text{sub}}H_m^\circ(T_0)$ with the temperature of measurement. They yield an average value of $\Delta_{\text{sub}}H_m^\circ(T_0) = (650.4 \pm 6.3)$ kJ · mol⁻¹. Carrera *et al.* [64CAR/WAL] reported a third-law standard enthalpy of sublimation of $\Delta_{\text{sub}}H_m^\circ(T_0) = (653.1 \pm 4.6)$ kJ · mol⁻¹ based on an analysis of all 94 of their most reliable vapour pressures. Our value of $\Delta_{\text{sub}}H_m^\circ(T_0) = (650.4 \pm 6.3)$ kJ · mol⁻¹ from analysis of a five point subset of their vapour pressures is in good agreement.

Since $\Delta_{\text{sub}}H_m^\circ(T_0) = [\Delta_fH_m^\circ(\text{g}, T_0) - \Delta_fH_m^\circ(\text{cr}, T_0)]$ and $\Delta_fH_m^\circ(\text{cr}, T_0) = 0$, we then have a value of $\Delta_fH_m^\circ(\text{Ru}, \text{g}, T_0)$. This can be combined with the calculated statistical thermodynamic entropy of Ru(g) to yield a calculated value of $\Delta_fG_m^\circ(\text{Ru}, \text{g}, T_0)$.

X.3.2. Evaluation from high-temperature data

There are some systems for which low-temperature heat capacities (and thus entropies) have not been measured, but for which high-temperature thermal and Gibbs energy results are available. These can be analysed by a variant of the third-law method to yield approximate values of $\Delta_r H_m^\circ(T_0)$ and $\Delta_r S_m^\circ(T_0)$.

Our fundamental equation for the third-law analysis, Eq. (X.55), can be rearranged into the form

$$\begin{aligned} \frac{\Delta_r G_m^\circ(T)}{T} - \frac{\Delta_r H_m^\circ(T_0)}{T} &= -\Delta_r S_m^\circ(T_0) - [\Delta_r S_m^\circ(T) - \Delta_r S_m^\circ(T_0)] \\ &\quad + \frac{\Delta_r H_m^\circ(T) - \Delta_r H_m^\circ(T_0)}{T}, \end{aligned}$$

where $\Delta_r G_m^\circ(T)$ is known, and both $[\Delta_r S_m^\circ(T) - \Delta_r S_m^\circ(T_0)]$ and $[\Delta_r H_m^\circ(T) - \Delta_r H_m^\circ(T_0)]$ can be calculated from high-temperature thermal (relative enthalpy) results. This equation has two unknowns, $\Delta_r S_m^\circ(T_0)$ and $\Delta_r H_m^\circ(T_0)$. One approach is to use a least-squares fit to obtain values of $\Delta_r S_m^\circ(T_0)$ and of $\Delta_r H_m^\circ(T_0)$ from all of the experimental temperatures. This would yield greater uncertainties than in the case discussed in Section X.3.1.

As an example we will reanalyse the same vapour pressure data for ruthenium that were used in the preceding section. Rearrangement of the last equation for the case of sublimation yields:

$$\begin{aligned} \frac{\Delta_{\text{sub}} H_m^\circ(T_0)}{T} - \Delta_{\text{sub}} S_m^\circ(T_0) &= \frac{\Delta_{\text{sub}} G_m^\circ(T)}{T} - \left[\frac{\Delta_{\text{sub}} H_m^\circ(T) - \Delta_{\text{sub}} H_m^\circ(T_0)}{T} \right] \\ &\quad + [\Delta_{\text{sub}} S_m^\circ(T) - \Delta_{\text{sub}} S_m^\circ(T_0)] \\ &= -R \ln p + \sum^*, \end{aligned}$$

where:

$$\sum^* = - \left[\frac{\Delta_{\text{sub}} H_m^\circ(T) - \Delta_{\text{sub}} H_m^\circ(T_0)}{T} \right] + [\Delta_{\text{sub}} S_m^\circ(T) - \Delta_{\text{sub}} S_m^\circ(T_0)]$$

Table X.8 contains values of \sum^* at round values of the temperature, which were calculated from the tabulated critically assessed thermodynamic values of Hultgren *et al.* [73HUL/DES].

Table X.9 contains the results obtained by reanalysis of the five selected vapour pressures. Values of \sum^* at each experimental temperature were obtained by graphical interpolation from a plot of \sum^* against T .

By using a linear least-squares analysis of the values in Table X.9, we obtain:

$$\frac{\Delta_{\text{sub}} H_m^\circ(T_0)}{T} - \Delta_{\text{sub}} S_m^\circ(T_0) = \frac{(654.250 \pm 51.995) \times 10^3}{T} - (159.69 \pm 24.70)$$

with a correlation coefficient of 0.9975. Thus this calculation yields $\Delta_{\text{sub}} S_m^\circ(T_0) = (159.69 \pm 24.70) \text{ J} \cdot \text{K}^{-1} \cdot \text{mol}^{-1}$ and $\Delta_{\text{sub}} H_m^\circ(T_0) = (654.250 \pm 51.995) \text{ kJ} \cdot \text{mol}^{-1}$. This value

Table X.8: Thermodynamic values for the reanalysis of sublimation data for ruthenium.

T (K)	$[\Delta_{\text{sub}}H_{\text{m}}^{\circ}(T) - \Delta_{\text{sub}}H_{\text{m}}^{\circ}(T_0)]/T$ (J · K ⁻¹ · mol ⁻¹)	$[\Delta_{\text{sub}}S_{\text{m}}^{\circ}(T) - \Delta_{\text{sub}}S_{\text{m}}^{\circ}(T_0)]$ (J · K ⁻¹ · mol ⁻¹)	\sum^* (J · K ⁻¹ · mol ⁻¹)
1800	-2.5639	-4.1547	-1.5908
2000	-3.2175	-5.1087	-1.8912
2200	-3.8930	-6.1212	-2.2282
2400	-4.5815	-7.1797	-2.5982

 Table X.9: Recalculation of ruthenium vapour pressures [64CAR/WAL] by the third-law extrapolation method without fixing the entropies of Ru(cr) and Ru(g) at $T_0 = 298.15$ K.

T (K)	$-R \ln p$ (J · K ⁻¹ · mol ⁻¹)	\sum^* (J · K ⁻¹ · mol ⁻¹)	$-R \ln p + \sum^*$ (J · K ⁻¹ · mol ⁻¹)
1940	180.82	-1.79 ₄	179.03
2023	163.98	-1.92 ₇	162.05
2107	153.31	-2.07 ₀	151.24
2199	138.50	-2.22 ₈	136.27
2324	125.60	-2.44 ₆	123.15

of $\Delta_{\text{sub}}H_{\text{m}}^{\circ}(T_0)$ is in very good agreement with the value obtained by a standard third-law extrapolation (*cf.* Section X.3.1), (650.4 ± 6.3) kJ · mol⁻¹ but is considerably more uncertain. The larger uncertainty arises because two parameters are now being determined by the same five data points whereas in the standard third-law extrapolation only $\Delta_{\text{sub}}H_{\text{m}}^{\circ}(T_0)$ was determined. It is possible to reduce these large uncertainties somewhat by using more of the published vapour pressures in the calculation. However, the same basic conclusion will still be reached, *i.e.*, that the third law calculation of a standard enthalpy of reaction will always yield significantly larger uncertainties when no reliable values of the standard entropies are available than when the calculation is constrained using the standard entropies.

For the examples just given involving the sublimation of ruthenium metal, both types of third-law extrapolations give values of $\Delta_{\text{sub}}H_{\text{m}}^{\circ}(T_0)$ in good agreement. However, consider a case where either the vapour pressures or high-temperature calorimetric data have a

temperature-dependent systematic error (or, if the calorimetric “data” were estimated and these estimated values were systematically in error). An analysis of such data by the standard third-law method as described in Section X.3.1 would yield values of $\Delta_r H_m^\circ(T_0)$ that vary with the temperature of the measurements. It would thus be obvious that there was an error in one or more of the input values for the calculations.

In contrast, if the calculations were done as described in the present section, then the errors due to certain types of systematic errors could be adsorbed into the coefficients of the linear fit. Consequently, both $\Delta_{\text{sub}} H_m^\circ(T_0)$ and $\Delta_{\text{sub}} S_m^\circ(T_0)$ would be in error, but it would not be obvious to the person doing the calculations. The standard third-law method should be considered more trustworthy in most cases, and it should be used when sufficient calorimetric data are available.

X.3.3. A brief comparison of enthalpies derived from the second and third-law methods

The starting point for a second-law calculation of the standard enthalpy of reaction from Gibbs energy of reaction data is

$$\Delta_r G_m^\circ(T) = \Delta_r H_m^\circ(T) - T \Delta_r S_m^\circ(T). \quad (\text{X.1})$$

where $\Delta_r H_m^\circ(T)$ is extracted from a linear or higher-order fit of the Gibbs energy of reaction data as a function of temperature. If a linear fit is appropriate, then the assessed value of $\Delta_r H_m^\circ(T)$ refers to the mean temperature of the measurements T_{av} . The standard enthalpy of reaction is then calculated from the integration of Eq. (X.4) from T_0 to the mean temperature of the high-temperature Gibbs energy of reaction measurements:

$$\Delta_r H_m^\circ(T_0) = \Delta_r H_m^\circ(T_{\text{av}}) - \int_{T_0}^{T_{\text{av}}} \Delta_r C_{p,m}^\circ(T) dT$$

Carrera *et al.* [64CAR/WAL] have compared values of $\Delta_{\text{sub}} H_m^\circ(T_0)$ derived from second and third-law analyses of their vapour pressures. There is no point in repeating those calculations and we merely cite their results. They performed five series of measurements and a separate analysis of each data set gave third-law values of $\Delta_{\text{sub}} H_m^\circ(T_0)$ ranging from (648.1 ± 2.5) to (656.5 ± 3.3) kJ · mol⁻¹. In contrast, their analysis by the second-law method of these same five data sets gave values of $\Delta_{\text{sub}} H_m^\circ(T_0)$ ranging from (600.0 ± 22.2) to (659.4 ± 10.9) kJ · mol⁻¹. Quite clearly, the third-law based values are more precise and more consistent than the second-law based values.

Although third-law based values of $\Delta_r H_m^\circ(T_0)$ are usually more precise and consistent than second-law based values, this better consistency is not in itself a proof that the original Gibbs energy measurements were completely accurate since there are certain types of systematic errors that do not affect these consistency checks. Agreement of second-law and third-law based values of $\Delta_r H_m^\circ(T_0)$ within their “experimental” precision is usually a better indication that the high-temperature Gibbs energy data and the corresponding calorimetric data are of high quality.

X.4. Estimation methods

Experimental or estimated values of $C_{p,m}^\circ$ and S_m° are needed in order to calculate high-temperature equilibrium constants either with Eqs. (X.6) or (X.16), or with Eq. (X.19) (which assumes a temperature independent heat capacity of reaction). The same situation applies to the electrostatic models described in Section X.2.4.

Therefore, estimation methods for $C_{p,m}^\circ(T)$ and $S_m^\circ(T)$ will be described here. For a broader presentation of thermodynamic estimation techniques, the reader is referred to the discussions in references [86NOR/MUN, Section 11-8], [93KUB/ALC, Chapter 3], [61LEW/RAN, pp.515–525], and [52LAT, Appendix III].

Recently, heat capacities have been measured for several aqueous electrolytes and non-electrolytes to about 720 K. See the article by Wood *et al.* [94WOO/CAR] for references to many of the original studies. Since these measurements do not yet include the majority of aqueous electrolytes and non-electrolytes, estimated values are still required for most applications.

X.4.1. Estimation methods for heat capacities

X.4.1.1. Heat capacity estimations for solid phases

Kopp's rule of additivity [86NOR/MUN, Eq. (11-52)] may be used to estimate the heat capacity of a solid phase as the sum of the molar heat capacities of the elements present:

$$C_{p,m}^\circ = \sum_i \nu_i C_{p,m}^\circ(i).$$

This rule is only valid for elements which are also solid in their standard state. However, effective contributions can be used for elements that are not solid in the standard state and adjustments can be made to the entropies of the solid light elements to improve the accuracy of the estimated values. Sturtevant [59STU, pp.557–558] reported the following effective atomic contributions (in units of $\text{J} \cdot \text{K}^{-1} \cdot \text{mol}^{-1}$) for the light elements: C, 7.53; H, 9.62; B, 11.3; Si, 15.9; O, 16.7; F, 20.9; P, 22.6; S, 22.6; and 25.9 for the heavier atoms.

Kubaschewski, Alcock and Spencer [93KUB/ALC] reported a technique similar to that of Latimer's method for standard entropies (*cf.* Section X.4.2.1, p.483) to estimate heat capacities of solids at 298.15 K by adding the contributions from the cationic and anionic groups present in a solid phase. Cationic and anionic contributions are listed in [93KUB/ALC, their Tables IX and X]. Coefficients for temperature functions of the type

$$C_{p,m}^\circ(T) = a + bT - cT^{-2}$$

may be estimated by their approach if the melting temperature of the solid phase is known [93KUB/ALC, their Eqs. (117) and (118)].

Parameter estimates for the same type of heat capacity function for oxide minerals were made by Helgeson *et al.* [78HEL/DEL, Eqs. (78), (80) and (85)] using the sum of the heat capacities for the constituent oxides.

For estimations on chalcogenides, the discussion given by Mills should be consulted [74MIL, Section 2.3.3]. For a discussion of the chalcogenides of rare earths and actinides, see Ref. [74MIL, Section 3.3.2.a].

X.4.1.2. Heat capacity estimations for aqueous species

For standard partial molar heat capacities of aqueous ions the estimation methods are mainly of two types:

- Correlations between $C_{p,m}^{\circ}(T_0)$ and standard partial molar ionic entropies at 298.15 K. The method of Criss and Cobble [64CRI/COB, 64CRI/COB2] will be described because of its historical interest. The equations of Helgeson and co-workers [81HEL/KIR, 88SHO/HEL, 97SHO/SAS, 97SVE/SHO] are modern correlations of this kind.
- Electrostatic models of ion hydration. These types of $C_{p,m}^{\circ}(T)$ estimations are described as alternative temperature functions for the heat capacity (Section X.2.4).

The first type of estimation methods (correlations between $C_{p,m}^{\circ}(T_0)$ and ionic entropies at 298.15 K) are limited to a few ion types, which do not yet include metal ligand complexes, and which sometimes exclude neutral aqueous species. Therefore these methods are not always useful unless further assumptions are made. For example, Baes and Mesmer [81BAE/MES] assigned partial molar heat capacities for a mononuclear hydrolysis product equal to that of another metal cation having the same ionic radius as that of the unhydrolysed cation of interest, and having the same charge as the hydrolysis product of interest. Another approximation for metal-ligand complexes, which was used by Lemire and Tremaine [80LEM/TRE], is to use the correlation parameters for simple cations and anions.

X.4.1.2.1. Criss and Cobble's method

The method developed by Criss and Cobble [64CRI/COB, 64CRI/COB2] is of interest because it was widely used during the 1970s and there are many publications which have used it. It has however several associated problems which are discussed below, and nowadays it has been largely superseded by the correlation equations of Helgeson and co-workers described in Section X.4.1.2.3.

Criss and Cobble [64CRI/COB, 64CRI/COB2] observed that by assigning a specific value to the standard partial molar ionic entropy of H^+ at each temperature, for simple ions a linear correspondence could be obtained between the standard partial molar ionic entropies at 298.15 K and at other temperatures,

$$S_m^{\circ,abs}(i, T) = a(T) + b(T)S_m^{\circ,abs}(i, T_0), \quad (X.56)$$

where $a(T)$ and $b(T)$ are temperature dependent parameters which differ for different ion types (*i.e.*, for simple cations, simple anions, oxyanions, and acid oxyanions),

and $S_m^{\circ, \text{abs}}(i, T)$ are “absolute” partial molar entropies (referred to a specific value for $S_m^{\circ, \text{abs}}(\text{H}^+, \text{aq}, T)$). At 298.15 K the optimum value of $S_m^{\circ, \text{abs}}(\text{H}^+, \text{aq}, T_0)$ was found to be equal to $-20.9 \text{ J} \cdot \text{K}^{-1} \cdot \text{mol}^{-1}$ [64CRI/COB, 64CRI/COB2], and therefore the relationship between “absolute” and conventional entropies at 298.15 K is

$$\begin{aligned} S_m^{\circ}(i, T_0) &= S_m^{\circ, \text{abs}}(i, T_0) - z_i S_m^{\circ, \text{abs}}(\text{H}^+, \text{aq}, T_0), \\ &= S_m^{\circ, \text{abs}}(i, T_0) + 20.9 z_i, \end{aligned} \quad (\text{X.57})$$

where z_i is the charge of the ion i .

A related type of correlation was given by Couture and Laidler several years earlier [57COU/LAI], in which $S_m^{\circ}(T_0)$ was related to the mass of the ion and a term in the inverse of the ionic radius (of the same basic form as the Born solvation term). In that study $S_m^{\circ, \text{abs}}(\text{H}^+, \text{aq}, T_0) = -23.0 \text{ J} \cdot \text{K}^{-1} \cdot \text{mol}^{-1}$, which is similar to Criss and Cobble’s value [64CRI/COB, 64CRI/COB2].

Criss and Cobble [64CRI/COB] found that one set of $a(T)$ and $b(T)$ was appropriate for simple cations, another for simple anions, a third set for oxyanions and a fourth for their oxyacids. They tabulated values of $a(T)$, $b(T)$ and $S_m^{\circ, \text{abs}}(\text{H}^+, \text{aq}, T)$ at 298.15, 333.15, 373.15 and 423.15 K.

The practical importance of Eq. (X.56) is that ionic partial molar heat capacities can be estimated from the ionic partial molar entropies of these ions averaged between two temperatures. Criss and Cobble [64CRI/COB2] calculated (*cf.* our Eq. (X.5))

$$C_{p,m}^{\circ, \text{abs}}|_{T_0}^T(i) = \frac{S_m^{\circ, \text{abs}}(i, T) - S_m^{\circ, \text{abs}}(i, T_0)}{\ln(T/T_0)}, \quad (\text{X.58})$$

in which case the “constant $\Delta_r C_{p,m}^{\circ}$ ” equations, Eqs. (X.19) and (X.20), may be used to calculate equilibrium constants at higher temperatures. By substituting Eq. (X.56) into Eq. (X.58), Criss and Cobble obtained average “absolute” heat capacities:

$$\begin{aligned} C_{p,m}^{\circ, \text{abs}}|_{T_0}^T(i) &= \frac{a(T) - (1 - b(T))S_{p,m}^{\circ, \text{abs}}(i, T_0)}{\ln(T/T_0)} \\ &= \alpha(T) + \beta(T)S_{p,m}^{\circ, \text{abs}}(i, T_0), \end{aligned} \quad (\text{X.59})$$

where

$$C_{p,m}^{\circ, \text{abs}}(i, T) = C_{p,m}^{\circ}(i, T) + z_i C_{p,m}^{\circ, \text{abs}}(\text{H}^+, \text{aq}, T) \quad (\text{X.60})$$

with

$$C_{p,m}^{\circ, \text{abs}}(\text{H}^+, \text{aq}, T_0) = 117.1 \text{ J} \cdot \text{K}^{-1} \cdot \text{mol}^{-1}.$$

Two extra digits were retained from the conversion of $28 \text{ cal} \cdot \text{K}^{-1} \cdot \text{mol}^{-1}$ to this value.

An alternative procedure is to estimate values for conventional standard partial molar ionic entropies at higher temperatures (Eqs. (X.56) and (X.57)), and to do a least-squares fit on these values to the constant heat capacity equation:

$$S_m^{\circ}(i, T) = S_m^{\circ}(i, T_0) + C_{p,m}^{\circ}|_{T_0}^T(i) \ln(T/T_0). \quad (\text{X.22})$$

Table X.10: Heat capacity parameters for Eq. (X.61). Units of A are $\text{J} \cdot \text{K}^{-1} \cdot \text{mol}^{-1}$, whereas B is unitless.

Species	A	B
Cations	174.1	−0.523
Anions including OH^-	−236.4	0.179
Oxyanions	−607	2.20
Acid oxyanions	−569	3.07

This method was used for example by Lemire and Tremaine [80LEM/TRE].

Similarly to Eq. (X.56), Criss and Cobble found a linear correlation between “absolute” standard partial molar ionic heat capacities and “absolute” standard partial molar ionic entropies at 298.15 K,

$$\begin{aligned} C_{p,m}^{\circ,\text{abs}}(i, T_0) &= A + BS_{\text{m}}^{\circ,\text{abs}}(i, T_0) \\ &= A + B(S_{\text{m}}^{\circ}(i, T_0) - 20.9z_i), \end{aligned}$$

and, using Eq. (X.60),

$$C_{p,m}^{\circ}(i, T_0) = A + BS_{\text{m}}^{\circ}(i, T_0) - z_i(20.9B + 117.1). \quad (\text{X.61})$$

The last equation relates conventional standard partial molar ionic heat capacities to conventional standard partial molar ionic entropies and to the electrical charge of aqueous ionic species. Criss and Cobble [64CRI/COB2] give the A and B parameters listed in our Table X.10.

For temperatures above 373 K, Criss and Cobble [64CRI/COB2] noted that $a(T)$ and $b(T)$ in Eqs. (X.56) and (X.59) could each be assumed to be linear functions of the temperature[†]:

$$\begin{aligned} a(T) &= a_1 + b_1T \\ b(T) &= a_2 + b_2T. \end{aligned}$$

However, these equations imply that the standard partial molar ionic heat capacities are also approximately linear functions of the temperature at $T \leq 500$ K [64CRI/COB2, 70LEW, 78TAY] which is in direct disagreement with experimental evidence which shows

[†] Tremaine *et al.* [77TRE/MAS] note that the value of $a(T)$ at 573 K for simple anions including OH^- should be $-47.2 \text{ cal} \cdot \text{mol}^{-1} \cdot \text{K}^{-1}$ instead of the value of $-49.2 \text{ cal} \cdot \text{mol}^{-1} \cdot \text{K}^{-1}$ given in [64CRI/COB2] which is presumably a misprint.

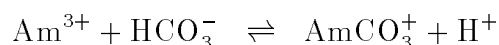
that they go through a maximum as a function of temperature and decrease asymptotically towards $-\infty$ at the critical point of water (see for example Figure 4 in Ref. [82PAT/SLO]). For this reason the $a(T)$ and $b(T)$ parameters of Criss and Cobble are not recommended for use above 423 K.

Note that Criss and Cobble [64CRI/COB2] recommended these linear equations for $373 \text{ K} < T < 473 \text{ K}$ and Taylor [78TAY] for $T < 523 \text{ K}$.

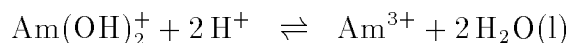
Criss and Cobble's equation, our Eq. (X.61), has been criticised by Shock and Helgeson [88SHO/HEL] since it does not agree very well with some more recent experimental data for M^{3+} and some M^{2+} , especially for aqueous ions whose $S_{\text{m}}^{\circ}(T_0)$ are less than about $-125 \text{ J} \cdot \text{K}^{-1} \cdot \text{mol}^{-1}$.

X.4.1.2.2. Isocoulombic method

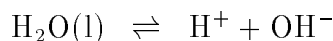
For neutral aqueous species and metal complexes, the isocoulombic approach (Section X.2.2.3) might be used to estimate a value for their $C_{p,\text{m}}^{\circ}(i)$. For example, for the estimation of the heat capacity for AmCO_3^+ , the isoelectric reaction



can be combined with the reactions



and



to yield the isocoulombic reaction,



If the assumption is made that $\Delta_{\text{r}}C_{p,\text{m}}^{\circ} = 0$ for this last reaction, then,

$$\begin{aligned} 0 &= C_{p,\text{m}}^{\circ}(\text{AmCO}_3^+, \text{aq}, T_0) + C_{p,\text{m}}^{\circ}(\text{OH}^-, \text{aq}, T_0) + C_{p,\text{m}}^{\circ}(\text{H}_2\text{O}, \text{l}, T_0) \\ &\quad - C_{p,\text{m}}^{\circ}(\text{HCO}_3^-, \text{aq}, T_0) - C_{p,\text{m}}^{\circ}(\text{Am}(\text{OH})_2^+, \text{aq}, T_0). \end{aligned}$$

As the heat capacities of $\text{H}_2\text{O}(\text{l})$, OH^- and HCO_3^- have been determined experimentally, and as the heat capacity for the hydrolysis product, $\text{Am}(\text{OH})_2^+$, can be estimated with Criss and Cobble's method, our Eq. (X.61) (using the parameters for cations and an estimated entropy for $\text{Am}(\text{OH})_2^+$), the heat capacity for AmCO_3^+ can then be estimated directly without a need to estimate its ionic entropy or to make further assumptions.

X.4.1.2.3. Other correlation methods

There are not many alternatives to Eq. (X.61), which was derived from equations proposed by Criss and Cobble [64CRI/COB2]. Helgeson and co-workers presented correlations for similar ions with equal charge, *cf.* [81HEL/KIR, Eq. (282)] and [88SHO/HEL, Eq. (91)],

$$C_{p,m}^{\circ}(i, T_0) = a + bS_m^{\circ}(i, T_0), \quad (\text{X.62})$$

where the parameters a and b are tabulated by Shock and Helgeson [88SHO/HEL]. These values should only be used with the same $S_m^{\circ}(i, T_0)$ used by Shock and Helgeson to derive them.

It seems rather strange to us that the parameters of Shock and Helgeson [88SHO/HEL] for the light and heavy tripositive rare earth ions should differ so greatly. These large differences may be a computational artifact because $C_{p,m}^{\circ}(T_0)$ was poorly determined at that time for those M^{3+} ions. We note that Shock and Helgeson [88SHO/HEL] derived values for the standard partial molar ionic heat capacities for the aqueous tripositive rare earth ions in the range -132.6 to $-199.6 \text{ J} \cdot \text{K}^{-1} \cdot \text{mol}^{-1}$, with values for the light rare earths generally being more negative than those for the heavy. However, a reanalysis by Rard [92RAR] of all the available heat capacities for aqueous rare earth chlorides and perchlorates gave values for the ionic heat capacities $C_{p,m}^{\circ}(T_0)$ that ranged from -50 to $-110 \text{ J} \cdot \text{K}^{-1} \cdot \text{mol}^{-1}$ for the lighter rare earth ions and from -40 to $-72 \text{ J} \cdot \text{K}^{-1} \cdot \text{mol}^{-1}$ for the heavier rare earths. In addition, Xiao and Tremaine [96XIA/TRE] reported experimental values of $C_{p,m}^{\circ}(T_0) = -(101 \pm 2) \text{ J} \cdot \text{K}^{-1} \cdot \text{mol}^{-1}$ for La^{3+} and $-74 \text{ J} \cdot \text{K}^{-1} \cdot \text{mol}^{-1}$ for Gd^{3+} , which differ significantly from Shock and Helgeson's values of -156 and $-150 \text{ J} \cdot \text{K}^{-1} \cdot \text{mol}^{-1}$, respectively. Differences at some other temperatures are even larger. Thus the values of $C_{p,m}^{\circ}(T_0)$ reported by Shock and Helgeson are probably too negative by about 50 to $100 \text{ J} \cdot \text{K}^{-1} \cdot \text{mol}^{-1}$ or more. Consequently, Eq. (X.62) should not be used for M^{3+} ions.*

Modified equations of this type were proposed by Khodakovskiy [69KHO],

$$C_{p,m}^{\circ}(i, T_0) = a - d|z_i| - \frac{2}{3}S_m^{\circ}(i, T_0)$$

and

$$S_m^{\circ}(i, T) = \frac{a(T - T_0)}{T_0} - \frac{d(T - T_0)}{T_0}|z_i| + [1 + 0.00224(T - T_0)]S_m^{\circ}(i, T_0),$$

for conventional standard state properties. He found that one set of coefficients worked well for cations, a different set worked well for non-oxygenated anions (mainly halides) and unionised dissolved gases (Ar , Kr , N_2 , O_2 , H_2 , H_2S), and a third set worked well for oxyacids and their oxyanions. These equations have the advantage of working for some dissolved gases also. Khodakovskiy's recommended values of a and d for each of these three cases are given in Table X.11.

* Note added in press: Recently Shock *et al.* [97SHO/SAS] have re-evaluated the parameters for Eq. (X.62) excluding rare earth cations.

Table X.11: Parameters for Khodakovskiy's equations [69KHO]. Units of a and d are $\text{J} \cdot \text{K}^{-1} \cdot \text{mol}^{-1}$.

Cases	a	d
Cations	212.5	124.7
Non-oxygenated anions and dissolved gases	212.5	311.3
Oxyacids and oxyanions	334.7	311.3

Unfortunately, these various correlations do not yet include inorganic complexes and, therefore, extra assumptions are needed to use them for reactions that involve metal complexes. Some preliminary work in this area was done by Cobble [53COB2] for halide, cyanide, and a few other complexes by using “hydration corrected” entropies.

Another method proposed is a heat capacity correlation among redox couples [85JAC/HEL]:

$$\frac{C_{p,m,\text{oxd1}}^{\circ}(T) - C_{p,m,\text{red1}}^{\circ}(T)}{z_{\text{oxd1}} - z_{\text{red1}}} = \frac{C_{p,m,\text{oxd2}}^{\circ}(T) - C_{p,m,\text{red2}}^{\circ}(T)}{z_{\text{oxd2}} - z_{\text{red2}}}.$$

If the heat capacity temperature functions for a redox couple are known (say $\text{Fe}^{2+}/\text{Fe}^{3+}$) and $C_{p,m}^{\circ}(T)$ for a member of another couple is known, then this method allows the estimation of the unknown temperature variation for the heat capacity of the other member of the second redox couple. However, the reliability of this estimation method has been tested for only a few aqueous systems.

X.4.1.3. Heat capacity estimation methods for reactions in aqueous solutions

The Ryzhenko-Bryzgalin model, which is described in Section X.2.4.3, may be used to estimate $\Delta_r C_{p,m}^{\circ}$, *cf.* Eq. (X.48), and for “isocoulombic” reactions, $\Delta_r C_{p,m}^{\circ}$ may be estimated to be equal to zero, as discussed in Sections X.2.2.3 and X.4.1.2.2.

Smith *et al.* [86SMI/POP] have proposed a set of average values of $\Delta_r C_{p,m}^{\circ}$ that may be used for the estimation of this quantity for proton dissociation reactions of acid oxyanions.

Sverjensky [87SVE] has proposed correlations between the $\Delta_r C_{p,m}^{\circ}$ for metal complexation reactions with halide and hydroxide ions and the value of $C_{p,m}^{\circ}$ for the metal cation.*

* Note added in press: Recently Sverjensky, Shock and Helgeson [97SVE/SHO] have proposed correlations for $\Delta_r C_{p,m}^{\circ}$ for complex formation reactions between divalent cations and monovalent ligands.

X.4.2. Entropy estimation methods

X.4.2.1. Entropy estimation methods for solid phases

For ionic compounds Latimer's method [52LAT] involves estimating entropies by adding empirically estimated ionic contributions. Based on later experimental data, Naumov *et al.* [71NAU/RYZ, Tables I-2 and I-3] prepared a revised table of parameters to be used with Latimer's method.

Langmuir [78LAN] described improved parameters for estimating entropy values for solid compounds containing the UO_2^{2+} moiety. In his procedure, the contributions of UO_2^{2+} to the entropy of $\gamma\text{-UO}_3$, $\beta\text{-UO}_2(\text{OH})_2$ and schoepite were used to estimate the contribution of UO_2^{2+} to the entropies of other uranium compounds.

Although Latimer [52LAT] and Naumov *et al.* [71NAU/RYZ] suggested a value of $39.3 \text{ J} \cdot \text{K}^{-1} \cdot \text{mol}^{-1}$ for the entropy of each water of hydration in a crystalline solid hydrate, Langmuir [78LAN] considered the value of $44.7 \text{ J} \cdot \text{K}^{-1} \cdot \text{mol}^{-1}$, the value for the entropy of ice I from the compilation of Robie and Waldbaum [68ROB/WAL], to be more appropriate.

Ionic contributions to the entropy also have slightly different values for the different sources of parameters for Latimer's method. Thus, the entropies in the literature, calculated by Latimer's method, may vary significantly, depending on the exact set of parameters used in the estimation. Table X.12 presents the parameter values selected for the NEA's uranium review [92GRE/FUG].

Also, for some compounds, especially binary solids, better entropy values may be estimated by comparison with values for closely related solids than by Latimer's method. For chalcogenides the reader is referred to the discussion given by Mills [74MIL, Section 2.4.2].

Helgeson and co-workers [78HEL/DEL] gave entropy estimation techniques for oxide minerals using the sum of the entropies for the constituent oxides [78HEL/DEL, their Eqs. (62) and (75)].

For some elements and ions, including most of the rare earths and actinides, the metals and ions have magnetic contributions to their entropies that depend mainly on their ground state electronic configurations. The S_{mag}° values range from 0.0 to $23.56 \text{ J} \cdot \text{K}^{-1} \cdot \text{mol}^{-1}$ for various rare earth and actinide ions[†] M^{2+} , M^{3+} , and M^{4+} at 298.15 K. Values for the total entropy $S_{\text{m}}^\circ(T_0)$ vary by $39 \text{ J} \cdot \text{K}^{-1} \cdot \text{mol}^{-1}$ for $\text{RCl}_3(\text{cr})$ across the series, for R_2O_3 by $49 \text{ J} \cdot \text{K}^{-1} \cdot \text{mol}^{-1}$ ($24.5 \text{ J} \cdot \text{K}^{-1} \cdot \text{mol}^{-1}$ per rare earth ion), and for R^{3+} by $57 \text{ J} \cdot \text{K}^{-1} \cdot \text{mol}^{-1}$ [77SPE/RAR, 92RAR]. It is clear that S_{mag}° is a significant fraction of the total variation of $S_{\text{m}}^\circ(T_0)$ across the rare earth series, and it must be taken into consideration for any accurate scheme for estimating $S_{\text{m}}^\circ(T_0)$. At 298.15 K there are three different structural types of $\text{RCl}_3(\text{cr})$ and three of $\text{R}_2\text{O}_3(\text{cr})$ for the rare earth series, so there are also structural factors that affect series trends.

For lanthanides and actinides and their cations, the $4f$ or $5f$ electrons are shielded by their outer electrons from the electric fields of their neighbouring ions, so their or-

[†] "M", "R" and "AN" are used as general abbreviations for metal, rare earth (lanthanum and the lanthanides), and actinide respectively.

Table X.12: Contributions to entropies of solids ($\text{J} \cdot \text{K}^{-1} \cdot \text{mol}^{-1}$), mainly from Refs. [71NAU/RYZ] and [92GRE/FUG]. The values in parentheses were not directly based on experimental values, but were estimated by Naumov, Ryzhenko and Khodakovsky [71NAU/RYZ].

Anion	Average cation charge			
	+1	+2	+3	+4
OH^-	30.5	19.2	17.5	(19.2)
O^{2-}	8.4	2.5	2.1	1.3
F^-	23.0	17.6	16.1	20.1
Cl^-	43.9	32.6	29.3	33.1
Br^-	56.1	45.2	41.8	49.8
I^-	63.2	54.4	55.2	51.0
IO_3^-	104.6	(92)		
CO_3^{2-}	64.9	49.4		
NO_3^-	90.8	73.2		
SO_3^{2-}	83.3	62.3	50.2	(46) ^(a)
SO_4^{2-}	92.9	67.8	57.3	(50)
PO_4^{3-}	79.5	62.8	57.3	(50) ^(a)
PO_3^-	66.9	54.0	(50.0)	(48) ^(a)
HPO_4^-	87.9	72.4	66.9	(63)
H_2O	44.7			
$\text{UO}_2^{2+ \text{(b)}}$	94.7			
$\text{U}^{(c)}$	66.9			

(a) Estimated by [92GRE/FUG].

(b) Treated as a dipositive ion for the purpose of selecting anion contributions.

(c) For uranium compounds not containing $\text{U}^{\text{VI}}\text{O}_2^{2+}$.

bital angular momentum is not quenched and Russell-Saunders coupling applies; thus the J quantum number remains a valid measure of total angular momentum. If this is true, the degeneracies of the lanthanide and actinide cations are not altered significantly by their ionic environments and thus the J retain approximately their free-ion values. Consequently, the magnetic (electronic) entropies are then fully developed by room temperature and take the values $S_{\text{mag}}^{\circ} = R \ln(2J + 1)$. For a few cases (*e.g.*, Sm^{3+} and Eu^{3+}) S_{mag}° also contains small contributions from low-lying excited electronic levels that can become thermally occupied at room temperature. Hinchey and Cobble [70HIN/COB2] noted that excited level term contributions add an extra $0.3 \text{ J} \cdot \text{K}^{-1} \cdot \text{mol}^{-1}$ to $S_{\text{mag}}^{\circ}(T_0)$ for Sm^{3+} and $9.3 \text{ J} \cdot \text{K}^{-1} \cdot \text{mol}^{-1}$ for Eu^{3+} . Table X.13 contains a listing of S_{mag}° for various M^{2+} , M^{3+} , and M^{4+} .

The electronic levels contribute to the total heat capacities through the Schottky heat capacity term, $C_{\text{Sch}}(T)$, see Ref. [83WES]. It is mathematically related to the Einstein heat capacity function.

For most lanthanide and actinide ions, the maximum in $C_{\text{Sch}}(T)$ appears at a temperature around 50 to 150 K, and this contribution to $C_{p,m}^{\circ}(T)$ becomes fairly small at temperatures near 298.15 K. For systems with low-lying excited electronic levels that can become thermally occupied, this is no longer true. For example, $C_{\text{Sch}}(T)$ for $\text{EuCl}_3(\text{cr})$ is essentially zero up to about 60 K, it increases to slightly greater than R up to 200 K, and then it very slowly decreases at higher temperatures [83WES]. Hinchey and Cobble [70HIN/COB2] noted that $C_{\text{Sch}}(T_0) = 1.7 \text{ J} \cdot \text{K}^{-1} \cdot \text{mol}^{-1}$ for Sm^{3+} and $8.7 \text{ J} \cdot \text{K}^{-1} \cdot \text{mol}^{-1}$ for Eu^{3+} . Schottky contributions to the heat capacities are still significant at T_0 for some rare earth sesquioxides [83WES].

Westrum [83WES] has shown that for a particular type of solid containing a tripositive lanthanide ion (RCl_3 , R_2O_3 , $\text{R}(\text{OH})_3$, R_2S_3), values of the “lattice entropy”, $S_{\text{lat}}^{\circ}(T_0) = S_{\text{m}}^{\circ}(T_0) - S_{\text{mag}}^{\circ}$, show a very smooth variation with the molar volume for an isostructural series of compounds with the same anion. These molar volumes can be calculated from crystallographic unit cell parameters. Note that each series of RX_3 or R_2X_3 (where “X” represents either a halogen, a chalcogen or an OH-group) undergoes one or more structural changes in going from light to heavy rare earths except for a few cases like $\text{R}(\text{OH})_3$; the smooth variation of $S_{\text{lat}}^{\circ}(T_0)$ with the molar volume applies only for compounds of the same stoichiometry with a common structure.

When S_{mag}° is added to interpolated values of S_{lat}° , the resulting $S_{\text{m}}^{\circ}(T_0)$ are generally highly accurate, frequently to within $0.5 \text{ J} \cdot \text{K}^{-1} \cdot \text{mol}^{-1}$ of experimental values for the rare earth compounds. The uncertainties in estimated values may be much greater for many actinide compounds, where available thermodynamic data are much less complete.

X.4.2.2. Entropy estimation methods for aqueous species

Several methods are available to estimate entropies of aqueous species and entropies of reaction at 298.15 K. These methods use correlations between ionic entropies and a combination of crystallographic radii, molar volumes and mass, electrical charge, *etc.*

For some aqueous ions, including most of the rare earths and actinides, there are mag-

Table X.13: Magnetic (electronic) contributions to entropies at 298.15 K.

4f or 5f configu- ration	Ground state ^(a)	S_{mag}° ^(b) (J · K ⁻¹ · mol ⁻¹)	Ions
f ⁰	¹ S ₀	0.0	La ³⁺ , Ce ⁴⁺ , Th ⁴⁺ , Pa ⁵⁺ , U ⁶⁺ (UO ₂ ²⁺), Ac ³⁺
f ¹	² F _{5/2}	14.90	Ce ³⁺ , Th ³⁺ , Pa ⁴⁺ , U ⁵⁺ , Np ⁶⁺ , Pu ⁷⁺
f ²	³ H ₄	18.27	Pr ³⁺ , U ⁴⁺ , Np ⁵⁺ , Pu ⁶⁺ , Pa ³⁺
f ³	⁴ I _{9/2}	19.14	Nd ³⁺ , U ³⁺ , Np ⁴⁺ , Pu ⁵⁺
f ⁴	⁵ I ₄	18.27	Pm ³⁺ , Np ³⁺ , Pu ⁴⁺
f ⁵	⁶ H _{5/2}	14.90	Pu ³⁺ , Am ⁴⁺
f ⁵	⁶ H _{5/2}	15.2	Sm ³⁺
f ⁶	⁷ F ₀	0.00	Sm ²⁺ , Am ³⁺ , Cm ⁴⁺
f ⁶	⁷ F ₀	9.3	Eu ³⁺
f ⁷	⁸ S _{7/2}	17.29	Eu ²⁺ , Gd ³⁺ , Tb ⁴⁺ , Am ²⁺ , Cm ³⁺ , Bk ⁴⁺
f ⁸	⁷ F ₆	21.33	Tb ³⁺ , Bk ³⁺ , Cf ⁴⁺
f ⁹	⁶ H _{15/2}	23.05	Dy ³⁺ , Cf ³⁺
f ¹⁰	⁵ I ₈	23.56	Dy ²⁺ , Ho ³⁺ , Es ³⁺
f ¹¹	⁴ I _{15/2}	23.05	Er ³⁺ , Es ²⁺ , Fm ³⁺
f ¹²	³ H ₆	21.33	Tm ³⁺ , Fm ²⁺
f ¹³	² F _{7/2}	17.29	Tm ²⁺ , Yb ³⁺ , Md ²⁺
f ¹⁴	¹ S ₀	0.00	Yb ²⁺ , Lu ³⁺ , No ²⁺
—	¹ S ₀	0.00	Y ³⁺

(a) Term symbols were taken from Refs. [70HIN/COB, 70HIN/COB2, 86EDE/GOF].

(b) The S_{mag}° were calculated from $S_{\text{mag}}^{\circ} = R \ln(2J + 1)$. Values for S_{mag}° for Sm³⁺ and Eu³⁺ contain contributions from thermally-populated higher electronic states. Similar contributions may be present for some of the actinide ions.

netic contributions to their entropies that depend mainly on the electronic configuration of their ground state (*cf.* Section X.4.2.1, *p.*483).

Hinchey and Cobble [70HIN/COB2] calculated the ionic entropies of the aqueous tripositive rare earth ions (lanthanides and yttrium) from available thermodynamic data for hydrated rare earth chlorides. These data include low-temperature heat capacities for the crystals, and enthalpies and Gibbs free energies of solution. They found that $[S_m^\circ - S_{\text{mag}}^\circ]$ was a linear function of r^{-2} within the scatter of the then available values. Here r is the crystal radius for rare earth ions for a CN[†] of 6, and S_{mag}° is the magnetic contribution described in Section X.4.2.1 and listed in Table X.13. However, they had to estimate Gibbs free energies of solution for seven of the hydrated salts and entropies for six of them. In addition, some of the experimental enthalpies of solution later proved to be inaccurate. Spedding, Rard and Habenschuss [77SPE/RAR] recalculated these ionic entropies and included more complete and accurate data that were published after Hinchey and Cobble's report. Spedding, Rard and Habenschuss [77SPE/RAR] found that $[S_m^\circ(T_0) - S_{\text{mag}}^\circ]$ actually had a tilted S shape as a function of r^{-2} , and this S shape correlated fairly well with the overall hydration of the rare earth ions.

Powell and Latimer [51POW/LAT] found that $(S_m^\circ - \frac{3}{2}R \ln M)$ was a linear function of r^{-2} for aqueous ions of various stoichiometries, whereas Couture and Laidler [57COU/LAI] found that $(S_m^{\circ, \text{abs}}(T_0) - \frac{3}{2}R \ln M)$ was a linear function of $z^2/(Nr_{\text{adj}})$ for oxyanions, where M is the mass of the oxyanion under consideration, N the number of coordinated oxygen atoms present in this anion, and r_{adj} the covalent radius of the central atom plus the van der Waals radius of an oxygen. Here $S_m^{\circ, \text{abs}}(T_0) = (S_m^\circ(T_0) + 23.0|z|)$ changed the conventional scale to an "absolute" scale by using $23.0 \text{ J} \cdot \text{K}^{-1} \cdot \text{mol}^{-1}$ for the "absolute entropy" of H^+ . Related equations are those of Cobble [53COB, 53COB3] and (without the mass term) Cobble [53COB2], Powell [54POW], Helgeson *et al.* [69HEL, Eq. (26)], [88SHO/HEL, Eq. (55)], [81HEL/KIR, Eq. (283)], [85JAC/HEL, Eqs. (22) and (25)], and also Ruaya [88RUA, Eq. (6)], Sassani and Shock [92SAS/SHO], and Shock *et al.* [97SHO/SAS].

The importance of Powell and Latimer's [51POW/LAT] and Couture and Laidler's [57COU/LAI] work is that they showed that entropies of very different types of ions could be correlated using ionic mass, charge type, and simple structural features. The $\frac{3}{2}R \ln M$ term is derived from the statistical thermodynamic calculation of the absolute entropy of a gas phase ion. An entropy of an aqueous ion can be considered as the sum of its gas phase entropy and the entropy of hydration of that ion by liquid water. The entropy of hydration should mainly depend on the sign and charge of the ion and the ionic radius. The presence of the $\frac{3}{2}R \ln M$ is then justified by assuming this is a gas phase feature that is not lost when the ion becomes hydrated in aqueous solutions.

The same type of mass dependence was included by David [86DAV, 86DAV2] in his comprehensive analysis of ionic entropies of the aqueous tripositive lanthanide and actinide ions. David [86DAV, his Fig. (10)] found that the adjusted entropy,

$$S_{\text{adj}}^\circ(T_0) = S_m^\circ(T_0) - S_{\text{mag}}^\circ - \frac{3}{2}R \ln M$$

[†] CN is used as an abbreviation for "coordination number".

was a simple and symmetrical function of the $CN = 8$ tripositive rare earth crystal radii. This curve was *S*-shaped, in agreement with the findings of Spedding, Rard and Habenschuss [77SPE/RAR], and that shape was understandable in terms of changes of total hydration of the rare earth ions as a function of the ionic radius. David also noted that the hydrated radii of actinide ions AN^{3+} were essentially proportional to those for rare earths R^{3+} , and thus the curve for rare earths can be used to estimate $S_{adj}^{\circ}(T_0)$ for AN^{3+} with a fairly high degree of confidence. An experimental value of $S_{adj}^{\circ}(T_0)$ is available only for Pu^{3+} among the actinides; although it falls slightly off the curve based upon values for the for R^{3+} , it does agree with its interpolated position on the $S_{adj}^{\circ}(T_0)$ curve for AN^{3+} within its uncertainty limits. These estimated values of $S_{adj}^{\circ}(T_0)$ for AN^{3+} were then used by David for calculation of his $S_m^{\circ}(T_0)$ values.

David [86DAV,86DAV2] also estimated $S_m^{\circ}(T_0)$ values for all possible R^{2+} , AN^{2+} , R^{4+} , and AN^{4+} . The dipositive ion values were based on $S_{adj}^{\circ}(T_0)$ for Ca^{2+} and Sr^{2+} with $CN = 6$, and those for the tetrapositive ions were based on Ce^{4+} and Th^{4+} with $CN = 8$. Since there are insufficient data to establish series trends as a function of ionic radii in these cases, David's estimated entropies have much greater uncertainties than for the tripositive R^{3+} and AN^{3+} ions.

Powell and Latimer [51POW/LAT] found that the entropies of a variety of non-electrolytes in aqueous solution could be represented by the equation

$$S_m^{\circ}(T_0) = \frac{3}{2}R \ln M + S_{int}^{\circ} + 41.8 - 0.92 V_m,$$

where V_m is the molar volume of the non-electrolyte in $cm^3 \cdot mol^{-1}$ for its pure liquid state, and S_{int}° is the "internal" contribution to the entropy as calculated for an ideal gas using statistical thermodynamic methods for rotational, vibrational, and electronic contributions. In general, non-polar inorganic gases (inert gases, halogens, O_2), a few polar gases (H_2O , HF , NO , N_2O , COS), and some saturated alkanes (CH_4 , C_2H_6) were well represented by this equation, with deviations of only 1 to 5 $J \cdot K^{-1} \cdot mol^{-1}$. However, a number of other polar gases and liquids (H_2S , CO , SO_2 , CO_2 , NH_3 , CH_3OH , C_2H_5OH) and also N_2 showed deviations of 10 to 25 $J \cdot K^{-1} \cdot mol^{-1}$. Cobble [53COB3] gave an extended version of this equation which is valid for small and medium sized organic molecules, but it fails for larger molecules. A more general and accurate correlation for non-electrolytes is certainly needed.

An alternative to the Powell and Latimer equation has been proposed by Laidler [56LAI], Eqs. (X.63) and (X.64) below. The relative merits of this and Powell and Latimer type of equations have been discussed by Scott and Hughus [57SCO/HUG] and Laidler [57LAI]. The following two empirical equations have been proposed for the estimation of the partial molar entropy of ions in aqueous solution

$$S_m^{\circ,abs}(i, T_0) = \frac{3}{2}R \ln M_i + 42.68 - 4.853 \times 10^{-9} \frac{z_i^2}{r_{u,i}} \quad (X.63)$$

and

$$S_m^{\circ,abs}(i, T_0) = \frac{3}{2}R \ln M_i + 152.7 - 1.347 \times 10^{-17} \frac{z_i}{r_{eff,i}^2} \quad (X.64)$$

where r_u is Pauling's univalent radius [60PAU, Table 13-3] converted from units of Å to metre, and r_{eff} is an effective ion radius. The “ordinary” and absolute entropy scales differ by the *assigned* values of the entropy of H^+ , which are -23.0 and $0.0 \text{ J} \cdot \text{K}^{-1} \cdot \text{mol}^{-1}$, respectively. Hence these two entropies for an ion i of charge z_i are related by the equation

$$S_{\text{m}}^{\circ, \text{abs}}(i, T_0) = S_{\text{m}}^{\circ}(i, T_0) - 23.0 z_i \quad (\text{X.65})$$

The equations above are able to describe the absolute ion entropies within 10 to 15 $\text{J} \cdot \text{K}^{-1} \cdot \text{mol}^{-1}$. From the discussion given in [57SCO/HUG] and [57LAI] it is clear that the theoretical foundations of both the Powell and Latimer and the Laidler type of equations are rather weak. However they provide some guidelines for entropy estimations.

For aqueous complex ions of uranium, Langmuir [78LAN, Figure 1] gave a simple correlation between $S_{\text{m}}^{\circ}(i, T_0)$ and the ionic charge, z_i . The parameters for this correlation were obtained by fitting data to a 4th degree polynomial of z_i (see also [80LAN/HER, Fig. 1] for Th(IV) complexes).

For halide and hydroxide complexes, Helgeson gave two equations that relate the entropy of a complex with either crystallographic radii only ([81HEL/KIR, Eq. (283)] for neutral complexes, or effective electrostatic radii [88SHO/HEL, Eq. (58)] for ionic species), or in combination with the stoichiometry of the complex, see Ref. [85JAC/HEL, Eqs. (22) and (25)], and also [88RUA, Eq. (6)].

The following methods are available to estimate standard reaction entropies:

- For hydrolysis reactions, Baes and Mesmer gave correlations for the reaction entropy for the first mononuclear hydrolysis product [81BAE/MES, their Eq. (11)], for the polynuclear products (their Eq. (20)), and for stepwise mononuclear hydrolysis (their Eq. (23)).
- Entropies of dissociation for a group of aqueous metal complexes (halide, *etc.*) may be estimated with equations similar to that given by Helgeson for charged and neutral metal chloride complexes, see Ref. [69HEL, Eq. (27)] and Ref. [81HEL/KIR, Eq. (283)] for neutral complexes.*
- Electrostatic models of complex formation were compared by Langmuir [79LAN]. The simplest model [79LAN, Eq. (4)] was used for making crude estimations of the entropy of formation of sulphate and fluoride complexes, *cf.* [79LAN, Figures 12 and 14].
- The Ryzhenko-Bryzgalin model as described in Section X.2.4.3 (*cf.* Eq. (X.46)).
- Sverjensky [87SVE] has proposed correlations between the $\Delta_{\text{r}}S_{\text{m}}^{\circ}$ for metal complexation reactions with halide ions and the values of S_{m}° for the metal cation and the ligand.

* Note added in press: Sverjensky, Shock and Helgeson [97SVE/SHO] have recently proposed correlations for $\Delta_{\text{r}}S_{\text{m}}^{\circ}$ for complex formation reactions involving monovalent ligands as well as SO_4^{2-} and CO_3^{2-} .

X.4.3. Examples

Criss and Cobble's publications [64CRI/COB, 64CRI/COB2] appeared before the heat capacity for Co^{2+} and Th^{4+} had been determined experimentally, and therefore these ions are suitable to do test calculations with Eqs. (X.61) and (X.62). For Co^{2+} , the standard partial molar entropy given by NBS, $-113 \text{ J} \cdot \text{K}^{-1} \cdot \text{mol}^{-1}$ [82WAG/EVA], is used here:

Reference	$C_{p,m}^{\circ}(\text{Co}^{2+}, \text{aq}, 298.15 \text{ K})/$ ($\text{J} \cdot \text{K}^{-1} \cdot \text{mol}^{-1}$)
[78SPI/SIN] (experimental)	$-25 \pm (2 \text{ to } 3)$
Eq. (X.61)	+21
Eq. (X.62)	-38

For Th^{4+} , the NBS tables [82WAG/EVA] give an entropy of $-422.6 \text{ J} \cdot \text{K}^{-1} \cdot \text{mol}^{-1}$. For this example Eq. (X.62) is not applicable since there are insufficient data for M^{4+} ions to determine values of a and b . The estimation with Eq. (X.61) gives an ionic heat capacity for Th^{4+} of $-30 \text{ J} \cdot \text{K}^{-1} \cdot \text{mol}^{-1}$, as compared with the experimental value of $-(1 \pm 11) \text{ J} \cdot \text{K}^{-1} \cdot \text{mol}^{-1}$ [76MOR/MCC].

These results give some indication on the accuracy expected from these kinds of estimations.

A more practical example is to predict high-temperature equilibrium constants for a reaction such as



The entropy and heat capacity for water at 298.15 K are taken from CODATA [89COX/WAG], and the corresponding values for U^{4+} from the NEA-TDB review [92GRE/FUG], while the values for H^{+} are zero by the hydrogen ion convention. Therefore, only the standard partial molar entropy and heat capacity at 298.15 K for UOH^{3+} will be estimated here.

Langmuir's equation [78LAN, p.554] gives an estimate of $-218 \text{ J} \cdot \text{K}^{-1} \cdot \text{mol}^{-1}$ for the standard partial molar ionic entropy of uranium species with an electrical charge of +3. In contrast, Shock and Helgeson's equation which ignores magnetic contributions to the entropy [88SHO/HEL, Eq. (58)], using a ionic radius of $0.97 \times 10^{-10} \text{ m}$ for UOH^{3+} (equal to that of U^{4+}), gives an estimate of $-207 \text{ J} \cdot \text{K}^{-1} \cdot \text{mol}^{-1}$.

In order to use Eq. (10) in Ref. [81BAE/MES], the U-O distance of $2.42 \times 10^{-10} \text{ m}$ given in [81BAE/MES, Table 2] may be used. The logarithm of the equilibrium constant is also needed, and the recommended value in the NEA-TDB uranium report will be used, $\log_{10} K_1^{\circ}(\text{X.66}, 298.15 \text{ K}) = -(0.54 \pm 0.06)$ [92GRE/FUG]. This

results in an entropy of reaction of $+128 \text{ J} \cdot \text{K}^{-1} \cdot \text{mol}^{-1}$. Finally, adding the entropy values for $\text{H}_2\text{O}(\text{l})$ and U^{4+} , the value of $-219 \text{ J} \cdot \text{K}^{-1} \cdot \text{mol}^{-1}$ is obtained for the estimate of $S_{\text{m}}^{\circ}(\text{UOH}^{3+}, \text{aq}, 298.15 \text{ K})$.

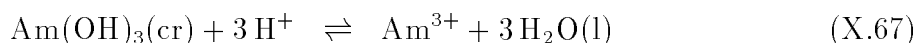
Thus, the estimated values for the standard partial molar entropy of UOH^{3+} are:

Reference/Method	$S_{\text{m}}^{\circ}(\text{UOH}^{3+}, \text{aq}, T_0) / (\text{J} \cdot \text{K}^{-1} \cdot \text{mol}^{-1})$
[78LAN, p.554]	-218
[81BAE/MES, their Eq. (10)]	-219
[88SHO/HEL, their Eq. (58)]	-207

To estimate the standard partial molar heat capacity for UOH^{3+} with Criss and Cobble's equation, our Eq. (X.61), the standard partial molar ionic entropy is needed. The value of $-219 \text{ J} \cdot \text{K}^{-1} \cdot \text{mol}^{-1}$ will be used as a "selected estimation". The derived heat capacity is then $-30 \text{ J} \cdot \text{K}^{-1} \cdot \text{mol}^{-1}$. The change in heat capacity of Reaction (X.66) is therefore estimated at $-57 \text{ J} \cdot \text{K}^{-1} \cdot \text{mol}^{-1}$. This small calculated heat capacity of reaction agrees with our discussion on isoelectric reactions (*cf.* Sections X.2.2.3, p.437).

A comparison between experimental values for the equilibrium constant of Reaction (X.66) [78NIK] and the calculated high-temperature values with Eq. (X.19) (*i.e.*, constant $\Delta_{\text{r}}C_{p,\text{m}}^{\circ}$) is given in Figure X.18.

The solubility reaction

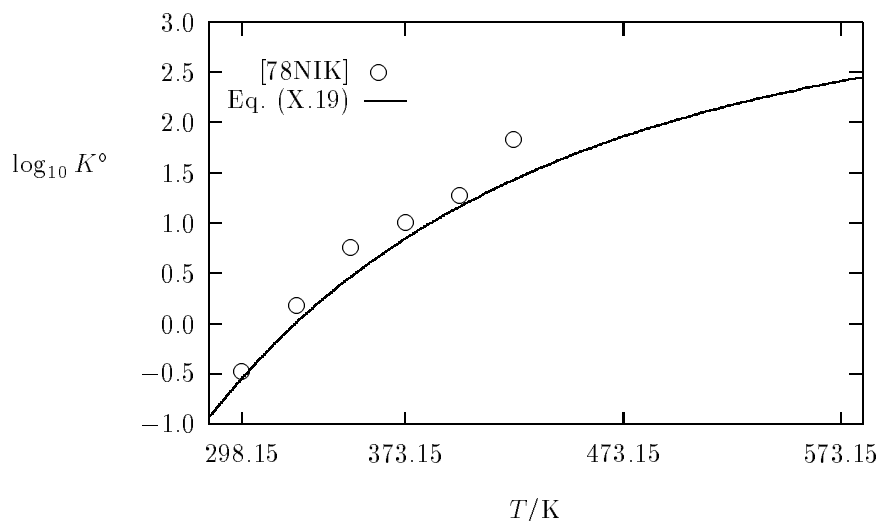


is used as an example for an equilibrium involving a solid phase. As before, the properties of water are taken from CODATA [89COX/WAG]. For the entropy of $\text{Am}(\text{OH})_3(\text{cr})$ the method of Latimer [52LAT] will be used with the following entropy contributions: Am^{3+} : $71 \text{ J} \cdot \text{K}^{-1} \cdot \text{mol}^{-1}$ (estimated from [52LAT, Appendix III, Figure 7]); OH^{-} with +3 cation: $17.6 \text{ J} \cdot \text{K}^{-1} \cdot \text{mol}^{-1}$ [71NAU/RYZ, Table I-3]. The magnetic contribution to S_{m}° is zero in this case. Therefore, $S_{\text{m}}^{\circ}(\text{Am}(\text{OH})_3, \text{cr}, T_0) = 71 + 3 \times 17.6 = 124 \text{ J} \cdot \text{K}^{-1} \cdot \text{mol}^{-1}$.

For the estimation of the heat capacity of $\text{Am}(\text{OH})_3(\text{cr})$, the method described in Chapter 3 of Ref. [93KUB/ALC] will be used. The contribution to the heat capacity for Am^{3+} is estimated as $29 \text{ J} \cdot \text{K}^{-1} \cdot \text{mol}^{-1}$ (from the trend between Th and U of Table IX in Ref. [93KUB/ALC]), and that of OH^{-} in a solid compound is given as $30.96 \text{ J} \cdot \text{K}^{-1} \cdot \text{mol}^{-1}$ [93KUB/ALC, Table X]. The estimated value is therefore $C_{p,\text{m}}^{\circ}(\text{Am}(\text{OH})_3, \text{cr}, T_0) = 122 \text{ J} \cdot \text{K}^{-1} \cdot \text{mol}^{-1}$.

The standard partial molar entropy of Am^{3+} was estimated as $-(201 \pm 13) \text{ J} \cdot \text{K}^{-1} \cdot \text{mol}^{-1}$ by Fuger and Oetting [76FUG/OET]. Using this value, the standard partial molar heat capacity estimated by Criss and Cobble's equation, our Eq. (X.61), is then $C_{p,\text{m}}^{\circ}(\text{Am}^{3+}, \text{aq}, T_0) = -39 \text{ J} \cdot \text{K}^{-1} \cdot \text{mol}^{-1}$. Shock and Helgeson's equation, our Eq. (X.62)

Figure X.18: Equilibrium constants from Nikolaeva [78NIK] for Reaction (X.66), $\text{U}^{4+} + \text{H}_2\text{O(l)} \rightleftharpoons \text{UOH}^{3+} + \text{H}^+$, compared with the calculated values using the “constant $\Delta_r C_{p,m}^\circ$ ” equation, Eq. (X.19), with $\log_{10} K^\circ(T_0) = -0.54$ and the estimated values (see text) of $\Delta_r C_{p,m}^\circ = -57 \text{ J} \cdot \text{K}^{-1} \cdot \text{mol}^{-1}$ and $\Delta_r S_m^\circ(T_0) = +128 \text{ J} \cdot \text{K}^{-1} \cdot \text{mol}^{-1}$.



[88SHO/HEL], with the correlation parameters for the heavy rare earths would result in $C_{p,m}^\circ(\text{Am}^{3+}, \text{aq}, T_0) = -162 \text{ J} \cdot \text{K}^{-1} \cdot \text{mol}^{-1}$ instead. However, this value has no experimental or theoretical basis and the values of $C_{p,m}^\circ(\text{R}^{3+}, \text{aq}, T_0)$ for rare earth ions derived by Shock and Helgeson [88SHO/HEL] seem to be much too negative (*cf.* the comments on $C_{p,m}^\circ$ estimation methods for aqueous species in p.481, Section X.4.1.2.3); consequently the heat capacity obtained with the method of Criss and Cobble will be used here.

Therefore, for Reaction (X.67) the following values are estimated:

$$\begin{aligned} \Delta_r S_m^\circ(T_0) &= 3 \times 69.95 + (-201) - 124 = -115 \text{ J} \cdot \text{K}^{-1} \cdot \text{mol}^{-1} \\ \Delta_r C_{p,m}^\circ(T_0) &= 3 \times 75.35 + (-39) - 122 = 65 \text{ J} \cdot \text{K}^{-1} \cdot \text{mol}^{-1}. \end{aligned}$$

X.5. Concluding remarks

Second-law extrapolation procedures must be used with caution in the absence of experimental heat capacities. When fitting high-temperature equilibrium constants, more than one equation should be tested (for example both the “constant $\Delta_r C_{p,m}^\circ$ ” equation, Eq. (X.19), and the Revised Helgeson-Kirkham-Flowers model, Eq. (X.32)), and the resulting reaction properties obtained at 298.15 K with different methods (*e.g.*, entropy and heat capacity) should be compared, as should their uncertainties and the difference between the calculated and experimental equilibrium constants at all temperatures.

Acknowledgements

When extrapolating equilibrium constants to higher temperatures from lower temperature data, several methods should also be tested and the results compared with each other (*cf.* Figures X.8 to X.10). Comparison of the results from these alternative methods will give a good estimate of the magnitude of the extrapolation error. This uncertainty, which differs for different methods of extrapolation, gives increased uncertainty to the thermodynamic reaction properties at higher temperatures compared to 298.15 K.

A similar attitude should be adopted with estimated thermodynamic properties which are used to make temperature extrapolations. If possible, several estimation methods should be compared. It is unfortunate that there are only a few estimation methods of $C_{p,m,i}^{\circ}$ for aqueous species, all of which have a limited field of application. This necessitates the use of less reliable methods like the DQUANT equation, Eq. (X.31), and the isocoulombic approach (*cf.* Section X.4.1.2.2). The measurement of aqueous solution heat capacities should be given a high priority.

X.6. Acknowledgements

Thanks are due to Kenneth Jackson (Lawrence Livermore National Laboratory) for his many suggestions and computer calculations which allowed us to check the numerical results of some computer programs used in this work.

We are grateful to Hans Wanner (Swiss Federal Nuclear Safety Inspectorate) for many corrections and improvements to the manuscript. Robert Silva (Lawrence Livermore National Laboratory) is acknowledged for suggestions and comments. B.N. Ryzhenko (Vernadsky Institute of Geochemistry and Analytical Chemistry) has kindly provided photocopies of a few pages of Ref. [66NIK]. We thank Kaname Miyahara (PNC, Japan) for pointing out a few misprints. We are specially grateful to Peter Tremaine (Memorial University, Newfoundland) for his critical review of our draft manuscript.

Major support for the contributions of Joseph A. Rard was from the Office of Basic Energy Sciences, Division of Geosciences, and the Office of Environmental Restoration and Waste Management (EM 30) of the U. S. Department of Energy. His contribution was performed under the auspices of the U. S. Department of Energy by the Lawrence Livermore National Laboratory under contract No. W-7405-ENG-48.

Chapter XI

Cellular Automaton Models of Reaction-Transport Processes

Theo KARAPIPERIS ¹
Paul Scherrer Institut
CH-5232 Villigen PSI
Switzerland

XI.1. Introduction

In many processes occurring in geological media mass transport and chemical reactions are intricately connected. The range of these processes includes natural phenomena, such as the chemical weathering of rocks and the diagenetic changes caused by ground-water flow, as well as procedures of technological interest, such as oil recovery and containment of contaminant migration. In case of a failure in a nuclear waste repository, the released radionuclides will be transported by flowing water, while they decay radioactively, sorb on solid surfaces and react chemically with each other and the host rock. Modelling coupled transport and chemical reactions in their full complexity is a formidable task and a great deal of ingenuity is required to identify the most important features and processes in any given situation.

In spatially extended geological systems, however, complexity at the macroscopic level need not reflect particularly intricate aspects of the microscopic dynamics. On the contrary, it is well-known that relatively simple microscopic properties can lead to very rich macroscopic behaviour. Thus, the motion of fluids (laminar and turbulent flow, shock waves, flow in porous media) can be understood in terms of local mass, momentum and energy conservation. The random collisions of the molecules of a few chemical species in solution can couple with their chemical reaction kinetics to produce a wide variety of

¹ Present address: European Parliament, Rue Belliard 97-113, B-1047 Brussels, Belgium.

striking behaviour (oscillations of the concentrations in time, stationary spatial patterns or non-linear travelling waves).

In theoretical models of such phenomena the essential microscopic properties are usually embedded in macroscopic *partial differential equations* (e.g., the continuity equation and the Navier-Stokes equations for fluid motion or the reaction-diffusion equations for the concentrations of dissolved species). The macroscopic attributes described by these equations (fluid velocity, solute concentration) are related to the underlying microscopic quantities by an averaging operation which extends over a volume element small on the typical volume scale of interest, but large compared with the average volume per molecule. In the process of averaging, such information as microscopic fluctuations is discarded. A basic premise of the macroscopic approach is that spatial and temporal variations are sufficiently slow for different parts of the system to be assumed in a state of local thermodynamic equilibrium at all times. The macroscopic equations are usually non-linear and have to be solved numerically. When iterating a numerical algorithm in a computer, round-off errors (arising when real numbers are truncated to finite computer words) can accumulate exponentially, leading to overflows. Guaranteeing the *stability* of numerical algorithms is a tedious procedure for non-linear problems. In contrast to the macroscopic approach, *molecular dynamics* deals with the motion of individual molecules under the influence of realistic intermolecular potentials. In this approach one addresses problems of a more fundamental nature, such as understanding at a molecular level the phenomenological coefficients of macroscopic models [80BOO/YIP]. Obviously the length and time scales relevant to molecular dynamics are much shorter than those typical of a macroscopic description.

There is a large class of problems involving natural systems that lie in the intermediate region between the macroscopic and the microscopic description. These naturally include problems with a characteristic length scale that is much larger than that of molecular events ($\sim 1 \text{ \AA} = 10^{-8} \text{ cm}$), but also much smaller than macroscopic length scales (for example, bulk properties of a rock, such as porosity, can be typically defined on a scale of $\sim 1 \text{ cm}$). We refer to such an intermediate scale as *mesoscopic*. Thus, processes taking place at pore level in a rock (typical pores have linear dimensions of the order of $100 \text{ }\mu\text{m} = 10^{-2} \text{ cm}$), such as changes in porosity due to precipitation/dissolution, belong intrinsically to this intermediate class of problems. Differential equations have been employed in mesoscopic modelling of natural systems, but only under convenient assumptions concerning the often very irregular boundaries (by assigning, for example, the flow in porous media to a network of capillary tubes of simple geometry [92DUL]). Even at typically macroscopic scales some kind of intermediate description may be indispensable when the complexity of the boundary conditions or the variability of certain quantities in space and time call for a degree of detail that cannot be afforded by the standard macroscopic equations.

The type of problems addressed at field scale (several metres or more) are of a very different nature from those solved by typical mesoscopic models. The spatial discretisation appropriate for field-scale problems is much coarser than the spatial detail that has to be accounted for at the mesoscopic scale. This is dictated in the first place by reasons

of computational feasibility, but also and most importantly for conceptual reasons: the evolution equations for macroscopic quantities, such as solute concentrations, can usually be expressed in terms of macroscopic bulk parameters, which are defined by averaging out finer details. Contact between modelling at different scales is established at the interface where mesoscopic models provide the relations between bulk parameters and their evolution in time, which cannot be derived or are known only empirically at the macroscopic level. The same is true about different time scales, where the times typical of geological phenomena may often render irrelevant the kinetics of specific reactions. As we shall see later in this chapter, there are notable exceptions where certain phenomena cannot be modelled in terms of purely macroscopic parameters and a mesoscopic description is indispensable, irrespective of the computational resources that this may require.

In this chapter we are going to present a new and promising method of modelling mass transport and chemical reactions at the mesoscopic level. The basic concept in this approach is that of a *cellular automaton*, i.e., *a dynamical system consisting of an integer field defined on the sites of a regular spatial lattice and evolving in discrete time steps according to a local updating rule; the rule determines the new value of the field at a certain site of the lattice according to the current values of the sites within a neighbourhood surrounding the site in question* [86WOL]. In the case of a system of dissolved species migrating in a porous or fractured medium and reacting with each other as well as with the host rock, one can think of the lattice as spanning the rock volume of interest and the local rule as modelling the collisions and the chemical reactions of the solute particles. Transport and chemical reactions are modelled in a way that preserves a limited number of microscopic features (most notably, microscopic fluctuations and correlations, as well as reaction kinetics), which are expected to influence the macroscopic behaviour we wish to describe. Moreover, since the behaviour of the solute particles upon contact with the solid boundaries is modelled in a physically motivated manner, the complexity of the boundaries has no bearing on modelling feasibility or even computational efficiency. The synchronous evolution of a cellular automaton reflects the *local* and *parallel* character of the natural processes it models: molecules migrate and react simultaneously at different locations inside the rock and each molecule reacts only with molecules in its immediate neighbourhood. The parallel and local properties of cellular automata map naturally onto the architecture of massively parallel computers. In the latter, a large number of processors (up to several tens of thousands) run in parallel, manipulating data from their local memories; data are transferred between processors via sophisticated communications networks which are particularly efficient for transfers between neighbouring processors. Massively parallel architectures are expected to dominate the design of new computers in the coming years since they offer the only way to improve by orders of magnitude, on the performance of current scalar and vector computers (it takes an electromagnetic signal some nanoseconds to traverse a typical length of 1 m and this sets an absolute upper limit to the clock frequency of serial processors).

The remainder of this chapter is organised as follows: The development of cellular automata (CA) from their initial inception as models of biological systems, to their present implementation in the simulation of a wide range of physical phenomena is outlined in

the next section. In the same section we illustrate the basic concepts with the help of elementary examples. Following that, we present CA models for coupled transport and chemical reactions and describe their applications to reaction-transport systems ranging from the simplest and better understood to increasingly more complex and realistic ones. In the final section we evaluate the potential of the CA approach and indicate possible future developments. It should be emphasised that this chapter has a rather pedagogical orientation. The author will allow a certain personal bias in the selection and presentation of the relevant material and does not expect this work to be seen as a review article, even more so since reviews and extensive compilations of articles are already available [84FAR/TOF, 89MAN/BOC, 90GUT, 95CHE/DAW].

XI.2. Cellular automata

XI.2.1. Historical development

The theory of *automata* was envisaged by John von Neumann as a systematic mathematical and logical framework that would unify the basic principles of natural and artificial information processing systems [87ASP/BUR, 90ASP]. The idea of a unified approach appeared in the early days of the digital computer and was motivated by the plausible analogy between computers (as well as other communications and control devices) and self-regulating biological systems (cells, the human nervous system, organisms capable of reproduction and evolution). Typical questions addressed were those of reliability (*i.e.*, the ability to detect errors and minimise their effect) and of the minimal complexity that enables an automaton to construct other, equally complicated automata. A *universal constructor*, *i.e.*, an automaton that can construct any other automaton would be equivalent to the *universal Turing machine*, the theoretical prototype of a general-purpose computer. A computer *A* is called “universal” if, given any other computer *B*, there is always an appropriate piece of software which enables *A* to emulate *B* in the sense that the two devices deliver the same output for any given input [89PEN]. Following initial difficulties with a three-dimensional *kinematic automaton* that would physically assemble its duplicate out of a pool of elementary parts, von Neumann heeded the advice of Stanislaw Ulam and considered the abstract setting of *cellular automata*, *i.e.*, two-dimensional square arrays of cells, each of which assumed one out of the same finite set of states ². Although cellular automata could be directly translated into parallel computer structures in theory, the size and power consumption of hardware components available at the time rendered a physical implementation of the cellular automaton paradigm impractical. Interestingly, von Neumann’s name is usually associated only with the *serial computers* developed in his lifetime; essentially, he also laid the theoretical foundations for the *massively parallel computers* built later, when integrated circuit technology drastically enhanced the processing and memory storage capacity of single chips.

Although von Neumann’s program of a comprehensive theory of automata was never

² It is possible that other people arrived at similar ideas independently (see, *e.g.*, [69ZUS]), but von Neumann’s work is by far the most extensive, albeit itself incomplete, on published record.

completed, cellular automata (CA) developed their own dynamic in the 1970's and 1980's. Information concerning CA implementations in special-purpose hardware and general-purpose computers can be found in Refs. [84HIL, 84PRE/DUF, 87TOF/MAR, 90BOG]. Largely as a result of the ongoing dramatic rise in available computing power in general, and the advent of massively parallel computers in particular, CA algorithms are increasingly employed to simulate natural phenomena. A wide field of applications opened when CA were applied to the simulation of fluid dynamics [90DOO/FRI, 91DOO], following the realisation that a certain class of CA approximate the Navier-Stokes equations [86FRI/HAS]³. The CA of this class have come to be known as *lattice gas automata* (LGA). A wide range of flow phenomena have been modelled in the meantime, including the flow of multiphase mixtures (*e.g.*, oil and water) [88ROT/KEL, 91SOM/REM] and phase transitions (*e.g.*, liquid-gas) [90APP/ZAL, 93APP/ZAL], turbulence [88SUC/SAN], magnetohydrodynamics (*i.e.*, the motion of electrically conducting fluids, such as plasmas, in the presence of a magnetic field) [87CHE/MAT, 87MON/DOO], colloidal suspensions [88LAD/COL] and flow in porous media [87BAL/HAY, 88ROT]. Due to the simplicity of their dynamics, LGA have been used as models to address fundamental problems in kinetic theory, such as the long-time behaviour of time correlation functions [76HAR/PAZ, 89FRE, 89FRE/ERN] and the relation of transport coefficients (*e.g.*, viscosity, thermal conductivity) to the time integral of correlation functions [87RIV, 90ERN/DUF, 92ERN/DAS]. CA have also been used to model various physicochemical processes of engineering interest (carbonation of concrete [91BRI/BON], catalytic CO(g) oxidation on platinum surfaces [92WU/KAP], polymer chains in solution [90VIA/KOE], charged-particle transport in semiconductors [92KOM/ZAN]), biological functions (*e.g.*, the immune response [85KAU/URB] or the biochemistry of the cell [93HAS/KAP]) and astrophysical phenomena [93PER/LEJ].

What interests us here are CA simulations of systems of molecules that move by means of diffusion and/or advection and react chemically with each other and with the surrounding medium (*e.g.*, reactive chemicals diffusing in a gel or solutes migrating in a porous medium). CA models of mass transport with chemical reactions were developed either along lines similar to the LGA models of fluid dynamics [89DAB/BOO, 90DAB/LAW, 91LAW/DAB] or independently [90BLA, 93KAR, 94KAR/BLA]. Before we describe these models in detail, we shall illustrate the basic concepts by means of a few elementary examples, which will also demonstrate the capacity of simple CA rules to produce interesting complex behaviour.

XI.2.2. Elementary examples

“Life” is a mathematical game, in which a two-dimensional square array of cells displays a lot of the lively activity typical of an assembly of living organisms [70GAR]. Beginning with some initial configuration of live cells (state ‘1’), one follows the evolution of the

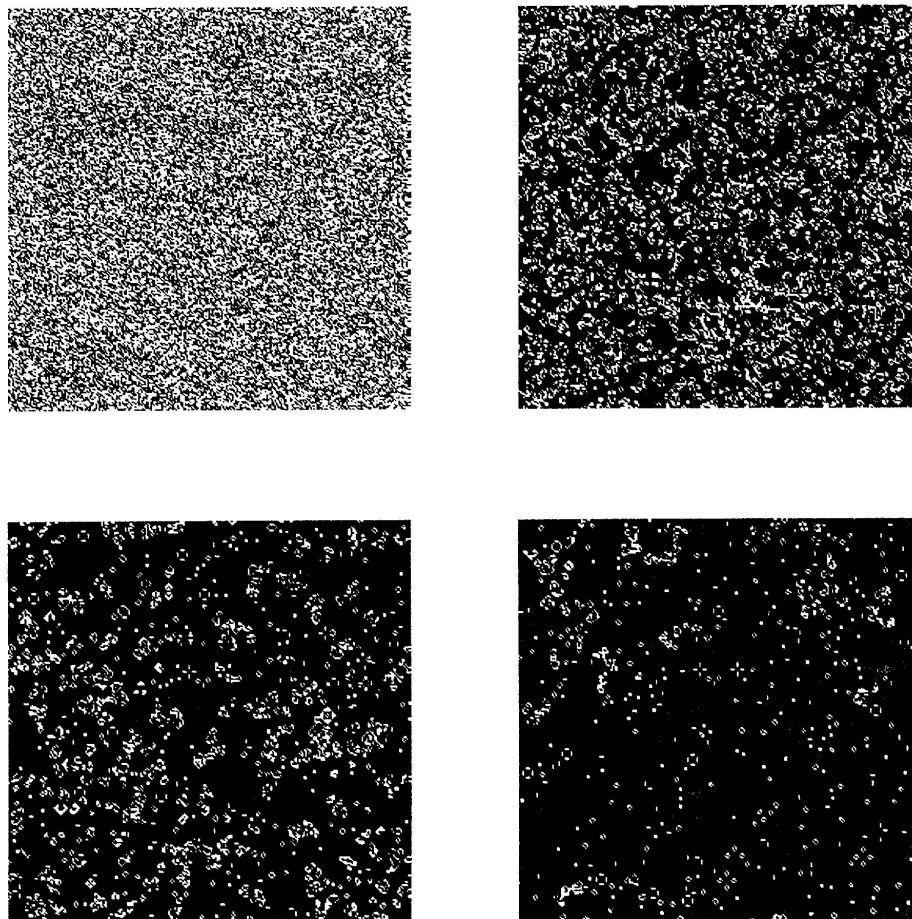
³ Although there is no general prescription for finding the microscopic rules that will simulate a given set of macroscopic equations, the CA approach has been applied to the numerical solution of various partial differential equations of physical interest [87BOG/LEV, 88CHE/CHE, 90CHE/MAT].

population as previously dead sites (state ‘0’) come to life (if there are exactly 3 live cells among the 8 neighbours on the square surrounding them) and live cells persist (if 2 or 3 of their 8 neighbours are alive) or die (otherwise). This evolution rule was chosen by John Conway, the inventor of the game, so as to avoid the more common scenarios of rapid uncontrolled growth or extinction of the population. Typical snapshots from the evolution of an originally random population of 50% live cells are shown in Fig. XI.1. Following an initial burst of activity and occasional later flares, most configurations settle down to a sparse distribution of stationary and oscillating patterns (last frame in Fig. XI.1). Propagating patterns (“gliders”) and configurations that grow without limit (“glider guns”) are less common, but contribute to the unpredictability of “Life”. When a glider meets another group of live cells a new pattern is in general created. Thus glider crashes can be designed to produce glider guns, which in turn emit streams of fresh gliders. An “eater” is a pattern that annihilates other patterns upon colliding with them. One can build logical gates (NOT, AND, OR) out of glider guns and eaters. It turns out that one can construct an arbitrary computer out of such gates, so that “Life” is capable of universal computation in the sense of the universal computer defined in Section XI.2.1 [82BER/CON]. It is a remarkable fact that a CA with no more than two possible states per site and a very simple evolution rule can perform all the complicated tasks that a general-purpose computer can.

As a second example we mention the CA implementation of the “billiard-ball” model of computation. In the latter, the elastic collisions of a gas of hard spheres with each other, and their reflections by a set of “mirrors” are used to construct a universal computer [82FRE/TOF]. We consider a square lattice of cells, as before, each with two possible states and we divide them in 2×2 blocks. Given such a partition of the lattice, we define the updating rule of a 2×2 block as specified in Fig. XI.2a (complemented with all possible rotations of the transitions indicated) [84MAR2]. Between successive applications of the rule, we shift the partitioning grid along the diagonal by $\sqrt{2}$ times the lattice spacing (from the solid to the dashed lines in Fig. XI.2b, where the legend “solid” or “dotted” indicates the partitioning for the next application of the rule). If we let ‘1’s and ‘0’s denote particles and empty sites respectively, iteration of the above rule makes particles propagate and collide elastically with each other (Fig. XI.2b). Two adjacent blocks filled with particles form a stable configuration that acts as a mirror. It has been shown [84MAR2] that the CA we have just described is equivalent to the billiard-ball model and is consequently a universal computer. This is an example of a reversible CA, *i.e.*, one whose evolution can be traced backwards in time, in direct analogy with the microscopic reversibility of physical laws. The realisation that reversible universal computers are feasible has far-reaching implications for the physical limitations of computers, since it appears to remove the lower boundary on dissipation associated with standard irreversible logic elements [73BEN, 84MAR2].

As a last example, we show in Fig. XI.3 different stages in the evolution of a CA which develops spatial structures similar to the concentration patterns observed in certain chemical experiments. The simulation is performed with a triangular lattice of cells that exist in three different states: “activated” (white), “receptive” (black) and “quiescent” (grey).

Figure XI.1: Initial random distribution of 50% live cells and distribution after 10, 100 and 1000 iterations of “Life”.



During one update, all receptive cells among the nearest neighbours of an activated cell become active, while the activated cell itself turns quiescent. A quiescent cell cannot be excited until it becomes receptive after two time steps [83MAD/FRE]. Different patterns, such as circular waves and spirals, develop depending on the initial configuration. The one- and two-armed spirals in Fig. XI.3 arise from isolated lines of active cells buffered by lines of quiescent cells. It can be seen that, when the spirals collide, they halt each other along their line of contact, but continue to spread unhindered elsewhere. Similar patterns have been observed in experiments with autocatalytic chemical reactions [72WIN, 73ZHA/ZAI]. We are going to return to the subject of autocatalytic reactions in the next section.

Having seen how simple CA can simulate the motion and collisions of particles, as well as effects reminiscent of complex chemical systems, we can now proceed to describe in

Figure XI.2: (a) Updating rule for CA implementation of “billiard-ball” model of computation; (b) Propagation and collision of particles according to this rule (reprinted with permission from Ref. [84MAR2], Figs. 4 and 12).

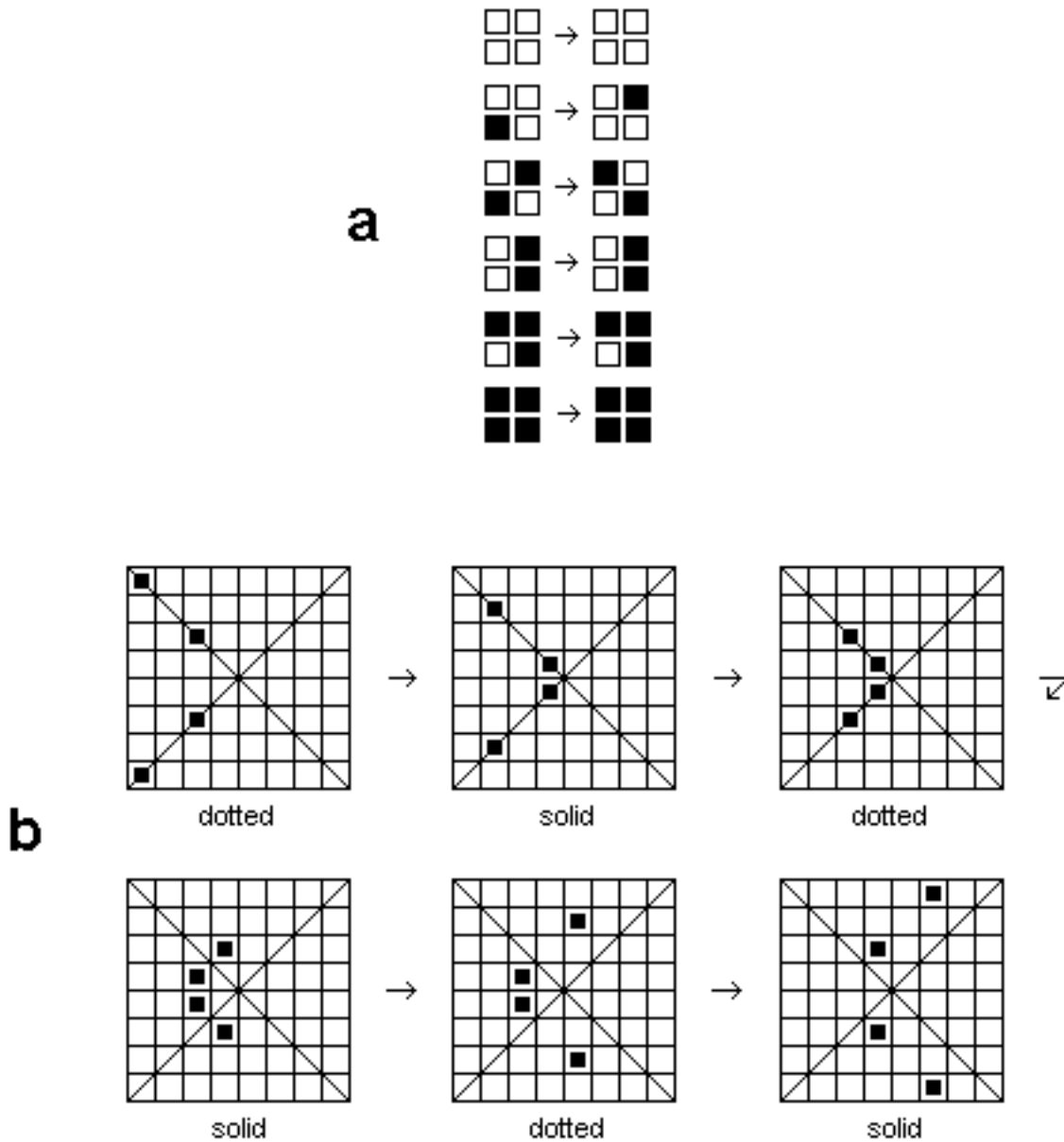
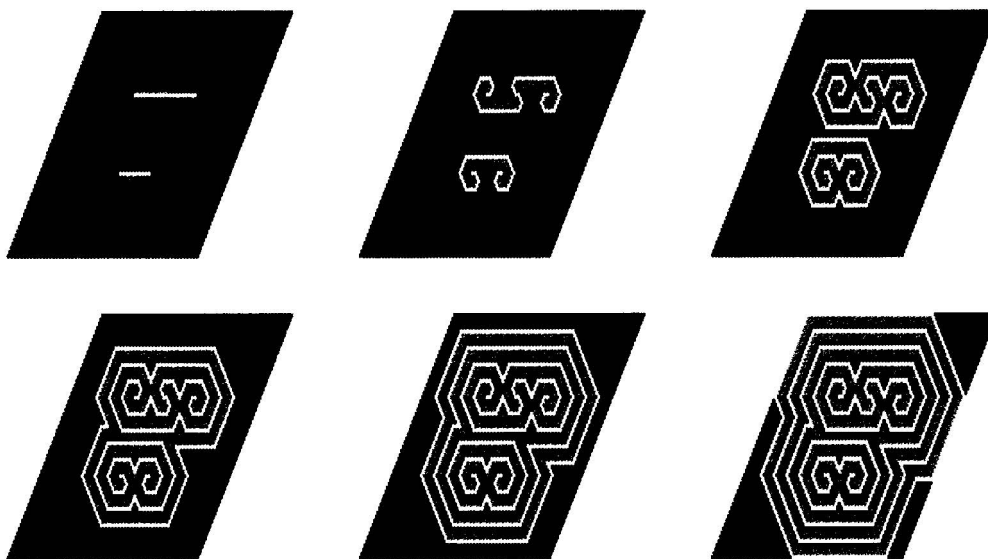


Figure XI.3: One- and two-armed spirals evolving out of isolated lines of activated cells (white) buffered by lines of quiescent cells (grey).



detail more elaborate CA models that couple these processes.

XI.3. Cellular automata for transport with chemical reactions

XI.3.1. Models

XI.3.1.1. Transport

From a macroscopic point of view, solutes migrate in a porous medium by means of *advection*, *molecular diffusion* and *kinematic dispersion* [86MAR3]. Advection takes place when a solute is carried along by the flow of the solvent; it is characterised by a velocity, which, for sufficient dilution, coincides with the Darcy velocity of the pure solvent. Molecular diffusion is the macroscopic manifestation of the Brownian motion of the solute particles caused by random impacts with fluid molecules; in an ideal solution it is described by Fick's law, which introduces the *coefficient of molecular diffusion*. Finally, kinematic dispersion is the spreading of the solutes around the mean advective displacement due to microscopic variations in flow velocity inside individual pores, but also between pores of different aperture and length; kinematic dispersion is commonly accounted for in the transport equation by a diffusion term, which can be combined with the analogous term for molecular diffusion to define an effective overall diffusion coefficient. In what follows, we shall use “diffusion” to describe the combined effect.

The breakdown of transport into advection and diffusion is rather arbitrary and becomes

less meaningful as we focus on the finer structure of the porous medium. At the mesoscopic level, particle transport can be thought of as a single process which consists of a collection of particles performing independent random walks ⁴. We assume that particles move between the sites of a regular spatial lattice. In discrete time steps, particles jump to one of their nearest-neighbour sites with a certain probability. If the particles jump in all directions with the same probability, then the random walk manifests itself at the macroscopic level as pure diffusion. If on the other hand particles tend to jump preferentially in a given direction, this leads macroscopically to combined advection (in the favoured direction) and diffusion [70FEL]. We consider for simplicity a one-dimensional lattice, since extensions to higher dimensions are straightforward. Let the lattice spacing and the time step be λ and τ respectively. We refer to sites on the lattice by their location in space, *e.g.*, site x . During one time step, each particle moves to the next site on the right with a certain probability p , to the next site on the left with probability q (of course $p + q \leq 1$) or remains stationary, with probability $1 - p - q$. It is useful to see the system as a fixed array of sites; the state of site x at time t is given by the integer field $N(x, t)$, the number of particles at that site, at the given time; the evolution of $N(x, t)$ is determined by the rule defining the random walk. The array of sites, together with the integer field and the evolution rule, constitute a CA that models the transport of solute particles.

We run the simulation on an ensemble of lattices subject to the same mesoscopic laws (*i.e.*, same p and q), with macroscopically identical initial and boundary conditions. Let us first assume that p and q are constant in space and time. If we define the particle density $\rho(x, t)$ as the ensemble average of $N(x, t)$, it can be easily seen that ρ evolves in time according to the difference equation

$$\rho(x, t + \tau) = p\rho(x - \lambda, t) + (1 - p - q)\rho(x, t) + q\rho(x + \lambda, t) \quad (\text{XI.1})$$

which can be readily rearranged to

$$\begin{aligned} \frac{\rho(x, t + \tau) - \rho(x, t)}{\tau} = & -V \frac{\rho(x + \lambda, t) - \rho(x - \lambda, t)}{2\lambda} \\ & + D \frac{\rho(x + \lambda, t) - 2\rho(x, t) + \rho(x - \lambda, t)}{\lambda^2}, \end{aligned} \quad (\text{XI.2})$$

with the parameters V and D defined as

$$V \equiv (p - q) \frac{\lambda}{\tau}, \quad D \equiv (p + q) \frac{\lambda^2}{2\tau}. \quad (\text{XI.3})$$

⁴ We intentionally talk about solute “particles” and their “density”, rather than about solute “molecules” and “concentration”, as it is clear that, in the foreseeable future, the number of particles in all CA simulations of experimentally or naturally realisable processes must, for practical reasons, fall short of the number of molecules actually involved by several orders of magnitude. Contact with the real process is established by rescaling the density at the level of the output [93KAR, 94KAR/BLA].

If we take the continuum limit $\lambda \rightarrow 0$, $\tau \rightarrow 0$ and $p - q \rightarrow 0$, while keeping λ^2/τ and $(p - q)\lambda/\tau$ finite, Eq. (XI.2) goes over to the transport equation

$$\frac{\partial \rho(x, t)}{\partial t} = -V \frac{\partial \rho(x, t)}{\partial x} + D \frac{\partial^2 \rho(x, t)}{\partial x^2} . \quad (\text{XI.4})$$

The right hand side of Eq. (XI.4) contains an advective and a diffusive term. We identify V as the *advection velocity* and D as the *diffusion coefficient*. The continuum limit is taken in such a way that V and D , as defined by Eq. (XI.3), remain finite. Eq. (XI.2) is the forward-time centred-space finite difference approximation to the transport equation (XI.4). It is clear that, by making p and q species dependent, we can have species with different transport properties move on the same lattice. If V and D are not homogeneous, the system can be modelled by making p and q position dependent (then, if V and D are defined according to Eq. (XI.3), the advection velocity has to be defined by $\tilde{V}(x) \equiv V(x) - dD(x)/dx$).

Boundary conditions are modelled by mimicking the behaviour of actual molecules when they reach boundaries with the specified properties. Thus, when particles reach an impermeable boundary, they bounce back or remain stationary. The “free-flow” boundary condition, according to which only advection carries particles across the boundary ($\partial \rho(x, t)/\partial t = 0$, for x at the boundary), is simulated by cancelling the outgoing diffusive flux with an equal and opposite diffusive flux, coming from a fictitious reservoir on the other side of the boundary. A fixed density at the boundary is modelled by choosing the number of particles at boundary sites from a distribution consistent with the specified average value; this simulates the situation where the boundary sites are in contact with a particle reservoir of the appropriate density. A periodic boundary condition is often computationally convenient and is justified when the precise behaviour of the boundary sites is not important, *e.g.*, with translationally invariant homogeneous systems or when the boundary is too far away to influence the region of interest.

In a typical simulation of the kind described above, it cannot be excluded that, at a certain point in the simulation, a large number of particles are found at the same lattice site. Given the total number of particles initially present and the rate at which particles enter and leave the system, an upper limit can be calculated in advance of the simulation. This limit is however of little value in practice since it is highly unlikely to ever be reached in an actual simulation. It is often desirable in computer simulations to allow *a priori*, only a limited number of particles per site. This makes it possible to program at bit level and construct look-up tables of all conceivable input-output combinations that may occur at a site. One is then able to produce very efficient CA simulations on dedicated hardware [87TOF/MAR], but also to substantially improve performance on serial and vector computers [90SHI/DOO]. A restriction to the the number of particles per site is imposed in LGA models of fluid dynamics in the form of an *exclusion principle*: a small number of velocities are assigned to each lattice site (*e.g.*, in a single-speed model, the vectors of magnitude λ/τ pointing to the nearest neighbours) and at most one particle per site is allowed to have a given velocity. As a result, the state of an LGA is defined by

a Boolean field that gives the occupation numbers (0 or 1) of the velocity states at each site.

One can also model diffusion with very efficient CA algorithms which obey an exclusion principle [91CHO/DRO]. We consider again a one-dimensional lattice and assign two possible velocities to each site: $\mathbf{c}_1 = (\lambda/\tau)\hat{\mathbf{e}}_1$ pointing to the right and $\mathbf{c}_2 = (\lambda/\tau)\hat{\mathbf{e}}_2$ to the left ($\hat{\mathbf{e}}_1$ and $\hat{\mathbf{e}}_2$ are unit vectors). One evolution step of the automaton consists of two elementary operations: First, a rotation operator acts independently on different nodes and causes the velocity configuration at each of them to remain intact or rotate by π with probability p and $1 - p$, respectively; following this, particles propagate to the next lattice site along the direction of their velocity. Let the Boolean variable $N_i(x, t)$ denote the number of particles with velocity \mathbf{c}_i at site x and time t . Then the ensemble average $\rho_i(x, t)$ of $N_i(x, t)$ satisfies the discrete evolution equation

$$\begin{pmatrix} \rho_1(x, t + \tau) \\ \rho_2(x, t + \tau) \end{pmatrix} = p \begin{pmatrix} \rho_1(x - \lambda, t) \\ \rho_2(x + \lambda, t) \end{pmatrix} + (1 - p) \begin{pmatrix} \rho_2(x - \lambda, t) \\ \rho_1(x + \lambda, t) \end{pmatrix} . \quad (\text{XI.5})$$

The first (second) term on the right hand side of Eq. (XI.5) accounts for particles that propagate to the next site without (after) being rotated. We define the particle density $\rho(x, t) \equiv \sum_i \rho_i(x, t)$.

Since the number of particles is conserved, a continuity equation holds in the form

$$\rho(x, t) - \rho(x, t - \tau) + \sum_{i=1}^2 J_i(x, t) = 0 , \quad (\text{XI.6})$$

where $J_i(x, t) \equiv \rho_i(x + \lambda\hat{\mathbf{e}}_i, t) - \rho_{3-i}(x, t)$ is the net flux of particles traversing the lattice link from x to $x + \lambda\hat{\mathbf{e}}_i$ in the time between $t - \tau$ and t . Taking the continuum limit of Eqs. (XI.5) and (XI.6) ($\lambda \rightarrow 0$, $\tau \rightarrow 0$, keeping λ^2/τ finite), we arrive, after some simple algebraic manipulations, at the diffusion equation (Eq. (XI.4) without the advection term) with

$$D \equiv \frac{p}{1 - p} \cdot \frac{\lambda^2}{2\tau} . \quad (\text{XI.7})$$

Species with different diffusion coefficients can be simulated on the same lattice by adjusting p . Diffusion in two and three dimensions is treated in Ref. [91CHO/DRO]. The advantage of this algorithm is that it can be readily implemented on special-purpose computers and its performance on vector supercomputers exceeds that of the previous algorithm by more than an order of magnitude. On the other hand, the exclusion principle induces correlations between particles and these in turn give rise to non-linear terms in the transport equations derived from models with biased random walks [87BOG/LEV]. As a result, models with an exclusion principle are not able to model advection without introducing at the same time unwanted terms in the transport equation.

Modelling diffusion and advection with CA would be an exercise of little practical interest, were it not to be coupled with chemical reactions, a task that we immediately proceed to fulfil.

XI.3.1.2. Chemical reactions

In the full coupled problem, an evolution step consists of a transport operation followed by a chemical reaction operation. We first consider a system with no restriction on the number of particles per site. Transport takes place as described above for such a system. Particles of various solute species move on the lattice and, when sufficient numbers of them meet at a site, they react with a certain probability. A reaction is more likely to occur the more the particles of each reactant that are present. If a reaction takes place, then the appropriate number of products (reactants) are added to (subtracted from) the local inventory of particles.

We consider a system of species s_α and reactions r . We write all reactions in the one-way form by separating, in the case of reversible reactions, the forward from the reverse process:

$$\sum_{\alpha} \nu_{\alpha r, i} s_{\alpha} \rightarrow \sum_{\alpha} \nu_{\alpha r, f} s_{\alpha} \quad (\text{XI.8})$$

where $\nu_{\alpha r, i}$ and $\nu_{\alpha r, f}$ are the stoichiometric coefficients of the initial and final state of the reaction, respectively. The summations run over all species, but the $\nu_{\alpha r, i}$ ($\nu_{\alpha r, f}$) vanish for species not present among the reactants (products). If reaction r involves only species in solution, we let it proceed with probability

$$P_r \prod_{\alpha} \prod_{m=1}^{\nu_{\alpha r, i}} (N_{\alpha}(x, t) - m + 1) \quad , \quad (\text{XI.9})$$

where P_r is a constant and $N_{\alpha}(x, t)$ is the number of particles of species s_{α} at site x and time t . For example, if r is the reaction $a + 2b \rightarrow c$, it takes place with probability $P_r N_a N_b (N_b - 1)$. Of course, the reaction probability has to be ≤ 1 ; since N_a and N_b are finite in a simulation, we can always ensure that $P_r N_a N_b (N_b - 1) \leq 1$ by choosing P_r sufficiently small. We shall see shortly that it is the ratio P_r/τ that is physically meaningful, so τ has to be chosen correspondingly small, with a concomitant increase in the number of iterations. In the case of reactions between solutes and mineral surfaces, the reaction rule has to be modified so that precipitation takes place with a probability defined as before, but only if solid is already present or the solution is saturated.

We wish to derive an evolution equation for the particle density $\rho_{\alpha}(x, t)$, defined as an ensemble average of $N_{\alpha}(x, t)$. To this end we have to make two important assumptions. In evaluating the average of the product in Eq. (XI.9), we assume that there are no correlations between the N_{α} for different species (*molecular chaos*). The resulting simple averages (*e.g.*, $\overline{N_b(N_b - 1)}$ in the example above) can be expressed in terms of the densities, if the N_{α} do not vary appreciably over several lattice spacings (*smoothness assumption*); then we can evaluate $\rho_{\alpha}(x, t)$ by averaging locally around x over a uniform distribution of particles (the crucial fact is that, for a uniform particle distribution, $N_{\alpha}(x, t)$ obeys a Poisson distribution parametrised with $\rho_{\alpha}(x, t)$ [70FEL]). We thus arrive at the discrete equation [94KAR/BLA]

$$\rho_{\alpha}(x, t + \tau) = \tilde{\rho}_{\alpha}(x, t) + \sum_r (\nu_{\alpha r, f} - \nu_{\alpha r, i}) P_r \prod_{\beta} \tilde{\rho}_{\beta}^{\nu_{\beta r, i}}(x, t) \quad , \quad (\text{XI.10})$$

where the sum is over all reactions r , the products over all species β and

$$\tilde{\rho}_\alpha(x, t) \equiv p_\alpha \rho_\alpha(x - \lambda, t) + (1 - p_\alpha - q_\alpha) \rho_\alpha(x, t) + q_\alpha \rho_\alpha(x + \lambda, t) , \quad (\text{XI.11})$$

is the result of the transport operation on the particle distribution at time t ; here p_α and q_α are the species-dependent displacement probabilities.

Upon taking the continuum limit as before, with the additional limiting procedure $P_r \rightarrow 0$ so that P_r/τ remains finite, we obtain the standard transport equations for reacting solutes

$$\begin{aligned} \frac{\partial \rho_\alpha(x, t)}{\partial t} = & -V_\alpha \frac{\partial \rho_\alpha(x, t)}{\partial x} + D_\alpha \frac{\partial^2 \rho_\alpha(x, t)}{\partial x^2} \\ & + \sum_r (\nu_{\alpha r, f} - \nu_{\alpha r, i}) k_r \prod_\beta \rho_\beta^{\nu_{\beta r, i}}(x, t) \end{aligned} \quad (\text{XI.12})$$

where

$$V_\alpha \equiv (p_\alpha - q_\alpha) \frac{\lambda}{\tau} , \quad D_\alpha \equiv (p_\alpha + q_\alpha) \frac{\lambda^2}{2\tau} , \quad k_r \equiv P_r/\tau . \quad (\text{XI.13})$$

k_r is the *rate constant* of reaction r .

We emphasize that the CA simulations are not subject to the assumptions which were introduced above with the purpose of deriving the macroscopic equations. The simulations account for microscopic effects of correlations and fluctuations that are typically averaged out by the macroscopic approach. The results of the discrete model were compared carefully to the solution of the reaction-transport PDE's in Ref. [94KAR/BLA]. Two essential sources of discrepancy were encountered: (i) correlations between the particles that arise as a result of chemical reactions, and (ii) statistical fluctuations. Systematic study shows that the effect of chemically induced correlations disappears as the continuum limit is approached (for details see [94KAR/BLA]). If one sees CA algorithms only as numerical tools for the solution of macroscopic equations, correlations of this type are no more than numerical artefacts associated with the particular method of solution. This is to be contrasted with the potentially observable effect that statistical fluctuations can have on the behaviour of reaction-diffusion systems, as it will be illustrated in Section XI.3.2. Of course, physical systems are after all discrete and so correlations will manifest themselves at some level. Here the discrete model could provide a more accurate model than afforded by the PDE's.

In reaction-diffusion models with an exclusion principle one needs to ensure careful book-keeping of the occupied velocity states before and after a reaction. In general there are several species on the lattice and the rotation and propagation operations described previously are applied to each of them independently. The dynamics of different species is coupled by chemical reactions of the type given by Eq. (XI.8). We concentrate, for illustration purposes, on an effective single-species system, assuming the concentrations of other species to be kept constant by contact with an appropriate reservoir [89DAB/BOO,

90DAB/LAW, 91LAW/DAB]. In the notation of Eq. (XI.8), there is one active species, s_1 , and the reactions r are identified by the stoichiometric coefficients $\nu_{1r,i}$ and $\nu_{1r,f}$. We denote, for simplicity, s_1 by X and $\nu_{1r,i}$, $\nu_{1r,f}$ by α , β , respectively. The reaction probability $P(\alpha\beta)$ is independent of the initial and final velocity states: if, for a given initial configuration, there are $n_{\alpha\beta}$ possible final velocity configurations of the reaction $\alpha X \rightarrow \beta X$, each occurs with the same probability $P(\alpha\beta)/n_{\alpha\beta}$.

Introducing indices i_k to differentiate between the m different velocity states ($i_k = 1, \dots, m$; $m = 2$ for a one-dimensional lattice, 4 for a two-dimensional square lattice etc.), we note that a reaction configuration is fully defined in terms of α , β and the velocity states i_1, \dots, i_q ($q \equiv |\alpha - \beta|$) of the particles that are created or destroyed, depending on whether $\alpha < \beta$ or $\alpha > \beta$, respectively. With each configuration thus defined we associate a random Boolean variable $\gamma_{\alpha\beta}(i_1 \dots i_q)$ which takes the value 1 when the reaction takes place (with probability $P(\alpha\beta)/n_{\alpha\beta}$) and is 0 otherwise. If we then define N_i as before, we can write the effect of the chemical reaction operation as follows:

$$\begin{aligned} N_i \rightarrow N_i &+ \sum_{\alpha, \beta (\alpha < \beta)} \sum'_{i_1, \dots, i_\alpha \neq i} Q(\{N_i\}, i_1 \dots i_\alpha) \sum'_{j_2, \dots, j_q \neq i} \gamma_{\alpha\beta}(i j_2 \dots j_q) \\ &- \sum_{\alpha, \beta (\alpha > \beta)} \sum'_{i_2, \dots, i_\alpha \neq i} Q(\{N_i\}, i i_2 \dots i_\alpha) \sum'_{j_2, \dots, j_q = i_2}^{i_\alpha} \gamma_{\alpha\beta}(i j_2 \dots j_q), \end{aligned} \quad (\text{XI.14})$$

where

$$Q(\{N_i\}, i_1 \dots i_\alpha) \equiv \prod_{k=1}^{\alpha} N_{i_k} \prod'_{l \neq 1, \dots, \alpha} (1 - N_{i_l}) \quad (\text{XI.15})$$

populates the initial state with particles of velocities i_1, \dots, i_α . The primes constrain the indices of the summation or multiplication to be distinct. In Eq. (XI.14), N_i increases (decreases) by 1 if a particle with velocity i is among the $|\alpha - \beta|$ particles produced (destroyed).

We take the ensemble average of the Eq. (XI.14), defining ρ_i as the average of N_i and $\rho \equiv \sum_i \rho_i$. Assuming that we can factorise the expectation value of products of random variables and taking the continuum limit for a homogeneous system ($\tau \rightarrow 0$, $P(\alpha\beta) \rightarrow 0$, keeping $P'(\alpha\beta) \equiv P(\alpha\beta)/\tau$ finite), we deduce the rate law

$$\frac{d\rho(t)}{dt} = \sum_{n=0}^m \kappa_n \rho^n(t) \quad , \quad (\text{XI.16})$$

where

$$\kappa_n \equiv (-1)^n \binom{m}{n} m^{-n} \sum_{\alpha=0}^n (-1)^\alpha \binom{n}{\alpha} \sum_{\beta \neq \alpha} (\beta - \alpha) P'(\alpha\beta) \quad . \quad (\text{XI.17})$$

Identifying the κ_n with the macroscopic rate constants, one can solve the resulting system of linear equations for the reaction probabilities $P(\alpha\beta)$. For an inhomogeneous system

we obtain the standard reaction-diffusion equations. The generalisation to multi-species systems is straightforward [91DAB/BOO, 91KAP/LAW, 92KAP/LAW]. The exclusion principle permits the utilisation of very efficient programming techniques, as described earlier. In the model described in Refs. [89DAB/BOO, 90DAB/LAW, 91LAW/DAB], there are different sets of mesoscopic reaction rules which are consistent with the same macroscopic kinetics. It is possible, however, to construct the reaction probabilities so as to allow only those particle number changes that are specified by the macroscopic mechanism [92WU/KAP, 93GRU/KAP].

XI.3.2. Applications

In this subsection CA modelling will be illustrated by means of applications to various reaction-transport processes. Our goal is to demonstrate the versatility of the method, as well as its ability to describe aspects of the microscopic dynamics, especially when the latter have macroscopic consequences that lie beyond the scope of the standard averaged equations. Thus when microscopic fluctuations determine, under certain conditions, the macroscopic behaviour of physical systems, the mesoscopic level of description afforded by CA models becomes indispensable.

XI.3.2.1. $a + b \rightarrow c$

We first consider a homogeneous system consisting of equal amounts of two mobile species, which combine to form an inert species. There is no external supply of reactants, so the two active species will deplete each other until there are only inert particles left. We are interested in the time dependence of the reactant particle density as the final inert state is approached. A system of this kind was analysed in connection with the mutual annihilation of magnetic monopoles and antimonopoles produced in the early universe [83TOU/WIL], but the analysis was relevant to a much wider range of phenomena. Other relevant physical processes include the recombination of electron-hole pairs in semiconductors [80VAR/OCO] and, conceivably, chemical reactions of the type $a + b \rightleftharpoons c$, if the reverse reaction can be reduced to a negligible rate by varying a physical parameter such as the temperature [78OVC/ZEL].

For a homogeneous system, we write the macroscopic densities of a and b as $\rho_a(t)$ and $\rho_b(t)$. If the two densities are initially equal, the particular kinetics implies that they will remain so at later times. Then the macroscopic rate equation assumes the simple form

$$\frac{d\rho_a(t)}{dt} = -k_1\rho_a^2(t) \quad , \quad (\text{XI.18})$$

k_1 being the rate constant. According to Eq. (XI.18), ρ_a has the long-time behaviour t^{-1} .

We consider a lattice populated by a - and b -particles subject to the irreversible reaction $a + b \rightarrow c$. The species c plays no active rôle in the evolution of the system. Initially the lattice is occupied by a uniform random distribution of equal numbers of a and b . We define the densities $\rho_a(t)$ and $\rho_b(t)$ by dividing the total numbers of a - and b -particles by

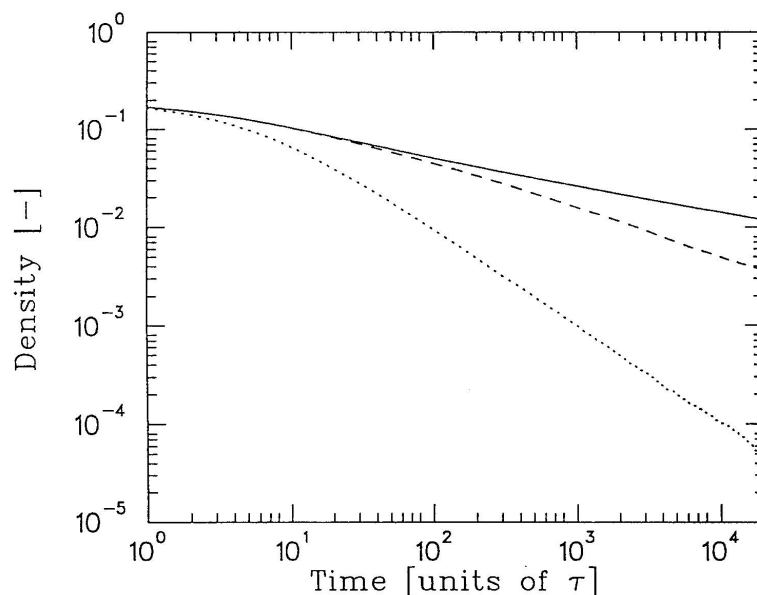
the number of sites in the lattice. When N_a a -particles and N_b b -particles meet at a site, they react with probability $P_1 N_a N_b$, where $P_1 = \tau k_1$. Each time a reaction takes place, one particle of each reactant is subtracted, so that the overall numbers and densities of a and b remain equal to each other. We consider three different cases: (i) the reactants diffuse with the same diffusion coefficient D , (ii) the reactants diffuse as before, but one of them is additionally subject to advection with a constant velocity V , and (iii) transport is replaced by a random redistribution of the reactants on the lattice. The last case emulates the instantaneous mixing implicitly assumed by the macroscopic rate equation.

The results of our simulations on a one-dimensional lattice are shown in Fig. XI.4. The asymptotic time dependence of ρ_a is $t^{-1/4}$, $t^{-1/2}$ and t^{-1} , respectively, in the three cases listed above. In the well-mixed third case, the result coincides naturally with that of the macroscopic equation. When the mixing is less fast, as in the other two cases, a slower depletion mechanism takes over. This happens because, as the bulk of particles disappear in mutual annihilation, the microscopic fluctuations present already in the initial state play an increasingly important rôle. Let us first consider the case of pure diffusion. The time exponent $-1/4$ (which is specific to a one-dimensional system; for d dimensions one finds $-d/4$ for $d < 4$ and 1 for $d \geq 4$) can be understood as follows [83TOU/WIL]: At any given time t in the evolution of an infinite system, particle transport has not had the time to dissolve fluctuations on a length scale longer than $l_D = \sqrt{Dt}$. For $\rho_a(0) = \rho_b(0) = \rho_0$, a part of the system of length l_D contains initially $\sim \rho_0 l_D$ particles of each species and the difference between the numbers of a - and b -particles is of the order of $\sqrt{\rho_0 l_D}$. Thus the surplus density of the species in excess is of the order of $\sqrt{\rho_0 l_D}/l_D = \rho_0^{1/2} (Dt)^{-1/4}$. We see that the decay of initial fluctuations results in a $t^{-1/4}$ decline of the density which is bound to dominate over the t^{-1} decline due to bulk depletion for long times. For very long times the system breaks up in segregated regions of a - or b -particles formed by the remaining excess particles after the bulk has annihilated; the reaction then proceeds only along the boundaries of these regions. It turns out that the relative drift between the reactants mixes them faster than diffusion and the asymptotic decline of the density follows a $t^{-1/2}$ law. This can be easily seen if the length scale \sqrt{Dt} swept out by diffusion is replaced by the advective scale Vt [85KAN/RED]. *It is clear that, with the exception of the unphysical case of infinitely fast transport, the correct long-time decline of the density can only be captured if microscopic fluctuations are explicitly accounted for.* To the extent that a mesoscopic model is called for, it is obviously desirable that it should be able, like the model used here, to account for advection, which was seen to alter qualitatively the behaviour of the physical system under consideration.

XI.3.2.2. Autocatalytic reactions

As we saw in Section XI.3.1, CA can be used to model species of different transport properties, as well as complex chemical reactions. We are now going to consider reaction-diffusion systems in which the difference between the diffusion coefficients of the reactants and a certain degree of complexity in the reactions play an essential rôle in the observed phenomena. The reactions of interest here contain autocatalytic steps, in which the

Figure XI.4: a -density for a one-dimensional, homogeneous system reacting via $a + b \rightarrow c$, as a function of time: (a) only diffusion (solid line), (b) diffusion+relative advection (dashed line), and (c) random redistribution (dotted line).

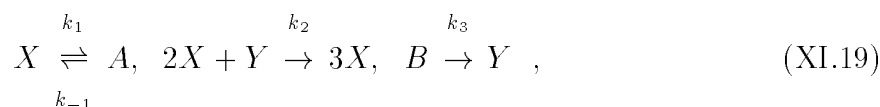


catalyst is one of the products (*e.g.*, $2X + Y \rightarrow 3X$). When autocatalytic systems are maintained far from chemical equilibrium (*e.g.*, by suppressing reverse reactions and by removing or adding reactants), they can experience phase transitions to states with remarkable spatial or temporal structures. A classic example is the Belousov-Zhabotinsky reaction (*i.e.*, the oxidation of citric, malonic or bromomalonic acid by bromate in acidic aqueous solution, with variable valence ions, such as $\text{Ce}^{+4}/\text{Ce}^{+3}$ or $\text{Fe}^{+3}/\text{Fe}^{+2}$, acting as catalysts [58BEL2, 64ZHA, 70ZAI/ZHA]), which, under appropriate conditions, displays oscillations in the concentrations of the oxidised and reduced forms of the catalyst, as well as periodic propagation of concentration waves. The emergence of ordered states far from equilibrium is of extreme importance in chemistry and biology [77NIC/PRI, 89MUR].

There is a certain class of steady spatial structures which are sustained by the combined effect of reaction kinetics and diffusion. The earliest example was proposed by Alan Turing in 1952 [52TUR]. A crucial condition for the formation of such patterns is that two species have different diffusion coefficients. Then it is possible that a uniform steady state, which would be stable in the absence of diffusion, becomes unstable and goes over to a stationary spatial concentration pattern when the ratio of diffusion coefficients exceeds a certain critical value. The faster species, the *inhibitor*, hinders by chemical action the production of the slower one, the *activator*, and confines the latter to restricted regions of

space, giving rise to a pattern of inhomogeneous concentration. The inhibitor itself forms a complementary pattern of high and low concentration. One can apply linear stability analysis to the reaction-diffusion equations to derive the range of wavelengths that become unstable for given values of the macroscopic parameters. The emerging pattern is an example of *spatial symmetry breaking* since it defines a new length scale that does not depend on the geometrical properties of the system, but rather on intrinsic properties described by the diffusion coefficients and the reaction rates (including feed and removal rates of reactants, as well as prescribed concentrations of external reactants). Sustained concentration patterns were obtained recently with the chlorite-iodide-malonic acid reaction in open reactors, in which the reactants diffuse into an inert gel from adjacent reservoirs of constant and uniform concentrations [90CAS/DUL, 91KEP/CAS, 91QUY/SWI].

One of the simplest reaction systems that are subject to the Turing instability under appropriate conditions is

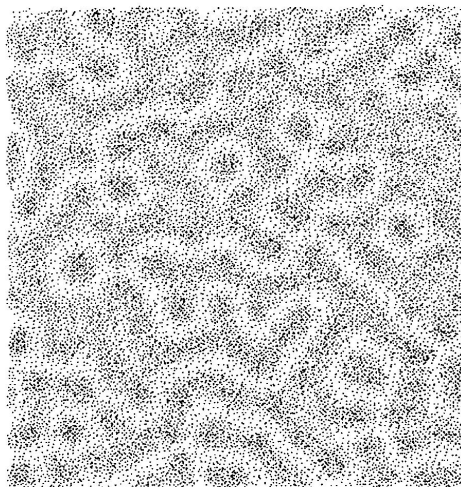


which was conceived by J. Schnackenberg in his search for simple systems admitting periodic solutions [79SCH2]. The concentrations of A and B are held fixed, for example by external supply or removal of reactants. The system (XI.19) can be analysed analytically and is known to exhibit a Turing instability for a wide range of parameter values [89MUR]. If the first reaction in (XI.19) is also made irreversible, the system may still oscillate, but it may also evolve towards infinite concentrations (*e.g.*, $X \rightarrow 0$, $Y \rightarrow \infty$, with X^2Y finite); the system $X \rightarrow A$, $2X + Y \rightarrow 3X$, $B \rightarrow Y$ had been used earlier by E. E. Selkov to model the phosphofructokinase catalysed production of ADP from an ATP substrate, as a possible source of glycolytic oscillations [68SEL, Eq. (II)]. Replacing the last reaction in Selkov's scheme with the pair of reactions $B + X \rightarrow Y + D$, $E \rightarrow X$, we obtain the "Brusselator", one of the earliest systems employed to illustrate the possibility of symmetry breaking instabilities [68PRI/LEF].

Simulations of the above reaction systems have been performed with CA models [91KAP/LAW, 92KAP/LAW, 93DRO/FRA, 93KAR, 94KAR/BLA]. The pattern in Fig. XI.5 was obtained from a random, macroscopically homogeneous initial state after a few thousand iterations of a CA simulation of the Schnackenberg model on a two-dimensional lattice with periodic boundary conditions [93KAR, 94KAR/BLA]. Given the rest of the macroscopic parameters, linear stability analysis predicts in this case that the Turing instability occurs if the ratio of diffusion coefficients $d \equiv D_Y/D_X$ exceeds the critical value $d_{crit} = 19.7$. The simulation was performed with $d = 30$, for which the macroscopic analysis predicts a window of unstable wavelengths consistent with the observed pattern.

Whereas reaction-diffusion equations describe the evolution of the macroscopically averaged particle densities, CA simulations incorporate microscopic fluctuations at all stages of the evolution. Fluctuations are expected to have an enhanced influence on the dynamics of the system near *bifurcation points*, such as near the onset of the Turing instability in

Figure XI.5: Spatial concentration pattern obtained from two-dimensional simulation of the Schnackenberg model.

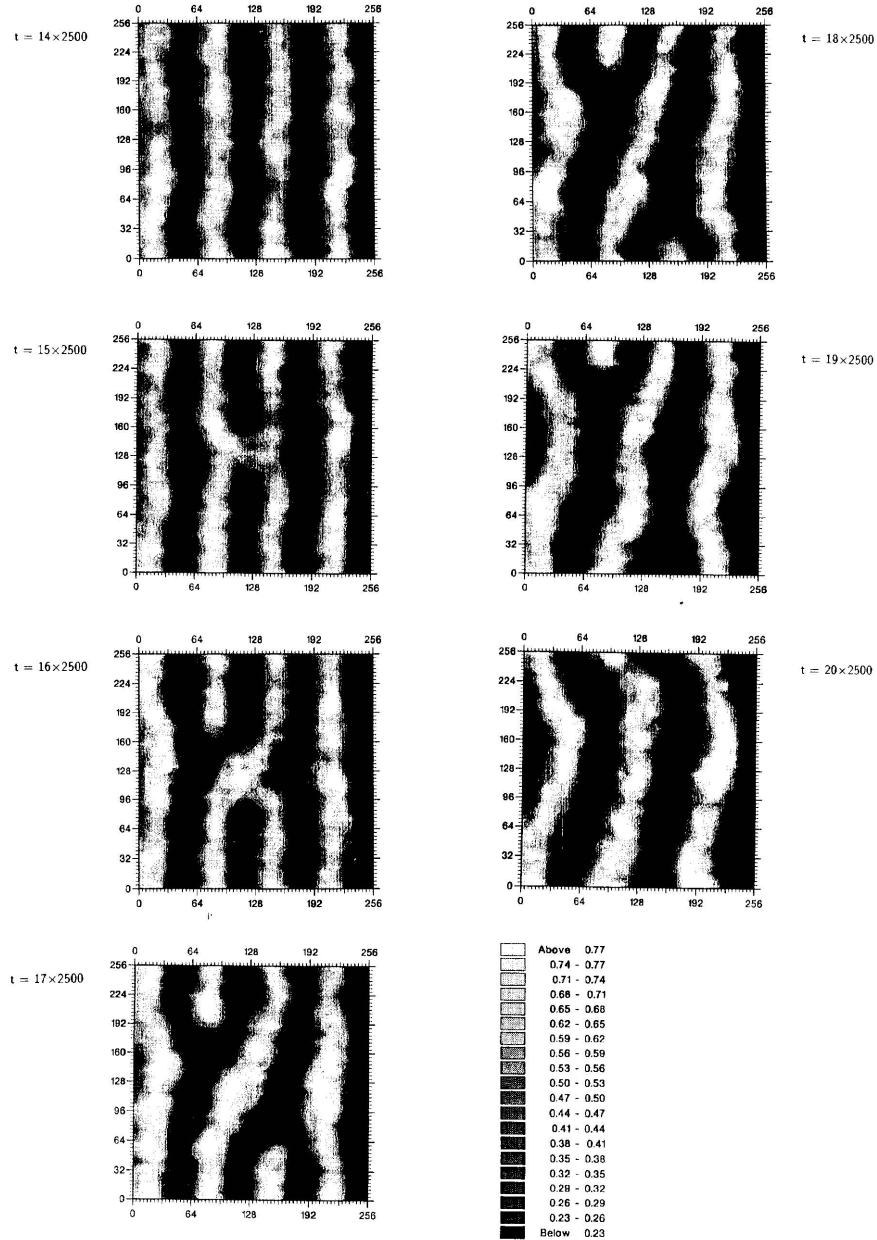


parameter space. The computational efficiency of CA models with an exclusion principle allows their application to detailed investigations of the rôle of fluctuations in particular chemical systems. Thus, in two-dimensional simulations of the Schnackenberg model, as well as of the Selkov model, transient patterns appear also below the critical value of the diffusion coefficient ratio [91KAP/LAW, 92KAP/LAW, 93DRO/FRA]. In that region pattern formation is not possible according to the macroscopic reaction-diffusion equations. Apparently, below the critical ratio, the homogeneous state is destabilised by density fluctuations which effectively widen the range of unstable wavenumbers. For parameter values for which the macroscopic equations predict a Turing instability, the patterns obtained by CA simulation generally display a certain roughness and are less regular than the ones derived from the reaction-diffusion equations. Whereas the latter patterns are strictly stationary after a certain time, the former are continually perturbed by fluctuations which occasionally destabilise a sustained structure and induce reorganisation of the pattern (Fig. XI.6).

XI.3.2.3. Reactions with mineral surfaces

We now move to chemical reactions taking place in heterogeneous systems, where different phases are in contact with each other. Thus, solutes often react with the surfaces of the water-conducting channels along which they are transported. The reaction may be in the form of mineral *precipitation* and *dissolution*, which leads to changes in rock properties (*e.g.*, the porosity) with a direct impact on the transport of the reacting solutes. Alternatively, the solid surface may act as a *catalyst* by adsorbing one or more reactants from the liquid or gaseous phase and modifying them so that they react more readily. In both

Figure XI.6: Turing pattern reorganisation (from four to three stripes) caused by density fluctuations. The density pattern shown here (see grey scale) is unpublished work by D. Dab and was obtained with the Maginu model [75MAG, 79MAG] simulated on a 256×256 lattice with parameter values $k = 0.9$, $c = 0.45$, $s = 10$, $D_x = 1$ and $D_y = 19$, as described in Refs. [91DAB/BOO, 92DAB].



cases, inhomogeneities in the spatial distribution of reactants play a crucial rôle in the evolution of the system, while moving boundaries may further complicate the situation. Due to its ability to treat spatially and temporally varying parameters with no additional effort, the CA approach is particularly appropriate for modelling systems of the kind described here. We shall illustrate this by means of two simple CA models of heterogeneous processes.

We first consider the precipitation/dissolution reaction



where a and b are aqueous species, c is a mineral and K_1 , K_2 are the rate constants. For constant and uniform porosity ε , the standard reaction-transport equations for this system are

$$\begin{aligned} \varepsilon \frac{\partial C_a(x, t)}{\partial t} &= -\varepsilon V_a \frac{\partial C_a(x, t)}{\partial x} + \varepsilon D_a \frac{\partial^2 C_a(x, t)}{\partial x^2} + \zeta \left(K_1 - \varepsilon^2 K_2 C_a(x, t) C_b(x, t) \right) \\ \frac{\partial C_c(x, t)}{\partial t} &= -\zeta \left(K_1 - \varepsilon^2 K_2 C_a(x, t) C_b(x, t) \right) \quad , \end{aligned} \quad (\text{XI.21})$$

where C_a and C_b are the concentrations of the solutes in mol per m³ of water, C_c is the “concentration” of solid in mol per m³ of rock and ζ is a constant with

$$\zeta = \begin{cases} 1, & \text{if } C_c(x, t) > 0 \text{ or } C_a(x, t) C_b(x, t) > \mathcal{K} \\ 0, & \text{otherwise} \end{cases} \quad , \quad (\text{XI.22})$$

$\mathcal{K} \equiv K_1/\varepsilon^2 K_2$ being the *solubility product*. The equation for C_b is analogous to the one for C_a .

In the simulation, the a - and b -particles are mobile, whereas the c -particles are stationary. The reaction rule depends on the local numbers of a and b as in the case of the reaction $a + b \rightarrow c$ considered above, but it additionally depends on the numbers of reactants through the conditions for the onset of precipitation. Precipitation may namely occur only if there is solid already present or if the solution is saturated (the definition of ζ above is the mathematical equivalent of this statement). This leads to the following mesoscopic rule: If one or more c -particles are present at a site, one of them goes into solution in the form of an a - and a b -particle with probability P_1 . If N_a a -particles and N_b b -particles are present, then they may precipitate and form a c -particle only if at least one c -particle is already present or if the product of the densities of a and b (calculated by averaging over an ensemble of macroscopically identical systems) is greater than P_1/P_2 . If one or both of these conditions are fulfilled, precipitation is allowed to take place with probability $P_2 N_a N_b$. Particle densities are related to the physical quantities in Eq. (XI.21) by $C_a = \gamma \rho_a$, $C_b = \gamma \rho_b$ and $C_c = \gamma \varepsilon \rho_c$, where the scaling factor γ can be fixed by the

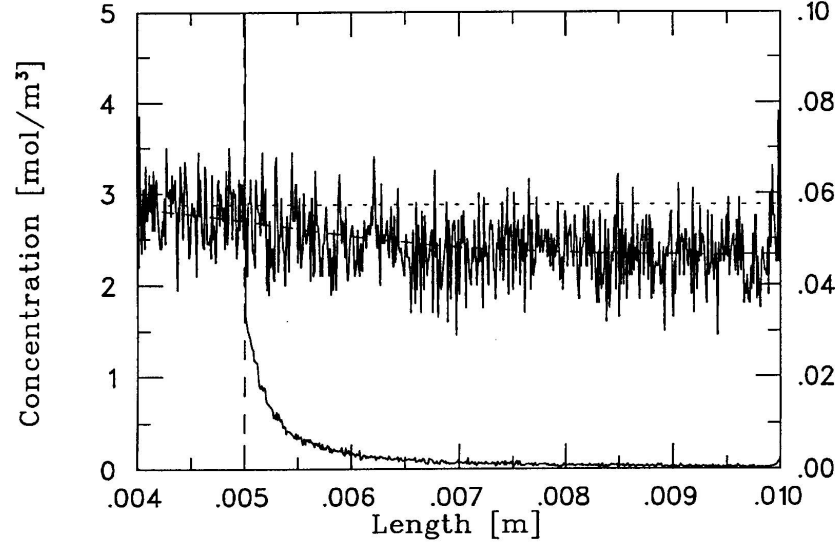
physical data and the initial conditions of the simulation. The reaction parameters are related to the rate constants by $P_1 = \tau K_1 / \gamma \varepsilon$ and $P_2 = \gamma \varepsilon \tau K_2$.

The CA model described above is now applied to a system with one-dimensional geometry (with translational invariance assumed in the other two dimensions). We look at the dissolution of a block of porous rock by an inert fluid flowing through it [95KAR, 95KAR2]. We consider a piece of rock of length of 1 cm, with a uniform porosity of $\varepsilon = 65\%$. The left half of the rock is occupied at time $t = 0$ by a soluble mineral with a density of 2.71 g/cm^3 and a molecular weight of 100. The rate constants for dissolution and precipitation are $K_1 = 1.3 \times 10^{-3} \text{ mol} \cdot \text{m}^{-3} \cdot \text{s}^{-1}$ and $K_2 = 0.93 \text{ m}^3 \cdot \text{mol}^{-1} \cdot \text{s}^{-1}$, respectively; they are compatible with a solubility product of $K = 10^{-2.48} \text{ mol}^2 \cdot \text{m}^{-6} = 10^{-8.48} (\text{mol/l})^2$. The physical and chemical parameters are chosen to be consistent with calcite (CaCO_3) as a typical mineral in the geological systems of interest. The value of K_1 in particular follows from the value of the dissolution rate per unit surface of mineral, $K_{1s} = 6.5 \times 10^{-11} \text{ mol} \cdot \text{cm}^{-2} \cdot \text{s}^{-1} = 6.5 \times 10^{-7} \text{ mol} \cdot \text{m}^{-2} \cdot \text{s}^{-1}$ obtained in an investigation of the pH dependence of the dissolution rate of various carbonates at 25°C using a fluidized bed reactor [89CHO/GAR]. To obtain the dissolution rate per unit volume of mineral, we have multiplied K_{1s} by a surface area to volume ratio of 20 cm^{-1} , which corresponds to grains of size 0.3-0.4 cm. It is clear that K_1 is inversely proportional to the grain size and a good knowledge of the latter is necessary for modelling dissolution kinetics in particular situations. The value of K_2 is then calculated from $K_2 = K_1 / \varepsilon^2 K$ and is consistent within 2-3% with the value of K_{2s} found independently in Ref. [89CHO/GAR]. The dissolved species Ca^{2+} and CO_3^{2-} move with an advection velocity of $V = 10^{-5} \text{ m/s} = 0.86 \text{ m/day}$ and a diffusion coefficient of $D = 10^{-9} \text{ m}^2/\text{s}$. For the simulation we choose $\lambda = 10^{-5} \text{ m}$, $\tau = 0.05 \text{ s}$ and $\gamma = 1.0 \text{ mol/m}^3$.

Fig. XI.7 shows the profiles of C_c and C_a at time $t = 10^4 \text{ s} = 2.8 \text{ h}$.

In the simulation we obtain net precipitation of solid downstream from the original solid edge. Due to fluctuations in the solute densities, the product of these densities occasionally exceeds the saturation threshold and precipitation ensues. This effect is absent from the macroscopic description, where the edge remains sharp. The net precipitation of solid in the right half of the lattice is accompanied by a reduction in solute concentration relative to the prediction of the macroscopic equations. Of course the amount of solid that is found downstream of the edge is tiny on the scale of the total amount of solid, but the consequences can be more serious for the concentration of solutes. In Fig. XI.7, of 7.3 million solid particles initially present, about 750 have been removed from the solid block and about 110 have precipitated in the right half of the lattice. This suffices however to produce a 20% suppression in the solute concentration, as a comparison of the dotted and dashed curves shows. Simulations show that the downstream precipitation of solid and the suppression of solute concentration diminish as we reduce the magnitude of the statistical fluctuations by increasing the size of the ensemble over which we average. Since the particles of our simulations do not model individual molecules of the actual system, the interpretation of statistical fluctuations and their consequences is not immediately obvious. We can assume a phenomenological point of view, allowing for microscopic processes not explicitly accounted for to contribute to the fluctuations present in our

Figure XI.7: Profile of solute concentration (horizontal dotted line and solid line running on the average parallel to it: reaction transport equations and CA, respectively; the short-dashed line is a smoothed version of the solid line; axis labelled on the right) and the “concentration” of solid per m^3 of rock (vertical long-dashed line and solid line running partly parallel to it: reaction transport equations and CA, respectively; axis labelled on the left).



model. Then one has to normalise the amplitudes of the fluctuations by comparing the size of the resulting effects with real systems. The impact of the observed effect will therefore depend on the problem at hand. For times long enough for precipitation/dissolution to cause changes in the porosity, it is likely to influence those changes, to a degree however that remains to be investigated.

Remarkably, the effect described above occurs only in the presence of advection and is absent when diffusion is the only transport mechanism. The dependence of the effect on the physical parameters of the problem was studied in Ref. [95KAR2]. It was found there that the suppression of solute concentration downstream from the solid edge persists up to the longest times t for which the simulation can be performed without exceeding a week of CPU time. If one varies the relative time scales for transport (especially advection) and reactions, then the effect of fluctuations is washed out when the reaction kinetics is not fast enough to keep up with transport. The effect appears clearly only when transport is slow relative to the kinetics. These observations underline the important role of advection in the interplay between transport and chemistry. The ability of the mesoscopic model used here to account for advection clearly opens a wide field of interesting phenomena to be investigated.

As another example of a heterogeneous process we take up the catalytic oxidation of CO(g) on platinum (Pt) surfaces. This process was investigated in Ref. [92WU/KAP] from the point of view of the interplay between sorption kinetics, reactions and surface phase transformations. The basic process consists of the following steps: gaseous CO and O₂ adsorb on sites of the Pt(cr) surface and O₂ molecules dissociate to O atoms, which oxidise adsorbed CO to form CO₂. The adsorption rates of CO(g) and O₂(g) depend on the availability of free surface sites. Adsorbed CO and O may of course desorb before they react, but, once they react, CO₂ desorbs rapidly. If ρ_1 and ρ_2 are the densities of adsorbed CO and O respectively (note that 1 and 2 are here species labels, the summation over velocity states having already been performed) and ρ_0 the (constant) density of adsorption sites (free + occupied), one can write down schematically the rate equations

$$\begin{aligned}\frac{d\rho_1}{dt} &= k_1 p_{\text{CO}} (\rho_0 - \rho_1 - \rho_2) - k_{-1} \rho_1 - k_0 \rho_1 \rho_2 \\ \frac{d\rho_2}{dt} &= k_2 p_{\text{O}_2} (\rho_0 - \rho_1 - \rho_2)^2 - k_{-2} \rho_2^2 - k_0 \rho_1 \rho_2 \quad ,\end{aligned}\tag{XI.23}$$

where k_1 (k_{-1}) and k_2 (k_{-2}) are the adsorption (desorption) rate constants of CO and O₂, p_{CO} and p_{O_2} are the respective partial pressures and k_0 is the rate constant for the surface reaction $\text{CO} + \text{O} \rightarrow \text{CO}_2$. The first term on the right hand side of both rate equations makes explicit the dependence of adsorption rates on the density of free sites.

If the CO-O reaction takes place on the Pt(100) crystallographic plane, then the surface may undergo phase transformations, depending on the fraction of sites covered by CO. Thus, if the surface is in the hexagonally ordered phase (hex) and the CO coverage exceeds $\sim 90\%$ a transition occurs to the (1×1) phase characterised by a square lattice of surface atoms on which CO molecules occupy alternate sites. When the CO coverage falls below $\sim 30\%$ the reverse surface transformation takes place. Since a reorganisation of the surface affects the sorption rates and, hence, the oxidation kinetics, the coupling between the different processes can induce oscillations in the surface concentration of the reactants and the fraction of sites in each phase. These oscillations proceed by means of the appearance and growth of domains of one phase in the midst of the other, coupled with the diffusion of adsorbed particles across the domains. Such oscillatory behaviour has been observed experimentally [84NOR/BIN].

The model of Ref. [92WU/KAP] applies an exclusion principle, as described in Section XI.3.1, making sure, however, that the reactive transitions at the mesoscopic level are only those implied by the rate law Eq. (XI.23). Extending the notation used earlier for one-species systems, we introduce the probability $P(\boldsymbol{\alpha}\boldsymbol{\beta})$ for the transition $\alpha_1 \text{CO} + \alpha_2 \text{O} \rightarrow \beta_1 \text{CO} + \beta_2 \text{O}$, with $\boldsymbol{\alpha} \equiv (\alpha_1, \alpha_2)$ and $\boldsymbol{\beta} \equiv (\beta_1, \beta_2)$. $P(\boldsymbol{\alpha}\boldsymbol{\beta})$ is written as

$$\begin{aligned}P(\boldsymbol{\alpha}\boldsymbol{\beta}) &= p_1(\boldsymbol{\alpha}) \delta_{\beta_1, \alpha_1+1} \delta_{\beta_2, \alpha_2} + p_2(\boldsymbol{\alpha}) \delta_{\beta_1, \alpha_1-1} \delta_{\beta_2, \alpha_2} + p_3(\boldsymbol{\alpha}) \delta_{\beta_1, \alpha_1} \delta_{\beta_2, \alpha_2+2} \\ &\quad + p_4(\boldsymbol{\alpha}) \delta_{\beta_1, \alpha_1} \delta_{\beta_2, \alpha_2-2} + p_5(\boldsymbol{\alpha}) \delta_{\beta_1, \alpha_1-1} \delta_{\beta_2, \alpha_2-1} \quad .\end{aligned}\tag{XI.24}$$

In Eq. (XI.24), the $p_i(\boldsymbol{\alpha})$, $i = 1, \dots, 5$, are the probabilities for CO adsorption and

desorption, O adsorption and desorption, and CO oxidation, respectively:

$$\begin{aligned}
 p_1(\boldsymbol{\alpha}) &= \begin{cases} \bar{k}_1(m - \alpha_1 - \alpha_2) , & \text{if } \alpha_1 + \alpha_2 < m , \\ 0 , & \text{if } \alpha_1 + \alpha_2 \geq m , \end{cases} \\
 p_2(\boldsymbol{\alpha}) &= \bar{k}_{-1}\alpha_1 , \\
 p_3(\boldsymbol{\alpha}) &= \begin{cases} \frac{1}{2}\bar{k}_2(m - \alpha_1 - \alpha_2)(m - 1 - \alpha_1 - \alpha_2) , & \text{if } \alpha_1 + \alpha_2 < m - 1 , \\ 0 , & \text{if } \alpha_1 + \alpha_2 \geq m - 1 , \end{cases} \quad (\text{XI.25}) \\
 p_4(\boldsymbol{\alpha}) &= \frac{1}{2}\bar{k}_{-2}\alpha_2(\alpha_2 - 1) , \\
 p_5(\boldsymbol{\alpha}) &= \bar{k}_0\alpha_1\alpha_2 .
 \end{aligned}$$

If one chooses the parameters \bar{k}_i according to

$$\begin{aligned}
 \bar{k}_0 &= k_0 , \quad \bar{k}_1 = k_1 p_{\text{CO}} , \quad \bar{k}_{-1} = k_{-1} \\
 \bar{k}_2 &= \frac{m}{m-1} k_2 p_{\text{O}_2} , \quad \bar{k}_{-2} = \frac{m}{m-1} k_{-2} , \quad (\text{XI.26})
 \end{aligned}$$

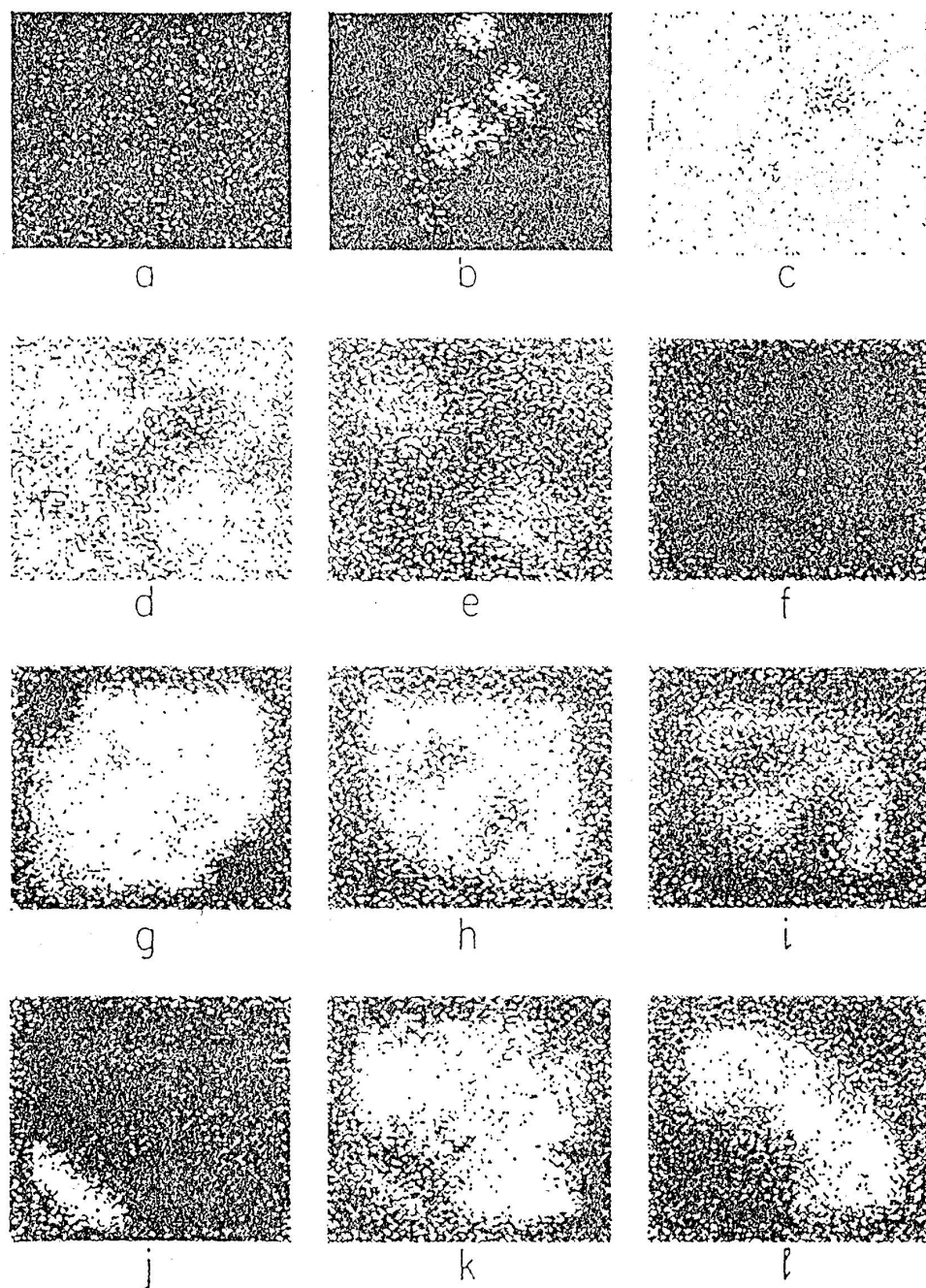
one obtains upon averaging and taking the continuum limit rate equations very similar, but not identical, to Eq. (XI.23). There is a clear connection between the different terms in the rate equations (XI.23) and the corresponding expressions for the $p_i(\boldsymbol{\alpha})$, which are reminiscent of Eq. (XI.9) ⁵. Eqs. (XI.24), (XI.25) and (XI.26) define the mesoscopic reaction dynamics.

The phase transformations of the surface can also be modelled by a CA rule. Thus one ascribes each site to one of two phases and allows it to make a transition to the other phase with a certain probability, if the local CO coverage crosses a certain critical value. The CO coverage at a site is defined by counting the number of CO molecules in a neighbourhood consisting of the site itself and its nearest neighbours. The phase transition couples back to the adsorption and reaction kinetics, since the reaction rates k_i have different values for each phase.

Fig. XI.8 shows the oscillations in the CO surface density obtained for a particular choice of the physicochemical parameters [92WU/KAP]. Initially most of the sites are in the hex phase which adsorbs O much more weakly than the (1×1) phase. As a result the CO density increases (Fig. XI.8a), the critical coverage for transition to the (1×1) phase is locally exceeded and domains of that phase begin to appear and spread (Fig. XI.8b). These domains adsorb O at a high rate and cause oxidative depletion of the CO molecules that are originally present in their interior, as well as of those that arrive there by diffusion. Thus the new phase wins gradually over and the density of adsorbed CO diminishes (Fig. XI.8c). When, however, the CO coverage falls locally below a certain critical value, domains of the original phase begin to appear and spread (Figs. XI.8d,e) and the CO density increases again (Fig. XI.8f). Thus the relatively

⁵ The α_i in Eq. (XI.25) cannot exceed, however, the number of possible velocity states and obey a binomial distribution at equilibrium, whereas the N_α in Eq. (XI.9) are unrestricted and have a Poisson equilibrium distribution.

Figure XI.8: Oscillations in CO surface density obtained from two-dimensional simulation of CO catalytic oxidation on the Pt(100) plane. (reprinted with permission from Ref. [92WU/KAP], Fig. 5). The frames (a)-(l) are for times $t = 100$ -1200 at equally spaced time intervals of 100 time steps. The simulation was carried out on a 100×100 hexagonal lattice with periodic boundary conditions. For the values of system parameters used in the simulation the reader is referred to [92WU/KAP].



simple CA we are considering here is capable of reproducing the experimentally observed oscillatory behaviour. Moreover, as the Pt surface oscillates in space and time between the two phases, which are characterized by different reaction rate constants, the present application illustrates the capacity of CA models to describe systems with spatially and temporally varying parameters.

It should be remarked that both models of heterogeneous processes that we have presented are relatively simple. They already show the potential of the mesoscopic method to describe interesting physical behaviour, but they should rather be taken as the basis for more elaborate and realistic models.

XI.4. Conclusion

The models of reaction-transport phenomena discussed in this chapter occupy a position intermediate between the standard macroscopic approach of partial differential equations (PDE's) and the fully microscopic approach of molecular dynamics. We have indicated with several examples that there is a wide range of physical phenomena for which the mesoscopic point of view provides the necessary amount of detail (that PDE's cannot afford) and optimises the use of resources (by neglecting inessential details of the microscopic dynamics). Cellular automata (CA) describe transport and chemical reactions at an elementary level, keeping, however, only those aspects of the microscopic dynamics which are important for the problem at hand. Due to their simplicity, CA models are conceptually transparent and can be transcribed into simple computer code. This is a significant advantage when it comes to modelling complex geometries and boundary conditions or the kinetics of arbitrary chemical reactions. CA algorithms iterate integer variables and are therefore free of round-off errors and associated instabilities. This remains true for the stochastic CA models considered here, since real numbers appear only as bounded probabilities. By being faithful to the local and parallel character of the physical processes they model, cellular automata are suitable for implementation on massively parallel computers. It should be emphasised that it was largely the dramatic progress in computer hardware and architecture in recent years that made CA modelling of natural phenomena technically possible.

The models we have discussed simulate the transport of particles as a random walk on a regular spatial lattice. When the particles meet at a lattice site, they react chemically and are transformed according to a local probabilistic rule. Radioactive decay, sorption on conduit walls and the dissolution of solids are also modelled by simple probabilistic rules. We have presented a model which places no restriction on the number of particles that can be found at a site, as well as one derived from lattice gas automata for fluid dynamics, which allows only a small set of possible velocity states to each particle. The "particles" in both models are mathematical abstractions of the actual molecules of the physical system. The number of particles is large enough to make statistical concepts meaningful, but is still many orders of magnitude smaller than the real number of molecules involved. Mesoscopic modelling relies crucially on the assumption that this is legitimate, provided that the macroscopic behaviour of interest does not depend on the details of the microscopic

dynamics, but follows from general properties of the latter. Of the two models, the former has the merit of being able to account for advection by imparting a directional bias to the random walk and of modelling chemical reactions in a more transparent and flexible way. The lattice gas model, on the other hand, offers substantial computational advantages: thanks to the limited number of allowed particle configurations at a site, it can be programmed at bit level (thus making optimal use of computer memory and processing power) and updating can be optimised by using look-up tables (which contain stored all elementary events that can take place at any site). The ability to describe advection and a relative ease in the inclusion of various chemical reactions are indispensable for modelling coupled transport and reaction phenomena in geological media, but computational performance is an important criterion of the usefulness of a model as a practical tool. Despite the recent advances in computer resources, computational efficiency still has to be reckoned with, especially for problems of the complexity we wish to address. It is therefore desirable to combine the advantages of the simple and more flexible model with the experience accumulated with numerous specific applications of lattice gas models.

In the simulations discussed here, the transport of solutes was modelled assuming that their advection followed a given velocity field. If the solute concentration is small enough, the velocity field coincides with that of pure water flowing under the given mechanical conditions. The dynamics of water flow is governed by the Navier-Stokes equations, which for a porous medium go over to Darcy's law. Although the applications presented here involved only uniform flows, the transport model without an exclusion principle was formulated for an arbitrary flow field. In general the problem of solute transport can be solved by a two-step procedure, where one first solves the appropriate hydrodynamic equations and then uses the resulting velocity field as an input parameter to the model describing solute transport. This approach is conceptually similar to the Lagrangian approach for modelling tracer transport in geological formations (*e.g.*, Ref. [82PRI/NAY]). Chemical reactions can be added and the full algorithm iterated in time. If the porosity and the permeability of a porous medium change substantially as a result of chemical reactions, the influence of these changes on water flow have to be explicitly considered.

To quantify computational efficiency in CA simulations, one usually introduces the concept of site updates per second (u.p.s.). The density of particles has an influence on updating speed, but, except for simulations with very different particle densities, it is useful to compare the performance of various algorithms in terms of u.p.s. We consider first the model with no *a priori* limitation on the number of particles per site. The simulation of the reaction $a + b \rightarrow c$ that produced the solid curve in Fig. XI.4, had an average performance of 1.2×10^6 u.p.s. and required about 16 CPU hours on a massively parallel Connection Machine (CM-200). The pattern shown in Fig. XI.5 took about 30 CPU hours at a rate of 2×10^4 u.p.s. on a VAX-9000 in scalar mode (the simulation of the reaction $a + b \rightarrow c$ on the same computer was roughly a factor of 4 less efficient than on CM-200). The simulations can be made faster by utilising a low-level instruction set available on the Connection Machine, but this would impair the transparency of the code. The potential of application-specific optimisation becomes clear if we compare the above rates with those achieved with specialised lattice gas models. Thus, the reaction $a + b \rightarrow c$

was simulated with a lattice gas model using a look-up table on a CRAY-YMP at a rate of 2×10^7 u.p.s., while a four times higher rate was attained on a CM-2a (typically slower than CM-200 by a factor of 2) [91CHO/DRO2]. It should be mentioned, however, that the code without limitation on particle number was applied unmodified to the case with advection (the dashed curve in Fig. XI.4) at no cost in performance, whereas advection lies beyond the scope of the lattice gas model.

The relative merits of different CA models and standard numerical methods for the solution of the corresponding PDE's depends on the specific applications. Thus, with present-day computers, pattern formation in autocatalytic reaction systems can be studied in general more efficiently with conventional methods; if, however, one is interested in the rôle of fluctuations, the mesoscopic approach provides a powerful alternative. It is, therefore, important to seek areas of applications where each method maximises its advantages. CA models are very well suited for describing transport with inhomogeneous and time-varying parameters. They also naturally describe the chemical kinetics of systems which are not in chemical equilibrium. According to the discussion in the Introduction, the guaranteed stability of CA algorithms is a valuable asset when non-linear processes come into play. Finally, the ability of cellular automata to accommodate arbitrary boundary conditions (including moving boundaries) has not been sufficiently exploited so far. Among potential applications suitable for CA modelling, of particular theoretical and practical interest are the interaction of solutes with the solid surfaces of porous and fractured media and the coupling of porosity changes, induced by precipitation/dissolution, with solute transport. CA models appear to be particularly called for when, for example, the physical processes of interest show strong variations in space [92SAR/BRA] or when chemical reactions are slow compared to transport [90WOL]. It is in such cases, where conventional methods are confronted with serious conceptual and technical problems, that cellular automata can best utilise their potential for incorporating microscopic detail in the macroscopic description of the physical world.

XI.5. Acknowledgements

A large fraction of the author's original work presented in this article was performed in collaboration with B. Blankleider, now at Flinders University (Australia). The author has also benefited a great deal from discussions with U. Berner, J. Hadermann, F. Neall (PSI, Switzerland), B. Chopard, M. Droz (Université de Genève), J.-P. Boon and D. Dab (Université Libre de Bruxelles). D. Dab kindly provided one unpublished figure. Partial financial support by NAGRA is gratefully acknowledged.

Chapter XII

Modelling Solute Transport Using the Double Porous Medium Approach

Andreas JAKOB
Paul Scherrer Institut
Würenlingen and Villigen
CH-5232 Villigen PSI (Switzerland)

XII.1. Introduction

We encounter transport phenomena in every day life: when heating water for coffee, when using electric implements; even the soil-water rising in plants is a transport phenomenon. These flow or transport processes include heat flow, electric current, mass transfer, or more complex processes such as the movement of chemically reactive, viscous and heat-conductive fluids, galvano electric effects, *etc.* Such processes are governed by laws which will be partially addressed in this chapter. It is evident that a sound theoretical understanding of the principles of these transport *processes*¹ is essential for those who work in pure or applied physics, physical chemistry, soil physics, meteorology, biology and those dealing with the long-term behaviour of hazardous waste repositories.

The basic physics of transport phenomena is described by non-equilibrium thermodynamics, which is the frame for the macroscopic description of irreversible processes. We confine our discussion to laminar flows and transport processes only; turbulent flow is not considered in the following. The treatment of transport phenomena as such is part of macroscopic physics and is related to other macroscopic disciplines like fluid dynamics and electrodynamics. The media in which transport phenomena occur are regarded as

¹ Words written in *italics* are explained in a glossary at the end of this chapter.

continua, and processes on a microscopic scale are not considered. The advantage of using macroscopic equations is obvious. A microscopic description would typically require a system of about 10^{23} coupled differential equations (the set of equations of motion) to be solved with the pertinent number of parameters. It would be a hopeless task to try to solve such a system of equations in a reasonable time span. Instead one must replace the microscopic quantities by the macroscopic continuum quantities by using a carefully chosen *REV* (*Representative Elementary Volume*). This procedure is based on the idea that there exists a scale for the *porous medium* below which the microscopic equations have to be allied, and above which the geometry of the phases can be averaged. By doing this, the porous medium is replaced by a fictitious continuum at the macroscopic scale. The unknown details on the microscopic scale are replaced by a few averaged parameter values at the macroscopic scale. These averaged parameter values can be measured in suitable experiments and used in macroscopic equations to arrive at a predictive model.

The first objective of this chapter is to give a short and rather qualitative overview of the large domain of non-equilibrium thermodynamics. Our aim is to present some transport phenomena which can be described by similar mathematical equations. However, it is not our purpose to present a formal description of all the effects and to discuss their consequences in detail. This can be found in a textbook. Our approach is not a sophisticated one; after the introduction, we will restrict the transport phenomena to those which are described by Fick's law - *i.e.*, by mass transport due to a concentration gradient.

Using a simple continuum model² for transport of a solute in porous media we will highlight some aspects of the concept of Fickian dispersion but also mention its principal limitations. One such limitation is the still-open question of the scaling-up of the values for the dispersivity tensor obtained from small-scale experiments. We will see that the Peclet number (*cf. p.535*) is of little importance for this problem contrary to the Reynolds number in fluid dynamics (*cf. footnote on page 536*). Other limitations are due to the effects of a fracture network or channelling.

For the solute/rock interactions, we will restrict ourselves to sorption processes which can be formulated with the help of an isotherm formalism and we will neglect more complicated processes such as precipitation and dissolution, redox-reactions, *etc.*

As an additional important transport mechanism we will discuss the influence of unlimited and limited matrix diffusion in the frame of the double porosity medium concept. When molecular diffusion of a solute into the adjacent rock matrix beneath a fracture is sufficiently fast, the effect of matrix diffusion can be estimated with high precision using the effective surface sorption approximation. Its efficiency and simplicity makes this approximation an appreciated and fast "tool" for a modeller.

Physics describes reality with the help of *models*, and models are abstractions, *i.e.* descriptions which consider only certain aspects of nature. Moreover, a given physi-

² At this point we would like to refer to the article by T. Karapiperis in this book (Chapter XI), wherein coupled transport and chemical reactions are modelled by means of a cellular automaton in discrete space and time. This approach is especially appropriate for the class of problems lying in the intermediate region between the macroscopic and microscopic length scales (≈ 1 cm and ≈ 1 Å, respectively), such as, *e.g.*, the evolution of porosity as a result of solute-mineral reactions.

cal phenomenon can be described by different models using different assumptions and approximations and with different degrees of sophistication according to the individual requirements. Both the complexity and the accuracy of models are important issues. In order to decide on the adequacy and accuracy of models, they have to be compared with experiments, and differences have to be ascertained. With this procedure one tries to quantify the quality of a given model, *e.g.* by determining the minimum value of the χ^2 -merit function by fitting experimental data with a suitable model. A real test for a model, however, is its predictive capacity for experimental data or even of new phenomena. Therefore, in the last section, we will discuss experimental data from various experiments and compare them with different continuum concepts. By starting with a simple model (*e.g.* the “equivalent porous medium model”), comparing the model with experimental data, ascertaining the differences quantitatively, refining the concept (*e.g.*, using the “double porosity medium model”) and arriving at a deeper knowledge, we will demonstrate the iterative procedure of modelling and also point out open questions and unresolved problems.

XII.2. Classification of transport phenomena

There are different ways to organise a discussion of transport phenomena. A simple classification based on the entity being transported results in the following scheme:

- transport of momentum [Ns],
- transport of energy (heat) [Nm],
- transport of electrical charge [C],
- transport of mass [kg].

It is a natural tendency among *closed physical systems* out of equilibrium to approach a state of equilibrium by transport of an entity. These are the spatial inhomogeneities (a difference) of a quantity which start the transport of another (*extensive*³) quantity. Transport - a flow (or current or transfer) - of a quantity occurs due to a “driving force”. Examples of driving forces are, *e.g.*, a spatial difference in the velocity field, in temperature, in the concentration or, in a generalised thermodynamic potential. If a given (thermodynamic) state is not too far away from equilibrium, it is reasonable to assume a linear relationship between flux⁴ and driving force. This means that in a first approximation, the flux is a linear function of the driving force⁵. This phenomenological relationship

³ The transported quantity is *extensive*, whereas the quantity causing transport is *intensive*.

⁴ By the term “flux” we mean “rate of flow per unit area” (*e.g.*, [Current density] = $\frac{C}{m^2s}$, or [Diffusive flux] = $\frac{mole}{m^2s}$).

⁵ Certain irreversible processes should be described by non-linear relations. However, the adequate description of such processes is beyond the scope of this chapter and will not be considered here. Thus, “ordinary” transport phenomena, such as heat conduction and electric current are approximated by linear relations, even if the experimental conditions are rather extreme, whereas chemical reactions must be described by non-linear relations.

Table XII.1: Table of coupled processes.

Flux	Driving force (gradient of)			
	Hydraulic head	Temperature	Electric potential	Concentration
Volume/Fluid	Darcy's law	Thermal osmosis	Electro osmosis	Chemical osmosis
Energy/Heat	Thermal filtration	Fourier's law	Peltier effect	Dufour effect
Electric charge	Rouss effect	Seebeck effect	Ohm's law	Sedimentation current
Mass	Ultrafiltration	Soret effect	Electrophoresis	Fick's law

between the gradient $\vec{\nabla}$ of a quantity φ - the driving force - and the flux \vec{j} ⁶ is of the form:

$$\vec{j} = -\mathbf{C} \cdot \vec{\nabla} \varphi \quad (\text{XII.1})$$

with the transport coefficient \mathbf{C} . For example, a velocity gradient causes a momentum flux; a temperature gradient a heat flux; or a gradient of the electrical potential the transport of charge, *etc.* But things are even more complicated. It is a well-known fact that electrically charged particles (*e.g.*, ions) also carry mass. Hence, an electric current, due to the gradient of the electrical potential, is automatically coupled with mass transfer, a process established in science and technology under the name of electrophoresis or electro-osmosis. In addition, a concentration gradient causes mass transport, a process which is accompanied by a viscous flow, known as chemical osmosis. Indeed, experiments show that transport of an entity may be caused by different gradients, and therefore Eq. (XII.1) should actually be expressed as a sum of all possible gradients. Taking into account all combinations of gradients and fluxes, we end up with a matrix (the scheme) of the coupled transport processes.

There are practical reasons why volume/fluid flux rather than momentum flux is considered in Table XII.1. Hence, the hydraulic head gradient instead of the velocity gradient enters the scheme. (The word “law” for the effects in the diagonal of the matrix of coupled processes is traditional and also used here.)

The quantities \mathbf{C} in Eq. (XII.1) are phenomenological (transport) or kinetic coefficients and have to be determined experimentally. These coefficients are functions of the medium, composition, temperature, pressure, *etc.* More precisely, the transport coefficients of Table XII.1 are second rank tensors, and it is assumed that they are dependent on the local properties of a solid or mobile phase and possibly also on the local value of φ , but not on $\vec{\nabla} \varphi$. As examples, some of the (diagonal) coefficients are listed below:

- the hydraulic conductivity \mathbf{K} [m/s] in the case of volume/fluid flux,
- the thermal conductivity κ [W · m⁻¹ · (°K)⁻¹] for transport of energy/heat,

⁶ In most cases φ is a *scalar* and \vec{j} a *vector*. If, in addition, the medium is *isotropic*, \vec{j} points in the direction of the most rapid decrease of $\varphi(\vec{r})$, which is the reason for the minus sign in Eq. (XII.1). (However, if φ is the velocity \vec{v} , then $\vec{\nabla} \vec{v}$ and \vec{j} are *tensors*.)

- the electrical conductivity σ $[(\Omega \cdot \text{m})^{-1}]$ for transport of electrical charge,
- the diffusivity D $[\text{m}^2/\text{s}]$ for transport of mass.

For a homogeneous material, \mathbf{C} can only depend on position through any dependence of φ . For *isotropic* materials, \mathbf{C} must have a form which is independent of all spatial directions; hence all sets of orthogonal axes must be principal axes of the coefficient matrix \mathbf{C} which is only possible when $C_{ij} = C\delta_{ij}$.

As mentioned before, to consider each process and its effect in the matrix of coupled processes (Table XII.1) in detail would be beyond the scope of this chapter. If additional information on particular processes are requested, more details can be obtained from the relevant literature [59LAN/LIF, 60BIR/STE, 86MAR3, 88BRO/HER, 89DAG, 91BEA/BAC, 94BAT].

XII.3. Mass transport due to a concentration gradient

Following these general remarks on transport phenomena we now focus on mass transport as a result of a concentration gradient⁷ and we will discuss in more detail some mechanisms which can have a strong influence on mass transport, such as dispersion, sorption, matrix diffusion, *etc.* For the following we assume that transport of a dissolved substance takes place in a (fractured) porous medium.

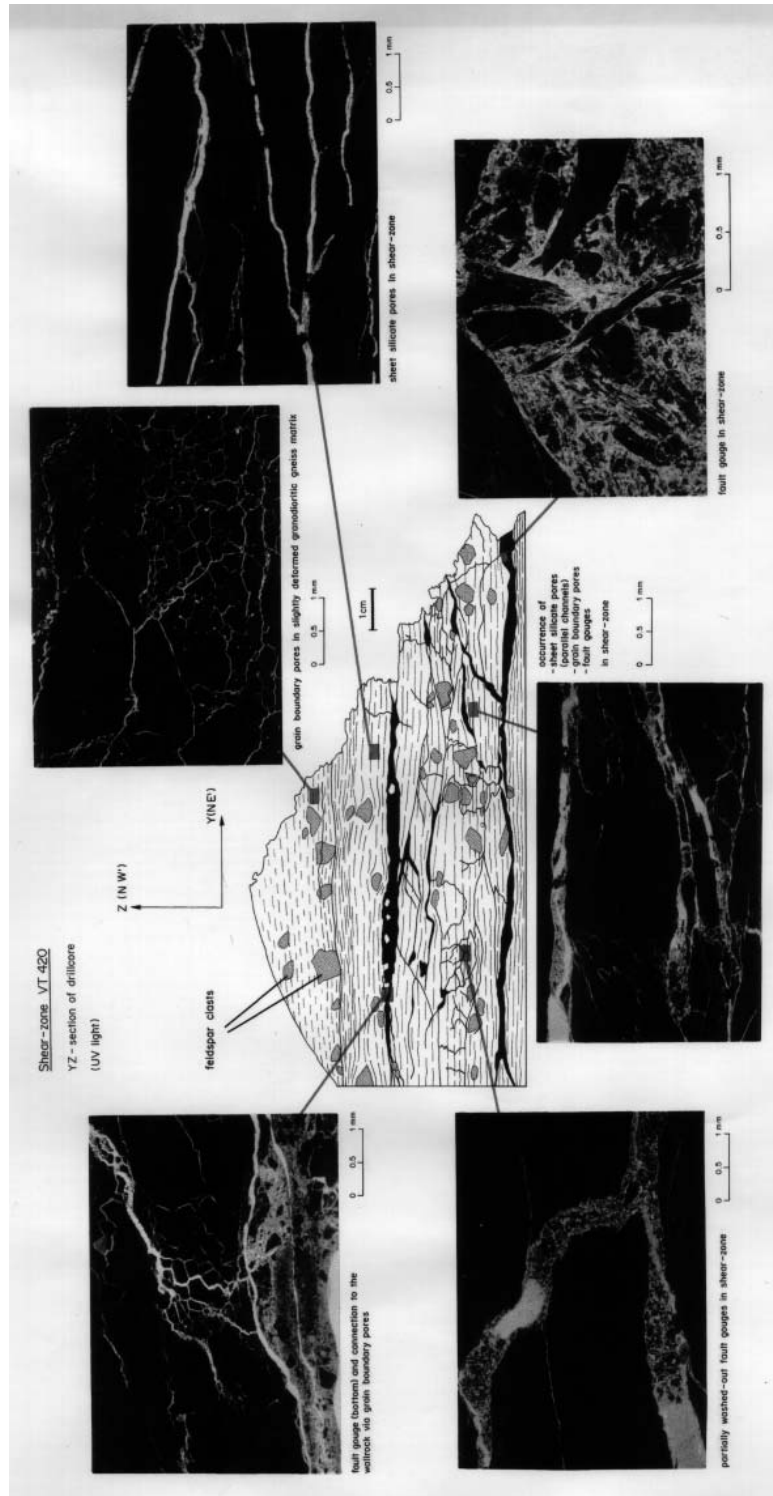
Structural geological studies of bore cores give information about the mineral composition, the heterogeneities of the rock, and on the degree of anisotropy and persistency of flow paths. Such investigations also allow assumptions to be made about the porosity and the maximum penetration depth for matrix diffusion. When viewed from the local scale, it seems that geological systems are too complex - even for a description using rather sophisticated models. This is because complicated flow patterns can be recognised which may be associated with grain boundaries of minerals and pore spaces; other flow paths are simple cracks with or without mineral infill. For illustration, we have included some pictures where individual macroscopic features are magnified and disintegrated into micro-structures (see Figure XII.1). This gives an impression of the variability of flow paths and patterns as they appear in a drillcore from granitic rock.

XII.3.1. Fickian dispersion

In a uniform fluid flow field of a single phase, a spherical domain contaminated by a tracer would progress without any spreading. However, slow mixing will occur due to Brownian motion of the particles, *i.e.* by molecular diffusion. Therefore, the shape of such a traced domain will remain spherical, and the whole domain will increase but with an average

⁷ In 1931 Hartley [31HAR] showed that it is the gradient of the chemical potential rather than the gradient of the concentration which pushes the diffusion process. For our purposes the concentration of a dissolved species will be assumed to be low, so that the gradient of the thermodynamic activity of the dissolved species can be well approximated by the gradient of its concentration. In such a case a concentration gradient can be assumed for the driving force for mass transfer.

Figure XII.1: Sections through a drillcore of granite from the Grimsel underground laboratory (Switzerland). There is a relation between macroscopic deformation features (cleavage trajectories stippled, fault gauges black in the sketch) and the microscopic distribution of flow paths in the micrographs (reprinted with permission from [91BOS/MAZ]).



concentration decreasing with time. Normally, media in which transport takes place are heterogeneous - they are “disordered” on a microscopic scale (*e.g.*, porous media) - and show an additional mixing which is often larger by orders of magnitude than the spreading due to pure molecular diffusion. Such additional spreading of an initially narrow tracer pulse is due to mechanical dispersion. This mechanism is part of the hydrodynamic dispersion, \mathbf{D} , which is the sum of the coefficient for mechanical dispersion \mathbf{D}_{mech} [m^2/s] and that for the molecular diffusion \mathbf{D}_{diff} [m^2/s]:

$$\mathbf{D} = \mathbf{D}_{\text{mech}} + \mathbf{D}_{\text{diff}} . \quad (\text{XII.2})$$

With the term mechanical dispersion we denote the drift of tracer particles in a liquid due to microscopic variations of the fluid flow field. Friction of fluid particles on surfaces of the solid phase reduce irreversibly the velocity of these particles. The size and the orientation of micropores have a statistical distribution, therefore, also changing the direction of flowing particles and, at the same time, causing spreading of a substance at right angles to the main flow direction. Dispersive effects are regarded separately from convection, but this is rather arbitrary because averaging over a domain of a porous medium yields a macroscopic dispersive tracer flux in addition to an averaged macroscopic advective tracer flux. The mechanical dispersion is the result of a real and highly complex - and in principle unknown - velocity field on the microscopic scale. Variations in the velocity field mainly cause solute dispersion. It would therefore be completely inadequate to take into account only convection and molecular diffusion as mixing phenomena. For the mathematical treatment of mechanical dispersion, it is very common to assume an expression analogous to that for molecular diffusion - hence, a formula which is also of the Fickian type:

$$\vec{j}_{\text{mech}} = -\varepsilon \mathbf{D}_{\text{mech}} \cdot \vec{\nabla} C . \quad (\text{XII.3})$$

In this equation \vec{j}_{mech} means the (mechanical) dispersive flux in a porous medium (with porosity ε) which is mass per unit area of porous medium and unit time of a migrating species. We can see that the expression for the Fickian dispersion may not be appropriate. Eq. (XII.3) implies that \mathbf{D}_{mech} is a property of matter as is the diffusivity. However, as mentioned above, dispersion is a consequence of a velocity distribution and hence cannot be a property of matter only. It is dependent on the structure of the inhomogeneities of the solid phase which causes the velocity distribution and the fluid flow field.

The most simple geometry for modelling transport of a solute is that of a porous medium assumed to be macroscopically *homogeneous* and isotropic. For the following considerations we will use Cartesian co-ordinates and we will put its origin so that the z -axis coincides with the direction of the averaged pore water velocity - $\langle \vec{v} \rangle$. In a concept with such a simple underlying geometry, the transport coefficients are constant in space and time, and the dispersion tensor is diagonal. Moreover, in such a case the tensor \mathbf{D}_{mech} is a function of two scalar quantities only and \mathbf{D}_{diff} is also a scalar quantity, representing the pore diffusivity:

$$\begin{aligned}
 \mathbf{D} &= (D_{ij}) \\
 &= \begin{pmatrix} D_T + D_{\text{diff}} & 0 & 0 \\ 0 & D_T + D_{\text{diff}} & 0 \\ 0 & 0 & D_L + D_{\text{diff}} \end{pmatrix} \\
 &= \begin{pmatrix} a_T < |\vec{v}| > + D_{\text{diff}} & 0 & 0 \\ 0 & a_T < |\vec{v}| > + D_{\text{diff}} & 0 \\ 0 & 0 & a_L < |\vec{v}| > + D_{\text{diff}} \end{pmatrix}. \quad (\text{XII.4})
 \end{aligned}$$

$D_L = a_L < |\vec{v}| >$ is called the coefficient for the longitudinal dispersion, whereas $D_T = a_T < |\vec{v}| >$ is the coefficient for the transverse dispersion, both being macroscopic quantities and having the dimension $[\text{m}^2/\text{s}]$. The tensor \mathbf{D} is anisotropic even for isotropic media, because the mixing is larger in the direction of the velocity vector than in transverse directions. Therefore Eq. (XII.4) is only valid for uniform flow; otherwise the principal axes (being linked to the mobile and not to the solid phase) for \mathbf{D} would vary over the flow domain.

The mass balance equation governing the transport of a non-reactive (non-sorbing) and non-decaying solute by a fluid with constant density and viscosity through a porous medium is given by (note: the porosity ε cancels out if it is constant):

$$\frac{\partial C}{\partial t} = -\text{div } \vec{j}_{\text{conv}} - \text{div } \vec{j}_{\text{disp}} = -\vec{\nabla} \cdot (\vec{v} C) + \vec{\nabla} \cdot (\mathbf{D} \cdot \vec{\nabla} C). \quad (\text{XII.5})$$

This expression is called the transport equation for convection (advection⁸) and dispersion and is, in general, three-dimensional. Advection/convection describes the mean transport rate of a solute and hydrodynamic dispersion explains the variation of the mean. Due to lack of data, one may have to use a simplified geometry for the transport. The equation is often reduced to two or even one dimension, but this restriction should be justified on the basis of plume observations in the laboratory or in field experiments.

Let us now briefly discuss the one dimensional case, neglecting molecular diffusion. Flow takes place in the z -direction. Eq. (XII.5) is then reduced to:

$$\frac{\partial C}{\partial t} = a_L < |\vec{v}| > \frac{\partial^2 C}{\partial z^2} - < |\vec{v}| > \frac{\partial C}{\partial z}. \quad (\text{XII.6})$$

This equation has been extensively used to describe the transient distribution of solute concentrations. Its popularity is based on the fact that it describes successfully a variety of contaminant transport observations and also that an analytical solution can be obtained for simple initial and boundary conditions.

⁸ We use convection and advection as synonyms.

In our example, at $t = 0$ a short tracer pulse with release time T ($T \ll t$, where t is the time of interest) is injected at concentration C_0 [mol/m³] into a semi-infinite medium ($0 \leq z \leq +\infty$) which is initially free of solute: hence $C(z, 0) = 0$, $\forall z$. We require as a boundary condition downstream at infinity ($z \rightarrow +\infty$) that the concentration should vanish for all times. An analytical solution can be obtained with the help of Laplace transforms:

$$C(z, t) = \frac{\Delta m}{\varepsilon F \sqrt{4\pi a_L <|\vec{v}|> t}} \cdot \exp\left(-\frac{(z - <|\vec{v}|> t)^2}{4a_L <|\vec{v}|> t}\right), \quad (\text{XII.7})$$

$$\text{for } t \gg \frac{a_L}{<|\vec{v}|>}$$

where $\Delta m = \varepsilon F <|\vec{v}|> T C_0$ [mol] and F [m²] is the cross-sectional area of the flow. The spatial form of the solution (XII.7) is a symmetric Gauss curve with mean value $<z> = <|\vec{v}|> t$, the transport distance due to convection only, and the standard deviation

$$\sigma_{z,t} = \sqrt{2a_L <|\vec{v}|> t} = \sqrt{2a_L <z>}. \quad (\text{XII.8})$$

σ [m] characterises the spreading due to mechanical dispersion and is proportional to the square root of the travelling length $<z>$, but not to velocity. For a fixed observation point along the migration pathway at $<z> = L$, we obtain an asymmetric curve

$$C(L, t) = \frac{\Delta m}{\varepsilon F <|\vec{v}|> \sqrt{4\pi a_L \frac{t}{<|\vec{v}|>}}} \cdot \exp\left(-\frac{\left(t - \frac{L}{<|\vec{v}|>}\right)^2}{4a_L \frac{t}{<|\vec{v}|>}}\right). \quad (\text{XII.9})$$

From this equation we determine the time when the peak maximum concentration passes location L :

$$t_{\max} = \frac{L}{<|\vec{v}|>} \left[\sqrt{1 + \left(\frac{a_L}{L}\right)^2} - \frac{a_L}{L} \right] \approx \frac{L}{<|\vec{v}|>} \left(1 - \frac{a_L}{L} \right). \quad (\text{XII.10})$$

Here we made use of the condition $a_L \ll L$ ⁹ so that powers in a_L/L higher than the linear term can be neglected. If we remember that $t^{\text{conv}} = L / <|\vec{v}|>$ holds, we can rewrite Eq. (XII.10):

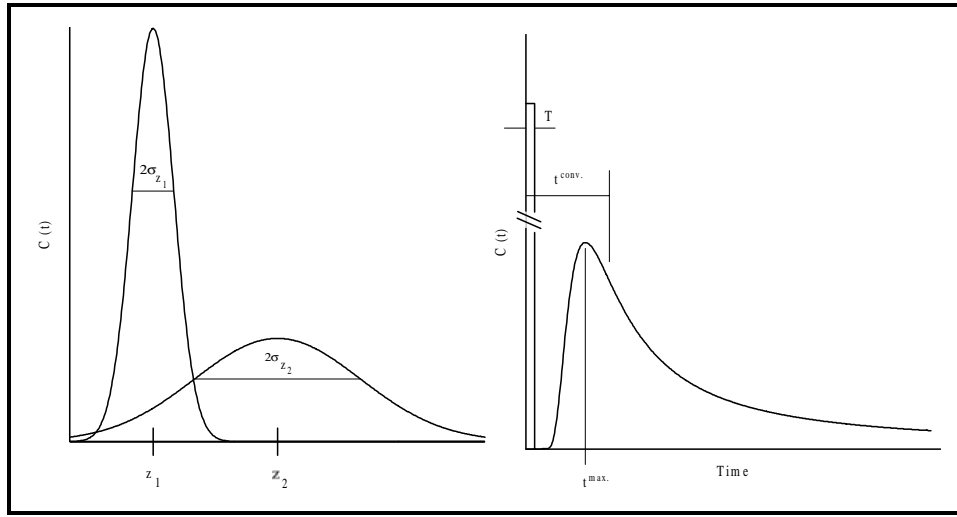
$$t_{\max} = t^{\text{conv}} \left(1 - \frac{a_L}{L} \right) < t^{\text{conv}}. \quad (\text{XII.11})$$

Hence, due to mechanical dispersion, the arrival time of the peak maximum at distances $L > a_L$ is shifted by the term a_L/L to shorter times. For the maximum peak height we get at the observation point $z = L$:

$$C_{\max}(L, t) = \frac{\Delta m}{\varepsilon F \sqrt{4\pi a_L L}} \left(1 + \frac{a_L}{4L} \right) \approx \frac{\Delta m}{\varepsilon F \sqrt{4\pi a_L L}}. \quad (\text{XII.12})$$

⁹ This is a necessary condition for using a macroscopic continuum approach for modelling transport of a solute in a porous medium.

Figure XII.2: Spreading and shape of the peak due to mechanical dispersion for a short tracer pulse with initial release time T . The travelling time for the tracer pulse due to convection only is $t^{\text{conv}} = z / \langle |\vec{v}| \rangle$. The left sketch outlines the spatial tracer concentration profile for a fixed time t . For short migration distances, the tracer distribution is narrow and high; for larger distances, it decreases and becomes wider. According to Eq. (XII.7) the distribution is Gaussian and, hence, has a symmetric shape. 2σ is defined by the two points where the curve has its maximum slope. The relative height of these points (equivalent with the two points of inflection) is $\exp(-1/2)$. The right sketch illustrates the temporal tracer concentration distribution at a fixed location. Due to the time dependence of σ the shape of the curve is asymmetric and the peak position is slightly earlier than the convection time t^{conv} .



From this expression we easily see that, due to Fickian dispersion, the peak height is:

- proportional to the total released mass Δm ,
- inversely proportional to the porosity ε and the flow area F ,
- inversely proportional to the square root of the travel distance L of the solute and, finally,
- inversely proportional to the square root of the (longitudinal) dispersivity a_L .

The most important results of this brief discussion are depicted for illustration purposes in Figure XII.2.

Let us briefly address the boundary condition problem. In our example we have chosen a concentration boundary condition upstream which, in the model, causes a mass transfer

due to dispersion in addition to the advective mass transfer across the boundary. For a short tracer pulse with release time T , the total mass released Δm is composed of the advective and dispersive parts according to

$$\Delta m = \Delta m_{\text{adv}} + \Delta m_{\text{disp}} , \quad (\text{XII.13})$$

where

$$\Delta m_{\text{adv}} = \varepsilon F C_0 < |\vec{v}| > T \quad (\text{XII.14})$$

and

$$\Delta m_{\text{disp}} \approx \frac{2}{\sqrt{\pi}} \varepsilon F C_0 \sqrt{a_L < |\vec{v}| > T} \propto \sqrt{T} ; \text{ for } T \ll \frac{a_L}{< |\vec{v}| >} . \quad (\text{XII.15})$$

As T approaches zero, the solute release is purely dispersive, caused by the large concentration gradient which strongly dominates advection. However, this is an effect of the advection/dispersion model only. If the release time becomes sufficiently large, corresponding to a constant concentration input with actual duration \tilde{T} , the additional released mass due to dispersion becomes constant and is given by

$$\lim_{\tilde{T} \rightarrow \infty} \Delta m_{\text{disp}} = \varepsilon F C_0 a_L . \quad (\text{XII.16})$$

About 95% of the asymptotic value of Δm_{disp} will have entered the migration zone when the advective transport distance is

$$< |\vec{v}| > \tilde{T} = < z > \geq 8 a_L . \quad (\text{XII.17})$$

This means that for larger distances the influence of the upstream concentration boundary condition has worn off. Eqs. (XII.16) and (XII.17) show that the dispersive mass transfer across the upstream boundary is negligible for a concentration boundary condition if the release time \tilde{T} allows a sufficiently large advective transport distance. Because only linear mass balance relations are considered, a concentration pulse at the observation time $t = \tilde{T}$ with release time T can be described as the linear superposition (difference) of two step functions with release time \tilde{T} and $(\tilde{T} - T)$, respectively. In this case the total dispersive mass transfer across the upstream boundary sums up exactly to zero giving rise to the relation $\Delta m = \Delta m_{\text{adv}}$ in Eq. (XII.7).

It is important to investigate the conditions under which dispersion cannot be taken into account by the simple convection-dispersion equation.

For very slow convection the spreading due to mechanical dispersion may be negligible compared to the effect of molecular diffusion. However, when the velocity is so large that turbulence occurs, Darcy's law is no longer applicable. To estimate the effect of molecular diffusion, a dimensionless quantity - the Peclet number - is defined

$$Pe = \frac{< |\vec{v}| > l}{D_{\text{diff}}} \quad (\text{XII.18})$$

where l is a characteristic length of the porous medium (*e.g.*, the pore size) and D_{diff} is the molecular diffusion coefficient. The Peclet number is a measure of the competition between convection and molecular diffusion:

- If $Pe < 0.3$: Convection is so slow that dispersive effects are dominated by molecular diffusion. Hydrodynamic dispersion therefore is practically isotropic, meaning that a spherical domain of solute will remain spherical, but with increased size for increased time.
- For $0.3 < Pe < 5$: Both processes are about equally important.
- For $5 < Pe < 300$: Convection becomes more and more important and induces increased mechanical dispersion. However, molecular diffusion cannot be neglected.
- For $300 < Pe < 10^5$: The regime of pure mechanical dispersion is reached; molecular diffusion is - for all practical purposes - negligible.
- If $Pe > 10^5$: The flow is highly turbulent, and, in addition to the Peclet number, the Reynolds number¹⁰ should also be taken into account.

If molecular diffusion can be neglected an alternative Peclet number may be defined as

$$Pe = \frac{\langle |\vec{v}| \rangle l}{D_{\text{mech}}} \quad (\text{XII.19})$$

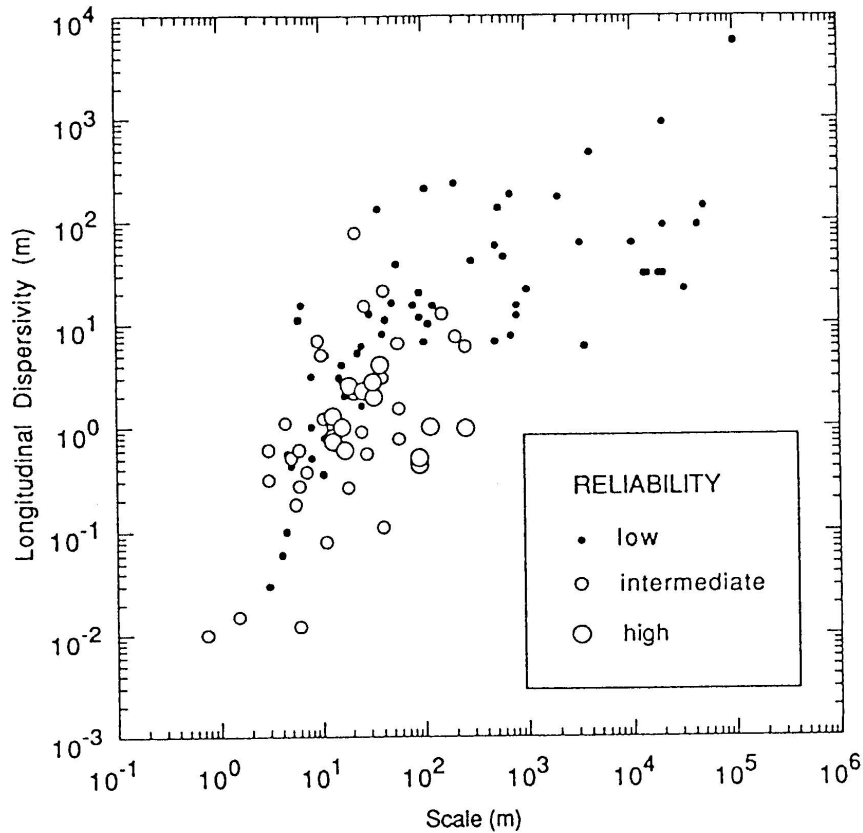
This is the transport Peclet number, which is a measure of the competition between convection and mechanical dispersion. The smaller the (transport) Peclet number, the greater the (mechanical) dispersive contribution. In the one-dimensional case, where transverse dispersion is judged to be of little importance, Eq. (XII.19) is reduced to $Pe = l/a_L$ where l is considered as the observation distance. Empirically the transport Peclet number has to be greater than about 5, otherwise the microscopic quantities cannot be replaced by macroscopic continuum quantities such as D_{mech} , and the continuum transport Eq. (XII.5) is no longer appropriate.

The applicability of the simple convection-dispersion equation for describing solute transport in heterogeneous porous media has been thoroughly investigated.

For experiments in more or less homogeneous laboratory columns it was found that the convection-dispersion equation reproduces the experimental data quite well using values for the dispersivity in the order of mm up to cm.

¹⁰ Every flow of a viscous liquid which is not frictionless can be characterised by a dimensionless number, the Reynolds number $Re = \frac{\nu l}{\mu/\rho}$, where ν is the mean velocity, l is the hydraulic diameter of the flow domain and μ/ρ is the kinematic viscosity. The Reynolds number is given by the ratio of the inertial forces and friction forces; for large Re the inertial forces are dominant and flow is turbulent, and for small values of Re flow is laminar. Large/small only makes sense with regard to a reference point, *e.g.* Re_{crit} where laminar flow turns towards turbulent flow. Typical values for Re_{crit} are of the size 1000 ... 10000 depending on the roughness of the bounding walls and on the upstream boundary condition. Flow fields in the geosphere are characterised by Reynolds numbers which are orders of magnitude smaller than the critical value; hence, such flow fields can be considered as laminar.

Figure XII.3: Longitudinal dispersivity *vs.* scale with data classified by reliability. Reprinted with permission from [92GEL/WEL].



However, for heterogeneous experiments, especially for the case of a stratified porous medium with flow strictly parallel to the stratification, it was shown [80MAT/MAR] that the solute transport cannot be described adequately by the convection-dispersion equation, even when considering large transport times. However, for flow not strictly parallel to the bedding, this theoretical study has shown that Fickian dispersion will occur asymptotically for large transport times.

XII.3.2. Scale dependent dispersivity

Experimental as well as theoretical investigations clearly indicate that dispersivities determined on a field-scale are typically several orders of magnitude larger than values obtained on the laboratory-scale using the same material. Such a scale dependence of the dispersivity is documented, *e.g.*, in [77OAK/EDW, 81PIC/GRI, 92GEL/WEL] and is illustrated by Figure XII.3.

The variation of the dispersivity reflects the influence of differing degrees of the spatial heterogeneities of a medium and, hence, also in local heterogeneities in the hydraulic conductivity. In field experiments, the (longitudinal) dispersivity is of the order of some

meters up to several hundred meters, or even kilometres, depending on the size of the heterogeneities. By using the Peclet number, it is **not** possible to rescale the results from one type of experiment to another with the help of a similarity law for the real physical systems. **Consequently, laboratory measurements of dispersion cannot be used for the extrapolation to large scale experiments.** This scaling problem may severely limit the predictive capability of models being calibrated on experiments on the laboratory scale.

Knowledge of transverse dispersion is much less profound than that of longitudinal dispersion. Data indicate that values for transverse dispersion are typically an order of magnitude smaller and can therefore be estimated as a few tenths of the value for a_L .

XII.3.3. The problem of local averaging

So far we have used a simple formalism for transport of a solute in a porous medium. For illustration purposes we may think in terms of a column experiment with sand as the solid material. A necessary condition for the use of the continuum approach is, as previously outlined, that a REV can be determined which is much smaller than the domain of interest (the length of the column in our example) and larger than the scale of the microscopic heterogeneities (the size of the pores or the size of the grains). Hence, the REV is large enough to encompass all geometrical heterogeneities. At this point the question arises whether the continuum approach is also applicable to fractured porous rock. We define fractured porous rock as a porous medium with void geometry composed by the pore spaces and also by a network of more or less open fractures. Modelling the solute flow in fractured porous rock is largely a problem of defining the geometry of all the fractures. In reality not all systems of fractures constitute a network. Often the fracture density (the number of fractures per unit volume of porous medium) is too low and/or the extent of the fractures (trace length) is too small to constitute a fracture network. Therefore, measurements of the hydraulic conductivity performed tend to be erratic and very sensitive to the volume of fractured porous rock. Such variations of the hydraulic conductivity in a fractured porous medium cause a nonuniform velocity field, whereas the variations in the velocity - as mentioned earlier - mainly cause mixing due to mechanical dispersion. In such a case, a REV can hardly be defined, because its volume may be even larger than the volume of interest, and a formalism based on a continuum approach cannot be developed. In order to describe a transient solute distribution for a system of sparsely connected fractures we would require information on every individual fracture, but this can never be achieved. However, if information on geometrical quantities such as orientation, aperture, *etc.* can be obtained as statistical values, a statistical description of the solute behaviour can be achieved. If the number of individual fractures is large (ten thousands or even more), as when considering solute transport over larger distances, only statistical distributions for individual parameters can be derived and *no local averaging* can be performed over a REV.

One approach is to treat the fractured porous medium as an equivalent porous medium, which is appropriate when the individual fractures are densely interconnected and fluid

flow through large regions is considered. In this way, the domain of fractured porous rock can be characterised by a conductivity tensor, and flow and transport can be treated as in a porous medium.

An alternative approach would be the treatment of flow and transport through a number of discrete and interconnected fractures. In the first approach, we consider mixing phenomena like dispersion to be of the Fickian type, hence as spatially invariant, while in the second approach dispersion is strongly non-Fickian. Because a fluid always flows along the least resistive flowpath, a fraction of the solute may be transported in a few preferential flow paths much faster than with the mean transport time. Moreover, the hydraulics and transport properties of such channels may be completely different from those averaging over the whole domain of interest. Further information concerning these problems can be found in [93BEA/TSA].

XII.3.4. Sorption equations used in transport modelling

The geosphere is an exceedingly complex system; not only is it composed of solid, liquid and often gaseous phases, but each of these phases may include reacting inorganic, and organic, components. This strongly heterogeneous character of the geosphere determines and influences the physical and chemical behaviour of the system, and has a direct and strong impact on solute transport. Understanding the physical and chemical transformation of the solute is one of the key problems for modelling the rock-solute complex. Typical phenomena involved in the physical and chemical transformation of solutes are various forms of sorption processes, precipitation, dissolution, oxidation-reduction reactions, volatilisation, maybe biodegradation in the presence of micro-organisms, *etc.* Given such a high degree of complexity of a solute-rock system, a comprehensive, complete and accurate description with predictive capabilities can never be reached. Nevertheless, in the past major efforts have been made to understand some of these processes and mechanisms, and many models have been developed to describe experimental data adequately and to deduce new information from them.

Some processes, such as volatilisation, irreversible¹¹ precipitation or dissolution could roughly be taken into account by the net source/sink terms in the transport equations. Other processes are much more complicated, as described in other chapters in this book¹².

Let us now turn our attention towards the description of sorption processes. The term sorption in general refers to the distribution of a solute between an immobile phase and a solution. Examples are physical sorption, chemisorption, *e.g.* surface complexation, ion exchange, isotopic exchange; or ion exclusion, molecular filtration, mineralisation, *etc.* Hence, the term sorption includes a broad variety of physical-chemical processes. Physical adsorption, for example, is a process where solute adheres to the surface of the solid phase.

¹¹ Whether a process is considered reversible or irreversible (or: instantaneous or non-instantaneous = kinetics) depends on the timescale involved.

¹² For a more comprehensive overview on the theoretical framework concerning the chemical transformation and immobilisation of solutes onto surfaces at the solid/liquid interface of geological media, the reader is referred to the chapter by S.A. Banwart in this book (Chapter VII).

The bonding is caused by Van-der-Waals forces and is weaker than when sorption occurs through covalent or ionic bonding as in chemisorption/surface complexation. The capacity to form surface complexes depends on the species dissolved, the pH of the solution, the composition of the water, the minerals of the solid phase present, *etc.* Anions, as well as cations, may form surface complexes. Ion exchange is a process by which charged particles of the solute replace ions on the surface or within the structure of the solid phase. If the process involves isotopes of the same element, the process is called isotopic exchange. Processes such as ion exclusion and molecular filtration are phenomena associated with solute flow; they do not represent a direct uptake of solute species onto the solid phase as the processes mentioned before. For both processes the mobility of the solute species is restricted by either constrictions along the flow pathway, as in the case of molecular filtration, or by surface charges resulting in a repulsion of similarly charged ions as in the case of ion exclusion. It is conceivable that positively charged solute particles (cations) may reduce the influence of a negatively charged surface resulting in weaker repulsion of migrating ions, less sorption and, hence, less retardation. The term mineralisation describes a direct uptake of ions by the solid phase and includes also precipitation of solids.

The nature of all the processes mentioned leads to retardation of migrating solute species¹³. However, since it is often very difficult to quantify these reactions or even to estimate the relative importance of different sorption processes, simplifications are normally employed. Nevertheless, some characteristics of the sorption mechanisms can be recognised. Most experiments show that the capacity for sorption of a solid phase for a dissolved species tends to increase with increased concentration of the dissolved species (but there are examples where this is not the case).

From a thermodynamic point of view, sorption processes can be divided into reversible and irreversible processes depending on the time scale involved. Furthermore, sorption reactions may be slow or they can rapidly reach an equilibrium state with no further concentration changes with time. The latter is the domain where the sorption isotherm formalism is used. An equilibrium sorption isotherm cannot be used to describe processes with slow reaction kinetics.

The simplest and most widely used equilibrium sorption isotherm is given by a linear relationship between the amount of solute on the solid phase S [mol/kg] and the concentration of solute C [mol/m³] in the mobile phase according to (for the following discussion we omit the subscript f and p for simplicity):

$$S = K_d C . \quad (\text{XII.20})$$

Here K_d is the sorption equilibrium distribution coefficient with units [m³/kg], which is a measure of the retardation of a migrating solute. The concept of the linear sorption

¹³ Sorption processes constitute the main retardation mechanisms for migrating radionuclides. It is mainly sorption (and not *e.g.* dispersion) which decreases the mobility of certain nuclides in such a way that radioactive decay gets a chance to reduce the maximum concentration of these nuclides by orders of magnitude. Indeed, sorption of dissolved matter is considered as the key process for delayed transport.

isotherm is based on the following assumptions

1. the solutes are present in low concentrations,
2. the system is at equilibrium,
3. the reaction is reversible,
4. the temperature is constant, and
5. no other chemical processes are occurring¹⁴.

This description is one of those most commonly used, because it often leads to simple analytical solutions for the transport equations. Another reason that the K_d -concept has survived is that for many solutes the experimental sorption data may be described well by a linear sorption isotherm. When there is no linear relationship between S and C other types of sorption isotherms have to be used. There are several types, some of them purely empirical, others with a certain theoretical background, *cf.* Chapter VII.

The Freundlich isotherm [26FRE] is an example of a non-linear relationship between S and C

$$S = KC^N \quad (\text{XII.21})$$

where K [$\text{mol}^{1-N} \cdot \text{m}^{3N} \cdot \text{kg}^{-1}$] and N [-]¹⁵, with $0 < N \leq 1$ [80SPO2] are constant. The linear form of Eq. (XII.21) $\log_{10} S = \log_{10} K + N \log_{10} C$ is often fitted to experimental data. The Freundlich isotherm has been widely used to model sorption of solutes by soils. A serious limitation of the Freundlich isotherm is that, as for the linear isotherm, there is no maximum amount of sorbed solute on the solid phase. At low concentrations of the mobile phase, the distribution coefficient becomes large, which means strong retardation for flowing solutes but smaller retardation at higher concentrations. The linear isotherm is a special case where the Freundlich exponent is unity.

The Langmuir isotherm [18LAN] is another type of non-linear isotherm originally introduced to describe the adsorption of gases on different solid phases. It is given by the following formula:

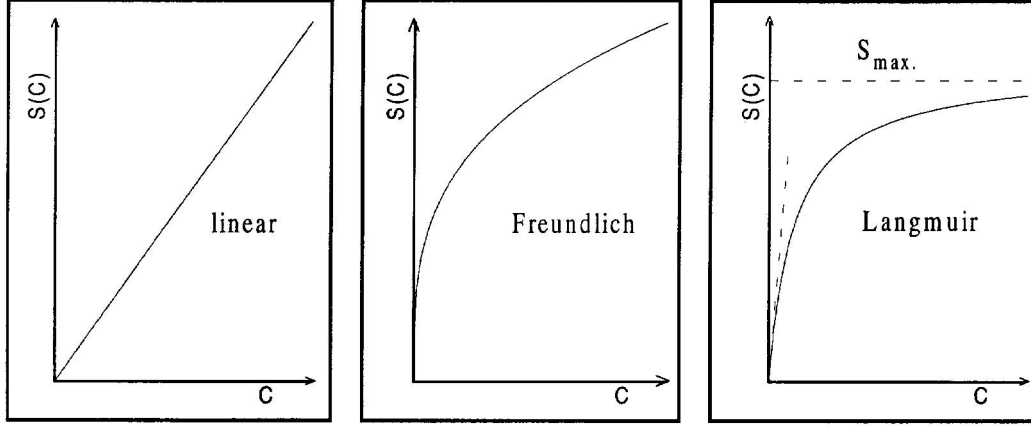
$$S = \frac{\tilde{K} S_{\max} \cdot C}{1 + \tilde{K} C} = S_{\max} \frac{C}{\frac{1}{\tilde{K}} + C} \quad (\text{XII.22})$$

\tilde{K} [m^3/mol], S_{\max} [mol/kg] are phenomenological coefficients. For this isotherm the underlying assumptions are:

¹⁴ This means that processes like precipitation/dissolution, ion exchange *etc.* which cannot be described in terms of a linear sorption isotherm formalism, but which occur in many systems and also influence the retardation cannot be properly modelled.

¹⁵ [-] denotes a dimensionless quantity.

Figure XII.4: Schematic $S(C)$ vs. C diagrams for the linear, Freundlich and (one site) Langmuir isotherm. For the Langmuir isotherm the linear behaviour for small concentration values is indicated in the figure.



1. the sorption capacity is restricted due to a finite number of sorption sites. The maximum sorption is reached when the surface of the solid phase is covered with a monolayer of solute molecules,
2. all sorption sites are equivalent, and
3. the rate of desorption is independent of the occupation of neighbouring sites.

For low concentration $C \ll S_{\max}$, where S_{\max} is the saturation concentration, the Langmuir isotherm has a linear behaviour while for high concentration $S(C)$ becomes a constant $= S_{\max}$. \tilde{K} is a measure of the “bond strength” for sorbed solute on the solid phase surfaces. In the past there have been different attempts to refine the Langmuir isotherm, *e.g.* by introducing two different types of surface sites; one site may have a high bonding strength while the other has a lower one. Such a two-site Langmuir isotherm is given by:

$$S = S_{\max}^{(1)} \frac{C}{\frac{1}{\tilde{K}^{(1)}} + C} + S_{\max}^{(2)} \frac{C}{\frac{1}{\tilde{K}^{(2)}} + C} \quad (\text{XII.23})$$

In this formula the superscripts (1) and (2) refer to the two types of site. There are experimental data supporting such a model. However, for each type of sorption site two freely adjustable parameters \tilde{K} and S_{\max} occur in the sorption model and have to be determined from suitable experimental data. Figure XII.4 shows the schematic representation of the three different equilibrium sorption isotherms.

The sorption description reviewed above is based on the assumption that the reaction time for sorption is much smaller than the water transit time for the REV. Therefore, kinetic effects are strongly dependent on the time scale involved and play no role for certain problems. In the frame of a safety assessment for a repository for radioactive waste, where, typically, the time spans of interest are of the order of tens of thousands of years or even more, kinetic effects with rate constants of hours or even months are completely negligible. But for small scale laboratory experiments this might not be the case. To model slow sorption/desorption processes of a solute, it is more appropriate to use a kinetic model.

To account for sorption kinetics in transport modelling, it is common to use phenomenological relationships which may lack an adequate microscopic, deterministic representation. The most simple description is the reversible first-order kinetic sorption model given by:

$$\frac{dS}{dt} = k_s C - k_r S, \quad (\text{XII.24})$$

where S [mol/kg] is again the amount of solute sorbed onto solid phase surfaces and C [mol/m³] is the concentration of solute in the mobile phase. k_s [m³·kg⁻¹·s⁻¹] and k_r [s⁻¹] are the rates for sorption and desorption, respectively. Eq. (XII.24) accounts for the rate of solute sorption by the solid phase as a result of the difference between the actual concentration of solute in the mobile phase and what already has been sorbed. This differential equation describes a reversible non-equilibrium sorption process. If k_r is equal to zero, no desorption of solute occurs, and the sorption process becomes irreversible. If k_s and k_r are large while k_s/k_r is finite, the equilibrium linear sorption model is obtained. If the concentration in the liquid phase is regarded as constant ($C = \text{const.}$), assuming that initially no solute is sorbed onto the solid phase ($S(0) = 0$) and the rate for desorption is $k_r \neq 0$, we obtain the following analytical solution for Eq. (XII.24):

$$S(t) = \frac{k_s}{k_r} \cdot C \left(1 - e^{-k_r t}\right). \quad (\text{XII.25})$$

At steady-state, or dynamic equilibrium, where $\dot{S} = 0$ holds for Eq. (XII.24) we get:

$$S(t) = \frac{k_s}{k_r} \cdot C := K_d \cdot C. \quad (\text{XII.26})$$

Hence, the first order reversible sorption kinetic model is reduced to the linear isotherm with $K_d := k_s/k_r$.

If sorption is limited one obtains a special case of a first order kinetic model:

$$\frac{dS}{dt} = \tilde{k}_s (S_{\max} - S) \cdot C - k_r \cdot S. \quad (\text{XII.27})$$

In Eq. (XII.27) the sorption is proportional to the number of sites ($S_{\max} - S$) still accessible for sorption, whereas the rate for desorption is proportional to the concentration of sorbed

solute. For $C = \text{const.}$ we get the analytical solution:

$$S(t) = \frac{\frac{\tilde{k}_s}{\tilde{k}_r} S_{\max} \cdot C}{1 + \frac{\tilde{k}_s}{\tilde{k}_r} \cdot C} \left(1 - e^{-\left(\tilde{k}_s \cdot C + \tilde{k}_r\right)t} \right), \quad (\text{XII.28})$$

which in the steady-state results in the Langmuir isotherm (XII.22), if $\tilde{K} := \frac{\tilde{k}_s}{\tilde{k}_r}$; ($[\tilde{k}_s] = \frac{\text{m}^3}{\text{mol} \cdot \text{s}}$).

We can also formulate a reversible non-linear kinetic equation similar to the Freundlich isotherm:

$$\frac{dS}{dt} = \hat{k}_s \cdot C^N - k_r \cdot S \quad (\text{XII.29})$$

Eq. (XII.29) describes sorption processes where the forward reaction is non-linear and the reverse reaction is linear. Again, \hat{k}_s [$\text{mol}^{1-N} \cdot \text{m}^{3N} \cdot \text{kg}^{-1} \cdot \text{s}^{-1}$] and k_r are rate coefficients and N a dimensionless quantity. In principle, \hat{k}_s and k_r need not be constant and may be dependent on the solute concentration of the liquid phase. The isotherm for constant solute concentration C of the mobile phase is equal to:

$$S(t) = \frac{\hat{k}_s}{k_r} \cdot C^N \left(1 - e^{-k_r t} \right) \quad (\text{XII.30})$$

and, as before, at steady-state, *i.e.* $\dot{S} = 0$ holds, the Freundlich isotherm (XII.21) is obtained. In this case the Freundlich isotherm coefficient K is the ratio of the rate coefficients \hat{k}_s/k_r .

Finally, we briefly mention the kinetic product model proposed by Enfield [74ENF]:

$$\frac{dS}{dt} = a \cdot C^b \cdot S^d \quad (\text{XII.31})$$

where a , b and d are phenomenological constants. There is no theoretical foundation for this expression which was empirically found by modelling the mobility of phosphorus in soil. Like the Freundlich isotherm it does not limit the sorption to a maximum value. Because no desorption rate occurs in this formula, it may be regarded as an irreversible sorption equation.

Although a number of other kinetic models [68GOU, 81AND/RUB] exist, we will not discuss them here. The intrinsic value of a particular sorption model is strongly dependent on the type of transport problem being investigated. Many problems may be tackled with the help of a simple equilibrium model, while others may require more sophisticated, and time-dependent, models. Finally, the choice of a model suitable for describing sorption processes is dependent on the type of knowledge available and the accuracy required. It makes little sense to use a n -site Langmuir kinetic model, if the values for the phenomenological parameters are unknown or if transport is prevalingly advective (convective) and the sorption processes only play a minor role.

XII.3.5. The double porosity medium concept

In this section we discuss the influence of an additional important transport process - molecular diffusion of a solute into the porous rock matrix, briefly called matrix diffusion. For this we have to expand our model to the so-called double porosity medium concept. So far we have assumed that transport of a solute happens only within a water saturated porous medium or within a water-carrying fracture. Such a fracture could be considered as open or as partially filled with altered rock material, *e.g.* clay minerals or sand grains, and with a flow porosity ε_f [-] between 0 and 1. Now, we will assume that a solute is allowed to diffuse into the connected pore space of the host rock surrounding a water bearing fracture and altered by geological processes. Such a domain for molecular diffusion is characterised by the matrix porosity ε_p [-] with values, again between zero and unity and we speak now of transport of the solute in a double porosity medium. However, the dual porosity model is also widely used in non-fractured media. Hence, advection is not coupled automatically to fracture flow. In the double porosity medium concept, the fluid phase is divided into one mobile and one immobile part, with a diffusive mass transfer between them as the consequence of a difference in the solute concentration between the mobile and the immobile regions. The dual porosity medium model can be extended by introducing additional processes such as instantaneous mass exchange described by a linear or non-linear sorption isotherm in both the mobile and the immobile phases, and by introducing radioactive decay for non-stable solutes.

As a first step we will derive the system of coupled transport equations - one for transport in the fracture and the second for the molecular diffusion in the adjacent rock matrix. We will neglect dispersive effects in the fracture to demonstrate and discuss the influence of matrix diffusion on solute transport. We will first consider unlimited matrix diffusion of sorbing solutes, where the boundary in the rock matrix is infinitely far away from the interface fracture/porous rock, so that boundary effects play no role. This makes the mathematical treatment of the transport equations relatively simple. Then we will discuss limited matrix diffusion and also present a useful and simple approximation of matrix diffusion, the effective surface sorption approximation. Finally we will reintroduce dispersion and demonstrate the power, but also the limitations of this concept, on a few selected examples where the double porosity medium approach is confronted with experimental data.

Let us start with the derivation of the transport equations for a double porosity medium. According to the mass conservation equation, see *e.g.* [91BEA/BAC], for the variation in time of the total concentration of a species i in a porous medium we can write:

$$\frac{\partial C^i}{\partial t} = - \sum_{\alpha} \vec{\nabla} \cdot \text{flux}_{\alpha} - \text{sinks} + \text{sources} . \quad (\text{XII.32})$$

The total flux is the sum of different terms, one term describing advection, another representing dispersion *etc.* To take solute/rock interactions into account, it is useful to split the total concentration of species i into

- a) a mobile part C_f^i [mol/m³]; the concentration of species i in the liquid phase

and

- b) an immobile part S_f^i [mol/m²] which is the amount of species i per unit area of solid phase:

$$\frac{\partial C^i}{\partial t} = \frac{\partial}{\partial t} [\varepsilon_f C_f^i + \xi_f S_f^i] . \quad (\text{XII.33})$$

C_f^i is the ratio of dissolved amount/quantity of species i , and the volume accessible for the flowing liquid; S_f^i is given by the ratio of absorbed species i , and the surface accessed by the flowing liquid. ε_f [-] denotes the flow porosity and is the ratio of the volume of flowing liquid and total volume (the latter being the sum of volume of flowing liquid and volume of solid phase). ξ_f [m⁻¹] is the specific sorbing surface of the water-conducting zone¹⁶ and is given by the ratio of sorbing surface and total volume of the water conducting zone.

Eq. (XII.32) is written in form of two coupled partial differential equations: one equation for transport in the water conducting zone and another equation for the transport in the rock matrix adjacent to the fracture.

The transport equation for a volume element of the water conducting feature is given by:

$$\begin{aligned} \frac{\partial}{\partial t} [\varepsilon_f C_f^i + \xi_f S_f^i] &= \vec{\nabla} \cdot \varepsilon_f [\mathbf{D} \cdot \vec{\nabla} - \vec{\nu}_f] C_f^i \\ &+ \varepsilon_f \left[\frac{d\vec{F}_f}{dV_f} \cdot \varepsilon_p \mathbf{D}_p^i \cdot \vec{\nabla} C_p^i \right]_{\text{interface}} + Q_f^i \end{aligned} \quad (\text{XII.34})$$

and that for a volume element of the matrix by:

$$\frac{\partial}{\partial t} [\varepsilon_p C_p^i + (1 - \varepsilon_p) \rho S_p^i] = \vec{\nabla} \cdot \varepsilon_p \mathbf{D}_p^i \cdot \vec{\nabla} C_p^i + Q_p^i . \quad (\text{XII.35})$$

The left hand side of Eq. (XII.34) describes the variations with time t of the total concentration of species i in the liquid phase C_f^i and on solid phase S_f^i .

Q_f^i represents a net source/sink term (mass per unit volume of the water conducting zone and unit time); Q_p^i in Eq. (XII.35) a net source/sink term (mass per unit volume of porous rock and unit time) respectively, *e.g.* radioactive decay and ingrowth in the case of a nuclide chain.

The first term of the right hand side is minus the divergence of the flux in the water-conducting zone and is composed of

- a) a flux term for the hydrodynamic dispersion $\vec{j}_{\text{disp}}^i = -\varepsilon_f \mathbf{D} \cdot \vec{\nabla} C_f^i$, where \mathbf{D} in general is a second rank tensor taking into account molecular diffusion and the fact that the direction of the dispersive flux is not only determined by the concentration gradient but also by the geometry of a possible fracture infill and

¹⁶ ξ_f is the sum of the flow wetted surface of a possible fracture infill and the fracture surface itself. Therefore, only those parts of the fracture surface which are not covered by fracture infill and not part of the rock pore space are considered.

- b) a flux term representing advection $\vec{j}_{\text{adv}}^i = +\varepsilon_f \vec{v}_f C_f^i$, where \vec{v}_f is the velocity vector of the liquid flow field.

A sink/source term describing the diffusive mass transfer of species i across the interface between the water-conducting zone and the porous rock matrix is given by $-\varepsilon_f \left[\frac{d\vec{F}_f}{dV_f} \cdot \varepsilon_p \mathbf{D}_p^i \cdot \vec{\nabla} C_p^i \right]_{\text{interface}}$, with the second rank diffusion tensor \mathbf{D}_p^i taking into account that the direction of the diffusive flux is not only given by the concentration gradient, but also by the rock pore geometry. In this expression $\frac{d\vec{F}_f}{dV_f}$ is a vector representing the ratio of the surface area of the water conducting and altered rock zone, and the volume element of the water conducting zone. Its orientation is perpendicular to the surface element and points towards the altered rock zone. In the case of a planar fracture geometry this ratio is $1/b$ where b [m] is half of the fracture aperture. The factor ε_f takes into account that, due to partial coverage of the interface surface by a fracture infill¹⁷, only the fraction ε_f ¹⁸ of the altered zone is accessible for diffusion¹⁹. The matrix porosity ε_p [-] is equal to the ratio of volume of stagnant liquid and total volume. C_p^i [mol/m³] is the amount of dissolved species i per unit volume of stagnant liquid. This term links the transport equation for advection and dispersion (XII.34) with that for matrix diffusion (XII.35).

At this point a problem could arise because the diffusive outflux across the interface is given by

$$\vec{j}_f^i = +\varepsilon_f \varepsilon_p \mathbf{D}_p^i \cdot \vec{\nabla} C_p^i \Big|_{\text{interface}} \quad (\text{XII.36})$$

and the diffusive influx in the matrix by

$$\vec{j}_p^i = -\varepsilon_p \mathbf{D}_p^i \cdot \vec{\nabla} C_p^i \Big|_{\text{interface}} \quad (\text{XII.37})$$

hence, $-\vec{j}_f^i \neq \vec{j}_p^i$. Although the flux $[\frac{\text{mol}}{\text{m}^2 \cdot \text{s}}]$ is not continuous at the interface, mass is conserved, since the mass flow per total volume \dot{M}_f^i $[\frac{\text{mol}}{\text{m}^3 \cdot \text{s}}]$ is equal to that in the porous rock zone \dot{M}_p^i

$$|\dot{M}_f^i| = -\frac{d\vec{F}_f}{dV_f} \vec{j}_f^i = \left(\varepsilon_f \frac{d\vec{F}_f}{dV_f} \right) \vec{j}_p^i = \dot{M}_p^i. \quad (\text{XII.38})$$

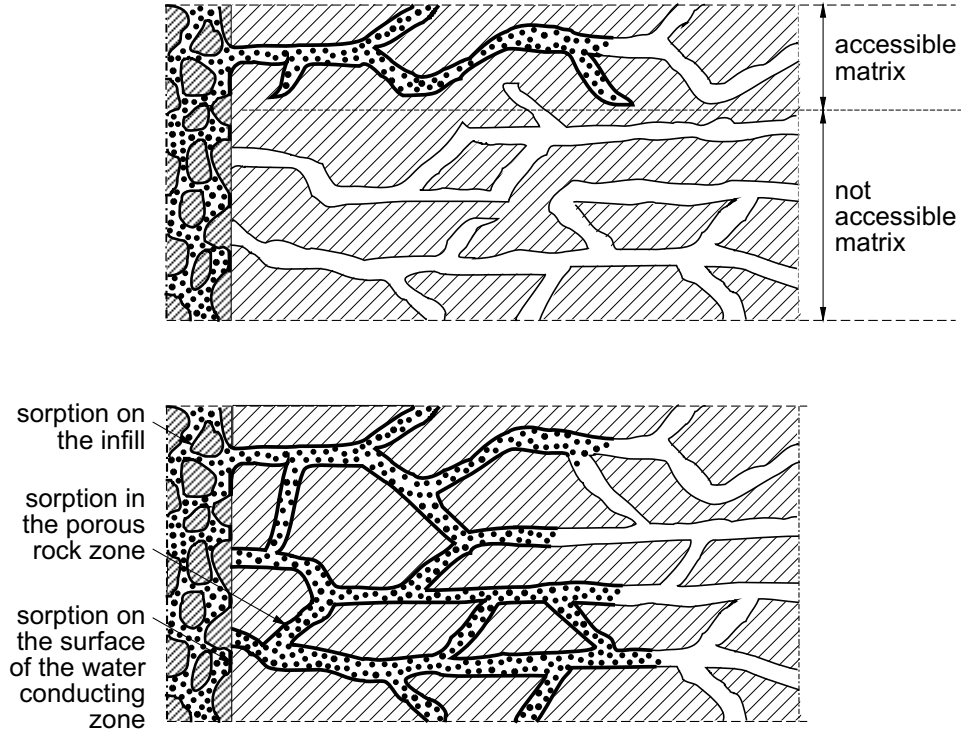
In this equation the factor $\left(\varepsilon_f \frac{d\vec{F}_f}{dV_f} \right)$ takes into account the restricted portion of porous rock matrix available by diffusion.

¹⁷ For simplicity the fracture infill is considered as being not porous. Otherwise, a third type of porosity has to be taken into account and a third transport equation would be necessary to describe contaminant transport from the flowing liquid into the fracture infill.

¹⁸ The term ε_f represents the ratio of (uncovered) fracture surface accessible to matrix diffusion and total fracture surface and is approximated - for simplicity - by the flow porosity ε_f .

¹⁹ This may be a reasonable assumption if pores which are blocked by a fracture infill for diffusion from the fracture interface cannot be reached by diffusing solute via unblocked pores. However, if pore interconnection and fast diffusion in the flow direction allow such blocked pores to be reached, the factor ε_f has to be omitted.

Figure XII.5: Sketch of the influence of a possible fracture infill in the water-conducting zone on matrix diffusion. In the upper part, matrix diffusion is reduced due to covering of matrix pores by the fracture infill. Whether such a picture is a realistic representation will depend on the system being considered. However, from a safety assessment point of view it is certainly conservative. In the lower part, the whole matrix is accessible to matrix diffusion due to pore interconnections in the matrix. In such a case the leading factor ε_f of the sink/source term for diffusing transfer across the interface in Eq. (XII.34) has to be dropped.

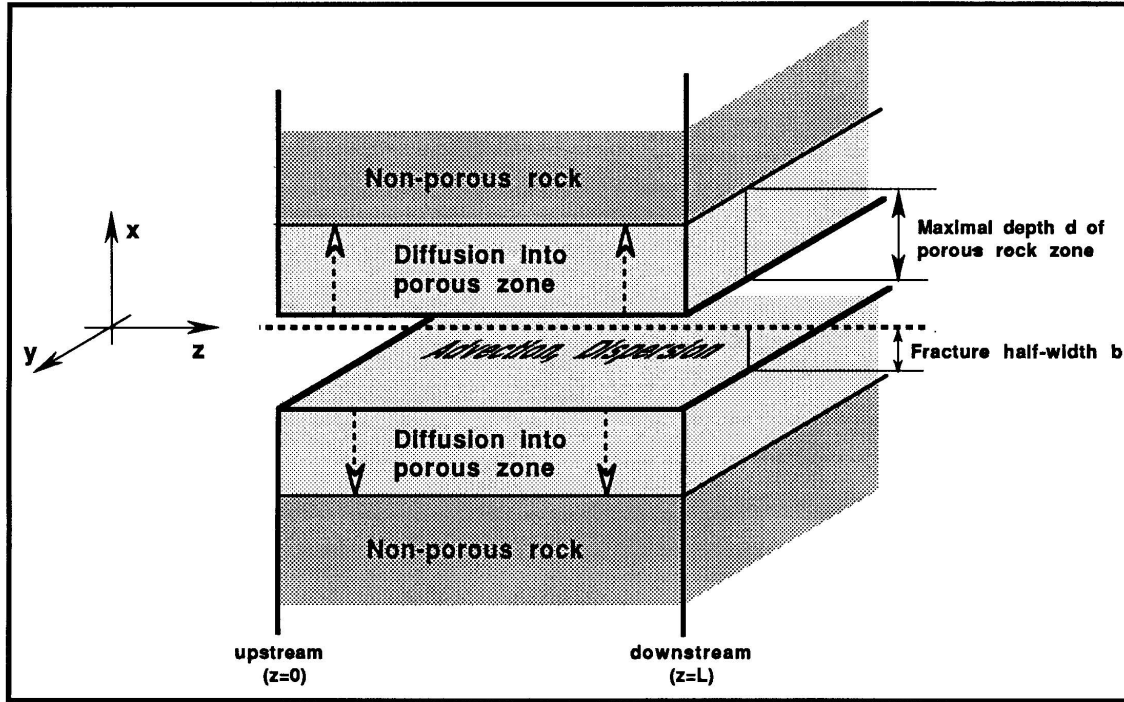


The second transport Eq. (XII.35) represents diffusive transport of a species i into stagnant water of the connected pore space of the altered rock matrix, where ρ [kg/m³] is the averaged solid phase density, and S_p^i [mol/kg] the ratio of the mass of absorbed species i in the rock matrix and the unit mass of porous rock.

For the following considerations we will make some principal assumptions and approximations. It is clear that they have to be formulated differently for different physical problems. Very often it is not necessary or, due to the lack of appropriate data, it is useless to attempt to develop a full three-dimensional formalism. In such a case a two- or even one-dimensional description may be sufficient to encompass the most relevant mechanisms and processes²⁰.

²⁰ In principle, such conceptual restrictions and approximations have to be estimated quantitatively

Figure XII.6: The (x,z) -geometry for transport in a fractured rock. Advection/dispersion takes place in z -direction and matrix diffusion in x -direction. The fracture aperture is $2b$. A limitation on matrix diffusion could result if a hydrothermal altered zone beneath the fracture is embedded in a zone of fresh unaltered rock with very low porosity being considered in the model as non-porous. The porosity of the altered zone can easily be an order of magnitude larger than that of the non-porous rock zone.



In Figure XII.6 we have sketched the geometry for flow and transport in a planar fracture. However, in nature, fractures are neither planar nor do they extend as single fractures over the whole distance to be considered (see also Figure XII.1).

Let us - with the help of Figure XII.6 - specify the underlying assumptions and approximations, providing the basis for a simplification of the transport problem.

- Perpendicular to the fracture plane, in x -direction in Figure XII.6, hydrodynamic dispersion (molecular diffusion only if there is no fracture infill) is responsible for fast mixing of the solute so that the concentration distribution perpendicular to the fracture plane can be approximated by an averaged concentration. Therefore we

or, at least, motivated qualitatively. This means, in a rigid sense, that results from, say, a one-dimensional model have to be compared with results from two- or three-dimensional models. In certain disciplines such comparisons between competing models were made periodically within international benchmarking studies such as, *e.g.*, INTRACON [86INT].

assume that the fracture aperture is much smaller than its length.

- To restrict the flow within the fracture to a 1D-problem we further assume that the solute is released uniformly along the y -axis resulting in a zero concentration gradient in this direction.
- In the matrix we only consider diffusive processes occurring perpendicularly to the fracture. This approximation is surely reasonable because of the much lower hydraulic conductivity, if transport in the fracture is much faster than in the matrix. The volume of the porous rock matrix, accessible to diffusion may be limited or unlimited.
- Very often, molecular diffusion can be neglected along the flow path (in z -direction), when compared to mechanical dispersion and advection, *i.e.*, the Peclet number (XII.18) is much larger than unity.

Thus the water velocity vector along the flow path is reduced to ν_f ; the second rank tensor for the hydrodynamic dispersion is degenerated to the mechanical dispersion only and this is represented by a single scalar quantity according to Eq. (XII.4)

$$\mathbf{D} \approx a_L \nu_f, \quad (\text{XII.39})$$

where a_L [m] is the longitudinal dispersion length.

In order to calculate the time- and space-dependent concentration in the water-conducting feature C_f^i and in the stagnant pore water of the rock matrix C_p^i , reasonable assumptions about the relationship between the concentration in the mobile phase C and the concentration on the solid phase S have to be made. For host rocks considered in a safety assessment of a repository for radioactive waste, water velocities are of the order of a few meters per year, hence very small; and thus, typical transport times (neglecting retarding mechanisms at all) are of the order of hundreds of years. Sorption kinetics in such a case certainly plays a minor role; however, kinetics may become important when modelling laboratory experiments on a much smaller time scale.

- Therefore let us, for the sake of simplicity, assume that sorption kinetics plays no role, *i.e.* we assume instantaneous sorption equilibrium with a sorption isotherm of the form:

$$S_{f,p}^i = f(C_{f,p}^i) \quad (\text{XII.40})$$

where $f(C)$ may be any function, which in general has different forms for the fracture and the matrix.

Considering these additional approximations and introducing Eq. (XII.40) into the set of coupled transport equations we get:

$$\frac{\partial C_f^i}{\partial t} = \frac{1}{R_f^i(C_f^i)} \left[a_L \nu_f \frac{\partial^2 C_f^i}{\partial z^2} - \nu_f \frac{\partial C_f^i}{\partial z} + \frac{1}{b} \varepsilon_p D_p^i \frac{\partial C_p^i}{\partial x} \right]_{x=b} + \frac{Q_f^i}{\varepsilon_f} \quad (\text{XII.41})$$

$$\frac{\partial C_p^i}{\partial t} = \frac{1}{R_p^i(C_p^i)} \left[D_p^i \frac{\partial^2 C_p^i}{\partial x^2} + \frac{Q_p^i}{\varepsilon_p} \right] \quad (\text{XII.42})$$

where we used the following abbreviations for the concentration dependent retardation functions $R_f^i(C_f^i)$ and $R_p^i(C_p^i)$

$$R_f^i = 1 + \frac{\xi_f}{\varepsilon_f} \frac{df(C_f^i)}{dC_f^i} \quad (\text{XII.43})$$

$$R_p^i = 1 + \frac{1 - \varepsilon_p}{\varepsilon_p} \rho \frac{df(C_p^i)}{dC_p^i} . \quad (\text{XII.44})$$

In the case of a linear sorption isotherm of the form $S(C) = K \cdot C$ where $K = \text{const.}$ for the retardation functions (XII.43) and (XII.44) we get the following constants:

$$R_f^i = 1 + \frac{\xi_f}{\varepsilon_f} K_a^i \quad (\text{in the fracture}) \quad (\text{XII.45})$$

$$R_p^i = 1 + \frac{1 - \varepsilon_p}{\varepsilon_p} \rho K_d^i \quad (\text{in the matrix}) , \quad (\text{XII.46})$$

where ξ_f/ε_f [m^{-1}] is the sorbing surface of the water conducting zone per unit volume of flowing water; K_a^i [m] is the surface based and K_d^i [m^3/kg] the volume based sorption equilibrium distribution coefficients. For more complicated isotherms as, *e.g.* the Freundlich or Langmuir isotherms (Figure XII.7), one must use concentration dependent retardation functions. Hence different parts of a migrating solute plume will move with different rates and its shape will change with time even when neglecting dispersive effects and matrix diffusion. Often, solutes have a finite natural (stable) background concentration in the transport domain. This is assumed to be constant in time and space. Therefore the cumulative solute concentration $C_{\text{total}} = C_{\text{solute}} + C_{\text{background}}$ enters the equations for the retardation functions, thereby avoiding the unrealistic special feature of the Freundlich isotherm that $R(C)$ becomes infinitely large for concentrations approaching zero.

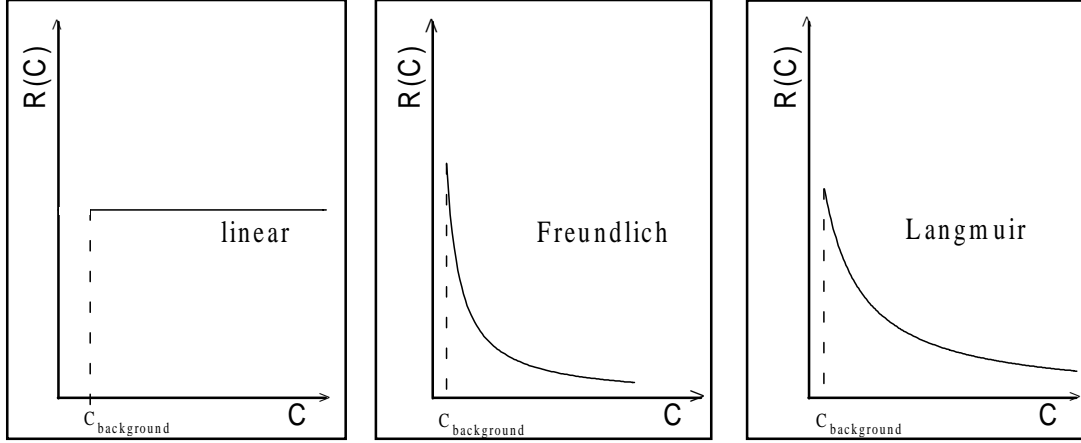
Because both transport equations are first order in time and second order in space, we have to specify for each differential equation one initial and two boundary conditions depending on the physical problem at hand.

The following is used as a common initial condition for both differential equations:

$$\text{a)} \quad C_f^i(z, t) = C_p^i(z, x, t) = C_{\text{background}}^i ; t \leq 0 \text{ and } \forall z, x , \quad (\text{XII.47})$$

meaning that the whole domain of interest has originally a certain solute concentration which may, of course, be zero. As examples, we mention the ^{235}U and ^{238}U content of groundwater flowing through crystalline (granitic) rock.

Figure XII.7: The qualitative behaviour of the retardation functions $R(C)$ for three often used isotherms as depicted in the diagrams.



The continuity condition is as follows:

- b) At the interface fracture/porous (altered) rock matrix, we assume continuity in the concentration; this is given by:

$$C_f^i(z, t) = C_p^i(z, b, t) ; \forall z ; t > 0 , \quad (\text{XII.48})$$

and continuity in flow (but not in the flux) is implicitly included in Eq. (XII.34) and (XII.41), respectively.

The boundary conditions are as follows:

- c) In the porous rock matrix, we choose a no-flow boundary condition at a certain distance $b + d$ [m]; d being the maximum depth for matrix diffusion:

$$D_p^i \frac{\partial C_p^i}{\partial x} \Big|_{|x|=b+d} = 0 ; \forall t . \quad (\text{XII.49})$$

The matrix diffusion is limited if a finite value is assumed for d , so that for sufficiently long time scales the whole accessible rock matrix becomes saturated. If d is so large that only parts of the porous rock close to the interface are invaded by the solute during the time span considered, we have unlimited matrix diffusion. (A limitation of matrix diffusion could result from the presence of a hydrothermally altered zone beneath the fracture embedded in a zone of fresh, unaltered rock with very low porosity which in the model is considered as non-porous.)

With the conditions (XII.47) - (XII.49) the second transport equation - the diffusion equation - can be solved; the corresponding boundary conditions for the transport equation in the fracture must also be fixed:

- d) At the inlet - this means at the upstream boundary - we use the following form of the mixed von-Neumann/Dirichlet (also called Fourier type of) boundary condition²¹ specifying the solute flux:

$$\left(C_f^i - a_L \frac{\partial C_f^i}{\partial z} \right) \Big|_{z=0} = f(t) \cdot \Theta(T_L - t) ; t > 0 . \quad (\text{XII.50})$$

In this expression $\Theta(w)$

$$\Theta(w) = \begin{cases} 0 & ; w < 0 \\ 1 & ; w \geq 0 \end{cases} \quad (\text{XII.51})$$

is the Heaviside step function and $f(t)$ is a time-dependent input function with units [mol/m³] which describes the release of the solute. T_L [s] is the release time for the solute (or species i). The Heaviside step function switches the release function $f(t)$ during the period $[0, T_L]$.

- e) At the downstream boundary, there are different possible boundary conditions: if the transport domain is considered as a semi-infinite medium $[0, \infty)$ a zero concentration boundary condition is often used.

$$\lim_{z \rightarrow \infty} C_f^i(z, t) = 0 ; \forall t . \quad (\text{XII.52})$$

This boundary condition may also be used for the solute breakthrough in a field experiment where, at $z = L$ (L finite), the solute becomes strongly and instantaneously diluted by uncontaminated fracture water.

Another possible boundary condition is the zero dispersive flow condition which corresponds to a free outflow at the outlet at $z = L$:

$$a_L \frac{\partial C_f^i(z = L, t)}{\partial z} = 0 ; \forall t . \quad (\text{XII.53})$$

This boundary condition may be appropriate for modelling column experiments but may also be consistent with a solute transfer to a non-dispersive porous medium.

In most cases it is not possible to obtain an analytical solution of the coupled system of partial and, in general, non-linear differential Eqs. (XII.41) and (XII.42) (for analytical

²¹ A boundary condition is of the von-Neumann type, if the flux in direction normal to the bounding surface of the physical system is known. If the value of the quantity on the boundary is specified, then we have a boundary condition of the Dirichlet type. However, also a mixture of both types of boundary conditions is possible.

solutions, see also [81TAN/FRI, 82SUD/FRI, 85AHN/CHA]). Therefore it is necessary to solve the system of equations numerically. In principle, it is possible to obtain solutions with the help of a number of numerical methods such as finite differences, finite elements, spectral method, random walk, or with the help of the method of line approximations. For certain methods (*e.g.* finite differences, method of lines, *etc.*) one has to take into consideration that the system of partial differential equations may be stiff, especially if processes with very different time scales are taken into account, *e.g.* when chemical reactions are included in the transport problem.

Here, we do not want to go deeper into detail; for further information the reader is referred to textbooks on numerical mathematics, especially for solving partial differential equations of the parabolic type [82LAP/PIN, 93VRE/KOR].

XII.3.6. Effects of matrix diffusion and the effective surface sorption approximation

In a former section we saw that sorption processes still cannot be explained sufficiently well; hence, assumptions on the reversibility and rate of equilibration are made. The sorption capacity and distribution ratio for different solutes and different rocks are in general measured in small scale laboratory experiments (batch sorption experiments). These data are then used to estimate - often via an isotherm formalism - the retardation for a given solute in the rock. For fractured porous rock it is assumed that flow takes place mainly in more or less open fractures, and that the solute only interacts with the fracture surfaces. Possible penetration of the solute into the rock is neglected, and hence, fluid transport through the intact rock matrix between these fractures is also neglected. Retardation in such a case is due to surface sorption. However, with this description the retardation capacity of the rock may be considerably underestimated, because microfissures, connected or unconnected pores do exist even in very dense rocks, such as crystalline rocks (see also Figure XII.1). Solutes not only flow with the groundwater in connected fractures, but also diffuse into the adjacent rock pores. Diffusion of a solute from fractures where the liquid is flowing into such water-filled micro-fissures and dead-end pores acts as a sink for a solute, because rock pores temporarily store the solute. Depending on the solute concentration in the fracture, the concentration gradient in the matrix may change its sign with time, and the diffusion direction then points towards the fracture, showing that the rock matrix can also act as a solute source. The solute may be sorbed on inner surfaces of the pore space and micro-fissures. Both processes, diffusion into the rock matrix and sorption of the solute onto the inner surfaces, slow the rate of migration of the solute and are therefore additional mechanisms for retardation and dilution of the solute concentration in the water-conducting system.

Matrix diffusion has been discussed in connection with groundwater dating [75FOS], in the petroleum engineering literature with the exploitation of oil reservoirs, but has also gained much attention in the context of radioactive waste disposal. Non-sorbing species may penetrate a few tens of centimetres of crystalline rock matrix, if the contact time exceeds 1000 years; however, strongly sorbing species penetrate only fractions of a millimetre in the same time span. Matrix diffusion can enhance the retardation by many

orders of magnitude with respect to retardation by surface sorption only, especially when the diffusion process is combined with a high sorption capacity on the inner surfaces of the rock matrix.

Let us discuss, more quantitatively, how matrix diffusion affects solute transport for a simplified transport problem. We will study the influence of (unlimited) matrix diffusion taking into account only one-dimensional advection and neglecting dispersive effects. For simplicity, the solute is assumed to sorb linearly onto fissure surfaces and pore surfaces of the adjacent rock. Fracture infills and additional sinks for the solute, *e.g.* radioactive decay, will be neglected for the purpose of simplicity. The geometry of the model (see also Figure XII.6), the transport Eqs. (XII.41), (XII.42), the initial (XII.47) and the boundary conditions (XII.49), (XII.50), (XII.52) are described in the previous section.

The solutions of the two transport equations are obtained by using the Laplace transformation technique. Here, we do not go deeper into detail of the formalism and only mention the results. Both solutions are linear combinations of the complementary error function $erfc$ ²², and one has to distinguish between three different solutions depending on whether the solute release has been terminated or not.

In the fracture we get as the solution:

$$\frac{C_f^i(z, t)}{C_0^i} = \begin{cases} 0 & ; \quad 0 < t \leq \beta^i z \\ erfc\left(\frac{\alpha^i z}{2\sqrt{t-\beta^i z}}\right) & ; \quad \beta^i z < t \leq T^i + \beta^i z \\ erfc\left(\frac{\alpha^i z}{2\sqrt{t-\beta^i z}}\right) - erfc\left(\frac{\alpha^i z}{2\sqrt{t-T^i-\beta^i z}}\right) & ; \quad T^i + \beta^i z < t \end{cases} \quad (\text{XII.54})$$

and in the porous rock

$$\frac{C_p^i(z, x, t)}{C_0^i} = \begin{cases} 0 & ; \quad 0 < t \leq \beta^i z \\ erfc\left(\frac{\delta^i}{2\sqrt{t-\beta^i z}}\right) & ; \quad \beta^i z < t \leq T^i + \beta^i z \\ erfc\left(\frac{\delta^i}{2\sqrt{t-\beta^i z}}\right) - erfc\left(\frac{\delta^i}{2\sqrt{t-T^i-\beta^i z}}\right) & ; \quad T^i + \beta^i z < t \end{cases} \quad (\text{XII.55})$$

We have used the following abbreviations:

$$\alpha^i = \frac{\varepsilon_p \sqrt{D_p^i R_p^i}}{b \nu_f}, \quad (\text{XII.56})$$

$$\beta^i = \frac{R_f^i}{\nu_f}, \quad (\text{XII.57})$$

and

$$\delta^i = \alpha^i z + \sqrt{\frac{R_p^i}{D_p^i}} (x - b). \quad (\text{XII.58})$$

From Eqs. (XII.54) and (XII.55) we can see that the solution in the porous rock is reached by substituting $\alpha^i z$ by δ^i in the expression for the relative concentration in the fracture; the solution (XII.55) is equal to the solution in the fracture for $x \rightarrow b$.

²² $erfc(x) = 1 - erf(x)$, where $erf(x) = \frac{2}{\sqrt{\pi}} \int_0^x e^{-\xi^2} d\xi$ and $erf(-x) = -erf(x)$.

Let us first discuss the behaviour of the concentration profile in the fracture for large transport times, *i.e.*, when matrix diffusion becomes important. We distinguish two cases:

1. For long release times T^i (or for constant input) we can calculate the solute breakthrough time t_0^i , which is defined as the time at which the concentration in the fracture at a given position - say z - has reached half of the input concentration C_0^i . The value of the (complementary) error function is $1/2$, if its argument is also approximately half. Hence for t_0^i [s] we find:

$$t_0^i \approx \frac{R_f^i}{\nu_f} z + 4.4 \tau_0^i . \quad (\text{XII.59})$$

In this result the first term of the right hand side is the transport time due to advection only, and we conclude that matrix diffusion gives rise to an additional retardation of $4.4 \tau_0^i$ ($[\tau_0^i] = \text{s}$) where τ_0^i is given by:

$$\tau_0^i = \left(\frac{z}{\nu_f} \right)^2 \left(\frac{\varepsilon_p}{2b} \right)^2 R_p^i D_p^i . \quad (\text{XII.60})$$

2. For short release times, where $T^i \ll t - (R_f^i/\nu_f) z$, we can expand the (complementary) error function into a Taylor series taking into account only linear terms. By means of some straightforward algebra we arrive at the following expression for the concentration in the water-conducting features:

$$\frac{C_f^i(z, t)}{C_0^i} \approx T^i \sqrt{\frac{\tau_0^i}{\pi \left(t - \frac{R_f^i}{\nu_f} z \right)^3}} \exp \left(-\frac{\tau_0^i}{t - \frac{R_f^i}{\nu_f} z} \right) . \quad (\text{XII.61})$$

Asymptotically, this means for $t \gg \frac{R_f^i}{\nu_f} z$ we obtain for the concentration at z in the fracture:

$$\frac{C_f^i(z, t)}{C_0^i} \approx T^i \sqrt{\frac{\tau_0^i}{\pi \left(t - \frac{R_f^i}{\nu_f} z \right)^3}} \propto t^{-\frac{3}{2}} . \quad (\text{XII.62})$$

For the peak maximum at z we set the first derivative of Eq. (XII.61) with respect to time equal to zero and obtain:

$$t(z)_{f, \max}^i \approx \frac{R_f^i}{\nu_f} z + \frac{2}{3} \tau_0^i . \quad (\text{XII.63})$$

The additional retardation for the peak maximum due to matrix diffusion in the case of a short step (pulse) input is approximately six times smaller than that in Eq. (XII.59).

According to Eq. (XII.60) the additional retardation of the peak is enhanced, if

- the square of the migration distance and/or of the matrix porosity becomes larger,
- a tracer is more strongly sorbing in the rock matrix (larger value for R_p^i),
- the square of the water velocity and/or the fracture aperture becomes smaller.

The maximum of the relative concentration at $t_{f,\max}^i$ is reached at:

$$\frac{C_f^i(z, t_{f,\max}^i)}{C_0^i} \approx 0.23 \frac{T^i}{\tau_0^i} \approx \frac{T^i}{4 \tau_0^i} \quad (\text{XII.64})$$

and the peak reduction is enhanced, if τ_0^i becomes large (assuming that $T^i \ll t - \frac{R_f^i}{\nu_f} z$ holds). However, the dependence on T^i in Eq. (XII.64) is due to the normalisation procedure only. The breakthrough curve $C_f^i(z, t)$ is dependent on the product $C_0^i T^i$ corresponding to the released mass of solute and not on the shape of the release function. For illustration purposes we have plotted these results in Figure XII.8.

For completeness sake we also add the expression for the peak-maximum at (z, x) in the porous rock matrix for $t \gg T + \beta^i z$. In analogy to the formalism for the concentration profile in the fracture for the peak-maximum we find:

$$t(z, x)_{p,\max} = \beta^i z + \frac{2}{3} \left[\tau_0^{i1/2} + \frac{1}{2} \sqrt{\frac{R_p^i}{D_p^i}} (x - b) \right]^2. \quad (\text{XII.65})$$

The term $\frac{1}{6}(x - b)^2 \frac{R_p^i}{D_p^i} := \gamma^i$ [s] represents the matrix diffusion time and accounts for the time span to reach the maximum concentration at x in the porous rock zone. Finally, the mixed term in Eq. (XII.65) accounts for the change of the concentration profile in the water conducting zone due to matrix diffusion. As with the advection time $\beta^i z$ and the matrix delay time τ_0^i , the matrix diffusion time γ^i is a third important quantity to characterise transport problems in the framework of the double porosity medium approach.

The peak-maximum for the concentration in the matrix at $t_{p,\max}$ is given by:

$$\frac{C_p^i(z, x, t_{p,\max})}{C_0^i} \approx 0.23 \frac{T}{\left[\tau_0^{i1/2} + \frac{1}{2} \sqrt{\frac{R_p^i}{D_p^i}} (x - b) \right]^2} \quad (\text{XII.66})$$

Finally we mention that the concept of unlimited matrix diffusion encompasses the idea that with increased time the whole rock matrix is available for the diffusing solute. The no-diffusive flux boundary condition (XII.49) states that at $|x| = b + d$ there is a plane impermeable to matrix diffusion. This means physically that solutes diffusing into the porous rock from fractures are essentially restricted to a region beneath the fracture and are reflected at that boundary. From a safety assessment point of view, limited matrix

Figure XII.8: Effects of matrix diffusion in a 1D-advection model and neglecting (longitudinal) dispersion for a non-decaying solute migrating in a semi-infinite medium. In the upper part of the figure the breakthrough curves are shown at z for a rectangular input pulse of $T^i = 1$ hour (dashed line) transported a) purely advectively (solid line-rectangle, with a peak arrival time of $(R_f^i/\nu_f)z = 25$ hours) and b) taking into account also unlimited matrix diffusion. According to Eq. (XII.63) the peak maximum is shifted by $\Delta t \approx (2/3)\tau_0^i$ ($\tau_0^i = 10$ hours) and lowered to $0.23 T^i/\tau_0^i$. In a \log_{10} - \log_{10} plot, shown in the right upper corner, the asymptotic $t^{-3/2}$ behaviour of the breakthrough curve according to (XII.62) can clearly be recognised. In the lower part of the figure the breakthrough curves for a constant input (dashed line) are plotted. First tracer arrival time is again 25 hours taking into consideration only advection. According to Eq. (XII.59) the additional retardation due to matrix diffusion is now $\Delta t \approx 4.4\tau_0^i$.

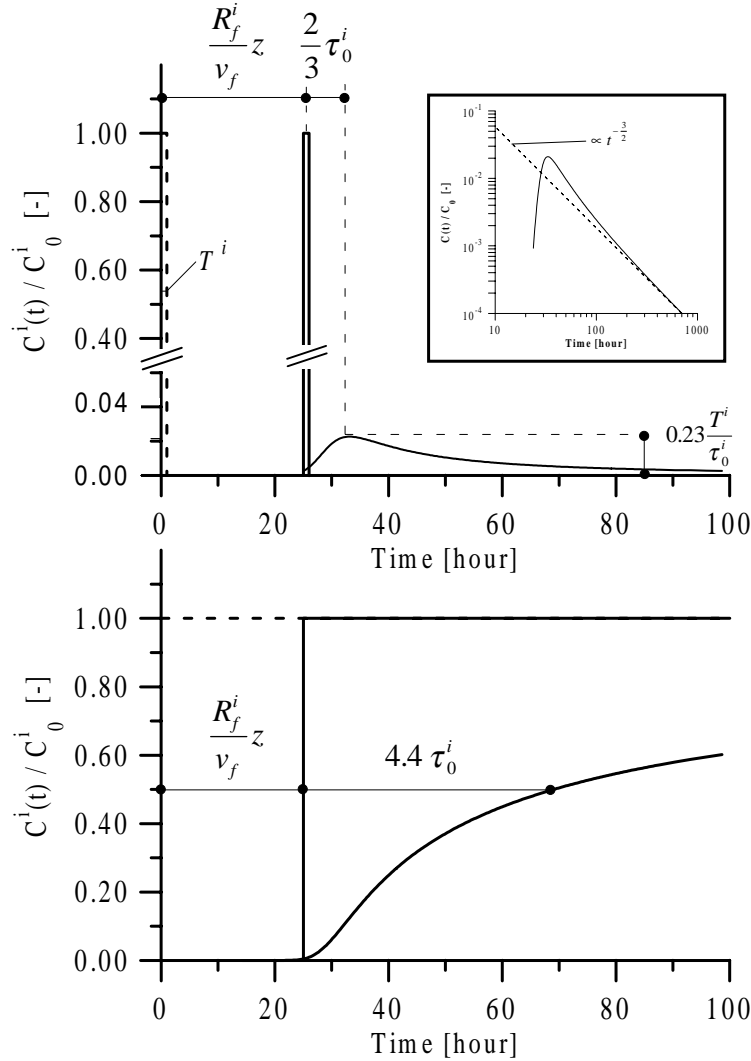
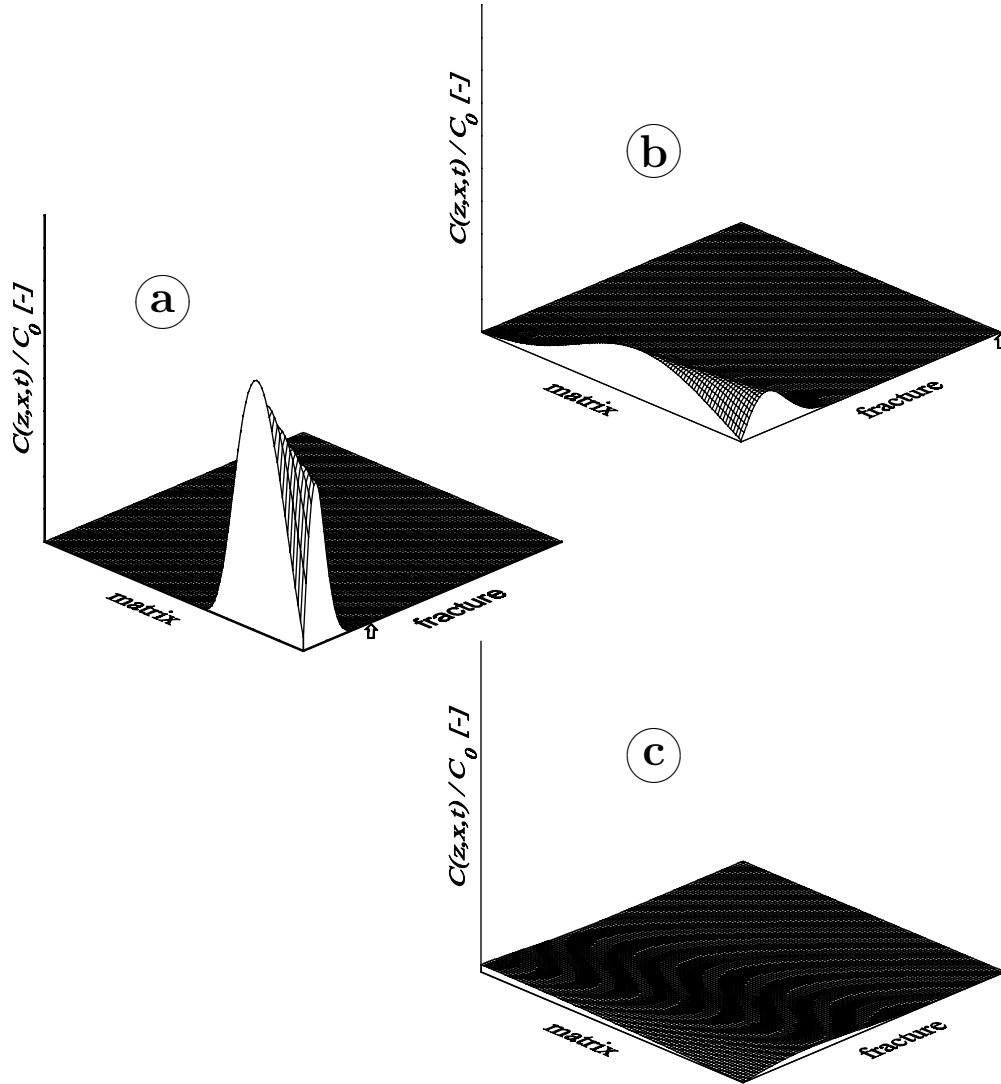


Figure XII.9: The influence of (limited) matrix diffusion for a migrating stable solute taking into account only 1D-advection, 1D-matrix diffusion, neglecting dispersion, and including sorption onto fracture surfaces and onto inner surfaces of the porous rock matrix. The plots show the relative solute concentration $C(z, x, t)/C_0$ [-] as a function of space and time. The fracture upstream boundary (inlet) is at the left, the downstream boundary (outlet) at the right, respectively. Shown is the solute distribution at three different times, increasing from (a) to (c). The arrows indicate the migration distance for the original rectangular input-pulse (top hat) taking into account only advection and fracture surface sorption. Plot (b) is drawn at the advection time $t_{\text{adv}} = (R_f/|\vec{v}_f|)L_{\text{migr}}$; in plot (c) at t_{adv} , four times this value. Matrix diffusion accounts for a marked spreading of the solute in the porous rock matrix and to a strong retardation in the fracture downstream. In plot (c) also an effect of the limitation of matrix diffusion can be recognised: a finite solute concentration at the zero-diffusive flux boundary in the porous rock matrix.



diffusion is a more conservative assumption than the model of unlimited matrix diffusion and results in higher solute concentration in the fracture.

We have already seen that the solute concentration in the porous rock is a function of time and space. If the penetration depth to which the solute is allowed to diffuse is small enough, the kinetics of matrix diffusion can fairly well be ignored in comparison with the long transport times for advection and dispersion, and an effective (fracture) surface sorption approximation may be justified. The concentration in the connected pore spaces in the porous rock adjusts “instantaneously” to the concentration in the water-carrying zone. Therefore we assume a priori the continuity equation to be:

$$C_f^i(z, t) = C_p^i(z, x, t) ; \forall z, x ; t > 0 . \quad (\text{XII.67})$$

The system of transport Eqs. (XII.41) and (XII.42) is reduced to a single partial differential equation for solute transport in the fracture with only an effective retardation factor (assuming linear sorption) which can be defined as follows:

$$R_{\text{eff}}^i = \frac{\text{Total quantity of solute}}{\text{Quantity of solute in solution in the flowing liquid}}$$

Defining

$$K_a^i \equiv \frac{\text{Quantity of solute sorbed per unit area of flow wetted surface}}{\text{Quantity of solute in solution per unit volume of solution}} [\text{m}]$$

as the surface-based sorption equilibrium distribution coefficient and analogously

$$K_d^i \equiv \frac{\text{Quantity of solute sorbed per unit mass of solid}}{\text{Quantity of solute in solution per unit volume of solution}} [\text{m}^3/\text{kg}]$$

as the volume-based sorption equilibrium distribution coefficient and using

$$\begin{aligned} \frac{\xi_f}{\varepsilon_f} &= \frac{\text{Total area of flow wetted surface}}{\varepsilon_f * \text{Total volume of water conducting zone}} \\ &= \frac{\text{Total area of flow wetted surface}}{\text{Total volume of flowing liquid}} , \end{aligned}$$

$$\begin{aligned} \frac{d}{b} \varepsilon_p &= \frac{\varepsilon_f 2 d F_{\text{fracture}} \varepsilon_p}{\varepsilon_f 2 b F_{\text{fracture}}} \\ &= \frac{\text{Total pore volume of the matrix accessible for diffusion}}{\text{Total volume of flowing liquid}} , \end{aligned}$$

$$\begin{aligned} \frac{\rho_{\text{solid}} (1 - \varepsilon_p) d}{b} &= \frac{\varepsilon_f \rho_{\text{solid}} (1 - \varepsilon_p) 2 d F_{\text{fracture}}}{\varepsilon_f 2 b F_{\text{fracture}}} \\ &= \frac{\text{Total accessible mass of the rock matrix}}{\text{Total volume of flowing liquid}} , \end{aligned}$$

where F_{fracture} is the surface of the water conducting zone, we get the effective retardation factor R_{eff}^i :

$$\begin{aligned} R_{\text{eff}}^i &= 1 + \frac{\xi_f}{\varepsilon_f} K_a^i + \varepsilon_p \frac{d}{b} \left(1 + \rho_{\text{solid}} \frac{(1 - \varepsilon_p)}{\varepsilon_p} K_d^i \right) \\ &= R_f^i + \varepsilon_p \frac{d}{b} R_p^i \end{aligned} \quad (\text{XII.68})$$

Comparing (XII.68) with (XII.45) we see that the additional term is due to limited bulk sorption which is obtained instantaneously. If there is no matrix sorption, *i.e.* $K_d^i = 0$ and $R_p^i = 1$ the additional term is reduced to $(\varepsilon_p d)/b$ representing only the amount of nuclides in the pore water. The advantage of the effective surface sorption approximation is evident: The coupled system of transport equations is reduced to a single partial differential equation for transport in the fracture requiring much less numerical expenditure.

With the help of the matrix diffusion time γ^i (see Eq. (XII.65) ff.) we are able to estimate the times required to equilibrate the porous rock zone accessible for matrix diffusion so that the R_{eff}^i -concept may be used.

- If the release time T^i is large compared to the matrix diffusion time γ^i , then the concentration gradient within the porous rock zone becomes flattened, and the effective surface sorption approximation may be used.
- If, however, the release time T^i , **and** the spreading due to dispersion at the downstream boundary, which is approximately given by $\frac{2\sigma^i(z=L)}{\nu_f} R_f^i$, **and** the spreading due to matrix diffusion, which is approximately $1.4 \tau_0^i(z=L)^{23}$, are small compared to the matrix diffusion time γ^i , we have an indication that the porous rock zone is not equilibrated and the effective surface sorption approximation is not applicable.

Let us now discuss the effect of limited matrix diffusion and the effective surface sorption approximation with the help of a special example. Imagine a deep-lying repository for radioactive waste. Long after the final closure of the repository ^{237}Np , and many other nuclides, will be released into the geosphere. For the following considerations we will partially adopt parameter values from a study of geospheric nuclide transport for a Swiss model repository. A release time $T = 12$ million years and a constant inlet concentration of $C_0(t) = 10^{-7}$ M is assumed and the nuclide's half life is 2.14 million years. We assume a zero concentration boundary at $L = 2050$ m and an observation point after $z = 500$ m. For simplicity we will limit our consideration to one dimension only. In addition to advection and matrix diffusion we also include longitudinal dispersion. For the relevant transport parameters the values in Table XII.2 are assumed.

In Figure XII.10 several calculations are shown, using the transport code RANCHMD [90RAN], with varying porous rock matrix thickness d , as indicated in the legend.

The figure shows the impact of limited matrix diffusion on ^{237}Np breakthrough. A first calculation is made excluding matrix diffusion considering only advection and dispersion as

²³ Further information concerning the factor 1.4 can be found in [94HEE/HAD2] - Appendix 1.

Figure XII.10: The effect of limited matrix diffusion on ^{237}Np breakthrough. d is the depth of the porous rock matrix. For comparison purposes the unlimited case, including also a calculation with no radioactive decay, is shown.

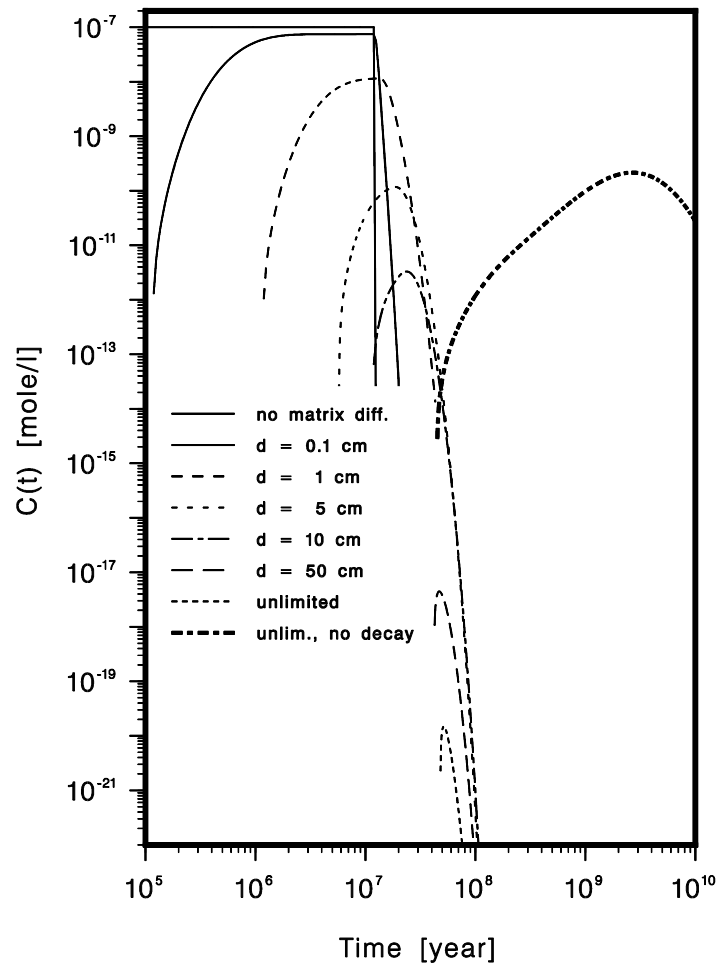


Table XII.2: Values for some transport parameters used in the double porosity medium approximation (see text).

Fracture aperture (no infill assumed)	$2b$	[m]	10^{-4}
Longitudinal dispersion length	a_L	[m]	100
Water velocity	ν_f	[m/year]	2.84
Matrix porosity	ε_p	[-]	$3.5 \cdot 10^{-2}$
Diffusion constant	D_p	[m ² /s]	$1.4 \cdot 10^{-11}$
Solid density	ρ_{solid}	[kg/m ³]	2700
Surface-based sorption constant (in the fracture)	K_a	[m]	0
Volume-based sorption constant (in the matrix)	K_d	[m ³ /kg]	0.1

the solute transport mechanisms. According to Eq. (XII.8) the spreading due to dispersion is $2\sigma_z^i(t) \approx \sqrt{8a_L z}/(\nu_f/R_f^i)$ and the nuclide front reaches the observation point only after about 220 years. Therefore the spreading cannot be recognised in the figure - the trailing edge is practically vertical. For the next curve the spreading is marked both, for the rising and for the trailing parts of the curve. Although the depth of the matrix is only one millimetre, matrix diffusion also causes a decrease of the peak maximum due to the combined effect of enhanced solute retardation and radioactive decay. For increased values of the matrix penetration depth, the peak maximum is more and more lowered and shifted to later times. Due to the additional retardation through matrix diffusion, the spreading due to dispersion alone also becomes more and more pronounced. Hence, it is the interaction of dispersion and matrix diffusion which enforces the solute spreading. Furthermore, a calculation for unlimited matrix diffusion was also made. In this, the maximum concentration is lowered by another three orders of magnitude. Finally, a calculation made assuming no decay for the solute illustrates the dilution capacity of matrix diffusion: the maximum concentration is lowered by three orders of magnitude, and the peak arrival time is shifted to later times by more than two orders of magnitude. It is the additional retardation which may become very important in the frame of a safety

assessment; if transport times become large compared to the half-life of the nuclide, radioactive decay will decrease the original nuclide inventory. Finally, we would like to mention the conservative aspect of limited, compared to unlimited matrix diffusion. Solute concentrations in the fracture may be higher by orders of magnitude, if solute uptake by the matrix is restricted to a limited domain beneath the fracture.

In another series of calculations we illustrate the quality of the effective surface sorption approximation (Figure XII.11).

Solid lines in Figure XII.11 correspond to calculations including matrix diffusion and dashed lines to the effective surface sorption approximation (essa). An excellent agreement between the two models can be seen in the plot for penetration depths to, say, 10 cm. This is a consequence of the very limited volume of porous rock matrix available for molecular diffusion and the rapid equilibration between fracture water and liquid in the matrix pore space for the given length of the released nuclide pulse. However, if the porous rock beneath the fracture is not equilibrated fast enough, *i.e.* if the extension of this domain is comparable to the penetration depth ($x_{1\%} - b$), it is not possible to represent matrix diffusion by an effective retardation factor or function. The single porous medium approach is not applicable, because matrix diffusion is now a time-dependent transport process.

XII.3.7. Modelling methodology and further examples

In the following, we will highlight the power of the double porosity medium concept with the help of some examples; but we will also point out the principal deficiencies of the models used.

As a first example we will study the calculations for the migration experiments performed in the Grimsel underground laboratory in central Switzerland. There, for several years tracer migration experiments have been performed as a joint undertaking of NAGRA²⁴, PNC and PSI [92FRI/ALE]. Their aim is to develop the know-how for field experiments under conditions comparable to those of possible sites for a radioactive waste repository and to gain a better understanding of the processes relevant to radionuclide transport in the geosphere. Some 400 m below the surface, a hydraulic dipole field is generated in a well-characterised fracture zone in a granitic rock (see Figure XII.12). A wide variety of stable and radio-tracers is used; non-sorbing tracers such as uranine, ³He, ⁴He, ⁸²Br, ¹²³I, weakly sorbing tracers such as ²²Na and ²⁴Na, and moderately strongly sorbing ones, such as ⁸⁵Sr, ⁸⁶Rb, ¹³⁷Cs, The migration experiments are accompanied by extensive laboratory investigations on petrography, water-rock and nuclide-rock interaction [89BRA/AKS]. Thus, values for parameters are available from independent experiments, and hence the best fit-parameter values from the migration model can be tested for consistency with the laboratory data. In addition to the experimental activities, extensive modelling work is also performed, *e.g.* [94HEE/HAD2, 94HEE/HAD3, 96HAD/HEE]. We

²⁴ NAGRA: National Cooperative for the Disposal of Radioactive Waste (Switzerland),
PNC: Power Reactor and Nuclear Fuel Development Corporation (Japan),
PSI: Paul Scherrer Institute (Switzerland).

Figure XII.11: Comparison of the effective surface sorption approximation **essa** (dashed lines) with calculations assuming matrix diffusion (solid lines) for various penetration depths d .

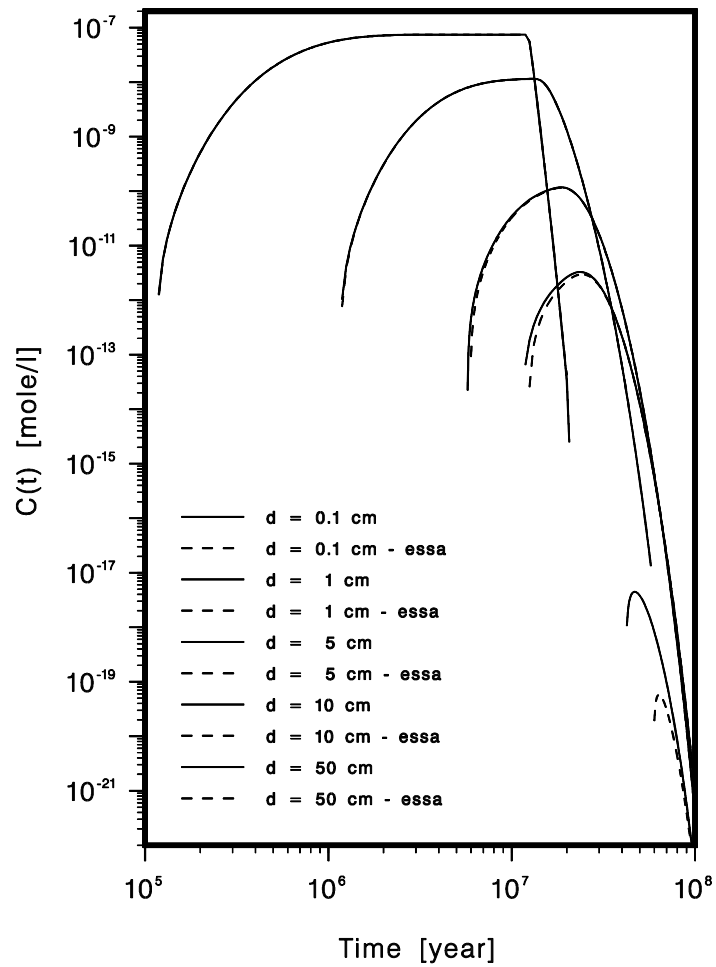
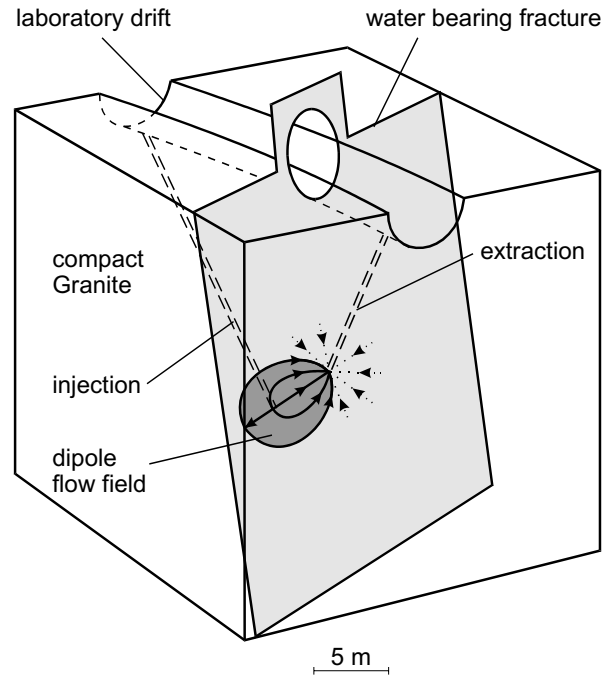


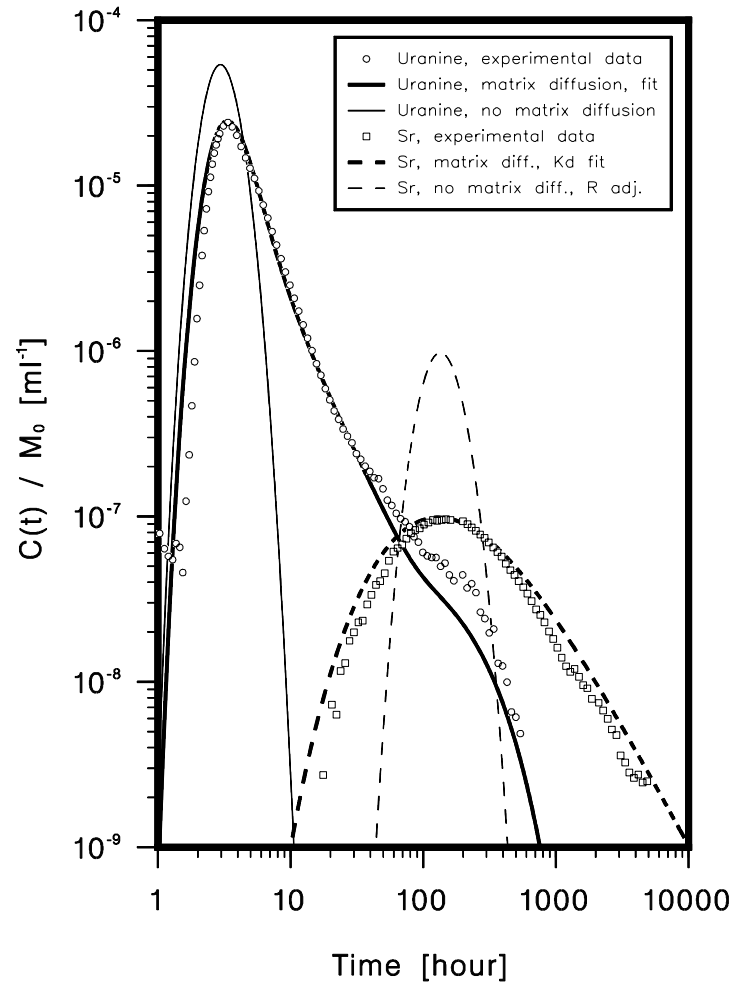
Figure XII.12: Schematic overview of the Grimsel migration experiment showing the laboratory drift, some of the boreholes drilled for the hydrogeological characterisation and the tracer experiments. Within the migration shear zone an artificial dipole flow field is established as depicted in the figure.



have chosen data for a conservative tracer - uranine - and a moderately sorbing tracer - strontium - to illustrate the effects of limited matrix diffusion.

As can be seen in Figure XII.13, good reproduction of the experimental data can only be obtained by including matrix diffusion in the model.

Figure XII.13: Effect of matrix diffusion on tracer breakthrough for a conservative (uranine) and for a weakly sorbing tracer (strontium). (Figure according to [94HEE/HAD2]). The curves refer to the best-fits with matrix diffusion. The calculations demonstrate that it is cogently necessary to include this process in the model.



From the fitting procedure the following values were obtained:

a) from modelling the conservative tracer (uranine)²⁵:

			Geological investigations
$2b$	[m]	$\left(9.3 \pm_{3.0}^{4.6}\right) \cdot 10^{-5}$	
a_L	[m]	$\left(25 \pm_4^5\right) \cdot 10^{-2}$	
ε_p	[-]	$\left(6.2 \pm_{3.2}^{6.8}\right) \cdot 10^{-2}$	$\left(12 \pm_5^8\right) \cdot 10^{-2}$
D_p	[m ² /s]	$\left(2.5 \pm_{2.0}^{11}\right) \cdot 10^{-11}$	$\left(7.5 \pm_4^8\right) \cdot 10^{-11}$

For comparison purposes also values for the rock porosity and the diffusion constant deduced from geological investigations are presented at the right end of the table (taken from [94HEE/HAD2] - Appendix 5).

b) from modelling of the sorbing tracer (strontium) we obtain in addition²⁶:

K_d	[m ³ /kg]	$\left(21 \pm_{14}^{38}\right) \cdot 10^{-3}$
-------	----------------------	---

This value can now be compared with those from independent, *e.g.* batch sorption experiments for K_d (Table XII.3). It may be questioned if it is reasonable to compare values from experiments which have been made with so different time and concentration scales. In the case of strontium, independent measurements for K_d were performed and are listed below together with the value obtained from the Grimsel migration experiment.

The K_d values are consistent within the estimated uncertainty range indicating that for “nuclides sorbing rapidly, and not too strongly, and exhibiting a reversible cation exchange process on fault gouge, the laboratory sorption coefficients can reasonably well

²⁵ No infill in the water conducting zone was assumed. ε_p and D_p could be determined separately because the breakthrough curve was measured long enough until the prominent bump at the end of the experiment indicating limited matrix diffusion. The parameters are median values of log-normal distributions and the errors correspond to one geometric standard deviation - expressing therefore relative uncertainty limits.

²⁶ The parameters determined with uranine are assumed to be valid also for strontium hence, leaving K_d as the only freely adjustable parameter.

Table XII.3: Comparison of the volume-based sorption equilibrium distribution coefficient, K_d , for strontium from different laboratory experiments and from the Grimsel migration experiment. The large positive errors of the K_d values from the batch and the rock-water interaction experiments originate in the extrapolation of the laboratory results to the conditions in the migration fracture. The errors of the K_d from the migration experiment correspond to one geometric standard deviation (taken from [94HEE/HAD2]).

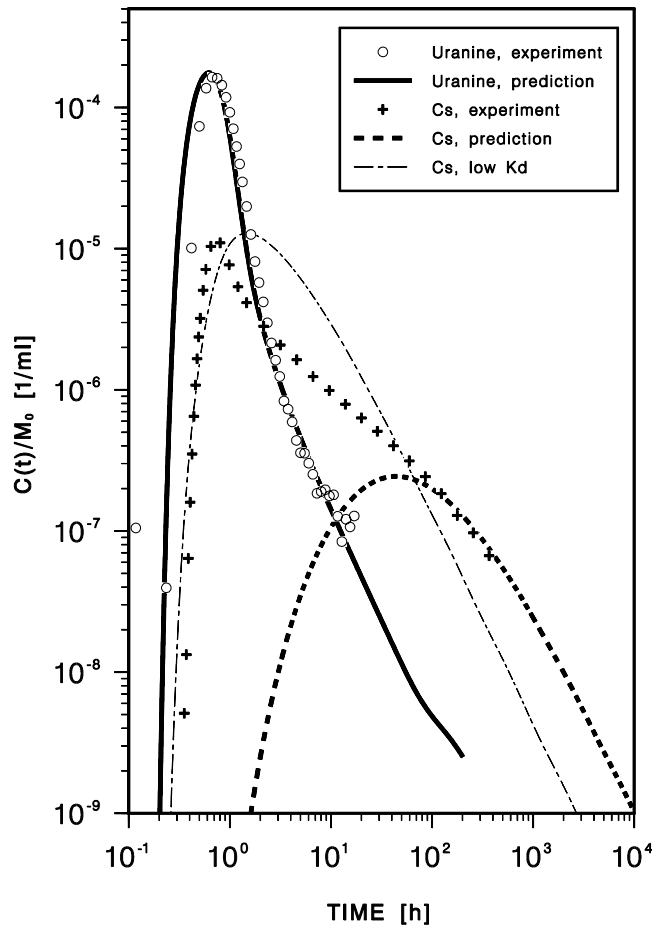
Experiment	$K_d \cdot 10^3 \text{ [m}^3\text{/kg]}$
Batch (grain size < 63 μm)	$41 \pm_4^{39}$
Batch (grain size < 250 μm)	$25 \pm_1^{22}$
Batch (loosely disaggregated)	$13 \pm_1^{19}$
Rock-water interaction (loosely disaggregated)	$8 \pm_2^8$
Migration experiment	$21 \pm_{14}^{38}$

be extrapolated to field conditions. Adequate care in selecting and preparing the rock sample is, of course, a necessary requirement” [94HEE/HAD2]. Note, for strontium it was not possible to determine values for ε_p and K_d because the breakthrough curve was not monitored long enough until the bump in the trailing edge indicating limited matrix diffusion appeared.

In order to illustrate the predictive qualities of the double porosity medium approximation the breakthrough curves for uranine and cesium were calculated for other experimental conditions. These new experiments were then made in the same fracture but using a smaller and faster dipole flow field where the transport times were much shorter. The values of the sorption distribution coefficient K_d and the parameters characterising the fracture and matrix from the modelling within the longer dipole field were used. In Figure XII.14 the predictions and the experimental data are compared with each other.

For uranine the agreement is excellent, indicating that the average fracture properties for the small dipole flow field are the same as for the longer ones and that the model is consistent. However, for cesium the fast breakthrough was not predicted at all. A calculation with a smaller K_d -value could fairly well reproduce the rising edge but failed completely to describe the trailing part of the breakthrough curve. This fact indicates that neglecting slow sorption kinetics for cesium (not covered by effects of matrix diffusion) might be the reason for the marked discrepancy between model and observed data. In experiments in a slower and longer dipole field, the effects of sorption kinetics could not

Figure XII.14: Prediction of uranine and cesium breakthrough in the Grimsel migration experiment using the double-porosity medium concept for a smaller and faster dipole flow field. The transport parameters were calibrated first on breakthrough curves for both tracers in the same fracture but in a longer dipole field. The experimental data are shown as circles or crosses. For uranine there is an excellent agreement between the model and the experimental data. This is not the case for cesium where the model does not match the measurements, especially not in the rising part. The shape of the peak region of the cesium breakthrough curve may indicate slow sorption kinetics.



be observed. For a safety assessment of a nuclear waste repository, sorption kinetics would certainly be less important due to the much longer time-scale being involved here.

Experiments similar to the ones at the Grimsel underground laboratory were performed in Sweden in the early 80's with extensive migration experiments at a test site near lake Finnsjön 140 km north of Stockholm. The tracer tests were made in granitic rock at a depth of about 100 m in a highly permeable fracture zone. One of the migration distances was about 30 m, and among the tracers used there were inactive iodide, strontium and cesium. The experiments are documented in detail in [81GUS/KLO, 84GUS/KLO]. In the past, several attempts to model these experiments were made, especially by teams participating in INTRACON [86INT]. A further detailed analysis was performed by PSI and is documented in [94JAK/HAD]. We have selected two calculations from this study as examples to demonstrate the iterative character of such modelling work. A first calculation was done using only the single-/double-porosity medium concept.

Figure XII.15 illustrates that the single-porosity medium approach reproduces the measured data only roughly and represents a somewhat 'averaged' behaviour. Including matrix diffusion results only in slightly different values of the fitting parameters and does not improve the overall-quality of the fit (*e.g.* smaller value for the χ^2 -merit function). Only by introducing a second preferential flow path with its own set of freely adjustable fitting-parameters do we obtain a much better representation of the experimental data, especially in the rising edge of the breakthrough curve (Figure XII.16); hence, this model seems closer to the "experimental reality".

In order to judge a given model we have to compare the extracted best-fitting parameter values also with the model's underlying assumptions.

As seen from Table XII.4 the value for the longitudinal dispersivity in the case of a one-flow-path system is approximately equal to the migration distance. Such a value is very large for an experiment of this type and indicates that the advection-dispersion equation may not be useful. By introducing a second flow path this quantity is reduced to a reasonable value. The study showed that it was only by including the full information of the experiment that further improvements could be reached, *e.g.*, also pump flow variations at both boundaries - up- and downstream - had to be taken into account. Such variations in the pumping rates had a critical influence on the extracted best-fit parameter values and could partially be identified as wiggles and peaks in the experimental breakthrough curve.

We would like to finish this chapter with some remarks on the double-porosity medium approximation as it was demonstrated in this section. This approach is still used worldwide for modelling both laboratory and field experiments and for safety assessment purposes. An advantage of the concept is that it is easy to understand the underlying physics and chemistry. The model is also capable of accurately fitting even complex experiments. Past experience has shown it to be a versatile, efficient and also appropriate tool for modelling, because it covers the most important transport processes such as advection, dispersion, matrix diffusion, sorption, *etc.*; it is also flexible enough to take into consideration various flow geometries such as the planar fracture (parallel plate representation), vein geometry and superposition of flow paths. It is the simplicity of this concept, its

Figure XII.15: Plot of a best-fit curve for iodide breakthrough in a Finnsj n migration experiment in the frame of a single-porosity medium approximation. Also shown are the experimental data as indicated in the legend.

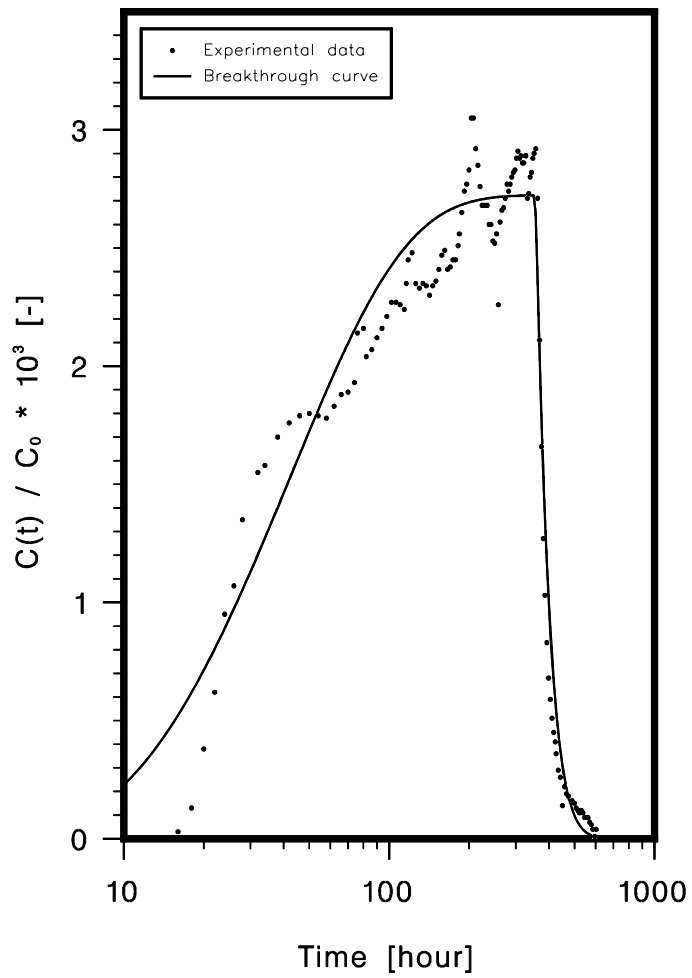


Figure XII.16: A calculation using the same experimental data as in Figure XII.15 but including a second preferential flow path. The tracer breakthrough concentration in the fracture is given by the superposition of the contribution of both flow paths. The full-drawn curve is the best-fit with this model.

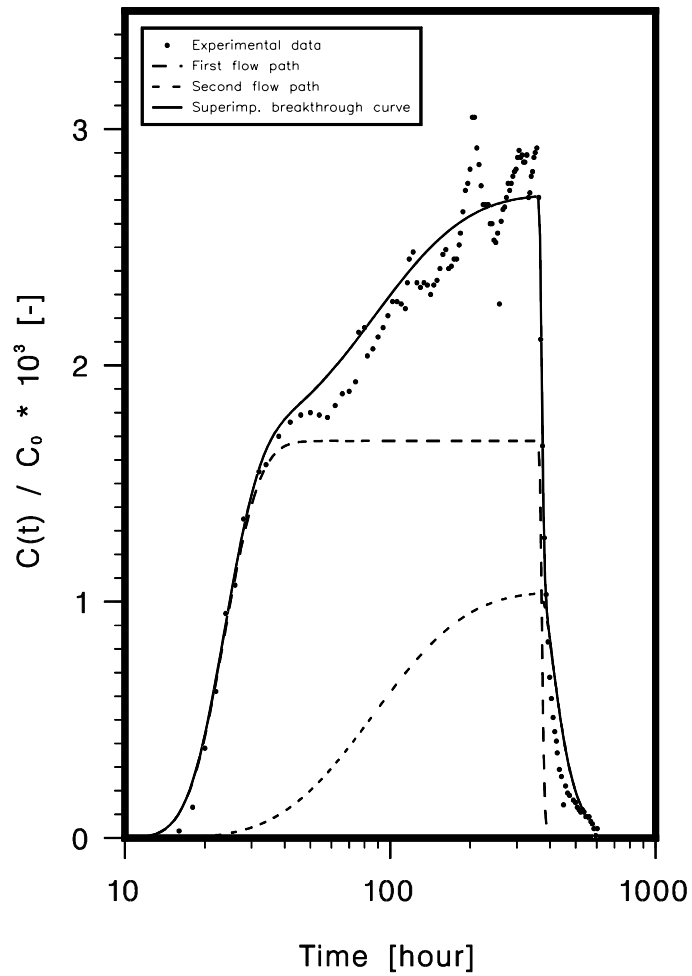


Table XII.4: Values of the best-fitting parameters and the minimum value for the χ^2 -merit function for two alternative calculations for iodide breakthrough in the Finnsjön migration experiment assuming either one or two preferential flow path(s). $a^{(i)}$, $i = 1, 2$ are the weighting factors for each flow path; they sum up to unity. (Superscripts denote the first and second flow path.)

Parameter	Unit	1 flow path	2 flow paths
$a^{(1)}$	[-]	1.0	0.617 ± 0.031
$a^{(2)}$	[-]	-	0.383 ± 0.031
$a_L^{(1)}$	[m]	31.8 ± 9.7	9.47 ± 0.07
$a_L^{(2)}$	[m]	-	8.70 ± 3.77
$ \nu_f^{(1)} \cdot 10^{-4}$	[m/year]	0.530 ± 0.017	1.08 ± 0.04
$ \nu_f^{(2)} \cdot 10^{-4}$	[m/year]	-	0.254 ± 0.025
$\chi^2 \cdot 10^5$	[-]	0.459	0.242

versatility and applicability to a broad variety of real-world observations in the context of solute transport in geological media, which has established the usefulness of the double porosity medium model.

XII.4. Acknowledgments

The author would like to express his indebtedness to I. Grenthe, J. Hadermann, W. Heer, and J. Pearson for reviewing and valuable criticism during the preparation of this chapter.

XII.5. Glossary

For our purposes we denote as a *continuum* a part of the space (body) which is occupied by mass. All quantities describing the behaviour of a body, such as the density, temperature etc., have to be continuous functions in space and time. The behaviour of a material as a whole is relevant for the investigations, and any microscopic (molecular) consideration is disregarded. This description does not reflect the real physical situation; it is only a convenient abstraction of a real world fact and permits the mathematical treatment of

physical quantities as continuous functions. In such a concept only averaged properties are taken into account and microscopic fluctuations are not considered (see also REV).

Extensive quantities depend on the size of the physical system. They are proportional to the system dimensions such as volume, mass, *etc.* and thus are additive. If two or more separate physical systems are combined to a unified system, then the extensive quantities are the sum of those of the constituent systems.

An *intensive quantity*, such as, *e.g.*, pressure, density, *etc.* is independent of the system dimensions. Intensive quantities are continuous functions of the space and time variable, since the values of these quantities have to be specified at each point in the system. These values may change from point to point, and such quantities are not additive.

As examples for extensive and intensive quantities we mention:

Extensive variables	Intensive variables
Number of particles N Volume V (total) Energy E Entropy S Internal energy U Mass m Charge q	Temperature T Pressure p Chemical potential μ Velocity ν Specific heat Density ρ

A *model* is an abstraction of a real world phenomenon. In a given model, a state of a physical object, the forces which interact between physical objects, and events are represented by mathematical formulae which contain variables and constants. Such (mathematical) variables or constants represent physical quantities. In this sense a model is only a hypothesis of the temporal behaviour of a physical object under the effect of forces being totally independent and artificial to the physical objects, forces and events considered. A model incorporates a large number of assumptions or simplifications about the real world phenomena and is therefore never a complete nor an exact description of a real world phenomenon, *cf.* Chapter .

A *porous medium* is defined according to Bear and Bachmat [91BEA/BAC] as “... a portion of space occupied by heterogeneous or multiphase matter. At least one of the phases comprising this matter is not solid. They may be gaseous and/or liquid phases. The solid phase is called the solid matrix. That space within the porous medium domain that is not part of the solid matrix is referred to as void (or pore) space.”

A fracture can be seen as a part of the void space but with the property that the fracture aperture or fracture width is much smaller than its length. The aperture is an important parameter for transport modelling, although this quantity is not a constant along the fracture and may be difficult or impossible to determine. The aperture is an averaged model parameter and has nothing to do with the actual openings for transport of a solute. Fractures may be partially filled with, *e.g.*, clay minerals and other materials reducing

the real fracture width. Such infills may strongly influence the transport properties of fractures.

Matter is denoted as *homogeneous* with regard to a certain property, if this property does not vary in space, hence, is translation-invariant. If this property is independent of direction at a considered point, the medium is said to be *isotropic* at that point. Hence, it is rotation-invariant. An example of a homogeneous but anisotropic medium is a Weiss-domain in ferromagnetic materials where all the elementary magnets are aligned.

A *process* is defined as the act of changing a physical system from a given state to another. Only the initial and the final states are fixed; in general, nothing is said about intermediate states. A system in equilibrium neither changes its mass nor its energy. In other words, none of its properties changes with time.

A *REV* (Representative Elementary Volume) is the selected minimum volume of material over which a physical quantity can be averaged so that its value is not sensitive to small variations of the REV and variations of its size. The size of such a REV strongly depends on the geometry of the material and represents (generally speaking) the smallest possible volume which contains the full complexity of the physical system. In practice, it is very cumbersome to determine the size of a REV, as it is strongly site-specific. For further consideration of this problem of REV-formation we refer to literature [91BEA/BAC], and [86MAR3].

Closed systems have boundaries which are permeable for energy transfer in both directions but not for the transfer of matter. Such systems have a fixed mass and composition but a variable total energy.

Open systems are characterised by walls which allow transfer of both matter and energy in both directions, to and from the system. Such systems have neither a fixed mass and composition nor a fixed energy level.

For completeness we mention three important categories of mathematical quantities underlying the physics of transport phenomena:

1. A *scalar* is a tensor of zero order. A scalar quantity is characterised by its magnitude only and shows no direction dependence hence being specified by one single numerical value. Changing the co-ordinate system does not affect its value being an invariant. Examples of scalar quantities are concentration, pressure, density and temperature.
2. A *vector* is a tensor of the first order and is characterised by its magnitude and its direction. In a 3-dimensional space it may be decomposed into three scalar quantities. Changing the co-ordinate system does not affect a vector only its components. Velocity and momentum are examples of vector quantities.
3. A *second rank tensor* is a mathematical entity which is characterised by its magnitude and two directions. A second rank tensor may be resolved into 9 scalar quantities which are dependent on the co-ordinate system; however the tensor is invariant. Diffusivity and viscosity stress are examples of tensors of the second order.

Chapter XIII

The Pillars of Safety

Jörg HADERMANN
Paul Scherrer Institut
CH-5232 Villigen PSI (Switzerland)

XIII.1. Introduction

Disposal of nuclear wastes arising from medicine, industry, research and nuclear power production is a global challenge to society. Both from the perspective of volume and from activity the wastes from the latter dominate by far. In the present section we restrict ourselves to high-level radioactive wastes and the direct disposal of spent fuel elements. Since the planning stage of nuclear energy production, consideration and preference have been given to geological disposal (*e.g.*, [57NAT]), though a broad spectrum of disposal options has been explored in the early years (*e.g.*, [74BAT]), ranging from extraterrestrial to disposal in ice sheets.

The long-term safety of a geological repository relies on a series of barriers: the engineered and the geological barrier systems. The purpose of the first is to contain the wastes for a period of time such that short-lived nuclides have decayed to insignificance, and then to limit the release rate of surviving radionuclides. The purpose of the second barrier is to retard radionuclide migration so that the radioactive inventory is substantially reduced by decay, and dilute the concentration of the most long-lived nuclides. In a safety assessment, it has to be shown that both mechanisms lead to acceptable dose expositions or risks for the future generations of man. In the following we will shortly, and necessarily incompletely, outline the salient elements of a safety assessment and discuss the most important factors for safety.

The first step in a safety assessment is a *scenario analysis*. This specifies possible events and processes controlling repository system behaviour (Table XIII.1) and provides a broad description of their characteristics and sequencing [92NEA]. As a result possible futures of the repository system are identified as well as the classes of models required

for a quantitative safety assessment. For example, radionuclides might be transported in flowing groundwater through the geosphere; however, a sufficiently high gas production from corrosion of repository materials might call for multiphase flow models. A practical illustration of scenario identification and evaluation is given in [91SKI] in the context of examining methods and requirements for future repository licensing.

Given a scenario, a *model chain* is established describing the temporal evolution of the repository system and, specifically, the release and transport of radionuclides to the biosphere, and appropriate parameter values or distributions are determined. It has to be noted that parameters are mostly model dependent and, therefore, special attention has to be paid to the consistency between models and parameters. This is especially true when a discrimination is made between detailed research models and simplified performance assessment models. For example, if sorption distribution ratios were extracted from experiments with the aid of a dual porosity medium model and have made their way into a sorption data base, it is pointless to use such data in a fast-running code based on a single porosity model. A typical example of the model chain for a groundwater scenario is given in Figure XIII.1. The driving force is the hydraulics describing the subsurface water movements. On one hand, water carries the corroding agents into the engineered barrier system, on the other it transports the leached radionuclides to the biosphere. Hence, the three parts of the model chain are water transport, engineered barrier performance and radionuclide transport.

The temporal scale of safety assessments extends far into the future. For this reason the question of model validation (we stress: for the intended use, performance assessment) has received special attention over the last decade. Consequently, a great effort has been spent in testing models by laboratory and field experiments and through consideration of natural analogues. Going into details would lead too far and the reader is referred to the contributions of a recent symposium [94GEO]. Models for safety assessment do not need to predict the future accurately, they have rather to give an upper bound of consequences in possible futures. They are firmly based on fundamental principles like momentum and mass conservation. Also, during the past years no new processes had to be conjectured to explain experiments. However, there remain open issues; we mention two of them: On the side of radionuclide transport the problem of scaling up from field to repository scales and the influence of heterogeneities is largely unresolved [96NEA], and on the side of geochemistry it is the applicability of thermodynamic concepts [91GRE]. Within safety assessment, the impact of such shortcomings is investigated through uncertainty and sensitivity analyses.

Finally, the results from scenario analysis and model calculations are combined into an *integrated safety assessment* allowing a comparison with safety criteria. Several such integral assessments have been performed to date (the newest ones are [88PAG, 92PRE, 92SKB, 93VIE/HAU, 94KRI]). These assessments show that safety criteria can be met if the sites are chosen appropriately and the repositories are carefully designed, and they have identified areas where additional research will decrease the broad band of uncertainties most effectively. A discussion of research needs from the perspective of disposal of vitrified high-level waste is given in [93HAD/MCC].

Table XIII.1: Example compilation of features, events and processes for a deep geological repository.

1.	NATURAL PHENOMENA	1.4	GEOMORPHOLOGICAL
1.1	EXTRA TERRESTRIAL	1.4.1	Land slide
1.1.1	Meteorite Impact	1.4.2	Denudation (aeolian and fluvial)
1.1.2	Solar insolation	1.4.3	River, stream, channel erosion (downcutting)
1.2	GEOLOGICAL	1.4.4	River meander
1.2.1	Plate movement/ tectonic change	1.4.5	Freshwater sediment transport and deposition
1.2.2	Changes in the Earth's magnetic field	1.4.6	Coastal erosion and estuarine development
1.2.3	Magmatic activity (intrusive, extrusive)	1.4.7	Marine sediment transport and deposition
1.2.4	Metamorphic activity	1.4.8	River meander
1.2.5	Diagenesis	1.4.9	Chemical denudation and weathering
1.2.6	Uplift and subsidence (orogenic, isostatic)	1.4.10	Frost weathering
1.2.7	Diapirism	1.5	HYDROLOGICAL
1.2.8	Seismicity	1.5.1	River flow and lake level changes
1.2.9	Fault activation	1.5.2	Site flooding
1.2.10	Fault generation	1.5.3	Recharge to groundwater
1.2.11	Rock heterogeneity (permeability, mineralogy), affecting water and gas flow	1.5.4	Groundwater discharge (to surface water, springs, soils, wells, and marine)
1.2.12	Undetected features (faults, fracture networks, shear zones, brecciation, gas pockets)	1.5.5	Groundwater flow (Darcy, non-Darcy, intergranular fracture, channelling and preferential pathways)
1.2.13	Natural gas intrusion	1.5.6	Groundwater conditions (saturated/unsaturated)
1.3	CLIMATOLOGICAL	1.5.7	Saline or freshwater intrusion
1.3.1	Precipitation, temperature, and soil water balance	1.5.8	Effects at saline-freshwater interface
1.3.2	Extremes of precipitation, snow melt and associated flooding	1.5.9	Natural thermal effects
1.3.3	Coastal surge, storms, and hurricanes	1.6	TRANSPORT AND GEOCHEMICAL
1.3.4	Sea-level rise/fall	1.6.1	Advection and dispersion
1.3.5	Periglacial effects (permafrost, high seasonality)	1.6.2	Diffusion
1.3.6	Glaciation (erosion/deposition, glacial loading, hydro-geological change)	1.6.3	Matrix diffusion
1.3.7	No ice age		

Table XIII.1 (continued)

1.6.4	Gas mediated transport	2.1.3	Shaft or access tunnel seal failure and degradation
1.6.5	Multiphase flow and gas driven flow	2.1.4	Stress field changes, settling, subsidence or caving
1.6.6	Solubility limit	2.1.5	Dewatering of host rock
1.6.7	Sorption (linear/non-linear, reversible/irreversible)	2.1.6	Material defects (<i>e.g.</i> , early canister failure)
1.6.8	Dissolution, precipitation, and crystallisation	2.1.7	Common cause failures
1.6.9	Colloid formation, dissolution, and transport	2.1.8	Poor quality construction
1.6.10	Complexing agents	2.1.9	Design modification
1.6.11	Fracture mineralisation and weathering	2.1.10	Thermal effects (concrete hydration)
1.6.12	Accumulation in soils and organic debris	2.2	OPERATION AND CLOSURE
1.6.13	Mass, isotopic and species dilution	2.2.1	Radioactive waste disposal error
1.6.14	Chemical gradients (electrochemical effects and osmosis)	2.2.2	Inadequate backfill or compaction voidage
1.7	ECOLOGICAL	2.2.3	Co-disposal of reactive wastes (deliberate)
1.7.1	Plant uptake	2.2.4	Inadvertent inclusion of undesirable materials
1.7.2	Animal uptake	2.2.5	Heterogeneity of waste forms (chemical, physical)
1.7.3	Uptake by deep rooting species	2.2.6	Accidents during operation
1.7.4	Soil and sediment bioturbation	2.2.7	Sabotage
1.7.5	Pedogenesis	2.2.8	Repository flooding during operation
1.7.6	Chemical transformations	2.2.9	Abandonment of unsealed repository
1.7.7	Microbial interactions	2.2.10	Poor closure
1.7.8	Ecological change (<i>e.g.</i> , forest fire cycles)	2.2.11	Post-closure monitoring
1.7.9	Ecological response to climate (<i>e.g.</i> , desert formation)	2.2.12	Effects of phased operation
1.7.10	Plant and animal evolution		
2.	HUMAN ACTIVITIES	2.3	POST-CLOSURE SUB SURFACE ACTIVITIES (INTRUSION)
2.1	DESIGN AND CONSTRUCTION	2.3.1	Recovery of repository materials
2.1.1	Undetected past intrusions (boreholes, mining)	2.3.2	Malicious intrusion (sabotage, act of war)
2.1.2	Investigation borehole seal failure and degradation	2.3.3	Exploratory drilling
		2.3.4	Exploitation drilling
		2.3.5	Geothermal energy production

Table XIII.1 (continued)

2.3.6	Resource mining	3.2	CHEMICAL
2.3.7	Tunnelling	3.2.1	Metallic corrosion (pitting/uniform, internal and external agents, gas generation, <i>e.g.</i> , H ₂)
2.3.8	Underground construction	3.2.2	Interactions of host materials and groundwater with repository material (<i>e.g.</i> , concrete carbonation, sulphate attack)
2.3.9	Archaeological investigation	3.2.3	Interactions of waste and repository materials with host materials (electrochemical, corrosive agents)
2.3.10	Injection of liquid wastes	3.2.4	Non-radioactive solute plume in geosphere (effect on redox, pH, and sorption)
2.3.11	Groundwater abstraction	3.2.5	Cellulosic degradation
2.3.12	Underground nuclear testing	3.2.6	Introduced complexing agents and cellulose
2.4	POST-CLOSURE SURFACE ACTIVITIES	3.2.7	Microbiological (effects on corrosion/ degradation, solubility/ complexation, gas generation, <i>e.g.</i> , CH ₄ CO ₂)
2.4.1	Loss of records	3.3	MECHANICAL
2.4.2	Dams and reservoirs, built/drained	3.3.1	Canister or container movement
2.4.3	Rivers rechanneled	3.3.2	Changes in in-situ stress field
Z.4.4	Irrigation	3.3.3	Embrittlement and cracking
2.4.5	Altered soil or surface water chemistry	3.3.4	Subsidence/collapse
2.4.6	Land use changes	3.3.5	Fracturing
2.4.7	Agricultural and fisheries practice changes	3.3.6	Gas effects (pressurisation, disruption, explosion, fire)
2.4.8	Demographic change, urban development	3.4	RADIOLOGICAL
2.4.9	Anthropogenic climate change (greenhouse effect)	3.4.1	Radiolysis
2.4.10	Quarrying, near surface extraction	3.4.2	Material property changes
3.	WASTE AND REPOSITORY EFFECTS	3.4.3	Nuclear criticality
3.1	THERMAL (nuclear and chemical)	3.4.4	Radioactive decay and ingrowth (chain decay)
3.1.1	Differential elastic response		
3.1.2	Non-elastic response		
3.1.3	Host rock fracture aperture changes		
3.1.4	Induced hydrological changes (fluid pressure, density convection, viscosity)		
3.1.5	Induced chemical changes (solubility, sorption, species equilibrium, mineralisation)		

Figure XIII.1: Typical model chain for the groundwater scenario.

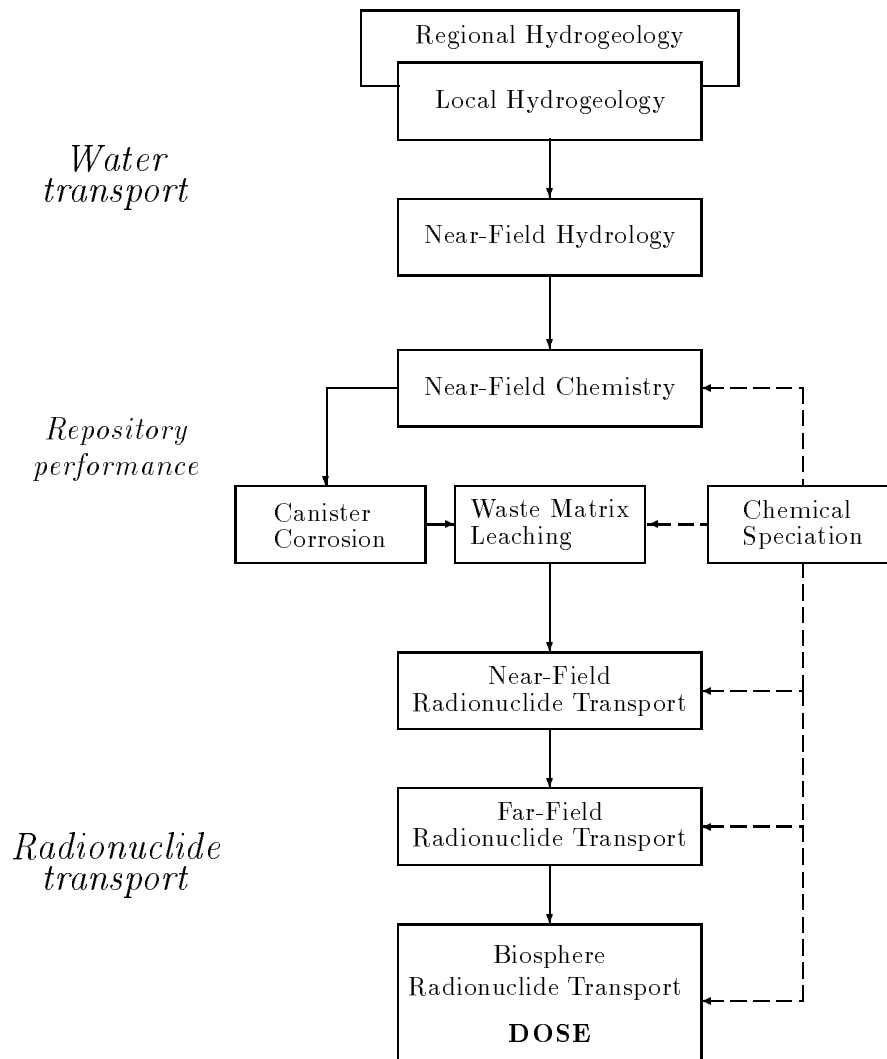
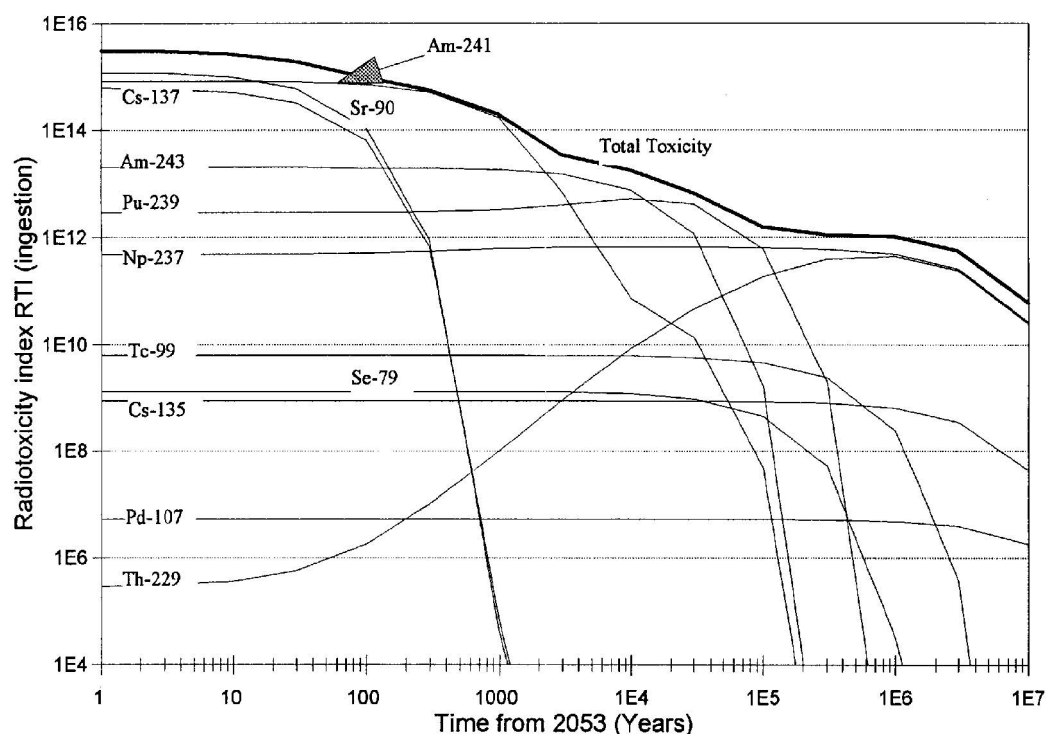


Figure XIII.2: Radiotoxicity index (RTI) for vitrified high-level wastes from 120 GWyr electricity production as a function of time. RTI is defined here, as the dose, in units of 0.1 mSv/yr, one would get by ingestion of the whole radioactive inventory. 0.1 mSv/yr is a sensible safety goal. It must be stressed that RTI is a purely calculational number; the safety of, or the risk from, a repository system cannot be judged from RTI. Of concern are those radionuclides having half-lives longer than about 50 000 years. (Adapted from [94KRI2], courtesy D.F. McGinnes).



Having broadly outlined the methods used in a safety assessment, the question arises as to which factors the conclusion mentioned above is based on. To put the question into a quantitative form, we ask: What are the main mechanisms which convert the extremely high radiotoxicity potential of a repository, as given for example in Figure XIII.2, into acceptable doses for man. The integrated assessments show three main pillars of safety. A word of caution is necessary, here. For simplicity reasons, we consider the different mechanisms separately. In a safety assessment (and in nature) they are coupled, and their impact depends also on the position in parameter space.

XIII.2. Reduction of release rate at the source

In principle, two features contribute to such a reduction.

First, a long-lived waste package (waste glass or spent fuel enclosed in a massive canister) contributes to an absolute containment allowing for decay of the main portion of radioactive inventory. Now, the distribution of half-lives and the geochemical behaviour of relevant radionuclides is such that (except for very unlikely scenarios) a variation of life-time of the waste package between several 100 years and a few 100 000 years has little influence on doses to man.

Therefore, two classes of canisters have been considered. The first guarantees extremely long containment and a typical canister material is copper. This option has been chosen for disposal of spent fuel, *e.g.*, [92SKB, 93VIE/HAU]. Copper is thermodynamically stable in pure water. In a crystalline groundwater with low concentration of corroding agents, the life-time of a well manufactured canister is tens of millions of years. Of concern, therefore, is earlier canister failure by changed groundwater composition, rock displacement or manufacture defects, and such initial defects are postulated in order to obtain a radionuclide release. Compared to vitrified waste, spent fuel contains higher amounts of transuranium radionuclides which decay completely (*e.g.* ^{238}Pu , ^{241}Pu) or to a very large extent (*e.g.* ^{239}Pu , ^{240}Pu) if canister life-time is 100 000 years. It is also noteworthy that spent fuel contains the original inventory of ^{129}I with a half-life of 1.6×10^7 years. Whereas ^{129}I is absent in vitrified waste since it is released to the atmosphere during reprocessing, it dominates the early doses to man from spent fuel [94NEA] because of its long half-life, its solubility, its negligible sorption on solid surfaces, and because of the assumption of early canister failure. In the same context the option of disposal in salt domes might also be mentioned: After a relatively short time the disposal caverns are sealed by convergence of the rock, and improbable scenarios have to be postulated for getting a non-zero source term.

The second class of materials yields a much shorter absolute containment, in the order of a few 1000 years. However, the material is chosen such that the corrosion products yield favourable chemical conditions; a typical representative is steel, *e.g.*, [94KRI]. This leads to the second feature reducing release rates at the source.

Chemical elements can not be dissolved in groundwaters in arbitrary high amounts. Since the host rock of a repository is chosen such that water flow through the repository region is minimal, the release of many radionuclides is solubility limited. This is true for the dissolution of the spent fuel matrix as well as the vitrified waste. Hence, there is an incentive to keep geochemical conditions at the source such that solubility limitations are most effective. Generally, these are reducing groundwater conditions and, therefore, the choice of steel. For solubility limited radionuclides the release rate R_N can be estimated crudely by

$$R_N = QC_L \quad (\text{XIII.1})$$

where Q is the water exchange rate in the neighbourhood of the waste package and C_L the elemental solubility limit. Q depends on the hydrology of the host rock and its hetero-

Table XIII.2: Maximum release rates from the near-field for some isotopes, with and without solubility limitation. The models and data are those of the reference case from [94KRI] (courtesy E. Curti).

Nuclide	Half-life [yr]	Release rate [mol/yr] with solubility limit	Release rate [mol/yr] without solubility limit
^{239}Pu	$2 \cdot 10^4$	$5 \cdot 10^{-9}$	$1 \cdot 10^{-8}$
^{237}Np	$2 \cdot 10^6$	$2 \cdot 10^{-7}$	$9 \cdot 10^{-5}$
^{107}Pd	$6 \cdot 10^6$	$4 \cdot 10^{-9}$	$4 \cdot 10^{-4}$
^{99}Tc	$2 \cdot 10^5$	$3 \cdot 10^{-4}$	$1 \cdot 10^{-2}$
^{79}Se	$7 \cdot 10^4$	$3 \cdot 10^{-6}$	$1 \cdot 10^{-3}$

geneity, and on the properties of the backfill surrounding the waste package. Eq. (XIII.1) shows one of the reasons why a repository is to be sited in a low permeability rock (or in the unsaturated zone in a desert). Quantitative calculation of C_L is a difficult task, and the major problems are addressed in previous sections. In passing we just mention that a sufficiently high concentration of complexing agents in the groundwater such as dissolved organic materials could have a strong detrimental effect on the solubility limitation. To appreciate the impact of solubility limitations, Table XIII.2 is given. Comparing the second and the third column shows that taking this mechanism into account reduces the release rate of specific nuclides by many orders of magnitude.

Neglecting radioactive decay for a moment, we see from mass conservation:

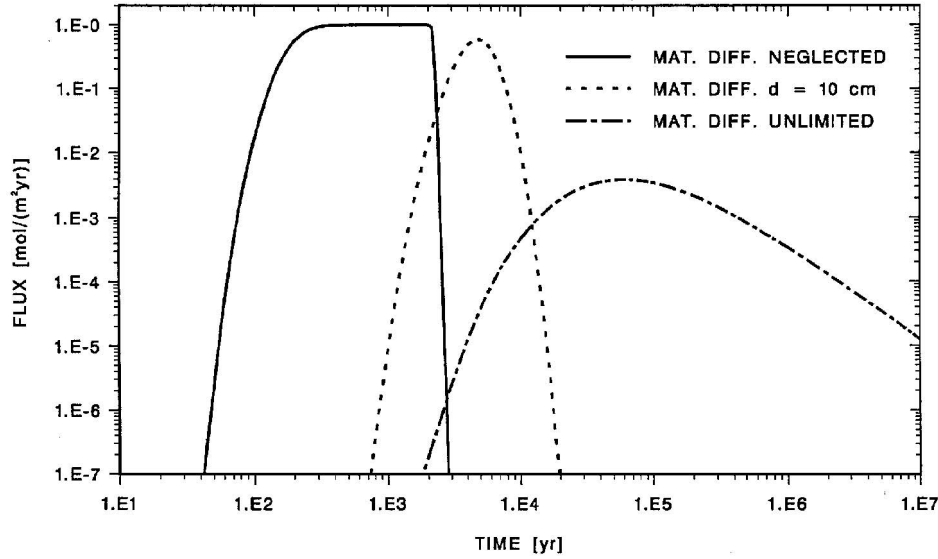
$$\int_0^\infty (\text{release rate}) d(\text{time}) = \text{total mass} \quad (\text{XIII.2})$$

that is, solubility limitations not only decrease release rates but also extend them to correspondingly longer times. Taking radioactive decay into account, results in a higher portion of the inventory decay at the source. The effect of a changed shape of the release rate on doses to man depends on the characteristics of geosphere transport. Roughly speaking, if the total release time is small compared to the geosphere transit time the effect is minimal, if it is comparable or larger than the geosphere transport time the effect is maximal.

XIII.3. Retardation during transport

The safety relevant feature of retardation during transport is that longer transport times allow for decay of larger portions of the nuclide inventory. We may distinguish between

Figure XIII.3: Typical effect of physical retardation by matrix diffusion. The full line shows a breakthrough curve without, and the two other lines with inclusion of matrix diffusion. For the dashed line diffusion is limited to 10 cm porous rock matrix adjacent to the fracture, for the dash-dotted line matrix diffusion is unlimited. Radioactive decay is not considered. For all, the input into the geosphere is a constant over 2000 years. The parameters are as given in the text below (courtesy W. Heer).



physical and chemical retardation.

The first arises when nuclides advected in a water carrying zone are diffusing into portions of rock with stagnant waters. The driving force is the concentration gradient. This process, conventionally called matrix diffusion, is a very efficient retardation mechanism; Figure XIII.3 shows, for some stable isotope, that matrix diffusion shifts the breakthrough curve to much longer times and decreases the peak (by dilution, see Section XIII.4). For a relatively short-lived nuclide, ^{90}Sr say, with a half-life of around 30 years, the inventory would decay to insignificance.

If tracer transit time is large compared to injection duration, the shape of the injection is irrelevant. The effect of hydrodynamic dispersion in the water conducting zones can be neglected compared to that of matrix diffusion, provided water velocity is sufficiently low and migration distance sufficiently large. If matrix diffusion is unlimited in space, the peak retardation can be estimated (see Eq. (28b) in Ref. [94HEE/HAD]) by

$$R \equiv \frac{t_m}{t_w} = 1 + \frac{D_p}{6} \cdot \frac{z}{\nu} \left(\frac{\varepsilon_p}{b} \right)^2 \quad (\text{XIII.3})$$

where t_m is the peak time, t_w the water transit time, D_p the matrix pore diffusion constant,

ε_p the matrix porosity, b the half-width of the water conducting fracture, ν the water velocity, and z the migration distance. For typical values of $D_p = 10^{-11} \text{ m}^2 \cdot \text{s}^{-1}$, $\varepsilon_p = 1\%$, $b = 50 \text{ } \mu\text{m}$, $\nu = 1 \text{ m/yr}$ and $z = 200 \text{ m}$, we obtain $R = 420$, a high retardation.

If matrix diffusion is limited to an alteration zone adjacent to the water conducting fracture which is rapidly saturated with diffusing nuclei, the retardation factor is given (see Eq. (23a) in Ref. [94HEE/HAD]) by

$$R = 1 + \varepsilon_p \frac{d}{b} \quad (\text{XIII.4})$$

where d is the width of the alteration zone. Assuming $d = 10 \text{ cm}$, we obtain, with the above values, $R = 21$. This clearly shows the importance of an extended rock matrix available for diffusion. In Figure XIII.3 the results from a numerical solution of the transport equations are presented. The reader is invited to check the simple estimates above against this numerical solution. Whereas there is little doubt that matrix diffusion is a process operating in fractured media, there is debate on the spatial scales of connected matrix pore spaces.

We conclude these considerations by mentioning that matrix diffusion also has its importance in groundwater dating with conservative tracers: In heterogeneous media the water transit time as determined from measurements of hydraulic conductivities and heads might be much less than tracer transit time.

The second, very important retardation mechanism is sorption. Sorption retards migration of nuclei in the backfill of the engineered repository system as well as in the geosphere. Since sorption is a fast process compared to the migration time scales, in safety assessments, sorption enters the nuclide transport equations in the form of equilibrium distribution ratios or, more generally, equilibrium isotherms. This can be seen from the general structure of the transport equations. From mass balance in a representative elementary volume (REV) we have, *e.g.*, [92BEA/VER];

$$\frac{\partial}{\partial t} I_{\text{tot}} = f(\text{fluxes}) + \text{sinks} + \text{sources} \quad (\text{XIII.5})$$

where I_{tot} is the total nuclide inventory and f is a well-defined function of the geometry of the medium and the various processes inducing nuclide fluxes. I_{tot} can be split into a mobile contribution entering the fluxes, I_m , and an immobile contribution, I_s . The relationship between I_s and I_m is given by the isotherm provided dissolved nuclei are the only mobile contribution. Isotherms can be measured or might be based on surface complexation models; we will not address pertaining problems here, but stress that the approach is correct, granted that solid and liquid phase are properly characterised and chosen.

When sorption is taken into account, the retardation factors, Eqs. (XIII.3) and (XIII.4) get modified, under the simplifying assumption of a linear isotherm:

$$R = R_f + \frac{D_p R_p}{6} \cdot \frac{z}{\nu} \left(\frac{\varepsilon_p}{b} \right)^2 \quad (\text{XIII.6})$$

and

$$R = R_f + \frac{d}{b} (\varepsilon_p + \rho_b K_d) \quad (\text{XIII.7})$$

Here, we have defined a term for retardation by sorption on the surface of water conducting fractures, $R_f = 1 + K_a/b$, where K_a is the surface based distribution constant (we may think of fracture coating materials), and a retardation factor for diffusion in the rock matrix, $R_p = 1 + \rho_b K_d/\varepsilon_p$, where K_d is the volume based distribution constant describing sorption on the accessible surfaces of the matrix and ρ_b the bulk density. For actinides under reducing conditions and crystalline rocks, typical values are $K_d = 1 \text{ m}^3 \cdot \text{kg}^{-1}$, $K_a = 10 \text{ cm}$ and $\rho_b = 2600 \text{ kg} \cdot \text{m}^{-3}$. With the values given previously, we obtain: $R_f = 2000$, $R_p = 2.6 \cdot 10^5$, from Eq. (XIII.6) $R = 1 \cdot 10^8$, and from Eq. (XIII.7) $R = 5 \cdot 10^6$, respectively.

From these numbers, one sees the following: The retardation from sorption on fracture surfaces can be neglected. This is understandable since surfaces of fracture coatings are much smaller than the pore surfaces of the matrix. Secondly, matrix diffusion combined with sorption on inner rock surfaces is an extremely efficient retardation mechanism, and the very longest-lived nuclei, only, will survive transport if both mechanisms are operating in full.

However, we conclude this section by a word of caution. Nuclides might be sorbed on colloids which for size reasons might not diffuse into the matrix pore spaces. Description of nuclide transport by colloids is still in debate, and especially the question of irreversible sorption on colloids is open [90GRA]. Not fully resolved is also the issue whether sorption data from static batch sorption experiments can be transferred *tel-quel* to the dynamic migration situation in the field, though recent investigations show encouraging results, see Table XIII.3.

XIII.4. Dilution

Whereas the previous two mechanisms eventually reduce nuclide fluxes to the biosphere by allowing for decay during release and transport, dilution reduces the concentration of the surviving inventory by mixing contaminated and fresh water. Three mechanisms lead to dilution.

The first is hydrodynamic dispersion in the host rock caused by spatial variability of water velocities. Dispersion smears out the nuclide breakthrough curve and so contributes to dilution. If nuclide transit time is large compared to half-life, dispersion becomes important since only the fast-running proportion of the nuclides survives decay. In safety assessments dispersion is not a very important parameter for most nuclides, which is fortunate since dispersion on the large repository scale is not well understood [89DAG].

Second is dilution caused by matrix diffusion. Also here, through diffusion kinetics, the concentration-time distribution is smeared out and a dilution in the fracture water results. For short nuclide pulses compared to diffusion times, this type of dilution becomes important.

Table XIII.3: Comparison of different sorption distribution constants as measured in the laboratory by static batch and dynamic bore-core experiments and in the field. If samples are well prepared and field experiments carefully interpreted the agreement is acceptable. Data were taken from [94HEE/HAD].

Experiment		$K_d [10^{-3} \text{ m}^3 \cdot \text{kg}^{-1}]$	
		Na	Sr
Laboratory	Batch Sorption ($< 63 \mu\text{m}$)	$1.3^{+1.5}_{-0.4}$	41^{+39}_{-4}
	Batch Sorption ($< 250 \mu\text{m}$)	$0.85^{+0.76}_{-0.04}$	25^{+22}_{-1}
	Batch Sorption (loosely disaggregated)	$0.43^{+0.60}_{-0.02}$	13^{+19}_{-1}
	Rock Water Interaction (\approx loosely dis.)	$0.13^{+0.13}_{-0.02}$	$7.6^{+8.2}_{-1.7}$
	Dynamic Infiltration	0.1 - 0.3	(a)
Field	Hydrogeochemical	$0.21^{+0.2}_{-0.1}$	7.8^{+8}_{-5}
	Migration	$0.13^{+0.16}_{-0.07}$	21^{+38}_{-14}

(a) not determined

Of extraordinary importance, however, is the dilution along the pathway to man by large bodies of freshwater. These might be aquifers into which the small amounts of contaminated groundwaters infiltrate (then mixing is related to hydrodynamic dispersion), lakes or rivers on the surface or the sea. This is the reason why sub-seabed disposal leads to remarkably low doses [88PAG]. This is also seen in Table XIII.4 where dose conversion factors are given for a continuous release of 1 Bq/yr from the geosphere into the biosphere recipient (adapted from [92SKB]). An estimate of the dilution factor F is given by

$$F = Q_B/Q_R \quad (\text{XIII.8})$$

where Q_B is the water flow in the biosphere recipient and Q_R the water flow through the repository. Both quantities are evidently very site specific; Q_R depends on the local

Table XIII.4: Dose conversion factor (Sv/Bq) for a hypothetical release of all nuclides to a well or all to the Baltic Sea. The Table also gives an idea of the nuclides to be considered in a safety analysis. Adapted from [92SKB].

Nuclide	Half-life [yr]	Well	Baltic Sea
C-14	5730	$4.2 \cdot 10^{-13}$	$3.5 \cdot 10^{-17}$
Cl-36	$3 \cdot 10^5$	$2.0 \cdot 10^{-13}$	$2.0 \cdot 10^{-18}$
Ni-59	75000	$8.0 \cdot 10^{-14}$	$2.0 \cdot 10^{-19}$
Se-79	65000	$5.4 \cdot 10^{-12}$	$2.9 \cdot 10^{-16}$
Sr-90	29	$2.2 \cdot 10^{-11}$	$8.2 \cdot 10^{-18}$
Zr-93	$1.5 \cdot 10^6$	$2.7 \cdot 10^{-13}$	$5.9 \cdot 10^{-19}$
Tc-99	$2.1 \cdot 10^5$	$1.7 \cdot 10^{-13}$	$1.8 \cdot 10^{-19}$
Pd-107	$6.5 \cdot 10^6$	$7.0 \cdot 10^{-14}$	$2.0 \cdot 10^{-19}$
Sn-126	$1 \cdot 10^5$	$3.1 \cdot 10^{-12}$	$3.8 \cdot 10^{-16}$
I-129	$1.6 \cdot 10^7$	$4.9 \cdot 10^{-11}$	$4.1 \cdot 10^{-16}$
Cs-135	$2.3 \cdot 10^6$	$1.6 \cdot 10^{-12}$	$1.1 \cdot 10^{-17}$
Cs-137	30	$8.6 \cdot 10^{-12}$	$6.1 \cdot 10^{-17}$
Ra-226	1600	$1.8 \cdot 10^{-10}$	$7.2 \cdot 10^{-16}$
Th-229	7340	$6.0 \cdot 10^{-10}$	$2.0 \cdot 10^{-15}$
Th-230	75400	$7.5 \cdot 10^{-11}$	$1.9 \cdot 10^{-16}$
Th-232	$1.4 \cdot 10^{10}$	$4.0 \cdot 10^{-10}$	$2.0 \cdot 10^{-15}$
Pa-231	32800	$1.0 \cdot 10^{-8}$	$2.0 \cdot 10^{-14}$
U-233	$1.6 \cdot 10^5$	$1.6 \cdot 10^{-10}$	$4.3 \cdot 10^{-16}$
U-234	$2.4 \cdot 10^5$	$1.6 \cdot 10^{-10}$	$4.2 \cdot 10^{-16}$
U-235	$7 \cdot 10^8$	$1.5 \cdot 10^{-10}$	$4.0 \cdot 10^{-16}$
U-236	$2.3 \cdot 10^7$	$1.5 \cdot 10^{-10}$	$4.1 \cdot 10^{-16}$
U-238	$4.5 \cdot 10^9$	$1.4 \cdot 10^{-10}$	$3.8 \cdot 10^{-16}$
Np-237	$2.1 \cdot 10^6$	$2.2 \cdot 10^{-10}$	$5.9 \cdot 10^{-16}$
Pu-239	24000	$4.3 \cdot 10^{-10}$	$4.2 \cdot 10^{-16}$
Pu-240	6540	$4.3 \cdot 10^{-10}$	$4.2 \cdot 10^{-16}$
Pu-241	14	$7.9 \cdot 10^{-12}$	$7.9 \cdot 10^{-18}$
Pu-242	$3.8 \cdot 10^5$	$3.9 \cdot 10^{-10}$	$3.7 \cdot 10^{-16}$
Am-241	432	$4.1 \cdot 10^{-10}$	$7.8 \cdot 10^{-16}$

hydrology and Q_B might be the flow in a large river or in a well drilled for water consumption. It must be noted that the estimate, Eq. (XIII.8), is an upper bound, assuming complete mixing.

We have roughly sketched the important factors leading to the low consequences revealed in recent safety assessments. A comprehensive assessment is a major multidisciplinary task. Although there is no doubt that a carefully designed and sited repository fulfills the safety criteria, there is still much work ahead for the involved scientists and engineers to determine site-specific parameters and to reduce uncertainty bands such that an optimisation of the repository system becomes feasible.

Chapter XIV

Trace Element Modelling

Jordi BRUNO
QuantiSci
Parc Tecnologic del Vallés
E-08290 Cerdanyola (Spain)

XIV.1. Why are we concerned about trace metals ?

The development of the industrial societies is very much linked to the discovery and use of metals. Metal consumption has increased by 300% in the last fifty years, in spite of some deceleration during the latest economical recessions [91MEA/MEA]. Anthropogenic releases of metals like: Pb, Hg, Zn, Cd, Cu, and Cr, have increased threefold compared to their background pre-industrial fluxes. In the case of radionuclides, anthropogenic fluxes were virtually non-existent prior to the Manhattan project and man-made transuranium elements were not present in our environment prior to 1945. These factors have resulted in increased concentrations of trace metals (including radionuclides) in the various environmental reservoirs. Therefore, there is a growing need to understand and predict the consequences associated with the increased metal fluxes, particularly their effects on the biosphere.

The environmental impact of any metal is directly related to its bioavailability. The action of a metal on a biotic system will be dependent on its ability to be absorbed and excreted, its redox state and electrochemical behaviour and consequently, its speciation. As research is intensified in the role of trace metals in biological systems, the classical distinction between essential and toxic metals becomes fuzzier and strongly dependent of the metal concentration. Figure XIV.1 includes some of the trace elements which are considered to be biologically interesting. Elements which are in bold type have been determined as being essential. The effect of a metal in the biosphere is a function of the amount released (concentration) and in which chemical form this metal is released (speciation).

establish the main fluxes, sources and sinks of metals in natural systems. These can also be used to differentiate between major and minor components of the system under study. In general, we can say that the major components will define the chemical properties of the system, to which the chemistry of the minor components will be linked. The examples we will describe in this Chapter will try to illustrate this obvious, but quite often neglected principle.

The application of equilibrium models to the geochemical behaviour of trace elements was initiated mainly by the need of speciation in seawater. This was done by extending the equilibrium models of major components to trace element calculations [72MOR/MOR, 72ZIR/YAM]. A chemical description of the behaviour of trace metals in seawater was made by Ahrlund [96AHR], by applying the concepts of hard and soft donors and acceptors. This concept has been used in trace element biochemistry to assess their potential toxicological effects [91FRA/WIL]. In recent years, the role of abiotic and biotic surfaces and their influence on trace metal scavenging and speciation has become more important [87STU]. Also, surface complexation models have been incorporated into geochemical modelling, *cf.* Chapter VII.

Geochemical modelling has been developed to rationalise our observations of the geochemistry of natural systems. This is called interpretative modelling, which is the theoretical and mathematical construction we use to explain past and present experimental observations. However, as we become more and more aware of the impact of men's actions in the geosphere and biosphere, we want to use the geochemical models to predict the most probable outcome of the design and performance of our engineered solutions to various environmental problems. This is called predictive modelling. There has been a wealth of discussion about the terminology and use of predictive modelling (see [92NOR] for example). They reflect a very old controversy in science, between purism and pragmatism. Modelling always requires approximations, *c.f.* Chapter I, and it is used *e.g.*, to make a choice between different technical solutions based on their impact on the environment. This is particularly relevant for trace metals, when we realise that for many of them anthropogenic inputs are larger than natural ones.

The main objectives of this Chapter will be to describe the methodology of trace element geochemical modelling. We will specifically discuss the differences between interpretative and predictive modelling, and the uncertainties involved. We will elaborate on the use of kinetic and equilibrium models and when to use them. Finally, in a later section of this Chapter, we will try to illustrate these principles by some selected case studies, where we have been professionally involved.

XIV.3. The methodology of geochemical modelling

XIV.3.1. The building blocks

Any application of geochemical modelling is based on the following sequence, which is not strictly linear, but includes a lot of feed-back and iteration, as discussed in Chapter I of this book:

$$\begin{array}{ccccccc} \text{System Data} & \rightarrow & \text{Conceptual model} & \rightarrow & \text{Thermodynamic/kinetic databases} \\ & & \rightarrow & \text{Computerised models} & \rightarrow & \text{Model data.} \end{array}$$

These constitute the building blocks of geochemical modelling and the outcome of the final result, the model data, depends very much on how careful we are in designing and putting the building blocks together. The system data can be defined as the basis of the modelling application, while the conceptual model and the associated thermodynamic and kinetic databases constitute the structure of the model. Finally, the computerised models are the tools we will use to raise our model building. They have to be efficient and reliable, but they do not constitute geochemical models by themselves !

We will try now to develop some of the main aspects of the various building blocks.

XIV.3.2. The system data

To build the foundations of geochemical models is normally the hardest work and this is rarely performed by the “modellers”. Normally, the system data is the outcome of some previous investigations and analysis of the system under consideration and they have often been obtained with scopes which go beyond the chemical modelling application. The data the modeller will be confronted with are hydrogeological data, mineralogical data, soil investigations, analytical data from waters and solid phases, isotopic data, atmospheric deposition data, and so on. Unfortunately, the geochemical modeller cannot be expert in all the different techniques and methodologies, but he/she has to listen to the experts and rely on their judgement. The various parts of the system data evolve into partial conceptual models which are pieces in the puzzle that will finally form the overall conceptual geochemical model. The partial and total solutions of this puzzle are some of the most challenging and rewarding endeavours of the geochemical modeller.

However, it has to be clear from the beginning that the foundations are often not as stable as one would wish. The collection, analysis and interpretation of system data have uncertainties which will influence the outcome of the model. We can already state that there are rarely unique solutions to the geochemical problems and therefore we have to be aware of the uncertainties that occur throughout the model exercise.

The uncertainties in the system data for the subsurface environment can be particularly large. We might say that this is a demonstration of an “uncertainty” principle for large geophysical/geochemical systems: we cannot obtain the model data without disturbing the system itself. Therefore, it is important to realise the main uncertainties involved in subsurface system investigations and to be able to deal with them in our models. The

most important one is due to spatial heterogeneity of the systems which will strongly influence both the chemistry and water transport, *c.f.* Chapter XII.

XIV.3.3. The chemical and physical variability of subsurface environments

According to Barcelona [90BAR], the conditions given in Table XIV.1 are typical for subsurface systems.

XIV.3.3.1. Physical conditions

Temperature, pressure and flow conditions vary substantially in groundwaters. Temperature and, to a lesser extent pressure, affect both the kinetic and thermodynamic constraints on the system under investigation. Reaction paths and rates may vary with temperature and depth. This is particularly relevant in situations where we have a heat source in the waste matrix, *i.e.*, in nuclear waste repositories and landfills with high microbial activity. Degassing effects during groundwater sampling are almost inevitable and may affect the important carbonate equilibria, hence the pH and the chemical equilibrium speciation. However, we know both the fundamental relationships and most of the data required to take these effects into account.

XIV.3.3.2. Biological conditions

The subsurface environment is not an abiotic medium, as was previously assumed. Wilson and McNabb [83WIL/MCN] have suggested that the biotic population below the root zone is larger than the biomass present in surface waters. The existence of a widespread subterranean biosphere has been confirmed by the studies performed in conjunction with site investigations for nuclear waste disposal and a recent review [93PED] has updated our knowledge on, what K. Pedersen calls, “the deep subterranean biosphere”. Thermophilic bacteria populations have been identified at depths down to 4000 m in a deep borehole in Sweden [94SZE/SZE]. In general bacteria populations range between 10^2 and 10^8 bacteria per ml of groundwater. It has also been shown that bacteria can act both as reagents and catalysts in important chemical processes, like water/rock interactions and redox processes. However, our capability to account for microbiologically mediated processes in geochemical modelling is still very limited.

XIV.3.3.3. Variability of chemical conditions

The subsurface environment represents a continuous transition from oxic conditions to the original reducing state. This fact is one of the main reasons for the space variability of the chemical conditions in the subsurface environment. Again, measuring the redox conditions of a certain groundwater zone without disturbing it, is difficult, but not impossible [87WIK]. In fact, the lack of ability to measure redox potentials in subsurface environments has resulted in an overcritical attitude from some geochemists towards redox

Table XIV.1: Ranges of physical, biological and chemical variables in subsurface environments, *c.f.* [90BAR].

Variable	Causes/effects	Natural	Disturbed
Temperature	Mixing, reaction paths and rates, solubility considerations	3° to 20°C	3° to 35°C
Pressure	Gas solubility, permeability and porosity	1 to 10 bar	1 to 1000 bar
Flow velocity (m · d ⁻¹)	Recharge, pumping, mixing	< 1 to 1000	< 1 to 1000
Biomass	Catalytic or transformation potential	10 ¹ to 10 ⁸ (cells · g ⁻¹)	10 ⁴ to 10 ⁹ (cells · g ⁻¹)
Activity	Turnover rates	0.1 to 1 μg · l ⁻¹ · hr ⁻¹	?
V _{max} Glucose (Specific Gravity)	Metabolic status	0.03-0.06 × 10 ⁻⁹ (glucose · h ⁻¹ · cell ⁻¹)	?
<hr/>			
Gradients:	Site Scale (m to km)	Large Scale (km to 10 ³ km)	
<hr/>			
<i>Horizontal</i>			
O ₂	-0.01 to +0.5 (mg · l ⁻¹ · m ⁻¹)	0.3 to 1 (mg · l ⁻¹ · km ⁻¹)	
Fe ²⁺	0.01 to 0.1 (mg · l ⁻¹ · m ⁻¹)	0.02 to 0.2 (mg · l ⁻¹ · km ⁻¹)	
Eh	-3 to 1 (mV · m ⁻¹)	-0.5 to -180 (mV · km ⁻¹)	
<i>Vertical</i>			
O ₂	-0.2 to +0.77 (mg · l ⁻¹ · m ⁻¹)	—	
Fe ²⁺	-0.01 to 0.05 (mg · l ⁻¹ · m ⁻¹)	—	
Eh	-2 to -40 (mV · m ⁻¹)	—	

measurements in natural water systems [84LIN/RUN]. However, there is experimental information indicating that redox measurements in groundwater are indeed possible, if done with due care [92GRE/STU]. This does not imply that natural water systems are entirely at redox equilibrium, oxidising and reducing species are frequently found in disequilibrium in the system under study. Such disequilibria are always related to slow equilibria. They may also relate to microbially mediated reactions and our tools are still very limited to account for these processes. As we will describe later, multielectron redox reactions are slow, compared to most other homogeneous processes. Therefore the rate of equilibrium in redox systems has to be considered in the conceptual modelling approach. We will try to define how redox disequilibrium may be taken into account in the following sections.

Temporal variations of the groundwater chemical constituents are also observed. In areas close to recharge zones, this may be the result of seasonal variations on the intruding surface water. In deeper environments, temporal variations are often the result of the disturbances created by the investigations (pumping), again a consequence of our particular “uncertainty” principle. These disturbances are both a function of the sampling frequency and the time required; several sampling strategies have been devised in order to minimise these effects. Normally, conservative tracers, either present in the groundwater or originally added, are used to monitor these potential disturbances. The conceptual chemical model will be strongly dependent on how well we are able to take time-variability effects into account.

The temporal variability is more difficult to assess when studying dynamic systems, *e.g.*, leachates from landfills. They are very dependent on the variations in the source (“the garbage of the day”) and the microbial activity.

In summary, spatial and temporal variability of the chemical condition is inherent in the systems we attempt to model. Groundwater sampling strategies can be devised to minimise the associated uncertainties and the degree of accuracy of our models will be strongly dependent on how well we can do this.

XIV.3.4. Getting a feeling for the system. The conceptual model

As already mentioned at the beginning of this Chapter, the construction of the conceptual geochemical model is the most challenging and rewarding endeavour of the modelling. The definition of the conceptual framework of the geochemical model is the result of a series of primary analyses of the geochemical data. They range from spatial and temporal plots of the hydrogeological and chemical data, mineralogical determinations, microbial identifications, to initial mass balance calculations to identify the main water/rock interactions. It is necessary to perform this task in close co-operation with the field scientists, in order not to depart too far from reality.

The basic principle is the following: in order to understand and model trace element geochemistry, we have first to understand and model the main driving geochemical forces in the system under consideration, because these will control the trace element geochemistry. In order to determine the major hydrogeochemical driving forces of the system we will have to answer the following questions:

1. What does the geology of the system look like ? Which are the main spatial geological variabilities of the system ?
2. What is the local groundwater flow regime ? What does the regional flow regime look like ? Do we have information about the water residence times in the various parts of the system ?
3. Which is the spatial and temporal variability of the major component geochemistry of the system ?
4. Which are the main fissure fillings and mineral coatings identified in the boreholes ? How are the trace metals associated to them ? In which proportion ?
5. How do trace elements correlate to the major geochemical components of the system ?

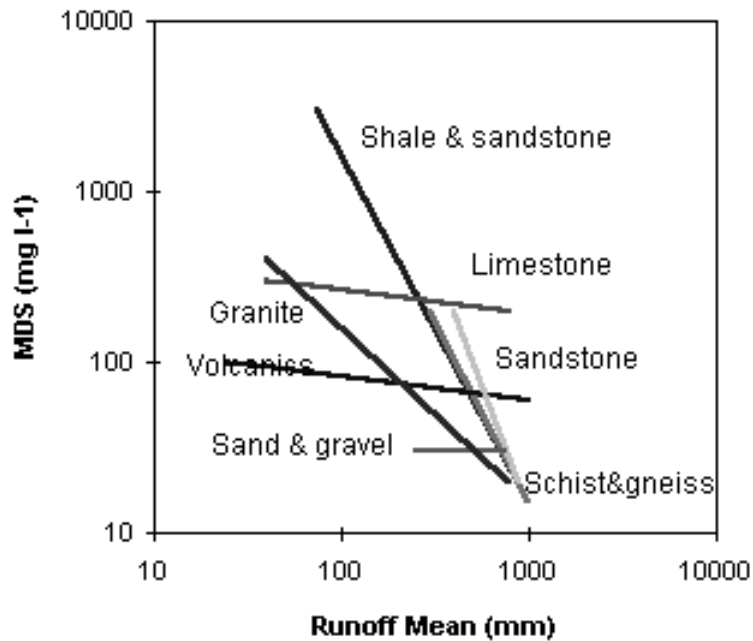
The degree of information in answering these questions will be decisive for our capability to establish a sound geochemical basis for the trace elements in the interpretative modelling. In the case of predictive modelling, many of these questions cannot be answered *a priori* and have to be assessed in the light of previous experiences from similar systems. In the next sections we will elaborate on the questions which have to be addressed in order to build the conceptual model.

XIV.3.4.1. The geological setting

It is obvious that the geochemical modelling depends on the geological setting of the system. Water/rock interactions are dependent on the facies encountered. The way in which meteoric water gains solutes through interactions with the soil will have a great influence on the geochemistry of shallow waters and this in turn will influence the composition of groundwaters through percolation and mixing. Information on water residence times is critical to assess these factors. The chemistry of natural water systems with residence times under 10^2 years depends very much on the result of the percolation of rain water through the soil. Therefore, they will carry the signature of the components added by wet and dry atmospheric deposition and by the fast soil/water processes. For trace metals we often cannot neglect the contribution from atmospheric deposition to the system under study. As an example, atmospheric inputs of trace metals in the North Sea oscillate between 7200-58000 ton/year for Zn, 110-430 ton/year for Cd and 70-1400 ton/year for Cr. This is bound to influence the trace element geochemistry of the surrounding areas.

There are some general patterns in the way the chemistry of waters is influenced by the geological medium, and Appelo and Postma [93APP/POS] have made an excellent summary of this information. A plot of the amount of dissolved solids *vs.* the mean annual runoff for different rock types gives an indication of the major water/rock interactions and how they are related to the kinetics of the interactions and the residence times, as shown in Figure XIV.2.

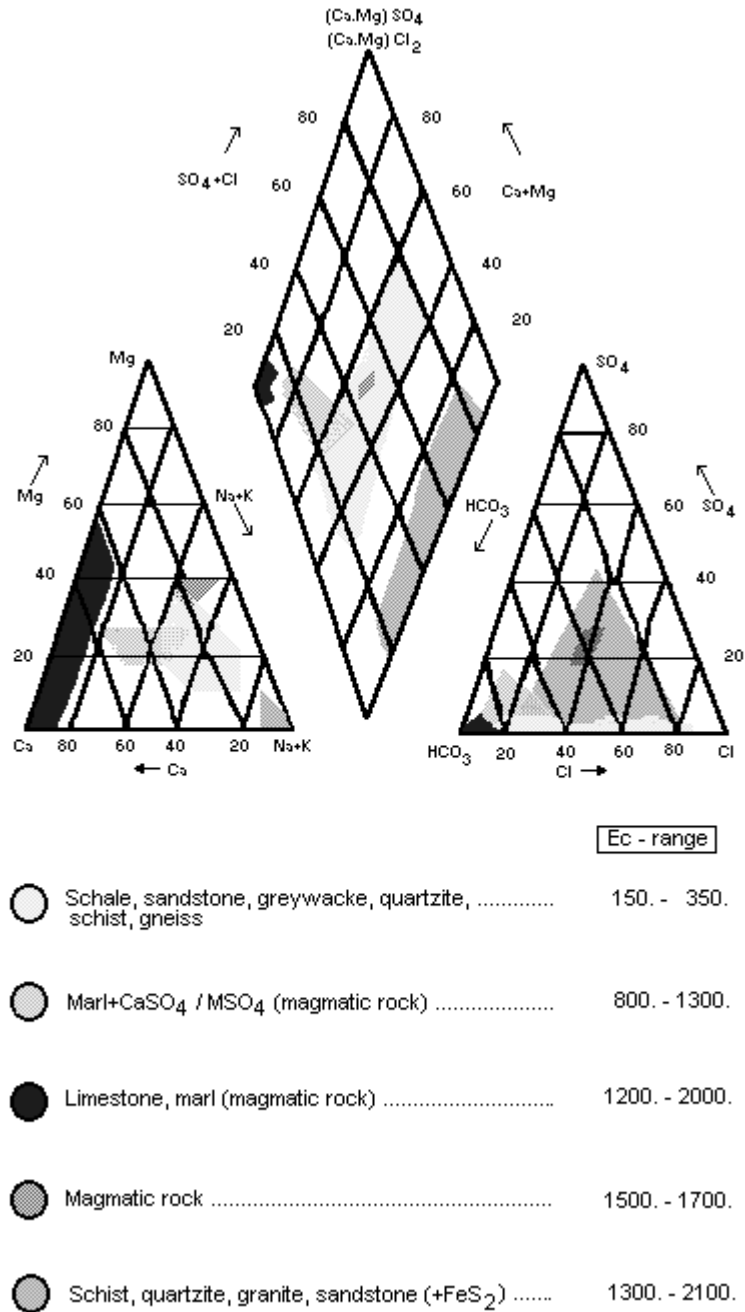
Figure XIV.2: Concentration of dissolved solids as a function of mean annual runoff for different rock types.



Sand and gravel are formed by quartz grains. Quartz has a very low rate of dissolution in comparison with the short residence times of the percolating water. The geochemistry of this zone will therefore only be influenced by atmospheric deposition and evapotranspiration. Volcanic rocks and limestone contain more soluble minerals and their dissolved concentrations are more or less independent of the runoff. This indicates that the kinetics of dissolution of these minerals is fast compared to the residence times of the waters. This is especially true for carbonate phases in contact with water. For granites and sandstones the dissolved concentrations are very much dependent on the annual runoff. This is an indication of slow dissolution rates, but still comparable to the residence times of water. Granite and sandstones are mainly composed of feldspars, mica and quartz, all with slow dissolution kinetics at low temperature.

The main geochemical patterns of groundwaters can be illustrated in Piper plots. These are diagrams summarising information on major element geochemistry which we will use to determine the chemical behaviour of the trace metals. How the major element geochemistry is determined by the surrounding rock type is illustrated in Figure XIV.3, giving a plot of the composition of European bottled waters and their relation to rock types, [85ZUU/WEI]. The strong dependence of the composition of the different waters on their origin is apparent.

Figure XIV.3: A Piper plot of European bottled waters and their relationship to the parent rock type, illustrating the variability of chemical compositions and their intimate relationship with the water/rock interactions. From [85ZUU/WEI].



XIV.3.4.2. The hydrogeological condition

The geochemistry of the systems will to a large extent be influenced by the way in which water flows into and out from it. The requirements about the detail of this information will be strongly dependent on the scale of the model. For the development of a conceptual geochemical model one must understand the local flow regime in the system, as well as its connection to the regional flow regimes. Furthermore, the information about the residence time of the water in the various zones of the system will be critical to ascertain which are the main geochemical driving forces and to which extent water/rock interactions and redox processes are kinetically or thermodynamically controlled. This is in spite of the difficulties in determining water residence times under groundwater conditions.

The previous Section already indicated how the different rock types influence the composition of the waters, depending on the residence time. We will try to develop this more quantitatively, because this is useful for the selection of a proper geochemical model. The residence time of water in one part of a system, τ_R , is defined as the average time a small water volume resides in a specific hydrological zone. Therefore, processes like weathering and heterogeneous redox reactions and their probability to attain equilibrium will be strongly dependent on this parameter. A quantitative estimate of the time needed to reach equilibrium is given by the characteristic reaction time, τ_{char} . This concept introduced by Morgan and Stone [85MOR/STO] in lake environments has been shown to be useful in determining to what extent equilibrium is expected under a given hydrological condition. The characteristic reaction time is defined as the “half-life” of a certain chemical reaction, under the conditions of interest. A first comparison of τ_R and τ_{char} will give an indication about the processes which are expected to be in equilibrium and the ones that will be kinetically controlled. Hence, if $\tau_R \gg \tau_{\text{char}}$, equilibrium models will be a satisfactory choice for the description of the system, but if $\tau_R \ll \tau_{\text{char}}$, kinetic models will have to be used.

Let us summarise the typical characteristic reactions times of the most common geochemical processes. Table XIV.2 shows the information derived from primary data given in the quoted references.

By comparing the average residence times of water in the various reservoirs (Table XIV.3) with the characteristic reaction times of chemical processes relevant for the geochemistry of the systems it is possible to state the following general rules:

1. Most homogeneous reactions in aqueous media are fast compared to the average residence times of water, therefore they can be treated as equilibrium reactions. The only exception is redox reactions which involve multielectron transfer and/or structural rearrangement (*i.e.*, Cr(III)/Cr(VI), S(-II)/S(VI), V(III)/V(V)). These homogeneous processes have to be described kinetically and the influence of potential catalysts (solid surfaces, biota) have to be taken into account.
2. Most heterogeneous, water/rock, interactions have characteristic reaction times larger than, or comparable to the average residence time of water. Therefore, most heterogeneous processes must be described using kinetic models. The exceptions are

Table XIV.2: Characteristic reaction times for geochemical processes derived from primary data from [76BAE/MES, 76BUS/CLE, 80DAV/LEC, 80RIM/BAR, 84HEL/MUR, 86MCK/BAR, 91BRU/CAS, 91CHO/CLA, 94LAS/SOL].

Reaction type	Example	$\log_{10} \tau_{\text{char}}$ (sec)
<i>Homogeneous reactions:</i>		
Inorganic complexation (OH^- , CO_3^{2-} , PO_4^{3-} , ...)	$\text{Me}^{z+} + q \text{H}_2\text{O} \rightarrow \text{Me}(\text{OH})^{(z-q)+} + q \text{H}^+$	-6 to -1
LMW organic complexation	$\text{Me}^{z+} + \text{edta}^{4-} \rightarrow \text{Me}(\text{edta})^{(z-4)} + z \text{H}^+$	-2 to 2
Humic and fulvic acids	$\text{Me}^{z+} + \text{HA} \rightarrow \text{MeHA}$	-1 to 3
Redox reactions: one electron transfer, minor structural rearrangement	$\text{Fe(II)} + \text{O}_2 \rightarrow \text{Fe(III)}$	3 to 8
Redox reactions: multielectron transfer, structural rearrangement	$\text{Cr(III)} + \text{O}_2 \rightarrow \text{Cr(VI)}$	8 to 11
<i>Heterogeneous reactions:</i>		
Oxyhydroxide dissolution	$\text{Fe}_2\text{O}_3(\text{s}) + 3 \text{HCO}_3^- + 2 \text{H}^+ \rightarrow \text{FeCO}_3\text{OH}(\text{aq}) + \text{Fe}(\text{CO}_3)_2^- + 2 \text{H}_2\text{O}$	9 to 12
Oxyhydroxide precipitation	$\text{Fe}^{3+} + 3 \text{H}_2\text{O} \rightarrow \text{Fe}(\text{OH})_3(\text{s}) + 3 \text{H}^+$	-12 to 10
Carbonate dissolution	$\text{CaCO}_3(\text{s}) + \text{H}^+ \rightarrow \text{Ca}^{2+} + \text{HCO}_3^-$	3 to 5
Carbonate precipitation	$\text{Ca}^{2+} + \text{HCO}_3^- \rightarrow \text{CaCO}_3(\text{s}) + \text{H}^+$	0 to 2
Aluminosilicate dissolution	$\text{KAlSi}_3\text{O}_8(\text{s}) + 4 \text{H}^+ + 4 \text{H}_2\text{O} \rightarrow \text{K}^+ + \text{Al}^{3+} + 3 \text{H}_4\text{SiO}_4$	12 to 14
Redox reactions: one electron transfer	$> \text{FeO-Fe}^+ + \text{e}^- \rightarrow \text{FeO-Fe}$	2 to 4
Redox reactions: multielectron transfer	$\text{FeS}_2 + 3.5 \text{O}_2(\text{g}) + \text{H}_2\text{O} \rightarrow \text{Fe}^{2+} + 2 \text{SO}_4^{2-} + 2 \text{H}^+$ $\text{UO}_2(\text{s}) + 0.5 \text{O}_2(\text{g}) + 2 \text{HCO}_3^- \rightarrow \text{UO}_2(\text{CO}_3)_2^{2-}$	9 to 11

Table XIV.3: Average residence times of water in main reservoirs. [79FRE/CHE].

Reservoir	$\log_{10} \tau_R$ (seconds)
Oceans and seas	11
Lakes and reservoirs	8.5
Swamps	7.5 - 8.5
Rivers	6
Soil moisture	6 - 7.5
Shallow groundwaters	6 - 8.5
Deep groundwaters	9.5 - 12
Icecaps and glaciers	8.5 - 11.5
Atmospheric water	5.9
Biospheric water	5.8

the precipitation and dissolution of amorphous oxyhydroxides (*i.e.*, $\text{Fe}(\text{OH})_3(\text{am})$, $\text{SiO}_2(\text{am})$, $\text{UO}_3 \cdot x\text{H}_2\text{O}(\text{am})$) and the precipitation and dissolution of carbonates ($\text{CaCO}_3(\text{s})$, $\text{MnCO}_3(\text{s})$, $\text{MgCO}_3(\text{s})$, $\text{FeCO}_3(\text{s})$). These processes can be treated assuming equilibrium, particularly in reservoirs with longer residence times (oceans, deep groundwaters). In the case of amorphous metal hydrous oxides, the rate of ageing to crystalline phases is strongly dependent on pH. In the pH range of natural waters the characteristic reaction times are 20-200 days ($\log \tau_R = 6.2 - 7.2$ seconds). Therefore, these reactions are in general kinetically controlled.

XIV.3.4.3. A quantitative description of local disequilibrium. The Peclet, Damkohler and Lichtner parameters

Recently, Steefel and Lasaga [90STE/LAS] have proposed the use of non-dimensional parameters like the Peclet and Damkohler numbers to indicate the relative importance of kinetics and advective and dispersive flux. The Peclet number is given by the expression:

$$P_e = \frac{v \cdot l}{D_h} \quad (\text{XIV.1})$$

where v is the true velocity, l is the length of the hydrological pathway under consideration and D_h , is the longitudinal dispersion constant, an element of the dispersion tensor, which is defined as the sum of the mechanical dispersion and the molecular diffusion. Depending on the relationship between the Peclet number and the dispersion and diffusion coefficients, we can estimate the relative importance of advective and dispersive fluxes in the system under study.

The Damkohler number is given by:

$$D_a = \frac{A_\theta \cdot k \cdot l}{v} \quad (\text{XIV.2})$$

where A_θ is the reactive rock surface, k is a rate constant and v and l have the same meaning as above. If the Damkohler number D_a is > 1 , the rate of the process under consideration is larger than the flow velocity and consequently the aqueous phase is considered to be largely in equilibrium with the reacting mineral phase. If D_a is ≤ 1 , then the rate of reaction is lower than the advection term, resulting in local disequilibrium.

In a series of papers, Lichtner [85LIC, 88LIC] has presented an analytical solution to the local disequilibrium problem, in the form of a steady-state solution for the case where the reaction front is located at the position l from the origin:

$$C(x) = C_{eq} - (C_{eq} - C_l)e^{-\gamma(x-l)} \quad (\text{XIV.3})$$

The parameter γ is defined as:

$$\gamma = \frac{v}{2D_h} \cdot \left[\left(1 + \frac{4D_h A_\theta k}{\nu^2} \right)^{0.5} - 1 \right] \quad (\text{XIV.4})$$

The Lichtner parameter

$$L = \frac{4D_h A_\theta k}{\nu^2} \quad (\text{XIV.5})$$

is a dimensionless quantity which combines both the Peclet and Damkohler numbers, and provides an approximate measure of the relative importance of reaction rate, dispersion and advection, for determining the concentration profile of a certain solute through the reaction path length l . The quantity γ^{-1} is the approximate distance from the reaction front at which the fluid is in equilibrium with the mineral involved in the reaction. If the reaction rate k is large, then γ^{-1} tends to zero and equilibrium occurs on the local scale. When the Lichtner parameter is sufficiently small then the reaction zone will be spread out over a finite distance, which is defined as the equilibration length. It is important to realise that all these parameters are directly dependent on the length l of the system. Therefore, disequilibrium at a certain (micro)scale may be overrun by equilibrium at the larger scale, hence defining the true scale of the system is essential.

As a general conclusion, we may say that the understanding of the hydrogeological setting will be critical to ascertain to which extent kinetic and thermodynamic models may be applied to the system under study. Here, a knowledge about the residence time of water in the reservoir(s) under study, and in the flow-length of interest, is very important in order to define the structure of the model.

The next step in the establishment of a conceptual model is to incorporate the interactions between the trace elements of interest and the major chemical phases.

XIV.3.4.4. *The interaction of trace metals with major component solid phases*

An underlying principle throughout this Chapter is the assumption that trace element geochemistry is mainly controlled by the chemical behaviour of the major components. This is an assumption which is well sustained by the increasing amount of information available regarding the mineralogy of phases including trace elements. The release of metals from waste such as different nuclear waste forms (borosilicate glasses, spent fuel, concrete containment), and incinerator ashes in concrete, is basically controlled by the dissolution of the waste matrix itself, and the “selective” release of trace components is more the exception than the rule. Once the trace elements have been released, they will be found associated to the main components of the system, bound to the predominant (and sufficiently strong) ligands in the aqueous phase, and also to the predominant and strong “ligands” in the solid phases present. Bonding to the solid phase occurs through surface groups, hence, interfacial phenomena, and the size of exposed surface *etc.*, are important factors for the modelling, *c.f.* Chapter VII. The surface ligands are associated to the most “dynamic” solids present in the system (phases that dissolve or precipitate under the time scales of the study). Trace metals associated to the bulk phases may precipitate and/or dissolve during the time scale of our studies, depending on the availability of solid surfaces. Trace metals will interact with the solids that are coating the fissures, pores and any surface in contact with water. These coatings have large surfaces and higher and more rapid sorption than the bulk of the rock solid phases. Freshly precipitated solid phases have large specific surface areas, hence the sorption capacity is much larger than that of aged solid phases.

The chemical interactions of trace metals with solid phases can be of three kinds:

1. Adsorption, when the trace metal interacts with the surface of a solid phase already formed.
2. Surface precipitation, as the trace metal saturates all the available surface of the already formed solid phase, the activity of the host solid phase is changed. This triggers a further precipitation of the host solid phase over the sorbed trace metal.
3. Coprecipitation, this is defined as the simultaneous precipitation of the major component and trace metal phases forming a single solid phase. Coprecipitation may also occur as the result of the further precipitation of the major component solid phases as they age. Wersin *et al.* [89WER/CHA] demonstrated by ESR spectroscopy that surface precipitation and coprecipitation are identical processes in the case of Mn-Fe carbonates.

The differentiation between these processes is difficult, and by and large phenomenological. There seems to be a continuum between these phenomena in nature.

However, the affinity of a certain trace metal for a certain solid surface is of chemical character. In this context, surface complexation models can be used to ascertain which are the stronger surface ligands. The interaction between solutes and solid surfaces, (adsorption-surface precipitation-coprecipitation), will depend on the strength of

Table XIV.4: Characteristic reaction times for the processes describing the interaction of trace metals with major component solid phases.

Process	Example	$\log_{10} \tau_{\text{char}}$ (sec)
Adsorption	$M^{z+} + >\text{FeOH} \rightarrow >\text{FeOM}^{(z-1)+} + \text{H}^+$	-3 to 5
Surface precipitation	$>\text{FeOM}^{(z-1)+} + M^{z+} + x \text{H}_2\text{O} \rightarrow$ $>\text{FeOM}(\text{OH})_x = M^{(2z-1-x)+} + x \text{H}^+$	5 to 6
Coprecipitation	$xM^{z+} + (1-x)\text{Fe}^{3+} + (3-3x+zx)\text{H}_2\text{O} \rightarrow$ $M_x\text{Fe}_{(1-x)}(\text{OH})_{(3-3x+zx)}(\text{s}) + (3-3x+zx)\text{H}^+$	5 to 7
Co-dissolution	$M_x\text{Fe}_{(1-x)}(\text{OH})_{(3-3x+zx)}(\text{s})$ $+ x \text{HCO}_3^- + x(z-1)\text{H}^+ \rightarrow$ $x \text{MCO}_3^{(z-2)+} + (1-x)\text{Fe}(\text{OH})_3(\text{s}) + zx \text{H}_2\text{O}$	5.5 to 6
Ageing of Iron(III) Oxyhydroxide	$\text{Fe}(\text{OH})_3(\text{s}) \rightarrow 0.5 \text{Fe}_2\text{O}_3(\text{s}) + 1.5 \text{H}_2\text{O}$	6.2 to 7.2

this bonding and the availability of the mineral surfaces. A more detailed discussion is given in Chapter VII.

We may establish some general rules to describe the strength of the interactions between trace metals and solid surfaces. These are based on the development of surface complexation models which take into account the adsorption reactions of trace elements with metal oxides and carbonates. As a result of research effort during recent years, there is a wealth of data concerning the kinetics and thermodynamics of these processes. The recent compilations of sorption data [80DAV/LEC, 87COM/MID, 87SCH/STU, 90DZO/MOR], together with recent sorption data of Th(IV) on silica [95OES] and U(VI) on iron(III) oxyhydroxides [94WAI/PAY], have been used to compare the relative strength of the adsorption of different trace elements with various surface types. The selected surface types have been alumina, silica, rutile, iron(III) oxyhydroxides, and calcite. The data are plotted in Figure XIV.4, as the logarithm of the intrinsic adsorption constant, as a function of the surface type. In spite of the scatter of the data, one observes that iron(III) oxyhydroxides (HFO) and calcite form stronger surface complexes with the majority of the trace elements studied than the rest of the solid surfaces. Therefore, they will be the most relevant surface ligands among the dynamic (precipitating/dissolving) solid phases.

We may now use the concept of characteristic reaction times to describe when and how the different processes operate in the natural systems we are trying to model.

Figure XIV.4: Plot of $\log_{10} K_{\text{int}}$ for the surface complexation reactions of trace elements with various solid surfaces. Data from the compilations by [80DAV/LEC], [87COM/MID], [87SCH/STU], and [90DZO/MOR], together with recent sorption data of Th(IV) on silica [95OES] and U(VI) on iron(III) oxyhydroxides [94WAI/PAY].

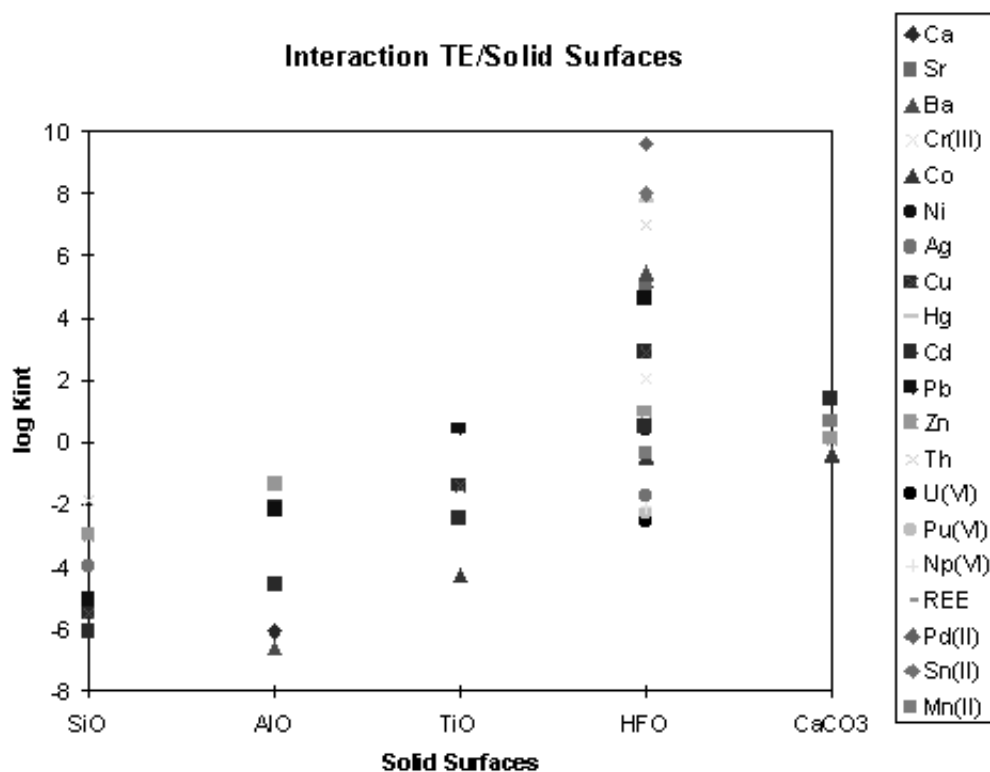


Table XIV.4 shows characteristic reaction times for the processes describing the interaction of trace metals with major component solid phases. We have also included the characteristic reaction time for the ageing of iron(III) oxyhydroxides, since this is a process which clearly controls the transition from sorption to coprecipitation [95BRU/PAB].

By comparing the characteristic reaction times with the average residence times of water in the various reservoirs given in Table XIV.4, we can draw some useful conclusions:

- Adsorption will be the dominant metal/solid phase interaction in reservoirs with short residence times: rivers, soil solutions and shallow groundwaters.
- Surface precipitation/coprecipitation will be important when modelling trace metal behaviour in reservoirs with longer residence times: oceans and deep groundwaters. In this case the ageing of the dynamic solid phases will be a critical factor.

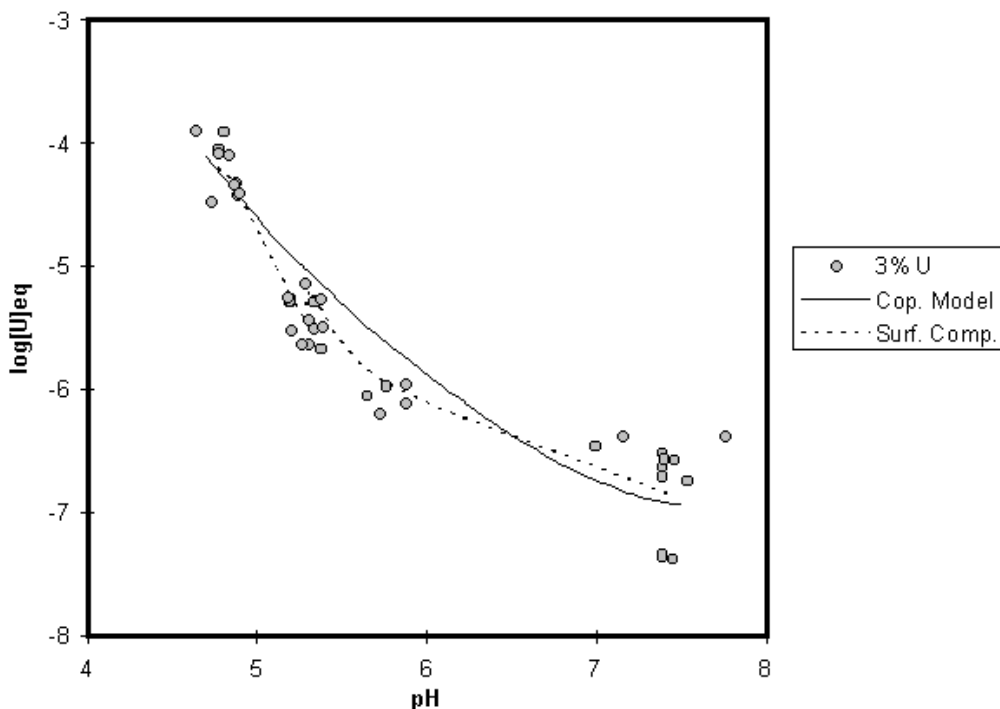
We will now attempt to describe how the interactions can be modelled using the present

Table XIV.5: Comparison of the surface complexation model by [90DZO/MOR] and the conditional solubility constant (coprecipitation) approach for the system: uranium(VI) – iron(III) oxyhydroxides. Surface complexation parameters taken from [94WAI/PAY].

Surface complexation model		Coprecipitation model (Conditional solubility constant model)	
Equilibria			
$>\text{FeOH}_2^+ \rightleftharpoons >\text{FeOH} + \text{H}^+$	K_1	$\text{Cop-UO}_2(\text{OH})_2 + 2 \text{H}^+ \rightleftharpoons \text{UO}_2^{2+} + 2 \text{H}_2\text{O}$	K^*
$>\text{FeOH} \rightleftharpoons >\text{FeO}^- + \text{H}^+$	K_2		
$>\text{Fe}_s(\text{OH})_2 + \text{UO}_2^{2+} \rightleftharpoons (>\text{Fe}_s\text{O}_2)\text{UO}_2^0 + 2 \text{H}^+$	K_s		
$>\text{Fe}_w(\text{OH})_2 + \text{UO}_2^{2+} \rightleftharpoons (>\text{Fe}_w\text{O}_2)\text{UO}_2^0 + 2 \text{H}^+$	K_w		
Parameters			
Specific surface area of the solid	$600 \text{ m}^2 \cdot \text{g}^{-1}$	Molar fraction trace metal / major metal	$\chi = (1\text{-}3) \cdot 10^{-2}$
Density of coordination sites: strong and weak sites (mol sites / mol “FeOOH”)	strong = $1.8 \cdot 10^{-3}$ weak = 0.873	Solubility constant of the pure trace solid phase;	$\log_{10} K_{s,0} = 6.1$
Acidity constants of the surface of the solid	$\log_{10} K_1 = -6.51$ $\log_{10} K_2 = -9.13$		
Surface complexation constants for the trace metal binding to strong and weak sites	$\log_{10} K_s = -2.57$ $\log_{10} K_w = -6.28$		

thermodynamic and kinetic models. Recently, Dzombak and Morel [90DZO/MOR] have published a compilation of the surface complexation data for anions and cations with iron(III) oxyhydroxides. They have demonstrated the common features of the various thermodynamic approaches used to model surface complexation, which undoubtedly enhances the utility of surface complexation models to describe the adsorption of trace metals onto solid phases. However, one of the most critical parameters in these models is the determination of the reactive surface, which is needed to determine the amount of surface ligands (surface co-ordination sites). We have recently studied the kinetics and thermodynamics of the interaction of U(VI) with iron(III) oxyhydroxides [95BRU/PAB], and attempted to model these laboratory results with different surface complexation models. As an alternative we have used the coprecipitation approach to describe trace metal behaviour, a comparison between the two models is given in Table XIV.5.

Figure XIV.5: Measured *vs.* calculated uranium concentrations from a 3% in mole U(VI)-Fe(III) oxyhydroxide coprecipitate, comparison between surface complexation and conditional solubility constant approach from [95BRU/PAB].



One of the most striking results is that both the surface complexation model proposed by Dzombak and Morel [90DZO/MOR] and the conditional solubility constant model provide a similar and equally satisfactory description of the experimental observations. This is apparent in Figure XIV.5, where the laboratory data for the uranium(VI)/iron(III)-oxyhydroxides interaction are compared to the model data obtained using both the surface complexation approach proposed by Dzombak and Morel [90DZO/MOR] and the conditional solubility constants approach [95BRU/PAB]. Although, the surface complexation model appears to be more “mechanistically correct”, the number of empirical parameters involved (see Table XIV.5) make it difficult to use in heterogeneous geological systems. The clear advantage of the conditional solubility model is that it does not require the determination of the reactive mineral surface. Only an estimate of the mole fraction of trace metal bound to the solid is needed. This can be derived a priori by using mass balances calculations.

In some of the examples to be explored later on, we will see that the conditional solubility model appears to describe quite nicely (and simply) the behaviour of trace metals in different geochemical environments.

XIV.4. The objective of geochemical modelling efforts. Interpretation *vs.* prediction

“Predictions are very difficult...Particularly, about the future” (Niels Bohr).

At this point, it is important to ponder about the use and application of geochemical models. Particularly relevant is the application of predictive geochemical modelling related to the safe disposal of high level nuclear waste. All nuclear waste management alternatives require the evaluation of the performance of the disposal system for periods of time longer than tens of thousands of years. This clearly exceeds the normal planning horizon conceived in most engineering systems. Therefore, the geochemical models have to be able to produce reasonable and defensible predictions about the geochemical evolution of the repository system over long periods of time. There are two main areas of application to the performance assessment of nuclear waste disposal systems. The first one is concerned with the evolution of the disposal environment itself due to internal (geological) or external (anthropogenic) disturbances. The second area of application is related to the prediction of the transport and fate of the radionuclides initially contained within the various waste matrices. In both cases the predictive modelling methodology is quite similar, as illustrated in the following examples.

XIV.4.1. An example of assessing the potential impact of an anthropogenic disturbance on a high-level nuclear waste repository. The effects of acid rain in the granitic geosphere

There has been some concern of the potential effects of soil and groundwater acidification on the geochemical stability of a HLNW repository, particularly in areas subject to extensive past and present acidification due to fossil fuel combustion. In Fennoscandia the dominant type of bedrocks are granite, gneiss and quartz. Because of their poor buffering capacity granitic/gneiss systems are sensitive to acidification. A contributing factor is that rock/water interactions are slow processes. Consequently, the flux of atmospheric acidification is transferred to the hydrosphere where it results in the acidification of surface waters, lakes in particular. In the long term, the acidic flux is transferred to the groundwater reservoir. It is necessary to evaluate the possible impact of this acidification process on the repository system. The disposal system can be disturbed in two ways:

- The geological stability of the granitic formations can be affected due to the increased rates of chemical weathering.
- The chemical composition of the groundwater could be altered if the acid buffering capacity is largely depleted.

The methodology to model this is as follows (detail is given in Ref. [91NEB/BRU]):

1. We have to devise different fossil fuel use and combustion scenarios in order to calculate the rates of acid deposition into Fennoscandia, as well as the estimated

times of the disturbance. Energy use and consumption scenarios have been largely explored and current estimates indicate that fossil fuel consumption will continue for the next 350 years [89GRA/CRU].

2. Three different sub-scenarios are used depending on the balance between emission control and consumption during the next centuries (mild, moderate and severe control). These sub-scenarios are generated by the IIASA international agency as part of their RAINS acidification model [89ALC/SHA].
3. The concentration of $\text{SO}_2(\text{g})$ and $\text{CO}_2(\text{g})$ in the atmosphere as a result of the various fossil fuel combustion scenarios is calculated by taking into consideration their atmospheric chemistry and residence times, which are well known.
4. The impact of the atmospheric acidic fluxes on the acid buffering capacity of the granitic soils is calculated by taking into consideration the main chemical processes which control the acid buffer capacity of these soils: a) ion exchange buffer capacity, which is at present quite low in the Fennoscandian soils; b) kinetic buffering capacity as given by the slow dissolution of feldspars and the secondary precipitation of $\text{Al}(\text{OH})_3(\text{s})$.
5. Finally, the cumulative effect on the geological stability of the repository is estimated by calculating the so called Net Surface Lowering, which is given by the difference between the amount of granite weathered, as calculated from laboratory measurements of feldspar dissolution, and the new soil formed, estimated from geological observations on the rates of soil formation.

The outcome of this predictive modelling on the impact of soil acidification on the stability of a granitic repository is given in Table XIV.6, where the total acid load received by the soils, the amount of silicate weathering and the resulting Net Surface Lowering are calculated for the next 60 000 years (estimated lifetime of a HLNW repository prior to the next Ice Age in Scandinavia) depending on the different emission control scenarios for fossil fuel combustion. The main outcome of this predictive modelling exercise is to point out that if control emissions are relaxed the known buffering capacity of the granitic soils will be depleted before fossil fuel combustion is exhausted resulting in a severe and irreversible damage to this ecosystem. An additional consequence might be a substantial increase on the rates of weathering and erosion, with a cumulative Net Surface Lowering of some hundred meters in the next 60 000 years.

This is a typical example of the use of predictive geochemical modelling: to give comparative estimates of the result of an anthropogenic disturbance on the fragile proton (un)balance in granitic soils. The main geochemical processes controlling the generation, transport and fate of the acidic fluxes in the various reservoirs are now quite well understood. There has been a substantial scientific effort to understand the critical reactions that contribute to the acid buffering capacity of this particular kind of soil and even if some detailed processes remain unclear, we now realise that the fast cation exchange capacity and the slower silicate weathering are the main buffer mechanisms which control

Table XIV.6: Results from modelling the effect of soil acidification on the stability of a granitic nuclear waste repository [91NEB/BRU].

	Severe emission control	Moderate emission control	Mild emission control
Total Acid load (mole m ⁻²)	1500	1600	2000
Total Weathered Silicate (mole m ⁻²)	2900	2900	90 000
Total Net Surface Lowering (m)	4	4	130
Acting soil buffering capacity after recovery of pre- industrial levels	cation exchange	cation exchange	gibbsite

the acidity of the soils. The effect of increased acidity of the soil and soil solution on the rates of silicate weathering is not completely understood. The chemical effects are quite well studied and there is a wealth of data which indicate that there is a fractional dependence of the rates of silicate weathering on the proton concentration: $R_w = K_w[H^+]^r$, with $0.2 < r < 0.7$ [90STU/WOL]. This would imply a limited effect of the increased acidification on the rates of silicate weathering. However, the physical effects of loss of vegetation and increased denudation are reported to result in increased weathering rates of acidified soils as compared to undisturbed ones [86PAC]. Therefore, as a part of our predictive modelling exercise we have described the system by assuming that the physical result of increased acidification is that the soil system behaves as in ideal kinetic studies in the laboratory, where almost all the silicate surface is available for reaction. This results in an increase in silicate weathering rates which are two to three orders of magnitude larger than the ones actually measured in the field [90SCH]. This approximation therefore results in an estimate of the upper boundary of the effect caused by uncontrolled fossil fuel combustion. However, the main fact remains unchanged: once the cation exchange buffer capacity of a granitic soil is depleted the ecological effects are serious and irreversible.

This model has been extended to the groundwater compartment in order to study the influence of the increased acid fluxes on the chemical composition of granitic groundwaters [94WER/BRU]. Once more, we identified the main processes which affect the acid buffer

capacity of a granitic groundwater:

- Rock/water interactions as given by the nature of the fracture filling materials: feldspar, calcite, and gibbsite weathering.
- Cation exchange reactions involving clay minerals.
- Pyrite oxidation to produce iron(III) oxyhydroxide
- Decomposition of organic matter.

The predicted evolution of the groundwater acid buffering capacity as a consequence of the increased soil acidity flux was modelled by using the STEADYQL code [89FUR/WES, 90FUR/WES]. This model allows the combination of fast (equilibrium) reactions with slow (kinetically controlled) ones, by including the relevant thermodynamic and kinetic data. The main outcome of this exercise was to establish that calcite weathering plays a critical role for the acid buffer capacity of granitic groundwaters. Once the calcite weathering capacity is depleted, the aquifer becomes irreversibly damaged. This process plays for the granitic groundwater system a critical role analogous to the cation exchange buffer capacity in the soil system. Depending on the various scenarios studied, we estimated that the time needed to deplete the calcite buffering capacity down to 500 meters depth is in the range of ten thousands to hundreds of thousands of years.

Again this modelling exercise contained some unrealistic idealisations of the physical properties of the system selected to provide a conservative estimate. In this way we were able to identify the critical geochemical processes and estimate their effect under the most unfavourable conditions.

XIV.4.2. An example of calculating the maximum release concentrations of critical radionuclides from spent fuel disposal. How information from natural system studies can be used to narrow down unrealistic predictions.

One of the most common applications of trace element thermodynamic modelling is the calculation of maximum release concentrations from nuclear waste under disposal conditions. These kinds of calculations are known under the name of Radionuclide Solubility Limit (RSL) calculations. The methodology used is simple, although it contains some critical assumptions:

- The system is governed by thermodynamics and the most stable phases are the ones that precipitate. As we have already discussed this is normally an exception in geochemical systems, where usually the less stable solid phases are kinetically favoured (the Ostwald principle) and are the first to precipitate. The usual sequence of precipitation and ageing with time for hard metal ions in granitic groundwater environments is:

amorphous oxyhydroxide → oxides/carbonates/hydroxocarbonates →
silicates/phosphates.

Figure XIV.6: Idealised view of the time dependence of the formation of hard metal ion solid phases under granitic groundwater conditions and the resulting equilibrium concentrations. Time and concentration scales are relative and should not be taken at their absolute values.

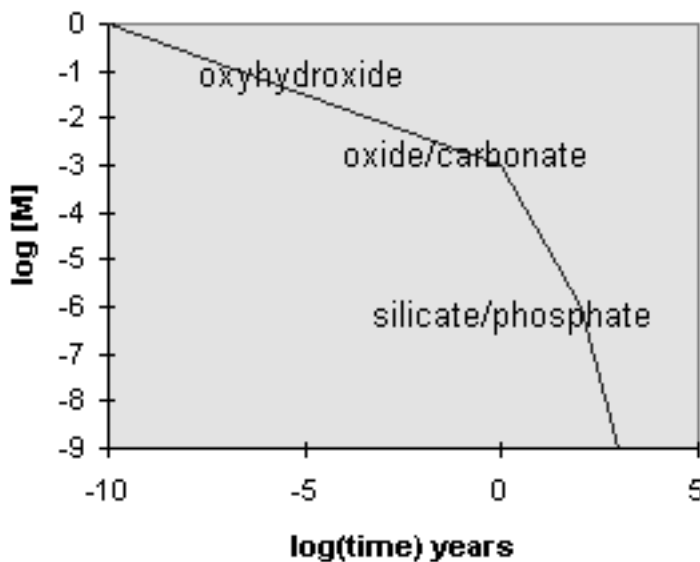


Figure XIV.6 shows an idealised view of the evolution of the equilibrium metal concentrations with time as the formation of different metal solid phases proceeds.

As we have already discussed in the previous sections it is useful to set the time frame of these processes in the perspective of their characteristic reaction times. This information can then be compared with the information on the residence times of water in the various parts of a repository system. We will use the information from Tables XIV.2 and XIV.4 for this discussion.

The precipitation of amorphous oxyhydroxide phases is a fast process with characteristic reaction times in the range of seconds. The ageing of the metal oxyhydroxides to crystalline oxides is a slower process with characteristic reaction times in the range of months. Finally, the alteration of the oxide phases to silicate and/or phosphate phases is an even slower process (average characteristic reaction times of tens to hundreds of years), which is strongly dependent on the hydrological condition of the system (S/V: solid surface/water volume ratio). The rate is accelerated by temperature and the stoichiometry of the final alteration product depends strongly on the silicate/phosphate ratio in the water.

The kinetic constraints on the evolution of radionuclide solid phases imply that from a safety assessment point of view, it is most proper to calculate Radionuclide Solubility Limits (RSL) by assuming equilibrium with crystalline oxide phases because the time scales involved in the different solid precipitation and alteration processes are comparable

with groundwater residence times in the different parts of the repository. Most chemical and geological information indicates that hard metal ions (*i.e.* actinides) are present in nature as silicates and/or phosphates, but other phases should also be considered.

The selection of the solubility limiting phase has to be not only realistic but also well documented. This point may be illustrated by looking into the Am(III) *vs.* REE(III)[†] solubility limits under disposal conditions, a case that has been already discussed in Chapter IV.

The establishment of RSL for safety assessment purposes requires that the phases selected under the conditions of the assessment have a well documented “pedigree”, as well as detailed information about their thermodynamic properties. The solubility limiting phase for americium(III) under granitic groundwater conditions is a typical case where various alternatives are possible under the kinetic constraints previously discussed. It may precipitate as Am(III) hydroxide, carbonate or hydroxocarbonate. The occurrence and stability of these phases has been the source of some scientific dispute. Fortunately, the work from the NEA Am-TDB has settled the issue and the ranges of occurrence and stability of these phases are now well understood [95SIL/BID]. A crucial factor in this assessment has been the characterisation of the mixed hydroxocarbonato phase by various spectroscopic techniques. From this work it is now clear that AmCO₃OH(s) is the solubility limiting phase under granitic groundwater conditions (see for example Figure V.12, p.163 in [95SIL/BID]).

In the case of rare earth elements, and particularly for samarium(III), a radionuclide of concern in the disposal of spent nuclear fuel, the situation is somewhat different. Recently, a compilation of thermodynamic data for the REE has been prepared [95SPA/BRU]. The information collected concerning the occurrence and stability of REE(III) hydroxides, oxides and carbonates may be summarised as follows:

- Data on the occurrence and stability of REE(III) hydroxides are quite satisfactory and this includes the stability constant for Sm(OH)₃(s).
- The stability constants for the REE(III) carbonates, (REE)₂(CO₃)₃(s), have also been determined and their rationalisation in terms of ionic strength corrections show the expected trends. In the case of Sm(III) the solubility product is calculated from three independent measurements with a satisfactory agreement (details [95SPA/BRU]).
- The occurrence of mixed REE(III) hydroxocarbonates is a more complex matter. A detailed evaluation of the geological and chemical literature available indicates that the formation of these phases in the lanthanide series is controlled by the ionic radius of the REE, the partial pressure of CO₂(g) and the temperature. The normal carbonates are favoured for REE with decreasing ionic radius, temperature and increasing *p*CO₂.

[†] REE: rare earth elements.

Under these circumstances the modeller is confronted to a dilemma between what it is reasonable to expect from chemical reasoning (*i.e.* the analogy between REE and actinide(III) elements) and the requirements to make predictions which do not underestimate the solubility (and therefore, the mobility) of the trace element in question. The normal choice will be in these circumstances, the selection of a solubility limiting phase which gives us a conservative (over)estimate of the solubility of the trace element. This is not satisfactory from the chemical reasoning point of view but it gives an indication of the maximum risks associated to the release of the element in question.

So, from a predictive geochemical modelling point of view we have to live with the different behaviour shown by the individual phases of apparently analogous ions. The next question to ask ourselves is: How reasonable is it to assume that the solubility of trace elements, like radionuclides in the disposal system, is controlled by the precipitation of pure individual phases ?

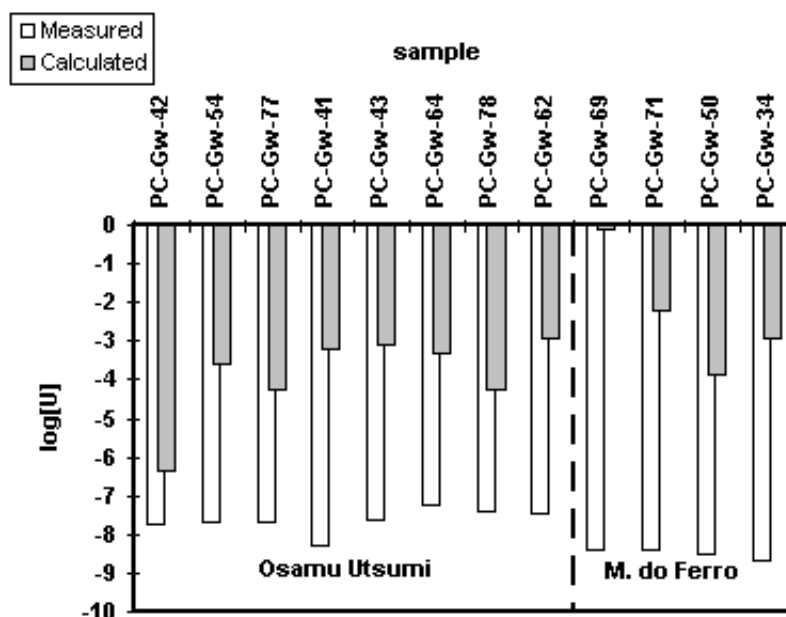
From the discussions at the initial sections of this Chapter, it follows that the fate of trace elements in aquatic systems is mainly controlled by the cycling of the main geochemical components (Fe, C, P, Si and S). The critical questions are then: how can we integrate this linkage in our geochemical predictive modelling of Radionuclide Solubility Limits (RSL) ? and to what extent do we feel comfortable about the assumptions ?

The integration of radionuclide coprecipitation in the calculation of RSL implies a detailed knowledge of its kinetic and thermodynamic constraints, as well as documented proof that the processes in natural systems are analogous to those in the disposal situation and that they can be satisfactorily modelled.

This point will be illustrated by discussing the coprecipitation of uranium(VI) with iron(III) oxyhydroxides. This is a well documented chemical phenomenon which has been identified both in geological and laboratory systems. It is a critical process because it will limit the uranium solubility and consequently its release under oxic conditions. Furthermore, if the phenomenon is well sustained it could be a critical factor controlling the release of some other more critical radionuclides (*e.g.* neptunium(V)) under oxic conditions. In addition, the kinetics and thermodynamics of the coprecipitation process have been studied and their fundamentals are established [95BRU/PAB]. The remaining issue is to what extent do we have indications that such an approach can be used to model the behaviour of U(VI) in the oxic zone of redox fronts in nature.

Fortunately, such redox fronts are encountered in uranium ore deposits close to the surface (most of them are, Cigar Lake being an exception). Within the various international Natural Analogue projects (for more information see [94MIL/ALE]), there have been several exercises intended to test geochemical modelling capabilities (codes and associated data bases) to predict RSL in geochemical environments analogous to the ones expected in repository conditions. These exercises were primarily aimed at reproducing the conditions and uncertainties encountered by geochemical modellers when trying to calculate the radionuclide solubility and speciation. They have been useful also in illustrating some of the major challenges and limitations of the present modelling tools and the associated databases. The prediction of trace element solubilities is compared with the actual measurements in the site which normally result in the identification of critical

Figure XIV.7: Calculated uranium concentrations by assuming equilibrium with U_3O_8 versus measured uranium content in the selected groundwaters at Poços de Caldas [91BRU/CRO].



uncertainties in the chemical assumptions and/or the necessary thermodynamic data.

Two of the natural analogue sites where there is a documented mineralogical association of U with Fe(III) oxyhydroxides are Poços de Caldas (Brazil) and El Berrocal (Spain). The initial predictions of U solubilities in these environments resulted in much higher estimated concentrations than those actually found in the field measurements. However, a calculation of the uranium solubility by using a revised chemical model which includes coprecipitation, and the available mineralogical information resulted in a much better agreement with the observed U concentrations. The comparison between measured and predicted U concentrations in both sites is given in Figures XIV.7, XIV.8 and XIV.9.

Similar improvement has been noted when the solubilities of trace components like Sr, Ba and Mn are calculated by assuming their mineralogically documented association to calcites in these sites (see [96BRU/DUR, 96BRU/DUR2] for details).

This development gives us some hopes that by combining fundamental geochemical laboratory work, together with the observations from well characterised sites, we will build up our confidence and capabilities to narrow the gap between predictive RSL modelling and the observations from relevant systems in nature. This should improve the level of realism in chemical risk assessments and enhance the possibility to implement technically sound solutions to the environmental problems related to the transport and fate of toxic metals and other pollutants.

Figure XIV.8: Calculated uranium concentrations by assuming U(VI)/Fe(OH)_3 coprecipitation of *versus* measured uranium content in the selected groundwaters at Poços de Caldas. Details in [96BRU/DUR2].

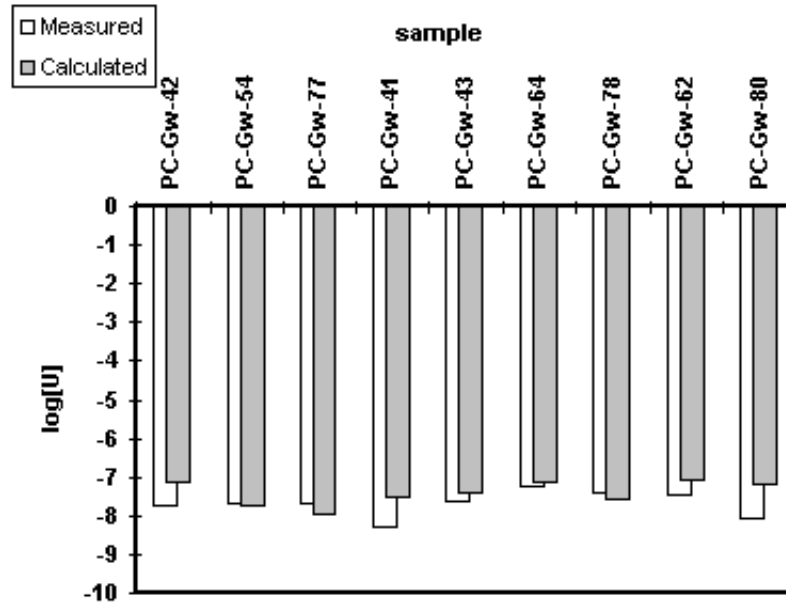
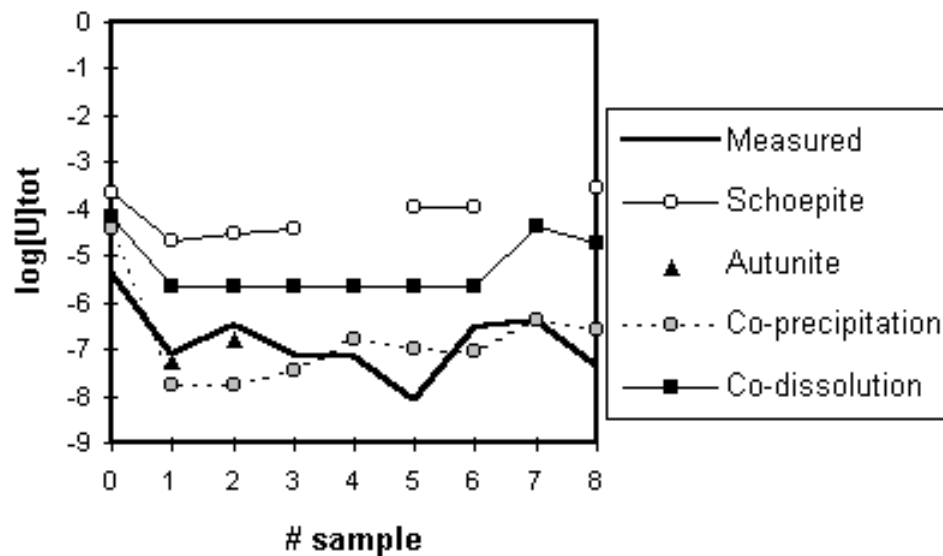


Figure XIV.9: El Berrocal. Calculated solubilities by using individual (schoepite/autunite) solid phases and by assuming U(VI)/Fe(OH)_3 coprecipitation compared with the measured uranium concentrations. Ref. [96BRU/DUR].



XIV.5. Acknowledgments

This chapter is a recollection of my working experience in the application of geochemical models. There are many people from whom I have learned and with whom I have enjoyed collaboration at various levels: to all of them my deepest recognition. However, there are a few people I would like to mention, in a chronological order, for their specific contributions: Ingmar Grenthe, teacher, advisor, mentor and friend with whom I grew professionally and personally. Ignasi Puigdoménech, who introduced me into the world of chemical modelling. Kastriot Spahiu, who taught me a great deal on solution thermodynamics and electrolyte theory. Kirk Nordstrom who showed me the excitement of the transition pathway from solution chemistry to geochemistry, although he should not feel responsible for my deviations from dogma. Werner Stumm, who introduced me with great intellectual generosity into the surface of things, showing that surfaces can indeed be very deep. My grateful recognition to Ignasi Casas, Amaia Sandino, Erik Östhols, Steve Banwart, Susan Carroll, Pepa Nebot, Paul Wersin, Joan de Pablo, Lara Duro and Esther Cera for their personal contributions to some of the work presented in this chapter. Dr. Jörg Haderman is acknowledged for a careful review and many useful comments.

The work presented here would not have been possible without the support of Fred Karlson, Lars Werme, Peter Wikberg and Patrik Sellin from SKB (Sweden), as well as Julio Astudillo and Pedro Hernan from ENRESA (Spain).

Chapter XV

Authors List

This chapter contains an alphabetical list of the authors of the references cited in this book, *cf.* Chapter XVI. The reference codes given with each name corresponds to the publications of which the person is the author or a co-author. Note that inconsistencies may occur due to different interpretations of foreign alphabets. These inconsistencies are not corrected in this volume.

Author	References
Aagard, P.	[84HEL/MUR]
Aberg, M.	[70ABE], [83ABE/FER]
Ackermann, R.J.	[76OET/RAN]
Adams, F.	[90BRO/GUC]
Adamson, A.W.	[54ADA], [90ADA]
Aguilera, M.	[72ZUN/GAL]
Ahn, J.	[85AHN/CHA]
Ahrland, S.	[57AHR/GRE], [58AHR/CHA], [67AHR], [68AHR], [73AHR], [78AHR], [79AHR], [82AHR], [96AHR]
Aiken, G.R.	[85AIK/MCK]
Akhachinskiy, V.V.	[81CHI/AKH]
Aksoyoglu, S.	[89BRA/AKS]
Alberts, J.J.	[83ALB/GIE]
Alcamo, J.	[89ALC/SHA]
Alcock, C.B.	[76ALC/JAC], [93GUR/VEY], [93KUB/ALC]
Alcock, R.M.	[80HAR/BUR]
Alegret, S.	[84ALE/ESC], [86EPH/ALE]
Alexander, R.	[94MIL/ALE]
Alexander, W.R.	[89BRA/AKS], [92ALE/DAY], [92FRI/ALE]
Allard, B.	[89EPH/BOR], [89EPH/BOR2], [89XU/EPH], [92ARS/BOR], [93EPH/ALL], [93NOR/EPH], [94EPH/ALL], [94KRA/ALL], [94NOR/EPH], [94PET/EPH], [95EPH/PET]
Allen, F.H.	[79ALL/BEL]
Allison, J.D.	[94ALL/PER]
Allred, A.L.	[61ALL]
Althaus, E.	[70ALT/KAR]
Altmann, R.S.	[87BUF/ALT], [88ALT/BUF], [90BUF/ALT]
Amster, J.L.	[77MEA/CRE]
Ananthaswamy, J.	[84ANA/ATK]
Anderegg, G.	[77AND], [94AND/KHO]
Anderson, G.M.	[91AND/CAS]
Anderson, J.	[95CHA/AND]
Anderson, M.A.	[81AND/RUB]
Anderson, O.L.	[91AND/ISA]
Andersson, J.O.	[85SUN/JAN]
Ansara, I.	[81CHI/AKH]
Appelo, C.A.J.	[93APP/POS]
Appert, C.	[90APP/ZAL], [93APP/ZAL]
Apps, J.A.	[90APP/NEI]
Arai, S.	[77ARA/KUM]
Aral, K.	[83CHE/ARA]
Archer, D.G.	[90ARC/WAN], [91ARC]
Ardakani, M.S.	[72ARD/STE]
Arnek, R.	[65ARN], [67ARN/KAK]
Arsenie, I.	[89EPH/BOR], [89EPH/BOR2], [92ARS/BOR]

Author	References
<hr/>	
Ashida, T.	[95PAS/KIM]
Asper, R.	[77OSW/ASP]
Aspray, W.	[87ASP/BUR], [90ASP]
Atkins, P.W.	[89ATK]
Atkinson, G.	[84ANA/ATK]
Atkinson, P.W.	[90ATK]
Ayora, C.	[96BRU/DUR2]
Baccasin F.	[92OTT/DEL]
Bachmat, Y.	[91BEA/BAC]
Backes, C.A.	[88TIP/BAC]
Baes, C.F., Jr.	[76BAE/MES], [81BAE/MES]
Baeyens, B.	[89BRA/AKS], [92FRI/ALE]
Bailey, S.M.	[82WAG/EVA]
Bajo, C.	[89BRA/AKS]
Balasubramanian, K.	[87BAL/HAY]
Balfour, F.W.	[83LEV/KAM]
Ball, J.W.	[79NOR/PLU], [84NOR/BAL]
Bancroft, G.M.	[90BAN/HYL]
Banwart, S.	[94BAN], [96BAN/TUL], [96DEN/STJ], [96MAL/BAN]
Barbero, J.A.	[86TRE/SWA]
Barcelona, M.J.	[90BAR]
Bard, J.A.	[85BAR/PAR]
Barin, I.	[93BAR]
Barnes, H.L.	[63BAR/ERN], [80RIM/BAR], [86MCK/BAR]
Bartschat, B.M.	[92BAR/CAB]
Batchelor, G.K.	[94BAT]
Bates, R.G.	[70BAT/STA], [73BAT]
Bear, J.	[91BEA/BAC], [92BEA/VER], [93BEA/TSA]
Beasley, M.L.	[77HAI/LLO]
Beck, M.T.	[90BEC/NAG]
Belitz, K.	[94ORE/SHR]
Bellard, S.	[79ALL/BEL]
Belonoshko, A.B.	[94BEL]
Belousov, B.P.	[58BEL2]
Belousov, E.A.	[84PRO/EIN], [85PRO/BEL]
Benedetti, M.F.	[95BEN/MIL]
Bennet, C.H.	[73BEN]
Benzi, R.	[88SUC/SAN]
Berg, R.L.	[75BER/VAN], [75BER/VAN2]
Bergerhoff, G.	[83BER/SIE]
Berlekamp, E.R.	[82BER/CON]
Berman, R.G.	[85BER/BRO2], [86BER/ENG], [88BER]
Berner, U.	[92PEA/BER], [95BER]
Bertha, E.L.	[78BER/CHO]

Author	References
Beverkog, B.	[96BEV/PUI]
Bicking, M.	[86EPH/ALE]
Bidaux, R.	[89MAN/BOC]
Bidoglio, G.	[91BID/GRE], [95SIL/BID]
Biedermann, G.	[53BIE/SIL], [75BIE], [82BIE/BRU]
Bilinski, H.	[82BIL/SCH]
Binder, P.E.	[84NOR/BIN]
Bird, D.K.	[78HEL/DEL]
Bird, R.B.	[60BIR/STE]
Bischoff, H.	[92KRA/BIS]
Blaakmeer, J.	[86RIE/BOL]
Blankleider, B.	[90BLA], [94KAR/BLA]
Blencoe, J.G.	[82SCH/KER]
Boccaro, N.	[89MAN/BOC]
Boccio, J.R.	[94WOO/CAR]
Bockris, J.O'M.	[77BOC/RED]
Boghosian, B.M.	[87BOG/LEV], [90BOG]
Boissonade, J.	[90CAS/DUL], [91KEP/CAS]
Bolt, G.H.	[86RIE/BOL], [89HIE/RIE]
Bond, A.M.	[80BON/HEF]
Bonn, B.A.	[93BON/FIS]
Bonner, F.T.	[45HAR/BON]
Bonomi, E.	[91BRI/BON]
Boon, J.-P.	[80BOO/YIP], [89DAB/BOO], [90DAB/LAW], [91DAB/BOO], [91LAW/DAB]
Boran, D.A.	[83HAR/BOR]
Borén, H.	[89EPH/BOR], [89EPH/BOR2], [92ARS/BOR]
Bossart, P.	[91BOS/MAZ], [92FRI/ALE]
Bourcier, W.L.	[88JAC/WOL], [90WOL/JAC], [93BOU/KNA]
Bradbury, M.H.	[89BRA/AKS], [92FRI/ALE], [92SAR/BRA]
Bradley, D.J.	[79BRA/PIT]
Brandberg, F.	[92BRU/STU]
Bratsch, S.G.	[89BRA]
Bredehoeft, J.D.	[92KON/BRE]
Breger, I.A.	[83HAT/BRE]
Bresnahan, W.T.	[78BRE/GRA]
Brewer, L.	[61LEW/RAN], [80BRE/LAM2]
Brezonik, P.L.	[83MIL/TUS], [83TUS/BRE]
Brice, L.K.	[83BRI]
Brice, M.D.	[79ALL/BEL]
Brieger, L.M.	[91BRI/BON]
Brodkey, R.S.	[88BRO/HER]
Broekaert, J.A.C.	[90BRO/GUC]
Bromley, L.A.	[73BRO]

Author	References
Brønsted, J.N.	[22BRO], [22BRO2]
Brookins, D.G.	[88BRO]
Brown, I.D.	[83BER/SIE]
Brown, P.R.	[90OSC/GIL], [90OSC/IZA]
Brown, T.H.	[85BER/BRO2], [86BER/ENG]
Bruno, J.	[82BIE/BRU], [86BRU], [87BRU/CAS], [91BRU/CAS], [91BRU/CRO], [91NEB/BRU], [92BRU/SEL], [92BRU/STU], [92BRU/WER], [92SAN/BRU], [93BRU/CAC], [94WER/BRU], [94WER/SPA], [95BRU/PAB], [95SPA/BRU], [96BRU/DUR], [96BRU/DUR2], [96MAL/BAN]
Bruton, C.J.	[90WOL/JAC], [94VIA/BRU], [97BRU/VIA]
Bryant, E.	[89KIM/BUC]
Bryzgalin, O.V.	[82BRY/RAF], [83BRY], [85RYZ/BRY], [85RYZ/SHA], [86BRY], [87RYZ/BRY], [89BRY], [91RYZ/BRY]
Buckau, G.	[89KIM/BUC], [92BUC/KIM], [94CZE/BUC], [96CZE/KIM]
Buehler, Ch.	[92FRI/ALE]
Buffle, J.	[77BUF/GRE], [80BUF], [83STA/BUF], [84BUF/STA], [84STA/BUF], [87BUF/ALT], [87BUF/VUI], [88ALT/BUF], [88BUF], [90BUF/ALT]
Bunzl, K.	[80MAR/WOL]
Burch, T.E.	[94LAS/SOL]
Burgess, C.	[80HAR/BUR]
Burks, A.	[87ASP/BUR]
Burnison, B.K.	[94BUR]
Busenberg, E.	[76BUS/CLE], [82PLU/BUS], [90NOR/PLU]
Busey, R.H.	[78BUS/MES], [82PAT/SLO], [84PAT/BUS], [84PIT/PEI]
Byrne, R.H.	[93BYR/KIM]
Cabaniss, S.E.	[83CAB/SHU], [84CAB/SHU], [88CAB/SHU], [89CAB/MOR], [92BAR/CAB]
Caceci, M.	[91MOU/CAC], [93BRU/CAC]
Caceci, M.S.	[85CAC]
Campbell, J.E.	[80CRA/GUZ]
Capdevila, H.	[92CAP/VIT], [95CAP/VIT]
Carlsen, L.	[85CAR]
Caroll, S.A.	[93CAR]
Carrera, N.J.	[64CAR/WAL]
Carter, R.W.	[94WOO/CAR]
Cartwright, B.A.	[79ALL/BEL]
Casabonne, J.M.	[89PET/DRA]
Casas, I.	[87BRU/CAS], [91BRU/CAS], [93BRU/CAC], [96BRU/DUR2]
Castet, S.	[91AND/CAS], [91CAS]
Castets, V.	[90CAS/DUL], [91KEP/CAS]
Cera, E.	[96BRU/DUR]
Chakrabarti, C.L.	[80LI/VIC]

Authors List

Author	References
Chambré, P.L.	[85AHN/CHA]
Chapman, N.A.	[91CHA/MCK], [94MIL/ALE], [95CHA/AND]
Charlet, L.	[89WER/CHA], [94CHA]
Charlot, G.	[57CHA], [71CHA/COL]
Chase, M.W.	[85CHA/DAV]
Chatt, J.	[58AHR/CHA]
Chatterjee, N.	[93SAX/CHA]
Chatterjee, N.D.	[74CHA/JOH], [82HAL/CHA], [94CHA/MIL]
Chen Q.	[91CHE/XU]
Chen, C.H.	[75CHE]
Chen, C.M.	[83CHE/ARA]
Chen, H.	[87CHE/MAT], [88CHE/CHE], [90CHE/MAT]
Chen, K.	[82COB/MUR]
Chen, S.	[88CHE/CHE], [95CHE/DAW]
Chen, X.	[92IZA/OSC], [93CHE/GIL], [93CHE/GIL2], [93GIL/OSC]
Chen, Y.	[77SEN/CHE], [86FIT/STE]
Chermak, J.A.	[89CHE/RIM]
Chernikova, G.E.	[75FED/CHE]
Cherry, J.A.	[79FRE/CHE]
Chesal, L.A.	[83HAR/BOR]
Cheshire, M.V.	[87GOO/CHE]
Chiotti, P.	[81CHI/AKH]
Chopard, B.	[91CHO/DRO], [91CHO/DRO2]
Choppin, G.	[95MOU/MOU2]
Choppin, G.R.	[78BER/CHO], [84TOR/CHO], [91CHO/CLA], [92CHO/DU], [94ERT/MOH], [95RAO/CHO]
Chou, I.M.	[73EUG/CHO]
Chou, L.	[89CHO/GAR]
Christ, C.L.	[65GAR/CHR]
Christensen, J.J.	[64CHR/IZA], [89IZA/CHR], [89IZA/CHR2], [90OSC/GIL], [90OSC/IZA]
Churney, K.L.	[82WAG/EVA]
Ciavatta, L.	[75CIA/GRI], [80CIA], [81CIA/FER], [87CIA/IUL], [88CIA], [90CIA]
Clark, S.B.	[91CHO/CLA]
Clarke, E.C.W.	[66CLA/GLE]
Clearfield, A.	[63HEI/CLE]
Clemency, C.V.	[76BUS/CLE]
Clinnick, M.L.	[88JAC/WOL]
Cobble, J.W.	[53COB], [53COB2], [53COB3], [64CRI/COB], [64CRI/COB2], [70HIN/COB], [70HIN/COB2], [82COB/MUR]
Coello, J.	[86COE]
Colin, F.	[87DEC/COL]
Collins, B.J.	[83CAB/SHU], [83SHU/COL], [84CAB/SHU]

Author	References
<hr/>	
Collumeau, A.	[71CHA/COL]
Colvin, M.E.	[88LAD/COL]
Comans, R.N.J.	[87COM/MID]
Combes, P.	[92MAR/COM]
Conway, J.H.	[82BER/CON]
Cordfunke, E.H.P.	[78COR/OHA]
Cornell, R.M.	[88COR]
Cosovic, B.	[88ULR/STU]
Cotton, F.A.	[87COT/WIL], [88COT/WIL]
Countryman, R.	[71SCH/COU]
Couture, A.M.	[57COU/LAI]
Couturier, Y.	[84COU/MIC]
Cowan, C.E.	[87PET/HOS]
Cox, B.G.	[74COX/HED]
Cox, J.D.	[89COX/WAG]
Cramer, S.	[89EPH/MAR]
Cranwell, R.M.	[80CRA/GUZ]
Cremers, A.	[91MAE/ELE]
Crerar, D.A.	[77MEA/CRE]
Criss, C.M.	[64CRI/COB], [64CRI/COB2]
Cross, J.E.	[91BRU/CRO]
Crovisier, J.L.	[91DAU/CRO]
Crutzen, P.J.	[89GRA/CRU]
Cvitaš, T.	[88MIL/CVI]
Czerwinski, K.R.	[94CZE/BUC], [96CZE/KIM], [96KIM/CZE]
Dab, D.	[89DAB/BOO], [90DAB/LAW], [91DAB/BOO], [91LAW/DAB], [92DAB]
Dagan, G.	[89DAG]
Dal Negro, A.	[92OTT/DEL]
Das, S.P.	[92ERN/DAS]
Daux, V.	[91DAU/CRO]
David, F.	[86DAV], [86DAV2]
Davies, C.A.	[85CHA/DAV]
Davies, J.A.	[84NOR/BIN]
Davies, N.R.	[58AHR/CHA]
Davis, J.A.	[80DAV/LEC]
Davis, R.	[43HAR/DAV]
Dawson, S.P.	[95CHE/DAW]
Day, H.W.	[73DAY], [80DAY/KUM]
Dayal, R.	[92ALE/DAY]
De Kepper, P.	[90CAS/DUL], [91KEP/CAS]
De Levie, R.	[90LEV]
De Marsily, G.	[80MAT/MAR], [86MAR3], [92MAR/COM], [93BEA/TSA]
De Pablo, J.	[93BRU/CAC], [95BRU/PAB]

Author	References
De Pazzis, O.	[76HAR/PAZ]
De Visser, C.	[76DES/VIS]
De Wit, J.C.M.	[90WIT/RIE], [93NED/WIT], [93WIT/RIE], [93WIT/RIE2]
Debyser, Y.	[80DER/MOR]
Decambox, P.	[91MOU/DEC]
Decarreau, A.	[87DEC/COL]
Decnop-Weever, L.G.	[78KRA/DEC]
Delahay, P.	[50DEL/POU]
Delany, J.M.	[78HEL/DEL], [88JAC/WOL], [90WOL/JAC]
Delgado, J.	[96BRU/DUR2]
Della Giusta, A.	[92OTT/DEL]
Della Mea, G.	[89PET/DRA]
Dempsey, B.A.	[83DEM/OME]
Deng, Y.	[96DEN/STJ]
Dennis, L.W.	[83HAT/BRE]
Dereppe, J.	[80DER/MOR]
Desai, P.D.	[73HUL/DES]
Desnoyers, J.E.	[76DES/VIS]
Deutsch, W.J.	[87PET/HOS]
Dickson, A.G.	[90DIC/WES]
Doolen, G.	[90DOO/FRI], [91DOO]
Doolen, G.D.	[87MON/DOO], [88CHE/CHE], [90SHI/DOO], [95CHE/DAW]
Doubleday, A.	[79ALL/BEL]
Downey, J.R.	[85CHA/DAV]
Dran, J.C.	[89PET/DRA]
Drever, J.I.	[82DRE]
Drowart, J.	[84GRO/DRO]
Droz, M.	[91CHO/DRO], [91CHO/DRO2], [93DRO/FRA]
Drummond, S.E.	[88PAL/DRU]
Du, J.	[96TAO/DU]
Du, M.	[92CHO/DU]
Duff, M.	[84PRE/DUF]
Dufty, J.W.	[90ERN/DUF]
Dullien, F.A.L.	[92DUL]
Dulos, E.	[90CAS/DUL], [91KEP/CAS]
Dunkle, S.A.	[88PLU/PAR]
Dunn, L.A.	[69DUN/MAR]
Duplay, J.	[92TAR/DUP]
Duro, L.	[95BRU/PAB], [96BRU/DUR], [96BRU/DUR2], [96MAL/BAN]
Dyatkina, M.E.	[50SYR/DYA]
Dyrssen, D.	[73DYR/HAN], [83PLE/JOS]
Dzombak, D.A.	[86DZO/FIS], [86FIS/DZO], [90DZO/MOR]
Eagleson, K.	[92ALE/DAY]
Earnshaw, A.	[84GRE/EAR]

Author	References
Edelstein, N.M.	[86EDE/GOF]
Edworthy, D.J.	[77OAK/EDW]
Ehrhardt, H.	[73EHR/JOH]
Eikenberg, J.	[91BRU/CRO], [92ALE/DAY], [92FRI/ALE]
Eintrop, R.V.	[84PRO/EIN]
Ekelund, R.	[70EKE/SIL]
Enfield, C.G.	[74ENF]
Eng, T.	[94ENG/HUD]
Engebretson, R.R.	[94ENG/WAN]
Engi, M.	[86BER/ENG]
Ephraim, J.	[86EPH/ALE], [86EPH/MAR], [86MAR/EPH], [88MAR/RED], [89XU/EPH], [94PET/EPH]
Ephraim, J.H.	[89EPH/BOR], [89EPH/BOR2], [89EPH/MAR], [89EPH/XU], [90EPH/MAR], [91EPH], [91EPH/RED], [93EPH/ALL], [93MAT/EPH], [93NOR/EPH], [94EPH/ALL], [94KRA/ALL], [94NOR/EPH], [95EPH/PET], [95MAR/RED], [95MAT/EPH]
Eremin, N.I.	[71VOL/PAV]
Eriksson, G.	[75ERI], [79ERI], [92ERI/HAC]
Ernst, M.H.	[89FRE/ERN], [90ERN/DUF], [92ERN/DAS]
Ernst, W.G.	[63BAR/ERN]
Erten, H.N.	[94ERT/MOH]
Escalas, M.T.	[84ALE/ESC]
Eugster, H.P.	[73EUG/CHO]
Evans, B.W.	[65EVA]
Evans, W.H.	[82WAG/EVA]
Falck, W.E.	[91FAL]
Fanghänel, Th.	[94FAN/KIM], [95NEC/FAN]
Farmer, D.	[84FAR/TOF]
Feder, G.L.	[83MCK/FED]
Fedorov, V.A.	[71FED/KAL], [75FED/CHE], [75KUT/LES]
Fei, Y.	[87SAX/FEI], [87SAX/FEI2], [93SAX/CHA]
Feller, W.	[70FEL]
Felmy, A.R.	[90FEL/RAI]
Fernelius, W.C.	[77FER]
Ferri, D.	[81CIA/FER], [82BIE/BRU], [83ABE/FER], [85FER/GRE]
Fierz, Th.	[92FRI/ALE]
Figuerola, E.	[95BRU/PAB]
Filella, M.	[90BUF/ALT]
Fiquet, G.	[91RIC/FIQ]
Fish, W.	[85FIS/MOR], [86DZO/FIS], [86FIS/DZO], [93BON/FIS]
Fisher, J.R.	[71FIS/ZEN], [76HAA/FIS], [78ROB/HEM]
Fitch, A.	[84FIT/STE], [86FIT/STE]
Fitzgerald, P.J.	[83SHU/COL]
Flaig, W.	[60FLA]

Author	References
Flannery, B.P.	[87PRE/FLA]
Fleming, G.W.	[83FLE/PLU], [88PLU/PAR]
Flotow, H.E.	[84FLO/HAS]
Flowers, G.C.	[81HEL/KIR]
Forsling, W.	[81OHM/FOR], [91ROE/SJO]
Foster, S.S.D.	[75FOS]
Frachebourg, L.	[93DRO/FRA]
Franck, E.U.	[56FRA], [61FRA], [81MAR/FRA]
Frantz, J.D.	[84FRA/MAR]
Fraústo da Silva, J.J.R.	[70FRA/LOU], [91FRA/WIL]
Frederic, W.J., Jr.	[88KIM/FRE]
Fredkin, E.	[82FRE/TOF]
Freedman, W.L.	[83MAD/FRE]
Freeman, R.D.	[84FRE]
Freeze, R.A.	[79FRE/CHE]
Frenkel, D.	[88LAD/COL], [89FRE], [89FRE/ERN]
Freundlich, H.	[26FRE]
Frick, U.	[92FRI/ALE]
Frind, E.O.	[81TAN/FRI], [82SUD/FRI]
Frisch, U.	[86FRI/HAS], [90DOO/FRI]
Fruvip, D.J.	[85CHA/DAV]
Frydman, M.	[58FRY/NIL]
Fu, C.	[90SHI/DOO]
Fuger, J.	[76FUG/OET], [83FUG/PAR], [92FUG/KHO], [92GRE/FUG], [96MER/FUG]
Fulton, R.W.	[90FEL/RAI]
Furrer, G.	[89FUR/WES], [90FUR/WES]
Fyfe, W.S.	[58FYF/TUR]
Galindo, G.	[72ZUN/GAL]
Gallagher, J.S.	[84HAA/GAL]
Gamble, D.S.	[70GAM], [72GAM], [73GAM/SCH], [80GAM/UND], [85GAM/MAR], [88GAM/LAN]
Gamsjäger, H.	[65GAM/STU], [81REI/JOH]
Ganor, J.	[94LAS/SOL]
Gardner, M.	[70GAR]
Garrels, R.M.	[60GAR], [65GAR/CHR], [74TAR/GAR], [77TAR/GAR], [89CHO/GAR]
Garvin, D.	[87GAR/PAR]
Gaus, P.L.	[87COT/WIL]
Gelhar, L.W.	[92GEL/WEL]
Gerassimov, Ya.I.	[68LAV/GER], [72GER/LAV]
Gergely, A.	[91KIS/SOV]
Ghosal, M.	[80PER/REU]
Ghose, S.	[65GHO]

Author	References
Gibbons, J.J.	[86ROY/GIB]
Gibbs, G.V.	[82GIB]
Giesy, J.P.	[83ALB/GIE]
Giffaut, E.	[92CAP/VIT]
Gillam, A.H.	[82GIL/RIL], [83GIL/WIL], [86GIL/WIL]
Gillespie, S.E.	[89IZA/CHR], [89IZA/CHR2], [90OSC/GIL], [90OSC/IZA], [92IZA/OSC], [93CHE/GIL], [93CHE/GIL2], [93GIL/OSC]
Gimeno, M.J.	[96BRU/DUR2]
Gjessing, E.T.	[90PER/GJE]
Glaser, J.	[83ABE/FER]
Glaus, M.A.	[95GLA/HUM]
Gleiser, M.	[73HUL/DES]
Glew, D.N.	[66CLA/GLE]
Goblet, P.	[92MAR/COM]
Goffart, J.	[86EDE/GOF]
Goldberg, E.D.	[54GOL]
Goldberg, J.E.	[96BRU/DUR2]
Goodman, B.A.	[87GOO/CHE]
Gordon, G.	[87KAT/GOR]
Gordon, T.M.	[73GOR]
Gould, R.F.	[68GOU]
Graedel, T.E.	[89GRA/CRU]
Granberg, I.	[83GRA/SJO]
Grant, C.L.	[78BRE/GRA]
Grauer, R.	[88GRA], [90GRA], [94GRA]
Grechikhina, N.K.	[67VAS/GRE], [67VAS/GRE2]
Greene, M.A.	[86ROY/GIB]
Greenwood, H.J.	[86BER/ENG]
Greenwood, N.N.	[84GRE/EAR]
Gregor, J.E.	[87GRE/POW], [88GRE/POW]
Grenthe, I.	[57AHR/GRE], [81CIA/FER], [82BIE/BRU], [83ABE/FER], [85FER/GRE], [86GRE/RIG], [91BID/GRE], [91GRE], [91GRE/LAG], [92GRE/FUG], [92GRE/STU], [94PLY/GRE], [95PAS/KIM], [96PLY/GRE]
Greter, F.L.	[77BUF/GRE]
Griffiths, K.	[84NOR/BIN]
Grimaldi, M.	[75CIA/GRI]
Grisak, G.E.	[81PIC/GRI]
Grønvold, F.	[84GRO/DRO]
Gruner, D.	[93GRU/KAP]
Güçer, S.	[90BRO/GUC]
Guggenheim, E.A.	[35GUG], [66GUG]
Gurney, R.W.	[38GUR], [53GUR]
Gurvich, L.V.	[85HIL/GUR], [93GUR/VEY]

Author	References
<hr/>	
Gustafsson, E.	[81GUS/KLO], [84GUS/KLO], [96BAN/TUL]
Gustafsson, J.P.	[94GUS]
Gutowitz, H.	[90GUT]
Guy, R.K.	[82BER/CON]
Guzowski, R.V.	[80CRA/GUZ]
Haar, L.	[84HAA/GAL]
Haas, J.L., Jr.	[76HAA/FIS], [82HEM/HAA], [83ROB/HAA]
Habenschuss, A.	[77SPE/RAR]
Hack, K.	[92ERI/HAC]
Hadermann, J.	[93HAD/MCC], [94HEE/HAD], [94HEE/HAD2], [94HEE/HAD3], [94JAK/HAD], [96HAD/HEE]
Haerdi, W.	[77BUF/GRE], [83STA/BUF], [84STA/BUF]
Haire, R.G.	[77HAI/LLO]
Halbach, H.	[82HAL/CHA]
Hale, J.D.	[64CHR/IZA]
Hallberg, R.O.	[88HAL/OES]
Halow, I.	[82WAG/EVA]
Hamilton, E.	[92ALE/DAY]
Hansen, E.H.	[69HAN/SCH]
Hansen, L.D.	[64CHR/IZA]
Hansson, I.	[73DYZ/HAN]
Hardy, J.	[76HAR/PAZ]
Harker, D.	[38KOS/HAR]
Harned, H.S.	[35HAR/MAN], [43HAR/DAV], [45HAR/BON], [58HAR/OWE]
Hartley, F.R.	[80HAR/BUR]
Hartley, G.S.	[31HAR]
Harvey, G.R.	[83HAR/BOR]
Harvie, C.E.	[84HAR/MOL]
Haschke, J.M.	[84FLO/HAS]
Hasslacher, B.	[86FRI/HAS], [90DOO/FRI], [90SHI/DOO], [93HAS/KAP]
Hatcher, P.G.	[83HAT/BRE]
Hauser, W.	[94FAN/KIM]
Hautojärvi, A.	[93VIE/HAU]
Havel, J.	[69HAV]
Hawkins, D.T.	[73HUL/DES]
Hayano, S.	[80SAI/HAY]
Hayes, K.F.	[88PAP/HAY]
Hayes, M.H.B.	[89HAY/MCC]
Hayot, F.	[87BAL/HAY]
Hazen, R.M.	[88HAZ]
He, S.	[93HE/MOR]
Hedlund, T.	[87HED/SJO], [88HED]
Hedwig, G.R.	[74COX/HED]
Heer, W.	[92FRI/ALE], [94HEE/HAD], [94HEE/HAD2], [94HEE/HAD3], [96HAD/HEE]

Author	References
Heftter, G.T.	[80BON/HEF]
Heistand, R.N.	[63HEI/CLE]
Helgeson, H.C.	[67HEL], [69HEL], [74HEL/KIR], [78HEL/DEL], [79HEL], [81HEL/KIR], [82HEL], [84HEL/MUR], [85JAC/HEL], [88SHO/HEL], [88TAN/HEL], [89SHO/HEL], [89SHO/HEL2], [92JOH/OEL], [92SHO/OEL], [97SVE/SHO]
Hemingway, B.S.	[76OPE/HEM], [78ROB/HEM], [79KRU/ROB], [81HEM/KRU], [82HEM/HAA], [84ROB/HEM3], [95ROB/HEM]
Hemley, J.J.	[80HEM/MON]
Hepler L.G.	[91CHE/XU]
Hepler, L.G.	[78SPI/SIN], [88HOV/HEP]
Herbelin, A.L.	[94HER/WES]
Herbillon, A.	[87DEC/COL]
Hering, J.G.	[88HER/MOR], [90HER/STU], [93MOR/HER]
Herman, J.S.	[80LAN/HER]
Herrmann, A.G.	[83HER]
Hershey, H.C.	[88BRO/HER]
Hesselmann, K.	[91KNA/KUB]
Hiemstra, T.	[89HIE/RIE]
Hietanen, S.	[76HIE/HOG], [85FER/GRE]
Higgo, J.J.W.	[93HIG/KIN]
Higgs, H.	[79ALL/BEL]
Hildenbrand, D.L.	[85HIL/GUR]
Hill, P.G.	[69KEE/KEY]
Hillis, W.D.	[84HIL]
Hinchey, R.J.	[70HIN/COB], [70HIN/COB2]
Hirata, S.	[81HIR]
Hoard, J.L.	[71SCH/COU]
Hochella, M.F., Jr.	[90HOC/WHI]
Hoehn, E.	[89BRA/AKS], [92FRI/ALE]
Högfeldt, E.	[76HIE/HOG], [82HOG], [83HOG], [93HOG]
Hohl, H.	[80WES/HOH]
Holden, L.J.	[83RYA/HOL]
Holland, T.J.B.	[89HOL], [90HOL/POW]
Holley, C.E., Jr.	[84HOL/RAN]
Holmes, H.F.	[88MES/MAR], [90HOL/MES]
Holtzclaw, K.M.	[77SPO/HOL]
Homann, K.	[88MIL/CVI]
Hordijk, L.	[89ALC/SHA]
Hostetler, C.J.	[87PET/HOS]
Hostettler, J.D.	[84HOS]
Hovey, J.K.	[88HOV/HEP]
Huang, W.L.	[77IRV/HUA]

Authors List

Author	References
Hubbard, W.N.	[83FUG/PAR]
Hudson, J.	[94ENG/HUD]
Hudson, J.A.	[92HUD]
Huffman, E.H.	[43SHO/HUF]
Hugus, Z Z., Jr.	[57SCO/HUG]
Hultgren, R.	[73HUL/DES]
Hummel, W.	[92PEA/BER], [95GLA/HUM]
Hummelink, T.	[79ALL/BEL]
Hummelink-Peters, B.G.	[79ALL/BEL]
Hundt, R.	[83BER/SIE]
Hurley, M.A.	[88TIP/BAC], [90TIP/RED], [92TIP/HUR]
Hyde, K.E.	[93PAL/HYD]
Hyland, M.M.	[90BAN/HYL]
Ingri, N.	[67ING/KAK], [71WAR/ING]
Interesse, F.S.	[78RUG/SCI], [79RUG/INT]
Iorish, V.S.	[93GUR/VEY]
Irving, A.J.	[77IRV/HUA]
Irving, H.	[53IRV/WIL], [56IRV/ROS]
Isaak, D.L.	[91AND/ISA]
Iuliano, M.	[87CIA/IUL]
Ivanovich, M.	[92OSM/IVA]
Izatt, R.M.	[64CHR/IZA], [89IZA/CHR], [89IZA/CHR2], [90OSC/GIL], [90OSC/IZA], [92IZA/OSC], [93CHE/GIL], [93CHE/GIL2], [93GIL/OSC]
Jackman, T.E.	[84NOR/BIN]
Jackson, K.J.	[85JAC/HEL], [88JAC/WOL], [90WOL/JAC], [93BOU/KNA]
Jacob, K.T.	[76ALC/JAC]
Jakob, A.	[94HEE/HAD3], [94JAK/HAD]
James, F.	[75JAM/ROO]
Janccky, D.R.	[95CHE/DAW]
Jansson, B.	[85SUN/JAN]
Jaycock, M.J.	[81JAY/PAR]
Jenne, E.A.	[79NOR/PLU]
Jensen, K.A.	[71JEN]
Johannes, W.	[73EHR/JOH], [74CHA/JOH], [81REI/JOH]
Johnson, D.A.	[95JOH/NEL]
Johnson, J.W.	[91JOH/NOR], [92JOH/OEL], [92SHO/OEL]
Jones, B.F.	[90NOR/PLU]
Jordan, J.	[85BAR/PAR]
Jordana, S.	[96BRU/DUR]
Josefsson, B.	[83PLE/JOS]
Kakolowicz, W.	[67ARN/KAK], [67ING/KAK]
Kallay, N.	[88MIL/CVI]
Kalosh, T.N.	[71FED/KAL]

Author	References
Kamgar-Parsi, B.	[83LEV/KAM], [84KES/SEN]
Kang, K.	[85KAN/RED]
Kapral, R.	[90DAB/LAW], [91KAP/LAW], [91LAW/DAB], [92KAP/LAW], [92WU/KAP], [93GRU/KAP], [93HAS/KAP]
Karapiperis, T.	[93KAR], [94KAR/BLA], [95KAR], [95KAR2]
Karlsson, F.	[95PED/KAR]
Karotke, E.	[70ALT/KAR]
Karpov, I.K.	[68KAR/KAS]
Karthein, R.	[89WER/CHA]
Kashik, S.A.	[68KAR/KAS]
Katakis, D.	[87KAT/GOR]
Kaufman, M.	[85KAU/URB]
Keech, D.A.	[77SPO/HOL]
Keenan, J.H.	[69KEE/KEY]
Keil, R.	[89BRA/AKS]
Kell, G.S.	[84HAA/GAL]
Keller, J.M.	[88ROT/KEL]
Kelley, K.K.	[73HUL/DES]
Kennard, O.	[79ALL/BEL]
Kerrick, D.M.	[72KER], [82SCH/KER]
Kestin, J.	[84KES/SEN]
Keyes, F.G.	[69KEE/KEY]
Khan, S.U.	[72SCH/KHA]
Khodakovskiy, I.L.	[69KHO], [72SER/NIK], [75KHO/YEL]
Khodakovsky, I.L.	[71NAU/RYZ], [92FUG/KHO]
Kholeif, S.	[94AND/KHO]
Kieffer, S.W.	[79KIE], [79KIE2], [79KIE3], [80KIE]
Kim, H.-T.	[88KIM/FRE]
Kim, J.I.	[89KIM/BUC], [91KIM/SEK], [92BUC/KIM], [93KIM], [94CZE/BUC], [94FAN/KIM], [95NEC/FAN], [95PAS/KIM], [96CZE/KIM], [96KIM/CZE]
Kim, K.-H.	[93BYR/KIM]
King, L.H.	[70RAS/KIN]
Kiniburgh, D.G.	[90WIT/RIE]
Kinney, P.	[77WIL/KIN]
Kinniburgh, D.	[93HIG/KIN]
Kinniburgh, D.G.	[95BEN/MIL]
Kirkham, D.H.	[74HEL/KIR], [81HEL/KIR]
Kirkpatrick, R.J.	[81LAS/KIR]
Kiss, T.	[91KIS/SOV]
Klein, C.	[83MIY/KLE]
Klein, L.W.	[90CHE/MAT]
Kleinhempel, D.	[70KLE]
Klenze, R.	[89KIM/BUC], [92BUC/KIM], [94FAN/KIM]

Authors List

Author	References
Klockars, C.E.	[81GUS/KLO], [84GUS/KLO]
Knacke, O.	[91KNA/KUB]
Knauss, K.G.	[90WOL/JAC], [93BOU/KNA]
Koelman, A.	[90VIA/KOE]
Kometer, K.	[92KOM/ZAN]
Konikow, L.F.	[92KON/BRE]
Konings, R.J.M.	[92GRE/FUG]
Kononova, M.M.	[66KON]
Koopal, L.K.	[86RIE/BOL], [90NED/RIE], [90WIT/RIE], [92NED/RIE], [93NED/WIT], [93WIT/RIE], [93WIT/RIE2], [94NED/RIE], [95BEN/MIL]
Kopajtic, Z.	[91LOO/KOP]
Koren, B.	[93VRE/KOR]
Koskinen, L.	[93VIE/HAU]
Kossiakoff, A.	[38KOS/HAR]
Kotrly, S.	[85KOT/SUC]
Kozlovskii, E.V.	[80VAS/KOZ]
Kragten, J.	[78KRA/DEC]
Kramer, J.R.	[79BER/KRA]
Kramer-Schnabel, U.	[92KRA/BIS]
Krantz-Rülcker, C.	[94KRA/ALL]
Krauskopf, K.B.	[56KRA2]
Krupka, K.M.	[76OPE/HEM], [79KRU/ROB], [81HEM/KRU]
Kubaschewski, O.	[83KUB], [91KNA/KUB], [93KUB/ALC]
Kuchitsu, K.	[88MIL/CVI]
Kumada, K.	[77ARA/KUM]
Kumin, H.J.	[80DAY/KUM]
Kutuzova, M.Ja.	[75KUT/LES]
Kuznechikhina, M.A.	[75FED/CHE]
Kuznezova, T.I.	[75FED/CHE]
Laaksoharju, M.	[94WER/BRU], [96BAN/TUL]
Laaksuharju, M.	[92GRE/STU]
Labonne, N.	[95MOU/MOU2]
Ladd, A.J.C.	[88LAD/COL]
Laffitte, M.	[82LAF]
Lagerman, B.	[87BRU/CAS], [91GRE/LAG]
Laidler, K.J.	[56LAI], [57COU/LAI], [57LAI]
Lamoreaux, R.H.	[80BRE/LAM2]
Lamport, L.	[94LAM]
Landau, L.D.	[59LAN/LIF]
Langford, C.H.	[80GAM/UND], [85GAM/MAR], [88GAM/LAN]
Langmuir, D.	[71LAN/WHI], [78LAN], [79LAN], [80LAN/HER], [90NOR/PLU]
Langmuir, I.	[18LAN]

Author	References
Lapidus, L.	[82LAP/PIN]
Lasaga, A.C.	[81LAS/KIR], [90STE/LAS], [94LAS/SOL]
Latimer, W.M.	[51POW/LAT], [52LAT]
Lavrentev, V.I.	[68LAV/GER], [72GER/LAV]
Lawniczak, A.	[90DAB/LAW], [91KAP/LAW], [91LAW/DAB], [92KAP/LAW], [93GRU/KAP], [93HAS/KAP], [95CHE/DAW]
LeBlanc, J.C.	[80TRE/LEB]
Leckie, J.O.	[80DAV/LEC], [88PAP/HAY], [93STI/PAR]
Ledin, A.	[89XU/EPH]
Lee, Y.C.	[88CHE/CHE]
Lefever, R.	[68PRI/LEF]
Leigh, G.J.	[90LEI]
Lejeune, A.	[93PER/LEJ]
Lemire, R.J.	[80LEM/TRE], [92GRE/FUG]
Leschishina, L.E.	[75KUT/LES]
Levelt Sengers, J.M.H.	[83LEV/KAM], [84KES/SEN]
Levermore, C.D.	[87BOG/LEV]
Lewenhagen, J.	[96MAL/BAN]
Lewis, D.	[70LEW]
Lewis, G.N.	[61LEW/RAN]
Li, J.	[96TAO/DU]
Li, W.C.	[80LI/VIC]
Li, Y.-H.	[91LI]
Li, Y.-X.	[91DAB/BOO]
Lichtner, P.C.	[85LIC], [88LIC]
Lifshitz, E.M.	[59LAN/LIF]
Lightfoot, E.N.	[60BIR/STE]
Lin, J.S.	[93RIC/LIN]
Lindberg, R.D.	[84LIN/RUN]
Linder, P.W.	[83MUR/LIN]
Lindsay, W.T., Jr.	[80LIN]
Linklater, C.M.	[92ALE/DAY], [96BRU/DUR2]
Lloyd, M.H.	[77HAI/LLO]
Lobanov, G.A.	[69LOB/VAS]
Long, F.A.	[52LON/MCD]
Lonnquist, G.	[82PRI/NAY]
Lourdes Sadler Simões, M.	[70FRA/LOU]
Lövgren, L.	[90LOE/SJO]
Luce, R.W.	[80HEM/MON]
Lundeen, S.R.	[88JAC/WOL]
Lundquist, K.	[83PLE/JOS]
Lytle, C.R.	[83PER/LYT], [83PER/LYT2]
Maccarthy, P.	[85AIK/MCK]
Maciel, G.E.	[83HAT/BRE]

Author	References
Mackenzie, F.T.	[90MOR/MAC]
Madore, B.F.	[83MAD/FRE]
Maeda, M.	[86MAE]
Maes, A.	[91MAE/ELE]
Maginu, K.	[75MAG], [79MAG]
Majer, V.	[94WOO/CAR]
Malcolm, G.N.	[61MAL/PAR]
Malcolm, R.L.	[81THU/MAL], [86EPH/ALE], [89HAY/MCC], [91MAL]
Malmström, M.	[96MAL/BAN]
Manceau, A.	[87DEC/COL]
Manneville, P.	[89MAN/BOC]
Manning, P.G.	[73MAN/RAM]
Mannweiler, G.E.	[35HAR/MAN]
Mantoura, R.F.C.	[75MAN/RIL], [86TUR/VAR], [87TUR/VAR]
Mantovani, M.	[89BRA/AKS]
Marchon, M.J.C.	[71CHA/COL]
Margolus, N.	[84MAR2], [87TOF/MAR]
Marinenko, J.W.	[80HEM/MON]
Marinsky, J.A.	[80MAR/WOL], [80SLO/MAR], [84ALE/ESC], [84MAR/RED], [84MAR/RED2], [84MER/MAR], [85GAM/MAR], [85MAR], [86EPH/ALE], [86EPH/MAR], [86MAR/EPH], [88MAR/RED], [89EPH/MAR], [90EPH/MAR], [90MAR/RED], [91EPH/RED], [93MAR], [95MAR/RED], [95MAT/EPH]
Marshall, W.L.	[68QUI/MAR], [68QUI/MAR2], [68QUI/MAR3], [68QUI/MAR4], [69DUN/MAR], [70MAR], [72MAR], [81MAR/FRA], [84FRA/MAR], [88MES/MAR]
Martell, A.E.	[64RAJ/MAR], [64SIL/MAR], [71SIL/MAR], [74MAR/SMI], [75MAR/SMI], [75SMI/MAR], [76SMI/MAR], [77MAR/SMI], [82MAR/SMI], [89SMI/MAR]
Marx, G.	[92KRA/BIS]
Masiar, P.	[91KAP/LAW], [92KAP/LAW]
Matheron G.	[80MAT/MAR]
Mathuthu, A.	[86EPH/ALE], [88MAR/RED]
Mathuthu, A.S.	[93MAT/EPH], [95MAR/RED], [95MAT/EPH]
Matijvić, E.	[77SAP/PAT]
Matthaeus, W.H.	[87CHE/MAT], [90CHE/MAT]
Matthiessen, A.	[91MAT2]
Mattigod, S.V.	[79MAT/SPO]
Mauchien, P.	[91MOU/DEC]
May, H.M.	[90NOR/PLU]
Maya, L.	[82MAY], [83MAY]
Mazurek, M.	[89BRA/AKS], [91BOS/MAZ]
McCarthy, P.	[89HAY/MCC]
McCombie, C.	[93HAD/MCC]

Authors List

Author	References
McCue, M.C.	[76MOR/MCC]
McCurdy, K.G.	[78SPI/SIN]
McDevit, W.F.	[52LON/MCD]
McDonald, R.A.	[85CHA/DAV]
McKibben, M.A.	[86MCK/BAR]
McKinley, I.G.	[91BRU/CRO], [91CHA/MCK], [92ALE/DAY], [92FRI/ALE], [94MIL/ALE]
McKnight, D.M.	[83MCK/FED], [85AIK/MCK]
McNabb, J.F.	[83WIL/MCN]
Meadows, D.H.	[91MEA/MEA]
Meadows, D.L.	[91MEA/MEA]
Means, J.L.	[77MEA/CRE]
Medvedev, V.A.	[89COX/WAG], [92FUG/KHO]
Meinrath, G.	[93MEI/TAK]
Merle, Y.	[84MER/MAR]
Merli, L.	[96MER/FUG]
Mesmer, R.E.	[76BAE/MES], [78BUS/MES], [81BAE/MES], [82PAT/SLO], [84PAT/BUS], [88MES/MAR], [90DIC/WES], [90HOL/MES], [91AND/CAS], [91MES/PAL]
Meyer, J.	[89BRA/AKS]
Michard, G.	[84COU/MIC]
Middelburg, J.J.	[87COM/MID]
Miles, C.J.	[83MIL/TUS]
Miller, K.	[94CHA/MIL]
Miller, W.M.	[94MIL/ALE]
Millero, F.J.	[82THU/MIL], [83MIL2], [90ROY/RIC]
Milligan, W.O.	[77HAI/LLO]
Mills, I.	[88MIL/CVI]
Mills, K.C.	[74MIL]
Milne, C.J.	[95BEN/MIL]
Mironov, V.E.	[71FED/KAL], [71VOL/PAV]
Miyano, T.	[83MIY/KLE]
Møller, N.	[84HAR/MOL]
Mohammed, A.K.	[94ERT/MOH]
Mokeev, A.A.	[80VAS/KOZ]
Montgomery, D.	[87MON/DOO]
Montoya, J.W.	[80HEM/MON]
Moon, H.	[94YOO/MOO]
Moore, J.G.	[69KEE/KEY]
Moore, R.M.	[88JAC/WOL]
Moreaux, C.	[80DER/MOR]
Morel, F.	[72MOR/MOR]
Morel, F.M.M.	[76WES/ZAC], [84WAI/MOR], [85FIS/MOR], [86DZO/FIS], [86FIS/DZO], [88HER/MOR], [89CAB/MOR], [90DZO/MOR], [92BAR/CAB], [93MOR/HER]

Author	References
Morgan, J.	[72MOR/MOR]
Morgan, J.J.	[81STU/MOR], [85MOR/STO], [96STU/MOR]
Morse, J.W.	[90MOR/MAC], [93HE/MOR]
Morss, L.R.	[76MOR/MCC], [83MOR/WIL]
Mortensen, K.	[94OST/MOR]
Motherwell, W.D.S.	[79ALL/BEL]
Moulin, C.	[91MOU/DEC], [95MOU/MOU], [95MOU/MOU2]
Moulin, V.	[91MOU/CAC], [91MOU/DEC], [95MOU/MOU], [95MOU/MOU2]
Muller, A.B.	[92GRE/FUG]
Munoz, J.L.	[86NOR/MUN], [94NOR/MUN]
Muñoz, M.	[87BRU/CAS]
Murphy, W.M.	[84HEL/MUR]
Murray, J.D.	[89MUR]
Murray, K.	[83MUR/LIN]
Murray, R.C., Jr.	[82COB/MUR]
Nagy, K.L.	[94LAS/SOL]
Nagypál, I.	[90BEC/NAG]
Nahon, D.	[87DEC/COL]
Naumov, G.B.	[71NAU/RYZ], [72SER/NIK]
Navratil, J.D.	[92FUG/KHO]
Naymik, T.	[82PRI/NAY]
Neall, F.B.	[94NEA]
Nebot, J.	[91NEB/BRU]
Nebot, P.	[93BRU/CAC]
Neck, V.	[95NEC/FAN]
Nederlof, M.M.	[90NED/RIE], [90WIT/RIE], [92NED/RIE], [93NED/WIT], [94NED/RIE]
Neil, J.M.	[90APP/NEI]
Néker-Neumann, E.	[85FER/GRE]
Nelson, P.G.	[95JOH/NEL]
Nesbitt, H.W.	[78HEL/DEL]
Nguyen-Trung, C.	[92GRE/FUG]
Nicolis, G.	[77NIC/PRI]
Nikitin, A.A.	[72SER/NIK]
Nikolaeva, N.M.	[69NIK/TOL], [76NIK], [76PIR/NIK], [78NIK]
Nikol'skiy, B.P.	[66NIK]
Nilsson, A.C.	[92GRE/STU]
Nilsson, A.-C.	[96BAN/TUL]
Nilsson, G.	[58FRY/NIL]
Nitsch, K.H.	[70ALT/KAR]
Noonan, M.J.	[83WIL/MCN]
Nordén, M.	[93NOR/EPH], [94NOR], [94NOR/EPH], [95EPH/PET]
Nordman, H.	[93VIE/HAU]

Author	References
Nordstrom, D.K.	[79NOR/PLU], [84NOR/BAL], [86NOR/MUN], [90NOR/PLU], [92NOR], [93STI/PAR], [94NOR/MUN]
Norman, D.I.	[86SMI/POP]
Norton, D.	[91JOH/NOR]
Norton, P.R.	[84NOR/BIN]
Novotný, P.	[85SOH/NOV]
Nriagu, J.O.	[75NRI]
Nuttall, R.L.	[82WAG/EVA]
Oakes, D.B.	[77OAK/EDW]
O'Connor, P.	[80VAR/OCO]
Oda, H.	[91AND/ISA]
Odier, M.	[71ODI/PLI]
Oelkers, E.H.	[92JOH/OEL], [92SHO/OEL]
Oestlund, P.	[88HAL/OES]
Oetting, F.L.	[76FUG/OET], [76OET/RAN], [83FUG/PAR]
O'Hare, P.A.G.	[78COR/OHA]
Öhman, L.-O.	[81OHM/FOR], [87HED/SJO]
Olbsicht, W.	[94CHA/MIL]
Olson, D.L.	[83SHU/COL]
Omelia, C.R.	[83DEM/OME]
Omenetto, N.	[91BID/GRE]
Openshaw, R.E.	[76OPE/HEM]
Oreskes, N.	[94ORE/SHR]
Orszag, S.	[90DOO/FRI]
Ortiz, N.R.	[80CRA/GUZ]
Oscarson, J.L.	[89IZA/CHR], [89IZA/CHR2], [90OSC/GIL], [90OSC/IZA], [92IZA/OSC], [93CHE/GIL], [93CHE/GIL2], [93GIL/OSC]
Osmond, J.K.	[92OSM/IVA]
Österberg, R.	[94OST/MOR]
Östhols, E.	[95OES]
Oswald, H.R.	[77OSW/ASP]
Ottonello, G.	[87OTT], [92OTT/DEL]
Ovchinnikov, A.A.	[78OVC/ZEL]
Owen, B.B.	[58HAR/OWE]
Paccagnella, A.	[89PET/DRA]
Paces, T.	[86PAC]
Palmer, D.A.	[83PAL/ELD], [88MES/MAR], [88PAL/DRU], [90DIC/WES], [91MES/PAL], [92PAL/WES], [93PAL/HYD], [93PAL/WES]
Palombari, R.	[75CIA/GRI]
Pando, C.	[93GIL/OSC]
Pandolfo, P.	[92SAR/BRA]
Papelis, C.	[88PAP/HAY]
Paquet, H.	[87DEC/COL]
Parfitt, G.D.	[81JAY/PAR]

Authors List

Author	References
Park, K.K.	[94YOO/MOO]
Park, Y.J.	[94YOO/MOO]
Parker, A.J.	[74COX/HED]
Parker, V.B.	[82WAG/EVA], [83FUG/PAR], [87GAR/PAR]
Parkhurst, D.L.	[80PAR/THO], [88PLU/PAR], [90NOR/PLU], [90PLU/PAR]
Parks, G.A.	[93STI/PAR]
Parrish, R.S.	[87PER/PAR]
Parrishi, R.S.	[84PER/REU]
Parsons, R.	[85BAR/PAR]
Parthasarathy, N.	[87BUF/VUI]
Parton, H.N.	[61MAL/PAR]
Pashalidis, I.	[95PAS/KIM]
Patel, R.C.	[77SAP/PAT]
Patterson, C.S.	[82PAT/SLO], [84PAT/BUS]
Pauling, L.	[60PAU]
Paviet, P.	[94FAN/KIM]
Pavlov, L.N.	[71VOL/PAV]
Pawlak, Z.	[90OSC/IZA]
Paxéus, N.	[85PAX/WED], [91PAX/WED]
Payne, T.E.	[94WAI/PAY]
Pearson, F.J.	[92PEA/BER]
Pedersen, K.	[93PED], [95PED/KAR], [96BAN/TUL]
Peiper, J.C.	[82PEI/PIT], [84PIT/PEI]
Peirano, P.	[72ZUN/GAL]
Pena, J.	[96BRU/DUR2]
Penrose, R.	[89PEN]
Perdang, J.M.	[93PER/LEJ]
Perdue, E.M.	[78PER], [79PER], [80PER/REU], [83PER/LYT], [83PER/LYT2], [84PER/REU], [87PER/PAR], [90PER/GJE], [94ALL/PER]
Perrin, D.D.	[79PER3], [82PER]
Perron, G.	[76DES/VIS]
Peterson, S.R.	[87PET/HOS]
Petit, J.C.	[89PET/DRA], [91DAU/CRO]
Pettersson, C.	[89EPH/BOR], [89EPH/BOR2], [91PET], [92PET], [94PET/EPH], [95EPH/PET]
Peuravuori, J.	[91PEU/PIH]
Phillips, C.S.G.	[65PHI/WIL]
Phillips, S.L.	[83PHI/SIL], [84PHI/SIL]
Phutela, R.C.	[87PHU/PIT]
Pickens, J.F.	[81PIC/GRI]
Picker, P.	[76DES/VIS]
Pigford, T.H.	[85AHN/CHA]
Pihlaja, K.	[91PEU/PIH]

Authors List

Author	References
Pinder, G.F.	[82LAP/PIN]
Pirozhkov, A.V.	[76PIR/NIK]
Pitzer, K.S.	[61LEW/RAN], [73PIT], [79BRA/PIT], [79PIT], [82PEI/PIT], [83PIT], [84PIT/PEI], [87PHU/PIT], [91PIT]
Plante, E.R.	[64CAR/WAL]
Plechanov, N.	[83PLE/JOS]
Plichon, V.	[71ODI/PLI]
Plummer, L.N.	[79NOR/PLU], [80PAR/THO], [82PLU/BUS], [83FLE/PLU], [88PLU/PAR], [90NOR/PLU], [90PLU/PAR]
Plyasunov, A.V.	[94PLY/GRE], [96PLY/GRE]
Pomeau, Y.	[76HAR/PAZ], [86FRI/HAS]
Popp, C.J.	[86SMI/POP]
Popper, K.	[59POP]
Porto, R.	[87CIA/IUL]
Postma, D.	[93APP/POS]
Pourbaix, M.	[50DEL/POU], [74POU]
Powell, H.K.J.	[87GRE/POW], [88GRE/POW], [91POW/TOW]
Powell, R.	[90HOL/POW]
Powell, R.E.	[51POW/LAT], [54POW]
Press, W.H.	[87PRE/FLA]
Preston, C.M.	[84PRE/SCH]
Preston, K.	[84PRE/DUF]
Prewitt, C.T.	[69SHA/PRE]
Prickett, T.A.	[82PRI/NAY]
Prigogine, I.	[68PRI/LEF], [77NIC/PRI]
Prokuev, V.A.	[84PRO/EIN], [85PRO/BEL]
Prue, J.E.	[69PRU]
Pruss, A.	[93WAG/PRU]
Puigdomenech, I.	[83PUI], [91BRU/CAS], [95SIL/BID], [96BEV/PUI]
Qi, P.	[91BID/GRE]
Quint, J.R.	[94WOO/CAR]
Quist, A.S.	[68QUI/MAR], [68QUI/MAR2], [68QUI/MAR3], [68QUI/MAR4]
Quyang, Q.	[91QUY/SWI]
Rafal'skiy, R.P.	[82BRY/RAF]
Rai, D.	[90FEL/RAI]
Rainville, D.P.	[82RAI/WEB]
Rajan, K.S.	[64RAJ/MAR]
Ramamoorthy, S.	[73MAN/RAM]
Rand, M.H.	[66RAN], [75RAN], [76OET/RAN], [81CHI/AKH], [84HOL/RAN], [95SIL/BID]
Randall, M.	[61LEW/RAN]
Randers, J.	[91MEA/MEA]
Rao, L.	[95RAO/CHO]

Author	References
Rard, J.A.	[77SPE/RAR], [92RAR]
Rashid, M.A.	[70RAS/KIN]
Ray, S.	[80VAR/OCO]
Read, D.	[91BRU/CRO]
Reddy, A.K.N.	[77BOC/RED]
Reddy, M.M.	[84MAR/RED], [84MAR/RED2], [88MAR/RED], [90MAR/RED], [90TIP/RED], [91EPH/RED], [95MAR/RED]
Redner, S.	[85KAN/RED]
Rehfeldt K.R.	[92GEL/WEL]
Reiterer, F.	[80REI], [81REI/JOH]
Rem, P.C.	[91SOM/REM]
Remy, H.	[50REM], [50REM2], [50REM3]
Rengemo, T.	[58FRY/NIL]
Reuter, J.H.	[80PER/REU], [84PER/REU]
Rhee, D.S.	[92BUC/KIM], [96CZE/KIM]
Rice, J.A.	[93RIC/LIN]
Rice, O.K.	[40RIC]
Rice, S.A.	[90ROY/RIC]
Richet, P.	[91RIC/FIQ]
Riglet, C.	[86GRE/RIG], [89RIG/ROB]
Riley, J.P.	[75MAN/RIL], [82GIL/RIL], [86TUR/VAR], [87TUR/VAR]
Rimstidt, J.D.	[80RIM/BAR], [89CHE/RIM]
Rivet, J.-P.	[87RIV]
Robbins, J.E.	[82SAV/ROB]
Robie, R.A.	[68ROB/WAL], [76OPE/HEM], [78ROB/HEM], [79KRU/ROB], [81HEM/KRU], [84ROB/HEM3], [95ROB/HEM]
Robinson, G.R., Jr.	[82HEM/HAA], [83ROB/HAA]
Robinson, P.	[95CHA/AND]
Robinson, R.A.	[59ROB/STO], [70BAT/STA]
Robouch, P.	[89RIG/ROB], [91BID/GRE]
Robouch, P.B.	[95SIL/BID]
Rodgers, J.R.	[79ALL/BEL]
Rönngren, L.	[91ROE/SJO]
Roots, M.	[75JAM/ROO]
Rossotti, F.J.C.	[61ROS/ROS], [71ROS/ROS]
Rossotti, H.	[56IRV/ROS], [61ROS/ROS], [69ROS]
Rossotti, H.S.	[71ROS/ROS]
Rothman, D.H.	[88ROT], [88ROT/KEL]
Roy, L.N.	[86ROY/GIB], [90ROY/RIC]
Roy, R.	[82ROY]
Roy, R.N.	[86ROY/GIB], [90ROY/RIC]
Ruaya, J.R.	[88RUA]
Rubin, A.J.	[81AND/RUB]
Rudolph, G.	[95NEC/FAN]

Author	References
Ruggiero, P.	[78RUG/SCI], [79RUG/INT]
Runnels, D.D.	[84LIN/RUN]
Rustig, J.	[84NOR/BIN]
Ryan, D.K.	[83RYA/HOL]
Ryzhenko, B.N.	[71NAU/RYZ], [81RYZ], [85RYZ/BRY], [85RYZ/SHA], [87RYZ/BRY], [91RYZ/BRY]
Šucha, L.	[85KOT/SUC]
Saam, W.F.	[87BAL/HAY]
Saar, R.A.	[80SAA/WEB]
Saito, Y.	[80SAI/HAY]
Saluja, P.P.S.	[87PHU/PIT]
Salvatore, F.	[81CIA/FER], [82BIE/BRU], [85FER/GRE]
Sandino, A.	[91BRU/CRO], [92SAN/BRU]
Santangelo, P.	[88SUC/SAN]
Sapieszko, R.S.	[77SAP/PAT]
Sarazin, G.	[84COU/MIC]
Sarrot, F.-A.	[92SAR/BRA]
Sassani, D.C.	[92SAS/SHO], [97SHO/SAS]
Sato, M.	[92SAT]
Saul, A.	[89SAU/WAG]
Savage, D.	[82SAV/ROB]
Saxena, S.K.	[87SAX/FEI], [87SAX/FEI2], [88SAX], [89SAX/ZHA], [93SAX/CHA]
Scatchard, G.	[36SCA], [76SCA]
Scheidt, R.W.	[71SCH/COU]
Scherbaum, F.	[94CZE/BUC]
Schindler, P.	[65GAM/STU], [82BIL/SCH]
Schindler, P.W.	[67SCH], [87SCH/STU], [90LOE/SJO], [91ROE/SJO]
Schnakenberg, J.	[79SCH2]
Schnitzer, M.	[67SCH/SKI], [69HAN/SCH], [72SCH/KHA], [73GAM/SCH], [77SEN/CHE], [78SCH], [84PRE/SCH]
Schnoor, J.L.	[90SCH]
Schott, J.	[91AND/CAS]
Schramke, J.K.	[82SCH/KER]
Schubert, J.	[48SCH]
Schulten, H.R.	[94SCH]
Schumm, R.H.	[82WAG/EVA]
Schwarzenbach, G.	[52SCH]
Schweingruber, M.	[82SCH], [84SCH]
Sciacovelli, O.	[78RUG/SCI], [79RUG/INT]
Scott, P.C.	[57SCO/HUG]
Seidel, H.	[73EHR/JOH]
Sekine, T.	[91KIM/SEK]
Selkov, E.E.	[68SEL]

Authors List

Author	References
Sellin, P.	[91BRU/CRO], [92BRU/SEL]
Senesi, N.	[77SEN/CHE], [90SEN], [94SEN]
Sengers, J.V.	[83LEV/KAM], [84KES/SEN]
Sergeyeva, E.I.	[72SER/NIK], [92FUG/KHO]
Shannon, R.D.	[69SHA/PRE], [76SHA]
Shapkin, A.I.	[85RYZ/SHA], [91RYZ/BRY]
Shaw, R.	[89ALC/SHA]
Shchigolev, B.M.	[65SHC]
Shea, M.A.	[91CHA/MCK]
Shen, G.	[93SAX/CHA]
Shierman, G.R.	[77TRE/MAS]
Shimomura, T.	[90SHI/DOO]
Shock, E.L.	[88SHO/HEL], [89SHO/HEL], [89SHO/HEL2], [92SAS/SHO], [92SHO/OEL], [97SHO/SAS], [97SVE/SHO]
Shomate, C.H.	[43SHO/HUF]
Shrader-Fechette, K.	[94ORE/SHR]
Shuman, M.S.	[73SHU/WOO], [83CAB/SHU], [83SHU/COL], [84CAB/SHU], [88CAB/SHU]
Sievers, R.	[83BER/SIE]
Sigg, L.	[94SIG/XUE]
Sillén, L.G.	[52SIL], [53BIE/SIL], [58FRY/NIL], [59SIL], [61SIL], [64SIL/MAR], [67ING/KAK], [70EKE/SIL], [71SIL], [71SIL/MAR]
Silva, R.J.	[95SIL/BID]
Silvester, L.F.	[83PHI/SIL], [84PHI/SIL]
Simonson, J.M.	[88MES/MAR], [91MES/PAL]
Singer, M.	[82SIN]
Singh, P.P.	[78SPI/SIN]
Sips, R.	[48SIP]
Sitte, P.	[79SIT]
Sjöberg, S.	[83GRA/SJO], [87HED/SJO], [90LOE/SJO], [91ROE/SJO]
Skagius, K.	[94ENG/HUD], [95CHA/AND]
Skinner, S.I.M.	[67SCH/SKI]
Skogerboe, R.K.	[81SKO/WIL]
Slocum, G.H.	[82PAT/SLO]
Slota, P.	[80SLO/MAR]
Smellie, J.	[94MIL/ALE]
Smellie, J.A.T.	[91CHA/MCK]
Smith, B.	[93HIG/KIN]
Smith, P.A.	[92FRI/ALE]
Smith, R.G., Jr.	[76SMI]
Smith, R.M.	[74MAR/SMI], [75MAR/SMI], [75SMI/MAR], [76SMI/MAR], [77MAR/SMI], [82MAR/SMI], [89SMI/MAR]
Smith, R.W.	[86SMI/POP]

Author	References
Söhnel, O.	[85SOH/NOV]
Soler, J.M.	[94LAS/SOL]
Sollins, P.	[89FUR/WES], [90FUR/WES]
Somers, J.A.	[91SOM/REM]
Sóvágó, I.	[91KIS/SOV]
Spahiu, K.	[81CIA/FER], [82BIE/BRU], [83SPA], [85SPA], [94WER/SPA], [95SPA/BRU]
Spedding, F.H.	[77SPE/RAR]
Spencer, P.J.	[73SPE], [81SPE], [93KUB/ALC]
Spieler, P.	[92SAR/BRA]
Spitzer, J.J.	[78SPI/SIN]
Sposito, G.	[77SPO/HOL], [79MAT/SPO], [80SPO2], [89SPO]
Staples, B.R.	[70BAT/STA]
Staub, C.	[83STA/BUF], [84BUF/STA], [84STA/BUF]
Steefel, C.I.	[90STE/LAS]
Stenström, T.H.	[94SZE/SZE]
Stephansson, O.	[94ENG/HUD]
Stevenson, F.J.	[72ARD/STE], [76STE], [77STE], [82STE], [84FIT/STE], [86FIT/STE]
Stewart, W.E.	[60BIR/STE]
Stipp, S.L.S.	[93STI/PAR]
Stjernström, M.	[96DEN/STJ]
Stokes, R.H.	[59ROB/STO]
Stone, A.T.	[85MOR/STO]
Storms, E.K.	[84HOL/RAN]
Strübel, G.	[91STR/ZIM]
Stuber, H.U.	[65GAM/STU]
Stumm, W.	[81STU/MOR], [87SCH/STU], [87STU], [88ULR/STU], [89WER/CHA], [90HER/STU], [90STU/WOL], [92BRU/STU], [92BRU/WER], [92GRE/STU], [96STU/MOR]
Sturtevant, J.M.	[59STU]
Succi, S.	[88SUC/SAN]
Sudicky, E.A.	[81TAN/FRI], [82SUD/FRI]
Sun, Z.	[91ROE/SJO]
Sundman, B.	[85SUN/JAN]
Sverjensky, D.A.	[87SVE], [89SHO/HEL2], [92SHO/OEL], [97SHO/SAS], [97SVE/SHO]
Sway, K.	[86TRE/SWA]
Swift, R.S.	[89HAY/MCC]
Swinney, H.L.	[91QUY/SWI]
Syrkin, Y.K.	[50SYR/DYA]
Syverud, A.N.	[85CHA/DAV]
Szewzyk, R.	[94SZE/SZE]
Szewzyk, U.	[94SZE/SZE]

Author	References
<hr/>	
Takamatsu, T.	[83TAK/YOS]
Takeishi, H.	[93MEI/TAK]
Tanford, C.	[61TAN], [67TAN]
Tang, D.H.	[81TAN/FRI]
Tanger, IV, J.C.	[88TAN/HEL]
Tao, Z.	[96TAO/DU]
Tardy, Y.	[74TAR/GAR], [77TAR/GAR], [78TAR], [92TAR/DUP]
Tauc, T.	[80VAR/OCO]
Taylor, D.F.	[78TAY]
Tercier, M.L.	[87BUF/VUI]
Tessier, A.	[90BUF/ALT]
Testini, C.	[78RUG/SCI]
Teukolsky, S.A.	[87PRE/FLA]
Theus, G.J.	[83CHE/ARA]
Theyssier, M.	[91MOU/DEC]
Thomas, R.	[85KAU/URB]
Thompson, P.T.	[94WOO/CAR]
Thorstenson, D.C.	[80PAR/THO]
Thurman, E.M.	[81THU/MAL], [83MCK/FED], [85THU]
Thurmond, V.	[82THU/MIL]
Tipping, E.	[88TIP/BAC], [90TIP/RED], [92TIP/HUR], [93HIG/KIN], [93TIP], [93TIP2], [94TIP]
Tits, J.	[91MAE/ELE]
Tobe, M.L.	[72TOB]
Toffoli, T.	[82FRE/TOF], [84FAR/TOF], [87TOF/MAR]
Tokar, J.M.	[83HAR/BOR]
Tolpygina, L.N.	[69NIK/TOL]
Torres, R.A.	[83TOR], [84TOR/CHO]
Toussaint, D.	[83TOU/WIL]
Town, R.M.	[91POW/TOW]
Trauth-Badaud, D.	[87DEC/COL]
Treadwell, F.P.	[14TRE]
Treadwell, W.D.	[47TRE]
Tremaine, P.R.	[77TRE/MAS], [80LEM/TRE], [80TRE/LEB], [86TRE/SWA], [88HOV/HEP], [96XIA/TRE]
Trescases, J.J.	[87DEC/COL]
Trotignon, L.	[89PET/DRA]
Truitt, R.E.	[81TRU/WEB]
Tsang, C.F.	[93BEA/TSA]
Tullborg, E.-L.	[96BAN/TUL]
Turing, A.M.	[52TUR]
Turner, D.R.	[86TUR/VAR], [87TUR/VAR]
Turner, F.J.	[58FYF/TUR]
Turner, P.J.	[82COB/MUR]
Tuschall, J.R., Jr.	[83MIL/TUS], [83TUS/BRE]

Authors List

Author	References
Tweed, C.J.	[92ALE/DAY]
Ulrich, H.J.	[88ULR/STU]
Underdown, A.W.	[80GAM/UND]
Urbain, J.	[85KAU/URB]
Valensi, G.	[74VAL]
Van den Berg, C.M.G.	[79BER/KRA], [84BER4]
Van der Weiden, M.J.J.	[85ZUU/WEI]
Van Eldik, R.	[83PAL/ELD]
Van Elewijck, F.	[91MAE/ELE]
Van Loon, L.R.	[91LOO/KOP], [95GLA/HUM]
Van Panthaleon van Eck, C.L.	[53PAN]
Van Riemsdijk, W.H.	[86RIE/BOL], [89HIE/RIE], [90NED/RIE], [90WIT/RIE], [92NED/RIE], [93NED/WIT], [93WIT/RIE], [93WIT/RIE2], [94NED/RIE], [95BEN/MIL]
Van Rysselberghe, P.	[50DEL/POU]
Van Wandruszka, R.	[94ENG/WAN]
Vancuysen, J.	[91MAE/ELE]
Vanderzee, C.E.	[75BER/VAN], [75BER/VAN2]
Vardeny, Z.	[80VAR/OCO]
Varney, M.S.	[86TUR/VAR], [87TUR/VAR]
Vasil'ev, V.P.	[62VAS], [67VAS], [67VAS/GRE], [67VAS/GRE2], [69LOB/VAS], [78VAS/YAS2], [80VAS/KOZ]
Velde, B.	[66VEL]
Ventry, L.S.	[83RYA/HOL]
Verdes, G.	[90VER]
Verhoogen, J.	[58FYF/TUR]
Verruijt, A.	[92BEA/VER]
Vetterling, W.T.	[87PRE/FLA]
Veyts, I.V.	[93GUR/VEY]
Viani, B.E.	[90WOL/JAC], [94VIA/BRU], [97BRU/VIA]
Vianney, J.M.	[90VIA/KOE]
Vichniac, G.Y.	[89MAN/BOC]
Victor, D.M.	[80LI/VIC]
Vieno, T.	[93VIE/HAU]
Vitorge, P.	[86GRE/RIG], [89RIG/ROB], [92CAP/VIT], [95CAP/VIT]
Vogel, K.M.	[90ROY/RIC]
Vogl, P.	[92KOM/ZAN]
Volokhov, Yu.A.	[71VOL/PAV]
Von Massow, R.	[77TRE/MAS]
Vreugdenhil, C.B.	[93VRE/KOR]
Vuileumier, J.J.	[87BUF/VUI]
Wadsten, T.	[88HAL/OES]
Wagman, D.D.	[73HUL/DES], [82WAG/EVA], [89COX/WAG]
Wagner, W.	[89SAU/WAG], [93WAG/PRU]
Wahlberg, O.	[70EKE/SIL]

Authors List

Author	References
Waite, T.D.	[84WAI/MOR], [90WAI], [94WAI/PAY]
Waldbaum, D.R.	[68ROB/WAL], [76OPE/HEM]
Walker, R.F.	[64CAR/WAL]
Wallin, B.	[96BAN/TUL]
Wang, P.	[90ARC/WAN]
Wanner, H.	[88WAN], [90WAN], [92GRE/FUG], [95SIL/BID]
Warnqvist, B.	[67ING/KAK], [71WAR/ING]
Watson, D.G.	[79ALL/BEL]
Watson, I.D.	[61MAL/PAR]
Watts, D.W.	[74COX/HED]
Waychumas, G.A.	[94WAI/PAY]
Weare, J.H.	[84HAR/MOL]
Weast, R.C.	[87WEA]
Weber, J.H.	[78BRE/GRA], [80SAA/WEB], [81TRU/WEB], [82RAI/WEB]
Wedborg, M.	[85PAX/WED], [91PAX/WED]
Wedepohl, K.H.	[78WED]
Welty, C.	[92GEL/WEL]
Werne, C.O.	[95CHA/AND]
Wershaw, R.L.	[83MCK/FED], [85AIK/MCK], [86WER]
Wersin, P.	[89WER/CHA], [92BRU/STU], [92BRU/WER], [94WER/BRU], [94WER/SPA]
Wesolowski, D.J.	[90DIC/WES], [92PAL/WES], [93PAL/WES]
Westall, J.	[79WES], [80WES/HOH], [89FUR/WES], [90FUR/WES]
Westall, J.C.	[76WES/ZAC], [83MCK/FED], [86WES], [87WES], [94HER/WES]
Westrum, E.F., Jr.	[83WES], [84GRO/DRO]
Whewell, R.J.	[71ROS/ROS]
Whiffen, D.H.	[79WHI2]
White, A.F.	[90HOC/WHI], [90WHI]
White, H.J., Jr.	[87GAR/PAR]
Whitfield, M.	[86TUR/VAR], [87TUR/VAR]
Whittemore, D.O.	[71LAN/WHI]
Wiborgh, M.	[94ENG/HUD], [95CHA/AND]
Wigley, T.M.L.	[79NOR/PLU]
Wikberg, P.	[87WIK], [92GRE/STU], [96BAN/TUL]
Wilczek, F.	[83TOU/WIL]
Wilkins, R.G.	[74WIL]
Wilkinson, G.	[87COT/WIL], [88COT/WIL]
Williams, C.W.	[83MOR/WIL]
Williams, R.J.P.	[53IRV/WIL], [65PHI/WIL], [91FRA/WIL]
Williamson, A.T.	[44WIL]
Willis, M.	[97SHO/SAS]
Wilson, B.H.	[83WIL/MCN]
Wilson, D.E.	[77WIL/KIN]
Wilson, J.T.	[83WIL/MCN]

Authors List

Author	References
Wilson, M.A.	[83GIL/WIL], [86GIL/WIL]
Wilson, S.A.	[81SKO/WIL]
Wimmer, H.	[92BUC/KIM]
Winfree, A.T.	[72WIN]
Wingefors, S.	[95CHA/AND]
Winkler, H.G.F.	[70ALT/KAR]
Wolery, T.J.	[79NOR/PLU], [83WOL], [88JAC/WOL], [90WOL/JAC]
Wolf, A.	[80MAR/WOL]
Wolfram, S.	[84FAR/TOF], [86WOL], [90DOO/FRI]
Wollast, R.	[89CHO/GAR], [90STU/WOL], [90WOL]
Wood, R.H.	[94WOO/CAR]
Wood, S.A.	[90WOO]
Woodwark, G.P., Jr.	[73SHU/WOO]
Wu, X.G.	[92WU/KAP]
Wyllie, J.	[77IRV/HUA]
Xi, R.H.	[92KRA/BIS]
Xiao, C.	[96XIA/TRE]
Xu Y.	[91CHE/XU]
Xu, H.	[89EPH/XU], [89XU/EPH]
Xu, N.	[94WAI/PAY]
Xue, H.	[94SIG/XUE]
Yamamoto, T.	[72ZIR/YAM]
Yamauchi, S.	[84FLO/HAS]
Yasinskii, F.N.	[78VAS/YAS2]
Yasunishi, A.	[79YAS/YOS]
Yelkin, A.Ye.	[75KHO/YEL]
Yip, S.	[80BOO/YIP]
Yoon, T.H.	[94YOO/MOO]
Yoshida, F.	[79YAS/YOS]
Yoshida, T.	[83TAK/YOS]
Yungman, V.S.	[85HIL/GUR]
Zachary, J.L.	[76WES/ZAC]
Zador, S.	[76ALC/JAC]
Zaikin, A.N.	[70ZAI/ZHA], [73ZHA/ZAI]
Zaleski, S.	[90APP/ZAL], [93APP/ZAL]
Zandler, G.	[92KOM/ZAN]
Zeldovich, Ya.B.	[78OVC/ZEL]
Zen, E.	[71FIS/ZEN]
Zhabotinsky, A.M.	[64ZHA], [70ZAI/ZHA], [73ZHA/ZAI]
Zhang, J.	[89SAX/ZHA]
Zimmer, S.H.	[91STR/ZIM]
Zirino, A.	[72ZIR/YAM]
Zunino, H.	[72ZUN/GAL]
Zuse, K.	[69ZUS]
Zuurdeg, B.W.	[85ZUU/WEI]

Chapter XVI

Reference List

- [14TRE] Treadwell, F.P., Kurzes Lehrbuch der analytischen Chemie: I. Band: Qualitative Analyse, 8. Aufl. Franz Deuticke, Leipzig und Wien 1914.
- [18LAN] Langmuir, I., The adsorption of gases on plane surfaces of glass, mica, and platinum, J. Am. Chem. Soc., **40** (1918) 1361–1402.
- [22BRO] Brønsted, J.N., Studies on solubility. IV. The principle of the specific interaction of ions, J. Am. Chem. Soc., **44** (1922) 877–898.
- [22BRO2] Brønsted, J.N., Calculation of the osmotic and activity functions in solutions of uni-univalent salts, J. Am. Chem. Soc., **44** (1922) 938–948.
- [26FRE] Freundlich, H., Colloid and capillary chemistry, Methuen, London, 1926.
- [31HAR] Hartley, G.S., Theory of the velocity of diffusion of strong electrolytes in dilute solution, Phil. Mag., **12** (1931) 473–488.
- [35GUG] Guggenheim, E.A., The specific thermodynamic properties of aqueous solutions of strong electrolytes, Philos. Mag., **19** (seventh series) (1935) 588–643.
- [35HAR/MAN] Harned, H.S., Mannweiler, G.E., The thermodynamics of ionized water in sodium chloride solutions, J. Am. Chem. Soc., **57** (1935) 1873–1876.
- [36SCA] Scatchard, G., Concentrated solutions of strong electrolytes, Chem. Rev., **19** (1936) 309–327.
- [38GUR] Gurney, R.W., Exchange forces and electrostatic forces between ions in solution, J. Chem. Phys., **6** (1938) 499–505.
- [38KOS/HAR] Kossiakoff, A., Harker, D., The calculation of the ionization constants of inorganic oxygen acids from their structures, J. Am. Chem. Soc., **60** (1938) 2047–2055.
- [40RIC] Rice, O.K., Electronic structure and chemical bonding. With special reference to inorganic chemistry, New York: McGraw-Hill Book Company, Inc., 1940, 511p.

Reference List

- [43HAR/DAV] Harned, H.S., Davis, R., The ionization constant of carbonic acid in water and the solubility of carbon dioxide in water and aqueous salt solutions from 0 to 50°C, *J. Am. Chem. Soc.*, **65** (1943) 2030–2037.
- [43SHO/HUF] Shomate, C.H., Huffman, E.H., Heats of formation of MgO, MgCl₂, MgCl₂·H₂O, MgCl₂·2H₂O, MgCl₂·4H₂O and MgCl₂·6H₂O, *J. Am. Chem. Soc.*, **65** (1943) 1625–1629.
- [44WIL] Williamson, A.T., The exact calculation of heats of solution from solubility data, *Trans. Faraday Soc.*, **40** (1944) 421–436.
- [45HAR/BON] Harned, H.S., Bonner, F.T., The first ionization of carbonic acid in aqueous solutions of sodium chloride, *J. Amer. Chem. Soc.*, **67** (1945) 1026–1031.
- [47TRE] Treadwell, W.D., *ed.*, Tabellen zur qualitativen Analyse, 18. Auflage Franz Deuticke, Wien 1947.
- [48SCH] Schubert, J., The use of ion exchangers for the determination of physical-chemical properties of substances, particularly radiotracers, in solution, *J. Phys. Coll. Chem.*, **52** (1948) 340–351.
- [48SIP] Sips, R., On the structure of a catalyst surface, *J. Chem. Phys.*, **16** (1948) 490–495.
- [50DEL/POU] Delahay, P., Pourbaix, M., van Rysselberghe, P., Potential-pH diagrams, *J. Chem. Edu.*, **27** (1950) 683–688.
- [50REM] Remy, H., Lehrbuch der anorganischen Chemie, Band I & II, 5. Aufl. Akademische Verlagsgesellschaft Geest & Portig K.G., Leipzig 1949, 1950.
- [50REM2] Remy, H., Lehrbuch der anorganischen Chemie, Band II, 5. Aufl. Akademische Verlagsgesellschaft Geest & Portig K.G., Leipzig 1949, 1950, *p.*342.
- [50REM3] Remy, H., Lehrbuch der anorganischen Chemie, Band I, 5. Aufl. Akademische Verlagsgesellschaft Geest & Portig K.G., Leipzig 1949, 1950, *p.*465.
- [50SYR/DYA] Syrkin, Y.K., Dyatkina, M.E., Structure of molecules and the chemical bond, (translated and revised by Partridge, M.A. and Jordan, D.O.), London: Butterworths Sci. Publ., 1950, 509p.
- [51POW/LAT] Powell, R.E., Latimer, W.M., The entropy of aqueous solutes, *J. Chem. Phys.*, **19** (1951) 1139–1141.
- [52LAT] Latimer, W.M., The oxidation states of the elements and their potentials in aqueous solutions, 2nd ed., New York: Prentice-Hall Inc., 1952, 392p.
- [52LON/MCD] Long, F.A., McDevit, W.F., Activity coefficients of nonelectrolyte solutes in aqueous salt solutions, *Chem. Rev.*, **51** (1952) 119–169.
- [52SCH] Schwarzenbach, G., The chelate effect, *Helv. Chim. Acta*, **35** (1952) 2344–2359.

Reference List

- [52SIL] Sillén, L.G., Redox diagrams, *J. Chem. Edu.*, **29** (1952) 600–608.
- [52TUR] Turing, A.M., The chemical basis of morphogenesis, *Phil. Trans. Roy. Soc., London*, **B 237** (1952) 37–72.
- [53BIE/SIL] Biedermann, G., Sillén, L.G., Studies on the hydrolysis of metal ions. IV. Liquid junction potentials and constancy of activity factors in $\text{NaClO}_4\text{-HClO}_4$ ionic medium, *Arkiv Kemi*, **5** (1953) 425–440.
- [53COB] Cobble, J.W., Empirical considerations of entropy. I. The entropies of the oxy-anions and related species, *J. Chem. Phys.*, **21** (1953) 1443–1446.
- [53COB2] Cobble, J.W., Empirical considerations of entropy. II. The entropies of inorganic complex ions, *J. Chem. Phys.*, **21** (1953) 1446–1450.
- [53COB3] Cobble, J.W., Empirical considerations of entropy. III. A structural approach to the entropies of aqueous organic solutes and complex ions, *J. Chem. Phys.*, **21** (1953) 1451–1456.
- [53GUR] Gurney, R.W., *Ionic processes in solution*, McGraw-Hill Book Company, Inc., (1953) London, 275p.
- [53IRV/WIL] Irving, H., Williams, R.J.P., The stability of transition-metal complexes, *J. Chem. Soc.*, (1953) 3192–3210.
- [53PAN] van Panthaleon van Eck, C.L., The relation between the stability of metal complexes in solution and the ionization potential of their metal component, *Rec. Trav. Chim.*, **72** (1953) 50–56.
- [54ADA] Adamson, A.W., A proposed approach to the chelate effect, *J. Am. Chem. Soc.*, **76** (1954) 1578–1579.
- [54GOL] Goldberg, E.D., Marine geochemistry. I. Chemical scavengers of the sea, *J. Geol.*, **62** (1954) 249–265.
- [54POW] Powell, R.E., The entropies of aqueous ions, *J. Phys. Chem.*, **58** (1954) 528–533.
- [56FRA] Franck, E.U., Hochverdichteter Wasserdampf. II. Ionendissoziation von KCl in H_2O bis 750°C , *Z. Phys. Chem. N.F.*, **8** (1956) 107–126 (in German).
- [56IRV/ROS] Irving, H., Rossotti, H., Some relationships among the stabilities of metal complexes, *Acta Chem. Scand.*, **10** (1956) 72–93.
- [56KRA2] Krauskopf, K.B., Factors controlling the concentrations of thirteen rare metals in sea water, *Geochim. Cosmochim. Acta*, **9** (1956) 1–32.
- [56LAI] Laidler, K.J., The entropies of ions in aqueous solution. I. Dependence on charge and radius, *Can. J. Chem.*, **34** (1956) 1107–1113.

Reference List

- [57AHR/GRE] Ahrland, S., Grenthe, I., The stability of metal halide complexes in aqueous solution. III. The chloride, bromide and iodide complexes of bismuth, *Acta Chem. Scand.*, **11** (1957) 1111–1130.
- [57CHA] Charlot, G., *L'analyse qualitative et les réactions en solution*, 4th. ed. Aufl. Masson, Paris, 1957.
- [57COU/LAI] Couture, A.M., Laidler, K.J., The entropies of ions in aqueous solution: II. An empirical equation for oxy-anions, *Can. J. Chem.*, **35** (1957) 202–206.
- [57LAI] Laidler, K.J., Comments on “Partial molal entropies of ions in aqueous solution” by P. C. Scott and Z Z. Hugus, *J. Chem. Phys.*, **27** (1957) 1423–1424.
- [57NAT] National Academy of Sciences, National Research Council, The disposal of radioactive waste on land, Publication 519, Washington, 1957.
- [57SCO/HUG] Scott, P.C., Hugus, Z Z., Jr., Partial molal entropies of ions in aqueous solution, *J. Chem. Phys.*, **27** (1957) 1421–1423.
- [58AHR/CHA] Ahrland, S., Chatt, J., Davies, N.R., The relative affinities of ligand atoms for acceptor molecules and ions, *Q. Rev.*, **12** (1958) 265–276.
- [58BEL2] Belousov, B.P., *Sbornik Referatov po Radiatsionni Meditsine* (Megdiz, Moscow, 1958), p.145 (in Russian); English translation of extended version, in: *Oscillations and Travelling Waves in Chemical Systems* (Field, R.J., Burger, M., eds.), New York: Wiley, (1985) pp.605–613.
- [58FRY/NIL] Frydman, M., Nilsson, G., Rengemo, T., Sillén, L.G., Some solution equilibria involving calcium sulfite and carbonate: III. The acidity constants of H_2CO_3 and H_2SO_3 , and $\text{CaCO}_3 + \text{CaSO}_3$ equilibria in NaClO_4 medium at 25°C , *Acta Chem. Scand.*, **12** (1958) 868–872.
- [58FYF/TUR] Fyfe, W.S., Turner, F.J., Verhoogen, J., Metamorphic reactions and metamorphic facies, *Geological Soc. of America Mem.*, **73** (1958) 259pp.
- [58HAR/OWE] Harned, H.S., Owen, B.B., *The physical chemistry of electrolytic solutions*, Third edition, Reinhold Publishing Corporation, New York (1958), 803p.
- [59LAN/LIF] Landau, L.D., Lifshitz, E.M., *Course of theoretical physics*, Vol. 6. Fluid mechanics, Pergamon Press, Oxford, 1959.
- [59POP] Popper, K., *Logik der Forschung*, 8. Aufl. J.C.M. Mohr, Tübingen 1984; *The Logic of Scientific Discovery*, Basic Books, New York 1959.
- [59ROB/STO] Robinson, R.A., Stokes, R.H., *Electrolyte solutions*, London: Butterworths, 2nd ed., 1959, 559p.
- [59SIL] Sillén, L.G., Graphic presentation of equilibrium data, in: *Treatise on Analytical Chemistry*, Part I, Sect. B, Vol. 1 (Kolthoff, I.M., Elving, P.J., eds.), New York: John Wiley & Sons, Inc., 1959, pp.277–317.

Reference List

- [59STU] Sturtevant, J.M., Calorimetry, Chapter X, in: *Technique of organic chemistry*, Vol. **I**, Part **I**, Physical methods of organic chemistry, 3rd ed. (Weissberger, A., *ed.*), New York: Interscience Publ. Inc., 1959, *pp.*523–654.
- [60BIR/STE] Bird, R.B., Stewart, W.E., Lightfoot, E.N., *Transport phenomena*, John Wiley and Sons, New York, 1960.
- [60FLA] Flaig, W., Comparative chemical investigations on natural humic compounds and their model substances, *Sci. Proc. Roy. Dublin Soc.*, **4** (1960) 49–62.
- [60GAR] Garrels, R.M., *Mineral Equilibria at Low Temperature and Pressure*, Harper and Row, New York, 1960.
- [60PAU] Pauling, L., *The nature of the chemical bond, and the structure of molecules and crystals: An introduction to modern structural chemistry*, Ithaca, New York: Cornwell University Press, 3rd ed., 1960, 644*p.*
- [61ALL] Allred, A.L., Electronegativity values from thermochemical data, *J. Inorg. Nucl. Chem.*, **17** (1961) 215–221.
- [61FRA] Franck, E.U., Überkritisches Wasser als elektrolytisches Lösungsmittel, *Angew. Chem.*, **73** (1961) 309–322.
- [61LEW/RAN] Lewis, G.N., Randall, M., Pitzer, K.S., Brewer, L., *Thermodynamics*, 2nd ed., New York: McGraw-Hill, 1961, 723*p.*
- [61MAL/PAR] Malcolm, G.N., Parton, H.N., Watson, I.D., Enthalpies and entropies of formation of mercury(II)-halide 1:1 complex ions, *J. Phys. Chem.*, **65** (1961) 1900–1902.
- [61ROS/ROS] Rossotti, F.J.C., Rossotti, H., *The determination of stability constants and other equilibrium constants in solution*, New York: McGraw-Hill, 1961.
- [61SIL] Sillén, L.G., The physical chemistry of sea water, in: *Oceanography* (Sears, M. *ed.*), Washington, D.C.: American Association for the Advancement of Science, Publ., **67**, 1961, *pp.*549–581.
- [61TAN] Tanford, C., *Physical chemistry of macromolecules*, John Wiley & Sons, Inc., New York, 1961, *pp.*457–525.
- [62VAS] Vasil'ev, V.P., Influence of ionic strength on the instability constants of complexes, *Russ. J. Inorg. Chem.*, **7** (1962) 924–927.
- [63BAR/ERN] Barnes, H.L., Ernst, W.G., Ideality and ionization in hydrothermal fluids: the system MgO-H₂O-NaOH, *Am. J. Sci.*, **261** (1963) 129–150.
- [63HEI/CLE] Heistand, R.N., Clearfield, A., The effect of specific swamping electrolytes upon the formation constant of the monochloroiron(III) complex, *J. Am. Chem. Soc.*, **85** (1963) 2566–2570.

Reference List

- [64CAR/WAL] Carrera, N.J., Walker, R.F., Plante, E.R., Vapor pressures of ruthenium and osmium, *J. Res. Nat. Bur. Stand.*, **68A** (1964) 325–330.
- [64CHR/IZA] Christensen, J.J., Izatt, R.M., Hansen, L.D., Hale, J.D., Thermodynamics of metal halide coordination. II. ΔH° and ΔS° values for stepwise formation of HgX_2 (X=Cl, Br, I) in aqueous solution at 8, 25, and 40° C, *Inorg. Chem.*, **3** (1964) 130–133.
- [64CRI/COB] Criss, C.M., Cobble, J.W., The thermodynamic properties of high temperature aqueous solutions. IV. Entropies of the ions up to 200° and the correspondence principle, *J. Am. Chem. Soc.*, **86** (1964) 5385–5390.
- [64CRI/COB2] Criss, C.M., Cobble, J.W., The thermodynamic properties of high temperature aqueous solutions. V. The calculation of ionic heat capacities up to 200°. Entropies and heat capacities above 200°, *J. Am. Chem. Soc.*, **86** (1964) 5390–5393.
- [64RAJ/MAR] Rajan, K.S., Martell, A.E., Equilibrium studies of uranyl complexes-I: Interaction of uranyl ion with some hydroxycarboxylic and aminocarboxylic acids, *J. Inorg. Nucl. Chem.*, **26** (1964) 789–798.
- [64SIL/MAR] Sillén, L.G., Martell, A.E., Stability constants of metal-ion complexes, Special Publ. No. **17**, Chemical Society, London, 1964, 754p.
- [64ZHA] Zhabotinsky, A.M., Periodic course of oxidation of malonic acid in solution (investigation of the kinetics of the reaction of Belousov), *Biophysics (Biofizika)*, **9** (1964) 329–335 (orig. *pp.*306–311).
- [65ARN] Arnek, R., A calorimetric and potentiometric study of the systems Cl^- - Hg^{2+} and Br^- - Hg^{2+} at 25°C in 3 M NaClO_4 medium, *Arkiv för Kemi*, **24** (1965) 531–550.
- [65EVA] Evans, B.W., Application of a reaction-rate method to the breakdown equilibria of muscovite and muscovite plus quartz, *Am. J. Sci.*, **263** (1965) 647–667.
- [65GAM/STU] Gamsjäger, H., Stuber, H.U., Schindler, P., Zur Thermodynamik der Metallcarbonate: I. Löslichkeitskonstanten und Freie Bildungsenthalpie von Cadmiumcarbonat, ein Beitrag zur Thermodynamik des Systems Cd^{2+} - H_2O - CO_2 , *Helv. Chim. Acta*, **48** (1965) 723.
- [65GAR/CHR] Garrels, R.M., Christ, C.L., *Solutions, minerals and equilibria*, San Francisco: Freeman, Cooper & Co, 1965, 450p.
- [65GHO] Ghose, S., Mg^{2+} - Fe^{2+} order in an orthopyroxene, $\text{Mg}_{0.93}\text{Fe}_{1.07}\text{Si}_2\text{O}_6$, *Z. Kristallogr.*, **122** (1965) 81–99.
- [65PHI/WIL] Phillips, C.S.G., Williams, R.J.P., *Inorganic chemistry*, Chapter 5, Oxford: Clarendon Press, 1965.
- [65SHC] Shchigolev, B.M., *Mathematical analysis of observations*, Amer. Elsevier Publ. Company Inc., 1965.

Reference List

- [66CLA/GLE] Clarke, E.C.W., Glew, D.N., Evaluation of thermodynamic functions from equilibrium constants, *Trans. Faraday Soc.*, **62** (1966) 539–547.
- [66GME] Gmelin-Institut, Gmelins Handbuch der Anorganischen Chemie: Nickel, Teil B, Lieferung 3, Weinheim/Bergstr.: Verlag Chemie, 1966.
- [66GUG] Guggenheim, E.A., Applications of statistical mechanics, Oxford: Clarendon Press, 1966, 211p.
- [66KON] Kononova, M.M., Soil organic matter, Pergamon, Elmsford, New York (1966) 544pp.
- [66NIK] Nikol'skiy, B.P. (*ed.*), Spravochnik khimika (Chemist's handbook), 2nd ed., Vol. 1, Moscow: Khimiya, 1966, in Russian.
- [66RAN] Rand, M.H., Thermochemical properties, in: Plutonium: Physico-chemical properties of its compounds and alloys, *Atomic Energy Rev.*, **4**, Special Issue Nbr. 1 (1966) 7–51.
- [66VEL] Velde, B., Upper stability of muscovite, *Am. Mineral.*, **51** (1966) 921–929.
- [67AHR] Ahrland, S., Enthalpy and entropy changes by formation of different types of complexes, *Helv. Chim. Acta*, **50** (1967) 306–318.
- [67ARN/KAK] Arnek, R., Kakolowicz, W., Thermochemical studies of hydrolytic reactions. 3. A thermochemical study of hydrolyzed $\text{Hg}(\text{ClO}_4)_2$ solutions, *Acta Chem. Scand.*, **21** (1967) 1449–1456.
- [67GME] Gmelin-Institut, Gmelins Handbuch der Anorganischen Chemie: Nickel, Teil AI, Weinheim/Bergstr.: Verlag Chemie, 1967, 641p.
- [67HEL] Helgeson, H.C., Thermodynamics of complex dissociation in aqueous solution at elevated temperatures, *J. Phys. Chem.*, **71** (1967) 3121–3136.
- [67ING/KAK] Ingri, N., Kakolowicz, W., Sillén, L.G., Warnqvist, B., High-speed computers as a supplement to graphical methods-V. HALTAFALL, a general program for calculating the composition of equilibrium mixtures, *Talanta*, **14** (1967) 1261.
- [67SCH] Schindler, P.W., Heterogeneous equilibria involving oxides, hydroxides, carbonates, and hydroxide carbonates, in: Equilibrium concepts in natural water systems, *Adv. Chem. Ser.*, Nr. **67**, Washington, D.C.: Amer. Chem. Soc., 1967, pp.196–221.
- [67SCH/SKI] Schnitzer, M., Skinner, S.I.M., Organo-metallic interactions in soils. 7. Stability constants of Pb(II)-, Ni(II)-, Mn(II)-, Co(II)-, Ca(II)-, and Mg(II)-fulvic acid complexes, *Soil Sci.*, **103** (1967) 247–251.
- [67TAN] Tanford, C., Physical chemistry of macromolecules, (1967), New York, John Wiley & Sons, Inc., 710p.

Reference List

- [67VAS] Vasil'ev, V.P., On the calculation of the standard heat effects of the reactions in solution, *Zh. Fiz. Khim.*, **41** (1967), 121–125 (in Russian).
- [67VAS/GRE] Vasil'ev, V.P., Grechikhina, N.K., Solubility of oxychloride of bismuth in perchloric acid solutions and standard isobaric potential of Bi^{3+} ion in aqueous solution, *Zh. Neorg. Khim.*, **12** (1967) 605–609 (in Russian).
- [67VAS/GRE2] Vasil'ev, V.P., Grechikhina, N.K., Solubility of BiOCl and BiONO_3 in aqueous solution of nitric and perchloric acids, *Zh. Neorg. Khim.*, **12** (1967) 1372–1380 (in Russian).
- [68AHR] Ahrland, S., Thermodynamics of complex formation between hard and soft acceptors and donors, *Structure and Bonding*, **5** (1968) 117–149.
- [68GOU] Gould, R.F., Adsorption from aqueous solutions, *Adv. Chem. Ser.*, Vol. 79, Am. Chem. Soc., Washington DC, 1968.
- [68KAR/KAS] Karpov, I.K., Kashik, S.A., Computer calculation of standard isobaric-isothermal potentials of silicates by multiple regression from a crystallochemical classification, *Geochem. International*, **5** (1968) 706–713.
- [68LAV/GER] Lavrentev, V.I., Gerassimov, Ya.I., Thermochemical properties, in: *Niobium: Physico-chemical properties of its compounds and alloys*, *Atomic Energy Rev.*, Special Issue Nbr. 2 (1968) 7–44.
- [68PRI/LEF] Prigogine, I., Lefever, R., Symmetry breaking instabilities in dissipative systems. II, *J. Chem. Phys.*, **48** (1968) 1695–1700.
- [68QUI/MAR] Quist, A.S., Marshall, W.L., Electrical conductances of aqueous sodium chloride solutions from 0 to 800° and at pressures to 4000 bars, *J. Phys. Chem.*, **72** (1968), 684–703.
- [68QUI/MAR2] Quist, A.S., Marshall, W.L., Electrical conductances of aqueous hydrogen bromide solution from 0 to 800° and at pressures to 4000 bars, *J. Phys. Chem.*, **72** (1968) 1545–1552.
- [68QUI/MAR3] Quist, A.S., Marshall, W.L., Electrical conductances of aqueous sodium bromide solutions from 0 to 800° and at pressures to 4000 bars, *J. Phys. Chem.*, **72** (1968) 2100–2105.
- [68QUI/MAR4] Quist, A.S., Marshall, W.L., Ionization equilibria in ammonia-water solutions to 700° and to 4000 bars of pressure, *J. Phys. Chem.*, **72** (1968) 3122–3128.
- [68ROB/WAL] Robie, R.A., Waldbaum, D.R., Thermodynamic properties of minerals and related substances at 298.15°K (25.0°C) and one atmosphere (1.013 bars) pressure and at higher temperatures, *U.S. Geological Survey Bull.*, No. 1259, 1968, 256p.
- [68SEL] Selkov, E.E., Self-oscillations in glycolysis: 1. A simple kinetic model, *Eur. J. Biochem.*, **4** (1968) 79–86.

Reference List

- [69COM] Comité International des Poids et des Mesures., The International Practical Temperature Scale of 1968, *Metrologia*, **5** (1969) 35–47.
- [69DUN/MAR] Dunn, L.A., Marshall, W.L., Electrical conductances of aqueous sodium iodide and the comparative thermodynamic behaviour of aqueous sodium halide solutions to 800° and 4000 bars, *J. Phys. Chem.*, **73** (1969) 723–728.
- [69HAN/SCH] Hansen, E.H., Schnitzer, M., Molecular weight measurements of polycarboxylic acids in water by vapor pressure osmometry, *Anal. Chim. Acta*, **46** (1969) 247–254.
- [69HAV] Havel, J., Spectrophotometric study of complex formation of uranyl with oxalic acid, *Coll. Czech. Chem. Commun.*, **34** (1969) 3248–3265.
- [69HEL] Helgeson, H.C., Thermodynamics of hydrothermal systems at elevated temperatures and pressures, *Am. J. Sci.*, **267** (1969) 729–804.
- [69KEE/KEY] Keenan, J.H., Keyes, F.G., Hill, P.G., Moore, J.G., *Steam Tables*, New York: John Wiley & Sons, 1969, 162p.
- [69KHO] Khodakovskiy, I.L., Thermodynamics of aqueous solutions of electrolytes at elevated temperatures (entropies of ions in aqueous solutions at elevated temperatures), *Geokhimiya*, (**1**) (1969) 57–63, in Russian; Engl. transl.: *Geochem. Int.*, **6** (1969) 29–34.
- [69LOB/VAS] Lobanov, G.A., Vasil'ev, V.P., Heat of water ionization in solutions of some 1-1 electrolytes at 25°C, *Izv. Vysshikh Uchebn. Zaved. SSSR. Khimiya i Khim. Teknol.*, **12** (1969), 740–743 (in Russian).
- [69NIK/TOL] Nikolaeva, N.M., Tolpygina, L.N., Hydrolysis of aluminum salts at elevated temperatures, *Izv. Sibirskogo Otdeleniya Akad. Nauk. SSSR, Ser. Khim. Nauk*, (1969), 49–55 (in Russian); *Chem. Abstr.*, 71 (1969) 108625N.
- [69PRU] Prue, J.E., Ion pairs and complexes: free energies, enthalpies, and entropies, *J. Chem. Educ.*, **46** (1969) 12–16.
- [69ROS] Rossotti, H., *Chemical applications of potentiometry*, Princeton N.J.: D. Van Nostrand, 1969, 229p.
- [69SHA/PRE] Shannon, R.D., Prewitt, C.T., Effective ionic radii in oxides and fluorides, *Acta Cryst.*, **B25** (1969) 925–946.
- [69ZUS] Zuse, K., *Rechnender Raum*, Braunschweig: Vieweg, 1969.
- [70ABE] Aberg, M., On the structures of the predominant hydrolysis products of uranyl(VI) in solution, *Acta Chem. Scand.*, **24** (1970) 2901–2915.
- [70ALT/KAR] Althaus, E., Karotke, E., Nitsch, K.H., Winkler, H.G.F., An experimental re-examination of the upper stability limit of muscovite plus quartz, *Neues. Jahrb. Mineral. Monatsh.*, 1970, pp.325–336.

Reference List

- [70BAT/STA] Bates, R.G., Staples, B.R., Robinson, R.A., Ionic hydration and single ion activities in unassociated chlorides at high ionic strengths, *Analytical Chem.*, **42** (1970) 867–871.
- [70EKE/SIL] Ekelund, R., Sillén, L.G., Wahlberg, O., Fortran editions of Haltafall and Letagrop, *Acta Chem. Scand.*, **24** (1970) 3073.
- [70FEL] Feller, W., *An Introduction to Probability Theory and its Applications*, New York: Wiley, 1970.
- [70FRA/LOU] Fraústo da Silva, J.J.R., Lourdes Sadler Simões, M., Studies on uranyl complexes-IV: Simple and polynuclear uranyl complexes of some polyaminocarboxylic acids, *J. Inorg. Nucl. Chem.*, **32** (1970) 1313–1322.
- [70GAM] Gamble, D.S., Titration curves of fulvic acid: The analytical chemistry of a weak acid polyelectrolyte, *Can. J. Chem.*, **48** (1970) 2662–2669.
- [70GAR] Gardner, M., Mathematical games. The fantastic combinations of John Conway's new solitaire game "life", *Sc. Am.*, **223** (1970) 120–123.
- [70HIN/COB] Hinchey, R.J., Cobble, J.W., The thermodynamic functions for $\text{Pu}^{3+}(\text{aq})$ and the entropies for some trivalent actinide ions, *Inorg. Chem.*, **9** (1970) 922–926.
- [70HIN/COB2] Hinchey, R.J., Cobble, J.W., Standard-state entropies for the aqueous trivalent lanthanide and yttrium ions, *Inorg. Chem.*, **9** (1970) 917–921.
- [70KLE] Kleinhempel, D., Ein Beitrag zur Theorie des Huminstoffzustandes, *Albrecht-Thaer-Archiv*, **14** (1970) 3–14.
- [70LEW] Lewis, D., Studies of redox equilibria at elevated temperatures: I. The estimation of equilibrium constants and standard potentials for aqueous systems up to 374°C, *Arkiv för Kemi*, **32** (1970) 385–404.
- [70MAR] Marshall, W.L., Complete equilibrium constants, electrolyte equilibria, and reaction rates, *J. Phys. Chem.*, **74** (1970) 346–355.
- [70RAS/KIN] Rashid, M.A., King, L.H., Major oxygen-containing functional groups present in humic and fulvic acid fractions isolated from contrasting marine environments, *Geochim. Cosmochim. Acta*, **34** (1970) 193–201.
- [70ZAI/ZHA] Zaikin, A.N., Zhabotinsky, A.M., Concentration wave propagation in two-dimensional liquid-phase self-oscillating system, *Nature*, **225** (1970) 535–537.
- [71CHA/COL] Charlot, G., Collumeau, A., Marchon, M.J.C., Selected constants. Oxidation-reduction potentials of inorganic substances in aqueous solution, *Inter. Union Pure & Appl. Chem.*, London: Butterworths, 1971.
- [71FED/KAL] Fedorov, V.A., Kalosh, T.N., Mironov, V.E., Investigation of solubility of oxybromide of bismuth(III) in solutions of perchloric acid and standard isobaric potentials of BiOBr and hydrated ion Bi^{3+} , *Zh. Neorg. Khim.*, **16** (1971) 3006–3008 (in Russian).

Reference List

- [71FIS/ZEN] Fisher, J.R., Zen, E., Thermodynamic calculations from hydrothermal phase equilibrium data and the free energy of H₂O, *Am. J. Sci.*, **270** (1971) 297–314.
- [71JEN] Jensen, K.A. (*chairman*), Nomenclature of inorganic chemistry, 2nd ed., IUPAC Commission on Nomenclature of Inorganic Chemistry, Oxford: Pergamon Press, 1971, 110p.
- [71LAN/WHI] Langmuir, D., Whittemore, D.O., Variations in the stability of precipitated ferri oxyhydroxides, in: Nonequilibrium systems in natural water chemistry (Hem, J.D., *ed.*), *Adv. Chem. Ser.*, Nr. **106**, Washington, D.C.: Amer. Chem. Soc., 1971, *pp.*209-234.
- [71NAU/RYZ] Naumov, G.B., Ryzhenko, B.N., Khodakovsky, I.L., Handbook of thermodynamic data, Moscow: Atomizdat, 1971, in Russian; Engl. transl.: Report USGS-WRD-74-001 (Soleimani, G.J., translator; Barnes I., Speltz, V., *eds.*), U.S. Geological Survey, Menlo Park, California, USA, 1974, 328p.
- [71ODI/PLI] Odier, M., Plichon, V., Le cuivre en solution dans l'eau de mer: forme chimique et dosage, *Anal. Chim. Acta*, **55** (1971) 209–220.
- [71ROS/ROS] Rossotti, F.J.C., Rossotti, H.S., Whewell, R.J., The use of electronic computing techniques in the calculation of stability constants, *J. Inorg. Nucl. Chem.*, **33** (1971) 2051–2065.
- [71SCH/COU] Scheidt, R.W., Countryman, R., Hoard, J.L., Spectrochemistry of dioxovanadium(V) complexes. III. The crystal and molecular structures of trisodium(ethylenediaminetetraacetato)dioxovanadate(V) tetrahydrate, *J. Am. Chem. Soc.*, **93** (1971) 3878–3882.
- [71SIL] Sillén, L.G., Polynuclear complexes in solution, in: Coordination Chemistry (Martell, A.E., *ed.*), Vol. I., ACS Monograph, New York: Van Nostrand Reinhold Co., 1971, *pp.*491–541.
- [71SIL/MAR] Sillén, L.G., Martell, A.E., Stability constants of metal-ion complexes, *Suppl. No. 1*, Special Publ. No. 25, London: The Chemical Society, 1971, 865p.
- [71VOL/PAV] Volokhov, Yu.A., Pavlov, L.N., Eremin, N.I., Mironov, V.E., Hydrolysis of aluminum salts, *J. Appl. Chem. USSR*, **44** (1971) 243–246.
- [71WAR/ING] Warnqvist, B., Ingri, N., The HALTAFALL program – some corrections, and comments on recent experience, *Talanta*, **18** (1971) 457–458.
- [72ARD/STE] Ardakani, M.S., Stevenson, F.J., A modified ion-exchange technique for the determination of stability constants of metal-soil organic matter complexes, *Soil Sci. Soc. Am. Proc.*, **36** (1972) 884–890.
- [72GAM] Gamble, D.S., Potentiometric titration of fulvic acid. Equivalence point calculations and acidic functional groups, *Can. J. Chem.*, **50** (1972) 2680–2690.

Reference List

- [72GER/LAV] Gerassimov, Ya.I., Lavrentev, V.I., Thermochemical properties, in: Tantalum: Physico-chemical properties of its compounds and alloys, Atomic Energy Rev., Special Issue Nbr. 3 (1972) 7–39.
- [72KER] Kerrick, D.M., Experimental determination of muscovite + quartz stability with $p_{\text{(H}_2\text{O)}} < p_{\text{(total)}}$, Am. J. Sci., **272** (1972) 946–958.
- [72MAR] Marshall, W.L., A further description of complete equilibrium constants, J. Phys. Chem., **76** (1972) 720–731.
- [72MOR/MOR] Morel, F., Morgan, J., A numerical method for computing equilibria in aqueous chemical systems, Env. Sci. Technol., **6** (1972) 58–67.
- [72SCH/KHA] Schnitzer, M., Khan, S.U., Humic substances in the environment, Marcel Dekker, New York (1972) 327pp.
- [72SER/NIK] Sergeyeva, E.I., Nikitin, A.A., Khodakovskiy, I.L., Naumov, G.B., Experimental investigation of equilibria in the system $\text{UO}_3\text{-CO}_2\text{-H}_2\text{O}$ in 25–200°C temperature interval, Geochem. Int., **9** (1972) 900–910.
- [72TOB] Tobe, M.L., Inorganic reaction mechanisms, London: Thomas Nelson & Sons Ltd., 1972, 192p.
- [72WIN] Winfree, A.T., Spiral waves of chemical activity, Science, **175** (1972) 634–636.
- [72ZIR/YAM] Zirino, A., Yamamoto, T., pH dependent model for the chemical speciation of copper, zinc, cadmium and lead in seawater, Limnol. Oceanograph., **17** (1972) 661–671.
- [72ZUN/GAL] Zunino, H., Galindo, G., Peirano, P., Aguilera, M., Use of the resin exchange method for the determination of stability constants of metal-soil organic matter complexes, Soil Sci., **114** (1972) 229–233.
- [73AHR] Ahrland, S., Thermodynamics of the stepwise formation of metal-ion complexes in aqueous solution, Structure and Bonding, **15** (1973) 167–188.
- [73BAT] Bates, R.G., Determination of pH, theory and practice, New York: John Wiley & Sons, 1973, 479p.
- [73BEN] Bennet, C.H., Logical reversibility of computation, IBM Journal of Research and Development, **17** (1973) 525–532.
- [73BRO] Bromley, L.A., Thermodynamic properties of strong electrolytes in aqueous solutions, AIChE J., **19** (1973) 313–320.
- [73DAY] Day, H.W., The high temperature stability of muscovite plus quartz, Am. Mineral., **58** (1973) 255–262.
- [73DYR/HAN] Dyrssen, D., Hansson, I., Ionic medium effects in sea water - a comparison of acidity constants of carbonic acid and boric acid in sodium chloride and synthetic sea water, Marine Chem., **1** (1973) 137–149.

Reference List

- [73EHR/JOH] Ehrhardt, H., Johannes, W., Seidel, H., Hochdrucksynthese von Kupfer(II)-carbonat, *Z. Naturforsch.*, **28b** (1973) 682.
- [73EUG/CHO] Eugster, H.P., Chou, I.M., The depositional environments of Precambrian Banded Iron-formations, *Econ. Geol.*, **68** (1973) 1144–1168.
- [73GAM/SCH] Gamble, D.S., Schnitzer, M., The chemistry of fulvic acid and its reactions with metal ions, in: Trace metals and metal-organic interactions in natural waters (Singer, P.C., *ed.*), Ann Arbor, Mich. (Ann Arbor Science), (1973) *pp.*265–302.
- [73GOR] Gordon, T.M., Determination of internally consistent thermochemical data from phase equilibrium experiments, *J. Geol.*, **81** (1973) 199–208.
- [73HUL/DES] Hultgren, R., Desai, P.D., Hawkins, D.T., Gleiser, M., Kelley, K.K., Wagman, D.D., Selected values of the thermodynamic properties of the elements, American Society for Metals, Metals Park, Ohio, USA, 1973, 630p.
- [73MAN/RAM] Manning, P.G., Ramamoorthy, S., Equilibrium studies of metal - ion complexes of interest to natural waters - VII Mixed - ligand complexes of Cu(II) involving fulvic acid as primary ligand, *J. Inorg. Nucl. Chem.*, **35** (1973) 1577–1581.
- [73PIT] Pitzer, K.S., Thermodynamics of electrolytes: I. Theoretical basis and general equations, *J. Phys. Chem.*, **77** (1973) 268–277.
- [73SHU/WOO] Shuman, M.S., Woodward, G.P., Jr., Chemical constants of metal complexes from a complexometric titration followed with anodic stripping voltammetry, *Anal. Chem.*, **45** (1973) 2032–2035.
- [73SPE] Spencer, P.J., Thermochemical properties, in: Beryllium: Physico-chemical properties of its compounds and alloys, *Atomic Energy Rev.*, special issue 4, (1973) 7–44.
- [73ZHA/ZAI] Zhabotinsky, A.M., Zaikin, A.N., Autowave processes in a distributed chemical system, *J. Theor. Biol.*, **40** (1973) 45–61.
- [74BAT] Battelle Pacific Northwest Laboratories, High-level radioactive waste management alternatives, BNWL-1900, Richland, WA, 1974.
- [74CHA/JOH] Chatterjee, N.D., Johannes, W., Thermal stability and standard thermodynamic properties of synthetic 2M₁ muscovite, KAl₂[AlSi₃O₁₀](OH)₂, *Contrib. Mineral. Petrol.*, **48** (1974) 89–114.
- [74COX/HED] Cox, B.G., Hedwig, G.R., Parker, A.J., Watts, D.W., Solvation of ions. XIX. Thermodynamic properties for transfer of single ions between protic and dipolar aprotic solvents, *Aust. J. Chem.*, **27** (1974) 477–501.
- [74ENF] Enfield, C.G., Rate of phosphorus sorption by five Oklahoma soils, *Soil. Sci. Soc. Am. Proc.*, **38** (1974) 404–407.

Reference List

- [74HEL/KIR] Helgeson, H.C., Kirkham, D.H., Theoretical prediction of the thermodynamic behavior of aqueous electrolytes at high pressures and temperatures: I. Summary of the thermodynamic/electrostatic properties of the solvent, *Am. J. Sci.*, **274** (1974) 1089–1198.
- [74MAR/SMI] Martell, A.E., Smith, R.M., Critical stability constants, Vol. 1: Amino Acids, New York: Plenum Press, 1974, 469p.
- [74MIL] Mills, K.C., Thermodynamic data for inorganic sulphides, selenides and tellurides, London: Butterworths, 1974, 845p.
- [74POU] Pourbaix, M., Atlas of electrochemical equilibria in aqueous solutions, Nat. Ass. Corrosion Engineers, Houston, Texas, and CEBELCOR, Brussels, second edition, 1974.
- [74TAR/GAR] Tardy, Y., Garrels, R.M., A method of estimating the Gibbs energies of formation of layer silicates, *Geochim. Cosmochim. Acta*, **38** (1974) 1101–1116.
- [74VAL] Valensi, G., General chemistry, in: Atlas of electrochemical equilibria in aqueous solutions (Pourbaix, M., *ed.*), Houston, Texas: Nat. Ass. Corrosion Engineers, and Brussels: CEBELCOR, 2nd ed., 1974, pp.56–67.
- [74WIL] Wilkins, R.G., The study of kinetics and mechanism of reactions of transition metal complexes, Allyn and Bacon, Inc., Boston, 1974.
- [75BER/VAN] Berg, R.L., Vanderzee, C.E., The enthalpies of solution of zinc oxide in perchloric and hydrochloric acids and the standard enthalpy of formation of aqueous zinc ion, *J. Chem. Thermodyn.*, **7** (1975) 229–239.
- [75BER/VAN2] Berg, R.L., Vanderzee, C.E., Zinc perchlorate: enthalpies of dilution with water and some enthalpies of mixing with perchloric acid, *J. Chem. Thermodyn.*, **7** (1975) 219–228.
- [75BIE] Biedermann, G., Ionic media, in: Dahlem workshop on the nature of seawater. Dahlem Konferenzen, Berlin, (1975) 339–362.
- [75CHE] Chen, C.H., A method of estimation of standard free energies of formation of silicate minerals at 298.15 K, *Am. J. Sci.*, **275** (1975) 801–817.
- [75CIA/GRI] Ciavatta, L., Grimaldi, M., Palombari, R., Thermochemical studies on the formation of chloride, thiocyanate and mononuclear hydroxo complexes of mercury(II), *J. Inorg. Nucl. Chem.*, **37** (1975) 1685–1692.
- [75ERI] Eriksson, G., Thermodynamic studies of high temperature equilibria. XII. SOLGASMIX, a computer program for calculation of equilibrium compositions in multiphase systems, *Chem. Scr.*, **8** (1975) 100–103.
- [75FED/CHE] Fedorov, V.A., Chernikova, G.E., Kuznechikhina, M.A., Kuznezova, T.I., The formation of mixed chloride-sulfate and bromide-sulfate complexes of zinc and cadmium in solutions, *Zh. Neorg. Khim.*, **20** (1975) 2912–2915 (in Russian).

Reference List

- [75FOS] Foster, S.S.D., The chalk groundwater tritium anomaly - a possible explanation, *J. Hydr.*, **25** (1975) 159–165.
- [75GME] Gmelin-Institut, Gmelins Handbuch der Anorganischen Chemie: Zinn, Teil C2, Springer-Verlag, Berlin, Heidelberg, New York, 1975, p.60.
- [75JAM/ROO] James, F., Roots, M., MINUIT – A system for function minimization and analysis of the parameter errors and correlations, *Comput. Phys. Commun.*, **10** (1975) 343–367.
- [75KHO/YEL] Khodakovskiy, I.L., Yelkin, A.Ye., Measurement of the solubility of zincite in aqueous NaOH at 100, 150 and 200°C, *Geochem. Int.*, **12(5)** (1975) 127–133.
- [75KUT/LES] Kutuzova, M.Ja., Leschishina, L.E., Fedorov, V.A., The investigation of chloride-iodide complexes of cadmium, *Zh. Neorg. Khim.*, **20** (1975) 817–820 (in Russian).
- [75MAG] Maginu, K., Reaction-diffusion equation describing morphogenesis: I. Wave-form stability of stationary wave solutions in a one dimensional model, *Mathematical Biosciences*, **27** (1975) 17–98.
- [75MAN/RIL] Mantoura, R.F.C., Riley, J.P., The use of gel filtration in the study of metal binding by humic acids and related compounds, *Anal. Chim. Acta*, **78** (1975) 193–200.
- [75MAR/SMI] Martell, A.E., Smith, R.M., Critical Stability Constants, Vol. 2: Amines, New York: Plenum Press, 1975, 415p.
- [75NRI] Nriagu, J.O., Thermochemical approximations for clay minerals, *Am. Mineral.*, **60** (1975) 834–839.
- [75RAN] Rand, M.H., Thermochemical properties, in: Thorium: Physico-chemical properties of its compounds and alloys, *Atomic Energy Rev.*, special issue 5 (1975) 7–85.
- [75SMI/MAR] Smith, R.M., Martell, A.E., Critical stability constants, Vol. 2: Amines, New York: Plenum Press, 1975, 415p.
- [76ALC/JAC] Alcock, C.B., Jacob, K.T., Zador, S., Thermochemical properties, in: Zirconium: Physico-chemical properties of its compounds and alloys, *Atomic Energy Rev.*, Special Issue Nbr. 6 (1976) 7–65.
- [76BAE/MES] Baes, C.F., Jr., Mesmer, R.E., The hydrolysis of cations, New York: Wiley & Sons, 1976, 489p.
- [76BUS/CLE] Busenberg, E., Clemency, C.V., The dissolution kinetics of feldspars at 25°C and 1 atm CO₂ partial pressure, *Geochim. Cosmochim. Acta*, **41** (1976) 41–49.
- [76DES/VIS] Desnoyers, J.E., de Visser, C., Perron, G., Picker, P., Reexamination of the heat capacities obtained by flow microcalorimetry. Recommendation for the use of a chemical standard, *J. Solution Chem.*, **5** (1976) 605–616.

Reference List

- [76FUG/OET] Fuger, J., Oetting, F.L., The chemical thermodynamics of actinide elements and compounds: Part **2**. The actinide aqueous ions, Vienna: International Atomic Energy Agency, 1976, 65p.
- [76HAA/FIS] Haas, J.L., Jr., Fisher, J.R., Simultaneous evaluation and correlation of thermodynamic data, *Am. J. Sci.*, **276** (1976) 525–545.
- [76HAR/PAZ] Hardy, J., de Pazzis, O., Pomeau, Y., Molecular dynamics of a classical lattice gas: Transport properties and time correlation functions, *Phys. Rev.*, **A 13** (1976) 1949–1961.
- [76HIE/HOG] Hietanen, S., Högfeldt, E., A potentiometric study of the solid phases in the systems $\text{Hg(I)}\text{-HCO}_3^-$ and $\text{Hg(II)}\text{-HCO}_3^-$, *Chem. Scripta*, **9** (1976) 24–29.
- [76MOR/MCC] Morss, L.R., McCue, M.C., Partial molal entropy and heat capacity of the aqueous thorium(IV) ion. Thermochemistry of thorium nitrate pentahydrate, *J. Chem. Eng. Data*, **21(3)** (1976) 337–341.
- [76NIK] Nikolaeva, N.M., Investigation of hydrolysis and complexing at elevated temperatures, *Proc. Int. Corr. Conf. Ser. 1973, NACE-4* (1976) 146–152.
- [76OET/RAN] Oetting, F.L., Rand, M.H., Ackermann, R.J., The chemical thermodynamics of actinide elements and compounds: Part **1**. The actinide elements, Vienna: International Atomic Energy Agency, 1976, 111p.
- [76OPE/HEM] Openshaw, R.E., Hemingway, B.S., Robie, R.A., Waldbaum, D.R., Krupka, K.M., The heat capacities at low temperature and entropies at 298.15 K of low albite, analbite, microcline, and sanidine, *J. Res. U.S. Geol. Surv.*, **4** (1976) 195–204.
- [76PIR/NIK] Pirozhkov, A.V., Nikolaeva, N.M., Determination the stability constants of UO_2CO_3 at the temperature from 25 to 150°C, *Izv. Sib. Otd. Akad. Nauk SSSR*, (**5**) (1976) 55–59, in Russian.
- [76SCA] Scatchard, G., *Equilibrium in solution: Surface and colloid chemistry*, Cambridge, Massachusetts: Harvard University Press, 1976, 306p.
- [76SHA] Shannon, R.D., Revised effective ionic radii and systematic studies of interatomic distances in halides and chalcogenides, *Acta Cryst.*, **A32** (1976) 751–767.
- [76SMI] Smith, R.G., Jr., Evaluation of combined applications of ultrafiltration and complexation capacity techniques to natural waters, *Anal. Chem.*, **48** (1976) 74–76.
- [76SMI/MAR] Smith, R.M., Martell, A.E., *Critical stability constants*, Vol. 4: Inorganic complexes, New York: Plenum Press, 1976, 257p.
- [76STE] Stevenson, F.J., Stability constants of Cu^{2+} , Pb^{2+} , and Cd^{2+} complexes with humic acid, *Soil Sci. Soc. Am. Proc.*, **40** (1976) 665–672.

Reference List

- [76WES/ZAC] Westall, J.C., Zachary, J.L., Morel, F.M.M., MINEQL – A computer program for the calculation of chemical equilibrium compositions of aqueous systems. MIT Technical Note TN-18, Parsons Lab., M.I.T., Cambridge, Mass., 1976. See also [82SCH, 84SCH].
- [77AND] Anderegg, G., Critical survey of stability constants of EDTA complexes, IUPAC Chemical Data Series 14, Oxford: Pergamon Press, 1977, 42p.
- [77ARA/KUM] Arai, S., Kumada, K., An interpretation of the conductometric titration curve of humic acid, *Geoderma*, **19** (1977) 21–35.
- [77BOC/RED] Bockris, J.O'M., Reddy, A.K.N., Modern electrochemistry, New York: Plenum/Rossetta, 1977, 2 vols.
- [77BUF/GRE] Buffle, J., Greter, F.L., Haerdi, W., Measurement of complexation properties of humic and fulvic acids in natural waters with lead and copper ion-selective electrodes, *Anal. Chem.*, **49** (1977) 216–222.
- [77FER] Fernelius, W.C. (*chairman*), How to name an inorganic substance, IUPAC Commission on Nomenclature of Inorganic Chemistry, Oxford: Pergamon Press, 1977, 36p.
- [77HAI/LLO] Haire, R.G., Lloyd, M.H., Milligan, W.O., Beasley, M.L., Lattice parameters of $^{244}\text{Cm}(\text{OH})_3$ and the effect of self-irradiation on crystalline $^{241}\text{Am}(\text{OH})_3$ and $^{244}\text{Cm}(\text{OH})_3$, *J. Inorg. Nucl. Chem.*, **39** (1977) 843–847.
- [77IRV/HUA] Irving, A.J., Huang, W.L., Wyllie, J., Phase relation of portlandite, $\text{Ca}(\text{OH})_2$ and brucite, $\text{Mg}(\text{OH})_2$ to 33 kilobars, *Am. J. Sci.*, **277** (1977) 313–321.
- [77MAR/SMI] Martell, A.E., Smith, R.M., Critical stability constants, Vol. 3: Other Organic Ligands, New York: Plenum Press, 1977, 495p.
- [77MEA/CRE] Means, J.L., Crerar, D.A., Amster, J.L., Application of gel filtration chromatography to evaluation of Organo-metallic interactions in natural Waters, *Limnol. Oceanography*, **22** (1977) 957–965.
- [77NIC/PRI] Nicolis, G., Prigogine, I., Self-Organization in Nonequilibrium Systems, New York: Wiley, 1977.
- [77OAK/EDW] Oakes, D.B., Edworthy, D.J., Field measurements of dispersion coefficients in the United Kingdom, in: *Groundwater Quality, Measurement, Prediction and Protection*, Water Research Centre, Reading, England, 1977.
- [77OSW/ASP] Oswald, H.R., Asper, R., Bivalent metal hydroxides, in: *Preparation and crystal growth of material with layered structures* (Lieth, R.M.A., *ed.*), Dordrecht: D. Reidel Publ. Co., 1977, pp.71–140.
- [77SAP/PAT] Sapiieszko, R.S., Patel, R.C., Matijević, E., Ferric hydrous oxide sols: 2. Thermodynamics of aqueous hydroxo and sulfato ferric complexes, *J. Phys. Chem.*, **81** (1977) 1061–1068.

Reference List

- [77SEN/CHE] Senesi, N., Chen, Y., Schnitzer, M., The role of free radicals in the oxidation and reduction of fulvic acid, *Soil Biol. Biochem.*, **9** (1977) 397–403.
- [77SPE/RAR] Spedding, F.H., Rard, J.A., Habenschuss, A., Standard state entropies of the aqueous rare earth ions, *J. Phys. Chem.*, **81**(11) (1977) 1069–1074.
- [77SPO/HOL] Sposito, G., Holtzclaw, K.M., Keech, D.A., Proton binding in fulvic-acid extracted from sewage sludge soil mixtures, *J. Am. Soil Sci. Soc.*, **41** (1977) 1119–1125.
- [77STE] Stevenson, F.J., Nature of divalent transition metal complexes of humic acids as revealed by a modified potentiometric titration method, *Soil Sci.*, **123** (1977) 10–17.
- [77TAR/GAR] Tardy, Y., Garrels, R.M., Prediction of Gibbs energies of formation of compounds from the elements: II. Monovalent and divalent metal silicates, *Geochim. Cosmochim. Acta*, **41** (1977) 87–92.
- [77TRE/MAS] Tremaine, P.R., von Massow, R., Shierman, G.R., A calculation of Gibbs free energies for ferrous ions and the solubility of magnetite in H₂O and D₂O to 300°C, *Thermochim. Acta*, **19** (1977) 287–300.
- [77WIL/KIN] Wilson, D.E., Kinney, P., Effects of polymeric charge variations on the proton-metal ion equilibria of humic materials, *Limnol. Oceanogr.*, **22** (1977) 281–289.
- [78AHR] Ahrland, S., Solvation and complex formation in protic and aprotic solvents, in: *The chemistry of nonaqueous solvents* (Lagowski, J.J., *ed.*), Vol. VA, New York: Academic Press, 1978, pp.1–62.
- [78BER/CHO] Bertha, E.L., Choppin, G.R., Interaction of humic and fulvic acids with Eu(III) and Am(III), *J. Inorg. Nucl. Chem.*, **40** (1978) 655–658.
- [78BRE/GRA] Bresnahan, W.T., Grant, C.L., Weber, J.H., Stability constants for the complexation of copper(II) ions with water and soil fulvic acids measured by an ion selective electrode, *Anal. Chem.*, **50** (1978) 1675–1679.
- [78BUS/MES] Busey, R.H., Mesmer, R.E., Thermodynamic quantities for the ionization of water in sodium chloride media to 300°C, *J. Chem. Eng. Data*, **23** (1978) 175–176.
- [78COR/OHA] Cordfunke, E.H.P., O'Hare, P.A.G., The chemical thermodynamics of actinide elements and compounds: Part 3. Miscellaneous actinide compounds, Vienna: International Atomic Energy Agency, 1978, 83p.
- [78HEL/DEL] Helgeson, H.C., Delany, J.M., Nesbitt, H.W., Bird, D.K., Summary and critique of the thermodynamic properties of rock-forming minerals, *Am. J. Sci.*, **278A** (1978) 1–220.
- [78KRA/DEC] Kragten, J., Decnop-Weever, L.G., Hydroxide complexes of cerium(III), *Talanta*, **25** (1978) 147–150.

Reference List

- [78LAN] Langmuir, D., Uranium solution - mineral equilibria at low temperatures with applications to sedimentary ore deposits, *Geochim. Cosmochim. Acta*, **42** (1978) 547–569.
- [78NIK] Nikolaeva, N.M., The hydrolysis of U^{4+} ions at elevated temperatures, *Izv. Sib. Otd. Akad. Nauk SSSR, Ser. Khim. Nauk*, **9(4)** (1978) 91–95, in Russian; Engl. transl.: Report ORNL/TR-88/2, Oak Ridge National Laboratory, Oak Ridge, Tennessee, USA, 1988, 14p.
- [78OVC/ZEL] Ovchinnikov, A.A., Zeldovich, Ya.B., Role of density fluctuations in bimolecular reaction kinetics, *Chemical Physics*, **28** (1978) 215–218.
- [78PER] Perdue, E.M., Solution Thermochemistry of humic substances. 1. Acid-base equilibria of humic acid, *Geochim. Cosmochim. Acta*, **42** (1978) 1351–1358.
- [78ROB/HEM] Robie, R.A., Hemingway, B.S., Fisher, J.R., Thermodynamic properties of minerals and related substances at 298.15 K and 1 bar (10^5 Pascals) pressure and at higher temperatures, *US Geological Survey Bulletin*, **1452** (1978) 456p.
- [78RUG/SCI] Ruggiero, P., Sciacovelli, O., Testini, C., Interesse, F.S., Spectroscopic studies on soil organic fractions. II. IR and proton NMR spectra of methylated and Unmethylated fulvic acids, *Geochim. Cosmochim. Acta*, **42** (1978) 411–416.
- [78SCH] Schnitzer, M., Humic substances: Chemistry and reactions, in: *Soil organic matter* (Schnitzer, M., Khan, S.U., eds.), (1978) pp.1–64, Amsterdam (Elsevier).
- [78SPI/SIN] Spitzer, J.J., Singh, P.P., McCurdy, K.G., Hepler, L.G., Apparent molar heat capacities and volumes of aqueous electrolytes: $CaCl_2$, $Cd(NO_3)_2$, $CoCl_2$, $Cu(ClO_4)_2$, $Mg(ClO_4)_2$, and $NiCl_2$, *J. Solution Chem.*, **7** (1978) 81–86.
- [78TAR] Tardy, Y., Relationships among Gibbs free energies of formation of compounds, *Am. J. Sci.*, **279** (1978) 217–224.
- [78TAY] Taylor, D.F., Thermodynamic properties of metal-water systems at elevated temperatures, *J. Electrochem. Soc.*, **125** (1978) 808–812.
- [78VAS/YAS2] Vasil'ev, V.P., Yasinskii, F.N., The equation for the extrapolation of heat effects to zero ionic strength, *Zh. Neorg. Khim.*, **23** (1978) 579–584 (in Russian).
- [78WED] Wedepohl, K.H., (ed.), *Handbook of Geochemistry*, Vol. **2/3**, Springer-Verlag, Berlin 1978.
- [79AHR] Ahrland, S., Complex formation in protic and aprotic media, *Pure & Appl. Chem.*, **51** (1979) 2019–2039.
- [79ALL/BEL] Allen, F.H., Bellard, S., Brice, M.D., Cartwright, B.A., Doubleday, A., Higgs, H., Hummelink, T., Hummelink-Peters, B.G., Kennard, O., Motherwell, W.D.S., Rodgers, J.R., Watson, D.G., *The Cambridge Crystallographic Data Centre: Computer-Based Search, Retrieval, Analysis and Display of Information*, *Acta Cryst.*, **B35** (1979) 2331–2339.

Reference List

- [79BER/KRA] Van den Berg, C.M.G., Kramer, J.R., Determination of complexing capacities of ligands in natural waters and conditional stability constants of the copper complexes by means of manganese dioxide, *Anal. Chim. Acta*, **106** (1979) 113–120.
- [79BRA/PIT] Bradley, D.J., Pitzer, K.S., Thermodynamics of electrolytes. 12. Dielectric properties of water and Debye-Hückel parameters to 350 °C and 1 kbar, *J. Phys. Chem.*, **83** (1979) 1599–1603.
- [79ERI] Eriksson, G., An algorithm for the computation of aqueous multicomponent, multiphase equilibria, *Anal. Chim. Acta*, **112** (1979) 375–383.
- [79FRE/CHE] Freeze, R.A., Cherry, J.A., *Groundwater*, Prentice Hall Inc. Englewood Cliffs., New Jersey, 1979.
- [79HEL] Helgeson, H.C., Mass transfer among minerals and hydrothermal solutions, in: *Geochemistry of Hydrothermal Ore Deposits*, 2nd ed. (Barnes, H.L., ed.), New York: John Wiley & Sons, 1979, 568–610.
- [79KIE] Kieffer, S.W., Thermodynamics and lattice vibrations of minerals: 1. Mineral heat capacities and their relationships to simple lattice vibrational models, *Rev. Geophys. Space Phys.*, **17** (1979) 1–19.
- [79KIE2] Kieffer, S.W., Thermodynamics and lattice vibrations of minerals: 2. Vibrational characteristics of silicates, *Rev. Geophys. Space Phys.*, **17** (1979) 20–34.
- [79KIE3] Kieffer, S.W., Thermodynamics and lattice vibrations of minerals: 3. Lattice dynamics and an approximation for minerals with application to simple substances and framework silicates, *Rev. Geophys. Space Phys.*, **17** (1979) 35–59.
- [79KRU/ROB] Krupka, K.M., Robie, R.A., Hemingway, B.S., High-temperature heat capacities of corundum, periclase anorthite, $\text{CaAl}_2\text{Si}_2\text{O}_8$ glass, muscovite, pyrophyllite, KAlSi_3O_8 glass, grossular, $\text{NaAlSi}_3\text{O}_8$, *Am. Mineral.*, **64** (1979) 86–101.
- [79LAN] Langmuir, D., Techniques of estimating thermodynamic properties for some aqueous complexes of geochemical interest, in: *Chemical Modeling in Aqueous Systems: Speciation sorption, solubility, and kinetics* (Jenne, E.A., ed.), ACS Symp. Ser. **93**, Am. Chem. Soc., Washington D.C., 1979, pp.353–387.
- [79MAG] Maginu, K., Stability of spatially homogeneous periodic solutions of reaction-diffusion equations, *J. Differential Equations*, **31** (1979) 130–138.
- [79MAT/SPO] Mattigod, S.V., Sposito, G., Chemical modeling of trace metal equilibria in contaminated soil solutions using the computer program GEOCHEM, in: *Chemical Modeling in Aqueous Systems: Speciation sorption, solubility, and kinetics* (Jenne, E.A., ed.), ACS Symp. Ser. **93**, Am. Chem. Soc., Washington D.C., 1979, pp.837–856.

Reference List

- [79NOR/PLU] Nordstrom, D.K., Plummer, L.N., Wigley, T.M.L., Wolery, T.J., Ball, J.W., Jenne, E.A., *et al.*, A comparison of computerized chemical models for equilibrium calculations in aqueous systems, in: Chemical Modeling in Aqueous Systems: Speciation sorption, solubility, and kinetics (Jenne, E.A., *ed.*), ACS Symp. Ser. **93**, Am. Chem. Soc., Washington D.C., 1979, *pp.*857–892.
- [79PER] Perdue, E.M., Solution thermochemistry of humic substances: Acid-base equilibria of river water humic substances, in: Chemical modeling in aqueous systems: Speciation, sorption, solubility, and kinetics (Jenne, E.A., *ed.*), ACS Symp. Ser., **93** (1979) 99–114.
- [79PER3] Perrin, D.D., Stability constants of metal-ion complexes, Part B: Organic ligands, IUPAC Chemical Data Series No. **22**, Pergamon Press, 1979.
- [79PIT] Pitzer, K.S., Theory: Ion interaction approach, in: Activity coefficients in electrolyte solutions (Pytkowicz, R.M., *ed.*), Vol. **I**, Boca Raton: CRC Press, 1979, *pp.*157–208.
- [79RUG/INT] Ruggiero, P., Interesse, F.S., Sciacovelli, O., Proton and carbon-13 NMR studies on the importance of aromatic structures in fulvic and humic acids, *Geochim. Cosmochim. Acta*, **43** (1979) 1771–1775.
- [79SCH2] Schnakenberg, J., Simple chemical reaction systems with limit cycle behaviour, *J. Theor. Biol.*, **81** (1979) 389–400.
- [79SIT] Sitte, P., Unterwegs zu einem neuen Weltbild der Naturwissenschaften, *Naturwissenschaften*, **66** (1979) 273.
- [79WES] Westall, J., MICROQL. II. Computation of adsorption equilibria in BASIC. Technical Report, Swiss Federal Inst. of Technology, CH-8600 Debendorf, Switzerland, 1979.
- [79WHI2] Whiffen, D.H., Manual of symbols and terminology for physicochemical quantities and units, IUPAC Commission on physicochemical symbols, terminology and units, Oxford: Pergamon Press, 1979, 41p.
- [79YAS/YOS] Yasunishi, A., Yoshida, F., Solubility of carbon dioxide in aqueous electrolyte solutions, *J. Chem. Eng. Data*, **24** (1979) 11–14.
- [80BON/HEF] Bond, A.M., Hefter, G.T., Critical survey of stability constants and related thermodynamic data of fluoride complexes in aqueous solution, IUPAC Chemical Data Series **27**, Oxford: Pergamon Press, 1980, 67p.
- [80BOO/YIP] Boon, J.-P., Yip, S., Molecular Hydrodynamics, New York: McGraw-Hill, 1980.
- [80BRE/LAM2] Brewer, L., Lamoreaux, R.H., Molybdenum: Physico-chemical properties of its compounds and alloys, *Atomic Energy Review*, IAEA, Special issue **7** (1980) 144–146 and 327–329.

Reference List

- [80BUF] Buffle, J., A critical comparison of studies of complex formation between copper(II) and fulvic substances of natural waters, *Anal. Chim. Acta*, **118** (1980) 29–44.
- [80CIA] Ciavatta, L., The specific interaction theory in evaluating ionic equilibria, *Ann. Chim. (Roma)*, **70** (1980) 551–567.
- [80CRA/GUZ] Cranwell, R.M., Guzowski, R.V., Campbell, J.E., Ortiz, N.R., Risk methodology for geologic disposal of radioactive waste. Scenario selection procedure, Technical Report NUREG/CR-1667, Sandia Nat. Lab., Albuquerque, NM, 1980.
- [80DAV/LEC] Davis, J.A., Leckie, J.O., Surface Ionization and Complexation at the Oxide/Water Interface III. Adsorption of anions, *J. Colloid. Interf. Sci.*, **74** (1980) 32–43.
- [80DAY/KUM] Day, H.W., Kumin, H.J., Thermodynamic analysis of the aluminum silicate triple point, *Am. J. Sci.*, **280** (1980) 265–287.
- [80DER/MOR] Dereppe, J., Moreaux, C., Debyser, Y., Investigation of marine and terrestrial humic substances by ^1H and ^{13}C nuclear magnetic resonance and infrared spectroscopy, *Org. Geochem.*, **2** (1980) 117–124.
- [80GAM/UND] Gamble, D.S., Underdown, A.W., Langford, C.H., Copper(II) titration of fulvic acid ligand sites with theoretical, potentiometric and spectrophotometric analysis, *Anal. Chem.*, **52** (1980) 1901–1908.
- [80HAR/BUR] Hartley, F.R., Burgess, C., Alcock, R.M., *Solution equilibria*, Chichester: Ellis Horwood Ltd., 1980, 361p.
- [80HEM/MON] Hemley, J.J., Montoya, J.W., Marinenko, J.W., Luce, R.W., Equilibria in the system $\text{Al}_2\text{O}_3\text{-SiO}_2\text{-H}_2\text{O}$ and some general implications for alteration/mineralization processes, *Econ. Geol.*, **75** (1980) 210–228.
- [80KIE] Kieffer, S.W., Thermodynamics and lattice vibrations of minerals: 4. Application to chain and sheet silicates and orthosilicates, *Rev. Geophys. Space Phys.*, **18** (1980) 862–886.
- [80LAN/HER] Langmuir, D., Herman, J.S., The mobility of thorium in natural waters at low temperature, *Geochim. Cosmochim. Acta*, **44** (1980) 1753–1766.
- [80LEM/TRE] Lemire, R.J., Tremaine, P.R., Uranium and plutonium equilibria in aqueous solutions to 200°C, *J. Chem. Eng. Data*, **25** (1980) 361–370.
- [80LI/VIC] Li, W.C., Victor, D.M., Chakrabarti, C.L., Effect of pH and uranium concentration on interaction of uranium(VI) and uranium(IV) with organic ligands in aqueous solutions, *Anal. Chem.*, **52** (1980) 520–523.
- [80LIN] Lindsay, W.T., Jr., Estimation of concentration quotients for ionic equilibria in high temperature water: the model substance approach, in: *Proc. Int. Water*

Reference List

- Conf., 41st annual meeting of the Engineers Society of Western Pennsylvania, 1980, pp.284–294.
- [80MAR/WOL] Marinsky, J.A., Wolf, A., Bunzl, K., The binding of trace amounts of lead(II), copper(II), cadmium(II), zinc(II) and calcium(II) to soil organic matter, *Talanta*, **27** (1980) 461–468.
- [80MAT/MAR] Matheron G., de Marsily, G., Is transport in porous media always diffusive? A counterexample, *Water Resour. Res.*, **16** (1980) 901–917.
- [80PAR/THO] Parkhurst, D.L., Thorstenson, D.C., Plummer, L.N., PHREEQE: A computer program for geochemical calculations, Report USGS/WRI-80–96, US Geological Survey, Reston, VA, 1980, revised Jan. 1985, 193p.
- [80PER/REU] Perdue, E.M., Reuter, J.H., Ghosal, M., The operational nature of acidic functional group analyses and its impact on mathematical descriptions of acid-base equilibriums in humic substances, *Geochim. Cosmochim. Acta*, **44** (1980) 1841–1851.
- [80REI] Reiterer, F., Löslichkeitskonstanten und Freie Bildungsenthalpien neutraler Uebergangsmetallcarbonate, Diss. Montanuniversität Leoben, 1980.
- [80RIM/BAR] Rimstidt, J.D., Barnes, H.L., The kinetics of silica-water reactions, *Geochim. Cosmochim. Acta*, **50** (1980) 2509–2516.
- [80SAA/WEB] Saar, R.A., Weber, J.H., Lead(II) complexation by fulvic acid: How it differs from fulvic acid complexation of copper(II) and cadmium(II), *Geochim. Cosmochim. Acta*, **44** (1980) 1381–1384.
- [80SAI/HAY] Saito, Y., Hayano, S., Distribution of oxygen-containing functional groups and elements in humic acids from marine sediments, *J. Oceanogr. Soc. Jap.*, **36** (1980) 59–67.
- [80SLO/MAR] Slota, P., Marinsky, J.A., An electrochemical method for the determination of the effective volume of charged polymers in solution, in: *Ions in Polymers* (Eisenberg, A., *ed.*), *Adv. Chem. Ser.*, **187**, Am. Chem. Soc., Washington, D.C., 1980, pp.313–325.
- [80SPO2] Sposito, G., Derivation of the Freundlich equation for ion exchange reactions in soils, *Soil Sci. Soc. Am. J.*, **44** (1980) 652–654.
- [80TRE/LEB] Tremaine, P.R., LeBlanc, J.C., The solubility of magnetite and the hydrolysis and oxidation of Fe^{2+} in water to 300°C, *J. Solution Chem.*, **9** (1980) 415–442.
- [80VAR/OCO] Vardeny, Z., O'Connor, P., Ray, S., Tauc, T., Optical studies of excess carrier recombination in *a*-Si:H: Evidence for dispersive diffusion, *Phys. Rev. Lett.*, **44** (1980) 1267–1271.
- [80VAS/KOZ] Vasil'ev, V.P., Kozlovskii, E.V., Mokeev, A.A., Thermodynamics of reactions of formation of halogenid complexes of mercury(II) in aqueous solution, *Zh. Neorg. Khim.*, **25** (1980) 1765–1771, (in Russian).

Reference List

- [80WES/HOH] Westall, J., Hohl, H., A comparison of electrostatic models for the oxide/solution interface, *Adv. Coll. Interf. Sci.*, **12** (1980) 265–294.
- [81AND/RUB] Anderson, M.A., Rubin, A.J., Adsorption of inorganics at solid-liquid interfaces, *Sci. Publ.*, Ann Arbor, 1981.
- [81BAE/MES] Baes, C.F., Jr., Mesmer, R.E., The thermodynamics of cation hydrolysis, *Am. J. Sci.*, **281** (1981) 935–962.
- [81CHI/AKH] Chiotti, P., Akhachinskiy, V.V., Ansara, I., Rand, M.H., The chemical thermodynamics of actinide elements and compounds: Part 5. The actinide binary alloys, Vienna: International Atomic Energy Agency, 1981, 275p.
- [81CIA/FER] Ciavatta, L., Ferri, D., Grenthe, I., Salvatore, F., Spahiu, K., Studies on metal carbonate equilibria: 3. The lanthanum(III) carbonate complexes in aqueous perchlorate media, *Acta Chem. Scand.*, **A35** (1981) 403–413.
- [81GUS/KLO] Gustafsson, E., Klockars, C.E., Studies on groundwater transport in fractured crystalline rock under controlled conditions using non-radioactive tracers, SKB-TR-81-07, Swedish Nucl. Fuel Waste Manag. Co., Stockholm, Sweden, 1981.
- [81HEL/KIR] Helgeson, H.C., Kirkham, D.H., Flowers, G.C., Theoretical prediction of the thermodynamic behavior of aqueous electrolytes at high pressures and temperatures: IV. Calculation of activity coefficients, osmotic coefficients, and apparent molal and standard and relative partial molal properties to 600°C and 5 kb, *Am. J. Sci.*, **281** (1981) 1249–1516.
- [81HEM/KRU] Hemingway, B.S., Krupka, K.M., Robie, R.A., Heat capacities of the alkali feldspars between 350 and 1000 K from differential scanning calorimetry, the thermodynamic functions of the alkali feldspars from 298.15 to 1400 K, and the reaction quartz + jadeite = analbite, *Am. Mineral.*, **66** (1981) 1202–1215.
- [81HIR] Hirata, S., Stability constants for the complexes of transition-metal ions with fulvic and humic acids in sediments measured by gel filtration, *Talanta*, **28** (1981) 809–815.
- [81JAY/PAR] Jaycock, M.J., Parfitt, G.D., Chemistry of Interfaces, Chapter 2, Ellis Horwood, Chichester, 1981.
- [81LAS/KIR] Lasaga, A.C., Kirkpatrick, R.J. (*eds.*), Kinetics of geochemical processes, Reviews in Mineralogy, Vol. 8, Washington, D.C.: Mineral. Soc. Amer., 1981.
- [81MAR/FRA] Marshall, W.L., Franck, E.U., Ion product of water substance, 0–1000°C, 1–10000 bars. New international formulation and its background, *J. Phys. Chem. Ref. Data*, **10** (1981) 295–304.
- [81OHM/FOR] Öhman, L.-O., Forsling, W., Equilibrium and structural studies of silicon(IV) and aluminum(III) in aqueous solution: 3. A potentiometric study of aluminum(III) hydrolysis and aluminum(III) hydroxo carbonates in 0.6 M NaCl, *Acta Chem. Scand.*, **A35** (1981) 795–802.

Reference List

- [81PIC/GRI] Pickens, J.F., Grisak, G.E., Scale-dependent dispersion in a stratified granular aquifer, *Water Resour. Res.*, **17** (1981) 1191–1211.
- [81REI/JOH] Reiterer, F., Johannes, W., Gamsjäger, H., Semimicro determination of solubility constants: Copper(II) Carbonate and Iron(II) carbonate, *Mikrochim. Acta*, (1981) 62.
- [81RYZ] Ryzhenko, B.N., Equilibria in hydrothermal solutions, Moscow: Nauka, 1981, in Russian. 191p.
- [81SKO/WIL] Skogerboe, R.K., Wilson, S.A., Reduction of ionic species by fulvic acid, *Anal. Chem.*, **53** (1981) 228–232.
- [81SPE] Spencer, P.J., Thermochemical properties, in: *Hafnium: Physico-chemical properties of its compounds and alloys*, Atomic Energy Rev., Special Issue Nbr. 8 (1981) 9–53.
- [81STU/MOR] Stumm, W., Morgan, J.J., *Aquatic Chemistry. An introduction emphasizing chemical equilibria in natural waters*, 2nd ed., New York: John Wiley and Sons, (1981) 780p.
- [81TAN/FRI] Tang, D.H., Frind, E.O., Sudicky, E.A., Contaminant transport in fractured porous media: Analytical solution for a single fracture, *Water Resour. Res.*, **17** (1981) 555–564.
- [81THU/MAL] Thurman, E.M., Malcolm, R.L., Preparative isolation of aquatic humus substances, *Environ. Sci. Technol.*, **15** (1981) 463–466.
- [81TRU/WEB] Truitt, R.E., Weber, J.H., Determination of complexing capacity of fulvic acid for copper(II) and cadmium(II) by dialysis titration, *Anal. Chem.*, **53** (1981) 337–342.
- [82AHR] Ahrland, S., Solvation and complex formation - Competing and cooperative processes in solution, *Pure & Appl. Chem.*, **54** (1982) 1451–1468.
- [82BER/CON] Berlekamp, E.R., Conway, J.H., Guy, R.K., *Winning Ways for your Mathematical Games*, Vol. **2**, London: Academic Press, 1982.
- [82BIE/BRU] Biedermann, G., Bruno, J., Ferri, D., Grenthe, I., Salvatore, F., Spahiu, K., Modelling of the migration of lanthanoids and actinoids in ground water; the medium dependence of equilibrium constants, in: *Sci. Basis Nucl. Waste Management V* (Lutze, W., *ed.*), *Mat. Res. Soc. Symp. Proc.*, **11** (1982) 791–800.
- [82BIL/SCH] Bilinski, H., Schindler, P., Solubility and equilibrium constants of lead in carbonate solutions (25°C, $I = 0.3 \text{ mol} \cdot \text{dm}^3$), *Geochim. Cosmochim. Acta*, **46** (1982) 921–928.
- [82BRY/RAF] Bryzgalin, O.V., Rafal'skiy, R.P., Estimation of instability constants for ore-element complexes at elevated temperatures, *Geochem. Int.*, **19** (3) (1982) 158–168.

Reference List

- [82COB/MUR] Cobble, J.W., Murray, R.C., Jr., Turner, P.J., Chen, K., High-temperature thermodynamic data for species in aqueous solution, Report EPRI-NP-2400, Electric Power Research Institute, Palo Alto, California, 1982.
- [82DRE] Drever, J.I., The geochemistry of natural waters, Englewood Cliffs, N.J.: Prentice-Hall, 1982, 388p.
- [82FRE/TOF] Fredkin, E., Toffoli, T., Conservative logic, *Int. J. Theor. Phys.*, **21** (1982) 219–253.
- [82GIB] Gibbs, G.V., Molecules as models for bonding in silicates, *Am. Mineral.*, **67** (1982) 421–450.
- [82GIL/RIL] Gillam, A.H., Riley, J.P., Microscale functional group analysis of marine and sedimentary humic substances, *Anal. Chim. Acta*, **141** (1982) 287–299.
- [82HAL/CHA] Halbach, H., Chatterjee, N.D., The use of linear parametric programming for determination of internally consistent thermodynamic data for minerals, in: High-pressure researches in geoscience (Schreyer, W., *eds.*), E. Schweizerbart'sche Verlagsbuchhandlung, Stuttgart, 1982, 475–491.
- [82HEL] Helgeson, H.C., Errata: Thermodynamics of minerals, reactions, and aqueous solutions at high pressures and temperatures, *Am. J. Sci.*, **282** (1982) 1143–1149.
- [82HEM/HAA] Hemingway, B.S., Haas, J.L., Jr., Robinson, G.R., Jr., Thermodynamic properties of selected minerals in the system $\text{Al}_2\text{O}_3\text{-CaO-SiO}_2\text{-H}_2\text{O}$ at 298.15 K and 1 bar pressure and at higher temperatures, *US Geological Survey Bull.*, **1544** (1982) 70p.
- [82HOG] Högfelddt, E., Stability constants of metal-ion complexes. Part A: Inorganic ligands. IUPAC Chemical Data Series, No. 21. Pergamon Press, 1982, 310p.
- [82LAF] Laffitte, M. (*chairman*), A report of IUPAC commission I.2 on thermodynamics: Notation for states and processes, significance of the word “standard” in chemical thermodynamics, and remarks on commonly tabulated forms of thermodynamic functions, *J. Chem. Thermodyn.*, **14** (1982) 805–815.
- [82LAP/PIN] Lapidus, L., Pinder, G.F., Numerical solution of partial differential equations in science and engineering, John Wiley Sons, New York, 1982.
- [82MAR/SMI] Martell, A.E., Smith, R.M., Critical stability constants, Vol. 5: First supplement, New York: Plenum Press, 1982, 604p.
- [82MAY] Maya, L., Hydrolysis and carbonate complexation of dioxouranium(VI) in the neutral-pH range at 25°C, *Inorg. Chem.*, **21** (1982) 2895–2898.
- [82PAT/SLO] Patterson, C.S., Slocum, G.H., Busey, R.H., Mesmer, R.E., Carbonate equilibria in hydrothermal systems: first ionization of carbonic acid in NaCl media to 300°C, *Geochim. Cosmochim. Acta*, **46** (1982) 1653–1663.

Reference List

- [82PEI/PIT] Peiper, J.C., Pitzer, K.S., Thermodynamics of aqueous carbonate solutions including mixtures of sodium carbonate, bicarbonate and chloride, *J. Chem. Thermodyn.*, **14** (1982) 613–638.
- [82PER] Perrin, D.D., Ionisation constants of inorganic acids and bases in aqueous solution, 2nd ed., IUPAC Chemical Data Series **29**, Oxford: Pergamon Press, 1982, 180p.
- [82PLU/BUS] Plummer, L.N., Busenberg, E., The solubilities of calcite, aragonite and vaterite in CO₂-H₂O solutions between 0 and 90°C, and an evaluation of the aqueous model for the system CaCO₃-CO₂-H₂O, *Geochim. Cosmochim. Acta*, **46** (1982) 1011–1040.
- [82PRI/NAY] Prickett, T.A., Naymik, T., Lonquist, G., A “random-walk” solute transport model for selected groundwater quality evaluations, *Illinois State Water Survey, Bulletin* **65** (1982).
- [82RAI/WEB] Rainville, D.P., Weber, J.H., Complexing capacity of soil fulvic acid for Cu²⁺, Cd²⁺, Mn²⁺, Ni²⁺ and Zn²⁺ measured by dialysis titration: A model based on soil fulvic acid aggregation, *Can. J. Chem.*, **60** (1982) 1–5.
- [82ROY] Roy, R., *Radioactive Waste Disposal, Vol. 1: The Waste Package*, Pergamon Press, New York, 1982, *pp.* 88, 221.
- [82SAV/ROB] Savage, D., Robbins, J.E., The interaction of borosilicate glass and granodiorite at 100°C, 50 MPa, Implications for models of radionuclide release, In W. Lutze (*ed.*): *Scientific Bases for Nuclear Waste Management V*, North Holland, 1982, *p.* 145.
- [82SCH] Schweingruber, M., User’s guide for extended MINEQL (EIR version) – standard subroutine / data library package. Technical Report EIR TM-45-82-38, Swiss Federal Institute for Reactor Research, 1982. See also [76WES/ZAC].
- [82SCH/KER] Schramke, J.K., Kerrick, D.M., Blencoe, J.G., The experimental determination of the brucite = periclase + water equilibrium with a new volumetric technique, *Am. Mineral.*, **67** (1982) 269–276.
- [82SIN] Singer, M., The vitality of mythical numbers, in: *Judgement under uncertainty: Heuristics and biases* (Kahneman, D., *ed.*), Cambridge: Cambridge Univ. Press, 1982, reprinted 1993, *pp.* 408–413.
- [82STE] Stevenson, F.J., *Humus Chemistry, Genesis, Composition, Reactions*, Wiley-Interscience, New York, (1982).
- [82SUD/FRI] Sudicky, E.A., Frind, E.O., Contaminant transport in fractured porous media: Analytical solution for a system of parallel fracture, *Water Resour. Res.*, **18** (1982) 1634–1642.
- [82THU/MIL] Thurmond, V., Millero, F.J., Ionization of carbonic acid in sodium chloride solutions at 25°C, *J. Solution Chem.*, **11** (1982) 447–456.

Reference List

- [82WAG/EVA] Wagman, D.D., Evans, W.H., Parker, V.B., Schumm, R.H., Halow, I., Bailey, S.M., Churney, K.L., Nuttall, R.L., The NBS tables of chemical thermodynamic properties: Selected values for inorganic and C₁ and C₂ organic substances in SI units, *J. Phys. Chem. Ref. Data*, **11**, Suppl. No. **2** (1982) 1–392.
- [83ABE/FER] Aberg, M., Ferri, D., Glaser, J., Grenthe, I., Studies of metal carbonate equilibria. VIII. Structure of the hexakis(carbonato)tri[dioxouranate(VI)] ion in aqueous solution. An X-ray diffraction and ¹³C NMR study, *Inorg. Chem.*, **22** (1983) 3981–3985.
- [83ALB/GIE] Alberts, J.J., Giesy, J.P., Conditional stability constants of trace metals and naturally occurring humic materials: Application in equilibrium models and verification with field data, in: *Aquatic and terrestrial humic materials* (Christman, R.F., Gjessing, E.T., eds.), Ann Arbor, Mich. (Ann Arbor Science), (1983) *pp.*333.
- [83BER/SIE] Bergerhoff, G., Hundt, R., Sievers, R., Brown, I.D., The Inorganic Crystal Structure Data Base, *J. Chem. Inf. Comput. Sci.*, **23** (1983) 66–69.
- [83BRI] Brice, L.K., Le Chatelier's principle: The effect of temperature on the solubility of solids in liquids, *J. Chem. Educ.*, **60** (1983) 387–389.
- [83BRY] Bryzgalin, O.V., An electrostatic model for the instability constants of tungsten hydroxy complexes at elevated temperatures, *Geochem. Int.*, **20** (1) (1983) 150–157.
- [83CAB/SHU] Cabaniss, S.E., Shuman, M.S., Collins, B.J., Metal-organic binding: A comparison of models, in: *Developments in biogeochemistry* (Kramer, C.J.M., Duinker, J.C., eds.), **1** (1983) 165–179, (Martinus Nijhoff/Dr. W. Junk).
- [83CHE/ARA] Chen, C.M., Aral, K., Theus, G.J., Computer-calculated potential pH diagrams to 300°C, Vol. 2: Handbook of diagrams. Technical report EPRI-NP-3137, Electric Power Research Inst., Palo Alto, California, 1983.
- [83DEM/OME] Dempsey, B.A., Omelia, C.R., Proton and calcium complexation of four fulvic acid fractions, in: *Aquatic and terrestrial humic materials* (Christman, R.F., Gjessing, E.T., eds.), Ann Arbor, Mich. (Ann Arbor Science), (1983) *pp.*239–273.
- [83FLE/PLU] Fleming, G.W., Plummer, L.N., PHRQINPT – An interactive computer program for constructing input data sets to the geochemical simulation program PHREEQE. Technical Report USGS/WRI-83-4236, U.S. Geological Survey, 1983.
- [83FUG/PAR] Fuger, J., Parker, V.B., Hubbard, W.N., Oetting, F.L., The chemical thermodynamics of actinide elements and compounds: Part **8**. The actinide halides, Vienna: International Atomic Energy Agency, 1983, 267p.

Reference List

- [83GIL/WIL] Gillam, A.H., Wilson, M.A., Application of ^{13}C -NMR spectroscopy to the structural elucidation of dissolved marine humic substances and their phytoplanktonic precursors, in: Aquatic and terrestrial humic materials (Christman, R.F., Gjessing, E.T., *eds.*), Ann Arbor, Mich. (Ann Arbor Science), (1983) *pp.*25–35.
- [83GRA/SJO] Granberg, I., Sjöberg, S., Metal complexes with mixed ligands: 26. Complex formation between cadmium(II) imizadoles and chloride ions. A potentiometric and solubility study in mixed 3.0 M (Na)ClO₄,Cl media, Acta Chem. Scand., **A37** (1983) 415–422.
- [83HAR/BOR] Harvey, G.R., Boran, D.A., Chesal, L.A., Tokar, J.M., The structure of marine fulvic and humic acids, Mar. Chem., **12** (1983) 119–132.
- [83HAT/BRE] Hatcher, P.G., Breger, I.A., Dennis, L.W., Maciel, G.E., Solid-state carbon-13-NMR of sedimentary humic substances: New revelations on their chemical composition, in: Aquatic and terrestrial humic materials (Christman, R.F., Gjessing, E.T., *eds.*), 1983, *pp.*37–81.
- [83HER] Herrmann, A.G., Radioaktive Abfälle, Springer-Verlag, Berlin, 1983, *p.*40.
- [83HOG] Högfeldt, E., Stability constants of metal-ion complexes, Part A: Inorganic ligands, Pergamon Press, New York (1983).
- [83KBS] KBS-3, Final storage of spent nuclear fuel, Swedish Nuclear Fuel Supply Co., Division KBS, 1983, Stockholm, Sweden.
- [83KUB] Kubaschewski, O., Thermochemical properties, in: Titanium: Physico-chemical properties of its compounds and alloys, Atomic Energy Rev., Special Issue Nbr. 9 (1983) 3–71.
- [83LEV/KAM] Levelt Sengers, J.M.H., Kamgar-Parsi, B., Balfour, F.W., Sengers, J.V., Thermodynamic properties of steam in the critical region, J. Phys. Chem. Ref. Data, **12** (1983) 1–28.
- [83MAD/FRE] Madore, B.F., Freedman, W.L., Computer simulations of the Belousov-Zhabotinsky reaction, Science, **222** (1983) 615–616.
- [83MAY] Maya, L., Hydrolysis and carbonate complexation of dioxoneptunium(V) in 1.0 M NaClO₄ at 25°C, Inorg. Chem., **22** (1983) 2093–2095.
- [83MCK/FED] McKnight, D.M., Feder, G.L., Thurman, E.M., Wershaw, R.L., Westall, J.C., Complexation of copper by aquatic humic substances from different environments, Sci. Total Environ., **28** (1983) 65–76.
- [83MIL/TUS] Miles, C.J., Tuschall, J.R., Jr., Brezonik, P.L., Isolation of aquatic humus with diethylaminoethylcellulose, Anal. Chem., **55** (1983) 410–411.
- [83MIL2] Millero, F.J., The estimation of the pK_{HA}^* of acids in seawater using the Pitzer equations, Geochim. Cosmochim. Acta, **47** (1983) 2121–2129.

Reference List

- [83MIY/KLE] Miyano, T., Klein, C., Phase relations of orthopyroxene, olivine and grunerite in high-grade metamorphic iron-formation, *Am. Mineral.*, **68** (1983) 699–716.
- [83MOR/WIL] Morss, L.R., Williams, C.W., Enthalpies of formation of strontium dichloride and of the strontium ion (Sr^{2+}) in water and in $1 \text{ mol}\cdot\text{dm}^{-3}$ HCl, and an assessment of the enthalpies of formation of alkaline-earth dichlorides, *J. Chem. Thermodyn.*, **15** (1983) 279–285.
- [83MUR/LIN] Murray, K., Linder, P.W., Fulvic acids - Structure and metal binding. I. A random molecular model, *J. Soil Sci.*, **34** (1983) 511–523.
- [83PAL/ELD] Palmer, D.A., Van Eldik, R., The chemistry of metal carbonato and carbon dioxide complexes, *Cem. Rev.*, **83** (1983) 651–731.
- [83PER/LYT] Perdue, E.M., Lytle, C.R., A critical examination of metal-ligand complexation models: Application to defined multiligand mixtures, in: *Aquatic and terrestrial humic materials* (Christman, R.F., Gjessing, E.T., eds.), Ann Arbor, Michigan: Ann Arbor Science, 1983, pp.295–313.
- [83PER/LYT2] Perdue, E.M., Lytle, C.R., Distribution model for binding protons and metal ions by humic substances, *Environ. Sci. Technol.*, **17** (1983) 654–660.
- [83PHI/SIL] Phillips, S.L., Silvester, L.F., Use of balanced-like-charges approach to metal-bicarbonate reactions, *Inorg. Chem.*, **22** (1983) 3848–3851.
- [83PIT] Pitzer, K.S., Thermodynamics of unsymmetrical electrolyte mixtures. Enthalpy and heat capacity, *J. Phys. Chem.*, **87** (1983) 2360–2364.
- [83PLE/JOS] Plechanov, N., Josefsson, B., Dyrssen, D., Lundquist, K., Investigations on humic substances in natural waters, in: *Aquatic and terrestrial humic materials* (Christman, R.F., Gjessing, E.T., eds.), Ann Arbor, Michigan: Ann Arbor Science, 1983, pp.387–405.
- [83PUI] Puigdomenech, I., INPUT, SED and PREDOM: computer programs drawing equilibrium diagrams. Technical Report TRITA-OKK-3010, Dept. Inorg. Chem., The Royal Institute of Technology, 100 44 Stockholm, Sweden, 1983, 12p.
- [83ROB/HAA] Robinson, G.R., Jr., Haas, J.L., Jr., Heat capacity, relative enthalpy, and calorimetric entropy of silicate minerals: an empirical method of prediction, *Am. Mineral.*, **68** (1983) 541–553.
- [83RYA/HOL] Ryan, D.K., Holden, L.J., Ventry, L.S., Fluorescence quenching studies of Cu^{2+} complexation by humic materials: Theory and comparison of data treatments, *Abstr. Pap. Am. Chem. Soc.*, **193** (1983) abstract ENVR-91.
- [83SHU/COL] Shuman, M.S., Collins, B.J., Fitzgerald, P.J., Olson, D.L., Distribution of stability constants and dissociation rate constants among binding sites on estuarine copper-organic complexes: Rotated disk electrode studies and an affinity spectrum analysis of ion-selective electrode and photometric data, in:

Reference List

- Aquatic and terrestrial humic materials (Christman, R.F., Gjessing, E.T., *eds.*), (1983) *pp.*349–370, Ann Arbor, Mich. (Ann Arbor Sci.).
- [83SPA] Spahiu, K., Carbonate complex formation in lanthanoid and actinoid systems, Ph.D. thesis, The Royal Institute of Technology, Stockholm, Sweden, 1983.
- [83STA/BUF] Staub, C., Buffle, J., Haerdi, W., Application of ultrafiltration for the determination of stability constants of zinc(II) complexes with regards to metal speciation in natural water, 4th Internat. Conf. on Heavy Metals in the Environ., **2** (1983) 1227–1230.
- [83TAK/YOS] Takamatsu, T., Yoshida, T., Determination of stability constants of metal-humic acid complexes by potentiometric titration and ion-selective electrodes, *Soil Sci.*, **125** (1983) 377–386.
- [83TOR] Torres, R.A., Humic acid complexation of europium, americium, and plutonium, Diss. Florida State Univ., Diss. Abstr. Int. B, **43** (1983) 2901, Univ. Microfilm Int. Order N° DA8304084.
- [83TOU/WIL] Toussaint, D., Wilczek, F., Particle-antiparticle annihilation in diffusive motion, *J. Chem. Phys.*, **78** (1983) 2642–2647.
- [83TUS/BRE] Tuschall, J.R., Jr., Brezonik, P.L., Complexation of heavy metals by aquatic humus: A comparative study of five analytical methods, in: *Aquatic and terrestrial humic materials* (Christman, R.F., Gjessing, E.T., *eds.*), Ann Arbor, Michigan: Ann Arbor Science, 1983, *pp.*275–294.
- [83WES] Westrum, E.F., Jr., Lattice and Schottky contributions to the morphology of lanthanide heat capacities, *J. Chem. Thermodyn.*, **15** (1983) 305–325.
- [83WIL/MCN] Wilson, J.T., McNabb, J.F., Wilson, B.H., Noonan, M.J., Biotransformation of selected organic pollutants in groundwater, *Developments in Industrial Microbiology*, **24** (1983) 225–233.
- [83WOL] Wolery, T.J., EQ3NR: A computer program for geochemical aqueous speciation-solubility calculations: User's guide and documentation, Report UCRL-53414, Lawrence Livermore National Laboratory, Livermore, California, 1983, 191p.
- [84ALE/ESC] Alegret, S., Escalas, M.T., Marinsky, J.A., Gel speciation studies. II. An extension of earlier studies of protonation equilibria of cross-linked carboxymethyldextran, *Talanta*, **31** (1984) 683–687.
- [84ANA/ATK] Ananthaswamy, J., Atkinson, G., Thermodynamics of concentrated electrolyte mixtures. 4. Pitzer-Debye-Hückel limiting slopes for water from 0 to 100°C and from 1 atm to 1 kbar, *J. Chem. Eng. Data*, **29** (1984) 81–87.
- [84BER4] Van den Berg, C.M.G., Determination of the complexing capacity and conditional stability constants of complexes of copper(II) with natural organic ligands in seawater by cathodic stripping voltammetry of copper-catechol complex ions, *Marine Chem.*, **15** (1984) 1–18.

Reference List

- [84BUF/STA] Buffle, J., Staub, C., Measurement of complexation properties of metal ions in natural conditions by ultrafiltration: Measurement of equilibrium constants for complexation of zinc by synthetic and natural ligands, *Anal. Chem.*, **56** (1984) 2837–2842.
- [84CAB/SHU] Cabaniss, S.E., Shuman, M.S., Collins, B.J., Metal-organic binding: A comparison of models, in: *Complexation of Trace Metals in Natural Waters* (Kramer, C.J.M., Duinker, J.C., *eds.*) Martinus Nijhof and Dr W. Junk Publish., The Hague, Boston, Lancaster, 1984, *pp.*165–179.
- [84COU/MIC] Couturier, Y., Michard, G., Sarazin, G., Constantes de formation des complexes hydroxydés de l'aluminium en solution aqueuse de 20 a 70°C, *Geochim. Cosmochim. Acta*, **48** (1984) 649–659, in French.
- [84FAR/TOF] Farmer, D., Toffoli, T., Wolfram, S., *eds.*, Cellular Automata, Proc. of an Interdisciplinary Workshop, Los Alamos, March 1983, *Physica*, **D 10** (1984) Nos. 1 & 2.
- [84FIT/STE] Fitch, A., Stevenson, F.J., Comparison of models for determining stability constants of metal complexes with humic substances, *J. Am. Soil Sci. Soc.*, **48** (1984) 1044–1050.
- [84FLO/HAS] Flotow, H.E., Haschke, J.M., Yamauchi, S., The chemical thermodynamics of actinide elements and compounds: Part **9**. The actinide hydrides, Vienna: International Atomic Energy Agency, 1984, 115p.
- [84FRA/MAR] Frantz, J.D., Marshall, W.L., Electrical conductances and ionization constants of salts, acids, and bases in supercritical aqueous fluids: I. Hydrochloric acid from 100° to 700°C and at pressures to 4000 bars, *Am. J. Sci.*, **284** (1984) 651–667.
- [84FRE] Freeman, R.D., Conversion of standard (1 atm) thermodynamic data to the new standard-state pressure, 1 bar (10^5 Pa), *J. Chem. Eng. Data*, **29** (1984) 105–111.
- [84GRE/EAR] Greenwood, N.N., Earnshaw, A., *Chemistry of the elements*, Pergamon Press, Oxford 1984; *Chemie der Elemente*, VCH Verlagsgesellschaft, Weinheim 1988.
- [84GRO/DRO] Grønvold, F., Drowart, J., Westrum, E.F., Jr., The chemical thermodynamics of actinide elements and compounds: Part **4**. The actinide chalcogenides (excluding oxides), Vienna: International Atomic Energy Agency, 1984, 265p.
- [84GUS/KLO] Gustafsson, E., Klockars, C.E., Study of strontium and cesium migration in fractured crystalline rock, SKB-TR-84-07, Swedish Nucl. Fuel Waste Manag. Co., Stockholm, Sweden, 1984.
- [84HAA/GAL] Haar, L., Gallagher, J.S., Kell, G.S., NBS/NRC Steam tables, Thermodynamic and transport properties and computer programs for vapor and liquid states of water in SI units, Washington: Hemisphere Publ. Co., 1984, 320p.

Reference List

- [84HAR/MOL] Harvie, C.E., Møller, N., Weare, J.H., The prediction of mineral solubilities in natural waters: the Na-K-Mg-Ca-H-Cl-SO₄-OH-HCO₃-CO₂-H₂O system to high ionic strengths at 25°C, *Geochim. Cosmochim. Acta*, **48** (1984) 723–751.
- [84HEL/MUR] Helgeson, H.C., Murphy, W.M., Aagard, P., Thermodynamic and kinetic constraints on reaction rates among minerals and aqueous solutions II. Rate constants, effective surface area and the hydrolysis of feldspar, *Geochim. Cosmochim. Acta*, **48**(12) (1984) 2405–2432.
- [84HIL] Hillis, W.D., The connection machine: A computer architecture based on cellular automata, *Physica*, **D 10** (1984) 213–228.
- [84HOL/RAN] Holley, C.E., Jr., Rand, M.H., Storms, E.K., The chemical thermodynamics of actinide elements and compounds: Part **6**. The actinide carbides, Vienna: International Atomic Energy Agency, 1984, 101p.
- [84HOS] Hostettler, J.D., Electrode electrons, aqueous electrons, and redox potentials in natural waters, *Am. J. Sci.*, **284** (1984) 734–759.
- [84KES/SEN] Kestin, J., Sengers, J.V., Kamgar-Parsi, B., Levelt Sengers, J.M.H., Thermo-physical properties of fluid H₂O, *J. Phys. Chem. Ref. Data*, **13** (1984) 175–183.
- [84LIN/RUN] Lindberg, R.D., Runnels, D.D., Ground water redox reactions: an analysis of equilibrium state applied to Eh measurements and geochemical modeling, *Science*, **225** (1984) 925–927.
- [84MAR/RED] Marinsky, J.A., Reddy, M.M., Proton and metal ion binding to natural organic polyelectrolytes; I. Studies with model compounds, *Org. Geochem.*, **7** (1984) 207–214.
- [84MAR/RED2] Marinsky, J.A., Reddy, M.M., Proton and metal ion binding to natural organic polyelectrolytes; II. Preliminary investigation with a peat and a humic acid, *Org. Geochem.*, **7** (1984) 215–221.
- [84MAR2] Margolus, N., Physics-like models of computation, *Physica*, **10 D** (1984) 81–95.
- [84MER/MAR] Merle, Y., Marinsky, J.A., Gel speciation studies. I. The intrinsic dissociation constant of weakly acidic cation-exchange gels, *Talanta*, **31** (1984) 199–204.
- [84NOR/BAL] Nordstrom, D.K., Ball, J.W., Chemical models, computer programs and metal complexation in natural waters, in: *Developments in biogeochemistry* (Kramer, C.J.M., Duinker, J.C., eds.), **1** (1984) 149–164, (Martinus Nijhoff/Dr. W. Junk).
- [84NOR/BIN] Norton, P.R., Binder, P.E., Griffiths, K., Jackman, T.E., Davies, J.A., Rustig, J., Kinetic oscillations in oxidation of Co over Pt(100) – A study by Rutherford backscattering, nuclear microanalysis, LEED, and work function techniques, *J. Chem. Phys.*, **80** (1984) 3859–3865.

Reference List

- [84PAT/BUS] Patterson, C.S., Busey, R.H., Mesmer, R.E., Second ionization of carbonic acid in NaCl media to 250°C, *J. Solution Chem.*, **13** (1984) 647–661.
- [84PER/REU] Perdue, E.M., Reuter, J.H., Parrishi, R.S., A statistical model of proton binding by humus, *Geochim. Cosmochim. Acta*, **48** (1984) 1257–1263.
- [84PHI/SIL] Phillips, S.L., Silvester, L.F., A data base for nuclear waste disposal for temperatures up to 300°C, *High Temp. High Pressures*, **16** (1984) 81–91.
- [84PIT/PEI] Pitzer, K.S., Peiper, J.C., Busey, R.H., Thermodynamic properties of aqueous sodium chloride solutions, *J. Phys. Chem. Ref. Data*, **13** (1984) 1–102.
- [84PRE/DUF] Preston, K., Duff, M., *Modern Cellular Automata: Theory and Applications*, New York: Plenum, 1984.
- [84PRE/SCH] Preston, C.M., Schnitzer, M., Effects of chemical modifications and extractants on the carbon-13 NMR spectra of humic materials, *J. Am. Soil Sci. Soc.*, **48** (1984) 305–311.
- [84PRO/EIN] Prokuev, V.A., Eintrop, R.V., Belousov, E.A., The polarographic investigation of complexation of cadmium(II) in perchlorate-chloride solutions of magnesium and calcium, *Zh. Neorg. Khim.*, **29** (1984) 1599–1600 (in Russian).
- [84ROB/HEM3] Robie, R.A., Hemingway, B.S., Entropies of kyanite, andalusite and sillimanite: Additional constraints on the pressure and temperature of the Al_2SiO_5 triple point, *Am. Mineral.*, **69** (1984) 298–306.
- [84SCH] Schweingruber, M., Revision 1 of: User's guide for extended MINEQL (EIR version) - standard subroutine / data library package. Technical Report EIR AN-45-84-39, Swiss Federal Institute for Reactor Research, 1984.
- [84STA/BUF] Staub, C., Buffle, J., Haerdi, W., Measurement of complexation properties of metal ions in natural conditions by ultrafiltration: Influence of various factors on the retention of metals and ligands by neutral and negatively charged membranes, *Anal. Chem.*, **56** (1984) 2843–2849.
- [84TOR/CHO] Torres, R.A., Choppin, G.R., Europium(III) and americium(III) stability constants with humic acid, *Radiochim. Acta*, **35** (1984) 143–148.
- [84WAI/MOR] Waite, T.D., Morel, F.M.M., Ligand exchange and fluorescence quenching studies of the fulvic acid-iron interaction. Effects of pH and light, *Anal. Chim. Acta*, **162** (1984) 263–274.
- [85AHN/CHA] Ahn, J., Chambré, P.L., Pigford, T.H., Nuclide migration through a planar fissure with matrix diffusion, LBL-19429, April 1985, Earth Sci. Div., Lawrence Berkeley Laboratory.
- [85AIK/MCK] Aiken, G.R., McKnight, D.M., Wershaw, R.L., Maccarthy, P., *eds.*, Humic substances in soil, sediment, and water: Geochemistry, Isolation, and Characterization, (1985) 691p., (John Wiley & Sons).

Reference List

- [85BAR/PAR] Bard, J.A., Parsons, R., Jordan, J. (*eds.*) Standard Potentials in Aqueous Solution, International Union of Pure and Applied Chemistry, New York: Marcel Dekker, Inc., 1985, 834p.
- [85BER/BRO2] Berman, R.G., Brown, T.H., Heat capacity of minerals in the system $\text{Na}_2\text{O}-\text{K}_2\text{O}-\text{CaO}-\text{MgO}-\text{FeO}-\text{Fe}_2\text{O}_3-\text{Al}_2\text{O}_3-\text{SiO}_2-\text{TiO}_2-\text{H}_2\text{O}-\text{CO}_2$: Representation, estimation, and high temperature extrapolation, *Contrib. Mineral. Petrol.*, **89** (1985) 168–183.
- [85CAC] Caceci, M.S., The interactions of humic acid with europium(III). Complexation strength as a function of load and pH, *Radiochim. Acta*, **39** (1985) 51–56.
- [85CAR] Carlsen, L., Radionuclide-soil organic matter interactions (Final Report Part 1), European Applied Research Report, **6** (1985) 1419–1476.
- [85CHA/DAV] Chase, M.W., Davies, C.A., Downey, J.R., Frurip, D.J., McDonald, R.A., Syverud, A.N., JANAF thermochemical tables, 3rd ed., *J. Phys. Chem. Ref. Data*, **14**, suppl. 1 (1985).
- [85FER/GRE] Ferri, D., Grenthe, I., Hietanen, S., Néker-Neumann, E., Salvatore, F., Studies on metal carbonate equilibria: 12. Zinc(II) carbonate complexes in acid solution, *Acta Chem. Scand.*, **A39** (1985) 347–353.
- [85FIS/MOR] Fish, W., Morel, F.M.M., Propagation of error in fulvic titration data: A comparison of three analytical methods, *Can. J. Chem.*, **63** (1985) 1185–1193.
- [85GAM/MAR] Gamble, D.S., Marinsky, J.A., Langford, C.H., Humic-trace metal ion equilibria in natural waters, in: Ion exchange and solvent extraction (Marinsky, J.A., Marcus, Y., *eds.*), *Adv. Chem. Ser.*, **9**, Chapter 7, (1985), (Marcel Dekker).
- [85HIL/GUR] Hildenbrand, D.L., Gurvich, L.V., Yungman, V.S., The chemical thermodynamics of actinide elements and compounds: Part **13**. The gaseous actinide ions, Vienna: International Atomic Energy Agency, 1985, 187p.
- [85JAC/HEL] Jackson, K.J., Helgeson, H.C., Chemical and thermodynamic constraints on the hydrothermal transport and deposition of tin: I. Calculation of the solubility of cassiterite at high pressures and temperatures, *Geochim. Cosmochim. Acta*, **49** (1985) 1–22.
- [85KAN/RED] Kang, K., Redner, S., Fluctuation-dominated kinetics in diffusion-controlled reactions, *Phys. Rev.*, **A 32** (1985) 435–447.
- [85KAU/URB] Kaufman, M., Urbain, J., Thomas, R., Towards a logical analysis of the immune-response, *J. Theor. Biol.*, **114** (1985) 527–561.
- [85KOT/SUC] Kotrlý, S., Šücha, L., Handbook of chemical equilibria in analytical chemistry, New York: Ellis Horwood Ltd, Chichester 1985, 414p.
- [85LIC] Lichtner, P.C., Continuum model for simultaneous chemical reactions and mass transport in hydrothermal systems, *Geochim. Cosmochim. Acta*, **49** (1985) 779–800.

Reference List

- [85MAR] Marinsky, J.A., An interpretation of the sensitivity of weakly acidic (basic) polyelectrolyte (cross-linked and linear) equilibria to excess neutral salt, *J. Phys. Chem.*, **89** (1985) 5294–5302.
- [85MOR/STO] Morgan, J.J., Stone, A.T., Kinetics of Chemical Processes of Importance in Lacustrine Environments, in: *Chemical Processes in Lakes*, (Stumm, W., *ed.*), Wiley-Interscience, New York, 1985, 435 pp.
- [85PAX/WED] Paxéus, N., Wedborg, M., Acid-base properties of aquatic fulvic acid, *Anal. Chim. Acta*, **169** (1985) 87–98.
- [85PRO/BEL] Prokuev, V.A., Belousov, E.A., The potentiometric investigation of complexation of cadmium(II) with chloride ions in aqueous solutions of $\text{Mg}(\text{ClO}_4)_2$, *Zh. Neorg. Khim.*, **30** (1985) 1203–1205.
- [85RYZ/BRY] Ryzhenko, B.N., Bryzgalin, O.V., Reference neutrality points for the redox and acid-base properties of aqueous solutions at the parameters for hydrothermal ore formation, *Geochem. Int.*, **22** (1) (1985) 88–93.
- [85RYZ/SHA] Ryzhenko, B.N., Shapkin, A.I., Bryzgalin, O.V., Electrolytic dissociation of metal sulfates in water solution, *Geochem. Int.*, **22** (8) (1985) 5–11.
- [85SOH/NOV] Söhnle, O., Novotný, P., Densities of aqueous solutions of inorganic substances, Amsterdam: Elsevier, 1985, 335p.
- [85SPA] Spahiu, K., Studies on metal carbonate equilibria: 11. Yttrium(III) carbonate complex formation in aqueous perchlorate media of various ionic strengths, *Acta Chem. Scand.*, **A 39** (1985) 33–45.
- [85SUN/JAN] Sundman, B., Jansson, B., Andersson, J.O., The thermo-Calcdatabank system, *Calphad*, **9** (1985) 153–190.
- [85THU] Thurman, E.M., Organic geochemistry of natural waters, Dordrecht: Kluwer Acad. Publish., 1985, 497p.
- [85ZUU/WEI] Zuurdeg, B.W., Van der Weiden, M.J.J., Geochemical aspects of European bottled waters. Geothermics, thermal-mineral waters and hydrogeology, *Theophrastus Publ. Athens.*, 1985, 235–264.
- [86BER/ENG] Berman, R.G., Engi, M., Greenwood, H.J., Brown, T.H., Derivation of internally-consistent thermodynamic data by the technique of mathematical programming: a review with application to the system $\text{MgO-SiO}_2\text{-H}_2\text{O}$, *J. Petrol.*, **27** (1986) 1331–1364.
- [86BRU] Bruno, J., Stoichiometric and structural studies on the $\text{Be}^{2+}\text{-H}_2\text{O-CO}_2(\text{g})$ system, Ph.D. thesis, The Royal Institute of Technology, Stockholm, Sweden, 1986.
- [86BRY] Bryzgalin, O.V., Estimating dissociation constants in the supercritical region for some strong electrolytes from an electrostatic model, *Geochem. Int.*, **23** (2) (1986) 84–95.

Reference List

- [86COD] CODATA recommended values for the fundamental constants 1986., Committee on Data for Science and Technology (CODATA), Newsletter No. 38, Paris: International Council of Scientific Unions, 1986, 12p.
- [86COE] Coello, J., Studies on extraction equilibria from chloride solutions using tri-laurylamine. Techn. Lic. Thesis, Dept. Inorg. Chem., The Royal Institute of Technology, Stockholm, Sweden, 1986.
- [86DAV] David, F., Thermodynamic properties of the lanthanide and actinide ions in aqueous solution, *J. Less-Common Met.*, **121** (1986) 27–42.
- [86DAV2] David, F., Oxidation reduction and thermodynamic properties of curium and heavier actinide elements, in: *Handbook on the physics and chemistry of the actinides*, Vol. 4 (Freeman, A.J., Keller, C., *eds.*), Amsterdam: North-Holland, 1986, *pp.*97–128.
- [86DZO/FIS] Dzombak, D.A., Fish, W., Morel, F.M.M., Metal-humate interactions. 1. Discrete ligand and continuous distribution models, *Environ. Sci. Technol.*, **20** (1986) 669–675.
- [86EDE/GOF] Edelstein, N.M., Goffart, J., Magnetic properties, Chapter 18, in: *The chemistry of the actinide elements*, Vol. 2, 2nd. ed. (Katz, J.J., Seaborg, G.T., Morss, L.R., *eds.*), London: Chapman and Hall, 1986, *pp.*1361–1387.
- [86EPH/ALE] Ephraim, J., Alegret, S., Mathuthu, A., Bicking, M., Malcolm, R.L., Marinsky, J.A., A unified physicochemical description of the protonation and metal ion complexation equilibria of natural organic acids (humic and fulvic acids). 2. Influence of polyelectrolyte properties and functional group heterogeneity on the protonation equilibria of fulvic acid, *Environ. Sci. Technol.*, **20** (1986) 354–366.
- [86EPH/MAR] Ephraim, J., Marinsky, J.A., A unified physicochemical description of the protonation and metal ion complexation equilibria of natural organic acids (humic and fulvic acids). 3. Influence of polyelectrolyte properties and functional group heterogeneity on the copper ion binding equilibria of in armandale horizons Bh fulvic acid sample, *Environ. Sci. Technol.*, **20** (1986) 367–376.
- [86FIS/DZO] Fish, W., Dzombak, D.A., Morel, F.M.M., Metal-humate Interactions. 2. Application and comparison of models, *Environ. Sci. Technol.*, **20** (1986) 676–683.
- [86FIT/STE] Fitch, A., Stevenson, F.J., Chen, Y., Complexation of copper(II) with a soil humic acid: Response characteristics of the copper(II) ion-selective electrode and ligand concentration effects, *Org. Geochem.*, **9** (1986) 109–116.
- [86FRI/HAS] Frisch, U., Hasslacher, B., Pomeau, Y., Lattice-gas automata fo the Navier-Stokes equation, *Phys. Rev. Lett.*, **56** (1986) 1505–1508.
- [86GIL/WIL] Gillam, A.H., Wilson, M.A., Structural analysis of aquatic humic substances by NMR spectroscopy, in: *Organic marine geochemistry* (Sohn, M.L., *ed.*),

Reference List

- ACS Symp. Ser. **305**, Washington, D.C.: American Chemical Soc., 1986, 128–141.
- [86GRE/RIG] Grenthe, I., Riglet, C., Vitorge, P., Studies of metal-carbonate complexes: 14. Composition and equilibria of trinuclear neptunium(VI)- and plutonium(VI)-carbonates complexes, *Inorg. Chem.*, **25** (1986) 1679–1684.
- [86INT] INTRACOIN, International Nuclide Transport Code Intercomparison Study, Final reports level 1, September 1984, and levels 2 and 3, May 1986, The Swedish Nuclear Power Inspectorate (SKI), Stockholm, Sweden.
- [86MAE] Maeda, M., Estimation of medium effect on enthalpy changes for ionization of water and ammonium ion in aqueous solution, *J. Phys. Chem.*, **90** (1986) 1134–1137.
- [86MAR/EPH] Marinsky, J.A., Ephraim, J., A unified physicochemical description of the protonation and metal ion complexation equilibria of natural organic acids (humic and fulvic acids), 1. Analysis of the influence of polyelectrolyte properties on protonation equilibria in ionic media: Fundamental concepts, *Environ. Sci. Technol.*, **20** (1986) 349–354.
- [86MAR3] de Marsily, G., *Quantitative Hydrogeology: Groundwater Hydrology for Engineers*, San Diego: Academic Press, 1986.
- [86MCK/BAR] McKibben, M.A., Barnes, H.L., Oxidation of pyrite in low temperature acidic solutions: Rate laws and surface textures, *Geochim. Cosmochim. Acta*, **50** (1986) 1509–1520.
- [86NOR/MUN] Nordstrom, D.K., Munoz, J.L., *Geochemical Thermodynamics*, Palo Alto: Blackwell Sci. Publ., 1986, 477p.
- [86PAC] Paces, T., Weathering rates of gneiss and depletion of exchangeable cations in soil under environmental acidification, *J. Geol. Soc.*, **143** (1986) 673–677.
- [86RIE/BOL] van Riemsdijk, W.H., Bolt, G.H., Koopal, L.K., Blaakmeer, J., Electrolyte adsorption on heterogeneous surfaces: Adsorption models, *J. Coll. Interf. Sci.*, **109** (1986) 219–228.
- [86ROY/GIB] Roy, R.N., Gibbons, J.J., Roy, L.N., Greene, M.A., Thermodynamics of the unsymmetrical mixed electrolyte HCl-SrCl₂. Applications of Pitzer's equations, *J. Phys. Chem.*, **90** (1986) 6242–6247.
- [86SMI/POP] Smith, R.W., Popp, C.J., Norman, D.I., The dissociation of oxy-acids at elevated temperatures, *Geochim. Cosmochim. Acta*, **50** (1986) 137–142.
- [86TRE/SWA] Tremaine, P.R., Sway, K., Barbero, J.A., The apparent molar heat capacity of aqueous hydrochloric acid from 10 to 140°C, *J. Solution Chem.*, **15** (1986) 1–22.

Reference List

- [86TUR/VAR] Turner, D.R., Varney, M.S., Whitfield, M., Mantoura, R.F.C., Riley, J.P., Electrochemical studies of copper and lead complexation by fulvic acid. I. Potentiometric measurements and a critical comparison of metal binding models, *Geochim. Cosmochim. Acta*, **50** (1986) 289–297.
- [86WER] Wershaw, R.L., A new model for humic materials and their interactions with hydrophobic organic chemicals in soil-water or sediment-water systems, in: *Transport and transformation of organic contaminants* (Macalady, D.L., *ed.*), *J. Contaminant Hydrology*, **1** (1986) 29–45.
- [86WES] Westall, J.C., MICROQL: A chemical equilibrium program in BASIC. Version 2 for PCs. Report 86–02, Dept. of Chemistry, Oregon State University, Corvallis, OR, (1986) 44p.
- [86WOL] Wolfram, S., *ed.*, *Theory and Applications of Cellular Automata*, Adv. Series on Complex Systems, Vol. **1**, Singapore: World Scientific, 1986.
- [87ASP/BUR] Aspray, W., Burks, A., *eds.*, *Papers of John von Neumann on Computing and Computer Theory*, Charles Babbage Institute Reprint Series for the History of Computing, Cambridge: MIT Press, MA, 1987.
- [87BAL/HAY] Balasubramanian, K., Hayot, F., Saam, W.F., Darcy's law from lattice-gas hydrodynamics, *Phys. Rev.*, **A 36** (1987) 2248–2253.
- [87BOG/LEV] Boghosian, B.M., Levermore, C.D., A cellular automaton for Burgers' equation, *Complex Systems*, **1** (1987) 17–30.
- [87BRU/CAS] Bruno, J., Casas, I., Lagerman, B., Muñoz, M., The determination of the solubility of amorphous $\text{UO}_2(\text{s})$ and the mononuclear hydrolysis constants of uranium(IV) at 25°C, *Sci. Basis Nucl. Waste Management X*, (Bates, J.K., Seefeldt, W.B., *eds.*), held 1–4 December, 1986, in Boston, Massachusetts, *Mat. Rec. Soc. Symp. Proc.*, **84** (1987) 153–160.
- [87BUF/ALT] Buffle, J., Altmann, R.S., Interpretation of metal complexation by heterogeneous complexants, in: *Aquatic surface chemistry: Chemical processes at the particle-water interface* (Stumm, W., *eds.*), (1987) *pp.*351–383, (J. Wiley & Sons).
- [87BUF/VUI] Buffle, J., Vuileumier, J.J., Tercier, M.L., Parthasarathy, N., Voltammetric study of humic and fulvic substances. V. Interpretation of metal ion complexation measured by anodic stripping voltammetric methods, *Sci. Total Environ.*, **62** (1987) 75–96.
- [87CHE/MAT] Chen, H., Matthaeus, W.H., New cellular automaton model for magnetohydrodynamics, *Phys. Rev. Lett.*, **58** (1987) 1845–1848.
- [87CIA/IUL] Ciavatta, L., Iuliano, M., Porto, R., The hydrolysis of the La(III) ion in aqueous perchlorate solution at 60°C, *Polyhedron*, **6** (1987) 1283–1290.

Reference List

- [87COM/MID] Comans, R.N.J., Middelburg, J.J., Sorption of trace metals on calcite: Applicability of the surface precipitation model, *Geochim. Cosmochim. Acta*, **51** (1987) 2587–2591.
- [87COT/WIL] Cotton, F.A., Wilkinson, G., Gaus, P.L., Basic inorganic chemistry, 2nd edition, Chapter 3, 4, New York: John Wiley & Sons, 1987.
- [87DEC/COL] Decarreau, A., Colin, F., Herbillon, A., Manceau, A., Nahon, D., Paquet, H., Trauth-Badaud, D., Trescases, J.J., Domain Segregation in Ni-Fe-Mg-Smectites, *Clays and Clay Minerals*, **35** (1987) 1–10.
- [87GAR/PAR] Garvin, D., Parker, V.B., White, H.J., Jr., CODATA thermodynamic tables: Selections for some compounds of calcium and related mixtures: A prototype set of tables, Washington, D.C.: Hemisphere Publishing Corp., 1987, 356p.
- [87GOO/CHE] Goodman, B.A., Cheshire, M.V., Characterization of iron-fulvic acid complexes using Mössbauer and EPR spectroscopy, *Sci. Total Environ.*, **62** (1987) 229–240.
- [87GRE/POW] Gregor, J.E., Powell, H.K.J., Effects of extraction procedures on fulvic acid properties, *Sci. Total Environ.*, **62** (1987) 3–12.
- [87HED/SJO] Hedlund, T., Sjöberg, S., Öhman, L.-O., Equilibrium and structural studies of silicon(IV) and aluminum(III) in aqueous solution: 15. A potentiometric study of speciation and equilibria in the Al^{3+} - $\text{CO}_2(\text{g})$ - OH^- system, *Acta Chem. Scand.*, **A41** (1987) 197–207.
- [87KAT/GOR] Katakis, D., Gordon, G., Mechanisms of inorganic reactions, New York: Wiley-Interscience, 1987, 384p.
- [87MON/DOO] Montgomery, D., Doolen, G.D., Magnetohydrodynamic cellular automata, *Phys. Lett.*, **A 120** (1987) 229–231.
- [87OTT] Ottonello, G., Energies and interactions in binary (Pbnm) orthosilicates: A Born parametrization, *Geochim. Cosmochim. Acta*, **51** (1987) 3119–3135.
- [87PER/PAR] Perdue, E.M., Parrish, R.S., Fitting multisite binding equilibria to statistical distribution models: Turbo Pascal program for Gaussian models, *Comput. Geosci.*, **13** (1987) 587–601.
- [87PET/HOS] Peterson, S.R., Hostetler, C.J., Deutsch, W.J., Cowan, C.E., MINTEQA user's manual, Report NUREG/CR-4808, PNL-6106, 1987, U.S. Nuclear Regulatory Commission, Washington, D.C.
- [87PHU/PIT] Phutela, R.C., Pitzer, K.S., Saluja, P.P.S., Thermodynamics of aqueous magnesium chloride, calcium chloride, and strontium chloride at elevated temperatures, *J. Chem. Eng. Data*, **32** (1987) 76–80.
- [87PRE/FLA] Press, W.H., Flannery, B.P., Teukolsky, S.A., Vetterling, W.T., Numerical Recipes. The Art of Scientific Computing, Cambridge: Cambridge University Press, 1987.

Reference List

- [87RIV] Rivet, J.-P., Green-Kubo formalism for lattice gas hydrodynamics and Monte-Carlo evaluation of shear viscosities, *Complex Systems*, **1** (1987) 839–851.
- [87RYZ/BRY] Ryzhenko, B.N., Bryzgalin, O.V., Dissociation of acids under hydrothermal conditions, *Geochem. Int.*, **24** (8) (1987) 122–127.
- [87SAX/FEI] Saxena, S.K., Fei, Y., Fluids at crustal pressures and temperatures: I. Pure species, *Contrib. Mineral. Petrol.*, **95** (1987) 370–375.
- [87SAX/FEI2] Saxena, S.K., Fei, Y., High pressure and high temperature fluid fugacities, *Geochim. Cosmochim. Acta*, **15** (1987) 783–791.
- [87SCH/STU] Schindler, P.W., Stumm, W., The surface chemistry of oxides, hydroxides and oxide minerals, in: *Aquatic Surface Chemistry* (Stumm, W., *ed.*), New York, John Wiley & Sons, 1987, *pp.*83–110.
- [87STU] Stumm, W. (*ed.*), *Aquatic surface chemistry. Chemical processes at the particle-water interface*, John Wiley & Sons, New York, 1987.
- [87SVE] Sverjensky, D.A., Calculation of the thermodynamic properties of aqueous species and the solubilities of minerals in supercritical electrolyte solutions, in: *Thermodynamic Modelling of Geologic Materials: Minerals, Fluids and Melts* (Carmichael, I.S.E., Eugster, H.P., *eds.*), Washington, D.C.: Mineral. Soc. Am., 1987, *pp.*177–210.
- [87TOF/MAR] Toffoli, T., Margolus, N., *Cellular Automata Machines: A New Environment for Modeling*, Cambridge: MIT Press, 1987.
- [87TUR/VAR] Turner, D.R., Varney, M.S., Whitfield, M., Mantoura, R.F.C., Riley, J.P., Electrochemical studies of copper and lead complexation by fulvic acid. II. A critical comparison of potentiometric and polarographic measurements, *Sci. Total Environ.*, **60** (1987) 17–34.
- [87WEA] Weast, R.C. (*ed.*): *CRC Handbook of Chemistry and Physics*, 68rd *ed.* CRC Press, Boca Raton 1987.
- [87WES] Westall, J.C., Adsorption mechanisms in aquatic surface chemistry, in: *Aquatic Surface Chemistry*, (Stumm, W., *ed.*), New York, John Wiley & Sons, 1987, *pp.*3–32.
- [87WIK] Wikberg, P., The chemistry of deep groundwaters in crystalline rocks, Ph D Thesis, 1987, Dep. Inorg. Chem., The Royal Institute of Technology, Stockholm, Sweden.
- [88ALT/BUF] Altmann, R.S., Buffle, J., The use of differential equilibrium functions for interpretation of metal binding in complex ligand systems: Its relation to site occupation and site affinity distribution, *Geochim. Cosmochim. Acta*, **52** (1988) 1505–1519.

Reference List

- [88BER] Berman, R.G., Internally-consistent thermodynamic data for minerals in the system $\text{Na}_2\text{O-K}_2\text{O-CaO-MgO-FeO-Fe}_2\text{O}_3\text{-Al}_2\text{O}_3\text{-SiO}_2\text{-TiO}_2\text{-H}_2\text{O-CO}_2$, *J. Petrol.*, **29** (1988) 445–522.
- [88BRO] Brookins, D.G., Eh-pH diagrams for geochemistry, Springer-Verlag, Berlin, 1988, 176*p*.
- [88BRO/HER] Brodkey, R.S., Hershey, H.C., Transport phenomena. A unified approach, McGraw-Hill Book Company, New York, 1988.
- [88BUF] Buffle, J., Complexation reactions in aquatic systems: An analytical approach, Chichester: Ellis Horwood Ltd, 1988, 692*p*.
- [88CAB/SHU] Cabaniss, S.E., Shuman, M.S., Copper binding by dissolved organic matter: I. Suwannee River fulvic acid equilibria, *Geochim. Cosmochim. Acta*, **52** (1988) 185–193.
- [88CHE/CHE] Chen, H., Chen, S., Doolen, G.D., Lee, Y.C., Simple lattice gas models for waves, *Complex Systems*, **2** (1988) 259–267.
- [88CIA] Ciavatta, L., Private communication, cited by Grenthe *et al.* in the NEA-TDB review on uranium thermodynamics [92GRE/FUG], Università de Napoli, Naples, Italy, June 1988.
- [88COR] Cornell, R.M., The influence of some divalent cations on the transformation of ferrihydrite to more crystalline products, *Clay Minerals* **23** (1988) 329.
- [88COT/WIL] Cotton, F.A., Wilkinson, G., Advanced inorganic chemistry, 5*th* edition, New York: Wiley-Interscience, 1988.
- [88GAM/LAN] Gamble, D.S., Langford, C.H., Complexing equilibria in mixed ligand systems: Tests of theory with computer simulations, *Environ. Sci. Technol.*, **22** (1988) 1325–1336.
- [88GRA] Grauer, R., The chemical behaviour of montmorillonite in a repository back-fill, NTB 88-24E; Zum chemischen Verhalten von Montmorillonit in einer Endlagerverfüllung, PSI-Bericht Nr. 11 (1988).
- [88GRE/POW] Gregor, J.E., Powell, H.K.J., Protonation reactions of fulvic acids, *J. Soil Sci.*, **39** (1988) 243–252.
- [88HAL/OES] Hallberg, R.O., Oestlund, P., Wadsten, T., Inferences from a corrosion study of a bronze cannon, applied to high level nuclear waste disposal, *Appl. Geochem.*, **3** (1988) 273–280.
- [88HAZ] Hazen, R.M., A useful fiction: polyhedral modeling of mineral properties, *Am. J. Sci.*, **288-A** (1988) 242–269.
- [88HED] Hedlund, T., Studies of complexation and precipitation equilibria in some aqueous aluminium(III) systems, Ph.D. thesis, University of Umeå, Umeå, Sweden, 1988.

Reference List

- [88HER/MOR] Hering, J.G., Morel, F.M.M., Kinetics of trace metal complexation: Role of alkaline-earth metals, *Environ. Sci. Technol.*, **22** (1988) 1469–1478.
- [88HOV/HEP] Hovey, J.K., Hepler, L.G., Tremaine, P.R., Thermodynamics of aqueous aluminate ion: standard partial molar heat capacities and volumes of $\text{Al}(\text{OH})_4^-$ (aq) from 10 to 55°C, *J. Phys. Chem.*, **92** (1988) 1323–1332.
- [88JAC/WOL] Jackson, K.J., Wolery, T.J., Bourcier, W.L., Delany, J.M., Moore, R.M., Clinick, M.L., Lundeen, S.R., MCRT user's guide and documentation, Report UCID-21406 Rev. 1, Lawrence Livermore National Laboratory, Livermore, California, USA, 1988, 93p.
- [88KIM/FRE] Kim, H.-T., Frederic, W.J., Jr., Evaluation of Pitzer ion interaction parameters of aqueous electrolytes at 25°C: 1. Single salt parameters, *J. Chem. Eng. Data*, **33** (1988) 177–184.
- [88LAD/COL] Ladd, A.J.C., Colvin, M.E., Frenkel, D., Application of lattice-gas cellular automata to the Brownian-motion of solids in suspension, *Phys. Rev. Lett.*, **60** (1988) 975–978.
- [88LIC] Lichtner, P.C., The quasi-stationary state approximation to coupled mass-transport and fluids rock interaction in a porous medium, *Geochim. Cosmochim. Acta*, **52** (1988) 143–165.
- [88MAR/RED] Marinsky, J.A., Reddy, M.M., Ephraim, J., Mathuthu, A., Ion binding by humic and fulvic acids: A computational procedure based on functional site heterogeneity and the physical chemistry of polyelectrolyte solutions, SKB-TR-88-01, Swedish Nucl. Fuel Waste Manag. Co., Stockholm, Sweden, 1988.
- [88MES/MAR] Mesmer, R.E., Marshall, W.L., Palmer, D.A., Simonson, J.M., Holmes, H.F., Thermodynamics of aqueous association and ionization reactions at high temperatures and pressures, *J. Solution Chem.*, **17**(8) (1988) 699–718.
- [88MIL/CVI] Mills, I., Cvitaš, T., Homann, K., Kallay, N., Kuchitsu, K., Quantities, units and symbols in physical chemistry, IUPAC, Oxford: Blackwell Scientific Publications, 1988, 134p.
- [88PAG] PAGIS, Performance assessment of geological isolation systems for radioactive waste, EUR 11775 EN, CEC, Luxembourg, 1988.
- [88PAL/DRU] Palmer, D.A., Drummond, S.E., Potentiometric determination of the molal formation constants of ferrous acetate complexes in aqueous solutions to high temperatures, *J. Phys. Chem.*, **92** (1988) 6795–6800.
- [88PAP/HAY] Papelis, C., Hayes, K.F., Leckie, J.O., HYDRAQL: A program for the computation of chemical equilibrium composition of aqueous batch systems including surface complexation modeling of ion adsorption at the oxide/solution interface, Technical Report N°306, Environmental Engineering and Science, (1988) Stanford University.

Reference List

- [88PLU/PAR] Plummer, L.N., Parkhurst, D.L., Fleming, G.W., Dunkle, S.A., A computer program incorporating Pitzer's equations for calculation of geochemical reactions in brines, Water Resources Investigations Report 88-4153, U.S. Geol. Survey, Reston, Virginia, 1988, 310p.
- [88ROT] Rothman, D.H., Cellular-automaton fluids – A model for flow in porous-media, *Geophysics*, **53** (1988) 509–518.
- [88ROT/KEL] Rothman, D.H., Keller, J.M., Immiscible cellular-automaton fluids, *J. Stat. Phys.*, **52** (1988) 1119–1127.
- [88RUA] Ruaya, J.R., Estimation of instability constants of metal chloride complexes in hydrothermal solutions up to 300°C, *Geochim. Cosmochim. Acta*, **52** (1988) 1983–1996.
- [88SAX] Saxena, S.K., Assessment of thermal expansion, bulk modulus and heat capacity of enstatite and forsterite, *J. Phys. Chem. Solids*, **49** (1988) 1233–1235.
- [88SHO/HEL] Shock, E.L., Helgeson, H.C., Calculation of the thermodynamic and transport properties of aqueous species at high pressures and temperatures: Correlation algorithms for ionic species and equation of state predictions to 5 kb and 1000°C, *Geochim. Cosmochim. Acta*, **52** (1988) 2009–2036.
- [88SUC/SAN] Succi, S., Santangelo, P., Benzi, R., High-resolution lattice-gas simulation of two-dimensional turbulence, *Phys. Rev. Lett.*, **60** (1988) 2738–2740.
- [88TAN/HEL] Tanger, IV, J.C., Helgeson, H.C., Calculation of the thermodynamic and transport properties of aqueous species at high pressures and temperatures: Revised equations of state for the standard partial molal properties of ions and electrolytes, *Am. J. Sci.*, **288** (1988) 19–98.
- [88TIP/BAC] Tipping, E., Backes, C.A., Hurley, M.A., The complexation of protons, aluminium and calcium by aquatic humic substances: a model incorporating binding site heterogeneity and macroionic effects, *Wat. Res.*, **22** (1988) 597–611.
- [88ULR/STU] Ulrich, H.J., Stumm, W., Cosovic, B., Adsorption of aliphatic fatty acids on aquatic interfaces. Comparisons between two model surfaces: the mercury electrode and δ -Al₂O₃ colloids, *Environ. Sci. Technol.*, **22** (1988) 1–37.
- [88WAN] Wanner, H., The NEA Thermochemical Data Base Project, *Radiochim. Acta*, **44/45** (1988) 325–329.
- [89ALC/SHA] Alcamo, J., Shaw, R., Hordijk, L., The rains model of acidification, Kluwer Academic Publishers, (1989).
- [89ATK] Atkins, P.W., General Chemistry, New York: Scientific American Books, 1989, 989p.
- [89BRA] Bratsch, S.G., Standard electrode potentials and temperature coefficients in water at 298.15 K, *J. Phys. Chem. Ref. Data*, **18** (1989) 1–21.

Reference List

- [89BRA/AKS] Bradbury, M.H., Aksoyoglu, S., Alexander, W.R., Baeyens, B., Hoehn, E., Keil, R., Mantovani, M., Meyer, J., Mazurek, M., Bajo, C., Laboratory investigations in support of the migration experiment at the Grimsel test site, PSI-Bericht Nr. 28, Würenlingen und Villigen, 1989 and Nagra Technical Report NTB 88-23, NAGRA, Baden, 1989.
- [89BRY] Bryzgalin, O.V., Electrostatic-model estimates of electrolyte dissociation constants up to 800°C and 5 kbar, *Geochem. Int.*, **26** (3) (1989) 63–70.
- [89CAB/MOR] Cabaniss, S.E., Morel, F.M.M., Comment on “A unified physicochemical description of protonation and metal complexation equilibria of natural organic acids (humic and fulvic acids)”, and Marinsky, J.A., Reply on this comment, *Environ. Sci. Technol.*, **23** (1989) 746–748.
- [89CHE/RIM] Chermak, J.A., Rimstidt, J.D., Estimating the thermodynamic properties of silicate minerals at 298 K from the sum of polyhedral contributions, *Am. Mineral.*, **74** (1989) 1023–1031.
- [89CHO/GAR] Chou, L., Garrels, R.M., Wollast, R., Comparative study of the kinetics and mechanisms of dissolution of carbonate minerals, *Chemical Geology*, **78** (1989) 269–282.
- [89COX/WAG] Cox, J.D., Wagman, D.D., Medvedev, V.A., CODATA Key Values for Thermodynamics, New York: Hemisphere Publishing Corp., (1989), 271p.
- [89DAB/BOO] Dab, D., Boon, J.-P., in: Cellular Automata and Modeling of Complex Physical Systems (Manneville, P., *et al.*, eds.), Berlin: Springer, (1989) *pp.*257–273.
- [89DAG] Dagan, G., Flow and transport in porous formations, Springer-Verlag, Berlin, 1989.
- [89EPH/BOR] Ephraim, J.H., Borén, H., Pettersson, C., Arsenie, I., Allard, B., A novel description of the acid-base properties of an aquatic fulvic acid, *Environ. Sci. Technol.*, **23** (1989) 356–362.
- [89EPH/BOR2] Ephraim, J.H., Borén, H., Arsenie, I., Pettersson, C., Allard, B., A combination of acid-base titrations and derivatization for functional group determinations of an aquatic fulvic acid, *Sci. Total Environ.*, **81/82** (1989) 615–624.
- [89EPH/MAR] Ephraim, J.H., Marinsky, J.A., Cramer, S., Complex-forming properties of natural organic acids. Fulvic acid complexes with cobalt, zinc and europium, *Talanta*, **36** (1989) 437–443.
- [89EPH/XU] Ephraim, J.H., Xu, H., The binding of cadmium by an aquatic fulvic acid: A comparison of ultrafiltration with ion-exchange distribution and ion-selective electrode techniques, *Sci. Total Environ.*, **81/82** (1989) 625–634.
- [89FRE] Frenkel, D., in: Cellular Automata and Modeling of Complex Physical Systems (Manneville, P., *et al.*, eds.), Berlin: Springer, (1989) *pp.*144–154.

Reference List

- [89FRE/ERN] Frenkel, D., Ernst, M.H., Simulation of diffusion in a two-dimensional lattice-gas cellular automaton – A test of mode-coupling theory, *Phys. Rev. Lett.*, **63** (1989) 2165–2168.
- [89FUR/WES] Furrer, G., Westall, J., Sollins, P., The study of soil chemistry through quasi-steady-state models: I. Mathematical definition of model, *Geochim. Cosmochim. Acta*, **53** (1989) 595–601.
- [89GRA/CRU] Graedel, T.E., Crutzen, P.J., The changing atmosphere, *Sci. Am.*, **261** (1989) 86–93.
- [89HAY/MCC] Hayes, M.H.B., McCarthy, P., Malcolm, R.L., Swift, R.S., *eds.*, Humic substances: II. In search of structure, Wiley Interscience, New York (1989).
- [89HIE/RIE] Hiemstra, T., van Riemsdijk, W.H., Bolt, G.H., Multisite proton adsorption modelling at the solid/solution interface of (hydr)oxides: a new approach, *J. Coll. Interf. Sci.*, **133** (1989) 91–104.
- [89HOL] Holland, T.J.B., Dependence of entropy on volume for silicate and oxide minerals: A review and a predictive model, *Am. Mineral.*, **74** (1989) 5–13.
- [89IZA/CHR] Izatt, R.M., Christensen, J.J., Oscarson, J.L., Gillespie, S.E., Determination of thermodynamic data for modeling corrosion, Vol. 1: Sulfates (Revision 1). Technical Report EPRI-NP-5708, Electric Power Research Inst., Palo Alto, California, 1989.
- [89IZA/CHR2] Izatt, R.M., Christensen, J.J., Oscarson, J.L., Gillespie, S.E., Determination of thermodynamic data for modeling corrosion, Vol. 2: Chlorides and acetates. Technical Report EPRI-NP-5708, Electric Power Research Inst., Palo Alto, California, 1989.
- [89KIM/BUC] Kim, J.I., Buckau, G., Bryant, E., Klenze, R., Complexation of americium(III) with humic acid, *Radiochim. Acta*, **48** (1989) 135–143.
- [89MAN/BOC] Manneville, P., Boccara, N., Vichniac, G.Y., Bidaux, R., *eds.*, Cellular Automata and Modeling of Complex Physical Systems, Proc. of the Winter School, Les Houches, February 1989, Berlin: Springer, 1989.
- [89MUR] Murray, J.D., *Mathematical Biology*, New York: Springer, 1989.
- [89PEN] Penrose, R., *The emperor's new mind*, Oxford University Press, 1989.
- [89PET/DRA] Petit, J.C., Dran, J.C., Trotignon, L., Casabonne, J.M., Paccagnella, A., Della Mea, G., Mechanism of heavy element retention in hydrated layers formed on leached silicate glasses, *Scientific Basis for Nuclear Waste Management XII* (Lutze, W., Ewing, R. C., *eds.*), Mat. Res. Soc. Symp. Proc., Vol. **127** (1989) 33–40.
- [89RIG/ROB] Riglet, C., Robouch, P., Vitorge, P., Standard potentials of the ($\text{MO}_2^{2+}/\text{MO}_2^{+}$) and ($\text{M}^{4+}/\text{M}^{3+}$) redox systems for neptunium and plutonium, *Radiochim. Acta*, **46** (1989) 85–94.

Reference List

- [89SAU/WAG] Saul, A., Wagner, W., A fundamental equation for water covering the range from the melting line to 1273 K at pressures up to 25 000 MPa, *J. Phys. Chem. Ref. Data*, **18** (1989) 1537–1564.
- [89SAX/ZHA] Saxena, S.K., Zhang, J., Assessed high-temperature thermochemical data on some solids, *J. Phys. Chem. Solid*, **50** (1989) 723–727.
- [89SHO/HEL] Shock, E.L., Helgeson, H.C., Corrections to [88SHO/HEL], *Geochim. Cosmochim. Acta*, **53** (1989) 215.
- [89SHO/HEL2] Shock, E.L., Helgeson, H.C., Sverjensky, D.A., Calculation of the thermodynamic and transport properties of aqueous species at high pressures and temperatures: Standard partial molal properties of inorganic neutral species, *Geochim. Cosmochim. Acta*, **53** (1989) 2157–2183.
- [89SMI/MAR] Smith, R.M., Martell, A.E., Critical stability constants, Vol. 6: Second supplement, New York: Plenum Press, 1989, 643p.
- [89SPO] Sposito, G., The chemistry of soils, Oxford University Press., New York, 1989, p.11.
- [89WER/CHA] Wersin, P., Charlet, L., Karthein, R., Stumm, W., From adsorption to precipitation: Sorption of Mn^{2+} on $\text{FeCO}_3(\text{s})$, *Geochim. Cosmochim. Acta*, **53** (1989) 2787–2796.
- [89XU/EPH] Xu, H., Ephraim, J., Ledin, A., Allard, B., Effects of fulvic acid on the adsorption of Cd(II) on alumina, *Sci. Total Environ.*, **81/82** (1989) 653–660.
- [90ADA] Adamson, A.W., Physical Chemistry of Surfaces, John Wiley & Sons, New York, 1990.
- [90APP/NEI] Apps, J.A., Neil, J.M., Solubilities of aluminium hydroxides and oxyhydroxides in alkaline solutions, Chapter 32, in: Chemical modeling of aqueous systems II (Melchior, D.C., Bassett, R.L., *eds.*), ACS Symp. Ser., **416** (1990) 414–428.
- [90APP/ZAL] Appert, C., Zaleski, S., Lattice gas with a liquid-gas transition, *Phys. Rev. Lett.*, **64** (1990) 1–4.
- [90ARC/WAN] Archer, D.G., Wang, P., The dielectric constant of water and Debye-Hückel limiting law slopes, *J. Phys. Chem. Ref. Data*, **19** (1990) 371–411.
- [90ASP] Aspray, W., John von Neumann and the Origins of Modern Computing, Cambridge: MIT Press, MA, 1990.
- [90ATK] Atkinson, P.W., Physical Chemistry, Fourth Edition, Oxford University Press, 1990, 995p.
- [90BAN/HYL] Bancroft, G.M., Hyland, M.M., Spectroscopic studies of adsorption/reduction reactions of aqueous metal complexes on sulphide surfaces, in: Mineral-Water Interface Geochemistry (Hochella, M.F., Jr., White, A.F., *eds.*), Reviews in Mineralogy, Vol. 23, Mineral. Soc. Amer., Washington, D.C., 1990, pp.511–558.

Reference List

- [90BAR] Barcelona, M.J., Uncertainties in Groud Water Chemistry and Sampling Procedures, in: Chemical Modeling of Aqueous Systems II, (Melchior, D.C., Basset, R.L., *eds.*), ACS Symp. Ser., nr. 416, Am. Chem. Soc., Washington D.C., 1990, *pp.*310–320.
- [90BEC/NAG] Beck, M.T., Nagypál, I., Chemistry of complex equilibria, Horwood Limited Publishers, 1990, New York, 402*p.*
- [90BLA] Blankleider, B., A cellular automata model for coupling transport and chemical reactions, PSI Internal Report TM-41-90-13, Würenlingen and Villigen, 1990.
- [90BOG] Boghosian, B.M., Computational physics on the connection machine, *Comp. in Physics*, **4** (1990) 14–33.
- [90BRO/GUC] Broekaert, J.A.C., Güçer, S., Adams, F., *eds.*, Metal speciation in the environment, NATO ASI Series, Vol. **G32**, Springer, 1990, *p.*644.
- [90BUF/ALT] Buffle, J., Altmann, R.S., Filella, M., Tessier, A., Complexation by natural heterogeneous compounds: Site occupation distribution functions, a normalized description of metal complexation, *Geochim. Cosmochim. Acta*, **54** (1990) 1535–1553.
- [90CAS/DUL] Castets, V., Dulos, E., Boissonade, J., de Kepper, P., Experimental-evidence of a sustained standing Turing-type nonequilibrium chemical-pattern, *Phys. Rev. Lett.*, **64** (1990) 2953–2956.
- [90CHE/MAT] Chen, H., Matthaeus, W.H., Klein, L.W., Theory of multicolor lattice gas – A cellular automaton Poisson solver, *J. Comp. Phys.*, **88** (1990) 433–466.
- [90CIA] Ciavatta, L., The specific interaction theory in equilibrium analysis: Some empirical rules for estimating interaction coefficients of metal ion complexes, *Ann. Chim. Roma*, **80** (1990) 255–263.
- [90DAB/LAW] Dab, D., Lawniczak, A., Boon, J.-P., Kapral, R., Cellular-automaton model for reactive systems, *Phys. Rev. Lett.*, **64** (1990) 2462–2465.
- [90DIC/WES] Dickson, A.G., Wesolowski, D.J., Palmer, D.A., Mesmer, R.E., Dissociation constant of bisulfate ion in aqueous sodium chloride solutions to 250°C, *J. Phys. Chem.*, **94** (1990) 7978–7985.
- [90DOO/FRI] Doolen, G., Frisch, U., Hasslacher, B., Orszag, S., Wolfram, S. (*eds.*), Lattice gas methods for partial differential equations, Santa Fe Institute Studies in the Science of Complexity, Addison–Wesley, 1990.
- [90DZO/MOR] Dzombak, D.A., Morel, F.M.M., Surface complexation modeling: hydrous ferric oxide, Wiley Inters. Publ., New York, 1990, 393*p.*
- [90EPH/MAR] Ephraim, J.H., Marinsky, J.A., Ultrafiltration as a technique for studying metal-humate interactions: Studies with iron and copper, *Anal. Chim. Acta.*, **232** (1990) 171–180.

Reference List

- [90ERN/DUF] Ernst, M.H., Dufty, J.W., Hydrodynamics and time correlation-functions for cellular automata, *J. Stat. Phys.*, **58** (1990) 57–86.
- [90FEL/RAI] Felmy, A.R., Rai, D., Fulton, R.W., The solubility of $\text{AmOHCO}_3(\text{c})$ and the aqueous thermodynamics of the system $\text{Na}^+ - \text{Am}^{3+} - \text{HCO}_3^- - \text{CO}_3^{2-} - \text{OH}^- - \text{H}_2\text{O}$, *Radiochim. Acta*, **50** (1990) 193–204.
- [90FUR/WES] Furrer, G., Westall, J., Sollins, P., The study of soil chemistry through quasi steady-state models II. Acidity of soil solutions, *Geochim. Cosmochim. Acta*, **54** (1990) 2363–2374.
- [90GRA] Grauer, R., *Zur Chemie von Kolloiden: Verfügbare Sorptionsmodelle und zur Frage der Kolloidhaftung*, PSI-Bericht Nr. 65, Würenlingen, 1990; Nagra NTB 90-37, Wettingen, Switzerland, 1990.
- [90GUT] Gutowitz, H., *ed.*, Cellular Automata: Theory and Experiment, *Physica*, **D 45** (1990) Nos. 1–3.
- [90HER/STU] Hering, J.G., Stumm, W., Oxidation and reductive dissolution of minerals, in: *Mineral-Water Interface Geochemistry* (Hochella, M.F., Jr., White, A.F., *eds.*), *Reviews in Mineralogy*, Vol. 23, Mineral. Soc. Amer., Washington, D.C., 1990, *pp.* 427–465.
- [90HOC/WHI] Hochella, M.F., Jr., White, A.F. (*eds.*), *Mineral-Water Interface Geochemistry*, *Reviews in Mineralogy*, Vol. 23, Mineral. Soc. Amer., Washington, D.C., 1990.
- [90HOL/MES] Holmes, H.F., Mesmer, R.E., Isopiestic studies of aqueous solutions at elevated temperatures: 10. $[(1-y)\text{NaCl} + y\text{CsCl}](\text{aq})$, *J. Phys. Chem.*, **94** (1990) 7800–7805.
- [90HOL/POW] Holland, T.J.B., Powell, R., An enlarged and updated internally consistent thermodynamic dataset with uncertainties and correlations: the system $\text{K}_2\text{O} - \text{Na}_2\text{O} - \text{CaO} - \text{MgO} - \text{MnO} - \text{FeO} - \text{Fe}_2\text{O}_3 - \text{Al}_2\text{O}_3 - \text{TiO}_2 - \text{SiO}_2 - \text{C} - \text{H}_2 - \text{O}_2$, *J. Metamorphic Geol.*, **8** (1990) 89–124.
- [90LEI] Leigh, G.J., *Nomenclature of inorganic chemistry, recommendations 1990*, IUPAC Commission on Nomenclature of Inorganic Chemistry, Oxford: Blackwell Sci. Publ., 1990, 289p.
- [90LEV] de Levie, R., Notes on Gouy diffuse-layer theory, *J. Electroanal. Chem.*, **278** (1990) 17–24.
- [90LOE/SJO] Lövgren, L., Sjöberg, S., Schindler, P.W., Acid/base reactions and $\text{Al}(\text{III})$ complexation at the surface of goethite, *Geochim. Cosmochim. Acta*, **54** (1990) 1301–1306.
- [90MAR/RED] Marinsky, J.A., Reddy, M.M., Vapor-pressure osmometric study of the molecular weight and aggregation tendency of a reference-soil fulvic acid, *Anal. Chim. Acta*, **232** (1990) 123–130.

Reference List

- [90MOR/MAC] Morse, J.W., Mackenzie, F.T., *Geochemistry of Sedimentary Carbonates*, Elsevier, Amsterdam, 1990. *p*.41.
- [90NED/RIE] Nederlof, M.M., van Riemsdijk, W.H., Koopal, L.K., Determination of adsorption affinity distributions: A general framework for methods related to local isotherm approximations, *J. Coll. Interf. Sci.*, **135** (1990) 410–426.
- [90NOR/PLU] Nordstrom, D.K., Plummer, L.N., Langmuir, D., Busenberg, E., May, H.M., Jones, B.F., Parkhurst, D.L., Revised chemical equilibrium data for major water-mineral reactions and their limitations, in: *Chemical modeling of aqueous systems II* (Melchior, D.C., Basett, R.L., *eds.*), A.C.S. Symp. Ser. No. 416, Amer. Chem. Soc., Washington, D.C., 1990, *pp*.398–413.
- [90OSC/GIL] Oscarson, J.L., Gillespie, S.E., Christensen, J.J., Izatt, R.M., Brown, P.R., Thermodynamic quantities for the interactions of H^+ and Na^+ with $C_2H_3O_2^-$ and Cl^- in aqueous solutions from 275 to 320°C, in: *Proc. 1987 Symp. on Chemistry in High-Temperature Water* (Izatt, R.M., Oscarson, J.L., Lindh, G.H., *eds.*), Technical Report EPRI-NP-6005, Electric Power Research Inst., Palo Alto, California, 1990, *pp*.B2l.1–B2l.37.
- [90OSC/IZA] Oscarson, J.L., Izatt, R.M., Brown, P.R., Pawlak, Z., Gillespie, S.E., Christensen, J.J., Thermodynamic quantities for the interaction of SO_4^{2-} with H^+ and Na^+ in aqueous solution from 150 to 320°C, in: *Proc. 1987 Symp. on Chemistry in High-Temperature Water* (Izatt, R.M., Oscarson, J.L., Lindh, G.H., *eds.*), Technical Report EPRI-NP-6005, Electric Power Research Inst., Palo Alto, California, 1990, *pp*.B2m.1–B2m.36.
- [90PER/GJE] Perdue, E.M., Gjessing, E.T., *eds.*, *Organic acids in aquatic ecosystems*, Life Sciences Research Report, Vol. 48, John Wiley and Sons, New York (1990).
- [90PLU/PAR] Plummer, L.N., Parkhurst, D.L., Application of the Pitzer equations to the PHREEQE geochemical model, in: *Chemical modeling of aqueous systems II* (Melchior, D.C., Basett, R.L., *eds.*), A.C.S. Symp. Ser. No. 416, Amer. Chem. Soc., Washington, D.C., 1990, *pp*.128–137.
- [90RAN] Radionuclide chain transport with matrix diffusion - RANCHMD, OECD/NEA Data Bank, Paris (France).
- [90ROY/RIC] Roy, R.N., Rice, S.A., Vogel, K.M., Roy, L.N., Millero, F.J., Activity coefficients for $HCl + BaCl_2 + H_2O$ at different temperatures and effects of higher order electrostatic terms, *J. Phys. Chem.*, **94** (1990) 7706–7710.
- [90SCH] Schnoor, J.L., Kinetics of chemical weathering: a comparison of laboratory and field weathering rates, in: *Aquatic Chemical Kinetics*, (Stumm W., *ed.*), New York, John Wiley & Sons, 1990, 475–504.
- [90SEN] Senesi, N., Molecular and quantitative aspects of the chemistry of fulvic acid and its interaction with metal ions and organic chemicals. Part. I. The electron spin resonance approach, *Anal. Chim. Acta*, **232** (1990) 51–75.

Reference List

- [90SHI/DOO] Shimomura, T., Doolen, G.D., Hasslacher, B., Fu, C., in: Lattice Gas Methods for Partial Differential Equations (Doolen, G., Frisch, U., Hasslacher, B., Orszag, S., Wolfram, S., *eds.*), Santa Fe Institute Studies in the Science of Complexity, Addison-Wesley, (1990) *pp.*3–9.
- [90STE/LAS] Steefel, C.I., Lasaga, A.C., Evolution of Dissolution Patterns. Permeability Change Due to Coupled Flow and Reaction, in: Chemical Modeling of Aqueous Systems II, (Melchior, D.C, Basset, R.L., *eds.*), ACS Symp. Ser., nr. 416, Am. Chem. Soc., Washington D.C., 1990, 507p.
- [90STU/WOL] Stumm, W., Wollast, R., Coordination chemistry of weathering, *Rev. Geophys.*, **28**(1) (1990) 53–69.
- [90TIP/RED] Tipping, E., Reddy, M.M., Hurley, M.A., Modeling electrostatic and heterogeneity effects on proton dissociation from humic substances, *Environ. Sci. Technol.*, **24** (1990) 1700–1705.
- [90VER] Verdes, G., Solubilité des hydroxydes d'aluminium entre 20 et 300°C. Propriétés thermodynamiques des principales espèces naturelles du système $\text{Al}_2\text{O}_3\text{-H}_2\text{O}$: Ph. D. Diss., Paul Sabatier Univ., Toulouse, France, (1990) 267 p.
- [90VIA/KOE] Vianney, J.M., Koelman, A., Cellular-automaton-based simulation of 2D polymer dynamics, *Phys. Rev. Lett.*, **64** (1990) 1915–1918.
- [90WAI] Waite, T.D., Photo-redox processes at the mineral-water interface, in: Mineral-Water Interface Geochemistry (Hochella, M.F., Jr., White, A.F., *eds.*), Reviews in Mineralogy, Vol. 23, Mineral. Soc. Amer., Washington, D.C., 1990, *pp.*559–603.
- [90WAN] Wanner, H., Guidelines for the independent peer review of TDB reports, Report TDB-6, OECD Nuclear Energy Agency, Data Bank, Gif-sur-Yvette, France, March 1990, 8p.
- [90WHI] White, A.F., Heterogeneous electrochemical reactions associated with oxidation of ferrous oxide and silicate surfaces, in: Mineral-Water Interface Geochemistry (Hochella, M.F., Jr., White, A.F., *eds.*), Reviews in Mineralogy, Vol. 23, Mineral. Soc. Amer., Washington, D.C., 1990, *pp.*467–509.
- [90WIT/RIE] de Wit, J.C.M., van Riemsdijk, W.H., Nederlof, M.M., Kiniburgh, D.G., Koopal, L.K., Analysis of ion binding on humic substances and the determination of intrinsic affinity distributions, *Anal. Chim. Acta*, **232** (1990) 189–207.
- [90WOL] Wollast, R., Rate and mechanism of dissolution of carbonates in the system $\text{CaCO}_3\text{-MgCO}_3$, in: Aquatic Chemical Kinetics (Stumm, W., *ed.*), New York: Wiley, (1990) *pp.*431–445.
- [90WOL/JAC] Wolery, T.J., Jackson, K.J., Bourcier, W.L., Bruton, C.J., Viani, B.E., Knauss, K.G., Delany, J.M., Current status of the EQ3/6 software package

Reference List

- for geochemical modeling, in: Chemical modeling of aqueous systems II (Melchior, D.C., Bassett, R.L., *eds.*), A.C.S. Symp. Ser. No. 416, Amer. Chem. Soc., Washington, D.C., 1990, *pp.*104–116.
- [90WOO] Wood, S.A., The aqueous geochemistry of the rare-earth elements and yttrium. 1. Review of available low-temperature data for inorganic complexes and the inorganic REE speciation of natural waters, *Chem. Geol.*, **82** (1990) 159–186.
- [91AND/CAS] Anderson, G.M., Castet, S., Schott, J., Mesmer, R.E., The density model for estimation of thermodynamic parameters of reactions at high temperatures and pressures, *Geochim. Cosmochim. Acta*, **55** (1991) 1769–1779.
- [91AND/ISA] Anderson, O.L., Isaak, D.L., Oda, H., Thermoelastic parameters for six minerals at high temperature, *J. Geophys. Res.*, **96** (1991) 18037–18046.
- [91ARC] Archer, D.G., Thermodynamic properties of the NaBr + H₂O system, *J. Phys. Chem. Ref. Data*, **20** (1991) 509–555.
- [91BEA/BAC] Bear, J., Bachmat, Y., Introduction to modelling of transport phenomena in porous media, Kluwer Acad. Pub., Dordrecht, Boston, London 1991.
- [91BID/GRE] Bidoglio, G., Grenthe, I., Qi, P., Robouch, P., Omenetto, N., Complexation of Eu and Tb with fulvic acids as studied by time resolved laser induced fluorescence, *Talanta*, **38** (1991) 999–1008.
- [91BOS/MAZ] Bossart, P., Mazurek, M., Structural geology and water flow-paths in the migration shear-zone, NAGRA Techn. Report, NTB 91-12, NAGRA, Wettingen, Switzerland, 1991.
- [91BRI/BON] Brieger, L.M., Bonomi, E., A stochastic cellular automaton model of nonlinear diffusion and diffusion with reaction, *J. Comp. Phys.*, **94** (1991) 467–486.
- [91BRU/CAS] Bruno, J., Casas, I., Puigdomenech, I., The kinetics of dissolution of UO₂ under reducing conditions and the influence of an oxidized surface layer (UO_{2+x}). Application of a continuous flow-through reactor, *Geochim. Cosmochim. Acta*, **55** (1991) 647–658.
- [91BRU/CRO] Bruno, J., Cross, J.E., Eikenberg, J., McKinley, I.G., Read, D., Sandino, A., Sellin, P., Testing of geochemical models in the Poços de Caldas analogue study, SKB-TR-90-20, Swedish Nucl. Fuel Waste Manag. Co., Stockholm, Sweden, 1991.
- [91CAS] Castet, S., Solubilité de la boehmite et spéciation de l'aluminium dissous dans les solutions aqueuses à haute température (90–350°C). Détermination expérimentale et modélisation: Ph. D. thesis, Lab. of Geochemistry, Paul Sabatier Univ., Toulouse, France (1991).
- [91CHA/MCK] Chapman, N.A., McKinley, I.G., Shea, M.A., Smellie, J.A.T., The Poços de Caldas Project: Summary and implications for Radioactive Waste Management, NTB 90-33, SKB TR 90-24, UK DOE WR 90-055 (1991).

Reference List

- [91CHE/XU] Chen Q., Xu Y., Hepler L.G., Calorimetric study of the digestion of gibbsite, $\text{Al}(\text{OH})_3(\text{cr})$, and thermodynamics of aqueous aluminate ion, $\text{Al}(\text{OH})_4^-(\text{aq})$, *Can. J. Chem.*, **69** (1991) 1685–1690.
- [91CHO/CLA] Choppin, G.R., Clark, S.B., The kinetic interactions of metal ions with humic acids, *Mar. Chem.*, **36** (1991) 27–38.
- [91CHO/DRO] Chopard, B., Droz, M., Cellular automata model for the diffusion equation, *J. Stat. Phys.*, **64** (1991) 859–892.
- [91CHO/DRO2] Chopard, B., Droz, M., Microscopic study of the properties of the reaction front in an $A + B \rightarrow C$ reaction-diffusion process, *Europhys. Lett.*, **15** (1991) 459–465.
- [91DAB/BOO] Dab, D., Boon, J.-P., Li, Y.-X., Lattice-gas automata for coupled reaction-diffusion equations, *Phys. Rev. Lett.*, **66** (1991) 2535–2538.
- [91DAU/CRO] Daux, V., Crovisier, J.L., Petit, J.C., Rare earth elements behaviour during alteration of basaltic glasses: case of the weathering of icelandic hyaloclastites, *Scientific Basis for Nuclear Waste Management XIV* (Abrajo, T.A., Jr., Johnson, L.H., *eds.*), *Mat. Res. Soc. Symp. Proc.*, Vol. **212** (1991) 107–114.
- [91DOO] Doolen, G., *ed.*, Lattice Gas Methods for PDE's: Theory, Applications and Hardware, *Proc. of the NATO Advanced Research Workshop*, Los Alamos, September 1989, *Physica*, **D 47** (1991) Nos. 1 & 2.
- [91EPH] Ephraim, J.H., Europium binding by an aquatic fulvic acid. Interaction functions for the “average” sites in the fulvic acid molecule, *Sci. Total Environ.*, **108** (1991) 261–273.
- [91EPH/RED] Ephraim, J.H., Reddy, M.M., Marinsky, J.A., Ion binding by humic substances: Considerations based on the solution chemistry and heterogeneity of humic substances, in: *Humic substances in the aquatic and terrestrial environment* (Allard, B., Borén, H., Grimvall, A., *eds.*), *Lecture Notes in Earth Science*, **33** (1991) 263–276, Springer-Verlag, Berlin, Heidelberg.
- [91FAL] Falck, W.E., The incorporation of natural organic matter - cation interaction into the speciation code phreeqc, in: *Humic substances in the aquatic and terrestrial environment* (Allard, B., Borén, H., Grimvall, A., *eds.*), *Lecture Notes in Earth Science*, **33** (1991) 277–285, Springer-Verlag, Berlin, Heidelberg.
- [91FRA/WIL] Fraústo da Silva, J.J.R., Williams, R.J.P., *The Biological Chemistry of the Elements. The Inorganic Chemistry of Life*. Clarendon Press, Oxford, 1991, 561p.
- [91GRE] Grenthe, I., Thermodynamics in migration chemistry, *Radiochim. Acta*, **52/53** (1991) 425–432.

Reference List

- [91GRE/LAG] Grenthe, I., Lagerman, B., Studies on the metal carbonate equilibria: 22. A coulometric study of the uranium(VI)-carbonate system, the composition of the mixed hydroxide carbonate species, *Acta Chem. Scand.*, **45** (1991) 122–128.
- [91JOH/NOR] Johnson, J.W., Norton, D., Critical phenomena in hydrothermal systems: state, thermodynamic, electrostatic, and transport properties of H₂O in the critical region, *Am. J. Sci.*, **291** (1991) 541–648.
- [91KAP/LAW] Kapral, R., Lawniczak, A., Masiar, P., Oscillations and waves in a reactive lattice-gas automaton, *Phys. Rev. Lett.*, **66** (1991) 2539–2542.
- [91KEP/CAS] de Kepper, P., Castets, V., Dulos, E., Boissonade, J., Turing-type chemical patterns in the chlorite-iodide-malonic acid reaction, *Physica*, **D 49** (1991) 161–169.
- [91KIM/SEK] Kim, J.I., Sekine, T., Complexation of neptunium(V) with humic acid, *Radiochim. Acta*, **55** (1991) 187–192.
- [91KIS/SOV] Kiss, T., Sóvágó, I., Gergely, A., Critical survey of stability constants of complexes of glycine, *Pure & Applied Chem.*, **63** (1991) 597–638.
- [91KNA/KUB] Knacke, O., Kubaschewski, O., Hesselmann, K. (*eds.*), Thermochemical properties of inorganic substances, *2nd ed.*, Berlin: Springer-Verlag, 1991, Vols. I and II, 2412*p.*
- [91LAW/DAB] Lawniczak, A., Dab, D., Kapral, R., Boon, J.-P., Reactive lattice gas automata, *Physica*, **D 47** (1991) 132–158.
- [91LI] Li, Y.-H., Distribution patterns of the elements in the ocean: A synthesis, *Geochim. Cosmochim. Acta*, **55** (1991) 3223.
- [91LOO/KOP] Van Loon, L.R., Kopajtic, Z., Complexation of Cu²⁺, Ni²⁺ and UO₂²⁺ by radiolytic degradation products of bitumen, *Radiochim. Acta*, **54** (1991) 193–199.
- [91MAE/ELE] Maes, A., Van Elewijck, F., Vancluysen, J., Tits, J., Cremers, A., Cobalthexamine as an index cation for measuring the cation exchange capacity of humic acids, in: *Humic substances in the aquatic and terrestrial environment* (Allard, B., Borén, H., Grimvall, A., *eds.*), *Lecture Notes in Earth Sciences*, **33** (1991) 85–95, Springer-Verlag, Berlin.
- [91MAL] Malcolm, R.L., Factors to be considered in the isolation and characteristics of aquatic humic substances, in: *Humic substances in the aquatic and terrestrial environment* (Allard, B., Borén, H., Grimvall, A., *eds.*), *Lecture Notes in Earth Science*, **33** (1991) 9–36, Springer-Verlag, Berlin, Heidelberg.
- [91MAT2] Matthiessen, A., Kinetic aspects on the oxidation of humic substances, *Finnish Humus News*, **3** (1991) 317–322.

Reference List

- [91MEA/MEA] Meadows, D.H., Meadows, D.L., Randers, J., Mas alla de los limites del crecimiento, El Pais Aguilar, Madrid, 1991, 355 pp.
- [91MES/PAL] Mesmer, R.E., Palmer, D.A., Simonson, J.M., Ion association at high temperatures and pressures, in: Activity coefficients in electrolyte solutions (Pitzer, K.S., *ed.*), Boca Raton: CRC Press, 2nd ed., 1991, *pp.*491–529.
- [91MOU/CAC] Moulin, V., Caceci, M., Complexation behaviour of humic substances from granitic groundwater towards Am(III), in: Humic substances in the aquatic and terrestrial environment (Allard, B., Borén, H., Grimvall, A., *eds.*), Lecture Notes in Earth Science, **33** (1991) 305–313, Springer-Verlag, Berlin, Heidelberg.
- [91MOU/DEC] Moulin, C., Decambox, P., Mauchien, P., Moulin, V., Theyssier, M., On the use of laser-induced time-resolved spectrofluorometry for interaction studies between organic matter and actinides: Application to curium, Radiochim. Acta, **52/53** (1991) 119–125.
- [91NEB/BRU] Nebot, J., Bruno, J., The implications of soil acidification on a future HLNW repository. Part I: The effects of increased weathering, erosion and deforestation, SKB-TR-91-45, Swedish Nucl. Fuel Waste Manag. Co., Stockholm, Sweden, 1991.
- [91PAX/WED] Paxéus, N., Wedborg, M., Calcium binding to an aquatic fulvic acid, in: Humic substances in the aquatic and terrestrial environment (Allard, B., Borén, H., Grimvall, A., *eds.*), Lecture Notes in Earth Science, **33** (1991) 287–296, Springer-Verlag, Berlin, Heidelberg.
- [91PET] Pettersson, C., Properties of humic substances from groundwater and surface waters, Ph.D. Thesis, Dept. Water and Environmental Studies, Linköping University, Sweden, 1991.
- [91PEU/PIH] Peuravuori, J., Pihlaja, K., Humus and its structure. II. Are (lake) fulvic and humic acids definite entities, Finnish Humus News, **3** (1991) 115–126.
- [91PIT] Pitzer, K.S., Ion interaction approach: theory and data correlation, in: Activity coefficients in electrolyte solutions, 2nd Edition, (Pitzer K.S., *ed.*) CRC Press, (1991) *pp.*75–153.
- [91POW/TOW] Powell, H.K.J., Town, R.M., Interaction of humic substances with hydrophobic metal complexes: a study by anodic stripping voltammetry and spectrophotometry, Anal. Chim. Acta, **248** (1991) 95–102.
- [91QUY/SWI] Quyang, Q., Swinney, H.L., Transition from a uniform state to hexagonal and striped Turing patterns, Nature, **352** (1991) 610–612.
- [91RIC/FIQ] Richet, P., Fiquet, G., High-temperature heat capacity and premelting of minerals in the system MgO-CaO-Al₂O₃-SiO₂, J. Geophys. Res., **96** (1991) 445–456.

Reference List

- [91ROE/SJO] Rönngren, L., Sjöberg, S., Sun, Z., Forsling, W., Schindler, P.W., Surface reactions in aqueous metal sulfide systems, *J. Coll. Interf. Sci.*, **145** (1991) 396–404.
- [91RYZ/BRY] Ryzhenko, B.N., Bryzgalin, O.V., Shapkin, A.I., Dissociation of salts and bases in aqueous solution at 25°C and 1 bar, *Geochem. Int.*, **28** (5) (1991) 77–83.
- [91SKI] Swedish Nuclear Power Inspectorate, SKI Project-90, SKI Technical Report 91:23, Stockholm 1991.
- [91SOM/REM] Somers, J.A., Rem, P.C., Analysis of surface tension in two-phase lattice gases, *Physica*, **D 47** (1991) 39–46.
- [91STR/ZIM] Strübel, G., Zimmer, S.H., *Lexikon der Minerale*, F. Enke, Stuttgart 1991.
- [92ALE/DAY] Alexander, W.R., Dayal, R., Eagleson, K., Eikenberg, J., Hamilton, E., Linklater, C.M., McKinley, I.G., Tweed, C.J., A natural analogue of high pH cement pore waters from the Maqarin area of northern Jordan: II. Results of predictive geochemical calculations, *J. Geochem. Explor.*, **46** (1992) 133–146.
- [92ARS/BOR] Arsenie, I., Borén, H., Allard, B., Determination of the carboxylic content in humic substances by methylation, *Sci. Total Environ.*, **116** (1992) 213–220.
- [92BAR/CAB] Bartschat, B.M., Cabaniss, S.E., Morel, F.M.M., Oligoelectrolyte model for cation binding by humic substances, *Environ. Sci. Technol.*, **26** (1992) 284–294.
- [92BEA/VER] Bear, J., Verruijt, A., *Modeling groundwater flow and pollution*, Dordrecht: D. Reidel Publ. Comp., 1992.
- [92BRU/SEL] Bruno, J., Sellin, P., Radionuclide solubilities to be used in SKB 91, SKB-TR-92-13, Swedish Nucl. Fuel Waste Manag. Co., Stockholm, Sweden, 1992.
- [92BRU/STU] Bruno, J., Stumm, W., Wersin, P., Brandberg, F., On the influence of carbonate in mineral dissolution: Part I. The thermodynamics and kinetics of hematite dissolution in bicarbonate solutions at $T = 25^{\circ}\text{C}$, *Geochim. Cosmochim. Acta*, **56** (1992) 1139–1147.
- [92BRU/WER] Bruno, J., Wersin, P., Stumm, W., On the influence of carbonate in mineral dissolution: II. The solubility of $\text{FeCO}_3(\text{s})$ at 25°C and 1 atm total pressure, *Geochim. Cosmochim. Acta.*, **56** (1992) 1149–1155.
- [92BUC/KIM] Buckau, G., Kim, J.I., Klenze, R., Rhee, D.S., Wimmer, H., A comparative spectroscopic study of the fulvate complexation of trivalent transuranium ions, *Radiochim. Acta*, **57** (1992) 105–111.
- [92CAP/VIT] Capdevila, H., Vitorge, P., Giffaut, E., Stability of pentavalent plutonium. Spectrophotometric study of PuO_2^+ and Pu^{4+} disproportionation in perchloric media, *Radiochim. Acta*, **58/59** (1992) 45–52.

Reference List

- [92CHO/DU] Choppin, G.R., Du, M., *f*-Element complexation in brine solutions, *Radiochim. Acta*, **58/59** (1992) 101–104.
- [92DAB] Dab, D., Automates de gaz sur réseaux: une approche microscopique des systèmes réactifs, Thèse de Doctorat, Université Libre de Bruxelles, 1992.
- [92DUL] Dullien, F.A.L., *Porous Media: Fluid Transport and Pore Structure*, San Diego: Academic Press, 1992.
- [92ERI/HAC] Eriksson, G., Hack, K., *ChemSage Handbook*, RWTH-Aachen, Germany, 1992.
- [92ERN/DAS] Ernst, M.H., Das, S.P., Thermal cellular automata fluids, *J. Stat. Phys.*, **66** (1992) 465–483.
- [92FRI/ALE] Frick, U., Alexander, W.R., Baeyens, B., Bossart, P., Bradbury, M.H., Buehler, Ch., Eikenberg, J., Fierz, Th., Heer, W., Hoehn, E., McKinley, I.G., Smith, P.A., Grimsel test site, the radionuclide migration experiment. Overview of investigations 1985-1990, PSI-Bericht Nr. 120, Würenlingen und Villigen, 1992 and Nagra Technical Report NTB 91-04, NAGRA, Wettingen, Switzerland, 1992.
- [92FUG/KHO] Fuger, J., Khodakovsky, I.L., Sergeyeva, E.I., Medvedev, V.A., Navratil, J.D., *The chemical Thermodynamics of Actinide Elements and Compounds: Part 12. The Actinide Aqueous Inorganic Complexes*, Vienna: International Atomic Energy Agency, 1992, 224p.
- [92GEL/WEL] Gelhar, L.W., Welty, C., Rehfeldt K.R., A critical review of data on field-scale dispersion in aquifers, *Water Resour. Res.*, **28** (1992) 1955–1974.
- [92GRE/FUG] Grenthe, I., Fuger, J., Konings, R.J.M., Lemire, R.J., Muller, A.B., Nguyen-Trung, C., Wanner, H., *Chemical thermodynamics of uranium* (Wanner, H., Forest, I., *eds.*), Amsterdam: Elsevier Science Publishers B.V., 1992, 715p.
- [92GRE/STU] Grenthe, I., Stumm, W., Laaksuharju, M., Nilsson, A.C., Wikberg, P., Redox potentials and redox reactions in deep groundwater systems, *Chem. Geol.*, **98** (1992) 131–150.
- [92HUD] Hudson, J.A., *Rock Engineering Systems: Theory and Practice*, Ellis Horwood Ltd., Chichester, England, 1992, 185p.
- [92IZA/OSC] Izatt, R.M., Oscarson, J.L., Chen, X., Gillespie, S.E., Determination of thermodynamic data for modeling corrosion, Vol. 3: CO₂-NaOH-H₂O system. Technical Report EPRI-NP-5708, Electric Power Research Inst., Palo Alto, California, 1992.
- [92JOH/OEL] Johnson, J.W., Oelkers, E.H., Helgeson, H.C., SUPCRT92: a software package for calculating the standard molal thermodynamic properties of minerals, gases, aqueous species, and reactions from 1 to 5000 bar and 0 to 1000°C, *Comput. Geosci.*, **18** (1992) 899–947.

Reference List

- [92KAP/LAW] Kapral, R., Lawniczak, A., Masiar, P., Reactive dynamics in a multispecies lattice-gas automaton, *J. Chem. Phys.*, **96** (1992) 2762–2776.
- [92KOM/ZAN] Kometer, K., Zandler, G., Vogl, P., Lattice-gas cellular-automaton method for semiclassical transport in semiconductors, *Phys. Rev.*, **B 46** (1992) 1382–1394.
- [92KON/BRE] Konikow, L.F., Bredehoeft, J.D., Ground-water models cannot be validated, *Adv. Water Resources*, **15** (1992) 75–83.
- [92KRA/BIS] Kramer-Schnabel, U., Bischoff, H., Xi, R.H., Marx, G., Solubility products and complex formation equilibria in the systems uranyl hydroxide and uranyl carbonate at 25°C and $I = 0.1$ M, *Radiochim. Acta*, **56**(4) (1992) 183–188.
- [92MAR/COM] de Marsily, G., Combes, P., Goblet, P., Comment on “Ground-water models cannot be validated”, *Adv. Water Resources*, **15** (1992) 367–369.
- [92NEA] Nuclear Energy Agency, Systematic approaches to scenario development, OECD, Paris, 1992.
- [92NED/RIE] Nederlof, M.M., van Riemsdijk, W.H., Koopal, L.K., Comparison of semianalytical methods to analyze complexation with heterogeneous ligands, *Environ. Sci. Technol.*, **26** (1992) 763–771.
- [92NOR] Nordstrom, D.K., On the evaluation and application of geochemical models, in: 5th CEC Natural Analogue Working Group meeting, Toledo, Spain, 5-9 October 1992, CEC-EUR 15176, Brussels.
- [92OSM/IVA] Osmond, J.K., Ivanovich, M., Uranium series mobilization and surface hydrology, in: Uranium-series disequilibrium: Applications to Earth, Marine, and Environmental Sciences, 2nd edn. (Ivanovich, M., Harmon, R.S., eds.), Oxford: Clarendon Press, 1992, pp.259–289.
- [92OTT/DEL] Ottonello, G., Della Giusta, A., Dal Negro, A., Baccasin F., A structural energy model for C2/C pyroxenes in the system Na-Mg-Ca-Mn-Fe-Al-Cr-Ti-Si-O, in: Thermodynamic Data, (Saxena, S.K., ed.), Springer-Verlag, New York, 1992, pp.192–238.
- [92PAL/WES] Palmer, D.A., Wesolowski, D.J., Aluminum speciation and equilibria in aqueous solution: II. The solubility of gibbsite in acidic chloride solutions from 30 to 70°C, *Geochim. Cosmochim. Acta*, **56** (1992) 1093–1111.
- [92PEA/BER] Pearson, F.J., Berner, U., Hummel, W., Nagra thermochemical data base: II. Supplemental Data 05/92, Nagra Technical Report 91-18, Nagra, Wettingen, Switzerland, 1992, 284p.
- [92PET] Pettersson, C., Properties of humic substances from groundwater and surface waters, PhD. Thesis, Linköping University-Sweden, (1992).
- [92PRE] Preliminary performance assessment for the waste isolation pilot plant, December 1992, SAND 92-0700, Sandia National Laboratories, Albuquerque, 1992.

Reference List

- [92RAR] Rard, J.A., Thermodynamic properties of ions of the rare earth elements in aqueous solution, (1992) *draft*.
- [92ROM] Römpp Chemie Lexikon, 9. Aufl. (Falbe, J., Regitz, M., *eds.*), G. Thieme Verlag, Stuttgart, 1989-1992, p.5152.
- [92SAN/BRU] Sandino, A., Bruno, J., The solubility of $(\text{UO}_2)_3(\text{PO}_4)_2 \cdot 4\text{H}_2\text{O}(\text{s})$ and the formation of U(VI) phosphate complexes: Their influence in uranium speciation in natural waters, *Geochim. Cosmochim. Acta*, **56** (1992) 4135–4145.
- [92SAR/BRA] Sarrot, F.-A., Bradbury, M.H., Pandolfo, P., Spieler, P., Diffusion and adsorption studies of hardened cement paste and the effect of carbonation on diffusion rates, *Cement and Concrete Research*, **22** (1992) 439–444.
- [92SAS/SHO] Sassani, D.C., Shock, E.L., Estimation of standard partial molal entropies of aqueous ions at 25°C and 1 bar, *Geochim. Cosmochim. Acta*, **56** (1992) 3895–3908; *Errata*: **58** (1994) 2756–2758.
- [92SAT] Sato, M., Persistency-field Eh-pH diagrams for sulfides and their application to supergene oxidation and enrichment of sulfide ore bodies, *Geochim. Cosmochim. Acta*, **56** (1992) 3133–3156.
- [92SHO/OEL] Shock, E.L., Oelkers, E.H., Johnson, J.W., Sverjensky, D.A., Helgeson, H.C., Calculation of the thermodynamic properties of aqueous species at high pressures and temperatures. Effective electrostatic radii, dissociation constants and standard partial molal properties to 1000°C and 5 kbar, *J. Chem. Soc. Faraday Trans.*, **88** (1992) 803–826.
- [92SKB] SKB 91, Final disposal of spent fuel. Importance of the bedrock for safety, Report SKB-TR-92-20, Swedish Nuclear Fuel and Waste Management Co., 1992, 197p.
- [92TAR/DUP] Tardy, Y., Duplay, J., A method of estimating the Gibbs free energies of formation of hydrated and dehydrated clay minerals, *Geochim. Cosmochim. Acta*, **56** (1992) 3007–3029.
- [92TIP/HUR] Tipping, E., Hurley, M.A., A unifying model of cation binding by humic substances, *Geochim. Cosmochim. Acta*, **56** (1992) 3627–3641.
- [92WU/KAP] Wu, X.G., Kapral, R., Catalytic CO oxidation on Pt surfaces: a lattice-gas cellular automaton model, *Physica*, **A 188** (1992) 284–301.
- [93APP/POS] Appelo, C.A.J., Postma, D., *Geochemistry, groundwater and pollution*, Bakema, Rotterdam, 1993.
- [93APP/ZAL] Appert, C., Zaleski, S., Dynamical liquid-gas phase transition, *J. Phys. II, France*, **3** (1993) 309–337.
- [93BAR] Barin, I., *Thermochemical data of pure substances*, Weinheim: VCH Verlagsgesellschaft mbH, 2nd ed., 1993, 2 Vols.

Reference List

- [93BEA/TSA] Bear, J., Tsang, C.F., de Marsily, G., Flow and contaminant transport in fractured rock, Academic Press, Inc., San Diego, 1993.
- [93BON/FIS] Bonn, B.A., Fish, W., Measuring the electrostatic and site-specific associations of alkali metal cations with humic acid, *J. Soil Sci.*, **44** (1993) 335–345.
- [93BOU/KNA] Bourcier, W.L., Knauss, K.G., Jackson, K.J., Aluminum hydrolysis constants to 250°C from boehmite solubility measurements, *Geochim. Cosmochim. Acta*, **57** (1993) 747–762.
- [93BRU/CAC] Bruno, J., Caceci, M., Nebot, P., Casas, I., de Pablo, J., Heavy Metal Cycling in the Northwestern Mediterranean Coastal Zone and the Evaluation of Its Impact by Speciation, in: *Chemical Industry and the Environment Vol. 1.*, (Casal, J., *ed.*), Univ. Polit. Catalunya, 1993, 238 pp.
- [93BYR/KIM] Byrne, R.H., Kim, K.-H., Rare earth precipitation and coprecipitation behaviour: The limiting role of PO_4^{3-} on dissolved rare earth concentrations in seawater, *Geochim. Cosmochim. Acta*, **57** (1993) 519–526.
- [93CAR] Carroll, S.A., Precipitation of Nd-Ca carbonate solid solution at 25°C, *Geochim. Cosmochim. Acta*, **57** (1993) 3383–3393.
- [93CHE/GIL] Chen, X., Gillespie, S.E., Oscarson, J.L., Izatt, R.M., Calorimetric determination of thermodynamic quantities for chemical reactions in the system $\text{CO}_2\text{-NaOH-H}_2\text{O}$ from 225 to 325°C, in: *Proc. 1991 Symp. on Chemistry in High-Temperature Aqueous Solutions* (Izatt, R.M., Oscarson, J.L., Gillespie, S.E., *eds.*), Technical Report EPRI-TR-102706, Electric Power Research Inst., Palo Alto, California, 1993, pp.F6d.1–F6d.33.
- [93CHE/GIL2] Chen, X., Gillespie, S.E., Oscarson, J.L., Izatt, R.M., Enthalpy of dissociation of water at 325°C and $\log K$, ΔH , ΔS , and ΔC_p values for the formation of NaOH(aq) from 250 to 325°C, in: *Proc. 1991 Symp. on Chemistry in High-Temperature Aqueous Solutions* (Izatt, R.M., Oscarson, J.L., Gillespie, S.E., *eds.*), Technical Report EPRI-TR-102706, Electric Power Research Inst., Palo Alto, California, 1993, pp.F6e.1–F6e.26.
- [93DRO/FRA] Droz, M., Frachebourg, L., Turing structures in cellular automata models of reaction-diffusion systems, *Helv. Phys. Acta*, **66** (1993) 97–98.
- [93EPH/ALL] Ephraim, J.H., Allard, B., Influence of humic substances on the uptake of metal ions by naturally occurring materials, in: *Ion exchange and solvent extraction. A series of advances* (Marinsky, J.A., Marcus, Y., *eds.*), **11** (1993) 335–367, Marcel Dekker, New York.
- [93GIL/OSC] Gillespie, S.E., Oscarson, J.L., Chen, X., Izatt, R.M., Pando, C., Thermodynamic quantities for the interaction of Cl^- with Mg^{2+} , Ca^{2+} and H^+ in aqueous solution from 250 to 325°C, in: *Proc. 1991 Symp. on Chemistry in High-Temperature Aqueous Solutions* (Izatt, R.M., Oscarson, J.L., Gillespie, S.E., *eds.*), Technical Report EPRI-TR-102706, Electric Power Research Inst., Palo Alto, California, 1993, pp.B2d.1–B2d.31.

Reference List

- [93GRU/KAP] Gruner, D., Kapral, R., Lawniczak, A., Nucleation, domain growth, and fluctuation in a bistable chemical-system, *J. Chem. Phys.*, **99** (1993) 3938–3945.
- [93GUR/VEY] Gurvich, L.V., Veyts, I.V., Alcock, C.B., Iorish, V.S., *Thermodynamic Properties of Individual Substances*, Vol. 3, Parts 1 and 2, Boca Raton, Florida: CRC Press, 1993, 1120p.
- [93HAD/MCC] Hadermann, J., McCombie, C., Research needs in HLW disposal programmes, *Mat. Res. Soc. Symp. Proc.*, **294** (1993) 707.
- [93HAS/KAP] Hasslacher, B., Kapral, R., Lawniczak, A., Molecular Turing structures in the biochemistry of the cell, *Chaos*, **3** (1993) 7–13.
- [93HE/MOR] He, S., Morse, J.W., The carbonic acid system and calcite solubility in aqueous Na-K-Ca-Mg-Cl-SO₄ solutions from 0 to 90°C, *Geochim. Cosmochim. Acta*, **57** (1993) 3553–3554.
- [93HIG/KIN] Higgo, J.J.W., Kinniburgh, D., Smith, B., Tipping, E., Complexation of Co²⁺, Ni²⁺, UO₂²⁺ and Ca²⁺ by humic substances in groundwaters, *Radiochim. Acta*, **61** (1993) 91–103.
- [93HOG] Högfeldt, E., A three-parameter model for summarizing data in ion exchange, in: *Ion Exchange and Solvent Extraction*, Vol. 11, Dekker, New York, 1993, pp.120–150.
- [93KAR] Karapiperis, T., in: *Cellular Automata: Prospects in Astrophysical Applications* (Perdang, J.M., Lejeune, A., eds.), Singapore: World Scientific, (1993) pp.187–198.
- [93KIM] Kim, J.I., The chemical behaviour of transuranium elements and barrier functions in natural aquifer systems, in: *Scientific basis for nuclear waste management XVI* (Interrante, C.G., Pabalan, R.T., eds.), *MRS Symp. Proc.*, **294** (1993) 3–21.
- [93KUB/ALC] Kubaschewski, O., Alcock, C.B., Spencer, P.J., *Materials thermochemistry*, 6th ed., Oxford: Pergamon Press Ltd., 1993, 363p.
- [93MAR] Marinsky, J.A., A Gibbs-Donnan-based analysis of ion-exchange and related phenomena, in: *Ion exchange and solvent extraction. A series of advances* (Marinsky, J.A., Marcus, Y., eds.), **11** (1993) 237–334, Marcel Dekker, New York.
- [93MAT/EPH] Mathuthu, A.S., Ephraim, J.H., Calcium binding by fulvic acids studied by an ion selective electrode and an ultrafiltration method, *Talanta*, **40** (1993) 521–526.
- [93MEI/TAK] Meinrath, G., Takeishi, H., Solid-liquid equilibria of Nd³⁺ in carbonate solutions, *J. Alloys and Compounds*, **194** (1993) 93–99.
- [93MOR/HER] Morel, F.M.M., Hering, J.G., *Principles and applications of aquatic chemistry*, New York: John Wiley & Sons, Inc., 1993, 588p.

Reference List

- [93NED/WIT] Nederlof, M.M., de Wit, J.C.M., van Riemsdijk, W.H., Koopal, L.K., Determination of proton affinity distributions for humic substances, *Environ. Sci. Technol.*, **27** (1993) 846–856.
- [93NOR/EPH] Nordén, M., Ephraïm, J.H., Allard, B., The binding of strontium and europium by an aquatic fulvic acid - Ion exchange distribution and ultrafiltration studies, *Talanta* **40** (1993) 1425–1432.
- [93PAL/HYD] Palmer, D.A., Hyde, K.E., An experimental determination of ferrous chloride and acetate complexation in aqueous solutions to 300°C, *Geochim. Cosmochim. Acta*, **57** (1993) 1393–1408.
- [93PAL/WES] Palmer, D.A., Wesolowski, D.J., Aluminum speciation and equilibria in aqueous solution: III. Potentiometric determination of the first hydrolysis constant of aluminum(III) in sodium chloride solutions to 125°C, *Geochim. Cosmochim. Acta*, **57** (1993) 2929–2938.
- [93PED] Pedersen, K., The deep subterranean biosphere, *Earth Sci. Rev.*, **34** (1993) 243–260.
- [93PER/LEJ] Perdang, J.M., Lejeune, A., *eds.*, Cellular Automata: Prospects in Astrophysical Applications, Singapore: World Scientific, 1993.
- [93RIC/LIN] Rice, J.A., Lin, J.S., Fractal nature of humic materials, *Environ. Sci. Technol.*, **27** (1993) 413–414.
- [93SAX/CHA] Saxena, S.K., Chatterjee, N., Fei, Y., Shen, G., Thermodynamic data base for silicates and oxides, Springer-Verlag, Heidelberg, 1993, 428p.
- [93STI/PAR] Stipp, S.L.S., Parks, G.A., Nordstrom, D.K., Leckie, J.O., Solubility-product constant and the thermodynamic properties for synthetic otavite, $\text{CdCO}_3(\text{s})$, and aqueous association constants for the $\text{Cd(II)}\text{-CO}_2\text{-H}_2\text{O}$ system, *Geochim. Cosmochim. Acta*, **57** (1993) 2699–2713.
- [93TIP] Tipping, E., Modeling the competition between alkaline earth cations and trace metal species for binding by humic substances, *Environ. Sci. Technol.*, **27** (1993) 520–529.
- [93TIP2] Tipping, E., Modelling the binding of europium and the actinides by humic substances, *Radiochim. Acta*, **62** (1993) 141–152.
- [93VIE/HAU] Vieno, T., Hautajärvi, A., Koskinen, L., Nordman, H., TVO-92, Safety analysis of spent fuel disposal, YJT-92-33E, Technical Research Centre of Finland, Helsinki, 1993.
- [93VRE/KOR] Vreugdenhil, C.B., Koren, B., Numerical methods for advection-diffusion problems. Notes on Numerical Fluid Mechanics, Vol. 45, Vieweg, Braunschweig, Germany, 1993.

Reference List

- [93WAG/PRU] Wagner, W., Pruss, A., International equations for the saturation properties of ordinary water substance. Revised according to the international temperature scale of 1990. Addendum to J. Phys. Chem. Ref. Data 16, 893 (1987), J. Phys. Chem. Ref. Data, **22** (1993) 783–787.
- [93WIT/RIE] de Wit, J.C.M., van Riemsdijk, W.H., Koopal, L.K., Proton binding to humic substances. 1. Electrostatic effects, Environ. Sci. Technol., **27** (1993) 2005–2014.
- [93WIT/RIE2] de Wit, J.C.M., van Riemsdijk, W.H., Koopal, L.K., Proton binding to humic substances. 2. Chemical heterogeneity and adsorption models, Environ. Sci. Technol., **27** (1993) 2015–2022.
- [94ALL/PER] Allison, J.D., Perdue, E.M., Modeling metal-humic interactions with MINTEQA2, in: Humic Substances in the Global Environment and Implications on Human Health (Senesi, N., Miano, T.M., *eds.*) (1994) *pp.*927–942, Elsevier.
- [94AND/KHO] Anderegg, G., Kholeif, S., The extrapolation of experimental equilibrium constant data to zero ionic strength: critical review and new approach, Talanta, **41** (1994) 1507–1522.
- [94BAN] Banwart, S., Surface processes in water technology, in: Chemistry of Aquatic Systems: Local and Global Perspectives, (Bidoglio, G., Stumm, W., *eds.*), Kluwer, Dordrecht, 1994, *pp.*307–335.
- [94BAT] Batchelor, G.K., An introduction to fluid dynamics, Cambridge Univ. Press, 1994.
- [94BEL] Belonoshko, A.B., Molecular dynamics of MgSiO₃ perovskite at high pressures: Equation of state, structure and melting transition, Geochim. Cosmochim. Acta, **58** (1994) 4039–4047.
- [94BUR] Burnison, B.K., Solubility enhancement of fenvalerate by isolated DOC lake water fractions, Proc. of IHSS 6th International Meeting, Bari-Italy, 1992, (1994).
- [94CHA] Charlet, L., Reactions at the mineral-water interface, in: Chemistry of Aquatic Systems: Local and Global Perspectives, (Bidoglio, G., Stumm, W., *eds.*), Kluwer Academic, Dordrecht, 1994, *pp.*273–305.
- [94CHA/MIL] Chatterjee, N.D., Miller, K., Olbicht, W., Bayes estimation: A novel approach to derivation of internally consistent thermodynamic data for minerals, their uncertainties, and correlations, Phys. Chem. Minerals, **21** (1994) 50–62.
- [94CZE/BUC] Czerwinski, K.R., Buckau, G., Scherbaum, F., Kim, J.I., Complexation of the uranyl ion with aquatic humic acid, Radiochim. Acta, **65** (1994) 111–119.
- [94ENG/HUD] Eng, T., Hudson, J., Stephansson, O., Skagius, K., Wiborgh, M., Scenario development methodologies, Technical Report SKB-TR-94-28, Swedish Nucl. Fuel Waste Manag. Co., Stockholm, Sweden, 1994.

Reference List

- [94ENG/WAN] Engebretson, R.R., van Wandruszka, R., Microorganization in dissolved humic acids, *Environ. Sci. Technol.*, **28** (1994) 1934–1941.
- [94EPH/ALL] Ephraim, J.H., Allard, B., Copper binding by an aquatic fulvic acid: Heterogeneity considerations, *Environmental International*, **20** (1994) 89–95.
- [94ERT/MOH] Erten, H.N., Mohammed, A.K., Choppin, G.R., Variation of stability constants of thorium and uranium oxalate complexes with ionic strength, *Radiochim. Acta*, **66/67** (1994) 123–128.
- [94FAN/KIM] Fanghänel, Th., Kim, J.I., Paviet, P., Klenze, R., Hauser, W., Thermodynamics of radioactive trace elements in concentrated electrolyte solutions: hydrolysis of Cm^{3+} in NaCl-solutions, *Radiochim. Acta*, **66/67** (1994) 81–87.
- [94GEO] GEOVAL '94, Validation through model testing. Proceedings of an NEA/SKI symposium, Paris, France, 11-14 October, 1994, OECD.
- [94GRA] Grauer, R., Bereinigte Löslichkeitsprodukte von M(II)-Schwermetallcarbonaten, Interner Bericht TM-44-94-05, Paul Scherrer Institut, August 1994.
- [94GUS] Gustafsson, J.P., Sulphur, selenium and arsenic in forest soils - retention mechanisms and solid-phase speciation, Ph D Thesis, 1994, Dep. Land Water Resour., The Royal Institute of Technology, Stockholm, Sweden.
- [94HEE/HAD] Heer, W., Hadermann, J., Grimsel test site - Modelling radionuclide migration field experiments, PSI-Bericht Nr. 94-13, Würenlingen, 1994; Nagra NTB 94-18, Wettingen, Switzerland, 1994.
- [94HEE/HAD2] Heer, W., Hadermann, J., Modelling radionuclide migration field experiments, PSI-Bericht Nr. 94-13, Würenlingen and Villigen, 1994 and Nagra Technical Report NTB 94-18, NAGRA, Wettingen, Switzerland, 1994.
- [94HEE/HAD3] Heer, W., Hadermann, J., Jakob, A., Modelling the radionuclide migration experiments at the Grimsel test site, Proc. IAHR Symp. on transport and reactive processes in aquifers, Zurich, April 11-15, 1994, A. A. Balkema, Rotterdam, 1994.
- [94HER/WES] Herbelin, A.L., Westall, J.C., FITEQL - A computer program for determination of chemical equilibrium constants from experimental data. Version 3.1, Report 94-01, Department of Chemistry, Oregon State University, Corvallis, OR, 1994.
- [94JAK/HAD] Jakob, A., Hadermann, J., INTRAVAL Finnsjon Test: modelling results for some tracer experiments, PSI Bericht Nr. 94-12, Würenlingen und Villigen, September 1994 and Nagra Technical Report NTB 94-21, NAGRA, Wettingen, Switzerland, September 1994.
- [94KAR/BLA] Karapiperis, T., Blankleider, B., Cellular automaton model of reaction-transport processes, *Physica*, **D 78** (1994) 30–64.

Reference List

- [94KRA/ALL] Krantz-Rülcker, C., Allard, B., Ephraim, J.H., Acid-base properties of a soil fungus, *trichoderma harzianum*, *Environ. Sci. Technol.*, **28** (1994) 1502–1505.
- [94KRI] KRISTALLIN I, Safety Assessment Report, Nagra NTB 93-22, Wettingen, Switzerland, 1994.
- [94KRI2] KRISTALLIN I, Conclusions from the regional investigation programme for siting a HLW repository in the crystalline basement of Northern Switzerland, Nagra NTB 93-09E, Wettingen, Switzerland, 1994.
- [94LAM] Lamport, L., *L^AT_EX— A document preparation system. User’s guide and reference manual*, 2nd. ed., Reading, Massachusetts: Addison-Wesley, 1994, 272p.
- [94LAS/SOL] Lasaga, A.C., Soler, J.M., Ganor, J., Burch, T.E., Nagy, K.L., Chemical weathering rate laws and global geochemical cycles, *Geochim. Cosmochim. Acta*, **58** (1994) 2361–2386.
- [94MIL/ALE] Miller, W.M., Alexander, R., Chapman, N.A., McKinley, I.G., Smellie, J., *Natural Analogue Studies in the Geological Disposal of Radioactive Wastes, Studies in Environmental Science 57*, Elsevier, Amsterdam, 1994.
- [94NEA] Neall, F.B., “Kristallin-1. Results in perspective”, Nagra NTB 93-23, Wettingen, Switzerland, 1994.
- [94NED/RIE] Nederlof, M.M., van Riemsdijk, W.H., Koopal, L.K., Heterogeneity analysis for binding data using an adapted smoothing spline technique, *Environ. Sci. Technol.*, **28** (1994) 1037–1047.
- [94NOR] Nordén, M., The complexation of some radionuclides with natural organics - Implications for radioactive waste disposal, PhD. Thesis, Linköping University, (1994) Sweden.
- [94NOR/EPH] Nordén, M., Ephraim, J.H., Allard, B., The influence of a fulvic acid on the adsorption of Europium and strontium by alumina and quartz: Effects of pH and ionic strength, *Radiochim. Acta*, **65** (1994) 265–270.
- [94NOR/MUN] Nordstrom, D.K., Munoz, J.L., *Geochemical Thermodynamics*, 2nd. ed., Boston: Blackwell Sci. Publ., 1994.
- [94ORE/SHR] Oreskes, N., Shrader-Fechette, K., Belitz, K., Verification, validation, and confirmation of numerical models in the earth sciences, *Science* **263** (1994) 641–646.
- [94OST/MOR] Österberg, R., Mortensen, K., Fractal geometry of humic acids. Temperature-dependent restructuring studied by small-angle neutron scattering, in: *Humic substances in the Global Environment and Implications on Human Health* (Senesi, N., Miano, T.M., eds.), Elsevier, 1994, pp.127–132.

Reference List

- [94PET/EPH] Pettersson, C., Ephraim, J., Allard, B., On the composition and properties of humic substances isolated from deep groundwater and surface waters, *Org. Geochem.*, **21** (1994) 443–451.
- [94PLY/GRE] Plyasunov, A.V., Grenthe, I., The temperature dependence of stability constants for the formation of polynuclear cationic complexes, *Geochim. Cosmochim. Acta*, **58** (1994) 3561–3582.
- [94SCH] Schulten, H.R., A chemical structure for humic acid. Pyrolysis-gas chromatography/mass spectrometry and pyrolysis-soft ionization mass spectrometry evidence, in: *Humic Substances in the Global Environment and Implications on Human Health* (Senesi, N., Miano, T.M., *eds.*), Elsevier, Amsterdam, 1994, *pp.*43–56.
- [94SEN] Senesi, N., The fractal approach to the study of humic substances, in: *Humic substances in the Global Environment and Implications on Human Health* (Senesi, N., Miano, T.M., *eds.*), Elsevier, 1994, *pp.*3–41.
- [94SIG/XUE] Sigg, L., Xue, H., Metal speciation: concepts, analysis and effects, in: *Chemistry of Aquatic Systems: Local and Global Perspectives*, (Bidoglio, G., Stumm, W., *eds.*), Kluwer Academic, Dordrecht, 1994, *pp.*153–181.
- [94SZE/SZE] Szewzyk, U., Szewzyk, R., Stenström, T.H., Thermophilic anaerobic bacteria isolated from a 4000 m deep borehole, National Bacteriological Laboratory, Dep. Water Microb., S-105 21 Stockholm, 1994, Sweden.
- [94TIP] Tipping, E., WHAM - a chemical equilibrium model and computer code for waters, sediments, and soils incorporating a discrete site/electrostatic model of ion-binding by humic substances, *Comput. Geosci.*, **20** (1994) 973–1023.
- [94VIA/BRU] Viani, B.E., Bruton, C.J., Effect of cation exchange on major cation chemistry in the large scale redox experiment at Äspö, in: *Proceedings of the Äspö International Geochemistry Workshop* (Banwart, S., *ed.*), June 2-3 1994, Äspö Hard Rock Laboratory, International Cooperation Report 94-13, The Swedish Nuclear Fuel and Waste Management Company, Stockholm.
- [94WAI/PAY] Waite, T.D., Payne, T.E., Waychunas, G.A., Xu, N., Uranium(VI) adsorption to ferrihydrite: application of a surface complexation model, *Geochim. Cosmochim. Acta*, **58(24)** (1994) 5465–5478.
- [94WER/BRU] Wersin, P., Bruno, J., Laaksoharju, M., The implications of soil acidification on a future HLNW repository. Part II. Influence on deep granitic groundwater. The Klipperas study site as test case, SKB-TR-94-31, Swedish Nucl. Fuel Waste Manag. Co., Stockholm, Sweden, 1994.
- [94WER/SPA] Wersin, P., Spahiu, K., Bruno, J., Time evolution of dissolved oxygen and redox conditions in a HLW repository, SKB-TR-94-02, Swedish Nucl. Fuel Waste Manag. Co., Stockholm, Sweden, 1994.

Reference List

- [94WOO/CAR] Wood, R.H., Carter, R.W., Quint, J.R., Majer, V., Thompson, P.T., Boccio, J.R., Aqueous electrolytes at high temperatures: comparison of experiment with simulation and continuum models, *J. Chem. Thermodyn.*, **26** (1994) 225–249.
- [94YOO/MOO] Yoon, T.H., Moon, H., Park, Y.J., Park, K.K., Investigation of metal binding sites on soil fulvic acid using Eu(III) luminescence spectroscopy, *Environ. Sci. Technol.*, **28** (1994) 2139–2146.
- [95BEN/MIL] Benedetti, M.F., Milne, C.J., Kinniburgh, D.G., van Riemsdijk, W.H., Koopal, L.K., Metal ion binding to humic substances: Application of the non-ideal competitive adsorption model, *Environ. Sci. Technol.*, **29** (1995) 446–457.
- [95BER] Berner, U., KRISTALLIN-I: Estimates of solubility limits for safety relevant radionuclides, PSI-Bericht Nr. 95-07, NTB 94-08 (1995).
- [95BRU/PAB] Bruno, J., de Pablo, J., Duro, L., Figuerola, E., Experimental and modelling study of the U(VI)-Fe(OH)₃ surface precipitation-coprecipitation equilibria, *Geochim. Cosmochim. Acta*, **59** (1995) 4113–4123.
- [95CAP/VIT] Capdevila, H., Vitorge, P., Redox potentials of $\text{PuO}_2^{+2}/\text{PuO}_2^{+}$ and $\text{Pu}^{+4}/\text{Pu}^{+3}$ at different ionic strengths and temperatures. Entropy and heat capacity, *Radiochim. Acta*, **68** (1995) 51–62.
- [95CHA/AND] Chapman, N.A., Anderson, J., Robinson, P., Skagius, K., Werne, C.O., Wiborgh, M., Wingefors, S., SITE-94: systems analysis, scenario construction and consequence analysis definition for SITE-94, SKI Report 95:26, June 1995, Swedish Nuclear Power Inspectorate, Stockholm, Sweden.
- [95CHE/DAW] Chen, S., Dawson, S.P., Doolen, G.D., Janckey, D.R., Lawniczak, A., Lattice methods and their applications to reacting systems, *Computers & Chemical Engineering*, **19** (1995) 617–646.
- [95EPH/PET] Ephraim, J.H., Pettersson, C., Nordén, M., Allard, B., Potentiometric titrations of humic substances: do ionic strength effects depend on the molecular weight?, *Environ. Sci. Technol.*, **29** (1995) 622–628.
- [95GLA/HUM] Glaus, M.A., Hummel, W., Van Loon, L.R., Stability of mixed-ligand complexes of metal ions with humic substances and low molecular weight ligands, *Environ. Sci. Technol.*, **29** (1995) 2150–2153.
- [95JOH/NEL] Johnson, D.A., Nelson, P.G., Ligand-field stabilization energies of the first-row transition-metal dihalides and their bearing on the Irving-Williams rule, *J. Chem. Soc. Dalton Trans.*, 1995, 3483–3488.
- [95KAR] Karapiperis, T., Cellular automaton model of precipitation/dissolution coupled with solute transport, *Journal of Statistical Physics*, **81** (1995) 165–180.
- [95KAR2] Karapiperis, T., A mesoscopic investigation of coupled precipitation/dissolution and solute transport using a cellular automaton model, PSI Internal Report TM-44-95-03, Würenlingen and Villigen, 1995.

Reference List

- [95MAR/RED] Marinsky, J.A., Reddy, M.M., Ephraim, J.H., Mathuthu, A.S., Computational scheme for the prediction of metal ion binding by a soil fulvic acid, *Anal. Chimica Acta*, **302** (1995) 309–322.
- [95MAT/EPH] Mathuthu, A.S., Ephraim, J.H., Marinsky, J.A., Dissociation properties of Laurentide fulvic acid: Identifying the predominant acidic sites, *Talanta*, **42** (1995) 441–447.
- [95MOU/MOU] Moulin, V., Moulin, C., Fate of actinides in the presence of humic substances under conditions relevant to nuclear waste disposal, *Applied Geochem.*, **10** (1995) 573–580.
- [95MOU/MOU2] Moulin, V., Moulin, C., Choppin, G., Labonne, N., Interactions of natural organic substances with radionuclides: competition of other complexes, experimental results, in: *Binding Models Concerning Natural Organic Substances in Performance Assessment*, OECD Nuclear Energy Agency, Paris, 1995, *pp.*223–232.
- [95NEA] NEA, Binding models concerning natural organic substances in performance assessment, *Proceedings from the NEA Workshop*, OECD Nuclear Energy Agency, Paris, 1995.
- [95NEC/FAN] Neck, V., Fanghänel, Th., Rudolph, G., Kim, J.I., Thermodynamics of neptunium(V) in concentrated salt solutions; chloride complexation and ion interaction (Pitzer) parameters for the NpO_2^+ ion, *Radiochim. Acta*, **69** (1995) 39–47.
- [95OES] Östhols, E., Thorium sorption on amorphous silica, *Geochim. Cosmochim. Acta.*, **59** (1995) 1235–1250.
- [95PAS/KIM] Pashalidis, I., Kim, J.I., Ashida, T., Grenthe, I., Spectroscopy study of the hydrolysis of PuO_2^{2+} in aqueous solution, *Radiochim. Acta*, **68** (1995) 99–104.
- [95PED/KAR] Pedersen, K., Karlsson, F., Investigations of subterranean microorganisms. Their importance for performance assessment of radioactive waste disposal, SKB-TR-95-10, Swedish Nucl. Fuel Waste Manag. Co., Stockholm, Sweden, 1995.
- [95RAO/CHO] Rao, L., Choppin, G.R., Thermodynamic study of the complexation of neptunium(V) with humic acids, *Radiochim. Acta*, **69** (1995) 87–95.
- [95ROB/HEM] Robie, R.A., Hemingway, B.S., Thermodynamic properties of minerals and related substances at 298.15 K and 1 bar (10^5 Pascals) pressure and at higher temperatures, *US Geological Survey Bulletin*, **2131** (1995) 461*p.*
- [95SIL/BID] Silva, R.J., Bidoglio, G., Rand, M.H., Robouch, P.B., Wanner, H., Puigdomenech, I., *Chemical thermodynamics of americium*, Amsterdam: Elsevier Science Publishers B.V., 1995, 375*p.*

Reference List

- [95SPA/BRU] Spahiu, K., Bruno, J., A selected thermodynamic database for REE to be used in HLNW performance assessment exercises, SKB-TR-95-35, Swedish Nucl. Fuel Waste Manag. Co., Stockholm, Sweden, 1995.
- [96AHR] Åhrland, S., The relative affinities of ligand atoms for acceptor molecules and ions: a long story revisited, *Coord. Chem. Rev.*, **154** (1996) 13–18.
- [96BAN/TUL] Banwart, S., Tullborg, E.-L., Pedersen, K., Gustafsson, E., Laaksoharju, M., Nilsson, A.-C., Wallin, B., Wikberg, P., Organic carbon oxidation induced by large-scale shallow water intrusion into a vertical fracture zone at the Äspö Hard Rock Laboratory (Sweden), *J. Contaminat Hydrol.*, **21** (1996) 115–125.
- [96BEV/PUI] Beverskog, B., Puigdomenech, I., Revised Pourbaix diagrams for iron at 25–300°C, *Corrosion Sci.*, **38** (1996) 2121–2135.
- [96BRU/DUR] Bruno, J., Duro, L., Jordana, S., Cera, E., Revisiting Poços de Caldas. Application of the co-precipitation approach to establish realistic solubility limits for performance assessment, SKB-TR-96-04, Swedish Nucl. Fuel Waste Manag. Co., Stockholm, Sweden, 1996.
- [96BRU/DUR2] Bruno, J., Duro, L., Linklater, C.M., Goldberg, J.E., Gimeno, M.J., Pena, J., Ayora, C., Delgado, J., Casas, I., Testing of geochemical models for trace element mobility at El Berrocal. Topical Report 7 of El Berrocal Project, Enresa (Madrid), 1996.
- [96CZE/KIM] Czerwinski, K.R., Kim, J.I., Rhee, D.S., Buckau, G., Complexation of trivalent actinide ions (Am^{3+} , Cm^{3+}) with humic acid: The effect of ionic strength, *Radiochim. Acta*, **72** (1996) 179–187.
- [96DEN/STJ] Deng, Y., Stjernström, M., Banwart, S., Accumulation and remobilization of aqueous chromium(VI) at iron oxide surfaces: application of a thin-film continuous flow-through reactor, *J. Contaminant Hydrol.*, **21** (1996) 141–151.
- [96HAD/HEE] Hadermann, J., Heer, W., The Grimsel (Switzerland) migration experiment. Integrating field experiments, laboratory investigations and modelling, *J. Contam. Hydrol.*, **21** (1996) 87–100.
- [96KIM/CZE] Kim, J.I., Czerwinski, K.R., Complexation of metal ions with humic acid: Metal ion charge neutralization model, *Radiochim. Acta*, **73** (1996) 5–10.
- [96MAL/BAN] Malmström, M., Banwart, S., Lewenhagen, J., Duro, L., Bruno, J., The dissolution of biotite and chlorite at 25°C in the near neutral pH region, *J. Contaminant Hydrol.*, **21** (1996) 201–213.
- [96MER/FUG] Merli, L., Fuger, J., Thermochemistry of selected lanthanide and actinide hydroxycarbonates and carbonates, *Radiochim. Acta*, **74** (1996) 37–43.
- [96NEA] NEA, The international INTRAVAL project – Final results, OECD, Paris, 1996.

Reference List

- [96PLY/GRE] Plyasunov, A.V., Grenthe, I., Extrapolation of enthalpies of reaction in electrolyte systems to infinite dilution, *Acta Chem. Scand.*, **50** (1996) 571–579.
- [96STU/MOR] Stumm, W., Morgan, J.J., *Aquatic Chemistry*, 3rd edition, New York, John Wiley & Sons, 1996.
- [96TAO/DU] Tao, Z., Du, J., Li, J., Use of the ion exchange method for determination of stability constants of uranyl ions with three soil fulvic acids, *Radiochim. Acta*, **72** (1996) 51–54.
- [96XIA/TRE] Xiao, C., Tremaine, P.R., Apparent molar heat capacities and volumes of $\text{LaCl}_3(\text{aq})$, $\text{La}(\text{ClO}_4)_3(\text{aq})$, and $\text{Gd}(\text{ClO}_4)_3(\text{aq})$ between the temperatures 283 K and 338 K, *J. Chem. Thermodyn.*, **28** (1996) 43–66.
- [97BRU/VIA] Bruton, C.J., Viani, B.E., Sorption onto hydrous oxides: effect on major element fluid chemistry at Äspö, Sweden, in: *Integration of hydrochemical and hydrogeological models of Äspö*, (Laaksoharju, M, Wallin, B., eds.), Swedish Nucl. Fuel Waste Manag. Co., Stockholm, 1997, in preparation.
- [97SHO/SAS] Shock, E.L., Sassani, D.C., Willis, M., Sverjensky, D.A., Inorganic species in geologic fluids: Correlations among standard molal thermodynamic properties of aqueous ions and hydroxide complexes, *Geochim. Cosmochim. Acta*, **61** (1997) 907–950.
- [97SVE/SHO] Sverjensky, D.A., Shock, E.L., Helgeson, H.C., Prediction of the thermodynamic properties of aqueous metal complexes to 1000°C and 5 kb, *Geochim. Cosmochim. Acta*, **61** (1997) 1359–1412.